AWARD NUMBER: W81XWH-22-1-0238

TITLE: Receptors in Endosomes Mediate Chronic Pain Associated with Trauma, Inflammation, and Stress: Non-Opioid Targets for Sustained Relief of Pain

PRINCIPAL INVESTIGATOR: Nigel Bunnett, PhD

CONTRACTING ORGANIZATION: New York University, New York, NY

REPORT DATE: October 2023

TYPE OF REPORT: Annual

PREPARED FOR: U.S. Army Medical Research and Development Command
Fort Detrick, Maryland 21702-5012

DISTRIBUTION STATEMENT: Approved for Public Release;
Distribution Unlimited

The views, opinions and/or findings contained in this report are those of the author(s) and should not be construed as an official Department of the Army position, policy or decision unless so designated by other documentation.

REPORT DOCUMENTATION PAGE

Form Approved
OMB No. 0704-0188

Public reporting burden for this collection of information is estimated to average 1 hour per response, including the time for reviewing instructions, searching existing data sources, gathering and maintaining the data needed, and completing and reviewing this collection of information. Send comments regarding this burden estimate or any other aspect of this collection of information, including suggestions for reducing this burden to Department of Defense, Washington Headquarters Services, Directorate for Information Operations and Reports (0704-0188), 1215 Jefferson Davis Highway, Suite 1204, Arlington, VA 22202-4302. Respondents should be aware that notwithstanding any other provision of law, no person shall be subject to any penalty for failing to comply with a collection of information if it does not display a currently valid OMB control number. **PLEASE DO NOT RETURN YOUR FORM TO THE ABOVE ADDRESS.**

1. REPORT DATE	**2. REPORT TYPE**	**3. DATES COVERED**
October 2023	Annual	01Sep2022-31Aug2023

4. TITLE AND SUBTITLE

Receptors in Endosomes Mediate Chronic Pain Associated with Trauma, Inflammation, and Stress: Non-Opioid Targets for Sustained Relief of Pain

5a. CONTRACT NUMBER
W81XWH-22-1-0238

5b. GRANT NUMBER
PR212174

5c. PROGRAM ELEMENT NUMBER

6. AUTHOR(S)

Nigel Bunnett, PhD

E-Mail: nwb2@nyu.edu

5d. PROJECT NUMBER

5e. TASK NUMBER

5f. WORK UNIT NUMBER

7. PERFORMING ORGANIZATION NAME(S) AND ADDRESS(ES)

NEW YORK UNIVERSITY
70 Washington Square S
New York, NY 10010

8. PERFORMING ORGANIZATION REPORT NUMBER

9. SPONSORING / MONITORING AGENCY NAME(S) AND ADDRESS(ES)

U.S. Army Medical Research and Development Command
Fort Detrick, Maryland 21702-5012

10. SPONSOR/MONITOR'S ACRONYM(S)

11. SPONSOR/MONITOR'S REPORT NUMBER(S)

12. DISTRIBUTION / AVAILABILITY STATEMENT

Approved for Public Release; Distribution Unlimited

13. SUPPLEMENTARY NOTES

14. ABSTRACT

G-protein coupled-receptors (GPCRs) mediate pain. Damaged and diseased tissue secrete proteases that activate a GPCR, protease-activated receptor-2 (PAR_2) on sensory neurons. The activated sensory neurons release neuropeptides including substance P (SP) and calcitonin gene-related peptide (CGRP). SP activates the neurokinin-1 receptor (NK_1R) and CGRP activates calcitonin-like receptor (CLR), which produces pain. Endocytosis, which is the process of intracellular uptake of plasma membrane receptors, terminates plasma membrane signaling of GPCRs; however, evidence, including work supported by our original Peer Reviewed Medical Research Program (PRMRP) Award, indicates that GPCRs in intracellular sorting organelles, termed endosomes, can generate sustained signals that govern the transition from acute to chronic pain. PAR_2 is implicated in pain associated with inflammatory bowel disease (IBD). Endosomal signaling of PAR_2 in trigeminal nociceptors and Schwann cells mediates post-traumatic headache (PTH). For the Expansion Award we developed encapsulated small molecule GPCR antagonists, including FDA-approved drugs, into nanoparticles (NPs). Our NPs offer a fresh approach for the treatment of chronic pain, especially pain related to IBD and PTH, which disproportionately affects military personnel and veterans.

15. SUBJECT TERMS
None listed.

16. SECURITY CLASSIFICATION OF:			**17. LIMITATION OF ABSTRACT**	**18. NUMBER OF PAGES**	**19a. NAME OF RESPONSIBLE PERSON**
a. REPORT	**b. ABSTRACT**	**c. THIS PAGE**			USAMRDC
Unclassified	Unclassified	Unclassified	Unclassified	310	**19b. TELEPHONE NUMBER** *(include area code)*

TABLE OF CONTENTS

	Page
1. Introduction	4
2. Keywords	4
3. Accomplishments	4
4. Impact	10
5. Changes/Problems	10
6. Products	10
7. Participants & Other Collaborating Organizations	12
8. Special Reporting Requirements	14
9. Appendices	14

1. INTRODUCTION

The object of this research is to develop new treatments for the pain associated with inflammatory bowel disease (IBD) and post-traumatic headache (PTH) that afflict military personnel and the general population. The proposal aims to develop nanoparticle (NP) -encapsulated antagonists of G protein-coupled receptors (GPCRs) that signal from endosomes to cause pain associated with IBD and PTH. The NPs will be tested in preclinical mouse models of IBD and PTH, and also studied in human cells to assess translation to patients. Targeted receptors include protease-activated receptor-2 (PAR_2), a receptor for proteases that are generated during inflammation and injury, and calcitonin-like receptor (CLR), a receptor for calcitonin gene-related peptide (CGRP), which is released from nociceptors in inflamed and damaged tissues. During inflammation (*e.g.*, IBD) and injury (*e.g.*, PTH), proteases and neuropeptides are released that activate PAR_2 and CLR on nociceptors and ensheathing Schwann cells. PAR_2 and CLR traffic to endosomes and continue to signal by $G\alpha$- and β-arrestin (βARR)-mediated mechanisms that initiate and sustain pain. When encapsulated into NPs that are optimized for endosomal uptake/retention and for sustained cargo release in endosomes, PAR_2 and CLR antagonists prevent the transition from acute to chronic pain and reverse preexisting chronic pain of IBD and PTH. This approach provides superior efficacy when compared to conventional antagonists, which are usually designed to target cell surface receptors and are unable to effectively antagonize receptors in endosomes. Lyophilized NPs allow stable drug storage in resource-limited environments. Targeted NPs that encapsulate combinations of antagonists surmount the inherent redundancy of pain signaling. NPs offer the prospect of prophylactic and early intervention in far-forward operational environments.

2. KEYWORDS

Pain, Inflammation, Trauma, Neuropeptides, Proteases, Receptors, Signal Transduction, Trafficking, Endosomes, Nanomedicines, Drug Delivery

3. ACCOMPLISHMENTS

The objectives of the proposal are: **1.** Optimize NPs for efficient encapsulation of PAR_2 and CLR antagonists, stable long-term storage (lyophilized, room temperature), sustained stimulus-responsive (pH) release of cargo (days), efficient uptake/retention in endosomes and antagonism of eGPCRs. **2.** Determine the causative role of PAR_2 and CLR in IBD/IBS and PTH pain and identify the critical cell types by deletion of receptors in nociceptors and Schwann cells of mice. **3.** Analyze mechanisms of endosomal PAR_2 and CLR signaling in isolated nociceptors and Schwann cells. **4.** Assess efficacy, potency and duration of action of NP-encapsulated PAR_2 and CLR antagonists for inhibition of eGPCR signals and prevention/reversal of IBD/IBS and PTH pain in preclinical models in mice. **5.** Translate findings to humans by analysis of patient-derived nociceptors, Schwann cells and colon tissues.

Progress has been made in all three aims. Results have been published and manuscripts are under review and also have been prepared for submission.

Development and characterization of NPs. Four nanoparticle formulations have been developed containing antagonists of GPCRs for proteases and neuropeptides.

1. Soft polymer nanoparticles (DIPMA) were generated and used to encapsulate antagonists of CLR and the related substance P, neurokinin-1 receptor (NK_1R).
2. Dendrimer nanostar polymer NPs were generated and used to encapsulate antagonists of CLR and NK_1R.
3. Dendrimer PAMAM NPs coated with cholesterol (PAMAM-Chol) NPs were generated and used to encapsulate PAR_2 antagonists.
4. Polymeric pegylated NPs (Poly-PEG) were generated and used to encapsulated antagonists of CLR and PAR_2.

All NP formulations were analyzed to measure size, charge and polydispersity. Cargo loading and the kinetics of cargo release were measured. Toxicity was assessed. NP stability was determined and conditions for lyophilization and long-term storage were optimized. Fluorescent NPs were generated to study cellular uptake and retention in endosomes.

DIPMA NPs demonstrated rapid, pH-dependent cargo release in acidified early endosomes; cargo was released within minutes of encountering the acidic endosomal environment. DIMPA NPs were stable for up to

4 weeks. Nanostars, PAMAM-Chol and PEG-Poly NPs did not demonstrate pH-dependent cargo release. Nanostars released cargo over hours. PAMAM-Chol and PEG-Poly NPs released cargo over days. All NP formulations trafficked to endosomes of target cells, including neurons, Schwann cells and epithelial cells. NPs did not cause detectable cytotoxicity at the concentrations used to evaluate their effects on GPCR signaling, neuronal excitation, and pain in preclinical models.

NP antagonism of eGPCR signaling. An assay was developed to study the formation of GPCR signaling complexes in subcellular compartments of living cells with high spatial and temporal resolution. Assembly of signalosomes in subcellular compartments was monitored using NanoLuc Binary Technology Bioluminescence Resonance Energy Transfer (nbBRET) to measure proximity of PAR_2 or CLR and mini (m) Gα and βARR isoforms, and organelle markers. mGα proteins are N-terminally truncated forms of Gα that diffuse through the cytosol to interact with active GPCRs. NbBRET is based on a split luciferase assay whereby human PAR_2 or CLR was C-terminally tagged with the Natural Peptide (NP) fragment of NanoLuc (13 residue NanoBiT fragment) and HA-tagged localization markers of the plasma membrane (CAAX), early endosomes (FYVE), recycling endosomes (Rab4a, Rab11a), late endosomes (Rab7a), cis-Golgi network (giantin) and trans-Golgi network (TGN38) were tagged with large NanoBiT fragment (LgBiT). Luminescence occurs from a complex between PAR_2-NP and LgBiT markers, which serves as an energy donor for fluorophore-tagged isoforms of Venus-mGα or βARR-YFP. Both PAR2 and CLR were found to signal from early, late and recycling endosomes and the Golgi apparatus. NP-encapsulated antagonists abrogated signaling in intracellular compartments, demonstrating efficient targeting of eGPCRs.

Anti-nociceptive actions of NP encapsulated eGPCR antagonists in preclinical models of colonic and periorbital pain. The following studies have been completed and published, are under review or are in preparation for submission.

Mice expressing fluorescent PAR_2 reveal that endocytosis mediates colonic inflammation and pain. GPCRs regulate many pathophysiological processes and are major therapeutic targets. The impact of disease on the subcellular distribution and function of GPCRs is poorly understood. We investigated trafficking and signaling of protease-activated receptor-2 (PAR_2) in colitis. To localize PAR_2 and assess redistribution during disease, we generated knockin mice expressing PAR_2 fused to monomeric ultra-stable green fluorescent protein (muGFP). PAR_2-muGFP signaled and trafficked normally. PAR_2 mRNA was detected at similar levels in *Par$_2$-mugfp* and wild-type mice. Immunostaining with a GFP antibody and RNAScope® *in situ* hybridization using *F2rl1* (PAR_2) and *Gfp* probes revealed that PAR_2-muGFP was expressed in epithelial cells of the small and large intestine and in subsets of enteric and dorsal root ganglia neurons. In healthy mice, PAR_2-muGFP was prominently localized to the basolateral membrane of colonocytes. In mice with colitis, PAR_2-muGFP was depleted from the plasma membrane of colonocytes and redistributed to early endosomes, consistent with generation of proinflammatory proteases that activate PAR_2. PAR_2 agonists stimulated endocytosis of PAR_2 and recruitment of $G\alpha_q$, $G\alpha_i$ and β-arrestin2 to early endosomes of T84 colon carcinoma cells, assessed using bioluminescence resonance energy transfer and fluorescence microscopy. PAR_2 agonists increased paracellular permeability of colonic epithelial cells, induced colonic inflammation and hyperalgesia in mice, and stimulated proinflammatory cytokine release from segments of human colon. Knockdown of dynamin-2 (*Dnm2*), the major colonocyte isoform, and Dnm inhibition attenuated PAR_2 endocytosis, signaling complex assembly, and colonic inflammation and hyperalgesia. Thus, PAR_2 endocytosis sustains protease-evoked inflammation and nociception and PAR_2 in endosomes is a potential therapeutic target for colitis.

Nanomedicines targeting $PARr_2$ signaling in endosomes of colonocytes and nociceptors reverse colonic inflammatory pain. Although nanomedicines targeting diseased tissues, cells and organelles offer the prospect of improved therapeutic efficacy and minimal side effects, sequestration in liver and spleen, protein fouling and inability to selectively target organelles of diseased cells represent formidable challenges. Herein, we demonstrate that dendrimer and polymeric nanoparticles locally administered into the mouse colonic lumen accumulate and persist in endosomes of colonocytes and neurons. NPs encapsulating an antagonist of PAR_2, AZ3451, inhibit the assembly of PAR_2/Gα/β-arrestin signalosomes in endosomes and the Golgi apparatus and prevent PAR_2-induced hyperexcitability of nociceptors, a hallmark of pain. NP AZ3451 formulations reverse allodynia and proinflammatory cytokine and chemokine expression and normalize locomotor, exploratory and grooming behavior in preclinical models of inflammatory bowel disease. Unencapsulated AZ3451 is largely ineffective. Luminally administered nanomedicines provide an opportunity to target the organelle-specific signals in colonocytes and neurons that mediate disease, minimizing dosing and the side effects of systemic exposure.

Targeting of protease-activated receptor-2 in endosomes using nanoparticle-encapsulated antagonist provides long-lasting relief from oral cancer pain. Oral cancer is notoriously painful. Seventy percent of oral cancer patients experience high levels of pain that diminishes quality of life. This pain worsens with disease progression and responds poorly to opioids. PAR_2 is a GPCR implicated in oral cancer pain. Our investigation documented PAR_2 overexpression in oral cancer patients. By deleting the PAR_2 gene in an oral cancer mouse model, we observed a reduction in nociception, suggesting the involvement of sustained PAR2 signaling from endosomes in persistent oral cancer pain. We explored the use of nanoparticles (NPs) to deliver a PAR_2 antagonist, AZ3451, to endosomes as a therapeutic approach for sustained oral cancer pain management. A third-generation poly (amidoamine) dendrimer was functionalized with cholesterol to form an amphiphilic molecule that self-assembled into NPs for the encapsulation of AZ3451. The NPs were characterized for size (150 – 200 nm), zeta potential (65 – 72 mV), encapsulation efficiency (>99%), loading level (up to 40% w/w), release kinetics (>24 hr), and intracellular trafficking. Confocal imaging demonstrated uptake and retention of NPs in early endosomes of oral cancer cells, the sites of PAR_2 signaling. The AZ3451-loaded NPs showed significant reductions in mechanical and thermal nociception for more than 24 hours in two preclinical mouse models of oral cancer pain. These findings suggest that the proposed NPs delivering a PAR_2 antagonist to endosomes of oral cancer cells can achieve sustained anti-nociception. The study provides promising evidence for the potential of an endosome-targeted nanomedicine as a superior pain relief strategy for oral cancer patients.

Oral cancer induced TRPV1 sensitization is mediated by PAR_2 signaling in primary afferent neurons innervating the cancer microenvironment. Oral cancer patients report sensitivity to spicy foods and liquids. The mechanism responsible for chemosensitivity induced by oral cancer is not known. We simulate oral cancer-induced chemosensitivity in a xenograft oral cancer mouse model using two-bottle choice drinking and conditioned place aversion assays. An anatomic basis of chemosensitivity is shown in increased expression of TRPV1 in anatomically relevant trigeminal ganglion (TG) neurons in both the xenograft and a carcinogen (4-nitroquinoline 1-oxide)-induced oral cancer mouse models. The percent of retrograde labeled TG neurons that respond to TRPV1 agonist, capsaicin, is increased along with the magnitude of response as measured by calcium influx, in neurons from the cancer models. To address the possible mechanism of TRPV1 sensitivity in tongue afferents, we study the role of PAR_2, which can sensitize the TRPV1 channel. We show co-expression of TRPV1 and PAR_2 on tongue afferents and using a conditioned place aversion assay, demonstrate that PAR_2 mediates oral cancer-induced, TRPV1-evoked sensitivity in an oral cancer mouse model. The findings provide insight into oral cancer-mediated chemosensitivity.

CGRP signals from endosomes of Schwann cells elicit periorbital mechanical allodynia: relevance for migraine. Efficacy of monoclonal antibodies against CGRP or its receptor, CLR and receptor activity modifying protein-1 (RAMP1) implicates peripherally-released CGRP in migraine pain. However, the site and mechanism of CGRP-evoked migraine pain remain unknown. By cell-selective RAMP1 gene deletion, we reveal that CGRP released from mouse cutaneous trigeminal fibers targets CLR/RAMP1 on surrounding Schwann cells to evoke periorbital mechanical allodynia. CLR/RAMP1 activation in human and mouse Schwann cells generates long-lasting signals from endosomes that evoke cAMP-dependent formation of NO. NO, by gating Schwann cell transient receptor potential ankyrin 1 (TRPA1), releases ROS, which in a feed-forward manner sustain allodynia *via* nociceptor TRPA1. When encapsulated into NPs that release cargo in acidified endosomes, a CLR/RAMP1 antagonist provides superior inhibition of CGRP signaling and allodynia in mice. The CGRP-mediated neuronal/Schwann cell pathway is critical to mediate allodynia associated with neurogenic inflammation, thus contributing to the pro-migraine action of CGRP.

Exploiting drug delivery approaches to target subcellular CGRP-induced signalosomes for enhanced analgesia. While GPCRs are classically considered to signal from the plasma membrane, seminal findings have demonstrated that GPCR signaling continues from subcellular endosomes. Compartmentalized signaling is often explored in the context of early endosomes, and more recently the Golgi apparatus. However GPCRs enter many distinct intracellular compartments. As well as being a clinically-approved target for migraine pain, CGRP is a major analgesic target for non-opioid therapeutics. This pro-nociceptive peptide is key in both the peripheral and central transmission of nociception. We demonstrated that CGRP induces CGRP/RAMP1 to form its active conformation at the plasma membrane, multiple endosomal populations (late, recycling) as well as the Golgi apparatus. To enhance drug development targeting prolonged CGRP signalling, we have developed two NP-based therapeutics that utilize drug delivery methods for delayed release of olcegepant/BIBN4096BS. Hydrogen ion-pairing NPs (HIPs) were used to encapsulate olcegepant, while benzo-conjugated nanostars were used for delayed release kinetics through a covalent bond that cleaved upon acidic pH. We demonstrate that NPs can provide potent inhibition of CGRP-induced signalling at the plasma

membrane and intracellular signalling compartments. Upon intrathecal injection, both approaches had enhanced analgesia to free olcegepant. As well as providing evidence for CGRP-induced signalosomes in multiple subcellular compartments, these drug delivery approaches can be exploited to enhance analgesia for the treatment of chronic pain.

Sustained endosomal release of a neurokinin-1 receptor antagonist from nanostars provides long-lasting relief of chronic pain. Soft polymer nanoparticles designed to disassemble and release an antagonist of the neurokinin 1 receptor (NK_1R) in endosomes provide efficacious yet transient relief from chronic pain. These micellar nanoparticles are unstable and rapidly release cargo, which may limit the duration of analgesia. We examined the efficacy of stable star polymer nanostars containing the NK_1R antagonist aprepitant-amine for the treatment of chronic pain in mice. Nanostars continually released cargo for 24 h, trafficked through the endosomal system, and disrupted NK_1R endosomal signaling. After intrathecal injection, nanostars accumulated in endosomes of spinal neurons. Nanostar-aprepitant reversed mechanical, thermal and cold allodynia and normalized nociceptive behavior more efficaciously than free aprepitant in preclinical models of neuropathic and inflammatory pain. Analgesia was maintained for >10 h. The sustained endosomal delivery of antagonists from slow-release nanostars provides effective and long-lasting reversal of chronic pain.

Goals of Project. The table indicates approved Statement of Work tasks, date of completed tasks, and percentage of tasks accomplished by those dates.

Abbreviations: βARRs, β-arrestins; BLS, bright light stress; BRET, bioluminescence resonance energy transfer assay; CGRP, calcitonin gene-related peptide; CI, counter ion; CLR, calcitonin-like receptor; DRG, dorsal root ganglia; ERK, extracellular signal-regulated kinase; FRET, Förster resonance energy transfer; GPCR, G protein-coupled receptor; eGPCR, endosomal GPCR; HIP, hydrophobic ion pairing; IBD, inflammatory bowel disease; NP, nanoparticle; PAR2, protease-activated receptor-2; PKA, protein kinase A; PKC, protein kinase C; PTH, post-traumatic headache; RAMP1, receptor activity-modifying protein 1; TG, trigeminal ganglia; TNBS, trinitrobenzene sulphonic acid; TRPA1, transient receptor potential ankyrin 1 channel

Aim 1: Aim 1. To develop NP-encapsulated PAR_2 and CLR antagonists optimized for sustained pH-dependent cargo release, storage stability, endosomal uptake and retention, and antagonism of eGPCR signaling.	**Completion Date**	**Percentage Completed**
Major Task 1: Synthesize NPs		
Subtask 1: To synthesize NPs with different physicochemical properties • Pinkerton lab, site 4: synthesize DIPMA, HIP, PAMAM-Chol NPs	9/28/2023	75%
Subtask 2: To load cargo into NPs • Pinkerton lab, site 4: load NPs with PAR_2 and CLR antagonists, fluorophores	9/28/2023	75%
Major Task 2: Characterize NPs		
Subtask 1: To characterize the physicochemical properties of the NPs • Pinkerton lab, site 4: characterize size, structure, surface charge of the NPs	9/28/2023	75%
Subtask 2: To characterize NP storage properties • Pinkerton lab, site 4: assess storage stability at -20°, 4°C, 20°C	9/28/2023	75%
Subtask 3: To characterize NP loading and release • Pinkerton lab, site 4: assess encapsulation efficiency; pH-dependence; release	9/28/2023	75%
Major Task 3: Study NP cytotoxicity		
Subtask 1: To study cell viability following NP exposure with MTT assay • Schmidt lab, site 2: HEK293, mouse DRG, human Schwann cells	9/28/2023	75%
Major Task 4: Study NP cellular uptake and biodistribution		
Subtask 1: To study cell uptake of NPs into endosomes, lysosomes, Golgi structure • Bunnett lab, site 1: assess HEK293, mouse DRG neurons, human Schwann cells	9/28/2023	75%
Subtask 2: To study biodistribution of NPs from colon, peritoneum, face • Bunnett lab, site 1: assess HEK293, mouse DRG neurons, human Schwann cells	9/28/2023	75%
Major Task 5: Study NPs w/ antagonists for PAR_2 and CLR		
Subtask 1: To study assembly of PAR_2/ or CLR/βARR2/Gα signalosomes • Bunnett lab, site 1: image transfected HEK293 cells with BRET	9/28/2023	75%

Subtask 2: To study signaling pathways following PAR_2 and CLR agonists • Bunnett lab, site 1: image FRET biosensors for PKC, PKA, ERK	9/28/2023	75%
Milestone #1: Manuscript on properties of three types of NPs *Milestone #2: Manuscript on the effect of NPs on endosomal signaling*	9/28/2023	Milestone #1 100%, #2 100%
Aim 2. To investigate the hypothesis that PAR_2 signals from endosomes of colonic nociceptors, following cleavage by host- and microbiome-derived proteases, to mediate IBD pain and neurogenic inflammation**.**		
Major Task 1: Study mouse models of IBD/IBS pain		
Subtask 1: To study PAR_2 endocytosis in models of IBD/IBS pain • Bunnett lab, site 1: image PAR_2-muGFP in IBD/IBS colon	9/28/2023	100%
Subtask 2: To study colonic nociceptor activity in models of IBD/IBS pain • Schmidt lab, site 1: study activity of colonic afferent nociceptors w/ patch clamp	9/28/2023	25%
Subtask 3: To study nociception in IBD/IBS pain models • Bunnett lab, site 1: assess evoked and non-evoked nociception	9/28/2023	100%
Major Task 2: Identify cellular mediators of PAR_2-evoked IBD pain		
Subtask 1: To study assembly of PAR_2/ or CLR/βARR2/Gα signalosomes • Bunnett lab, site 1: image transfected HEK293 cells with BRET	9/28/2023	100%
Subtask 2: To study signaling pathways following PAR_2 and CLR agonist • Bunnett lab, site 1: image FRET biosensors for PKC, PKA, ERK	9/28/2023	50%
Major Task 3: PAR_2 sensitization of DRG nociceptors		
Subtask 1: To study DRG nociceptor hyperexcitability due to PAR_2 • Schmidt lab, site 2: use patch clamp recording to measure rheobase	9/28/2023	75%
Subtask 2: To study the role of eGPCR signaling on DRG nociceptor excitability • Schmidt lab, site 2: use patch clamp recording and endocytosis inhibitors	9/28/2023	75%
Major Task 4: NP antagonism of PAR_2 signaling/nociception in IBD pain model		
Subtask 1: Analyze endosomal PAR_2 signaling in IBD model • Bunnett lab, site 1: image transfected HEK293 cells with BRET • Bunnett lab, site 1: image FRET biosensors for PKC, PKA, ERK	9/28/2023	75%
Subtask 2: Nociceptor sensitization • Schmidt lab, site 2: measure effect of NPs with PAR_2 antagonists w/ patch clamp	9/28/2023	75%
Subtask 3: Evaluate evoked/non-evoked colonic nociception • Bunnett lab, site 2: effect of NPs w/ PAR_2-induced, TNBS colonic pain models	9/28/2023	75%
Major Task 5: Human translation/human subjects		
Subtask 1: Collect colonic mucosa and luminal fluid from veterans • Gaspari at VAMC, site 4: enroll IBD patients; IRB already approved	9/28/2023	25%
Subtask 2: Collect whole thickness colon from surgical patients • Schmidt, site 2: collect from NYU Langone Hospital; IRB already approved	9/28/2023	25%
Subtask 3: Collect DRG neurons through LiveOnNY • Schmidt, site 2: procure DRG neurons from organ donors; MTA in place	9/28/2023	0%
Subtask 4: PAR_2 transcript localization in human DRG • Bunnett, site 1: RNAScope® *in situ* hybridization	9/28/2023	0%
Subtask 5: PAR_2 transcript localization in normal and IBD colon • Bunnett, site 1: RNAScope® *in situ* hybridization	9/28/2023	0%
Milestone #1: Manuscript on role of endosomal PAR_2 in IBD *Milestone #2: Manuscript on PAR_2 in human colon/DRG in IBD* *Milestone #3: Manuscript on the effect of NPs on IBD pain*	9/28/2023	Milestone #1 100%, #2 0%, #3 100%
Aim 3. To investigate the hypothesis that PAR_2 and CLR signal from endosomes of trigeminal nociceptors and ensheathing Schwann cells to mediate PTH pain and neurogenic inflammation.		
Major Task 1: Study PAR_2 and CLR in a mouse model of PTH pain		
Subtask 1: To study role of PAR_2 endocytosis in PTH pain • Bunnett lab, site 1: image PAR_2-muGFP in TG neurons of PTH model	9/28/2023	0%
Subtask 2: To study evoked/non-evoked nociception due to PAR_2 • Schmidt lab, site 1: assess periorbital, paw withdrawal with PAR_2 agonist	9/28/2023	10%
Major Task 2: Identify mediators of PAR_2-evoked periorbital/PTH pain		
Subtask 1: To study the role of PAR_2 on sensory afferents in periorbital pain • Schmidt lab, site 1: assess nociception in *$Par_2Na_v1.8$* mice; *$Par_2^{fl/fl}$* control	9/28/2023	100%

Subtask 2: To study the role of PAR_2 on Schwann cells periorbital pain • Schmidt lab, site 2: periorbital allodynia in *Plp-Cre^{ERT+}/Par$_2^{fl/fl}$* and *Plp-Cre^{ERT}/Par$_2^{fl/fl}$* (control) mice and wild-type mice • Schmidt lab, site 2: periorbital allodynia in mice with selective deletion of periorbital PAR2 on Schwann cells using 4-hydroxytamoxifen	9/28/2023	50%
Subtask 3: To study the role of PAR_2 on Schwann cells in PTH pain • Bunnett lab, site 1: nociception in TBI/BLS using mice from Subtasks 1 and 2	9/28/2023	50%
Major Task 3: CGRP, TRPA1 in PAR_2-evoked periorbital and PTH pain		
Subtask 1: Study CGRP from TG in PAR_2-evoked and PTH pain • Bunnett lab, site 1: intraperitoneal olcegepant or vehicle (control) • Bunnett lab, site 1: study PAR_2-evoked and TBI/BLS-evoked nociception	9/28/2023	0%
Subtask 2: To study the role of CLR/RAMP1 on Schwann cells • Bunnett lab, site 1: periorbital allodynia in *Plp-Cre^{ERT+}/Ramp1$^{fl/fl}$* and *Plp-Cre^{ERT}/Ramp1$^{fl/fl}$* (control) mice treated with 4-hydroxytamoxifen • Bunnett lab, site 1: study PAR_2-evoked and TBI/BLS-evoked nociception	9/28/20239/	25%
Subtask 3: The study the role of TRPA1 in PAR_2- and TBI/BLS-evoked pain • Bunnett lab, site 1: sensory neuron deletion of TRPA1(*Adv-Cre/Trpa1$^{fl/fl}$*) in mice	9/28/2023	25%
Major Task 4: Endosomal PAR_2 signaling in TG and Schwann cells		
Subtask 1: To study assembly of PAR_2/ or CLR/βARR2/Gα signalosomes • Bunnett lab, site 1: mouse TG, human DRG and Schwann cells w/ BRET	9/28/2023	10%
Subtask 2: To study signaling pathways following PAR_2 and CLR agonist • Bunnett lab, site 1: mouse TG, human DRG and Schwann cells w/ FRET	9/28/2023	10%
Subtask 1: To study the role of PAR_2 endocytosis • Bunnett lab, site: endocytosis inhibitors and PAR_2 endosomal signaling	9/28/2023	10%
Major Task 6: PAR_2 sensitization of TG nociceptors		
Subtask 1: To study PAR_2 agonists and endocytosis inhibitors on rheobase • Schmidt lab, site 2: patch clamp recordings of mouse TG neurons	9/28/2023	25%
Major Task 7: NPs w/ PAR_2, CLR antagonists; control: antagonists, empty NPs		
Subtask 1: Endosomal PAR_2 signaling following NPs with antagonists • Bunnett lab, site 1: mouse TG, human DRG and Schwann cells w/ BRET, FRET	9/28/2023	0%
Subtask 2: Nociceptor sensitization following NP administration • Schmidt lab, site 2: patch clamp recording and NPs with PAR_2 antagonists	9/28/2023	0%
Subtask 3: Nociception • Schmidt lab, site 2: evoked/non-evoked nociception w/ PAR_2 agonist, CGRP • Bunnett lab, site 1: evoked/non-evoked nociception in PTH/BLS model	9/28/2023	0%
Major Task 7: Human translation/human subjects		
Subtask 1: Collect human TG nerves • Schmidt, site 2: collection of lingual nerves from human oral cancer patients	9/28/2023	50%
Subtask 2: Collect TG neurons from LiveOnNY • Schmidt, site 2: procure TG neurons from organ donors	9/28/2023	0%
Subtask 3: PAR_2 localization in human TG neurons and Schwann cells • Schmidt, site 2: immunofluorescence with antibodies to PGP9.5, PAR_2 and S100 • Bunnett, site 1: RNAScope® *in situ* hybridization to visualize target transcript	9/28/2023	50%
Subtask 4: NPs w/ PAR_2 antagonists; nociceptor sensitization; endocytosis • Schmidt lab, site 2: patch clamp recording and NPs with PAR_2 antagonists • Schmidt lab, site 2: patch clamp recording; endocytosis inhibitors	9/28/2023	25%
Milestone #1: Manuscript on endosomal PAR_2 in PTH *Milestone #2: Manuscript on PAR_2 expression in human TG and Schwann cells* *Milestone #3: Manuscript on sustained analgesic effect of NPs on PTH*	9/28/2023	Milestone#1 0%, #2 0%, #3 0%

Research Progress

Dissemination of Results. Results are disseminated by publications in peer reviewed journals, delivery of lectures and seminars to universities and at scientific meetings, and by posting newsworthy findings on university websites. Interviews with journalists representing specific and general journals enhance community outreach. The Bunnett and Schmidt laboratories meet as a group each week to evaluate progress, provide feedback on technical issues and results, arrange transfer of mice and chemical resources, and trouble-shoot problems. Technical methods specific to the project are discussed. Member of the laboratory including students, postdoctoral fellows, scientists and principal investigators attend this joint laboratory meeting.

Plans for Next Reporting Period. Priorities for the next reporting period include: the continued development of nanoparticles that accumulate and persist in diseased tissues; refinement of nanoparticles to allow cell specific targeting and prolonged release of antagonists; evaluation of the effects of nanoparticles in neurons and Schwann cells derived from patients; analysis of the effects of proteases released from the diseased human colon on eGPCR signaling; study of the efficacy of nanoparticles for the treatment of PTH in preclinical models.

4. IMPACT

Impact on principal discipline. The concepts that receptors function within endosomes to control disease processes, in particular chronic pain, and that nanoparticles allow delivery of drugs to endosomes to more effectively treat pain has implications for multiple forms of pain beyond the pain of inflammatory bowel disease and post-traumatic headache. Implications extend to inflammatory, neuropathic and cancer pain.

Impact on other disciplines. G protein-coupled receptors control most disease processes and one third of FDA-approved drugs target these receptors. The concepts that receptors in endosomes control disease and are the optimal therapeutic target have implications beyond pain. Nanoparticle formulations could enhance the treatment of diverse diseases, including inflammatory diseases, neurological diseases, diseases of the cardiovascular and pulmonary systems, and cancer.

Impact on technology transfer. Nothing to Report.

Impact on society. Nothing to Report.

5. CHANGES/PROBLEMS

Changes in approach and reasons for change. Nothing to Report.

Actual or anticipated problems or delays and actions or plans to resolve them. Nothing to Report.

Changes that had a significant impact on expenditures. Nothing to Report.

Significant changes in use or care of human subjects, vertebrate animals, biohazards, and/or select agents. Nothing to Report.

Significant changes in use or care of human subjects. Nothing to Report.

Significant changes in use or care of vertebrate animals. Nothing to Report.

Significant changes in use of biohazards and/or select agents. Nothing to Report.

6. PRODUCTS

* Papers included in appendix

All publications acknowledge federal support

Journal publications

Published Papers

1. *Tonello R, Anderson WB, Davidson S, Escriou V, Yang L, **Schmidt BL**, Imlach WL, **Bunnett NW**. The contribution of endocytosis to sensitization of nociceptors and synaptic transmission in nociceptive circuits. *Pain* 164, 1355-1374 (2023). PMC10182228. https://www.ncbi.nlm.nih.gov/pubmed/36378744
2. *Peach CJ, Edgington-Mitchell LE, **Bunnett NW**, **Schmidt BL**. Protease-activated receptors in health and disease. *Physiol Rev* 103, 717-785 (2023). PMC9662810. https://www.ncbi.nlm.nih.gov/pubmed/35901239
3. *Hegron A, Peach CJ, Tonello R, Seemann P, Teng S, Latorre R, Huebner H, Weikert D, Rientjes J, Veldhuis NA, Poole DP, Jensen DD, Thomsen ARB, **Schmidt BL**, Imlach WL, Gmeiner P, **Bunnett NW**. Therapeutic antagonism of the neurokinin 1 receptor in endosomes provides sustained pain relief. *Proc Natl Acad Sci U S A* 120, e2220979120 (2023). https://www.ncbi.nlm.nih.gov/pubmed/37216510
4. *Xie Y, Fontenot L, Chupina Estrada A, Nelson B, Wang J, Shih DQ, Ho W, Mattai SA, Rieder F, Jensen DD, **Bunnett NW**, Koon HW. Elafin Reverses Intestinal Fibrosis by Inhibiting Cathepsin S-Mediated Protease-Activated Receptor 2. *Cell Mol Gastroenterol Hepatol* 14, 841-876 (2022). PMC9425040. https://www.ncbi.nlm.nih.gov/pubmed/35840034
5. *Scheff NN, Wall IM, Nicholson S, Williams H, Chen E, Tu NH, Dolan JC, Liu CZ, Janal MN, **Bunnett NW**, **Schmidt BL.** Oral cancer induced TRPV1 sensitization is mediated by PAR(2) signaling in primary

afferent neurons innervating the cancer microenvironment. *Sci Rep* 12, 4121 (2022). PMC8904826. https://www.ncbi.nlm.nih.gov/pubmed/35260737

6. *Latorre R, Ramirez-Garcia PD, Hegron A, Grace JL, Retamal JS, Shenoy P, Tran M, Aurelio L, Flynn B, Poole DP, Klein-Cloud R, Jensen DD, Davis TP, **Schmidt BL**, Quinn JF, Whittaker MR, Veldhuis NA, **Bunnett NW**. Sustained endosomal release of a neurokinin-1 receptor antagonist from nanostars provides long-lasting relief of chronic pain. *Biomaterials* 285, 121536 (2022). PMC10064865. https://www.ncbi.nlm.nih.gov/pubmed/35533442
7. *Latorre R, Hegron A, Peach CJ, Teng S, Tonello R, Retamal JS, Klein-Cloud R, Bok D, Jensen DD, Gottesman-Katz L, Rientjes J, Veldhuis NA, Poole DP, **Schmidt BL**, Pothoulakis CH, Rankin C, Xie Y, Koon HW, **Bunnett NW**. Mice expressing fluorescent PAR(2) reveal that endocytosis mediates colonic inflammation and pain. *Proc Natl Acad Sci U S A* 119(2022). PMC8833192. https://www.ncbi.nlm.nih.gov/pubmed/35110404
8. *Keely SJ, Urso A, Ilyaskin AV, Korbmacher C, **Bunnett NW**, Poole DP, Carbone SE. Contributions of bile acids to gastrointestinal physiology as receptor agonists and modifiers of ion channels. *Am J Physiol Gastrointest Liver Physiol* 322, G201-G222 (2022). PMC8782647. https://www.ncbi.nlm.nih.gov/pubmed/34755536
9. *Kaiserman D, Zhao P, Rowe CL, Leong A, Barlow N, Joeckel LT, Hitchen C, Stewart SE, Hollenberg MD, **Bunnett N**, Suhrbier A, Bird PI. Granzyme K initiates IL-6 and IL-8 release from epithelial cells by activating protease-activated receptor 2. *PLoS One* 17, e0270584 (2022). PMC9321427. https://www.ncbi.nlm.nih.gov/pubmed/35881628
10. *Jimenez-Vargas NN, Yu Y, Jensen DD, Bok DD, Wisdom M, Latorre R, Lopez C, Jaramillo-Polanco JO, Degro C, Guzman-Rodriguez M, Tsang Q, Snow Z, **Schmidt BL**, Reed DE, Lomax AE, Margolis KG, Stein C, **Bunnett NW**, Vanner SJ. Agonist that activates the micro-opioid receptor in acidified microenvironments inhibits colitis pain without side effects. *Gut* 71, 695-704 (2022). PMC8608554. https://www.ncbi.nlm.nih.gov/pubmed/33785555
11. *Jaramillo-Polanco J, Lopez-Lopez C, Yu Y, Neary E, Hegron A, Canals M, **Bunnett NW**, Reed DE, Lomax AE, Vanner SJ. Opioid-Induced Pronociceptive Signaling in the Gastrointestinal Tract Is Mediated by Delta-Opioid Receptor Signaling. *J Neurosci* 42, 3316-3328 (2022). PMC9034783. https://www.ncbi.nlm.nih.gov/pubmed/35256532
12. *De Logu F, Nassini R, Hegron A, Landini L, Jensen DD, Latorre R, Ding J, Marini M, Souza Monteiro de Araujo D, Ramirez-Garcia P, Whittaker M, Retamal J, Titiz M, Innocenti A, Davis TP, Veldhuis N, **Schmidt BL**, **Bunnett NW**, Geppetti P. Schwann cell endosome CGRP signals elicit periorbital mechanical allodynia in mice. *Nat Commun* 13, 646 (2022). PMC8813987. https://www.ncbi.nlm.nih.gov/pubmed/35115501
13. *Caldwell A, Grundy L, Harrington AM, Garcia-Caraballo S, Castro J, **Bunnett NW**, Brierley SM. TGR5 agonists induce peripheral and central hypersensitivity to bladder distension. *Sci Rep* 12, 9920 (2022). PMC9200837. https://www.ncbi.nlm.nih.gov/pubmed/35705684

Under review and in preparation

Nanomedicines targeting PAR_2 signaling in endosomes of colonocytes and nociceptors reverse colonic inflammatory pain. Rocco Latorre, Shavonne Teng, Divya Bhansali, Parker Lewis, Rachel Pollard, Chloe J. Peach, Gokul SA Thanigai, Tracy Chiu, Dane D. Jensen, Nestor N Jimenez-Vargas, Abby Mocherniak, Michael M. Gaspari, Stephen J. Vanner, **Nathalie M. Pinkerton**, Kam Leong, **Brian L. Schmidt**, **Nigel W. Bunnett**

Targeting of protease-activated receptor-2 in endosomes using nanoparticle-encapsulated antagonist provides long-lasting relief from oral cancer pain. Divya Bhansali, Nguyen H. Tu, Kenji Inoue, Tianyu Li, Hung D. Tran, Dong H. Kim, Jessy Dong, Shavonne Teng, Dane D Jensen, John C. Dolan, Seiichi Yamano, **Nigel W. Bunnett**, Kam W. Leong, **Brian L. Schmidt**

Exploiting drug delivery approaches to target subcellular CGRP-induced signalosomes for enhanced analgesia. Chloe J. Peach, Rocco Latorre, Parker Lewis, Rachel Pollard, James Grace Nicholas Andrikopoulos, Thomas P. Davis, John F. Quinn, Nicholas A. Veldhuis, Michael R. Whittaker, **Brian L. Schmidt, Nathalie Pinkerton**, **Nigel W Bunnett**

Books

Thomsen ARB, Hahn H & **Bunnett NW**. Arrestin-Mediated Trafficking and Compartmentalized Biology of GPCRs. In: Arrestins. Structure and Function in Vision and Beyond. Edited by Gurevich VV. Academic Press. 2022.

Other. Nothing to Report

Websites. Nothing to Report

Technologies and techniques. Nothing to Report

Inventions and patents. Nothing to Report

Other products. Nothing to Report

7. PARTICIPANTS AND OTHER COLLABORATING ORGANIZATIONS:

Individuals who have worked on project

NEW YORK UNIVERSITY

Name:	Nigel Bunnett
Project Role:	PI
Researcher Identifier (e.g. ORCID ID):	0000-003-3367-0644
Nearest person month worked:	2.25 Calendar Months
Contribution to Project:	Conceived the project, designed experiments, analyzed results, wrote manuscripts
Funding Support:	W81XWH2210238 W81XWH1810431 R01DK118971 R01DE026806 R01DE029951 R01NS102722 1R01DK130293-01A1via Stanford R01DK128142 via UCLA

Name:	Nathalie Pinkerton
Project Role:	Co-PI
Researcher Identifier (e.g. ORCID ID):	0000-0001-9325-9764
Nearest person month worked:	2 Calendar Months
Contribution to Project:	Conceived the project, designed experiments, analyzed results, wrote manuscripts
Funding Support:	W81XWH2210238 3R01DE29951-01S2

Name:	Raquel Tonello
Project Role:	Associate Research Scientist
Researcher Identifier (e.g. ORCID ID):	0000-0002-2175-9804
Nearest person month worked:	5.3 Calendar Months
Contribution to Project:	Designed and completed experiments to assess nociception, analyzed results, wrote manuscripts
Funding Support:	W81XWH2210238 R01DK118971

	R01DE026806 R01DE029951

Name:	Alan Hegron
Project Role:	Assistant Research Scientist
Researcher Identifier (e.g. ORCID ID):	000-0002-7588-9209
Nearest person month worked:	3.3 Calendar Months
Contribution to Project:	Designed and completed experiments to assess endosomal signaling, analyzed results, wrote manuscripts
Funding Support:	W81XWH-22-1-0238 R01DK118971 R01DE026806 R01DE029951 R01NS102722 R01DK128142 via UCLA NYU# 2023-0495-Heptares

Name:	Rocco Latorre
Project Role:	Research Scientist
Researcher Identifier (e.g. ORCID ID):	0000-0003-2737-8233
Nearest person month worked:	1.19 Calendar Months
Contribution to Project:	Designed and completed experiments to assess nociception, analyzed results, wrote manuscripts
Funding Support:	W81XWH-2210238 W81XWH1810431 R01DK118971 R01DE026806 1R01DK130293-01A1via Stanford NYU# 2021-1141-Takeda

Name:	Nouha El Amri
Project Role:	Postdoctoral Research Scientist
Researcher Identifier (e.g. ORCID ID):	0009-0007-0904-4260
Nearest person month worked:	5 Calendar Months
Contribution to Project:	Designed and completed experiments to generate nanoparticles, analyzed results, wrote manuscripts
Funding Support:	W81XWH2210238 3R01DE29951-01S2

Other organizations. Nothing to Report

8. SPECIAL REPORTING REQUIREMENTS

This is a collaborative award between N.W. Bunnett (New York University) and B.L. Schmidt (New York University).

9. APPENDICES

Research Paper

PAIN®

The contribution of endocytosis to sensitization of nociceptors and synaptic transmission in nociceptive circuits

Raquel Tonello[a,b], Wayne B. Anderson[c], Steve Davidson[d], Virginie Escriou[e], Lei Yang[f], Brian L. Schmidt[a,b,f], Wendy L. Imlach[c,*], Nigel W. Bunnett[a,b]

Downloaded from http://journals.lww.com/pain by BhDMf5ePHKav1zEoum1tQfN4a+kJLhEZgbsIHo4XMi0hCywCX1AWnYQp/IlQrHD3i3D0OdRyi7TvSFl4Cf3VC4/OAVpDDa8K2+Ya6H515kE= on 09/29/2023

Abstract

Chronic pain involves sensitization of nociceptors and synaptic transmission of painful signals in nociceptive circuits in the dorsal horn of the spinal cord. We investigated the contribution of clathrin-dependent endocytosis to sensitization of nociceptors by G protein–coupled receptors (GPCRs) and to synaptic transmission in spinal nociceptive circuits. We determined whether therapeutic targeting of endocytosis could ameliorate pain. mRNA encoding dynamin (Dnm) 1 to 3 and adaptor-associated protein kinase 1 (AAK1), which mediate clathrin-dependent endocytosis, were localized to primary sensory neurons of dorsal root ganglia of mouse and human and to spinal neurons in the dorsal horn of the mouse spinal cord by RNAScope. When injected intrathecally to mice, Dnm and AAK1 siRNA or shRNA knocked down Dnm and AAK1 mRNA in dorsal root ganglia neurons, reversed mechanical and thermal allodynia and hyperalgesia, and normalized nonevoked behavior in preclinical models of inflammatory and neuropathic pain. Intrathecally administered inhibitors of clathrin, Dnm, and AAK1 also reversed allodynia and hyperalgesia. Disruption of clathrin, Dnm, and AAK1 did not affect normal motor functions of behaviors. Patch clamp recordings of dorsal horn neurons revealed that Dnm1 and AAK1 disruption inhibited synaptic transmission between primary sensory neurons and neurons in lamina I/II of the spinal cord dorsal horn by suppressing release of synaptic vesicles from presynaptic primary afferent neurons. Patch clamp recordings from dorsal root ganglion nociceptors indicated that Dnm siRNA prevented sustained GPCR-mediated sensitization of nociceptors. By disrupting synaptic transmission in the spinal cord and blunting sensitization of nociceptors, endocytosis inhibitors offer a therapeutic approach for pain treatment.

Keywords: Endocytosis, Synapse, Neurotransmission, GPCR, Sensitization

1. Introduction

Chronic pain is common, poorly understood, and difficult to treat. The analgesic properties of μ-opioid agonists, a common treatment, dwindle with time, and their usefulness is limited by life-threatening side effects.[36] The redundancy of pain signaling, where multiple receptors and channels activate the same neurons,[2] may limit the effectiveness of selective ligands for the treatment of multimodal forms of pain.

We investigated the contributions of clathrin-dependent endocytosis to sensitization of nociceptors and synaptic transmission in nociceptive circuits in the dorsal horn of the spinal cord. We hypothesized that disruption of endocytosis would reverse multiple modalities of pain. Mediators from damaged tissues activate G protein–coupled receptors (GPCRs), receptor tyrosine kinases, and ligand-gated ion channels at the peripheral endings of nociceptors to initiate pain.[2] The central terminals of nociceptors in the dorsal horn of the spinal cord release substance P, calcitonin gene–related peptide (CGRP), and glutamate, which activate GPCRs on spinal neurons that transmit signals centrally. Synaptic vesicle (SV) cycling is required for synaptic transmission.[6,37] Synaptic vesicle exocytosis at presynaptic terminals releases neurotransmitters into the synapse. Clathrin-dependent endocytosis retrieves SVs from the plasma membrane of presynaptic neurons, which replenishes the releasable SV pool and is necessary for sustained neurotransmission. Dynamin (Dnm) GTPase mediates fission of clathrin-coated SVs and is required for endocytosis. Of the 3 Dnm isoforms (*Dnm1*, *Dnm2*, *Dnm3*), Dnm1 and Dnm3 are expressed in the nervous system.[15] *Dnm1* deletion in mice impairs activity-dependent endocytosis of SVs at nerve terminals and disrupts neurotransmission during intense stimulation.[29] Although *Dnm3* deletion alone does not severely disrupt synaptic transmission, deletion of *Dnm3* and *Dnm1* depletes SVs and causes accumulation of clathrin-coated pits (CCPs) in presynaptic terminals.[29] Dynamin inhibitors recapitulate these effects.[24] Together with clathrin, adaptor protein 2 (AP2) constitutes the major coated protein of the endocytic vesicles.

Sponsorships or competing interests that may be relevant to content are disclosed at the end of this article.

[a] *Department of Molecular Pathobiology, Department of Neuroscience and Physiology, Neuroscience Institute, New York University, New York, NY, United States,* [b] *Pain Research Center, New York University, New York, NY, United States,* [c] *Department of Physiology and Monash Biomedicine Discovery Institute, Monash University, Melbourne, Australia,* [d] *Department of Anesthesiology, College of Medicine, University of Cincinnati, Cincinnati, United States,* [e] *Université de Paris, CNRS, INSERM, UTCBS, Paris, France,* [f] *NYU Dentistry Translational Research Center, New York University College of Dentistry, New York, NY, United States*

**Corresponding author. Address: Department of Physiology, Monash University, Melbourne, VIC, 3800, Australia. Tel.: +61 03 9905 1210. E-mail address: wendy.imlach@monash.edu (W.L. Imlach).*

Supplemental digital content is available for this article. Direct URL citations appear in the printed text and are provided in the HTML and PDF versions of this article on the journal's Web site (www.painjournalonline.com).

PAIN 164 (2023) 1355–1374

© 2022 International Association for the Study of Pain

http://dx.doi.org/10.1097/j.pain.0000000000002826

Copyright © 2022 by the International Association for the Study of Pain. Unauthorized reproduction of this article is prohibited.

Downloaded from http://journals.lww.com/pain by BhDMf5ePHKav1zEoum1tQfN4a+kJLhEZgbsIHo4XMi0hCywCX1AWnYQp/IlQrHD3i3D0OdRyi7TvSFl4Cf3VC4/OAVpDDa8K2+Ya6H515kE= on 09/29/2023

Adaptor-associated kinase 1 (AAK1) recruits clathrin and AP2 to the plasma membrane and phosphorylates the μ2 subunit of AP2 (AP2M1), thereby stimulating cargo binding and recruitment, vesicle assembly, and internalization.[9] Clathrin assembly promotes AAK1-dependent phosphorylation of AP2M1, which constitutes a feedforward loop for pit maturation.[32] Clathrin and Dnm also mediate endocytosis and sustained endosomal signaling of GPCRs, which underlies neuronal sensitization and nociception.[18–20,30,40]

The contribution of clathrin, Dnm, and AAK1 to nociception is not fully understood. A screen of knockout mice identified AAK1 as a mediator and target for neuropathic pain.[21] *Aak1* deletion and inhibition attenuated neuropathic pain in mice and rats. The α subunit of the AP2 complex (AP2α2) is expressed in CGRP+ve nociceptors and AP2 small hairpin RNA (shRNA) suppressed nociception in mice.[28] However, the distribution of Dnm and AAK1 isoforms in nociceptive circuits is unknown, and their role in nociception is unexplored. We used genetic and pharmacological approaches to investigate the contribution of endocytosis to nociception. Anatomical, electrophysiological, and behavioral studies support the hypothesis that Dnm and AAK1 are necessary for sensitization of nociceptors and for nociceptive transmission in the spinal cord and that disruption of endocytosis reverses nociception.

2. Methods

2.1. Animals

All experiments and procedures were in accordance with the guidelines recommended by the National Institute of Health, the International Association for the study of Pain, the National Centre for the Replacement, Refinement, and Reduction of Animals in Research ARRIVE guidelines, and were approved by the New York University Institutional Animal Care and Use Committee and the Monash University Animal Ethics Committee. Male and female C57BL/6 mice (8-10 weeks, Jackson Laboratory, Bar Harbor, ME) were housed 4 per cage at 22 ± 0.5°C under a controlled 14/10 hours of light/dark cycle with free access to food and water. Mice were randomly assigned to experimental groups, and the group size was based on our previous similar studies. Investigators were blind to treatments.

2.2. Collection of human tissues

The collection of dorsal root ganglia (DRG) from deidentified organ donors was reviewed by the Institutional Review Board of the University of Cincinnati (#00003152, Study ID 2015-5302) and was deemed to be exempt. Donor information is provided in Table S1 (available as supplemental digital content at http://links.lww.com/PAIN/B750). Dorsal root ganglia (L4, L5) were collected in the operating room within 90 minutes of aortic cross clamp and after removal of vital organs. Dorsal root ganglia were placed in N-Methyl-D-glucamine-artificial cerebrospinal fluid (ACSF) solution at 4°C and were dissected as described.[39] For RNAScope, DRG were immersion fixed in 4% paraformaldehyde in phosphate-buffered saline (PBS) overnight at 4°C, cryoprotected in 30% sucrose for 24 hours at 4°C, and embedded in optimal cutting temperature (OCT) compound (Tissue Tek). Frozen sections (14 μm sections) were mounted onto Superfrost Plus slides (Fisher, Suwanne, GA), dried (15 minutes), and stored at −20°C.

2.3. Collection of mouse tissues

Mice were anesthetized (5% isoflurane) and perfused through the ascending aorta with PBS and then 4% paraformaldehyde in PBS. Dorsal root ganglia, trigeminal ganglia (TG), and spinal cord were removed, postfixed in 4% paraformaldehyde in PBS at 4°C for 1 hour or overnight, respectively, placed in 30% sucrose solution for 24 hours at 4°C, and embedded in OCT. Frozen sections (10-12 μm) were mounted onto Superfrost Plus slides (Fisher), dried (15 minutes), and stored at −20°C.

2.4. RNAScope in situ hybridization and immunofluorescence

The RNAScope system (Advanced Cell Diagnostics, Newark, CA) was used per manufacturer's directions for fresh-frozen tissue except for omission of the initial on-slide fixation step. Probe hybridization and detection using the Multiplex Fluorescent Kit v2 followed the manufacturer's directions. Probes to *Mm-Dnm1* (#446931-C3), *Mm-Dnm2* (#451831-C1), *Mm-Dnm3* (#451841-C2), *Mm-Aak1* (#1097711-C1) (mouse), *Hs-Dnm1* (#1099091-C1), *Hs-Dnm2* (#821511-C1), *Hs-Dnm3* (#1105961-C2), and *Hs-AAK1* (#531971-C1) (human) were used. Sections were incubated with Opal 620 reagent (1:1000, cat#FP1495001KT, Akoya Biosciences, Marlborough, MA) for detection. To detect neurons, hybridized slides were incubated with NeuroTrace 500/525 Green Fluorescent Nissl Stain (1:500, cat#N21480, Invitrogen, Waltham, MA) (10 minutes, room temperature, RT). To detect satellite glial cells and peptidergic neurons, hybridized slides were incubated with rabbit antiglutamine synthetase antibody (GS, 1:1000, cat#ab49873, Abcam, Cambridge, MA) or rabbit anti-CGRP, (1:1000, cat#C8198, Sigma, St. Louis, MO), respectively (overnight, 4°C). Slides were washed and incubated with goat antirabbit Alexa Fluor 488 (1:1000; cat#A21206, Invitrogen, Waltham, MA) (1 hour, RT). Slides were washed and incubated with DAPI (1 μg/mL, 5 minutes) and mounted in ProLong Gold Antifade (Thermo Fisher, Waltham, MA). Sections were observed using a Leica SP8 confocal microscope with HCX PL APO 40x (NA 1.30) oil objective (Wetzlar, Germany).

2.5. RNAScope quantification

Dnm 1, 2, or 3 and *Aak1* were localized by RNAScope. Confocal images were analyzed using Fiji ImageJ (NIH) according to ACD Bio-Techne Technical Note. Regions of interest were defined by applying a threshold with the moments setting (Min & Max) and analyzing particles with size range from 0 to infinity. Regions of interest were overlaid on the original micrograph, and the number of dots per area were quantified. Results are expressed as dots per square millimeter tissue. A total of 3 images (×20 magnification) were analyzed for each mouse (N = 4 mice for control and treatment groups; 12 images analyzed per experimental group).

2.6. Quantitative real-time reverse transcription polymerase chain reaction

RNA was isolated from snap frozen mouse tissues using Direct-zol RNA MiniPrep kit (cat#R2051 Zymo Research). cDNA was prepared using MultiScribe Reverse Transcriptase (cat#4311235 Thermo Fisher). cDNA (50 ng) was amplified for 40 cycles by quantitative real-time reverse transcription polymerase chain reaction (qRT-PCR) using Dnm1 (DNM1, Mn00802468_m1), Dnm2 (DNM2, Mn00514582_m1), Dnm3 (DNM3, Mn00554098_m1), AAK1 (Mn01183675_m1), and GAPDH (Mn99999915_g1) primers, QuantStudio 3 Real-Time PCR System, and TaqMan Fast Advanced PCR Mastermix (cat#4444556 Thermo Fisher). All samples were analyzed at least in duplicate and normalized by GAPDH expression. The relative expression ratio per condition was calculated as described.[27]

Copyright © 2022 by the International Association for the Study of Pain. Unauthorized reproduction of this article is prohibited.

Downloaded from http://journals.lww.com/pain by BhDMf5ePHKav1zEoum1tQfN4a+kJLhEZgbsIHo4XMi0hCywCX1AWnYQp/IlQrHD3i3D0OdRyi7TvSFl4Cf3VC4/OAVpDDa8K2+Ya6H515kE= on 09/29/2023

2.7. Intrathecal administration of siRNA to mice

Cationic liposome and adjuvant anionic polymer (polyglutamate) were used to deliver small interfering RNA (siRNA).[35] The following siRNAs were used: ON-TARGETplus siRNA mouse Dnm1 siRNA (cat#L-043277-01-0005), mouse Dnm2 (cat#L-044919-02-0005), mouse Dnm3 (cat#L-059061-01-0005), mouse AAK1 (cat#L-065639-00-0005), or nontargeting control (CTR) siRNA (cat#D-001810-10-05) (Dharmacon, Lafayette, CO) (Table S2, available as supplemental digital content at http://links.lww.com/PAIN/B750). siRNAs (50 ng, 0.5 μL of 100 ng/μL stock) were mixed with 0.5 μL of adjuvant polyglutamate (0.1 μg/μL stock) and 1.5 μL of sterile 0.15 M NaCl. Liposome solution, cationic lipid 2-3-[bis-(3-amino-propyl)-amino]-propylamino-N-ditetradecylcarbamoylmethyl-acetamide (DMAPAP), and L-α-dioleoyl phosphatidylethanolamine (DOPE) (DMAPAP/DOPE, 1/1 M:M) (2.5 μL of 200 μM) was added to siRNA/adjuvant, vortexed for 1 minute, and incubated (30 minutes, RT). The siRNA lipoplexes were administered to conscious mice by intrathecal (i.t.) injection (L4-L5, 5 μL), 24 hours after complete Freund adjuvant (CFA) intraplantar (i.pl.) injection, or 10 days after spared nerve injury (SNI) surgery. *Dnm1*, *Dnm2*, *Dnm3*, and *Aak1* expression in DRG and spinal cord (L4-L5) were analyzed by RNAScope in situ hybridization, 24 or 48 hours after siRNA injection. For electrophysiology experiments, mouse Dnm1 siRNA, mouse AAK1 siRNA, or CTR siRNA were mixed with PEI (cat#765090, Sigma) and incubated for 10 minutes at RT. The siRNA–PEI complex was diluted in saline, and 5 μL was injected i.t. into mice 48 hours before laminectomy for spinal slice preparation.

2.8. Intrathecal administration of shRNA to mice

Mouse Dnm1 (cat# TL500548), AAK1 (cat# TL508098), shRNA plasmids, and noneffective 29-mer scrambled shRNA cassette in pGFP-C-shLenti Vector were from OriGene (Table S2, available as supplemental digital content at http://links.lww.com/PAIN/B750). The Dnm1 shRNA or AAK1 shRNA (1.25 μg) was mixed with polyethyleneimine-based transfection reagent (in vivo-jetPEI, 201-50 G; Polyplus, Illkirch, France) in an 8:1 N:P ratio (polyethyleneimine nitrogen to DNA phosphate ratio).[8] The shRNA in vivo jetPEI mixture were administered to conscious mice by i.t. injection (L4-L5, 5 μL), 24 hours after CFA injection (i.pl.) or 10 days after SNI surgery. Dnm1 and Aak1 expression in DRG (L4-L5) were analyzed by RNAScope in situ hybridization, 72 hours after shRNA injection.

2.9. Intrathecal administration of endocytosis inhibitors to mice

Dyngo4a (Dnm inhibitor, 50 nM), PitStop2 (clathrin inhibitor, 50 nM), inactive analogs (trademarks of Children's Medical Research Institute, Newcastle Innovation and Freie Universitat Berlin), LP935509 (AAK1 inhibitor, cat#HY-117626, MedChemExpress; 1-10 μg/5 μL), SGC-AAK1-1 (AAK1 inhibitor, cat#6528, Tocris; 1-10 μg/5 μL), or vehicle (PBS, 5% DMSO/PBS) was injected i.t. (5 μL, L4/L5) into conscious mice. The inhibitors were injected 48 hours after CFA injection (i.pl.) or 10 days after SNI surgery.

2.10. Inflammatory pain

Complete Freund adjuvant (1 mg/mL) or vehicle (0.9% NaCl) was administered by i.pl. injection (10 μL) into the right hindpaw of sedated mice (2% isoflurane). siRNA, shRNA, or inhibitors were injected i.t. 24 hours or 48 hours after CFA. Mechanical allodynia and thermal hyperalgesia were assessed.

2.11. Neuropathic pain

Spared nerve injury and sham surgeries were made, as described.[26] Briefly, mice were anesthetized with isoflurane. A skin and muscle incision were made in the thigh to expose the sciatic nerve innervating the left hindpaw. The tibial and common peroneal nerves were ligated and transected distal to the ligature. The third branch, the sural nerve, was left intact. For sham controls, the nerves were exposed but not ligated or transected. siRNA, shRNA, or inhibitors were injected i.t. at 10 days after the surgery. Mechanical and cold allodynia were assessed.

2.12. Mechanical allodynia

Mechanical allodynia was assessed by measuring hindpaw withdrawal response to von Frey filament stimulation using the up-and-down method.[13] Mice were acclimatized to the testing apparatus, which comprised individual clear Plexiglass boxes on an elevated wire mesh platform to facilitate access to the plantar surface of the hindpaws, for 1 hour/day for 2 days. A series of von Frey filaments (0.02, 0.07, 0.16, 0.4, 1.0, and 2 g; Stoelting, Wood Dale, IL) were applied perpendicular to the plantar surface of hindpaw. The test began with an application of 0.4-g filament. A positive response was defined as a clear paw withdrawal or shaking. Whenever a positive response occurred, the next lower filament was applied, and whenever a negative response occurred, the next higher filament was applied. The testing consisted of 6 stimuli, and the pattern of response was converted to a 50% von Frey threshold.[7]

2.13. Thermal hyperalgesia

The Hargreaves apparatus was used to evaluate hypersensitivity to heat (Ugo Basile).[17] Mice were acclimatized to the testing apparatus, which comprised individual clear Plexiglass chambers and a radiant heat source, for 1 hour/day for 2 days. The infrared intensity was set at 50% and cutoff time to a maximum of 30 seconds. The time between stimulus onset and paw withdrawal was measured automatically, giving an index of the thermal nociceptive threshold. Significant decreases in paw withdrawal latency were interpreted as evidence of thermal hyperalgesia. The latency, expressed in seconds, was evaluated before (basal) and at different time points after the treatment.

2.14. Cold allodynia

Cold allodynia was assessed by measuring the acute nociceptive response to the acetone evoked evaporative cooling.[38] A droplet (50 μL) of acetone, formed on the flat-tip needle of a syringe, was gently touched to the plantar surface of the mouse hind paw. The time spent licking and lifting of the paw over a period of 60 seconds was evaluated before (basal) and at different time points after the treatment.

2.15. Nonevoked behavior

Nonevoked behavior of mice was assessed using a behavioral spectrometer (Behavioral Instruments), a validated instrument for phenotyping rodents that avoids operator bias.[3] This approach has been used for studies of abhorrent behavior in mouse models of autism, restraint stress, and inflammatory, neuropathic, and

Copyright © 2022 by the International Association for the Study of Pain. Unauthorized reproduction of this article is prohibited.

Downloaded from http://journals.lww.com/pain by BhDMf5ePHKav1zEoum1tQfN4a+kJLhEZgbsIHo4XMi0hCywCX1AWnYQp/IlQrHD3i3D0OdRyi7TvSFl4Cf3VC4/OAVpDDa8K2+Ya6H515kE= on 09/29/2023

visceral pain.[3,5,23] The spectrometer comprised a 40-cm^2 arena with a CCD camera mounted in the center of the ceiling and a door aperture in the front area of the arena. Movement was assessed by a floor mounted vibration sensor and 32 wall-mounted infrared transmitter and receiver pairs. Mice were individually placed in the center of the behavioral spectrometer, and their behavior was recorded for 20 minutes and analyzed using a combination of video tracking analysis (Viewer3, BiObserve, Sankt Augustin, Germany) and vibration analysis. Total distance traveled in the open field (number of visits to a central area), average velocity of locomotion (centimeters/second), track length (centimeter), ambulation (% activity), time engaged in grooming (minutes), and wall distance (centimeter) were recorded and analyzed as described.[3]

2.16. Spinal slice preparation

Adult C57BL/6J mice were anesthetized (5% isoflurane), decapitated, and the lumbar region of the spinal cord with the dorsal root exposed by laminectomy was removed. Parasagittal spinal cord slices with the dorsal root attached (300 μm) were sectioned on a vibratome (Leica VT 1200s, Wetzlar, Germany) in ice cold (0-4˚C) oxygenated sucrose-based ACSF that contained the following (millimolar): 100 sucrose, 63 NaCl, 2.5 KCl, 1.2 NaH_2PO_4, 1.2 $MgCl_2$, 25 glucose, 25 $NaHCO_3$, and 5 Na ascorbate. Slices were then incubated for 15 minutes at 34˚C in NMDG-based recovery ACSF composed of the following (millimolar): 93 NMDG, 2.5 KCl, 1.2 NaH_2PO_4, 30 $NaHCO_3$, 20 HEPES, 25 glucose, 5 Na ascorbate, 2 thiourea, 3 Na pyruvate, 10 $MgSO_4$, and 0.5 $CaCl_2$ and adjusted to pH 7.4 with HCl. After the recovery incubation, slices were transferred to oxygenated ACSF with the following composition (millimolar): 125 NaCl, 2.5 KCl, 1.25 NaH_2PO_4, 1.2 $MgCl_2$, 2.5 $CaCl_2$, 25 glucose, and 25 $NaHCO_3$ for 45 minutes at 36˚C and then maintained at RT prior to transfer to the recording chamber. All ACSF solutions were equilibrated with 95% O_2 and 5% CO_2. Spinal cord slices were collected 48 hours after administration of siRNA (i.t). Some slices were preincubated with inhibitors of Dnm (Dyngo4a, 30 μM) or AAK1 (SGC-AAK1-1, 100 nM; LP-935509, 1 μM) for 10 minutes.

2.17. Spinal cord electrophysiology

Slices were transferred to the recording chamber and continuously superfused with ACSF equilibrated with 95% O_2/5% CO_2 at a rate of 2 mL/minute at RT. Dodt-contrast optics were used to identify dorsal horn neurons in the translucent substantia gelatinosa layer of the superficial dorsal horn. Evoked and spontaneous excitatory postsynaptic currents (eEPSCs and sEPSCs respectively) were recorded in whole-cell voltage clamp using a CsCl-based internal solution composed of the following (millimolar): 140 CsCl, 10 EGTA, 5 HEPES, 2 $CaCl_2$, 2 MgATP, 0.3 NaGTP, 5 QX-314.Cl, and 0.1% biocytin (osmolarity 285-295 mosmol/L). Patch clamp electrodes had resistances between 3 and 5 MΩ, and neurons were held at −65 mV (not corrected for the liquid junction potential of 4 mV). A bipolar stimulating electrode was placed in the dorsal root entry zone for electrical stimulation of evoked postsynaptic currents. For paired pulse experiments, evoked currents were elicited by 2 consecutive stimuli of identical strength separated by 40 milliseconds. Paired-pulse ratio (PPR) was calculated by dividing the second pulse by the first (PSC2/PSC1). All eEPSCs were recorded in gabazine (10 μM) and strychnine (0.5 μM). In experiments with endocytosis inhibitors, baseline recordings were made before superfusion of with inhibitors for 10 minutes, after which recordings were repeated in the presence of the inhibitor. In the inhibitor studies, the 1 Hz protocol was reduced to 8 pulses to prevent plastic changes at the synapse occurring between the baseline recording and postinhibitor recording.

2.18. Synaptic vesicle imaging

Lumbar spinal cord slices were incubated in Mg^{2+}-free ACSF that contained the following (millimolar): 125 NaCl, 2.5 KCl, 1.25 NaH_2PO_4, 25 $NaHCO_3$, 2.5 $CaCl_2$, 10 glucose, and 0.1 4-AP for 10 minutes to increase neuronal activity. Slices were transferred to Mg^{2+}-free ACSF with 4-AP containing 8 μM FM1-43 (Abcam, Australia) for 3 minutes, washed with ACSF for 2 minutes, and then incubated in 1 mM ADVASEP-7 (Sigma) for 2 minutes. Slices were washed with ACSF for 2 minutes, and the ADVASEP-7 incubation was repeated. Slices were placed in the recording chamber and washed for a further 15 minutes in ACSF before imaging. A bipolar stimulating electrode was placed in the dorsal root entry zone of the spinal cord and stimulated for 10 seconds at 1 Hz, 4 to 6 V to facilitate the release of vesicles from the presynaptic terminals. Optical recordings were completed on an upright fluorescence microscope (BX51W1, Olympus, Center Valley, PA) under ×40 magnification using a Cy3/TRITC filter set CCD camera (C11440 Orca Flash 4.0, Hamamatsu, Shizuoka, Japan). Image sequences were analyzed using Fiji NIH image software.

2.19. Transmission electron microscopy

Adult C57BL/6 mice were treated with Dnm1 or CTR siRNA (i.t). After 48 hours, mice were anaesthetized (5% isoflurane), decapitated, and the lumbar region of the spinal cord exposed by laminectomy and removed. Spinal cord slices were prepared and a bipolar stimulating electrode was placed in the dorsal root entry zone for electrical stimulation of evoked postsynaptic currents. Spinal cord sections were fixed in 2% paraformaldehyde, 2.5% glutaraldehyde, and 0.1 M sucrose in 0.1 M MBP (pH 7.4). Sections were postfixed in 1% OsO_4 and 1.5% $K_4Fe(CN)_6$ in ddH_2O, dehydrated in graded series of ethanol and propylene oxide, and embedded in EMbed 812 (Electron Microscopy Sciences, Hatfield, PA). Ultrathin sections (70 nm) were cut and stained with uranyl acetate and lead citrate. Stained grids were imaged with Talos120C transmission electron microscope (Thermo Fisher Scientific) and recorded using Gatan (4k × 4k) OneView Camera with software Digital Micrograph (Gatan Inc, Pleasanton, CA). Morphometry measurements were made using Image J by an investigator blinded to the experimental conditions. For analysis of SV numbers, 10,331 vesicles in total from 212 Dnm1 siRNA and 182 CTR siRNA synapses from 2 separate preparations. To eliminate bias that could arise from choosing synapses based on their size or SV number, synapses were selected based on the presence of an active zone. All SVs within the adjacent SV cluster were then counted. In experiments designed to assess the effects of Dnm1 siRNA treatment on the abundance of CCPs, 13276 vesicles (CCP + SV) in total were counted; results were expressed as the percentage of CCPs relative to the total of SVs + CCPs/synapse (n = 212 Dnm1 siRNA and 182 CTR siRNA synapses).

2.20. Trypsin-evoked nociception

Dnm1+2+3 or CTR siRNA was administered by i.t. injection as described above. After 48 hours, trypsin (10 μL, 80 nM) was

Copyright © 2022 by the International Association for the Study of Pain. Unauthorized reproduction of this article is prohibited.

Downloaded from http://journals.lww.com/pain by BhDMf5ePHKav1zEoum1tQfN4a+kJLhEZgbsIHo4XMi0hCywCX1AWnYQp/IlQrHD3i3D0OdRyi7TvSFl4Cf3VC4/OAVpDDa8K2+Ya6H515kE= on 09/29/2023

injected (i.pl.) into the right hindpaw. Mechanical allodynia was assessed 1 hour after trypsin injection.[20]

2.21. Trypsin-evoked hyperexcitability of nociceptors

Dnm1+2+3 or CTR siRNA was administered by i.t. injection as described above. After 48 hours, DRG (L3-L5) were removed and dispersed by incubation in collagenase (4 mg/mL, Gibco, Waltham, MA) and dispase (4.7 mg/mL, Gibco) for 15 minutes at 37°C and triturated with a 200-μL pipette tip. Neurons were plated onto coverslips coated with laminin (0.013 mg/mL) and poly-L-ornithine (0.1 mg/mL) in 12-well plates. Neurons were cultured in F12 medium (Sigma) containing 10% fetal bovine serum, penicillin, and streptomycin and maintained at 37°C in a humidified atmosphere of 95% air and 5% CO_2 until retrieval (16 hours) for patch clamp recordings. Small-diameter (<30 μm) neurons were selected for patch clamp recording. Changes in excitability were quantified by measuring rheobase. Whole-cell perforated patch clamp recordings were made using Amphotericin B (240 μg/mL, Sigma Aldrich) in current clamp mode at RT. The recording chamber was perfused with external solution at 2 mL/minute. Recordings were made using Multiclamp 700B amplifiers, digitized by Digidata 1440A, and processed using pClamp 10.7 software (Molecular Devices). Solutions had the following composition (millimolar): pipette—K-gluconate 110, KCl 30, HEPES 10, $MgCl_2$ 1, and $CaCl_2$ 2; pH 7.25 with 1 M KOH; external—NaCl 140, KCl 5, HEPES 10, glucose 10, $MgCl_2$ 1, and $CaCl_2$ 2; pH to 7.3 to 7.4 with 1 M NaOH. Neurons were preincubated with trypsin (100 nM) for 10 minutes and washed. Rheobase was measured at T = 0 or T = 30 minutes after washing.

2.22. Statistics

Data are presented as mean ± SEM. Groups of n = 6 to 10 mice were studied. Differences were assessed using the Student 2-tailed *t* test for 2 comparisons and 1-way or 2-way analysis of variance (ANOVA) and Sídák, Tukey, Newman–Keuls or Dunnett post hoc tests for multiple comparisons. $P < 0.05$ was considered significant at the 95% confidence level. Sample sizes and statistical tests are specified in figure legends.

3. Results

3.1. Dynamin 1 and Dynamin 3 are expressed in neurons of sensory ganglia and the spinal cord dorsal horn

We used RNAScope in situ hybridization to localize isoforms of *Dnm1*, *Dnm2*, and *Dnm3* mRNAs in DRG, TG, and spinal cord of mice. Neurons were identified by Nissl staining. Immunostaining for CGRP allowed identification of a subset of small-diameter peptidergic nociceptors of sensory ganglia.[2] CGRP+ve nociceptors express AP2α2, a key endocytosis protein that contributes to nociception.[28] Satellite glial cells of sensory ganglia were identified by immunostaining for GS. *Dnm1* and *Dnm3* mRNAs were expressed in neurons of DRG and TG (**Fig. 1A**; Fig. S1A, available as supplemental digital content at http://links.lww.com/PAIN/B750). *Dnm2* mRNA was detected in DRG and TG neurons at lower levels (**Fig. 1A**; Fig. S1A, available as supplemental digital content at http://links.lww.com/PAIN/B750). Although *Dnm1*, *Dnm2*, and *Dnm3* mRNAs were detected in CGRP+ve nociceptors (Fig. S2, available as supplemental digital content at http://links.lww.com/PAIN/B750). Dnm isoforms were expressed in most neurons regardless of CGRP expression and diameter. Dynamin isoforms were also found in nonneuronal cells within sensory ganglia, including GS+ve satellite glial cells (**Fig. 1A**). *Dnm1* and *Dnm3* mRNAs were mainly detected in neurons of deeper laminae of the dorsal horn of the spinal cord, although some neurons with cell bodies in the superficial laminae (LI, LII, LIII) also expressed *Dnm1* and *Dnm3* mRNAs (**Fig. 1B**). Fewer neurons in the spinal cord expressed *Dnm2* mRNA. Analysis of extracts of DRG, TG, and spinal cord by qRT-PCR confirmed the higher levels of expression of *Dnm1* and *Dnm3* compared with *Dnm2* mRNA (**Figs. 1C and D**; Fig. S1B, available as supplemental digital content at http://links.lww.com/PAIN/B750). *Dnm1* and *Dnm3* mRNAs were also localized to neurons of human DRG (**Fig. 1E**), which adds translational relevance to these findings.

3.2. Dynamin siRNA knockdown in dorsal root ganglia reverses inflammatory and neuropathic pain

To study the contribution of Dnm isoforms to nociception, we administered (i.t. injection) Dnm1, Dnm2, Dnm3, or CTR siRNAs to mice. RNAScope revealed that Dnm siRNA inhibited expression of *Dnm1*, *Dnm2*, and *Dnm3* mRNA in DRG neurons after 48 hours compared with CTR siRNA (**Figs. 2A and B**), although expression in the spinal cord was unaffected (Fig. S3A, B, available as supplemental digital content at http://links.lww.com/PAIN/B750).

We investigated the effects of Dnm knockdown in a preclinical model of inflammatory pain in mice induced by injection of CFA or vehicle (control) into the hindpaw (**Fig. 2C**). Dnm1, Dnm2, Dnm3, or CTR siRNA was administered 24 hours after CFA. Withdrawal responses of the CFA-injected (left, ipsilateral) and noninjected (right, contralateral) hindpaws to stimulation with von Frey filaments and radiant heat were assessed daily to evaluate mechanical allodynia and thermal hyperalgesia, respectively. Complete Freund adjuvant–induced inflammation reduced both the withdrawal threshold to von Frey filaments and the withdrawal latency to heat in the ipsilateral paw for at least 4 days, consistent with mechanical allodynia and thermal hyperalgesia (**Figs. 2D and E**; Fig. S4A, B, available as supplemental digital content at http://links.lww.com/PAIN/B750). Dnm1, Dnm2, or Dnm3 siRNAs partially reversed mechanical allodynia to a similar degree after 24 and 48 hours, with a larger effect at 48 hours when compared with CTR siRNA (**Fig. 2D**). When administered together, Dnm1+2+3 siRNAs reversed mechanical allodynia to 72 ± 15% of baseline at 48 hours ($P < 0.0001$ compared with CTR siRNA). Dnm1, Dnm2, or Dnm3 siRNAs reversed thermal hyperalgesia after 24 and 48 hours, with a larger effect at 24 hours (**Fig. 2E**). Dnm1+2+3 siRNAs reversed thermal hyperalgesia by 100 ± 4% at 24 hours ($P < 0.0001$). The antinociceptive actions of Dnm siRNA were lost after 72 hours (Fig. S4A, B, available as supplemental digital content at http://links.lww.com/PAIN/B750). None of the treatments (i.pl. CFA, i.t. siRNAs) affected withdrawal responses of the contralateral (noninjected) paw to mechanical stimuli (Fig. S4C-F, available as supplemental digital content at http://links.lww.com/PAIN/B750).

Neuropathic pain was induced by SNI surgery of the hindpaw, which induces allodynia; control mice underwent sham surgery. Dnm1, Dnm2, Dnm3, or CTR siRNA was administrated (i.t. injection) 10 days after surgery, and withdrawal responses of the operated (ipsilateral) and nonoperated (contralateral) hindpaws to von Frey filaments and cold were assessed daily to evaluate mechanical and cold allodynia, respectively (**Fig. 3A**). Dnm1 siRNA reversed

Copyright © 2022 by the International Association for the Study of Pain. Unauthorized reproduction of this article is prohibited.

Downloaded from http://journals.lww.com/pain by BhDMf5ePHKav1zEoum1tQfN4a+kJLhEZgbsIHo4XMi0hCywCX1AWnYQp/IlQrHD3i3D0OdRyi7TvSFl4Cf3VC4/OAVpDDa8K2+Ya6H515kE= on 09/29/2023

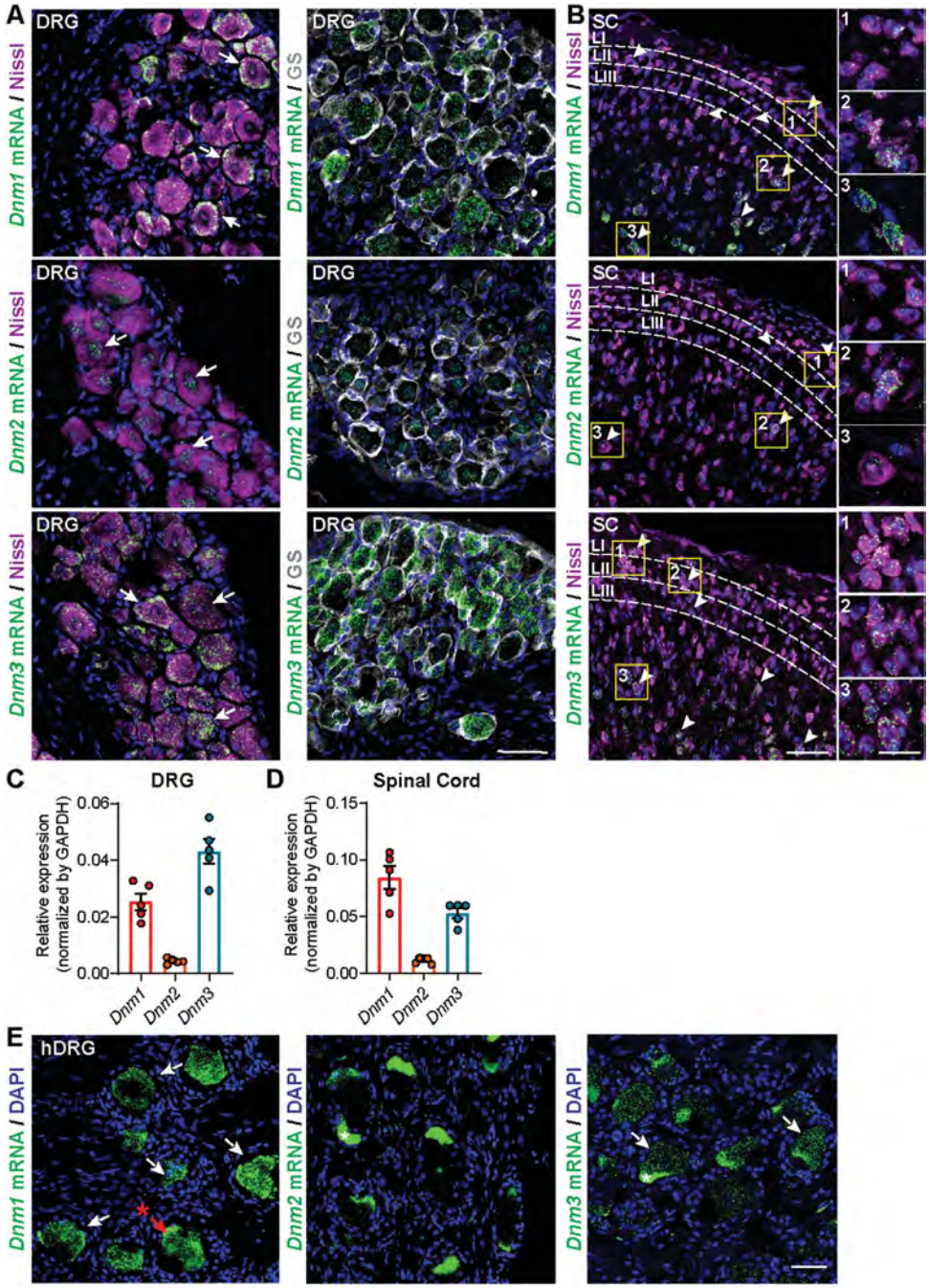

Figure 1. Localization of *Dnm* mRNA in DRG and spinal cord. RNAScope localization of *Dnm1*, *Dnm2*, and *Dnm3* mRNA in DRG (A) and dorsal horn of the spinal cord (SC) (B) of mice. Arrows indicate mRNA expression within DRG and spinal cord neurons. Scale bar, 50 μm and in the detail box 20 μm. Representative images, n = 5 mice per group. Quantification of expression of *Dnm1*, *Dnm2*, and *Dnm3* mRNA in the DRG (C) and spinal cord (D) of mice determined by qRT-PCR, n = 5 mice per group. RNAScope localization of *Dnm1*, *Dnm2*, and *Dnm3* mRNA in human DRG (E). Arrows indicate mRNA expression within DRG neurons. Scale bar, 50 μm. *Indicates fluorescent signal because of the presence of lipofuscin in human DRG neurons. Dnm, dynamin; DRG, dorsal root ganglia; DAPI, 4',6-diamidino-2-phenylindole; GAPDH, Glyceraldehyde-3-phosphate dehydrogenase; qRT-PCR, quantitative real-time reverse transcription polymerase chain reaction.

mechanical and cold allodynia after 24 and 48 hours when compared with CTR siRNA, although the inhibitory effects were lost after 72 hours (**Fig. 3B**). Dnm1+2+3 siRNAs strongly inhibited mechanical and cold allodynia at 24, 48, and 72 hours (**Fig. 3C**). The largest effect on mechanical allodynia was after 48 hours, when the response was 42 ± 5% of baseline ($P < 0.0001$). The largest effect on cold allodynia was after 24 hours, when the response was 70 ± 6% of baseline ($P < 0.0001$). None of the treatments (SNI surgery, i.t. siRNA) affected withdrawal responses of the contralateral (nonoperated) paw to mechanical stimuli (Fig. S5A, available as supplemental digital content at http://links.lww.com/PAIN/B750).

Nonevoked behavior was assessed using a behavioral spectrometer. Behavior was monitored for 20 minutes at 48 hours after administration (i.t. injection) of Dnm or CTR siRNA into SNI and sham mice. In mice receiving CTR siRNA, the number of visits to the center area was reduced in SNI compared with sham mice (**Figs. 3D and E**). Dnm1+2+3 siRNAs normalized the number of visits to the center area in SNI mice but had no effects

Copyright © 2022 by the International Association for the Study of Pain. Unauthorized reproduction of this article is prohibited.

Downloaded from http://journals.lww.com/pain by BhDMf5ePHKav1zEoum1tQfN4a+kJLhEZgbsIHo4XMi0hCywCX1AWnYQp/IlQrHD3i3D0OdRyi7TvSFl4Cf3VC4/OAVpDDa8K2+Ya6H515kE= on 09/29/2023

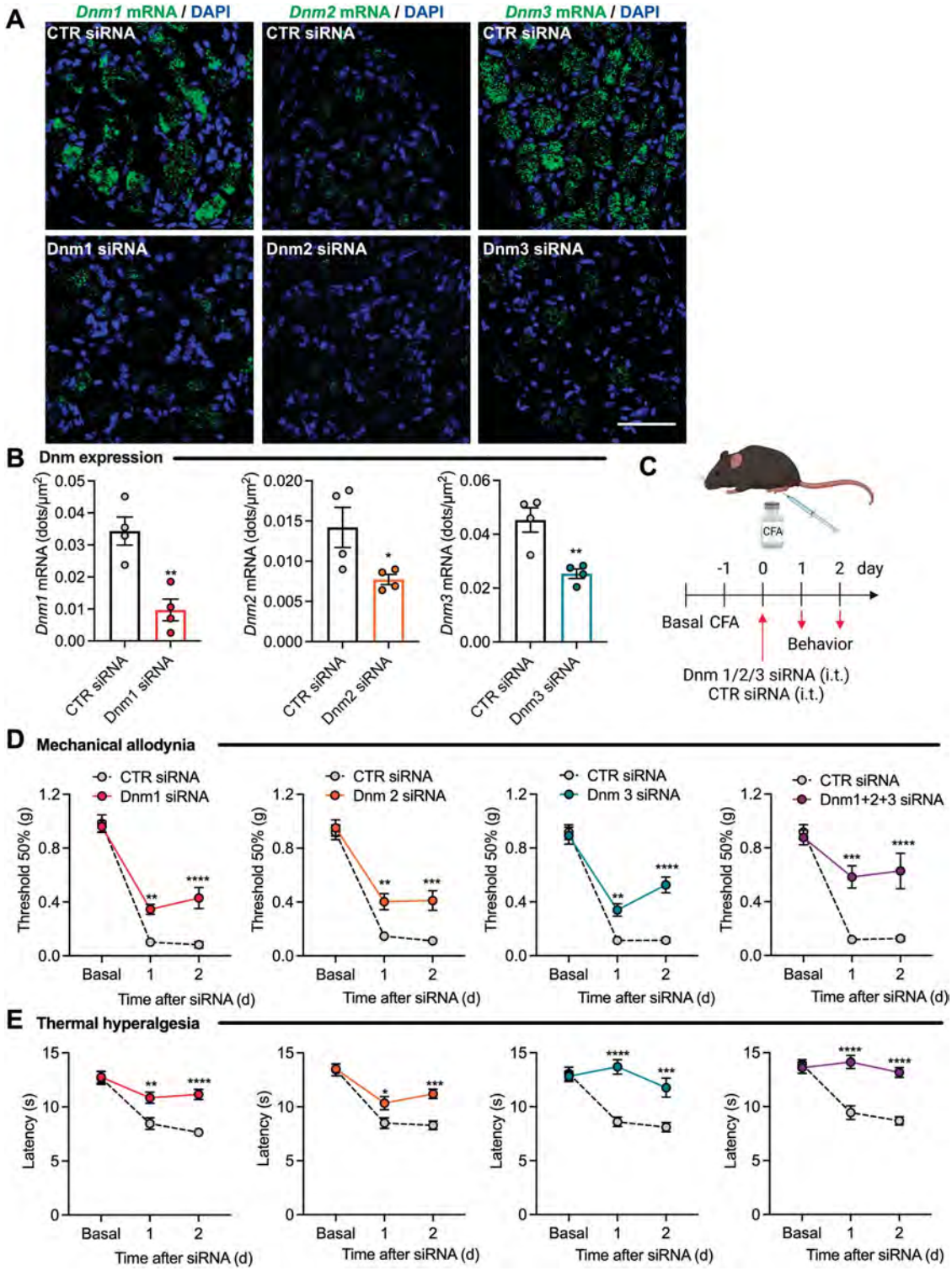

Figure 2. Dnm siRNA knockdown and inflammatory pain. RNAScope localization (A) and quantification (number of dots per area) (B) of *Dnm1*, *Dnm2*, and *Dnm3* mRNA expression in mouse DRG at 2 days after administration of Dnm1, Dnm2, Dnm3, or control (CTR) siRNA, n = 4 mice per group. Experimental timeline (C). Mechanical allodynia (D) and thermal hyperalgesia (E) induced by CFA measured 1 or 2 days after administration of Dnm1, Dnm2, Dnm3, or CTR siRNA, n = 8 mice per group. Mean ± SEM. $^{*}P < 0.05$, $^{**}P < 0.01$, $^{***}P < 0.001$, $^{****}P < 0.0001$ vs CTR siRNA. Parametric unpaired 2-tailed *t* test (B) or 2-way ANOVA, Sídák multiple comparisons test (D and E). ANOVA, analysis of variance; CFA, complete Freund adjuvant; Dnm, dynamin; DRG, dorsal root ganglia; DAPI, 4',6-diamidino-2-phenylindole.

in sham mice. In sham mice, Dnm1+2+3 siRNAs did not affect average velocity, track length, total activity, ambulation, grooming, or wall distance when compared with CTR siRNA (Fig. S5B, available as supplemental digital content at http://links.lww.com/PAIN/B750).

3.3. Adaptor associated kinase 1 siRNA knockdown in dorsal root ganglia reverses inflammatory and neuropathic pain

RNAScope revealed *Aak1* mRNA in neurons of DRG, TG, and spinal cord dorsal horn (**Fig. 4A**; Fig. S1A, available as supplemental digital content at http://links.lww.com/PAIN/B750).

Copyright © 2022 by the International Association for the Study of Pain. Unauthorized reproduction of this article is prohibited.

Downloaded from http://journals.lww.com/pain by BhDMf5ePHKav1zEoum1tQfN4a+kJLhEZgbsIHo4XMi0hCywCX1AWnYQp/IlQrHD3i3D0OdRyi7TvSFl4Cf3VC4/OAVpDDa8K2+Ya6H515kE= on 09/29/2023

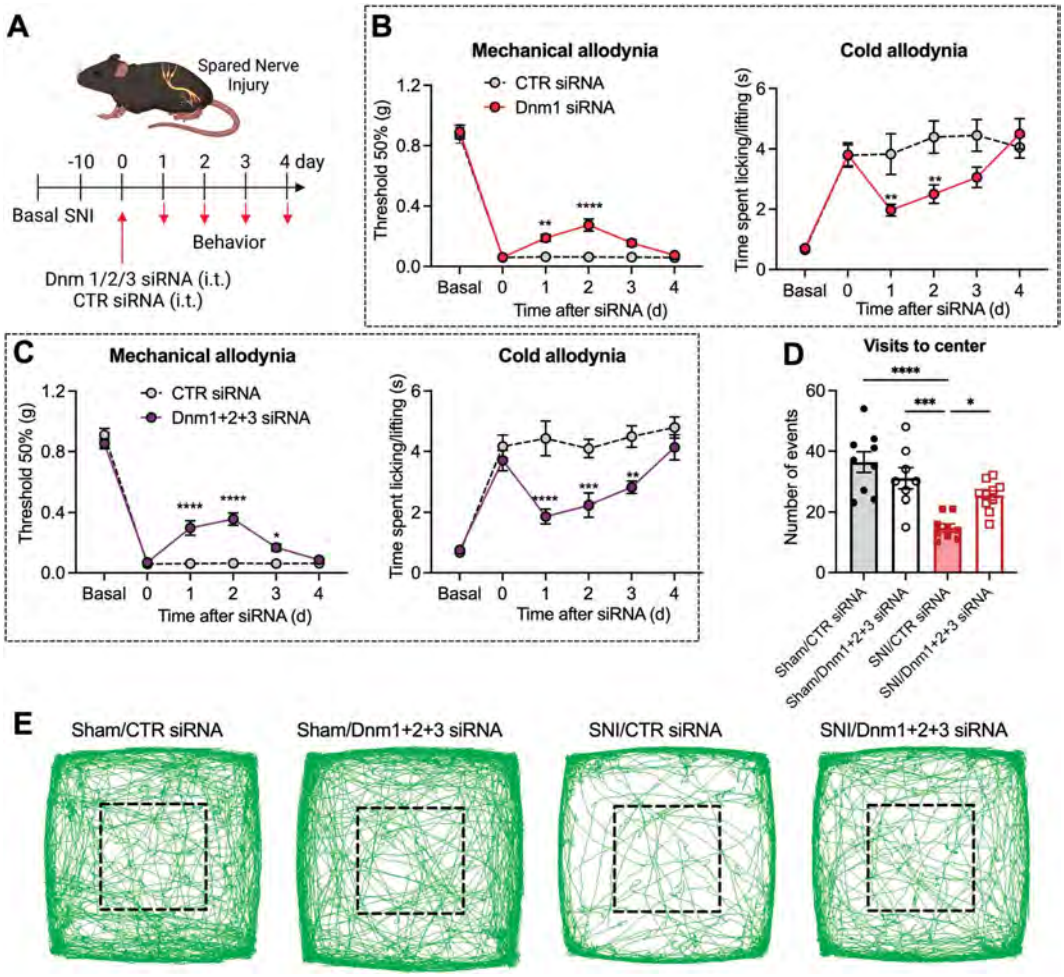

Figure 3. Dnm siRNA knockdown and neuropathic pain. Experimental timeline (A). Mechanical and cold allodynia in SNI mice measured 1 to 4 days after administration of Dnm1 or CTR siRNA (B) or Dnm1+2+3 or CTR siRNA (C), n = 10 mice per group. Nonevoked nociceptive behavior in SNI and sham control mice recorded for 20 minutes at 2 days after administration of Dnm1+2+3 or CTR siRNA. Visits to center area marked by black square (D) and representative images of the track records (E) are shown, n = 8 mice per group for Sham/Dnm1+2+3 siRNA, n = 9 mice per group for Sham/CTR siRNA and SNI/CTR siRNA and n = 10 mice per group for SNI/Dnm1+2+3 siRNA. Mean ± SEM. *$P < 0.05$, **$P < 0.01$, ***$P < 0.001$, ****$P < 0.0001$ vs CTR siRNA; Sham vs SNI; SNI/CTR siRNA vs SNI/Dnm1+2+3 siRNA. Two-way ANOVA, Sídák multiple comparisons test (B and C) or 1-way ANOVA, Tukey multiple comparisons test (D). ANOVA, analysis of variance; CTR, control; Dnm, dynamin; SNI, spared nerve injury.

Although *Aak1* mRNA was detected in CGRP+ve peptidergic nociceptors of DRG, most neurons expressed *Aak1* mRNA regardless of CGRP content or diameter (**Fig. 4B**). *Aak1* mRNA was also detected in GS+ve satellite glial cells of sensory ganglia. Quantitative real-time reverse transcription polymerase chain reaction analyses confirmed the expression of *Aak1* mRNA in DRG, TG, and spinal cord (**Fig. 4C**). Adaptor-associated kinase 1 mRNA was also localized to neurons of human DRG (**Fig. 4D**).

Adaptor-associated kinase 1 siRNA (i.t. injection) depleted *Aak1* mRNA in DRG neurons after 24 hours compared with CTR siRNA, determined by RNAScope (**Figs. 5A and B**); *Aak1* expression in the spinal cord was unaffected (Fig. S3A, B, available as supplemental digital content at http://links.lww.com/PAIN/B750). To evaluate the effects on nociception, AAK1 or CTR siRNA was administered (i.t. injection) to mice 24 hours after CFA or 10 days after SNI surgery (**Figs. 5C and D**). Adaptor-associated kinase 1 siRNA partially reversed CFA-evoked mechanical allodynia and almost completely reversed thermal hyperalgesia when compared with CTR siRNA (**Fig. 5C**). Adaptor-associated kinase 1 siRNA reversed mechanical allodynia to 52 ± 9% of baseline ($P < 0.0001$ compared with CTR siRNA) and thermal hyperalgesia to 92 ± 6% of baseline ($P < 0.01$) after 48 hours. Adaptor-associated kinase 1 siRNA partially reversed SNI-evoked mechanical and cold allodynia (**Fig. 5D**), and it reversed mechanical allodynia to 28 ± 4% of baseline at 48 hours ($P < 0.01$) and reversed cold allodynia to 54 ± 8% of baseline at 24 hours ($P < 0.01$). Furthermore, it did not affect withdrawal responses of the contralateral paw (Fig. S6A, B, available as supplemental digital content at http://links.lww.com/PAIN/B750). In mice receiving CTR siRNA, the number of visits to the center area of the field was reduced in SNI compared with sham mice. Adaptor-associated kinase 1 siRNA restored the number of visits to the center area in SNI mice but had no effects in sham mice (**Figs. 5E and F**). In sham mice, AAK1 siRNA did not affect any measured behavior (Fig. S6C, available as supplemental digital content at http://links.lww.com/PAIN/B750).

3.4. Dynamin and adaptor-associated kinase 1 inhibitors reverse inflammatory and neuropathic pain

Inhibitors of endocytosis offer a pharmacological approach for pain management. To investigate this hypothesis, we examined the effects of inhibitors of Dnm (Dyngo4a),[33] clathrin (PitStop2),[34] and AAK1 (LP935509,[21] SGC-AAK1-1[1]) on inflammatory and neuropathic pain.

Copyright © 2022 by the International Association for the Study of Pain. Unauthorized reproduction of this article is prohibited.

Downloaded from http://journals.lww.com/pain by BhDMf5ePHKav1zEoum1tQfN4a+kJLhEZgbsIHo4XMi0hCywCX1AWnYQp/IlQrHD3i3D0OdRyi7TvSFl4Cf3VC4/OAVpDDa8K2+Ya6H515kE= on 09/29/2023

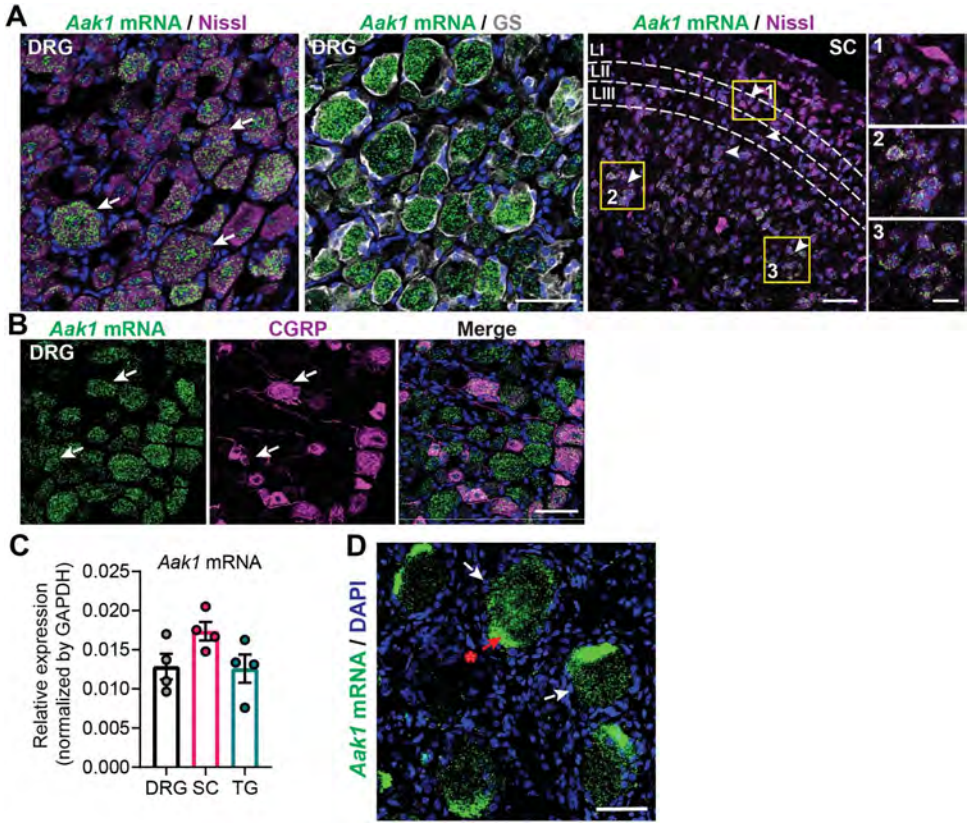

Figure 4. Localization of *Aak1* mRNA in DRG ganglia and spinal cord. RNAScope localization of *Aak1* mRNA in DRG and dorsal horn of the spinal cord of mice (A). Arrows indicate mRNA expression within DRG and spinal cord neurons. Scale bar, 50 μm and in the detail box 20 μm. Representative images, n = 5 mice per group. Localization of *Aak1* mRNA in CGRP +ve DRG neurons (B). Scale bar, 50 μm. Representative images, n = 3 mice per group. Quantification of expression of *Aak1* mRNA in the DRG, spinal cord, and TG of mice determined by qRT-PCR, n = 4 mice per group (C). RNAScope localization of *Aak1* mRNA in human DRG (D). Arrows indicate mRNA expression within DRG neurons. Scale bar, 50 μm. *Fluorescent signal because of the presence of lipofuscin in human DRG neurons. CGRP, calcitonin gene-related peptide; DRG, dorsal root ganglia; DAPI, DAPI, 4',6-diamidino-2-phenylindole; GAPDH, Glyceraldehyde-3-phosphate dehydrogenase; GS, Glutamine synthetase; qRT-PCR, quantitative real-time reverse transcription polymerase chain reaction; SC, spinal cord; TG, trigeminal ganglia.

Dyngo4a, PitStop2, inactive analogs (control) (5 μL, 50 μM), LP935509, SGC-AAK1-1 (5 μL, 1-10 μg), or vehicle (control) was administered (i.t. injection) 48 hours after CFA (**Fig. 6A**). Dyngo4a partially reversed mechanical allodynia and thermal hyperalgesia when compared with vehicle, with a maximum inhibitory effect at 1 hour of 80 ± 11% for mechanical allodynia ($P < 0.0001$ compared with vehicle) and 75 ± 6% for thermal hyperalgesia ($P < 0.05$) (**Figs. 6B and C**). PitStop2 reversed CFA-evoked mechanical allodynia and thermal hyperalgesia similarly to Dyngo4a (**Figs. 6B and C**). LP935509 dose-dependently inhibited mechanical allodynia, with a maximal effect for 10 μg at 2 hours of 78 ± 8% of baseline ($P < 0.0001$) (**Fig. 6D**). LP935509 almost completely reversed thermal hyperalgesia, with a maximal effect for 10 μg at 2 hours of 89 ± 7% of baseline ($P < 0.0001$) (**Fig. 6E**). Likewise, SGC-AAK1-1 reversed CFA-evoked mechanical allodynia and thermal hyperalgesia similarly to LP935509 (**Figs. 6F and G**).

Inhibitors of Dnm, clathrin, or AAK1 were administered (i.t. injection) 10 days after SNI surgery (**Fig. 6H**). Dyngo4a reversed SNI-evoked mechanical and cold allodynia with a maximum inhibitory effect at 1 hour of 61 ± 10% of baseline for mechanical allodynia and 69 ± 8% of baseline for cold allodynia ($P < 0.01$) (**Figs. 6I and J**). PitStop2 similarly reversed SNI-induced mechanical and cold allodynia (**Figs. 6I and J**). LP935509 and SGC-AAK1-1 partially reversed SNI-evoked mechanical and cold allodynia from 1 to 4 hours (**Figs. 6K–N**). Maximal inhibitory effects of LP935509 (10 μg) were at 2 hours for mechanical allodynia (79 ± 9% of baseline, $P < 0.0001$) and 1 hour for cold allodynia (61 ± 8% of baseline, $P < 0.0001$).

Inactive analogs of Dyngo4a and PitStop2 or vehicle did not affect CFA-evoked or SNI-evoked allodynia or hyperalgesia. None of the treatments affected withdrawal responses of the contralateral paw to mechanical stimuli (Figs. S7A–F, available as supplemental digital content at http://links.lww.com/PAIN/B750).

3.5. Dynamin 1 and adaptor-associated kinase 1 shRNA knockdown induces long-lasting reversal of inflammatory and neuropathic pain

To determine whether a more sustained knockdown of Dnm or AAK1 would have a larger and longer-lasting antinociceptive effect, we administered Dnm1, AAK1, or CTR shRNA to mice (i.t. injection). Dnm1 and AAK1 shRNA depleted *Dnm1* mRNA by 42 ± 6% and *Aak1* mRNA by 28 ± 4% (both $P < 0.01$ to CTR), respectively, in DRG neurons after 72 hours, determined by RNAScope. Dnm1, AAK1, or CTR shRNA was administered to mice 24 hours after CFA or 10 days after SNI surgery. Dnm1 and AAK1 shRNA caused a long-lasting reversal of CFA-evoked and SNI-evoked nociception that was fully sustained for at least 7 days (**Figs. 7A and B**). In CFA-treated mice, Dnm1 and AAK1 shRNA, respectively, reversed mechanical allodynia to 78 ± 8% and 71 ± 6% of baseline ($P < 0.0001$ compared with CTR shRNA) and

Copyright © 2022 by the International Association for the Study of Pain. Unauthorized reproduction of this article is prohibited.

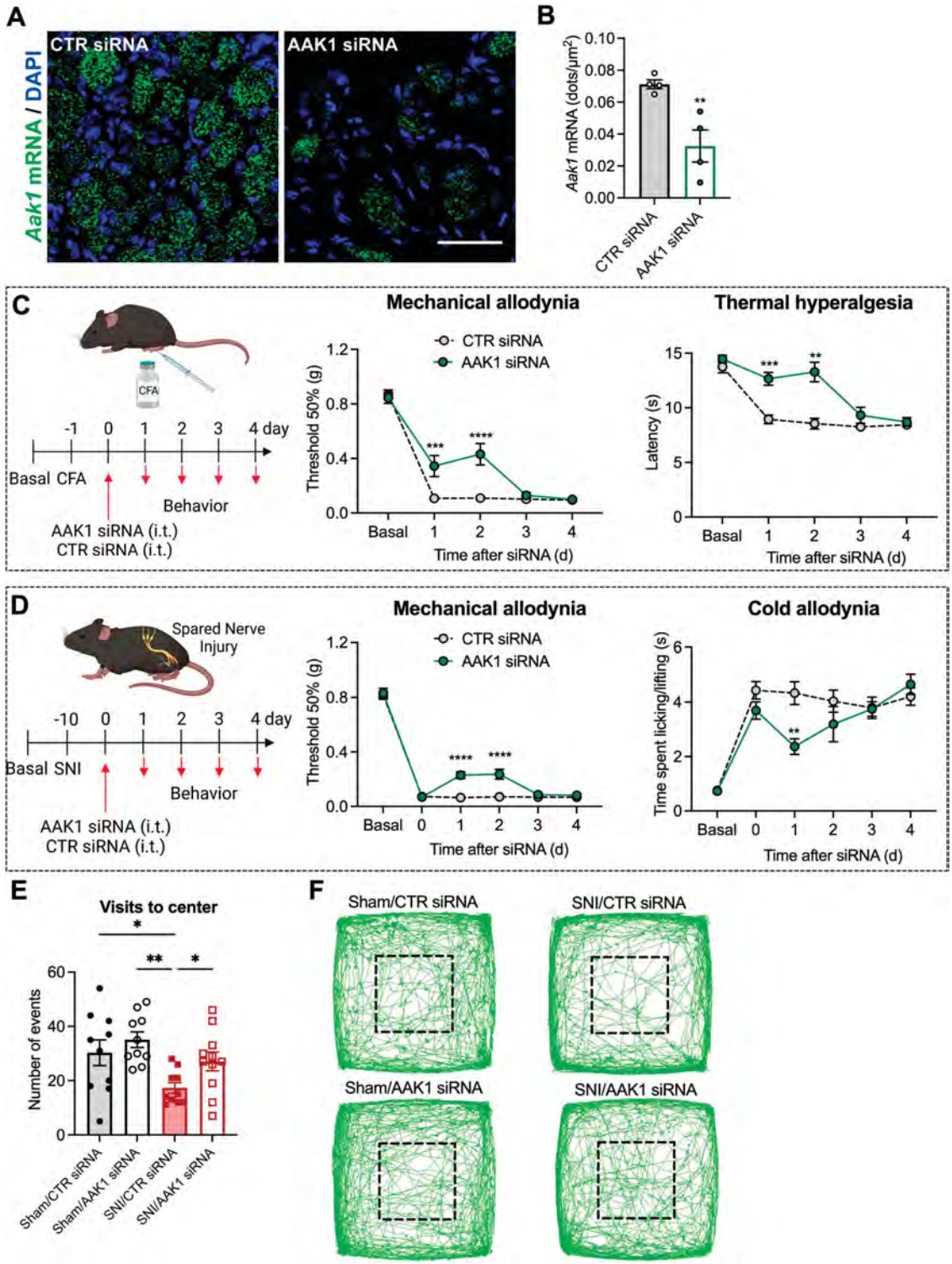

Figure 5. AAK1 siRNA knockdown and inflammatory and neuropathic pain. RNAScope localization (A) and quantification (number of dots per area) (B) of *Aak1* mRNA expression in mouse DRG at 1 day after administration of AAK1 or CTR siRNA, n = 4 mice per group. Experimental timeline for CFA-evoked inflammatory pain, and mechanical allodynia and thermal hyperalgesia induced by CFA measured 1 to 4 days after administration of AAK1 or CTR siRNA, n = 8 mice per group (C). Experimental timeline for SNI-evoked neuropathic pain, and mechanical and cold allodynia in SNI mice measured 1 to 4 days after administration of AAK1 or CTR siRNA, n = 10 mice per group (D). Nonevoked behavior in SNI and sham control mice recorded for 20 minutes at 2 days after the administration of AAK1 or CTR siRNA. Visits to center area marked by black square (E) and representative images of the track records (F) are shown, n = 10 mice per group for Sham/CTR siRNA, Sham/AAK1 siRNA and SNI/CTR siRNA and n = 11 mice per group for SNI/AAK1 siRNA. Mean ± SEM. $^{*}P < 0.05$, $^{**}P < 0.01$, $^{***}P < 0.001$, $^{****}P < 0.0001$ vs CTR siRNA. Parametric unpaired 2-tailed *t* test (B), 2-way ANOVA, Sídák multiple comparisons test (C and D) or 1-way ANOVA, Newman–Keuls multiple comparisons test (E). AAK1, adaptor-associated protein kinase 1; ANOVA, analysis of variance; CFA, complete Freund adjuvant; CTR, control; DRG, dorsal root ganglia; DAPI, 4',6-diamidino-2-phenylindole; SNI, spared nerve injury.

Downloaded from http://journals.lww.com/pain by BhDMf5ePHKav1zEoum1tQfN4a+kJLhEZgbsIHo4XMi0hCywCX1AWnYQp/IlQrHD3i3D0OdRyi7TvSFl4Cf3VC4/OAVpDDa8K2+Ya6H515kE= on 09/29/2023

Copyright © 2022 by the International Association for the Study of Pain. Unauthorized reproduction of this article is prohibited.

Downloaded from http://journals.lww.com/pain by BhDMf5ePHKav1zEoum1tQfN4a+kJLhEZgbsIHo4XMi0hCywCX1AWnYQp/IlQrHD3i3D0OdRyi7TvSFl4Cf3VC4/OAVpDDa8K2+Ya6H515kE= on 09/29/2023

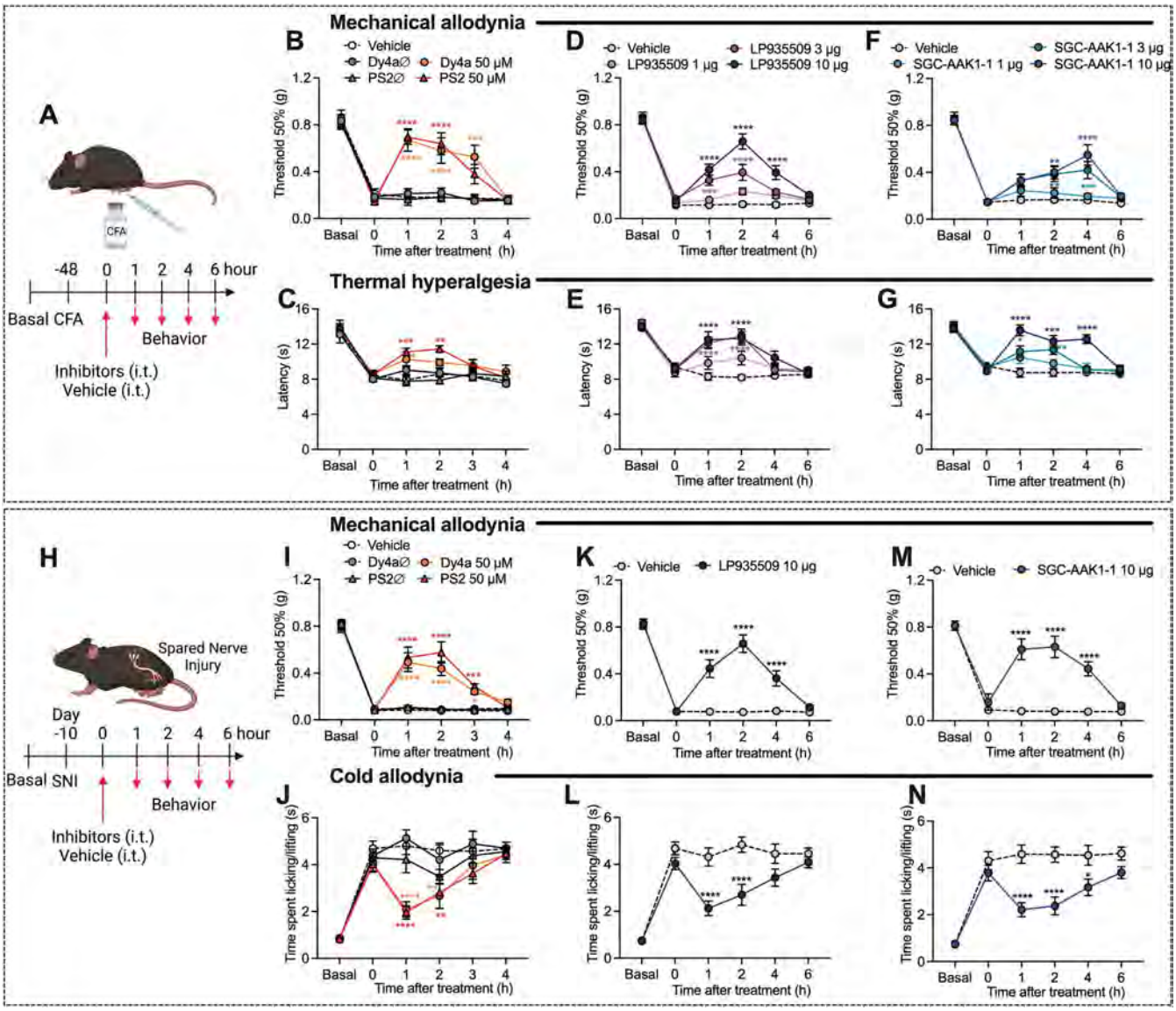

Figure 6. Effects of Dnm, clathrin, and AAK1 inhibitors on inflammatory and neuropathic pain. Experimental timeline for CFA-evoked inflammatory pain (A). Effects of Dyngo4a (Dy4a), PitStop2 (PS2), inactive analogs (Dy4aØ, PS2Ø) (all 5 µL, 50 µM, i.t.), or vehicle on CFA-evoked mechanical allodynia (B) and thermal hyperalgesia (C), n = 6 mice per group for vehicle and inactive analogs and n = 7 mice per group for Dyngo4a and PitStop2. Effects of LP935509 (5 µL, 1-10 µg, i.t.) or vehicle on CFA-evoked mechanical allodynia (D) and thermal hyperalgesia (E), n = 8 mice per group. Effects of SGC-AAK1-1 (5 µL, 1-10 µg, i.t.) or vehicle on CFA-evoked mechanical allodynia (F) and thermal hyperalgesia (G), n = 8 mice per group. Experimental timeline for SNI-evoked neuropathic pain (H). Effects of Dyngo4a, PitStop2, inactive analogs (5 µL, 50 µM, i.t.), or vehicle on SNI-evoked mechanical (I) and cold (J) allodynia, n = 7 mice per group for inactive analogs and n = 8 mice per group for vehicle, Dyngo4a and PitStop2. Effects of LP935509 (5 µL, 10 µg, i.t.) or vehicle on SNI-evoked mechanical (K) and cold (L) allodynia, n = 10 mice per group. Effects of SGC-AAK1-1 (5 µL, 10 µg, i.t.) or vehicle on SNI-evoked mechanical (M) and cold (N) allodynia, n = 10 mice per group. Mean ± SEM. $^{*}P < 0.05$, $^{**}P < 0.01$, $^{***}P < 0.001$, $^{****}P < 0.0001$ vs vehicle. Two-way ANOVA, Sídák multiple comparisons test. AAK1, adaptor-associated protein kinase 1; ANOVA, analysis of variance; CFA, complete Freund adjuvant; CTR, control; Dnm, dynamin; SNI, spared nerve injury.

thermal hyperalgesia to 86 ± 4% and 83 ± 4% of baseline ($P = 0.0001$; $P = 0.001$) after 72 hours. In SNI mice, Dnm1 and AAK1 shRNA, respectively, reversed mechanical allodynia to 69 ± 11% and 41 ± 5% of baseline ($P < 0.0001$ compared with CTR shRNA) and cold allodynia to 79 ± 4% and 97 ± 3% of baseline ($P < 0.0001$) after 72 hours (**Fig. 7D**). Dnm1 or AAK1 shRNA did not affect withdrawal responses of the contralateral paw to mechanical stimulation, heat or cold (Fig. S8A, B, available as supplemental digital content at http://links.lww.com/PAIN/B750).

Thus, Dnm and AAK1 siRNA, shRNA, and inhibitors reverse nociception in preclinical models of inflammatory and neuropathic pain without discernible effects on normal motor functions or behavior.

3.6. Dynamin 1 siRNA increases the threshold required to elicit dorsal root–evoked synaptic currents in spinal neurons

To investigate the contribution of Dnm to synaptic transmission in nociceptive circuits, dorsal root–evoked synaptic currents were recorded from spinal neurons in parasagittal slice preparations of mouse spinal cord 48 hours after injection of Dnm1 or CTR siRNA (i.t). Dorsal roots were stimulated, and eEPSCs were recorded in whole-cell voltage clamp in superficial dorsal horn (lamina I-II) neurons. The stimulus was incrementally increased from 1 to 10 V to assess the stimulus intensity required to elicit a synaptic response. The threshold voltage required to stimulate an eEPSC was higher in the Dnm1 siRNA

Copyright © 2022 by the International Association for the Study of Pain. Unauthorized reproduction of this article is prohibited.

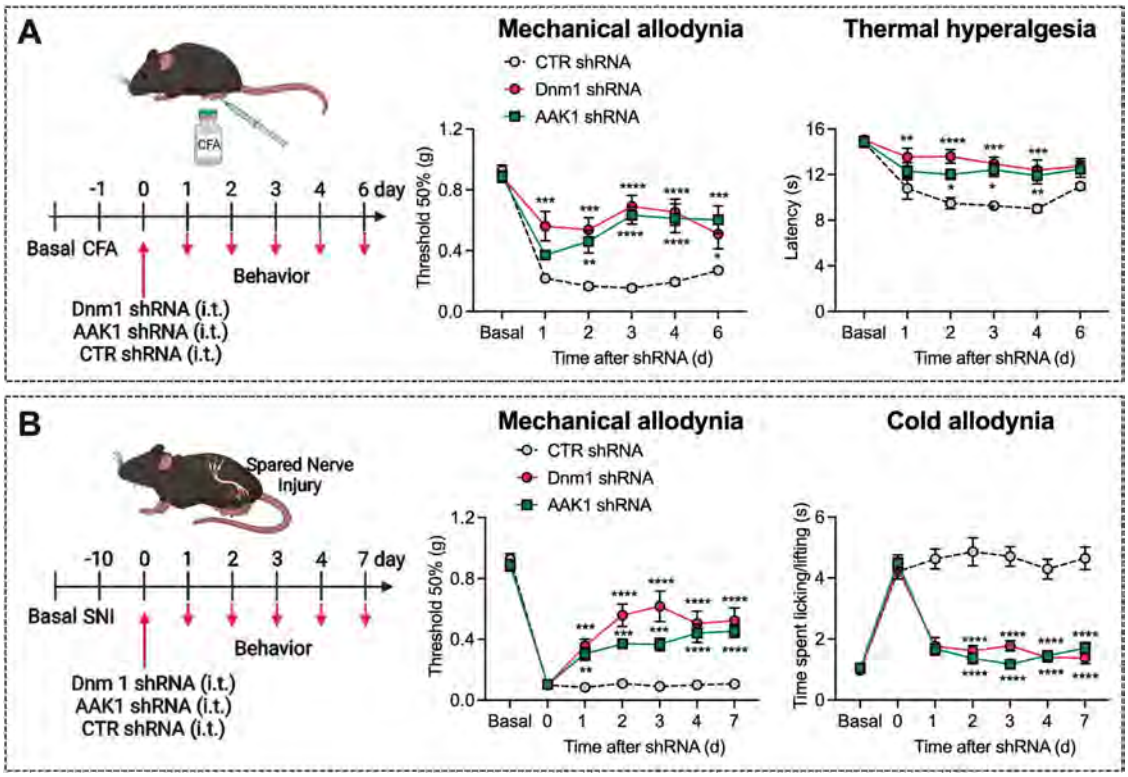

Figure 7. Dnm1 and AAK1 shRNA knockdown and inflammatory and neuropathic pain. Experimental timeline for CFA-evoked inflammatory pain, and mechanical allodynia and thermal hyperalgesia measured 1 to 6 days after administration of Dnm1, AAK1, or CTR shRNA, n = 8 mice per group (A). Experimental timeline for SNI-evoked neuropathic pain, and mechanical and cold allodynia measured 1 to 7 days after administration of Dnm1, AAK1, or CTR shRNA, n = 8 mice per group (B). Mean ± SEM. *$P < 0.05$, **$P < 0.01$, ***$P < 0.001$, ****$P < 0.0001$ vs CTR shRNA. Two-way ANOVA, Sídák multiple comparisons test. AAK1, adaptor-associated protein kinase 1; ANOVA, analysis of variance; CFA, complete Freund adjuvant; CTR, control; Dnm, dynamin; SNI, spared nerve injury.

group compared with the CTR siRNA group, and current amplitudes were higher in the control group at lower stimulus strength (**Figs. 8A and B**), which may be the result of increased release probability at higher stimulus intensities and recruitment of high threshold fibers. In the control group, the 50% maximal eEPSC amplitude was 2.7 V, and maximal amplitude was 5 V, above which the responses were not significantly different from one another. In the Dnm1 siRNA group, the 50% maximal eEPSC amplitude was 4.26 V, and the maximal eEPSC amplitude was 6 V (repeated-measures 1-way ANOVA, with Sidak multiple comparisons test).

3.7. Dynamin 1 siRNA reduces the probability of synaptic vesicle release and prevents sustained synaptic vesicle release from presynaptic primary afferent neurons

To investigate the effect of Dnm1 knockdown on the probability of SV release and to determine the contribution of presynaptic or postsynaptic sites, we measured paired-pulse ratios of eEPSCs in superficial neurons using a paired dorsal root stimulation at 40-ms intervals. Compared with controls, the paired-pulse ratio was depressed in the Dnm1 siRNA group ($P = 0.0042$, Mann–Whitney test), which indicates a presynaptic mechanism caused by a reduction in release probability from primary afferent neurons (**Figs. 8C and D**). The prominent expression of *Dnm1* mRNA in DRG neurons and the preferential knockdown of *Dnm1* mRNA in DRG neurons support a presynaptic mechanism.

Because a reduction in release probability is likely to affect the sustained responses to repetitive stimuli, we tested the eEPSC responses to 1 Hz stimulation of the dorsal roots. A 1 Hz frequency was chosen to allow repetitive activation of the slower latency C-fibers, which would be lost at higher frequencies, as well as A-fiber–mediated signals. In spinal cord from mice treated with CTR siRNA, consistent eEPSC amplitudes were observed throughout the 80-second train of stimuli, whereas the eEPSC amplitudes rapidly decreased after repeated stimulation in the Dnm1 siRNA group (**Figs. 8E and F**). This decrease was most apparent within the first 10 stimuli, where normalized amplitudes were significantly different between the 2 groups by the sixth stimulus (**Fig. 8G**).

Styryl dyes can be used to observe SV recycling.[10] Dye molecules reversibly partition into the plasma membrane outer leaflet but do not penetrate cells because of cationic charge. Upon stimulation and SV exocytosis, dye molecules internalize during compensatory endocytosis and label newly formed SVs. When labeled vesicles undergo exocytosis in dye-free medium, dye molecules dissociate from the plasma membrane and lose fluorescence. To further support findings from electrophysiological studies showing reduced SV release after *Dnm1* knockdown, FM1-47 was used to track SV recycling. Spinal cord slices were incubated in Mg^{2+}-free ACSF containing 4-aminopyridine (4-AP) to enhance calcium-dependent neurotransmitter release. Tissues were incubated with FM1-43 for 3 minutes, washed, and incubated with ADVASEP-7 to scavenge unincorporated FM1-43. The dorsal roots were stimulated at 1 Hz 4 to 6 V to facilitate SV release from presynaptic terminals, which were imaged by fluorescence microscopy. After 1 Hz dorsal root stimulation, fluorescence at individual synapses declined in the CTR siRNA group, representing exocytosis and consequent loss of labeled SVs. By contrast, synaptic fluorescence was maintained in the Dnm1 siRNA group (**Figs. 8H and I**).

Downloaded from http://journals.lww.com/pain by BhDMf5ePHKav1zEoum1tQfN4a+kJLhEZgbsIHo4XMi0hCywCX1AWnYQp/IlQrHD3i3D0OdRyi7TvSFl4Cf3VC4/OAVpDDa8K2+Ya6H515kE= on 09/29/2023

Copyright © 2022 by the International Association for the Study of Pain. Unauthorized reproduction of this article is prohibited.

Downloaded from http://journals.lww.com/pain by BhDMf5ePHKav1zEoum1tQfN4a+kJLhEZgbsIHo4XMi0hCywCX1AWnYQp/IlQrHD3i3D0OdRyi7TvSFl4Cf3VC4/OAVpDDa8K2+Ya6H515kE= on 09/29/2023

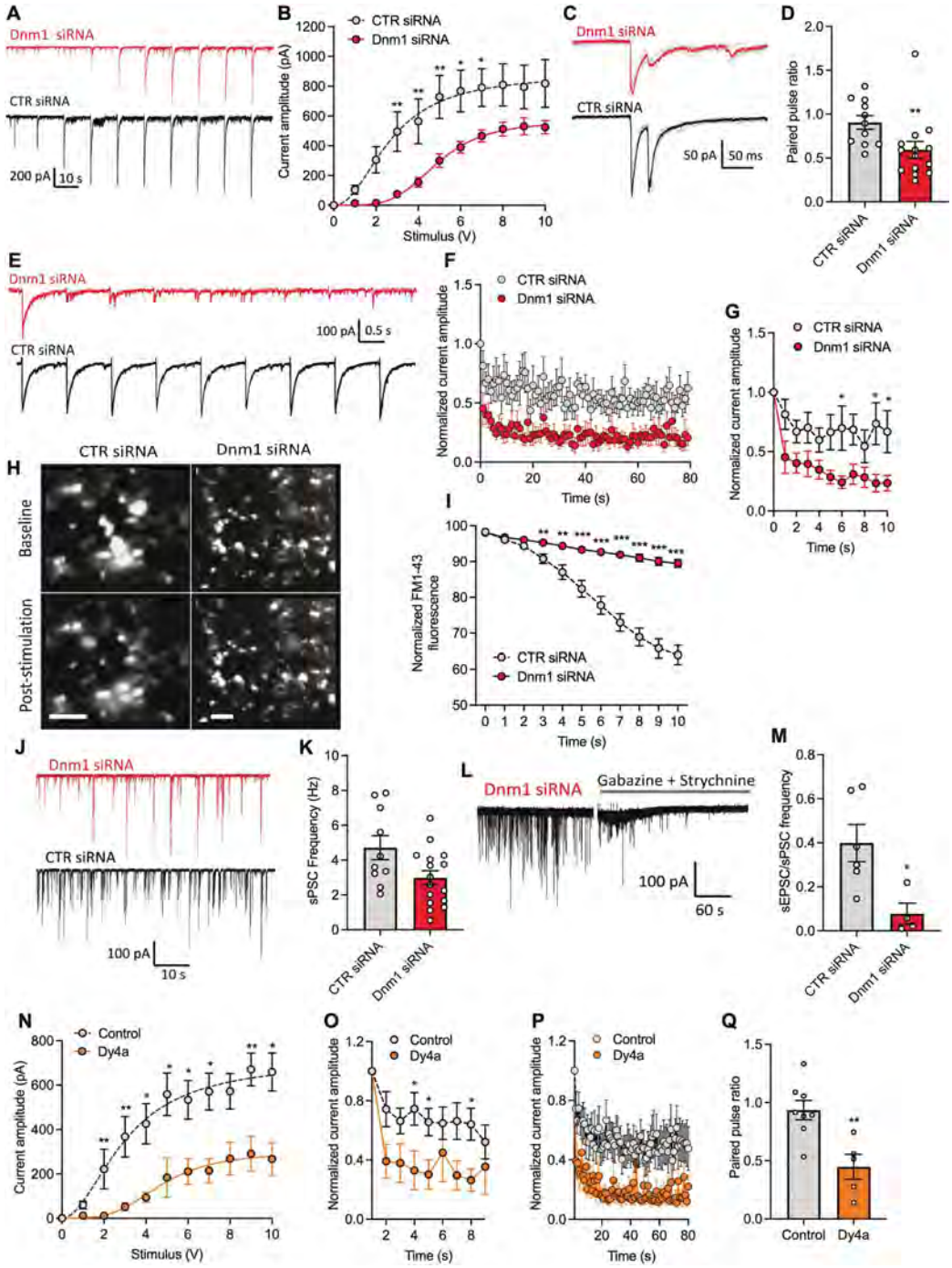

Figure 8. Contributions of Dnm1-mediated endocytosis to synaptic transmission in the spinal cord dorsal horn. Input–output responses of electrically evoked postsynaptic currents from spinal cord slices of mice at 2 days after intrathecal injection of Dnm1 or CTR siRNA. Representative traces show eEPSCs recorded in whole-cell voltage clamp from dorsal horn neurons in response to increasing intensity of presynaptic dorsal root electrical stimulus (1-10 V) (A). Mean eEPSC amplitude from Dnm1 (n = 14) and CTR (n = 10) siRNA-treated mice (B). Traces show averaged paired-pulse responses for neurons of Dnm1 and CTR siRNA-treated mice (C). Paired-pulse ratio of Dnm1 (n = 14) and CTR (n = 11) siRNA groups (D). Traces showing eEPSC responses to 1 Hz presynaptic stimulation in Dnm1 and CTR siRNA-treated groups (E). Normalized amplitude of eEPSCs over (F) 80 seconds and the initial 10 seconds (G) of 1 Hz presynaptic stimulation in Dnm1 (n = 11) and CTR (n = 8) siRNA-treated mice. Images of FM1-47 fluorescence detecting activity of individual synapses in the dorsal horn of Dnm1 and CTR siRNA mice pre- and post-1 Hz stimulation (H). Scale bar, 5 μm. Normalized FM1-47 fluorescence from the start of stimulation in Dnm1 (n = 36) and CTR (n = 33) siRNA groups (I). Traces show spontaneous postsynaptic currents (PSPs) recorded in voltage-clamped chloride-loaded spinal neurons (J). Frequency of sPSC events in spinal neurons from Dnm1 and CTR siRNA groups (K). Trace showing baseline sPSC events, which are reduced by GABA and glycine receptor antagonists (L). The frequency of sEPSCs as a proportion of total sPSCs is reduced in neurons from Dnm1 siRNA-treated mice (M). Input–output responses showing current amplitude in response to increasing stimulus intensity (1-10 V) in Dyngo4a-treated (30 μM, n = 5) and vehicle-treated (n = 13) spinal cord slices (N). Normalized amplitude of eEPSCs over the initial 8 seconds (O) and over 80 seconds (P) of 1 Hz stimulation in Dyngo4a-treated (n = 5) and vehicle-treated (n = 7) spinal cord slices. Paired-pulse ratio of Dyngo4a-treated (n = 5) and vehicle-treated (n = 8) spinal cord (Q). Mean ± SEM. $^{*}P < 0.05$, $^{**}P < 0.01$, $^{***}P < 0.001$ vs CTR. Two-way ANOVA, Sídák (B and G), or Dunnett (I) multiple comparisons test or Mann–Whitney test (D, M, N, O, Q). ANOVA, analysis of variance; CTR, control; Dnm, dynamin; eEPSC, evoked excitatory post-synaptic currents; GABA, Gamma-Aminobutyric Acid; sPSC, spontaneous post-synaptic currents.

Copyright © 2022 by the International Association for the Study of Pain. Unauthorized reproduction of this article is prohibited.

Downloaded from http://journals.lww.com/pain by BhDMf5ePHKav1zEoum1tQfN4a+kJLhEZgbsIHo4XMi0hCywCX1AWnYQp/IlQrHD3i3D0OdRyi7TvSFl4Cf3VC4/OAVpDDa8K2+Ya6H515kE= on 09/29/2023

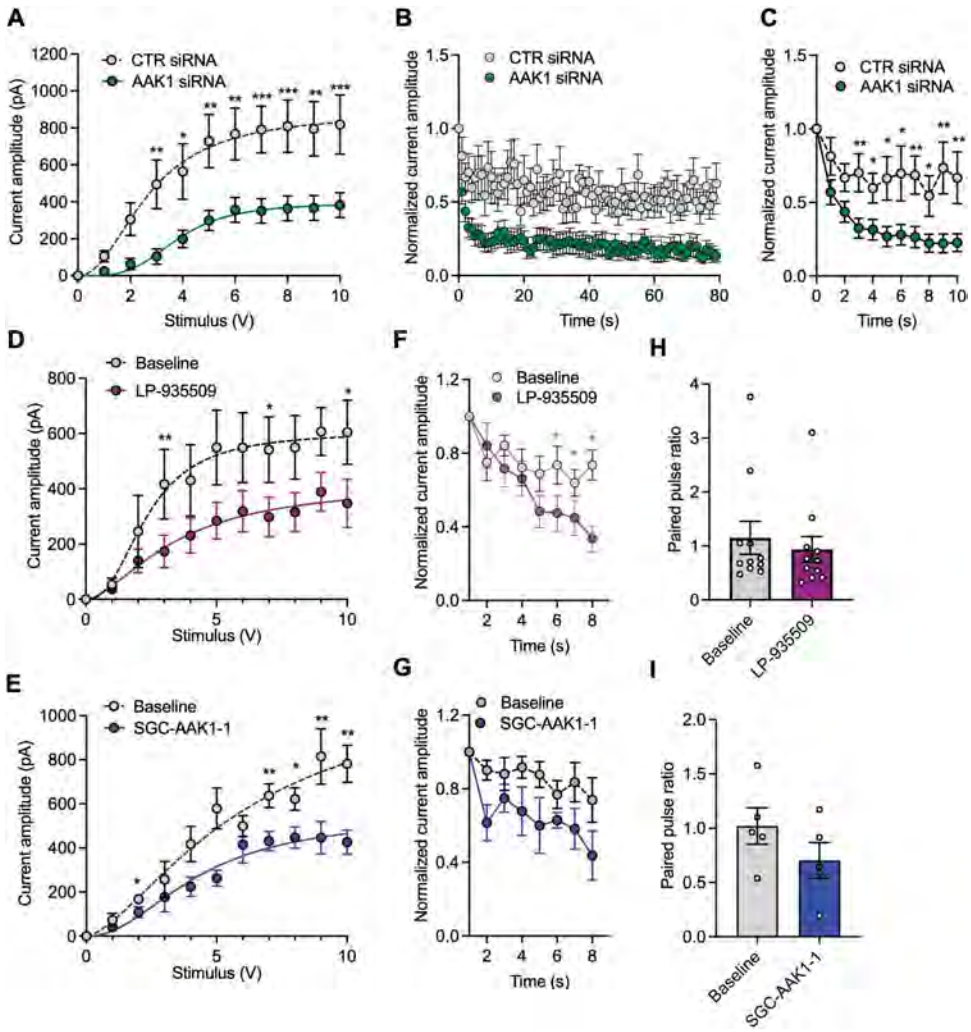

Figure 9. Contributions of AAK1-mediated endocytosis to synaptic transmission in the spinal cord dorsal horn. Input–output responses showing mean eEPSC amplitude of electrically evoked postsynaptic currents recorded from neurons from spinal cord slices of AAK-1 (n = 16) and CTR (n = 10) siRNA-treated mice (A). Normalized current amplitude of eEPSCs over 80 seconds (B) or the first 10 seconds (C) of 1 Hz dorsal root stimulation from lamina II neurons from AAK1 (n = 16) and CTR (n = 8) siRNA-treated mice. Effect of LP-935509 (1 μM, n = 9) (D) and SGC-AAK1-1 (100 nM, n = 4) (E) on eEPSC amplitude in response to increasing electrical stimulus of the dorsal root (1-10 V). Baseline recordings are shown in grey and responses following superfusion AAK1 inhibitor in red. Normalized current amplitude of eEPSCs over 8 seconds of 1 Hz dorsal root stimulation for baseline and after LP-935509 (F) and SGC-AAK1-1 (G) incubation. Paired-pulse ratios of LP-935509-treated (H) and SGC-AAK1-1–treated (I) slices compared with baseline. Mean ± SEM. $^{*}P < 0.05$, $^{**}P < 0.01$, $^{***}P < 0.001$ vs CTR siRNA or baseline. Two-way ANOVA, Sídák multiple comparisons test (A) or Paired Wilcoxon tests (D and G). AAK1, adaptor-associated protein kinase 1; ANOVA, analysis of variance; CTR, control; eEPSC, evoked excitatory post-synaptic currents.

3.8. Dynamin 1 siRNA inhibits spontaneous excitatory but not inhibitory events in the spinal cord

No significant difference in the frequency of spontaneous synaptic events (total sPSC, including sEPSCs and spontaneous inhibitory postsynaptic currents [sIPSCs]) were observed between Dnm1 and CTR siRNA groups (**Figs. 8J and K**), which suggests that the underlying network activity in the dorsal horn remains functional after Dnm1 knockdown. However, when the proportion of excitatory to inhibitory synaptic events was compared by measuring sEPSC frequency in the presence of antagonists of GABA (gabazine) and glycine (strychnine) receptors as a proportion of baseline sPSC frequency, there was a significant reduction in the excitatory component in the Dnm1 siRNA group ($P = 0.019$, Mann–Whitney test) (**Figs. 8L and M**). This change is likely to be the result of a reduction in spontaneous excitatory activity generated by primary afferent neurons, whereas the spontaneous glycinergic and GABAergic events that originate from inhibitory neurons in laminae II to III remain the same, leading to reduced nociceptive signaling.

3.9. Dynamin inhibition reduces the probability of synaptic vesicle release and prevents sustained release from presynaptic primary afferent neurons

To corroborate the findings with Dnm1 siRNA, we investigated the effect of the Dnm inhibitor Dyngo4a on synaptic transmission. Dyngo4a (30 μM) reduced eEPSC amplitude in response to dorsal root stimulation at increasing intensities compared with vehicle (DMSO/ACSF) (**Fig. 8N**). Dyngo4a reduced the sustained neurotransmitter release when afferent inputs were stimulated with a 1 Hz train of impulses (**Figs. 8O and P**). There was a decrease in paired-pulse ratio of eEPSCs in superficial dorsal horn neurons following incubation in Dyngo4a, which suggests that presynaptic release is driving these changes in synaptic activity (**Fig. 8Q**).

Copyright © 2022 by the International Association for the Study of Pain. Unauthorized reproduction of this article is prohibited.

Downloaded from http://journals.lww.com/pain by BhDMf5ePHKav1zEoum1tQfN4a+kJLhEZgbsIHo4XMi0hCywCX1AWnYQp/IlQrHD3i3D0OdRyi7TvSFl4Cf3VC4/OAVpDDa8K2+Ya6H515kE= on 09/29/2023

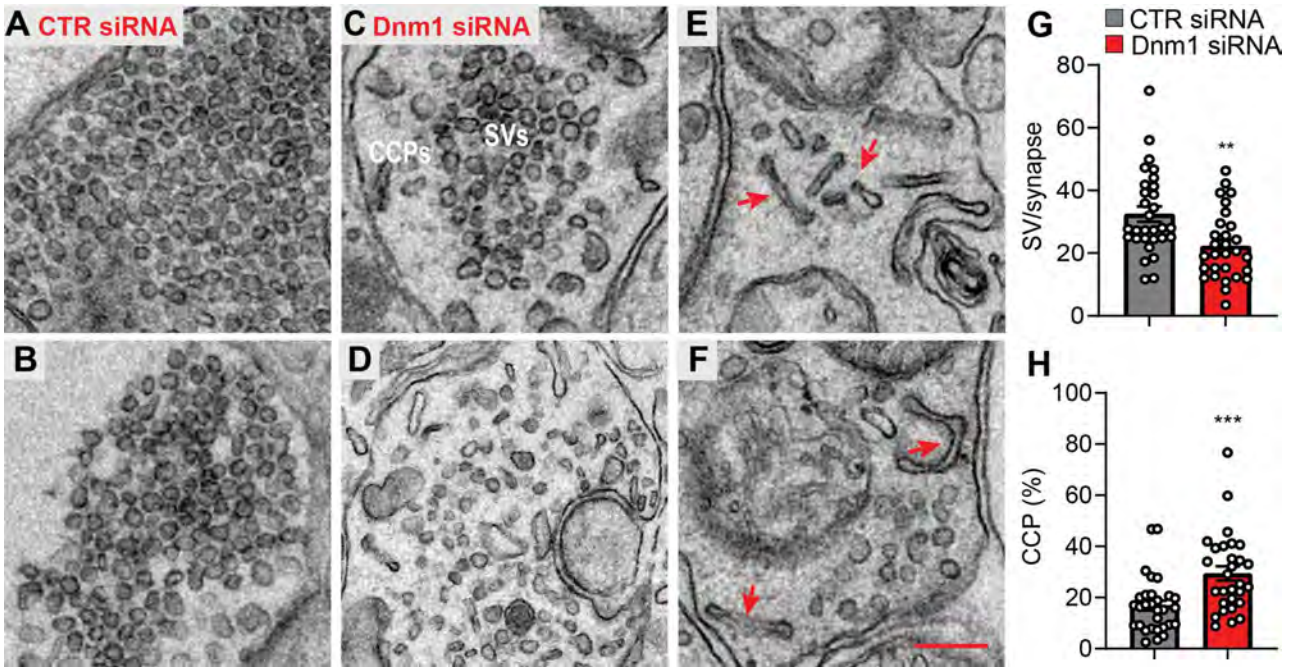

Figure 10. Ultrastructural analysis of spinal cord slices after *Dnm1* knockdown. Duplicate electron micrographs of spinal cord from mice at 2 days after the administration of CTR siRNA showing presynaptic terminals filled with abundant SVs (A and B). Duplicate low-power and high-power electron micrographs of spinal cord from mice at 2 days after the administration of Dnm1 siRNA (C–F). Images of presynaptic terminals reflect the range in the severity of the phenotype from nearly normal (C) to a major accumulation of CCPs with few remaining SVs (D). Red arrows show interconnected CCPs in synapses from Dnm1 siRNA-treated mice. Scale bars, 200 nm. Quantification of SVs in Dnm1 and CTR siRNA-treated neurons expressed as the number per synaptic profile (G). Quantification of CCPs expressed as the percentage of CCPs relative to the total of SVs + CCPs/synapse (Dnm1, n = 212; CTR n = 182 synapses) (H). Mean ± SEM. $^{**}P < 0.01$, $^{***}P < 0.001$ vs CTR siRNA. Parametric unpaired 2-tailed *t* test. CTR, control; Dnm, dynamin; CCP, clathrin-coated pit; SV, synaptic vesicle.

3.10. Adaptor-associated kinase 1 siRNA reduces the probability of synaptic vesicle release and prevents sustained release from presynaptic primary afferent neurons

We administered AAK1 or CTR siRNA to mice (i.t.) and recorded eEPSCs in response to stimulation of the dorsal roots. The threshold voltage required to stimulate an eEPSC was higher in the AAK1 siRNA group, and current amplitudes were higher in the control group at lower stimulus strength (**Fig. 9A**). Adaptor-associated protein kinase 1 siRNA also suppressed sustained neurotransmitter release when afferent inputs were stimulated with a 1 Hz train (**Figs. 9B and C**).

3.11. Adaptor-associated kinase 1 inhibitors reduce the probability of synaptic vesicle release and prevent sustained release from presynaptic primary afferent neurons

The AAK1 inhibitors LP-935509 (1 μM) or SCG-AAK1-1 (100 nM) were bath applied following baseline recordings in the presence of the vehicle. Both compounds reduced eEPSC amplitude in response to dorsal root stimulation at increasing intensities compared with baseline control (**Figs. 9D and E**), but the effects were less significant than data from AAK-1 siRNA–treated animals (**Fig. 9A**). When afferent inputs were stimulated with a 1 Hz train in the presence of these compounds, there was a significant reduction in sustained release in the LP-935509–treated group compared with baseline control (**Fig. 9F**) but not in the SGC-AAK1-1 group (**Fig. 9G**). The train of stimuli were limited to 8 pulses in these experiments to avoid synaptic potentiation between the baseline control and drug treatment recordings. Paired-pulse ratios were not significantly different with either treatment (**Figs. 9H and I**).

Thus, Dnm1 and AAK1 siRNA and inhibitors deplete the readily releasable SV pool and suppress SV release from presynaptic terminals, which disrupts neurotransmission in nociceptive circuits in the spinal cord.

3.12. Dynamin 1 siRNA reduces the number of synaptic vesicles in spinal cord synapses

Transmission electron microscopy was used to examine the effects of knockdown of *Dnm* mRNA on SV recycling in the dorsal horn. A characteristic feature of synapses in mice treated with Dnm1 siRNA was a reduction in the number of SVs and an increase in the proportion of clathrin-coated vesicular profiles when compared with synapses in mice treated with CTR siRNA (**Figs. 10A–H**). Many of the coated profiles in Dnm1 siRNA-treated mice appeared to be interconnected clathrin-coated buds (**Figs. 10E and F**). These results are in line with the effects of Dnm1 deletion on the morphological appearance of synapses.[29]

3.13. Dynamin siRNA attenuates activation of nociceptors

In addition to inhibiting synaptic transmission, endocytosis inhibitors curtail signaling of GPCRs, including protease-activated receptor-2 (PAR_2), in nociceptors and thereby blunt persistent nociception.[20] To examine the role of Dnm in GPCR-evoked nociception, Dnm or CTR siRNA was administered (i.t.) 48 hours before injection of trypsin (10 μL, 80 nM i.pl.; PAR_2 agonist). In mice receiving CTR siRNA, trypsin induced mechanical allodynia after 60 minutes (**Fig. 11A**). Dnm1+2+3 siRNA inhibited trypsin-evoked allodynia. To ascertain whether these effects depend on disruption of trypsin-evoked sensitization of nociceptors, we measured the rheobase (minimal input current to fire action potential) of small diameter DRG neurons by patch-clamp recording. Dorsal root ganglia were preincubated with trypsin (100 nM, 10 minutes),

Copyright © 2022 by the International Association for the Study of Pain. Unauthorized reproduction of this article is prohibited.

Downloaded from http://journals.lww.com/pain by BhDMf5ePHKav1zEoum1tQfN4a+kJLhEZgbsIHo4XMi0hCywCX1AWnYQp/IlQrHD3i3D0OdRyi7TvSFl4Cf3VC4/OAVpDDa8K2+Ya6H515kE= on 09/29/2023

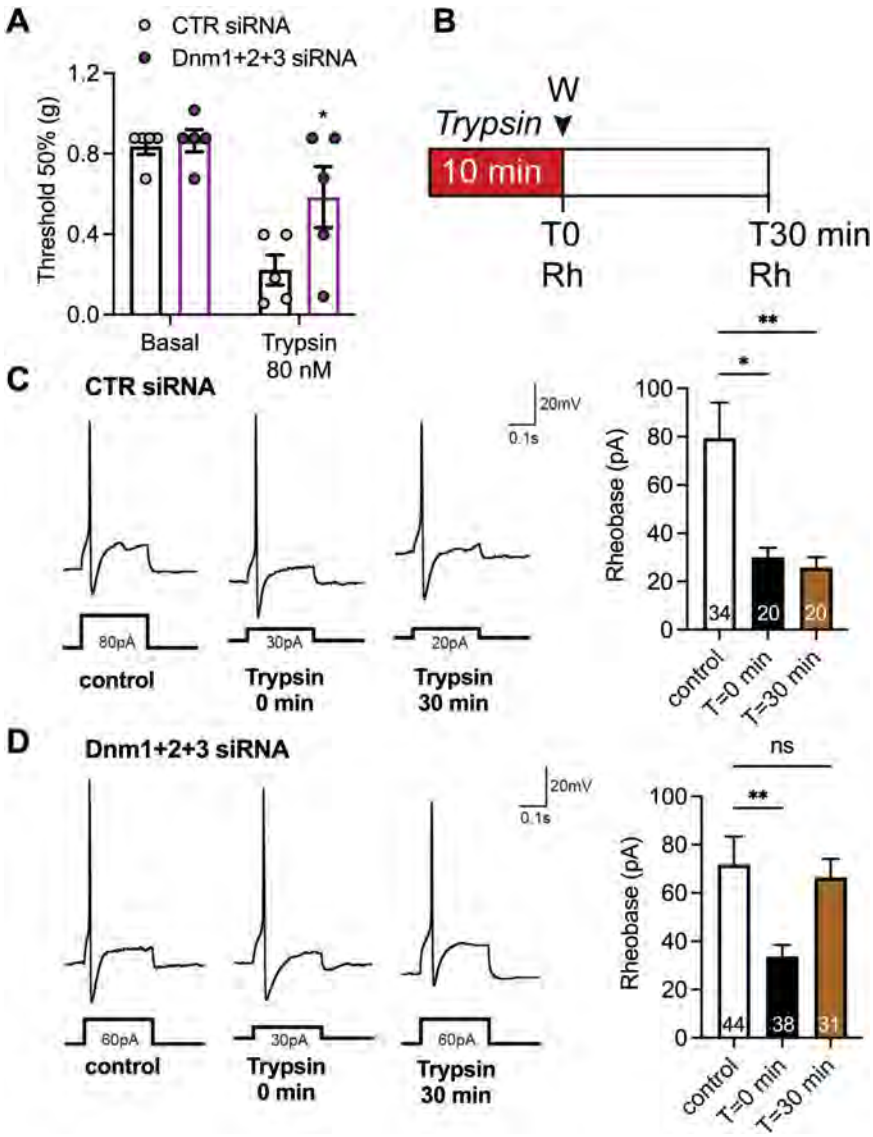

Figure 11. Dnm-mediated sensitization of nociceptors. Effects of trypsin (80 nM, 10 μL, i.pl.) on mechanical allodynia in mice at 2 days after intrathecal injection of Dnm1+2+3 or CTR siRNA (A). Mechanical allodynia was measured at 60 minutes after trypsin, n = 5 mice per group. Experimental timeline for electrophysiology experiments (B). Representative traces of rheobase (Rh) and mean rheobase response of DRG neurons at 2 days after the administration of CTR siRNA (C) or Dnm1+2+3 siRNA (D). DRG neurons were challenged with trypsin and washed. Rheobase was measured at T = 0 and T = 30 minutes following trypsin challenge. Numbers in bars denote neurons measured. Mean ± SEM. $^{*}P < 0.05$, $^{**}P < 0.01$ vs control or CTR siRNA. Two-way ANOVA, Sídák multiple comparisons test (B) or 1-way ANOVA, Dunnett multiple comparisons test (C and D). ANOVA, analysis of variance; CTR, control; Dnm, dynamin; DRG, dorsal root ganglia.

washed, and rheobase was measured 0 or 30 minutes later (**Fig. 11B**). In DRG from CTR siRNA mice, trypsin decreased the rheobase at 0 and 30 minutes (control 79 ± 15 pA; 0 minutes 30 ± 4 pA, $P = 0.002$ vs control; 30 minutes 26 ± 4 pA, $P = 0.001$ vs control, 1-way ANOVA, Dunnett test, **Fig. 11C**). Dnm1+2+3 siRNA did not block the initial effects of trypsin (control 72 ± 12 pA, 0 minutes 34 ± 5 pA, $P = 0.003$ vs control) but prevented the sustained effects of trypsin (30 minutes, 68 ± 8 pA, $P = 0.7$ vs control, **Fig. 11D**). Thus, trypsin causes an immediate and a sustained hyperexcitability of nociceptors; the sustained effect requires PAR_2 endosomal signaling.

4. Discussion

We report a major role for Dnm and AAK1 in synaptic transmission within nociceptive circuits in the dorsal horn of the spinal cord. *Dnm1*, *Dnm3*, and *Aak1* mRNA were expressed in mouse and human DRG, including in peptidergic nociceptors. Intrathecal siRNA or shRNA downregulated *Dnm* and *Aak1* mRNA in DRG neurons and reversed nociception in preclinical models of inflammatory and neuropathic pain. Dnm, clathrin, and AAK1 inhibitors replicated the effects of siRNA, supporting selectivity. Dnm1 and AAK1 knockdown and inhibition blunted electrically evoked synaptic transmission between primary sensory neurons and dorsal horn neurons. These changes were coincident with the accumulation of SVs within presynaptic nerve terminals. The results support the hypothesis that Dnm and AAK1 mediate the endocytosis of SVs in nociceptive circuits and thereby sustain nociceptive transmission (**Fig. 12**). Disruption of this process ameliorates pain.

The conclusion that Dnm mediates synaptic transmission in nociceptive spinal circuits is supported by the expression of

Copyright © 2022 by the International Association for the Study of Pain. Unauthorized reproduction of this article is prohibited.

Downloaded from http://journals.lww.com/pain by BhDMf5ePHKav1zEoum1tQfN4a+kJLhEZgbsIHo4XMi0hCywCX1AWnYQp/IlQrHD3i3D0OdRyi7TvSFl4Cf3VC4/OAVpDDa8K2+Ya6H515kE= on 09/29/2023

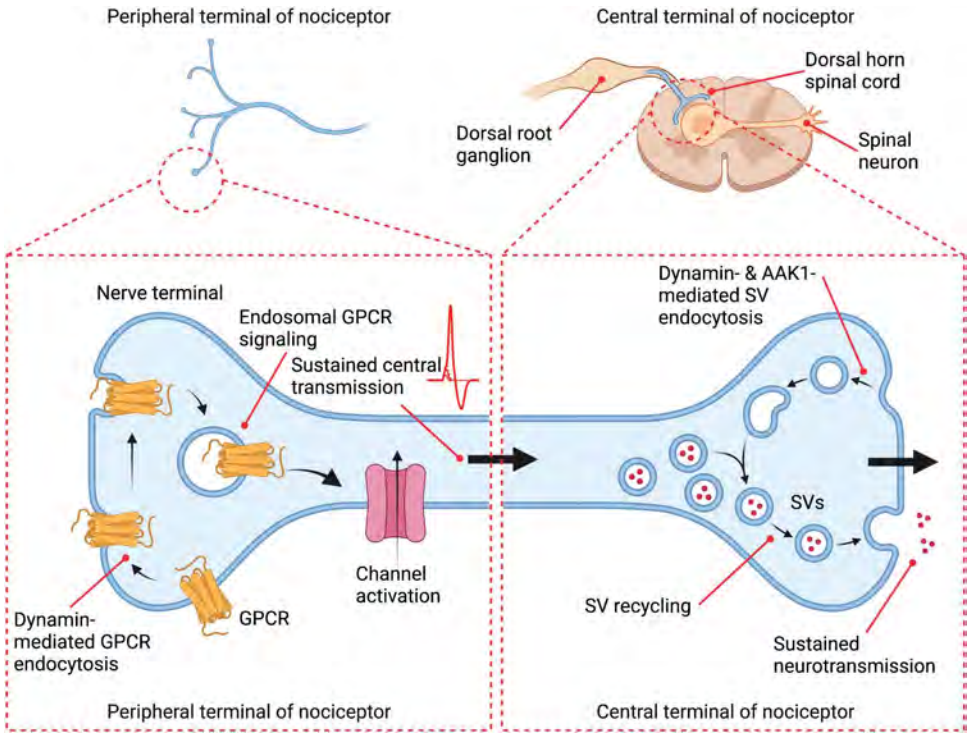

Figure 12. Hypothesized contributions of endocytosis in nociceptors to pain transmission. The role of endocytosis for GPCR signaling in the periphery and SV recycling centrally are depicted. At the peripheral terminals of nociceptors, clathrin-mediated and Dnm-mediated endocytosis of GPCRs, such as PAR_2, enables sustained endosomal signaling that is necessary for the activation of ion channels and ongoing central transmission. At the central terminals of nociceptors, Dnm-mediated and AAK1-mediated endocytosis of SVs replenishes the releasable pool of SVs that is necessary for sustained synaptic transmission. AAK1, adaptor-associated protein kinase 1; Dnm, dynamin; GPCR, G protein–coupled receptor; PAR_2, protease-activated receptor-2; SV, synaptic vesicle.

Dnm1 and *Dnm3* mRNA in DRG and spinal cord neurons. *Dnm1* and *Dnm3* mRNA were also expressed in human DRG neurons, providing translational relevance. Single-nucleus RNA sequencing in mouse and human DRG tissue identified *Dnm1* and *Dnm3* in all sensory neuron subtypes.[25,31] *Dnm1* and *Dnm3* mRNA were coexpressed with CGRP in peptidergic nociceptors. Peptidergic nociceptors are sensitized during pain and release neuropeptides that mediate pain transmission in the spinal cord.[2,16] However, Dnm isoforms were expressed by most primary sensory neurons and by satellite glial cells and thus participate in multiple processes. Intrathecal Dnm siRNA or shRNA downregulated *Dnm* mRNA in DRG neurons and reversed nociception in mice with persistent inflammatory and neuropathic pain. Isoform-selective knockdown had antinociceptive actions, suggesting redundancy. Differences in the magnitude of the antinociceptive actions of Dnm siRNA in models of inflammatory and neuropathic pain could be attributable to different mechanisms of nociceptive transmission; further studies are required to investigate this possibility. Simultaneous knockdown of all Dnm isoforms was more efficacious and sustained than knockdown of individual isoforms and also normalized behavioral changes in a model of neuropathic pain. Dnm1 shRNA had large antinociceptive actions that were fully sustained for at least 7 days in mouse models of inflammatory and neuropathic pain. A limitation of this study is that knockdown was assessed at the level of mRNA rather than protein. Future studies will investigate the correlation between the antinociceptive actions of shRNA and the degree of protein knockdown over time.

Electrophysiological studies support the conclusion that clathrin and Dnm sustain synaptic transmission in nociceptive circuits by mediating the endocytosis and replenishing the releasable pool of SVs of presynaptic terminals. Dnm1 knockdown and inhibition suppressed eEPSCs in superficial dorsal horn neurons and depressed the paired-pulse ratio of eEPSCs, which implicates a presynaptic mechanism caused by a reduction in the probability of neurotransmitter release from primary afferent neurons. The finding that Dnm1 siRNA disrupted the maintenance of eEPSCs during repetitive stimulation of dorsal roots implicates Dnm in sustained synaptic transmission in nociceptive circuits. The imaging of SV recycling with a styryl dye revealed that Dnm1 siRNA disrupts SV recycling, which would be secondary to disruption of SV endocytosis. Ultrastructural studies showed that *Dnm1* mRNA knockdown reduced the number of SVs and caused an accumulation of CCPs in presynaptic nerve terminals of dorsal horn synapses. These morphological changes are consistent with the role of Dnm in SV endocytosis and are in accordance with reported changes in SVs and CCPs in neurons cultured from *Dnm1* and *Dnm1+3* knockout mice.[14,29] Thus, behavioral, electrophysiological, and morphological studies support the conclusion that Dnm is necessary for endocytosis of SVs in presynaptic nerve terminals in nociceptive circuits in the dorsal horn. This process enables SV recycling, which is required for ongoing neurotransmission that underlies nociceptive signaling within the spinal cord.

Adaptor-associated kinase 1 participates in clathrin-mediated endocytosis[9,32] and is a target for treatment of neuropathic pain.[21] Anatomical, behavioral, and electrophysiological studies support the hypothesis that AAK1, like Dnm, mediates endocytosis of SVs in presynaptic neurons of nociceptive circuits in the dorsal horn and is thus necessary

Copyright © 2022 by the International Association for the Study of Pain. Unauthorized reproduction of this article is prohibited.

Downloaded from http://journals.lww.com/pain by BhDMf5ePHKav1zEoum1tQfN4a+kJLhEZgbsIHo4XMi0hCywCX1AWnYQp/IlQrHD3i3D0OdRyi7TvSFl4Cf3VC4/OAVpDDa8K2+Ya6H515kE= on 09/29/2023

for ongoing synaptic transmission of nociceptive signals. *Aak1* mRNA was prominently expressed by primary sensory neurons of DRG, including peptidergic nociceptors, and in neurons of the spinal cord. In line with these results, the α-subunit isoform of the AP2 complex, which is activated by the AAK1 phosphorylation, is preferentially expressed within CGRP+ve nociceptors.[28] Single-nucleus RNA sequencing studies demonstrated the expression of *Aak1* in all DRG sensory neuron subtypes of mouse and human.[25,31] Intrathecal AAK1 siRNA downregulated the *Aak1* mRNA expression in DRG neurons, reversed mechanical and thermal nociception in mice with inflammatory and neuropathic pain, and suppressed electrically evoked synaptic currents and neurotransmitter release from presynaptic afferent neurons in the spinal cord. Adaptor-associated kinase 1 shRNA had large and long-lasting antinociceptive actions. The observations that 2 distinct inhibitors of AAK1 replicated the effects of AAK1 siRNA by reversing nociceptive behavior and reducing the probability of SV release supports selectivity. These results accord with genetic and pharmacological studies that revealed a major role of AAK1 in neuropathic pain through global deletion or systemic antagonism of AAK1.[21] The current research identifies an anatomical site and mechanism of the pronociceptive actions of AAK1. The results support the hypothesis that AAK1 mediates SV endocytosis in presynaptic terminals of nociceptors in the dorsal horn of the spinal cord, which underlies SV recycling and sustained synaptic transmission of pain.

The observation that Dnm and AAK1 siRNA preferentially knockdown *Dnm* and *Aak1* mRNA in DRG, rather than the spinal cord, supports the hypothesis that Dnm and AAk1 mediate pain transmission by regulating presynaptic neurotransmission in the dorsal horn. The lack of discernible knockdown in the spinal cord may be attributable to poor tissue penetration and targeting of neurons in deeper laminae that are the main site of *Dnm* and *Aak1* mRNA expression. The current studies do not preclude an important role for endocytosis in spinal neurons, which deserves further investigation.

In addition to mediating endocytosis of SVs in presynaptic nerve terminals, Dnm and AAK1 may contribute to nociception by mediating endosomal signaling of pronociceptive GPCRs in primary afferent neurons and spinal neurons (**Fig. 12**). Clathrin and Dnm mediate endocytosis of PAR_2 by nociceptors and endocytosis of substance P and CGRP receptors by spinal neurons.[18,20,40] Endosomal signaling of these GPCRs activates kinases that mediate sustained activation of neurons, which is necessary for nociception. Accordingly, inhibitors of Dnm and lipid-conjugated or nanoparticle-encapsulated antagonists that target GPCRs in endosomes have sustained antinociceptive effects.[11,18,20,22,23,40] In this study, we observed that trypsin evokes mechanical allodynia in mice, which is known to be mediated by PAR_2.[20] Trypsin caused an immediate and a sustained increase in excitability of nociceptors. Intrathecal Dnm1+2+3 siRNA inhibited mechanical allodynia and sustained hyperexcitability of nociceptors. These results are in agreement with the effects of Dyngo4a on trypsin-evoked nociception.[20] These findings support the hypothesis that Dnm also contributes to nociception by mediating the endosomal signaling of PAR_2 (and other GPCRs) that underlies neuronal hyperexcitability and pain.

Is endocytosis in nociceptors a potential target for the treatment of pain? An advantage is that targeting endocytosis may surmount the redundancy of pain mechanisms. A plethora of mediators initiate and maintain pain, which might explain the lack of efficacy of some highly selective inhibitors. A disadvantage of targeting Dnm and AAK1 is their widespread distribution and multiple roles beyond pain. We enhanced selectivity by administering siRNA, shRNA, and antagonists into the intrathecal space, which preferentially targeted DRG neurons. Notably, Dnm and AAk1 siRNA, shRNA, and inhibitors did not affect normal motor functions in mice with inflammatory or neuropathic pain, assessed by measuring withdrawal responses of the contralateral paw. These treatments also did not affect multiple behaviors in sham-operated mice, monitored using a behavioral spectrometer. Moreover, these treatments preferentially blocked electrically evoked synaptic transmission, with no effects on basal synaptic transmission. The systemic administration of Dnm inhibitors could disrupt essential cellular processes that depend upon endocytosis. Indeed, deletion of Dnm 1 and Dnm3 is lethal in mice.[14,29] However, global deletion of *Aak1* and systemic administration of the AAK1 antagonist LP935509 inhibits nociception in mice and rats without effects on normal motor function.[21] The AAK1 antagonist LX9211 was safe and well tolerated in healthy subjects in phase 1 clinical trials.[4] The AAK1 inhibitor SGC-AAK1-1 shows improved selectivity over the LX9211[1]; to our knowledge, its therapeutic potential has not been evaluated beyond the current study. Another limitation is that we assessed nociception and did not evaluate the unpleasant emotional aspects of pain, which requires assessment of affective responses to painful stimuli.[12]

This study defined the contribution of Dnm and AAK1 to SV endocytosis in presynaptic terminals of nociceptive circuits in the spinal cord, which is necessary for sustained transmission of nociceptive signals. It also confirmed the contribution of endocytosis to GPCR-mediated sensitization of nociceptors. Disruption of endocytosis and consequent inhibition of nociceptor sensitization and nociceptive neurotransmission offers a nonopioid approach to treat pain.

Conflict of interest statement

N. W. Bunnett is a founding scientist of Endosome Therapeutics Inc. Research in N. W. Bunnett laboratory is partly supported by Takeda Pharmaceuticals Inc. The remaining authors have no conflicts of interest to declare.

Acknowledgments

(1) The authors thank Daniel P. Poole, Nicholas A. Veldhuis and Phillip Robinson for valuable discussion. (2) The authors thank the NYU DART Microscopy Laboratory for consultation and assistance with electron microscopy; this Core is partially supported by NYU Cancer Center Support Grant NIH/NCI P30CA016087. Figure 10E was made using BioRender. (3) Supported by grants from the National Institutes of Health (NS102722, DE026806, DK118971, DE029951, N. W. Bunnett, B. L. Schmidt; RF1 NS113881, S. Davidson), Department of Defense (W81XWH1810431, W81XWH-22-1-0239, Expansion Award, N. W. Bunnett, B. L. Schmidt), National Health and Medical Research Council (NHMRC APP1125877, APP1139586, W. L. Imlach) and Australian Research Council (ARC DP190102854, W. L. Imlach).
Data availability: Contact the corresponding author to obtain original data.

Appendix A. Supplemental digital content

Supplemental digital content associated with this article can be found online at http://links.lww.com/PAIN/B750.

Copyright © 2022 by the International Association for the Study of Pain. Unauthorized reproduction of this article is prohibited.

Article history:
Received 23 June 2022
Received in revised form 25 October 2022
Accepted 8 November 2022
Available online 14 November 2022

Downloaded from http://journals.lww.com/pain by BhDMf5ePHKav1zEoum1tQfN4a+kJLhEZgbsIHo4XMi0hCywCX1AWnYQp/IlQrHD3i3D0OdRyi7TvSFl4Cf3VC4/OAVpDDa8K2+Ya6H515kE= on 09/29/2023

References

[1] Agajanian MJ, Walker MP, Axtman AD, Ruela-de-Sousa RR, Serafin DS, Rabinowitz AD, Graham DM, Ryan MB, Tamir T, Nakamichi Y, Gammons MV, Bennett JM, Counago RM, Drewry DH, Elkins JM, Gileadi C, Gileadi O, Godoi PH, Kapadia N, Muller S, Santiago AS, Sorrell FJ, Wells CI, Fedorov O, Willson TM, Zuercher WJ, Major MB. WNT activates the AAK1 kinase to promote clathrin-mediated endocytosis of LRP6 and establish a negative feedback loop. Cell Rep 2019;26:79–93.e8.

[2] Basbaum AI, Bautista DM, Scherrer G, Julius D. Cellular and molecular mechanisms of pain. Cell 2009;139:267–84.

[3] Brodkin J, Frank D, Grippo R, Hausfater M, Gulinello M, Achterholt N, Gutzen C. Validation and implementation of a novel high-throughput behavioral phenotyping instrument for mice. J Neurosci Methods 2014; 224:48–57.

[4] Bundrant L, Hunt TL, Banks P, Gopinathan S, Boehm KA, Kassler-Taub K, Tyle P, Wilson A, Warner C, Wason S. Results of two phase 1, randomized, double-blind, placebo-controlled, studies (ascending single-dose and multiple-dose studies) to determine the safety, tolerability, and pharmacokinetics of orally administered LX9211 in healthy participants. Clin Ther 2021;43:1029–50.

[5] Castro J, Harrington AM, Lieu T, Garcia-Caraballo S, Maddern J, Schober G, O'Donnell T, Grundy L, Lumsden AL, Miller P, Ghetti A, Steinhoff MS, Poole DP, Dong X, Chang L, Bunnett NW, Brierley SM. Activation of pruritogenic TGR5, MrgprA3, and MrgprC11 on colon-innervating afferents induces visceral hypersensitivity. JCI Insight 2019; 4:131712.

[6] Chanaday NL, Cousin MA, Milosevic I, Watanabe S, Morgan JR. The synaptic vesicle cycle revisited: new insights into the modes and mechanisms. J Neurosci 2019;39:8209–16.

[7] Chaplan SR, Bach FW, Pogrel JW, Chung JM, Yaksh TL. Quantitative assessment of tactile allodynia in the rat paw. J Neurosci Methods 1994; 53:55–63.

[8] Cheng CF, Cheng JK, Chen CY, Rau RH, Chang YC, Tsaur ML. Nerve growth factor-induced synapse-like structures in contralateral sensory ganglia contribute to chronic mirror-image pain. PAIN 2015;156: 2295–309.

[9] Conner SD, Schmid SL. Identification of an adaptor-associated kinase, AAK1, as a regulator of clathrin-mediated endocytosis. J Cell Biol 2002; 156:921–9.

[10] Cousin MA, Robinson PJ. Mechanisms of synaptic vesicle recycling illuminated by fluorescent dyes. J Neurochem 2002;73:2227–39.

[11] De Logu F, Nassini R, Hegron A, Landini L, Jensen DD, Latorre R, Ding J, Marini M, Souza Monteiro de Araujo D, Ramirez-Garcia P, Whittaker M, Retamal J, Titiz M, Innocenti A, Davis TP, Veldhuis N, Schmidt BL, Bunnett NW, Geppetti P. Schwann cell endosome CGRP signals elicit periorbital mechanical allodynia in mice. Nat Commun 2022;13:646.

[12] Deuis JR, Dvorakova LS, Vetter I. Methods used to evaluate pain behaviors in rodents. Front Mol Neurosci 2017;10:284.

[13] Dixon WJ. Efficient analysis of experimental observations. Annu Rev Pharmacol Toxicol 1980;20:441–62.

[14] Ferguson SM, Brasnjo G, Hayashi M, Wolfel M, Collesi C, Giovedi S, Raimondi A, Gong LW, Ariel P, Paradise S, O'Toole E, Flavell R, Cremona O, Miesenbock G, Ryan TA, De Camilli P. A selective activity-dependent requirement for dynamin 1 in synaptic vesicle endocytosis. Science 2007; 316:570–4.

[15] Ferguson SM, De Camilli P. Dynamin, a membrane-remodelling GTPase. Nat Rev Mol Cell Biol 2012;13:75–88.

[16] Finnerup NB, Kuner R, Jensen TS. Neuropathic pain: from mechanisms to treatment. Physiol Rev 2021;101:259–301.

[17] Hargreaves K, Dubner R, Brown F, Flores C, Joris J. A new and sensitive method for measuring thermal nociception in cutaneous hyperalgesia. PAIN 1988;32:77–88.

[18] Jensen DD, Lieu T, Halls ML, Veldhuis NA, Imlach WL, Mai QN, Poole DP, Quach T, Aurelio L, Conner J, Herenbrink CK, Barlow N, Simpson JS, Scanlon MJ, Graham B, McCluskey A, Robinson PJ, Escriou V, Nassini R, Materazzi S, Geppetti P, Hicks GA, Christie MJ, Porter CJH, Canals M, Bunnett NW. Neurokinin 1 receptor signaling in endosomes mediates sustained nociception and is a viable therapeutic target for prolonged pain relief. Sci Transl Med 2017;9:eaal3447.

[19] Jimenez-Vargas NN, Gong J, Wisdom MJ, Jensen DD, Latorre R, Hegron A, Teng S, DiCello JJ, Rajasekhar P, Veldhuis NA, Carbone SE, Yu Y, Lopez-Lopez C, Jaramillo-Polanco J, Canals M, Reed DE, Lomax AE, Schmidt BL, Leong KW, Vanner SJ, Halls ML, Bunnett NW, Poole DP. Endosomal signaling of delta opioid receptors is an endogenous mechanism and therapeutic target for relief from inflammatory pain. Proc Natl Acad Sci U S A 2020;117:15281–92.

[20] Jimenez-Vargas NN, Pattison LA, Zhao P, Lieu T, Latorre R, Jensen DD, Castro J, Aurelio L, Le GT, Flynn B, Herenbrink CK, Yeatman HR, Edgington-Mitchell L, Porter CJH, Halls ML, Canals M, Veldhuis NA, Poole DP, McLean P, Hicks GA, Scheff N, Chen E, Bhattacharya A, Schmidt BL, Brierley SM, Vanner SJ, Bunnett NW. Protease-activated receptor-2 in endosomes signals persistent pain of irritable bowel syndrome. Proc Natl Acad Sci U S A 2018;115:E7438–47.

[21] Kostich W, Hamman BD, Li YW, Naidu S, Dandapani K, Feng J, Easton A, Bourin C, Baker K, Allen J, Savelieva K, Louis JV, Dokania M, Elavazhagan S, Vattikundala P, Sharma V, Das ML, Shankar G, Kumar A, Holenarsipur VK, Gulianello M, Molski T, Brown JM, Lewis M, Huang Y, Lu Y, Pieschl R, O'Malley K, Lippy J, Nouraldeen A, Lanthorn TH, Ye G, Wilson A, Balakrishnan A, Denton R, Grace JE, Lentz KA, Santone KS, Bi Y, Main A, Swaffield J, Carson K, Mandlekar S, Vikramadithyan RK, Nara SJ, Dzierba C, Bronson J, Macor JE, Zaczek R, Westphal R, Kiss L, Bristow L, Conway CM, Zambrowicz B, Albright CF. Inhibition of AAK1 kinase as a novel therapeutic approach to treat neuropathic pain. J Pharmacol Exp Ther 2016;358:371–86.

[22] Latorre R, Hegron A, Peach CJ, Teng S, Tonello R, Retamal JS, Klein-Cloud R, Bok D, Jensen DD, Gottesman-Katz L, Rientjes J, Veldhuis NA, Poole DP, Bunnett NW, Schmidt BL, Pothoulakis CH, Rankin C, Xie Y, Koon HW, Bunnett NW. Mice expressing fluorescent PAR2 reveal that endocytosis mediates colonic inflammation and pain. Proc Natl Acad Sci U S A 2022;119:e2112059119.

[23] Latorre R, Ramirez-Garcia PD, Hegron A, Grace JL, Retamal JS, Shenoy P, Tran M, Aurelio L, Flynn B, Poole DP, Klein-Cloud R, Jensen DD, Davis TP, Schmidt BL, Quinn JF, Whittaker MR, Veldhuis NA, Bunnett NW. Sustained endosomal release of a neurokinin-1 receptor antagonist from nanostars provides long-lasting relief of chronic pain. Biomaterials 2022; 285:121536.

[24] Lu W, Ma H, Sheng ZH, Mochida S. Dynamin and activity regulate synaptic vesicle recycling in sympathetic neurons. J Biol Chem 2009;284: 1930–7.

[25] Nguyen MQ, von Buchholtz LJ, Reker AN, Ryba NJ, Davidson S. Single-nucleus transcriptomic analysis of human dorsal root ganglion neurons. Elife 2021;10:e71752.

[26] Pertin M, Gosselin RD, Decosterd I. The spared nerve injury model of neuropathic pain. Methods Mol Biol 2012;851:205–12.

[27] Pfaffl MW. A new mathematical model for relative quantification in real-time RT-PCR. Nucleic Acids Res 2001;29:e45.

[28] Powell R, Young VA, Pryce KD, Sheehan GD, Bonsu K, Ahmed A, Bhattacharjee A. Inhibiting endocytosis in CGRP(+) nociceptors attenuates inflammatory pain-like behavior. Nat Commun 2021;12:5812.

[29] Raimondi A, Ferguson SM, Lou X, Armbruster M, Paradise S, Giovedi S, Messa M, Kono N, Takasaki J, Cappello V, O'Toole E, Ryan TA, De Camilli P. Overlapping role of dynamin isoforms in synaptic vesicle endocytosis. Neuron 2011;70:1100–14.

[30] Ramirez-Garcia PD, Retamal JS, Shenoy P, Imlach W, Sykes M, Truong N, Constandil L, Pelissier T, Nowell CJ, Khor SY, Layani LM, Lumb C, Poole DP, Lieu T, Stewart GD, Mai QN, Jensen DD, Latorre R, Scheff NN, Schmidt BL, Quinn JF, Whittaker MR, Veldhuis NA, Davis TP, Bunnett NW. A pH-responsive nanoparticle targets the neurokinin 1 receptor in endosomes to prevent chronic pain. Nat Nanotechnol 2019; 14:1150–9.

[31] Renthal W, Tochitsky I, Yang L, Cheng YC, Li E, Kawaguchi R, Geschwind DH, Woolf CJ. Transcriptional reprogramming of distinct peripheral sensory neuron subtypes after axonal injury. Neuron 2020; 108:128–44.e9.

[32] Ricotta D, Conner SD, Schmid SL, von Figura K, Honing S. Phosphorylation of the AP2 mu subunit by AAK1 mediates high affinity binding to membrane protein sorting signals. J Cell Biol 2002;156:791–5.

[33] Robertson MJ, Deane FM, Robinson PJ, McCluskey A. Synthesis of dynole 34-2, dynole 2-24 and Dyngo 4a for investigating dynamin GTPase. Nat Protoc 2014;9:851–70.

[34] Robertson MJ, Deane FM, Stahlschmidt W, von Kleist L, Haucke V, Robinson PJ, McCluskey A. Synthesis of the Pitstop family of clathrin inhibitors. Nat Protoc 2014;9:1592–606.

[35] Schlegel A, Largeau C, Bigey P, Bessodes M, Lebozec K, Scherman D, Escriou V. Anionic polymers for decreased toxicity and enhanced in vivo delivery of siRNA complexed with cationic liposomes. J Controlled Release 2011;152:393–401.

Copyright © 2022 by the International Association for the Study of Pain. Unauthorized reproduction of this article is prohibited.

[36] Shipton EA, Shipton EE, Shipton AJ. A Review of the opioid epidemic: what do we do about it? Pain Ther 2018;7:23–36.
[37] Sudhof TC. The synaptic vesicle cycle. Annu Rev Neurosci 2004;27:509–47.
[38] Tonello R, Fusi C, Materazzi S, Marone IM, De Logu F, Benemei S, Goncalves MC, Coppi E, Castro-Junior CJ, Gomez MV, Geppetti P, Ferreira J, Nassini R. The peptide Phα1β, from spider venom, acts as a TRPA1 channel antagonist with antinociceptive effects in mice. Br J Pharmacol 2017;174:57–69.
[39] Valtcheva MV, Copits BA, Davidson S, Sheahan TD, Pullen MY, McCall JG, Dikranian K, Gereau RW. Surgical extraction of human dorsal root ganglia from organ donors and preparation of primary sensory neuron cultures. Nat Protoc 2016;11:1877–88.
[40] Yarwood RE, Imlach WL, Lieu T, Veldhuis NA, Jensen DD, Klein Herenbrink C, Aurelio L, Cai Z, Christie MJ, Poole DP, Porter CJH, McLean P, Hicks GA, Geppetti P, Halls ML, Canals M, Bunnett NW. Endosomal signaling of the receptor for calcitonin gene-related peptide mediates pain transmission. Proc Natl Acad Sci U S A 2017;114:12309–14.

Downloaded from http://journals.lww.com/pain by BhDMf5ePHKav1zEoum1tQfN4a+kJLhEZgbsIHo4XMi0hCywCX1AWnYQp/IlQrHD3i3D0OdRyi7TvSFl4Cf3VC4/OAVpDDa8K2+Ya6H515kE= on 09/29/2023

Copyright © 2022 by the International Association for the Study of Pain. Unauthorized reproduction of this article is prohibited.

american physiological society
PHYSIOLOGICAL REVIEWS
REVIEW ARTICLE

PROTEASE-ACTIVATED RECEPTORS IN HEALTH AND DISEASE

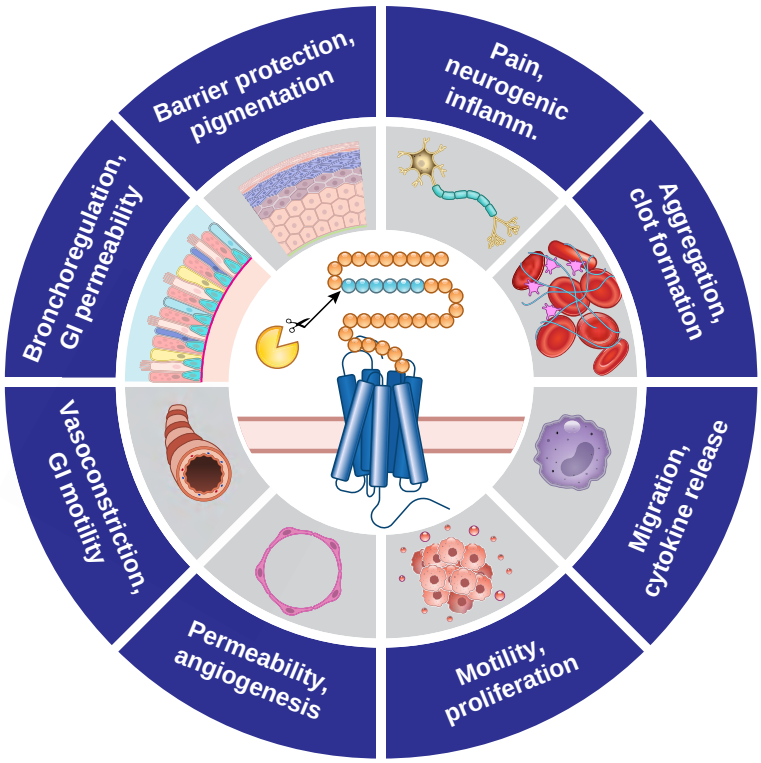

AUTHORS

Chloe J. Peach, Laura E. Edgington-Mitchell, Nigel W. Bunnett, Brian L. Schmidt

CORRESPONDENCE

nwb2@nyu.edu

KEY WORDS

antagonists; disease; homeostasis; proteases; receptors

CLINICAL HIGHLIGHTS

1) PARs are widely expressed on platelets, epithelial cells, endothelial cells, smooth muscle cells, innate and adaptive immune cells, neurons, and cancer cells and contribute to the physiology and pathology of every organ system.
2) PAR activation by proteases, including coagulation factors, position the receptor as a key target for major causes of death including coronary artery disease, cerebrovascular disease, cancer, and, more recently, SARS-CoV-2 infection.
3) Drugs, including peptidic, small molecules, and antibodies, have been developed to target PAR_1, PAR_2, and PAR_4. Vorapaxar, a PAR_1 antagonist, has been tested for the treatment of acute coronary syndrome and the prevention of atherothrombotic events; vorapaxar has been approved for specific indications.
4) Given their central role in highly prevalent diseases including coronary artery disease and cerebrovascular disease, PARs will continue to be attractive targets for drug development; however, much of our knowledge regarding PAR physiology is based on genetically engineered mouse models. There are species differences with PAR function, therefore the translation of laboratory findings to clinical management will require an increase in the number of studies involving humans.

PEACH ET AL., 2023, *Physiol Rev* 103: 717–785
July 28, 2022; Copyright © 2023 the American Physiological Society.
https://doi.org/10.1152/physrev.00044.2021

Downloaded from journals.physiology.org/journal/physrev at New York Univ (216.165.095.084) on September 28, 2023.

american physiological society
PHYSIOLOGICAL REVIEWS
Physiol Rev 103: 717–785, 2023
First published July 28, 2022; doi:10.1152/physrev.00044.2021
REVIEW ARTICLE

PROTEASE-ACTIVATED RECEPTORS IN HEALTH AND DISEASE

Chloe J. Peach,[1,2] Laura E. Edgington-Mitchell,[3,4] Nigel W. Bunnett,[1,2] and Brian L. Schmidt[1,4]

[1]Department of Molecular Pathobiology, College of Dentistry, New York University, New York, New York; [2]Department of Neuroscience and Physiology and Neuroscience Institute, Grossman School of Medicine, New York University, New York, New York; [3]Department of Biochemistry and Pharmacology, Bio21 Molecular Science and Biotechnology Institute, The University of Melbourne, Parkville, Victoria, Australia; and [4]Bluestone Center for Clinical Research, Department of Oral and Maxillofacial Surgery, New York University College of Dentistry, New York, New York

Abstract

Proteases are signaling molecules that specifically control cellular functions by cleaving protease-activated receptors (PARs). The four known PARs are members of the large family of G protein-coupled receptors. These transmembrane receptors control most physiological and pathological processes and are the target of a large proportion of therapeutic drugs. Signaling proteases include enzymes from the circulation; from immune, inflammatory epithelial, and cancer cells; as well as from commensal and pathogenic bacteria. Advances in our understanding of the structure and function of PARs provide insights into how diverse proteases activate these receptors to regulate physiological and pathological processes in most tissues and organ systems. The realization that proteases and PARs are key mediators of disease, coupled with advances in understanding the atomic level structure of PARs and their mechanisms of signaling in subcellular microdomains, has spurred the development of antagonists, some of which have advanced to the clinic. Herein we review the discovery, structure, and function of this receptor system, highlight the contribution of PARs to homeostatic control, and discuss the potential of PAR antagonists for the treatment of major diseases.

antagonists; disease; homeostasis; proteases; receptors

1. INTRODUCTION 717
2. PAR DISCOVERY AND GENE AND PROTEIN... 719
3. CELL TYPE EXPRESSION OF PARS 723
4. ACTIVATION AND SIGNALING OF PARS IN... 729
5. PARS IN PHYSIOLOGY AND PATHOLOGY 739
6. DRUG DEVELOPMENT TARGETING PARS 757
7. CONCLUSIONS 760

CLINICAL HIGHLIGHTS

1) PARs are widely expressed on platelets, epithelial cells, endothelial cells, smooth muscle cells, innate and adaptive immune cells, neurons, and cancer cells and contribute to the physiology and pathology of every organ system.
2) PAR activation by proteases, including coagulation factors, position the receptor as a key target for major causes of death including coronary artery disease, cerebrovascular disease, cancer, and, more recently, SARS-CoV-2 infection.
3) Drugs, including peptidic, small molecules, and antibodies, have been developed to target PAR_1, PAR_2, and PAR_4. Vorapaxar, a PAR_1 antagonist, has been tested for the treatment of acute coronary syndrome and the prevention of atherothrombotic events; vorapaxar has been approved for specific indications.
4) Given their central role in highly prevalent diseases including coronary artery disease and cerebrovascular disease, PARs will continue to be attractive targets for drug development; however, much of our knowledge regarding PAR physiology is based on genetically engineered mouse models. There are species differences with PAR function, therefore the translation of laboratory findings to clinical management will require an increase in the number of studies involving humans.

1. INTRODUCTION

Proteases are critically important regulators of homeostasis and mediators of disease. The coordinated cascade of proteolytic events that lead to the formation of a blood clot illustrates the importance of proteases in homeostatic control. The requirement of proteases for the entry of viruses into cells exemplifies their contributions to diseases of global relevance. In line with their important regulatory roles, the activity of proteases is tightly controlled; most proteases are formed as inactive zymogens, and activity is further regulated by endogenous inhibitors or by intracellular and extracellular acidity. Herein, we review another aspect of the regulatory role of proteases: their ability to function as hormones or paracrine substances that regulate cells by cleaving and activating protease-activated receptors (PARs). PARs

0031-9333/23 Copyright © 2023 the **American Physiological Society.**

Downloaded from journals.physiology.org/journal/physrev at New York Univ (216.165.095.084) on September 28, 2023.

are a subfamily of four G protein-coupled receptors (GPCRs), the largest family of cell surface receptors and the target of one-third of therapeutic drugs. All PARs share the main features of GPCRs, with seven transmembrane (TM) domains, three extracellular loop (ECL) and three intracellular loop (ICL) domains, an extracellular NH_2-terminal domain, and an intracellular COOH-terminal domain. However, proteases activate PARs by a unique mechanism. Although some proteases can dock with their receptors, binding per se does not lead to signaling. Instead, proteolysis either reveals a tethered ligand domain that binds to and activates the cleaved PAR or results in a conformational change that initiates signaling (**FIGURE 1**). Synthetic peptides that mimic the tethered ligand sequence, referred to herein as activating peptides, can directly activate some PARs without the need for proteolysis. Activating peptides are useful tools for studying PAR activation and are a starting point for the development of selective ligands.

The prototypical PAR, PAR_1, was discovered as a mediator of thrombin-induced aggregation of platelets and revealed a major role for PARs in hemostasis in the circulatory system. PARs are now known to mediate the hormone-like actions of diverse proteases, including enzymes from the circulation and those secreted by inflammatory, immune, epithelial, and cancer cells. Proteases from commensal and

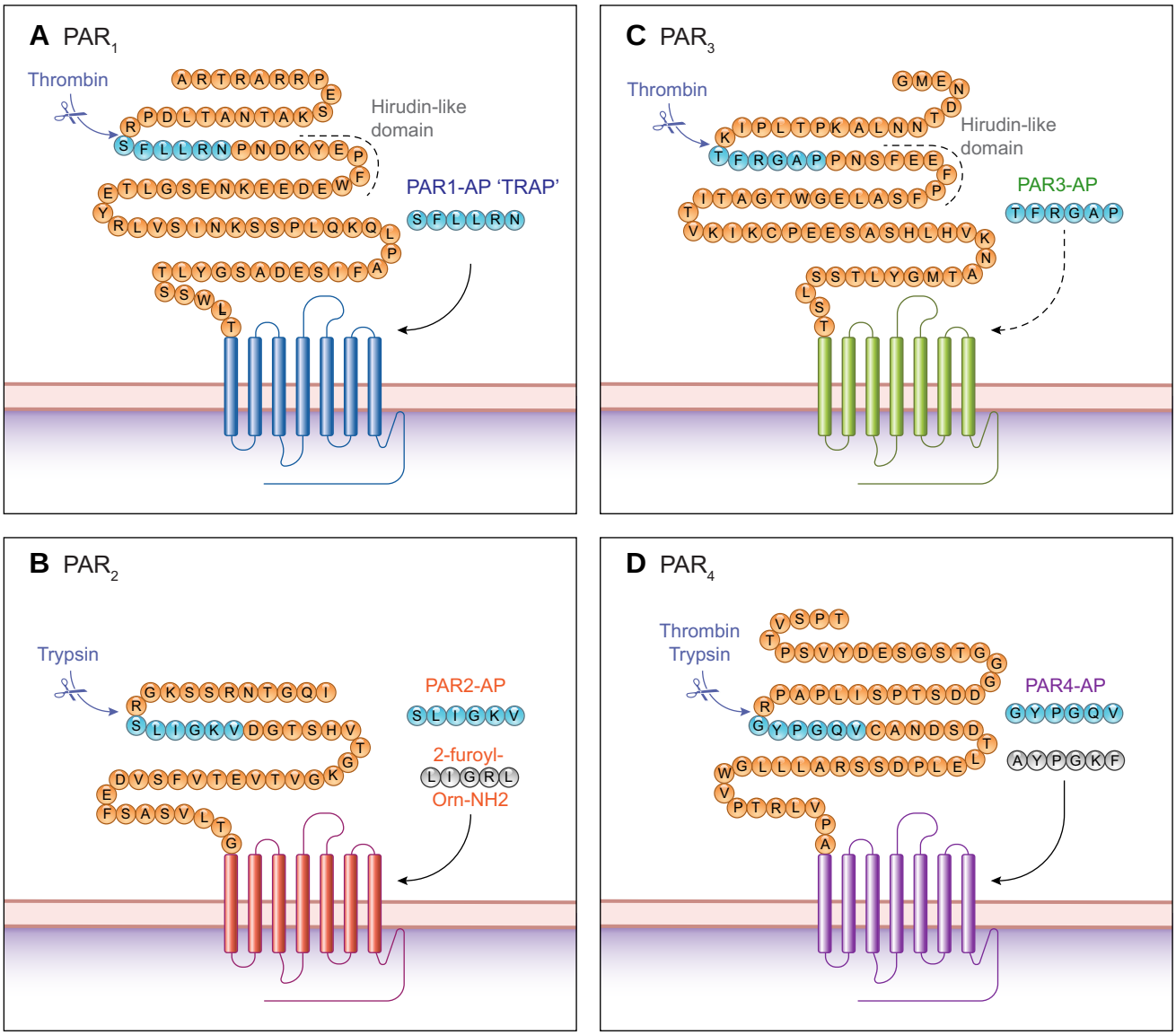

FIGURE 1. Canonical protease-activated receptor (PAR) cleavage sites and activation mechanisms. *A–D*: NH_2-terminal domains of PAR_{1-4} highlighting the canonical cleavage site for thrombin or trypsin in the human receptors. Cleavage can reveal a tethered ligand (blue) from which soluble activating peptides (APs) were derived; PAR_3-AP is unable to activate PAR_3. APs have been modified to generate selective and potent activating peptides (e.g., for PAR_2 and PAR_4; gray). TRAP, thrombin receptor-activating peptide.

Downloaded from journals.physiology.org/journal/physrev at New York Univ (216.165.095.084) on September 28, 2023.

pathogenic microorganisms can also activate PARs. Proteases and PARs are known to control most tissues and organ systems and to regulate important homeostatic and disease processes. This review summarizes the discovery, structure, and function of PARs in the major cell types and organ systems. The review then highlights the mechanisms by which activated PARs engage the intracellular signaling machinery to control physiological and pathological processes and discusses how new knowledge about the structure and function of PARs has informed the development of selective antagonists, some of which have advanced to the clinic.

2. PAR DISCOVERY AND GENE AND PROTEIN STRUCTURE

The key features of the gene and protein structure of PARs are summarized in **TABLE 1**.

2.1. Discovery and Gene Structure

2.1.1. PAR_1.

The concept that proteases can act as hormonal regulators of cellular functions is illustrated by the ability of thrombin to aggregate human platelets by cleaving PAR_1. The search for the platelet thrombin receptor was motivated by a desire to develop treatments for vascular diseases and coagulopathies, in which thrombin was implicated. Schmidt hypothesized in 1872 that a protease would mediate the conversion of fibrinogen to fibrin; thrombin was ultimately identified as the responsible protease (1). Thrombin also promotes platelet activation and aggregation. In 1990, two groups reported that microinjection of poly(A)$^+$ mRNA from two thrombin-responsive cell lines, hamster lung fibroblasts (2) and human umbilical vein endothelial cells (HUVECs; Ref. 3), into *Xenopus* oocytes led to thrombin responsiveness. Platelets were not used as the source of mRNA because they contain little nucleic acid. An expression cloning

Table 1. ***Summary of the key properties of PARs, highlighting the gene and protein structure, mechanisms of activation, and sites of expression of human receptors***

	PAR_1	PAR_2	PAR_3	PAR_4
Amino acids*	425	397	374	385
Gene name	*F2r*	*F2rl1*	*F2rl2*	*F2rl3*
Gene structure	2 exons	2 exons	2 exons	2 exons
Chromosome	5q13.3	5q13.3	5q13.3	19p13.11
Highest transcript expression	Spleen, gall bladder, skin, endometrium, and lung	Colon, duodenum, stomach, small intestine, and gall bladder	Fat, stomach, thyroid, colon, and thyroid	Fat, stomach, thyroid, colon, and thyroid
Canonical cleavage site	Arg^{41}/Ser^{42}	Arg^{36}/Ser^{37}	Lys^{38}/Thr^{39}	Arg^{47}/Gly^{48}
Exposed canonical NH_2-terminal domain	$S^{42}FLLRN$	$S^{37}LIGKV$	$T^{39}FRGAP$	$G^{48}YPGQV$
Canonical activating				
Peptides	SFLLRN ($hPAR_1$)	SLIGKV ($hPAR_2$)	TFRGAP ($hPAR_3$) inactive	GYPGQV ($hPAR_4$)
Analogs		2-furoyl-LIGRLO-NH_2		AYPGKF
Activating proteases (canonical and biased)	Thrombin APC Plasmin MMP1 Proteinase-3 Elastase FVIIa FXa	Trypsin Tryptase Elastase Proteinase-3 Cathepsin G Cathepsin S FXa KLK-4 Chymase Legumain	Thrombin APC	Thrombin Trypsin Plasmin Cathepsin G Cathepsin S KLK-14

APC, activated protein C; MMP, matrix metalloprotease; PAR, protease-activated receptor. *Including the signal sequence, obtained from UniProt.

Downloaded from journals.physiology.org/journal/physrev at New York Univ (216.165.095.084) on September 28, 2023.

approach in which cDNA from human erythroleukemic cell lines (HEL; Dami) was injected into *Xenopus* oocytes led to cloning of the thrombin receptor (4). *F2r*, the official HUGO Gene Nomenclature Committee gene symbol for PAR_1, contains two exons separated by a large intron. The second exon contains most of the coding sequence, including the critical thrombin cleavage site. *F2r* exhibits ubiquitous expression with the highest expression levels in the spleen, gall bladder, skin, endometrium, and lung.

2.1.2. PAR_2.

Different PAR variants were hypothesized given the expansive role of serine proteases in physiological processes. In 1994, low-stringency screening of a mouse genomic library using probes corresponding to TM2 and TM6 of the bovine substance K receptor revealed a gene for which the predicted GPCR was homologous to PAR_1 and thus designated PAR_2. PAR_2 is not a second thrombin receptor; α-thrombin did not activate PAR_2 in an oocyte system, but trypsin did. The trypsin cleavage site on PAR_2 was comparable to the thrombin cleavage site on PAR_1. The HUGO symbol for the PAR_2 gene is *F2rl1*. *F2rl1* encodes a 397 amino acid protein. PAR_2 and PAR_1 share ~30% identity, but some key differences explain different mechanisms of activation and signaling. The extracellular NH_2 terminus of PAR_2 is similar to that of PAR_1 at the cleavage site but shorter and lacking the acidic residues responsible for thrombin affinity. The intracellular COOH terminus of PAR_1 and PAR_2 is also dissimilar, which likely accounts for different signaling properties (5). The genes for PAR_1 and PAR_2 share a common locus, leading to the proposal that they arose from a gene-duplication event (6). The PAR_2 gene spans over 13 kb. The two exons are separated by an intron of ~10 kb. *F2rl1* is expressed widely in the colon, duodenum, stomach, small intestine, and gall bladder.

2.1.3. PAR_3.

To explain the cellular effects of thrombin not mediated by PAR_1, investigators sought to discover other thrombin receptors. The second thrombin receptor, PAR_3, was discovered in a study that characterized the phenotype of mice in which the gene for PAR_1 was deleted (6). Differential genomic blotting using cDNA probes that encompassed the PAR_1 and PAR_2 genes was used to identify the human PAR_3 gene. The query did not reveal an associated gene with PAR_1-specific probes; however, the PAR_2-specific probes induced a band that was identified as PAR_3. Confirmation came when the protein that represented the band produced phosphatidylinositol 4,5-bisphosphate (PIP_2) hydrolysis when activated by thrombin (6). The PAR_3 gene *F2rl2* is almost identical to PAR_1 and PAR_2. *F2rl2* contains two exons. Like PAR_1 and PAR_2, the second exon contains the protease cleavage site. PAR_3 transcripts are present in both platelets and endothelial cells. PAR_3 shows biased expression in the fat, stomach, thyroid, colon, and thyroid.

2.1.4. PAR_4.

Human PAR_4 was cloned in 1998 in an expressed sequence tag (EST) database. The full-length cDNA was then isolated from a lymphoma cell cDNA library (7). The amino acid sequences for PAR_1, PAR_2, and PAR_3 were used to query available databases. An EST sequence matched the TM4 domain of the PARs. Translation of the identified sequence identified PAR_4 as a GPCR of 385 amino acids with 33% identity with PAR_1, PAR_2, and PAR_3. However, the extracellular NH_2 terminus and intracellular COOH terminus of PAR_4 do not resemble the homologous regions of the remaining PARs. The PAR_4 gene *F2rl3* does not exhibit the same characteristics common to the genes of the other PAR types. The gene is not on the same chromosome as the other PARs, and the intron is smaller. PAR_4 likely resulted from a combination of gene duplication and translocation events (8). The PAR_4 gene is expressed in most tissues, with the highest expression level in fat, stomach, thyroid, colon, and thyroid.

2.1.5. Interspecies gene homology.

Like other GPCRs, the PAR genes are clustered (9, 10). The PAR_1, PAR_2, and PAR_3 genes are on chromosome 5q13.3 for humans and chromosome 13 for mice. The PAR_4 gene is on chromosome 19p13.11 in humans and chromosome 8 in mice. PAR gene evolution has been characterized in the context of phylogenetics, chromosomal location, selective pressure, and functional divergence (11). Phylogenetic tree analysis suggests that $PARs_{1-4}$ originate from four invertebrates. A maximum likelihood tree of the PAR family shows that PAR_1 and PAR_2 cluster into one subfamily while PAR_3 and PAR_4 cluster into another. The genes for PAR_1 show evidence of environmental adaptation, while PAR_2, PAR_3, and PAR_4 are highly conserved in vertebrates.

2.2. Protein Structure

PARs are classified within the family of class A rhodopsin-like GPCRs. A brief summary of the structures shared by all PARs will expedite structural comparisons between PAR types. All four PARs comprise seven TM helices, an extracellular NH_2-terminal domain, three ICL

Downloaded from journals.physiology.org/journal/physrev at New York Univ (216.165.095.084) on September 28, 2023.

and three ECL domains, and an intracellular COOH terminus (**FIGURES 1** and **2**). Posttranslational modifications of PARs include phosphorylation, ubiquitination, palmitoylation, and *N*-glycosylation. GPCR stability is bolstered by a disulfide bond across cysteines between TM3 and ECL3. *N*-glycosylation occurs at the following sites: the mature NH_2 termini of all four PARs, ECL2 of PAR_1 and PAR_2, and the ECL3 of PAR_3.

2.2.1. PAR_1.

Human and murine PAR_1 possess a canonical thrombin cleavage site at Arg^{41}/Ser^{42} (4). Cleavage reveals the tethered ligand SFLLRN as the new NH_2 terminus of the human receptor (4). Adjacent to this canonical cleavage site, PAR_1 contains a hirudin-like domain that mediates high-affinity thrombin binding (7). Mutation of this domain reduces the potency of thrombin to induce Ca^{2+} signaling (12). Other proteases that cleave the canonical site include factor Xa (FXa; Ref. 13) and FVIIa (14; **FIGURE 2*A***). Advances in protein engineering and crystallography enabled elucidation of a 2.2 Å resolution structure of PAR_1 bound to its antagonist vorapaxar (sect. 6.1). PAR_1 was stabilized to permit crystallization by insertion of T4 lysozyme into ICL3, mutation of *N*-linked glycosylation sites in ECL2, and removal of the NH_2-terminal exodomain. Key structural features included a conserved disulphide bond between helix III and ECL2 and two antiparallel β-strands, which are formed by residues situated toward the NH_2 terminus of Cys254 loop outward toward $Phe^{6.44}$ (numbered according to the Ballesteros-Weinstein scheme). $Phe^{6.44}$ is a position that is conserved across class A (i.e., rhodopsin-like) GPCRs (15). PAR_1 differs from other class A GPCRs with regard to its transmission of the signal from the extracellular side to the cytoplasmic domains that interact with G

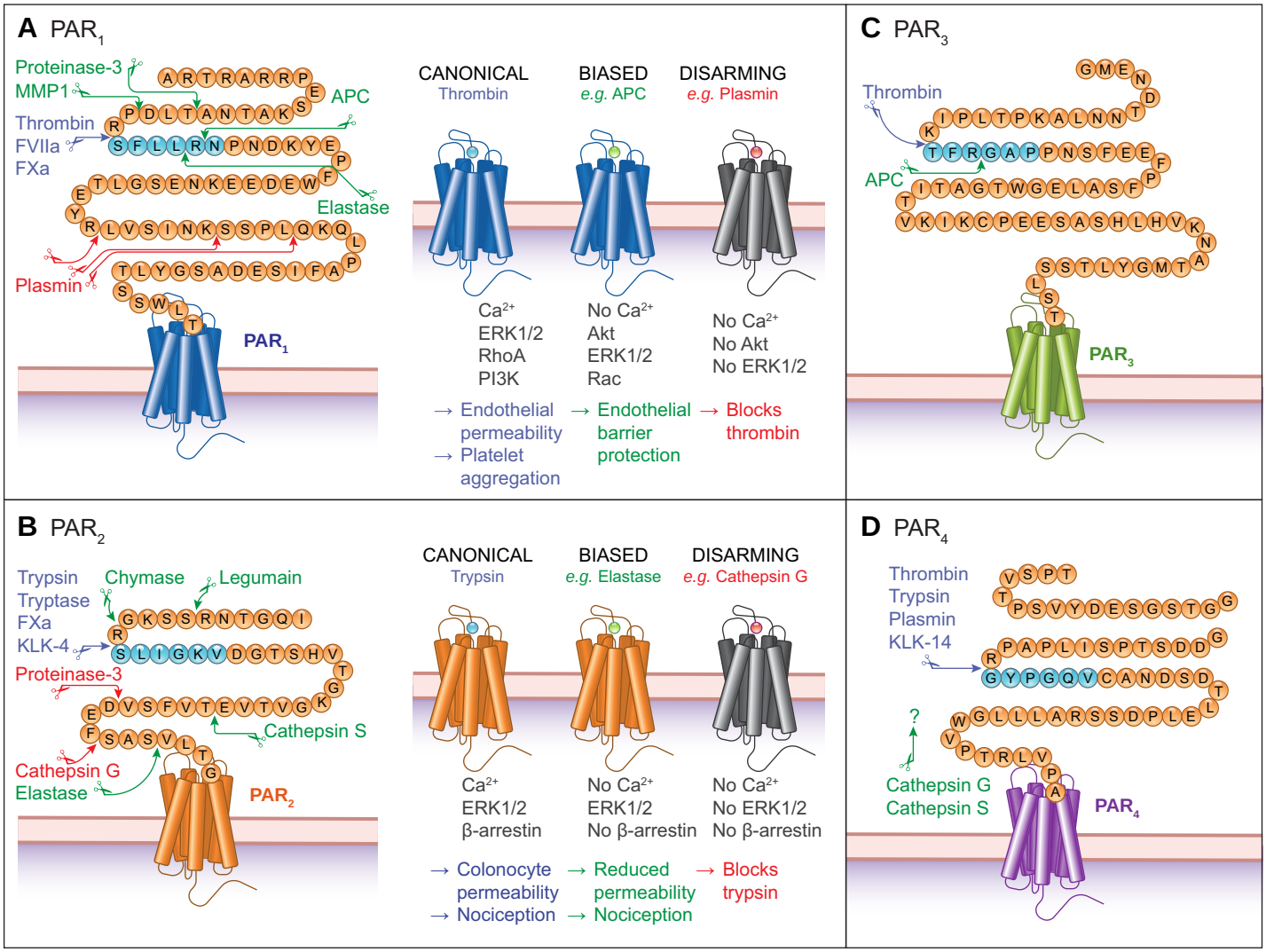

FIGURE 2. Cleavage by noncanonical proteases. *A–D*: NH_2-terminal domains of protease-activated receptors 1 to 4 (PAR_{1-4}) showing cleavage sites for proteases that activate PARs by canonical (blue) or biased (green) mechanisms or those that disarm the receptor (red). Residues are shown for the human receptors without the predicted signal sequence. APC, activated protein C; MMP, matrix metalloproteases.

Downloaded from journals.physiology.org/journal/physrev at New York Univ (216.165.095.084) on September 28, 2023.

proteins, as well as associated structural rearrangements (16, 17). Interactions between TM5, TM6, and TM7, and conserved motifs in the former two TMs, facilitate structural rearrangement upon receptor activation in class A GPCRs. However, the interactions between TMs 5, 6, and 7 and the conserved motifs in TM6 and TM7 are different in the PARs. In this regard, the β_2 adrenergic receptor (β_2-AR) serves as a good comparator to the PARs. The TM6 motif is FxxCWxP, and the TM7 motif is NPxxY, whereby the amino acid identity of X is not critical. Based on differences in the active and inactive states of β_2-AR, Phe$^{6.44}$, along with Ile$^{3.40}$ and Pro$^{5.50}$, is important for G-protein binding and undergo rearrangement. PAR_1 also contains Phe$^{6.44}$. However, the interaction between Phe322$^{6.44}$, Ile190$^{3.40}$, and Pro282$^{5.50}$ in PAR_1 during the switch between the active and inactive state is different from the interaction between the associated amino acid residues within β_2-AR. For many GPCRs, the Trp residue within the motif FxxCW$^{6.48}$xP operates as a molecular switch following receptor activation; however, all PARs are characterized by Phe$^{6.48}$. For PAR_1, the DP$^{7.50}$xxY in the above-referenced TM7 motif (which is NP$^{7.50}$xxY in other class A GPCRs) mediates sodium sensitivity.

The crystal structure of PAR_1 was consistent with the hypothesis that thrombin cleavage exposes a tethered ligand that interacts superficially with the heptahelical bundle, rather than deep within the TM core (18). Support for superficial activation was provided by mutagenesis experiments. The substitution of the tethered ligand binding region of ECL2 (Asn259 to Ala268) on human PAR_1 with the associated *Xenopus* ECL2 sequences increased basal activity by 10-fold (19).

2.2.2. PAR_2.

PAR_2 was discovered as a receptor for trypsin (5, 20, 21). Trypsin cleaves human PAR_2 at Arg^{36}/Ser^{37} to reveal the tethered ligand SLIGKV. Trypsin cleaves mouse PAR_2 at Arg^{38}/Ser^{39}, exposing the tethered ligand SLIGRL (5). The PAR_2 canonical site (**FIGURE 2*B***) is also cleaved by tryptase (22, 23), FXa (24), KLK-14 (25), KLK-4 (26), and KLK-5 (27).

Crystal structures of PAR_2 in complex with two antagonists and a blocking antibody were reported in 2017 (28). For thermostabilization, nine mutations were introduced into PAR_2. Crystallization was optimized by replacing residues 1–54 in the NH_2 terminus with T4 lysozyme, replacing residues 270–275 on ICL3 with cytochrome b_{562}RIL, mutating Asn222 to Gln, and truncating the COOH terminus after Lys377. The crystal structure of PAR_2 revealed similarities and differences with PAR_1. The ECL2 of PAR_2 fills the top half of the binding pocket, similar to the PAR_1 structure (29). On PAR_2, His227^{ECL2} and Tyr156$^{3.33}$ form a hydrogen bond; this intermolecular interaction is not present on PAR_1.

The crystal structures for PAR_1 and PAR_2 provide a possible explanation for the selectivity of the antagonist vorapaxar for PAR_1 and the antagonist AZ8838 for PAR_2. Vorapaxar does not bind PAR_2 because of the interaction between TM5, TM6, and TM7. Inward movement of TM5 and TM6 leads to steric clashes between vorapaxar and Tyr242$^{5.38}$, Phe243$^{5.39}$, His310$^{6.58}$, and Tyr311$^{6.59}$; therefore, the vorapaxar binding pocket on PAR_2 is eliminated. With regard to the selectivity of AZ8838 for PAR_2, the hydroxyl group of AZ8838 makes a hydrogen bond to a side chain on His135$^{2.64}$. While His135$^{2.64}$ is present on PAR_3 and PAR_4, it is not present on PAR_1, and the corresponding amino acid is Tyr162$^{2.64}$. If His135$^{2.64}$ is replaced with Tyr, AZ8838 no longer inhibits PAR_2. The binding site for AZ8838 is buried in the crystal structure, which leads to slow binding kinetics. AZ8838 inhibition, as measured with Ca^{2+} conductance and β-arrestin recruitment, requires 1 hour for complete inhibition. The crystal structure of PAR_2 also provided information regarding receptor activation. For all four PARs, the residue equivalent to Asp228^{ECL2} in PAR_2 is critical to activation.

The final crystal structure of PAR_2 to be characterized was PAR_2 bound to a monoclonal antibody, MAB3949. The antibody binds the following extracellular PAR_2 residues: 59–63 from the NH_2 terminus, 220 and 232–234 from ECL2, and 315–319 from TM6 and ECL3. Residues 57–62 on the NH_2 terminus are important to the PAR_2-binding epitope. MAB3949 antagonizes PAR_2 activation by trypsin or SLIGRL as measured by an increase in intracellular Ca^{2+}.

2.2.3. PAR_3.

The canonical thrombin cleavage site of human PAR_3 is Lys^{38}/Thr^{39} (30). Similarly to PAR_1, this is followed by a hirudin-like domain. There are questions regarding the signaling capacity of PAR_3. In oocytes expressing PAR_3, thrombin, FXa, trypsin, elastase, and chymotrypsin evoke Ca^{2+} signaling (30). Thrombin cleavage reveals the NH_2-terminal sequence of TFRGAP (**FIGURE 2*C***). However, peptides that mimic this NH_2-terminal sequence fail to initiate any signaling response via PAR_3.

2.2.4. PAR_4.

PAR_4 is the most structurally divergent of the PARs. PAR_4 is considered the "low-affinity" thrombin receptor. Thrombin and trypsin cleave human PAR_4 at Arg^{47}/Gly^{48} to reveal the tethered ligand GYPGQV (7, 8) (**FIGURE 2*D***). PAR_4 lacks a hirudin-like thrombin-binding domain, instead it contains an anionic cluster (DDED) that

Downloaded from journals.physiology.org/journal/physrev at New York Univ (216.165.095.084) on September 28, 2023.

interacts with thrombin to facilitate cleavage (31). The lack of the hirudin site explains the low potency for thrombin activation of PAR_4 (4, 7, 30). PAR_1 and PAR_4 act together to mediate platelet responses to a range of thrombin concentrations. Whereas low-thrombin concentrations lead to PAR_1-mediated platelet activation, high-thrombin concentrations maximally activate platelets through PAR_4 (32). The NH_2 terminus and COOH terminus share little with the corresponding regions of the other PARs. PAR_4 shares only three amino acids (CHD) with the common sequence (ITTCHDV) present in PAR_1, PAR_2, and PAR_3 in ECL2, the region that binds the tethered ligand (7). ECL2 is key to the activity of PAR_4. A series of Asp residues within ECL2 mediate the interaction and activation of platelets. Following cleavage, the tethered ligand that consists of the sequence GYPGQV binds ECL2. PAR_4 does not have the high-affinity binding domain for thrombin that is present in PAR_1 and PAR_3. PAR_4 lacks the hirudin-like binding domain present in PAR_1 and PAR_3; however, a series of anionic residues including Asp57, Asp59, Glu62, and Asp65 increase the K_m of α-thrombin fourfold and impede thrombin dissociation (33).

Less is known regarding the structure of PAR_3 and PAR_4. The crystal structures of fragments of murine PAR_3 and PAR_4 reveal information regarding cleavage by thrombin (34). Thrombin is characterized by an active site and two exosites. Binding at exosite I orients the substrate toward the active site. Thrombin Trp^{60d} acts like a swinging gate and permits diffusion of the substrate to the active site. Upon binding of PAR_3 to exosite I, the 60-loop on thrombin rotates 3.8 Å upward, a movement that allows Trp^{60d} to rotate 180°. This open gate makes the active site accessible.

A further key finding from the crystal structures of PAR_3 and PAR_4 was that cleaved PAR_3 and intact PAR_4 do not overlap when bound to thrombin, a finding that suggests that a ternary complex is structurally feasible. Thus cleaved PAR_3 can be bound to the thrombin exosite I and still allow for thrombin/PAR_4 binding. In this manner, PAR_3 can act as an allosteric modulator to promote cleavage of PAR_4 (34). Exosite I on thrombin plays a critical role in the allosteric regulation of the active site. This role is best exemplified by hirudin, a potent natural anticoagulant found in leech saliva. When the COOH-terminal tail of hirudin is bound to exosite I, the active site of thrombin is accessible (35). Hirudin binds thrombin at both exosite I and the active site and prevents activation of fibrinogen. PAR_1 has a hirudin-like region that is rich in aromatic and acidic residues (DKYEPF). PAR_1 residues Tyr52, Glu53, and Phe55, which are similar to Phe56, Glu57, and Ile59 of hirudin, facilitate the interaction with thrombin and bind its anion-binding exosite. In the case of cleaved PAR_1, the hirudin-like domain remains bound to exosite I of thrombin. In humans, PAR_1 and PAR_4 can form heterodimers. Cleaved PAR_1 facilitates the association between platelets and thrombin while leaving the active site of thrombin free to bind PAR_4. In this manner, PAR_1 enhances the cleavage of PAR_4 by thrombin. The allosteric role of PAR_1 in mouse platelets, which lack PAR_1, is taken up by PAR_3. Cleaved PAR_3 binds exosite I of thrombin, similarly to hirudin (36). Mouse PAR_3 enhances cleavage of PAR_4 by opening the active site with the shift in 60-loop and flip of Trp^{60d} described above (8, 37). With PAR_3 bound to the exosite I of thrombin, diffusion of PAR_4 to the active site is enhanced; this configuration thus favors hydrolysis. PAR_3 has a short cytoplasmic domain, which could also limit its involvement in signaling.

2.3. Summary

PARs are a family of G protein-coupled receptors. Common elements of all four PARs include seven TM helices, an extracellular NH_2-terminal domain, three ICL and three ECL domains, and an intracellular COOH terminus. The location of NH_2-terminal domain cleavage and the remaining peptide fragment determines subsequent cellular signaling and physiological activity. PAR_2 differs from the other three PARs by lacking an extracellular NH_2-terminal domain that is cleaved by thrombin. The crystal structures of PAR_1 and PAR_2 have been revealed with the use of antagonists, monoclonal antibodies, mutagenesis, and domain removal. Less is known about the structure of PAR_3 and PAR_4. PAR_4 is an outlier with regard to the structure of the NH_2 terminus and COOH terminus; it also lacks the hirudin-like binding domain of PAR_1 and PAR_3. PAR_1 and PAR_3 enhance binding and cleavage of PAR_4.

3. CELL TYPE EXPRESSION OF PARS

One challenge in reporting the cellular expression of PARs is concern over the specificity of GPCR antibodies (38). Evidence of expression of PARs should thus include analysis of transcript, as well as functional responses (e.g., Ca^{2+} imaging) to selective agonists and antagonists. Another approach to localize PARs with high specificity has been to study knockin mice expressing PARs fused to a fluorescent protein. With the use of this approach, PAR_2-GFP has been detected in intestinal epithelial cells and a subpopulation of primary sensory neurons of dorsal root ganglia with high specificity and sensitivity (39). **TABLE 1** and **FIGURE 3** summarize the distribution of PARs in different cells, tissues, and organs.

Downloaded from journals.physiology.org/journal/physrev at New York Univ (216.165.095.084) on September 28, 2023.

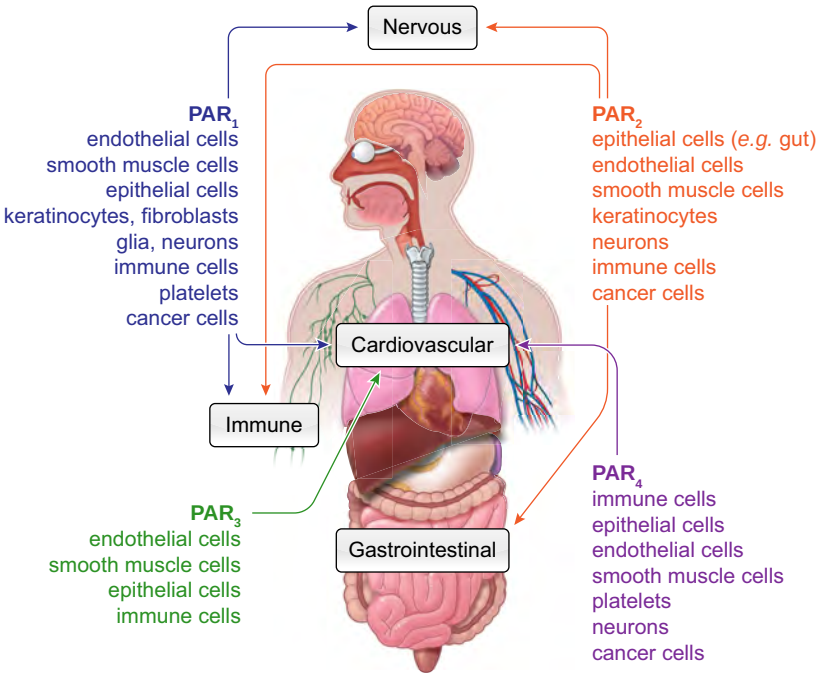

FIGURE 3. Patterns of protease-activated receptors (PAR) expression. Sites of $PAR_{1\text{-}4}$ expression across different organ systems (arrows) and cell types (listed).

3.1. Epithelial Cells

Epithelial cells of the skin, airway, gastrointestinal (GI) tract, urinary tract, and exocrine and endocrine glands differentially express PARs, which contribute to the physiology and pathology of these tissues (sect. 5).

3.1.1. Cutaneous epithelia.

The presence of proteases, protease inhibitors, and PARs in the skin suggests a major role for this system in cutaneous biology (sect. 5.2). PARs regulate the function of keratinocytes, which interact with nerves, melanocytes, Langerhans cells, and immune cells of the skin. PARs also contribute to keratinocyte maturation, replication, wound repair, migration, inflammation, and immune response. PAR_1 and PAR_2 activation have opposing effects on keratinocyte growth but similar effects on differentiation. PAR_1 activation enhances keratinocyte growth, whereas PAR_2 activation inhibits cell growth (40).

PAR_2 activity in keratinocytes was discovered based on functional assays and localization of immunoreactive receptors (41, 42). PAR_2 was detected in keratinocytes but not fibroblasts, while PAR_1 was detected in both cell types. PAR_2 on keratinocytes is activated by tissue factor (TF)/coagulation factor VIIa (FVIIa), as well as FXa is generated by TF/FVIIa (43). In keratinocytes, PAR_2 activation evokes release of Ca^{2+} from store-operated calcium entry (SOCE), which makes use of Ca^{2+} release-activated channels in the plasma membrane, such as ORAI1, also known as calcium release-activated calcium (CRAC) channel protein 1. Keratinocytes regulate the local immune response in the skin, and PARs contribute to immune regulation. In differentiated human primary keratinocytes, PAR_2 upregulates the release of inflammatory mediators, which involves the transient receptor potential vanilloid 1 (TRPV1) channel (44). Activation of PAR_2 on human primary keratinocytes depletes Ca^{2+} stores. However, the effect requires both TRPV1 and the inositol 1,4,5-trisphosphate (IP_3) receptor on the endoplasmic membrane, rather than SOCE.

3.1.2. Respiratory epithelia.

All four PARs are expressed in the human lung (45) (sect. 5.3). In the human lung, immunoreactive PAR_2 is localized to bronchial smooth muscle and epithelium (46).

3.1.3. Gastrointestinal epithelia.

Across species, PARs are expressed in GI epithelia (sect. 5.4). PAR_2 is highly expressed in the intestinal mucosa, including at the apical membrane of enterocytes where it can be cleaved by luminal trypsin (47). In situ hybridization in the mouse reveals PAR_2 transcript in epithelial cells of the small intestine, where it is primarily localized to the upper two-thirds of the intestinal villi and less so in the crypts.

Downloaded from journals.physiology.org/journal/physrev at New York Univ (216.165.095.084) on September 28, 2023.

3.1.4. Genitourinary epithelia.

PAR_1 and PAR_2 are expressed in the kidney. PAR_1 expression in the kidney epithelium regulates inflammation (48). PAR_2 is strongly expressed in the epithelium of the ureter (49). Activation of PAR_2 inhibits rhythmic beating of the ureter. PAR_2 is expressed in renal cortical collecting duct cells and in cultured M-1 mouse cortical collecting duct cells (50).

3.2. Endothelial Cells

Our understanding of PAR physiology has largely been driven by the study of thrombin-mediated PAR signaling in endothelial cells. For example, the observation that the tethered ligand alone could act as a receptor agonist was demonstrated in human platelets and endothelial cells (4). PAR endothelial signaling affects homeostasis and contributes to cerebrovascular disease, cardiovascular disease, and carcinogenesis (sect. 5.2). The effects of activation on platelets and endothelial cells exemplify the role of PAR activation in hemostasis. PAR_1, PAR_3, and PAR_4 mediate the effects of thrombin following blood vessel trauma. Thrombin activation of PARs leads to cytokine production by endothelial cells (51–53). Vitamin K-dependent coagulation proteases (e.g., FVIIa, FXa) except for FIXa, as well as thrombin, activate PARs on the surface of endothelial cells. PAR_1 and PAR_4 expression by endothelial cells in mice serve redundant roles; endothelial cells that do not express PAR_1 or PAR_4 show no response to thrombin (54). PAR_1 (4), PAR_2 (55, 56), PAR_3 (57), and PAR_4 (58) are expressed on human endothelial cells. Thrombin activates PAR_1, PAR_3, and PAR_4 but not PAR_2. PAR_1 on endothelial cells is a clinically important target due to its potential role in thrombosis. Quantitative phosphoproteomics have been used to study the effects of thrombin activation PAR_1 and of PAR_1 antagonism on endothelial cells, including the finding that the antagonist properties of vorapaxar and parmodulin-2 are distinct (59).

Human dermal microvascular endothelial cells (HMEC-1) have revealed the effects of PAR_1 activation and downstream trafficking (60). PAR_1 activation on endothelial cells leads to the secretion of inflammatory cytokines including interleukin (IL)-1, IL-6, tumor necrosis factor (TNF)-α, and cell adhesion molecules including selectins, intracellular adhesion molecule 1 (ICAM-1), and vascular cell adhesion molecule 1 (VCAM-1). PAR_1 is the effector receptor for endothelial protein C receptor (EPCR), which is responsible for the cytoprotective effects of activated protein C (APC). This includes anti-inflammation, antiapoptotic effects, and protection of endothelial barrier functions (61–63). PAR_1 exists in the native and cleaved form within intracellular pools of endothelial cells. When endothelial cells are exposed to an agonist, both native and cleaved PAR_1 will translocate to the cell surface (64, 65).

PAR_1 on endothelial cells exhibits biased agonism (sect. 4). APC is a serine protease that proteolytically inactivates FVa and FVIIIa; it therefore opposes coagulation and is also involved in inflammation. APC leads to endothelial barrier protection, as measured by zymogen-affected permeability of an endothelial cell monolayer. Based on its effects on systemic inflammation, recombinant human APC was approved for treatment of sepsis in patients (66). APC cleaves PAR_1; however, PAR_1 remains on the endothelial cell surface, as opposed to PAR_1 cleavage by thrombin (66, 67) (sect. 4.8). When thrombin cleaves PAR_1, the receptor internalizes for lysosomal degradation. While the two activators of PAR_1 have differential effects, thrombin and APC can cleave the same scissile bond on PAR_1 (68). APC can, however, also cleave downstream from the canonical site at Arg^{46}/Asn^{47} (**FIGURE 2**).

3.3. Smooth Muscle Cells

Before the discovery and characterization of PARs, thrombin was well-known to cause vasoconstriction and induce biogenesis in vascular smooth cells (69, 70). Activation of “the thrombin receptor” on smooth muscle cells (SMCs) by thrombin led to our early understanding of the selectivity of activating peptides for PARs (71). PARs are also expressed on SMCs in the respiratory system (72), GI tract (73, 74), and vasculature (75, 76). PAR activation on SMCs leads to protein phosphorylation, gene expression, contraction, relaxation, and mitogenesis. PAR_2 is expressed by human vascular SMCs and contributes to proliferation and migration (77). Vascular SMCs express PAR_1, PAR_3, and PAR_4, which mediate thrombin-induced proliferation and migration (78).

3.4. Platelets

Thrombin is the most potent activator of platelets. In 1967, Davey and Luscher (79) showed that thrombin’s catalytic activity was responsible for its action at the thrombin receptor on platelets. In the late 1970s and early 1980s, evidence was building that thrombin activation of platelets produced downstream signaling that involved GTP-binding proteins and second messengers, signaling processes that would later be characterized as a consequence of PAR activation (80). In 1990, a receptor for serine protease was identified in leukocytes (81). The authors proposed the name “effector cell protease receptor-1” for this receptor. The authors made the seminal finding that activation involved release of the NH_2

Downloaded from journals.physiology.org/journal/physrev at New York Univ (216.165.095.084) on September 28, 2023.

terminus of the receptor and rearrangement of the tethered ligand into a pocket within the receptor. Soon after the thrombin receptor was cloned, it was discovered that thrombin-induced cleavage of the NH_2 terminus and receptor activation by the tethered ligand led to granule secretion, shape change, and platelet activation (82). PAR_1 activation leads to the secretion of mediators that alter platelet function, including ATP and ADP. The search for a second thrombin-responsive receptor was motivated by data that showed thrombin-mediated effects following activation of platelets from PAR_1 knockout mice. Further investigation of effects not mediated by PAR_1 led to cloning and characterization of PAR_3 (30).

PAR expression on platelets is species specific. In spite of this, thrombin receptor subtypes work in concert in mice and humans. Human platelets do not express PAR_2. Rat platelets do not express PAR_1 or PAR_2. Similarly, mouse platelets express PAR_3 and PAR_4; in mice, PAR_3 is the high-affinity receptor. Knockout of either PAR subtype affects platelet activation by thrombin (83). However, mice deficient in PAR_3 do not exhibit spontaneous bleeding or have abnormally long bleeding times. Human platelets express PAR_1 and PAR_4; in the case of humans, PAR_1 acts as the high-affinity receptor. The role of the dual thrombin receptor system is not known. Coughlin and colleagues (83) hypothesized that the role of two PARs might allow for ligands other than thrombin to activate the receptors, or for thrombin to signal through different pathways with distinct kinetics. An example is the expression of PAR_3 on Dami cells (derived from a patient with megaloblastic leukemia) but not on human platelets. This suggests that PAR_3 is expressed by hematopoietic cells in the megakaryocyte lineage; however, expression is lost on megakaryocytes as the cells mature into platelets (84).

Although thrombin activates both PAR_1 and PAR_4, the affinity for PAR_1 is higher and the cellular consequences are different. PAR_4 lacks the hirudin-like binding site. Glycoprotein Ib and PAR_3 mediate binding of thrombin to PAR_1 and PAR_4, respectively (85, 86). Activation of PAR_1 or PAR_4 leads to secretion and aggregation of human platelets, and if both PARs are inhibited, platelets do not respond to even high doses of thrombin. This suggested that PAR_1 and PAR_4 were responsible for the action of thrombin on platelets (84), while PAR_3 does not participate in human platelet activation.

Mouse knockout models and heterologous expression systems have been used to elucidate the downstream mechanisms following activation of the PARs on platelets; however, species differences in expression of PARs limit the inference of the result to effects expected in human platelets. Activation of PAR_1 and PAR_4 results in human platelet aggregation, secretion, and increased intracellular Ca^{2+} (84). The differences between PAR_1 and PAR_4 activation remain a question. However, work has shown that PAR_1 has a dominant role in fibrinolysis, whereas PAR_4 mediates clot elasticity (87).

Proteases besides thrombin can activate PARs on platelets. For example, cathepsin G from neutrophils activates PAR_4, whereas cathepsin G does not activate PAR_1. Cathepsin G/PAR_4 activation leads to secretion from platelets and platelet aggregation (see Supplemental Table S4; all Supplemental material is available at https://doi.org/10.6084/m9.figshare.19739830). The effect mediated by PAR_4 can be blocked with an antibody against the thrombin cleavage site and desensitization with an activating peptide (88). Human kallikreins (KLKs) are another family of proteases that activate PARs and induce platelet aggregation. Activating peptides for both PAR_1 and PAR_4 generate a strong Ca^{2+} signal (25). The advantage of a Ca^{2+} assay over platelet aggregation is that the latter allows for a sequential and concurrent evaluation of activation of PAR_1 and PAR_4 on platelets.

3.5. Neurons and Glial Cells

In 1978, it was demonstrated that a glial-derived protease inhibitor induced neurite outgrowth in neuroblastoma cells (89). Neurite outgrowth is a cytoarchitectural change consistent with differentiation in neurons and glial cells. In contrast, thrombin was shown to reduce neurite outgrowth a decade later (90). Hirudin, the thrombin inhibitor, led to neurite outgrowth of neuroblastoma cells (91). Thrombin was known to bind to a receptor on neuroblastoma cells, and the binding resulted in an increase in cGMP (92). Collectively, these findings pointed to PAR_1 expression on neurons. Subsequently, data supported PAR expression in the central nervous system (CNS) on neurons and astrocytes; PAR_1 is highly expressed in the former and moderately expressed in the latter (93). PAR_1 on astrocytes responds to activation by thrombin in the same way that PAR_1 responds to activation on human platelets (94). On astrocytes, the strongest expression of PAR_1 is on the cell body and the distal neuronal endplate that innervates capillaries. Human astrocytes in culture respond to PAR_1 activation by increasing intracellular Ca^{2+}.

Of the four PARs, the role of PAR_2 on sensory neurons and its role in neurogenic inflammation and pain is best characterized (95, 96) (sect. 5.5). Activation of PAR_2 induces neurogenic inflammation and pain and sensitizes ion channels including TRPV1 (97). PAR_2 is expressed on peripheral nerve endings and the cell body of dorsal root ganglia (DRG); however, PAR_2 does not appear to be expressed in the central terminals in the spinal cord (98). While most of the work on PAR_2 expression in sensory ganglia has been done in DRG, PAR_2 has also been shown to be strongly expressed in

Downloaded from journals.physiology.org/journal/physrev at New York Univ (216.165.095.084) on September 28, 2023.

trigeminal ganglia (99). Trigeminal neurons innervating the nasal mucosa in rats were retrograde labeled, and then labeled ganglia were stained for PAR_2. Over 40% of trigeminal neurons were positive for PAR_2. Functional evidence also showed PAR_2 was expressed in trigeminal ganglia (100). Administration of the PAR_2-activating peptide SLIGRL-NH_2 produced c-Fos expression in the trigeminal nucleus caudalis of the caudal brainstem and superior cervical spinal cord. Further evidence for PAR_2 expression in the trigeminal ganglia was provided by experiments showing that activation of PAR_2 on rat trigeminal neurons leads to functional competence of δ-opioid receptor, which is inactive under basal conditions (101).

The question regarding expression of PAR_2/*F2rl1* on neurons has been controversial. Despite functional in vitro and in vivo data that supported PAR_2 expression on neurons, confirmation of expression was complicated by the nonspecific nature of antibodies for PAR_2. A publication by Price and colleagues in 2020 (102) clarified the conflicting functional and anatomic results; the publication also resolved some of the controversial ideas with regard to neuronal PAR_2 and pain. The first demonstration of the role of PAR_2 in pain was published by Vergnolle and colleagues in 2001 (96). This publication was one of the first to use a genetic knockout model to confirm the role of a receptor in mediating nociception. The authors showed that activation of PAR_2 with SLIGRL produced mechanical allodynia and thermal hyperalgesia. Subsequently, there were publications over two decades that confirmed the role of PAR_2 in somatic and visceral hyperalgesia; however, RNA sequencing data also showed extremely low levels of expression of *F2rl1* (103, 104). Price and colleagues (102) demonstrated that *F2rl1* is expressed on a small subset of neurons using available RNA sequencing data. Approximately 4% of DRG neurons express *F2rl1*. Using RNAScope, the authors showed that *F2rl1* is expressed on nonpeptidergic neurons that express *P2rx3*. These *F2rl1*-expressing neurons also coexpress *Il31ra* and *nppb* (naturietic precursor peptide b), genes that mediate itch. The authors used a conditional knockout with the *Pirt* promoter, where $F2rl^{flox}$ mice were crossed with $Pirt^{Cre}$ mice. The promoter for *Pirt* is expressed in primary sensory neurons in the DRG and TG; however, it is not expressed in glia or skin (106). Using the conditional knockout mice, the authors showed that activation of *F2rl1* on neurons by three different agonists produces mechanical allodynia, agonists including at-LIGRL, neutrophil elastase, and compound 48/80, which leads to mast cell degranulation of tryptase. The dose of at-LIGRL (<10 μM) is specific for PAR_2 (107). Thermal hyperalgesia was induced by at-LIGRL through PAR_2. In contrast, compound 48/80 and neutrophil elastase produced thermal hyperalgesia; however, neuronal PAR_2 was not required. This key result shows that activation of nonneuronal PAR_2 by endogenous proteases mediates the thermal effect. Before this study, most studies that reported on the role of neuronal PAR_2 in pain have used reflexive assays. Price and colleagues (102) used the facial grimace assay that measures the affective component of nociception (108). They showed that at-LIGRL injected into the paw produces nociception measured by facial grimace. The nociception is dependent on neuronal *F2rl1*. The investigators also looked at the role of PAR_2 in itch. Using the at-LIGRL dose specific for PAR_2 as well as *F2rl1*-/-, they showed that the low at-LIGRL dose induces pain but not itch. This finding is consistent with the work of Dong and colleagues (109) who showed that SLIGRL mediates itch through activation of murine MrgprC11. Homolog to the human mas-related GPCR member X1 (MRGPRX1), this pruritogenic receptor is an orphan receptor expressed by sensory neurons. The authors showed that the pentapeptide SLIGR specifically activated PAR_2 and not MrgprC11; this induced nociception but not pain.

PAR_4 was shown to be expressed on sensory neurons in 2002 (110). While PAR_4 was later shown to be strongly expressed in the gut, it was first shown to be expressed on visceral primary afferent neurons in 2009 (111).

Following early studies looking at PAR expression on sensory neurons, motor neurons, and the brain, investigators started to look at PAR expression on neurons that innervate the GI tract. Myenteric neurons strongly (>60%) express PAR_1 and PAR_2, at the transcript and protein level (23). PAR_1 and PAR_2 expression was studied in neurons isolated from the guinea pig small intestine. These neurons responded to mast cell tryptase and trypsin, proteases that have a central role in trauma and inflammation, as measured by Ca^{2+} imaging. The neurons also responded to agonist peptides selective for PAR_1 [AF(pF)RchaCitY-NH_2 and TFLLRN-NH_2] and PAR_2 (SFLLRN-NH_2). The response of these myenteric neurons to PAR_2 agonists was further characterized in the guinea pig ileum (112). SLIGRL-NH_2 or trypsin activation of the myenteric neurons produced prolonged depolarization in tetrodotoxin-resistant manner, which suggested direct activation of PAR_2 on myenteric neurons. Myenteric neurons have been classified into two types based on electrophysiologic parameters: AH/type 2 (less excitable, one to two spikes following depolarizing current pulses) and S/type 1 (more excitable, repetitive spikes following depolarizing current pulses) (113, 114).

3.6. Immune and Inflammatory Cells

The interpretation of studies that report PAR expression on leukocytes should consider the cellular treatment such as centrifugation, purification, or even repeated

Downloaded from journals.physiology.org/journal/physrev at New York Univ (216.165.095.084) on September 28, 2023.

pipetting; each step can lead to PAR upregulation (115). Early evidence suggested that leukocytes express PARs (116) (sect. 5.6). Activation of PAR_1 on mast cells, either from trypsin or the activating peptide, produced a change in mast cell activity and secretion of IL-6 (117, 118). PAR_1 is expressed on memory $CD4^+$ and $CD8^+$ T cells (119).

Work with neutrophils and thrombin led to the speculation that there were additional PARs beyond PAR_1. Neutrophils were known to respond to thrombin and that response was mediated by a proteolytically activated receptor. It was also known that a peptide analog of the NH_2-terminal region following its cleavage could activate neutrophils in the absence of thrombin (4). Work with thrombin and its activating peptide, thrombin receptor-activating peptide (TRAP), led to the suggestion of additional PARs, including PAR_2 (120). The peptide sequence for TRAP (SFLLRN) and the specific PAR_2-activating peptide (SLIGRL) share homology (20).

Cutaneous human primary skin mast cells and the human mast cell line 1 (HMC-1) express all four PARs; however, PAR_2 mediates the action of mast cells. PAR_2 agonists cause the release of histamine by mast cells. Tryptase and PAR_2 colocalize on the surface of mast cells (121). Human mast cells express PAR_2, which, when activated, leads to mast cell degranulation. Tryptase, which is released by degranulation, cleaves PAR_2 (121–123).

There is functional and anatomic evidence for PAR_2 expression in human eosinophils. PAR_2 and eosinophils mediate airway disease. While there is a transcript for PAR_2 and PAR_3 in human eosinophils, there is no transcript for PAR_1 or PAR_4. Human eosinophils respond to trypsin and the activating peptide for PAR_2, but not thrombin or the activating peptides for PAR_1, PAR_3, and PAR_4 (124). In a subsequent study, eosinophils were isolated from human blood. Tryptase caused release of interleukin-6 (IL-6) and IL-8 from eosinophils (125). A later study used RT-PCR, Western blotting, and flow cytometry to analyze expression of the PARs in human eosinophils, neutrophils, and mononuclear cells (126). In contrast to the earlier study that did not detect PAR_1 in eosinophils, this study, which used complementary techniques, showed expression of PAR_1 and PAR_2. Similarly, mononuclear cells showed expression of PAR_1 and PAR_2. Neutrophils expressed PAR_2, which had been shown in an earlier study in which a PAR_2-activating peptide led to an increase in intracellular Ca^{2+} and a change in cellular morphology (127).

PAR_2 on T lymphocytes is involved with leukocyte rolling and adhesion (128, 129). PAR_2 is also expressed in the Jurkat T-cell leukemia line (130). PAR_2 is not expressed on B cells (131). With the use of a preparation that involves exteriorization of the midjejunum and in vivo microscopy, it was demonstrated that activation of PAR_2 contributes to leukocyte rolling, adhesion, and extravasation (132). Trypsin-mediated activation of neutrophils (133), eosinophils (124, 126), and lymphocytes (134) leads to the release of reactive oxygen species.

Differential expression of PARs on human monocytes was studied using RT-PCR and flow cytometric analysis to measure expression of PARs; Ca^{2+} imaging then demonstrated functional expression (135). PAR_3, and a lower level of PAR_1, are expressed by human monocytes. When monocytes were treated with granulocyte-macrophage colony-stimulating factor (GM-CSF) to differentiate into macrophages, or with GM-CSF and IL-4 to differentiate into dendritic cells, both macrophages and dendritic cells expressed PAR_1, PAR_2, and PAR_3.

PAR_4 is present on the surface of rat neutrophils (110). In a separate in vivo study measuring neutrophil function, they demonstrated that PAR_4 on neutrophils participated in the features of inflammation including edema and granulocyte recruitment. Carrageenan-induced inflammation was reduced with a PAR_4 antagonist. Conversely, injection of the PAR_4 agonist produced paw edema and granulocyte recruitment (136).

3.7. Cancer Cells

Soon after their discovery, PARs were detected in cancer cells (sect. 5.7), including expression of PAR_2 in lung and colon adenocarcinoma cells (21) and expression of PAR_1 in pancreatic tumor cells (137). The role of thrombin in metastasis was demonstrated in metastatic breast cancers (138). PAR_1 was expressed in metastatic breast carcinoma cell lines but not in nonmetastatic breast carcinoma cell lines. For metastatic cell lines, PAR_1 correlated with metastatic potential. A key study recently used data from The Cancer Genome Atlas and the Genotype-Tissue Expression projects to highlight PARs overexpressed by human cancer cells (139).

PAR_1 and PAR_2 are not only expressed by cancer cells but also by nonmalignant cells in the tumor microenvironment that support carcinogenesis (140). The key finding of this study was that PAR_1 and PAR_2 are upregulated and showed moderate to strong staining by stromal fibroblasts that express smooth muscle actin. Myofibroblasts are known to be critical for carcinogenesis (141).

3.8. Summary

PARs are widely expressed on epithelial cells (skin, respiratory system, GI tract, urinary tract, and exocrine and endocrine glands), endothelial cells, platelets, smooth muscle cells, neurons, glial cells, innate and adaptive immune and inflammatory cells, and cancer cells. PAR expression on the different cell type positions PARs

Downloaded from journals.physiology.org/journal/physrev at New York Univ (216.165.095.084) on September 28, 2023.

to contribute to homeostasis and pathology. Our understanding of PAR physiology has been driven by the study of the effect of PAR activation on different cell types. PAR expression and function differ across species.

4. ACTIVATION AND SIGNALING OF PARS IN HEALTH AND DISEASE

4.1. Canonical and Biased Mechanisms of PAR Activation

PAR activation entails hydrolysis of peptide bonds in the extracellular NH_2-terminal domain, revealing a sequence of amino acids (tethered ligand) that can interact with the orthosteric site within the TM domains of the cleaved receptor. While a growing variety of proteases are known to cleave PARs, their canonical sites are defined by the protease linked to their discovery. Biased signaling is a phenomenon whereby different ligands stabilize conformations of the same receptor that favor distinct signaling pathways. Biased signaling is of particular interest for proteases that cleave PARs at different sites and reveal distinct tethered ligands or stabilize unique receptor conformations (**FIGURE 2**). Biased mechanisms of PAR activation trigger different downstream signaling pathways and physiological outcomes. For example, APC cleaves PAR_1 at both the canonical Arg^{41}/Ser^{42} site and distal at Arg^{46}/Asn^{47} (142) (see Supplemental Table S1). Whereas thrombin leads to endothelial permeability, APC stabilizes the endothelial barrier with anti-inflammatory and cytoprotective effects (sect. 5.1; see **FIGURE 6**).

Noncanonical cleavage sites can occur proximal and distal to the canonical cleavage site. In some cases, cleavage reveals a distinct peptide that retains some residues of the canonical tethered ligand but includes a sequence that can independently activate the receptor. Matrix metalloprotease 1 (MMP1) is a matrix-degrading enzyme released by platelets that modulates platelet survival and hemostatic function. MMP1 cleaves PAR_1 at Asp^{39}/Pro^{40}, two residues proximal to the canonical thrombin cleavage site, to reveal PR-SFLLRN (143) (**FIGURE 2**; see Supplemental Table S1). This activates signaling pathways that regulate platelet motility and aggregation. Proteinase-3 cleaves PAR_1 at Ala^{36}/Thr^{37}, revealing TLDPR-SFLLRN (144). Proteinase-3 cleavage causes biased signaling, leading to ERK1/2 phosphorylation but lacking Ca^{2+} mobilization (**FIGURE 2**; see Supplemental Table S1). Activating peptides mimicking the PAR_1-tethered ligand revealed by MMP1 or proteinase-3 reproduce signaling pathways observed by protease exposure. Similarly, cathepsin S cleaves PAR_2 at Glu^{56}/Thr^{57}, distal to the canonical site, which reveals a distinct tethered ligand (145) (**FIGURE 2**; see Supplemental Table S2). Cathepsin S and its activating peptide are biased for $G\alpha_s$ signaling, while lacking Ca^{2+} signaling or β-arrestin recruitment.

Some proteases can activate PARs without exposing a tethered ligand, presumably by stabilizing unique active conformations. Elastase cleaves PAR_1 and PAR_2 distal to their canonical site at Leu^{45}/Arg^{46} and Ser^{67}/Val^{68}, respectively (144, 146, 147) (**FIGURE 2**). While elastase does not initiate PAR_2-mediated Ca^{2+} signaling, it activates ERK1/2 (146) and protein kinase D (PKD; Refs. 146, 148) (see Supplemental Table S2). The activating peptide for elastase initiates PAR_1 signaling as a tethered ligand (144). In contrast, the elastase/PAR_2-activating peptide does not signal in its own right (146). Legumain, an asparaginyl endopeptidase resident in late endosomes, also leads to biased PAR_2 signaling. Cleavage at Asn^{30}/Arg^{31} reveals RSSKGR-SLIGKV (149), leading to ERK, Ca^{2+}, and cyclic adenosine monophosphate (cAMP) signaling without β-arrestin recruitment (**FIGURE 2**; see Supplemental Table S2). Likewise, the activating peptide for legumain/PAR_2 cleavage does not initiate signaling (149).

4.2. Proteolytic Disarming of PARs

Cleavage distal to the canonical site of activation can "disarm" PARs by permanently removing the canonical cleavage site and destroying the tethered ligand sequence. If these cleavage events do not themselves activate PARs, they can render the cleaved receptor unresponsive to proteases that activate PARs by canonical mechanisms. Mass spectrometry studies show plasmin, calpain, elastase, cathepsin G, and proteinase-3 cleave PAR_1 at multiple sites distal of the canonical site (150). Plasmin, for example, can cleave at both the canonical site and distal at Arg^{70}/Leu^{71}, Lys^{76}/Ser^{77}, and Lys^{82}/Gln^{83} (68). Plasmin desensitizes PAR_1 Ca^{2+} signaling in response to thrombin (see Supplemental Table S1). Cathepsin G cleaves PAR_2 at Phe^{64}/Ser^{65} and renders the receptor unresponsive to trypsin; it does not, however, prevent signaling in response to the activating peptide SLIGKV (151). Nonmammalian proteases also disarm PARs. Streptococcal pyrogenic exotoxin B (SpeB), a virulence factor secreted from Group A streptococcus, cleaves PAR_1 at Leu^{44}/Leu^{45} within the SFLLRN tethered ligand (152). SpeB inhibits thrombin-induced ERK1/2 signaling in endothelial cells and prevents thrombin-evoked platelet aggregation. Bacterial proteases can also disarm PAR_2. Elastolytic metalloproteinase (Epa) from *Pseudomonas aeruginosa* cleaves PAR_2 at Ser^{37}/Leu^{38} to reveal LIGKV and disrupt the canonical tethered ligand (153).

Downloaded from journals.physiology.org/journal/physrev at New York Univ (216.165.095.084) on September 28, 2023.

4.3. Tethered Ligands and Soluble Activating Peptides

Structure/function studies of the interaction between the tethered ligand domain and the cleaved receptor provide insights into the mechanism of intramolecular activation of PARs. The PAR_1 tethered ligand interacts with ECL2 Glu160, as identified by mutagenesis (154). This was corroborated by the PAR_1 crystal structure in complex with an orthosteric antagonist (29) (sect. 2.2). A synthetic peptide mimicking the PAR_1 tethered ligand (TRAP) can directly activate PAR_1 without requiring receptor cleavage (4). Modified versions of SFLLRN have a varying capacity to activate PAR_1 and aggregate platelets (155). The potency depends on peptide length, whereby reduction from 14 to 5 residues enables platelet aggregation while reducing potency fivefold (156, 157). At least five amino acids are required to activate PAR_1 (155, 156) and PAR_2 (158). In contrast, PAR_3 does not itself respond to activating peptides TFRGAP-NH_2 (human) or SFNGGP-NH_2 (murine) (159). The PAR_4-activating peptide was modified to AYPGKF to enhance its potency (160). Other modifications of activating peptides can enhance biological activity. Modification of the PAR_2-activating peptide to 2-furoyl-LIGKV-OH enhances bioavailability by protection from endogenous aminopeptidases (161), leading to development of 2-furoyl-LIGRLO-NH_2, a potent and selective PAR_2 agonist (162).

Activating peptides have been widely used to probe PAR functions. While they usually recapitulate the actions of proteases, there are some differences. Thrombin aggregates platelets and stimulates Ca^{2+} in all species, whereas SFLLRN only activates PARs in guinea pigs, monkeys, and humans (40). Signaling kinetics also differ; thrombin-induced Ca^{2+} signaling in platelets is more sustained than SFLLRN or GYPGQV (163). Activating peptides exhibit varying degrees of subtype selectivity, which can complicate the interpretation of their effects. PAR_4-activating peptides cannot activate PAR_1 and PAR_2 (164). In contrast, the PAR_1-activating peptide activates both PAR_1 and PAR_2 (165). This lack of selectivity raises the possibility that tethered ligands from different PAR subtypes could activate another via transactivation and coactivation (**FIGURE 4*A***). For example, PAR_1-PAR_2 heterodimers have been directly observed using biophysical techniques (166). PAR_1-PAR_4 heterodimers also occur via TM4 interactions induced by thrombin (167). Activating peptides can also activate non-PARs, such as the activation of MrgprC11 by the PAR_2-activating peptide (109).

PAR_3 does not respond to synthetic peptides that mimic the putative tethered ligand. PAR_3 signaling remains an enigma. Autonomous PAR_3-mediated signaling was shown in response to thrombin using HEK293 cells lacking PAR_1 (168). However, thrombin can have additional functions, such as integrin-induced chemotaxis (169). Thus observed ERK phosphorylation and IL-8 release could be PAR_3 independent. PAR_3-activating peptides can also signal through other PAR subtypes (as in **FIGURE 4*A***). PAR_3 acts as a cofactor in platelets, signaling via PAR_4 (86). PAR_3 activation could also act through PAR_1, as the PAR_3-activating peptide initiates ERK1/2 signaling that was abolished by a PAR_1 antagonist or using PAR_1 knockout fibroblasts (170). PAR_3 modulation of thrombin/PAR_1 signaling causes biased signaling in endothelial cells, whereby siRNA against PAR_3 corresponds with increased endothelial barrier permeability independently of Ca^{2+} signaling (171).

4.4. Accessory Proteins for PAR Activation

Interactions with other membrane proteins can bias the outcomes of PAR activation. This concept is illustrated by the role of EPCR in APC-mediated activation of PAR_1 (63, 172) (sect. 3.2). APC activates PAR_1, yet it leads to divergent phenotypic outcomes compared to thrombin. APC also cleaves PAR_3 distal from its canonical site in an EPCR-dependent manner with a barrier-protective phenotype (173). EPCR binds the other PAR_1-cleaving proteases FXa (174) and FVIIa (14, 175). FXa/EPCR interactions reduce endothelial cell permeability in a manner sensitive to the EPCR inhibitor RCR252 (174).

Other membrane proteins can modulate the protease activity or PAR-signaling pathways. For example, integrins are receptors linking the extracellular matrix (ECM) with the cytoskeleton. Plasmin interacts with $\alpha_9\beta_1$-integrin, leading to enhanced migration blocked by a PAR_1 inhibitor (e.g., RWJ 58259) (176). Coexpression of another integrin subtype, $\alpha_{IIb}\beta_3$-integrin, enhances MMP2-mediated cleavage of PAR_1 (177). Thrombin interacts with $\alpha_V\beta_5$-integrin, a membrane protein localized in the same region as PAR_1 in lung carcinoma cells (178).

Other GPCRs can also modulate PAR signaling (reviewed in Ref. 179; **FIGURE 4*B***). In addition to heteromers between PAR subtypes, PAR_1 can interact with β-adrenoceptors expressed by cardiac fibroblasts and cardiomyocytes (180). Considering PAR_1 is the highest GPCR expressed in numerous fibroblast subtypes (181), modulation could have important implications in cardiac dysfunction with β-adrenoceptor overstimulation. PAR_4 interacts with $G\alpha_i$-coupled $P2Y_1$ and $P2Y_{12}$ purinergic receptors to induce platelet activation (182). There is also evidence that PAR_1 forms a heteromer with chemokine receptor 4 (CXCR4) (183).

Downloaded from journals.physiology.org/journal/physrev at New York Univ (216.165.095.084) on September 28, 2023.

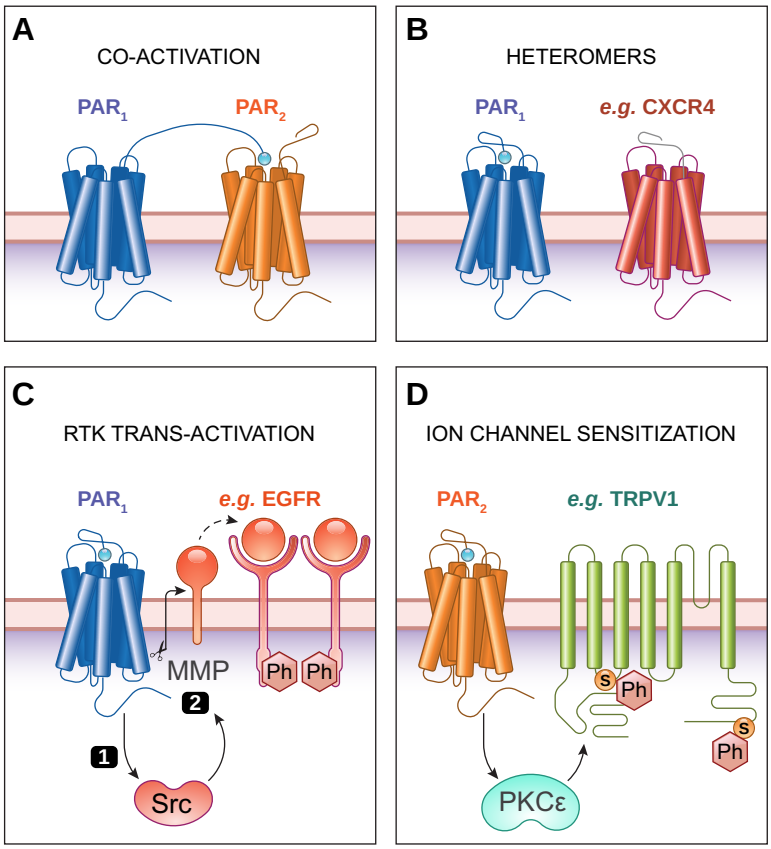

FIGURE 4. Modulation of protease-activated receptors (PAR) signaling. *A*: heteromers can form between different PAR subtypes, such as PAR_1 and PAR_2. Tethered ligands from one subtype can transactivate another. *B*: heteromers can form with other G protein-coupled receptors (GPCRs), such as between the chemokine receptor 4 (CXCR4; shown) or with β-adrenoceptors in cardiac fibroblasts. *C*: GPCRs transactivate receptor tyrosine kinases (RTKs), such as the epidermal growth factor receptor (EGFR). PAR_1-mediated Src activation can phosphorylate (Ph) EGFR (*1*). PAR_1 also activates matrix metalloproteases (MMPs) that liberate membrane-tethered EGFR ligands, such as amphiregulin (*2*). *D*: PAR signaling can modulate ion channel signaling, such as PAR_2-mediated sensitization of transient receptor potential vanilloid 1 (TRPV1) in sensory neurons. TRPV1 sensitization is mediated by PKC activation downstream of PAR_2, causing phosphorylation (Ph) of TRPV1 (Ser residues 502 and 800 in human TRPV1).

4.5. Pathways of Canonical and Biased PAR Signaling

PARs activate multiple pathways of intracellular signaling, which depend on the activating proteases and the receptor in question (see Supplemental Tables S1–S4). PARs couple to multiple subtypes of heterotrimeric guanosine triphosphate-binding proteins (G proteins) that are composed of Gα and Gβγ subunits. GPCR activation causes the Gα subunit to exchange GDP for GTP, leading to dissociation of "active" GTP-bound Gα protein from the Gβγ subunits. Subsequent signaling cascades are typically determined by the Gα protein subtype, where PAR_1 and PAR_2 interact with $G\alpha_{q/11}$, $G\alpha i_{/o}$, and $G\alpha_{12/13}$ (184).

4.5.1. Calcium.

$G\alpha_{q/11}$ activates phospholipase C (PLC) to hydrolyze PIP_2 into IP_3 and diacylglycerol. IP_3 initiates Ca^{2+} release from the endoplasmic reticulum. Ca^{2+} mobilization was monitored upon first characterization of thrombin/PAR_1 (4), trypsin/PAR_2 (5, 21), thrombin/PAR_3 (30), and thrombin/PAR_4 (8). This leads to protein kinase C (PKC) activation; e.g., PKCε recruitment to the plasma membrane of DRG neurons in response to thrombin (185). Multiple regions of PAR receptors are involved in $G\alpha_q/Ca^{2+}$ signaling, including PAR_1 helix 8 (186) or a PAR_2 palmitoylation site (187). PAR_1-mediated Ca^{2+} signaling is sensitive to thapsigargin, a Ca^{2+}/ATPase transporter inhibitor (188). It can also be modulated by store-operated Ca^{2+} influx via TRPC (189). In endothelial cells, thrombin and activating peptides for PAR_1 and PAR_2 induce $G\alpha_q$-mediated Ca^{2+}, with no role of $G\alpha_i$ (190). While many proteases induce Ca^{2+} signaling [e.g., legumain-activated PAR_2 (149)], some proteases do not mobilize Ca^{2+} [e.g., elastase/PAR_2 (146, 148)].

Ca^{2+} signaling has distinct consequences depending on cell type. For example, PAR_1-mediated Ca^{2+} signaling in astrocytic end feet is important for protease influx upon disturbance of the blood-brain barrier (93). With respect to platelets, Ca^{2+} signaling is linked to platelet aggregation. Two rare patients with deficiencies in $G\alpha_q$ or PLC-β2 had a mild bleeding disorder with mucosal bleeding and bruising. This was accompanied by reduced Ca^{2+} signaling via PAR_1 and PAR_4 in platelets (191). A racially dimorphic mutation in platelet PAR_4 that is prevalent in Black populations enhances Ca^{2+} signaling, with elevated platelet aggregation in response to AYPGKF (192). This Thr120Ala mutation (rs773902) in TM2 implicated responses to therapeutics, with resistance to inhibition by selective PAR_4 antagonist YD-3 (193).

Ca^{2+}-signaling kinetics differ between PAR subtypes. PAR_4 has a slower, sustained Ca^{2+}-signaling profile,

Downloaded from journals.physiology.org/journal/physrev at New York Univ (216.165.095.084) on September 28, 2023.

compared to rapid, transient Ca^{2+} mobilization in response to PAR_1 (84, 194, 195) or PAR_2 (196). Akin to Ca^{2+} kinetics, platelet aggregation induced by the PAR_4-activating peptide is slower than thrombin/PAR_1 (197). There are also distinctions in kinetics between proteases, whereby FXa Ca^{2+} mobilization in endothelial cells is more delayed than thrombin (13, 198, 199). Other factors can influence Ca^{2+}-signaling kinetics, such as TRPV4 coexpression resulting in more sustained Ca^{2+} in response to PAR_2 (200).

4.5.2. MAPK kinases.

PAR activation leads to the phosphorylation of mitogen-activated protein kinases (MAPK), including ERK1/2 or p38 MAPK. Canonical ERK1/2 signaling is downstream of $G\alpha_q/Ca^{2+}$ for PAR_2 (201) and PAR_4 (197). Trypsin causes PKC-dependent ERK1/2 activation inhibited by a nonselective PKC inhibitor and a PKC-β inhibitor (201). Trypsin-mediated PAR_2 ERK1/2 signaling is also reduced by inhibitors of Src, $G\alpha_i$, and Rho kinase (202). Activation of PAR_2-mediated nuclear or cytosolic ERK1/2 is sensitive to $G\alpha_q$ and $G\beta\gamma$ inhibitors (203). ERK1/2 is linked to chemotactic pathways, as PAR_2 is expressed in motile cells (e.g., macrophages, tumor cells). PAR_2-activating peptide induces cytoskeletal rearrangements and extended polarized pseudopodia in a manner sensitive to an inhibitor of MEK1/2, a kinase upstream of ERK1/2 (204). siRNA against PAR_2 demonstrated its role in cancer cell migration, where ERK1/2 activation peaks within 15 minutes and remains elevated in response to FXa or activating peptides (140). Other physiological consequences are linked to ERK1/2, such as PAR_2-mediated hypersensitivity in DRG neurons. Likewise, incubation with a MEK1/2 inhibitor inhibited the development of mechanical hypersensitivity (205). Considering PAR_1 is an oncogene in metastatic breast cancer, cell proliferation is also a consequence of ERK1/2 signaling. Janus kinase 2 (JAK2) is another kinase upstream of Ras/Raf/MEK/ERK in thrombin-stimulated vascular SMC growth (206). Thrombin/PAR_1 also activates p38 MAPK in vascular SMCs (207). PAR_1 p38 MAPK activation leads to increased endothelial permeability, downstream of Src-mediated activation of E3 ubiquitin ligase (208).

Despite lacking Ca^{2+} signaling, elastase and proteinase-3 activate ERK1/2 via PAR_1 and $G\alpha_{i/o}$ signaling (144). Similarly, elastase triggers Ca^{2+}-independent PAR_2 ERK1/2 phosphorylation in a Rho kinase-dependent manner (146). ERK1/2 signaling can be modulated by other receptors. PAR_1 heteromerization with CXCR4 (**FIGURE 4*B***) modulates thrombin-induced Ca^{2+} and ERK1/2 signaling in endothelial cells (183). Via TM2 PAR_1/CXCR4 interactions, ERK1/2 phosphorylation kinetics are modulated where CXCR4 siRNA reduces ERK1/2 phosphorylation.

4.5.3. PI3K/Akt.

$G\alpha_q$-mediated PI3K activation phosphorylates Akt (also known as protein kinase B), a Ser/Thr-specific kinase that regulates cell survival and proliferation. For PAR_2, this leads to chemotaxis downstream of $G\alpha_q/Ca^{2+}$-activated PI3K (209). Trypsin-mediated Akt activation can enhance motility in tumor metastasis via actin polymerization promoting microvesicle generation in MDA-MB-231 cancer cells (210). PAR_2/Akt also maintains intestinal epithelium homeostasis by inhibiting cytokine-induced apoptosis in colonic epithelial cells, in a manner sensitive to MEK1/2 and PI3K inhibitors (211). In response to various proteases, PI3K/Akt signaling also regulates platelet aggregation downstream of PAR_1 (212) and PAR_4 (213). MMP2 potentiates thrombin-induced platelet aggregation in a PI3K-dependent manner (214). Later identified to reveal "DPR-TRAP," MMP2 triggers $G\alpha_q$ and $G\alpha_{12/13}$ signaling that lead to Akt activation in platelets, as well as p38 MAPK and Ca^{2+} (177). Key phenotypic differences between APC- and thrombin-induced PAR_1 signaling in endothelial cells have been attributed to Akt signaling. APC or its activating peptide "TR47" cause Akt phosphorylation in endothelial cells, whereas thrombin or "TRAP" did not (142). Likewise, mice expressing PAR_1 Arg46Asn exhibit reduced Akt phosphorylation, whereas mutating the canonical site have reduced Ca^{2+} signaling (215).

4.5.4. Adenylyl cyclase and cAMP.

Whereas $G\alpha_s$ increases cAMP via activation of adenylyl cyclase, $G\alpha_{i/o}$ inhibits local cAMP production. PAR_1 activation leads to reduced forskolin-induced cAMP in platelets (155). PAR_2 also reduces cAMP formation in SMCs, such as in response to tryptase (216) or its activating peptide (217). There are disagreements regarding PAR_2-induced cAMP changes across cell types. Unlike PAR_1, the same study suggests PAR_2 does not modulate cAMP (184). In contrast, there is evidence of $PAR_2/G\alpha_s$ signaling in response to trypsin in a manner sensitive to PAR_2 antagonist I-343 (203). Cathepsin S is biased for $G\alpha_s$ signaling, while lacking Ca^{2+} signaling or β-arrestin recruitment (145). Legumain also leads to cAMP accumulation (149). In addition to monitoring cAMP, studies demonstrate the concentration dependence of PAR_1- or PAR_2-$G\alpha_i$ coupling, with rapid $G\alpha_i$ recruitment to PAR_1 and evidence for preassembled complexes (218). PAR_4 can induce $G\alpha_i$-mediated reduction in cAMP. Activating peptides for PAR_1 (SFLLRN) and PAR_4 (AYPGKF) inhibit adenylyl cyclase in platelets in an ADP-dependent manner (219). This is reduced by an antagonist of the $P2Y_{12}$ receptor, a receptor for ADP. Platelets from a patient lacking $P2Y_{12}$

Downloaded from journals.physiology.org/journal/physrev at New York Univ (216.165.095.084) on September 28, 2023.

no longer respond to thrombin with respect to cAMP inhibition, resulting in reduced platelet aggregation (219). There is evidence that PAR_4/$P2Y_{12}$ interactions occur via TM4 (214).

4.5.5. Cytoskeletal changes via Rho GTPase.

$G\alpha_{12/13}$ activation modulates the cytoskeleton via RhoGEFs, RhoA, and phosphorylation of myosin light chain (MLC). Early studies demonstrated that thrombin activates $G\alpha_{12/13}$ [e.g., platelets (220), endothelial cells (221)]. Thrombin-mediated RhoGEF activation regulates the cytoskeleton (222). In endothelial cells, thrombin-mediated activation of RhoA increases endothelial permeability important for vascular inflammation (223) via rearrangement of the cytoskeleton (224). Changes in endothelial permeability induced by thrombin or PAR_1-activating peptide are sensitive to inhibitors of $G\alpha_{12/13}$-mediated Rho kinase (190). Cytoskeletal changes can also involve cofilin, an actin filament-severing protein that leads to cytoskeletal reorganization and chemotaxis. PAR_2 activates cofilin by dephosphorylation independently of $G\alpha_q/Ca^{2+}$; this is reduced in the absence of β-arrestin (225). PAR_1 and PAR_2 activate RhoA via both $G\alpha_{q/11}$ and $G\alpha_{12/13}$ (185). PAR_4 also leads to changes in cell shape in a $G\alpha_{12/13}$-dependent manner in response to AYPGKF, sensitive to a ROCK inhibitor or CRISPR/Cas9-mediated knockout of RhoA (226). In contrast to the rapid, transient recruitment of $G\alpha_i$ to PAR_1 and PAR_2, $G\alpha_{12/13}$ coupling is delayed and sustained (218, 227). Gα subtypes interact with different interfaces on the cytoplasmic face of GPCRs. While inhibition of PAR_1 helix 8 reduces $G\alpha_q$ signaling, there is no effect on $G\alpha_{12/13}$-mediated changes in platelet shape or transepithelial resistance (228).

There are contrasting effects of thrombin and APC on endothelial barrier permeability. Whereas thrombin increases permeability by a RhoA pathway, APC/EPCR stabilizes the endothelial barrier by a Rac1 pathway (229). Phosphoproteomic studies comparing thrombin and APC in endothelial cells demonstrate differences in numerous phosphorylation targets that modulate adherens junctions, such as afadin and adducin-1 (230). Other proteases exhibit bias with respect to cytoskeletal changes. Despite cleaving noncanonical sites, elastase and proteinase-3 induce MAPK signaling and actin stress fiber formation in endothelial cells (144). MMP1/PAR_1 also demonstrate bias, causing migration through cytoskeletal changes via Rho activation and MAPK (143). This was shown in platelets (143), endothelial cells (231), and SMCs (232), in addition to triggering cancer cell invasiveness (233). Whereas thrombin induces a contractile phenotype, MMP1 triggers migration and proliferation (232). MMP1 migration is PAR_1 dependent, blocked by a cell-penetrating pepducin (sect. 6.2) or inhibitor RWJ-56110 (231). Other factors can modulate cytoskeletal responses, such as protease concentration. Whereas high thrombin concentrations disrupt endothelial barriers, picomolar concentrations are protective in a PAR_1-dependent manner (234). Posttranslational modifications can also alter Gα coupling, whereby lacking PAR_1 ECL2 glycosylation reduces $G\alpha_{12/13}$-dependent RhoA activation and stress fiber formation in contrast to $G\alpha_q$ signaling (235). Heteromer PAR_1/PAR_3 formation can also increase $G\alpha_{12/13}$ signaling without affecting Ca^{2+} pathways, causing increased endothelial permeability and $PAR_1/G\alpha_{12/13}$ coupling (171).

4.5.6. β-Arrestin recruitment.

β-Arrestins mediate desensitization and endocytosis of many GPCRs. Whereas PAR_2 endocytosis requires β-arrestin recruitment (**FIGURE 5**; sect. 4.8) (201), β-arrestin is not required for endocytosis of PAR_1 (236) or PAR_4 (237). With respect to PAR_1, β-arrestin interactions are phosphorylation independent (236) with slow, sustained kinetics (238). Rapid β-arrestin recruitment to PAR_2, on the other hand, peaks within minutes (227). PAR_1/PAR_2 heteromer formation results in increased β-arrestin recruitment (166). Some proteases that activate PAR_2 are unable to recruit β-arrestin, such as elastase (146, 147), cathepsin S (145), and legumain (149).

4.6. Sustained PAR Signaling in Subcellular Compartments

GPCRs were conventionally considered to signal predominantly from the plasma membrane, where GPCRs interact with extracellular ligands and couple to intracellular G proteins and β-arrestins. Plasma membrane signaling is often transient, where β-arrestin-mediated desensitization and endocytosis were viewed to terminate cell surface GPCR signaling. However, it is now clear that GPCRs, including PARs, can continue to signal from within the cell (239). Moreover, different signaling outcomes can originate from receptors in distinct subcellular regions.

When activated by canonical mechanisms, PAR_1 (240), PAR_2 (122, 201, 241, 242), and PAR_4 (237) all undergo clathrin-mediated endocytosis (sect. 4.8). While it is unknown whether extracellular proteases internalize alongside PARs, fluorescent PAR_2-activating peptides rapidly internalize (243). The capacity of PAR_2 to signal from endosomes has been extensively studied. Trypsin and activating peptides induce the assembly of PAR_2, G protein, and β-arrestin signalosomes in model cell lines (HEK, KNRK), colonocyte cell lines, and DRG neurons (201, 203). Endosomal PAR_2 signaling leads to activation

Downloaded from journals.physiology.org/journal/physrev at New York Univ (216.165.095.084) on September 28, 2023.

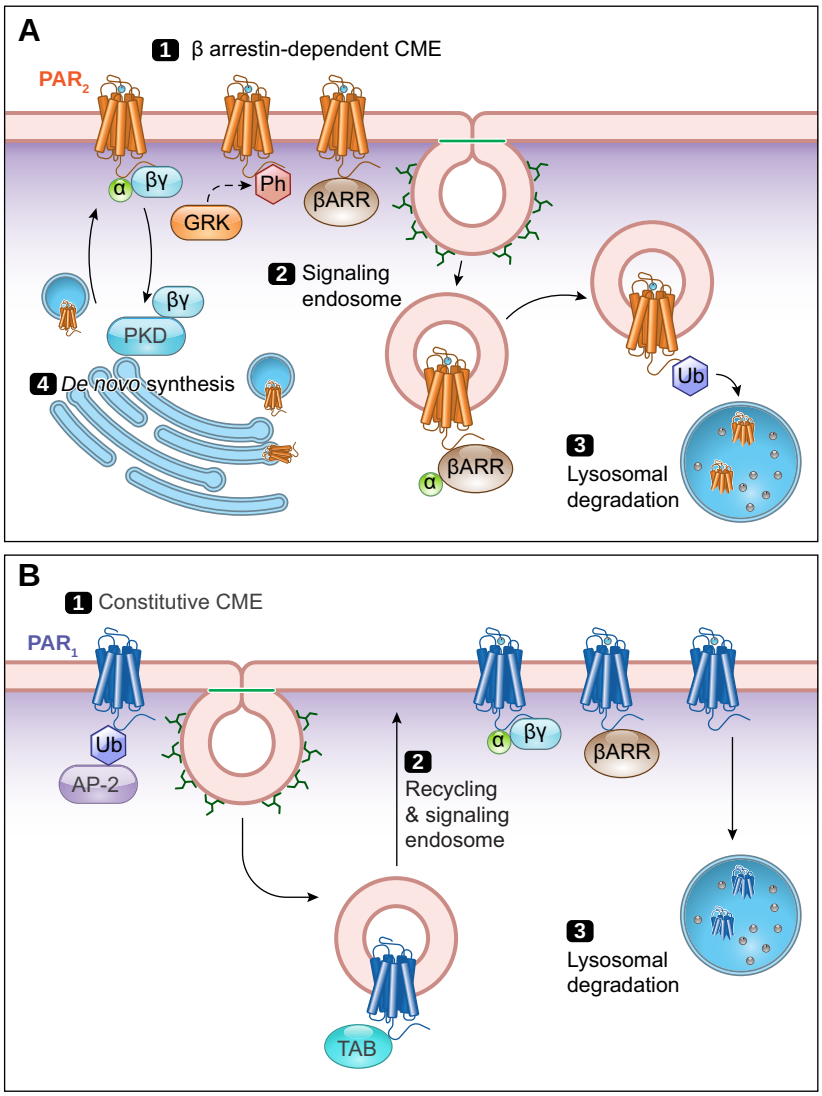

FIGURE 5. Trafficking of protease-activated receptors (PARs). *A*: PAR_2 activation leads to Gα/βγ recruitment, phosphorylation (Ph; red) by G protein-coupled receptor (GPCR)-regulated kinase (GRK), and β-arrestin (βARR) recruitment (*1*). This triggers clathrin-mediated endocytosis (CME). Internalized PAR_2 continues to signal from endosomes (*2*). Ubiquitination (Ub; blue) of the COOH terminus triggers trafficking to lysosomes for degradation (*3*). To replace the cleaved receptor, PAR_2 signaling induces Gβγ-mediated activation of PKD in the Golgi apparatus, which mobilizes newly synthesized PAR_2 to repopulate the plasma membrane (*4*). *B*: PAR_1 is subject to constitutive CME upon ubiquitination and AP-2 recruitment (*1*). In contrast to PAR_2, it is not subject to βARR-dependent endocytosis. PAR_1 can signal from endosomes in a ubiquitin-driven manner with adaptor proteins TABs to drive p38 MAPK signaling (*2*). Uncleaved PAR_1 is returned to the plasma membrane via recycling endosomes. Cleaved PAR_1 signals with Gα/βγ. Similarly, PAR_1 is then degraded in the lysosome (*3*).

of ERK1/2 in the cytosol and nucleus, mediating the effects of trypsin and tryptase on paracellular permeability of colonocytes (244) and excitability of nociceptors (203). PAR_1 and PAR_4 also signal from endosomes. Ubiquitinated PAR_1 in endosomes interacts with adaptor proteins to mediate p38 MAPK signaling (208). Although β-arrestin knockdown has no effect on PAR_4 endocytosis, siRNA targeting a subunit of adaptor protein-2 (AP-2) or mutations in PAR_4 ICL3 inhibit internalization. Inhibition of PAR_4 endocytosis enhances ERK1/2 phosphorylation, whereas internalization is required for Akt signaling (237). Some proteases do not cause PAR_2 internalization, including elastase (146, 147), cathepsin S (145), and legumain (149). As such, inhibiting endocytosis has no effect on signaling or nociceptive responses initiated by these proteases (203).

PAR signaling can also be modulated by receptor localization in membrane microdomains, including lipid rafts. PAR_1 and EPCR colocalize in cholesterol-rich lipid rafts in endothelial cells (245). Lipid rafts are vital for the protective barrier effects of APC since methyl-β-cyclodextrin, a cholesterol-chelating agent that disrupts lipid rafts, blocks the cytoprotective effects of APC (246). Filipin, which also disrupts lipid rafts, inhibits thrombin and MLC kinase-mediated cytoskeletal changes in endothelial cells (247). Cavaeloe ("little caves") are specialized lipid rafts. Disruption of caveolae using siRNA against caveolin-1 has no effect on thrombin-mediated cytoskeletal changes (247). In contrast, the cytoprotective effects of APC via Rac1 activation and protection from endothelial barrier permeability are abolished in cells lacking caveolin-1 (229).

4.7. Downstream Targets of PAR Signaling

4.7.1. Transactivation with receptor tyrosine kinases.

GPCRs transactivate receptor tyrosine kinases (RTKs) and vice versa. A seminal study of GPCR/RTK

Downloaded from journals.physiology.org/journal/physrev at New York Univ (216.165.095.084) on September 28, 2023.

transactivation investigated PAR-mediated upregulation of epidermal growth factor receptor (EGFR) signaling (248; **FIGURE 4C**). Rapid RTK phosphorylation is observed in response to thrombin and PAR_1-activating peptide (248). Considering these agonists could act through multiple PAR subtypes, it was later shown to be PAR_1 dependent (249). PAR/EGFR transactivation can occur through multiple mechanisms. PAR activation can stimulate the release of EGFR agonists following MMP activation (250), cleaving amphiregulin (heparin-binding EGF) to enable EGFR activation (**FIGURE 4C**). Additionally, Src kinase can mediate thrombin- or TRAP-induced EGFR transactivation, as demonstrated using an Src kinase inhibitor or immunoprecipitation (249, 251). PAR_2/EGFR transactivation is also observed in HT-29 colon cancer cells, where PAR_2 activation by trypsin or PAR_2-activating peptide leads to Src kinase activation and MMP-dependent release of an EGFR ligand (252). In lung-derived A-549 epithelial cells, SLIGRL-mediated activation of PAR_2 leads to EGFR phosphorylation, as well as delayed, persistent p38 MAPK activation blocked by the EGFR inhibitor PD153035 (253). PAR_2-mediated EGFR transactivation is also seen in epithelial cells via an Src-dependent mechanism (254). Src-mediated PAR_2/EGFR transactivation is observed in response to trypsin or activating peptide in ovarian cancer cells that endogenously overexpress PAR_2 with an enhanced migratory and invasive phenotype. PAR_2 transactivates EGFR through $G\alpha_{q/11}$, $G\alpha_{12/13}$, and β-arrestin but not $G\alpha_s$ or $G\alpha_i$ (255). In lung cancer cells, coinhibition with the EGFR inhibitor gefitinib and 2pal-18S leads to synergistic inhibition of EGFR phosphorylation, ERK1/2 phosphorylation, and tumor growth (255).

PARs can also transactivate platelet-derived growth factor receptors (PDGFRs). PAR_1 and PDGFRs are coexpressed in the spinal cord, where thrombin-induced hyperalgesia is reduced in the presence of recombinant mouse PDGFR/Fc chimera (256). PAR_2-induced Src signaling mediates PDGFR transactivation, leading to chemotaxis in monocytes, fibroblasts, and endothelial cells (257). PAR_2 also transactivates the hepatocyte growth factor (HGF) receptor Met involved in liver cancer metastasis (258). PAR_2 activation causes Met transactivation in hepatocarcinoma cells independently of HGF release. PAR_2-mediated cell invasion via ERK1/2 is sensitive to Met inhibition following siRNA knockdown or pharmacological inhibition with SU 11274 or PHA 665752. In endothelial cells, thrombin/PAR_1 signaling also transactivates the vascular endothelial growth factor (VEGF) receptor 2 via MAPK phosphatase and ERK1/2 signaling (259).

4.7.2. TRP ion channels.

Numerous studies have shown PAR activation sensitizes TRP channels, which is relevant to protease-evoked neurogenic inflammation and pain (sect. 5.5; **FIGURE 4D**). PAR_2 activation sensitizes TRPV1 in DRG neurons, which results in thermal hyperalgesia (97, 260, 261). The TRPV1 antagonist capsazepine blocks thermal hyperalgesia induced by selective PAR_2 agonists (262). Mechanistically, PAR_2-mediated TRPV1 sensitization is mediated by PKCε and protein kinase A (PKA) (97, 260, 261). TRPV1 sensitization in response to activating peptides for PAR_1 or PAR_4 is also mediated by PKCε signaling (185). PAR_2-mediated TRPV1 potentiation in response to SLIGRL is absent in PAR_2 knockout mice (109). PAR_2-mediated sensitization of TRP channels is responsible for chemotherapy-induced neuropathy following paclitaxel exposure (263). Pain responses are inhibited by a selective PAR_2 antagonist, as well as inhibitors of PKCε and PKA. Paclitaxel-induced hyperalgesia is reduced by inhibitors of TRPV4 (RN1734), TRPV1 (capsazepine, SB366791), and TRPA1 (HC030031).

PAR_2 also sensitizes TRPV4 signaling, with relevance to pain (147, 200, 264). PAR_2-induced mechanical allodynia is absent in TRPV4 knockout mice (264). PAR_2-activating peptide leads to enhanced firing of colonic DRG neurons in response to TRPV4 agonists (265). PAR_2 activation induces a sustained TRPV4-mediated Ca^{2+} influx from extracellular ions (200, 266). Dependent on the TRPV4 Tyr110 residue, this is sensitive to inhibitors of PLA_2 and arachidonic-derived lipid mediators, the latter suggesting links to the release of TRPV4 agonists such as epoxyeicosatrienoic acid (200). Trypsin and PAR_2 agonist-mediated sensitization of mouse aorta contractions via TRPV4 is reduced in the presence of PKC inhibitor Go6983 (267). In the hippocampus, the PAR_2 agonist AC55541 also leads to long-term depression following PKA-dependent TRPV4 phosphorylation (268). TRPV4 sensitization has been shown for different proteases cleaving PAR_2, including cathepsin S (145). Cathepsin S/PAR_2-evoked sensitization of TRPV4 is dependent on adenylyl cyclase and PKA. Elastase evokes PAR_2-dependent sensitization of TRPV4 by a similar mechanism (147). TRPV4 potentiation by PAR_2 is inhibited in the presence of the EGFR kinase inhibitor AG1478 in the mouse aorta (267). TRPV4 sensitization is also observed in response to PAR_1 activation in endothelial cells, whereby TRPV4 contributes to sustained Ca^{2+} signaling and endothelial junction remodeling (269). There are also links between PAR_4 and TRP channel sensitization. DRG neurons do not signal in response to PAR_4-selective AYPGKF. Instead, AYPGKF reduces capsaicin-induced Ca^{2+} signaling and reverts inflammatory hyperalgesia in a dose-dependent manner (270). In response to PAR_4

Downloaded from journals.physiology.org/journal/physrev at New York Univ (216.165.095.084) on September 28, 2023.

agonist peptide AYPGKF-NH_2, Ca^{2+} mobilization is reduced when stimulated with pronociceptive PAR_2 agonists or TRPV4 agonist 4αPDD in colonic sensory neurons (111). This endogenously acts to reduce nociception.

PAR_2 also potentiates responses to TRPA1 (271). TRPA1 is expressed on sensory neurons, including those that innervate the intestine, where it mediates mechanosensation (272). TRPA1 is activated by allyl isothiocyanate (AITC), the spicy component of mustard that also activates TRPV1. Covalent modification of cytosolic NH_2-terminal TRPA1 residues (Cys621, Cys641, Cys665) leads to channel activation (273). TRPA1 sensitization is partly mediated by increased channel insertion into the membrane (274). PKA phosphorylates four serine residues (Ser86, Ser317, Ser428, Ser972) proposed to contribute to TRPA1 sensitization. Potentiated currents are sensitive to inhibitors or PIP_2 or PLC, showing that PAR_2 sensitizes TRPA1 via membrane hydrolysis of PIP_2. In comparison to TRPV1 sensitization, the mechanism of PAR_2-mediated sensitization of TRPA1 does not involve PKC. Studies have also shown that PAR_2 sensitizes responses to acid-sensing ion channel 3 (ASIC3). Potentiation by PAR_2-activating peptide causes a dose-dependent increase in acetic acid-induced hyperalgesia in rats in a PAR_2-specific manner (275).

4.7.3. Genes.

It is well-established that PAR signaling leads to transcriptional changes that alter gene expression. Early studies showed thrombin or FXa stimulation activates NF-κB, a known regulator of gene transcription (13). Gene expression microarrays have since demonstrated hundreds of genes are regulated by PAR_1 (276) or PAR_2 (277) signaling. Considering their central role in the immune system, PAR activation leads to the upregulation of proinflammatory cytokines and chemokines across cell types. For example, IL-6 and IL-8 are released from HUVECs in response to FXa and thrombin (199). IL-8 secretion induced by thrombin has also been attributed to PAR_3 activation in lung epithelial cells and human astrocytoma cells (168). Activation of both PAR_1 and PAR_2 leads to IL-8 expression in epithelial cells through NF-κB- and ERK1/2-dependent pathways (278). In human lung A-549 epithelial cells, PAR_2 stimulation leads to prostaglandin E2 (PGE_2) formation (253, 279). PAR_2-mediated IL-8 upregulation in A-549 cells is sensitive to MEK, JNK, and EGFR inhibitors (280). Treating mice with a PAR_2 agonist leads to the release of IL-4, IL-6, IL-13, and TNF-α, many of which are reduced in β-arrestin knockout mice (281). Studies have demonstrated PAR_2-dependent release, as CXCL8, IL-8, IL-6, CTGF, and CSF2 are released in response to the PAR_2 agonist and inhibited by I-191 (282). SLIGRL-mediated activation of PAR_2 in A-549 epithelial cells upregulates cyclooxygenases (COX-1, COX-2) (253). PAR_2 activation in A-549 cells upregulates prostaglandin E synthetase isoform 1 (mPGE-1) and COX-2, dependent on prostanoids formed via MEK/ERK/$cPLA_2$/COX-1 (279).

Noncanonical proteases can alter gene expression, such as downstream of APC/PAR_1/EPCR in HUVECs (63). This alters expression of genes encoding the nuclear hormone receptor TR3, the immunomodulatory monocyte chemoattractant MCP-1, and a negative regulator of calcineurin (63). Granzyme K also causes a concentration-dependent release of IL-6, IL-8, and MCP-1 from human lung fibroblasts, sensitive to PAR_1 or ERK1/2 inhibitors (283). KLK-5 leads to PAR_2/NF-κB signaling and changes in microRNA expression in oral cells (284). In addition to distinctions between proteases, gene expression is modulated by other membrane proteins. For example, PAR_2 is expressed alongside Toll-like receptor 4 (TLR4) in macrophages and colonic epithelial cells. Functional cross talk between PAR_2 and TLR4 can induce NF-κB signaling (285). Growth factors are also released in response to PAR activation, such as the release of PDGF in response to FXa stimulation of vascular smooth muscle (286). PAR_1-activating peptide induces PDGF secretion from epithelial cells derived from the lung (287). PAR_2-activating peptide and FXa stimulate the expression of connective tissue growth factor involved in its profibrotic events in endothelial cells (174).

Genes involving the ECM network of proteoglycans and glycosaminoglycan chains are also modulated by PAR signaling. FXa and thrombin activation increases expression of ECM-associated proteins that modulate adhesion, Cyr61, and CTGF (13). PAR_1 signaling also induces ECM production, whereby FXa and thrombin both stimulate procollagen gene expression in mouse fibroblasts, absent in the PAR_1-deficient mouse fibroblasts (288). Thrombin also increases expression of a glycosaminoglycan biosynthesizing enzyme via PAR_1 RTK transactivation (289).

PARs therefore act as the first step that triggers "feed-forward signaling" through a multitude of downstream outcomes mediated by other receptors. These signaling events can have different kinetics and degrees of signal amplification, which enable both a rapid and prolonged response to proteases. For example, TRP channel sensitization and RTK transactivation are rapid (seconds to minutes), whereas transcriptional regulation is more sustained (minutes to hours). The release of agonists acting through other receptors can also have a variable timeframe, such as prostanoids secreted from epithelial cells. Considering there is context dependence across even different cell lines, we have a limited understanding of feed-forward signaling in endogenous human systems.

Downloaded from journals.physiology.org/journal/physrev at New York Univ (216.165.095.084) on September 28, 2023.

4.8. Termination and Recovery of PAR Signaling

4.8.1. PAR desensitization.

Desensitization rapidly terminates signaling of PARs. There are distinct mechanisms through which PAR signaling is terminated that differ in their kinetics and downstream outcomes. These mechanisms include receptor desensitization due to irreversible proteolysis and G-protein uncoupling, endocytosis-mediated trafficking and subsequent receptor degradation. Once cleaved, PARs can no longer respond to proteases due to removal of the cleavage site. This is a rapid process occurring on a timescale of seconds to minutes. For example, exposure of DRG neurons to tryptase prevents subsequent Ca^{2+} responses to trypsin (95). Similarly, exposure to trypsin prevents subsequent thrombin/PAR_1 activation in Jurkat cells (159). Protease-cleaved PARs can, however, still respond to activating peptide, as shown for thrombin-activated PAR_1 (290).

Another method of PAR desensitization involves endocytosis. Relative to desensitization, endocytosis and degradation are slower. The trafficking of many GPCRs is regulated by phosphorylation of the COOH-terminal domain by GPCR kinases (GRKs). The COOH terminus of PAR_1 (291, 292) and PAR_2 (242) are rapidly phosphorylated at Ser/Thr residues in response to activation. GPCR phosphorylation is often required for β-arrestin recruitment and receptor endocytosis. However, PAR_1 recruitment of β-arrestin is phosphorylation independent (236). Despite this, mutagenesis of PAR_1 Ser/Thr residues causes reduced endocytosis, slower desensitization, and more robust signaling (291, 293, 294). Accordingly, enhancing PAR_1 phosphorylation by GRK overexpression reduces thrombin-induced signaling (291, 295). There are also differences between GRK isoforms, whereby the termination of PAR_1 signaling involves GRK5 (295). Another mechanism of PAR desensitization involves regulators of G-protein signaling (RGS proteins). RGS proteins are cytoplasmic GTPase-activating proteins that accelerate GTP hydrolysis, thereby reducing GPCR signaling. These directly interact with PAR_1 at ICL3, reducing Ca^{2+}-activated chloride currents and ERK1/2 phosphorylation (296, 297). This is also observed for PAR_2 (298) and PAR_4 (299).

Some studies have solely attributed β-arrestin to receptor desensitization. Although not required for PAR_1 endocytosis, β-arrestin overexpression reduces thrombin-induced IP_3 production (236). Similarly, phosphatidylinositol hydrolysis is reduced upon β-arrestin overexpression in cells expressing PAR_1 (300). On the other hand, studies have linked β-arrestin knockdown to signaling. In a pathway-specific manner, thrombin-induced PI3K and Akt signaling is reduced by dominant-negative β-arrestin without affecting ERK1/2 (212). PAR_1/β-arrestin coupling is linked to APC-mediated cytoprotective signaling, in contrast to thrombin-mediated ERK1/2 and Rho GTPase endothelial disruption (301). FVIIa/PAR_1-mediated Akt phosphorylation is also reduced in endothelial cells with β-arrestin siRNA (14). Contradicting studies have also been shown for PAR_2. Implicating its role in desensitization, numerous PAR_2-expressing cell types lacking β-arrestin have increased phosphatidylinositol hydrolysis (302). Likewise, mutant PAR_2 unable to interact with β-arrestin (Ser636Ala/Thr366Ala) has sustained Ca^{2+} and ERK1/2 signaling kinetics (201). β-Arrestin knockout cells expressing PAR_2 have prolonged Ca^{2+} signaling in response to SLIGRL or trypsin (187). β-Arrestin knockdown also causes distinct kinetics in ERK1/2 phosphorylation with a sustained signaling profile in response to trypsin in the absence of desensitization (302). In contrast, other studies have shown that ERK1/2 phosphorylation is reduced in the absence of β-arrestin (146). This is also shown for PAR_2-mediated inflammation, as β-arrestin knockout mice have reduced proinflammatory cytokine production or leukocyte recruitment in response to a PAR_2 agonist (281). There is evidence for direct interactions between PAR_2, β-arrestin, and ERK1/2 using coimmunoprecipitation (201), as well as between β-arrestin and PI3K, albeit with an inhibitory outcome on Akt signaling (209).

While there are distinctions between PAR_2 and PAR_1/PAR_4 trafficking, each subtype undergoes clathrin-mediated endocytosis (**FIGURE 5**). Fluorophore-labeled PAR_2 shows β-arrestin recruitment to the plasma membrane within 5 minutes of trypsin stimulation, followed by receptor/β-arrestin internalization within 10 minutes in KNRK cells (241). PAR_2 is internalized into $Rab5^+$ endosomes (303). There has since been evidence using BRET between luciferase-tagged PAR_2 and fluorescent subcellular markers to demonstrate trafficking in response to trypsin within 5–10 minutes sensitive to dominant-negative dynamin (203). This was demonstrated in colonocytes using BRET, as well as in vivo using mice expressing PAR_2 fused to green fluorescent protein (39).

Unlike PAR_2 (**FIGURE 5*A***), the trafficking of PAR_1 and PAR_4 away from the plasma membrane occurs through distinct mechanisms. PAR_1 endocytosis is phosphorylation and β-arrestin independent (236, 300, 304, 305; **FIGURE 5*B***). PAR_1 is subject to dynamin-mediated endocytosis into clathrin-coated pits (240) and rapidly internalizes in response to SFLLRN (306) or thrombin (307). Unlike PAR_2, PAR_1 is also subject to constitutive endocytosis (293). PAR_1 constitutive endocytosis is regulated by ubiquitylation, whereby mutating ubiquitinated Lys residues causes enhanced constitutive endocytosis (304). This is mediated by interactions of AP-2 with a COOH-

Downloaded from journals.physiology.org/journal/physrev at New York Univ (216.165.095.084) on September 28, 2023.

terminal tyrosine motif in PAR_1 that can be mutated to AKKAA (305, 306). However, cultured cells may secrete proteases that endogenously activate PARs by an autocrine mechanism. These proteases could activate PAR_1, evoke endocytosis, and thus account for spontaneous PAR turnover. PAR_4 is internalized with slower kinetics than PAR_1 in response to stimulation, albeit similarly independent of phosphorylation or β-arrestin (194, 237). PAR_4 endocytosis is, however, clathrin mediated with inhibition by dominant-negative dynamin (237). PAR_4 is also internalized from the plasma membrane via AP-2 binding, instead of through a highly conserved tyrosine motif in the ICL3 (237).

4.8.2. PAR lysosomal targeting and downregulation.

PARs are activated in an irreversible manner and are ultimately degraded rather than recycled. There are differences between PAR_1 and PAR_2 with respect to pathways that lead to receptor degradation. PAR_2 is ubiquitinated and then targeted to lysosomes for degradation (308–310). PAR_2 signaling leads to phosphorylation and activation of c-Cbl, an E3 ligase, that directly ubiquitinates PAR_2 Lys residues (310). In the absence of Lys residues or in cells expressing dominant-negative c-Cbl, PAR_2 is retained in endosomes without degradation. Lysosomal PAR_2 degradation then occurs via a component of ESCRT-0, the HGF-regulated tyrosine kinase substrate (HRS) (309). As observed for endocytosis, not all proteases cause lysosomal degradation. Trypsin and its activating peptide lead to colocalization with a lysosomal marker within 2 hours, whereas elastase does not (311).

In contrast, PAR_1 is targeted to lysosomes in an ubiquitin-independent manner through an ESCRT-III–dependent pathway (312). PAR_1 is directed to lysosomes via interactions with a Tyr-based motif in ICL2, interacting with adaptor protein ALG-2-interacting protein X (ALIX) in multivesicular bodies. Direct interactions with an ESCRT complex bypass the requirement for ubiquitination. siRNA against ALIX, or PAR_1 mutagenesis to Tyr206Ala, highlights the importance of this interaction for rapid lysosomal sorting. PAR_1 lysosomal sorting is also regulated by palmitoylation at Cys residues in the COOH terminus (313). In the absence of this palmitoylation site, there is increased constitutive internalization and degradation mediated by AP-3. PAR_1 lysosomal degradation is modulated by tumor suppressor α-arrestin domain-containing protein-3 (ARRDC3), a protein that acts via ALIX to mediate PAR_1 degradation (314). Invasive breast cancers exhibit a loss of ARRDC3, thus reducing lysosomal degradation for sustained, aberrant PAR_1 signaling.

In terms of the other PAR subtypes, initial studies have identified PAR_4 in lysosomes after agonist stimulation (237). Although in a similar localization to PAR_1, this is independent of the COOH terminus. PAR_4 degradation is mediated through a conserved tyrosine motif in ICL3 involved in AP-2 interactions.

4.8.3. Recovery of PAR signaling.

Many GPCRs for hormones and neurotransmitters recycle from endosomes to the plasma membrane, typically involving Rab11 GTPases that control vesicle formation; this recycling mediates resensitization. Constitutive PAR_1 endocytosis is considered to enable rapid recovery of signaling by returning uncleaved PAR_1 to the plasma membrane (292, 315). Uncleaved PAR_1 is directed to the plasma membrane via Rab11b-dependent sorting, in opposition with Rab11a-mediated targeting for lysosomal degradation (316). The requirement of constitutive PAR_1 internalization for resensitization to signaling is demonstrated in endothelial cells. Mutating the tyrosine motif responsible for AP-2 interactions, or using siRNA against AP-2, prevents endothelial cells from gaining responsiveness to thrombin (306).

Following protease stimulation, PARs are not recycled to return to the plasma membrane given their nature of irreversible cleavage. This was investigated with respect to PAR_1 using a "P/S" chimera with the COOH terminus of neurokinin 1 receptor (NK_1R, substance P receptor) (317, 318). Whereas wild-type PAR_1 was destined for lysosomal degradation, the protease-stimulated chimera recycled to the plasma membrane, allowing persistent signaling to thrombin and activating peptide.

Recovery of PAR_2 signaling at the cell surface occurs by a different mechanism that requires mobilization of intact receptors from Golgi stores in a Rab11-dependent manner (303, 308) (**FIGURE 5*A***). Dominant-negative Rab11 Ser25Asn causes receptor retention in the Golgi apparatus, whereas Rab11a overexpression accelerates trafficking from the Golgi to the plasma membrane (303). PAR_2 translocation from the Golgi is Gβγ and PKD dependent and is responsible for recovery of signaling at the cell surface (148, 319). This mechanism of recovery is similar to when PAR_2 is activated by canonical (trypsin) or biased (cathepsin S, elastase) mechanisms (148, 319). This process underlies sustained protease- and PAR_2-evoked pain since inhibitors of Gβγ and PKD attenuate mechanical allodynia in response to proteases in mice.

4.9. Summary

Proteases with varying selectivity can cleave PARs at distinct sites, leading to divergent pathways of receptor signaling and trafficking. Biased signaling can arise from

Downloaded from journals.physiology.org/journal/physrev at New York Univ (216.165.095.084) on September 28, 2023.

exposure of different tethered ligands or stabilization of unique receptor conformations. Alternatively, proteases can disarm PARs by removal of cleavage sites or tethered ligand domains. Synthetic peptides that mimic tethered ligand domains (activating peptides) have been instrumental in delineating PAR signaling pathways and the complex modulation of PARs in heteromeric complexes with other GPCRs. While less is known for PAR_3, the other PAR subtypes activate signaling pathways linked to Ca^{2+}, cAMP, MAPK/ERK, PI3K/Akt, and Rho GTPases. PARs can also induce RTK transactivation, ion channel sensitization, and changes in gene expression. PARs also undergo endocytosis to regulate their localization and turnover with distinctions between mechanisms governing PAR_1 and PAR_2.

5. PARS IN PHYSIOLOGY AND PATHOLOGY

There are several challenges to delineating the function of PARs in health and disease states. Multiple proteases are capable of activating PARs, and, in some instances, the relevant proteases are not known. Although thrombin is an established agonist of PAR_1 in the circulatory system, the proteases that activate PAR_2 in different healthy and diseased tissues are not well understood. Since proteases are regulated through control of their activity, rather than expression, insight into the proteases that activate PARs requires profiling activated proteases. Activity-based probes that irreversibly bind to activated proteases are valuable tools for profiling proteases that are activated in diseased tissues (320). Pharmacological studies of PARs are hampered by the inadequate potency and selectivity of some PAR antagonists and the promiscuity of certain activating peptides that signal through multiple PAR subtypes. Genetic deletion studies, particularly cell-specific deletion of PARs, have provided valuable insights into functions, although compensatory changes can complicate the interpretation of results. Section 5 will discuss the role of PARs by the organ system in health and disease states.

5.1. PARs in the Circulatory System

5.1.1. Physiology.

The role of PARs in hemodynamic maintenance was proposed soon after their discovery, by the finding that intravenous administration of trypsin or thrombin produced endothelium-dependent acute hypotension in dogs (321). However, the effects of PAR activation on the vascular system (**FIGURE 6*A***) depend on species, age, whether endothelial cells or vascular SMCs are studied, and the proteases under investigation. For example, canonical activation of PAR_1 by thrombin produces a contractile, dedifferentiated phenotype, whereas biased activation of PAR_1 by MMP1 leads to dedifferentiation and hyperplasia of SMCs (232).

PAR_1 and PAR_4 mediate thrombin signaling in platelets and thrombosis (322; **FIGURE 6*B***). PAR_1-mediated contraction is endothelium dependent and mediated by prostacyclin and nitric oxide (NO), an effect observed in humans (323, 324). PAR_1 activation contributes to vascular permeability and edema, which involves substance P activation of NK_1R on endothelial cells, the first evidence that thrombin mediated neurogenic inflammation (325). PAR_2 activation leads to vasodilation by release of NO and endothelin from endothelial cells (326, 327). At a systems level, PAR_2 activation induces hypotension by the L-arginine/NO pathway. The vasodilatory effects of PAR_2 activation are greater than for PAR_1 and PAR_4 (164). PAR_2-mediated vasodilation has been proposed to protect against heart ischemia, disseminated intravascular coagulation, and endotoxemia (328).

Proteases that participate in coagulation that can cleave PARs include thrombin, APC, TF-FVIIa, and TF-FVIIa-FXa. TF-FVIIa generates FXa, which can cleave PAR_1 and PAR_2. The complex of TF-FVIIa-Xa and EPCR can also cleave PAR_1 or PAR_2 (329). The APC-EPCR complex, as part of the protein C pathway, can cleave PAR_1 (63; **FIGURE 6*C***). FVIIa-EPCR can cleave PAR_1 on endothelial cells (330). TF-FVIIa cleaves and signals through PAR_2, which contributes to several pathologic conditions, especially cancer. PAR_2 signaling following cleavage by TF-FVIIa affects integrin function and angiogenesis (331). The ternary complex TF-FVIIA-FXa cleaves PAR_2. The TF pathway inhibitor inhibits the ternary complex; therefore, PAR signaling is also reduced (332). Thrombin activation of platelets leads to the secretion of endostatin, which inhibits angiogenesis. This effect is mediated by PAR_4 (333).

The processes of thrombosis and inflammation are interlinked and reciprocal (334). Coagulation mediates both processes, where the factors and associated proteases activate PARs. For example, mannose-binding lectin-associated serine protease-1 (MASP-1) can activate PAR_1 and PAR_4 on platelets and endothelial cells, while MASP-2 activates the complement system starting with C4 and C2 (335, 336). Thrombin activates PAR_1, PAR_3, and PAR_4, and plasmin activates PAR_1 and PAR_4. PAR_2 is cleaved by trypsin, tryptase, TF, FVIIa, and FXa (43). Thrombin activation of PAR_1 and PAR_4 in humans leads to procoagulant activity through the release of α-granules and dense granules from platelets, which facilitates inflammation.

Following activation by the proteases associated with coagulation, PARs mediate a myriad of cellular effects on leukocytes that contribute to their role in the innate

Downloaded from journals.physiology.org/journal/physrev at New York Univ (216.165.095.084) on September 28, 2023.

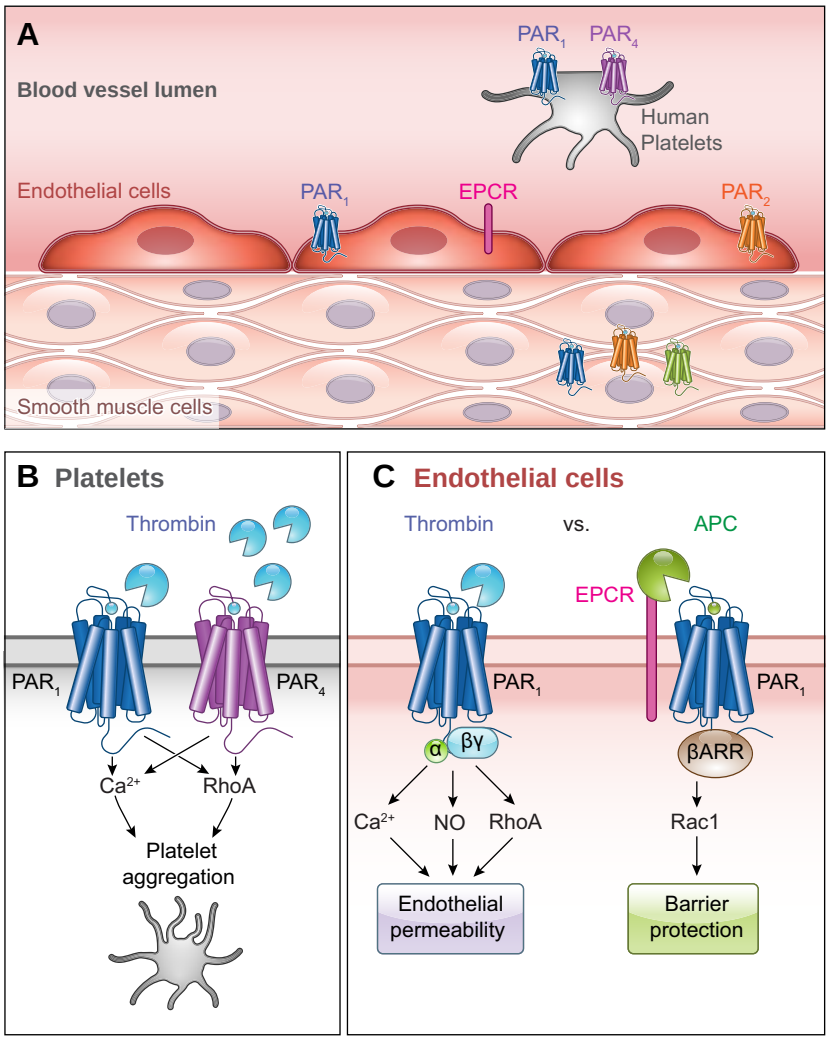

FIGURE 6. Role of protease-activated receptors (PARs) in the circulatory system. *A*: PARs are expressed in various cell types in the vasculature and circulation. *B*: human platelets expressing PAR_1 and PAR_4 respond to low- or high-thrombin concentrations to aggregate platelets. *C*: endothelial PAR_1 has distinct signaling outcomes in response to thrombin or activated protein C (APC) bound to endothelial protein C receptor (EPCR). NO, nitric oxide.

immune system. Activation of PAR_1 on murine mast cells increases adhesion to fibronectin and laminin (117). Thrombin/PAR_1 signaling mediates inflammation by endothelial cell activation, which leads to monocyte activation and increases the permeability of endothelial cells. Activation of PAR_2 on eosinophils leads to the generation of superoxide anion and degranulation (124, 126). Similarly, activation of PAR_2 either by trypsin or the activating peptide SLIGKV leads to degranulation of histamine from mast cells (121, 337). Activation of PARs leads to leukocyte recruitment, an effect that was demonstrated by injection of proteases and activating peptides into the airways of mice (specifically, thrombin activation of PAR_4), which leads to the recruitment of polymorphonuclear cells (338). Catalytic activity of thrombin is not required for activation and chemotaxis of innate immune cells; the mechanism likely involves integrin activation (169, 339, 340). PARs also contribute to the adaptive immune response that follows coagulation. Activation of PAR_2 of T_H2 lymphocytes in mice leads to secretion of IL-31, which activates neurons and enhances neuroimmune signaling (341). The activation of PAR_1 on T lymphocytes leads to the secretion of IL-6 and IL-8 (342).

In addition to differences in PAR subtype expressed by platelets (rat/mouse: PAR_3, PAR_4; human: PAR_1, PAR_4; sect. 3.4), there are species differences in the signaling pathways and platelet response to PAR activation. This must be considered as drugs are developed for the treatment of diseases that are a consequence of dysregulation of the coagulation system. Both thrombin and SFLLRN, which activate PAR_1, have the following effect on platelets: activation of PLC, PI3K, and PKC, inhibition of adenylyl cyclase, and tyrosine phosphorylation of platelet proteins including a 47-kDa protein known as P47 or pleckstrin (343). While thrombin produces platelet aggregation and an increase in cytosolic Ca^{2+} in all species, SFLLRN activates PAR in guinea pigs, monkeys, and human platelets (40).

The activation of PAR_1 and PAR_4 on human platelets by their selective activating peptides has divergent effects with angiogenesis (333). Activation of both PARs

Downloaded from journals.physiology.org/journal/physrev at New York Univ (216.165.095.084) on September 28, 2023.

leads to platelet aggregation; activation of PAR_4 alone leads to platelet retraction (344). Activation of PAR_1 induces VEGF release and suppresses endostatin release. In contrast, activation of PAR_4 results in endostatin release, as occurs in the rat, and suppresses VEGF secretion. PAR_1 is not expressed by rat or mouse platelets; however, rat platelets demonstrate a response to PAR_1 agonists (345, 346). Moreover, in vivo effects (gastric ulcer healing) are observed in rats in response to a PAR_1 antagonist (333). As such, studies in rodent platelets should be extrapolated with caution to humans.

5.1.2. Pathology.

Cells including monocytes, macrophages, lymphocytes, vascular SMCs, and platelets contribute to circulatory system pathology. PARs expressed on vascular SMCs, macrophages, and platelets contribute to diseases of the circulatory system, especially atherosclerosis and thrombosis.

In addition to its contribution to atherosclerosis, PAR_2 on monocytes, macrophages, and endothelial cells contributes to vessel stability and health. PAR_2 on monocytes mediates the effects of ischemia on vessel walls (347). Moreover, inflammation upregulates PAR_2 on the endothelial cells (324, 348). Accordingly, PAR_2 is upregulated in human coronary atheromas. Similarly, atherosclerotic aortas from mice that are *ApoE*-/- exhibit upregulation of PAR_2 (349). Plaques from PAR_2-/- mice are characterized by reduced levels of MMP9 and smooth muscle actin, along with increased collagen content in the plaques. Activation of PAR_2 induces expression of inflammatory cytokines in macrophages (350). On the other hand, PAR_2 stabilizes atherosclerotic plaques through the following: plaque progression is halted and stabilized, vascular inflammation and the associated macrophage response are reduced, and the adhesion between macrophages and vascular SMCs is lowered. Decreased adhesion between macrophages and vascular SMCs leads to reciprocal effects of the two cell types; namely, decreased expression of VCAM-1 and ICAM-1 by vascular SMCs and reduced TNF-α and MCP-1 expression by macrophages. PAR_2 further affects plaque stability through new blood vessel formation and revascularization (351, 352).

PAR_1 and PAR_4 on platelets facilitate aggregation and subsequent thrombosis. When thrombin cleaves PAR_1, PLCγ leads to increased intracellular Ca^{2+}, in addition to the activation of integrin $\alpha_{IIb}\beta_3$ that leads to platelet aggregation. Antiplatelet therapy has been investigated extensively to reduce the generation of thrombi. Vorapaxar is a PAR_1 antagonist approved for the treatment of patients who have suffered a myocardial infarction (sect. 6.1). Despite the central role of thrombin activation of PARs in atherosclerosis, platelet activation by mediators other than thrombin is sufficient to produce atheromas (353). This finding was demonstrated using ApoE-/- mice, which are prone to develop atherosclerotic plaques. The role of PAR_4 was demonstrated using PAR_4-/- mice. Mouse platelets require PAR_4 for activation by thrombin, and platelets from PAR_4-/- mice do not respond to thrombin, as measured by Ca^{2+} mobilization (322, 354). The investigators showed that atheromas on the aorta of the mice did not differ in size, extent, or location between PAR_4-/- and WT mice.

Due to the differential expression and signaling of PAR_1 and PAR_4 on platelets and their role in forming a clot (**FIGURE 6*B***), the two PARs are an attractive target for the development of antagonists to treat cardiovascular disease and cerebrovascular disease. Studies related to PAR_1 led to the development of vorapaxar, which is selective for PAR_1 but not PAR_4. PAR_1 mediates strong blood clotting, while the effect of PAR_4 activation leads only to platelet aggregation, a response similar to that seen with weaker agonists such as epinephrine and ADP (163).

Most publications on the role of PARs on vascular SMCs report effects on these cells harvested from the aorta, and few studies have focused on cerebral arterioles. Misaki et al. (355) studied the response of SMCs from rat cerebral arterioles. Thrombin and PAR_1-activating peptide induce increased Ca^{2+} mobilization from intracellular sources and contraction. On the other hand, PAR_2 induced a decrease in Ca^{2+} thought to be mediated by endothelium-derived NO and Ca^{2+} sequestration. A rabbit double subarachnoid hemorrhage model was studied to understand the role of thrombin and PAR_1 activation. PAR_1 was found to have an autoregulatory role because thrombin led to upregulation of PAR_1, which enhanced the contractile response to thrombin. The aforementioned effects could be prevented with intracisternal PAR_1 antagonist. In contrast, activating peptides for PAR_2 and PAR_4 did not induce a contractile response in the subarachnoid hemorrhage model. Previous reports have confirmed thrombin-induced upregulation of PAR_1 in isolated rings of the basilar artery (356).

In addition to vessel narrowing and coagulation, PARs contribute to systolic dysfunction, overload, and fibrosis. Ischemia increases expression of PAR_1 and PAR_2, while cardiac overload leads to overexpression of PAR_2 (357, 358). Investigators used cardiomyocyte-specific PAR_1 overexpression in a mouse model to show that PAR_1 is responsible for systolic dysfunction and enlargement of the left ventricle (359). Genetic deletion or pharmacological antagonism of PAR_1 abrogates cardiac systolic dysfunction and fibrosis (360). More recently, investigators have

Downloaded from journals.physiology.org/journal/physrev at New York Univ (216.165.095.084) on September 28, 2023.

used more refined models and measures of cardiac dysfunction to confirm the role of PAR_1 in congestive heart failure (361). Renin-overexpressing hypertensive (Ren-Tg) mice, in which the liver secretes high levels of renin that yield elevated levels of renin and angiotensin II in the plasma, exhibit elevated blood pressure and congestive heart failure. Experiments with the selective PAR_1 antagonist SCH79797 implicated PAR_1 in the resultant circulatory pathology. In this pathological Ren-Tg mouse model, PAR_1 antagonism had several effects: decreased systolic blood pressure, reduced cardiac hypertrophy, and fibrosis. Additional effects included fewer monocytes and macrophages, along with proinflammatory and profibrotic cytokines. Thrombin or FXa produces cardiac inflammation and remodeling through PAR_1 (362). Thrombin or FXa activates PAR_1 in cardiac fibroblasts to phosphorylate ERK1/2. Given the finding that PAR_1 antagonism does not affect systolic blood pressure or vascular tone, the role of PAR_1 inhibition in reducing cardiac hypertrophy and fibrosis is independent of blood pressure mechanisms.

PAR activation contributes to the related processes of inflammation and thromboembolic events that characterize pathologic conditions affecting the circulatory system. For example, SARS-CoV-2 is associated with a pathologic increase in cytokines (i.e., cytokine storm), which include interferon-γ, TNF-α, IL-1, IL-6, and IL-2, and coagulation factors (363, 364). Following infection by SARS-CoV-2, the increase in cytokines leads to the upregulation of coagulation factors including TF (365). Moreover, the high level of cytokines can lead to massive engagement of macrophages, resulting in macrophage activation syndrome. This perpetuates activation of coagulation factors, disinhibition of coagulation through the loss of inhibitors, venous thrombosis, pulmonary embolism, and multiple organ failure, a process that leads to death in persons with severe SARS-CoV-2 infections (366, 367). Because of its role in coagulation and its expression on endothelial cells and the lung, PAR_1 has been thought to play a prominent role in the hypercoagulable state and lung pathology associated with SARS-CoV-2 infection (368). Due to PAR_2 expression on lung epithelial cells, neutrophils, and fibroblasts (sect. 3), PAR_2 is likely to contribute directly or indirectly to the cytokine storm, innate immune response, organ inflammation, and ultimate organ failure that characterize SARS-CoV-2 infection.

5.2. PARs in the Integumentary System

5.2.1. Physiology.

Three layers comprise the skin: epidermis, dermis, and subcutis. The outer layer or the epidermis consists of five strata: stratum corneum, stratum lucidum, stratum granulosum, stratum spinosum, and stratum basale. PAR expression occurs early in development. As an example, PAR_2 shows up in the epidermis at embryonic *day 17* in mice. For context, PAR_2 is first expressed in the CNS and cardiac muscle at embryonic *day 12* (369).

Shortly after its discovery, PAR_2 was shown to be expressed by keratinocytes (sect. 3.1); expression was confirmed with Ca^{2+} imaging. PAR_2 is highly expressed by keratinocytes that comprise the granular layer; however, there is expression in basal and spinous layers (42). PAR_2 localizes to lipid rafts in human and mouse keratinocytes (370). Within the stratum corneum, there are three families of proteases produced: human tissue KLKs, cysteine proteases, and aspartate proteases. There are eight KLKs that are expressed in the stratum corneum; all KLKs are tryptic proteases, except KLK-7, which is chymotryptic (371). Activation of PAR_2 on keratinocytes by KLK-5 and KLK-14 mediates homeostatic functions in the skin including barrier protection, immune response, inflammation, pigmentation, and tumor surveillance (372, 373). PAR activation by KLKs on keratinocytes also leads to pigmentation, differentiation, and cornification. KLK-5 and KLK-14 cleave PAR_2 and favor keratinocyte maturation, rather than keratinocyte proliferation (373, 374).

5.2.1.1. DIFFERENTIATION. Stem cells generate keratinocytes that progress from the immature to the mature stage, followed by cell death and cornification. PAR_2 activation participates in keratinocyte progression through these different steps (370). The role of PAR_2 in differentiation of keratinocytes is equivocal; some publications support the concept that PAR_2 activation leads to differentiation, while others show that PAR_2 activation opposes differentiation. Based on the evidence that Ca^{2+} mediates differentiation, investigators expected that PAR_2 activation would promote differentiation given its mobilization of intracellular Ca^{2+}. One of the earliest papers that looked at the roles of PAR_1 and PAR_2 activation on differentiation found that the PARs exhibited divergent effects (40). Thrombin activation of PAR_1 increased cell growth and decreased differentiation. PAR_2 activation inhibited both cell growth and differentiation. Opposing work has shown that PAR_2 activation promotes differentiation (375).

5.2.1.2. BARRIER FUNCTION. Before the description of the role of PAR_2 in cutaneous barrier function, PAR_2 activation was shown to disrupt the barrier in the cornea, vagina, respiratory system, kidney, and GI tract. Skin barrier protection involves keratinocyte cornification, lamellar body section, and formation of intercellular junctions. PAR_2 activation delays barrier recovery. The reverse, that is barrier recovery following PAR_2 antagonism, has been shown. In PAR_2-/- mice, barrier recovery is accelerated

Downloaded from journals.physiology.org/journal/physrev at New York Univ (216.165.095.084) on September 28, 2023.

(370). PAR_2 regulates lamellar body secretion. PAR_2 activation suppressed lamellar body secretion and barrier recovery; PAR_2-mediated alterations of actin mediated the decrease in lamellar body secretion (376).

5.2.1.3. INFLAMMATION AND IMMUNE RESPONSES. Immune cells within the skin contribute to protection mediated by PARs. Activation of PAR_1 on monocytes and T lymphocytes leads to the production of IL-6 and IL-8. PAR_2, expressed by eosinophils, mast cells, monocytes, and neutrophils, leads to the secretion of IL-6, IL-8, IL-13, IL-1β, ICAM-1, thymic stromal lymphopoietin, and TNF-α. PAR_1- and PAR_2-mediated production of inflammatory mediators cause inflammation within the deeper layers of the skin (342).

PAR_2 activation induces an inflammatory response, which is observed at the tissue level and is manifested as edema, vascular permeability, and mobilization of granulocytes. PAR_2, which mediates neurogenic inflammation in the skin, contributes to smooth muscle contraction, vasodilation, and plasma extravasation (377). The PAR_2-mediated inflammatory effect is balanced by the anti-inflammatory effect of PAR_1 activation. As in **FIGURE 6C**, EPCR acts as a coreceptor for the anticoagulant APC. APC cleaves PAR_1 and is antiapoptotic and neuroprotective (61). When APC binds to EPCR and activates PAR_1, keratinocyte proliferation and barrier protection are reinforced, along with reduced inflammation (378, 379).

PAR_2 activation on keratinocytes mediates phagocytosis. Activation by trypsin, SLIGRL, or SLIGKV mediates ingestion of microspheres and bioparticles (380). The mechanisms by which PAR_2 activation increases phagocytosis involve actin polymerization, α-actinin reorganization, cellular morphological changes, and protease activity. PAR_2 activation of keratinocytes, in this case the simian virus-transformed human keratinocyte SVK14 cell line, also leads to the secretion of cytokines, including IL-8 (381).

5.2.1.4. PIGMENTATION. Evidence supporting the role of PAR_2 in skin color includes the finding that pigmented human skin exhibits higher expression of PAR_2 and its canonical activator, trypsin, relative to lighter human skin; moreover, dark skin exhibits increased PAR_2-mediated phagocytosis (382). PAR_2 activation by trypsin and SLIGRL on keratinocytes upregulates melanosome transfer and phagocytosis (383).

5.2.2. Pathology.

5.2.2.1. INFLAMMATORY SKIN DISORDERS. Of the PAR subtypes, PAR_2 features prominently in inflammatory skin disorders. These disorders are common: acne affects 50% of teenagers, atopic dermatitis (AD) affects ~20% of the population, rosacea affects 10% of adults, and psoriasis affects ~3% of the population (384).

PAR_2 has a clear role in AD. AD is characterized by increased expression of PAR_2 in keratinocytes and associated nerve fibers (377). Skin affected by AD contains a higher concentration of tryptase, which induces itch through PAR_2. KLK-5 and KLK-14, which cleave PAR_2, are upregulated in skin samples from patients with AD. Not all KLKs are capable of cleaving PAR_2, for example, KLK-7 or KLK-8 (385). Komatsu et al. (385) generated their data from lesional and nonlesional skin samples harvested from the same six patients, with patients serving as their own control. In a separate study, investigators found that activated PAR_2 in diseased skin from patients with AD leads to upregulation of ICAM-1 through the NF-κB pathway.

PAR_2 activation resulting from proteases secreted by the house dust mite also contributes to AD. Investigators used a PAR_2-overexpressing mouse in which the gene for PAR_2 was inserted into the start codon of the grainyhead-like-3 gene $Grhl3^{Par2/+}$ to study the role of house dust mite in AD (386, 387). The AD model was generated by repeated application of an extract of house dust mite to the nape of the neck. The AD mouse model exhibited spontaneous eczema and an intense pruritic-like behavioral response and impaired skin barrier. DRG harvested from the overexpressing mice exhibited a greater response to SLIGRL, which can activate PAR_2 and MrgprC11. The authors propose that the PAR_2-overexpressing mice are a more accurate model of pediatric AD compared to flaky tail mice, or the SPINK5-/-, and flaggrin-/- mouse models (388–390). PAR_2 activation of T_H2 cells in the PAR_2-overexpressing mice leads to secretion of IL-31, which activates neurons and enhances neuroimmune signaling.

Netherton syndrome is a rare autosomal recessive skin disease associated with skin inflammation, scaling, and itch as well as with dehydration and growth abnormalities. Patients exhibit a mutation in the gene for serine protease inhibitor Kazal-type 5 (SPINK5), also known as lympho-epithelial Kazal-type-related inhibitor (LEKTI). LEKTI regulates desquamation and inhibits three KLK-related peptidases: KLK-5, KLK-7, and KLK-14. With the loss of the serine protease inhibitors, there is increased activation of PAR_2 by the KLKs. PAR_2 then signals through NF-κB (388). The KLK-5/PAR_2 cascade leads to an increase in thymic stromal lymphopoietin production, which generates a proallergic microenvironment. This leads to the formation of eczematous skin lesions and a systemic T_H2 response; an unweighted T_H2 response contributes to allergy (391). Thymic stromal lymphopoietin released by keratinocytes induces Langerhans cells to accelerate sensitization to allergens from sources such as cockroaches and dust mites that activate PAR_2 and

Downloaded from journals.physiology.org/journal/physrev at New York Univ (216.165.095.084) on September 28, 2023.

contribute to a disruption of the skin barrier. Allergens disrupt the skin barrier through several mechanisms including increased protease activity, delayed barrier recovery, and delayed lamellar body secretion. These PAR_2-mediated effects explain why PAR_2 antagonists normalize the time required for barrier recovery (392).

5.2.2.2. ITCH. PAR_2 activation produces itch (393). Injection of PAR_2 agonist into humans induces pain, followed by itch (377). Most patients suffering from chronic itch have AD or psoriasis (394). There are differences in the role of PAR_2 in itch associated with AD versus psoriasis. Nattkemper and colleagues (395) performed RNA sequencing on skin from 25 patients with AD and 25 patients with psoriasis; 30 patients without skin lesions provided site-matched skin biopsies, which served as controls. For the patients with psoriasis or AD, the pruritic, lesional skin was compared to nonpruritic, nonlesional skin. Pruritic skin from patients with AD overexpressed *F2rl1* (the gene for PAR_2); however, pruritic psoriatic skin did not.

PAR_2 contributes to itch associated with several disorders besides AD and psoriasis, including uremia, dermatophyte infection, and liver failure (396, 397). Uremic pruritis is associated with end-stage renal disease. A recent study evaluated differences in serine protease activity and PAR_2 expression in patients with end-stage renal disease without uremic pruritis, patients with end-stage renal disease and uremic pruritis, and healthy controls. They found a significant positive correlation between elevated PAR_2 expression and uremic pruritis, as measured with a visual analog scale (397).

Dermatophytes are fungi that infect the skin. These organisms secrete itch- and pain-inducing proteases. For example, PAR_2 is activated by Der p1 (cysteine proteases), p3 (trypsins), and p9 (serine proteases) secreted by the house dust mites *Dermatophagoides pteronyssinus* and *Dermatophagoides farina* (398–400).

Cholestatic liver disease, characterized by reduced or blocked flow of bile from the liver, is associated with itch. A rat model was developed in which the bile duct was ligated; the rats ultimately exhibit cirrhosis and hepatic encephalopathy (396). In this model, the roles of proteases and PAR_2 were investigated by administering gabexate mesylates, lima bean trypsin inhibitor, and the PAR_2 antagonist FSLLRY-NH_2. The protease inhibitors and PAR_2 antagonist attenuated the scratching behavior. DRG removed from the rat bile duct ligation model demonstrated PAR_2 upregulation and greater TRPV1 activity. Furthermore, there were more peptidergic neurons that expressed PAR_2 and TRPV1; medium-sized neurons exhibited expression of TRPV1. PAR_2 activation leads to TRPV1 phosphorylation and subsequent sensitization with a rapid decrease in activation threshold through PKCε and PKA (260).

5.3. PARs in the Respiratory System

5.3.1. Physiology.

All four PARs are expressed in the lungs (45, 53). PAR_2 is expressed on the apical surface of ciliated columnar epithelial cells in the trachea, main bronchi, and first-order bronchi. PAR_2 staining is less commonly seen on airway smooth muscle. PAR_1 immunoreactivity is faint on epithelium and SMCs.

The differential actions of PAR_1 and PAR_2 in the lung have been studied with activating peptides. SFLLRN-NH_2 activates PAR_1 and PAR_2, while SLIGRL-NH_2 is specific to PAR_2. In preparations of mouse bronchi from which the epithelium has been denuded, SLIGRL-NH_2 does not cause contraction; however, SFLLRN-NH_2 does cause contraction through activation of PAR_1. One of the early studies that reported on the role of PAR_2 in the bronchi, that is bronchodilation, was by Cocks et al. in 1999 (74). The authors proposed that PAR_2 activation was protective for the bronchi, which is PGE_2 dependent. In a bronchial ring preparation, constriction can be induced with the muscarinic agonist carbachol. Subsequent relaxation in the preparation is induced by the mouse-activating peptide SLIGRL-NH_2 and trypsin; PAR_2-mediated bronchorelaxation is rapid and concentration dependent. PAR_2 activation inhibited bronchoconstriction. This protective action in the bronchi points to the role of PAR_2 has in reactive airway disease.

In addition to regulation of bronchoconstriction and bronchodilation, PAR_2 regulates ciliary beating, which facilitates mucociliary clearance. Mucociliary clearance is a mechanism of defense against inhaled pathogens. Expression and subsequent activation of PAR_2 on different regions of the cell (apical versus basolateral) determine sinonasal epithelial functions such as ciliary beating frequency (401).

5.3.2. Pathology.

The four PAR variants are expressed in the lung by different cell types including cells in the epithelium and blood vessels. PARs contribute to pathologic conditions in the lungs that usually involve a combination of fibrosis, proliferation, edema, and inflammation.

PAR_1 is expressed on lung epithelium and lung fibroblasts (402–404; sect. 3.1). PAR_1 activation on epithelium leads to inflammation through the release of cytokines. Activation of PAR_1 on fibroblasts drives differentiation to myofibroblasts and subsequent generation of proteins that form the ECM (231, 405). A common cause of iatrogenic lung injury involves the administration of high-volume ventilation, which induces pulmonary edema. This outcome involves PAR_1, transforming growth factor-β (TGFβ), and the $\alpha_V\beta_6$-integrin (406). Thrombin is a PAR_1

Downloaded from journals.physiology.org/journal/physrev at New York Univ (216.165.095.084) on September 28, 2023.

agonist active during lung injury (407, 408). TGFβ is normally latent and activated by $\alpha_V\beta_6$. PAR_1 regulates TGFβ activity through RhoA and Rho kinase signaling (sect. 4.5). The $PAR_1/\alpha_V\beta_6$ /TGFβ axis mediates a distinct form of lung injury that is induced by bleomycin, a chemotherapeutic agent that induces DNA double-strand breaks. Bleomycin leads to increased lung permeability and edema. In PAR_1-/- mice, TGFβ activation and the lung permeability induced by bleomycin are reduced (406, 409). Exposure of airway SMCs to thrombin leads to proliferation through ERK2 activation, which is inhibited by activation of cAMP-dependent protein kinases by forskolin. PAR_1 has a role in pulmonary fibrosis; however, PAR_2 is required. Simultaneous antagonism of PAR_1 and PAR_2 is not more effective than antagonism of either PAR alone (410).

Much of the pathology of the respiratory system involves bronchoconstriction and bronchodilation. Investigating the role of PARs in constriction and dilation in lung pathology is challenging. The effect of PAR activation on airway smooth muscle, i.e., contraction versus dilation, as well as the effect of proteases versus activating peptides, is species dependent. Moreover, airway preparation variability affects the results. In rat trachea-derived smooth muscle cells, the activating peptides for PAR_1, PAR_2, PAR_3, and PAR_4 were tested, along with thrombin and trypsin (411). To test whether PARs induce dilation, precontraction was induced by carbachol. PAR_1-, PAR_2-, and PAR_4-activating peptides, along with trypsin and thrombin, produced dilation, which was indomethacin dependent. PAR_1- and PAR_4-activating peptides induced dilation that was preceded by a rapid and transient contraction. The contractile effect was not induced by thrombin or trypsin.

Fresh human lung tissue is difficult to obtain for translational experiments. However, bronchial rings can be obtained from patients who require pneumonectomy or lobectomy for carcinoma. Intact human bronchial rings obtained from such patients were used to test the effect of α-thrombin on bronchial tone. α-Thrombin increased bronchial tone, which did not depend on the respiratory epithelium. Transcripts for PAR_1, PAR_2, and PAR_3 were present, while protein for only PAR_1 and PAR_2 could be detected (412). Experiments on isolated rat airways, including the trachea and main bronchi and first-order bronchi, revealed that epithelium must be present to induce smooth muscle contraction and relaxation (413). Trypsin and thrombin did not have an effect on the airway. This study also revealed differences in the actions of proteases or activating peptide. PAR_1-activating peptide caused contraction of the airway, while PAR_2- and PAR_4-activating peptides caused airway dilation; the effect of the PAR_2-activating peptide was greater than the effect of the PAR_4-activating peptide. The effect of PAR_2 activation was inhibited by redox states of hemoglobin, which was independent of hemoglobin's NO- and CO-scavenging properties.

PAR_2 expressed by circulating immune cells also contributes to asthma. In fact, PAR_2 on $CD14^{++}CD16^{+}$ monocytes in the blood of asthma patients has been proposed as a biomarker for asthma severity (414). Monocytes are classified according to expression of CD14 (the lipopolysaccharide coreceptor) and CD16 (the Fcγ receptor). $CD14^{++}CD16^{+}$ are intermediate monocytes. Concentration of these monocytes is increased in patients with type 2 diabetes and sarcoidosis (415, 416).

The prominent role of PARs in inflammation contributes to scar formation and fibrosis in the lungs (417, 418). PAR_3 (along with PAR_1) on alveolar epithelium plays a role in the epithelial-to-mesenchymal transition (45). PAR_3 is overexpressed in the lungs of patients with idiopathic pulmonary fibrosis and in mice with bleomycin-induced lung fibrosis. PAR_1 and PAR_3 colocalize within alveolar type II cells, which comprise 60% of alveolar epithelial cells. PAR_3 is overexpressed primarily on alveolar type II cells and is thought to contribute to lung fibrosis. Activation of PAR_3 on alveolar type II cells leads to secretion of IL-8 (168) (sect. 4.7). In the lung, the PAR_2/EGFR axis also leads to secretion of IL-8 (280). PAR_4 contributes to the role that EGFR plays in mediating the transition from epithelial cells to mesenchyme. This transition contributes to lung fibrosis (53).

5.4. PARs in the Gastrointestinal System

5.4.1. Physiology.

The site of highest PAR expression is in the GI system (sect. 3). The GI system contains and is subject to more proteases (from exocrine pancreas, inflammatory cells, microorganisms) than any other location or organ in the body; therefore, PARs are anatomically set up to contribute to GI homeostasis, including enterocyte renewal, permeability, barrier function, motility, immune response, cytokine function, neurogenic inflammation, and sensation. Within the GI system, PARs are most highly expressed in the small intestine, colon, liver, and pancreas; however, other sites within the GI system that exhibit PAR expression include the oral cavity, salivary glands, exocrine pancreas, and liver (419). At a cellular level, PARs are expressed on enterocytes (basolateral and apical membranes), endothelial cells, SMCs, immune cells, and neurons. Most reports on PAR function address the roles of PAR_1, PAR_2, and PAR_4; we know little about the expression and function of PAR_3 in the GI system.

Based on the role of PAR_1 in electrolyte transport on epithelial cells, such as renal proximal tubule cells, PAR_1 was proposed to contribute to intestinal epithelial cell function. The role of PAR_1 in intestinal epithelial cells

Downloaded from journals.physiology.org/journal/physrev at New York Univ (216.165.095.084) on September 28, 2023.

was demonstrated in 2001 using a nontransformed, chloride-secreting human epithelial crypt cell line (SCBN) (420). PAR_1 activation on the basolateral surface of the SCBN cells led to chloride secretion that is directed toward the apical portion of the cell; a mechanism that is mediated by the release of intracellular stores of Ca^{2+}.

5.4.1.1. EPITHELIAL RENEWAL. Similar to their role in organ development, PARs contribute to epithelial cell renewal and turnover. PAR_2 is involved in human colonocyte homeostasis and maintenance (211). Intestinal cell homeostasis involves cellular proliferation and differentiation from stem cells within the base of mucosal crypts; the cells undergo differentiation, maturation, and ultimately senescence as they migrate to the mucosal surface. Trypsin activation of PAR_2 on enterocytes stabilizes yes-associated protein 1 (YAP), a transcriptional regulator and member of the Hippo signaling pathway. YAP activation contributes to cellular turnover (421). PAR_2 contributes to colon carcinogenesis, which involves YAP1, an oncogene. PAR_2 also regulates proliferation of intestinal stem cells through activation of glycogen synthase kinase-3β (422).

5.4.1.2. BARRIER FUNCTION. The critical function of the GI system is the movement of nutrients and water from the lumen into the vasculature and lymphatic system, while also serving as a barrier to bacteria; accordingly, GI permeability, transcellular and paracellular, is central to homeostasis. The protease/PAR axis regulates transcellular and paracellular permeability (**FIGURE 7*A***).

PAR_1 and PAR_2 contribute to intestinal epithelial barrier function and ionic transport (423). PAR_1 agonists disrupt tight junctional zonula occludens (ZO). PAR_1 activation disrupts ZO-1 and apoptotic nuclear condensation, mechanisms that involve caspase-3, tyrosine kinase, and MLC kinase (423). Most of the work on PARs and enterocyte paracellular permeability has focused on PAR_2. PAR_2 mediates intestinal epithelial inflammation across multiple species (424–426). Activation of PAR_2 on enterocytes by a low dose of SLIGRL leads to increased paracellular permeability through calmodulin activation, which leads to MLC phosphorylation and ZO-1 disruption (427). Paracellular permeability is mediated through activation of PAR_2 on capsaicin-sensitive sensory neurons and subsequent neurogenic inflammation (428). Intraperitoneal PAR_2 activation (that is, activation of PAR_2 on the basolateral surface) leads to paracellular permeability (**FIGURE 7*B***), which involves ERK1/2 and β-arrestin (sect. 4.5).

If homeostasis of the tight junctions is lost, toxins and bacteria migrate between enterocytes, which then generates an inflammatory response. The inflammatory response, characterized by increased epithelial permeability and bacterial translocation, follows PAR_2 activation in the colon (425). Indirect evidence also confirms that PAR_2 mediates colonic permeability. Ampicillin, a broad-spectrum antibiotic that inhibits growth of Gram-positive and Gram-negative bacteria, was given to animals in the drinking water (429). The antibiotic reduced serine protease activity and PAR_2 expression. PAR_2 activity was restored with trypsin administration. The results of this study show the relationship between bacteria, luminal proteases, PAR_2 expression, and colonocyte paracellular permeability. Moreover, apical expression of PAR_2 changes with antibiotics (429).

5.4.1.3. MOTILITY. Interpretation of the effect of PAR activation on GI motility needs to be considered in the context of the cell, tissue (e.g., gastric versus colon), or whole animal that is studied. Species differences should also be considered, along with the assay. An in vitro assay quantifies circular muscle activity by measuring endoluminal pressure and uses isometric tension as an index of longitudinal muscle activity. As an example of the importance of tissue specificity in considering GI motility, activation of PAR_2 reduces the amplitude of rhythmic contractions of the circular and longitudinal muscle of the rat colon. PAR_2 is expressed (shown by immunofluorescence) in the muscularis externa of the rat colon as well as the mucosa; therefore, activation of PAR_2 at either site could impact GI motility. The investigators ruled out the effect of PAR_2 on the mucosa by removing this tissue (122). The literature contains equivocal results with regard to PAR activation and motility. For example, activation of PAR_2 in the mouse and rat stomach, by trypsin and activating peptides, leads to stimulation of gastric motility, as demonstrated with a gastric longitudinal muscle preparation (327). In another study, PAR_2 activation, along with PAR_1 activation, in the mouse gastric fundus produces relaxation followed by contraction (72). Relaxation requires small-conductance Ca^{2+}-activated potassium channels (SK or small potassium). Ryanodine also inhibited the effect. In a separate study, PAR_2 activation in the rat colon inhibits the amplitude of rhythmic contractions (122). Colonic myocytes respond, as measured by an increase in Ca^{2+}, to numerous PAR_2 agonists including trypsin, SLIGRL-NH_2, mast cell tryptase, and filtrate collected from degranulated mast cells. The PAR_2-mediated effect on gastric motility is Ca^{2+} dependent.

PAR_1 and PAR_2 activity, induced by either selective activating peptides or trypsin for the latter PAR, cause contraction in the guinea pig and human gall bladder (430). Contraction of the gall bladder strips was measured with an isometric transducer. RT-PCR confirmed expression of PAR_1 and PAR_2 in the gall bladder.

Downloaded from journals.physiology.org/journal/physrev at New York Univ (216.165.095.084) on September 28, 2023.

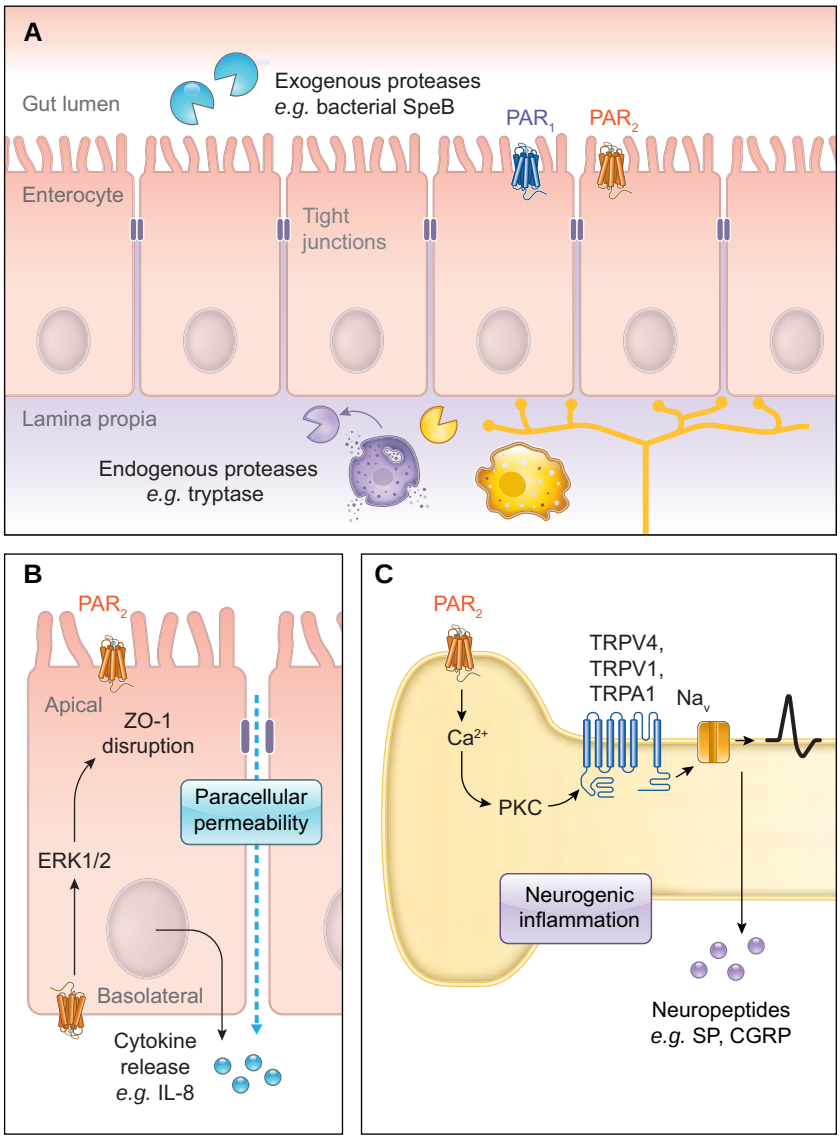

FIGURE 7. Protease-activated receptor (PAR) signaling in the gastrointestinal system. *A*: colonocytes express PAR_1 and PAR_2. The apical membrane facing the gut lumen is exposed to proteases, including digestive enzymes and proteases from commensal and pathogenic microorganisms. The basolateral membrane is exposed to proteases released by immune cells, epithelial cells, blood vessels, and other cell types. *B*: activation of PAR_2 at the basolateral region of cells leads to ERK1/2 signaling that causes paracellular permeability via disruption of tight junctions. *C*: PAR_2 activation on sensory neurons, including those that innervate the gut, leads to Ca^{2+} mobilization. Subsequent PKC activation sensitizes transient receptor potential (TRP) channels, leading to ionic influx and activation of voltage-gated channels to trigger action potentials. This also triggers release of neuropeptides, such as substance P (SP) or calcitonin gene-related peptide (CGRP), which mediate neurogenic inflammation and pain. ZO-1, zona occludens.

Contraction did not depend on tetrodotoxin or atropine; therefore, the effects of PAR_1 and PAR_2 activation were direct. PAR_4 activation had no effect on gall bladder contraction.

5.4.1.4. SECRETION. PAR_2 activation has effects on secretion in the stomach; PAR_2 activation stimulates mucus secretion that involves TRPV1+ neurons. PAR_2 activation also increases gastric mucosal blood flow and has an inhibitory effect on gastric acid secretion. Activation of PAR_2 in the stomach, but not in the duodenum, leads to secretion of mucus. The mechanism involves the release of calcitonin gene-related peptide (CGRP) and tachykinins on sensory neurons (431) (**FIGURE 7C**). PAR_2 is expressed on gastric chief cells and leads to secretion of pepsinogen. PAR_2 on pancreatic and parotid gland acinar cells leads to secretion of amylase (432). Ablation of TRPV1+ neurons reversed the gastric mucosal secretion induced by PAR_2 activation. PAR_2 activation leads to exocrine secretion by the salivary glands and the pancreas.

5.4.1.5. SENSATION. Pain homeostasis is a balance of nociceptive and antinociceptive mechanisms, including visceral sensitivity in the GI system. PAR_4 activation is antinociceptive in a number of visceral hypersensitivity models. PAR_4 has also been shown to reverse nociception in the somatic system (270). Activation of PAR_4 by the activating peptide AYPGKF-NH_2 inhibits the Ca^{2+} current induced by capsaicin in rat DRG sensory neurons. At a behavioral level, the PAR_4-activating peptide heightened mechanical and thermal nociceptive thresholds. The PAR_4-mediated antinociceptive effect that was

Downloaded from journals.physiology.org/journal/physrev at New York Univ (216.165.095.084) on September 28, 2023.

demonstrated in the somatic system is also seen in DRG that innervate the colon (433). Activation of PAR_4 was shown to counterbalance the excitatory effects of PAR_2-induced excitability in dissociated neurons, as measured by whole cell patch-clamp recording. Antagonism of PAR_2-mediated nociception by PAR_4 activation was also shown at a systems level (111). PAR_2 sensitizes TRPV4, which contributes to visceral hypersensitivity. When the PAR_4-activating peptide was injected into the colon, there was reduced visceral hypersensitivity. A combination of PAR_2 and TRPV4 agonists induced allodynia and hyperalgesia, as measured by visceromotor responses that occurs following colorectal distension. PAR_4 agonism reversed the allodynia and hyperalgesia.

5.4.2. Pathology.

5.4.2.1. ORAL CAVITY. Soon after the discovery of PARs, these receptors were found to contribute to the physiology and pathology of the GI system, especially the intestines. More recently, the role of PARs in pathologic conditions of the oral cavity, including teeth, has emerged. Pulpitis, inflammation of the dental pulp, causes odontogenic (i.e., tooth) pain. This process is mediated by PAR_1 (434). In the setting of pulpitis, PAR_1 can be activated by KLK, a serine protease that cleaves kininogen to generate bradykinin and a well-established algogen (i.e., a mediator that is responsible for pain). KLK produces pulpal inflammation by generating a Ca^{2+} flux that upregulates COX-2 and production of PGE_2. SCH79797, the PAR_1 antagonist, reverses KLK-induced pulpitis. PAR_1 in periodontal tissues (i.e., the tissues supporting teeth) mediates inflammatory and reparative processes. Activation of PAR_1 on oral epithelial cells by Arg-gingipain leads to an increase in IL-1α, IL-1β, IL-6, TNF-α, and CXCL5. Chronic periodontitis causes downregulation of PAR_1 expression, which leads to an increase in IL-6, IL-8, TNF-α, IFN-γ, and MMP2 in crevicular fluid (435). On the other hand, periodontal therapy leads to an increase in PAR_1 expression by epithelial cells. Thrombin activates PAR_1 on oral epithelial cells, which attracts granulocytes through chemokine induction and contributes to the inflammation that characterizes periodontal disease. Trypsin-like cysteine proteases in the gingipains family are secreted by *Porphyromonas gingivalis*. These proteases cleave PAR_1 on monocytes, which generates secretion of cytokines (436) and contributes to periodontal disease (437).

5.4.2.2. INFLAMMATORY BOWEL DISEASE. Inflammatory bowel disease (IBD), which includes Crohn's disease and ulcerative colitis, is characterized by dysmotility, a process that contributes to overgrowth of bacteria, increased intestinal permeability, bacterial translocation, inflammation (which reciprocally worsens dysmotility), diarrhea, and constipation. Inflammation affects sensory and motor neuronal function, which further impacts motility. Inflammation is responsible for sensory and motor neuronal hypertrophy, hyperplasia, axonal degeneration, and necrosis.

GI dysmotility results in constipation and diarrhea. Intestinal inflammation suppresses spontaneous phasic contractions and contributes to ultrarapid propulsion (438). Peristalsis involves ascending contraction and descending relaxation. PARs mediate contraction, relaxation and/or both (i.e., biphasic; 419, 439, 440). In a dextran sulfate sodium (DSS)-induced colitis model in rats, both trypsin and the PAR_2-activating peptide SLIGRL-NH_2 pathologically altered relaxation (441).

Permeability of the gut contributes to GI pathology, including Crohn's disease and ulcerative colitis. Of all the PARs, PAR_2 is the most prominent subtype that contributes to permeability (**FIGURE 8*B***). The role of PAR_2 in GI pathology, including permeability, has been demonstrated in preclinical models and patients. PAR_2 is overexpressed in patients with IBD (442). Trypsin administered into the colon produces an inflammatory reaction that contributes to permeability (425). GI inflammation is characterized by high levels of trypsinogen I-II, which activate PAR_2. Trypsinogen IV, a human trypsin that is resistant to inhibitors and proteolytic breakdown, activates PAR_2 and PAR_4 (443). In a pathologic context, activation of PAR_2 leads to fluid secretion and inflammation through neurogenic inflammation mediated by CGRP and substance P (444, 445). Along with endogenous proteases, microbial proteases contribute to increased intestinal permeability (446). In IBD patients, *Enterococcus faecalis* produces gelatinase, which breaks down E-cadherin through PAR_2 activation and leads to increased permeability (447). *Serratia marcescens* produces serralysin that activates PAR_2.

As PAR_2 is so widely expressed in the GI system (epithelium, SMCs, endothelium, enteric neurons, fibroblasts, and infiltrating immune cells; sect. 3), the cellular source and associated PAR_2 activity that contributes to IBD is in question. The role of PAR_2 on some of the cell types has been addressed using a variety of models. The role of PAR_2 on bone marrow-derived blood cells was shown to contribute to a trinitrobenzenesulfonic acid (TNBS)-induced colitis model, which recapitulates human IBD (448). PAR_2-/- recipient mice did not develop colitis induced by DSS or TNBS. PAR_2 on bone marrow-derived cells plays an important role in the latter model but not the former. In patients with IBD-associated colitis and patients with Hirschsprung's-associated enterocolitis, PAR_1 and PAR_2 are overexpressed and thought to contribute to their pathology (449).

Downloaded from journals.physiology.org/journal/physrev at New York Univ (216.165.095.084) on September 28, 2023.

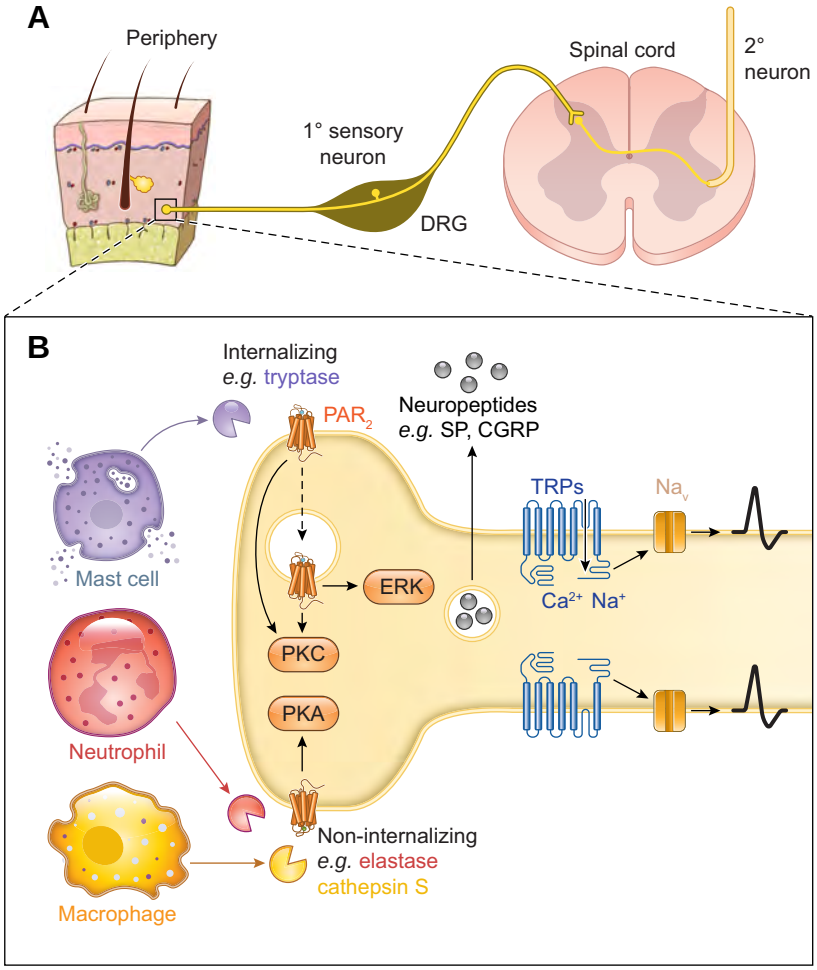

FIGURE 8. Protease-activated receptor (PAR) signaling in pain. *A*: primary (1°) sensory neurons with cell bodies in dorsal root ganglia (DRG) project fibers to peripheral tissues and the dorsal horn of the spinal cord. Second-order (2°) neurons in the dorsal horn transmit painful signals centrally. *B*: proteases that are released from immune cells cleave PAR_2 expressed on sensory nerve fibers in the periphery. Some proteases (e.g., mast cell tryptase) trigger PAR_2 endocytosis and trafficking to signaling endosomes that generate signals leading to sensitization or activation of ion channels. Other proteases (e.g., neutrophil elastase, macrophage cathepsin S, and legumain) activate PAR_2 by biased mechanisms that do not evoke endocytosis; PAR_2 signals from the plasma membrane to sensitize or activate ion channels. Neurons can release substance P (SP) and calcitonin gene-related peptide (CGRP) locally, causing neurogenic inflammation, and centrally, leading to pain transmission. TRP, transient receptor potential.

5.4.2.3. IRRITABLE BOWEL SYNDROME. Irritable bowel syndrome (IBS) affects over 10% of the population and consists of symptoms that include abdominal pain, abdominal bloating, and dysregulated bowel movements. The latter is used to distinguish different types of IBS: IBS-D (IBS with diarrhea); IBS-C (IBS with constipation); IBS-M (IBS with diarrhea and constipation); and IBS-U (IBS with neither diarrhea nor constipation). Because of the role of proteases in visceral pain, the role of proteases in IBS is expected. Sources of proteases in IBS include tryptase from mast cells and trypsin from the pancreas as well as epithelial and endothelial cells (443).

Investigators have used biopsies from patients with IBS to understand the role of proteases and PARs in the etiology of IBS and associated symptoms, especially pain. Studies by several groups have demonstrated the following: *1*) colonic biopsy supernatant collected from patients diagnosed with IBS contains proteases and shows proteolytic activity at an Arg site; and *2*) proteases in this supernatant produce hyperalgesia through PAR_2 (450). Evaluation of the proteases in the supernatant reveals increased levels of trypsin and tryptase, without an increase in the quantity of mast cells. Investigators applied the supernatant to dissociated DRG neurons and measured the neuronal response with Ca^{2+} imaging. Supernatants collected from the four subgroups of IBS patients led to an increase in Ca^{2+} signaling in DRG neurons. There was no distinction between tissue removed from the ascending colon or rectum. The general serine protease inhibitor FUT-175 reversed the effect. The level of expression of α-1-antiproteinase in the supernatants was unaltered; it is inferred that the increased proteolytic activity was not due to decreased inhibition. DRG neurons from PAR_2-/- did not exhibit a Ca^{2+} response. This finding implicates PAR_2 on neurons. In addition to the in vitro results, the investigators demonstrated that the supernatant had an in vivo effect. Supernatants induced visceral hypersensitivity, which recapitulates the human condition. Moreover, the supernatant produced both somatic thermal hyperalgesia and mechanical allodynia. These nociceptive effects were PAR_2 dependent. IBS is characterized by decreased expression of PAR_4, based on its expression in healthy control patients relative to IBS patients. Soon after the discovery that PAR_2 contributes to somatic nociception, it was shown that activation of PAR_2 by either trypsin or its activating peptide produces abdominal contractions

Downloaded from journals.physiology.org/journal/physrev at New York Univ (216.165.095.084) on September 28, 2023.

(a measure of visceral nociception), as well as c-Fos expression in the relevant spinal cord level (451, 452). Human colonic biopsies from IBS patients were kept in oxygenated media for 24 hours, and the supernatant was subsequently collected. The supernatant produced hypersensitivity through PAR_2 (450).

IBS pain is typically chronic and maintained by continued PAR_2 signaling in endosomes (203; sect. 4.6). Supernatant from colonic mucosal biopsies contained proteases that led to the activation and endocytosis of PAR_2. Activation of PAR_2 from endosomes sustained nociceptor activation. A PAR_2 antagonist was conjugated with cholestanol to allow the passage of the antagonist through the plasma membrane and into the endosomes (sect. 6.2), with enhanced inhibition of nociception. The investigators studied trypsin, elastase, and cathepsin S and their effect on PAR_2 endocytosis, nociceptor sensitivity, and allodynia.

Supernatants generated from colonic biopsies from patients with IBS were demonstrated to act through PAR_1 (453). Proteases at high concentrations included elastase 3a, cathepsin L, and proteasome α-subunit-4. The supernatants generated from colonic samples were then tested on submucosal plexus preparations from humans and guinea pigs and neuronal responses were assessed with Ca^{2+} imaging. The role of PAR_1 in IBS was shown with human thoracic DRG neurons, which were also tested with supernatant from human colonic biopsies. The thoracic DRG neurons responded to a PAR_1 agonist but not to PAR_2 or PAR_4 activation. The results were confirmed with a PAR_1 antagonist (454).

5.4.2.4. VISCERAL PAIN. Visceral pain is a symptom associated with many common GI disorders including IBS, gastroenteritis, and IBD. Similar to somatic pain, visceral pain is mediated primarily by peptidergic (i.e., those fibers that express and secrete substance P and CGRP) unmyelinated C-fibers and thinly myelinated Aδ-fibers. Anatomically relevant sensory nerve fibers innervating the colon identified by retrograde tracing express TRPA1 and PAR_2 (455).

TRPV4 is also required for PAR_2-induced visceral mechanical hyperalgesia (265; sect. 4.7). TRPV4, like TRPA1, responds to mechanical stimulation (456). In 2007, it was shown that PAR_2 sensitizes the response of TRPV4 to mechanical stimulation in the somatic system; however, it was not clear whether this effect occurred with visceral hyperalgesia (264). Somatic nociception and visceral nociception differ in their mechanisms (457). Anatomic and functional studies reveal that TRPV4 and PAR_2 are coexpressed and colocalized on spinal afferent neurons that innervate the colon. Administration of a PAR_2 antagonist potentiates this hyperalgesia. The effect of PAR_2-induced visceral hyperalgesia was not observed in TRPV4-/- mice. Whole cell patch-clamp electrophysiology recording of Fast Blue-labeled DRG neurons showed that pretreatment of neurons with a PAR_2 agonist led to increased current density following application of the TRPV4 agonist 4αPDD.

Cathepsins have several roles including antigen presentation and pain modulation through spinal microglial cells (458). In addition, cathepsins contribute to visceral pain. Activity-based probes were used to demonstrate the role of cathepsin S in colitis-related pain. Cathepsin S cleaves the transmembrane chemokine fractalkine, which mediates allodynia alongside cathepsin S itself (459). Stimulation of primary afferent neurons leads to secretion of fractalkine. This process requires cathepsin S from activated microglial cells. Microglial cathepsin S liberates fractalkine, leading to p38 MAPK phosphorylation in microglia, which, in turn, causes release of pronociceptive mediators from neurons. The cathepsin S inhibitor morpholinurea-leucine-homophenylalanine-vinyl phenyl sulfone (LHVS) reverses hyperalgesia and allodynia in neuropathic rats. The authors conclude that cathepsin S in microglial cells, but not cathepsin B and cathepsin L, maintains rather than initiates mechanical hypersensitivity. Activity-based probes were also used to demonstrate that cathepsin S is responsible for cleaving PAR_2 and contributes to visceral hyperalgesia (460). A series of probes were used to label cathepsin B, cathepsin L, and cathepsin S. Cathepsin S was localized to macrophages in the colon, spinal cells, and microglia in mouse models of colitis. Two models of colitis were studied: piroxicam-induced in IL-10-/- mice and TNBS-induced colitis. The former recapitulates Crohn's disease, while the latter allows for the study of genetic knockout mice.

5.4.2.5. EXTRAINTESTINAL PATHOLOGY. PARs contribute to pathology related to the hepatobiliary system. Thrombin activation of PAR_1 contributes to hepatocellular injury through lipopolysaccharide, an endotoxin in the cell wall of gram-negative bacteria (461–463). Hepatocellular damage secondary to lipopolysaccharide involves neutrophils. Lipopolysaccharide is increased in the setting of sepsis. Sepsis leads to activation of coagulation factors, including thrombin, which contribute to hepatocellular injury. Thrombin also leads to an increase in neutrophil degranulation that further contributes to lipopolysaccharide-induced injury. Activation of PAR_1 by TRAP recapitulated the effect of thrombin following hepatocellular injury induced by lipopolysaccharide (464).

PAR_2 has a dual role, protective and injurious, in pancreatitis. Acute pancreatitis leads to multiple organ failure that affects the lungs (pulmonary dysfunction is the most common cause of death with pancreatitis), kidneys, heart, nervous system, and coagulation system. PAR_2 is upregulated in acute pancreatitis, as shown in a rat

Downloaded from journals.physiology.org/journal/physrev at New York Univ (216.165.095.084) on September 28, 2023.

pancreatitis model induced by taurocholate in rats (465). Ion exchange, especially Cl^-/HCO_3^- exchange, is critical for pancreatic function. Pancreatic epithelial duct cells express PAR_2 and mediate ion channel function following activation by trypsin (466).

Our understanding of pancreatitis has become more refined with the use of fluorescently quenched activity-based probes. Legumain is a cysteine protease found in lysosomes and is capable of cleaving PAR_2 (149) (sect. 4.1). Legumain was implicated in pancreatitis when increased legumain expression was identified in patients with this disease (467). The use of an activity-based probe was used to show that legumain contributed to acute (up to 12 hours) and chronic (5 weeks) pancreatitis, in a model that was induced with caerulein (468). The source of legumain was localized to $CD68^+$ macrophages, rather than pancreatic acinar cells. Increased legumain activity was confirmed in tissues from patients with pancreatitis. The authors propose that macrophages that express legumain might be the source of inflammation, which ultimately could lead to pancreatic cancer.

5.4.2.6. PATHOLOGIC INFECTION. In 2011, *Clostridium difficile* infection occurred in ~500,000 Americans and caused nearly 29,000 deaths; it is the leading cause of death due to enteritis (469, 470). *C. difficile* infection is often iatrogenic following antibiotic administration. *C. difficile* secretes multiple toxins including an enterotoxin [toxin A (TxA)] and a cytotoxin (toxin B), which produce diarrhea. TxA is responsible for other effects including fluid secretion, enterocyte damage, edema, and myeloperoxidase (MPO) activity. MPO activity is used as an index of colonic inflammation (471). PAR_2 is pivotal for translating the toxic effects of TxA into signs and symptoms of *C. difficile* infection (472). *C. difficile* colitis can be induced by administration of TxA into the small intestine of mice, which recapitulates infection in humans. TxA administration leads to the following: fluid secretion, infiltration of neutrophils, edema, and cellular damage. In PAR_2-deficient mice, these effects are significantly reduced. Tryptase, which must be activated by dipeptidyl peptidase I (DPPI), is secreted by mast cells and activates PAR_2 (**FIGURE 2**). Mast cell tryptase contributes to long-term hyperexcitability on submucosal neurons (473). Similar to PAR_2 deletion, DPPI deletion reverses fluid secretion, granulocyte infiltration, and the pathologic changes (e.g., edema and necrosis) induced by TxA. Antagonists of trypsin and tryptase can mimic the effects of deletion of PAR_2 and DPPI. While the studies were done in mice, the mechanisms are likely similar in humans. TxA leads to increased expression and activity of PAR_2 in human colonocytes; trypsin IV expression is also increased by TxA. PAR_2-mediated TxA-induced colitis involves neurogenic inflammation through the NK_1R. Trypsinogen IV or brain trypsin can activate PAR_1, PAR_2, and PAR_4. This human trypsin is resistant to inhibitors (475). Trypsinogen IV was identified in the brain and is a splice variant of mesotrypsinogen (476). Trypsinogen IV is also expressed in normal human colonic mucosa (443).

5.5. PARs in the Nervous System

5.5.1. Physiology.

The early evidence to suggest that PARs mediated nervous system physiology included the finding that thrombin induced a change in neuron morphology and neurite retraction; moreover, continued activation by thrombin led to neuronal apoptosis (90). Within a few years of demonstrating thrombin's effects on neurons, PAR_1 was shown to be responsible (477–479). Additional studies confirmed that continuous exposure of neurons to thrombin led to apoptosis from PAR_1 activation (480–483). In 1994 it was demonstrated that granzyme A, a serine protease released by T lymphocytes, activates PAR_1 on neurons and astrocytes (484). Activation of PAR_1 by thrombin or granzyme A results in neurite retraction, an action that can be inhibited by function-inhibiting antibodies to PAR_1. Thrombin also produced a change in the morphology, proliferation, and differentiation of neuroblastoma cells (485) and astrocytes (90, 483, 486).

Following the discovery of PAR_2 expression on neurons (sect. 3.5), the role of PAR_2 in neurogenic inflammation would soon follow (**FIGURE 7**). Neurogenic inflammation is characterized by arteriolar vasodilation, opening of gaps in postcapillary venules, plasma extravasation, and neutrophil infiltration into tissues (73, 487–489). It was known that neurogenic inflammation was mediated by neuropeptides. Also, arteriolar vasodilation is mediated by CGRP through activation of the $CGRP_1$ receptor, now known as CLR/RAMP1 (490, 491). Gap formation between endothelial cells was mediated by substance P, which activates NK_1R and leads to plasma extravasation and neutrophil mobilization (492, 493). In 2000, the link between PAR_2 and neurogenic inflammation was demonstrated (95). The authors showed that PAR_2 was coexpressed with neuropeptides on DRG, providing anatomic evidence for the role of PAR_2 in neurogenic inflammation. Functional evidence was provided by data confirming that PAR_2 stimulation led to secretion of CGRP and substance P and tissue edema. The PAR_2-activating peptide $SLIGRL\text{-}NH_2$ led to paw edema and infiltration of neutrophils, effects that could be inhibited by antagonists of CLR/RAMP1 and NK_1R. In the same year, it was shown independently that the same PAR_2-activating peptide $SLIGRL\text{-}NH_2$ produced another feature of neurogenic inflammation, nociception (431;

Downloaded from journals.physiology.org/journal/physrev at New York Univ (216.165.095.084) on September 28, 2023.

FIGURE 7). PAR_2 agonism produced thermal, but not mechanical, hyperalgesia, as measured by paw withdrawal. Moreover, the animals exhibited nociceptive behavior including biting and licking. The hyperalgesic effect had a rapid onset and was not lost following mast cell degranulation, suggesting that activation of PAR_2 on sensory afferents directly led to neuronal activation and hyperalgesia. Hyperalgesia induced by PAR_2 agonism was independently demonstrated (96).

The roles of PAR_1, PAR_3, and PAR_4 in nociception are poorly characterized compared to PAR_2. PAR_1 is not expressed by TRPV1+ neurons (260). PAR_1 and PAR_4, at the appropriate protease concentration, mediate antinociception (494, 495). McNaughton and colleagues (185) have characterized the expression and function of PARs besides PAR_2 on neurons that mediate nociception. PAR_1 and PAR_4 are expressed on small peptidergic neurons and larger myelinated neurons; the former location is proposed to mediate nociception, and the latter site is proposed to mediate antinociception.

Mesotrypsin, which is encoded by PRSS3 and also known as brain trypsin, is a serine protease that is resistant to inhibitors. Mesotrypsin is isolated from the brain. PAR_1 on astrocytes in rats is activated by mesotrypsin, which has been proposed to contribute to physiologic and pathologic conditions in the brain (496). Wang et al. (496) did not find that PAR_2 is activated by mesotrypsin; however, other investigators have shown that mesotrypsin activates PAR_2 to induce inflammation and pain (475).

A looming question in the GPCR field has been how ligand binding and/or cleavage of the receptor leads to membrane depolarization. A recent paper addressed this question by studying how PAR_1 activation on nodose ganglia neurons mediated a change in current (497). PARs on pulmonary sensory neurons are involved with neuronal excitability, similar to their role on peripheral sensory neurons. C-fiber activation in the lungs contributes to inflammatory disease. TRP channels have been proposed to possibly mediate membrane depolarization. Undem and colleagues (497) showed that PAR_1 activation leads to an increase in intracellular Ca^{2+} that involves TRPA1 but not TRPV1. PAR_1 is expressed by mouse nodose C-fibers but not jugular ganglion neurons. In some nodose C-fibers, TRPA1 contributes to the intracellular Ca^{2+} increase following selective activation of PAR_1 by TFLLR but not membrane depolarization. The PAR_1-mediated action potential discharge depended on the PLCβ3 isozyme of PLC. The investigators showed that neither TRPA1 nor TRPV1 are required for PLC-dependent activation. C-fiber neurons from wild-type and TRPA1/TRPV1 double knockout mice exhibited the same action potential number and peak discharge frequency when activated by TFLLR. Another example of regulation of TRP channel activity by PARs is reflected by the increase in vascular permeability following activation of PAR_1, which is mediated through TRPV4 (269; sect. 4.7).

The analysis of pulmonary jugular and nodose ganglia in response to PAR_2 activation also sheds light on the question of how activation of PAR_2 leads to neuronal activation. PAR_2 activation leads to hyperexcitability of pulmonary jugular and nodose ganglia neurons through regulation of large-conductance Ca^{2+}-activated potassium (BK or big potassium; also known as KCa1.1) channels in the rat (498). BK channels respond to an increase in Ca^{2+} conductance, which leads to opening of potassium channels and neuronal repolarization. The second messengers PLC, PKC, PKA, and MEK/ERK were not involved in PAR_2-mediated regulation of BK channels. Like sensitization of TRP channels by PAR_2 activation on sensory neurons (261) (sect. 4.7), PAR_2 is activated by serine proteases secreted by house dust mites on vagal pulmonary sensory neurons. These are anatomically relevant pulmonary sensory neurons identified by DiI labeling. These proteases secreted from house dust mites sensitize the response to capsaicin, as measured by Ca^{2+} fluorimetry, in a PLC- and PKC-mediated manner (499). The action of PAR_2 on nociceptors has also pointed to a role in inhibition of potassium channels, which mediate neuronal activation and nociception (500). Inhibition of the M current was mediated by PLC, Ca^{2+}, and PIP_2.

PAR_1 agonists have neuroprotective effects on CNS neurons in conditions of hypoglycemia, as well as oxidative and environmental stress (480). Brain astrocytes undergo morphological changes, proliferate and secrete endothelin-1 and nerve growth factor upon activation of PAR_1 (479, 501, 502). Activation of PAR_1 and PAR_3 by APC has neuroprotective effects. APC is a serine protease that along with its neuroprotective effects, has anticoagulant properties (sects. 3.1 and 4.1). Mutated forms of APC have been generated to disambiguate APC's anticoagulant and neuroprotective properties, as well as whether effects are observed in rodents are observed in human cells. 3K3A-APC is a mutated form of human APC (503–505). 3K3A-APC has less than 10% of APC's anticoagulant properties, but it has APC's cell signaling and neuroprotective effects in models of amyotrophic lateral sclerosis (506), traumatic brain injury (507), and stroke (508). Both APC and 3K3A-APC exert their neuroprotective effects through PAR_1 and PAR_3 (508–513). APC induces proliferation of neural progenitor cells (NPCs) in ischemic (514) and traumatic injury (515) mouse models; the proliferative effect is not observed in PAR_1 knockout mice. Fetal human neural stem and progenitor cells divide and differentiate when treated with human 3K3A-APC, similar to the cellular effects observed in

Downloaded from journals.physiology.org/journal/physrev at New York Univ (216.165.095.084) on September 28, 2023.

response to fibroblast growth factor and brain-derived growth factor (516). At the same time, 3K3A-APC inhibits differentiation of astroglial cells (517). This response, neuronal differentiation and astrogliosis, is the opposite of that found with CNS injury and pathology; therefore, mutated forms of APC might hold potential for therapy. The neuroprotective effects of APC require both PAR_1 and PAR_3 in most cell types; however, only PAR_1 is required in other cell types (509–511, 518). The neurogenic effects of 3K3A-APC in human neural progenitor cells is mediated through PAR_1- and/or PAR_3-sphingosine-1-phosphate receptor-1 (S1PR1)-mediated Akt signaling (519). Activation of S1PR1 is involved in the proliferation and migration of neural progenitors, likely through PI3K/Akt signaling (520).

5.5.2. Pathology.

Thrombin and PARs contribute to a number of neurologic diseases, including, but not limited to, ischemia, hemorrhage, HIV-associated dementia, Alzheimer's disease, and traumatic head injury. As tissue plasminogen activator is effective with occlusive stroke, the role of serine proteases on CNS neuronal function following ischemic injury is of interest. When thrombin is infused into the caudate putamen, the resulting cellular features are consistent with those seen following trauma, such as the formation of a glial scar (521, 522). PAR_1 mediates glial proliferation, retraction of neurites, and cell death (90). Thrombin also precipitates seizures when it is injected into the basal ganglia of rats. PAR_1 and PAR_2 activation induces neuronal inflammation and cytotoxicity (523, 524).

Neurologic conditions affect PAR_1 expression. Trauma, such as nerve transection, impacts PAR_1 expression; for example, facial nerve transection produces a decrease in PAR_1 mRNA expression in facial motoneurons (525). Ischemia, on the other hand, leads to an increase in the expression of PAR_1 in hippocampal neurons and glia (526). In the CNS, thrombin activation of PAR_1 on glial cells produces neuroinflammation (527).

PAR_1 is upregulated in HIV encephalitis and in the brains of patients with HIV-associated neurocognitive disorders (528). HIV-infected macrophages are a source of proteases that can activate PAR_2, including cathepsin B and cathepsin G (529). Trypsin, the canonical activator of PAR_2, is absent from the CNS. CNS mast cells secrete tryptase that cleave PAR_2 in the nervous system. Furin, a PAR_2 protease that cleaves at the canonical site, is neuroprotective in the setting of HIV (530). Activation of PAR_2 in the brain prevents neuronal death and prevents behavioral changes associated with HIV (523).

5.6. PARs in the Immune System

5.6.1. Physiology.

PARs are an ideal immune system regulator, based on cellular expression and the change in local concentrations of proteases that accompany tissue injury, inflammation, and barrier compromise. PAR expression on epithelial surfaces that line the skin and internal organs (sect. 3.1), as well as on nerves that innervate these tissues (sect. 3.5), allows these GPCRs to serve as sensors for proteases secreted by microorganisms such as fungi, mites, and bacteria. Expression of PARs on immune cells allows these cells to alter their activity and development based on protease activation.

The link between coagulation and inflammation has long been appreciated. A thrombin-like receptor, rather than the thrombin receptor itself, produced immune cell activation and chemotaxis. Evidence for a thrombin-like receptor came from neutrophils, as inactivated thrombin could produce neutrophil chemotaxis (531–533). This finding led to the hypothesis that proteases at sites of inflammation could generate fragments of thrombin, which did not have proteolytic activity but could activate processes associated with inflammation, such as leukocyte chemotaxis. Supporting evidence showed that if the cleavage site of the thrombin receptor was inactivated with antibodies, thrombin could still induce neutrophil chemotaxis. While it was recognized that proteolytic activity was not required for neutrophil chemotaxis, it was also known that the actions of thrombin could occur through a receptor that was not the thrombin receptor. The PAR_1-activating peptide TRAP was shown to increase intracellular Ca^{2+} but did not require a proteolytically activated thrombin receptor (i.e., PAR_1), which had been described 4 years earlier (4). Experiments showed that there was a receptor that caused neutrophil chemotaxis that did not require proteolysis. Evidence from neutrophils in 1995 suggested that neutrophils have a receptor that was activated by a protease that was not thrombin (120). It was known that neutrophils did not stain for an antibody to the thrombin receptor (127). An inactive mutant of thrombin (Ser195Ala) produced neutrophil chemotaxis of the same amplitude as that produced by thrombin. Neutrophil chemotaxis was not impacted by antibodies to the cleavage site of PAR_1. Moreover, TRAP did not stimulate neutrophil chemotaxis (120). Hirudin, or the COOH-terminal fragments of hirudin, inhibited thrombin-induced neutrophil chemotaxis (532, 533). Translational relevance is seen with increased expression of PAR_2 on neutrophils in patients with sepsis (534). Early experimental results showed that TRAP produced an increase in Ca^{2+}, while thrombin did not, in certain cells. When alanine was substituted on

Downloaded from journals.physiology.org/journal/physrev at New York Univ (216.165.095.084) on September 28, 2023.

positions 1, 2, 3, and 5, the response of neutrophils to TRAP was reduced. This finding was a surprise based on what was anticipated for thrombin receptor agonist activity. There were further distinctions between the response to TRAP and thrombin. While serine in position 1 is not essential for thrombin activation, there was diminished activity if leucine in position 4 is replaced by alanine (156). The solution to this question came 3 years later when it was shown that TRAP could activate PAR_2 (41, 165) (sect. 4.3). PAR_2 was cloned from endothelial cells and shown to be thrombin insensitive. PAR_2 was also upregulated when exposed to inflammatory mediators (348). The effect of IL-1α and TNF-α on the expression of PAR_2 on endothelial cells further supported the role of PAR_2 in the inflammatory response (165).

Activation of PAR_2 mediates the migration of leukocytes through lymph nodes. Thrombin activates dendritic cells, which affects their migration through lymph nodes in models of endotoxemia. PAR_2 signaling mediates the uptake of antigens and T-cell trafficking by dendritic cells (535). Following PAR_2 activation of $CD11c^{high}$ dendritic cells, these cells showed increased expression of major histocompatibility complex class II and CD86 and migration toward draining lymph nodes. Furthermore, activated T cells, which included $CD4^+$ and $CD8^+$ T cells, also migrated to draining lymph nodes. The role of PAR_2 was confirmed using global knockout mice and a PAR_2-specific-activating peptide (536). As mentioned previously, there are also distinctions between in vivo rodent models with respect to inflammation.

5.6.2. Pathology.

PARs contribute to the pathologic effects of systemic inflammation, including platelet activation, endothelial cell damage, leukocytosis, organ damage, and death. The effect of PARs on inflammatory disease is not straightforward, as PAR activation can improve or worsen inflammatory disease. Infusion of lipopolysaccharide induces a state of endotoxemia, and this model is commonly used to study the contribution of PARs to systemic inflammation; however, this model may not accurately recapitulate systemic inflammation in conditions such as bacterial sepsis in humans. The roles of PAR_1, PAR_2, and PAR_4 have been studied in an endotoxemia model generated in global knockout mice. Mice deficient in one of these PARs were studied, along with double knockouts for PAR_1/PAR_2 and PAR_2/PAR_4 (537).

PAR_2 has a central role in the development of inflammatory diseases. PAR_2 is expressed by lymphocytes, neutrophils, eosinophils, and monocytes; endogenous and exogenous inflammatory mediators upregulate PAR_2. Activation of PAR_2 leads to erythema, edema, and pain. The interaction of PAR_2 with the cytoplasmic domain of TF contributes to its role in inflammation. Sustained activation of the innate immune system contributes to disseminated intravascular coagulation that is associated with sepsis. Disseminated intravascular coagulation is defined by uncontrolled generation of blood clots, which leads to occlusion of smaller blood vessels, and is characterized with thrombin-antithrombin and antithrombin III levels, along with microvascular fibrin deposition. The condition can occur in the setting of sepsis, trauma, pregnancy, and cancer. In a lipopolysaccharide infusion model, deletion of PAR_2 did not impact the outcome or measurements of glucose, alanine transaminase, creatinine, or lipase in the serum of a mouse model; however, fever was reduced (538).

The role of PAR_2 in neurogenic inflammation is well characterized (**FIGURE 7**). Its presence on sensory afferent neurons that innervate cutaneous and mucosal epithelia enables PAR_2 to mediate the clinical manifestations of inflammation including edema, redness, warmth, and pain. Sensory neurons extend from the periphery to the spinal cord, where activation of PAR_2 at both locations leads to the secretion of the substance P and CGRP (95, 539). Edema is mediated by plasma extravasation, which involves substance P release and activation of the NK_1R on endothelial cells in postcapillary venules. Plasma extravasation is accompanied by granulocyte infiltration. Increased blood flow leads to an elevated temperature, redness, and edema, clinical features attributed to substance P. Several clinical features of neurogenic inflammation can be reduced or blocked by depletion of PAR_2 or through the use of a PAR_2 antagonist. For example, injection of carrageenan leads to paw edema; this is not present in *F2rl1*-/- mice or mice treated with a cell-penetrating PAR_2 pepducin antagonist (540). PAR_2-mediated neurogenic inflammation is regulated by insulin; insulin reduces the PAR_2-mediated inflammatory effect in an insulin-deficient murine type I diabetes model (541).

5.7. PARs in Cancer

The hallmarks of cancer, as described by Hanahan and Weinberg (542), include sustained proliferative signaling, evasion of growth suppression, resisting cell death, replicative immortality, angiogenesis, and invasion and metastasis. PARs, especially PAR_1 and PAR_2, play a role in these hallmarks (**FIGURE 9**). This was first described for thrombin-mediated cancer cell invasion via PAR_1 (reviewed in Ref. 543).

5.7.1. Proliferation.

PAR_1 agonists induce cell proliferation and motility in cancers. Tumor-associated macrophages also play a role in the contribution of PAR_1 to carcinogenesis. PAR_1

Downloaded from journals.physiology.org/journal/physrev at New York Univ (216.165.095.084) on September 28, 2023.

activation on macrophages leads to the secretion of growth factors and thrombin (544). Trypsin, tryptase, and thrombin within the cancer microenvironment activate PAR_1, as well as PAR_2, to drive the differentiation of monocytes into macrophages.

PAR_2 and its activating proteases (e.g., trypsin, mast cell tryptase, type II transmembrane serine protease (TMPRSS2), uPA, FXa, FVIIa, tissue factor or factor III, matriptase, and KLKs) are upregulated in human cancers including colorectal cancer, lung adenocarcinoma, glioma, cutaneous squamous cell carcinoma (SCC), and oral SCC (545–550).

PAR_2, acting through direct and indirect mechanisms, is a mitogenic factor in cancers. Direct mechanisms involve Ca^{2+} release, activation of PKCα, and activation of ERK1/2 (sect. 4.5). One indirect mechanism involves transactivation of EGFR (sect. 4.7), which then activates ERK1/2 and NF-κB. Trypsin activation of PAR_2 leads to engagement of integrin $\alpha_5\beta_1$ to bind fibronectin, which stimulates proliferation of human gastric carcinoma cells (551, 552). Downregulation of the microRNA miR-34a is an indirect mechanism through which PAR_2 contributes to cancer cell proliferation. The G_1/S checkpoint regulator cyclin D1 is negatively regulated by miR-34a. PAR_2 activation suppresses miR-34a through TGFβ, which leads to disinhibition of cyclin D1, activation of E2F transcription factors, and induction of cellular proliferation in colon cancer cells. Knockdown of PAR_2 in cells used to generate a xenograft model yielded tumors of decreased weight (553). PAR_1 can also indirectly contribute to cellular proliferation. PAR_1 activation by an activating peptide leads to downregulation of $p21^{Cip1/Waf1}$ and upregulation of cyclin D1. $p21^{Cip1/Waf1}$, also known as cyclin-dependent kinase inhibitor 1, mediates cell cycle arrest following DNA damage through p53 (554).

EGFR is transactivated by GPCRs, including PAR_2, which contributes to proliferation in several types of cancers (252, 555). EGFR internalization, which depends on dynamin fission in clathrin-independent pathways and nuclear translocation, leads to tumor progression (556–558). PAR_2-EGFR transactivation affects survival in patients with colon, cervical, and gastric cancer (252, 555, 559). A 2020 study made use of data from The Cancer Genome Atlas and found that PAR_2 is overexpressed in ovarian cancer relative to normal tissue (255). Transactivation of PAR_2 induces expression of transcription factors including *FOS*, *MYC*, and *STAT3*, along with *PTGS2* through MEK-ERK1/2 signaling, which increases PGE_2. Transactivation of EGFR and the increase in PGE_2 lead to increased ovarian cancer cell migration and invasion.

5.7.2. Motility, invasion, and metastasis.

Cancers express PARs (sect. 3.7), as well as their respective activating proteases, therefore there is a molecular basis for autocrine regulation that contributes to the hallmarks of cancer. The finding that activation of PAR_1 and PAR_2 by their activating peptides across different prostate cancer cell lines leads to increased expression and activity of proteases provides further evidence for an

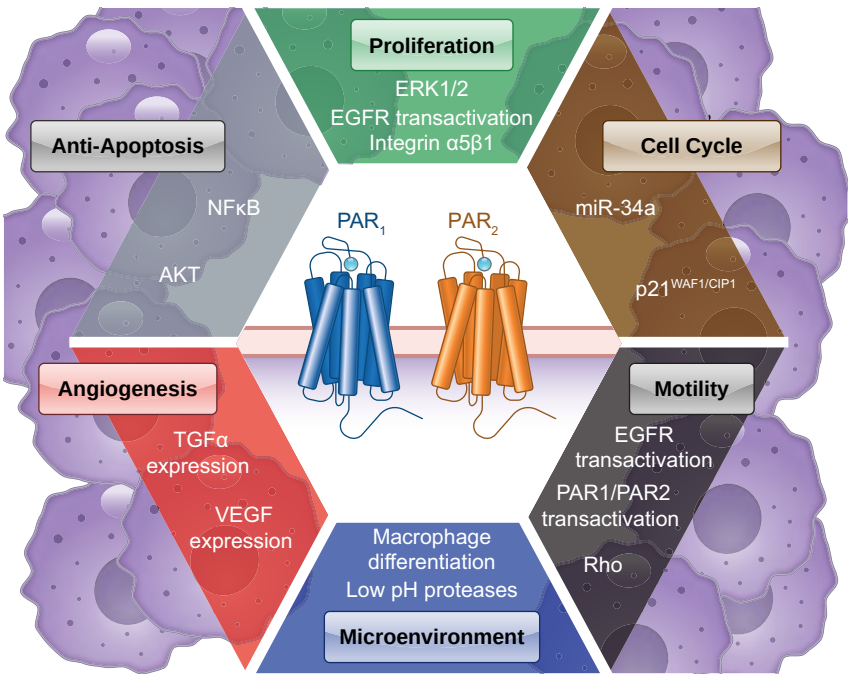

FIGURE 9. Protease-activated receptor (PAR) signaling in cancer. Proteases and PARs contribute to numerous pathways involved in the "hallmarks of cancer" (542). The acidic tumor microenvironment can enhance protease activity. PARs activate downstream signaling pathways and transactivate other receptors that promote cancer. EGFR, epidermal growth factor receptor; TGFα, transforming growth factor-α.

Downloaded from journals.physiology.org/journal/physrev at New York Univ (216.165.095.084) on September 28, 2023.

autocrine function between PARs and proteases in cancer (560). The same effect, secretion and increased activity of proteases, is seen with activation of PAR_1 by thrombin or PAR_1-activating peptide in oral SCC (561).

PAR_1 mediates both invasion and metastasis. Expression of PAR_1 is low or absent in normal breast tissue, benign breast lesions, and noninvasive breast carcinoma; however, PAR_1 is overexpressed in breast cancers (138, 562, 563). A causative role for PAR_1 in breast cancer invasion and metastasis has been demonstrated. In an experiment using PAR_1 antisense treatment of a breast cancer cell line that exhibits aggressive metastatic behavior, the antisense treatment reduced invasion in a Matrigel migration assay (564).

Thrombin activation of PAR_1 mediates cancer cell attachment to platelets and endothelial cells in melanoma (565–568). While PAR_2 expression in human melanomas is comparable to levels in benign melanocytic nevi, PAR_1 expression is increased in atypical nevi and melanoma compared to common melanocytic nevi (569). The effect of thrombin on cancer cell motility is thought to be mediated by PAR_1; however, a potentially intriguing mechanism that drives cancer cell motility involves thrombin activation of PAR_1 and transactivation of PAR_2. This finding was revealed by desensitizing PAR_2 using an activating peptide; when PAR_2 was desensitized, the migratory effect of thrombin was reduced. PAR_2 is transactivated following thrombin activation of PAR_1, exposure of the PAR_1 tethered ligand, and formation of a PAR_1-PAR_2 heterodimer (**FIGURE 4*A***), a process that contributed to cancer cell metastasis in melanoma and prostate cancer. Once TF generates and activates FVIIa and FXa, both factors can activate PAR_1 and PAR_2. The roles of PAR_1 and PAR_2 in cancer cell migration were demonstrated with interfering RNAs to deplete breast cancer cells of the two PARs. The studies demonstrated that coagulant proteases FVIIa and FXa signal through PAR_2, and not PAR_1, to mediate breast cancer cell migration and invasion. PAR_2 and TF show increased expression within the invasive component of human breast cancer tissues (549).

PAR_2 activation produces several processes associated with carcinogenesis including migration (140), angiogenesis (351, 570), and signaling; however, the responsible activating proteases are less clearly defined. TF is the primary activator of the coagulation cascade. TF is responsible for generating coagulation factors (i.e., proteases) on the plasma membrane of cancer cells. Proteases degrade proteins, adhesion molecules, and the ECM; proteases also activate kinases and growth factors. Proteases are regulated by endogenous inhibitors. Proteases are commonly overexpressed in cancer. The lysosomal cysteine protease cathepsin S is unique because it is active at the pH consistent of the extracellular environment. Accordingly, cathepsin S can activate PAR_2 in the setting of cancer. Cathepsin S is overexpressed in several cancers including cancer of the GI system [hepatocellular carcinoma (571), pancreatic cancer (572), colon cancer (573), prostate cancer (574, 575), uveal melanoma (576), astrocytoma (577), and glioblastoma (578)]. Elevated cathepsin S expression within breast cancer, at the primary site, correlates with reduced metastasis-free survival in breast cancer patients (579). The role of cathepsin S and PAR_2 in mediating the processes of cancer has been investigated with hepatocellular carcinoma. When cathepsin S expression is inhibited with siRNA, there was inhibition of cancer proliferation, invasion, and angiogenesis as measured by in vitro assays and tumor volume in a mouse model (571). Silencing cathepsin S also induces apoptosis in cells; this process is mediated by PAR_2 regulation of NF-κB signaling. Serum levels of cathepsin S correlate with cancer behavior (tumor, size, venous invasion) in humans (580). Cathepsin S expression was also found to correlate with poor survival in patients with glioblastoma; expression was higher in grade IV tumors relative to grade I–III tumors. In the normal human brain, cathepsin S expression is low or absent (578).

5.7.3. Angiogenesis.

PAR_1 activation leads to an increase in VEGF expression at the transcript and protein level, a key mediator of angiogenesis (581). The role of PAR_2 in regulating VEGF in cancers has been demonstrated with solid cancers, including breast, stomach, and pancreas (582–584). A series of in vitro studies have supported the role of PAR_2 in mediating angiogenesis in pancreatic cancer. PAR_2 activation regulates angiogenesis in pancreatic cancer through induced TGF-α and VEGF-A expression; the former is mediated by integrin-linked kinase/hypoxia-inducible factor-1α and the latter by MEK (582). TGF-α activates EGFR. Activated EGFR contributes to proliferation, differentiation, and invasion (585). PAR_2 also directly activates EGFR (552). As mentioned, thrombosis is a well-established feature of cancer. Factors that mediate thrombosis, including TF and FVII, activate PAR_2. Blocking TF/PAR_2 signaling on cancer cells decreases vessel density (586). PAR_2 deficiency, but not PAR_1 deficiency, decreases the transformation rate of adenoma to adenocarcinoma in a spontaneous breast cancer development model based on the oncogenic middle T-antigen protein, a model that recapitulates human breast cancer development (587). PAR_2 regulates angiogenesis in models besides cancer, including a mouse model of hindlimb ischemia (588).

Because of the role of PARs in several stages of carcinogenesis, PARs are attractive targets for the

Downloaded from journals.physiology.org/journal/physrev at New York Univ (216.165.095.084) on September 28, 2023.

treatment of cancer. Liposomal delivery of PAR_1 siRNA blocked melanoma proliferation and metastasis in a xenograft model. The most immediate advantage of liposomes over viruses for the delivery of siRNA is that the former does not generate the cytokine storm associated with viruses (589). PAR antagonists have been combined with chemotherapeutics to produce a combined or possibly synergistic effect. A PAR_1 inhibitor in the form of a pepducin (sect. 6.2) has been combined with the chemotherapeutic agent taxotere. The pepducin/taxotere combination reduces melanoma growth and metastasis (590). PAR_1 is an ideal cancer target because it is expressed by breast carcinoma (sect. 3.7) but not by benign tissues. MMP1 contributes to progression of several cancers including breast, colon, and esophageal. The MMP1-PAR_1-Akt axis participates in breast cancer progression. A pepducin, P1pal-7, was developed to inhibit PAR_1 and disrupt MMP1-PAR_1-Akt signaling. The advantage of pepducin is its selective cytotoxicity in breast cancer cells; benign breast cells were not affected. When the pepducin was combined with taxotere, as it often is for breast cancer, the combination of drugs was synergistic and highly effective in a breast cancer xenograft model. The mechanism of the two drugs involved inhibition of tumor growth and induction of apoptosis through blockade of Akt, which is required for cell survival.

5.8. Summary

Due to their extensive tissue expression and their activation by proteases, PARs are central to the normal function and pathological states affecting every organ system. Moreover, in the case of the nervous system, PARs serve a protective role. The related and dependent processes of coagulation and inflammation, which are both regulated by PARs, lead to thromboembolic events that characterize diseases affecting the vascular system in the periphery, brain, lungs, and heart. Accordingly, PARs are considered high-value targets for drug development to reduce major causes of morbidity and death including cardiovascular and cerebrovascular disease.

6. DRUG DEVELOPMENT TARGETING PARS

6.1. Existing PAR Agonists and Antagonists: Peptides, Small Molecules, and Antibodies

Preclinical studies that implicated PARs in disease spurred drug discovery efforts to develop PAR antagonists from the late 1990s. The development of PAR antagonists was initially met with skepticism in light of the intramolecular mechanisms of proteolytic activation by a tethered ligand, as this was deemed challenging to inhibit. However, PARs have since been successfully antagonized by peptidic compounds based on activating peptide sequences, as well as small molecules and PAR-directed antibodies (**FIGURE 10**). Antagonists can disrupt PAR signaling by several mechanisms. Orthosteric PAR antagonists block the intermolecular interaction between the tethered ligand domain and the cleaved receptor. Allosteric PAR antagonists interact with a site different from that occupied by the tethered ligand and either suppress or amplify PAR signaling (negative or positive allosteric modulators, respectively). Antagonists can also interact with the cleavage site to suppress proteolytic activation or with protease binding sites (if present) to disrupt binding and efficient proteolysis.

6.1.1. PAR_1.

PAR_1 antagonists were developed as antithrombotic drugs to prevent protease-mediated platelet aggregation. PAR_1 antagonists include peptidic (e.g., BMS-200261, RWJ-58259) and nonpeptidic molecules (e.g., FR-171113, SCH 530348/Vorapaxar, E555/atopaxar, F 16618; Refs. 591–596). Antagonistic antibodies can also target various PAR_1 domains, including the NH_2 terminus immediately distal to the canonical cleavage site (597) and the hirudin-like thrombin-binding domain (598).

Peptidomimetic antagonists are analogs of activating peptides designed to compete with the orthosteric site of the intramolecular interaction. BMS-200261 was developed as a peptidic antagonist arising from NH_2-terminal acylation of tetrapeptides mimicking SFLLR binding (591). BMS-200261 had a nanomolar IC_{50} with the ability to reduce platelet aggregation induced by SFLLRN-NH_2. RWJ-56110 was discovered as a potent, selective PAR_1 antagonist that interfered with Ca^{2+} signaling, platelet aggregation, and cell proliferation (599).

Small molecule antagonists were pursued to overcome the limitations of peptidomimetics, such as their limited bioavailability. Vorapaxar (SCH 530348) was the first small molecule inhibitor of PAR_1 (600). Vorapaxar occupies the orthosteric binding site (Ref. 29; sect. 2.2). Atopaxar (E5555) is a small molecule inhibitor that interacts with ECL2 of PAR_1 (601). Vorapaxar was Food and Drug Administration-approved in 2014 as a first-in-class oral PAR_1 antagonist. Vorapaxar, however, led to increased bleeding in Phase II trials (602). This was attributed to its slow kinetic dissociation (603). This increased bleeding risk led to a general “black box warning” against serious bleeding and its withdrawal from European Union recommendations. On-target side

Downloaded from journals.physiology.org/journal/physrev at New York Univ (216.165.095.084) on September 28, 2023.

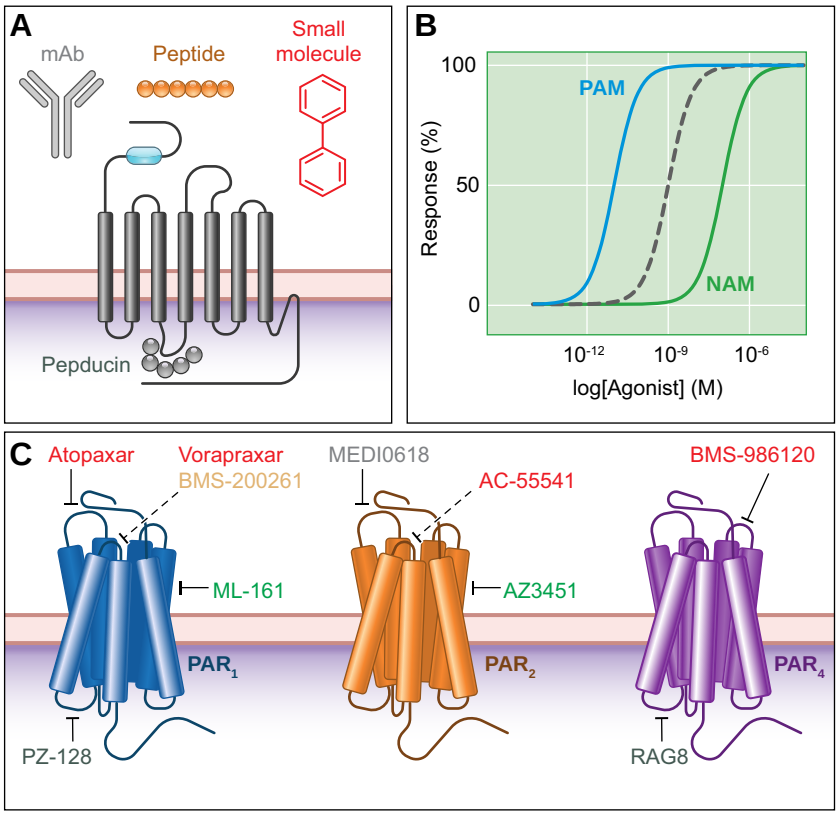

FIGURE 10. Therapeutic targeting of protease-activated receptors (PARs). *A*: multiple drug classes have been developed to target PAR signaling, including peptidic and small molecule antagonists and monoclonal antibodies (mAbs). *B*: receptor signaling can be modified by allosteric modulators that either enhance agonist activity [positive allosteric modulator (PAM)] or decrease signaling [negative allosteric modulator (NAM)]. *C*: examples of PAR inhibitors, including mAbs (gray), peptides (yellow), small molecules (red), NAMs (green), or pepducins targeting intracellular loops (blue). These can target allosteric sites or the orthosteric binding site of the tethered ligand (dashed).

effects are a liability of PAR_1 agonists considering its widespread distribution. For example, PAR_1 expression on endothelial cells was attributed to the intracranial bleeding that occurs with PAR_1 antagonism. PAR_1 activation maintains endothelial cell integrity via APC; thus antagonism also impacts platelet aggregation and vessel wall integrity (604). While PAR_4 has a central role in hemostasis, it is not as widely expressed. Accordingly, PAR_4 has the potential as a more tractable target for inhibitors for cardiovascular indications. Additionally, APC-like agonists were developed as an alternative due to their neuroprotective functions (605, 606). 3K3A-APC, an analog of APC (607), has since demonstrated promising outcomes with successful data emerging from clinical trials (608, 609).

Negative allosteric modulators have been developed to inhibit PAR_1 signaling. For example, ML 161 is a small molecular negative allosteric modulator with potent inhibition (IC_{50}: ~0.3 μM) of SFLLRN-induced P-selectin expression in platelets (610). Parmodulins are a class of small molecule inhibitors developed as allosteric PAR_1 antagonists that interfere with Gα-protein binding (611). This key study demonstrated bias, with preferential inhibition of $G\alpha_q$ signaling compared to $G\alpha_{12/13}$ in response to PAR_1. Unlike vorapaxar, parmodulins can maintain cytoprotective APC signaling while inhibiting thrombin-mediated signaling. Whereas an antagonist inhibits any signaling response, a partial agonist leads to a submaximal response relative to the full receptor agonist (612). Partial agonism can be a useful pharmacological property for drugs by preventing the endogenous full agonist from signaling, while producing a weak signal that can maintain basal activity. Having been investigated as antagonists, parmodulins were also shown to be partial agonists. Parmodulins themselves can trigger cytoprotective APC-like signaling in the endothelium and activate Gβγ, PI3K, and NF-κB (613).

6.1.2. PAR_2.

The contributions of PAR_2 to neurogenic inflammation, pain, and other disease processes catalyzed the search for PAR_2 antagonists (reviewed in Ref. 614). The first PAR_2 antagonists, FSLLRY-NH_2 and LSIGRL-NH_2, were peptidic and based on modifications of the canonical tethered ligand domain (196). Other peptide antagonists included K-12940 (615) and K-14585, which showed evidence of partial agonism (616). These compounds favored inhibition against activating peptides rather than trypsin, which limited further development. Peptidic C-391 showed micromolar potency and antagonism of hyperalgesia in vivo (617).

The poor bioavailability and potency of peptidic antagonists led to the development of nonpeptidic ligands,

Downloaded from journals.physiology.org/journal/physrev at New York Univ (216.165.095.084) on September 28, 2023.

including full agonist AC-55541 and partial agonist AC-98170 (262, 618). Modifications were introduced to make molecules more drug-like by developing GB110 and GB83 with selectivity for PAR_2 over PAR_1 (619). This led to the discovery of the biased antagonist GB88 (620). GB88 was an antagonist in $G\alpha_q$-mediated Ca^{2+} signaling, but a partial agonist with respect to cAMP inhibition, ERK1/2 phosphorylation, and Rho kinase signaling (621).

Small molecular PAR_2 antagonists have been developed by Heptares Therapeutics and AstraZeneca, where structural studies have mapped the interaction of these antagonists with PAR_2 (28; sect. 2.2). AZ3541 is a negative allosteric modulator that binds outside the helix domains. AZ8838 binds in a pocket near the extracellular surface and exhibits slow binding kinetics. Vertex Pharmaceuticals also developed a series of imidazopyridazine compounds that inhibit PAR_2 signaling (622). In subsequent studies, antagonist I-191 shows improved potency relative to GB88 (282). This also included I-287, a negative allosteric modulator that inhibits $G\alpha_q$ and $G\alpha_{12/13}$ pathways without affecting $G\alpha_{i/o}$ or β-arrestin2 signaling (623). Crucially, this led to reduced inflammation in vivo. The value of small molecule PAR_2 inhibitors with oral bioavailability, subtype selectivity, and high potency is evident from the variety of pathologies that implicate PAR_2 signaling (sect. 5).

There have been successful examples of antibodies developed against PAR_2. Boehringer Ingelheim developed a humanized blocking antibody against the PAR_2 protease cleavage site with picomolar affinity (624). AstraZeneca developed a monoclonal antibody against PAR_2, MEDI0618, that is undergoing Phase I clinical trials as the first in human safety trial for chronic pain (NCT04198558; Ref. 614).

6.1.3. PAR_1 and PAR_2.

Bivalent compounds simultaneously target more than one receptor. A bivalent antagonist of PAR_1 and PAR_2 was developed by appending PAR_1-selective RWJ-58259 to PAR_2-selective antagonists based on the imidazopyridine scaffold and joined by a polyethylene glycol linker (625). The optimal bivalent antagonist compound 13d successfully reduced Ca^{2+} signaling in endothelial cells and cancer cells.

6.1.4. PAR_4.

Given the liabilities of PAR_1-targeted antagonists, recent drug discovery programs have investigated PAR_4 antagonists as improved antiplatelet therapeutics (reviewed in Ref. 626). Bristol-Myers Squibb developed BMS-986120, a potent, selective, first-in-class small molecule PAR_4 antagonist (627). This study crucially demonstrated reduced bleeding risk in monkeys compared to typical platelet drugs. BMS-986120 has since completed numerous Phase I clinical trials, including positive results on human thrombin formation ex vivo (628).

6.2. *Subcellular Targeting of PAR Antagonists*

The realization that PARs can signal at the plasma membrane and from intracellular domains prompted the development of antagonists targeted at subcellular microdomains.

6.2.1. Plasma membrane targeting.

Cell-penetrating antagonists were developed to penetrate cells and inhibit PARs from an intracellular site. Pepducins are peptidic compounds derived from an intracellular region of PARs. These have a palmitoyl modification as a lipid chain to aid association with the plasma membrane. Pepducins were developed against PAR_1 using peptide sequences based on the ICL3 of PAR_1 and named according to their length (629). Whereas P1pal-13 (palmitate-AVANRSKKSRALF) is an agonist, P1pal-12S (palmitate-RSLSSSAVANRS) is a full antagonist for PAR_1. Interactions with ICL3 interfere with Gα protein binding. This PAR_1 pepducin antagonist, later designated PZ-128, was successful in Phase II clinical trials in patients with coronary artery disease (630).

Pepducins have also been developed against PAR_4. Based on a COOH-terminal motif of PAR_4, "RAG8" (RAGLFQRS) was developed. This is coupled to a palmitoylated region as a cell-penetrating peptide (213). This reduces PAR_4-mediated Ca^{2+} signaling, Akt phosphorylation, and binding to β-arrestin but not MAPK signaling. Given the structural differences between PAR_1 and PAR_4 in this region, RAG8 is PAR_4 selective. Importantly, PAR_1-mediated activation is not affected. When the COOH-terminal sequence of PAR_4 is coupled to RAG8, platelet activation is blocked in vitro and clot consolidation blocked in vivo.

6.2.2. Endosomal membrane targeting.

The discovery that PAR_2 can continue to signal from endosomes and that sustained endosomal signaling mediates long-term nociceptor hyperexcitability and pain prompted the development of endosomally targeted PAR_2 antagonists (203). Tripartite antagonists comprising cholestanol, a PEG linker, and a cargo of I-343 PAR_2 antagonist accumulate in endosomes. These abrogate endosomal signaling and protease-evoked hyperexcitability of nociceptors (sect. 5.5).

Downloaded from journals.physiology.org/journal/physrev at New York Univ (216.165.095.084) on September 28, 2023.

This antagonist also blocks the effects of proteases released from mucosal biopsies on nociceptor hyperexcitability, raising the possibility of using endosome-targeted PAR_2 antagonists for the treatment of IBS pain.

6.3. Future of Drugs Targeting PARs

Vorapaxar is the only PAR-directed drug approved for clinical use. Given the roles of other PARs in pathology in many organ systems (sect. 5), there remain ample opportunities to target PARs for the treatment of diverse diseases. However, the therapeutic targeting of PARs faces several challenges. The widespread expression of PARs (sect. 3) and their roles in essential physiological processes (sect. 5) increase the risks of severe on-target side effects (i.e., mediated by the same receptor). For example, vorapaxar (PAR_1-selective antagonist) effectively inhibits platelet aggregation and can be used to treat thrombotic events, but a small number of patients experienced intracranial bleeds due to the impact on endothelial cell function (602). One approach to limiting on-target side effects is to administer drugs to particular tissues using biomaterials, such as nanoparticles. The incorporation of vorapaxar into cardiac stents would be expected to provide beneficial local protection against inappropriate coagulation without detrimental systemic actions. Similarly, inhaled drugs that preferentially target the airway epithelium, or oral drugs that target the intestinal epithelium, might be useful approaches for treatment of inflammatory diseases of the airway and intestine, minimizing side effects in other tissues.

Another approach that has been used to minimize on-target side effects has been to design ligands that preferentially target receptors in diseased tissue. This approach has been exploited to develop agonists of the μ-opioid receptor that preferentially activate receptors in the acidified microenvironment of diseased tissues (e.g., sites of inflammation and cancer). An analog of fentanyl designed to preferentially interact with μ-opioid receptors in acidic environments provides analgesia without the well-known on-target side effects of respiratory depression and constipation mediated by μ-opioid receptors in normal tissues (631). Given the established roles of PARs in inflamed tissues and cancer, which are usually associated with extracellular acidification, pH-dependent PAR ligands could provide another layer of selectivity.

The concept of biased signaling has attracted considerable attention for GPCR drug development. For example, biased ligands (antagonists or agonists) targeting GPCR signaling pathways that mediate detrimental events but sparing those that mediate beneficial outcomes could provide effective therapy while minimizing side effects. However, a prerequisite for the successful development of biased ligands is that the signaling pathways that mediate the detrimental versus beneficial outcomes of GPCR signaling are known and sufficiently distinct, which is not always the case. The complexities of PAR signaling complicate whether an antagonist or agonist would benefit. For example, a PAR_1 agonist with respect to APC-induced PAR_1 signaling, but an antagonist for thrombin-induced signaling, would be ideal for circulatory pathologies (sect. 5.1). To better target PARs in pathology, it therefore remains vital to understand how PARs function with respect to in vivo physiology and in vitro molecular pharmacology, progressing studies from isolated models to represent the human condition.

6.4. Summary

A range of peptidic, small molecules, and antibody-based therapeutics have been developed against PAR_1, PAR_2, and more recently PAR_4. Vorapaxar is the only PAR-directed drug approved for use in patients, as a first-in-class antiplatelet drug acting through PAR_1. They have since been drugs in clinical trials, including a small molecule inhibitor of PAR_4 as an alternative antiplatelet drug to reduce bleeding risk (BMS-986120), the recombinant APC-like agonist (3K3A-APC), as well as an antibody against PAR_2 for the treatment of pain (MEDI0618). Considering the range of pathologies that PAR signaling implicates, increased understanding of PARs at a molecular level in the human setting will be instrumental in developing better drugs across disease states.

7. CONCLUSIONS

The discovery that thrombin causes the aggregation of platelets by cleaving PAR_1 provided the impetus for intensive investigations of the receptor-mediated actions of proteases. They resulted in the identification of the family of four widely expressed PARs. These GPCRs are now known to regulate mechanisms of homeostasis and disease in most tissues and organs. Antagonists of PAR_1 have advanced to the clinic for the treatment of coagulation disorders, and antagonists of PAR_2 and PAR_4 are in clinical development. Structural studies of PAR_1 and PAR_2 complexed to antagonists have provided an understanding of the mechanisms of activation and antagonism. Future structural studies of PARs in their activated state and complexed with signaling partners and regulatory proteins (e.g., G proteins, β-arrestins) will further enhance the development of selective ligands that may advance to approved drugs. The original concept that proteases activate PARs by cleavage at a single site

Downloaded from journals.physiology.org/journal/physrev at New York Univ (216.165.095.084) on September 28, 2023.

and that cleavage at different sites merely disarms the receptor has been superseded by the realization that proteases can activate PARs by diverse noncanonical mechanisms. Thus proteases that cleave PARs at distinct sites can activate PARs by biased mechanisms leading to unique cellular responses. The four PARs can, therefore, be considered as molecular integrators of the biological actions of a very large number of proteases, many of which likely derive from microorganisms. Proteases from the microbiome could regulate host cell functions by cleaving PARs. This might be of particular importance in the colon, where proteases from commensal and pathogenic bacteria are likely to regulate colonocyte function in health and disease states by cleaving PARs. It is evident that there are major differences between signaling cascades of PAR subtypes, despite structural and genetic similarities. In particular, PAR_3 signaling in its own right remains a major question. The realization that proteases and PARs can signal from subcellular microdomains, which differ depending on the mechanism of PAR activation, adds additional complexity. This also provides an opportunity of developing antagonists that preferentially target PARs in subcellular microdomains with enhanced selectivity and efficacy. The rapidly evolving field of protease and PAR signaling is likely to provide new insights into physiological control and mechanisms of disease, with multiple opportunities for therapeutic intervention.

SUPPLEMENTAL DATA

Supplemental Tables S1–S5 are available at https://doi.org/10.6084/m9.figshare.19739830.

CORRESPONDENCE

Correspondence: N. W. Bunnett (nwb2@nyu.edu).

ACKNOWLEDGMENTS

Parts of the figures were created with BioRender.com, with permission.

GRANTS

Work in the authors' laboratories is supported by grants from the National Institutes of Health (NS102722, DE026806, DK118971, and DE029951 to N.W.B. and B.L.S.), Department of Defense (W81XWH1810431 and W81XWH2210239 to N.W.B. and B.L.S.), the Leon Levy Foundation for the Leon Levy Fellowship in Neuroscience (to C.J.P.), the Grimwade Fellowship funded by the Russell and Mab Grimwade Miegunyah Fund at the University of Melbourne (to L.E.E.), and a DECRA Fellowship from the Australian Research Council (ARC; DE180100418 to L.E.M.).

DISCLOSURES

N. W. Bunnett is a founding scientist of Endosome Therapeutics Inc. None of the other authors has any conflicts of interest, financial or otherwise, to disclose.

AUTHOR CONTRIBUTIONS

N.W.B. conceived and designed research; C.J.P., L.E.E., N.W.B., and B.L.S. prepared figures; C.J.P., L.E.E., N.W.B., and B.L.S. drafted manuscript; C.J.P., L.E.E., N.W.B., and B.L.S. edited and revised manuscript; C.J.P., L.E.E., N.W.B., and B.L.S. approved final version of manuscript.

REFERENCES

1. Schmidt A. Neue Untersuchungen ueber die Fasserstoffesgerinnung. **Pflüger Arch** 6: 413–538, 1872. doi:10.1007/BF01612263.

2. Van Obberghen-Schilling E, Chambard JC, Lory P, Nargeot J, Pouyssegur J. Functional expression of Ca2(+)-mobilizing alpha-thrombin receptors in mRNA-injected Xenopus oocytes. **FEBS Lett** 262: 330–334, 1990. doi:10.1016/0014-5793(90)80221-4.

3. Pipili-Synetos E, Gershengorn MC, Jaffe EA. Expression of functional thrombin receptors in xenopus oocytes injected with human endothelial cell mRNA. **Biochem Biophys Res Commun** 171: 913–919, 1990. doi:10.1016/0006-291X(90)90770-N.

4. Vu TK, Hung DT, Wheaton VI, Coughlin SR. Molecular cloning of a functional thrombin receptor reveals a novel proteolytic mechanism of receptor activation. **Cell** 64: 1057–1068, 1991. doi:10.1016/0092-8674(91)90261-V.

5. Nystedt S, Emilsson K, Wahlestedt C, Sundelin J. Molecular cloning of a potential proteinase activated receptor. **Proc Natl Acad Sci U S A** 91: 9208–9212, 1994. doi:10.1073/pnas.91.20.9208.

6. Connolly AJ, Ishihara H, Kahn ML, Farese RV Jr, Coughlin SR. Role of the thrombin receptor in development and evidence for a second receptor. **Nature** 381: 516–519, 1996. doi:10.1038/381516a0.

7. Xu WF, Andersen H, Whitmore TE, Presnell SR, Yee DP, Ching A, Gilbert T, Davie EW, Foster DC. Cloning and characterization of human protease-activated receptor 4. **Proc Natl Acad Sci U S A** 95: 6642–6646, 1998. doi:10.1073/pnas.95.12.6642.

8. Kahn ML, Zheng YW, Huang W, Bigornia V, Zeng D, Moff S, Farese RV Jr, Tam C, Coughlin SR. A dual thrombin receptor system for platelet activation. **Nature** 394: 690–694, 1998. doi:10.1038/29325.

9. Somers GR, Hammet F, Woollatt E, Richards RI, Southey MC, Venter DJ. Chromosomal localization of the human P2y6 purinoceptor gene and phylogenetic analysis of the P2y purinoceptor family. **Genomics** 44: 127–130, 1997. doi:10.1006/geno.1997.4841.

10. Yang-Feng TL, Xue FY, Zhong WW, Cotecchia S, Frielle T, Caron MG, Lefkowitz RJ, Francke U. Chromosomal organization of

Downloaded from journals.physiology.org/journal/physrev at New York Univ (216.165.095.084) on September 28, 2023.

adrenergic receptor genes. **Proc Natl Acad Sci U S A** 87: 1516–1520, 1990. doi:10.1073/pnas.87.4.1516.

11. Jin M, Yang HW, Tao AL, Wei JF. Evolution of the protease-activated receptor family in vertebrates. **Int J Mol Med** 37: 593–602, 2016. doi:10.3892/ijmm.2016.2464.

12. Ishii K, Gerszten R, Zheng YW, Welsh JB, Turck CW, Coughlin SR. Determinants of thrombin receptor cleavage. Receptor domains involved, specificity, and role of the P3 aspartate. **J Biol Chem** 270: 16435–16440, 1995. doi:10.1074/jbc.270.27.16435.

13. Riewald M, Kravchenko VV, Petrovan RJ, O'Brien PJ, Brass LF, Ulevitch RJ, Ruf W. Gene induction by coagulation factor Xa is mediated by activation of protease-activated receptor 1. **Blood** 97: 3109–3116, 2001. doi:10.1182/blood.V97.10.3109.

14. Kondreddy V, Pendurthi UR, Xu X, Griffin JH, Rao LV. FVIIa (Factor VIIa) induces biased cytoprotective signaling in mice through the cleavage of PAR (protease-activated receptor)-1 at xanonical Arg41 (Arginine41) site. **Arterioscler Thromb Vasc Biol** 40: 1275–1288, 2020. doi:10.1161/ATVBAHA.120.314244.

15. Isberg V, de Graaf C, Bortolato A, Cherezov V, Katritch V, Marshall FH, Mordalski S, Pin JP, Stevens RC, Vriend G, Gloriam DE. Generic GPCR residue numbers–aligning topology maps while minding the gaps. **Trends Pharmacol Sci** 36: 22–31, 2015. doi:10.1016/j.tips.2014.11.001.

16. Rasmussen SG, Choi HJ, Fung JJ, Pardon E, Casarosa P, Chae PS, Devree BT, Rosenbaum DM, Thian FS, Kobilka TS, Schnapp A, Konetzki I, Sunahara RK, Gellman SH, Pautsch A, Steyaert J, Weis WI, Kobilka BK. Structure of a nanobody-stabilized active state of the beta(2) adrenoceptor. **Nature** 469: 175–180, 2011. doi:10.1038/nature09648.

17. Rasmussen SG, DeVree BT, Zou Y, Kruse AC, Chung KY, Kobilka TS, Thian FS, Chae PS, Pardon E, Calinski D, Mathiesen JM, Shah ST, Lyons JA, Caffrey M, Gellman SH, Steyaert J, Skiniotis G, Weis WI, Sunahara RK, Kobilka BK. Crystal structure of the beta2 adrenergic receptor-Gs protein complex. **Nature** 477: 549–555, 2011. doi:10.1038/nature10361.

18. Gerszten RE, Chen J, Ishii M, Ishii K, Wang L, Nanevicz T, Turck CW, Vu TK, Coughlin SR. Specificity of the thrombin receptor for agonist peptide is defined by its extracellular surface. **Nature** 368: 648–651, 1994. doi:10.1038/368648a0.

19. Nanevicz T, Wang L, Chen M, Ishii M, Coughlin SR. Thrombin receptor activating mutations. Alteration of an extracellular agonist recognition domain causes constitutive signaling. **J Biol Chem** 271: 702–706, 1996. doi:10.1074/jbc.271.2.702.

20. Nystedt S, Emilsson K, Larsson AK, Strombeck B, Sundelin J. Molecular cloning and functional expression of the gene encoding the human proteinase-activated receptor 2. **Eur J Biochem** 232: 84–89, 1995. doi:10.1111/j.1432-1033.1995.tb20784.x.

21. Böhm SK, Kong W, Brömme D, Smeekens SP, Anderson DC, Connolly A, Kahn M, Nelken NA, Coughlin SR, Payan DG, Bunnett NW. Molecular cloning, expression and potential functions of the human proteinase-activated receptor-2. **Biochem J** 314: 1009–1016, 1996. doi:10.1042/bj3141009.

22. Molino M, Barnathan ES, Numerof R, Clark J, Dreyer M, Cumashi A, Hoxie JA, Schechter N, Woolkalis M, Brass LF. Interactions of mast cell tryptase with thrombin receptors and PAR-2. **J Biol Chem** 272: 4043–4049, 1997. doi:10.1074/jbc.272.7.4043.

23. Corvera CU, Dery O, McConalogue K, Gamp P, Thoma M, Al-Ani B, Caughey GH, Hollenberg MD, Bunnett NW. Thrombin and mast cell tryptase regulate guinea-pig myenteric neurons through proteinase-activated receptors-1 and -2. **J Physiol** 517: 741–756, 1999. doi:10.1111/j.1469-7793.1999.0741s.x.

24. Rana S, Yang L, Hassanian SM, Rezaie AR. Determinants of the specificity of protease-activated receptors 1 and 2 signaling by factor Xa and thrombin. **J Cell Biochem** 113: 977–984, 2012. doi:10.1002/jcb.23427.

25. Oikonomopoulou K, Hansen KK, Saifeddine M, Tea I, Blaber M, Blaber SI, Scarisbrick I, Andrade-Gordon P, Cottrell GS, Bunnett NW, Diamandis EP, Hollenberg MD. Proteinase-activated receptors, targets for kallikrein signaling. **J Biol Chem** 281: 32095–32112, 2006. doi:10.1074/jbc.M513138200.

26. Ramsay AJ, Dong Y, Hunt ML, Linn M, Samaratunga H, Samaratunga H, Clements J, Hooper JD, Hooper JD. Kallikrein-related peptidase 4 (KLK4) initiates intracellular signaling via protease-activated receptors (PARs). KLK4 and PAR-2 are co-expressed during prostate cancer progression. **J Biol Chem** 283: 12293–12304, 2008. doi:10.1074/jbc.M709493200.

27. Stefansson K, Brattsand M, Roosterman D, Kempkes C, Bocheva G, Steinhoff M, Egelrud T. Activation of proteinase-activated receptor-2 by human kallikrein-related peptidases. **J Invest Dermatol** 128: 18–25, 2008. doi:10.1038/sj.jid.5700965.

28. Cheng RK, Fiez-Vandal C, Schlenker O, Edman K, Aggeler B, Brown DG, Brown GA, Cooke RM, Dumelin CE, Dore AS, Geschwindner S, Grebner C, Hermansson NO, Jazayeri A, Johansson P, Leong L, Prihandoko R, Rappas M, Soutter H, Snijder A, Sundstrom L, Tehan B, Thornton P, Troast D, Wiggin G, Zhukov A, Marshall FH, Dekker N. Structural insight into allosteric modulation of protease-activated receptor 2. **Nature** 545: 112–115, 2017. doi:10.1038/nature22309.

29. Zhang C, Srinivasan Y, Arlow DH, Fung JJ, Palmer D, Zheng Y, Green HF, Pandey A, Dror RO, Shaw DE, Weis WI, Coughlin SR, Kobilka BK. High-resolution crystal structure of human protease-activated receptor 1. **Nature** 492: 387–392, 2012. doi:10.1038/nature11701.

30. Ishihara H, Connolly AJ, Zeng D, Kahn ML, Zheng YW, Timmons C, Tram T, Coughlin SR. Protease-activated receptor 3 is a second thrombin receptor in humans. **Nature** 386: 502–506, 1997. doi:10.1038/386502a0.

31. Nieman MT. Protease-activated receptor 4 uses anionic residues to interact with α-thrombin in the absence or presence of protease-activated receptor 1. **Biochemistry** 47: 13279–13286, 2008. doi:10.1021/bi801334s.

32. Duvernay MT, Temple KJ, Maeng JG, Blobaum AL, Stauffer SR, Lindsley CW, Hamm HE. Contributions of protease-activated receptors PAR1 and PAR4 to thrombin-induced GPIIbIIIa activation in human platelets. **Mol Pharmacol** 91: 39–47, 2017. doi:10.1124/mol.116.106666.

33. Jacques SL, Kuliopulos A. Protease-activated receptor-4 uses dual prolines and an anionic retention motif for thrombin recognition and cleavage. **Biochem J** 376: 733–740, 2003. doi:10.1042/bj20030954.

34. Bah A, Chen Z, Bush-Pelc LA, Mathews FS, Di Cera E. Crystal structures of murine thrombin in complex with the extracellular fragments of murine protease-activated receptors PAR3 and PAR4. **Proc Natl Acad Sci U S A** 104: 11603–11608, 2007. doi:10.1073/pnas.0704409104.

35. Vindigni A, White CE, Komives EA, Di Cera E. Energetics of thrombin-thrombomodulin interaction. **Biochemistry** 36: 6674–6681, 1997. doi:10.1021/bi962766a.

Downloaded from journals.physiology.org/journal/physrev at New York Univ (216.165.095.084) on September 28, 2023.

36. Vijayalakshmi J, Padmanabhan KP, Mann KG, Tulinsky A. The isomorphous structures of prethrombin2, hirugen-, and PPACK-thrombin: changes accompanying activation and exosite binding to thrombin. **Protein Sci** 3: 2254–2271, 1994. doi:10.1002/pro.5560031211.

37. Scarborough RM, Naughton MA, Teng W, Hung DT, Rose J, Vu TK, Wheaton VI, Turck CW, Coughlin SR. Tethered ligand agonist peptides. Structural requirements for thrombin receptor activation reveal mechanism of proteolytic unmasking of agonist function. **J Biol Chem** 267: 13146–13149, 1992. doi:10.1016/S0021-9258(18)42184-9.

38. Adams MN, Pagel CN, Mackie EJ, Hooper JD. Evaluation of antibodies directed against human protease-activated receptor-2. **Naunyn Schmiedebergs Arch Pharmacol** 385: 861–873, 2012. doi:10.1007/s00210-012-0783-6.

39. Latorre RA, Hegron A, Peach CJ, Teng SA, Tonello RA, Retamal JA, Klein-Cloud RA, Bok D, Jensen DA, Gottesman-Katz L, Rientjes J, Veldhuis NA, Poole DA, Schmidt BL, Pothoulakis CH, Rankin CO, Xie Y, Koon HA, Bunnett NA. Mice expressing fluorescent PAR(2) reveal that endocytosis mediates colonic inflammation and pain. **Proc Natl Acad Sci U S A** 119: e2112059119, 2022. doi:10.1073/pnas.2112059119.

40. Derian CK, Eckardt AJ, Andrade-Gordon P. Differential regulation of human keratinocyte growth and differentiation by a novel family of protease-activated receptors. **Cell Growth Differ** 8: 743–749, 1997.

41. Santulli RJ, Derian CK, Darrow AL, Tomko KA, Eckardt AJ, Seiberg M, Scarborough RM, Andrade-Gordon P. Evidence for the presence of a protease-activated receptor distinct from the thrombin receptor in human keratinocytes. **Proc Natl Acad Sci U S A** 92: 9151–9155, 1995. doi:10.1073/pnas.92.20.9151.

42. Steinhoff M, Corvera CU, Thoma MS, Kong W, McAlpine BE, Caughey GH, Ansel JC, Bunnett NW. Proteinase-activated receptor-2 in human skin: tissue distribution and activation of keratinocytes by mast cell tryptase. **Exp Dermatol** 8: 282–294, 1999.

43. Camerer E, Huang W, Coughlin SR. Tissue factor- and factor X-dependent activation of protease-activated receptor 2 by factor VIIa. **Proc Natl Acad Sci U S A** 97: 5255–5260, 2000. doi:10.1073/pnas.97.10.5255.

44. Gouin O, L'Herondelle K, Buscaglia P, Le Gall-Ianotto C, Philippe R, Legoux N, Mignen O, Buhe V, Leschiera R, Sakka M, Kerfant N, Carre JL, Le Garrec R, Lefeuvre L, Lebonvallet N, Misery L. Major role for TRPV1 and InsP3R in PAR2-elicited inflammatory mediator production in differentiated human keratinocytes. **J Invest Dermatol** 138: 1564–1572, 2018. doi:10.1016/j.jid.2018.01.034.

45. Wygrecka M, Didiasova M, Berscheid S, Piskulak K, Taborski B, Zakrzewicz D, Kwapiszewska G, Preissner KT, Markart P. Protease-activated receptors (PAR)-1 and -3 drive epithelial-mesenchymal transition of alveolar epithelial cells–potential role in lung fibrosis. **Thromb Haemost** 110: 295–307, 2013. doi:10.1160/TH12-11-0854.

46. D'Andrea MR, Derian CK, Leturcq D, Baker SM, Brunmark A, Ling P, Darrow AL, Santulli RJ, Brass LF, Andrade-Gordon P. Characterization of protease-activated receptor-2 immunoreactivity in normal human tissues. **J Histochem Cytochem** 46: 157–164, 1998. doi:10.1177/002215549804600204.

47. Kong W, McConalogue K, Khitin LM, Hollenberg MD, Payan DG, Bohm SK, Bunnett NW. Luminal trypsin may regulate enterocytes through proteinase-activated receptor 2. **Proc Natl Acad Sci U S A** 94: 8884–8889, 1997. doi:10.1073/pnas.94.16.8884.

48. Cunningham MA, Rondeau E, Chen X, Coughlin SR, Holdsworth SR, Tipping PG. Protease-activated receptor 1 mediates thrombin-dependent, cell-mediated renal inflammation in crescentic glomerulonephritis. **J Exp Med** 191: 455–462, 2000. doi:10.1084/jem.191.3.455.

49. Moffatt JD, Cocks TM. The role of protease-activated receptor-2 (PAR2) in the modulation of beating of the mouse isolated ureter: lack of involvement of mast cells or sensory nerves. **Br J Pharmacol** 128: 860–864, 1999. doi:10.1038/sj.bjp.0702871.

50. Bertog M, Letz B, Kong W, Steinhoff M, Higgins MA, Bielfeld-Ackermann A, Fromter E, Bunnett NW, Korbmacher C. Basolateral proteinase-activated receptor (PAR-2) induces chloride secretion in M-1 mouse renal cortical collecting duct cells. **J Physiol** 521: 3–17, 1999.

51. Chi L, Li Y, Stehno-Bittel L, Gao J, Morrison DC, Stechschulte DJ, Dileepan KN. Interleukin-6 production by endothelial cells via stimulation of protease-activated receptors is amplified by endotoxin and tumor necrosis factor-alpha. **J Interferon Cytokine Res** 21: 231–240, 2001. doi:10.1089/107999001750169871.

52. Fujiwara M, Jin E, Ghazizadeh M, Kawanami O. Differential expression of protease-activated receptors 1, 2, and 4 on human endothelial cells from different vascular sites. **Pathobiology** 71: 52–58, 2004. doi:10.1159/000072962.

53. Jesmin S, Gando S, Zaedi S, Sakuraya F. Differential expression, time course and distribution of four PARs in rats with endotoxin-induced acute lung injury. **Inflammation** 30: 14–27, 2007. doi:10.1007/s10753-006-9017-8.

54. Kataoka H, Hamilton JR, McKemy DD, Camerer E, Zheng YW, Cheng A, Griffin C, Coughlin SR. Protease-activated receptors 1 and 4 mediate thrombin signaling in endothelial cells. **Blood** 102: 3224–3231, 2003. doi:10.1182/blood-2003-04-1130.

55. Hwa JJ, Ghibaudi L, Williams P, Chintala M, Zhang R, Chatterjee M, Sybertz E. Evidence for the presence of a proteinase-activated receptor distinct from the thrombin receptor in vascular endothelial cells. **Circ Res** 78: 581–588, 1996. doi:10.1161/01.RES.78.4.581.

56. Mirza H, Yatsula V, Bahou WF. The proteinase activated receptor-2 (PAR-2) mediates mitogenic responses in human vascular endothelial cells. **J Clin Invest** 97: 1705–1714, 1996. doi:10.1172/JCI118597.

57. Schmidt VA, Nierman WC, Maglott DR, Cupit LD, Moskowitz KA, Wainer JA, Bahou WF. The human proteinase-activated receptor-3 (PAR-3) gene. Identification within a Par gene cluster and characterization in vascular endothelial cells and platelets. **J Biol Chem** 273: 15061–15068, 1998. doi:10.1074/jbc.273.24.15061.

58. Fujiwara M, Jin E, Ghazizadeh M, Kawanami O. Activation of PAR4 induces a distinct actin fiber formation via p38 MAPK in human lung endothelial cells. **J Histochem Cytochem** 53: 1121–1129, 2005. doi:10.1369/jhc.4A6592.2005.

59. Van Den Eshof BL, Hoogendijk AJ, Simpson PJ, Van Alphen FP, Zanivan S, Mertens K, Meijer AB, Van Den Biggelaar M. Paradigm of biased PAR1 (protease-activated receptor-1) activation and inhibition in endothelial cells dissected by phosphoproteomics. **Arterioscler Thromb Vasc Biol** 37: 1891–1902, 2017. doi:10.1161/ATVBAHA.117.309926.

60. Asteriti S, Daniele S, Porchia F, Dell'Anno MT, Fazzini A, Pugliesi I, Trincavelli ML, Taliani S, Martini C, Mazzoni MR, Gilchrist A. Modulation of PAR(1) signalling by benzimidazole compounds. **Br J Pharmacol** 167: 80–94, 2012. doi:10.1111/j.1476-5381.2012.01974.x.

61. Domotor E, Benzakour O, Griffin JH, Yule D, Fukudome K, Zlokovic BV. Activated protein C alters cytosolic calcium flux in human brain

Downloaded from journals.physiology.org/journal/physrev at New York Univ (216.165.095.084) on September 28, 2023.

endothelium via binding to endothelial protein C receptor and activation of protease activated receptor-1. **Blood** 101: 4797–4801, 2003. doi:10.1182/blood-2002-12-3680.

62. Mosnier LO, Griffin JH**.** Inhibition of staurosporine-induced apoptosis of endothelial cells by activated protein C requires protease-activated receptor-1 and endothelial cell protein C receptor. **Biochem J** 373: 65–70, 2003. doi:10.1042/bj20030341.

63. Riewald M, Petrovan RJ, Donner A, Mueller BM, Ruf W**.** Activation of endothelial cell protease activated receptor 1 by the protein C pathway. **Science** 296: 1880–1882, 2002. doi:10.1126/science.1071699.

64. Hoxie JA, Ahuja M, Belmonte E, Pizarro S, Parton R, Brass LF**.** Internalization and recycling of activated thrombin receptors. **J Biol Chem** 268: 13756–13763, 1993. doi:10.1016/S0021-9258(18)86921-6.

65. Woolkalis MJ, DeMelfi TM Jr, Blanchard N, Hoxie JA, Brass LF**.** Regulation of thrombin receptors on human umbilical vein endothelial cells. **J Biol Chem** 270: 9868–9875, 1995. doi:10.1074/jbc.270.17.9868.

66. Schuepbach RA, Feistritzer C, Brass LF, Riewald M**.** Activated protein C-cleaved protease activated receptor-1 is retained on the endothelial cell surface even in the presence of thrombin. **Blood** 111: 2667–2673, 2008. doi:10.1182/blood-2007-09-113076.

67. Shapiro MJ, Coughlin SR**.** Separate signals for agonist-independent and agonist-triggered trafficking of protease-activated receptor 1. **J Biol Chem** 273: 29009–29014, 1998. doi:10.1074/jbc.273.44.29009.

68. Kuliopulos A, Covic L, Seeley SK, Sheridan PJ, Helin J, Costello CE**.** Plasmin desensitization of the PAR1 thrombin receptor: kinetics, sites of truncation, and implications for thrombolytic therapy. **Biochemistry** 38: 4572–4585, 1999. doi:10.1021/bi9824792.

69. Walz DA, Anderson GF, Ciaglowski RE, Aiken M, Fenton JW 2nd. Thrombin-elicited contractile responses of aortic smooth muscle. **Proc Soc Exp Biol Med** 180: 518–526, 1985. doi:10.3181/00379727-180-42211.

70. Huang CL, Ives HE**.** Growth inhibition by protein kinase C late in mitogenesis. **Nature** 329: 849–850, 1987. doi:10.1038/329849a0.

71. Hollenberg MD, Yang SG, Laniyonu AA, Moore GJ, Saifeddine M**.** Action of thrombin receptor polypeptide in gastric smooth muscle: identification of a core pentapeptide retaining full thrombin-mimetic intrinsic activity. **Mol Pharmacol** 42: 186–191, 1992.

72. Cocks TM, Sozzi V, Moffatt JD, Selemidis S**.** Protease-activated receptors mediate apamin-sensitive relaxation of mouse and guinea pig gastrointestinal smooth muscle. **Gastroenterology** 116: 586–592, 1999. doi:10.1016/S0016-5085(99)70180-0.

73. Hollenberg MD, Saifeddine M, Al-Ani B**.** Proteinase-activated receptor-2 in rat aorta: structural requirements for agonist activity of receptor-activating peptides. **Mol Pharmacol** 49: 229–233, 1996.

74. Cocks TM, Fong B, Chow JM, Anderson GP, Frauman AG, Goldie RG, Henry PJ, Carr MJ, Hamilton JR, Moffatt JD**.** A protective role for protease-activated receptors in the airways. **Nature** 398: 156–160, 1999. doi:10.1038/18223.

75. Magazine HI, King JM, Srivastava KD**.** Protease activated receptors modulate aortic vascular tone. **Int J Cardiol** 53, *Suppl*: S75–S80, 1996. doi:10.1016/0167-5273(96)02569-7.

76. Hamilton JR, Nguyen PB, Cocks TM**.** Atypical protease-activated receptor mediates endothelium-dependent relaxation of human coronary arteries. **Circ Res** 82: 1306–1311, 1998. doi:10.1161/01.RES.82.12.1306.

77. Wei M, Liu Y, Zheng M, Wang L, Ma F, Qi Y, Liu G**.** Upregulation of protease-activated receptor 2 promotes proliferation and migration of human vascular smooth muscle cells (VSMCs). **Med Sci Monit** 25: 8854–8862, 2019. doi:10.12659/MSM.917865.

78. Schror K, Bretschneider E, Fischer K, Fischer JW, Pape R, Rauch BH, Rosenkranz AC, Weber AA**.** Thrombin receptors in vascular smooth muscle cells–function and regulation by vasodilatory prostaglandins. **Thromb Haemost** 103: 884–890, 2010. doi:10.1160/TH09-09-0627.

79. Davey MG, Luscher EF**.** Actions of thrombin and other coagulant and proteolytic enzymes on blood platelets. **Nature** 216: 857–858, 1967. doi:10.1038/216857a0.

80. Haslam RJ, Davidson MM**.** Potentiation by thrombin of the secretion of serotonin from permeabilized platelets equilibrated with Ca2+ buffers. Relationship to protein phosphorylation and diacylglycerol formation. **Biochem J** 222: 351–361, 1984. doi:10.1042/bj2220351.

81. Altieri DC, Edgington TS**.** Identification of effector cell protease receptor-1. A leukocyte-distributed receptor for the serine protease factor Xa. **J Immunol** 145: 246–253, 1990.

82. Norton KJ, Scarborough RM, Kutok JL, Escobedo MA, Nannizzi L, Coller BS**.** Immunologic analysis of the cloned platelet thrombin receptor activation mechanism: evidence supporting receptor cleavage, release of the N-terminal peptide, and insertion of the tethered ligand into a protected environment. **Blood** 82: 2125–2136, 1993.

83. Hamilton JR, Cornelissen I, Coughlin SR**.** Impaired hemostasis and protection against thrombosis in protease-activated receptor 4-deficient mice is due to lack of thrombin signaling in platelets. **J Thromb Haemost** 2: 1429–1435, 2004. doi:10.1111/j.1538-7836.2004.00783.x.

84. Kahn ML, Nakanishi-Matsui M, Shapiro MJ, Ishihara H, Coughlin SR**.** Protease-activated receptors 1 and 4 mediate activation of human platelets by thrombin. **J Clin Invest** 103: 879–887, 1999. doi:10.1172/JCI6042.

85. De Candia E, Hall SW, Rutella S, Landolfi R, Andrews RK, De Cristofaro R**.** Binding of thrombin to glycoprotein Ib accelerates the hydrolysis of Par-1 on intact platelets. **J Biol Chem** 276: 4692–4698, 2001. doi:10.1074/jbc.M008160200.

86. Nakanishi-Matsui M, Zheng YW, Sulciner DJ, Weiss EJ, Ludeman MJ, Coughlin SR**.** PAR3 is a cofactor for PAR4 activation by thrombin. **Nature** 404: 609–613, 2000. doi:10.1038/35007085.

87. Vretenbrant K, Ramstrom S, Bjerke M, Lindahl TL**.** Platelet activation via PAR4 is involved in the initiation of thrombin generation and in clot elasticity development. **Thromb Haemost** 97: 417–424, 2007. doi:10.1160/TH06-07-0397.

88. Sambrano GR, Huang W, Faruqi T, Mahrus S, Craik C, Coughlin SR**.** Cathepsin G activates protease-activated receptor-4 in human platelets. **J Biol Chem** 275: 6819–6823, 2000. doi:10.1074/jbc.275.10.6819.

89. Schurch-Rathgeb Y, Mongard D**.** Brain development influences the appearance of glial factor-like activity in rat brain primary cultures. **Nature** 273: 308–309, 1978. doi:10.1038/273308a0.

90. Gurwitz D, Cunningham DD**.** Thrombin modulates and reverses neuroblastoma neurite outgrowth. **Proc Natl Acad Sci U S A** 85: 3440–3444, 1988. doi:10.1073/pnas.85.10.3440.

Downloaded from journals.physiology.org/journal/physrev at New York Univ (216.165.095.084) on September 28, 2023.

91. Monard D, Niday E, Limat A, Solomon F. Inhibition of protease activity can lead to neurite extension in neuroblastoma cells. **Prog Brain Res** 58: 359–364, 1983. doi:10.1016/S0079-6123(08)60037-0.

92. Snider RM, McKinney M, Fenton JW 2nd, Richelson E. Activation of cyclic nucleotide formation in murine neuroblastoma N1E-115 cells by modified human thrombins. **J Biol Chem** 259: 9078–9081, 1984. doi:10.1016/S0021-9258(17)47267-X.

93. Junge CE, Lee CJ, Hubbard KB, Zhang Z, Olson JJ, Hepler JR, Brat DJ, Traynelis SF. Protease-activated receptor-1 in human brain: localization and functional expression in astrocytes. **Exp Neurol** 188: 94–103, 2004. doi:10.1016/j.expneurol.2004.02.018.

94. Debeir T, Vige X, Benavides J. Pharmacological characterization of protease-activated receptor (PAR-1) in rat astrocytes. **Eur J Pharmacol** 323: 111–117, 1997. doi:10.1016/S0014-2999(97)00018-6.

95. Steinhoff M, Vergnolle N, Young SH, Tognetto M, Amadesi S, Ennes HS, Trevisani M, Hollenberg MD, Wallace JL, Caughey GH, Mitchell SE, Williams LM, Geppetti P, Mayer EA, Bunnett NW. Agonists of proteinase-activated receptor 2 induce inflammation by a neurogenic mechanism. **Nat Med** 6: 151–158, 2000. doi:10.1038/72247.

96. Vergnolle N, Bunnett NW, Sharkey KA, Brussee V, Compton SJ, Grady EF, Cirino G, Gerard N, Basbaum AI, Andrade-Gordon P, Hollenberg MD, Wallace JL. Proteinase-activated receptor-2 and hyperalgesia: a novel pain pathway. **Nat Med** 7: 821–826, 2001. doi:10.1038/89945.

97. Amadesi S, Nie J, Vergnolle N, Cottrell GS, Grady EF, Trevisani M, Manni C, Geppetti P, McRoberts JA, Ennes H, Davis JB, Mayer EA, Bunnett NW. Protease-activated receptor 2 sensitizes the capsaicin receptor transient receptor potential vanilloid receptor 1 to induce hyperalgesia. **J Neurosci** 24: 4300–4312, 2004. doi:10.1523/JNEUROSCI.5679-03.2004.

98. Alier KA, Endicott JA, Stemkowski PL, Cenac N, Cellars L, Chapman K, Andrade-Gordon P, Vergnolle N, Smith PA. Intrathecal administration of proteinase-activated receptor-2 agonists produces hyperalgesia by exciting the cell bodies of primary sensory neurons. **J Pharmacol Exp Ther** 324: 224–233, 2008. doi:10.1124/jpet.107.129171.

99. Dinh QT, Cryer A, Dinh S, Trevisani M, Georgiewa P, Chung F, Geppetti P, Heppt W, Klapp BF, Fischer A. Protease-activated receptor 2 expression in trigeminal neurons innervating the rat nasal mucosa. **Neuropeptides** 39: 461–466, 2005. doi:10.1016/j.npep.2005.07.003.

100. Kawabata A, Itoh H, Kawao N, Kuroda R, Sekiguchi F, Masuko T, Iwata K, Ogawa A. Activation of trigeminal nociceptive neurons by parotid PAR-2 activation in rats. **Neuroreport** 15: 1617–1621, 2004. doi:10.1097/01.wnr.0000134991.97051.6b.

101. Patwardhan AM, Diogenes A, Berg KA, Fehrenbacher JC, Clarke WP, Akopian AN, Hargreaves KM. PAR-2 agonists activate trigeminal nociceptors and induce functional competence in the delta opioid receptor. **Pain** 125: 114–124, 2006. doi:10.1016/j.pain.2006.05.007.

102. Hassler SN, Kume M, Mwirigi J, Ahmad A, Shiers S, Wangzhou A, Ray P, Belugin SN, Naik DK, Burton MD, Vagner J, Boitano S, Akopian AN, Dussor G, Price TJ. The cellular basis of protease activated receptor type 2 (PAR2) evoked mechanical and affective pain. **JCI Insight** 5: e137393, 2020. doi:10.1172/jci.insight.137393.

103. Ray P, Torck A, Quigley L, Wangzhou A, Neiman M, Rao C, Lam T, Kim JY, Kim TH, Zhang MQ, Dussor G, Price TJ. Comparative transcriptome profiling of the human and mouse dorsal root ganglia: an RNA-seq-based resource for pain and sensory neuroscience research. **Pain** 159: 1325–1345, 2018. doi:10.1097/j.pain.0000000000001217.

104. Usoskin D, Furlan A, Islam S, Abdo H, Lonnerberg P, Lou D, Hjerling-Leffler J, Haeggstrom J, Kharchenko O, Kharchenko PV, Linnarsson S, Ernfors P. Unbiased classification of sensory neuron types by large-scale single-cell RNA sequencing. **Nat Neurosci** 18: 145–153, 2015. doi:10.1038/nn.3881.

105. Li CL, Li KC, Wu D, Chen Y, Luo H, Zhao JR, Wang SS, Sun MM, Lu YJ, Zhong YQ, Hu XY, Hou R, Zhou BB, Bao L, Xiao HS, Zhang X. Somatosensory neuron types identified by high-coverage single-cell RNA-sequencing and functional heterogeneity. **Cell Res** 26: 967, 2016. doi:10.1038/cr.2016.90.

106. Kim YS, Chu Y, Han L, Li M, Li Z, LaVinka PC, Sun S, Tang Z, Park K, Caterina MJ, Ren K, Dubner R, Wei F, Dong X. Central terminal sensitization of TRPV1 by descending serotonergic facilitation modulates chronic pain. **Neuron** 81: 873–887, 2014. doi:10.1016/j.neuron.2013.12.011.

107. Boitano S, Hoffman J, Tillu DV, Asiedu MN, Zhang Z, Sherwood CL, Wang Y, Dong X, Price TJ, Vagner J. Development and evaluation of small peptidomimetic ligands to protease-activated receptor-2 (PAR2) through the use of lipid tethering. **PLoS One** 9: e99140, 2014. doi:10.1371/journal.pone.0099140.

108. Langford DJ, Bailey AL, Chanda ML, Clarke SE, Drummond TE, Echols S, Glick S, Ingrao J, Klassen-Ross T, Lacroix-Fralish ML, Matsumiya L, Sorge RE, Sotocinal SG, Tabaka JM, Wong D, van den Maagdenberg AM, Ferrari MD, Craig KD, Mogil JS. Coding of facial expressions of pain in the laboratory mouse. **Nat Methods** 7: 447–449, 2010. doi:10.1038/nmeth.1455.

109. Liu Q, Weng HJ, Patel KN, Tang Z, Bai H, Steinhoff M, Dong X. The distinct roles of two GPCRs, MrgprC11 and PAR2, in itch and hyperalgesia. **Sci Signal** 4: ra45, 2011. doi:10.1126/scisignal.2001925.

110. Vergnolle N, Derian CK, D'Andrea MR, Steinhoff M, Andrade-Gordon P. Characterization of thrombin-induced leukocyte rolling and adherence: a potential proinflammatory role for proteinase-activated receptor-4. **J Immunol** 169: 1467–1473, 2002. doi:10.4049/jimmunol.169.3.1467.

111. Augé C, Balz-Hara D, Steinhoff M, Vergnolle N, Cenac N. Protease-activated receptor-4 (PAR4): a role as inhibitor of visceral pain and hypersensitivity. **Neurogastroenterol Motil** 21: 1189–e1107, 2009. doi:10.1111/j.1365-2982.2009.01310.x.

112. Linden DR, Manning BP, Bunnett NW, Mawe GM. Agonists of proteinase-activated receptor 2 excite guinea pig ileal myenteric neurons. **Eur J Pharmacol** 431: 311–314, 2001. doi:10.1016/S0014-2999(01)01447-9.

113. Bornstein JC, Furness JB, Kunze WA. Electrophysiological characterization of myenteric neurons: how do classification schemes relate? **J Auton Nerv Syst** 48: 1–15, 1994. doi:10.1016/0165-1838(94)90155-4.

114. Wood JD. Application of classification schemes to the enteric nervous system. **J Auton Nerv Syst** 48: 17–29, 1994. doi:10.1016/0165-1838(94)90156-2.

115. Johansson U, Lawson C, Dabare M, Syndercombe-Court D, Newland AC, Howells GL, Macey MG. Human peripheral blood monocytes express protease receptor-2 and respond to receptor activation by production of IL-6, IL-8, and IL-1{beta}. **J Leukoc Biol** 78: 967–975, 2005. doi:10.1189/jlb.0704422.

116. Mari B, Imbert V, Belhacene N, Far DF, Peyron JF, Pouyssegur J, Van Obberghen-Schilling E, Rossi B, Auberger P. Thrombin and

Downloaded from journals.physiology.org/journal/physrev at New York Univ (216.165.095.084) on September 28, 2023.

thrombin receptor agonist peptide induce early events of T cell activation and synergize with TCR cross-linking for CD69 expression and interleukin 2 production. **J Biol Chem** 269: 8517–8523, 1994. doi:10.1016/S0021-9258(17)37225-3.

117. Gordon JR, Zhang X, Stevenson K, Cosford K**.** Thrombin induces IL-6 but not TNFalpha secretion by mouse mast cells: threshold-level thrombin receptor and very low level FcepsilonRI signaling synergistically enhance IL-6 secretion. **Cell Immunol** 205: 128–135, 2000. doi:10.1006/cimm.2000.1714.

118. Strukova SM, Chistov IV, Umarova BA, Dugina TN, Storozhevykh TP, Pinelis VG, Glusa E**.** Modulation of mast cell activity by a peptide agonist of the thrombin receptor: role of nitric oxide. **Biochemistry (Mosc)** 64: 658–664, 1999.

119. Hurley A, Smith M, Karpova T, Hasley RB, Belkina N, Shaw S, Balenga N, Druey KM, Nickel E, Packard B, Imamichi H, Hu Z, Follmann D, McNally J, Higgins J, Sneller M, Lane HC, Catalfamo M**.** Enhanced effector function of CD8(+) T cells from healthy controls and HIV-infected patients occurs through thrombin activation of protease-activated receptor 1. **J Infect Dis** 207: 638–650, 2013. doi:10.1093/infdis/jis730.

120. Jenkins AL, Howells GL, Scott E, Le Bonniec BF, Curtis MA, Stone SR**.** The response to thrombin of human neutrophils: evidence for two novel receptors. **J Cell Sci** 108: 3059–3066, 1995. doi:10.1242/jcs.108.9.3059.

121. Moormann C, Artuc M, Pohl E, Varga G, Buddenkotte J, Vergnolle N, Brehler R, Henz BM, Schneider SW, Luger TA, Steinhoff M**.** Functional characterization and expression analysis of the proteinase-activated receptor-2 in human cutaneous mast cells. **J Invest Dermatol** 126: 746–755, 2006. doi:10.1038/sj.jid.5700169.

122. Corvera CU, Déry O, Mcconalogue K, Böhm SK, Khitin LM, Caughey GH, Payan DG, Bunnett NW**.** Mast cell tryptase regulates rat colonic myocytes through proteinase-activated receptor 2. **J Clin Invest** 100: 1383–1393, 1997. doi:10.1172/JCI119658.

123. D'Andrea MR, Rogahn CJ, Andrade-Gordon P**.** Localization of protease-activated receptors-1 and -2 in human mast cells: indications for an amplified mast cell degranulation cascade. **Biotech Histochem** 75: 85–90, 2000. doi:10.3109/10520290009064152.

124. Miike S, Mcwilliam AS, Kita H**.** Trypsin induces activation and inflammatory mediator release from human eosinophils through protease-activated receptor-2. **J Immunol** 167: 6615–6622, 2001. doi:10.4049/jimmunol.167.11.6615.

125. Temkin V, Kantor B, Weg V, Hartman ML, Levi-Schaffer F**.** Tryptase activates the mitogen-activated protein kinase/activator protein-1 pathway in human peripheral blood eosinophils, causing cytokine production and release. **J Immunol** 169: 2662–2669, 2002. doi:10.4049/jimmunol.169.5.2662.

126. Bolton SJ, McNulty CA, Thomas RJ, Hewitt CR, Wardlaw AJ**.** Expression of and functional responses to protease-activated receptors on human eosinophils. **J Leukoc Biol** 74: 60–68, 2003. doi:10.1189/jlb.0702351.

127. Howells GL, Macey MG, Chinni C, Hou L, Fox MT, Harriott P, Stone SR**.** Proteinase-activated receptor-2: expression by human neutrophils. **J Cell Sci** 110: 881–887, 1997. doi:10.1242/jcs.110.7.881.

128. Lopez ML, Soriano-Sarabia N, Bruges G, Marquez ME, Preissner KT, Schmitz ML, Hackstein H**.** Expression pattern of protease activated receptors in lymphoid cells. **Cell Immunol** 288: 47–52, 2014. doi:10.1016/j.cellimm.2014.02.004.

129. Mari B, Guerin S, Far DF, Breitmayer JP, Belhacene N, Peyron JF, Rossi B, Auberger P**.** Thrombin and trypsin-induced Ca(2+) mobilization in human T cell lines through interaction with different protease-activated receptors. **FASEB J** 10: 309–316, 1996. doi:10.1096/fasebj.10.2.8641564.

130. Joyce DE, Chen Y, Erger RA, Koretzky GA, Lentz SR**.** Functional interactions between the thrombin receptor and the T-cell antigen receptor in human T-cell lines. **Blood** 90: 1893–1901, 1997. doi:10.1182/blood.V90.5.1893.

131. Bushell TJ, Cunningham MR, McIntosh KA, Moudio S, Plevin R**.** Protease-activated receptor 2: are common functions in glial and immune cells linked to inflammation-related CNS disorders? **Curr Drug Targets** 17: 1861–1870, 2016. doi:10.2174/1389450117666151209115232.

132. Vergnolle N, Hollenberg MD, Sharkey KA, Wallace JL**.** Characterization of the inflammatory response to proteinase-activated receptor-2 (PAR2)-activating peptides in the rat paw. **Br J Pharmacol** 127: 1083–1090, 1999. doi:10.1038/sj.bjp.0702634.

133. Williams JD, Topley N, Alobaidi HM, Harber MJ**.** Activation of human polymorphonuclear leucocytes by particulate zymosan is related to both its major carbohydrate components: glucan and mannan. **Immunology** 58: 117–124, 1986.

134. Lim SY, Tennant GM, Kennedy S, Wainwright CL, Kane KA**.** Activation of mouse protease-activated receptor-2 induces lymphocyte adhesion and generation of reactive oxygen species. **Br J Pharmacol** 149: 591–599, 2006. doi:10.1038/sj.bjp.0706905.

135. Colognato R, Slupsky JR, Jendrach M, Burysek L, Syrovets T, Simmet T**.** Differential expression and regulation of protease-activated receptors in human peripheral monocytes and monocyte-derived antigen-presenting cells. **Blood** 102: 2645–2652, 2003. doi:10.1182/blood-2002-08-2497.

136. Houle S, Papez MD, Ferazzini M, Hollenberg MD, Vergnolle N**.** Neutrophils and the kallikrein-kinin system in proteinase-activated receptor 4-mediated inflammation in rodents. **Br J Pharmacol** 146: 670–678, 2005. doi:10.1038/sj.bjp.0706371.

137. Kaufmann R, Schafberg H, Nowak G**.** Proteinase-activated receptor-2-mediated signaling and inhibition of DNA synthesis in human pancreatic cancer cells. **Int J Pancreatol** 24: 97–102, 1998. doi:10.1007/BF02788566.

138. Even-Ram S, Uziely B, Cohen P, Grisaru-Granovsky S, Maoz M, Ginzburg Y, Reich R, Vlodavsky I, Bar-Shavit R**.** Thrombin receptor overexpression in malignant and physiological invasion processes. **Nat Med** 4: 909–914, 1998. doi:10.1038/nm0898-909.

139. Arakaki AK, Pan WA, Trejo JA**.** GPCRs in cancer: protease-activated receptors, endocytic adaptors and signaling. **Int J Mol Sci** 19: 1886–1824, 2018. doi:10.3390/ijms19071886.

140. Morris DR, Ding Y, Ricks TK, Gullapalli A, Wolfe BL, Trejo J**.** Protease-activated receptor-2 is essential for factor VIIa and Xa-induced signaling, migration, and invasion of breast cancer cells. **Cancer Res** 66: 307–314, 2006. doi:10.1158/0008-5472.CAN-05-1735.

141. Schmitt-Graff A, Desmouliere A, Gabbiani G**.** Heterogeneity of myofibroblast phenotypic features: an example of fibroblastic cell plasticity. **Virchows Arch** 425: 3–24, 1994.

142. Mosnier LO, Sinha R, Burnier L, Bouwens E, Griffin JH**.** Biased agonism of protease-activated receptor 1 by activated protein C caused by noncanonical cleavage at Arg46. **Blood** 120: 5237–5246, 2012. doi:10.1182/blood-2012-08-452169.

143. Trivedi V, Boire A, Tchernychev B, Kaneider NC, Leger AJ, O'Callaghan K, Covic L, Kuliopulos A**.** platelet matrix

Downloaded from journals.physiology.org/journal/physrev at New York Univ (216.165.095.084) on September 28, 2023.

metalloprotease-1 mediates thrombogenesis by activating PAR1 at a cryptic ligand site. **Cell** 137: 332–343, 2009. doi:10.1016/j.cell.2009.02.018.

144. Mihara K, Ramachandran R, Renaux B, Saifeddine M, Hollenberg MD**.** Neutrophil elastase and proteinase-3 trigger G protein-biased signaling through proteinase-activated receptor-1 (PAR1). **J Biol Chem** 288: 32979–32990, 2013. doi:10.1074/jbc.M113.483123.

145. Zhao P, Lieu T, Barlow N, Metcalf M, Veldhuis NA, Jensen DD, Kocan M, Sostegni S, Haerteis S, Baraznenok V, Henderson I, Lindström E, Guerrero-Alba R, Valdez-Morales EE, Liedtke W, McIntyre P, Vanner SJ, Korbmacher C, Bunnett NW**.** Cathepsin S causes inflammatory pain via biased agonism of PAR2 and TRPV4. **J Biol Chem** 289: 27215–27234, 2014. doi:10.1074/jbc.M114.599712.

146. Ramachandran R, Mihara K, Chung H, Renaux B, Lau CS, Muruve DA, Defea KA, Bouvier M, Hollenberg MD**.** Neutrophil elastase acts as a biased agonist for proteinase-activated receptor-2 (PAR2). **J Biol Chem** 286: 24638–24648, 2011. doi:10.1074/jbc.M110.201988.

147. Zhao P, Lieu T, Barlow N, Sostegni S, Haerteis S, Korbmacher C, Liedtke W, Jimenez-Vargas NN, Vanner SJ, Bunnett NW**.** Neutrophil elastase activates protease-activated receptor-2 (PAR2) and transient receptor potential vanilloid 4 (TRPV4) to cause inflammation and pain. **J Biol Chem** 290: 13875–13887, 2015. doi:10.1074/jbc.M115.642736.

148. Zhao P, Pattison LA, Jensen DD, Jimenez-Vargas NN, Latorre R, Lieu T, Jaramillo JO, Lopez-Lopez C, Poole DP, Vanner SJ, Schmidt BL, Bunnett NW**.** Protein kinase D and Gβγ mediate sustained nociceptive signaling by biased agonists of protease-activated receptor-2. **J Biol Chem** 294: 10649–10662, 2019. doi:10.1074/jbc.RA118.006935.

149. Tu NH, Jensen DD, Anderson BM, Chen E, Jimenez-Vargas NN, Scheff NN, Inoue K, Tran HD, Dolan JC, Meek TA, Hollenberg MD, Liu CZ, Vanner SJ, Janal MN, Bunnett NW, Edgington-Mitchell LE, Schmidt BL**.** Legumain induces oral cancer pain by biased agonism of protease-activated receptor-2. **J Neurosci** 41: 193–210, 2021. doi:10.1523/JNEUROSCI.1211-20.2020.

150. Loew D, Perrault C, Morales M, Moog S, Ravanat C, Schuhler S, Arcone R, Pietropaolo C, Cazenave JP, Van Dorsselaer A, Lanza F**.** Proteolysis of the exodomain of recombinant protease-activated receptors: prediction of receptor activation or inactivation by MALDI mass spectrometry. **Biochemistry** 39: 10812–10822, 2000. doi:10.1021/bi0003341.

151. Dulon S, Candé C, Bunnett NW, Hollenberg MD, Chignard M, Pidard D**.** Proteinase-activated receptor-2 and human lung epithelial cells. **Am J Respir Cell Mol Biol** 28: 339–346, 2003. doi:10.1165/rcmb.4908.

152. Ender M, Andreoni F, Zinkernagel AS, Schuepbach RA**.** Streptococcal SpeB cleaved PAR-1 suppresses ERK phosphorylation and blunts thrombin-induced platelet aggregation. **PLoS One** 8: e81298, 2013. doi:10.1371/journal.pone.0081298.

153. Dulon S, Leduc D, Cottrell GS, D'Alayer J, Hansen KK, Bunnett NW, Hollenberg MD, Pidard D, Chignard M**.** Pseudomonas aeruginosa elastase disables proteinase-activated receptor 2 in respiratory epithelial cells. **Am J Respir Cell Mol Biol** 32: 411–419, 2005. doi:10.1165/rcmb.2004-0274OC.

154. Nanevicz T, Ishii M, Wang L, Chen M, Chen J, Turck CW, Cohen FE, Coughlin SR**.** Mechanisms of thrombin receptor agonist specificity. **J Biol Chem** 270: 21619–21625, 1995. doi:10.1074/jbc.270.37.21619.

155. Vassallo RR, Kieber-Emmons T, Cichowski K, Brass LF**.** Structure-function relationships in the activation of platelet thrombin receptors by receptor-derived peptides. **J Biol Chem** 267: 6081–6085, 1992. doi:10.1016/S0021-9258(18)42664-6.

156. Chao BH, Kalkunte S, Maraganore JM, Stone SR**.** Essential groups in synthetic agonist peptides for activation of the platelet thrombin receptor. **Biochemistry** 31: 6175–6178, 1992. doi:10.1021/bi00142a001.

157. Hui KY, Jakubowski JA, Wyss VL, Angleton EL**.** Minimal sequence requirement of thrombin receptor agonist peptide. **Biochem Biophys Res Commun** 184: 790–796, 1992. doi:10.1016/0006-291X(92)90659-9.

158. Maryanoff BE, Santulli RJ, Mccomsey DF, Hoekstra WJ, Hoey K, Smith CE, Addo M, Darrow AL, Andrade-Gordon P**.** Protease-activated receptor-2 (PAR-2): structure-function study of receptor activation by diverse peptides related to tethered-ligand epitopes. **Arch Biochem Biophys** 386: 195–204, 2001. doi:10.1006/abbi.2000.2207.

159. Hansen KK, Saifeddine M, Hollenberg MD**.** Tethered ligand-derived peptides of proteinase-activated receptor 3 (PAR3) activate PAR1 and PAR2 in Jurkat T cells. **Immunology** 112: 183–190, 2004. doi:10.1111/j.1365-2567.2004.01870.x.

160. Faruqi TR, Weiss EJ, Shapiro MJ, Huang W, Coughlin SR**.** Structure-function analysis of protease-activated receptor 4 tethered ligand peptides. Determinants of specificity and utility in assays of receptor function. **J Biol Chem** 275: 19728–19734, 2000. doi:10.1074/jbc.M909960199.

161. Ferrell WR, Lockhart JC, Kelso EB, Dunning L, Plevin R, Meek SE, Smith AJ, Hunter GD, McLean JS, McGarry F, Ramage R, Jiang L, Kanke T, Kawagoe J**.** Essential role for proteinase-activated receptor-2 in arthritis. **J Clin Invest** 111: 35–41, 2003. doi:10.1172/JCI16913.

162. Mcguire JJ, Saifeddine M, Triggle CR, Sun K, Hollenberg MD**.** 2-Furoyl-LIGRLO-amide: a potent and selective proteinase-activated receptor 2 agonist. **J Pharmacol Exp Ther** 309: 1124–1131, 2004. doi:10.1124/jpet.103.064584.

163. Andersen H, Greenberg DL, Fujikawa K, Xu W, Chung DW, Davie EW**.** Protease-activated receptor 1 is the primary mediator of thrombin-stimulated platelet procoagulant activity. **Proc Natl Acad Sci U S A** 96: 11189–11193, 1999. doi:10.1073/pnas.96.20.11189.

164. Hollenberg MD, Saifeddine M, Al-Ani B, Gui Y**.** Proteinase-activated receptor 4 (PAR4): action of PAR4-activating peptides in vascular and gastric tissue and lack of cross-reactivity with PAR1 and PAR2. **Can J Physiol Pharmacol** 77: 458–464, 1999. doi:10.1139/cjpp-77-6-458, 10.1139/y99-090.

165. Blackhart BD, Emilsson K, Nguyen D, Teng W, Martelli AJ, Nystedt S, Sundelin J, Scarborough RM**.** Ligand cross-reactivity within the protease-activated receptor family. **J Biol Chem** 271: 16466–16471, 1996. doi:10.1074/jbc.271.28.16466.

166. Lin H, Trejo J**.** Transactivation of the PAR1-PAR2 heterodimer by thrombin elicits β-arrestin-mediated endosomal signaling. **J Biol Chem** 288: 11203–11215, 2013. doi:10.1074/jbc.M112.439950.

167. Arachiche A, Mumaw MM, De La Fuente M, Nieman MT**.** Protease-activated receptor 1 (PAR1) and PAR4 heterodimers are required for PAR1-enhanced cleavage of PAR4 by α-thrombin. **J Biol Chem** 288: 32553–32562, 2013. doi:10.1074/jbc.M113.472373.

168. Ostrowska E, Reiser G**.** The protease-activated receptor-3 (PAR-3) can signal autonomously to induce interleukin-8 release. **Cell Mol Life Sci** 65: 970–981, 2008. doi:10.1007/s00018-008-7555-y.

Downloaded from journals.physiology.org/journal/physrev at New York Univ (216.165.095.084) on September 28, 2023.

169. Bar-Shavit R, Sabbah V, Lampugnani M, Marchisio P, , Fenton J 2nd, Vlodavsky I, Dejana E. An Arg-Gly-Asp sequence within thrombin promotes endothelial cell adhesion. **J Cell Biol** 112: 335–344, 1991. doi:10.1083/jcb.112.2.335.

170. Kaufmann R, Schulze B, Krause G, Mayr L, Settmacher U, Henklein P. Proteinase-activated receptors (PARs)–the PAR3 Neo-N-terminal peptide TFRGAP interacts with PAR1. **Regul Pept** 125: 61–66, 2005. doi:10.1016/j.regpep.2004.07.032.

171. Mclaughlin JN, Patterson MM, Malik AB. Protease-activated receptor-3 (PAR3) regulates PAR1 signaling by receptor dimerization. **Proc Natl Acad Sci U S A** 104: 5662–5667, 2007. doi:10.1073/pnas.0700763104.

172. Bae JS, Yang L, Manithody C, Rezaie AR. The ligand occupancy of endothelial protein C receptor switches the protease-activated receptor 1-dependent signaling specificity of thrombin from a permeability-enhancing to a barrier-protective response in endothelial cells. **Blood** 110: 3909–3916, 2007. doi:10.1182/blood-2007-06-096651.

173. Burnier L, Mosnier LO. Novel mechanisms for activated protein C cytoprotective activities involving noncanonical activation of protease-activated receptor 3. **Blood** 122: 807–816, 2013. doi:10.1182/blood-2013-03-488957.

174. Schuepbach RA, Riewald M. Coagulation factor Xa cleaves protease-activated receptor-1 and mediates signaling dependent on binding to the endothelial protein C receptor. **J Thromb Haemost** 8: 379–388, 2010. doi:10.1111/j.1538-7836.2009.03682.x.

175. Kondreddy V, Wang J, Keshava S, Esmon CT, Rao LV, Pendurthi UR. Factor VIIa induces anti-inflammatory signaling via EPCR and PAR1. **Blood** 131: 2379–2392, 2018. doi:10.1182/blood-2017-10-813527.

176. Majumdar M, Tarui T, Shi B, Akakura N, Ruf W, Takada Y. Plasmin-induced migration requires signaling through protease-activated receptor 1 and integrin α9β1. **J Biol Chem** 279: 37528–37534, 2004. doi:10.1074/jbc.M401372200.

177. Sebastiano M, Momi S, Falcinelli E, Bury L, Hoylaerts MF, Gresele P. A novel mechanism regulating human platelet activation by MMP-2–mediated PAR1 biased signaling. **Blood** 129: 883–895, 2017. doi:10.1182/blood-2016-06-724245.

178. Zhu L, Wang X, Wu J, Mao D, Xu Z, He Z, Yu A. Cooperation of protease-activated receptor 1 and integrin αvβ5 in thrombin-mediated lung cancer cell invasion. **Oncol Rep** 28: 553–560, 2012. doi:10.3892/or.2012.1851.

179. Lin H, Liu AP, Smith TH, Trejo J. Cofactoring and dimerization of proteinase-activated receptors. **Pharmacol Rev** 65: 1198–1213, 2013. doi:10.1124/pr.111.004747.

180. Jaffré F, Friedman AE, Hu Z, Mackman N, Blaxall BC. β-Adrenergic receptor stimulation transactivates protease-activated receptor 1 via matrix metalloproteinase 13 in cardiac cells. **Circulation** 125: 2993–3003, 2012. doi:10.1161/CIRCULATIONAHA.111.066787.

181. Snead AN, Insel PA. Defining the cellular repertoire of GPCRs identifies a profibrotic role for the most highly expressed receptor, protease-activated receptor 1, in cardiac fibroblasts. **FASEB J** 26: 4540–4547, 2012. doi:10.1096/fj.12-213496.

182. Smith TH, Li JG, Dores MR, Trejo J. Protease-activated receptor-4 and purinergic receptor P2Y12 dimerize, co-internalize, and activate Akt signaling via endosomal recruitment of β-arrestin. **J Biol Chem** 292: 13867–13878, 2017. doi:10.1074/jbc.M117.782359.

183. Gao X, Cheng YH, Enten GA, DeSantis AJ, Gaponenko V, Majetschak M. Regulation of the thrombin/protease-activated receptor 1 axis by chemokine (CXC motif) receptor 4. **J Biol Chem** 295: 14893–14905, 2020. doi:10.1074/jbc.RA120.015355.

184. McCoy KL, Traynelis SF, Hepler JR. PAR1 and PAR2 couple to overlapping and distinct sets of G proteins and linked signaling pathways to differentially regulate cell physiology. **Mol Pharmacol** 77: 1005–1015, 2010. doi:10.1124/mol.109.062018.

185. Vellani V, Kinsey AM, Prandini M, Hechtfischer SC, Reeh P, Magherini PC, Giacomoni C, McNaughton PA. Protease activated receptors 1 and 4 sensitize TRPV1 in nociceptive neurones. **Mol Pain** 6: 61, 2010. doi:10.1186/1744-8069-6-61.

186. Swift S, Leger AJ, Talavera J, Zhang L, Bohm A, Kuliopulos A. Role of the PAR1 receptor 8th helix in signaling. **J Biol Chem** 281: 4109–4116, 2006. doi:10.1074/jbc.M509525200.

187. Thibeault PE, Ramachandran R. Role of the helix-8 and C-terminal tail in regulating proteinase activated receptor 2 signaling. **ACS Pharmacol Transl Sci** 3: 868–882, 2020. doi:10.1021/acsptsci.0c00039.

188. Kim YV, Di Cello F, Hillaire C, Kim KS. Differential Ca^{2+} signaling by thrombin and protease-activated receptor-1-activating peptide in human brain microvascular endothelial cells. **Am J Physiol Cell Physiol** 286: C31–C42, 2004. doi:10.1152/ajpcell.00157.2003.

189. Tiruppathi C, Freichel M, Vogel SM, Paria BC, Mehta D, Flockerzi V, Malik AB. Impairment of store-operated Ca2+ entry in TRPC4-/- mice interferes with increase in lung microvascular permeability. **Circ Res** 91: 70–76, 2002. doi:10.1161/01.RES.0000023391.40106.A8.

190. Mclaughlin JN, Shen L, Holinstat M, Brooks JD, Dibenedetto E, Hamm HE. Functional selectivity of G protein signaling by agonist peptides and thrombin for the protease-activated receptor-1. **J Biol Chem** 280: 25048–25059, 2005. doi:10.1074/jbc.M414090200.

191. Vaidyula VR, Rao AK. Role of Galphaq and phospholipase C-beta2 in human platelets activation by thrombin receptors PAR1 and PAR4: studies in human platelets deficient in Galphaq and phospholipase C-beta2. **Br J Haematol** 121: 491–496, 2003. doi:10.1046/j.1365-2141.2003.04296.x.

192. Tourdot BE, Conaway S, Niisuke K, Edelstein LC, Bray PF, Holinstat M. Mechanism of race-dependent platelet activation through the protease-activated receptor-4 and Gq signaling axis. **Arterioscler Thromb Vasc Biol** 34: 2644–2650, 2014. doi:10.1161/ATVBAHA.114.304249.

193. Edelstein LC, Simon LM, Lindsay CR, Kong X, Teruel-Montoya R, Tourdot BE, Chen ES, Ma L, Coughlin S, Nieman M, Holinstat M, Shaw CA, Bray PF. Common variants in the human platelet PAR4 thrombin receptor alter platelet function and differ by race. **Blood** 124: 3450–3458, 2014. doi:10.1182/blood-2014-04-572479.

194. Shapiro MJ, Weiss EJ, Faruqi TR, Coughlin SR. Protease-activated receptors 1 and 4 are shut off with distinct kinetics after activation by thrombin. **J Biol Chem** 275: 25216–25221, 2000. doi:10.1074/jbc.M004589200.

195. Covic L, Gresser AL, Kuliopulos A. Biphasic kinetics of activation and signaling for PAR1 and PAR4 thrombin receptors in platelets. **Biochemistry** 39: 5458–5467, 2000. doi:10.1021/bi9927078.

196. Al-Ani B, Wijesuriya SJ, Hollenberg MD. Proteinase-activated receptor 2: differential activation of the receptor by tethered ligand and soluble peptide analogs. **J Pharmacol Exp Ther** 302: 1046–1054, 2002. doi:10.1124/jpet.302.3.1046.

Downloaded from journals.physiology.org/journal/physrev at New York Univ (216.165.095.084) on September 28, 2023.

197. Thibeault PE, LeSarge JC, Arends D, Fernandes M, Chidiac P, Stathopulos PB, Luyt LG, Ramachandran R. Molecular basis for activation and biased signaling at the thrombin-activated GPCR proteinase activated receptor-4 (PAR4). **J Biol Chem** 295: 2520–2540, 2020. doi:10.1074/jbc.RA119.011461.

198. Bono F, Schaeffer P, Hérault JP, Michaux C, Nestor AL, Guillemot JC, Herbert JM. Factor Xa activates endothelial cells by a receptor cascade between EPR-1 and PAR-2. **Arterioscler Thromb Vasc Biol** 20: e107–e112, 2000. doi:10.1161/01.atv.20.11.e107.

199. Daubie V, Cauwenberghs S, Senden NH, Pochet R, Lindhout T, Buurman WA, Heemskerk JW. Factor Xa and thrombin evoke additive calcium and proinflammatory responses in endothelial cells subjected to coagulation. **Biochim Biophys Acta** 1763: 860–869, 2006. doi:10.1016/j.bbamcr.2006.04.010.

200. Poole DP, Amadesi S, Veldhuis NA, Abogadie FC, Lieu T, Darby W, Liedtke W, Lew MJ, Mcintyre P, Bunnett NW. Protease-activated receptor 2 (PAR2) protein and transient receptor potential vanilloid 4 (TRPV4) protein coupling is required for sustained inflammatory signaling. **J Biol Chem** 288: 5790–5802, 2013. doi:10.1074/jbc.M112.438184.

201. Defea KA, Zalevsky J, Thoma MS, Déry O, Mullins RD, Bunnett NW. βArrestin–dependent endocytosis of proteinase-activated receptor 2 is required for intracellular targeting of activated Erk1/2. **J Cell Biol** 148: 1267–811281, 2000. doi:10.1083/jcb.148.6.1267.

202. Ramachandran R, Mihara K, Mathur M, Rochdi MD, Bouvier M, Defea K, Hollenberg MD. Agonist-biased signaling via proteinase activated receptor-2: differential activation of calcium and mitogen-activated protein kinase pathways. **Mol Pharmacol** 76: 791–801, 2009. doi:10.1124/mol.109.055509.

203. Jimenez-Vargas NN, Pattison LA, Zhao P, Lieu T, Latorre R, Jensen DD, Castro J, Aurelio L, Le GT, Flynn B, Herenbrink CK, Yeatman HR, Edgington-Mitchell L, Porter CJ, Halls ML, Canals M, Veldhuis NA, Poole DP, McLean P, Hicks GA, Scheff N, Chen E, Bhattacharya A, Schmidt BL, Brierley SM, Vanner SJ, Bunnett NW. Protease-activated receptor-2 in endosomes signals persistent pain of irritable bowel syndrome. **Proc Natl Acad Sci U S A** 115: E7438–E7447, 2018. doi:10.1073/pnas.1721891115.

204. Ge L, Ly Y, Hollenberg M, DeFea K. A beta-arrestin-dependent scaffold is associated with prolonged MAPK activation in pseudopodia during protease-activated receptor-2-induced chemotaxis. **J Biol Chem** 278: 34418–34426, 2003. doi:10.1074/jbc.m300573200.

205. Tillu DV, Hassler SN, Burgos-Vega CC, Quinn TL, Sorge RE, Dussor G, Boitano S, Vagner J, Price TJ. Protease-activated receptor 2 activation is sufficient to induce the transition to a chronic pain state. **Pain** 156: 859–867, 2015. doi:10.1097/j.pain.0000000000000125.

206. Madamanchi NR, Li S, Patterson C, Runge MS. Thrombin regulates vascular smooth muscle cell growth and heat shock proteins via the JAK-STAT pathway. **J Biol Chem** 276: 18915–18924, 2001. doi:10.1074/jbc.M008802200.

207. Kanda Y, Mizuno K, Kuroki Y, Watanabe Y. Thrombin-induced p38 mitogen-activated protein kinase activation is mediated by epidermal growth factor receptor transactivation pathway. **Br J Pharmacol** 132: 1657–1664, 2001. doi:10.1038/sj.bjp.0703952.

208. Grimsey NJ, Aguilar B, Smith TH, Le P, Soohoo AL, Puthenveedu MA, Nizet V, Trejo J. Ubiquitin plays an atypical role in GPCR-induced p38 MAP kinase activation on endosomes. **J Cell Biol** 210: 1117–1131, 2015. doi:10.1083/jcb.201504007.

209. Wang P, Defea KA. Protease-activated receptor-2 simultaneously directs β-arrestin-1-dependent inhibition and Gαq-dependent activation of phosphatidylinositol 3-kinase. **Biochemistry** 45: 9374–9385, 2006. doi:10.1021/bi0602617.

210. Das K, Prasad R, Roy S, Mukherjee A, Sen P. The protease activated receptor 2 promotes Rab5a mediated generation of pro-metastatic microvesicles. **Sci Rep** 8: 1886, 2018. doi:10.1038/s41598-018-20099-5.

211. Iablokov V, Hirota CL, Peplowski MA, Ramachandran R, Mihara K, Hollenberg MD, Macnaughton WK. Proteinase-activated receptor 2 (PAR2) decreases apoptosis in colonic epithelial cells. **J Biol Chem** 289: 34366–34377, 2014. doi:10.1074/jbc.M114.610485.

212. Goel R, Phillips-Mason PJ, Raben DM, Baldassare JJ. α-Thrombin induces rapid and sustained Akt phosphorylation by β-arrestin1-dependent and -independent mechanisms, and only the sustained Akt phosphorylation is essential for G1 phase progression. **J Biol Chem** 277: 18640–18648, 2002. doi:10.1074/jbc.M108995200.

213. Ramachandran R, Mihara K, Thibeault P, Vanderboor CM, Petri B, Saifeddine M, Bouvier M, Hollenberg MD. Targeting a proteinase-activated receptor 4 (PAR4) carboxyl terminal motif to regulate platelet function. **Mol Pharmacol** 91: 287–295, 2017. doi:10.1124/mol.116.106526.

214. Falcinelli E, Guglielmini G, Torti M, Gresele P. Intraplatelet signaling mechanisms of the priming effect of matrix metalloproteinase-2 on platelet aggregation. **J Thromb Haemost** 3: 2526–2535, 2005. doi:10.1111/j.1538-7836.2005.01614.x.

215. Sinha RK, Wang Y, Zhao Z, Xu X, Burnier L, Gupta N, Fernández JA, Martin G, Kupriyanov S, Mosnier LO, Zlokovic BV, Griffin JH. PAR1 biased signaling is required for activated protein C in vivo benefits in sepsis and stroke. **Blood** 131: 1163–1171, 2018. doi:10.1182/blood-2017-10-810895.

216. Berger P, Perng DW, Thabrew H, Compton SJ, Cairns JA, McEuen AR, Marthan R, Tunon De Lara JM, Walls AF. Tryptase and agonists of PAR-2 induce the proliferation of human airway smooth muscle cells. **J Appl Physiol (1985)** 91: 1372–1379, 2001. doi:10.1152/jappl.2001.91.3.1372.

217. Sriwai W, Mahavadi S, Al-Shboul O, Grider JR, Murthy KS. Distinctive G protein-dependent signaling by protease-activated receptor 2 (PAR2) in smooth muscle: feedback inhibition of RhoA by cAMP-independent PKA. **PLoS One** 8: e66743, 2013. doi:10.1371/journal.pone.0066743.

218. Ayoub MA, Trinquet E, Pfleger KD, Pin JP. Differential association modes of the thrombin receptor PAR1 with Galphai1, Galpha12, and beta-arrestin 1. **FASEB J** 24: 3522–3535, 2010. doi:10.1096/fj.10-154997.

219. Kim S, Foster C, Lecchi A, Quinton TM, Prosser DM, Jin J, Cattaneo M, Kunapuli SP. Protease-activated receptors 1 and 4 do not stimulate Gi signaling pathways in the absence of secreted ADP and cause human platelet aggregation independently of Gisignaling. **Blood** 99: 3629–3636, 2002. doi:10.1182/blood.V99.10.3629.

220. Offermanns S, Laugwitz KL, Spicher K, Schultz G. G proteins of the G12 family are activated via thromboxane A2 and thrombin receptors in human platelets. **Proc Natl Acad Sci U S A** 91: 504–508, 1994. doi:10.1073/pnas.91.2.504.

221. Garcia JGN, Davis HW, Patterson CE. Regulation of endothelial cell gap formation and barrier dysfunction: role of myosin light chain phosphorylation. **J Cell Physiol** 163: 510–522, 1995. doi:10.1002/jcp.1041630311.

222. Majumdar M, Seasholtz TM, Buckmaster C, Toksoz D, Brown JH. A Rho exchange factor mediates thrombin and Gα12-induced

Downloaded from journals.physiology.org/journal/physrev at New York Univ (216.165.095.084) on September 28, 2023.

cytoskeletal responses. **J Biol Chem** 274: 26815–26821, 1999. doi:10.1074/jbc.274.38.26815.

223. Mehta D, Rahman A, Malik AB**.** Protein kinase C-α signals Rho-guanine nucleotide dissociation inhibitor phosphorylation and Rho activation and regulates the endothelial cell barrier function. **J Biol Chem** 276: 22614–22620, 2001. doi:10.1074/jbc.M101927200.

224. Holinstat M, Mehta D, Kozasa T, Minshall R, Malik AB**.** Protein kinase Calpha-induced p115RhoGEF phosphorylation signals endothelial cytoskeletal rearrangement. **J Biol Chem** 278: 28793–28798, 2003. doi:10.1074/jbc.M303900200.

225. Zoudilova M, Kumar P, Ge L, Wang P, Bokoch GM, DeFea KA**.** Beta-arrestin-dependent regulation of the cofilin pathway downstream of protease-activated receptor-2. **J Biol Chem** 282: 20634–20646, 2007. doi:10.1074/jbc.M701391200.

226. Vanderboor CM, Thibeault PE, Nixon KC, Gros R, Kramer J, Ramachandran R**.** Proteinase-activated receptor 4 activation triggers cell membrane blebbing through RhoA and β-arrestin. **Mol Pharmacol** 97: 365–376, 2020. doi:10.1124/mol.119.118232.

227. Ayoub MA, Pin JP**.** Interaction of protease-activated receptor 2 with G proteins and β-arrestin 1 studied by bioluminescence resonance energy transfer. **Front Endocrinol** 4: 196, 2013. doi:10.3389/fendo.2013.00196.

228. Dowal L, Sim DS, Dilks JR, Blair P, Beaudry S, Denker BM, Koukos G, Kuliopulos A, Flaumenhaft R**.** Identification of an antithrombotic allosteric modulator that acts through helix 8 of PAR1. **Proc Natl Acad Sci U S A** 108: 2951–2956, 2011. doi:10.1073/pnas.1014863108.

229. Russo A, Soh UJ, Paing MM, Arora P, Trejo J**.** Caveolae are required for protease-selective signaling by protease-activated receptor-1. **Proc Natl Acad Sci U S A** 106: 6393–6397, 2009. doi:10.1073/pnas.0810687106.

230. Lin Y, Wozniak JA, Grimsey NJ, Girada S, Patwardhan A, Molinar-Inglis O, Smith TH, Lapek JD, Gonzalez DJ, Trejo JA**.** Phosphoproteomic analysis of protease-activated receptor-1 biased signaling reveals unique modulators of endothelial barrier function. **Proc Natl Acad Sci USA** 117: 5039–5048, 2020. doi:10.1073/pnas.1917295117.

231. Tressel SL, Kaneider NC, Kasuda S, Foley C, Koukos G, Austin K, Agarwal A, Covic L, Opal SM, Kuliopulos A**.** A matrix metalloprotease-PAR1 system regulates vascular integrity, systemic inflammation and death in sepsis. **EMBO Mol Med** 3: 370–384, 2011. doi:10.1002/emmm.201100145.

232. Austin KM, Nguyen N, Javid G, Covic L, Kuliopulos A**.** Noncanonical matrix metalloprotease-1-protease-activated receptor-1 signaling triggers vascular smooth muscle cell dedifferentiation and arterial stenosis. **J Biol Chem** 288: 23105–23115, 2013. doi:10.1074/jbc.M113.467019.

233. Boire A, Covic L, Agarwal A, Jacques S, Sherifi S, Kuliopulos A**.** PAR1 is a matrix metalloprotease-1 receptor that promotes invasion and tumorigenesis of breast cancer cells. **Cell** 120: 303–313, 2005. doi:10.1016/j.cell.2004.12.018.

234. Bae JS, Kim YU, Park MK, Rezaie AR**.** Concentration dependent dual effect of thrombin in endothelial cells via Par-1 and Pi3 kinase. **J Cell Physiol** 219: 744–751, 2009. doi:10.1002/jcp.21718.

235. Soto AG, Smith TH, Chen B, Bhattacharya S, Cordova IC, Kenakin T, Vaidehi N, Trejo J**.** N-linked glycosylation of protease-activated receptor-1 at extracellular loop 2 regulates G-protein signaling bias. **Proc Natl Acad Sci U S A** 112: E3600–E3608, 2015. doi:10.1073/pnas.1508838112.

236. Chen CH, Paing MM, Trejo J**.** Termination of protease-activated receptor-1 signaling by β-arrestins is independent of receptor phosphorylation. **J Biol Chem** 279: 10020–10031, 2004. doi:10.1074/jbc.M310590200.

237. Smith TH, Coronel LJ, Li JG, Dores MR, Nieman MT, Trejo J**.** Protease-activated receptor-4 signaling and trafficking is regulated by the clathrin adaptor protein complex-2 independent of β-arrestins. **J Biol Chem** 291: 18453–18464, 2016. doi:10.1074/jbc.M116.729285.

238. Ayoub MA, Maurel D, Binet V, Fink M, Prezeau L, Ansanay H, Pin JP**.** Real-time analysis of agonist-induced activation of protease-activated receptor 1/Galphai1 protein complex measured by bioluminescence resonance energy transfer in living cells. **Mol Pharmacol** 71: 1329–1340, 2007. doi:10.1124/mol.106.030304.

239. Thomsen AR, Jensen DD, Hicks GA, Bunnett NW**.** Therapeutic targeting of endosomal G-protein-coupled receptors. **Trends Pharmacol Sci** 39: 879–891, 2018. doi:10.1016/j.tips.2018.08.003.

240. Trejo J, Altschuler Y, Fu HW, Mostov KE, Coughlin SR**.** Protease-activated receptor-1 down-regulation. **J Biol Chem** 275: 31255–31265, 2000. doi:10.1074/jbc.M003770200.

241. Déry O, Thoma MS, Wong H, Grady EF, Bunnett NW**.** Trafficking of proteinase-activated receptor-2 and β-arrestin-1 tagged with green fluorescent protein. **J Biol Chem** 274: 18524–18535, 1999. doi:10.1074/jbc.274.26.18524.

242. Ricks TK, Trejo J**.** Phosphorylation of protease-activated receptor-2 differentially regulates desensitization and internalization. **J Biol Chem** 284: 34444–34457, 2009. doi:10.1074/jbc.M109.048942.

243. Hollenberg MD, Renaux B, Hyun E, Houle S, Vergnolle N, Saifeddine M, Ramachandran R**.** Derivatized 2-furoyl-LIGRLO-amide, a versatile and selective probe for proteinase-activated receptor 2: binding and visualization. **J Pharmacol Exp Ther** 326: 453–462, 2008. doi:10.1124/jpet.108.136432.

244. Jacob C, Yang PC, Darmoul D, Amadesi S, Saito T, Cottrell GS, Coelho AM, Singh P, Grady EF, Perdue M, Bunnett NW**.** Mast cell tryptase controls paracellular permeability of the intestine. Role of protease-activated receptor 2 and beta-arrestins. **J Biol Chem** 280: 31936–31948, 2005. doi:10.1074/jbc.M506338200.

245. Bae JS, Yang L, Rezaie AR**.** Receptors of the protein C activation and activated protein C signaling pathways are colocalized in lipid rafts of endothelial cells. **Proc Natl Acad Sci U S A** 104: 2867–2872, 2007. doi:10.1073/pnas.0611493104.

246. Bae JS, Rezaie AR**.** Protease activated receptor 1 (PAR-1) activation by thrombin is protective in human pulmonary artery endothelial cells if endothelial protein C receptor is occupied by its natural ligand. **Thromb Haemost** 100: 101–109, 2008. doi:10.1160/TH08-02-0127.

247. Carlile-Klusacek M, Rizzo V**.** Endothelial cytoskeletal reorganization in response to PAR1 stimulation is mediated by membrane rafts but not caveolae. **Am J Physiol Heart Circ Physiol** 293: H366–H375, 2007. doi:10.1152/ajpheart.01044.2006.

248. Daub H, Weiss FU, Wallasch C, Ullrich A**.** Role of transactivation of the EGF receptor in signalling by G-protein-coupled receptors. **Nature** 379: 557–560, 1996. doi:10.1038/379557a0.

249. Sabri A, Short J, Guo J, Steinberg SF**.** Protease-activated receptor-1–mediated DNA synthesis in cardiac fibroblast is via epidermal growth factor receptor transactivation. **Circ Res** 91: 532–539, 2002. doi:10.1161/01.RES.0000035242.96310.45.

Downloaded from journals.physiology.org/journal/physrev at New York Univ (216.165.095.084) on September 28, 2023.

250. Prenzel N, Zwick E, Daub H, Leserer M, Abraham R, Wallasch C, Ullrich A. EGF receptor transactivation by G-protein-coupled receptors requires metalloproteinase cleavage of proHB-EGF. **Nature** 402: 884–888, 1999. doi:10.1038/47260.

251. Schauwienold D, Sastre AP, Genzel N, Schaefer M, Reusch HP. The transactivated epidermal growth factor receptor recruits Pyk2 to regulate Src kinase activity. **J Biol Chem** 283: 27748–27756, 2008. doi:10.1074/jbc.M801431200.

252. Darmoul D, Gratio V, Devaud H, Laburthe M. Protease-activated receptor 2 in colon cancer: trypsin-induced MAPK phosphorylation and cell proliferation are mediated by epidermal growth factor receptor transactivation. **J Biol Chem** 279: 20927–20934, 2004. doi:10.1074/jbc.M401430200.

253. Kawao N, Nagataki M, Nagasawa K, Kubo S, Cushing K, Wada T, Sekiguchi F, Ichida S, Hollenberg MD, Macnaughton WK, Nishikawa H, Kawabata A. Signal transduction for proteinase-activated receptor-2-triggered prostaglandin E2 formation in human lung epithelial cells. **J Pharmacol Exp Ther** 315: 576–589, 2005. doi:10.1124/jpet.105.089490.

254. van der Merwe JQ, Hollenberg M, MacNaughton WK. EGF receptor transactivation and MAP kinase mediate proteinase-activated receptor-2-induced chloride secretion in intestinal epithelial cells. **Am J Physiol Gastrointest Liver Physiol** 294: G441–G451, 2008. doi:10.1152/ajpgi.00303.2007.

255. Jiang Y, Zhuo X, Fu X, Wu Y, Mao C. Targeting PAR2 overcomes gefitinib resistance in non-small-cell lung cancer cells through inhibition of EGFR transactivation. **Front Pharmacol** 12: 625289, 2021. doi:10.3389/fphar.2021.625289.

256. Narita M, Usui A, Narita M, Niikura K, Nozaki H, Khotib J, Nagumo Y, Yajima Y, Suzuki T. Protease-activated receptor-1 and platelet-derived growth factor in spinal cord neurons are implicated in neuropathic pain after nerve injury. **J Neurosci** 2510000–10009, 2005. doi:10.1523/JNEUROSCI.2507-05.2005.

257. Siegbahn A, Johnell M, Nordin A, Aberg M, Velling T. TF/FVIIa transactivate PDGFRβ to regulate PDGF-BB–induced chemotaxis in different cell types. **Arterioscler Thromb Vasc Biol** 28: 135–141, 2008. doi:10.1161/ATVBAHA.107.155754.

258. Kaufmann R, Oettel C, Horn A, Halbhuber KJ, Eitner A, Krieg R, Katenkamp K, Henklein P, Westermann M, Bohmer FD, Ramachandran R, Saifeddine M, Hollenberg MD, Settmacher U. Met receptor tyrosine kinase transactivation is involved in proteinase-activated receptor-2-mediated hepatocellular carcinoma cell invasion. **Carcinogenesis** 30: 1487–1496, 2009. doi:10.1093/carcin/bgp153.

259. Chandrasekharan UM, Waitkus M, Kinney CM, Walters-Stewart A, Dicorleto PE. Synergistic induction of mitogen-activated protein kinase phosphatase-1 by thrombin and epidermal growth factor requires vascular endothelial growth factor receptor-2. **Arterioscler Thromb Vasc Biol** 30: 1983–1989, 2010. doi:10.1161/ATVBAHA.110.212399.

260. Dai Y, Moriyama T, Higashi T, Togashi K, Kobayashi K, Yamanaka H, Tominaga M, Noguchi K. Proteinase-activated receptor 2-mediated potentiation of transient receptor potential vanilloid subfamily 1 activity reveals a mechanism for proteinase-induced inflammatory pain. **J Neurosci** 24: 4293–4299, 2004. doi:10.1523/JNEUROSCI.0454-04.2004.

261. Amadesi S, Cottrell GS, Divino L, Chapman K, Grady EF, Bautista F, Karanjia R, Barajas-Lopez C, Vanner S, Vergnolle N, Bunnett NW. Protease-activated receptor 2 sensitizes TRPV1 by protein kinase Cepsilon- and A-dependent mechanisms in rats and mice. **J Physiol** 575: 555–571, 2006. doi:10.1113/jphysiol.2006.111534.

262. Gardell LR, Ma JN, Seitzberg JG, Knapp AE, Schiffer HH, Tabatabaei A, Davis CN, Owens M, Clemons B, Wong KK, Lund B, Nash NR, Gao Y, Lameh J, Schmelzer K, Olsson R, Burstein ES. Identification and characterization of novel small-molecule protease-activated receptor 2 agonists. **J Pharmacol Exp Ther** 327: 799–808, 2008. doi:10.1124/jpet.108.142570.

263. Chen Y, Yang C, Wang ZJ. Proteinase-activated receptor 2 sensitizes transient receptor potential vanilloid 1, transient receptor potential vanilloid 4, and transient receptor potential ankyrin 1 in paclitaxel-induced neuropathic pain. **Neuroscience** 193: 440–451, 2011. doi:10.1016/j.neuroscience.2011.06.085.

264. Grant AD, Cottrell GS, Amadesi S, Trevisani M, Nicoletti P, Materazzi S, Altier C, Cenac N, Zamponi GW, Bautista-Cruz F, Lopez CB, Joseph EK, Levine JD, Liedtke W, Vanner S, Vergnolle N, Geppetti P, Bunnett NW. Protease-activated receptor 2 sensitizes the transient receptor potential vanilloid 4 ion channel to cause mechanical hyperalgesia in mice. **J Physiol** 578: 715–733, 2007. doi:10.1113/jphysiol.2006.121111.

265. Sipe WE, Brierley SM, Martin CM, Phillis BD, Cruz FB, Grady EF, Liedtke W, Cohen DM, Vanner S, Blackshaw LA, Bunnett NW. Transient receptor potential vanilloid 4 mediates protease activated receptor 2-induced sensitization of colonic afferent nerves and visceral hyperalgesia. **Am J Physiol Gastrointest Liver Physiol** 294: G1288–G1298, 2008. doi:10.1152/ajpgi.00002.2008.

266. Grace MS, Lieu T, Darby B, Abogadie FC, Veldhuis N, Bunnett NW, Mcintyre P. The tyrosine kinase inhibitor bafetinib inhibits PAR2-induced activation of TRPV4 channelsin vitroand painin vivo. **Br J Pharmacol** 171: 3881–3894, 2014. doi:10.1111/bph.12750.

267. Saifeddine M, El-Daly M, Mihara K, Bunnett NW, Mcintyre P, Altier C, Hollenberg MD, Ramachandran R. GPCR-mediated EGF receptor transactivation regulates TRPV4 action in the vasculature. **Br J Pharmacol** 172: 2493–2506, 2015. doi:10.1111/bph.13072.

268. Shavit-Stein E, Artan-Furman A, Feingold E, Ben Shimon M, Itzekson-Hayosh Z, Chapman J, Vlachos A, Maggio N. Protease activated receptor 2 (PAR2) induces long-term depression in the hippocampus through transient receptor potential vanilloid 4 (TRPV4). **Front Mol Neurosci** 10: 42, 2017. doi:10.3389/fnmol.2017.00042.

269. Peng S, Grace MS, Gondin AB, Retamal JS, Dill L, Darby W, Bunnett NW, Abogadie FC, Carbone SE, Tigani T, Davis TP, Poole DP, Veldhuis NA, Mcintyre P. The transient receptor potential vanilloid 4 (TRPV4) ion channel mediates protease activated receptor 1 (PAR1)-induced vascular hyperpermeability. **Lab Invest** 100: 1057–1067, 2020. doi:10.1038/s41374-020-0430-7.

270. Asfaha S, Cenac N, Houle S, Altier C, Papez MD, Nguyen C, Steinhoff M, Chapman K, Zamponi GW, Vergnolle N. Protease-activated receptor-4: a novel mechanism of inflammatory pain modulation. **Br J Pharmacol** 150: 176–185, 2007. doi:10.1038/sj.bjp.0706975.

271. Dai Y, Wang S, Tominaga M, Yamamoto S, Fukuoka T, Higashi T, Kobayashi K, Obata K, Yamanaka H, Noguchi K. Sensitization of TRPA1 by PAR2 contributes to the sensation of inflammatory pain. **J Clin Invest** 117: 1979–1987, 2007. doi:10.1172/JCI30951.

272. Brierley SM, Hughes PA, Page AJ, Kwan KY, Martin CM, O'Donnell TA, Cooper NJ, Harrington AM, Adam B, Liebregts T, Holtmann G, Corey DP, Rychkov GY, Blackshaw LA. The ion channel TRPA1 is required for normal mechanosensation and is modulated by algesic stimuli. **Gastroenterology** 137: 2084–2095.e3, 2009. doi:10.1053/j.gastro.2009.07.048.

Downloaded from journals.physiology.org/journal/physrev at New York Univ (216.165.095.084) on September 28, 2023.

273. Hinman A, Chuang HH, Bautista DM, Julius D. TRP channel activation by reversible covalent modification. **Proc Natl Acad Sci U S A** 103: 19564–19568, 2006. doi:10.1073/pnas.0609598103.

274. Schmidt M, Dubin AE, Petrus MJ, Earley TJ, Patapoutian A. Nociceptive signals induce trafficking of TRPA1 to the plasma membrane. **Neuron** 64: 498–509, 2009. doi:10.1016/j.neuron.2009.09.030.

275. Wu J, Liu TT, Zhou YM, Qiu CY, Ren P, Jiao M, Hu WP. Sensitization of ASIC3 by proteinase-activated receptor 2 signaling contributes to acidosis-induced nociception. **J Neuroinflammation** 14: 150, 2017. doi:10.1186/s12974-017-0916-4.

276. McLaughlin JN, Mazzoni MR, Cleator JH, Earls L, Perdigoto AL, Brooks JD, Muldowney JA, Vaughan DE, Hamm HE. Thrombin modulates the expression of a set of genes including thrombospondin-1 in human microvascular endothelial cells. **J Biol Chem** 280: 22172–22180, 2005. doi:10.1074/jbc.M500721200.

277. Suen JY, Gardiner B, Grimmond S, Fairlie DP. Profiling gene expression induced by protease-activated receptor 2 (PAR2) activation in human kidney cells. **PLoS One** 5: e13809, 2010. doi:10.1371/journal.pone.0013809.

278. Wang H, Moreau F, Hirota CL, Macnaughton WK. Proteinase-activated receptors induce interleukin-8 expression by intestinal epithelial cells through ERK/RSK90 activation and histone acetylation. **FASEB J** 24: 1971–1980, 2010. doi:10.1096/fj.09-137646.

279. Nagataki M, Moriyuki K, Sekiguchi F, Kawabata A. Evidence that PAR2-triggered prostaglandin E2 (PGE2) formation involves the ERK-cytosolic phospholipase A2-COX-1-microsomal PGE synthase-1 cascade in human lung epithelial cells. **Cell Biochem Funct** 26: 279–282, 2008. doi:10.1002/cbf.1434.

280. Moriyuki K, Nagataki M, Sekiguchi F, Nishikawa H, Kawabata A. Signal transduction for formation/release of interleukin-8 caused by a PAR2-activating peptide in human lung epithelial cells. **Regul Pept** 145: 42–48, 2008. doi:10.1016/j.regpep.2007.08.002.

281. Nichols HL, Saffeddine M, Theriot BS, Hegde A, Polley D, El-Mays T, Vliagoftis H, Hollenberg MD, Wilson EH, Walker JK, Defea KA. beta-Arrestin-2 mediates the proinflammatory effects of proteinase-activated receptor-2 in the airway. **Proc Natl Acad Sci U S A** 109: 16660–16665, 2012. doi:10.1073/pnas.1208881109.

282. Jiang Y, Yau MK, Lim J, Wu KC, Xu W, Suen JY, Fairlie DP. A potent antagonist of protease-activated receptor 2 that inhibits multiple signaling functions in human cancer cells. **J Pharmacol Exp Ther** 364: 246–257, 2018. doi:10.1124/jpet.117.245027.

283. Cooper DM, Pechkovsky DV, Hackett TL, Knight DA, Granville DJ. Granzyme K activates protease-activated receptor-1. **PLoS One** 6: e21484, 2011. doi:10.1371/journal.pone.0021484.

284. Johnson JJ, Miller DL, Jiang R, Liu Y, Shi Z, Tarwater L, Williams R, Balsara R, Sauter ER, Stack MS. Protease-activated receptor-2 (PAR-2)-mediated Nf-κB activation suppresses inflammation-associated tumor suppressor microRNAs in oral squamous cell carcinoma. **J Biol Chem** 291: 6936–6945, 2016. doi:10.1074/jbc.M115.692640.

285. Rallabhandi P, Nhu QM, Toshchakov VY, Piao W, Medvedev AE, Hollenberg MD, Fasano A, Vogel SN. Analysis of proteinase-activated receptor 2 and TLR4 signal transduction. **J Biol Chem** 283: 24314–24325, 2008. doi:10.1074/jbc.M804800200.

286. Ko FN, Yang YC, Huang SC, Ou JT. Coagulation factor Xa stimulates platelet-derived growth factor release and mitogenesis in cultured vascular smooth muscle cells of rat. **J Clin Invest** 98: 1493–1501, 1996. doi:10.1172/JCI118938.

287. Shimizu S, Gabazza EC, Hayashi T, Ido M, Adachi Y, Suzuki K. Thrombin stimulates the expression of PDGF in lung epithelial cells. **Am J Physiol Lung Cell Mol Physiol** 279: L503–L510, 2000. doi:10.1152/ajplung.2000.279.3.L503.

288. Blanc-Brude OP, Archer F, Leoni P, Derian C, Bolsover S, Laurent GJ, Chambers RC. Factor Xa stimulates fibroblast procollagen production, proliferation, and calcium signaling via PAR1 activation. **Exp Cell Res** 304: 16–27, 2005. doi:10.1016/j.yexcr.2004.10.021.

289. Burch ML, Ballinger ML, Yang SN, Getachew R, Itman C, Loveland K, Osman N, Little PJ. Thrombin stimulation of proteoglycan synthesis in vascular smooth muscle is mediated by protease-activated receptor-1 transactivation of the transforming growth factor β type I receptor. **J Biol Chem** 285: 26798–26805, 2010. doi:10.1074/jbc.M109.092767.

290. Hammes SR, Coughlin SR. Protease-activated receptor-1 can mediate responses to SFLLRN in thrombin-desensitized cells: evidence for a novel mechanism for preventing or terminating signaling by PAR1's tethered ligand. **Biochemistry** 38: 2486–2493, 1999. doi:10.1021/bi982527i.

291. Ishii K, Chen J, Ishii M, Koch WJ, Freedman NJ, Lefkowitz RJ, Coughlin SR. Inhibition of thrombin receptor signaling by a G-protein coupled receptor kinase. Functional specificity among G-protein coupled receptor kinases. **J Biol Chem** 269: 1125–1130, 1994. doi:10.1016/S0021-9258(17)42230-7.

292. Hein L, Ishii K, Coughlin SR, Kobilka BK. Intracellular targeting and trafficking of thrombin receptors. A novel mechanism for resensitization of a G protein-coupled receptor. **J Biol Chem** 269: 27719–27726, 1994. doi:10.1016/S0021-9258(18)47045-7.

293. Shapiro MJ, Trejo J, Zeng D, Coughlin SR. Role of the thrombin receptor's cytoplasmic tail in intracellular trafficking. **J Biol Chem** 271: 32874–32880, 1996. doi:10.1074/jbc.271.51.32874.

294. Hammes SR, Shapiro MJ, Coughlin SR. Shutoff and agonist-triggered internalization of protease-activated receptor 1 can be separated by mutation of putative phosphorylation sites in the cytoplasmic tail. **Biochemistry** 38: 9308–9316, 1999. doi:10.1021/bi9902236.

295. Tiruppathi C, Yan W, Sandoval R, Naqvi T, Pronin AN, Benovic JL, Malik AB. G protein-coupled receptor kinase-5 regulates thrombin-activated signaling in endothelial cells. **Proc Natl Acad Sci U S A** 97: 7440–7445, 2000. doi:10.1073/pnas.97.13.7440.

296. Ghil S, Mccoy KL, Hepler JR. Regulator of G protein signaling 2 (RGS2) and RGS4 form distinct G protein-dependent complexes with protease activated-receptor 1 (PAR1) in live cells. **PLoS One** 9: e95355, 2014. doi:10.1371/journal.pone.0095355.

297. Lee J, Ghil S. Regulator of G protein signaling 8 inhibits protease-activated receptor 1/G i/o signaling by forming a distinct G protein-dependent complex in live cells. **Cell Signal** 28: 391–400, 2016. doi:10.1016/j.cellsig.2016.01.015.

298. Kim K, Lee J, Ghil S. The regulators of G protein signaling RGS16 and RGG18 nhibit protease-activated receptor 2/Gi/o signaling through distinct interactions with Gα in live cells. **FEBS Lett** 592: 3126–3138, 2018. doi:10.1002/1873-3468.13220.

299. Kim Y, Ghil S. Regulators of G-protein signaling, RGS2 and RGS4, inhibit protease-activated receptor 4-mediated signaling by forming a complex with the receptor and Gα in live cells. **Cell Commun Signal** 18: 86. 2020. doi:10.1186/s12964-020-00552-7.

300. Paing MM, Stutts AB, Kohout TA, Lefkowitz RJ, Trejo J. β-Arrestins regulate protease-activated receptor-1 desensitization but not

Downloaded from journals.physiology.org/journal/physrev at New York Univ (216.165.095.084) on September 28, 2023.

internalization or down-regulation. **J Biol Chem** 277: 1292–1300, 2002. doi:10.1074/jbc.M109160200.

301. Soh UJ, Trejo J. Activated protein C promotes protease-activated receptor-1 cytoprotective signaling through -arrestin and dishevelled-2 scaffolds. **Proc Natl Acad Sci U S A** 108: E1372–E1380, 2011. doi:10.1073/pnas.1112482108.

302. Stalheim L, Ding Y, Gullapalli A, Paing MM, Wolfe BL, Morris DR, Trejo J. Multiple independent functions of arrestins in the regulation of protease-activated receptor-2 signaling and trafficking. **Mol Pharmacol** 67: 78–87, 2005. doi:10.1124/mol.104.006072.

303. Roosterman D, Schmidlin F, Bunnett NW. Rab5a and rab11a mediate agonist-induced trafficking of protease-activated receptor 2. **Am J Physiol Cell Physiol** 284: C1319–C1329, 2003. doi:10.1152/ajpcell.00540.2002.

304. Wolfe BL, Marchese A, Trejo J. Ubiquitination differentially regulates clathrin-dependent internalization of protease-activated receptor-1. **J Cell Biol** 77: 905–916, 2007. doi:10.1083/jcb.200610154.

305. Chen B, R DM, Grimsey N, Canto I, Barker BL, Trejo J. Adaptor protein complex-2 (AP-2) and epsin-1 mediate protease-activated receptor-1 internalization via phosphorylation- and ubiquitination-dependent sorting signals. **J Biol Chem** 286: 40760–40770, 2011. doi:10.1074/jbc.M111.299776.

306. Paing MM, Johnston CA, Siderovski DP, Trejo J. Clathrin adaptor AP2 regulates thrombin receptor constitutive internalization and endothelial cell resensitization. **Mol Cell Biol** 26: 3231–3242, 2006. doi:10.1128/MCB.26.8.3231-3242.2006.

307. Alvarez-Arce A, Lee-Rivera I, López E, Hernández-Cruz A, López-Colomé AM. Thrombin-induced calpain activation promotes protease-activated receptor 1 internalization. **Intl J Cell Biol** 2017: 1908310, 2017. doi:10.1155/2017/1908310.

308. Böhm SK, Khitin LM, Grady EF, Aponte G, Payan DG, Bunnett NW. Mechanisms of desensitization and resensitization of proteinase-activated receptor-2. **J Biol Chem** 271: 22003–22016, 1996. doi:10.1074/jbc.271.36.22003.

309. Hasdemir B, Bunnett N, Cottrell GS. Hepatocyte growth factor-regulated tyrosine kinase substrate (HRS) mediates post-endocytic trafficking of protease-activated receptor 2 and calcitonin receptor-like receptor. **J Biol Chem** 282: 29646–29657, 2007. doi:10.1074/jbc.M702974200.

310. Jacob C, Cottrell GS, Gehringer D, Schmidlin F, Grady EF, Bunnett NW. c-Cbl mediates ubiquitination, degradation, and down-regulation of human protease-activated receptor 2. **J Biol Chem** 280: 16076–16087, 2005. doi:10.1074/jbc.M500109200.

311. Hasdemir B, Murphy JE, Cottrell GS, Bunnett NW. Endosomal deubiquitinating enzymes control ubiquitination and down-regulation of protease-activated receptor 2. **J Biol Chem** 284: 28453–28466, 2009. doi:10.1074/jbc.M109.025692.

312. Dores MR, Chen B, Lin H, Soh UJ, Paing MM, Montagne WA, Meerloo T, Trejo J. ALIX binds a YPX3L motif of the GPCR PAR1 and mediates ubiquitin-independent ESCRT-III/MVB sorting. **J Cell Biol** 197: 407–419, 2012. doi:10.1083/jcb.201110031.

313. Canto I, Trejo J. Palmitoylation of protease-activated receptor-1 regulates adaptor protein complex-2 and -3 interaction with tyrosine-based motifs and endocytic sorting. **J Biol Chem** 288: 15900–15912, 2013. doi:10.1074/jbc.M113.469866.

314. Arakaki AK, Pan WA, Lin H, Trejo J. The α-arrestin ARRDC3 suppresses breast carcinoma invasion by regulating G protein–coupled receptor lysosomal sorting and signaling. **J Biol Chem** 293: 3350–3362, 2018. doi:10.1074/jbc.RA117.001516.

315. Ishii K, Hein L, Kobilka B, Coughlin SR. Kinetics of thrombin receptor cleavage on intact cells. Relation to signaling. **J Biol Chem** 268: 9780–9786, 1993. doi:10.1016/S0021-9258(18)98415-2.

316. Grimsey NJ, Coronel LJ, Cordova IC, Trejo J. Recycling and endosomal sorting of protease-activated receptor-1 is distinctly regulated by Rab11A and Rab11B proteins. **J Biol Chem** 291: 2223–2236, 2016. doi:10.1074/jbc.M115.702993.

317. Trejo J, Hammes SR, Coughlin SR. Termination of signaling by protease-activated receptor-1 is linked to lysosomal sorting. **Proc Natl Acad Sci U S A** 95: 13698–13702, 1998. doi:10.1073/pnas.95.23.13698.

318. Trejo J, Coughlin SR. The cytoplasmic tails of protease-activated receptor-1 and substance p receptor specify sorting to lysosomes versus recycling. **J Biol Chem** 274: 2216–2224, 1999. doi:10.1074/jbc.274.4.2216.

319. Jensen DD, Zhao P, Jimenez-Vargas NN, Lieu T, Gerges M, Yeatman HR, Canals M, Vanner SJ, Poole DP, Bunnett NW. Protein kinase D and Gβγ subunits mediate agonist-evoked translocation of protease-activated receptor-2 from the golgi apparatus to the plasma membrane. **J Biol Chem** 291: 11285–11299, 2016. doi:10.1074/jbc.M115.710681.

320. Edgington LE, Verdoes M, Bogyo M. Functional imaging of proteases: recent advances in the design and application of substrate-based and activity-based probes. **Curr Opin Chem Biol** 15: 798–805, 2011. doi:10.1016/j.cbpa.2011.10.012.

321. Ku DD. Mechanism of thrombin-induced endothelium-dependent coronary vasodilation in dogs: role of its proteolytic enzymatic activity. **J Cardiovasc Pharmacol** 8: 29–36, 1986. doi:10.1097/00005344-198601000-00005.

322. Sambrano GR, Weiss EJ, Zheng YW, Huang W, Coughlin SR. Role of thrombin signalling in platelets in haemostasis and thrombosis. **Nature** 413: 74–78, 2001. doi:10.1038/35092573.

323. Hollenberg MD, Laniyonu AA, Saifeddine M, Moore GJ. Role of the amino- and carboxyl-terminal domains of thrombin receptor-derived polypeptides in biological activity in vascular endothelium and gastric smooth muscle: evidence for receptor subtypes. **Mol Pharmacol** 43: 921–930, 1993.

324. Hamilton JR, Moffatt JD, Frauman AG, Cocks TM. Protease-activated receptor (PAR) 1 but not PAR2 or PAR4 mediates endothelium-dependent relaxation to thrombin and trypsin in human pulmonary arteries. **J Cardiovasc Pharmacol** 38: 108–119, 2001. doi:10.1097/00005344-200107000-00012.

325. Vergnolle N, Hollenberg MD, Wallace JL. Pro- and anti-inflammatory actions of thrombin: a distinct role for proteinase-activated receptor-1 (PAR1). **Br J Pharmacol** 126: 1262–1268, 1999. doi:10.1038/sj.bjp.0702408.

326. Al-Ani B, Saifeddine M, Hollenberg MD. Detection of functional receptors for the proteinase-activated-receptor-2-activating polypeptide, SLIGRL-NH2, in rat vascular and gastric smooth muscle. **Can J Physiol Pharmacol** 73: 1203–1207, 1995. doi:10.1139/y95-172.

327. Saifeddine M, Al-Ani B, Cheng CH, Wang L, Hollenberg MD. Rat proteinase-activated receptor-2 (PAR-2): cDNA sequence and activity of receptor-derived peptides in gastric and vascular tissue. **Br J Pharmacol** 118: 521–530, 1996. doi:10.1111/j.1476-5381.1996.tb15433.x.

Downloaded from journals.physiology.org/journal/physrev at New York Univ (216.165.095.084) on September 28, 2023.

328. Cicala C. Protease activated receptor 2 and the cardiovascular system. **Br J Pharmacol** 135: 14–20, 2002. doi:10.1038/sj.bjp.0704438.

329. Disse J, Petersen HH, Larsen KS, Persson E, Esmon N, Esmon CT, Teyton L, Petersen LC, Ruf W. The endothelial protein C receptor supports tissue factor ternary coagulation initiation complex signaling through protease-activated receptors. **J Biol Chem** 286: 5756–5767, 2011. doi:10.1074/jbc.M110.201228.

330. Mohan Rao LV, Esmon CT, Pendurthi UR. Endothelial cell protein C receptor: a multiliganded and multifunctional receptor. **Blood** 124: 1553–1562, 2014. doi:10.1182/blood-2014-05-578328.

331. Rothmeier AS, Liu E, Chakrabarty S, Disse J, Mueller BM, Ostergaard H, Ruf W. Identification of the integrin-binding site on coagulation factor VIIa required for proangiogenic PAR2 signaling. **Blood** 131: 674–685, 2018. doi:10.1182/blood-2017-02-768218.

332. Ahamed J, Belting M, Ruf W. Regulation of tissue factor-induced signaling by endogenous and recombinant tissue factor pathway inhibitor 1. **Blood** 105: 2384–2391, 2005. doi:10.1182/blood-2004-09-3422.

333. Ma L, Perini R, McKnight W, Dicay M, Klein A, Hollenberg M, Wallace JL. Proteinase-activated receptors 1 and 4 counter-regulate endostatin and VEGF release from human platelets. **Proc Natl Acad Sci U S A** 102: 216–220, 2005. doi:10.1073/pnas.0406682102.

334. Jackson SP, Darbousset R, Schoenwaelder SM. Thromboinflammation: challenges of therapeutically targeting coagulation and other host defense mechanisms. **Blood** 133: 906–918, 2019. doi:10.1182/blood-2018-11-882993.

335. Ekdahl KN, Teramura Y, Hamad OA, Asif S, Duehrkop C, Fromell K, Gustafson E, Hong J, Kozarcanin H, Magnusson PU, Huber-Lang M, Garred P, Nilsson B. Dangerous liaisons: complement, coagulation, and kallikrein/kinin cross-talk act as a linchpin in the events leading to thromboinflammation. **Immunol Rev** 271: 245–269, 2016.

336. Megyeri M, Makó V, Beinrohr L, Doleschall Z, Prohászka Z, Cervenak L, Závodszky P, Gál P. Complement protease MASP-1 activates human endothelial cells: PAR4 activation is a link between complement and endothelial function. **J Immunol** 183: 3409–3416, 2009. doi:10.4049/jimmunol.0900879.

337. He SH, Xie H, Fu YL. Activation of human tonsil and skin mast cells by agonists of proteinase activated receptor-2. **Acta Pharmacol Sin** 26: 568–574, 2005. doi:10.1111/j.1745-7254.2005.00079.x.

338. Moffatt JD, Lever R, Page CP. Effects of inhaled thrombin receptor agonists in mice. **Br J Pharmacol** 143: 269–275, 2004. doi:10.1038/sj.bjp.0705926.

339. Bar-Shavit R, Kahn A, Mudd M, Wilner G, Mann K, Fenton JW 2nd. Localization of a chemotactic domain in human thrombin. **Biochemistry** 23: 397–400, 1984. doi:10.1021/bi00298a001.

340. Bar-Shavit R, Kahn A, Mann K, Wilner GD. Identification of a thrombin sequence with growth factor activity on macrophages. **Proc Natl Acad Sci U S A** 83: 976–980, 1986. doi:10.1073/pnas.83.4.976.

341. Rabenhorst A, Hartmann K. Interleukin-31: a novel diagnostic marker of allergic diseases. **Curr Allergy Asthma Rep** 14: 423, 2014. doi:10.1007/s11882-014-0423-y.

342. Shpacovitch V, Feld M, Hollenberg MD, Luger TA, Steinhoff M. Role of protease-activated receptors in inflammatory responses, innate and adaptive immunity. **J Leukoc Biol** 83: 1309–1322, 2008. doi:10.1189/jlb.0108001.

343. Rasmussen UB, Gachet C, Schlesinger Y, Hanau D, Ohlmann P, Van Obberghen-Schilling E, Pouyssegur J, Cazenave JP, Pavirani A. A peptide ligand of the human thrombin receptor antagonizes alpha-thrombin and partially activates platelets. **J Biol Chem** 268: 14322–14328, 1993. doi:10.1016/S0021-9258(19)85244-4.

344. Kuriri FA, Burchall G, Alanazi F, Antonipillai J, Dobie G, Beachemin N, Jackson DE. mice lacking PECAM-1 and Ceacam1 have enhanced platelet secretion and thrombus growth: novel link with PAR4. **Thromb Haemost** 122: 961–973, 2022. doi:10.1055/a-1663-8108.

345. Wallace JL, McKnight W, Del Soldato P, Baydoun AR, Cirino G. Antithrombotic effects of a nitric oxide-releasing, gastric-sparing aspirin derivative. **J Clin Invest** 96: 2711–2718, 1995. doi:10.1172/JCI118338.

346. Ruef J, Kacharava A, Pohl J, Bode C, , Runge MS. Indications for the presence of an atypical protease-activated receptor on rat platelets. **Ann Hematol** 79: 604–611, 2000. doi:10.1007/s002770000211.

347. van den Hengel LG, Hellingman AA, Nossent AY, van Oeveren-Rietdijk AM, de Vries MR, Spek CA, van Zonneveld AJ, Reitsma PH, Hamming JF, de Boer HC, Versteeg HH, Quax PH. Protease-activated receptor (PAR)2, but not PAR1, is involved in collateral formation and anti-inflammatory monocyte polarization in a mouse hind limb ischemia model. **PLoS One** 8: e61923, 2013. doi:10.1371/journal.pone.0061923.

348. Nystedt S, Ramakrishnan V, Sundelin J. The proteinase-activated receptor 2 is induced by inflammatory mediators in human endothelial cells. Comparison with the thrombin receptor. **J Biol Chem** 271: 14910–14915, 1996. doi:10.1074/jbc.271.25.14910.

349. Hara T, Fukuda D, Tanaka K, Higashikuni Y, Hirata Y, Nishimoto S, Yagi S, Yamada H, Soeki T, Wakatsuki T, Shimabukuro M, Sata M. Rivaroxaban, a novel oral anticoagulant, attenuates atherosclerotic plaque progression and destabilization in ApoE-deficient mice. **Atherosclerosis** 242: 639–646, 2015. doi:10.1016/j.atherosclerosis.2015.03.023.

350. Zuo P, Zuo Z, Wang X, Chen L, Zheng Y, Ma G, Zhou Q. Factor Xa induces pro-inflammatory cytokine expression in RAW 264.7 macrophages via protease-activated receptor-2 activation. **Am J Transl Res** 7: 2326–2334, 2015.

351. Uusitalo-Jarvinen H, Kurokawa T, Mueller BM, Andrade-Gordon P, Friedlander M, Ruf W. Role of protease activated receptor 1 and 2 signaling in hypoxia-induced angiogenesis. **Arterioscler Thromb Vasc Biol** 27: 1456–1462, 2007. doi:10.1161/ATVBAHA.107.142539.

352. Sitaras N, Rivera JC, Noueihed B, Bien-Aime M, Zaniolo K, Omri S, Hamel D, Zhu T, Hardy P, Sapieha P, Joyal JS, Chemtob S. Retinal neurons curb inflammation and enhance revascularization in ischemic retinopathies via proteinase-activated receptor-2. **Am J Pathol** 185: 581–595, 2015. doi:10.1016/j.ajpath.2014.10.020.

353. Hamilton JR, Cornelissen I, Mountford JK, Coughlin SR. Atherosclerosis proceeds independently of thrombin-induced platelet activation in ApoE-/- mice. **Atherosclerosis** 205: 427–432, 2009. doi:10.1016/j.atherosclerosis.2009.01.018.

354. Furman MI, Benoit SE, Barnard MR, Valeri CR, Borbone ML, Becker RC, Hechtman HB, Michelson AD. Increased platelet reactivity and circulating monocyte-platelet aggregates in patients with stable coronary artery disease. **J Am Coll Cardiol** 31: 352–358, 1998. doi:10.1016/s0735-1097(97)00510-x.

355. Misaki T, Satoh Y, Saino T, Ogawa A. The role of protease-activated receptors on the intracellular calcium ion dynamics of vascular smooth muscles, with special reference to cerebral arterioles. **Arch Histol Cytol** 69: 49–60, 2006. doi:10.1679/aohc.69.49.

Downloaded from journals.physiology.org/journal/physrev at New York Univ (216.165.095.084) on September 28, 2023.

356. Kai Y, Hirano K, Maeda Y, Nishimura J, Sasaki T, Kanaide H. Prevention of the hypercontractile response to thrombin by proteinase-activated receptor-1 antagonist in subarachnoid hemorrhage. **Stroke** 38: 3259–3265, 2007. doi:10.1161/STROKEAHA.107.487769.

357. Liu J, Nishida M, Inui H, Chang J, Zhu Y, Kanno K, Matsuda H, Sairyo M, Okada T, Nakaoka H, Ohama T, Masuda D, Koseki M, Yamashita S, Sakata Y. Rivaroxaban suppresses the progression of ischemic cardiomyopathy in a murine model of diet-induced myocardial infarction. **J Atheroscler Thromb** 26: 915–930, 2019. doi:10.5551/jat.48405.

358. Kondo H, Abe I, Fukui A, Saito S, Miyoshi M, Aoki K, Shinohara T, Teshima Y, Yufu K, Takahashi N. Possible role of rivaroxaban in attenuating pressure-overload-induced atrial fibrosis and fibrillation. **J Cardiol** 71: 310–319, 2018. doi:10.1016/j.jjcc.2017.08.007.

359. Pawlinski R, Tencati M, Hampton CR, Shishido T, Bullard TA, Casey LM, Andrade-Gordon P, Kotzsch M, Spring D, Luther T, Abe J, Pohlman TH, Verrier ED, Blaxall BC, Mackman N. Protease-activated receptor-1 contributes to cardiac remodeling and hypertrophy. **Circulation** 116: 2298–2306, 2007. doi:10.1161/CIRCULATIONAHA.107.692764.

360. Sonin DL, Wakatsuki T, Routhu KV, Harmann LM, Petersen M, Meyer J, Strande JL. Protease-activated receptor 1 inhibition by SCH79797 attenuates left ventricular remodeling and profibrotic activities of cardiac fibroblasts. **J Cardiovasc Pharmacol Ther** 18: 460–475, 2013. doi:10.1177/1074248413485434.

361. Yokono Y, Hanada K, Narita M, Tatara Y, Kawamura Y, Miura N, Kitayama K, Nakata M, Nozaka M, Kato T, Kudo N, Tsushima M, Toyama Y, Itoh K, Tomita H. Blockade of PAR-1 signaling attenuates cardiac hypertrophy and fibrosis in renin-overexpressing hypertensive mice. **J Am Heart Assoc** 9: e015616, 2020. doi:10.1161/JAHA.119.015616.

362. Darrow AL, Fung-Leung WP, Ye RD, Santulli RJ, Cheung WM, Derian CK, Burns CL, Damiano BP, Zhou L, Keenan CM, Peterson PA, Andrade-Gordon P. Biological consequences of thrombin receptor deficiency in mice. **Thromb Haemost** 76: 860–866, 1996. doi:10.1055/s-0038-1650676.

363. Bindoli S, Felicetti M, Sfriso P, Doria A. The amount of cytokine-release defines different shades of Sars-Cov2 infection. **Exp Biol Med (Maywood)** 245: 970–976, 2020. doi:10.1177/1535370220928964.

364. Sriram K, Insel PA. Inflammation and thrombosis in COVID-19 pathophysiology: proteinase-activated and purinergic receptors as drivers and candidate therapeutic targets. **Physiol Rev** 101: 545–567, 2021. doi:10.1152/physrev.00035.2020.

365. Schouten M, Wiersinga WJ, Levi M, van der Poll T. Inflammation, endothelium, and coagulation in sepsis. **J Leukoc Biol** 83: 536–545, 2008. doi:10.1189/jlb.0607373.

366. McGonagle D, Sharif K, O'Regan A, Bridgewood C. The role of cytokines including interleukin-6 in COVID-19 induced pneumonia and macrophage activation syndrome-like disease. **Autoimmun Rev** 19: 102537, 2020. doi:10.1016/j.autrev.2020.102537.

367. Helms J, Tacquard C, Severac F, Leonard-Lorant I, Ohana M, Delabranche X, Merdji H, Clere-Jehl R, Schenck M, Fagot Gandet F, Fafi-Kremer S, Castelain V, Schneider F, Grunebaum L, Angles-Cano E, Sattler L, Mertes PM, Meziani F, CRICS TRIGGERSEP Group (Clinical Research in Intensive Care and Sepsis Trial Group for Global Evaluation and Research in Sepsis). High risk of thrombosis in patients with severe SARS-CoV-2 infection: a multicenter prospective cohort study. **Intensive Care Med** 46: 1089–1098, 2020. doi:10.1007/s00134-020-06062-x.

368. Rovai ES, Alves T, Holzhausen M. Protease-activated receptor 1 as a potential therapeutic target for COVID-19. **Exp Biol Med (Maywood)** 246: 688–694, 2021. doi:10.1177/1535370220978372.

369. Jenkins AL, Chinni C, De Niese MR, Blackhart B, Mackie EJ. Expression of protease-activated receptor-2 during embryonic development. **Dev Dyn** 218: 465–471, 2000. doi:10.1002/1097-0177(200007)218:3<465::AID-DVDY1013>3.0.CO;2-5.

370. Hachem JP, Houben E, Crumrine D, Man MQ, Schurer N, Roelandt T, Choi EH, Uchida Y, Brown BE, Feingold KR, Elias PM. Serine protease signaling of epidermal permeability barrier homeostasis. **J Invest Dermatol** 126: 2074–2086, 2006. doi:10.1038/sj.jid.5700351.

371. Lundwall A, Brattsand M. Kallikrein-related peptidases. **Cell Mol Life Sci** 65: 2019–2038, 2008. doi:10.1007/s00018-008-8024-3.

372. Rattenholl A, Steinhoff M. Proteinase-activated receptor-2 in the skin: receptor expression, activation and function during health and disease. **Drug News Perspect** 21: 369–381, 2008. doi:10.1358/dnp.2008.21.7.1255294.

373. Oikonomopoulou K, Hansen KK, Saifeddine M, Vergnolle N, Tea I, Blaber M, Blaber SI, Scarisbrick I, Diamandis EP, Hollenberg MD. Kallikrein-mediated cell signalling: targeting proteinase-activated receptors (PARs). **Biol Chem** 387: 817–824, 2006. doi:10.1515/bc.2006.104.

374. Oikonomopoulou K, Hansen KK, Saifeddine M, Vergnolle N, Tea I, Diamandis EP, Hollenberg MD. Proteinase-mediated cell signalling: targeting proteinase-activated receptors (PARs) by kallikreins and more. **Biol Chem** 387: 677–685, 2006. doi:10.1515/BC.2006.086.

375. Roelandt T, Heughebaert C, Hachem JP. Proteolytically active allergens cause barrier breakdown. **J Invest Dermatol** 128: 1878–1880, 2008. doi:10.1038/jid.2008.168.

376. Roelandt T, Heughebaert C, Verween G, Giddelo C, Verbeken G, Pirnay JP, Devos D, Crumrine D, Roseeuw D, Elias PM, Hachem JP. Actin dynamics regulate immediate PAR-2-dependent responses to acute epidermal permeability barrier abrogation. **J Dermatol Sci** 61: 101–109, 2011. doi:10.1016/j.jdermsci.2010.11.016.

377. Steinhoff M, Neisius U, Ikoma A, Fartasch M, Heyer G, Skov PS, Luger TA, Schmelz M. Proteinase-activated receptor-2 mediates itch: a novel pathway for pruritus in human skin. **J Neurosci** 23: 6176–6180, 2003. doi:10.1523/JNEUROSCI.23-15-06176.2003.

378. Julovi SM, Xue M, Dervish S, Sambrook PN, March L, Jackson CJ. Protease activated receptor-2 mediates activated protein C-induced cutaneous wound healing via inhibition of p38. **Am J Pathol** 179: 2233–2242, 2011. doi:10.1016/j.ajpath.2011.07.024.

379. Xue M, Campbell D, Sambrook PN, Fukudome K, Jackson CJ. Endothelial protein C receptor and protease-activated receptor-1 mediate induction of a wound-healing phenotype in human keratinocytes by activated protein C. **J Invest Dermatol** 125: 1279–1285, 2005. doi:10.1111/j.0022-202X.2005.23952.x.

380. Sharlow ER, Paine CS, Babiarz L, Eisinger M, Shapiro S, Seiberg M. The protease-activated receptor-2 upregulates keratinocyte phagocytosis. **J Cell Sci** 113: 3093–3101, 2000. doi:10.1242/jcs.113.17.3093.

381. Hou L, Kapas S, Cruchley AT, Macey MG, Harriott P, Chinni C, Stone SR, Howells GL. Immunolocalization of protease-activated receptor-2 in skin: receptor activation stimulates interleukin-8 secretion by keratinocytes in vitro. **Immunology** 94: 356–362, 1998. doi:10.1046/j.1365-2567.1998.00528.x.

Downloaded from journals.physiology.org/journal/physrev at New York Univ (216.165.095.084) on September 28, 2023.

382. Babiarz-Magee L, Chen N, Seiberg M, Lin CB. The expression and activation of protease-activated receptor-2 correlate with skin color. **Pigment Cell Res** 17: 241–251, 2004. doi:10.1111/j.1600-0749.2004.00133.x.

383. Seiberg M, Paine C, Sharlow E, Andrade-Gordon P, Costanzo M, Eisinger M, Shapiro SS. The protease-activated receptor 2 regulates pigmentation via keratinocyte-melanocyte interactions. **Exp Cell Res** 254: 25–32, 2000. doi:10.1006/excr.1999.4692.

384. Bangert C, Brunner PM, Stingl G. Immune functions of the skin. **Clin Dermatol** 29: 360–376, 2011. doi:10.1016/j.clindermatol.2011.01.006.

385. Komatsu N, Saijoh K, Kuk C, Shirasaki F, Takehara K, Diamandis EP. Aberrant human tissue kallikrein levels in the stratum corneum and serum of patients with psoriasis: dependence on phenotype, severity and therapy. **Br J Dermatol** 156: 875–883, 2007. doi:10.1111/j.1365-2133.2006.07743.x.

386. Buhl T, Ikoma A, Kempkes C, Cevikbas F, Sulk M, Buddenkotte J, Akiyama T, Crumrine D, Camerer E, Carstens E, Schon MP, Elias P, Coughlin SR, Steinhoff M. Protease-activated receptor-2 regulates neuro-epidermal communication in atopic dermatitis. **Front Immunol** 11: 1740, 2020. doi:10.3389/fimmu.2020.01740.

387. Smith L, Gatault S, Casals-Diaz L, Kelly PA, Camerer E, Metais C, Knaus UG, Eissner G, Steinhoff M. House dust mite-treated PAR2 over-expressor mouse: a novel model of atopic dermatitis. **Exp Dermatol** 28: 1298–1308, 2019. doi:10.1111/exd.14030.

388. Briot A, Deraison C, Lacroix M, Bonnart C, Robin A, Besson C, Dubus P, Hovnanian A. Kallikrein 5 induces atopic dermatitis-like lesions through PAR2-mediated thymic stromal lymphopoietin expression in Netherton syndrome. **J Exp Med** 206: 1135–1147, 2009. doi:10.1084/jem.20082242.

389. Saunders DP, Epstein JB, Elad S, Allemano J, Bossi P, van de Wetering MD, Rao NG, Potting C, Cheng KK, Freidank A, Brennan MT, Bowen J, Dennis K, Lalla RV, Mucositis Study Group of the Multinational Association of Supportive Care in Cancer/International Society of Oral Oncology (MASCC/ISOO). Systematic review of antimicrobials, mucosal coating agents, anesthetics, and analgesics for the management of oral mucositis in cancer patients. **Support Care Cancer** 21: 3191–3207, 2013. doi:10.1007/s00520-013-1871-y.

390. Kawasaki H, Nagao K, Kubo A, Hata T, Shimizu A, Mizuno H, Yamada T, Amagai M. Altered stratum corneum barrier and enhanced percutaneous immune responses in filaggrin-null mice. **J Allergy Clin Immunol** 129: 1538–1546.e6e1536, 2012. doi:10.1016/j.jaci.2012.01.068.

391. Yoo J, Omori M, Gyarmati D, Zhou B, Aye T, Brewer A, Comeau MR, Campbell DJ, Ziegler SF. Spontaneous atopic dermatitis in mice expressing an inducible thymic stromal lymphopoietin transgene specifically in the skin. **J Exp Med** 202: 541–549, 2005. doi:10.1084/jem.20041503.

392. Jeong SK, Kim HJ, Youm JK, Ahn SK, Choi EH, Sohn MH, Kim KE, Hong JH, Shin DM, Lee SH. Mite and cockroach allergens activate protease-activated receptor 2 and delay epidermal permeability barrier recovery. **J Invest Dermatol** 128: 1930–1939, 2008. doi:10.1038/jid.2008.13.

393. Chung K, Pitcher T, Grant AD, Hewitt E, Lindstrom E, Malcangio M. Cathepsin S acts via protease-activated receptor 2 to activate sensory neurons and induce itch-like behaviour. **Neurobiol Pain** 6: 100032, 2019. doi:10.1016/j.ynpai.2019.100032.

394. Feramisco JD, Berger TG, Steinhoff M. Innovative management of pruritus. **Dermatol Clin** 28: 467–478, 2010. doi:10.1016/j.det.2010.03.004.

395. Nattkemper LA, Tey HL, Valdes-Rodriguez R, Lee H, Mollanazar NK, Albornoz C, Sanders KM, Yosipovitch G. The genetics of chronic itch: gene expression in the skin of patients with atopic dermatitis and psoriasis with severe itch. **J Invest Dermatol** 138: 1311–1317, 2018. doi:10.1016/j.jid.2017.12.029.

396. Belghiti M, Estevez-Herrera J, Gimenez-Garzo C, Gonzalez-Usano A, Montoliu C, Ferrer-Montiel A, Felipo V, Planells-Cases R. Potentiation of the transient receptor potential vanilloid 1 channel contributes to pruritogenesis in a rat model of liver disease. **J Biol Chem** 288: 9675–9685, 2013. doi:10.1074/jbc.M113.455162.

397. Moon SJ, Kim HJ, Cho SB, Lee SH, Choi HY, Park HC, Ha SK. Epidermal proteinase-activated receptor-2 expression is increased in end-stage renal disease patients with pruritus: a pilot study. **Electrolyte Blood Press** 12: 74–79, 2014. doi:10.5049/EBP.2014.12.2.74.

398. Chua KY, Stewart GA, Thomas WR, Simpson RJ, Dilworth RJ, Plozza TM, Turner KJ. Sequence analysis of cDNA coding for a major house dust mite allergen, Der p 1. Homology with cysteine proteases. **J Exp Med** 167: 175–182, 1988. doi:10.1084/jem.167.1.175.

399. Stewart GA, Ward LD, Simpson RJ, Thompson PJ. The group III allergen from the house dust mite Dermatophagoides pteronyssinus is a trypsin-like enzyme. **Immunology** 75: 29–35, 1992.

400. King C, Simpson RJ, Moritz RL, Reed GE, Thompson PJ, Stewart GA. The isolation and characterization of a novel collagenolytic serine protease allergen (Der p 9) from the dust mite Dermatophagoides pteronyssinus. **J Allergy Clin Immunol** 98: 739–747, 1996. doi:10.1016/S0091-6749(96)70121-5.

401. McMahon DB, Workman AD, Kohanski MA, Carey RM, Freund JR, Hariri BM, Chen B, Doghramji LJ, Adappa ND, Palmer JN, Kennedy DW, Lee RJ. Protease-activated receptor 2 activates airway apical membrane chloride permeability and increases ciliary beating. **FASEB J** 32: 155–167, 2018. doi:10.1096/fj.201700114RRR.

402. Trejo J, Connolly AJ, Coughlin SR. The cloned thrombin receptor is necessary and sufficient for activation of mitogen-activated protein kinase and mitogenesis in mouse lung fibroblasts. Loss of responses in fibroblasts from receptor knockout mice. **J Biol Chem** 271: 21536–21541, 1996. doi:10.1074/jbc.271.35.21536.

403. Camerer E, Kataoka H, Kahn M, Lease K, Coughlin SR. Genetic evidence that protease-activated receptors mediate factor Xa signaling in endothelial cells. **J Biol Chem** 277: 16081–16087, 2002. doi:10.1074/jbc.M108555200.

404. Howell DC, Goldsack NR, Marshall RP, McAnulty RJ, Starke R, Purdy G, Laurent GJ, Chambers RC. Direct thrombin inhibition reduces lung collagen, accumulation, and connective tissue growth factor mRNA levels in bleomycin-induced pulmonary fibrosis. **Am J Pathol** 159: 1383–1395, 2001. doi:10.1016/S0002-9440(10)62525-4.

405. Bogatkevich GS, Tourkina E, Silver RM, Ludwicka-Bradley A. Thrombin differentiates normal lung fibroblasts to a myofibroblast phenotype via the proteolytically activated receptor-1 and a protein kinase C-dependent pathway. **J Biol Chem** 276: 45184–45192, 2001. doi:10.1074/jbc.M106441200.

406. Jenkins RG, Su X, Su G, Scotton CJ, Camerer E, Laurent GJ, Davis GE, Chambers RC, Matthay MA, Sheppard D. Ligation of protease-activated receptor 1 enhances alpha(v)beta6 integrin-dependent TGF-beta activation and promotes acute lung injury. **J Clin Invest** 116: 1606–1614, 2006. doi:10.1172/JCI27183.

Downloaded from journals.physiology.org/journal/physrev at New York Univ (216.165.095.084) on September 28, 2023.

407. Fuchs-Buder T, de Moerloose P, Ricou B, Reber G, Vifian C, Nicod L, Romand JA, Suter PM. Time course of procoagulant activity and D dimer in bronchoalveolar fluid of patients at risk for or with acute respiratory distress syndrome. **Am J Respir Crit Care Med** 153: 163–167, 1996. doi:10.1164/ajrccm.153.1.8542111.

408. Kipnis E, Guery BP, Tournoys A, Leroy X, Robriquet L, Fialdes P, Neviere R, Fourrier F. Massive alveolar thrombin activation in Pseudomonas aeruginosa-induced acute lung injury. **Shock** 21: 444–451, 2004. doi:10.1097/00024382-200405000-00008.

409. Pittet JF, Griffiths MJ, Geiser T, Kaminski N, Dalton SL, Huang X, Brown LA, Gotwals PJ, Koteliansky VE, Matthay MA, Sheppard D. TGF-beta is a critical mediator of acute lung injury. **J Clin Invest** 107: 1537–1544, 2001. doi:10.1172/JCI11963.

410. Lin C, von der Thusen J, Daalhuisen J, ten Brink M, Crestani B, van der Poll T, Borensztajn K, Spek CA. Protease-activated receptor (PAR)-2 is required for PAR-1 signalling in pulmonary fibrosis. **J Cell Mol Med** 19: 1346–1356, 2015. doi:10.1111/jcmm.12520.

411. Shapiro PS, Evans JN, Davis RJ, Posada JA. The seven-transmembrane-spanning receptors for endothelin and thrombin cause proliferation of airway smooth muscle cells and activation of the extracellular regulated kinase and c-Jun NH2-terminal kinase groups of mitogen-activated protein kinases. **J Biol Chem** 271: 5750–5754, 1996. doi:10.1074/jbc.271.10.5750.

412. Hauck RW, Schulz C, Schomig A, Hoffman RK, Panettieri RA Jr. alpha-Thrombin stimulates contraction of human bronchial rings by activation of protease-activated receptors. **Am J Physiol Lung Cell Mol Physiol** 277: L22–L29, 1999. doi:10.1152/ajplung.1999.277.1.l22.

413. Chow JM, Moffatt JD, Cocks TM. Effect of protease-activated receptor (PAR)-1, -2 and -4-activating peptides, thrombin and trypsin in rat isolated airways. **Br J Pharmacol** 131: 1584–1591, 2000. doi:10.1038/sj.bjp.0703738.

414. Shrestha Palikhe N, Nahirney D, Laratta C, Gandhi VD, Vethanayagam D, Bhutani M, Mayers I, Cameron L, Vliagoftis H. Increased protease-activated receptor-2 (PAR-2) expression on CD14++CD16+ peripheral blood monocytes of patients with severe asthma. **PLoS One** 10: e0144500, 2015. doi:10.1371/journal.pone.0144500.

415. Terasawa T, Aso Y, Omori K, Fukushima M, Momobayashi A, Inukai T. Bezafibrate, a peroxisome proliferator-activated receptor alpha agonist, decreases circulating CD14(+)CD16(+) monocytes in patients with type 2 diabetes. **Transl Res** 165: 336–345, 2015. doi:10.1016/j.trsl.2014.07.008.

416. Okamoto H, Mizuno K, Horio T. Circulating CD14+ CD16+ monocytes are expanded in sarcoidosis patients. **J Dermatol** 30: 503–509, 2003. doi:10.1111/j.1346-8138.2003.tb00424.x.

417. Chambers RC. Procoagulant signalling mechanisms in lung inflammation and fibrosis: novel opportunities for pharmacological intervention? **Br J Pharmacol** 153: 367–378, 2008. doi:10.1038/sj.bjp.0707506.

418. Mercer PF, Chambers RC. Coagulation and coagulation signalling in fibrosis. **Biochim Biophys Acta** 1832: 1018–1027, 2013. doi:10.1016/j.bbadis.2012.12.013.

419. Kawabata A, Kuroda R, Kuroki N, Nishikawa H, Kawai K. Dual modulation by thrombin of the motility of rat oesophageal muscularis mucosae via two distinct protease-activated receptors (PARs): a novel role for PAR-4 as opposed to PAR-1. **Br J Pharmacol** 131: 578–584, 2000. doi:10.1038/sj.bjp.0703590.

420. Buresi MC, Schleihauf E, Vergnolle N, Buret A, Wallace JL, Hollenberg MD, MacNaughton WK. Protease-activated receptor-1 stimulates Ca^{2+}-dependent Cl^- secretion in human intestinal epithelial cells. **Am J Physiol Gastrointest Liver Physiol** 281: G323–G332, 2001. doi:10.1152/ajpgi.2001.281.2.G323.

421. He L, Ma Y, Li W, Han W, Zhao X, Wang H. Protease-activated receptor 2 signaling modulates susceptibility of colonic epithelium to injury through stabilization of YAP in vivo. **Cell Death Dis** 9: 949, 2018. doi:10.1038/s41419-018-0995-x.

422. Nasri I, Bonnet D, Zwarycz B, d'Aldebert E, Khou S, Mezghani-Jarraya R, Quaranta M, Rolland C, Bonnart C, Mas E, Ferrand A, Cenac N, Magness S, Van Landeghem L, Vergnolle N, Racaud-Sultan C. PAR2-dependent activation of GSK3beta regulates the survival of colon stem/progenitor cells. **Am J Physiol Gastrointest Liver Physiol** 311: G221–G236, 2016. doi:10.1152/ajpgi.00328.2015.

423. Chin AC, Vergnolle N, MacNaughton WK, Wallace JL, Hollenberg MD, Buret AG. Proteinase-activated receptor 1 activation induces epithelial apoptosis and increases intestinal permeability. **Proc Natl Acad Sci U S A** 100: 11104–11109, 2003. doi:10.1073/pnas.1831452100.

424. Hyun E, Andrade-Gordon P, Steinhoff M, Vergnolle N. Protease-activated receptor-2 activation: a major actor in intestinal inflammation. **Gut** 57: 1222–1229, 2008. doi:10.1136/gut.2008.150722.

425. Cenac N, Coelho AM, Nguyen C, Compton S, Andrade-Gordon P, MacNaughton WK, Wallace JL, Hollenberg MD, Bunnett NW, Garcia-Villar R, Bueno L, Vergnolle N. Induction of intestinal inflammation in mouse by activation of proteinase-activated receptor-2. **Am J Pathol** 161: 1903–1915, 2002. doi:10.1016/S0002-9440(10)64466-5.

426. Gobbetti T, Cenac N, Motta JP, Rolland C, Martin L, Andrade-Gordon P, Steinhoff M, Barocelli E, Vergnolle N. Serine protease inhibition reduces post-ischemic granulocyte recruitment in mouse intestine. **Am J Pathol** 180: 141–152, 2012. doi:10.1016/j.ajpath.2011.09.031.

427. Cenac N, Chin AC, Garcia-Villar R, Salvador-Cartier C, Ferrier L, Vergnolle N, Buret AG, Fioramonti J, Bueno L. PAR2 activation alters colonic paracellular permeability in mice via IFN-gamma-dependent and -independent pathways. **J Physiol** 558: 913–925, 2004. doi:10.1113/jphysiol.2004.061721.

428. Cenac N, Garcia-Villar R, Ferrier L, Larauche M, Vergnolle N, Bunnett NW, Coelho AM, Fioramonti J, Bueno L. Proteinase-activated receptor-2-induced colonic inflammation in mice: possible involvement of afferent neurons, nitric oxide, and paracellular permeability. **J Immunol** 170: 4296–4300, 2003. doi:10.4049/jimmunol.170.8.4296.

429. Roka R, Demaude J, Cenac N, Ferrier L, Salvador-Cartier C, Garcia-Villar R, Fioramonti J, Bueno L. Colonic luminal proteases activate colonocyte proteinase-activated receptor-2 and regulate paracellular permeability in mice. **Neurogastroenterol Motil** 19: 57–65, 2007. doi:10.1111/j.1365-2982.2006.00851.x.

430. Lee MC, Huang SC. Proteinase-activated receptor-1 (PAR(1)) and PAR(2) but not PAR(4) mediate contraction in human and guinea-pig gallbladders. **Neurogastroenterol Motil** 20: 385–391, 2008. doi:10.1111/j.1365-2982.2007.01041.x.

431. Kawabata A, Kawao N, Kuroda R, Tanaka A, Itoh H, Nishikawa H. Peripheral PAR-2 triggers thermal hyperalgesia and nociceptive responses in rats. **Neuroreport** 12: 715–719, 2001. doi:10.1097/00001756-200103260-00020.

432. Kawabata A, Kuroda R, Nishida M, Nagata N, Sakaguchi Y, Kawao N, Nishikawa H, Arizono N, Kawai K. Protease-activated receptor-2 (PAR-2) in the pancreas and parotid gland: Immunolocalization and

Downloaded from journals.physiology.org/journal/physrev at New York Univ (216.165.095.084) on September 28, 2023.

involvement of nitric oxide in the evoked amylase secretion. **Life Sci** 71: 2435–2446, 2002. doi:10.1016/S0024-3205(02)02044-1.

433. Karanjia R, Spreadbury I, Bautista-Cruz F, Tsang ME, Vanner S. Activation of protease-activated receptor-4 inhibits the intrinsic excitability of colonic dorsal root ganglia neurons. **Neurogastroenterol Motil** 21: 1218–1221, 2009. doi:10.1111/j.1365-2982.2009.01353.x.

434. Hayama T, Kamio N, Okabe T, Muromachi K, Matsushima K. Kallikrein promotes inflammation in human dental pulp cells via protease-activated receptor-1. **J Cell Biochem** 117: 1522–1528, 2016. doi:10.1002/jcb.25437.

435. da Silva HA, Euzebio Alves VT, Spolidorio LC, Cesar Neto JB, Eichler RS, de Carvalho MH, Holzhausen M. Expression of protease activated receptor-1 in chronic periodontitis. **J Periodontol** 85: 1763–1769, 2014. doi:10.1902/jop.2014.140172.

436. Uehara A, Imamura T, Potempa J, Travis J, Takada H. Gingipains from Porphyromonas gingivalis synergistically induce the production of proinflammatory cytokines through protease-activated receptors with Toll-like receptor and NOD1/2 ligands in human monocytic cells. **Cell Microbiol** 10: 1181–1189, 2008. doi:10.1111/j.1462-5822.2008.01119.x.

437. Curtis MA, Kuramitsu HK, Lantz M, Macrina FL, Nakayama K, Potempa J, Reynolds EC, Aduse-Opoku J. Molecular genetics and nomenclature of proteases of Porphyromonas gingivalis. **J Periodontal Res** 34: 464–472, 1999. doi:10.1111/j.1600-0765.1999.tb02282.x.

438. Jouet P, Sarna SK, Singaram C, Ryan RP, Hillard CJ, Telford GL, Fink J, Henderson JD. Immunocytes and abnormal gastrointestinal motor activity during ileitis in dogs. **Am J Physiol Gastrointest Liver Physiol** 269: G913–G924, 1995. doi:10.1152/ajpgi.1995.269.6.g913.

439. Kawabata A, Kuroda R, Kuroki N, Nishikawa H, Kawai K, Araki H. Characterization of the protease-activated receptor-1-mediated contraction and relaxation in the rat duodenal smooth muscle. **Life Sci** 67: 2521–2530, 2000. doi:10.1016/S0024-3205(00)00835-3.

440. Mule F, Baffi MC, Cerra MC. Dual effect mediated by protease-activated receptors on the mechanical activity of rat colon. **Br J Pharmacol** 136: 367–374, 2002. doi:10.1038/sj.bjp.0704746.

441. Sato K, Ninomiya H, Ohkura S, Ozaki H, Nasu T. Impairment of PAR-2-mediated relaxation system in colonic smooth muscle after intestinal inflammation. **Br J Pharmacol** 148: 200–207, 2006. doi:10.1038/sj.bjp.0706717.

442. Kim JA, Choi SC, Yun KJ, Kim DK, Han MK, Seo GS, Yeom JJ, Kim TH, Nah YH, Lee YM. Expression of protease-activated receptor 2 in ulcerative colitis. **Inflamm Bowel Dis** 9: 224–229, 2003. doi:10.1097/00054725-200307000-00002.

443. Cottrell GS, Amadesi S, Grady EF, Bunnett NW. Trypsin IV, a novel agonist of protease-activated receptors 2 and 4. **J Biol Chem** 279: 13532–13539, 2004. doi:10.1074/jbc.M312090200.

444. Vergnolle N. Modulation of visceral pain and inflammation by protease-activated receptors. **Br J Pharmacol** 141: 1264–1274, 2004. doi:10.1038/sj.bjp.0705750.

445. Nguyen C, Coelho AM, Grady E, Compton SJ, Wallace JL, Hollenberg MD, Cenac N, Garcia-Villar R, Bueno L, Steinhoff M, Bunnett NW, Vergnolle N. Colitis induced by proteinase-activated receptor-2 agonists is mediated by a neurogenic mechanism. **Can J Physiol Pharmacol** 81: 920–927, 2003. doi:10.1139/y03-080.

446. Van Spaendonk H, Ceuleers H, Witters L, Patteet E, Joossens J, Augustyns K, Lambeir AM, De Meester I, De Man JG, Winter BY. Regulation of intestinal permeability: the role of proteases. **World J Gastroenterol** 23: 2106–2123, 2017. doi:10.3748/wjg.v23.i12.2106.

447. Maharshak N, Huh EY, Paiboonrungruang C, Shanahan M, Thurlow L, Herzog J, Djukic Z, Orlando R, Pawlinski R, Ellermann M, Borst L, Patel S, Dotan I, Sartor RB, Carroll IM. Enterococcus faecalis gelatinase mediates intestinal permeability via protease-activated receptor 2. **Infect Immun** 83: 2762–2770, 2015. doi:10.1128/IAI.00425-15.

448. Hyun E, Andrade-Gordon P, Steinhoff M, Beck PL, Vergnolle N. Contribution of bone marrow-derived cells to the pro-inflammatory effects of protease-activated receptor-2 in colitis. **Inflamm Res** 59: 699–709, 2010. doi:10.1007/s00011-010-0181-9.

449. Tomuschat C, O'Donnell AM, Coyle D, Puri P. Increased protease activated receptors in the colon of patients with Hirschsprung's disease. **J Pediatr Surg** 55: 1488–1494, 2020. doi:10.1016/j.jpedsurg.2019.11.009.

450. Cenac N, Andrews CN, Holzhausen M, Chapman K, Cottrell G, Andrade-Gordon P, Steinhoff M, Barbara G, Beck P, Bunnett NW, Sharkey KA, Ferraz JG, Shaffer E, Vergnolle N. Role for protease activity in visceral pain in irritable bowel syndrome. **J Clin Invest** 117: 636–647, 2007. doi:10.1172/JCI29255.

451. Vergnolle N, Wallace JL, Bunnett NW, Hollenberg MD. Protease-activated receptors in inflammation, neuronal signaling and pain. **Trends Pharmacol Sci** 22: 146–152, 2001. doi:10.1016/S0165-6147(00)01634-5.

452. Coelho AM, Vergnolle N, Guiard B, Fioramonti J, Bueno L. Proteinases and proteinase-activated receptor 2: a possible role to promote visceral hyperalgesia in rats. **Gastroenterology** 122: 1035–1047, 2002. doi:10.1053/gast.2002.32387.

453. Buhner S, Hahne H, Hartwig K, Li Q, Vignali S, Ostertag D, Meng C, Hormannsperger G, Braak B, Pehl C, Frieling T, Barbara G, De Giorgio R, Demir IE, Ceyhan GO, Zeller F, Boeckxstaens G, Haller D, Kuster B, Schemann M. Protease signaling through protease activated receptor 1 mediate nerve activation by mucosal supernatants from irritable bowel syndrome but not from ulcerative colitis patients. **PLoS One** 13: e0193943, 2018. doi:10.1371/journal.pone.0193943.

454. Desormeaux C, Bautzova T, Garcia-Caraballo S, Rolland C, Barbaro MR, Brierley SM, Barbara G, Vergnolle N, Cenac N. Protease-activated receptor 1 is implicated in irritable bowel syndrome mediators-induced signaling to thoracic human sensory neurons. **Pain** 159: 1257–1267, 2018. doi:10.1097/j.pain.0000000000001208.

455. Cattaruzza F, Spreadbury I, Miranda-Morales M, Grady EF, Vanner S, Bunnett NW. Transient receptor potential ankyrin-1 has a major role in mediating visceral pain in mice. **Am J Physiol Gastrointest Liver Physiol** 298: G81–G91, 2010. doi:10.1152/ajpgi.00221.2009.

456. Suzuki M, Mizuno A, Kodaira K, Imai M. Impaired pressure sensation in mice lacking TRPV4. **J Biol Chem** 278: 22664–22668, 2003. doi:10.1074/jbc.M302561200.

457. Cervero F, Laird JM. Visceral pain. **Lancet** 353: 2145–2148, 1999. doi:10.1016/S0140-6736(99)01306-9.

458. Clark AK, Gentry C, Bradbury EJ, McMahon SB, Malcangio M. Role of spinal microglia in rat models of peripheral nerve injury and inflammation. **Eur J Pain** 11: 223–230, 2007. doi:10.1016/j.ejpain.2006.02.003.

459. Clark AK, Yip PK, Malcangio M. The liberation of fractalkine in the dorsal horn requires microglial cathepsin S. **J Neurosci** 29: 6945–6954, 2009. doi:10.1523/JNEUROSCI.0828-09.2009.

Downloaded from journals.physiology.org/journal/physrev at New York Univ (216.165.095.084) on September 28, 2023.

460. Cattaruzza F, Lyo V, Jones E, Pham D, Hawkins J, Kirkwood K, Valdez-Morales E, Ibeakanma C, Vanner SJ, Bogyo M, Bunnett NW. Cathepsin S is activated during colitis and causes visceral hyperalgesia by a PAR2-dependent mechanism in mice. **Gastroenterology** 141: 1864–1874, 2011. doi:10.1053/j.gastro.2011.07.035.

461. Marra F, DeFranco R, Grappone C, Milani S, Pinzani M, Pellegrini G, Laffi G, Gentilini P. Expression of the thrombin receptor in human liver: up-regulation during acute and chronic injury. **Hepatology** 27: 462–471, 1998. doi:10.1002/hep.510270221.

462. Margaretten W, McKay DG, Phillips LL. The effect of heparin on endotoxin shock in the rat. **Am J Pathol** 51: 61–68, 1967.

463. Moulin F, Copple BL, Ganey PE, Roth RA. Hepatic and extrahepatic factors critical for liver injury during lipopolysaccharide exposure. **Am J Physiol Gastrointest Liver Physiol** 281: G1423–G1431, 2001. doi:10.1152/ajpgi.2001.281.6.G1423.

464. Copple BL, Moulin F, Hanumegowda UM, Ganey PE, Roth RA. Thrombin and protease-activated receptor-1 agonists promote lipopolysaccharide-induced hepatocellular injury in perfused livers. **J Pharmacol Exp Ther** 305: 417–425, 2003. doi:10.1124/jpet.102.046391.

465. Olejar T, Matej R, Zadinova M, Pouckova P. Expression of proteinase-activated receptor 2 during taurocholate-induced acute pancreatic lesion development in Wistar rats. **Int J Gastrointest Cancer** 30: 113–121, 2001. doi:10.1385/IJGC:30:3:113.

466. Nguyen TD, Moody MW, Steinhoff M, Okolo C, Koh DS, Bunnett NW. Trypsin activates pancreatic duct epithelial cell ion channels through proteinase-activated receptor-2. **J Clin Invest** 103: 261–269, 1999. doi:10.1172/JCI2539.

467. Chen R, Brentnall TA, Pan S, Cooke K, Moyes KW, Lane Z, Crispin DA, Goodlett DR, Aebersold R, Bronner MP. Quantitative proteomics analysis reveals that proteins differentially expressed in chronic pancreatitis are also frequently involved in pancreatic cancer. **Mol Cell Proteomics** 6: 1331–1342, 2007. doi:10.1074/mcp.M700072-MCP200.

468. Edgington-Mitchell LE, Wartmann T, Fleming AK, Gocheva V, van der Linden WA, Withana NP, Verdoes M, Aurelio L, Edgington-Mitchell D, Lieu T, Parker BS, Graham B, Reinheckel T, Furness JB, Joyce JA, Storz P, Halangk W, Bogyo M, Bunnett NW. Legumain is activated in macrophages during pancreatitis. **Am J Physiol Gastrointest Liver Physiol** 311: G548–G560, 2016. doi:10.1152/ajpgi.00047.2016.

469. Lessa FC, Mu Y, Bamberg WM, Beldavs ZG, Dumyati GK, Dunn JR, Farley MM, Holzbauer SM, Meek JI, Phipps EC, Wilson LE, Winston LG, Cohen JA, Limbago BM, Fridkin SK, Gerding DN, McDonald LC. Burden of Clostridium difficile infection in the United States. **N Engl J Med** 372: 825–834, 2015. doi:10.1056/NEJMoa1408913.

470. Hall AJ, Curns AT, McDonald LC, Parashar UD, Lopman BA. The roles of Clostridium difficile and norovirus among gastroenteritis-associated deaths in the United States, 1999–2007. **Clin Infect Dis** 55: 216–223, 2012. doi:10.1093/cid/cis386.

471. Bradley PP, Priebat DA, Christensen RD, Rothstein G. Measurement of cutaneous inflammation: estimation of neutrophil content with an enzyme marker. **J Invest Dermatol** 78: 206–209, 1982. doi:10.1111/1523-1747.ep12506462.

472. Cottrell GS, Amadesi S, Pikios S, Camerer E, Willardsen JA, Murphy BR, Caughey GH, Wolters PJ, Coughlin SR, Peterson A, Knecht W, Pothoulakis C, Bunnett NW, Grady EF. Protease-activated receptor 2, dipeptidyl peptidase I, and proteases mediate Clostridium difficile toxin A enteritis. **Gastroenterology** 132: 2422–2437, 2007. doi:10.1053/j.gastro.2007.03.101.

473. Reed DE, Barajas-Lopez C, Cottrell G, Velazquez-Rocha S, Dery O, Grady EF, Bunnett NW, Vanner SJ. Mast cell tryptase and proteinase-activated receptor 2 induce hyperexcitability of guinea-pig submucosal neurons. **J Physiol** 547: 531–542, 2003. doi:10.1113/jphysiol.2002.032011.

474. Roosterman D, Cottrell GS, Schmidlin F, Steinhoff M, Bunnett NW. Recycling and resensitization of the neurokinin 1 receptor. Influence of agonist concentration and Rab GTPases. **J Biol Chem** 279: 30670–30679, 2004. doi:10.1074/jbc.M402479200.

475. Knecht W, Cottrell GS, Amadesi S, Mohlin J, Skaregarde A, Gedda K, Peterson A, Chapman K, Hollenberg MD, Vergnolle N, Bunnett NW. Trypsin IV or mesotrypsin and p23 cleave protease-activated receptors 1 and 2 to induce inflammation and hyperalgesia. **J Biol Chem** 282: 26089–26100, 2007. doi:10.1074/jbc.M703840200.

476. Wiegand U, Corbach S, Minn A, Kang J, Muller-Hill B. Cloning of the cDNA encoding human brain trypsinogen and characterization of its product. **Gene** 136: 167–175, 1993. doi:10.1016/0378-1119(93)90460-K.

477. Jalink K, Moolenaar WH. Thrombin receptor activation causes rapid neural cell rounding and neurite retraction independent of classic second messengers. **J Cell Biol** 118: 411–419, 1992. doi:10.1083/jcb.118.2.411.

478. Suidan HS, Stone SR, Hemmings BA, Monard D. Thrombin causes neurite retraction in neuronal cells through activation of cell surface receptors. **Neuron** 8: 363–375, 1992. doi:10.1016/0896-6273(92)90302-T.

479. Beecher KL, Andersen TT, Fenton JW 2nd, Festoff BW. Thrombin receptor peptides induce shape change in neonatal murine astrocytes in culture. **J Neurosci Res** 37: 108–115, 1994. doi:10.1002/jnr.490370115.

480. Smith-Swintosky VL, Zimmer S, Fenton JW 2nd, Mattson MP. Opposing actions of thrombin and protease nexin-1 on amyloid beta-peptide toxicity and on accumulation of peroxides and calcium in hippocampal neurons. **J Neurochem** 65: 1415–1418, 1995. doi:10.1046/j.1471-4159.1995.65031415.x.

481. Vaughan PJ, Pike CJ, Cotman CW, Cunningham DD. Thrombin receptor activation protects neurons and astrocytes from cell death produced by environmental insults. **J Neurosci** 15: 5389–5401, 1995. doi:10.1523/JNEUROSCI.15-07-05389.1995.

482. Festoff BW, Smirnova IV, Ma J, Citron BA. Thrombin, its receptor and protease nexin I, its potent serpin, in the nervous system. **Semin Thromb Hemost** 22: 267–271, 1996. doi:10.1055/s-2007-999018.

483. Donovan FM, Pike CJ, Cotman CW, Cunningham DD. Thrombin induces apoptosis in cultured neurons and astrocytes via a pathway requiring tyrosine kinase and RhoA activities. **J Neurosci** 17: 5316–5326, 1997. doi:10.1523/JNEUROSCI.17-14-05316.1997.

484. Suidan HS, Bouvier J, Schaerer E, Stone SR, Monard D, Tschopp J. Granzyme A released upon stimulation of cytotoxic T lymphocytes activates the thrombin receptor on neuronal cells and astrocytes. **Proc Natl Acad Sci U S A** 91: 8112–8116, 1994. doi:10.1073/pnas.91.17.8112.

485. Cavanaugh KP, Gurwitz D, Cunningham DD, Bradshaw RA. Reciprocal modulation of astrocyte stellation by thrombin and protease nexin-1. **J Neurochem** 54: 1735–1743, 1990. doi:10.1111/j.1471-4159.1990.tb01228.x.

Downloaded from journals.physiology.org/journal/physrev at New York Univ (216.165.095.084) on September 28, 2023.

486. Grabham P, Cunningham DD. Thrombin receptor activation stimulates astrocyte proliferation and reversal of stellation by distinct pathways: involvement of tyrosine phosphorylation. **J Neurochem** 64: 583–591, 2002. doi:10.1046/j.1471-4159.1995.64020583.x.

487. Emilsson K, Wahlestedt C, Sun MK, Nystedt S, Owman C, Sundelin J. Vascular effects of proteinase-activated receptor 2 agonist peptide. **J Vasc Res** 34: 267–272, 1997. doi:10.1159/000159233.

488. Kawabata A, Kuroda R, Minami T, Kataoka K, Taneda M. Increased vascular permeability by a specific agonist of protease-activated receptor-2 in rat hindpaw. **Br J Pharmacol** 125: 419–422, 1998. doi:10.1038/sj.bjp.0702063.

489. Vergnolle N. Proteinase-activated receptor-2-activating peptides induce leukocyte rolling, adhesion, and extravasation in vivo. **J Immunol** 163: 5064–5069, 1999.

490. Brain SD, Williams TJ, Tippins JR, Morris HR, MacIntyre I. Calcitonin gene-related peptide is a potent vasodilator. **Nature** 313: 54–56, 1985. doi:10.1038/313054a0.

491. Hughes SR, Brain SD. A calcitonin gene-related peptide (CGRP) antagonist (CGRP8-37) inhibits microvascular responses induced by CGRP and capsaicin in skin. **Br J Pharmacol** 104: 738–742, 1991. doi:10.1111/j.1476-5381.1991.tb12497.x.

492. Bowden JJ, Garland AM, Baluk P, Lefevre P, Grady EF, Vigna SR, Bunnett NW, McDonald DM. Direct observation of substance P-induced internalization of neurokinin 1 (NK1) receptors at sites of inflammation. **Proc Natl Acad Sci U S A** 91: 8964–8968, 1994. doi:10.1073/pnas.91.19.8964.

493. Baluk P, Bertrand C, Geppetti P, McDonald DM, Nadel JA. NK1 receptors mediate leukocyte adhesion in neurogenic inflammation in the rat trachea. **Am J Physiol Lung Cell Mol Physiol** 268: L263–L269, 1995. doi:10.1152/ajplung.1995.268.2.l263.

494. Kawabata A, Kawao N, Kuroda R, Tanaka A, Shimada C. The PAR-1-activating peptide attenuates carrageenan-induced hyperalgesia in rats. **Peptides** 23: 1181–1183, 2002. doi:10.1016/S0196-9781(02)00053-0.

495. Asfaha S, Brussee V, Chapman K, Zochodne DW, Vergnolle N. Proteinase-activated receptor-1 agonists attenuate nociception in response to noxious stimuli. **Br J Pharmacol** 135: 1101–1106, 2002. doi:10.1038/sj.bjp.0704568.

496. Wang Y, Luo W, Wartmann T, Halangk W, Sahin-Toth M, Reiser G. Mesotrypsin, a brain trypsin, activates selectively proteinase-activated receptor-1, but not proteinase-activated receptor-2, in rat astrocytes. **J Neurochem** 99: 759–769, 2006. doi:10.1111/j.1471-4159.2006.04105.x.

497. Sun H, Meeker S, Undem BJ. Role of TRP channels in G_q-coupled protease-activated receptor 1-mediated activation of mouse nodose pulmonary C-fibers. **Am J Physiol Lung Cell Mol Physiol** 318: L192–L199, 2020. doi:10.1152/ajplung.00301.2019.

498. Moss CR 2nd, Gilbert CA, Gabriel SA, Gu Q. Protease-activated receptor-2 inhibits BK channel activity in bronchopulmonary sensory neurons. **Neurosci Lett** 589: 13–18, 2015. doi:10.1016/j.neulet.2015.01.020.

499. Gu Q, Lee LY. House dust mite potentiates capsaicin-evoked Ca2+ transients in mouse pulmonary sensory neurons via activation of protease-activated receptor-2. **Exp Physiol** 97: 534–543, 2012. doi:10.1113/expphysiol.2011.060764.

500. Linley JE, Rose K, Patil M, Robertson B, Akopian AN, Gamper N. Inhibition of M current in sensory neurons by exogenous proteases: a signaling pathway mediating inflammatory nociception. **J Neurosci** 28: 11240–11249, 2008. doi:10.1523/JNEUROSCI.2297-08.2008.

501. Perraud F, Besnard F, Sensenbrenner M, Labourdette G. Thrombin is a potent mitogen for rat astroblasts but not for oligodendroblasts and neuroblasts in primary culture. **Int J Dev Neurosci** 5: 181–188, 1987. doi:10.1016/0736-5748(87)90028-1.

502. Ehrenreich H, Costa T, Clouse KA, Pluta RM, Ogino Y, Coligan JE, Burd PR. Thrombin is a regulator of astrocytic endothelin-1. **Brain Res** 600: 201–207, 1993. doi:10.1016/0006-8993(93)91374-2.

503. Gale AJ, Tsavaler A, Griffin JH. Molecular characterization of an extended binding site for coagulation factor Va in the positive exosite of activated protein C. **J Biol Chem** 277: 28836–28840, 2002. doi:10.1074/jbc.M204363200.

504. Mosnier LO, Gale AJ, Yegneswaran S, Griffin JH. Activated protein C variants with normal cytoprotective but reduced anticoagulant activity. **Blood** 104: 1740–1744, 2004. doi:10.1182/blood-2004-01-0110, 10.1182/blood.V104.11.1740.1740.

505. Mosnier LO, Zlokovic BV, Griffin JH. The cytoprotective protein C pathway. **Blood** 109: 3161–3172, 2007. doi:10.1182/blood-2006-09-003004.

506. Zhang P, Huang W, Wang L, Bao L, Jia ZJ, Bauer SM, Goldman EA, Probst GD, Song Y, Su T, Fan J, Wu Y, Li W, Woolfrey J, Sinha U, Wong PW, Edwards ST, Arfsten AE, Clizbe LA, Kanter J, Pandey A, Park G, Hutchaleelaha A, Lambing JL, Hollenbach SJ, Scarborough RM, Zhu BY. Discovery of betrixaban (PRT054021), N-(5-chloropyridin-2-yl)-2-(4-(N,N-dimethylcarbamimidoyl)benzamido)-5-methoxybenzamide, a highly potent, selective, and orally efficacious factor Xa inhibitor. **Bioorg Med Chem Lett** 19: 2179–2185, 2009. doi:10.1016/j.bmcl.2009.02.111.

507. Walker CT, Marky AH, Petraglia AL, Ali T, Chow N, Zlokovic BV. Activated protein C analog with reduced anticoagulant activity improves functional recovery and reduces bleeding risk following controlled cortical impact. **Brain Res** 1347: 125–131, 2010. doi:10.1016/j.brainres.2010.05.075.

508. Guo H, Wang Y, Singh I, Liu D, Fernandez JA, Griffin JH, Chow N, Zlokovic BV. Species-dependent neuroprotection by activated protein C mutants with reduced anticoagulant activity. **J Neurochem** 109: 116–124, 2009. doi:10.1111/j.1471-4159.2009.05921.x.

509. Guo H, Liu D, Gelbard H, Cheng T, Insalaco R, Fernandez JA, Griffin JH, Zlokovic BV. Activated protein C prevents neuronal apoptosis via protease activated receptors 1 and 3. **Neuron** 41: 563–572, 2004. doi:10.1016/S0896-6273(04)00019-4.

510. Guo H, Singh I, Wang Y, Deane R, Barrett T, Fernandez JA, Chow N, Griffin JH, Zlokovic BV. Neuroprotective activities of activated protein C mutant with reduced anticoagulant activity. **Eur J Neurosci** 29: 1119–1130, 2009. doi:10.1111/j.1460-9568.2009.06664.x.

511. Liu D, Cheng T, Guo H, Fernandez JA, Griffin JH, Song X, Zlokovic BV. Tissue plasminogen activator neurovascular toxicity is controlled by activated protein C. **Nat Med** 10: 1379–1383, 2004. doi:10.1038/nm1122.

512. Cheng T, Petraglia AL, Li Z, Thiyagarajan M, Zhong Z, Wu Z, Liu D, Maggirwar SB, Deane R, Fernandez JA, LaRue B, Griffin JH, Chopp M, Zlokovic BV. Activated protein C inhibits tissue plasminogen activator-induced brain hemorrhage. **Nat Med** 12: 1278–1285, 2006. doi:10.1038/nm1498.

513. Wang Y, Thiyagarajan M, Chow N, Singh I, Guo H, Davis TP, Zlokovic BV. Differential neuroprotection and risk for bleeding from activated protein C with varying degrees of anticoagulant activity. **Stroke** 40: 1864–1869, 2009. doi:10.1161/STROKEAHA.108.536680.

Downloaded from journals.physiology.org/journal/physrev at New York Univ (216.165.095.084) on September 28, 2023.

514. Thiyagarajan M, Fernandez JA, Lane SM, Griffin JH, Zlokovic BV. Activated protein C promotes neovascularization and neurogenesis in postischemic brain via protease-activated receptor 1. **J Neurosci** 28: 12788–12797, 2008. doi:10.1523/JNEUROSCI.3485-08.2008.

515. Petraglia AL, Marky AH, Walker C, Thiyagarajan M, Zlokovic BV. Activated protein C is neuroprotective and mediates new blood vessel formation and neurogenesis after controlled cortical impact. **Neurosurgery** 66: 165–171, 2010. doi:10.1227/01.NEU.0000363148.49779.68.

516. Goldman SA, Kirschenbaum B, Harrison-Restelli C, Thaler HT. Neuronal precursors of the adult rat subependymal zone persist into senescence, with no decline in spatial extent or response to BDNF. **J Neurobiol** 32: 554–566, 1997. doi:10.1002/(SICI)1097-4695(19970605)32:6<554::AID-NEU2>3.0.CO;2-Z.

517. Nakamura M, Tsuji O, Bregman BS, Toyama Y, Okano H. Mimicking the neurotrophic factor profile of embryonic spinal cord controls the differentiation potential of spinal progenitors into neuronal cells. **PLoS One** 6: e20717, 2011. doi:10.1371/journal.pone.0020717.

518. Zhong Z, Ilieva H, Hallagan L, Bell R, Singh I, Paquette N, Thiyagarajan M, Deane R, Fernandez JA, Lane S, Zlokovic AB, Liu T, Griffin JH, Chow N, Castellino FJ, Stojanovic K, Cleveland DW, Zlokovic BV. Activated protein C therapy slows ALS-like disease in mice by transcriptionally inhibiting SOD1 in motor neurons and microglia cells. **J Clin Invest** 119: 3437–3449, 2009. doi:10.1172/jci38476.

519. Guo D, Zhou H, Wu Y, Zhou F, Xu G, Wen H, Zhang X. Involvement of ERK1/2/NF-kappaB signal transduction pathway in TF/FVIIa/PAR2-induced proliferation and migration of colon cancer cell SW620. **Tumour Biol** 32: 921–930, 2011. doi:10.1007/s13277-011-0194-1.

520. Kimura A, Ohmori T, Ohkawa R, Madoiwa S, Mimuro J, Murakami T, Kobayashi E, Hoshino Y, Yatomi Y, Sakata Y. Essential roles of sphingosine 1-phosphate/S1P1 receptor axis in the migration of neural stem cells toward a site of spinal cord injury. **Stem Cells** 25: 115–124, 2007. doi:10.1634/stemcells.2006-0223.

521. Nishino A, Suzuki M, Ohtani H, Motohashi O, Umezawa K, Nagura H, Yoshimoto T. Thrombin may contribute to the pathophysiology of central nervous system injury. **J Neurotrauma** 10: 167–179, 1993. doi:10.1089/neu.1993.10.167.

522. Motohashi O, Suzuki M, Shida N, Umezawa K, Sugai K, Yoshimoto T. Hirudin suppresses the invasion of inflammatory cells and the appearance of vimentin-positive astrocytes in the rat cerebral ablation model. **J Neurotrauma** 14: 747–754, 1997. doi:10.1089/neu.1997.14.747.

523. Noorbakhsh F, Tsutsui S, Vergnolle N, Boven LA, Shariat N, Vodjgani M, Warren KG, Andrade-Gordon P, Hollenberg MD, Power C. Proteinase-activated receptor 2 modulates neuroinflammation in experimental autoimmune encephalomyelitis and multiple sclerosis. **J Exp Med** 203: 425–435, 2006. doi:10.1084/jem.20052148.

524. Lee PR, Johnson TP, Gnanapavan S, Giovannoni G, Wang T, Steiner JP, Medynets M, Vaal MJ, Gartner V, Nath A. Protease-activated receptor-1 activation by granzyme B causes neurotoxicity that is augmented by interleukin-1beta. **J Neuroinflammation** 14: 131, 2017. doi:10.1186/s12974-017-0901-y.

525. Niclou SP, Suidan HS, Pavlik A, Vejsada R, Monard D. Changes in the expression of protease-activated receptor 1 and protease nexin-1 mRNA during rat nervous system development and after nerve lesion. **Eur J Neurosci** 10: 1590–1607, 1998. doi:10.1046/j.1460-9568.1998.00183.x.

526. Striggow F, Riek-Burchardt M, Kiesel A, Schmidt W, Henrich-Noack P, Breder J, Krug M, Reymann KG, Reiser G. Four different types of protease-activated receptors are widely expressed in the brain and are up-regulated in hippocampus by severe ischemia. **Eur J Neurosci** 14: 595–608, 2001. doi:10.1046/j.0953-816x.2001.01676.x.

527. Moller T, Hanisch UK, Ransom BR. Thrombin-induced activation of cultured rodent microglia. **J Neurochem** 75: 1539–1547, 2000. doi:10.1046/j.1471-4159.2000.0751539.x.

528. Boven LA, Vergnolle N, Henry SD, Silva C, Imai Y, Holden J, Warren K, Hollenberg MD, Power C. Up-regulation of proteinase-activated receptor 1 expression in astrocytes during HIV encephalitis. **J Immunol** 170: 2638–2646, 2003. doi:10.4049/jimmunol.170.5.2638.

529. Rodriguez-Franco EJ, Cantres-Rosario YM, Plaud-Valentin M, Romeu R, Rodriguez Y, Skolasky R, Melendez V, Cadilla CL, Melendez LM. Dysregulation of macrophage-secreted cathepsin B contributes to HIV-1-linked neuronal apoptosis. **PLoS One** 7: e36571, 2012. doi:10.1371/journal.pone.0036571.

530. Sachan V, Lodge R, Mihara K, Hamelin J, Power C, Gelman BB, Hollenberg MD, Cohen EA, Seidah NG. HIV-induced neuroinflammation: impact of PAR1 and PAR2 processing by Furin. **Cell Death Differ** 26: 1942–1954, 2019. doi:10.1038/s41418-018-0264-7.

531. Bizios R, Lai L, Fenton JW 2nd, Malik AB. Thrombin-induced thromboxane generation by neutrophils and lymphocytes: dependence on enzymic site. **J Cell Physiol** 132: 359–362, 1987. doi:10.1002/jcp.1041320224.

532. Morin A, Marchand-Arvier M, Doutremepuich C, Vigneron C. Effect of hirudin on the chemotactic properties of alpha-thrombin. **Haemostasis** 21, *Suppl* 1: 32–35, 1991. doi:10.1159/000216260.

533. Rowand JK, Marucha P, Berliner LJ. Hirudin C-terminal fragments inhibit thrombin induced neutrophil chemotaxis. **Thromb Haemost** 67: 289–291, 1992. doi:10.1055/s-0038-1648433.

534. Shpacovitch VM, Seeliger S, Huber-Lang M, Balkow S, Feld M, Hollenberg MD, Sarma VJ, Ward PA, Strey A, Gerke V, Sommerhoff CP, Vergnolle N, Steinhoff M. Agonists of proteinase-activated receptor-2 affect transendothelial migration and apoptosis of human neutrophils. **Exp Dermatol** 16: 799–806, 2007. doi:10.1111/j.1600-0625.2007.00605.x.

535. Fields RC, Schoenecker JG, Hart JP, Hoffman MR, Pizzo SV, Lawson JH. Protease-activated receptor-2 signaling triggers dendritic cell development. **Am J Pathol** 162: 1817–1822, 2003. doi:10.1016/S0002-9440(10)64316-7.

536. Ramelli G, Fuertes S, Narayan S, Busso N, Acha-Orbea H, So A. Protease-activated receptor 2 signalling promotes dendritic cell antigen transport and T-cell activation in vivo. **Immunology** 129: 20–27, 2010. doi:10.1111/j.1365-2567.2009.03144.x.

537. Camerer E, Cornelissen I, Kataoka H, Duong DN, Zheng YW, Coughlin SR. Roles of protease-activated receptors in a mouse model of endotoxemia. **Blood** 107: 3912–3921, 2006. doi:10.1182/blood-2005-08-3130.

538. Kazerani HR, Plevin R, Kawagoe J, Kanke T, Furman BL. Lack of effect of proteinase-activated receptor-2 (PAR-2) deletion on the pathophysiological changes produced by lipopolysaccharide in the mouse: comparison with dexamethasone. **J Pharm Pharmacol** 56: 1015–1020, 2004. doi:10.1211/0022357043923.

539. Suckow SK, Caudle RM. Identification and immunohistochemical characterization of colospinal afferent neurons in the rat. **Neuroscience** 153: 803–813, 2008. doi:10.1016/j.neuroscience.2008.02.046.

Downloaded from journals.physiology.org/journal/physrev at New York Univ (216.165.095.084) on September 28, 2023.

540. Sevigny LM, Zhang P, Bohm A, Lazarides K, Perides G, Covic L, Kuliopulos A. Interdicting protease-activated receptor-2-driven inflammation with cell-penetrating pepducins. **Proc Natl Acad Sci U S A** 108: 8491–8496, 2011. doi:10.1073/pnas.1017091108.

541. Hyun E, Ramachandran R, Cenac N, Houle S, Rousset P, Saxena A, Liblau RS, Hollenberg MD, Vergnolle N. Insulin modulates protease-activated receptor 2 signaling: implications for the innate immune response. **J Immunol** 184: 2702–2709, 2010. doi:10.4049/jimmunol.0902171.

542. Hanahan D, Weinberg RA. The hallmarks of cancer. **Cell** 100: 57–70, 2000. doi:10.1016/S0092-8674(00)81683-9.

543. Bar-Shavit R, Maoz M, Kancharla A, Jaber M, Agranovich D, Grisaru-Granovsky S, Uziely B. Protease-activated receptors (PARs) in cancer: novel biased signaling and targets for therapy. **Methods Cell Biol** 132: 341–358, 2016. doi:10.1016/bs.mcb.2015.11.006.

544. White MJ, Gomer RH. Trypsin, tryptase, and thrombin polarize macrophages towards a pro-fibrotic M2a phenotype. **PLoS One** 10: e0138748, 2015. doi:10.1371/journal.pone.0138748.

545. Ducroc R, Bontemps C, Marazova K, Devaud H, Darmoul D, Laburthe M. Trypsin is produced by and activates protease-activated receptor-2 in human cancer colon cells: evidence for new autocrine loop. **Life Sci** 70: 1359–1367, 2002. doi:10.1016/S0024-3205(01)01519-3.

546. Malfettone A, Silvestris N, Saponaro C, Ranieri G, Russo A, Caruso S, Popescu O, Simone G, Paradiso A, Mangia A. High density of tryptase-positive mast cells in human colorectal cancer: a poor prognostic factor related to protease-activated receptor 2 expression. **J Cell Mol Med** 17: 1025–1037, 2013. doi:10.1111/jcmm.12073.

547. Jin E, Fujiwara M, Pan X, Ghazizadeh M, Arai S, Ohaki Y, Kajiwara K, Takemura T, Kawanami O. Protease-activated receptor (PAR)-1 and PAR-2 participate in the cell growth of alveolar capillary endothelium in primary lung adenocarcinomas. **Cancer** 97: 703–713, 2003. doi:10.1002/cncr.11087.

548. Magnus N, Garnier D, Rak J. Oncogenic epidermal growth factor receptor up-regulates multiple elements of the tissue factor signaling pathway in human glioma cells. **Blood** 116: 815–818, 2010. doi:10.1182/blood-2009-10-250639.

549. Ryden L, Grabau D, Schaffner F, Jonsson PE, Ruf W, Belting M. Evidence for tissue factor phosphorylation and its correlation with protease-activated receptor expression and the prognosis of primary breast cancer. **Int J Cancer** 126: 2330–2340, 2010. doi:10.1002/ijc.24921.

550. Lam DK, Dang D, Flynn AN, Hardt M, Schmidt BL. TMPRSS2, a novel membrane-anchored mediator in cancer pain. **Pain** 156: 923–930, 2015. doi:10.1097/j.pain.0000000000000130.

551. Miyata S, Koshikawa N, Yasumitsu H, Miyazaki K. Trypsin stimulates integrin alpha(5)beta(1)-dependent adhesion to fibronectin and proliferation of human gastric carcinoma cells through activation of proteinase-activated receptor-2. **J Biol Chem** 275: 4592–4598, 2000. doi:10.1074/jbc.275.7.4592.

552. Michel N, Heuze-Vourc'h N, Lavergne E, Parent C, Jourdan ML, Vallet A, Iochmann S, Musso O, Reverdiau P, Courty Y. Growth and survival of lung cancer cells: regulation by kallikrein-related peptidase 6 via activation of proteinase-activated receptor 2 and the epidermal growth factor receptor. **Biol Chem** 395: 1015–1025, 2014. doi:10.1515/hsz-2014-0124.

553. Ma Y, Bao-Han W, Lv X, Su Y, Zhao X, Yin Y, Zhang X, Zhou Z, MacNaughton WK, Wang H. MicroRNA-34a mediates the autocrine signaling of PAR2-activating proteinase and its role in colonic cancer cell proliferation. **PLoS One** 8: e72383, 2013. doi:10.1371/journal.pone.0072383.

554. Naldini A, Carney DH, Pucci A, Carraro F. Human alpha-thrombin stimulates proliferation of interferon-gamma differentiated, growth-arrested U937 cells, overcoming differentiation-related changes in expression of p21CIP1/WAF1 and cyclin D1. **J Cell Physiol** 191: 290–297, 2002. doi:10.1002/jcp.10101.

555. Caruso R, Pallone F, Fina D, Gioia V, Peluso I, Caprioli F, Stolfi C, Perfetti A, Spagnoli LG, Palmieri G, Macdonald TT, Monteleone G. Protease-activated receptor-2 activation in gastric cancer cells promotes epidermal growth factor receptor trans-activation and proliferation. **Am J Pathol** 169: 268–278, 2006. doi:10.2353/ajpath.2006.050841.

556. Bazzani L, Donnini S, Finetti F, Christofori G, Ziche M. PGE2/EP3/SRC signaling induces EGFR nuclear translocation and growth through EGFR ligands release in lung adenocarcinoma cells. **Oncotarget** 8: 31270–31287, 2017. doi:10.18632/oncotarget.16116.

557. Antonny B, Burd C, De Camilli P, Chen E, Daumke O, Faelber K, Ford M, Frolov VA, Frost A, Hinshaw JE, Kirchhausen T, Kozlov MM, Lenz M, Low HH, McMahon H, Merrifield C, Pollard TD, Robinson PJ, Roux A, Schmid S. Membrane fission by dynamin: what we know and what we need to know. **EMBO J** 35: 2270–2284, 2016. doi:10.15252/embj.201694613.

558. Bazzani L, Donnini S, Giachetti A, Christofori G, Ziche M. PGE2 mediates EGFR internalization and nuclear translocation via caveolin endocytosis promoting its transcriptional activity and proliferation in human NSCLC cells. **Oncotarget** 9: 14939–14958, 2018. doi:10.18632/oncotarget.24499.

559. Hugo de Almeida V, Guimaraes ID, Almendra LR, Rondon AM, Tilli TM, de Melo AC, Sternberg C, Monteiro RQ. Positive crosstalk between EGFR and the TF-PAR2 pathway mediates resistance to cisplatin and poor survival in cervical cancer. **Oncotarget** 9: 30594–30609, 2018. doi:10.18632/oncotarget.25748.

560. Wilson SR, Gallagher S, Warpeha K, Hawthorne SJ. Amplification of MMP-2 and MMP-9 production by prostate cancer cell lines via activation of protease-activated receptors. **Prostate** 60: 168–174, 2004. doi:10.1002/pros.20047.

561. Liu Y, Gilcrease MZ, Henderson Y, Yuan XH, Clayman GL, Chen Z. Expression of protease-activated receptor 1 in oral squamous cell carcinoma. **Cancer Lett** 169: 173–180, 2001. doi:10.1016/S0304-3835(01)00504-3.

562. D'Andrea MR, Derian CK, Santulli RJ, Andrade-Gordon P. Differential expression of protease-activated receptors-1 and -2 in stromal fibroblasts of normal, benign, and malignant human tissues. **Am J Pathol** 158: 2031–2041, 2001. doi:10.1016/S0002-9440(10)64675-5.

563. Booden MA, Eckert LB, Der CJ, Trejo J. Persistent signaling by dysregulated thrombin receptor trafficking promotes breast carcinoma cell invasion. **Mol Cell Biol** 24: 1990–1999, 2004. doi:10.1128/MCB.24.5.1990-1999.2004.

564. Even-Ram SC, Maoz M, Pokroy E, Reich R, Katz BZ, Gutwein P, Altevogt P, Bar-Shavit R. Tumor cell invasion is promoted by activation of protease activated receptor-1 in cooperation with the alpha vbeta 5 integrin. **J Biol Chem** 276: 10952–10962, 2001. doi:10.1074/jbc.M007027200.

565. Villares GJ, Zigler M, Dobroff AS, Wang H, Song R, Melnikova VO, Huang L, Braeuer RR, Bar-Eli M. Protease activated receptor-1 inhibits the Maspin tumor-suppressor gene to determine the melanoma

Downloaded from journals.physiology.org/journal/physrev at New York Univ (216.165.095.084) on September 28, 2023.

metastatic phenotype. **Proc Natl Acad Sci U S A** 108: 626–631, 2011. doi:10.1073/pnas.1006886108.

566. Trikha M, Timar J, Zacharek A, Nemeth JA, Cai Y, Dome B, Somlai B, Raso E, Ladanyi A, Honn KV**.** Role for beta3 integrins in human melanoma growth and survival. **Int J Cancer** 101: 156–167, 2002. doi:10.1002/ijc.10521.

567. Raso E, Tovari J, Toth K, Paku S, Trikha M, Honn KV, Timar J**.** Ectopic alphaIIbbeta3 integrin signaling involves 12-lipoxygenase- and PKC-mediated serine phosphorylation events in melanoma cells. **Thromb Haemost** 85: 1037–1042, 2001. doi:10.1055/s-0037-1615960.

568. Nierodzik ML, Karpatkin S**.** Thrombin induces tumor growth, metastasis, and angiogenesis: Evidence for a thrombin-regulated dormant tumor phenotype. **Cancer Cell** 10: 355–362, 2006. doi:10.1016/j.ccr.2006.10.002.

569. Massi D, Naldini A, Ardinghi C, Carraro F, Franchi A, Paglierani M, Tarantini F, Ketabchi S, Cirino G, Hollenberg MD, Geppetti P, Santucci M**.** Expression of protease-activated receptors 1 and 2 in melanocytic nevi and malignant melanoma. **Hum Pathol** 36: 676–685, 2005. doi:10.1016/j.humpath.2005.04.008.

570. Belting M, Dorrell MI, Sandgren S, Aguilar E, Ahamed J, Dorfleutner A, Carmeliet P, Mueller BM, Friedlander M, Ruf W**.** Regulation of angiogenesis by tissue factor cytoplasmic domain signaling. **Nat Med** 10: 502–509, 2004. doi:10.1038/nm1037.

571. Wang X, Xiong L, Yu G, Li D, Peng T, Luo D, Xu J**.** Cathepsin S silencing induces apoptosis of human hepatocellular carcinoma cells. **Am J Transl Res** 7: 100–110, 2015.

572. Ogbomo SM, Shi W, Wagh NK, Zhou Z, Brusnahan SK, Garrison JC**.** 177Lu-labeled HPMA copolymers utilizing cathepsin B and S cleavable linkers: synthesis, characterization and preliminary in vivo investigation in a pancreatic cancer model. **Nucl Med Biol** 40: 606–617, 2013. doi:10.1016/j.nucmedbio.2013.01.011.

573. Gormley JA, Hegarty SM, O'Grady A, Stevenson MR, Burden RE, Barrett HL, Scott CJ, Johnston JA, Wilson RH, Kay EW, Johnston PG, Olwill SA**.** The role of Cathepsin S as a marker of prognosis and predictor of chemotherapy benefit in adjuvant CRC: a pilot study. **Br J Cancer** 105: 1487–1494, 2011. doi:10.1038/bjc.2011.408.

574. Fernández PL, Farré X, Nadal A, FernáNdez E, Peiró N, Sloane BF, Shi GP, Chapman HA, Campo EA, Cardesa A**.** Expression of cathepsins B and S in the progression of prostate carcinoma. **Int J Cancer** 95: 51–55, 2001. doi:10.1002/1097-0215(20010120)95:1<51::AID-IJC1009>3.0.CO;2-J.

575. Lindahl C, Simonsson M, Bergh A, Thysell E, Antti H, Sund M, Wikström P**.** Increased levels of macrophage-secreted cathepsin S during prostate cancer progression in TRAMP mice and patients. **Cancer Genomics Proteomics** 6: 149–159, 2009.

576. Paraoan L, Gray D, Hiscott P, Garcia-Finana M, Lane B, Damato B, Grierson I**.** Cathepsin S and its inhibitor cystatin C: imbalance in uveal melanoma. **Front Biosci (Landmark Ed)** 14: 2504–2513, 2009. doi:10.2741/3393.

577. Flannery T, Gibson D, Mirakhur M, McQuaid S, Greenan C, Trimble A, Walker B, McCormick D, Johnston PG**.** The clinical significance of cathepsin S expression in human astrocytomas. **Am J Pathol** 163: 175–182, 2003. doi:10.1016/S0002-9440(10)63641-3.

578. Flannery T, McQuaid S, McGoohan C, McConnell RS, McGregor G, Mirakhur M, Hamilton P, Diamond J, Cran G, Walker B, Scott C, Martin L, Ellison D, Patel C, Nicholson C, Mendelow D, McCormick D, Johnston PG**.** Cathepsin S expression: an independent prognostic factor in glioblastoma tumours–a pilot study. **Int J Cancer** 119: 854–860, 2006. doi:10.1002/ijc.21911.

579. Sevenich L, Bowman RL, Mason SD, Quail DF, Rapaport F, Elie BT, Brogi E, Brastianos PK, Hahn WC, Holsinger LJ, Massague J, Leslie CS, Joyce JA**.** Analysis of tumour- and stroma-supplied proteolytic networks reveals a brain-metastasis-promoting role for cathepsin S. **Nat Cell Biol** 16: 876–888, 2014. doi:10.1038/ncb3011.

580. Lee TK, Cheung VC, Lu P, Lau EY, Ma S, Tang KH, Tong M, Lo J, Ng IO**.** Blockade of CD47-mediated cathepsin S/protease-activated receptor 2 signaling provides a therapeutic target for hepatocellular carcinoma. **Hepatology** 60: 179–191, 2014. doi:10.1002/hep.27070.

581. Yin YJ, Salah Z, Maoz M, Even Ram SC, Ochayon S, Neufeld G, Katzav S, Bar-Shavit R**.** Oncogenic transformation induces tumor angiogenesis: a role for PAR1 activation. **FASEB J** 17: 163–174, 2003. doi:10.1096/fj.02-0316com.

582. Chang LH, Pan SL, Lai CY, Tsai AC, Teng CM**.** Activated PAR-2 regulates pancreatic cancer progression through ILK/HIF-alpha-induced TGF-alpha expression and MEK/VEGF-A-mediated angiogenesis. **Am J Pathol** 183: 566–575, 2013. doi:10.1016/j.ajpath.2013.04.022.

583. Liu Y, Mueller BM**.** Protease-activated receptor-2 regulates vascular endothelial growth factor expression in MDA-MB-231 cells via MAPK pathways. **Biochem Biophys Res Commun** 344: 1263–1270, 2006. doi:10.1016/j.bbrc.2006.04.005.

584. Zhang C, Gao GR, Lv CG, Zhang BL, Zhang ZL, Zhang XF**.** Protease-activated receptor-2 induces expression of vascular endothelial growth factor and cyclooxygenase-2 via the mitogen-activated protein kinase pathway in gastric cancer cells. **Oncol Rep** 28: 1917–1923, 2012. doi:10.3892/or.2012.1998.

585. Ciardiello F, Tortora G**.** EGFR antagonists in cancer treatment. **N Engl J Med** 358: 1160–1174, 2008. doi:10.1056/NEJMra0707704.

586. Versteeg HH, Schaffner F, Kerver M, Petersen HH, Ahamed J, Felding-Habermann B, Takada Y, Mueller BM, Ruf W**.** Inhibition of tissue factor signaling suppresses tumor growth. **Blood** 111: 190–199, 2008. doi:10.1182/blood-2007-07-101048.

587. Versteeg HH, Schaffner F, Kerver M, Ellies LG, Andrade-Gordon P, Mueller BM, Ruf W**.** Protease-activated receptor (PAR) 2, but not PAR1, signaling promotes the development of mammary adenocarcinoma in polyoma middle T mice. **Cancer Res** 68: 7219–7227, 2008. doi:10.1158/0008-5472.CAN-08-0419.

588. Milia AF, Salis MB, Stacca T, Pinna A, Madeddu P, Trevisani M, Geppetti P, Emanueli C**.** Protease-activated receptor-2 stimulates angiogenesis and accelerates hemodynamic recovery in a mouse model of hindlimb ischemia. **Circ Res** 91: 346–352, 2002. doi:10.1161/01.RES.0000031958.92781.9E.

589. Villares GJ, Zigler M, Wang H, Melnikova VO, Wu H, Friedman R, Leslie MC, Vivas-Mejia PE, Lopez-Berestein G, Sood AK, Bar-Eli M**.** Targeting melanoma growth and metastasis with systemic delivery of liposome-incorporated protease-activated receptor-1 small interfering RNA. **Cancer Res** 68: 9078–9086, 2008. doi:10.1158/0008-5472.CAN-08-2397.

590. Yang E, Boire A, Agarwal A, Nguyen N, O'Callaghan K, Tu P, Kuliopulos A, Covic L**.** Blockade of PAR1 signaling with cell-penetrating pepducins inhibits Akt-survival pathways in breast cancer cells and suppresses tumor survival and metastasis. **Cancer Res** 69: 6223–6231-42, 2009. doi:10.1158/0008-5472.CAN-09-0187.

591. Bernatowicz MS, Klimas CE, Hartl KS, Peluso M, Allegretto NJ, Seiler SM**.** Development of potent thrombin receptor antagonist

Downloaded from journals.physiology.org/journal/physrev at New York Univ (216.165.095.084) on September 28, 2023.

peptides. **J Med Chem** 39: 4879–4887, 1996. doi:10.1021/jm960455s.

592. Damiano BP, Derian CK, Maryanoff BE, Zhang HC, Gordon PA. RWJ-58259: a selective antagonist of protease activated receptor-1. **Cardiovasc Drug Rev** 21: 313–326, 2003.

593. Kato Y, Kita Y, Hirasawa-Taniyama Y, Nishio M, Mihara K, Ito K, Yamanaka T, Seki J, Miyata S, Mutoh S. Inhibition of arterial thrombosis by a protease-activated receptor 1 antagonist, FR171113, in the guinea pig. **Eur J Pharmacol** 473: 163–169, 2003. doi:10.1016/S0014-2999(03)01973-3.

594. Oestreich J. SCH-530348, a thrombin receptor (PAR-1) antagonist for the prevention and treatment of atherothrombosis. **Curr Opin Investig Drugs** 10: 988–996, 2009.

595. Serebruany VL, Kogushi M, Dastros-Pitei D, Flather M, Bhatt DL. The in-vitro effects of E5555, a protease-activated receptor (PAR)-1 antagonist, on platelet biomarkers in healthy volunteers and patients with coronary artery disease. **Thromb Haemost** 102: 111–119, 2009. doi:10.1160/TH08-12-0805.

596. Dumas M, Nadal-Wollbold F, Gaussem P, Perez M, Mirault T, Letienne R, Bourbon T, Grelac F, Le Grand B, Bachelot-Loza C. Antiplatelet and antithrombotic effect of F 16618, a new thrombin proteinase-activated receptor-1 (PAR1) antagonist. **Br J Pharmacol** 165: 1827–1835, 2012. doi:10.1111/j.1476-5381.2011.01668.x.

597. Brass LF, Vassallo RR, Belmonte E, Ahuja M, Cichowski K, Hoxie JA. Structure and function of the human platelet thrombin receptor. Studies using monoclonal antibodies directed against a defined domain within the receptor N terminus. **J Biol Chem** 267: 13795–13798, 1992. doi:10.1016/S0021-9258(19)49635-X.

598. Hung DT, Vu TK, Wheaton VI, Ishii K, Coughlin SR. Cloned platelet thrombin receptor is necessary for thrombin-induced platelet activation. **J Clin Invest** 89: 1350–1353, 1992. doi:10.1172/JCI115721.

599. Andrade-Gordon P, Maryanoff BE, Derian CK, Zhang HC, Addo MF, Darrow AL, Eckardt AJ, Hoekstra WJ, Mccomsey DF, Oksenberg D, Reynolds EE, Santulli RJ, Scarborough RM, Smith CE, White KB. Design, synthesis, and biological characterization of a peptide-mimetic antagonist for a tethered-ligand receptor. **Proc Natl Acad Sci U S A** 96: 12257–12262, 1999. doi:10.1073/pnas.96.22.12257.

600. Chackalamannil S, Wang Y, Greenlee WJ, Hu Z, Xia Y, Ahn HS, Boykow G, Hsieh Y, Palamanda J, Agans-Fantuzzi J, Kurowski S, Graziano M, Chintala M. Discovery of a novel, orally active himbacine-based thrombin receptor antagonist (SCH 530348) with potent antiplatelet activity. **J Med Chem** 51: 3061–3064, 2008. doi:10.1021/jm800180e.

601. Kogushi M, Matsuoka T, Kawata T, Kuramochi H, Kawaguchi S, Murakami K, Hiyoshi H, Suzuki S, Kawahara T, Kajiwara A, Hishinuma I. The novel and orally active thrombin receptor antagonist E5555 (Atopaxar) inhibits arterial thrombosis without affecting bleeding time in guinea pigs. **Eur J Pharmacol** 657: 131–137, 2011. doi:10.1016/j.ejphar.2011.01.058.

602. Morrow DA, Braunwald E, Bonaca MP, Ameriso SF, Dalby AJ, Fish MP, Fox KA, Lipka LJ, Liu X, Nicolau JC, Ophuis AJ, Paolasso E, Scirica BM, Spinar J, Theroux P, Wiviott SD, Strony J, Murphy SA. Vorapaxar in the secondary prevention of atherothrombotic events. **N Engl J Med** 366: 1404–1413, 2012. doi:10.1056/NEJMoa1200933.

603. Kosoglou T, Reyderman L, Tiessen RG, Van Vliet AA, Fales RR, Keller R, Yang B, Cutler DL. Pharmacodynamics and pharmacokinetics of the novel PAR-1 antagonist vorapaxar (formerly SCH 530348) in healthy subjects. **Eur J Clin Pharmacol** 68: 249–258, 2012. doi:10.1007/s00228-011-1120-6.

604. Feistritzer C, Schuepbach RA, Mosnier LO, Bush LA, Di Cera E, Griffin JH, Riewald M. Protective signaling by activated protein C is mechanistically linked to protein C activation on endothelial cells. **J Biol Chem** 281: 20077–20084, 2006. doi:10.1074/jbc.M600506200.

605. Zlokovic BV, Griffin JH. Cytoprotective protein C pathways and implications for stroke and neurological disorders. **Trends Neurosci** 34: 198–209, 2011. doi:10.1016/j.tins.2011.01.005.

606. Griffin JH, Zlokovic BV, Mosnier LO. Activated protein C, protease activated receptor 1, and neuroprotection. **Blood** 132: 159–169, 2018. doi:10.1182/blood-2018-02-769026.

607. Guo H, Zhao Z, Yang Q, Wang M, Bell R, Wang S, Chow N, Davis T, Griffin J, Goldman S, Zlokovic BV. An activated protein C analog stimulates neuronal production by human neural progenitor cells via a PAR1-PAR3-S1PR1-Akt pathway. **J Neurosci** 33: 6181–6190, 2013. doi:10.1523/JNEUROSCI.4491-12.2013.

608. Lyden P, Pryor KE, Coffey CS, Cudkowicz M, Conwit R, Jadhav A, Sawyer RN Jr, Claassen J, Adeoye O, Song S, Hannon P, Rost NS, Hinduja A, Torbey M, Lee JM, Benesch C, Rippee M, Rymer M, Froehler MT, Clarke Haley E, Johnson M, Yankey J, Magee K, Qidwai J, Levy H, Mark Haacke E, Fawaz M, Davis TP, Toga AW, Griffin JH, Zlokovic BV; NeuroNEXT Clinical Trials Network NN104 Investigators. Final results of the RHAPSODY Trial: a multi-center, phase 2 trial using a continual reassessment method to determine the safety and tolerability of 3K3A-APC, A recombinant variant of human activated protein C, in combination with tissue plasminogen activator, mechanical thrombectomy or both in moderate to severe acute ischemic stroke. **Ann Neurol** 85: 125–136, 2019. doi:10.1002/ana.25383.

609. Lyden PD, Pryor KE, Minigh J, Davis TP, Griffin JH, Levy H, Zlokovic BV. Stroke treatment with PAR-1 agents to decrease hemorrhagic transformation. **Front Neurol** 12: 593582, 2021. doi:10.3389/fneur.2021.593582.

610. Dockendorff C, Aisiku O, Verplank L, Dilks JR, Smith DA, Gunnink SF, Dowal L, Negri J, Palmer M, Macpherson L, Schreiber SL, Flaumenhaft R. Discovery of 1,3-diaminobenzenes as selective inhibitors of platelet activation at the PAR1 receptor. **ACS Med Chem Lett** 3: 232–237, 2012. doi:10.1021/ml2002696.

611. Aisiku O, Peters CG, De Ceunynck K, Ghosh CC, Dilks JR, Fustolo-Gunnink SF, Huang M, Dockendorff C, Parikh SM, Flaumenhaft R. Parmodulins inhibit thrombus formation without inducing endothelial injury caused by vorapaxar. **Blood** 125: 1976–1985, 2015. doi:10.1182/blood-2014-09-599910.

612. Kenakin TP. **A Pharmacology Primer** (5th ed.), edited by Kenakin TP. New York: Academic Press, 2019, p. 1.

613. De Ceunynck K, Peters CG, Jain A, Higgins SJ, Aisiku O, Fitch-Tewfik JL, Chaudhry SA, Dockendorff C, Parikh SM, Ingber DE, Flaumenhaft R. PAR1 agonists stimulate APC-like endothelial cytoprotection and confer resistance to thromboinflammatory injury. **Proc Natl Acad Sci U S A** 115: E982–E991, 2018.

614. Mcintosh KA, Cunningham MR, Bushell T, Plevin R. The development of proteinase-activated receptor-2 modulators and the challenges involved. **Biochem Soc Trans** 48: 2525–2537, 2020. doi:10.1042/BST20200191.

615. Kanke T, Kabeya M, Kubo S, Kondo S, Yasuoka K, Tagashira J, Ishiwata H, Saka M, Furuyama T, Nishiyama T, Doi T, Hattori Y, Kawabata A, Cunningham MR, Plevin R. Novel antagonists for proteinase-activated receptor 2: inhibition of cellular and vascular responsesin vitroandin vivo. **Br J Pharmacol** 158: 361–371, 2009. doi:10.1111/j.1476-5381.2009.00342.x.

Downloaded from journals.physiology.org/journal/physrev at New York Univ (216.165.095.084) on September 28, 2023.

616. Goh FG, Ng PY, Nilsson M, Kanke T, Plevin R. Dual effect of the novel peptide antagonist K-14585 on proteinase-activated receptor-2-mediated signalling. **Br J Pharmacol** 158: 1695–1704, 2009. doi:10.1111/j.1476-5381.2009.00415.x.

617. Boitano S, Hoffman J, Flynn AN, Asiedu MN, Tillu DV, Zhang Z, Sherwood CL, Rivas CM, Defea KA, Vagner J, Price TJ. The novel PAR2 ligand C391 blocks multiple PAR2 signalling pathwaysin vitroandin vivo. **Br J Pharmacol** 172: 4535–4545, 2015. doi:10.1111/bph.13238.

618. Seitzberg JG, Knapp AE, Lund BW, Mandrup Bertozzi S, Currier EA, Ma JN, Sherbukhin V, Burstein ES, Olsson R. Discovery of potent and selective small-molecule PAR-2 agonists. **J Med Chem** 51: 5490–5493, 2008. doi:10.1021/jm800754r.

619. Barry GD, Suen JY, Le GT, Cotterell A, Reid RC, Fairlie DP. Novel agonists and antagonists for human protease activated receptor 2. **J Med Chem** 53: 7428–7440, 2010. doi:10.1021/jm100984y.

620. Suen JY, Barry GD, Lohman RJ, Halili MA, Cotterell AJ, Le GT, Fairlie DP. Modulating human proteinase activated receptor 2 with a novel antagonist (GB88) and agonist (GB110). **Br J Pharmacol** 165: 1413–1423, 2012. doi:10.1111/j.1476-5381.2011.01610.x.

621. Suen JY, Cotterell A, Lohman RJ, Lim J, Han A, Yau MK, Liu L, Cooper MA, Vesey DA, Fairlie DP. Pathway-selective antagonism of proteinase activated receptor 2. **Br J Pharmacol** 171: 4112–4124, 2014. doi:10.1111/bph.12757.

622. Farmer LJ, Fournier PA, Lessard S, Lui B, St-Onge M, Sturino C, Szychowski J, Yannopoulos C. Vertex Pharmaceuticals Incorporated. Imidazopyridazines Useful as Inhibitors of the PAR-2 Signaling Pathway. Patent WO/2015048245 A1. 2013. https://patentimages.storage.googleapis.com/ad/79/74/681fbe11d4c20b/WO2015048245A1.pdf.

623. Avet C, Sturino C, Grastilleur S, Gouill CL, Semache M, Gross F, Gendron L, Bennani Y, Mancini JA, Sayegh CE, Bouvier M. The PAR2 inhibitor I-287 selectively targets Gαq and Gα12/13 signaling and has anti-inflammatory effects. **Commun Biol** 3: 1–13, 2020. doi:10.1038/s42003-019-0734-6.

624. Giblin P, Boxhammer R, Desai S, Kroe-Barrett R, Hansen G, Ksiazek J, Panzenbeck M, Ralph K, Schwartz R, Zimmitti C, Pracht C, Miller S, Magram J, , Litzenburger T. Fully human antibodies against the protease-activated receptor-2 (PAR-2) with anti-inflammatory activity. **Hum Antibodies** 20: 83–94, 2011. doi:10.3233/HAB-2011-0243.

625. Majewski MW, Gandhi DM, Rosas R, Kodali R, Arnold LA, Dockendorff C. Design and evaluation of heterobivalent PAR1–PAR2 ligands as antagonists of calcium mobilization. **ACS Med Chem Lett** 10: 121–126, 2019. doi:10.1021/acsmedchemlett.8b00538.

626. Liu S, Li S, Yuan D, Wang E, Xie R, Zhang W, Kong Y, Zhu X. Protease activated receptor 4 (PAR4) antagonists: research progress on small molecules in the field of antiplatelet agents. **Eur J Med Chem** 209: 112893, 2021. doi:10.1016/j.ejmech.2020.112893.

627. Wong PC, Seiffert D, Bird JE, Watson CA, Bostwick JS, Giancarli M, Allegretto N, Hua J, Harden D, Guay J, Callejo M, Miller MM, Lawrence RM, Banville J, Guy J, Maxwell BD, Priestley ES, Marinier A, Wexler RR, Bouvier M, Gordon DA, Schumacher WA, Yang J. Blockade of protease-activated receptor-4 (PAR4) provides robust antithrombotic activity with low bleeding. **Sci Transl Med** 9: eaaf5294, 2017. doi:10.1126/scitranslmed.aaf5294.

628. Wilson SJ, Ismat FA, Wang Z, Cerra M, Narayan H, Raftis J, Gray TJ, Connell S, Garonzik S, Ma X, Yang J, Newby DE. PAR4 (protease-activated receptor 4) antagonism with BMS-986120 inhibits human ex vivo thrombus formation. **Arterioscler Thromb Vasc Biol** 38: 448–456, 2018. doi:10.1161/ATVBAHA.117.310104.

629. Covic L, Misra M, Badar J, Singh C, Kuliopulos A. Pepducin-based intervention of thrombin-receptor signaling and systemic platelet activation. **Nat Med** 8: 1161–1165, 2002. doi:10.1038/nm760.

630. Gurbel PA, Bliden KP, Turner SE, Tantry US, Gesheff MG, Barr TP, Covic L, Kuliopulos A. Cell-penetrating pepducin therapy targeting PAR1 in subjects with coronary artery disease. **Arterioscler Thromb Vasc Biol** 36: 189–197, 2016. doi:10.1161/ATVBAHA.115.306777.

631. Jimenez-Vargas NN, Yu Y, Jensen DD, Bok DD, Wisdom M, Latorre R, Lopez C, Jaramillo-Polanco JO, Degro C, Guzman-Rodriguez M, Tsang Q, Snow Z, Schmidt BL, Reed DE, Lomax AE, Margolis KG, Stein C, Bunnett NW, Vanner SJ. Agonist that activates the micro-opioid receptor in acidified microenvironments inhibits colitis pain without side effects. **Gut** 71: 695–704, 2022. doi:10.1136/gutjnl-2021-324070.

Downloaded from journals.physiology.org/journal/physrev at New York Univ (216.165.095.084) on September 28, 2023.

PNAS RESEARCH ARTICLE | PHARMACOLOGY

Therapeutic antagonism of the neurokinin 1 receptor in endosomes provides sustained pain relief

Alan Hegron[a,b,c,1], Chloe J. Peach[a,b,c,1], Raquel Tonello[a,b,c,1], Philipp Seemann[d,1], Shavonne Teng[a,b,c], Rocco Latorre[a,b,c], Harald Huebner[d], Dorothee Weikert[d], Jeanette Rientjes[e], Nicholas A. Veldhuis[f], Daniel P. Poole[f], Dane D. Jensen[a,b,c,g], Alex R. B. Thomsen[a,b,c], Brian L. Schmidt[a,b,c,g], Wendy L. Imlach[h], Peter Gmeiner[d], and Nigel W. Bunnett[a,b,c,2]

Edited by Robert Lefkowitz, Howard Hughes Medical Institute, Durham, NC; received December 9, 2022; accepted April 4, 2023

The hypothesis that sustained G protein-coupled receptor (GPCR) signaling from endosomes mediates pain is based on studies with endocytosis inhibitors and lipid-conjugated or nanoparticle-encapsulated antagonists targeted to endosomes. GPCR antagonists that reverse sustained endosomal signaling and nociception are needed. However, the criteria for rational design of such compounds are ill-defined. Moreover, the role of natural GPCR variants, which exhibit aberrant signaling and endosomal trafficking, in maintaining pain is unknown. Herein, substance P (SP) was found to evoke clathrin-mediated assembly of endosomal signaling complexes comprising neurokinin 1 receptor (NK_1R), $G\alpha_{q/i}$, and βarrestin-2. Whereas the FDA-approved NK_1R antagonist aprepitant induced a transient disruption of endosomal signals, analogs of netupitant designed to penetrate membranes and persist in acidic endosomes through altered lipophilicity and pKa caused sustained inhibition of endosomal signals. When injected intrathecally to target spinal NK_1R+ve neurons in knockin mice expressing human NK_1R, aprepitant transiently inhibited nociceptive responses to intraplantar injection of capsaicin. Conversely, netupitant analogs had more potent, efficacious, and sustained antinociceptive effects. Mice expressing C-terminally truncated human NK_1R, corresponding to a natural variant with aberrant signaling and trafficking, displayed attenuated SP-evoked excitation of spinal neurons and blunted nociceptive responses to SP. Thus, sustained antagonism of the NK_1R in endosomes correlates with long-lasting antinociception, and domains within the C-terminus of the NK_1R are necessary for the full pronociceptive actions of SP. The results support the hypothesis that endosomal signaling of GPCRs mediates nociception and provides insight into strategies for antagonizing GPCRs in intracellular locations for the treatment of diverse diseases.

signaling | receptors | endocytosis | pain

G protein-coupled receptors (GPCRs) are seven transmembrane domain receptors for hormones and neurotransmitters. They control homeostatic and disease processes and are therapeutic targets for disease (1). Drug discovery has focused on targeting GPCRs at the cell surface. However, plasma membrane signaling of GPCRs is usually tightly regulated and may not exclusively mediate long-lasting pathology. After binding to extracellular ligands, GPCRs are phosphorylated by GPCR kinases (GRKs) and interact with βarrestins (βARRs), which uncouple GPCRs from G proteins and desensitize plasma membrane signaling (2, 3). βARRs also couple GPCRs to clathrin and adaptor protein-2, which leads to dynamin (Dnm)-mediated vesicle scission and mediates receptor endocytosis. Although endocytosis has been considered as a mechanism that terminates GPCR signaling, many GPCRs continue to signal after endocytosis, including most class B GPCRs that interact with βARRs with sustained kinetics and some class A GPCRs that exhibit transient interactions with βARRs (4–15). Within endosomes, GPCR, Gα, and/or βARR signaling complexes (signalosomes) generate second messengers and activate kinases in subcellular compartments. Endosomal signaling of GPCRs has been implicated in certain physiological and pathological processes, including hormonal control (4, 7) and pain transmission (9–11, 15–17). Thus, GPCRs in endosomes, rather than at the cell surface, might be the optimal therapeutic target (18).

Painful stimuli provoke the release of substance P (SP) from primary sensory neurons, which stimulates endocytosis of the neurokinin 1 receptor (NK_1R) in second-order spinal neurons and endothelial cells of postcapillary venules (9, 19). NK_1R signals in endosomes mediate sustained activation of spinal neurons and pain transmission (9, 17). The calcitonin-like receptor (15), protease-activated receptor 2 (11, 16), and ∂-opioid receptor (10) also signal from endosomes to control pain, which suggests a general role for endosomal GPCR signaling in pain. The hypothesis that endosomal GPCR signaling controls nociception derives from the use of endocytosis inhibitors, which suppress endosomal signaling

Significance

Sustained GPCR signaling from endosomes mediates pathologies, including pain. Optimal therapy requires development of antagonists that penetrate cells, are retained in endosomes, and disrupt endosomal signaling. To enhance membrane penetration and retention in acidified endosomes, analogs of the neurokinin 1 receptor (NK_1R) antagonist netupitant were synthesized with altered lipophilicity and acidity. Lipophilic and acidic analogs antagonized endosomal NK_1R signaling and provided potent, efficacious, and long-lasting pain relief in mice expressing human NK_1R. Mice expressing a truncated NK_1R, corresponding to a naturally occurring variant with aberrant signaling and trafficking, showed diminished nociceptive responses to substance P. The results identify criteria that will facilitate the design of antagonists of endosomal receptors and provide evidence for the contribution of endosomal signaling to disease.

Competing interest statement: N.W.B. is a founding scientist of Endosome Therapeutics Inc. Research in N.W.B.'s laboratory is funded, in part, by Takeda Pharmaceuticals International.

This article is a PNAS Direct Submission.

Copyright © 2023 the Author(s). Published by PNAS. This article is distributed under Creative Commons Attribution-NonCommercial-NoDerivatives License 4.0 (CC BY-NC-ND).

[1]A.H., C.J.P., R.T., and P.S. contributed equally to this work.

[2]To whom correspondence may be addressed. Email: nwb2@nyu.edu.

This article contains supporting information online at https://www.pnas.org/lookup/suppl/doi:10.1073/pnas.2220979120/-/DCSupplemental.

Published May 22, 2023.

Downloaded from https://www.pnas.org by NEW YORK UNIVERSITY LIBRARY-SERIALS on September 28, 2023 from IP address 216.165.95.84.

and nociception (9, 11). Preferential blockade of endosomal GPCRs has been achieved by antagonist conjugation to a transmembrane lipid or encapsulation into nanoparticles, which deliver antagonists to endosomes and provide sustained antinociception (9–11, 15, 17, 20–22). Pharmacokinetic considerations may restrict the usefulness of lipidated and nanoparticle-encapsulated GPCR antagonists. The criteria for rational design of small-molecule GPCR antagonists that penetrate plasma and endosomal membranes, disrupt assembly of multiprotein signalosomes in acidic endosomes, and reverse sustained endosomal signaling and nociception are ill-defined. Whether expression of GPCR variants unable to signal from endosomes confers resistance to pain is unknown.

The current study sought to define the criteria for designing GPCR antagonists that disrupt endosomal signalosomes and provide effective pain relief. The NK_1R antagonists aprepitant (AP) and netupitant (NT), which are both FDA approved for treatment of chemotherapy-induced nausea and vomiting (23, 24), were compared with NT analogs with differing lipophilicity (LogP, LogD) and acidity (pKa). Nociception was studied in mice either expressing the human NK_1R, which avoided interspecies differences in NK_1R antagonist potency (25), or a truncated human NK_1R that corresponds to a natural variant with aberrant G protein and βARR signaling (26–28). The results show that sustained antagonism of the endosomal NK_1R correlates with long-lasting antinociception, and that domains within the C-terminus of the NK_1R are necessary for the full pronociceptive actions of SP.

Results

SP-Induced Assembly of NK_1R, Gα, and βARR Signalosomes in Early Endosomes. Endosomal signaling of GPCRs is thought to entail the assembly of GPCR, Gα, and βARR signalosomes, where Gα subunits transduce signals and βARRs are scaffolds for GPCRs and signaling enzymes. A bioluminescence resonance energy transfer (BRET) assay was developed to simultaneously study recruitment of the NK_1R and isoforms of Gα or βARR to subcellular compartments of HEK293T cells. Conventional BRET is limited to studying the proximity of only two proteins. To surmount this limitation, NanoLuc Binary Technology BRET (NanoBiT-BRET, nbBRET) was used to simultaneously measure the proximity between the NK_1R, an effector (mini (m) Gα or βARR) plus a localization marker (16, 29) (Fig. 1*A*). mGα proteins are N-terminally truncated Gα proteins that diffuse through the cytosol and bind to active conformations of GPCRs (30, 31); $mG\alpha_{sq}$ and $mG\alpha_{si}$ were developed by mutating $mG\alpha_s$ residues to equivalent $G\alpha_q$ and $G\alpha_i$ residues. NbBRET entails a split luciferase assay in which full-length human NK_1R-407 was C-terminally tagged with the natural peptide fragment of NanoLuc (NP, 13 residue NanoBiT fragment), and a plasma membrane (CAAX) or early endosomal (FYVE) marker was tagged with large NanoBiT fragment (LgBiT). Luminescence occurs from a complex between NK_1R-NP and LgBiT-CAAX or LgBiT-FYVE, which serves as an energy donor for fluorophore-tagged Venus-mGα or βARR-YFP. SP (100 nM) increased nbBRET between NK_1R, $mG\alpha_{sq}$, or βARR2 and LgBiT-CAAX or LgBiT-FYVE, consistent with

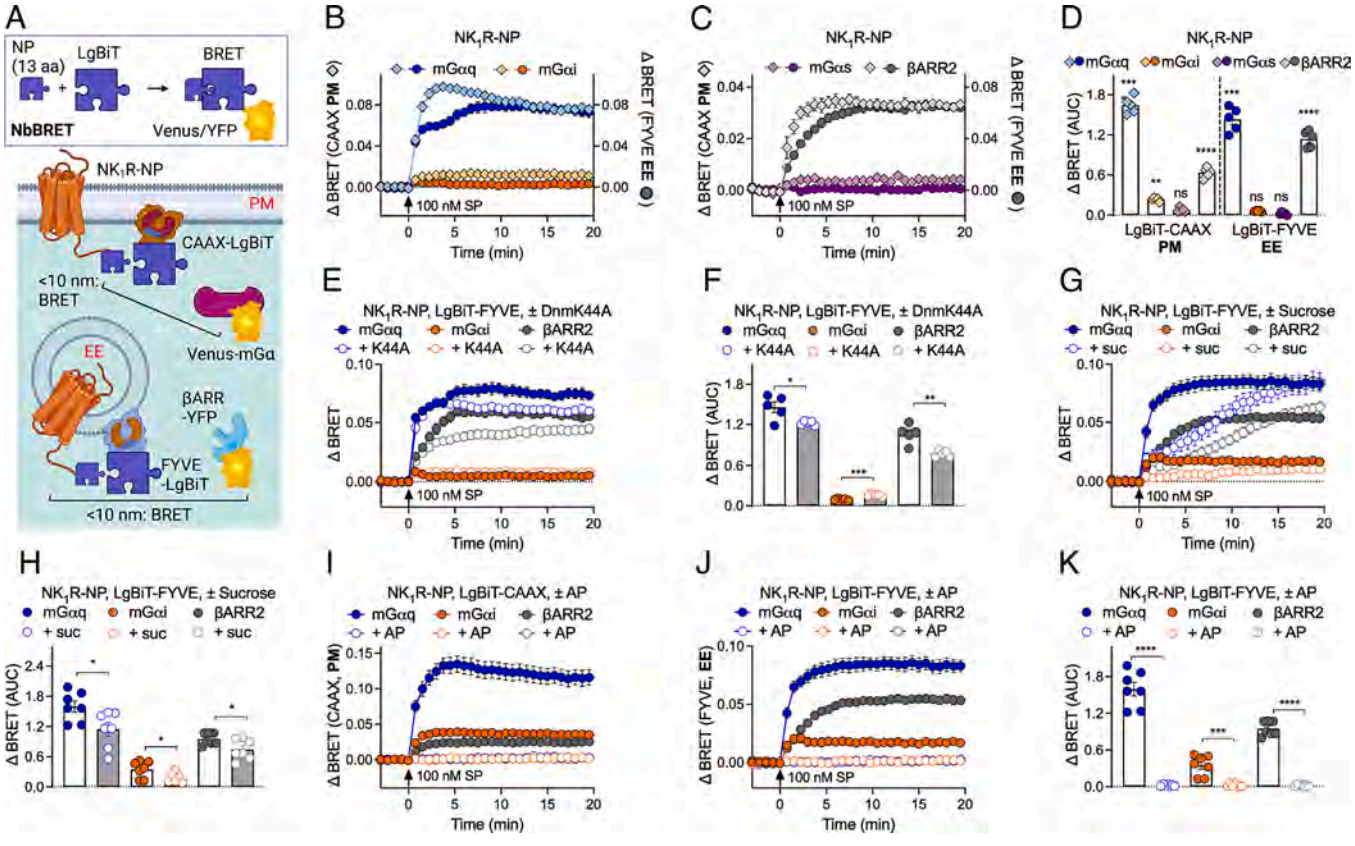

Fig. 1. Assembly of NK_1R signalosomes in HEK293T cells. (*A*) NanoBiT-BRET (nbBRET) uses a nanoluciferase split into two fragments (natural peptide, NP, and LgBiT) to detect BRET between receptor (NK_1R), mini Gα proteins (mGα) or βarrestin (βARR), and proteins resident to the plasma membrane (PM, CAAX) or early endosome (EE, FYVE). (*B–K*) Substance P (SP, 100 nM) induced nbBRET between NK_1R-NP, LgBiT-CAAX, or LgBiT-FYVE as well as Venus-$mG\alpha_{sq}$, Venus-$mG\alpha_{si}$, Venus-$mG\alpha_s$, or βARR2-YFP. (*E–H*) Effect of dominant-negative dynamin (DnmK44A; *E* and *F*) or hypertonic sucrose (0.45 M, 30 min, *G* and *H*). (*I–K*) Effect of aprepitant (AP, 100 nM, 30 min). AUC, area under curve. Mean ± SEM. N = 5 to 7 independent experiments. **P* < 0.05, ***P* < 0.01, ****P* < 0.001, *****P* < 0.0001. One-way ANOVA with Dunnett's test (*D*, *F*, *H*, and *K*).

Downloaded from https://www.pnas.org by NEW YORK UNIVERSITY LIBRARY-SERIALS on September 28, 2023 from IP address 216.165.95.84.

the recruitment of NK_1R, $mG\alpha_{sq}$, and βARR2 to the plasma membrane and early endosomes (Fig. 1 *B–D*). SP also stimulated a small increase in nbBRET between NK_1R, $mG\alpha_{si}$, and CAAX. Recruitment of $mG\alpha_{sq}$ and βARR2 to early endosomes lagged relative to recruitment to the plasma membrane. Recruitment of NK_1R, $mG\alpha_{sq}$, or βARR2 to the plasma membrane and endosomes was sustained for at least 20 min. Expression of a dominant-negative mutant of dynamin (DnmK44A), which harbors a mutation in the GTPase domain and selectively inhibits receptor endocytosis without affecting protein exocytosis (32), or pretreatment with hypertonic (0.45 M) sucrose, inhibited the recruitment of $NK_1R/mG\alpha_{sq}$, $NK_1R/mG\alpha_{si}$, and $NK_1R/\beta ARR2$ complexes to early endosomes (Fig. 1 *E–H*). Preincubation with the NK_1R antagonist AP (100 nM) abolished complex assembly at the plasma membrane and in early endosomes (Fig. 1 *I–K*).

NK_1R and effector (Gα, βARR) recruitment to intracellular compartments of HEK293T cells was confirmed using conventional BRET assays. To quantify the kinetics of NK_1R trafficking to subcellular compartments, NK_1R-407 tagged with *Renilla* luciferase-8 (Rluc8) was coexpressed with Venus-Kras (plasma membrane marker), Rab5a coupled to tandem *Renilla* green fluorescent protein (tdRGFP, early endosome), Venus-Rab11a (recycling endosome), Venus-Giantin (cis-Golgi network), or YFP-TGN38 (trans-Golgi network) (*SI Appendix*, Fig. S1*A*). SP (100 nM) decreased BRET between NK_1R-Rluc8 and Venus-Kras (*SI Appendix*, Fig. S1 *B* and *C*) and increased BRET between NK_1R-Rluc8 and tdRGFP-Rab5a, Venus-Rab11a, and Venus-Giantin, consistent with NK_1R trafficking from the plasma membrane to early and recycling endosomes and the cis-Golgi network (*SI Appendix*, Fig. S1 *D–I*). BRET between NK_1R-Rluc8 and YFP-TGN38 transiently decreased and then recovered (*SI Appendix*, Fig. S1 *J* and *K*). DnmK44A inhibited NK_1R-Rluc8 recruitment to early endosomes, recycling endosomes and the cis-Golgi network, implicating clathrin-dependent endocytosis. DnmK44A only partially inhibited SP-induced removal of the NK_1R from the plasma membrane, which may reflect the rapid recycling or mobilization of internalized NK_1R, incomplete disruption of endogenous Dnm, or involvement of additional (non-Dnm) mechanisms of receptor endocytosis. DnmK44A caused the BRET signal between NK_1R-Rluc8 and YFP-TGN38 to further decrease, which may implicate Dnm in maintaining a pool of NK_1R within the trans-Golgi network.

Enhanced bystander BRET (ebBRET), which capitalizes on the affinity of protein pairs tagged with *Renilla* fluorophores to improve sensitivity, was used to confirm the recruitment of mGα and βARR2 to the plasma membrane and early endosomes (*SI Appendix*, Fig. S2*A*) (33). EbBRET studies confirmed that SP stimulated recruitment of $mG\alpha_{sq}$, $mG\alpha_{si}$, and βARR2 to the plasma membrane and early endosomes (*SI Appendix*, Fig. S2 *B–G*). BRET between Gγ-GFP and Rluc2-Gα isoforms was measured to study the effects of SP on proximity of Gγ and Gα. SP deceased BRET between Gγ-GFP and Rluc2-$G\alpha_q$ or Rluc2-$G\alpha_i$, consistent with disassembly of the heterotrimeric Gα, Gβ, and Gγ complex or conformational rearrangement of the activated Gα subunit (*SI Appendix*, Fig. S2 *H* and *I*).

Considered together, these results support the hypothesis that SP induces the recruitment of the NK_1R, $mG\alpha_{sq}$, and βARR2 to endosomes, where a multiprotein signalosome may transduce intracellular signals.

Design, Synthesis, and Pharmacological Characterization of NT Analogs. Antagonists were designed to optimally inhibit NK_1R signaling in endosomes. The accumulation and retention of GPCR antagonists in endosomes likely depends on their lipophilicity and charge. Since the lumen of endosomes is acidic (pH 5.5 to 6.0), the degree of ligand protonation may differ between the cytoplasm and endosomal lumen, which could affect endosome membrane penetration and confer enrichment in endosomes and sustained receptor occupancy. Upon receptor binding, the protonation state of the ligand controls association and dissociation and, thus, binding affinity and the kinetic behavior. Furthermore, individual protonation states depending on environment-specific pH values may affect the conformation and, hence, ligand-binding properties of receptors. Ligands were designed with varying lipophilicity (LogP, LogD) and acidity (pKa) to promote accumulation or to take advantage of a potentially altered receptor conformation in endosomes at sufficient concentrations to extend the residence time at the endosomal NK_1R. To determine the criteria for design of antagonists of endosomal GPCRs, a series of structural analogs of the NK_1R antagonist NT ("PS" series) were developed. NT caused a concentration-dependent inhibition of $mG\alpha_{sq}$ recruitment to NK_1R-NP at the plasma membrane and in early endosomes (Fig. 2 *A–C*). NT had a lower potency in early endosomes (NT, FYVE pIC_{50} 7.70 ± 0.12, n = 5) compared to the plasma membrane (NT, CAAX pIC_{50} 8.19 ± 0.17, n = 5; unpaired *t* test, $P < 0.05$).

To better understand NT structure–activity relationships, the weakly basic pyridine nitrogen was replaced with a benzene ring (34) (Fig. 2 *D–G*). Initial investigations were directed to the synthesis and pharmacological investigation of carba-NT (PS15) with only one basic nitrogen. Further ligand modifications were guided by the crystal structure of the NT/NK_1R complex (PDB ID: 6HLP), which revealed that the $N(CH_3)$ group of the piperazine ring is ideally suited for further modifications (35). Examination of the binding pocket and subsequent docking studies indicated that a replacement of the $N(CH_3)$ group by O or CH_2 is possible, and the introduction of even large N-substituents is well tolerated. Hence, a series of carba-NT derivatives were synthesized to enable introduction of neutral (PS9, PS29), acidic (PS34), weakly basic (PS40), basic (PS21), and strongly basic (PS49) groups (Fig. 2*G* and Table 1). A maleimide group (PS26) was introduced to enable formation of a covalent bond to the NK_1R. Fluorescent tetramethylrhodamine (TAMRA) derivatives of NT were also prepared (PS67, PS68, PS69). Based on the preparation of NT (36), synthesis started from 2-bromo-4-fluoronitrobenzene to generate a biphenyl system using a Suzuki reaction (*SI Appendix*). Nucleophilic aromatic substitution allowed introduction of different saturated heterocyclic moieties. Reduction of the nitro group, *N*-methylation, and amide coupling reaction resulted in the introduction of a 1,3-bistrifluoromethylphenyl substituted isobutyric acid moiety and thus, final product formation. To characterize their binding affinity (K_d) at NK_1R, a BRET-based assay was developed using membranes from HEK293T cells expressing human NK_1R tagged at the N terminus with nanoluciferase (Nluc) and TAMRA-NT (*SI Appendix*, Fig. S3). Binding was measured at normal extracellular pH 7.4 or the acidic pH 6.0 of endosomes. At pH 7.4, TAMRA-NT analogs showed high affinities for Nluc-NK_1R (PS68, K_d 1.9 ± 0.39 nM, n = 12; PS69, K_d 0.81 ± 0.065 nM, n = 21). PS69 was then used as a fluorescent tracer to determine the affinity of SP (K_i 1.4 ± 0.46 μM, n = 6). The orthosteric NK_1R antagonists AP and NT inhibited binding with K_i values of 0.15 nM and 0.91 nM, respectively (Table 1). At pH 7.4, PS analogs retained binding with K_i values ranging from 0.72 nM (PS15) to 110 nM (PS21). Each NT analog also had nanomolar affinity for NK_1R at acidic pH 6.0, thus retaining the ability to antagonize SP/NK_1R binding in acidic endosomes. Most of the compounds showed slightly diminished binding affinities in the acidified environment. An approximately 2-fold and 20-fold increase in affinity was observed for weakly basic

Downloaded from https://www.pnas.org by NEW YORK UNIVERSITY LIBRARY-SERIALS on September 28, 2023 from IP address 216.165.95.84.

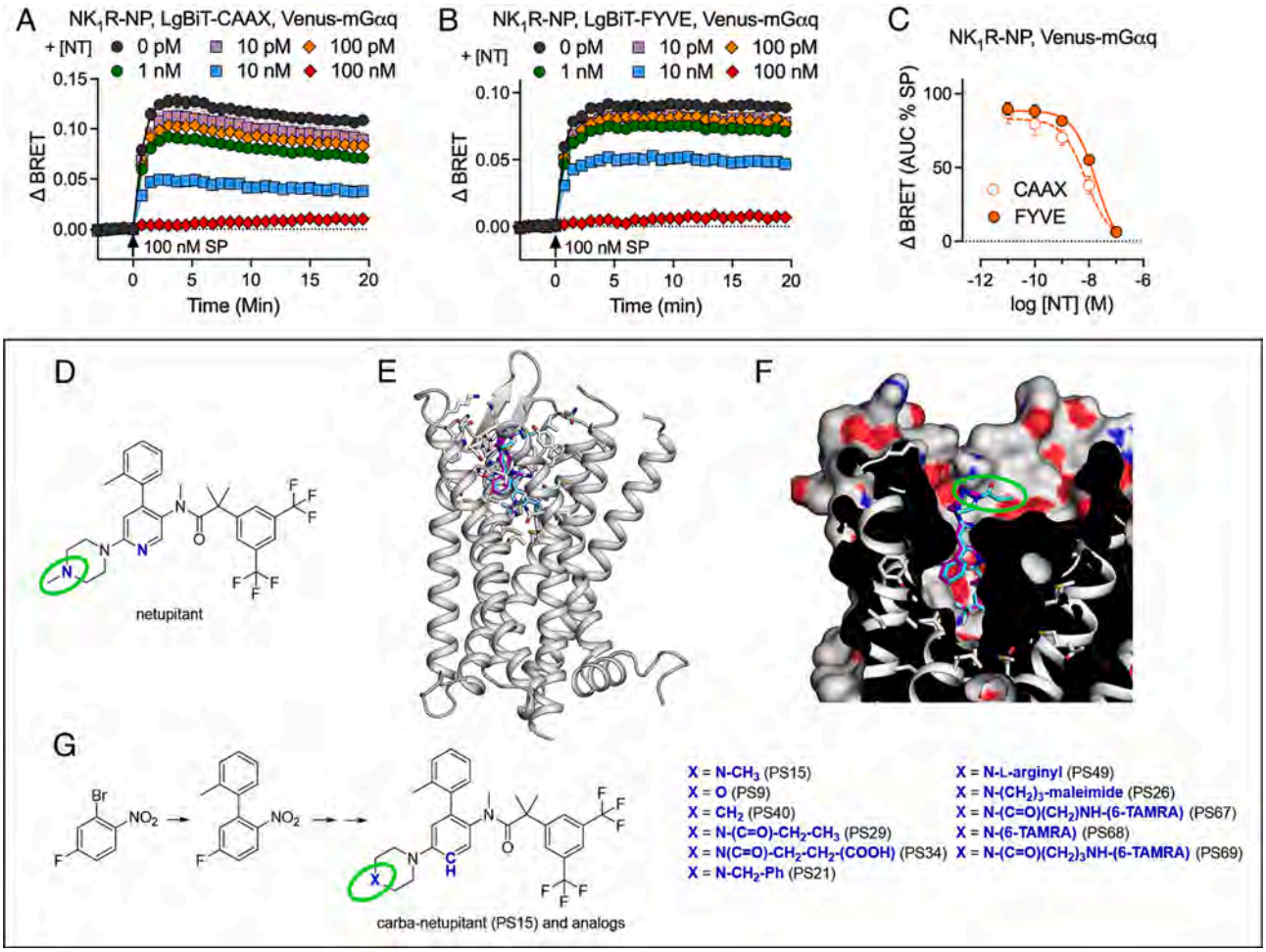

Fig. 2. Development of netupitant analogs. (*A–C*) Effect of graded concentrations of netupitant (NT, 30 min) on substance P (SP)–induced recruitment of mini $G\alpha_{sq}$ (mGαq) to the plasma membrane (CAAX, *A*) or early endosome (FYVE, *B*) on NanoBiT-BRET (nbBRET) with natural peptide (NP)–tagged NK_1R in HEK293T cells. (*D–G*) Design and synthesis of NT analogs. (*D*) Chemical formula of NT. (*E*) NK_1R crystal structure (PDB ID: 6HLP) in complex with NT (magenta) overlaid with the docked pose of PS29 (blue). Residues are displayed in a range of 8 Å relative to NT and PS29. F. NT (PDB ID: 6HLP) in complex with the NK_1R crystal structure (PDB ID: 6HLP) presented together with the docked pose of PS29. Receptor surface is clipped between the transmembrane helices 4, 5, and 6 to give better insight into the binding pocket and to show the outward reaching piperazine substituent of NT and PS29 (green circle), showing surface atoms and hetero atoms [oxygen (red), nitrogen (blue), sulfur (yellow)]. (*G*) Synthetic approach toward carba-NT derivatives. Structural changes compared to NT are highlighted in blue. Mean ± SEM. N = 4 to 9 independent experiments.

arylpiperidine PS40 [K_i (pH 7.4) = 71 nM; K_i (pH 6.0) = 36 nM] and the lipophilic and basic benzylamine PS21 [K_i (pH 7.4) = 110 nM; K_i (pH 6.0) = 4.4 nM], respectively, indicating that protonation affects ligand binding.

Inhibitory Actions of NK_1R Antagonists on SP-Induced Endosomal Signaling. The potency of NT analogs was determined by measuring inhibition of SP-induced inositol 1-phosphate (IP_1) accumulation. SP potently stimulated IP_1 accumulation (SP, EC_{50} 5.1 ± 1.1 nM, n = 8). To quantify antagonist potency (IC_{50}), HEK293T cells expressing the human NK_1R were preincubated with antagonists (90 min), challenged with SP (10 nM, ~EC_{80}, 90 min), and IP_1 accumulation was assessed. AP and NT inhibited SP-stimulated IP_1 accumulation with IC_{50} values of 170 nM and 178 nM, respectively (Table 1). PS analogs retained activity with IC_{50} values ranging from 91 nM (PS21) to 407 nM (PS49).

To evaluate whether NK_1R antagonists inhibit endosomal signaling, a Förster resonance energy transfer (FRET) biosensor targeted to the nucleus (Nuc-EKAR) was used to measure nuclear ERK activity, which emanates from NK_1R signaling in endosomes (9). HEK293T cells cotransfected with human NK_1R and NucEKAR were preincubated (30 to 90 min) with graded concentrations of NK_1R antagonists and challenged with SP (10 nM, ~ EC_{50}; *SI Appendix*, Fig. S2*J*). NT caused a concentration-dependent inhibition of SP-induced nuclear ERK activity (Fig. 3*A* and Table 1). NT was less potent than AP (Fig. 3*B*; NT, pIC_{50} 6.59 ± 0.12; AP, pIC_{50} 6.94 ± 0.17; n = 4 to 6). PS analogs with different physicochemical properties induced concentration-dependent inhibition of SP-induced activation of nuclear ERK with comparable potency (Fig. 3*C* and Table 1; pIC_{50} 6.16 to 6.72).

To determine the duration of antagonism (approximating to k_{off}), cells were preincubated with antagonists (30 to 90 min), washed, recovered for 2 or 4 h, and then challenged with SP. Most of the inhibitory effect of AP was lost within 2 h of recovery and is thus transient (Fig. 3 *D* and *E* and Table 1). In contrast, the inhibitory effects of NT and PS analogs were largely maintained after recovery for 2 h (Fig. 3 *D* and *E*) and 4 h, respectively (Fig. 3*F* and *SI Appendix*, Fig. S4 *A–F*). These results were consistent for two antagonist concentrations (*SI Appendix*, Fig. S4 *A–F*).

To assess the kinetics with which antagonists reverse endosomal NK_1R signaling (approximating to k_{on}), SP-evoked recruitment of mGα to early endosomes was studied by measuring ebBRET between Rluc8-$mG\alpha_{sq}$ and tdRFP-Rab5a. Cells were incubated

Downloaded from https://www.pnas.org by NEW YORK UNIVERSITY LIBRARY-SERIALS on September 28, 2023 from IP address 216.165.95.84.

Table 1. Pharmacological properties of NK_1R antagonists

	Compound properties					Binding affinity		Potency of inhibition		Kinetics of inhibition
	Derived*, † or calculated‡, §					BRET (Nluc-NK_1R)¶		IP_1 (HTRF)	Nuclear ERK (FRET)	Endosomal mini$G\alpha_{sq}$ (ebBRET)
	pKa*	pKa‡	LogP§	$LogD_{5.0}$†	$LogD_{7.0}$†	pK_i at pH 7.4	pK_i at pH 6.0	pIC_{50}	pIC_{50}	k (min^{-1}) for 10 μM
AP (neutral)	n.d.	n.d.	n.d.	n.d.	n.d.	9.82 ± 0.08 (5)	9.27± 0.06 (3)	6.77 ± 0.17 (4)	6.94 ± 0.17 (4)	0.15 ± 0.01 (4)
NT (basic)	6.81	6.51	7.22	n.d.	4.97	9.04 ± 0.07 (5)	9.07 ± 0.08 (3)	6.75 ± 0.10 (10)	6.59 ± 0.12 (6)	0.14 ± 0.02 (9)
PS15 (carba-NT)	6.95	7.44	7.54	3.85	5.06	9.14 ± 0.07 (4)	8.59 ± 0.04 (3)	6.50 ± 0.13 (5)	6.38 ± 0.09 (4)	0.23 ± 0.04 (9)
PS9 (neutral)	<3	2.23	7.66	n.d.	3.49	8.84 ± 0.08 (3)	8.45 ± 0.05 (3)	6.87 ± 0.07 (4)	6.29 ± 0.09 (4)	0.11 ± 0.04 (5)
PS40 (weakly basic)	4.31	4.13	8.73	n.d.	n.d.	7.15 ± 0.08 (4)	7.45 ± 0.12 (3)	6.78 ± 0.14 (7)	6.22 ± 0.15 (4)	n.d. – slow kinetics
PS29 (neutral)	<3	1.27	7.37	5.05	4.99	8.73 ± 0.07 (3)	8.31 ± 0.08 (5)	6.84 ± 0.18 (5)	6.46 ± 0.21 (4)	0.14 ± 0.02 (5)
PS21 (basic)	6.17	6.21	9.30	Not trace-able log D >> 5	Not trace-able log D >> 5	6.96 ± 0.02 (3)	8.36 ± 0.07 (3)	7.04 ± 0.11 (4)	6.50 ± 0.25 (4)	n.d. – slow kinetics
PS49 (basic)	>10	11.55	5.45	n.d.	n.d.	8.44 ± 0.08 (4)	7.59 ± 0.08 (6)	6.39 ± 0.09 (5)	6.36 ± 0.16 (5)	0.21 ± 0.01 (7)
PS34 (acidic)	n.d.	6.11	6.41	4.90	3.49	8.74 ± 0.03 (3)	8.69 ± 0.08 (5)	6.75 ± 0.11 (6)	6.16 ± 0.09 (5)	0.11 ± 0.01 (7)
PS26 (covalent)	n.d.	9.16	7.50	n.d.	n.d.	8.64 ± 0.08 (3)	7.91 ± 0.06 (3)	6.68 ± 0.17 (5)	6.72 ± 0.30 (4)	0.11 ± 0.02 (5)

*Free base titrated in 67% MeOH in H_2O (0.01 M HCl).
†LogD experiments with distribution between octanol and aqueous buffer solution at pH 5.0 and pH 7.0. n.d. not determined.
‡Calculated with Jaguar (Maestro Schroedinger).
§Calculated with QikProp (Maestro Schroedinger).
¶Determined by competition binding with fluorescent TAMRA-NT (PS69).

with SP (10 nM) for 5 min and then treated with NK_1R antagonists or vehicle (Fig. 3*G*). SP stimulated recruitment of $mG\alpha_{sq}$ to early endosomes that was maintained for at least 40 min. AP, NT, and PS analogs caused a concentration-dependent inhibition of $mG\alpha_{sq}$ recruitment, reaching equilibrium by 40 min (*SI Appendix*, Fig. S5). At a saturating concentration, PS15 induced a rapid disruption of the endosomal signal within 15 min, with a faster rate than AP, NT, or other analogs (Fig. 3 *G* and *H* and Table 1).

To evaluate the uptake of NT, HEK293T cells transiently expressing NK_1R-eGFP were incubated with TAMRA-NT (100 nM) and imaged using confocal microscopy. TAMRA-NT was taken up into cells within minutes regardless of NK_1R-eGFP expression (Fig. 3*I* and Movie S1). TAMRA-NT also colocalized with NK_1R-eGFP at the plasma membrane. Preincubation with SP prevented TAMRA-NT binding to NK1R-eGFP at the plasma membrane (Fig. 3*I* and Movie S2).

Thus, NT analogs penetrate cells and disrupt endosomal NK_1R signaling. Whereas the inhibitory actions of AP are rapidly reversed, NT analogs are long lasting and persist after washing cells to remove ligand.

Generation of Knockin Mice Expressing Full-Length hNK_1R-407 or Truncated hNK_1R-311. Differences in the potency of antagonists between human and mouse NK_1R, including for AP and NT, significantly hamper studies of the NK_1R in preclinical disease models (25). To circumvent this problem, knockin mice were generated in which the mouse NK_1R was replaced by the full-length human NK_1R (407 residues). A naturally occurring variant of the NK_1R has been described in several species, including human, that is truncated at residue 312 and lacks most of the intracellular C-terminal domain (26–28). To examine the function of this variant, knockin mice were generated in which mouse NK_1R was replaced by the truncated human variant (311 residues). This variant binds SP but displays diminished G protein signaling, interaction with βARRs, and internalization (9, 27). Thus, a comparison of SP-evoked nociception in NK_1R-407 and NK_1R-311 mice could give insight into the contribution of NK_1R endosomal signaling to pain.

Targeting constructs were designed to express tdTomato reporter (to detect NK_1R-expressing cells), a 2A peptide (cleavage would liberate tdTomato), and Flag-NK_1R-407 or Flag-NK_1R-311 (Fig. 4*A* and *SI Appendix*, Fig. S6*A*). Constructs were generated by homologous recombination using a 10 kb segment of mouse genomic DNA from a C57 BAC clone. Synthetic cDNAs encoding NK_1R-407 or NK_1R-311 were codon optimized for mouse. tdTomato followed by a 2A peptide was incorporated upstream and a neomycin cassette flanked by FRT sites was incorporated downstream from the NK_1R cDNAs. The cassette was inserted at the ATG site of mouse NK_1R and the first exon was deleted. Constructs were linearized and electroporated in Bruce4 (C57BL/6) ES cells. Screening of 200 clones revealed 8 to 14% ratio of recombination, which was confirmed by southern blotting (Fig. 4*B* and *SI Appendix*, Fig. S6*B*). Clones were analyzed using an internal probe annealing on the NEO cassette (Fig. 4*C* and *SI Appendix*, Fig. S6*C*). Sequencing of five NK_1R-407 and five NK_1R-311 clones confirmed correct insertion of tdTomato and integrity of FRT sites. Three clones were injected into mouse blastocysts, and male chimeras (black and white) were bred with wild-type C57BL/6 female mice to generate black F1 progeny; two clones gave germline transmission. Expression of NK_1R-407 and NK_1R-311 was confirmed by southern blotting of the heterozygotic F1 generation (Fig. 4*D* and *SI Appendix*, Fig. S4*D*) and RT-PCR of knockin mice. F1 mice were backcrossed for >10 generations to generate homozygotic NK_1R-407 and NK_1R-311 mice.

Characterization of hNK_1R-407 and hNK_1R-311 Mice. The expression of the NK_1R was verified in hNK_1R-407, hNK_1R-311, and wild-type mice using PCR and qRT-PCR with primers for mouse (m) or human (h) receptors, including primers specific to hNK_1R-407 but not hNK_1R-311 and primers that would

Downloaded from https://www.pnas.org by NEW YORK UNIVERSITY LIBRARY-SERIALS on September 28, 2023 from IP address 216.165.95.84.

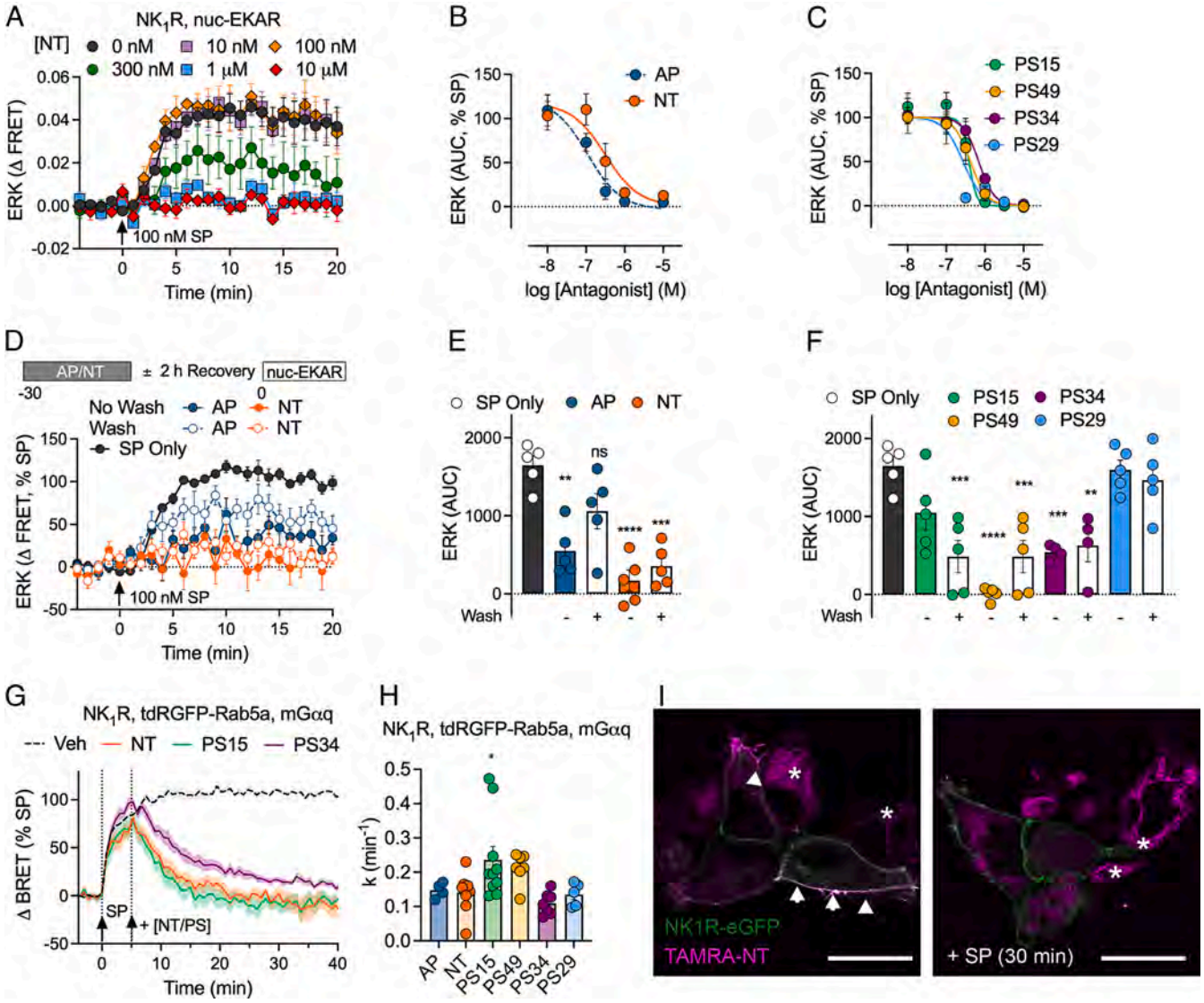

Fig. 3. Antagonism of NK_1R endosomal signaling in HEK293T cells. (*A*–*F*) FRET assays of substance P (SP)–induced activation of nuclear ERK activity measured using a nuclear EKAR biosensor. (*A*–*C*) Cells were preincubated (30 or 90 min) with graded concentrations of aprepitant (AP), netupitant (NT), PS15, PS29, PS34, or PS49 prior to SP (100 nM) challenge. (*D*–*F*) Duration of inhibition following antagonist removal and recovery. Cells were preincubated with antagonist for 30 min (AP, 100 nM; NT, 300 nM) or 90 min (NT analogs, 1 µM), washed, and recovered in agonist-free medium for 2 h (AP, NT) or 4 h (NT analogs; *SI Appendix*, Fig. S3), prior to stimulation with SP (100 nM). (*G* and *H*) Enhanced bystander BRET (ebBRET) measuring proximity between mini $G\alpha_{sq}$ (Venus-mGα_{sq}) and a *Renilla* luciferase–tagged endosomal marker (tdRGFP-Rab5a). Cells were stimulated with SP (100 nM, 5 min), then challenged with vehicle or saturating concentrations of NT, PS15, or PS34 (10 µM). EbBRET was measured for 40 min. Kinetics were fitted as a nonlinear exponential decay from antagonist addition to quantify the rate of antagonism. Mean±SEM. N = 4 to 9 independent experiments. 1-way ANOVA with Holm-Šídák's (*E*), Dunnett's (*F*) test against SP, or Dunnett's against NT (*H*). (*I*) Localization of fluorescent TAMRA-NT (PS68, 100 nM, 10 min, magenta) in HEK293T cells expressing NK_1R-eGFP (green), with or without preincubation with unlabeled SP (100 nM, 30 min). Arrow heads denote TAMRA-NT and NK_1R-eGFP colocalization at the plasma membrane. Asterisks denote uptake of TAMRA-NT into cells lacking NK_1R-eGFP. (Scale bar, 20 µm). Representative images, N = 3 experiments.

detect both hNK_1R-407 and hNK_1R-311. Primers specific to hNK_1R-407 detected the receptor in extracts of the spinal cord and colon from hNK_1R-407 mice, but not hNK_1R-311 or wild-type mice (Fig. 5 *A*–*C*). Primers common to hNK_1R-407 and hNK_1R-311 detected both receptors at similar levels in the spinal cord and colon of hNK_1R-407 and hNK_1R-311 mice but not in wild-type mice.

RNAScope® in situ hybridization was used to localize human and mouse NK_1R mRNAs in the spinal cord of mice. Probes were designed to specifically target both human NK_1R-407 and NK_1R-311 or mouse NK_1R. Neurons were identified by Nissl staining. Corroborating with the qRT-PCR results, a probe common to human NK_1R-407 and NK_1R-311 hybridized to spinal neurons of hNK_1R-407 and hNK_1R-311 but not in wild-type mice (Fig. 5*D*). Mouse NK_1R mRNA was detected in spinal neurons of wild-type mice (Fig. 5*D*).

SP-Evoked Nociception in hNK_1R-407 or hNK_1R-311 Mice. Since NK_1R-311 displays aberrant signaling by G proteins and βARRs and is resistant to SP-induced endocytosis (9, 27, 37), a comparison of the pronociceptive actions of SP between mice expressing full-length or truncated human NK_1R could provide insights into the contribution of NK_1R signaling and endocytosis to nociception. SP (0.1, 1, 3 µg/5 µL) was injected intrathecally to activate spinal neurons expressing the NK_1R in hNK_1R-407, hNK_1R-311, and wild-type mice. Paw withdrawal responses to stimulation with von Frey filaments were assessed over 1 h to evaluate mechanical allodynia. SP dose-dependently reduced withdrawal threshold

Downloaded from https://www.pnas.org by NEW YORK UNIVERSITY LIBRARY-SERIALS on September 28, 2023 from IP address 216.165.95.84.

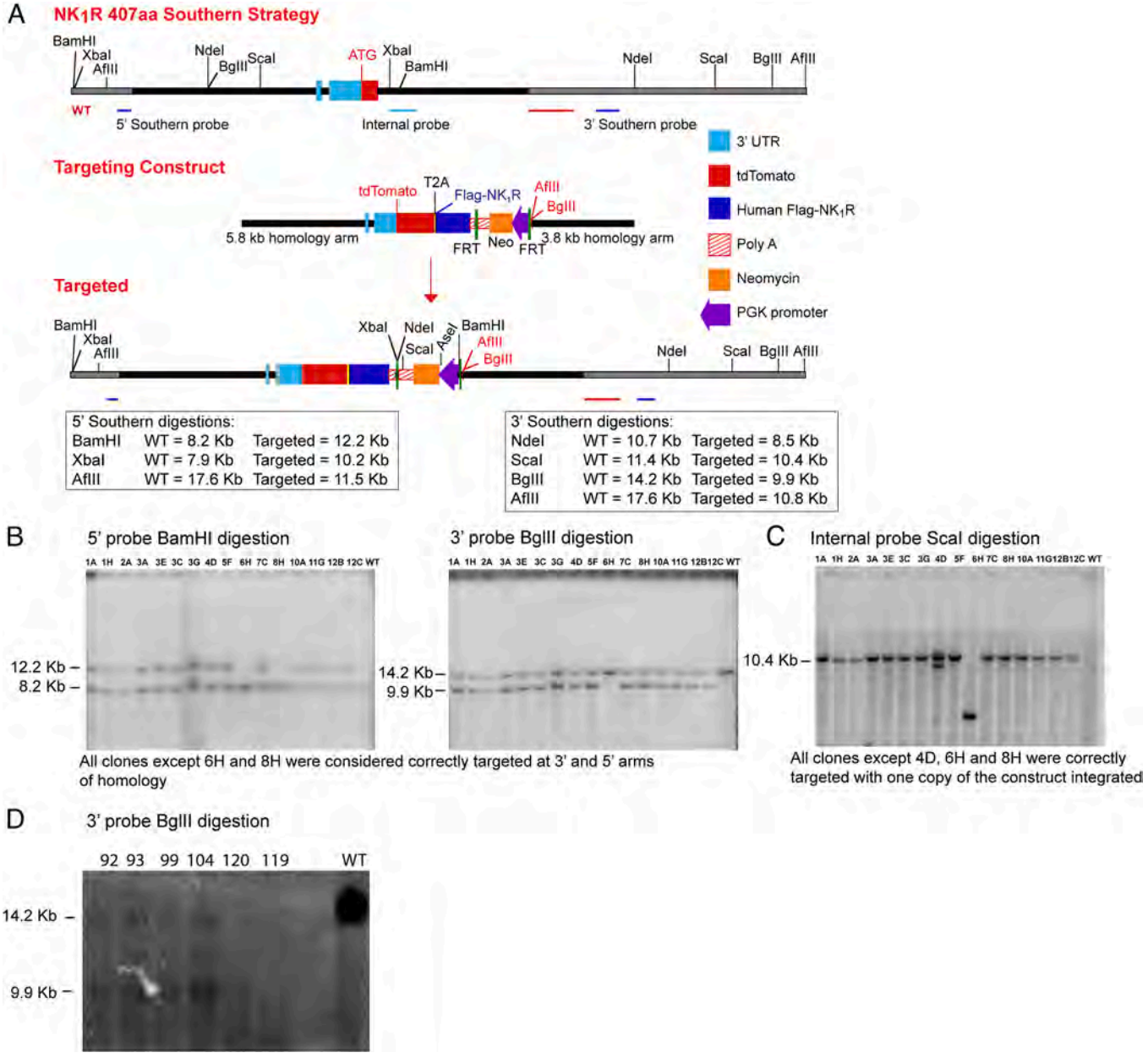

Fig. 4. Generation of knockin mice expressing hNK$_1$R-407. (*A*) NK$_1$R-407 Southern strategy and targeting construct comprising tdTomato, a T2A peptide cleavage site, Flag-hNK$_1$R-407, a downstream phosphoglycerine kinase neomycin cassette flanked by FRT sites, and downstream AflII and BglII sites. (*B* and *C*) Southern blots of selected clones with 5′, 3′, and internal probes confirming correct targeting. (*D*) Southern blot of F1 mice confirming NK$_1$R-407 expression. WT, wild-type.

to von Frey filaments in hNK$_1$R-407, hNK$_1$R-311, and wild-type mice, consistent with mechanical allodynia (Fig. 6 *A*–*C*). All doses of SP evoked mechanical allodynia, which was detected after 15 min, was maximal at 30 min, and returned to baseline at 60 min after injection. A comparison of mechanical allodynia between strains to the same dose of SP indicated identical mechanical allodynia in hNK$_1$R-407 and wild-type mice to all doses of SP (Fig. 6 *D*–*I*). Mechanical allodynia in hNK$_1$R-311 mice was less than that in NK$_1$R-407 and wild-type mice at all doses of SP, and this difference was significant at 1 μg SP (Fig. 6 *E* and *H*).

Although SP is the primary ligand for the NK$_1$R, SP can also activate the NK$_2$R and NK$_3$R, albeit with low affinity (25). To confirm that the SP nociceptive response was dependent on the NK$_1$R, AP (100 nM/5 μL) was coadministered with SP (1 μg/5 μL) by intrathecal injection. AP abolished SP-evoked mechanical allodynia in hNK$_1$R-407, hNK$_1$R-311, and wild-type mice (Fig. 6 *J* and *K*).

SP activates the NK$_1$R on spinal neurons to evoke receptor endocytosis and persistent neuronal excitation. Inhibitors of clathrin-mediated endocytosis, and lipidated or nanoparticle-encapsulated NK$_1$R antagonists that target endosomes, prevent sustained neuronal excitation, which thus requires NK$_1$R signaling in endosomes (9, 17). To obtain further evidence for the contribution of NK$_1$R endocytosis to nociception, spinal cord slices from NK$_1$R-407 and NK$_1$R-311 mice were superfused with SP (10 nM, 2 min), and action potential firing was assessed by cell-attached patch-clamp recording. SP induced a rapid-onset burst of action potential discharge that was similar in spinal neurons of NK$_1$R-407 and NK$_1$R-311 (Fig. 6 *L*–*N*). In NK$_1$R-407 mice, neuronal excitation persisted for 12 min after SP washout. In contrast, in NK$_1$R-311 mice, neuronal excitation returned to baseline by 4 min after SP

Downloaded from https://www.pnas.org by NEW YORK UNIVERSITY LIBRARY-SERIALS on September 28, 2023 from IP address 216.165.95.84.

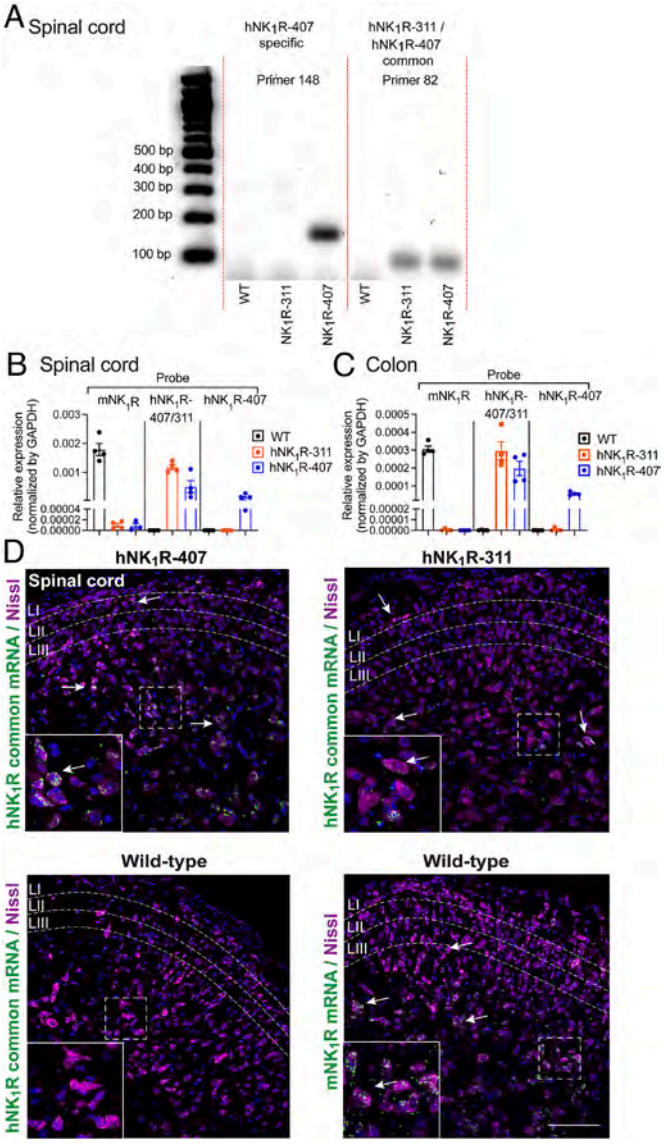

Fig. 5. Characterization of mice expressing hNK$_1$R-407 or hNK$_1$R-311. (*A*) PCR gels of the spinal cord from NK$_1$R-407, NK$_1$R-311, and WT mice probed with a primer (#148) specific for human NK$_1$R-407 or a primer (#82) that would detect both human NK$_1$R-407 and NK$_1$R-311. (*B* and *C*) qRT-PCR analysis of extracts of the spinal cord (*B*) and colon (*C*) probed with primers to mouse NK$_1$R, both human NK$_1$R-407 and NK$_1$R-311, or hNK$_1$R-407 alone. N = 4 mice. (*D*) RNAScope® in situ hybridization of sections of the spinal cord from NK$_1$R-407, NK$_1$R-311, or WT mice using probes to both human NK$_1$R-407 and NK$_1$R-311 or to mouse NK$_1$R, highlighting neurons with a Nissl stain (magenta). Representative images from n = 3 mice. Scale bar, 50 μm, and in detail box, 20 μm. L, lamina.

washout. AP prevented SP-induced excitation of spinal neurons in NK$_1$R-407 mice.

Attenuated SP-induced activation of spinal neurons and diminished nociception observed in mice expressing truncated NK$_1$R support the hypothesis that efficient coupling to G proteins, βARRs, and the endocytic machinery are necessary for SP-evoked pain.

Antinociceptive Effects of NK$_1$R Antagonists in hNK$_1$R-407 Mice. To assess whether effective antagonism of NK$_1$R signaling in endosomes correlates with antinociceptive activity, the effect of NK$_1$R antagonists was evaluated on capsaicin-induced mechanical allodynia in hNK$_1$R-407 mice. AP, NT, NT analogs (PS15, PS29, PS34, PS49) (10, 30, 100 or 300 nM, 5 μL) or vehicle (control) was injected intrathecally immediately before intraplantar injection of capsaicin. Withdrawal responses of the capsaicin-injected (right, ipsilateral) hindpaw to stimulation with von Frey filaments were assessed to evaluate mechanical allodynia. In vehicle-treated mice, capsaicin caused mechanical allodynia for 8 h (Fig. 7 A and B). Intrathecal AP (100 nM) inhibited capsaicin-evoked mechanical allodynia for 2 h. NT (100 nM) inhibited mechanical allodynia for 4 h. PS15, PS29, PS34, and PS49 (100 nM) had more efficacious and sustained antinociceptive effects. PS29 and PS34 completely prevented capsaicin-evoked mechanical allodynia for 4 h, with antinociceptive effects for at least 8 h. Higher doses of AP or NT (300 nM) did not further increase the magnitude or duration of the antinociception (Fig. 7 *C*, *D*, and *F*). In contrast, lower doses of PS34 (30 nM) still induced antinociception for 6 h. Thus, NT analogs that effectively inhibit endosomal signaling of the NK$_1$R also caused efficacious and persistent antinociception.

Discussion

The results support the hypothesis that SP stimulates recruitment of the NK$_1$R, mGα$_{sq}$, mGα$_{si}$, and βARR2 to early endosomes, where an NK$_1$R, mGα, and βARR signalosome may assemble and generate signals in subcellular compartments, including ERK activation in the nucleus. Although AP, NT, and NT analogs can disrupt complex formation and inhibit resultant signals, the actions of AP are rapidly reversed. NT analogs, in particular PS29 and PS34, demonstrate sustained antagonism of endosomal signaling and potent, efficacious, and long-lasting inhibition of nociception in mice expressing the human NK$_1$R. In mice expressing a truncated NK$_1$R variant with aberrant signaling and endosomal trafficking, SP is unable to cause sustained activation of spinal neurons and persistent nociception. The results identify criteria for the design of GPCR antagonists that are capable of penetrating endosomes and disrupting signalosomes and provide evidence for the contribution of endosomal NK$_1$R signaling in nociception.

NK$_1$R Signalosomes in Endosomes. BRET assays of NK$_1$R trafficking revealed that SP induces depletion of NK$_1$R from the plasma membrane and recruitment to early endosomes, recycling endosomes, and the Golgi apparatus. NK$_1$R trafficking was Dnm dependent because dominant-negative Dnm inhibited NK$_1$R endocytosis and accumulation in endosomes and the cis-Golgi apparatus. SP also stimulated the recruitment of mGα$_{sq}$, mGα$_{si}$, and βARR2, but not mGα$_s$, to the plasma membrane and early endosomes. A nbBRET assay allowed simultaneous evaluation of the proximity of the NK$_1$R, an effector (mGα, βARR2), and a plasma membrane or endosomal marker. These studies suggest that SP evokes assembly of NK$_1$R signalosomes with mGα$_{sq}$, mGα$_{si}$, or βARR2 in early endosomes. Although BRET assays can be used to infer signalosome assembly, the approach evaluates protein proximity rather than interaction. However, structural studies support the concept that GPCRs could physically associate with Gα and βARRs in endosomes, forming "megaplexes" that continue to signal (12, 13). GPCR signalosomes in endosomes generate second messengers and activate enzymes in specific intracellular compartments, including nuclear ERK and cytosolic protein kinase C and cAMP in the case of the NK$_1$R (9). Compartmentalized signals allow GPCRs, which often couple to a common set of effectors, to regulate specific cellular functions, including activity of spinal neurons that is required for the central transmission of pain (9). Further studies are required to evaluate the physiological relevance of recruitment of the NK$_1$R and isoforms of Gα and βARRs to endosomes, including stimulation of cells that endogenously express these proteins with biologically relevant concentrations of SP.

Downloaded from https://www.pnas.org by NEW YORK UNIVERSITY LIBRARY-SERIALS on September 28, 2023 from IP address 216.165.95.84.

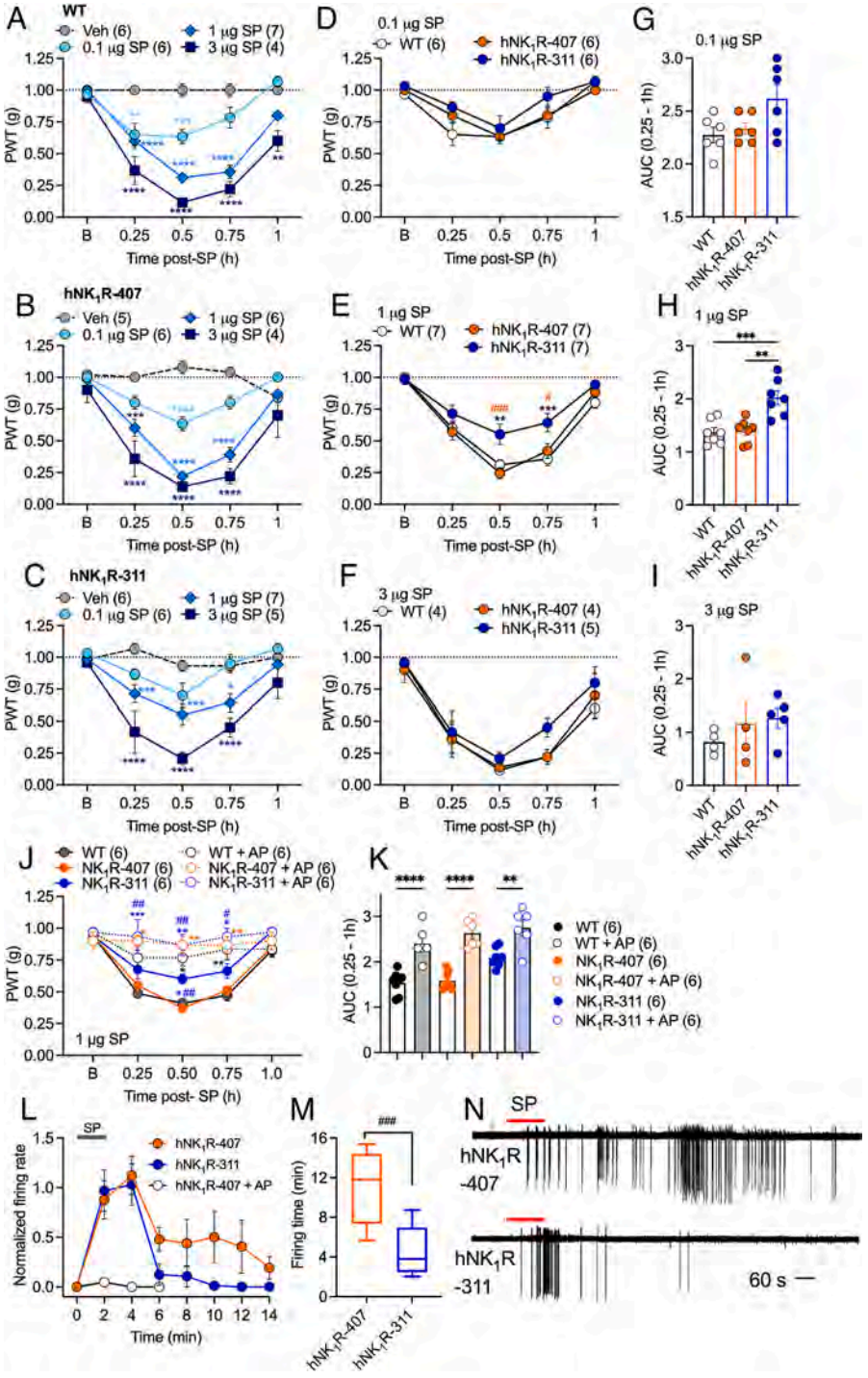

Fig. 6. SP-evoked nociception in hNK$_1$R-407, hNK$_1$R-311, and wild-type mice. (*A*–*C*) Substance P (SP; 0.1, 1, 3 µg/5 µL, intrathecal)–evoked mechanical allodynia in WT (*A*), NK$_1$R-407 (*B*), and NK$_1$R-311 (*C*) mice. Mechanical allodynia was measured 0.25 to 1 h after SP injection. (*D*–*F*) Mechanical allodynia to the same dose of SP in the three strains of mice. Paw withdrawal threshold (PWT) to stimulation with calibrated von Frey filaments was measured to assess mechanical allodynia. (*G*–*I*) AUC in the three strains of mice. (*J* and *K*) Effects of intrathecal injection of aprepitant (AP, 100 nM/5 µL) or vehicle on SP (1 µg/5 µL)-evoked mechanical allodynia in NK$_1$R-407, NK$_1$R-311, and WT mice. (*L*–*N*) Activation of spinal neurons in slice preparations of spinal cord from NK$_1$R-407 and NK$_1$R-311 mice after transient stimulation with SP (10 nM, 2 min). (*L*) Normalized firing rate. (*M*) Firing time. (*N*) Representative traces. Mean ± SEM; (N) denotes number of mice studied. $^*P < 0.05$, $^{**}P < 0.01$, $^{***}P < 0.001$, $^{****}P < 0.0001$ vs. Veh, WT; $^{\#}P < 0.05$, $^{\#\#}P < 0.01$, $^{\#\#\#}P < 0.001$ vs. NK$_1$R-407. Two-way ANOVA, Sídák's multiple comparison test (*A*–F and *J*), one-way ANOVA, Tukey's multiple comparison test (*G*–*I* and *K*), or parametric unpaired two-tailed *t* test (*M*).

Antagonism of NK$_1$R Signaling in Endosomes. Whereas GPCR signaling at the plasma membrane is tightly regulated by GRK-mediated receptor phosphorylation and interaction with βARRs, GPCR signaling in endosomes is often sustained. The mechanisms that terminate endosomal signaling are not fully understood. However, degradation of SP in acidic endosomes by the transmembrane peptidase endothelin–converting enzyme 1 disrupts signalosomes and terminates endosomal signaling of the NK$_1$R (38, 39). The observations that inhibitors of endocytosis block compartmentalized signaling and nociception provide a link between endosomal signaling and pain and suggest that GPCRs in endosomes are an optimal target for the treatment of pain (9, 11, 16). GPCR antagonists conjugated to the transmembrane lipid cholestanol or encapsulated into nanoparticles accumulate in early

Downloaded from https://www.pnas.org by NEW YORK UNIVERSITY LIBRARY-SERIALS on September 28, 2023 from IP address 216.165.95.84.

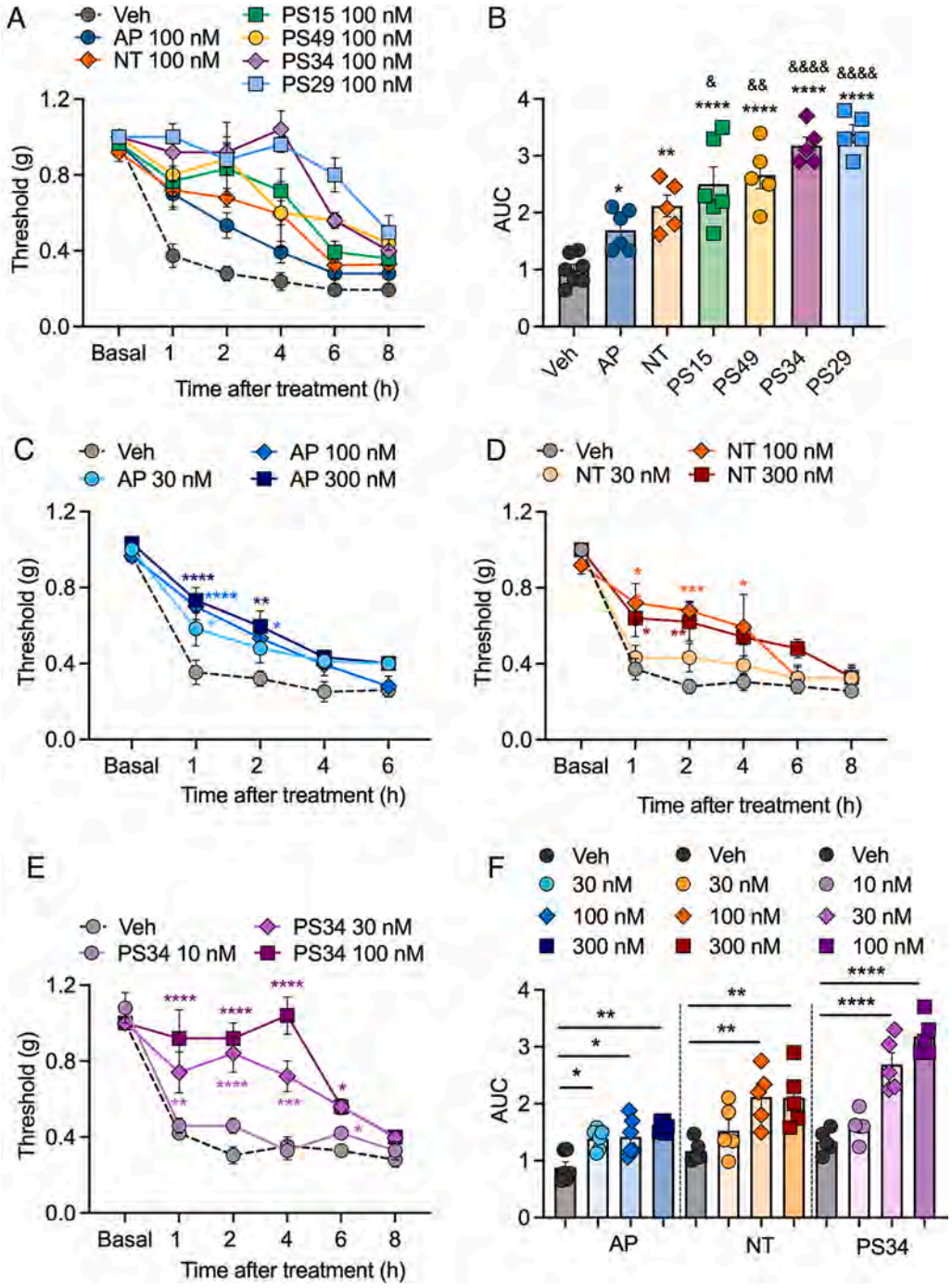

Fig. 7. Antagonism of capsaicin-evoked nociception in hNK_1R-407 mice. (*A*) Effects of intrathecal (i.t.) injection of aprepitant (AP), netupitant (NT), or NT analogs (PS15, PS49, PS34, PS29; 100 nM/5 μL) on capsaicin-induced mechanical allodynia in hNK_1R-407 mice. (*B*) AUC in the same groups of mice. (*C*–*E*) Dose–response effects of AP (30, 100, 300 nM/5 μL, i.t.), NT (30, 100, 300 nM/5 μL, i.t.), or PS34 (10, 30, 100 nM/5 μL, i.t.) on capsaicin-induced mechanical allodynia. (*F*) AUC in the same groups of mice. (N) denotes number of mice studied. $^{*}P < 0.05$, $^{**}P < 0.01$, $^{***}P < 0.001$, $^{****}P < 0.0001$ vs. Veh; $^{\&}P < 0.05$, $^{\&\&}P < 0.01$, $^{\&\&\&\&}P < 0.0001$ vs. AP, one-way ANOVA, Tukey's multiple comparison test (*B* and *F*) or two-way ANOVA, Sídák's multiple comparison test (*C*, *D*, and *E*).

endosomes, block endosomal signaling, and provide more efficacious and long-lasting relief from pain than conventional antagonists (9, 11, 15, 17, 22, 40). However, lipidated and nanoparticle-encapsulated drugs are not suited to systemic administration, and pharmacokinetic considerations may limit their usefulness. Thus, the current investigation sought to identify criteria for the rational design of small-molecule antagonists of the NK_1R. The structure of the NK_1R complexed with NT was used to design derivatives of NT (35). NT analogs of variable lipophilicity (LogP, LogD) and acidity (pKa) were synthesized based on the presumption that antagonists with altered physicochemical behavior would penetrate plasma and endosomal membranes and compounds with ideal properties are retained in proximity to NK_1R signalosomes. A similar approach has been used to design fluorinated analogs of fentanyl with a low pKa. These efficiently activate μ-opioid receptors in the acidified extracellular environment of damaged or diseased tissue, and thereby prevent pain without the detrimental on-target side effects usually evoked by engaging μ-opioid receptors in healthy tissues with normal extracellular pH (21, 41). A long residence time of antagonists in endosomes containing the NK_1R might be expected to abrogate endosomal signaling and prevent pain. NT analogs retained the ability to bind to the NK_1R in membrane preparations at extracellular (pH 7.4) and endosomal (pH 6.0) pH, and all potently inhibited SP-induced IP_1 formation. Lipophilic receptor antagonists may better diffuse into endosomes. Moreover, NK_1R conformation may change at a lower pH, conferring a strong and persistent receptor binding of suitable NT analogs. We suggest that PS29 and PS34 show favorable binding properties because such ligands are not charged at the lower pH in endosomes, leading to a more sustained inhibition of endosomal signaling. NT analogs

Downloaded from https://www.pnas.org by NEW YORK UNIVERSITY LIBRARY-SERIALS on September 28, 2023 from IP address 216.165.95.84.

also potently inhibited SP-induced activation of nuclear ERK, which requires endosomal NK_1R signaling (9). However, whereas AP caused only a transient inhibition of SP-induced activation of nuclear ERK that was rapidly reversed after washout, the inhibition by NT and all NT analogs was maintained after washing cells to remove extracellular drug. Moreover, NT and NT analogs rapidly reversed SP-induced recruitment of $mG\alpha_{sq}$ to endosomes. Notably, the NT analogs PS34 and PS29 caused a considerably larger and more sustained inhibition of capsaicin-evoked allodynia than that of AP and NT, which had smaller and more transient antinociceptive effects. The LogD values of PS29 ($LogD_{5.0}$ = 5.05, $LogD_{7.0}$ = 4.99) and PS34 indicate high lipophilicity. Despite its acidic functional group, the LogD value of PS34 at pH 5 ($LogD_{5.0}$ = 4.90, compared to $LogD_{7.0}$ = 3,49) indicates that deprotonation of PS34 in endosomes is not crucial. Hence, PS34 remains neutral and lipophilic in endosomes. The administration of antagonists by injection into the intrathecal space where they would readily access dorsal horn spinal neurons expressing the NK_1R likely minimizes the possibility that pharmacokinetic differences account for the large and prolonged analgesic actions of PS34 and PS29. Future pharmacokinetic studies are required to fully exclude this possibility. Pharmacokinetic and pharmacodynamic studies are also necessary to determine whether parenterally administered antagonists such as PS34 and PS29 access the NK_1R in endosomes of spinal neurons and effectively alleviate inflammatory and neuropathic pain.

Kinetics and Physicochemical Properties of NK_1R Antagonists. The most basic NT analogs, PS15 and PS49, show the fastest kinetics for the inhibition of endosomal signaling at high concentration. A rapid exchange between the protonated and nonprotonated forms under physiological conditions and pH-dependent protonation states, which are reflected by the experimental LogD values of PS15 ($LogD_{7.0}$ = 5.06, $LogD_{5.0}$ = 3.85), may promote their traffic to endosomes. Additionally, the exchange of the pyridine-core of NT to a more lipophilic benzene-ring (PS analogs) could accelerate the penetration of membranes.

SP-Induced Nociception in Mice Expressing Truncated NK_1R. mRNA encoding NK_1R-311, which lacks most of the intracellular C-terminus, is highly expressed in the human brain (26) and the immune system (42). Lacking critical Ser and Thr residues that are potential sites of GRK phosphorylation and interaction with βARRs, NK_1R-311 is unable to recruit βARRs and does not undergo SP-induced endocytosis (9). The C-terminal domain is also necessary for efficient Gα coupling, since NK_1R-311 responds only to high SP concentrations with reduced and delayed ERK signaling (27, 28). In knockin mice expressing human NK_1R-311, intrathecal injection of SP caused mechanical allodynia, although responses were smaller than those observed in mice expressing human NK_1R-407 or in wild-type mice, which were identical. Although SP caused an initial activation of spinal neurons from NK_1R-311 mice, the sustained response observed in neurons from NK_1R-407 mice was largely absent. Given that the sustained activation of spinal neurons is dependent on NK_1R endocytosis and consequent activation of ERK, the diminished response in neurons from NK_1R-311 mice may be attributable to diminished endocytosis and delayed ERK signaling. However, there are other possible explanations for the diminished nociception in NK_1R-311 mice. The inability of NK_1R-311 to respond to low concentrations of SP and efficiently couple to G proteins may also contribute to diminished nociception. Although altered levels of expression could explain abnormal nociception, the mRNA levels and distribution of the NK_1R were similar in NK_1R-311, NK_1R-407, and wild-type mice. It is also possible that SP may activate receptors other than the NK_1R. SP at high concentrations can activate NK_2R and NK_3R (25), but AP, which is selective for the NK_1R over NK_2R and NK_3R, abolished SP-evoked nociception in NK_1R-311, NK_1R-407, and wild-type mice. It is not possible to exclude the possibility that SP activates other types of GPCRs, such as the mouse Mas–related GPCR MrgprB2, which responds to high concentrations of SP and is antagonized by high concentrations of AP (43). Although MrgprB2 appears to mediate the effects of SP on mouse mast cells, further work is required to determine whether MrgprB2 could be involved in the central actions of SP on nociception in mice.

In summary, lipophilic and acidic NK_1R antagonists cause sustained disruption of endosomal signaling and long-lasting antinociception. The results provide insights into strategies for antagonizing GPCRs in intracellular locations, with implications for designing improved treatments for disease.

Materials and Methods

SI Appendix includes detailed methods.

Design, Synthesis, and Analysis of NT Analogs. The NT-bound NK_1R structure (PDB: 6HLP) (35) was used for molecular docking (44). NT analogs were synthesized by the Suzuki reaction and analyzed by chromatography and mass spectrometry. pKa was determined as described (45). TAMRA-NT binding to membranes from HEK293T cells expressing Nluc-NK_1R was measured using BRET (46). G-protein signaling was assessed by IP_1 assays (47, 48). TAMRA-NT uptake in cells expressing NK_1R-eGFP was studied by confocal microscopy.

BRET. NK_1R trafficking, mGα and βARR2 recruitment, and Gα/Gβγ dissociation were determined by BRET, ebBRET, and nbBRET (16).

FRET. Nuclear ERK activation was measured using nuc-EKAR FRET biosensor (9).

Generation and Characterization of Knockin Mice. Knockin mice were generated expressing full-length (407 aa) or truncated (311 aa) human NK_1R. PCR and RNAScope® probes to human NK_1R-407 and NK_1R-311, specific for human NK_1R-407, or specific for mouse NK_1R, were used to detect NK_1R mRNA. Nociception was studied after intrathecal injection of SP or NK_1R antagonists or intraplanar injection of capsaicin. Mechanical allodynia was assessed by measuring paw withdrawal response to von Frey filaments (9, 17, 49). Cell-attached patch-clamp recordings were made from spinal cord slices (9, 17, 49).

Statistics. Differences were assessed using Student's *t* test for two comparisons and 1- or 2-way ANOVA and Tukey's, Dunnett's, or Šidák's post-hoc test for multiple comparisons. $P < 0.05$ was considered significant at the 95% confidence level.

Data, Materials, and Software Availability. All study data are included in the article and/or *SI Appendix*.

ACKNOWLEDGMENTS. This study was supported by grants from NIH (NS102722, DE026806, DK118971, DE029951, N.W.B. and B.L.S.), Department of Defense (W81XWH1810431, W81XWH2210239, N.W.B. and B.L.S.), National Health and Medical Research Council (NHMRC APP1125877, APP1139586, W.L.I.), and Australian Research Council (ARC DP190102854, W.L.I.). C.J.P. is a Leon Levy Neuroscience Fellow. Cartoons were made with BioRender.

Author affiliations: [a]Department of Molecular Pathobiology, College of Dentistry, New York University, New York, NY 10010; [b]Department of Neuroscience and Physiology, Neuroscience Institute, New York University, New York, NY 10010; [c]Pain Research Center, College of Dentistry, New York University, New York, NY 10010; [d]Department of Chemistry and Pharmacy, Friedrich-Alexander Universität Erlangen-Nürnberg, 91058, Erlangen, Germany; [e]Gene Modification Platform, Monash University, Clayton, VIC 3168, Australia; [f]Drug Discovery Biology, Monash Institute of Pharmaceutical Sciences, Monash University, Parkville, VIC 3052, Australia; [g]NYU Dentistry Translational Research Center, College of Dentistry, New York University, New York, NY 10010; and [h]Department of Physiology and Monash Biomedicine Discovery Institute, Monash University, VIC 3800, Australia

Author contributions: A.H., C.J.P., R.T, P.S., S.T., R.L., H.H., D.W., J.R., N.A.V., D.P.P., D.D.J., B.L.S., W.L.I., P.G., and N.W.B. designed research; A.H., C.J.P., R.T., P.S., S.T., R.L., H.H., D.W., J.R., N.A.V., D.P.P., D.D.J., W.L.I., and P.G. performed research; A.R.B.T. contributed new reagents/analytic tools; A.H., C.J.P., R.T., P.S., S.T., R.L., H.H., D.W., J.R., N.A.V., D.P.P., D.D.J., W.L.I., P.G., and N.W.B. analyzed data; and A.H., C.J.P., R.T., P.S., B.L.S., W.L.I., P.G., and N.W.B. wrote the paper.

Downloaded from https://www.pnas.org by NEW YORK UNIVERSITY LIBRARY-SERIALS on September 28, 2023 from IP address 216.165.95.84.

1. D. Yang *et al.*, G protein-coupled receptors: Structure- and function-based drug discovery. *Signal Transduct. Target. Ther.* **6**, 7 (2021).
2. V. V. Gurevich, E. V. Gurevich, GPCR signaling regulation: The role of GRKs and arrestins. *Front. Pharmacol.* **10**, 125 (2019).
3. F. Dicker, U. Quitterer, R. Winstel, K. Honold, M. J. Lohse, Phosphorylation-independent inhibition of parathyroid hormone receptor signaling by G protein-coupled receptor kinases. *Proc. Natl. Acad. Sci. U.S.A.* **96**, 5476–5481 (1999).
4. D. Calebiro *et al.*, Persistent cAMP-signals triggered by internalized G-protein-coupled receptors. *PLoS Biol.* **7**, e1000172 (2009).
5. K. A. DeFea *et al.*, The proliferative and antiapoptotic effects of substance P are facilitated by formation of a beta -arrestin-dependent scaffolding complex. *Proc. Natl. Acad. Sci. U.S.A.* **97**, 11086–11091 (2000).
6. K. A. DeFea *et al.*, beta-arrestin-dependent endocytosis of proteinase-activated receptor 2 is required for intracellular targeting of activated ERK1/2. *J. Cell Biol.* **148**, 1267–1281 (2000).
7. A. Godbole, S. Lyga, M. J. Lohse, D. Calebiro, Internalized TSH receptors en route to the TGN induce local Gs-protein signaling and gene transcription. *Nat. Commun.* **8**, 443 (2017).
8. R. Irannejad *et al.*, Conformational biosensors reveal GPCR signalling from endosomes. *Nature* **495**, 534–538 (2013).
9. D. D. Jensen *et al.*, Neurokinin 1 receptor signaling in endosomes mediates sustained nociception and is a viable therapeutic target for prolonged pain relief. *Sci. Transl. Med.* **9**, eaal3447 (2017).
10. N. N. Jimenez-Vargas *et al.*, Endosomal signaling of delta opioid receptors is an endogenous mechanism and therapeutic target for relief from inflammatory pain. *Proc. Natl. Acad. Sci. U.S.A.* **117**, 15281–15292 (2020).
11. N. N. Jimenez-Vargas *et al.*, Protease-activated receptor-2 in endosomes signals persistent pain of irritable bowel syndrome. *Proc. Natl. Acad. Sci. U.S.A.* **115**, E7438–E7447 (2018).
12. A. H. Nguyen, R. J. Lefkowitz, Signaling at the endosome: Cryo-EM structure of a GPCR-G protein-beta-arrestin megacomplex. *FEBS J.* **288**, 2562–2569 (2021).
13. A. H. Nguyen *et al.*, Structure of an endosomal signaling GPCR-G protein-beta-arrestin megacomplex. *Nat. Struct. Mol. Biol.* **26**, 1123–1131 (2019).
14. M. Stoeber *et al.*, A genetically encoded biosensor reveals location bias of opioid drug action. *Neuron* **98**, 963–976.e5 (2018).
15. R. E. Yarwood *et al.*, Endosomal signaling of the receptor for calcitonin gene-related peptide mediates pain transmission. *Proc. Natl. Acad. Sci. U.S.A.* **114**, 12309–12314 (2017).
16. R. Latorre *et al.*, Mice expressing fluorescent PAR2 reveal that endocytosis mediates colonic inflammation and pain. *Proc. Natl. Acad. Sci. U.S.A.* **119**, e2112059119 (2022).
17. P. D. Ramirez-Garcia *et al.*, A pH-responsive nanoparticle targets the neurokinin 1 receptor in endosomes to prevent chronic pain. *Nat. Nanotechnol.* **14**, 1150–1159 (2019).
18. A. R. B. Thomsen, D. D. Jensen, G. A. Hicks, N. W. Bunnett, Therapeutic targeting of endosomal G-protein-coupled receptors. *Trends Pharmacol. Sci.* **39**, 879–891 (2018).
19. J. J. Bowden *et al.*, Direct observation of substance P-induced internalization of neurokinin 1 (NK1) receptors at sites of inflammation. *Proc. Natl. Acad. Sci. U.S.A.* **91**, 8964–8968 (1994).
20. D. Bhansali *et al.*, Nanotechnology for pain management: Current and future therapeutic interventions. *Nano Today* **39**, 101223 (2021).
21. N. N. Jimenez-Vargas *et al.*, Agonist that activates the micro-opioid receptor in acidified microenvironments inhibits colitis pain without side effects. *Gut* **71**, 695–704 (2022).
22. Q. N. Mai *et al.*, A lipid-anchored neurokinin 1 receptor antagonist prolongs pain relief by a three-pronged mechanism of action targeting the receptor at the plasma membrane and in endosomes. *J. Biol. Chem.* **296**, 100345 (2021).
23. P. K. Halik *et al.*, Radiochemical synthesis and evaluation of novel radioconjugates of neurokinin 1 receptor antagonist aprepitant dedicated for NK1R-positive tumors. *Molecules* **25**, 3756 (2020).
24. A. Rizzi *et al.*, In vitro and in vivo pharmacological characterization of the novel NK(1) receptor selective antagonist Netupitant. *Peptides* **37**, 86–97 (2012).
25. M. S. Steinhoff, B. von Mentzer, P. Geppetti, C. Pothoulakis, N. W. Bunnett, Tachykinins and their receptors: Contributions to physiological control and the mechanisms of disease. *Physiol. Rev.* **94**, 265–301 (2014).
26. J. P. Lai, A. Cnaan, H. Zhao, S. D. Douglas, Detection of full-length and truncated neurokinin-1 receptor mRNA expression in human brain regions. *J. Neurosci. Methods* **168**, 127–133 (2008).
27. J. P. Lai *et al.*, Differences in the length of the carboxyl terminus mediate functional properties of neurokinin-1 receptor. *Proc. Natl. Acad. Sci. U.S.A.* **105**, 12605–12610 (2008).
28. S. Spitsin, V. Pappa, S. D. Douglas, Truncation of neurokinin-1 receptor-Negative regulation of substance P signaling. *J. Leukoc. Biol.* 10.1002/JLB.3MIR0817-348R (2018).
29. A. S. Dixon *et al.*, Nanoluc complementation reporter optimized for accurate measurement of protein interactions in cells. *ACS Chem. Biol.* **11**, 400–408 (2016).
30. R. Nehme *et al.*, Mini-G proteins: Novel tools for studying GPCRs in their active conformation. *PLoS One* **12**, e0175642 (2017).
31. Q. Wan *et al.*, Mini G protein probes for active G protein-coupled receptors (GPCRs) in live cells. *J. Biol. Chem.* **293**, 7466–7473 (2018).
32. A. M. van der Bliek *et al.*, Mutations in human dynamin block an intermediate stage in coated vesicle formation. *J. Cell Biol.* **122**, 553–563 (1993).
33. Y. Namkung *et al.*, Monitoring G protein-coupled receptor and beta-arrestin trafficking in live cells using enhanced bystander BRET. *Nat. Commun.* **7**, 12178 (2016).
34. T. Hoffmann *et al.*, Design and synthesis of a novel, achiral class of highly potent and selective, orally active neurokinin-1 receptor antagonists. *Bioorg. Med. Chem. Lett.* **16**, 1362–1365 (2006).
35. J. Schoppe *et al.*, Crystal structures of the human neurokinin 1 receptor in complex with clinically used antagonists. *Nat. Commun.* **10**, 17 (2019).
36. F. Hoffmann-Emery, H. Hilpert, M. Scalone, P. Waldmeier, Efficient synthesis of novel NK1 receptor antagonists: Selective 1,4-addition of grignard reagents to 6-chloronicotinic acid derivatives. *J. Org. Chem.* **71**, 2000–2008 (2006).
37. F. Tuluc, J. P. Lai, L. E. Kilpatrick, D. L. Evans, S. D. Douglas, Neurokinin 1 receptor isoforms and the control of innate immunity. *Trends Immunol.* **30**, 271–276 (2009).
38. G. S. Cottrell *et al.*, Endosomal endothelin-converting enzyme-1: A regulator of beta-arrestin-dependent ERK signaling. *J. Biol. Chem.* **284**, 22411–22425 (2009).
39. D. Roosterman *et al.*, Endothelin-converting enzyme 1 degrades neuropeptides in endosomes to control receptor recycling. *Proc. Natl. Acad. Sci. U.S.A.* **104**, 11838–11843 (2007).
40. R. Latorre *et al.*, Sustained endosomal release of a neurokinin-1 receptor antagonist from nanostars provides long-lasting relief of chronic pain. *Biomaterials* **285**, 121536 (2022).
41. V. Spahn *et al.*, A nontoxic pain killer designed by modeling of pathological receptor conformations. *Science* **355**, 966–969 (2017).
42. J. P. Lai *et al.*, Full-length and truncated neurokinin-1 receptor expression and function during monocyte/macrophage differentiation. *Proc. Natl. Acad. Sci. U.S.A.* **103**, 7771–7776 (2006).
43. E. Azimi *et al.*, Dual action of neurokinin-1 antagonists on Mas-related GPCRs. *JCI Insight* **1**, e89362 (2016).
44. O. Trott, A. J. Olson, AutoDock Vina: Improving the speed and accuracy of docking with a new scoring function, efficient optimization, and multithreading. *J. Comput. Chem.* **31**, 455–461 (2010).
45. X. Liu *et al.*, An allosteric modulator binds to a conformational hub in the beta2 adrenergic receptor. *Nat. Chem. Biol.* **16**, 749–755 (2020).
46. A. Allikalt *et al.*, Fluorescent ligands for dopamine D2/D3 receptors. *Sci. Rep.* **10**, 21842 (2020).
47. J. Hellmann *et al.*, Structure-based development of a subtype-selective orexin 1 receptor antagonist. *Proc. Natl. Acad. Sci. U.S.A.* **117**, 18059–18067 (2020).
48. J. Xu *et al.*, Structural insights into ligand recognition, activation, and signaling of the alpha2A adrenergic receptor. *Sci. Adv.* **8**, eabj5347 (2022).
49. S. R. Chaplan, F. W. Bach, J. W. Pogrel, J. M. Chung, T. L. Yaksh, Quantitative assessment of tactile allodynia in the rat paw. *J. Neurosci. Methods* **53**, 55–63 (1994).

Downloaded from https://www.pnas.org by NEW YORK UNIVERSITY LIBRARY-SERIALS on September 28, 2023 from IP address 216.165.95.84.

cmgh
CELLULAR AND MOLECULAR GASTROENTEROLOGY AND HEPATOLOGY

ORIGINAL RESEARCH

Elafin Reverses Intestinal Fibrosis by Inhibiting Cathepsin S-Mediated Protease-Activated Receptor 2

Ying Xie,[1,2] Lindsey Fontenot,[1] Andrea Chupina Estrada,[1] Becca Nelson,[1] Jiani Wang,[1,2] David Q. Shih,[3] Wendy Ho,[1] S. Anjani Mattai,[4] Florian Rieder,[5] Dane D. Jensen,[7] Nigel W. Bunnett,[6] and Hon Wai Koon[1]

[1]Vatche and Tamar Manoukian Division of Digestive Diseases, David Geffen School of Medicine at the University of California Los Angeles, Los Angeles, California; [2]Department of Gastroenterology, The First Hospital of China Medical University, Shenyang City, Liaoning Province, China; [3]F. Widjaja Foundation, Inflammatory Bowel & Immunobiology Research Institute, Cedars-Sinai Medical Center, Los Angeles, California; [4]Department of Medicine, David Geffen School of Medicine at the University of California Los Angeles, Los Angeles, California; [5]Department of Gastroenterology, Hepatology, and Nutrition, Digestive Diseases and Surgery Institute, Cleveland Clinic Foundation, Cleveland, Ohio; [6]Department of Molecular Pathobiology, Department of Neuroscience and Physiology, Neuroscience Institute, New York University, New York, New York; and [7]Bluestone Center for Clinical Research, New York University College of Dentistry, New York, New York

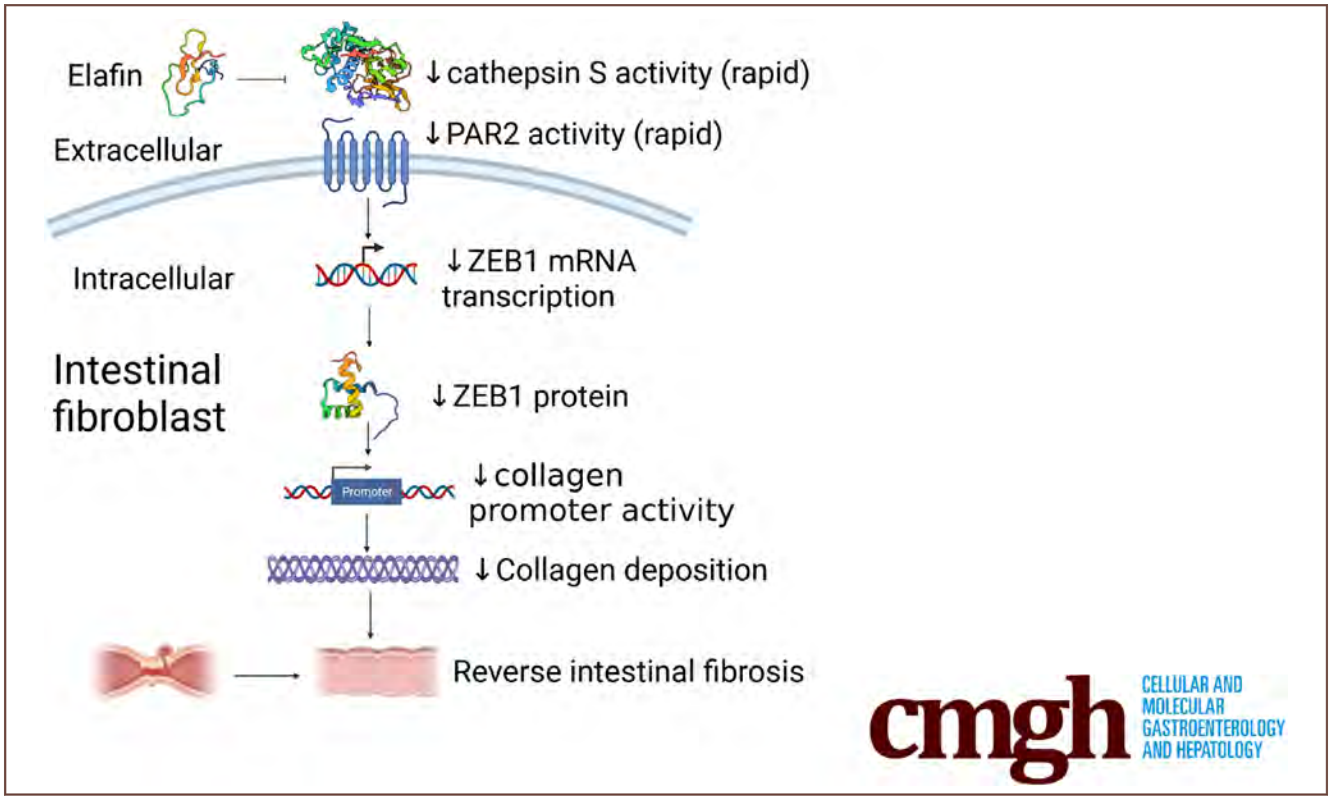

SUMMARY

Elafin inhibits cathepsin S and protease-activated receptor 2 activities and reduces collagen synthesis in intestinal fibroblasts.

BACKGROUND & AIMS: More than half of Crohn's disease patients develop intestinal fibrosis-induced intestinal strictures. Elafin is a human protease inhibitor that is downregulated in the stricturing intestine of Crohn's disease patients. We investigated the efficacy of elafin in reversing intestinal fibrosis and elucidated its mechanism of action.

METHODS: We developed a new method to mimic a stricturing Crohn's disease environment and induce fibrogenesis using stricturing Crohn's disease patient-derived serum exosomes to condition fresh human intestinal tissues and primary stricturing Crohn's disease patient-derived intestinal fibroblasts. Three mouse models of intestinal fibrosis, including SAMP1/YitFc mice, *Salmonella*-infected mice, and trinitrobenzene sulfonic acid–treated mice, were also studied. Elafin-Eudragit FS30D formulation and elafin-overexpressing construct and lentivirus were used.

RESULTS: Elafin reversed collagen synthesis in human intestinal tissues and fibroblasts pretreated with Crohn's disease patient-derived serum exosomes. Proteome arrays identified cathepsin S as a novel fibroblast-derived pro-fibrogenic protease. Elafin directly suppressed cathepsin S activity to inhibit protease-activated receptor 2 activity and Zinc finger E-box-binding homeobox 1 expression, leading to reduced collagen expression in intestinal fibroblasts. Elafin overexpression reversed ileal fibrosis in SAMP1/YitFc mice, cecal fibrosis in *Salmonella*-infected mice, and colonic fibrosis in trinitrobenzene sulfonic acid–treated mice. Cathepsin S, protease-activated receptor 2 agonist, and zinc finger E-box-binding homeobox 1 overexpression abolished the anti-fibrogenic effect of elafin in fibroblasts and all 3 mouse models of intestinal fibrosis. Oral elafin-Eudragit FS30D treatment abolished colonic fibrosis in trinitrobenzene sulfonic acid–treated mice.

CONCLUSIONS: Elafin suppresses collagen synthesis in intestinal fibroblasts via cathepsin S-dependent protease-activated receptor 2 inhibition and decreases zinc finger E-box-binding homeobox 1 expression. The reduced collagen synthesis leads to the reversal of intestinal fibrosis. Thus, modified elafin may be a therapeutic approach for intestinal fibrosis. *(Cell Mol Gastroenterol Hepatol 2022;14:841–876; https://doi.org/10.1016/j.jcmgh.2022.06.011)*

Keywords: Fibrosis; Protease; Receptor.

Intestinal stricture is a debilitating complication of inflammatory bowel disease (IBD).[1] Approximately 30%–50% of Crohn's disease (CD) patients develop intestinal strictures.[2,3] Anti–tumor necrosis factor (TNF) alpha neutralizing antibodies fail to reverse intestinal strictures in CD patients.[4] Strictureplasty can alleviate mild and simple bowel narrowing, but surgical resection may be needed to resolve severe and complex bowel obstructions.[5] However, surgery may adversely affect the patients' quality of life. Thus, new therapeutic approaches to intestinal fibrosis are needed.

To discover stricture-related targets, we compared colonic mRNA expression in stricturing and non-stricturing CD patients using whole-transcriptome RNA sequencing.[6] Consistent with a similar study,[4] stricturing CD patients have increased fibrosis-associated extracellular matrix gene and transcriptional regulator expression. However, we noted that these patients had impaired epithelial gene expression such as keratin, mucin, and antimicrobial peptide (elafin).[6]

IBD patients also carry specific patterns of microRNAs, proteins, and lipids in serum exosomes.[7] Exosomes are small vesicles in blood and body fluids.[8] Treatment of human intestinal fibroblasts with serum exosomes from stricturing CD patients (CDSE) caused increased mRNA expression of collagen type I alpha 2 (COL1A2) and alpha-smooth muscle actin.[6] Components in serum exosomes can regulate intestinal cell functions.[9] Although the pro-fibrogenic mechanism of CDSE is not fully understood, CDSE has lower miR205 expression than serum exosomes in non-stricturing CD patients.[6] The miR205 possesses anti-fibrogenic properties as its inhibition increases collagen expression in intestinal fibroblasts.[6] Collagen is a prominent extracellular matrix component in the CD intestinal strictures.[4,6] Therefore, CDSE treatment of intestinal fibroblasts can partially mimic a stricturing CD environment in vitro.

An antimicrobial peptide (cathelicidin) possesses anti-fibrogenic effects[10] but is cytotoxic.[11] Another human antimicrobial peptide (elafin) functions as a protease inhibitor.[12,13] IBD patients have increased elafin protein levels in circulation[6] but reduced elafin mRNA expression in the peripheral blood leukocytes.[14,15] Patients with ulcerative colitis have increased colonic elafin mRNA expression.[6,16] Several groups reported different colonic elafin mRNA and protein expression in CD patients.[6,17,18] Interestingly, stricturing CD patients have lower colonic elafin expression than non-stricturing CD patients.[6]

Elafin may also be used for therapeutic purposes. Elafin protects intestinal barrier function by inhibiting elastase activity.[19] Adenoviral delivery of elafin ameliorated chemically induced colitis.[20] In mice, oral administration of elafin-expressing *Lactococcus* inhibited colitis and gluten-related disorders.[8,21] Oral elafin formulation was as efficacious as lentiviral elafin overexpression in reversing obesity and diabetes in high-fat diet–treated mice.[22] Intravenous infusion of elafin to increase circulating levels (4.5 μg/mL) is also safe without affecting plasma elastase activity and cytokine levels in patients.[23] Therefore, elafin is an attractive therapeutic target against intestinal inflammation and fibrosis.

Elafin, an antiprotease, may be helpful against intestinal fibrosis because proteases participate in fibrogenesis. For example, tryptase can induce collagen expression in human colonic fibroblasts,[24] whereas *Salmonella*-infected mice have increased protease expression in fibrotic cecal tissues.[25] These previous studies provided a premise to explore whether elafin can inhibit fibrogenesis in intestinal fibroblasts via a specific antiprotease mechanism, leading to the amelioration of intestinal fibrosis.

This study discovered the functions of novel mediators of fibrogenesis. We elucidated a new anti-fibrogenic mechanism of elafin using primary stricturing CD patient-derived intestinal fibroblasts (CD-HIF), primary human colonic epithelial cells, Crohn's disease patient-derived peripheral blood mononuclear cells (PBMCs), fresh human intestinal tissues, and 3 CD-relevant mouse models of intestinal fibrosis, including well-established chronic trinitrobenzene

Abbreviations used in this paper: **ANOVA, analysis of variance; CD, Crohn's disease; CD-HIF, Crohn's disease patient-derived primary intestinal fibroblasts; CDSE, Crohn's disease patients' serum exosomes; COL1A2, collagen type I alpha 2; CTSS/Ctss, gene name of cathepsin S or CatS; HPMC, hydroxypropyl methylcellulose; IBD, inflammatory bowel disease; ODA, overall disease activity; PAR1/2, protease-activating receptor 1/2; PMBC, peripheral blood mononuclear cell; SLPI, secretory leukocyte protease inhibitor; TGF-β1, transforming growth factor beta 1; TNBS, trinitrobenzene sulfonic acid; TNF, tumor necrosis factor; ZEB1, zinc finger E-box-binding homeobox 1.**

Most current article

© 2022 The Authors. Published by Elsevier Inc. on behalf of the AGA Institute. This is an open access article under the CC BY license (http://creativecommons.org/licenses/by/4.0/).

2352-345X
https://doi.org/10.1016/j.jcmgh.2022.06.011

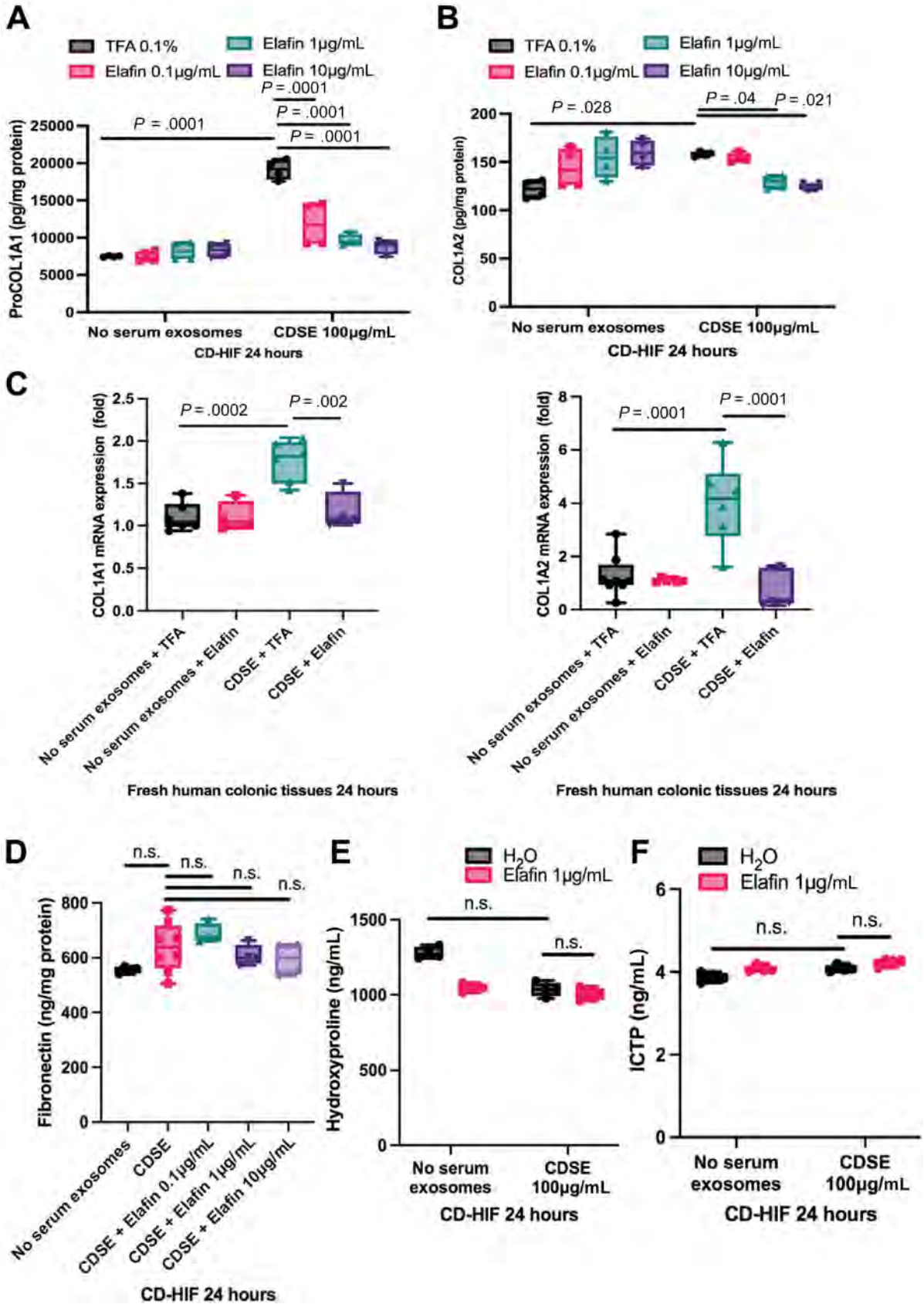
A
TFA 0.1%
Elafin 0.1µg/mL
Elafin 1µg/mL
Elafin 10µg/mL
P = .0001
P = .0001
P = .0001
P = .0001
ProCOL1A1 (pg/mg protein)
25000
20000
15000
10000
5000
0
No serum exosomes
CDSE 100µg/mL
CD-HIF 24 hours
B
TFA 0.1%
Elafin 0.1µg/mL
Elafin 1µg/mL
Elafin 10µg/mL
P = .028
P = .04
P = .021
COL1A2 (pg/mg protein)
200
150
100
50
0
No serum exosomes
CDSE 100µg/mL
CD-HIF 24 hours
C
P = .0002
P = .002
COL1A1 mRNA expression (fold)
2.5
2.0
1.5
1.0
0.5
0.0
No serum exosomes + TFA
No serum exosomes + Elafin
CDSE + TFA
CDSE + Elafin
Fresh human colonic tissues 24 hours
P = .0001
P = .0001
COL1A2 mRNA expression (fold)
8
6
4
2
0
No serum exosomes + TFA
No serum exosomes + Elafin
CDSE + TFA
CDSE + Elafin
Fresh human colonic tissues 24 hours
D
n.s.
n.s.
n.s.
n.s.
Fibronectin (ng/mg protein)
800
600
400
200
0
No serum exosomes
CDSE
CDSE + Elafin 0.1µg/mL
CDSE + Elafin 1µg/mL
CDSE + Elafin 10µg/mL
CD-HIF 24 hours
E
H2O
Elafin 1µg/mL
n.s.
n.s.
Hydroxyproline (ng/mL)
1500
1000
500
0
No serum exosomes
CDSE 100µg/mL
CD-HIF 24 hours
F
H2O
Elafin 1µg/mL
n.s.
n.s.
ICTP (ng/mL)
6
4
2
0
No serum exosomes
CDSE 100µg/mL
CD-HIF 24 hours

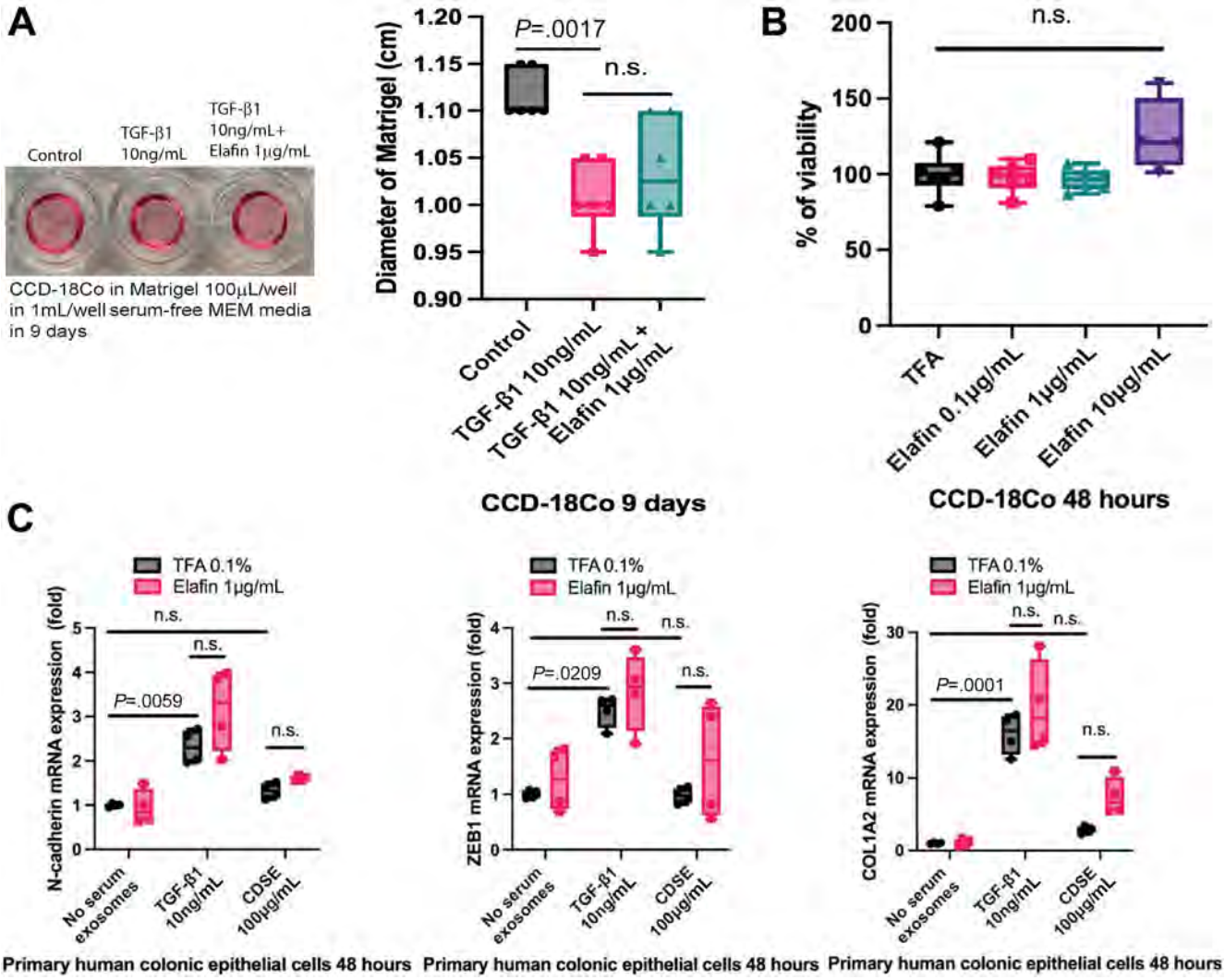

Figure 2. (*A*) Extracellular matrix (ECM) contraction assay. Human colonic CCD-18Co fibroblasts were embedded in 100 μL/well of Matrigel (Corning #356234) and covered by 1 mL/well serum-free minimal essential medium (MEM). TGF-β1 (10 ng/mL) and elafin (1 μg/mL) were added to the medium on day 0. The diameter of the Matrigel was measured on day 9. TGF-β1 treatment significantly reduced the Matrigel diameter, indicating increased ECM stiffness. Shrinkage was unaffected by elafin. Results were pooled from 3 independent experiments. Ordinary one-way ANOVA with Tukey test. (*B*) Human colonic CCD-18Co fibroblasts were treated with elafin for 48 hours, followed by addition of MTS assay reagent (G5421; Promega, Madison, WI). Absorbance was determined at 490 nm. Results were pooled from 4 independent experiments. Ordinary one-way ANOVA with Tukey test. (*C*) Serum-starved primary human colonic epithelial cells were pretreated with TGF-β1 (10 ng/mL) or CDSE (100 μg/mL) for 2 hours and then incubated with elafin for 48 hours. N-cadherin, ZEB1, and COL1A2 mRNA expression was determined by real-time reverse transcription polymerase chain reaction. TGF-β1, but not CDSE, induced N-cadherin, ZEB1, and COL1A2 mRNA expression, unaffected by elafin. Results were pooled from 4 independent experiments. Ordinary one-way ANOVA with Tukey test.

Figure 1. (***See previous page***). **(*A* and *B*) Primary stricturing CD patient-derived intestinal fibroblasts (CD-HIF) were pretreated with or without 100 μg/mL stricturing Crohn's disease patients' serum exosomes (CDSE).** Two hours later, elafin was added and further incubated for 24 hours. n = 4 patients; 4 independent experiments. Ordinary one-way ANOVA with Tukey test. (*C*) Fresh human colonic tissues from 4 colon cancer patients were incubated in serum-free RPMI1640 medium with or without 100 μg/mL CDSE. Two hours later, elafin (1 μg/mL) was added and incubated for 24 hours. n = 6 patients. Ordinary one-way ANOVA with Tukey test. (*D–F*) Primary stricturing CD-HIF were pretreated with or without 100 μg/mL CDSE. Two hours later, elafin was added and further incubated for 24 hours. ProCOL1A1, COL1A2, and fibronectin in cell lysates and hydroxyproline and C-telopeptide of type I collagen/ICTP in conditioned media were determined by ELISA. n = 4 patients; 4 independent experiments. Ordinary one-way ANOVA with Tukey test.

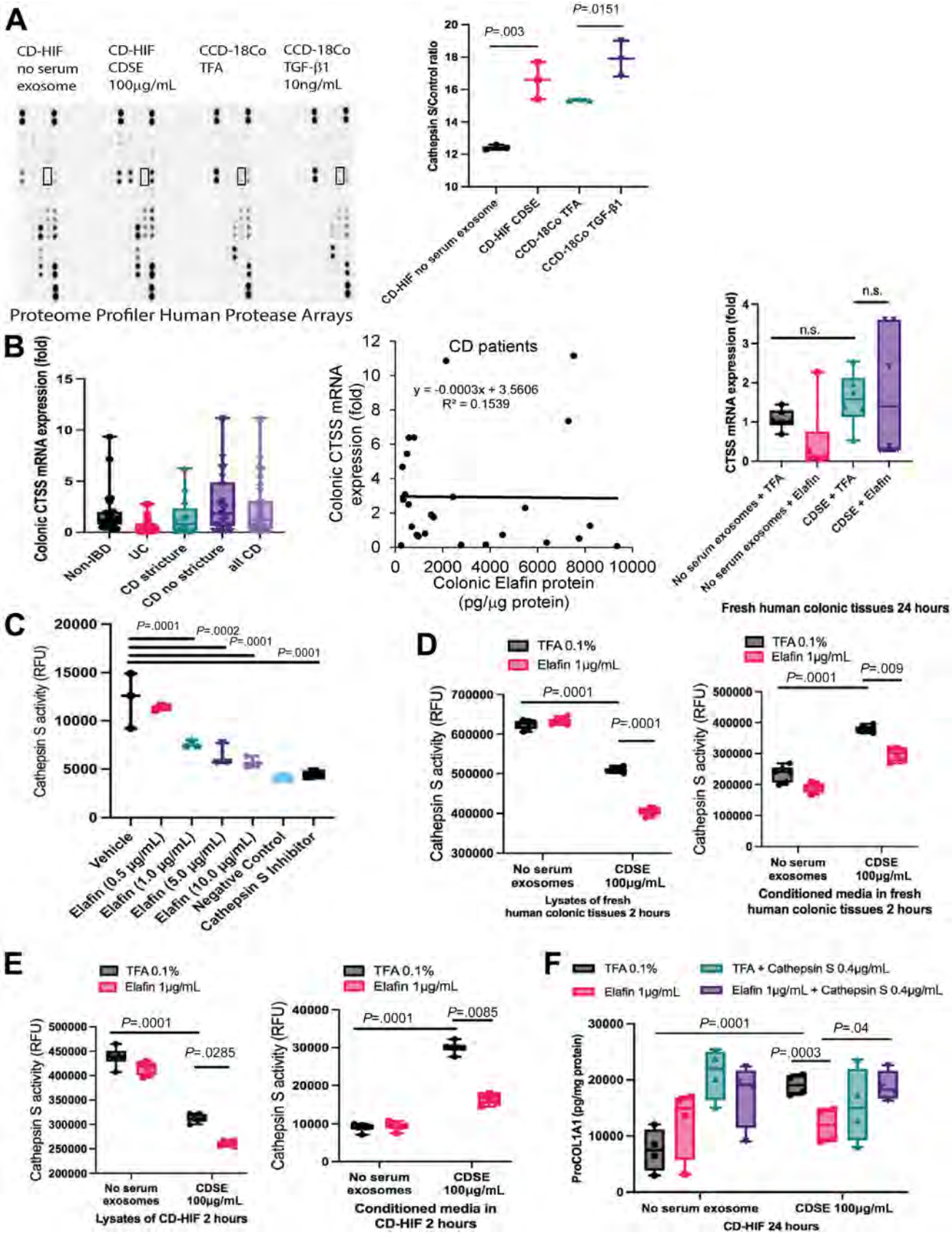
A
CD-HIF no serum exosome
CD-HIF CDSE 100µg/mL
CCD-18Co TFA
CCD-18Co TGF-β1 10ng/mL
Proteome Profiler Human Protease Arrays
Cathepsin S/Control ratio
P=.003
P=.0151
CD-HIF no serum exosome
CD-HIF CDSE
CCD-18Co TFA
CCD-18Co TGF-β1
B
Colonic CTSS mRNA expression (fold)
Non-IBD
UC
CD stricture
CD no stricture
all CD
CD patients
y = -0.0003x + 3.5606
R² = 0.1539
Colonic CTSS mRNA expression (fold)
Colonic Elafin protein (pg/µg protein)
CTSS mRNA expression (fold)
n.s.
n.s.
No serum exosomes + TFA
No serum exosomes + Elafin
CDSE + TFA
CDSE + Elafin
Fresh human colonic tissues 24 hours
C
Cathepsin S activity (RFU)
P=.0001
P=.0002
P=.0001
P=.0001
Vehicle
Elafin (0.5 µg/mL)
Elafin (1.0 µg/mL)
Elafin (5.0 µg/mL)
Elafin (10.0 µg/mL)
Negative Control
Cathepsin S Inhibitor
D
TFA 0.1%
Elafin 1µg/mL
Cathepsin S activity (RFU)
P=.0001
P=.0001
No serum exosomes
CDSE 100µg/mL
Lysates of fresh human colonic tissues 2 hours
TFA 0.1%
Elafin 1µg/mL
P=.0001
P=.009
Cathepsin S activity (RFU)
No serum exosomes
CDSE 100µg/mL
Conditioned media in fresh human colonic tissues 2 hours
E
TFA 0.1%
Elafin 1µg/mL
Cathepsin S activity (RFU)
P=.0001
P=.0285
No serum exosomes
CDSE 100µg/mL
Lysates of CD-HIF 2 hours
TFA 0.1%
Elafin 1µg/mL
Cathepsin S activity (RFU)
P=.0001
P=.0085
No serum exosomes
CDSE 100µg/mL
Conditioned media in CD-HIF 2 hours
F
TFA 0.1%
Elafin 1µg/mL
TFA + Cathepsin S 0.4µg/mL
Elafin 1µg/mL + Cathepsin S 0.4µg/mL
ProCOL1A1 (pg/mg protein)
P=.0001
P=.04
P=.0003
No serum exosome
CDSE 100µg/mL
CD-HIF 24 hours

sulfonic acid (TNBS)–mediated colitis,[26] *Salmonella*-infected mice with cecal Th1/Th17 cytokine activation,[27] and CD-like SAMP1/YitFc mice.[28,29] We also used an orally active elafin formulation to determine the feasibility of oral elafin therapy against intestinal fibrosis.

Results

Elafin Inhibited Collagen Synthesis in Activated Human Colonic Tissues and Fibroblasts

CDSE carries CD stricture-related mediators that induce fibrogenesis in intestinal fibroblasts.[6] CDSE induced procollagen I alpha 1 expression with modest COL1A2 protein induction in CD-HIF (Figure 1*A* and *B*). Similarly, CDSE pretreatment induced COL1A1 and COL1A2 mRNA expression in fresh colonic tissues from colon cancer patients (Figure 1*C*). Elafin abolished the induction of collagen expression in CDSE-pretreated CD-HIF and colonic tissues (Figure 1*A*–*C*).

Elafin did not affect the expression of extracellular matrix protein fibronectin and secretion of collagen degradation products (hydroxyproline and C-telopeptide of type I collagen/ICTP) in CDSE-treated CD-HIF (Figure 1*D*–*F*). In addition, elafin did not affect extracellular matrix contraction and cell viability of colonic fibroblasts (Figure 2*A* and *B*). Transforming growth factor beta 1 (TGF-β1), but not CDSE, induced N-cadherin, zinc finger E-box-binding homeobox 1 (ZEB1), and COL1A2 mRNA expression (Figure 2*C*). N-cadherin and ZEB1 are involved in epithelial-mesenchymal transition.[30,31] This epithelial-mesenchymal transition–like response was not affected by elafin treatment (Figure 2*C*). These findings suggested that elafin only regulates collagen synthesis in intestinal fibroblasts.

Activated Intestinal Fibroblasts Secreted Cathepsin S

We next attempted to discover the upstream target of elafin. Elafin inhibits protease activity, but the fibrosis-mediating protease in intestinal fibroblasts was previously unknown. Protease arrays showed that both CDSE and TGF-β1 induced cathepsin S secretion in the conditioned media of CD-HIF and CCD-18Co fibroblasts, respectively (Figure 3*A*). TGF-β1 activates CCD-18Co fibroblasts with increased collagen synthesis.[32] Cathepsin S is a cysteine protease that can degrade elastin.[33]

Colonic cathepsin S mRNA (CTSS) expression does not correlate with IBD, intestinal stricture, or colonic elafin protein expression in CD patients (Figure 3*B*, left and middle panels). In addition, elafin treatment did not affect CTSS mRNA expression in CDSE-treated fresh human colonic tissues (Figure 3*B*, right panel).

Elafin Inhibited Fibrogenesis by Reducing Cathepsin S Activity

We determined the direct interactions between elafin and cathepsin S proteins in cell-free conditions. Interestingly, elafin directly inhibited cathepsin S enzymatic activity in a dose-dependent manner (Figure 3*C*). The inhibitory concentrations against cathepsin S (1–10 μmol/L) were similar to the anti-fibrogenic concentrations of elafin in CDSE-treated CD-HIF (Figure 1*A*). CDSE reduced cathepsin S activity in lysates but increased cathepsin S activity in conditioned media of fresh human colonic tissues and CD-HIF (Figure 3*D* and *E*), suggesting that active cathepsin S was secreted into the conditioned media. Elafin reduced

Figure 3. (***See previous page***). **(*A, left panel*) Serum-starved CD-HIF were treated with 100 μg/mL CDSE for 2 hours.** Serum-starved CCD-18Co colonic fibroblasts were treated with 10 ng/mL TGF-β1 for 2 hours. Conditioned media were loaded to Proteome Profiler Human Protease Arrays (ARY021B; R&D Systems). A Bio-Rad ChemiDoc Imaging system captured the images. The *rectangles* highlighted the cathepsin S expression. (*A, right panel*) Quantification of cathepsin S signals (B7-8) and control signals (A1-2 and E1-2) using Bio-Rad Image Lab Software. Results were pooled from 3 independent experiments. Student *t* test was used to compare no serum exosome and CDSE groups. (*B, left panel*) Colonic cathepsin S mRNA expression in 40 non-IBD, 52 UC, 28 non-stricturing CD, and 15 stricturing CD patients was determined by real-time reverse transcription polymerase chain reaction. Ordinary one-way ANOVA test did not find any significant differences. (*B, middle panel*) Colonic cathepsin S mRNA (CTSS) expression in 43 CD patients is not correlated with colonic elafin mRNA expression. (*B, right panel*) Fresh human colonic tissues from 4 colon cancer patients were incubated in serum-free RPMI1640 media with or without 100 μg/mL CDSE. Two hours later, elafin (1 μg/mL) was added and incubated for 24 hours. Ordinary one-way ANOVA test did not find any significant differences. (*C*) Cathepsin S activity assay was performed by incubating 2 μL of CS substrate (200 μmol/L final concentration), 94 μL CS reaction buffer, 2 μL cathepsin S inhibitor provided by the assay kit, 1 μL cathepsin S (0.4 μg/mL final concentration), and 1 μL elafin (0.5–10 μg/mL final concentration) at 37°C for 1 hour. Cathepsin S activity was represented by relative fluorescence units (RFU). Results were pooled from 3 independent experiments. Ordinary one-way ANOVA with Tukey test. (*D*) Fresh human colonic tissues were pretreated with 100 μg/mL CDSE for 2 hours, followed by elafin 1 μg/mL for 2 hours. Conditioned media were collected. Each piece of tissue was homogenized in 500 μL CS cell lysis buffer. Next, 50 μg of tissue lysate supernatants in 50 μL CS lysis buffer or 50 μL of conditioned media were mixed with 2 μL CS substrates (200 μmol/L final concentration) and 48 μL CS reaction buffer and incubated for 1 hour. Cathepsin S activity was represented by relative fluorescence units (RFU). n = 6 patients. Ordinary one-way ANOVA with Tukey test. (*E*) CD-HIF in 96-well plates were pretreated with 100 μg/mL CDSE for 2 hours, followed by elafin 1 μg/mL for 2 hours. Conditioned media were collected. Cells were then lysed in 200 μL/well CS cell lysis buffer. Next, 50 μg of cell lysates in 50 μL CS lysis buffer or 50 μL of conditioned media were mixed with 2 μL of CS substrate (200 μmol/L final concentration) and 48 μL CS reaction buffer and incubated at 37°C for 1 hour. Cathepsin S activity was represented by relative fluorescence units (RFU). Results were pooled from 6 independent experiments. Ordinary one-way ANOVA with Tukey test. (*F*) Serum-starved CD-HIF were pretreated with either 0.1% TFA r 0.4 μg/mL cathepsin S (1183-CY-010; R&D Systems) for 30 minutes, followed by 100 μg/mL CDSE. Two hours later, elafin (1 μg/mL) was added and incubated for 24 hours. ProCOL1A1 protein was determined by ELISA. Results were pooled from 4 experiments. Ordinary one-way ANOVA with Tukey test.

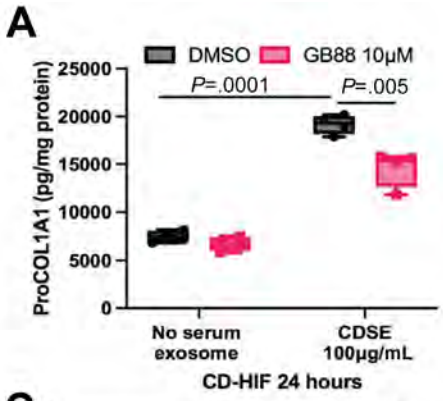

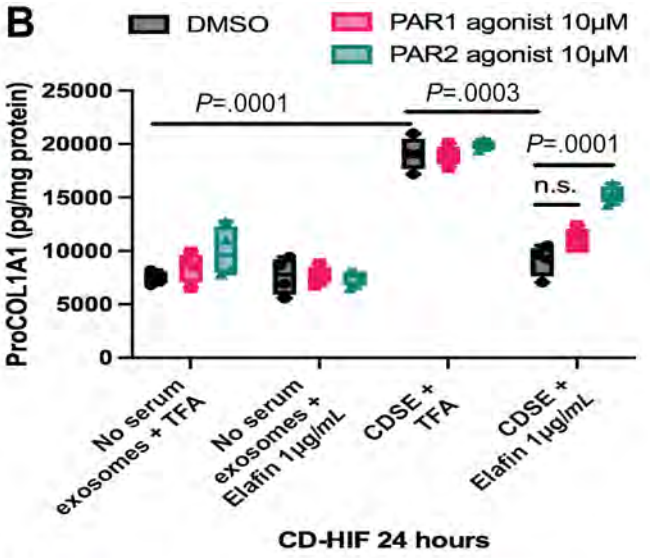

C

Over-expressed genes in CD stricture	log2(Fold Change)	Under-expressed genes in CD stricture	log2(Fold Change)
ACTG2	24.52	EIF3CL	-24.74
HSPB6	23.88	S100A10	-23.64
HSPA1A	23.72	S100A6	-23.64
MST1L	23.31	MUC5B	-12.12
PRELP	23.31	DEFA5	-11.87
ITGA2	23.29	MUC13	-11.76
CCR7	23.13	MUC1	-11.40
COL1A2	23.13	KRT19	-11.15
HSPG2	23.13	EIF2S3B	-11.12
ZEB1	23.13	MAPK3	-10.53
PPP1R12A	22.91	DEFA6	-10.12
ADAMTS1	22.35	PRDX5	-10.08
GPR107	22.35	PRDX2	-9.52
HSPA2	22.35	NFKBIA	-9.52
ZNF862	22.35	PI3	-9.52
GPR26	21.41	MUC17	-9.52
ITGB1	21.41		
FN1	11.88		

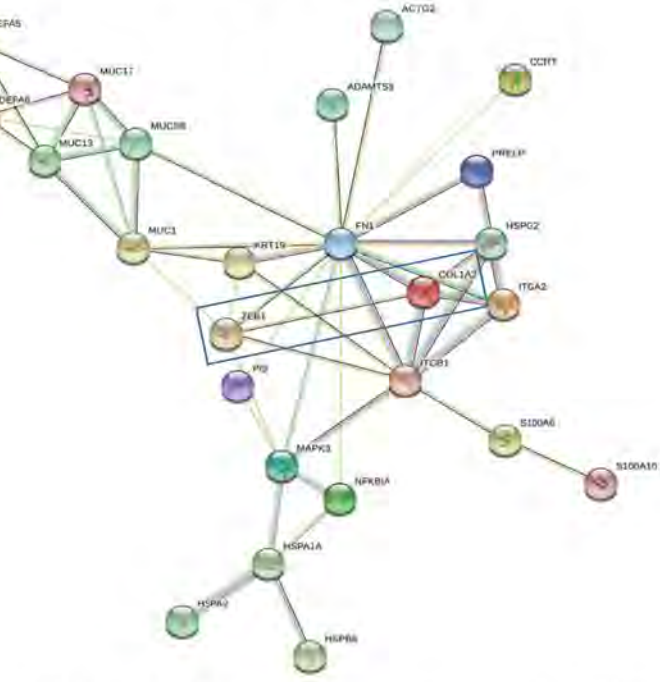

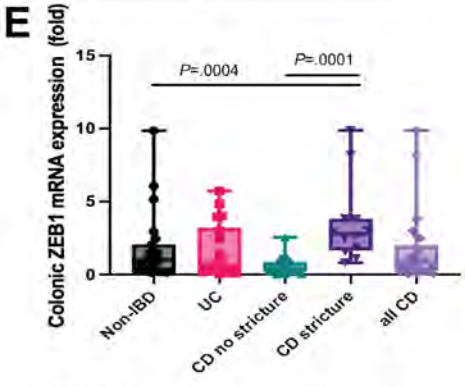

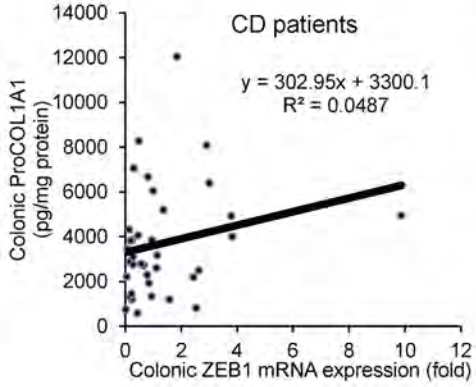

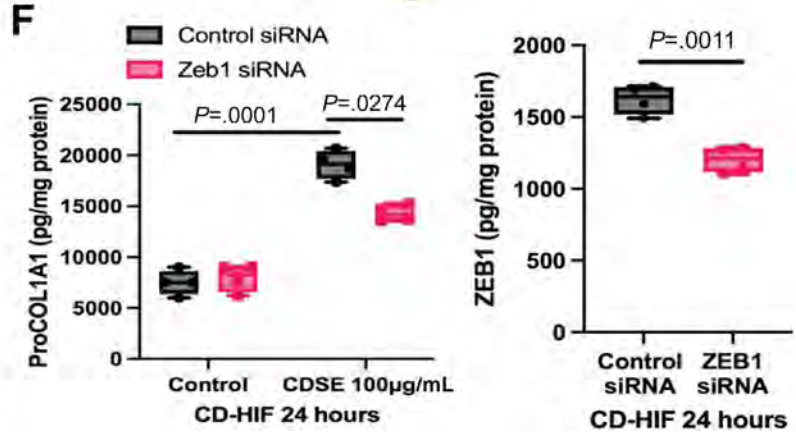

cathepsin S activity in lysates and conditioned media of CDSE-pretreated fresh human colonic tissues and CD-HIF (Figure 3*D* and *E*). Elafin might mediate the anti-fibrogenic effect by inhibiting cathepsin S activity as the addition of cathepsin S reversed elafin-mediated inhibition of ProCOL1A1 expression in CDSE-pretreated CD-HIF (Figure 3*F*).

Elafin Mediated Anti-Fibrogenic Effect via Protease-Activated Receptor 2 Inhibition

Because cathepsin S activates protease-activated receptor 2 (PAR2) activity,[34–36] we further determined the involvement of PAR2 in the anti-fibrogenic effect of elafin. PAR2 inhibitor GB88 significantly reduced ProCOL1A1 expression in CDSE-pretreated CD-HIF (Figure 4*A*). The elafin-mediated inhibition of ProCOL1A1 expression was abolished by a PAR2 agonist but not a PAR1 agonist (Figure 4*B*). These experiments suggested that elafin inhibits cathepsin S and then PAR2 activity, leading to reduced fibrogenesis.

Zinc Finger E-Box-Binding Homeobox 1 Is a Target in Intestinal Fibrosis

Whole-transcriptome RNA sequencing showed different colonic gene expressions in stricturing and non-stricturing CD patients.[6] To discover the downstream target of elafin, we ranked the differentially expressed genes (Figure 4*C*). STRING database analysis showed that ZEB1 is functionally associated with COL1A2 (Figure 4*D*) because ZEB1 regulates collagen promoter activity and expression.[37,38] Stricturing CD patients had significantly higher colonic ZEB1 mRNA expression than non-IBD and non-stricturing CD patients (Figure 4*E*, upper panel). In addition, colonic ZEB1 mRNA expression is positively correlated with ProCOL1A1 protein expression in CD patients (Figure 4*E*, lower panel), suggesting its association with intestinal fibrosis. ZEB1 regulates fibrogenesis as siRNA-mediated ZEB1 inhibition reduced collagen expression in CDSE-treated CD-HIF (Figure 4*F*, left panel). Transfection of ZEB1 siRNA was efficient in reducing ZEB1 protein expression (Figure 4*F*, right panel).

Elafin Suppressed Collagen Synthesis via Zinc Finger E-Box-Binding Homeobox 1 Inhibition

Although ZEB1 overexpression did not augment collagen synthesis in CDSE-pretreated CD-HIF, it abolished the anti-fibrogenic effect of elafin (Figure 5*A*). Transfection of the ZEB1-overexpressing construct efficiently increased ZEB1 protein expression (Figure 5*B*). Elafin might reduce ZEB1 protein expression via PAR2 inhibition because this inhibition was reversed by a PAR2 agonist (Figure 5*C*). These experiments indicated that elafin inhibits collagen synthesis via sequential inhibition of cathepsin S and PAR2 activity, followed by ZEB1 expression in intestinal fibroblasts.

Like CD-HIF, elafin inhibited ZEB1 mRNA expression in CDSE-treated fresh human colonic tissues (Figure 5*D*). However, intestinal strictures can occur in the ileum. Elafin inhibited CDSE-induced collagen and ZEB1 mRNA expression in fresh ileal tissues from stricturing CD patients (Figure 5*E* and *F*), suggesting that elafin may be useful for resolving ileal strictures in CD patients. Therefore, it is justified to use 3 mouse models of intestinal fibrosis to validate the mechanistic relationships between elafin, cathepsin S, PAR2, and Zeb1 in vivo.

Elafin Overexpression Inhibited Intestinal fibrosis in SAMP1/YitFc, Salmonella, and Trinitrobenzene Sulfonic Acid Mouse Models

SAMP1/YitFc mice are an established mouse model for studying CD because they develop spontaneous CD-like ileitis with preexisting ileal fibrosis at 40 weeks of age (Figure 6*A*).[28] There was no significant change in body weight in SAMP1/YitFc mice from 10 to 42 weeks of age (Figure 6*B*). In addition, the young 10-week-old SAMP1/YitFc mice developed spontaneous ileitis but not fibrosis (Figure 6*C*).

There is no consensus approach to characterize intestinal fibrosis. Therefore, we attempted to include commonly reported fibrosis- and inflammation-related parameters to compare disease activity between groups and models. Lentiviral elafin overexpression reversed preexisting ileal fibrosis with lowered histology score, fibrosis score, and overall disease activity (ODA) in SAMP1/YitFc mice from 40

Figure 4. (***See previous page***). **(*A* and *B*) Serum-starved CD-HIF were pretreated with 0.8% DMSO, 10 μmol/L PAR2 inhibitor GB88 (HY-120261; MCE), 10 μmol/L PAR1 agonist TRAP-6 (HY-P0078; MCE), or 10 μmol/L PAR2 agonist SLIGKV-NH_2 (HY-P0283; MCE).** An hour later, the fibroblasts were exposed to 100 μg/mL CDSE. Two hours later, elafin (1 μg/mL) was added and incubated for 24 hours. Results were pooled from 4 experiments. Ordinary one-way ANOVA with Tukey test. (*C*) The most differentially expressed genes found in whole-transcriptome RNA sequencing in the colonic tissues of 2 stricturing and 2 non-stricturing CD patients. (*D*) STRING database analysis shows protein interaction association between the most differentially expressed genes in stricturing versus non-stricturing CD patients. (*E, upper panel*) Colonic ZEB1 mRNA expression in 40 non-IBD, 52 UC, 28 non-stricturing CD, and 15 stricturing CD patients. Stricturing CD patients have significantly higher colonic ZEB1 mRNA expression than non-stricturing CD patients. Ordinary one-way ANOVA with Tukey test. (*E, lower panel*) Positive correlation between colonic ZEB1 mRNA and collagen (ProCOL1A1) protein expression in 43 CD patients. (*F*) Serum-starved CD-HIF were transfected with either control (sc-37007; Santa Cruz Biotechnology, Dallas, TX) or ZEB1 (sc-38643; Santa Cruz Biotechnology) siRNA via lipofectamine 3000 overnight, followed by 100 μg/mL CDSE for 24 hours. ZEB1 and ProCOL1A1 proteins were measured by ELISA. Results were pooled from 4 experiments. Ordinary one-way ANOVA with Tukey test for left panel. Student *t* test was used to compare ZEB1 expression between control siRNA and ZEB1 siRNA groups on right panel.

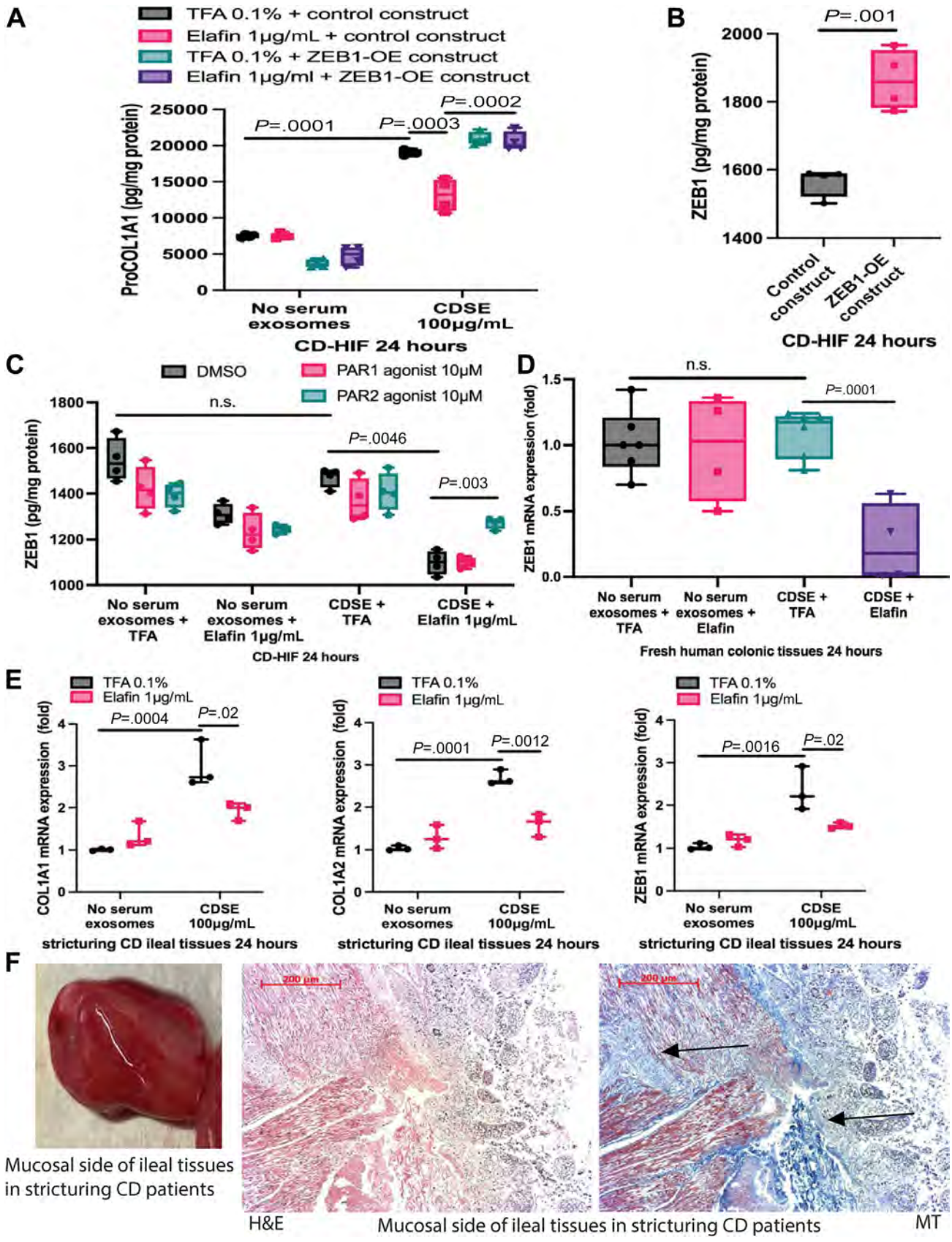
A
TFA 0.1% + control construct
Elafin 1µg/mL + control construct
TFA 0.1% + ZEB1-OE construct
Elafin 1µg/ml + ZEB1-OE construct
ProCOL1A1 (pg/mg protein)
P=.0001
P=.0003
P=.0002
No serum exosomes
CDSE 100µg/mL
CD-HIF 24 hours
B
P=.001
ZEB1 (pg/mg protein)
Control construct
ZEB1-OE construct
CD-HIF 24 hours
C
DMSO
PAR1 agonist 10µM
PAR2 agonist 10µM
ZEB1 (pg/mg protein)
n.s.
P=.0046
P=.003
No serum exosomes + TFA
No serum exosomes + Elafin 1µg/mL
CDSE + TFA
CDSE + Elafin 1µg/mL
CD-HIF 24 hours
D
ZEB1 mRNA expression (fold)
n.s.
P=.0001
No serum exosomes + TFA
No serum exosomes + Elafin
CDSE + TFA
CDSE + Elafin
Fresh human colonic tissues 24 hours
E
TFA 0.1%
Elafin 1µg/mL
COL1A1 mRNA expression (fold)
P=.0004
P=.02
No serum exosomes
CDSE 100µg/mL
stricturing CD ileal tissues 24 hours
COL1A2 mRNA expression (fold)
P=.0001
P=.0012
stricturing CD ileal tissues 24 hours
ZEB1 mRNA expression (fold)
P=.0016
P=.02
stricturing CD ileal tissues 24 hours
F
Mucosal side of ileal tissues in stricturing CD patients
200 µm
H&E
Mucosal side of ileal tissues in stricturing CD patients
MT

to 42 weeks (Figure 6*C*–*F*). The disease activity parameters of SAMP1/YitFc mice are shown in Table 1.

Similarly, *Salmonella* infection induced cecitis, followed by cecal fibrosis with mucosal disruption, immune cell infiltration, and collagen deposition on day 21 (Figure 7*A*).[39] There was no significant change in body weight in the infected mice from day 0 to day 21 (Figure 7*B*). Notably, lentiviral elafin overexpression (from day 14 to 21) ameliorated cecal fibrosis with lowered histology score, fibrosis score, and ODA in the infected mice (Figure 7*C*–*F*). The disease activity parameters of *Salmonella*–infected mice are shown in Table 2.

Multiple intracolonic TNBS injections induced colonic fibrosis (Figure 8*A*)[10,40] but did not cause weight loss in mice (Figure 8*B*). Intracolonic transfection of elafin-overexpressing constructs ameliorated colonic fibrosis with lowered histology score, fibrosis score, and ODA in the TNBS-treated mice within 7 days (Figure 8*C*–*F*). The disease activity parameters of TNBS-treated mice are shown in Table 3. In general, elafin overexpression consistently reduced intestinal fibrosis in these 3 mouse models.

Anti-TNFα neutralizing antibodies are widely used for treating intestinal inflammation among IBD patients. For comparison, injection of anti-TNFα neutralizing antibodies partially ameliorated colitis with moderately lowered histology score and ODA (Figure 8*C*, *D*, and *F*). However, this treatment failed to reverse colonic fibrosis because the fibrosis score remained high (Figure 8*C* and *E*).

Inhibition of Ctss, Protease-Activating Receptor 2, and Zinc Finger E-Box-Binding Homeobox 1 Ameliorated Intestinal Fibrosis in Vivo

As we demonstrated the involvement of cathepsin S, PAR2, and ZEB1 in the anti-fibrogenic effect of elafin in intestinal fibroblasts (Figures 3–5), we further validated their roles in intestinal development in vivo. Inhibition of Ctss, PAR2, and Zeb1 ameliorated ileal fibrosis in SAMP/YitFc mice (Figure 9*A*), cecal fibrosis in *Salmonella*-infected mice (Figure 10*A*), and colonic fibrosis in TNBS-treated mice (Figure 11*A*), with reduced histology scores (Figures 9*B*, 10*B*, and 11*B*), fibrosis scores (Figures 9*C*, 10*C*, and 11*C*), and ODAs (Figures 9*C*, 10*C*, and 11*C*) in all models. Therefore, cathepsin S, PAR2, and ZEB1 regulate intestinal fibrosis development in mice.

Anti-Fibrogenic Effect of Elafin Is Dependent on Ctss, Protease-Activating Receptor 2, and Zinc Finger E-Box-Binding Homeobox 1 Inhibition in Vivo

We further manipulated cathepsin S, PAR2, and ZEB1 in elafin-overexpressing mice to determine their involvement in the elafin-mediated anti-fibrogenic effect. Lentiviral Ctss and Zeb1 overexpression and PAR2 agonist reversed the anti-fibrogenic effect of elafin overexpression in SAMP1/YitFc mice (Figure 9*A*), *Salmonella*-infected mice (Figure 10*A*), and TNBS-treated mice (Figure 11*A*), with increased histology scores (Figures 9*B*, 10*B*, and 11*B*), fibrosis scores (Figures 9*C*, 10*C*, and 11*C*), and ODAs (Figures 9*C*, 10*C*, and 11*C*) in all models. The efficacies of pharmacologic and molecular manipulations are shown in Table 4. Overall, the anti-fibrogenic effect of elafin overexpression depends on cathepsin S, PAR2, and Zeb1.

Ctss-siRNA lentivirus diminished the intestinal tissue Ctss mRNA expression and cathepsin S activities in fibrotic mice (Tables 1–4, Figure 12*A*–*C*). Conversely, Ctss-overexpressing lentivirus reversed the elafin-mediated reduction of intestinal tissue Ctss mRNA expression and cathepsin S activities in elafin-overexpressing mice (Tables 1–4, Figure 12*A*–*C*). Thus, lentiviral manipulation of Ctss expression affected intestinal cathepsin S activity.

Lentiviral elafin, Ctss, and Zeb1 overexpression and PAR2 agonist did not affect the normal ileal histology and body weight in control non-fibrotic AKR mice (Figures 13 and 14*A*). Similarly, these manipulations did not affect body weight in fibrotic SAMP1/YitFc, *Salmonella*-infected, and TNBS-treated mice (Figure 14*B*–*D*).

Oral Elafin-Eudragit-Hydroxypropyl Methylcellulose Formulation Inhibited Colonic Fibrosis in Mice

We generated a clinically relevant elafin-Eudragit-hydroxypropyl methylcellulose (HPMC) formulation for oral administration (Figure 15*A*).[22] Oral elafin-Eudragit-

Figure 5. (*See previous page*). (*A*) Serum-starved CD-HIF were transfected with either control or ZEB1-overexpressing construct via lipofectamine 3000 overnight. Fibroblasts were then pretreated with 100 μg/mL CDSE. Two hours later, elafin (1 μg/mL) was added and incubated for 24 hours. Results were pooled from 4 independent experiments. Ordinary one-way ANOVA with Tukey test. (*B*) Efficiency of ZEB1-overexpressing construct transfection was determined by ELISA. Results were pooled from 4 experiments. Student *t* test was used to compare ZEB1 expression between control construct and ZEB1-overexpressing construct groups. (*C*) Serum-starved CD-HIF were pretreated with DMSO, 0.4 μg/mL cathepsin S, 10 μmol/L PAR1 agonist TRAP-6 (HY-P0078; MCE), or 10 μmol/L PAR2 agonist (HY-P0283; MCE) for 60 minutes, followed by addition of 100 μg/mL CDSE. Two hours later, some groups were treated with elafin (1 μg/mL) and incubated for 24 hours. Results were pooled from 4 independent experiments. Ordinary one-way ANOVA with Tukey test. (*D*) Fresh human colonic tissues from 4 colon cancer patients were incubated in serum-free RPMI1640 media with or without 100 μg/mL CDSE. Two hours later, elafin was added and further incubated for 24 hours. Results were pooled from 4 independent experiments. Ordinary one-way ANOVA with Tukey test. (*E*) Fresh human ileal tissues from 3 stricturing CD patients were incubated in serum-free RPMI1640 media with or without 100 μg/mL CDSE. Two hours later, elafin (1 μg/mL) was added and incubated for 24 hours. COL1A1, COL1A2, and ZEB1 mRNA expression were determined by real-time reverse transcription polymerase chain reaction. Ordinary one-way ANOVA with Tukey test. (*F*) Macroscopic and microscopic morphology of the fresh stricturing ileal tissue. Intense collagen deposition is found in the mucosal layer.

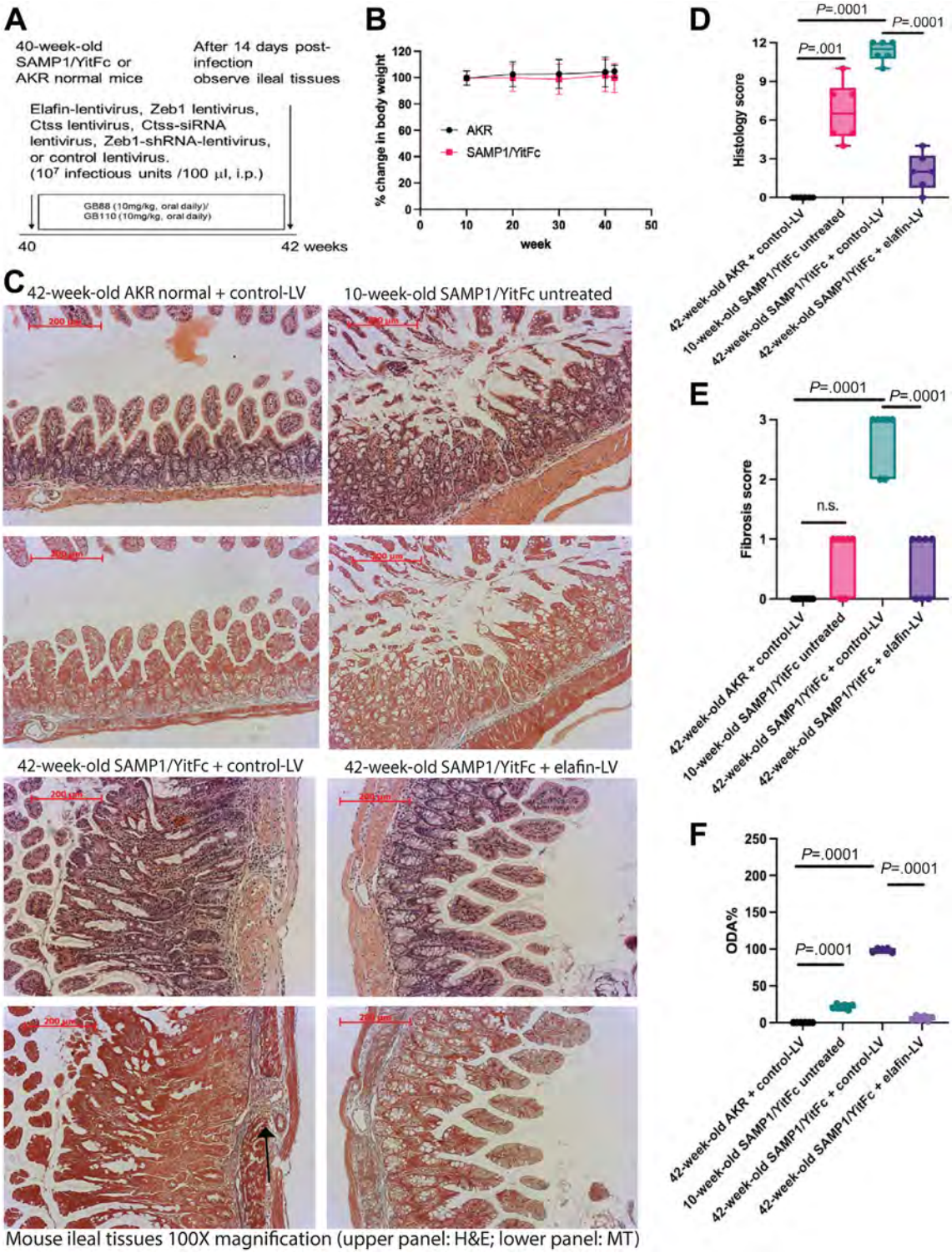

Figure 6. (*A*) Experimental plan. Control lentivirus, elafin-overexpressing lentiviruses, Ctss-overexpressing lentivirus, Ctss-siRNA lentivirus, Zeb1-shRNA lentivirus, and Zeb1-overexpressing lentivirus were injected into SAMP1/YitFc mice intraperitoneally once at 40 weeks of age. In addition, PAR2 agonist GB110 or PAR2 inhibitor GB88 was given via oral gavage from 40 to 42 weeks of age. Non-fibrotic 10-week-old SAMP1/YitFc mice and parental control 42-week-old AKR strain mice were used for comparison. Ileal tissues were collected for analysis 2 weeks after lentiviral injection. (*B*) Body weight. Six mice per group. Mean ± standard deviation. (*C*) H&E staining (*upper panels*) and Masson Trichrome (MT) staining (*lower panels*) of ileal tissues from 10 to 42 weeks of age. Blue color in MT staining (*arrows*) indicated collagen deposition in lamina propria. (*D*) Ileal histology scores. (*E*) Ileal fibrosis scores. (*F*) Ileal overall disease activities. Six mice per group. Ordinary one-way ANOVA with Tukey tests.

Table 1. Ileal Overall Disease Activity and Gene Expression Profile in SAMP1/YitFc Model

Ileal	HS score	FS score	Col1a2 mRNA	Col3a1 mRNA	Zeb1 mRNA	Vim mRNA	Acta2 mRNA	Tnf mRNA	Emr1 mRNA	ODA% Mean ± SD	Ctss mRNA
42-week-old AKR + control-LV											
Mean	0.0	0.0	1.1	1.1	1.1	1.1	0.8	1.1	1.1		1.0
SD	0.0	0.0	0.5	0.5	0.5	0.5	0.1	0.1	0.5		0.2
%	0	0	0	0	0	0	0	0	0	**0**	
10-week-old SAMP1Yit/Fc Untreated											
Mean	6.7	0.7	2.3	5.6	5.6	112.9	0.5	0.6	2.5		0.9
SD	2.3	0.5	4.5	6.3	6.3	117.3	0.1	0.2	1.4		0.4
%	59	26	6	20	21	23	0	0	40	**22 ± 3.3**	
42-week-old SAMP1Yit/Fc+ Control-LV											
Mean	11.3	2.7	21.0	24.0	23.0	486.0	2.5	2.6	4.5		1.0
SD	0.8	0.5	6.3	11.2	5.5	85.0	0.1	0.1	2.2		0.1
%	100	100	100	100	100	100	100	100	100	**100 ± 2.7**	100
compared with AKR											
P value	.0001	.0001	.0001	.0001	.0001	.0001	.0413	.0164	.0001		NS
42-week-old SAMP1Yit/Fc+ elafin-LV											
Mean	2.0	0.6	0.7	1.6	2.4	40.6	0.6	0.4	0.2		0.4
SD	1.4	0.5	0.3	0.3	0.6	18.0	0.1	0.1	0.1	**6 ± 3.1**	0.2
%	18	21	0	2	6	8	0	0	0		46
compared with SAMP control-LV											
P value	.0001	.0001	.0001	.0002	.0001	.0001	.0138	.0003	.0001	**.0001**	.002
42-week-old SAMP1Yit/Fc+ elafin-LV + Ctss-OE-LV											
Mean	10.8	2.6	6.3	23.0	164.3	404.0	8.5	3.6	5.9		0.8
SD	0.8	0.5	2.5	15.6	11.5	93.0	1.7	0.2	0.03		0.2
%	96	95	26	96	745	83	453	165	141	**211 ± 2.1**	80
compared with SAMP elafin-LV											
P value	.0001	.0001	.045	.0004	.0001	.0001	.0001	.0001	.0001	**.0001**	.040
42-week-old SAMP1Yit/Fc+ elafin-LV + GB110											
Mean	10.3	2.4	2.3	100.3	98.3	254.6	5.6	1.3	4.6		N/A
SD	0.8	0.5	0.3	11.1	9.1	46.2	1.5	0.4	0.1	**169 ± 2.3**	
%	91	89	6	433	444	52	284	15	104		
compared with SAMP elafin-LV											
P value	.0001	.0001	NS	.0001	.0001	.0001	.0001	NS	.0001	**.0001**	
42-week-old SAMP1Yit/Fc+ elafin-LV + Zeb1-OE-LV											
Mean	9.5	2.6	6.4	0.9	96.0	185.5	2.7	2.9	4.6		N/A
SD	1.6	0.5	0.3	0.2	3.4	11.5	0.9	1.2	1.2		
%	84	95	27	0	434	38	110	118	102	**112 ± 3.2**	

Table 1. Continued

Ileal	HS score	FS score	Col1a2 mRNA	Col3a1 mRNA	Zeb1 mRNA	Vim mRNA	Acta2 mRNA	Tnf mRNA	Emr1 mRNA	ODA% Mean ± SD	Ctss mRNA
compared with SAMP elafin-LV											
P value	.0001	.0001	.03	NS	.0001	.0020	.0042	.0017	.0001	**.0001**	
42-week-old SAMP1Yit/Fc+ Ctss-siRNA-LV											
Mean	4.8	1.4	5.4	14.1	1.2	12.1	3.4	2.3	5.0		0.5
SD	0.8	0.5	1.7	4.3	0.7	11.3	0.3	1.6	1.3		0.2
%	43	53	22	57	1	2	152	81	114	**58 ± 2.3**	48
compared with SAMP control-LV											
P value	.0001	.0027	.0001	NS	.0001	.0001	NS	NS	NS	**.0001**	.01
42-week-old SAMP1Yit/Fc+ GB88											
Mean	3.5	1.1	6.5	6.5	10.9	6.4	2.7	1.1	3.7		N/A
SD	0.5	0.7	4.2	3.3	2.6	1.8	0.7	0.6	0.5		
%	31	42	27	24	45	1	112	0	77	**39 ± 2.9**	
compared with SAMP control-LV											
P value	.0001	.0001	.0001	.0072	.0149	.0001	NS	.0189	NS	**.0001**	
42-week-old SAMP1Yit/Fc+ Zeb1-shRNA-LV											
Mean	4.5	1.1	12.8	11.3	5.1	12.0	2.5	1.8	5.2		N/A
SD	1.0	0.7	4.2	3.3	2.6	1.8	1.0	0.1	0.7		
%	40	42	59	45	18	2	100	48	119	**51 ± 3.8**	
compared with SAMP control-LV											
P value	.0001	.0001	.0059	NS	.0001	.0001	NS	NS	NS	**.0001**	

SD, standard deviation.

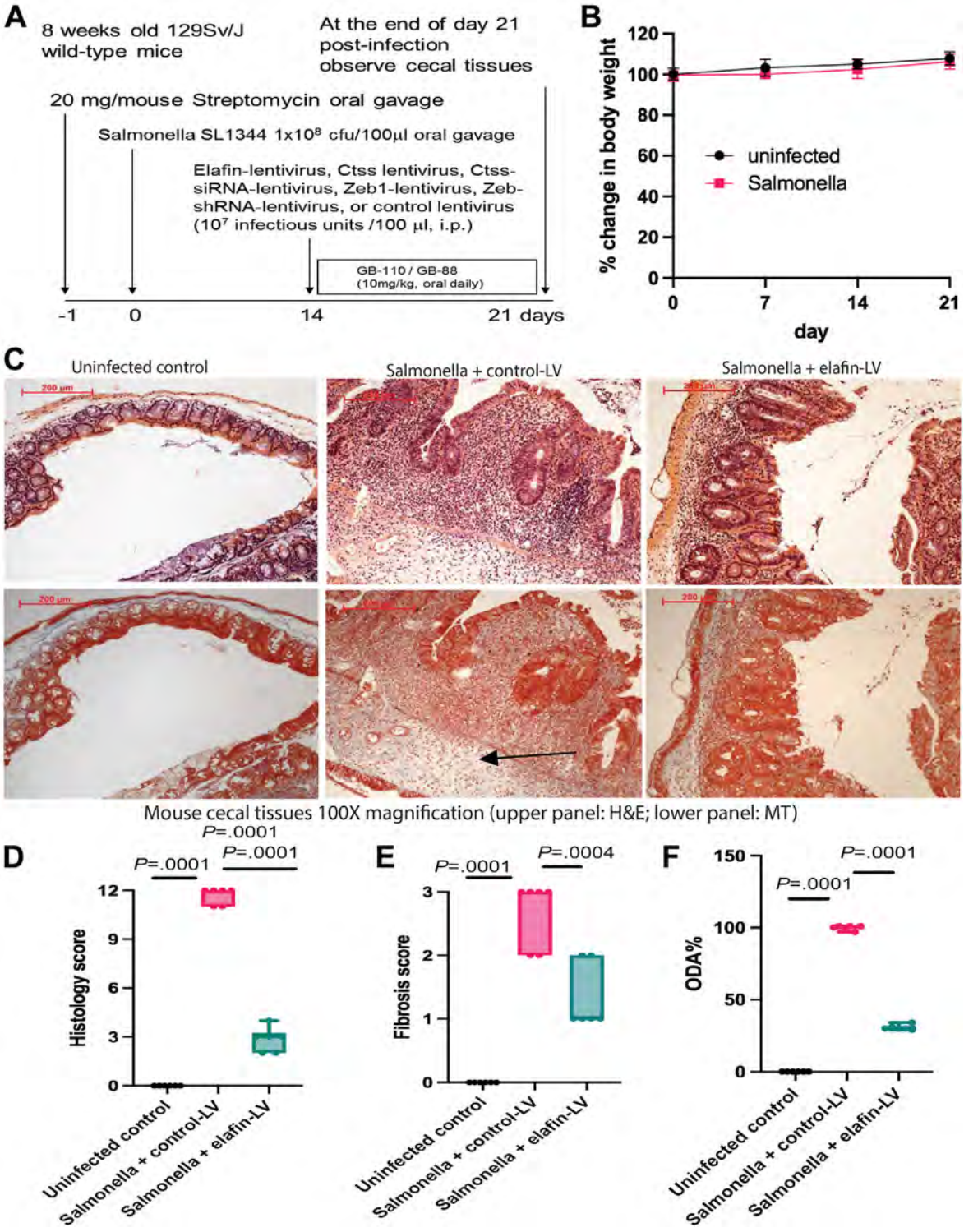

Figure 7. (*A*) Experimental plan. Eight-week-old male and female 129Sv/J mice were administered 20 mg streptomycin via oral gavage. Twenty-four hours later, mice were orally infected with *Salmonella typhimurium* SL1344 strain (1×10^8 colony-forming units) to induce cecal fibrosis. In addition, some mice received single intraperitoneal injection (10^7 infectious units/mouse) of control lentivirus or elafin-overexpressing lentiviruses on day 14. Cecal tissues were collected for analysis on day 21. (*B*) No significant change in body weight was noticed throughout the disease course in the infected mice. Six mice per group. Mean ± standard deviation. (*C*) H&E staining (*upper panels*) and Masson Trichrome (MT) staining (*lower panels*) of cecal tissues on day 21. Blue color in MT staining (*arrows*) indicated collagen deposition in cecal lamina propria of *Salmonella*-infected mice. (*D*) Cecal histology scores. (*E*) Cecal fibrosis scores. (*F*) Cecal overall disease activities. Lentiviral elafin expression reversed cecal fibrosis in *Salmonella*-infected mice. Six mice per group. Ordinary one-way ANOVA with Tukey tests.

Table 2. Cecal Overall Disease Activity and Gene Expression Profile in Salmonella Model

Cecal	HS score	FS score	Col1a2 mRNA	Zeb1 mRNA	Vim mRNA	Acta2 mRNA	Tnf mRNA	Emr1 mRNA	ODA% Mean ± SD	Ctss mRNA
Uninfected control										
Mean	0.0	0.0	1.0	1.0	1.1	1.0	1.0	1.0	0	1.1
SD	0.0	0.0	0.2	0.3	0.4	0.2	0.3	0.1		0.3
%	0	0	0	0	0	0	0	0		
Salmonella + control-LV										
Mean	11.7	2.8	5.3	3.8	7.9	2.2	216.6	22.5	100 ± 1.5	3.9
SD	0.5	0.4	0.3	0.4	2.9	0.2	40.0	2.3		0.7
%	100	100	100	100	100	100	100	100		100
Compared with uninfected										
P value	.0001	.0001	.0001	.0041	.0294	.0003	.0001	.0002		.0001
Salmonella + elafin-LV										
Mean	2.8	1.2	1.2	1.2	3.1	0.7	100.0	8.8	23 ± 1.6	1.8
SD	0.8	0.4	1.0	0.5	2.0	0.2	9.0	1.5		0.4
%	24	41	5	4	30	0	46	36		24
Compared with SAL + control-LV										
P value	.0001	.0004	.0002	.0084	NS	.0001	.0085	.0490	.0001	.0003
Salmonella + Ctss-OE-LV + elafin-LV										
Mean	10.5	2.8	11.6	3.8	7.4	1.6	87.6	12.6	97 ± 2.3	3.4
SD	0.8	0.4	3.2	1.1	1.6	0.6	75.4	4.6		1.2
%	90	100	245	101	94	49	40	54		82
Compared with SAL + elafin-LV										
P value	.0001	.0001	.0001	.008	NS	.0132	NS	NS	.0001	.01
Salmonella + GB110 + elafin-LV										
Mean	10.3	2.5	6.1	7.2	12.7	1.7	139.4	65.5	139 ± 2.4	N/A
SD	1.2	0.5	1.9	1.3	4.9	0.4	58.8	3.2		
%	89	88	117	223	171	61	64	300		
Compared with SAL + elafin-LV										
P value	.0001	.0028	.0001	.0001	.0003	.0039	NS	.0001	.0001	
Salmonella + Zeb1-LV + elafin-LV										
Mean	10.3	2.7	8.2	9.7	12.0	1.3	121.2	46.7	140 ± 2.9	N/A
SD	1.4	0.5	1.4	2.8	6.6	0.7	93.0	20.5		
%	89	94	167	314	161	24	56	212		
Compared with SAL + elafin-LV										
P value	.0001	.0004	.0001	.0001	.0010	NS	NS	.0001	.0001	
Salmonella + Ctss-siRNA-LV										
Mean	6.8	1.3	1.1	1.4	5.1	0.6	78.7	4.5	30 ± 2.6	0.7
SD	1.2	0.5	0.4	0.2	4.1	0.4	67.8	4.0		0.6
%	59	47	2	14	59	0	36	16		0
Compared with SAL + control-LV										
P value	.0001	.0004	.0001	.0196	NS	.0001	.001	.0029	.0001	.0001
Salmonella + GB88 + control-LV										
Mean	4.3	0.8	0.5	1.4	0.9	0.5	3.1	1.9	11 ± 2.7	N/A
SD	1.0	0.4	0.5	0.8	0.4	0.5	2.7	0.3		
%	37	29	0	14	0	0	1	4		
Compared with SAL + control-LV										
P value	.0001	.0001	.0001	.019	.0181	.0001	.0001	.0004	.0001	
Salmonella + Zeb1-shRNA-LV + control-LV										
Mean	4.2	0.5	0.7	1.6	1.0	0.5	2.8	0.7	9 ± 2.7	N/A
SD	0.4	0.5	0.3	0.1	0.1	0.2	2.4	0.5		
%	36	18	0	19	0	0	1	0		
Compared with SAL + control-LV										
P value	.0001	.0001	.0001	.0434	.0209	.0001	.0001	.0002	.0001	
Salmonella + ABX + control-LV										
Mean	10.00	2.50	4.67	2.45	6.07	1.98	191.52	25.37	86 ± 1.68	N/A
SEM	0.50	0.29	0.19	0.28	0.68	0.16	17.04	3.33		
%	64	88	85	51	74	82	88	113		
Compared with SAL + control-LV										
P value	NS	NS	NS	NS	NS	NS	NS	NS		

Table 2. Continued

Cecal	HS score	FS score	Col1a2 mRNA	Zeb1 mRNA	Vim mRNA	Acta2 mRNA	Tnf mRNA	Emr1 mRNA	ODA% Mean ± SD	Ctss mRNA
Salmonella + ABX + elafin-LV										
Mean	3.00	0.75	2.64	2.17	4.81	1.48	97.60	14.38	51 ± 1.62	N/A
SEM	0.71	0.25	0.43	0.31	0.83	0.17	3.09	2.19		
%	26	26	38	41	55	40	45	62		
Compared with SAL + elafin-LV										
P value	NS	NS	NS	NS	NS	NS	NS	NS		
Salmonella + miR205-5p-OE-LV + control-LV										
Mean	5.67	0.83	2.80	2.78	5.48	1.69	26.14	8.74	47 ± 0.92	N/A
SEM	0.21	0.17	0.31	0.26	0.34	0.15	3.96	0.94		
%	49	29	41	63	65	57	12	36		
Compared with SAL + control-LV										
P value	.0001	.0001	.0001	NS	NS	NS	.0001	.0001	.0001	
Salmonella + miR205-5p-OFF-LV + elafin-LV										
Mean	9.67	2.17	2.79	3.32	5.98	1.56	38.94	10.07	60 ± 0.86	N/A
SEM	0.21	0.17	0.22	0.61	0.91	0.24	5.51	1.24		
%	83	77	41	83	72	46	18	42		
Compared with SAL + elafin-LV										
P value	.0001	.0005	.0494	.0439	NS	.0244	.0015	.0205	.0001	

HPMC administration showed peak colonic elafin level at 6 hours and reversed colonic fibrosis with lowered histology and fibrosis scores in TNBS-treated mice (Figure 15*B*–*D*). Because multiple clinical and endoscopic disease activity scoring systems for IBD suggest the necessity to reduce severe disease activity to 22% to achieve remission (Table 5),[41] the overall disease activity at 7% reflected remission in the oral formulation-treated group (Figure 15*E*). Both elafin overexpression and elafin-Eudragit-HPMC formulation produced elafin in intestinal tissues (Figure 15*E*), reduced cathepsin S activity (Figure 12*C*), and Ctss and Zeb1 mRNA expression and lowered histology scores, fibrosis scores, and ODAs in fibrotic mice (Figure 15*D* and *E*).

Discussion

This report is the first to discover 3 novel targets of intestinal fibrosis (cathepsin S, PAR2, ZEB1). Although the protective role of elafin in mice with colitis was demonstrated previously,[20,42] we elucidated a novel anti-fibrogenic mechanism of elafin that involves these 3 targets.

The etiologies of intestinal fibrosis in the 3 mouse models of intestinal fibrosis have not been fully characterized. However, the anti-fibrogenic effects of elafin were robust, as shown by multiple cell and animal approaches. More importantly, elafin inhibited collagen mRNA expression in fresh ileal and colonic tissues from stricturing CD patients (Figures 1*C* and 5*E*), suggesting its potential efficacy against ileal and colonic strictures.

Elafin targets CDSE-induced cathepsin S because the extracellular cathepsin S is associated with the plasma membrane and cleaves near the N-terminus of PAR2,[33,35] which activates extracellular signal-regulated kinases.[43] The elafin-mediated extracellular signal-regulated kinase inactivation reflected diminished cathepsin S and PAR2 activity (Figure 16). Thus, elafin exerts anti-fibrogenic effects by inhibiting cathepsin S and PAR2 activities. Unfortunately, because of limited laboratory capacity, we cannot further characterize the molecular interactions between elafin and cathepsin S.

A previous x-ray crystallography study demonstrated that the primary contact region (from leucine position 20 to leucine position 26) and secondary contact region (from serine position 48 to alanine position 52) of elafin are bound at the active site of porcine pancreatic elastase non-covalently.[44] A modified elafin with A62D and M63L mutations lost its antiprotease activities without affecting antimicrobial properties.[45] On the other hand, substitutions of valines at positions 5 and 9 of the elafin amino acid sequence with glycine and glutamines abolished the antiprotease, but not anti-inflammatory, activities of elafin against neutrophil elastase and proteinase 3.[46] Interestingly, elafin and its closely related secretory leukocyte protease inhibitor (SLPI) possess C-terminal whey acidic protein regions and share similar but non-identical antiprotease, antimicrobial, and anti-inflammatory activities.[47,48] Thus, it is difficult to predict the exact region of mature elafin responsible for antiprotease activity against cathepsin S and other proteases.

Although this study discovered cathepsin S as a fibroblast-derived fibrogenic target, microbiota and host cells (epithelial cells and immune cells) can produce other proteases. For example, mast cell tryptase can mediate fibrogenesis in human colonic CCD-18Co fibroblasts.[24] However, the expression and activity of many proteases and antiproteases in IBD patients can be very complicated. In addition, many of them have multiple targets and

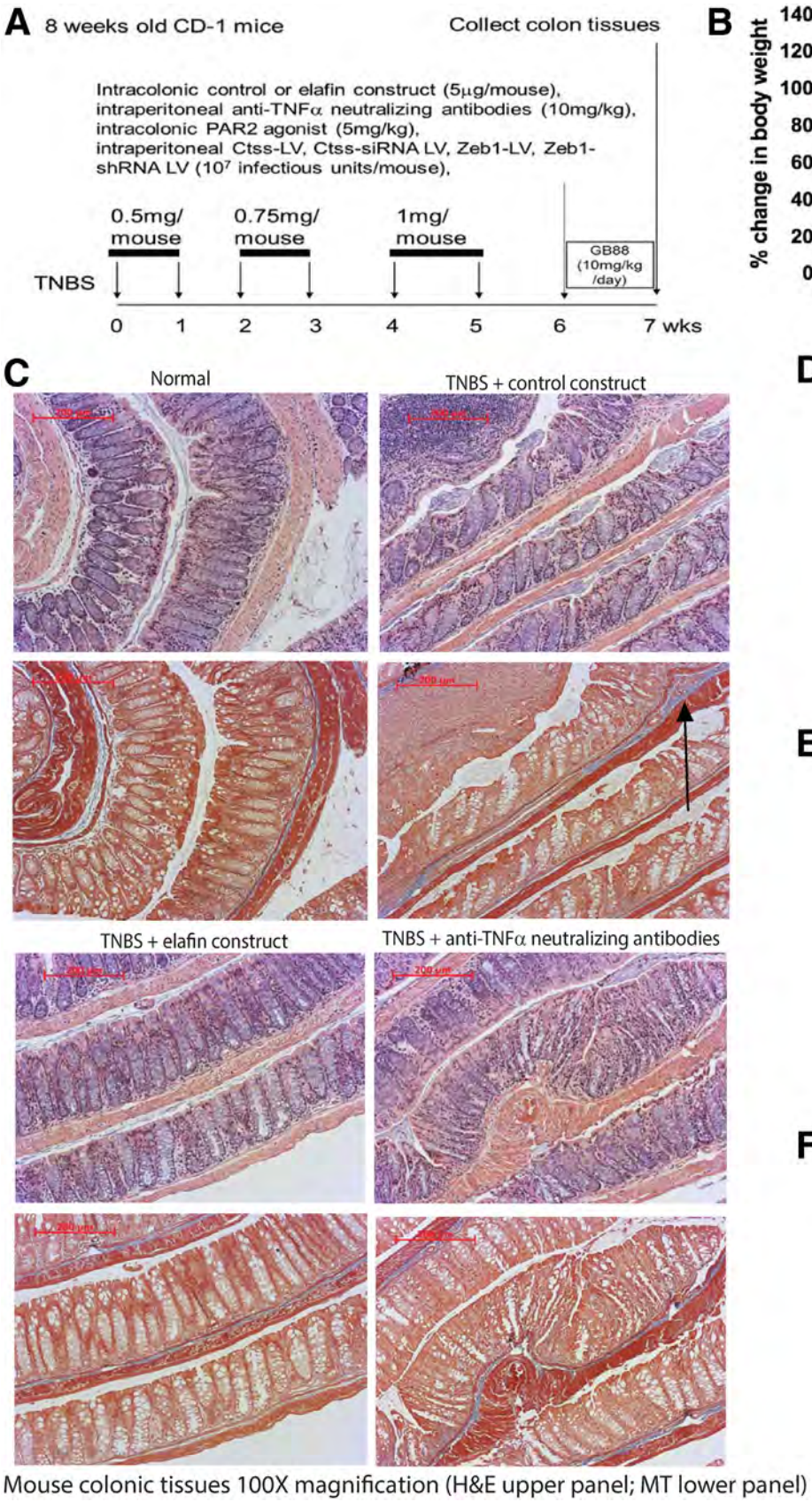

Mouse colonic tissues 100X magnification (H&E upper panel; MT lower panel)

functions. This area requires further investigation, but we could not further elucidate their interactions and involvement in CD strictures because of the limitations of assays and samples.

Elafin did not affect T-cell cytokine secretion in CDSE-preconditioned CD-PBMC (Table 6). Elafin also did not affect TNFα secretion in lipopolysaccharide-treated mouse macrophages.[22] Therefore, the anti-fibrogenic effect of elafin is independent of TNFα, because TNFα neutralization cannot reverse intestinal fibrosis in mice (Figure 8) and CD patients.[4] We speculate that the reduced Tnf mRNA expression in elafin-overexpressing mice might result from gut barrier protection. Elafin protects the epithelial barrier by inhibiting epithelial elastase 2A hyperactivity independent of PAR2.[19] Epithelial elastase 2A transgenic mice have colitis with increased colonic Tnf mRNA expression.[19] The relationship between the intestinal barrier and fibrosis development is unclear and beyond the scope of our study.

Although elafin and SLPI possess antiprotease, anti-inflammatory, and antimicrobial properties,[49] SLPI promotes cancer metastasis and is unsuitable for therapeutic development.[50] Elafin should not affect colorectal cancer risk because colonic elafin expression is not associated with the type, stage, and locations of the colorectal tumors or the survival of the patients (COADREAD database). Compared with non-IBD patients, CD patients do not have altered intestinal SLPI mRNA and protein expression.[17] SLPI deficiency does not affect bleomycin-induced lung fibrosis development in mice.[51] We speculate that SLPI is unlikely to exert anti-fibrogenic activities in activated fibroblasts because cathepsin S can cleave and inactivate SLPI.[52]

Eudragit-FS30D-HPMC polymer protects the therapeutic agent through the stomach and releases it in humans' mid-distal ileum and colon.[53] For example, Asacol is a Eudragit-coated mesalamine for treating IBD. Like elafin-overexpressing bacteria,[20,42] the elafin-Eudragit formulation maximized elafin delivery to the diseased intestine (Figure 15*E*). Both lentiviral elafin overexpression and elafin-Eudragit formulation increased circulating elafin levels in mice.[54] However, systemic delivery of elafin is unlikely to be useful for clinical applications because elafin has a short half-life in circulation because of rapid renal elimination.[55] IBD patients, including stricturing CD patients, have increased elafin expression in mesenteric fat and elevated circulating elafin levels.[6] Therefore, delivery of elafin to the fibrotic intestines should precisely confer anti-fibrogenic effects regardless of circulating elafin levels.

Direct exposure to elafin did not induce collagen mRNA expression in fresh human colonic tissues (Figure 1*C*), whereas lentiviral elafin overexpression did not cause ileal fibrosis in normal AKR mice (Figure 13). Therefore, we believe that elafin formulation delivery cannot initiate or promote intestinal fibrosis because intestinal fibrosis is a multifactorial process.[1]

Intestinal strictures are classified into inflammatory, fibrotic, and mixed phenotypes.[56] Anti-inflammatory drugs can diminish inflammatory strictures, but fibrotic strictures have no known anti-fibrogenic drugs. Imaging analysis is inaccurate in differentiating stricture phenotypes, whereas ileocolonoscopy may not access the strictures for evaluation, especially in sites with multiple strictures.[56] It is unfeasible to define phenotype-based therapy in current clinical practice because most CD patients' phenotypes are unknown. We believe that the elafin-Eudragit FS30D formulation can cover intestinal inflammation and fibrosis because the same formulation inhibited obesity and hyperglycemia in high-fat diet–treated mice,[22] which had low-grade chronic intestinal inflammation.[57]

In summary, elafin inhibits cathepsin S-dependent PAR2 activity and reduces ZEB1 and collagen expression in intestinal fibroblasts. The significance of this study is to gain insight into the mechanism of intestinal fibrosis and discover a potential anti-fibrogenic approach.

Methods

Frozen Human Colonic Tissues

Frozen colonic tissue samples of non-IBD, UC, and CD patients were collected from the Cedars-Sinai Medical Center during the surgical resection of diseased tissues from 2010 to 2014 prospectively and cryopreserved until the study.[40] The Cedars-Sinai Institutional Review Board (#3358 and #23705) and UCLA Institutional Review Board (11-001527) approved the study. Informed consent was obtained from all subjects by the Cedars-Sinai Medical Center. UCLA Institutional Review Board waived separate informed consent. Frozen human colonic tissues were used for comparing gene expression in non-IBD, UC, stricturing CD, and non-stricturing CD patients.[6]

Human Serum Samples

Serum samples of normal, UC, and CD patients were prospectively collected from UCLA from 2012 to 2015. The physicians requested the medically indicated blood collection. UCLA Institutional Review Board (IRB 12-001499) approved this study. Separate informed consent was waived by UCLA IRB because UCLA Pathology obtained written informed consent from all subjects. The pooled sera from 12

Figure 8. (***See previous page***). **(*A*) Experimental plan.** Eight-week-old male and female CD-1 mice were injected with 50 μL TNBS solution (to induce colitis) or 30% ethanol (vehicle) via weekly enema 6 times. After last TNBS injection, mice were held for 2 additional weeks to develop colonic fibrosis. Some mice were injected with either control construct or elafin-overexpressing construct intracolonically on day 9 after last TNBS injection. Anti-TNFα neutralizing antibodies were injected intraperitoneally on day 9 after last TNBS injection. (*B*) TNBS induced colitis slowly. No significant change in weight loss was noticed in TNBS-treated mice. Six mice per group. Mean ± standard deviation. (*C*) H&E staining (*upper panels*) and MT staining (*lower panels*) of colonic tissues. Blue color in MT staining (*arrows*) indicated collagen deposition. (*D*) Colonic histology scores. (*E*) Colonic fibrosis scores. (*F*) Colonic overall disease activities. Six mice per group. Ordinary one-way ANOVA with Tukey test.

Table 3. Colonic Overall Disease Activity and Gene Expression Profile in TNBS Model

Colonic	HS score	FS score	Col1a2 mRNA	Col3a1 mRNA	Zeb1 mRNA	Vim mRNA	Acta2 mRNA	Tnf mRNA	Emr1 mRNA	ODA% Mean ± SD	Ctss mRNA
Normal											
Mean	0.0	0.0	0.9	0.9	1.0	1.0	1.1	1.1	1.1	0	1.1
SD	0.0	0.0	0.2	0.4	0.3	0.3	0.2	0.3	0.6		0.3
%	0.0	0.0	0.0	0.0	0.0	0.0	0.0	0.0	0.0		
TNBS + control construct											
Mean	8.7	2.5	2.2	2.5	1.7	2.5	2.4	2.0	2.4	100 ± 3.2	0.9
SD	1.6	0.5	0.2	0.3	0.3	0.2	1.0	0.2	1.0		0.2
%	100	100	100	100	100	100	100	100	100		100
Compared with normal											
P value	.0001	.0001	.0372	.0059	.0477	.0349	.0019	.0364	.0364	.0001	NS
TNBS + elafin construct											
Mean	5.0	0.5	0.4	0.5	0.6	1.0	0.8	1.1	0.6	9 ± 2.7	0.5
SD	0.9	0.5	0.1	0.2	0.2	0.2	0.1	0.3	0.1		0.2
%	58	20	0	0	0	0	0	5	0		53
Compared with TNBS + control construct											
P value	.0003	.0001	.0008	.0002	.0002	.0394	.0001	NS	NS	.0001	.0191
TNBS + anti-TNFα NAB											
Mean	6.5	2.2	1.7	2.5	1.5	1.7	1.4	1.1	0.6	51 ± 3.6	N/A
SD	0.5	0.8	0.2	0.2	0.4	0.4	0.4	0.5	0.4		
%	75	87	66	100	70	43	19	0	0		
Compared with TNBS + control construct											
P value	NS	NS	NS	NS	NS	NS	.0249	.0364	.0364	.0001	
TNBS + elafin construct + Ctss-OE-LV											
Mean	11.2	2.7	1.8	2.0	2.2	1.3	1.8	1.4	2.6	85 ± 2.2	1.0
SD	0.8	0.5	0.9	1.1	0.6	0.2	0.3	0.3	0.5		0.2
%	129	107	69	67	170	20	53	32	117		108
Compared with TNBS + elafin construct											
P value	.0001	.0001	.0026	.0135	.0001	NS	.0396	NS	NS	.0001	.005
TNBS + elafin construct + PAR2 agonist											
Mean	8.8	2.3	3.3	2.7	2.0	4.0	1.9	0.5	2.9	114 ± 3.6	N/A
SD	1.2	0.5	1.2	1.3	0.4	0.5	0.6	0.2	1.9		
%	102	93	186	113	140	196	61	0	136		
Compared with TNBS + elafin construct											
P value	.0002	.0001	.0001	.0001	.0001	.0001	.0154	NS	NS	.0001	
TNBS + elafin construct + Zeb1-LV											
Mean	8.5	2.2	1.7	1.9	1.6	2.6	2.3	0.8	0.8	66 ± 4.0	N/A
SD	1.0	0.8	0.5	1.0	0.3	1.8	0.7	0.2	0.5		
%	98	87	61	64	85	103	93	0	0		
Compared with TNBS + elafin construct											
P value	.0007	.0010	.0457	.0194	.0009	.0309	.0002	NS	NS	.0001	

Table 3. Continued

Colonic	HS score	FS score	Col1a2 mRNA	Col3a1 mRNA	Zeb1 mRNA	Vim mRNA	Acta2 mRNA	Tnf mRNA	Emr1 mRNA	ODA% Mean ± SD	Ctss mRNA
TNBS + Ctss-siRNA-LV											
Mean	6.0	1.2	1.9	1.9	1.3	3.1	1.4	0.7	1.8	57 ± 2.6	0.5
SD	1.4	0.4	1.2	0.7	0.4	1.1	0.3	0.1	0.3		0.1
%	69	47	77	60	39	141	25	0	54		50
Compared with TNBS + control construct *P* value	.02	.0038	NS	NS	NS	NS	.0473	.0003	.0003	.0001	.011
TNBS + GB88											
Mean	3.0	0.3	0.7	0.9	1.0	1.7	0.9	1.4	2.6	27 ± 4.2	N/A
SD	1.9	0.5	0.1	0.0	0.5	0.9	0.6	1.0	1.3		
%	35	13	0	0	4	46	0	35	113		
Compared with TNBS + control construct *P* value	.0001	.0001	.0091	.0047	NS	NS	.0003	NS	NS	.0001	
TNBS + Zeb1-shRNA-LV											
Mean	3.5	0.5	1.2	1.1	1.0	1.3	0.6	0.9	1.9	20 ± 4.5	N/A
SD	2.0	0.5	0.1	0.0	0.1	0.2	0.2	0.2	0.2		
%	40	20	26	12	0	16	0	0	64		
Compared with TNBS + control construct *P* value	.0001	.0001	NS	.0239	.0332	NS	.0001	.0013	.0013	.0001	

Colonic	HS score	FS score	Col1a2 mRNA	Col3a1 mRNA	Zeb1 mRNA	Vim mRNA	Acta2 mRNA	Tnf mRNA	Emr1 mRNA	ODA% mean±sd	Ctss mRNA
Normal											
Mean	0.0	0.0	0.9	0.9	1.0	1.0	1.1	1.1	1.1	0	1.1
SD	0.0	0.0	0.2	0.4	0.3	0.3	0.2	0.3	0.6		0.3
%	0.0	0.0	0.0	0.0	0.0	0.0	0.0	0.0	0.0		
TNBS + control Eudragit-HPMC											
Mean	8.5	2.3	1.7	2.5	1.5	1.8	2.0	1.7	2.2	99 ± 3.3	1.0
SD	2.1	0.6	0.4	0.5	0.2	0.3	0.4	0.5	0.9		0.2
%	100	100	100	100	100	100	100	100	100		100
TNBS + Elafin Eudragit-HPMC											
Mean	2.8	0.4	0.8	0.5	0.8	1.1	1.2	0.7	1.1	7 ± 2.6	0.4
SD	2.0	0.6	0.1	0.1	0.4	0.5	0.4	0.2	0.6		0.1
%	33	18	0	0	0	0	13	0	0		42
Compared with TNBS + control Eudragit *P* value	.0013	.0007	.0001	.0001	.0061	.0234	NS	.0002	.0282	.0001	.0016

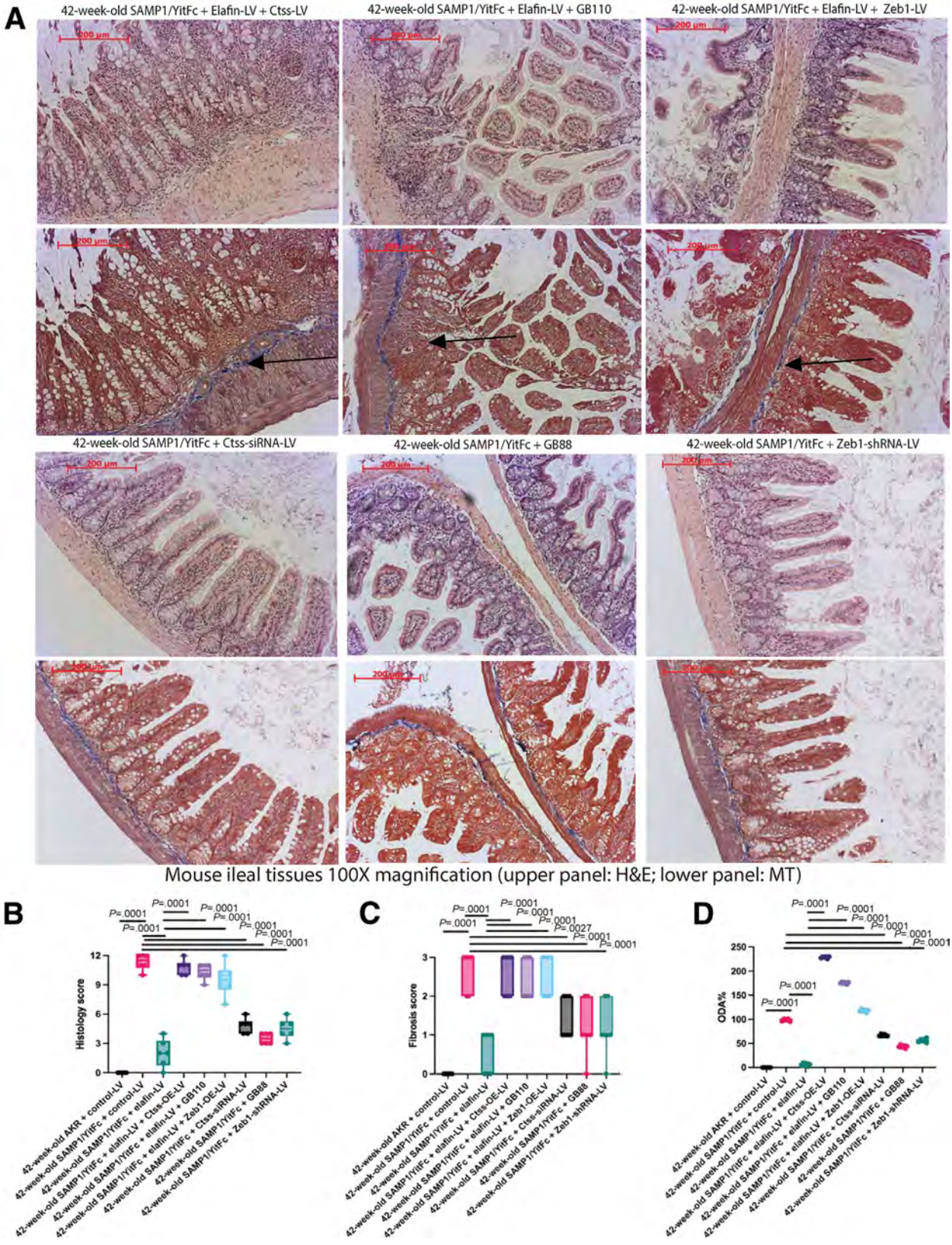

Figure 9. (*A*) H&E staining (*upper panels*) and MT staining (*lower panels*) of ileal tissues from SAMP1/YitFc mice at 42 weeks of age. Blue color in MT staining (*arrows*) indicated collagen deposition. (*B*) Ileal histology scores. (*C*) Ileal fibrosis scores. (*D*) Ileal overall disease activities. Prominent ileal fibrosis was found in elafin-overexpressing groups with lentiviral Ctss and Zeb1 overexpression and oral PAR2 agonist GB110 treatment. Ileal fibrosis was ameliorated with lentiviral Ctss and Zeb1 shRNA inhibition and oral PAR2 inhibitor GB88 treatment. Six AKR or SAMP1/YitFc mice per group. Ordinary one-way ANOVA with Tukey tests.

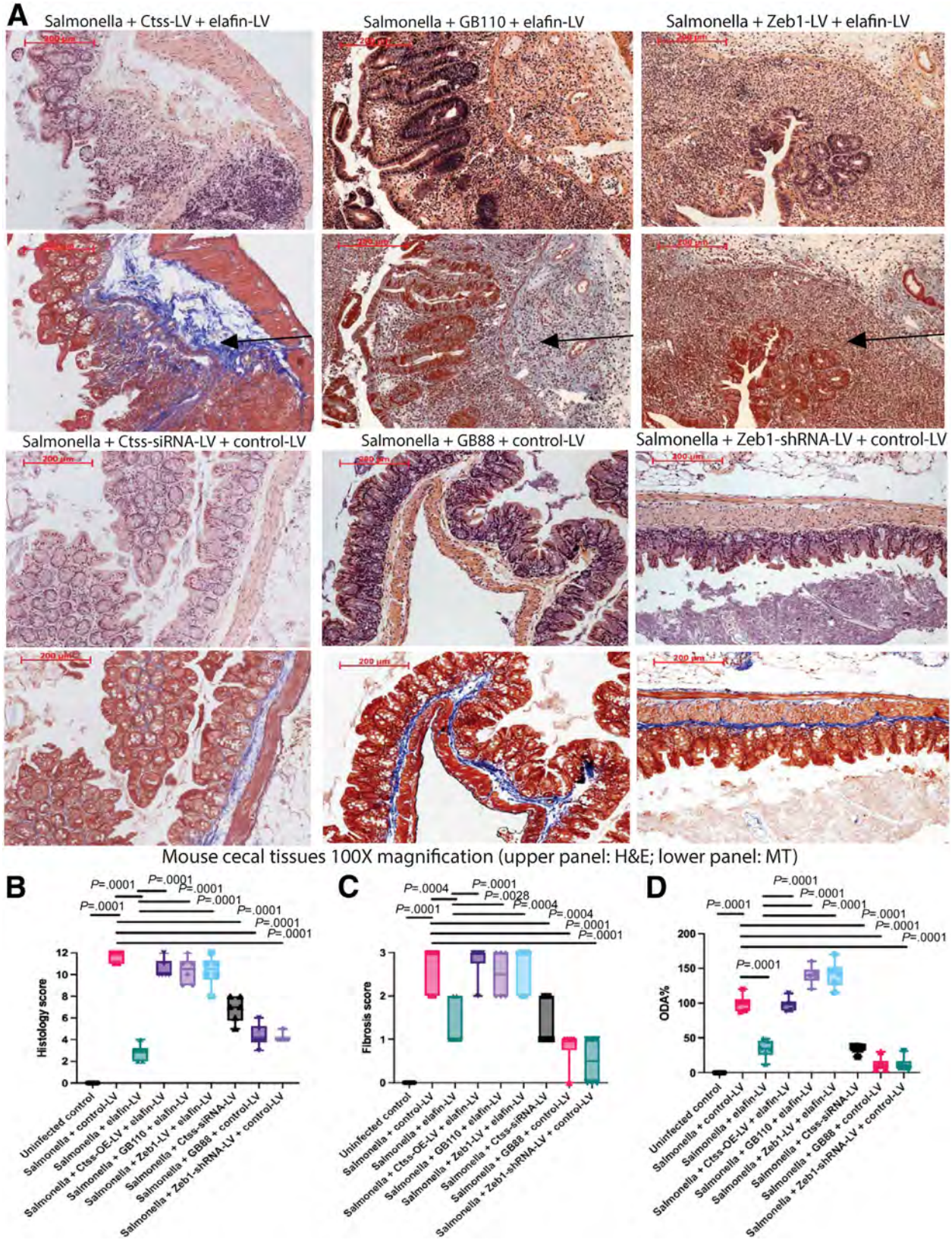

Figure 10. (*A*) H&E staining (*upper panels*) and Masson Trichrome (MT) staining (*lower panels*) of cecal tissues on day 21. Blue color in MT staining (*arrows*) indicated collagen deposition in cecal lamina propria of *Salmonella*-infected mice. Prominent cecal fibrosis was found in elafin-overexpressing groups with lentiviral Ctss and Zeb1 overexpression and oral PAR2 agonist GB110 treatment. Cecal fibrosis was ameliorated with lentiviral Ctss and Zeb1 shRNA inhibition and oral PAR2 inhibitor GB88 treatment. (*B*) Cecal histology scores. (*C*) Cecal fibrosis scores. (*D*) Cecal overall disease activities. Six uninfected or *Salmonella*-infected mice per group. Ordinary one-way ANOVA with Tukey tests.

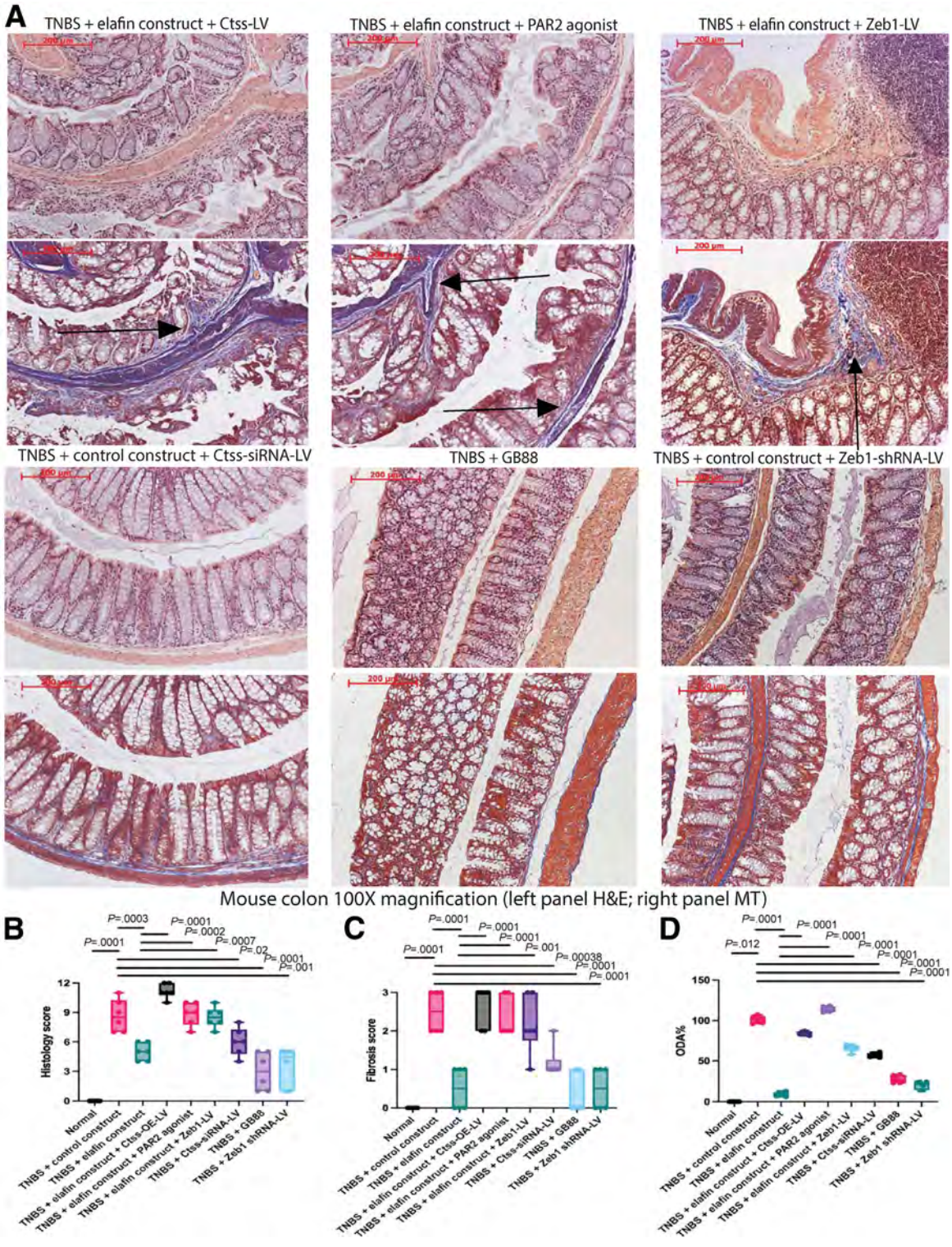

Figure 11. (*A*) TNBS-treated mice were injected with Ctss-overexpressing lentivirus, Ctss-siRNA lentiviruses, Zeb1-overexpressing lentivirus, or Zeb1-shRNA lentivirus on day 9 after last TNBS injection. Some mice were injected with 5 mg/kg PAR2 agonist SLIGKV-NH_2 intracolonically 9, 11, and 13 days after last TNBS injection. GB88 (10 mg/kg/day) was administered via oral gavage. Control or elafin-overexpressing construct was injected intracolonically. H&E staining (*upper panels*) and Masson Trichrome staining (*lower panels*) of colonic tissues are shown. Blue color in MT staining (*arrows*) indicated collagen deposition. (*B*) Colonic histology scores. (*C*) Colonic fibrosis scores. (*D*) Colonic overall disease activities. Prominent colonic fibrosis was found in elafin-overexpressing groups with lentiviral Ctss and Zeb1 overexpression and oral PAR2 agonist GB110 treatment. Colonic fibrosis was ameliorated with lentiviral Ctss and Zeb1 shRNA inhibition and oral PAR2 inhibitor GB88 treatment. Six mice per group. Ordinary one-way ANOVA with Tukey tests.

Table 4. Comparison of Overall Disease Activities and Gene Expression in Mice With Lentiviral and Pharmacologic Manipulations

Lentivirus/drugs	Target	SAMP ileal	Salmonella cecal	TNBS colonic	Overall target mRNA expression or ODA
Ctss-siRNA-LV	ODA	58%	30%	57%	48%
PAR2 inhibitor GB88	ODA	39%	11%	27%	26%
Zeb1-shRNA-LV	ODA	51%	9%	20%	27%
Ctss-siRNA-LV	Ctss	48%	0%	50%	33%
Ctss-siRNA-LV	Zeb1	1%	14%	39%	18%
PAR2 inhibitor GB88	Zeb1	45%	14%	4%	21%
Zeb1-shRNA-LV	Zeb1	18%	19%	0%	12%
Control-LV	ODA	100%	100%	100%	100%
Control-LV + Elafin	ODA	6%	23%	9%	13%
Ctss-LV + Elafin	ODA	211%	97%	85%	131%
GB110/PAR2 agonist	ODA	169%	139%	114%	141%
Zeb1-LV + Elafin	ODA	112%	140%	66%	106%
Control-LV	Ctss	100%	100%	100%	100%
Control-LV + Elafin	Ctss	46%	24%	53%	41%
Ctss-LV + Elafin	Ctss	80%	82%	108%	90%
Control-LV	Zeb1	100%	100%	100%	100%
Control-LV + Elafin	Zeb1	6%	4%	0%	3%
Ctss-LV + Elafin	Zeb1	745%	101%	170%	339%
GB110/PAR2 agonist	Zeb1	444%	223%	140%	269%
Zeb1-LV + Elafin	Zeb1	434%	314%	85%	278%

stricturing CD patients were used for preparing serum exosomes (CDSE).[6]

Serum exosomes were prepared by total exosome isolation reagent (#4478360; Thermo Fisher Scientific, Waltham, MA). In short, the serum sample (1 mL) was centrifuged at 2000*g* for 30 minutes to remove cells and debris. The supernatant was then mixed with 200 μL of total exosome isolation reagent and refrigerated at 4°C for 30 minutes. The mixture was then centrifuged at 10,000*g* for 10 minutes at room temperature. After removing the supernatant, the pellet was resuspended with 250 μL phosphate-buffered saline. The protein concentration in the serum exosomes was quantified by bicinchoninic acid protein assay (#23225; Thermo Fisher Scientific).

Fresh Human Intestinal Tissues

Fresh colonic tissues from colon cancer patients with normal histology and ileal tissues from stricturing CD patients with fibrotic morphology were obtained from UCLA Surgical Pathology from 2020 to 2021. UCLA IRB (12-001499) approved the study. Fresh human intestinal tissues were cut into 3 × 3 mm and incubated in serum-free RPMI1640 medium with or without 100 μg/mL CDSE. Two hours later, elafin (1 μg/mL) was added and incubated for 24 hours. Fresh human intestinal tissues were used for assessing elafin-mediated effects.

Baseline characteristics of all intestinal tissues and serum samples are shown in Table 7.

For inclusion criteria, IBD, intestinal strictures, and colon cancer were diagnosed by gastroenterologists as described previously.[6] For exclusion criteria, pregnant women, prisoners, minors younger than age 18, concurrent acute infection (cytomegalovirus infection, *Clostridium difficile* infection, and tuberculosis), and malignant conditions were excluded.

Intestinal Fibroblast and Epithelial Cell Culture

CD-HIFs were prepared from intestinal tissues in stricturing CD patients.[6] Baseline characteristics of the patients are shown in Table 7. In short, the intestinal mucosa was stripped from submucosa and muscularis propria and cut into 1 × 1 mm pieces. The mucosal tissues were washed with phosphate-buffered saline and then digested with 1 mg/mL collagenase II, 0.3 mg/ml DNase I, and 2 mg/mL hyaluronidase at 37°C for 30 minutes with shaking. Next, the dissociated cells were cleared through a 40-μm cell strainer and centrifuged at 10,000*g* for 5 minutes. After removing supernatants, the cell pellets were suspended with fibroblast medium (M2267; Cell Biologics, Chicago, IL) and cultured on gelatin-coated culture flasks. We cultured primary fibroblasts during passages 3–10 for experiments. Serum-starved CD-HIF were pretreated with 100 μg/mL CDSE for 2 hours to mimic the CD environment and induce fibrogenesis.[6]

Human colonic CCD-18Co fibroblasts (CRL-1459, ATCC) were cultured in minimal Eagle medium with 10% fetal bovine serum and 1% penicillin-streptomycin.[10,40] All cells

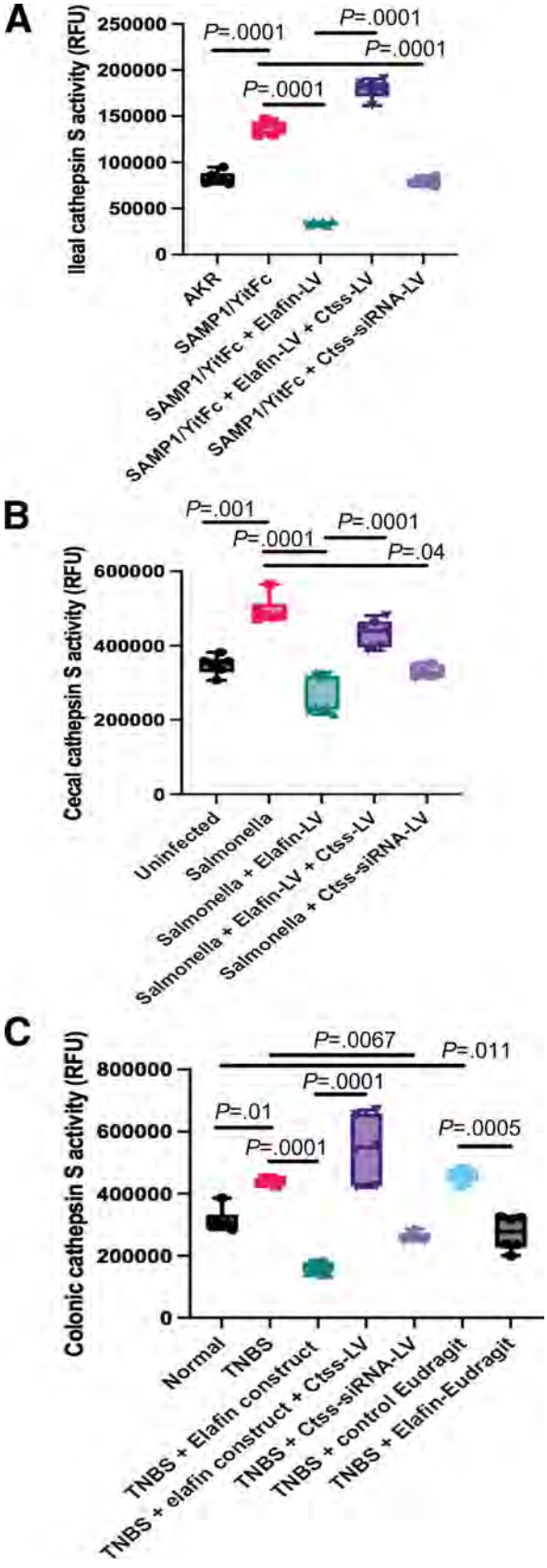

were grown to 80% confluence and then switched to serum-free medium overnight for experiments. Serum-starved fibroblasts were pretreated with either 0.1% trifluoroacetic acid as a vehicle or 10 ng/m: TGF-β1 for 2 hours, followed by incubation with elafin (#AS-61641; AnaSpec, Fremont, CA) for 2–24 hours. Details of other chemicals used in this study are shown in Table 8.

Primary human colonic epithelial cells (H6047; Cell Biologics) were cultured in epithelial cell medium (H6621; Cell Biologics) until 90% confluence. Then, the cells were switched to serum-free medium overnight for TGF-β1, CDSE, and elafin treatment.

At the end of the experiments, the cells were lysed with radioimmunoprecipitation assay buffer (#89900; Thermo Fisher Scientific) containing protease and phosphatase inhibitor cocktail (PPC1010; Sigma-Aldrich, St Louis, MO) for ELISA. We used ELISA to measure protein levels of Pro-COL1A1 (DY6220-05; R&D Systems, Minneapolis, MN), ERK1/2 phosphorylation (DYC1018B; R&D Systems), ZEB1 (MBS774017; MyBioSource, San Diego, CA), and COL1A2 (MBS2701496; MyBioSource) in cell lysates. Alternatively, the cells were lysed with Qiagen's RLT buffer for RNA experiments.

Protease Array

Serum-starved CD-HIF (1×10^7 cells/well) were treated with 100 μg/mL CDSE for 2 hours. Serum-starved CCD-18Co colonic fibroblasts (1×10^7 cells/well) were treated with 10 ng/mL TGF-β1 for 2 hours. Conditioned media 500 μL were loaded to Proteome Profiler Human Protease Array membranes (ARY021B; R&D Systems) and incubated with detection antibody overnight at 4° C with shaking. The membranes were then washed and incubated with streptavidin-horseradish peroxidase and substrate. A Bio-Rad ChemiDoc Imaging system (Hercules, CA) captured the luminescence signals emitted from the membranes and generated the images for analysis. Bio-Rad Image software quantified the signal intensities of individual proteases and references in images. We used Excel (Microsoft, Redmond, WA) to calculate the ratios of individual protease signals over reference signals.

Cathepsin S Activity Measurement

We used a fluorescence-based activity assay kit (ab65307; Abcam, Cambridge, UK) to measure the cathepsin S activity. This assay kit uses the preferred cathepsin-S substrate sequence VVR labeled with AFC (amino-4-trifluoromethyl coumarin). Cell lysates or other samples that contain cathepsin S will cleave the synthetic substrate

Figure 12. (*A*) Ileal cathepsin S activities in AKR and SAMP1/YitFc mice. (*B*) Cecal cathepsin S activities in uninfected and *Salmonella*-infected mice. (*C*) Colonic cathepsin S activities in normal and TNBS-treated mice. Fifty μg tissue lysates in 50 μL CS buffer per reaction. Six mice per group. Ordinary one-way ANOVA with Tukey tests.

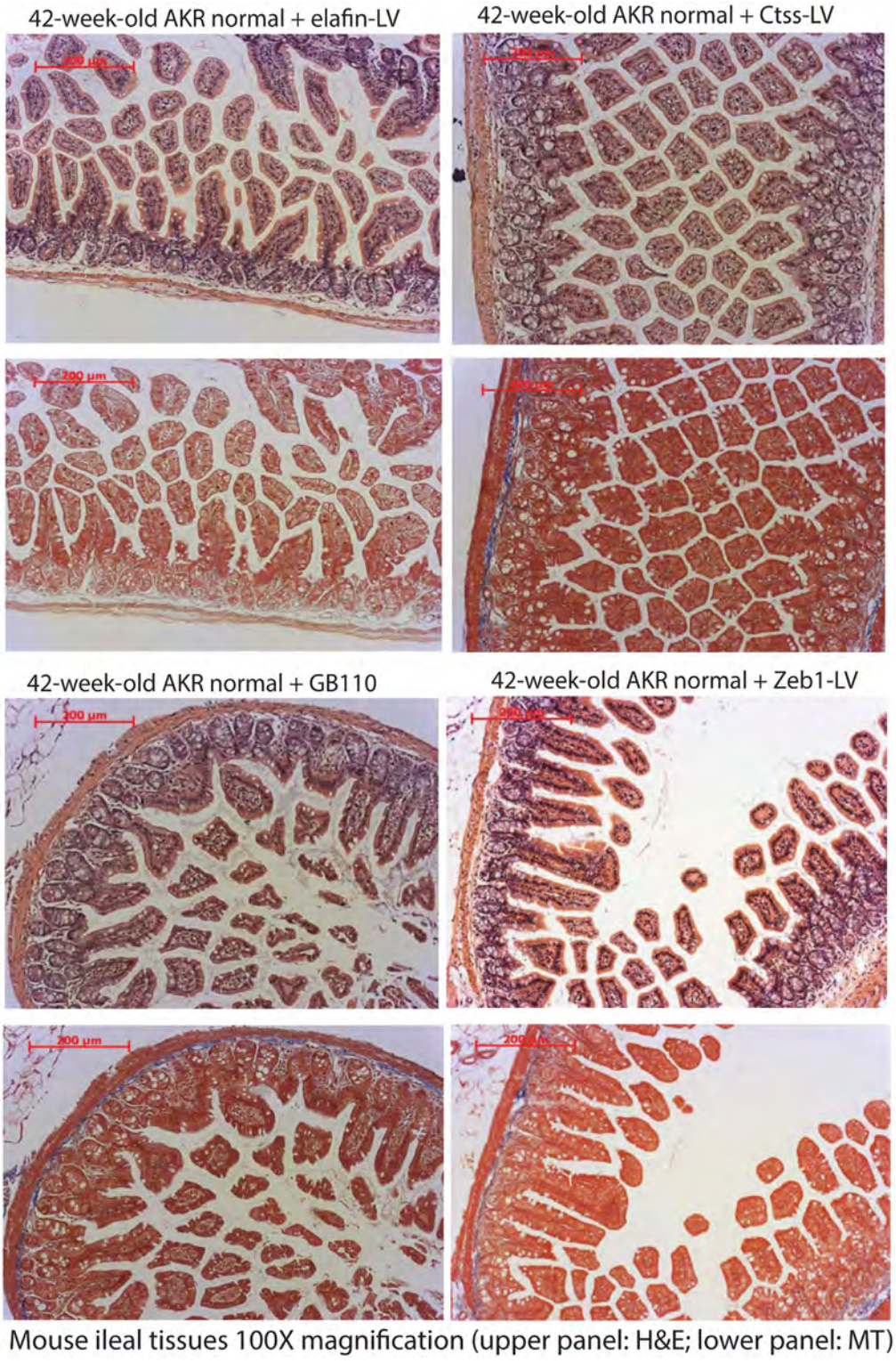

Figure 13. Elafin-overexpressing lentiviruses, Ctss-overexpressing lentivirus, and Zeb1-overexpressing lentivirus were injected into AKR mice intraperitoneally at 40 weeks of age. In addition, oral PAR2 agonist GB110 (10 mg/kg/day) was administered via oral gavage from 40 to 42 weeks of age. H&E staining (*upper panels*) and Masson Trichrome (MT) staining (*lower panels*) of ileal tissues did not find histologic injury or fibrosis. Six mice per group.

VVR-AFC to release free AFC. The released AFC can be quantified using a fluorometer or fluorescence plate reader.

We performed the cathepsin S activity assays in cell-free conditions to determine the direct interactions between purified elafin and cathepsin S proteins without interference from other cell components. Elafin (0.5–10 μg/mL final concentration), cathepsin S (0.4 μg/mL final concentration), and CS inhibitor (20 μmol/L final concentration, provided by the assay kit) were added to a mixture of CS reaction buffer and CS substrate buffer (200 μmol/L final concentration).

To measure cathepsin S activities in cells and tissues, cell culture media, cell lysates, and tissue lysates were first

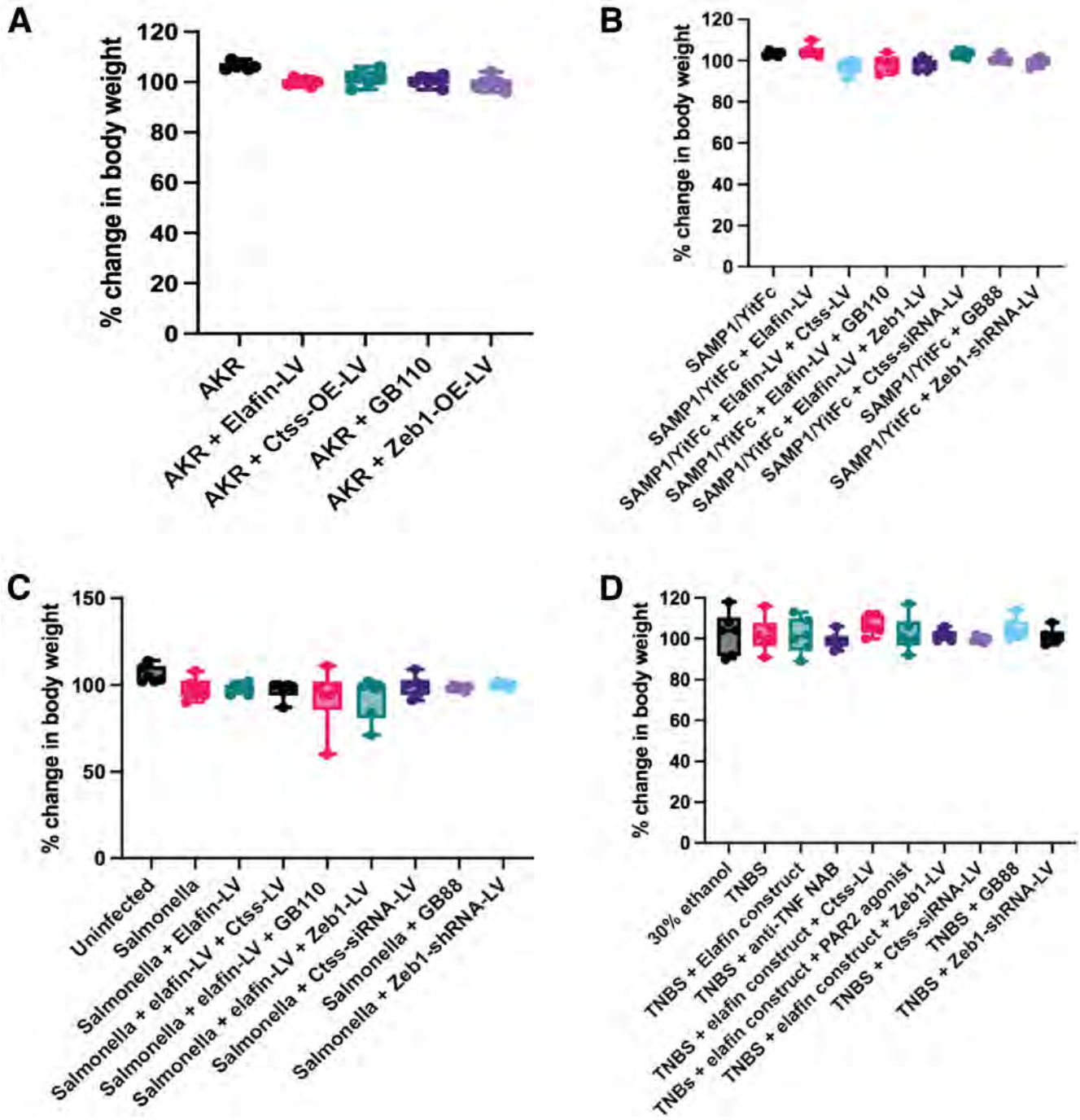

Figure 14. (*A*) Changes in body weight of AKR mice from 40 to 42 weeks of age. (*B*) Changes in body weight of SAMP/YitFc mice from 40 to 42 weeks of age. (*C*) Changes in body weight of uninfected and *Salmonella*-infected mice from day 14 to day 21. (*D*) Changes in body weight of normal and TNBS-treated mice from week 5 to week 7. Elafin overexpression and lentiviral/pharmacologic manipulations did not change body weight. n = 6 mice per group.

centrifuged for 10,000*g* at 4°C for 10 minutes and filtered through 40 μm to remove debris. The filtered supernatants were then added to a mixture of CS reaction buffer and CS substrate buffer (200 μmol/L final concentration).

The 100 μL/well mixture was incubated at 37°C for 1 hour. Relative fluorescence units were read with 400 nm excitation and 505 nm emission in clear-bottom dark-wall 96-well plates. Specific changes in protocols are mentioned in figure legends.

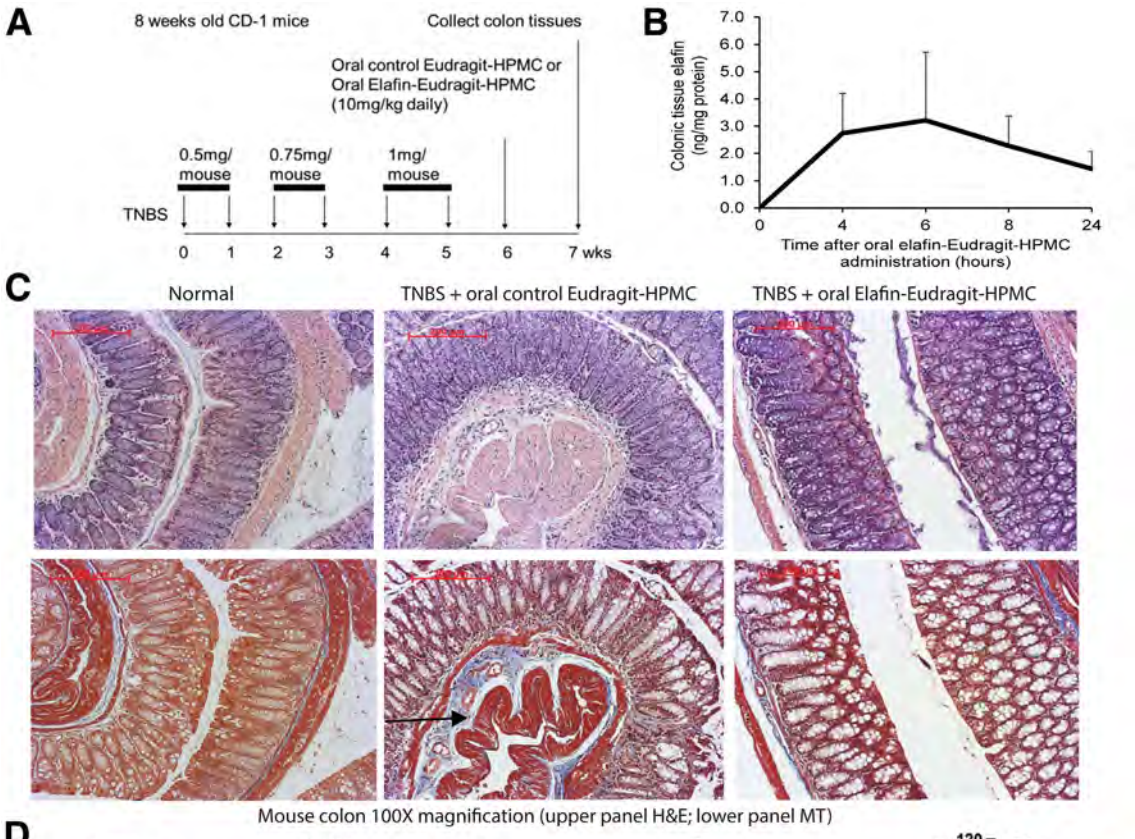

E

	SAMP1/YitFc + Elafin-LV	Salmonella + Elafin-LV	TNBS + Elafin construct	TNBS + Elafin-Eudragit-HPMC	mean	sd
Tissue elafin (ng/mg protein)	0.30±0.12 ileal	0.17±0.05 cecal	0.27±0.07 colonic	3.22±2.16 colonic peak	0.99	1.49
Ctss mRNA	46%	24%	53%	42%	41%	12%
Zeb1 mRNA	6%	4%	0%	0%	3%	3%
Histology score	18%	24%	58%	33%	33%	18%
Fibrosis score	21%	41%	20%	18%	25%	11%
ODA	6%	23%	9%	7%	11%	4%

Figure 15. (*A*) Experimental plan. The formulation was suspended in mildly acidified (pH 5) water containing 0.5% hydroxypropyl methylcellulose (HPMC) and administered to TNBS-treated mice via oral gavage. The Eudragit polymer releases its drug in the mid-distal ileum and colon under an alkaline environment at ~pH 8. (*B*) Elafin-Eudragit-HPMC (10 mg/kg) was administered to normal mice via oral gavage. Colonic tissue elafin levels were determined by ELISA (DY1747; R&D Systems). Mean ± standard deviation. (*C*) H&E staining (*upper panels*) and MT staining (*lower panels*) of colonic tissues. Blue color in MT staining (*arrows*) indicated collagen deposition. (*D*) Histology scores, fibrosis scores, overall disease activities, colonic Zeb1 mRNA expression, and changes in body weight. Six mice per group. Ordinary one-way ANOVA with Tukey tests. (*E*) Comparison of intestinal tissue elafin levels and efficiencies in regulating target genes and disease activities. Body weight changes in elafin treatment groups compared with their respective positive control groups. Mean ± standard deviation.

Table 5. Comparison of Clinical and Endoscopic Disease Activity Assessment Tools in IBD Patients % of IBD disease activity from severe to remission

Index	CDAI	HBI	PRO-2	St. Mark	Rachmilewitz	Mayo	SES-CD	CDEIS		
Assessment basis	symptom	symptom	symptom	symptom	symptom	both	endoscopic	endoscopic		
Disease	CD	CD	CD	UC	UC	UC	CD	CD		
High remission limit	149	4	7	3	4	2	2	3		
Low severe limit	451	17	35	15	18	11	16	13		
% of disease activity	33	24	20	20	22	18	13	23	Mean 22	Sd 5.82

CDAI, Crohn's disease activity index; CDEIS, Crohn's Disease Endoscopic Index of Severity; HBI, Harvey-Bradshaw Index; SES-CD, Simple Endoscopic Score for Crohn's Disease.
Defining Disease Severity in Inflammatory Bowel Diseases: Current and Future Directions

Crohn's Disease Patient-Derived Peripheral Blood Mononuclear Cells

CD-PBMCs from 3 CD patients (#70052; STEMCELL Technologies, Vancouver, Canada) were cultured in RPMI1640 medium containing 10% exosome-depleted fetal bovine serum (A2720803; Thermo Fisher Scientific) and 1% penicillin-streptomycin. Baseline characteristics are shown in Table 7. CD-PBMCs were preconditioned with 100 μg/mL stricturing CD or non-stricturing CDSE for 2 hours and then exposed to either 0.1% TFA or 1 μg/mL elafin for 6 hours. The cells were removed by centrifugation at 10,000*g* for 5 minutes at 4° C. The cell supernatants were collected for a 13-plex cytokine multiplex assay (HSTCMAG28SPMX13; Millipore Sigma, St Louis, MO).

Animal Experiments

All animal studies were approved by UCLA Institutional Animal Research Committee (#2007-116). All methods were compliant with the ARRIVE guidelines. Mice were randomized and assigned to cages by animal facility staff in a blinded manner and housed in the UCLA animal facility under standard environmental conditions. All interventions were performed during the light cycle.

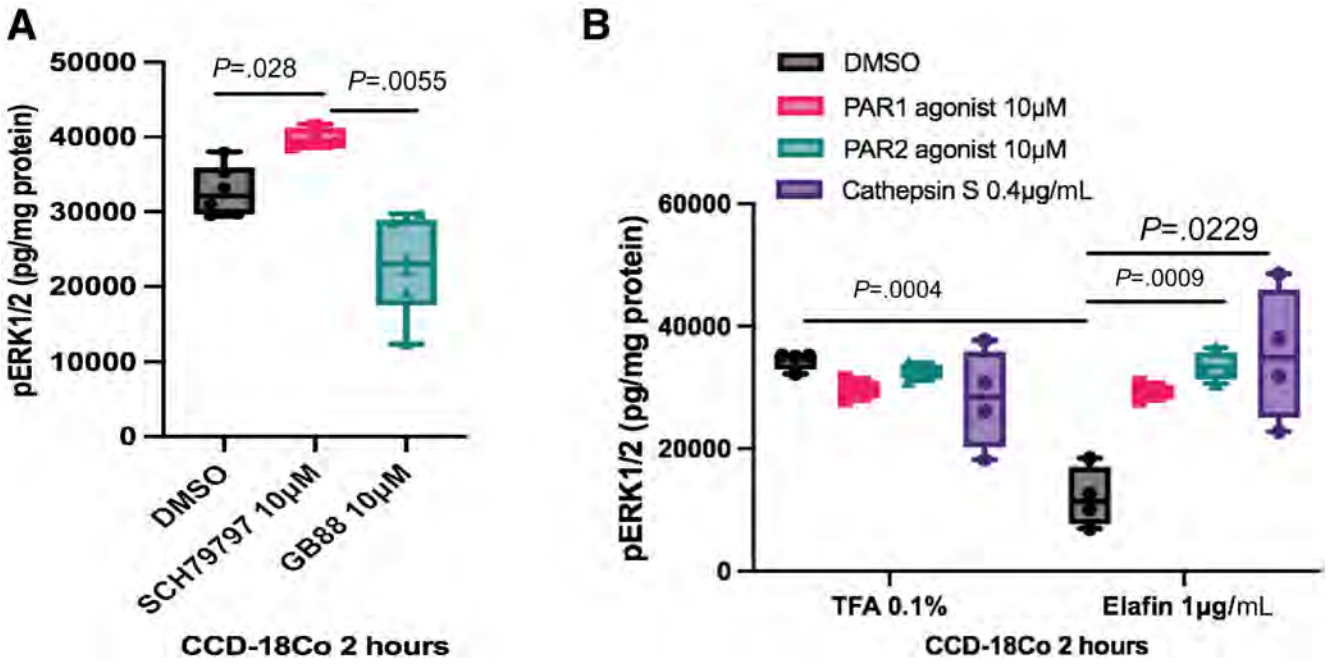

Figure 16. (*A*) Serum-starved CCD-18Co fibroblasts were treated with DMSO, PAR1 inhibitor (SCH79797), or PAR2 inhibitor (GB88) for 2 hours. PAR2 inhibitor GB88 inhibited ERK1/2 phosphorylation. Results were pooled from 3 independent experiments. Ordinary one-way ANOVA with Tukey test. (*B*) Serum-starved CCD-18Co fibroblasts were pretreated with DMSO, PAR1 agonist (10 μmol/L), PAR2 agonists (10 μmol/L), or cathepsin S (0.4 μg/mL) for 30 minutes, followed by incubation with elafin (1 μg/mL) for 2 hours. ERK1/2 phosphorylation was determined by ELISA. PAR2 agonist and cathepsin S reversed elafin-mediated inhibition of ERK phosphorylation. Results were pooled from 4 independent experiments. Ordinary one-way ANOVA with Tukey test.

Table 6. Cytokine Secretion in CD-PBMCs

CD PBMC 6 hours (*pg/mL*)		IFN-gamma mean	SD	IL-10 mean	SD	IL-13 mean	SD	IL-6 mean	SD	IL-7 mean	S	IL-8 mean	SD	TNFα mean	SD
no serum exosome	0.1% TFA	1.94	0.22	4.36	0.96	0.64	0.15	1.86	0.31	3.41	0.08	467.79	1.72	2.86	0.83
No serum exosome	Elafin 1μg/ml	2.69	0.44	4.77	0.42	0.62	0.09	1.85	0.04	3.90	0.08	539.54	58.15	3.58	0.32
CDS serum exosomes	0.1% TFA	2.22	0.40	3.71	0.36	0.82	0.34	1.75	0.05	3.35	0.70	583.98	11.30	3.80	0.21
CDS serum exosomes	Elafin 1μg/ml	3.09	0.37	3.65	0.29	0.84	0.05	1.99	0.14	3.66	0.32	591.44	14.63	4.41	0.40
CDNS serum exosomes	0.1% TFA	2.18	0.31	7.57	1.29	0.43	0.06	1.19	0.02	3.32	0.31	359.15	11.35	2.10	0.54
CDNS serum exosomes	Elafin 1μg/ml	1.64	0.07	7.12	0.63	0.57	0.12	1.04	0.02	2.39	0.35	256.31	20.34	1.59	0.12

NOTE. Results were pooled from 3 CD patients. Ordinary one-way ANOVA test did not find any significant differences.
IFN, interferon; IL, interleukin; PBMC, peripheral blood mononuclear cell; TNF, tumor necrosis factor.

SAMP1YitFc. We used 40-week-old male and female SAMP1/YitFc mice (#009355; Jackson Laboratories, Bar Harbor, ME). This model develops chronic ileitis with pre-existing ileal fibrosis around 40 weeks of age. We used 40-week-old AKR mice (#000648; Jackson Laboratories) as a parental normal control strain.[58]

Control lentivirus (PS100064V; OriGene, Rockville, MD), elafin-overexpressing lentiviruses (RC203136L1V; OriGene), Ctss-overexpressing lentivirus (#171210640196; Applied Biological Materials, Richmond, BC, Canada), Ctss-siRNA lentivirus (#171210940296; Applied Biological Materials), Zeb1-shRNA lentivirus (TL513177V; OriGene), and Zeb1-overexpressing lentivirus (MR223095L2V; OriGene) were injected to AKR or SAMP1/YitFc mice intraperitoneally once at 40 weeks of age. In addition, PAR2 agonist GB110 (HY-120528A; MedChemExpress [MCE], Monmouth Junction, NJ) or PAR2 inhibitor GB88 was given via oral gavage from 40 to 42 weeks of age. Ileal tissues were collected for analyses at 42 weeks of age.

Because SAMP1/YifFc mice were inefficient breeders and had low availability, we conducted the experiments in batches of 4 mice per batch. The SAMP1/YitFc mice were kept in cohousing during weeks 8–40 and then assigned to various groups in single housing conditions during weeks 40–42. We conducted 12 rounds of experiments in total.

Salmonella. We first treated 8-week-old male and female 129Sv/J mice (000691; Jackson Laboratories) with 20 mg streptomycin via oral gavage. The mice then received *Salmonella typhimurium* SL1344 strain (10^8 cfu) by oral gavage 1 day later. We used uninfected 8-week-old 129Sv/J mice for the control group and kept them along with the infection course. Cecal fibrosis develops from day 14 to day 21 after infection.[39]

Control lentivirus (PS100064V; OriGene), elafin-overexpressing lentiviruses (RC203136L1V; OriGene), Ctss-overexpressing lentivirus (#171210640196, Applied Biological Materials), Ctss-siRNA lentivirus (#171210940296; Applied Biological Materials), Zeb1-shRNA lentivirus (TL513177V; OriGene), and Zeb1-overexpressing lentivirus (MR223095L2V; OriGene) were injected into the infected mice intraperitoneally once on day 14 after infection. In addition, PAR2 agonist GB110 (HY-120528A; MCE) or PAR2 inhibitor GB88 was given daily via oral gavages from day 14 to day 21 after infection. Cecal tissues were collected for analyses on day 21 after infection.

All *Salmonella* infection experiments were conducted in 3 rounds with 3 male and 3 female mice. Mice were kept in cohousing throughout days 0–21 in the first 2 rounds. Because some mice died during the first 2 rounds of experiments, we conducted the third round to compensate for the loss of mice. Mice in the third round were kept in cohousing during days 0–14 and then single housing during days 14 and 21.

TNBS. We injected 8-week-old male and female outbred CD-1 mice (#022; Charles River Laboratories, Wilmington, MA) with TNBS solution in 30% ethanol via enema weekly 6 times (weeks 0, 1, 2, 3, 4, and 5). Thirty percent ethanol was used to help the penetration of TNBS into the colonic mucosa. Colonic fibrosis typically develops 1 week after the last injection (week 6). The normal control group was treated with 6 weekly injections of 30% ethanol via enema.

Some mice received a single intracolonic injection of 5 μg/mouse of either control construct (PS100001) or elafin-overexpressing construct (RC203136) from OriGene via InvivoJetPEI transfection reagent (201-10G; Polyplus, Illkirch-Graffenstaden, France) on the ninth day after the last TNBS injection. In addition, anti-TNFα neutralizing antibodies (BE0058; BioXCell, Lebanon, NH) were injected intraperitoneally.

TNBS-treated mice were injected with Ctss-overexpressing lentivirus (#171210640196) or Ctss-siRNA lentiviruses (#171210940296; Applied Biological Materials, Inc), Zeb1-overexpressing lentivirus (MR223095L2V), or Zeb1-shRNA lentivirus (TL513177V; OriGene) on the ninth day after the last TNBS injection. In addition, some mice were injected with 5 mg/kg PAR2 agonist SLIGKV-NH_2 (HY-P0283; MCE) intracolonically on days 9, 11, and 13 after the last TNBS injection. PAR2 inhibitor GB88 (10 mg/kg/day) was administered via oral gavage. Colonic tissues were collected 2 weeks after the last TNBS injection.

All TNBS colitis experiments were conducted in 2 rounds, with 3 male mice per group in the first round and 3

Table 7. Baseline Characteristics of Frozen Human Colonic Tissue Samples, Fresh Colonic Tissue Samples From Colon Cancer Patients, Fresh Ileal Tissue Samples From Stricturing CD Patients, Primary Stricturing CD Patient-Derived Intestinal Fibroblasts, Primary Peripheral Blood Mononuclear Cells From CD Patients, and Human Serum Samples

Colonic tissues (mean ± SD)	Non-IBD	UC	CD without stricture	CD with stricture
Elafin mRNA expression (fold)	5.7 ± 1.9	11.8 ± 2.7	5.4 ± 1	2.9 ± 2.3
Age at collection (*y*)	62 ± 13.9	43 ± 15.1	45 ± 19	36 ± 23.6
Gender (% male)	73	55	62	50
Histology score	2.6 ± 1.9	7.5 ± 2.9	8.8 ± 3.7	8.6 ± 4.6
Simple colitis activity score	N/A	6.8	N/A	N/A
Harvey Bradshaw Index	N/A	N/A	7.5 ± 1.2	5 ± 1.9
% of biologics	0	24	50	40
% of 6-mercaptopurine or steroid	0	51	66	33
Duration of disease (*y*)	26 ± 3	12 ± 2	8 ± 3	18 ± 3
n	40	52	28	15

Serum samples (mean ± SD)	Non-IBD	UC	CD without stricture	CD with stricture
Serum elafin levels (*pg/mL*)	7939 ± 791	12,987 ± 1124	7042 ± 520	11,263 ± 1818
Age at collection (*y*)	46 ± 12	40 ± 10	34 ± 11	40 ± 13
Gender (% male)	42	35	40	60
Harvey Bradshaw Index	N/A	N/A	3.7	5
Partial Mayo score	N/A	2.1 ± 0.4	N/A	N/A
% of biologics	N/A	13	40	46
% of 6-mercaptopurine or steroid	N/A	12	33	42
Duration of disease (*y*)	N/A	6 ± 2	11 ± 1.4	11 ± 2.3
n	12	23	33	20

Fresh colonic tissues from colon cancer

Patient	1	2	3	4	5	6
Age (*y*)	63	58	73	38	68	45
Gender	Female	Male	Female	Male	Male	Male
Disease	Adenocarcinoma	Moderately invasive adenocarcinoma	Moderately differentiated adenocarcinoma	Diverticulitis	Adenocarcinoma of descending colon	Adenocarcinoma of sigmoid colon
Disease location	Ascending colon	Proximal ascending colon	Ascending colon	Sigmoid colon	Descending colon	Sigmoid colon

CD-HIF	Fresh ileal tissues from CD patients							
Patient	1	2	3	4	Patient	1	2	3
Age (*y*)	41	45	66	68	Age (*y*)	41	45	48
Gender	Male	Female	Male	Female	Gender	Male	Female	Male
Disease	CD stricture	CD stricture	CD stricture	CD stricture	Disease	CD stricture	CD stricture	CD stricture
Disease location	Ileum	Ileum	Colon	Colon	Disease location	Ileum	Ileum	Ileum
					Medication	Budesonide	Stelara	Humira

Stemcell Technologies CD PBMC 70052

Lot	200871901C	1010113306	200971001C
Age (*y*)	48	25	32
Sex	Female	Female	Male
Ethnicity	Caucasian African American		Caucasian
Diagnosis date	42369	38353	40908
Process date	44062	42350	44084
Smoker	No	No	No

Table 7. Continued

		Stemcell Technologies CD PBMC 70052	
		VSL#3, Tri-	
		Previfem,	
Medications	Vitamin D	Tamiflu	None

female mice per group in the second round. Mice were kept in cohousing condition throughout weeks 1–7.

Production of Elafin-Eudragit-Hydroxypropyl Methylcellulose

In Texas, Southwest Research Institute produced the oral elafin-Eudragit-FS30D formulation via a material transfer agreement (MTA2019-00000337). First, elafin was coated with Eudragit FS30D polymer. This pH-responsive polymer is insoluble in acid but dissolves in a mildly alkaline environment (ie, pH 7 or above), which is optimal for colonic delivery. Next, elafin-Eudragit was packaged into microparticles using a Southwest Research Institute–patented spinning disk atomization technology. This packaging technology prevented leakage of elafin in acidic conditions. Finally, the elafin-Eudragit microparticles were dried. The resulting powder was suspended in 0.5% HPMC in water for oral gavage.

Table 8. Catalog and Batch Numbers of Reagents

	Catalog number	Lot number
Human PCR assays	Source: Thermo Fisher	
COL1A2	(Hs01028956_m1)	1811559
COL3A1	(Hs00943809_m1)	1771975
TGF-β1	(Hs00998133_m1)	1543822
N-cadherin	(Hs00983056_m1)	1248923
ZEB1	(Hs01566408_m1)	2005137
CTSS	(Hs00175407_m1)	1929800
18S (endogenous control)	(Hs99999901_s1)	1739902
Mouse PCR assays	Source: Thermo Fisher	
Col1a2	(Mm00483888_m1)	1782343
Col3a1	(Mm00802300_m1)	1763098
Tgf-β1	(Mm01178820_m1)	1313258
Zeb1	(Mm00495564_m1)	1868064
Vim	(Mm01333430_m1)	1910567
Acta2	(Mm00725415_s1)	2021653
Tnf	(Mm00443258_m1)	1980751
Emr1/Adgre1	(Mm00802529_m1)	1788225
Ctss	(Mm01255859_m1)	1883639
Gapdh (endogenous control)	(Mm99999915_g1)	1927287

Elafin-fibrosis project Elafin	Vendor Anaspec	Catalog # AS-61641	Purity 95%	Batch 2055773
Protease-activated receptor-2, amide SLIGKV-NH2	MCE	HY-P0283	98.33%	29492
2-Furoyl-LIGRLO-amide	MCE	HY-P1314	99.87%	57931
GB-110 hydrochloride	MCE	HY-120528A	99.94%	50389
GB-88	Eton Bioscience	2300100052	98.10%	1416435-96-5
SCH79797 hydrochloride	Sigma	SML1939	98%	57328
Control lentivirus Elafin overexpressing Lentivirus Mouse Zeb1 shRNA lentivirus Mouse Zeb1 overexpressing lentivirus Mouse Ctss siRNA lentivirus	OriGene OriGene OriGene OriGene ABMgood	PS1000064V RC203136L1V TL513177V MR223095L2V 171210940296	N/A N/A N/A N/A N/A	133EE26 SR156301 SR168040 SR180321 V21H18I
Mouse Ctss overexpressing lentivirus Control construct Human elafin overexpressing Construct Human ZEB1 overexpressing construct	ABMgood OriGene OriGene Origene	171210640196 PS100001 RC203136 RC217704	N/A N/A N/A N/A	V21H25I N/A N/A BJ10116-194610948

Histologic Evaluations

Intestinal tissue injury was evaluated with H&E staining, whereas extracellular matrix deposition was identified by Masson Trichrome staining. H&E- and Masson Trichrome–stained microphotographs were recorded at multiple locations and scored by 2 investigators blindly.[10,40] The chronic intestinal injury was scored in terms of mucosal transformation (0/3/6), round cell infiltration in the lamina propria mucosa (0-3), goblet cell death (0/1), tela submucosa fibrosa (0/1), and granuloma (0/1). These parameters result in a total score (0–12).[59] In addition, intestinal fibrosis was scored on a scale of normal, mild, moderate, and severe (0–3).[39]

Quantitative Real-Time Reverse Transcription Polymerase Chain Reaction

Total RNA was isolated by an RNeasy kit (#74104; Qiagen, Hilden, Germany) and reverse transcribed into cDNA (#4368813; Thermo Fisher Scientific). Polymerase chain reactions were run with cDNA, iTaq Universal SYBR Green Supermix (1725120; Bio-Rad), and TaqMan real-time polymerase chain reaction assays (Table 8) in a Bio-Rad CFX384 system.[60] After normalization with endogenous control genes, relative mRNA quantification was performed by comparing test and control groups. The fold changes are expressed as $2^{\Delta\Delta Ct}$. Fold-change values greater than 1 indicate a positive or an up-regulation. Conversely, fold-change values less than 1 indicate a negative or down-regulation.

Calculation of Overall Disease Activities

We converted histology scores, fibrosis scores, and intestinal gene expression into percentages to help compare between groups and models of intestinal fibrosis. It included several fibrosis-related and inflammation-related genes commonly reported by our and other intestinal fibrosis research groups. *Col1a2* and *Col3a1* are fibrosis signatures.[26,27,61,62] *Col3a1* was excluded in the *Salmonella* model because *Salmonella* infection did not affect cecal *Col3a1* mRNA expression.[27] *Acta2*, *Vim*, and *Zeb1* are fibroblasts and epithelial-mesenchymal transition markers.[38,63,64] *Tnf* and *Emr1* are inflammation markers.[40,65] The mRNA expression lower than the control group in negative percentage values was assigned 0, indicating complete inhibition. ODA is the average value of these parameters.

Power Analysis

The colonic tissue cohort of 40 non-IBD, 52 UC, and 43 CD patients provided adequate power to detect colonic elafin mRNA expression.[6] At least 3 mice per group were required to achieve a statistically significant difference in histology score between the TNBS group (8.33) and TNBS + anti-TNFα (6.4) group with standard deviation = 0.93, alpha = 0.5, and power = 0.8. Our study with 6 mice per group satisfied this requirement. We did not perform power analysis for in vitro experiments but followed the common practice of performing in vitro experiments 3 times or more independently.

Statistical Analysis

Results were expressed as mean ± standard deviation. We used Graphpad Prism 9 (San Diego, CA) to perform multiple-group comparisons using ordinary one-way analyses of variance (ANOVAs) with Tukey post hoc tests and two-group comparisons using Student *t* tests. The *P* values of statistical significance are shown in each figure or table.

References

1. Lenti MV, Di Sabatino A. Intestinal fibrosis. Mol Aspects Med 2019;65:100–109.
2. Cleynen I, Gonzalez JR, Figueroa C, Franke A, McGovern D, Bortlik M, Crusius BJ, Vecchi M, Artieda M, Szczypiorska M, Bethge J, Arteta D, Ayala E, Danese S, van Hogezand RA, Panes J, Pena SA, Lukas M, Jewell DP, Schreiber S, Vermeire S, Sans M. Genetic factors conferring an increased susceptibility to develop Crohn's disease also influence disease phenotype: results from the IBDchip European Project. Gut 2013;62:1556–1565.
3. Louis E, Collard A, Oger AF, Degroote E, Aboul Nasr El Yafi FA, Belaiche J. Behaviour of Crohn's disease according to the Vienna classification: changing pattern over the course of the disease. Gut 2001;49:777–782.
4. Kugathasan S, Denson LA, Walters TD, Kim MO, Marigorta UM, Schirmer M, Mondal K, Liu C, Griffiths A, Noe JD, Crandall WV, Snapper S, Rabizadeh S, Rosh JR, Shapiro JM, Guthery S, Mack R, Kellermayer R, Kappelman MD, Steiner S, Moulton DE, Keljo D, Cohen S, Oliva-Hemker M, Heyman MB, Otley AR, Baker SS, Evans JS, Kirschner BS, Patel AS, Ziring D, Trapnell BC, Sylvester FA, Stephens MC, Baldassano RN, Markowitz JF, Cho J, Xavier RJ, Huttenhower C, Aronow BJ, Gibson G, Hyams JS, Dubinsky MC. Prediction of complicated disease course for children newly diagnosed with Crohn's disease: a multicentre inception cohort study. Lancet 2017;389:1710–1718.
5. Rottoli M, Vallicelli C, Ghignone F, Tanzanu M, Vitali G, Gionchetti P, Rizzello F, Poggioli G. Predictors of early recurrence after strictureplasty for Crohn's disease of the small bowel during the years of biologics. Dig Liver Dis 2019;51:663–668.
6. Wang J, Ortiz C, Fontenot L, Xie Y, Ho W, Mattai SA, Shih DQ, Koon HW. High circulating elafin levels are associated with Crohn's disease-associated intestinal strictures. PLoS One 2020;15:e0231796.
7. Ayyar KK, Moss AC. Exosomes in intestinal inflammation. Front Pharmacol 2021;12:658505.
8. Galipeau HJ, Wiepjes M, Motta JP, Schulz JD, Jury J, Natividad JM, Pinto-Sanchez I, Sinclair D, Rousset P, Martin-Rosique R, Bermudez-Humaran L, Leroux JC, Murray JA, Smecuol E, Bai JC, Vergnolle N, Langella P, Verdu EF. Novel role of the serine protease inhibitor elafin in gluten-related disorders. Am J Gastroenterol 2014;109:748–756.

9. Zhang H, Wang L, Li C, Yu Y, Yi Y, Wang J, Chen D. Exosome-induced regulation in inflammatory bowel disease. Front Immunol 2019;10:1464.
10. Yoo JH, Ho S, Tran DH, Cheng M, Bakirtzi K, Kukota Y, Ichikawa R, Su B, Tran DH, Hing TC, Chang I, Shih DQ, Issacson RE, Gallo RL, Fiocchi C, Pothoulakis C, Koon HW. Anti-fibrogenic effects of the anti-microbial peptide cathelicidin in murine colitis-associated fibrosis. Cell Mol Gastroenterol Hepatol 2015;1:55–174 e1.
11. Scheenstra MR, van den Belt M, Tjeerdsma-van Bokhoven JLM, Schneider VAF, Ordonez SR, van Dijk A, Veldhuizen EJA, Haagsman HP. Cathelicidins PMAP-36, LL-37 and CATH-2 are similar peptides with different modes of action. Sci Rep 2019;9:4780.
12. Shaw L, Wiedow O. Therapeutic potential of human elafin. Biochem Soc Trans 2011;39:1450–1454.
13. Wiedow O, Schroder JM, Gregory H, Young JA, Christophers E. Elafin: an elastase-specific inhibitor of human skin—purification, characterization, and complete amino acid sequence. J Biol Chem 1990; 265:14791–14795.
14. Zhang W, Teng G, Wu T, Tian Y, Wang H. Expression and clinical significance of elafin in inflammatory bowel disease. Inflamm Bowel Dis 2017;23:2134–2141.
15. Zhang W, Teng GG, Tian Y, Wang HH. [Expression of elafin in peripheral blood in inflammatory bowel disease patients and its clinical significance]. Zhonghua Yi Xue Za Zhi 2016;96:1120–1123.
16. Flach CF, Eriksson A, Jennische E, Lange S, Gunnerek C, Lonnroth I. Detection of elafin as a candidate biomarker for ulcerative colitis by whole-genome microarray screening. Inflamm Bowel Dis 2006; 12:837–842.
17. Schmid M, Fellermann K, Fritz P, Wiedow O, Stange EF, Wehkamp J. Attenuated induction of epithelial and leukocyte serine antiproteases elafin and secretory leukocyte protease inhibitor in Crohn's disease. J Leukoc Biol 2007;81:907–915.
18. Curciarello R, Sobande T, Jones S, Giuffrida P, Di Sabatino A, Docena GH, MacDonald TT, Kok K. Human neutrophil elastase proteolytic activity in ulcerative colitis favors the loss of function of therapeutic monoclonal antibodies. J Inflamm Res 2020;13:233–243.
19. Motta JP, Rolland C, Edir A, Florence AC, Sagnat D, Bonnart C, Rousset P, Guiraud L, Quaranta-Nicaise M, Mas E, Bonnet D, Verdu EF, McKay DM, Buscail E, Alric L, Vergnolle N, Deraison C. Epithelial production of elastase is increased in inflammatory bowel disease and causes mucosal inflammation. Mucosal Immunol 2021; 14:667–678.
20. Motta JP, Magne L, Descamps D, Rolland C, Squarzoni-Dale C, Rousset P, Martin L, Cenac N, Balloy V, Huerre M, Frohlich LF, Jenne D, Wartelle J, Belaaouaj A, Mas E, Vinel JP, Alric L, Chignard M, Vergnolle N, Sallenave JM. Modifying the protease, antiprotease pattern by elafin overexpression protects mice from colitis. Gastroenterology 2011;140:1272–1282.
21. Bermudez-Humaran LG, Motta JP, Aubry C, Kharrat P, Rous-Martin L, Sallenave JM, Deraison C, Vergnolle N, Langella P. Serine protease inhibitors protect better than IL-10 and TGF-beta anti-inflammatory cytokines against mouse colitis when delivered by recombinant lactococci. Microb Cell Fact 2015;14:26.
22. Wang J, Ortiz C, Fontenot L, Mukhopadhyay R, Xie Y, Law IKM, Shih DQ, Mattai SA, Li Z, Koon HW. Elafin inhibits obesity, hyperglycemia, and liver steatosis in high-fat diet-treated male mice. Sci Rep 2020;10:12785.
23. Alam SR, Lewis SC, Zamvar V, Pessotto R, Dweck MR, Krishan A, Goodman K, Oatey K, Harkess R, Milne L, Thomas S, Mills NM, Moore C, Semple S, Wiedow O, Stirrat C, Mirsadraee S, Newby DE, Henriksen PA. Perioperative elafin for ischaemia-reperfusion injury during coronary artery bypass graft surgery: a randomised-controlled trial. Heart 2015;101:1639–1645.
24. Liu B, Yang MQ, Yu TY, Yin YY, Liu Y, Wang XD, He ZG, Yin L, Chen CQ, Li JY. Mast cell tryptase promotes inflammatory bowel disease-induced intestinal fibrosis. Inflamm Bowel Dis 2021;27:242–255.
25. Ehrhardt K, Steck N, Kappelhoff R, Stein S, Rieder F, Gordon IO, Boyle EC, Braubach P, Overall CM, Finlay BB, Grassl GA. Persistent Salmonella enterica Serovar Typhimurium infection induces protease expression during intestinal fibrosis. Inflamm Bowel Dis 2019;25:1629–1643.
26. Lawrance IC, Wu F, Leite AZ, Willis J, West GA, Fiocchi C, Chakravarti S. A murine model of chronic inflammation-induced intestinal fibrosis down-regulated by antisense NF-kappa B. Gastroenterology 2003; 125:1750–1761.
27. Grassl GA, Valdez Y, Bergstrom KS, Vallance BA, Finlay BB. Chronic enteric salmonella infection in mice leads to severe and persistent intestinal fibrosis. Gastroenterology 2008;134:768–780.
28. Pizarro TT, Pastorelli L, Bamias G, Garg RR, Reuter BK, Mercado JR, Chieppa M, Arseneau KO, Ley K, Cominelli F. SAMP1/YitFc mouse strain: a spontaneous model of Crohn's disease-like ileitis. Inflamm Bowel Dis 2011;17:2566–2584.
29. Kosiewicz MM, Nast CC, Krishnan A, Rivera-Nieves J, Moskaluk CA, Matsumoto S, Kozaiwa K, Cominelli F. Th1-type responses mediate spontaneous ileitis in a novel murine model of Crohn's disease. J Clin Invest 2001;107:695–702.
30. Loh CY, Chai JY, Tang TF, Wong WF, Sethi G, Shanmugam MK, Chong PP, Looi CY. The E-cadherin and N-cadherin switch in epithelial-to-mesenchymal transition: signaling, therapeutic implications, and challenges. Cells 2019;8.
31. Zhang P, Sun Y, Ma L. ZEB1: at the crossroads of epithelial-mesenchymal transition, metastasis and therapy resistance. Cell Cycle 2015;14:481–487.
32. Simmons JG, Pucilowska JB, Keku TO, Lund PK. IGF-I and TGF-beta1 have distinct effects on phenotype and proliferation of intestinal fibroblasts. Am J Physiol Gastrointest Liver Physiol 2002;283:G809–G818.
33. Cheng XW, Kuzuya M, Nakamura K, Di Q, Liu Z, Sasaki T, Kanda S, Jin H, Shi GP, Murohara T, Yokota M, Iguchi A. Localization of cysteine protease, cathepsin S, to the surface of vascular smooth muscle cells by

association with integrin alphanubeta3. Am J Pathol 2006;168:685–694.
34. Cattaruzza F, Lyo V, Jones E, Pham D, Hawkins J, Kirkwood K, Valdez-Morales E, Ibeakanma C, Vanner SJ, Bogyo M, Bunnett NW. Cathepsin S is activated during colitis and causes visceral hyperalgesia by a PAR2-dependent mechanism in mice. Gastroenterology 2011; 141:1864–1874 e1–e3.
35. Elmariah SB, Reddy VB, Lerner EA. Cathepsin S signals via PAR2 and generates a novel tethered ligand receptor agonist. PLoS One 2014;9:e99702.
36. Zhao P, Lieu T, Barlow N, Metcalf M, Veldhuis NA, Jensen DD, Kocan M, Sostegni S, Haerteis S, Baraznenok V, Henderson I, Lindstrom E, Guerrero-Alba R, Valdez-Morales EE, Liedtke W, McIntyre P, Vanner SJ, Korbmacher C, Bunnett NW. Cathepsin S causes inflammatory pain via biased agonism of PAR2 and TRPV4. J Biol Chem 2014;289:27215–27234.
37. Lee J, Jung E, Gestoso K, Heur M. ZEB1 mediates fibrosis in corneal endothelial mesenchymal transition through SP1 and SP3. Invest Ophthalmol Vis Sci 2020; 61:41.
38. Yao L, Conforti F, Hill C, Bell J, Drawater L, Li J, Liu D, Xiong H, Alzetani A, Chee SJ, Marshall BG, Fletcher SV, Hancock D, Coldwell M, Yuan X, Ottensmeier CH, Downward J, Collins JE, Ewing RM, Richeldi L, Skipp P, Jones MG, Davies DE, Wang Y. Paracrine signalling during ZEB1-mediated epithelial-mesenchymal transition augments local myofibroblast differentiation in lung fibrosis. Cell Death Differ 2019;26:943–957.
39. Johnson LA, Luke A, Sauder K, Moons DS, Horowitz JC, Higgins PD. Intestinal fibrosis is reduced by early elimination of inflammation in a mouse model of IBD: impact of a "Top-Down" approach to intestinal fibrosis in mice. Inflamm Bowel Dis 2012;18:460–471.
40. Xu C, Ghali S, Wang J, Shih DQ, Ortiz C, Mussatto CC, Lee EC, Tran DH, Jacobs JP, Lagishetty V, Fleshner P, Robbins L, Vu M, Hing TC, McGovern DPB, Koon HW. CSA13 inhibits colitis-associated intestinal fibrosis via a formyl peptide receptor like-1 mediated HMG-CoA reductase pathway. Sci Rep 2017;7:16351.
41. Peyrin-Biroulet L, Panes J, Sandborn WJ, Vermeire S, Danese S, Feagan BG, Colombel JF, Hanauer SB, Rycroft B. Defining disease severity in inflammatory bowel diseases: current and future directions. Clin Gastroenterol Hepatol 2016;14:348–354 e17.
42. Motta JP, Bermudez-Humaran LG, Deraison C, Martin L, Rolland C, Rousset P, Boue J, Dietrich G, Chapman K, Kharrat P, Vinel JP, Alric L, Mas E, Sallenave JM, Langella P, Vergnolle N. Food-grade bacteria expressing elafin protect against inflammation and restore colon homeostasis. Sci Transl Med 2012;4:158ra44.
43. Jimenez-Vargas NN, Pattison LA, Zhao P, Lieu T, Latorre R, Jensen DD, Castro J, Aurelio L, Le GT, Flynn B, Herenbrink CK, Yeatman HR, Edgington-Mitchell L, Porter CJH, Halls ML, Canals M, Veldhuis NA, Poole DP, McLean P, Hicks GA, Scheff N, Chen E, Bhattacharya A, Schmidt BL, Brierley SM, Vanner SJ, Bunnett NW. Protease-activated receptor-2 in endosomes signals persistent pain of irritable bowel syndrome. Proc Natl Acad Sci U S A 2018; 115:E7438–E7447.
44. Tsunemi M, Matsuura Y, Sakakibara S, Katsube Y. Crystal structure of an elastase-specific inhibitor elafin complexed with porcine pancreatic elastase determined at 1.9 A resolution. Biochemistry 1996;35:11570–11576.
45. Baranger K, Zani ML, Chandenier J, Dallet-Choisy S, Moreau T. The antibacterial and antifungal properties of trappin-2 (pre-elafin) do not depend on its protease inhibitory function. FEBS J 2008;275:2008–2020.
46. Small DM, Zani ML, Quinn DJ, Dallet-Choisy S, Glasgow AM, O'Kane C, McAuley DF, McNally P, Weldon S, Moreau T, Taggart CC. A functional variant of elafin with improved anti-inflammatory activity for pulmonary inflammation. Mol Ther 2015;23:24–31.
47. Kato A, Rooney AP, Furutani Y, Hirose S. Evolution of trappin genes in mammals. BMC Evol Biol 2010; 10:31.
48. Schalkwijk J, Wiedow O, Hirose S. The trappin gene family: proteins defined by an N-terminal transglutaminase substrate domain and a C-terminal four-disulphide core. Biochem J 1999;340(Pt 3):569–577.
49. Williams SE, Brown TI, Roghanian A, Sallenave JM. SLPI and elafin: one glove, many fingers. Clin Sci (Lond) 2006; 110:21–35.
50. Nugteren S, Samsom JN. Secretory leukocyte protease inhibitor (SLPI) in mucosal tissues: protects against inflammation, but promotes cancer. Cytokine Growth Factor Rev 2021;59:22–35.
51. Habgood AN, Tatler AL, Porte J, Wahl SM, Laurent GJ, John AE, Johnson SR, Jenkins G. Secretory leukocyte protease inhibitor gene deletion alters bleomycin-induced lung injury, but not development of pulmonary fibrosis. Lab Invest 2016;96:623–631.
52. Taggart CC, Lowe GJ, Greene CM, Mulgrew AT, O'Neill SJ, Levine RL, McElvaney NG. Cathepsin B, L, and S cleave and inactivate secretory leucoprotease inhibitor. J Biol Chem 2001;276:33345–33352.
53. Cole ET, Scott RA, Connor AL, Wilding IR, Petereit HU, Schminke C, Beckert T, Cade D. Enteric coated HPMC capsules designed to achieve intestinal targeting. Int J Pharm 2002;231:83–95.
54. Wang J, Ortiz C, Fontenot L, Mukhopadhyay R, Xie Y, Chen X, Feng H, Pothoulakis C, Koon HW. The therapeutic mechanism macrophage inflammatory protein 1 alpha (MIP-1alpha/CCL3) neutralizing antibody in Clostridium difficile infection in mice. J Infect Dis 2019.
55. Kaschwich M, Lutzen U, Zhao Y, Tjiong A, Marx M, Haenisch S, Wiedow O, Preuss S, Culman J, Zuhayra M. Biodistribution and pharmacokinetics of the (99m)Tc labeled human elastase inhibitor, elafin, in rats. Drug Metab Pharmacokinet 2016;31:146–155.
56. Bettenworth D, Nowacki TM, Cordes F, Buerke B, Lenze F. Assessment of stricturing Crohn's disease: current clinical practice and future avenues. World J Gastroenterol 2016;22:1008–1016.

57. Gulhane M, Murray L, Lourie R, Tong H, Sheng YH, Wang R, Kang A, Schreiber V, Wong KY, Magor G, Denman S, Begun J, Florin TH, Perkins A, Cuiv PO, McGuckin MA, Hasnain SZ. High fat diets induce colonic epithelial cell stress and inflammation that is reversed by IL-22. Sci Rep 2016;6:28990.
58. Menghini P, Di Martino L, Lopetuso LR, Corridoni D, Webster JC, Xin W, Arseneau KO, Lam M, Pizarro TT, Cominelli F. A novel model of colitis-associated cancer in SAMP1/YitFc mice with Crohn's disease-like ileitis. PLoS One 2017;12:e0174121.
59. Kruschewski M, Foitzik T, Perez-Canto A, Hubotter A, Buhr HJ. Changes of colonic mucosal microcirculation and histology in two colitis models: an experimental study using intravital microscopy and a new histological scoring system. Dig Dis Sci 2001; 46:2336–2343.
60. Koon HW, Shih DQ, Chen J, Bakirtzi K, Hing TC, Law I, Ho S, Ichikawa R, Zhao D, Xu H, Gallo R, Dempsey P, Cheng G, Targan SR, Pothoulakis C. Cathelicidin signaling via the Toll-like receptor protects against colitis in mice. Gastroenterology 2011;141: 1852–1863 e1, –e3.
61. Masterson JC, McNamee EN, Jedlicka P, Fillon S, Ruybal J, Hosford L, Rivera-Nieves J, Lee JJ, Furuta GT. CCR3 blockade attenuates eosinophilic ileitis and associated remodeling. Am J Pathol 2011; 179:2302–2314.
62. Ballengee CR, Stidham RW, Liu C, Kim MO, Prince J, Mondal K, Baldassano R, Dubinsky M, Markowitz J, Leleiko N, Hyams J, Denson L, Kugathasan S. Association between plasma level of collagen type III alpha 1 chain and development of strictures in pediatric patients with Crohn's disease. Clin Gastroenterol Hepatol 2019; 17:1799–1806.
63. Cheng F, Shen Y, Mohanasundaram P, Lindstrom M, Ivaska J, Ny T, Eriksson JE. Vimentin coordinates fibroblast proliferation and keratinocyte differentiation in wound healing via TGF-beta-Slug signaling. Proc Natl Acad Sci U S A 2016;113:E4320–E4327.
64. Shinde AV, Humeres C, Frangogiannis NG. The role of alpha-smooth muscle actin in fibroblast-mediated matrix contraction and remodeling. Biochim Biophys Acta Mol Basis Dis 2017;1863:298–309.
65. Koon HW, Kim YS, Xu H, Kumar A, Zhao D, Karagiannides I, Dobner PR, Pothoulakis C. Neurotensin induces IL-6 secretion in mouse preadipocytes and adipose tissues during 2,4,6,-trinitrobenzensulphonic acid-induced colitis. Proc Natl Acad Sci U S A 2009;106:8766–8771.

Received November 23, 2021. Accepted June 30, 2022.

Correspondence
Address correspondence to: Hon Wai Koon, PhD, Vatche and Tamar Manoukian Division of Digestive Diseases, David Geffen School of Medicine, University of California Los Angeles, Room 44-129, Center for Health Sciences Building, 10833 Le Conte Avenue, Los Angeles, California 90095. e-mail: hkoon@mednet.ucla.edu; fax: (310) 825-3542.

Acknowledgments
The authors thank China Scholarship Council (#202008210019) for supporting Dr Ying Xie's living expenses during her research at UCLA.

CRediT Authorship Contributions
Ying Xie, MD, PhD (Data curation: Lead; Investigation: Lead)
Lindsey Fontenot, BS (Data curation: Supporting; Investigation: Supporting)
Andrea Chupina Estrada (Data curation: Supporting; Investigation: Supporting)
Becca Nelson (Data curation: Supporting; Investigation: Supporting)
Jiani Wang, MD (Data curation: Supporting; Investigation: Supporting)
David Q. Shih, MD, PhD (Resources: Supporting)
Wendy Ho, MD (Resources: Supporting)
S. Anjani Mattai, MD (Resources: Supporting)
Florian Rieder, MD (Resources: Supporting)
Dane D. Jensen, PhD (Data curation: Supporting; Investigation: Supporting)
Nigel W. Bunnett, PhD (Data curation: Supporting; Investigation: Supporting)
Hon Wai Koon, PhD (Conceptualization: Lead; Supervision: Lead; Writing – original draft: Lead; Writing – review & editing: Lead)

Conflicts of interest
This author discloses the following: Nigel Bunnett is a founding scientist of Endosome Therapeutics Inc Research in the laboratory of NWB, which was funded, in part, by Takeda Pharmaceutics International. The remaining authors disclose no conflicts.

Funding
Supported by NIH (R01-DK128142 and R21-AI137663) grants, Crohn's & Colitis Foundation Senior Research Award (623027), and Eli and Edythe Broad Foundation to Hon Wai Koon. Nigel Bunnett was supported by grants from the National Institutes of Health (NS102722, DE026806, DK118971, NWB) and the Department of Defense (W81XWH1810431, NWB). The funder was not involved in the study design, data collection, analysis and interpretation, and manuscript writing. Dr Koon paid for the Grammarly service charge.

scientific reports

Check for updates

OPEN

Oral cancer induced TRPV1 sensitization is mediated by PAR_2 signaling in primary afferent neurons innervating the cancer microenvironment

Nicole N. Scheff[1], Ian M. Wall[2], Sam Nicholson[2], Hannah Williams[2], Elyssa Chen[2], Nguyen H. Tu[2], John C. Dolan[2], Cheng Z. Liu[3], Malvin N. Janal[4], Nigel W. Bunnett[5,6] & Brian L. Schmidt[1,5]✉

Oral cancer patients report sensitivity to spicy foods and liquids. The mechanism responsible for chemosensitivity induced by oral cancer is not known. We simulate oral cancer-induced chemosensitivity in a xenograft oral cancer mouse model using two-bottle choice drinking and conditioned place aversion assays. An anatomic basis of chemosensitivity is shown in increased expression of TRPV1 in anatomically relevant trigeminal ganglion (TG) neurons in both the xenograft and a carcinogen (4-nitroquinoline 1-oxide)-induced oral cancer mouse models. The percent of retrograde labeled TG neurons that respond to TRPV1 agonist, capsaicin, is increased along with the magnitude of response as measured by calcium influx, in neurons from the cancer models. To address the possible mechanism of TRPV1 sensitivity in tongue afferents, we study the role of PAR_2, which can sensitize the TRPV1 channel. We show co-expression of TRPV1 and PAR_2 on tongue afferents and using a conditioned place aversion assay, demonstrate that PAR_2 mediates oral cancer-induced, TRPV1-evoked sensitivity in an oral cancer mouse model. The findings provide insight into oral cancer-mediated chemosensitivity.

Oral cancer patients endure severe pain while undertaking routine oral functions that mechanically agitate soft tissue in the oral cavity such as eating and talking[1,2]. On the other hand, these same patients report low levels of spontaneous pain. Using xenograft and carcinogen-induced oral cancer mouse models and orofacial assays, we have modeled and studied the functional/mechanical pain observed in oral cancer patients[3]. Anecdotal clinical evidence reveals that some oral cancer patients also suffer from chemosensitivity, especially to spicy foods and liquids. We have not studied this symptom to date. Substances within spicy food activate the transient receptor vanilloid channel 1 (TRPV1). While afferent neurons throughout the different heterosegmental regions express TRPV1, the oral cavity is an ideal site to study TRPV1 sensitization in the setting of cancer. Exposure of the soft tissue of the oral cavity to capsaicin is consistent with the eating habits of numerous cultures. Accordingly, application of capsaicin to the tongue in a rodent oral cancer model mirrors the experience of oral cancer patients who eat or drink spicy ingredients. A model that utilizes subcutaneous injection of capsaicin does not accurately recapitulate the topical exposure to spicy substances that patients experience.

Little is known regarding cancer-induced chemosensitivity. However, various cancer pain models involving several species reveal that TRPV1 is upregulated on sensory neurons that innervate oral cancers. Moreover, TRPV1 mediates oral cancer pain[4–8]. For example, in an oral cancer pain model generated by inoculating squamous cell carcinoma into the gingiva of a rat, TRPV1 is overexpressed in the associated trigeminal ganglion

[1]Department of Neurobiology and Hillman Cancer Research Center, University of Pittsburgh, Pittsburgh, USA. [2]Department of Oral and Maxillofacial Surgery, Bluestone Center for Clinical Research, New York University (NYU) College of Dentistry, New York, USA. [3]Pathology Department, NYU Langone Health, New York, USA. [4]Department of Epidemiology and Health Promotion, NYU College of Dentistry, New York, USA. [5]Department of Molecular Pathobiology, NYU College of Dentistry, New York, USA. [6]Department of Neuroscience and Physiology, Neuroscience Institute, NYU Langone Health Neuroscience Institute, NYU Langone Health, New York, USA. ✉email: bls322@nyu.edu

(TG); mechanical allodynia and thermal hyperalgesia are observed in this model[9]. Agonists in the cancer microenvironment, including an elevated proton concentration, could activate TRPV1[10–13]. Rhabdomyosarcoma and osteosarcoma secrete lipophilic substances that activate TRPV1 on TG neurons[14]. In one of the most promising studies to date, selective ablation of TRPV1 fibers with intrathecal resiniferatoxin reversed cancer pain and restored function in a canine bone cancer model[15].

TRPV1 sensitization, rather than activation, is consistent with oral cancer pain during routine oral function, but not with spontaneous pain. TRPV1 sensitization occurs through phosphorylation of intracellular residues on the ion channel, a process that is modality specific[16]. Protease-activated receptor-2 (PAR_2), which has a prominent role in oral cancer pain[3,17], activates protein kinase C and A and leads to ion channel phosphorylation and sensitization of TRPV1[18]. The aim of our study was to determine whether oral cancer leads to TRPV1-mediated chemosensitivity, and whether the mechanism involves PAR_2, which is unknown in the setting of oral cancer. To study upregulation of TRPV1 on anatomically-relevant sensory neurons innervating the tongue, which we identified with the retrograde tracer DiI, in the setting of oral cancer, we used two oral cancer mouse models, the xenograft model with athymic nude mice and a carcinogen-induced oral cancer mouse model with wildtype C57BL/6 mice. We used PAR_2 knockout mice and conditioned place aversion (CPA) to assess the role of PAR_2 in oral cancer-induced TRPV1 sensitization. A better understanding of TRPV1 sensitization in the setting of cancer could provide insight into how TRPV1-mediated cancer nociception could be alleviated or preempted.

Results

Tongue primary afferents express TRPV1 protein that mediate aversion to capsaicin in the drinking water. A significant portion of sensory nerve innervation to the tongue arises from neurons in the V3 region of the TG. We determined the percentage of retrograde labeled tongue afferents that express TRPV1 in order to gauge the functional impact of TRPV1 activation on aversion behavior. Using a retrograde tracer, the subpopulation of TRPV1-positive TG neurons that innervate the tongue was 32.95 ± 3.5% (n = 3/sex/group, Fig. 1A,B). We found no positive staining in the TRPV1 KO mouse (Fig. 1A,B). A two-bottle drinking aversion test was used to measure TRPV1 mediated oral sensitivity. Two bottles, one that contained water with vehicle (0.1% ethanol) and the other containing water with 1 μM capsaicin, were available for 5 days to single sex socially housed male and female mice (n = 3/cage/sex). TRPV1 KO mice were used as a comparison. Total water consumption (mL) was the same across sex and genotype (sex by genotype: $F(1,16) = 0.013$, $p = 0.909$; independent samples t-test with pooled sexes: $t(16) = 0.152$ $p = 0.881$). However, capsaicin water was avoided in wildtype mice, where both male and female C57BL/6 mice drank less than half the volume of water containing capsaicin compared to TRPV1 KO mice (Fig. 1C, $t(16) = 7.023$, $p < 0.001$).

TRPV1-mediated aversion to capsaicin during oral cancer progression. TRPV1 activation is thought to be involved in cancer pain[19,20]; however, the effect of oral cancer on neuronal TRPV1 expression and sensitization is unclear. We have previously demonstrated a sex difference in pain secondary to oral cancer; male mice demonstrate significantly less oral cancer-induced nociceptive behavior due to a neutrophil-mediated endogenous opioid mechanism[21,22]. Thus, due to the potential confounding effects of the immune system on oral chemosensitivity, male mice were analyzed separately for behavioral experiments. We used the oral cancer tongue xenograft model in tandem with the two-bottle choice assay to determine oral chemosensitivity during tumor growth. Naïve athymic nude mice were housed 3 per cage and baseline consumption (vehicle water) was measured for 7 days followed by HSC-3 inoculation or sham injection. On post inoculation (PID) 3, one vehicle water was replaced with 1 μM capsaicin water and consumption was measured by weight every 7 days for 4 weeks (Fig. 2A). We found an interaction between time and treatment in female mice only ($F(3,12) = 10.22$, $p = 0.0013$). Tumor-bearing female athymic nude mice demonstrated greater aversion to 1 μM capsaicin in the drinking water compared to sham at 3 ($p = 0.0343$) and 4 ($p = 0.0001$) weeks post inoculation (Fig. 2B). Total water consumption was similar over levels of time and treatment (Fig. 2C; $F(3,12) = 1.389$, $p = 0.294$). Consistent with our previous studies, we found no interaction between time and treatment in tumor-bearing male mice (Suppl Fig. 1, $F(3,12) = 0.522$, $p = 0.675$). In addition to oral sensitivity, we tested the hypothesis that capsaicin is driving pain in the oral cavity secondary to oral cancer by assaying CPA in mice that were conditioned with oral swabbing of vehicle (0.1% EtOH) followed by low dose 500 nM capsaicin (Fig. 2D). Pre-conditioning (baseline) times did not differ between the vehicle-paired chamber and the capsaicin-paired chamber ($p = 0.39$). Tumor-bearing female mice treated with oral capsaicin displayed CPA (Fig. 2E, $F(1,8) = 14.13$, $p = 0.006$); they spent less time in the capsaicin-paired chamber compared with either the pre-conditioning baseline ($p = 0.019$) or post-conditioning vehicle-paired chamber ($p = 0.001$; Fig. 2E). Oral capsaicin had no effect on sham female mice (Fig. 2F; $F(1,8) = 3.02$, $p = 0.121$) or in tumor-bearing male mice (Suppl Fig. 1, $F(1,8) = 0.063$, $p = 0.808$) or sham male mice (Suppl Fig. 1, $F(1,8) = 1.187$, $p = 0.308$).

Oral cancer-induced increase in TRPV1 protein expression in tongue primary afferents. Previous findings in a bone cancer mouse model found increased TRPV1 expression in dorsal root ganglia (DRG) neurons innervating the bone[20]. We hypothesized that the increase in capsaicin-induced aversion behavior was due to an increase in TRPV1 protein expression in tongue trigeminal afferents. We analyzed TRPV1 protein expression in the xenograft and 4NQO-induced oral cancer models, as well as the associated controls (sham or Matrigel only and propylene glycol, respectively). Representative hematoxylin and eosin stained images of the cancer models and control tongues are shown in Fig. 3A. We used retrograde labeling from the tongue using DiI and immunohistochemistry in TG sections from tumor-bearing mice (n = 4/sex) compared to sham control (n = 4/sex). There was no interaction between sex and treatment ($F(1,12) = 1.744$, $p = 0.2112$), therefore, sexes were pooled. DiI + TRPV1 + neurons increased only in tumor-bearing mice (Fig. 3B,C; $t(14) = 2.187$,

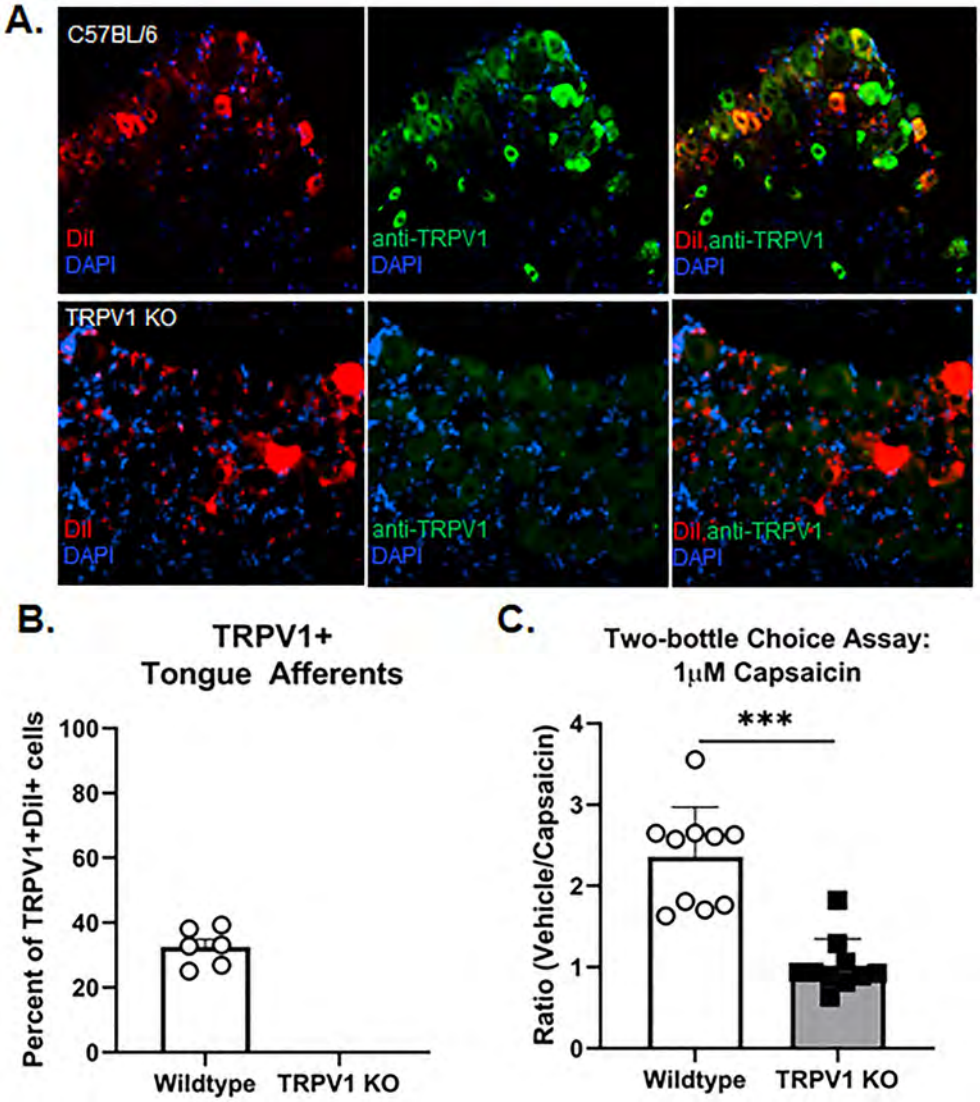

Figure 1. Tongue primary afferents express TRPV1 protein that mediates aversion to capsaicin in the drinking water. (**A**) Representative images of TRPV1-like immunoreactivity in TG sections from a retrograde labeled (DiI) female naïve C57BL/6 or female TRPV1 knockout (KO) mouse. (**B**) The pooled data indicate the percent of DiI + (red) neurons that were co-labeled with TRPV1 (green) from male and female C57BL/6 mice compared to TRPV1 KO mice (n = 3/sex). (**C**) There was a genotypic difference in TRPV1-mediated aversion to 1 μM capsaicin; wildtype C57BL/6 male and female mice (n = 5/sex) demonstrate an aversion to capsaicin in the drinking water compared to TRPV1 KO mice which demonstrated no preference. ***$p < 0.001$.

$p = 0.046$). We have previously demonstrated that the immune system plays an important role in oral cancer pain[23]. To determine if the lack of an intact immune system in athymic nude mice contributes to cancer-induced changes in TRPV1 expression, we measured TRPV1 expression in wildtype mice with 4NQO-induced oral SCC (oSCC, n = 4 female, 6 male) and vehicle treated mice (n = 4 female, 6 male). There was no interaction between sex and treatment ($F(1,16) = 0.918$, $p = 0.352$), therefore, sexes were pooled. Similar to the xenograft model, DiI + TRPV1 + cells increased only in tumor-bearing mice treated with 4NQO; Fig. 3D, $t(18) = 1.495$, $p = 0.0005$).

Oral cancer-induced increase in TRPV1 function. Next, we sought to determine cancer-induced changes in neuronal TRPV1 function. In dissociated retrograde labeled trigeminal neurons from mice, we quantified the percentage of retrograde labeled neurons that elicited a Ca^{2+} transient in response to 500 nM capsaicin as well as measured the magnitude of the capsaicin-evoked Ca^{2+} transient (Fig. 4A,B). We used neurons from mice with HSC-3 xenograft tumors (n = 6/sex) as well as 4NQO-treated mice with oSCC (n = 11 male,12 female). Sham athymic mice (n = 6/sex) and vehicle-treated C57BL/6 mice (n = 6/sex) respectively were used as controls. There was no interaction between sex and treatment for either model (xenograft: $F(1,19) = 2.066$, $p = 0.167$; 4NQO: $F(1.31) = 1.400$, $p = 0.246$), therefore, sexes were pooled. Oral cancer evoked an increase in TRPV1 function and magnitude of response compared to controls. The percent of DiI + neurons in which capsaicin evoked

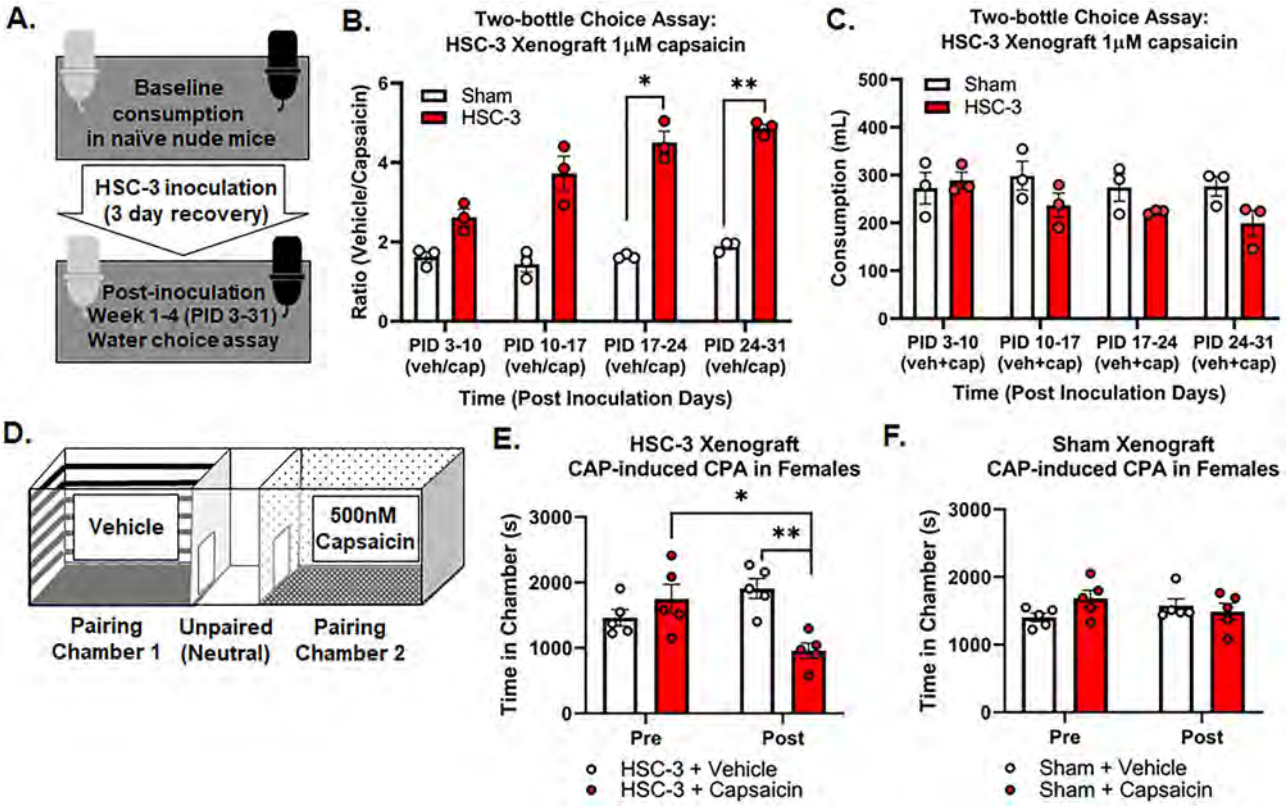

Figure 2. TRPV1-mediated aversion to capsaicin during oral cancer progression (**A**) Timeline for the two-bottle drinking assay using the oral cancer xenograft mouse model. Baseline water consumption using vehicle water (0.01% EtOH) was recorded prior to cancer cell injection into the tongue. (**B**) Tumor-bearing female athymic nude mice demonstrate greater aversion to 1 μM capsaicin in the drinking water compared to sham at 3 and 4 weeks post inoculation. We measured water consumed by cage; each cage housed 3 mice; each dot represents a cage of three female mice. Time x treatment, $p = 0.0013$. *$p < 0.05$, **$p < 0.01$ (**C**) There was a similar reduction in total consumption with cancer progression in tumor-bearing mice regardless of time and treatment. $p > 0.05$. (**D**) Standard CPA box in which mice were conditioned with either saline or 500 nM capsaicin oral swabbing on post inoculation days 22–24. Place aversion was measured on day 25 and CPA was assessed as the difference in time spent in the capsaicin-paired chamber compared to saline-paired chamber. (**E,F**) Tumor-bearing female mice (white and red bars) spent less time in the capsaicin-paired chamber compared to baseline. Time x treatment $p = 0.0056$, *$p < 0.05$, **$p < 0.01$. Capsaicin treatment had no effect in sham female mice. Time x treatment $p = 0.1207$.

a Ca^{2+} transient > 20% of baseline was increased in neurons from mice with HSC-3 xenograft ($t(21) = 6.829$, $p < 0.0001$ Fig. 4C) as well as 4NQO-treated mice with oSCC ($t(33) = 7.296$, $p < 0.0001$, Fig. 4D). The magnitude of the capsaicin-evoked Ca^{2+} transient, defined as the peak Ca^{2+} response minus baseline Ca^{2+} concentration, increased in mice with HSC-3 xenograft ($t(21) = 4.716$, $p = 0.0001$ Fig. 4C), as well as 4NQO-treated mice with oSCC ($t(33) = 5.508$, $p < 0.0001$; Fig. 4D) but not in their respective controls.

PAR_2-induced sensitization of the capsaicin-evoked Ca2+ transient. The tumor microenvironment is rich in protease and proteolytic peptides that directly activate PAR_2 on sensory neurons. PAR_2 activation has been shown to modulate TRPV1 activity[18,24]. To determine whether PAR_2 and TRPV1 are co-expressed in tongue trigeminal neurons, we localized the proteins by immunofluorescence in tissue sections and measured the capsaicin-evoked Ca^{2+} transients in TG cultures using selective PAR_2 pharmacology. Immunoreactive PAR_2 and TRPV1 were colocalized in retrograde labeled tongue afferents in sections from TG from adult C57BL/6 mice and PAR_2 KO mice (Fig. 5A); 33.8 ± 1.5% of retrograde labeled tongue afferents co-expressed PAR_2 and TRPV1 protein (n = 3 mice). No PAR_2 and TRPV1 immunoreactive overlap was identified in PAR_2 KO mice (n = 3 mice). Next, we examined whether PAR_2 activation sensitizes TRPV1-mediated Ca^{2+} transients in dissociated TG neurons. Capsaicin evoked a Ca^{2+} transient > 20% of baseline in 28.6 ± 2.5% of DiI + neurons responding to 30 mM KCl (n = 105 neurons total) in both wildtype and PAR_2KO mice; there was no difference in the number of capsaicin-responsive neurons between genotype. The magnitude of the Ca^{2+} transient evoked by capsaicin varied with the interaction of drug treatment and genotype ($F(2.54) = 5.952$, $p = 0.005$). Pre-treatment with the specific PAR_2 ligand, 2-F (100 nM), potentiated the response to capsaicin applied 5 min later by 123.52 ± 23.2% (n = 5/sex) in neurons from wild-type mice compared to neurons pre-treated with vehicle ($p < 0.0001$; Fig. 5B,C). Furthermore, pre-treatment with the PAR_2 antagonist, GB88 (10 μM), inhibited the 2-F-induced potentiation

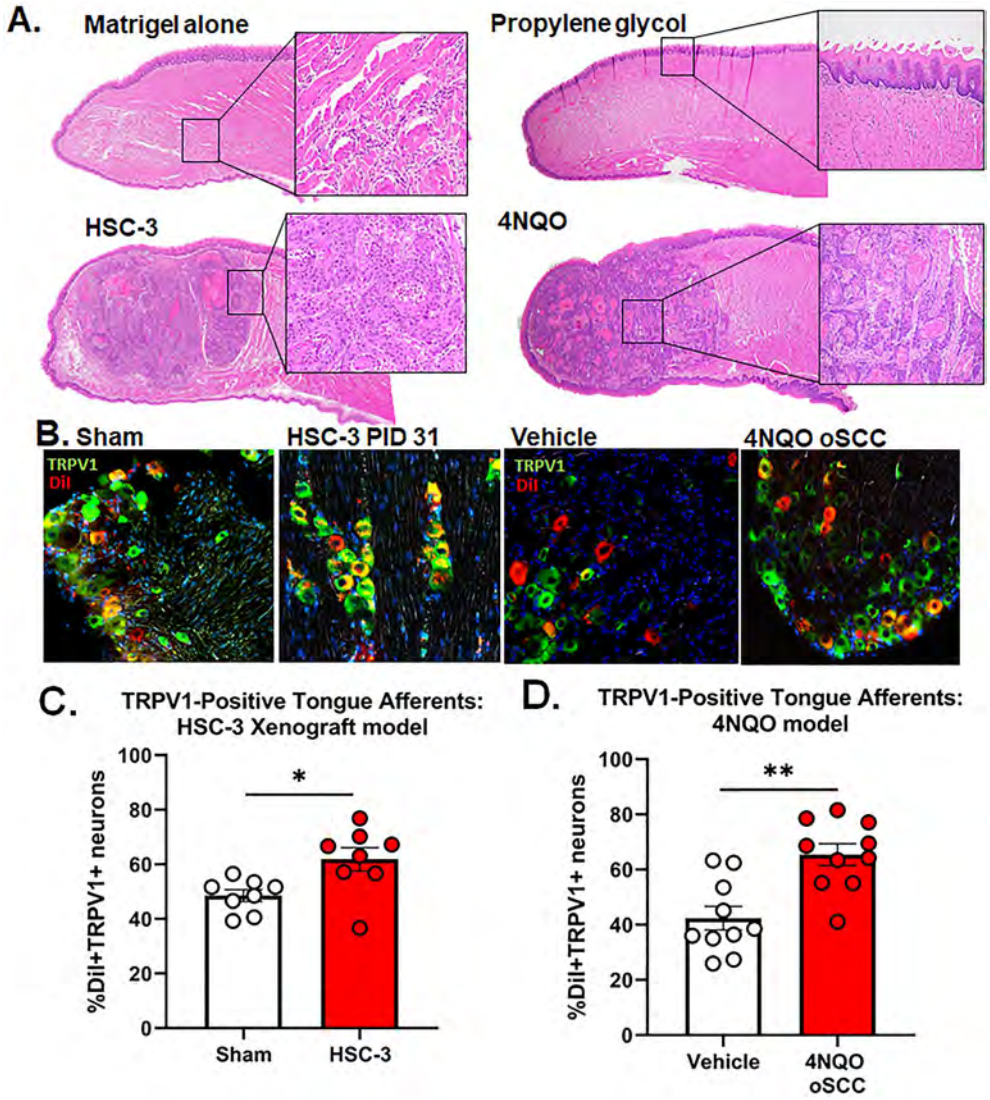

Figure 3. Oral cancer-induced increase in TRPV1 protein expression in tongue primary afferents. (**A**) Representative images of 5 µm tongue sections stained with hematoxylin and eosin from sham (*i.e.,* Matrigel alone) and HSC-3-tumor bearing mice at PID 31, as well as propylene glycol- and 4NQO-treated mice at week 28. (**B**) Representative images of TRPV1-like immunoreactivity in retrograde labeled (DiI) tongue primary afferent neurons from a section from female sham and HSC-3 xenograft at PID 31 as well as a vehicle treated and 4NQO-treated female mouse with oSCC, 10 × magnification. (**C**) Pooled data from male and female mice indicates an increased percentage of DiI + neurons co-labeled with TRPV1 (green) from HSC-3 xenograft (n = 4/sex) but not sham (n = 4/sex) mice at PID 31. *$p < 0.05$. (**D**) Pooled data from male and female mice indicates an increased percentage of DiI + neurons co-labeled with TRPV1 in 4NQO-induced oSCC (n = 4 female, 6 male) mice, but not vehicle treated mice (n = 4 female, 6 male).**$p < 0.01$.

of the capsaicin-evoked transient by 41.98 ± 17.7% only in neurons from wildtype mice (n = 5/sex; $p < 0.0001$). There was no effect of 2-F ($p = 0.160$) or GB88 ($p = 0.119$) on the capsaicin-evoked transient in PAR_2KO mice (n = 5/group/sex, Fig. 5B,C).

TRPV1-induced aversion behavior in the presence of oral cancer is mediated by PAR_2. Lastly, we sought to determine if PAR_2 mediates the TRPV1-evoked nociception secondary to oral cancer. We used CPA assay in tandem with the acute oral cancer pain model to test the hypothesis that PAR_2 activation is required for capsaicin-induced aversion behavior in the presence of oral cancer. The acute supernatant model was used to quantify oral cancer-induced nociceptive behavior in the absence of tumor burden and illness associated with carcinogenesis. We first tested whether HSC-3 cell line supernatant alone evokes aversion behavior in wildtype C57BL/6 and PAR_2KO female mice. Based on previous findings using hindpaw von Frey, HSC-3 supernatant-induced sensitization of primary afferents lasts for about 24 h[3]. While a "cell culture media only" injection group is the more appropriate for supernatant injection, multiple injections into the tongue per day

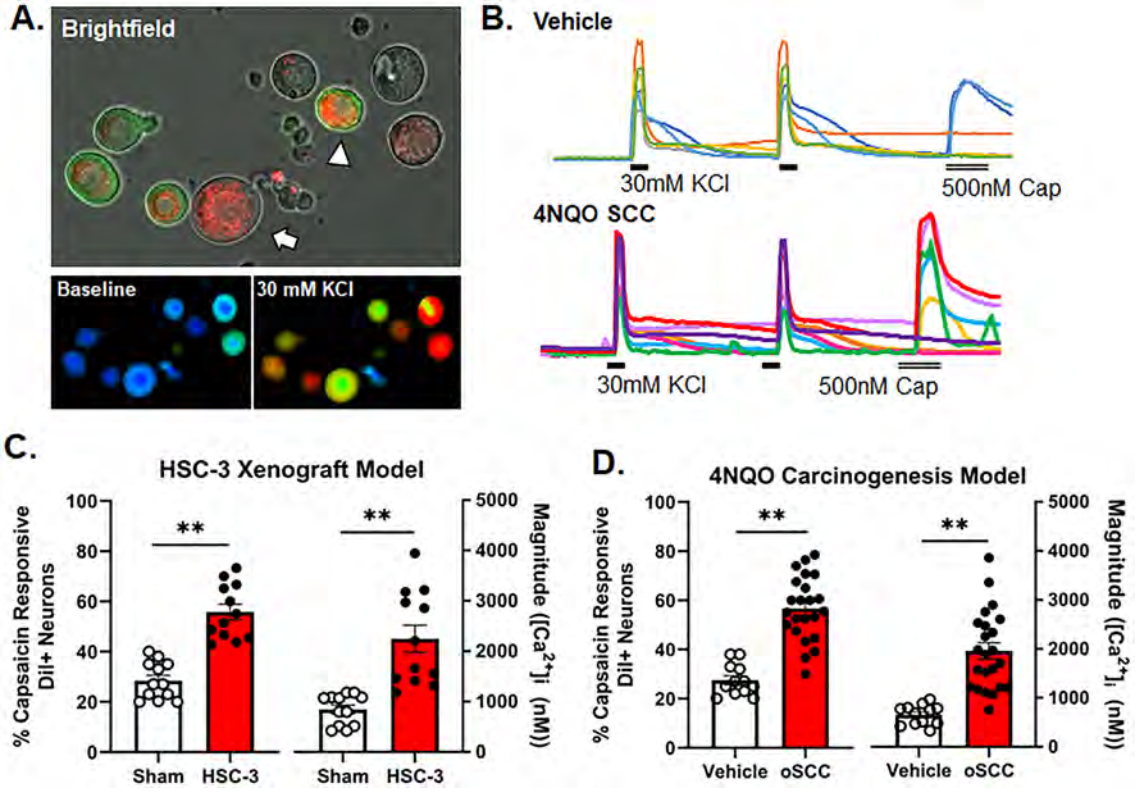

Figure 4. Oral cancer-induced increase in TRPV1 function (**A**) Image of dissociated TG neurons (bright field); a subset is retrograde labeled tongue afferents (DiI, white arrow) and IB4 nonpeptidergic (arrow head). (**B**) Traces of 30 mM KCl and 500 nM CAP-evoked transients from tumor bearing female mice. Ca^{2+} imaging was done at 20X magnification in fields containing ≥ 5 neurons and at least 2 coverslips were tested per mouse. For (**C**,**D**), which represent the HSC-3 xenograft and 4NQO models, respectively, each dot represents the average number of responders or the average Ca^{2+} transient magnitude of neurons tested from an individual mouse. The percentage of DiI + neurons that responded to CAP and the transient magnitude (peak-baseline) was increased in HSC-3 cancer-bearing mice (n = 12; 6/sex) compared to sham (n = 12; 6 mice/sex). **p < 0.01. $\Delta[Ca^{2+}]_i$ = change in intracellular Ca^{2+} concentration. The percentage of DiI + neurons that responded to CAP and the transient magnitude (peak-baseline) in CAP-evoked transients was increased in mice with 4NQO induced oSCC (n = 22; 10 male, 12 female) compared to vehicle-treated mice (n = 12; 6/sex).**p < 0.01.

over three days confounded the aversion behavior induced by the cancer supernatant. Therefore, for these CPA experiments, mice (n = 10/group) were conditioned with light anesthesia (2–2.5%) and no injection followed by either submucosal injection of cell line media or HSC-3 cell line supernatant (30 µl) into the tongue. Two-way ANOVA analyses showed that injection with cell line media does not evoke aversive behavior in either C57BL/6 ($F(1,18) = 0.581$, $p = 0.456$) or PAR_2KO ($F(1,18) = 0.175$, $p = 0.681$) mice (Fig. 6A,B). On the contrary, conditioning with HSC-3 cell culture supernatant evokes mild aversion behavior in C57BL/6 mice (Fig. 6C; interaction: $F(1,18) = 9.893$, $p = 0.006$; Holm Sidak: $p = 0.051$), but not in PAR_2KO mice (Fig. 6D; ($F(1,18) = 2.103$, $p = 0.164$). Oral cancer supernatant contains proteases which can activate neuronal PAR_2[3,17]. We hypothesize that low dose capsaicin swabbing potentiates oral cancer-induced aversion behavior in a PAR_2 dependent manner. To test this, mice were conditioned with no injection plus an oral swabbing of vehicle (0.01% EtOH) followed by HSC-3 cell line supernatant injection into the tongue plus, 1 h after injection, an oral swabbing of 500 nM capsaicin. Wildtype C57BL/6 mice demonstrated aversion to the chamber paired with HSC-3 supernatant plus capsaicin (Fig. 6E; interaction: $F(1,18) = 10.78$, $p = 0.004$; Holm Sidak: $p = 0.001$) whereas PAR_2KO mice did not (Fig. 6F; ($F(1,18) = 3.203$, $p = 0.090$). Furthermore, the percent time spent in the treatment chamber varied with the interaction of treatment and genotype (Fig. 6G; $F(2,54) = 4.401$, $p = 0.017$); C57BL/6 mice spent less time than PAR_2KO only in the HSC-3 supernatant plus capsaicin chamber ($p = 0.033$).

Discussion

We report that oral cancer sensitizes TRPV1 through a PAR_2-mediated mechanism. We propose that proteases cleave and activate PAR_2 on primary afferent neurons in the oral cancer microenvironment, which sensitizes TRPV1 on the same neurons. Back labeled, anatomically relevant oral nociceptors respond to oral cancer by overexpressing TRPV1. We study expression of TRPV1 in two oral cancer mouse models. The xenograft model is created with a human oral cancer cell line which has implications for the study of human oral cancer. The carcinogen-induced oral cancer mouse model involves transformation of oral keratinocytes to malignant oral keratinocytes, similar to what would occur in oral cancer patients, and can be generated in mice with an intact

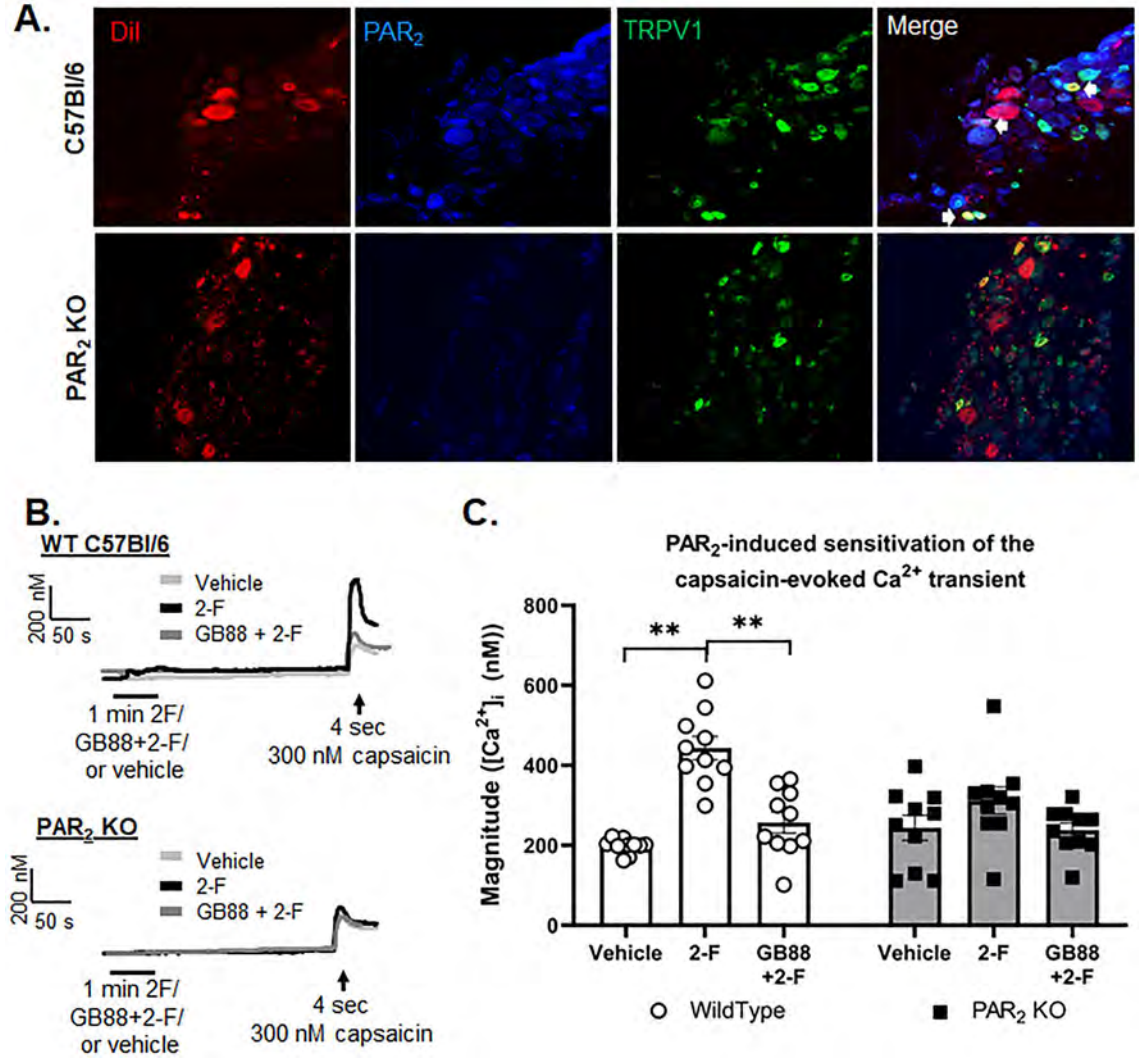

Figure 5. PAR_2-induced sensitization of the capsaicin-evoked Ca^{2+} transient. (**A**) Triple labeling of PAR_2 + TRPV1 + tongue primary afferent neurons using fast blue as retrograde tracer. (**B**) Representative traces from retrograde labeled tongue trigeminal neurons from (**C**) female wildtype C57BL/6 mouse or PAR_2 global knockout mouse. TGs were dissociated and neurons were loaded with Fura-2AM for Ca^{2+} imaging. After 30 s of baseline recording, neurons were treated for 1 min with either vehicle (normal bath, light gray), PAR_2 agonist, 2-F (100 nM, black) or pre-treatment with PAR_2 antagonist, GB88 (10 μM), followed by 2-F (dark gray). The drug was washed out for 5 min and the neuron was challenged with capsaicin (300 nM, 4 s). (**C**) Treatment with 2-F resulted in increased capsaicin-evoked Ca^{2+} transient amplitude (peak–baseline) in tongue neurons from male and female wildtype mice (n = 10; 5/sex). There was no effect of 2-F treatment in tongue neurons from PAR_2 KO mice (n = 10; 5/sex). $^{**}p < 0.01$.

immune system. Pharmacologic activation of PAR_2 on oral nociceptors prior to the application of capsaicin enhances calcium influx. We employed two operant assays—drinking aversion and CPA—to confirm capsaicin sensitivity in oral cancer models; we used the former assay to confirm that PAR_2 mediates oral cancer-induced capsaicin sensitivity.

Our results accord with those from two other studies that support the role of TRPV1 in oral cancer pain[19,25]. Ruparel and colleagues reported that three oral cancer cell lines, including HSC-3, a cell line we used in our study, secrete lipids that produce nocifensive behavior and thermal hypersensitivity through TRPV1[19]. The role of TRPV1 in bone cancer pain was demonstrated several years earlier when Mantyh and colleagues used pharmacologic antagonism and genetic disruption of TRPV1 to reverse spontaneous and functional pain in early and late stages of cancer progression[4]. Similar to our findings with tongue cancer and TG neurons, cancer-induced over expression of TRPV1 occurs in the DRG in a bone cancer pain model[20]. Cancer induces TRPV1-mediated functional changes as well. We demonstrated that back labeled neurons in two separate oral cancer models exhibit an elevated response to capsaicin. This effect is similar to the elevated response to capsaicin exhibited by neurons co-cultured with fibrosarcoma cells[26].

An understanding of the mechanism, and the second messengers that mediate TRPV1 sensitization, following PAR_2 activation might suggest a method for pharmacologic antagonism and treatment for oral cancer

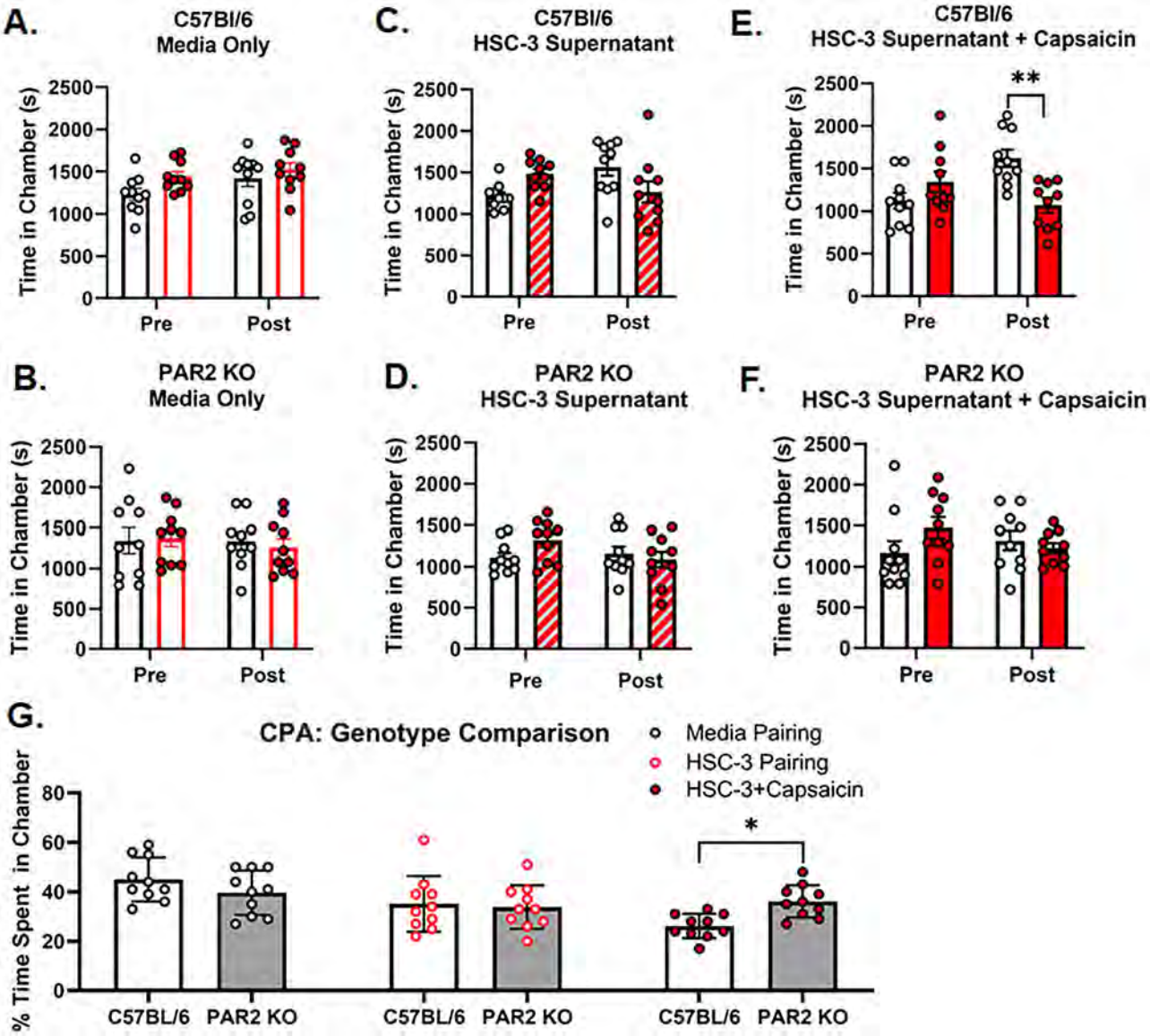

Figure 6. TRPV1-induced aversion behavior in the presence of oral cancer is mediated by PAR_2. C57BL/6 or PAR_2KO female mice were conditioned with either no injection or one of the following: saline injection, oral cancer supernatant injection into the tongue, or oral cancer supernatant followed by oral swabbing of 500 nM capsaicin 1 h post injection. The percent time spent in chamber was calculated as (time spent in the paired chamber / total time spent in both chambers post conditioning *100). (**A–F**) Conditioned place aversion was evident in C57BL/6 mice treated with HSC-3 supernatant + 500 nm capsaicin but not in other treatment types or PAR_2KO mice. *$p < 0.05$, **$p < 0.01$. (**G**) Conditioned place aversion was evident only in C57BL/6 mice in the chamber paired with HSC-3 supernatant + 500 nM capsaicin (genotype by treatment interaction, $p = 0.0170$).

pain. While the mechanism of PAR_2-mediated TRPV1 sensitization on tongue afferent neurons in the setting of oral cancer is not known, the mechanisms described for other conditions and neurons provide insight. PAR_2 sensitization of TRPV1 occurs in TG, DRG and nodose/jugular complex sensory ganglia[18,27,28]. Sensitization of TRPV1 involves phosphorylation by PKC and PKA, which enhances ion channel activity[29,30]. PKC mediates neuronal processing following cleavage of PAR_2[31]. PAR_2 activates PKC by producing diacylglycerol through phospholipase C following recruitment and activation of Gq proteins. Oral cancers secrete proteases that activate PAR_2, including legumain. In previous work we found that legumain cleaves PAR_2 and activates PKA; this cascade can subsequently phosphorylate and sensitize TRPV1[17,32]. PAR_2 also increases the open probability (P_O) of the capsaicin-induced single channel in vagal pulmonary sensory neurons[28]. PAR_2 activation increases the excitability of rat pulmonary capsaicin-induced chemoreflex in the lungs of rats[28]. Trypsin, which cleaves PAR_2, enhances the capsaicin-induced pulmonary chemoreflex response and potentiates the whole-cell inward current induced by capsaicin in isolated nodose/jugular small-diameter neurons that innervate the lungs[33]. Similar to our approach, Gu et al., studied anatomically, back labeled relevant sensory neurons. The in vivo effects of PAR_2 activation on the TRPV1-mediated tussive response have also been demonstrated in guinea pigs[24].

There are other mechanisms, in addition to PAR_2, by which oral cancer could sensitize TRPV1. Tumor necrosis factor alpha (TNFα), a pro-tumor inflammatory cytokine, is well known to potentiate TRPV1 activity leading to allodynia and thermal hyperalgesia in DRG[34] and Ca^{2+} influx in TG[35]. We have recently demonstrated that TNFα is overexpressed in human oral cancer tissues[36], secreted from human oral cancer cell lines and upregulated in cancer tongue tissues collected from mice treated with 4NQO[23]. Nerve growth factor (NGF) and adenosine triphosphate (ATP) are also secreted by oral cancer and can sensitize TRPV1[37,38]. TRPV1 can be sensitized through increased expression and/or receptor phosphorylation at key intracellular residues. NGF activates p38, which increases TRPV1 translation in the cell body and leads to subsequent anterograde transportation of the ion channel to nerve terminals in the periphery[39]. ATP sensitizes TRPV1 on TG neurons through phosphorylation of serine residues[27]. These TRPV1 sensitization mechanisms (PAR_2, ATP, NGF) likely overlap as it has been shown that PAR_2 activation by trypsin increases ATP secretion through TRPV1 sensitization[40].

Limitations of our study include the control used for the CPA experiments, our use of global knockout mice, and single sex behavioral experimental design. Because generation of the HSC-3 xenograft cancer model requires a nude athymic mouse, and we used PAR_2 knockout mice on a C57BL/6 background to study the role of PAR_2, we used the HSC-3 supernatant model[3]. With regard to our CPA control, our previous work demonstrates that HSC-3 supernatant-induced sensitization of primary afferents lasts for about 24 h[3]. While a media only injection group is a more appropriate control for the CPA experiments, multiple injections per day over three days would likely confound the aversive behavior induced by the cancer supernatant. To address this injection-related concern, we demonstrated in a separate experiment that a saline injection does not induce aversive behavior. To obviate the potential confound of multiple injections, we employed CPA using anesthesia only condition pairing. From our demonstration that back labeled tongue afferent fibers co-express PAR_2 and TRPV1, along with our demonstration that PAR_2 activation enhances the calcium influx induced by TRPV1, we infer that PAR_2 and TRPV1 on sensory neurons mediate the capsaicin sensitivity observed in our cancer model. However, there is a possibility that PAR_2 expression on non-neuronal cells could mediate capsaicin sensitivity. We did not use a conditional PAR_2 knockout selective for afferent fibers; for the current study, we used a global knockout mouse. Now that we have PAR_2-$Na_v1.8$ mice, we plan to use these mice in our future oral cancer and capsaicin sensitivity studies. Lastly, we used female mice only for the behavioral experiments to determine if TRPV1-induced aversion behavior in the presence of oral cancer is mediated by PAR_2. Including the present study, we have now demonstrated a sex difference in pain and chemosensitivity secondary to oral cancer. We hypothesize that male mice demonstrate significantly less oral cancer-induced nociceptive behavior due to a neutrophil-mediated endogenous opioid mechanism[21,22] and such, pre-treatment with naloxone in male mice may reveal the oral cancer-induced chemosensitivity during tumorigenesis.

In naïve mice, we found that 36% of lingual afferent fibers express TRPV1. Previous work by Elitt et al. and Wu et al. revealed TRPV1 expression in lingual TG neurons (25% and 17%, respectively)[41,42]. Capsaicin sensitivity might be greater in humans with oral cancer than in our mouse oral cancer model. A recent study revealed that TRPV1 expression is higher in human DRG than in mouse DRG; approximately 75% in the former and 32% in the latter[43]. Our study provides support for chemosensitivity testing in oral cancer patients to gain insight into neuronal plasticity in the context of oral cancer.

Methods

Animals. Male and female adult (6–20 weeks) athymic nude mice (NU/J, *Foxn1^{nu}*, stock #002019, Jackson Labs, Bar Harbor, ME, USA), and C57BL/6 mice (stock #027, Charles River, Wilmington, MA, USA), TRPV1 KO mice (B6.129X1-Trpv1^{tm1Jul}/J, stock #003770) and PAR_2KO mice (B6.Cg-*F2rl1^{tm1Mslb}*/J, stock #004993, Jackson Labs) were used. Mice were maintained on a 12:12 h light cycle and were housed in group cages in temperature-controlled rooms with access to food and water. Researchers were trained under the Animal Welfare Assurance Program. Experimental procedures were approved by the New York University Institutional Animal Care and Use Committee and were conducted in line with the National Institutes of Health guidelines for the use of laboratory animals in research.

Cell culture. Human oral cancer cell line, HSC-3 (human tongue oral SCC cell line, cell number JCRB0623, from the Japanese Collection of Research Bioresources Cell Bank), was utilized to produce the human oral cancer xenograft model in immunocompromised nude mice. Cells were maintained and cultured as previously described[44]. HSC-3 cells were cultured in 10 cm^2 cell culture dishes at 37 °C with 5% CO_2 in Dulbecco's modified Eagle's medium (DMEM, Gibco, Waltham, MA, USA) supplemented with 10% fetal bovine serum and penicillin/streptomycin (50 U/mL). When cells reached 70% confluency, the culture medium was removed, and cells were washed with 5 mL PBS without Ca^{2+} and Mg^{2+}. Cells were collected and resuspended in DMEM:matrigel (1:1; 1×10^5 cells/20 µL HSC-3) for tongue inoculation; HSC-3 cells were collected from passage 7. Supernatant was collected as previously described for the conditioned place aversion (CPA) nociceptive behavior assay[23]. Briefly, cells were cultured to 70% confluency, washed twice with 5 mL PBS without Ca^{2+} and Mg^{2+} and media was replaced with 3 mL of serum and antibiotic free culture media (DMEM for HSC-3). After 48 h, supernatant was removed and spun at 300 × g for 4 min to remove debris and injected into the lateral anterior portion of the tongue within 20 min.

Oral cancer xenograft model. A murine xenograft tongue cancer model was used to determine TRPV1 sensitization during oral carcinogenesis using the drinking choice behavior assay. Mice were inoculated with 1×10^5 HSC-3 cells prepared in DMEM:Matrigel (1:1, 30 µL) into the anterior lateral portion of the tongue, as previously described[21]. HSC-3 is a human tongue squamous cell carcinoma; the use of this cell line and the study of the xenograft model has the advantage of increased translational relevance. Cancer growth and associated

nociceptive behavior develops in approximately 10 days to 2 weeks following inoculation[21,25,37]. On post inoculation day (PID) 31, all mice were anesthetized with isoflurane followed by transcardial perfusion with cold Ca^{2+}/Mg^{2+} free Hank balanced salt solution (HBSS, Invitrogen) for TG harvest; harvested TG neurons were placed on ice cold HBSS for dissociation and acute culture. To prepare tissues for immunohistochemistry, mice were anesthetized with isoflurane followed by transcardial perfusion with ice cold PBS followed by 4% paraformaldehyde (PFA). The experimenters conducting the behavioral tests were blinded to the treatment groups; the allocation keys were held by NNS.

4-nitroquinoline-1-Oxide (4NQO) oral carcinogenesis model. To determine changes in TRPV1 expression and function during carcinogenesis in an animal with an intact immune system, which is an advantage of the carcinogen-induced oral cancer model, mice were offered carcinogen 4-nitroquinoline-1-oxide (4NQO; 100 µg/mL; Sigma Aldrich, St. Louis, MO, USA) in the drinking water or the equivalent dilution of the vehicle, propylene glycol for 16 weeks, which is required to induce transformation of oral keratinocytes to malignant keratinocytes[23]. The mice were then monitored weekly under light anesthesia for body weight, tumor incidence, location, and size for an additional 12 weeks. If mice lost greater than 20% body weight prior to week 28 following the start of exposure to 4NQO, they were euthanized and TG and tongue tissue were collected. By week 28, all mice were euthanized regardless of clinical evaluation and health status. Euthanasia, perfusion and TG and tongue tissue preparation was performed as described for the oral cancer xenograft model. Tongue tissue was harvested by using bone scissors to bilaterally cut the jaw and spring-loaded scissors were used to free the tongue muscle from the floor of mouth. The tongue was dissected back to the oropharyngeal region, fixed in 10% formalin, and processed for paraffin embedding and slide preparation. Four 5 µm hematoxylin & eosin-stained tongue sections separated by 100 µm were evaluated for the presence of papillary and invasive SCC[45,46]. Histopathologic analysis was performed by an oral and maxillofacial pathologist blinded to group identity; allocation keys were held by NNS While calcium microfluorimetry and immunohistochemical evaluation was completed on all samples, only mice with histologically confirmed invasive lesions were included in subsequent data analyses.

Drinking choice behavior assay. Mice were tested for TRPV1-mediated oral aversion to capsaicin using a paired-preference drinking aversion assay. A total of 36 athymic nude mice (18 males and 18 females) were used for these experiments. Mice were housed by sex in groups of three mice per cage. Cages were fitted with two water bottles, and positions of the bottles were swapped daily. Mice were acclimatized by ad libitum access to water with 0.1% ethanol vehicle in both bottles for one week. After acclimatization, mice were inoculated with HSC-3 cells freshly prepared in DMEM:Matrigel (1:1, 20 µL) or DMEM:Matrigel (1:1, 20µL) alone in the sham group. On PID 3, each cage was fitted with one bottle that contained vehicle (0.1% ethanol) and another bottle that contained 1 µM capsaicin (Sigma-Aldrich, St. Louis, MO). After seven days, the volume consumed from each bottle was measured by weight (1 mL water = 1 g). Fluid consumption was measured weekly for four weeks. An index measuring aversion to capsaicin was calculated individually for treatment group (sham/tumor-bearing) and sex as previously described[47]. Solutions and cages were replaced with fresh solutions following each measurement. Oral aversion to capsaicin was determined by two-way ANOVA (time by treatment).

Conditioned place aversion assay. CPA occurs by pairing a painful experience with a distinct context resulting in subsequent avoidance of the same contextual cues[48,49]. We use the CPA assay to measure aversive behaviors in response to three treatment groups, (1) injection of supernatant from oral cancer cell line culture, (2) low-dose capsaicin (500 nM, oral swabbing), and (3) supernatant injection followed by oral capsaicin swabbing. We performed a single trial CPA protocol. The 3-chamber CPA apparatus consists of two conditioning chambers with distinct tactile, visual, and olfactory cues, connected by a smaller neutral chamber that was brightly lit. The visual cues were horizontal stripe and dot wallpaper. The tactile cues were smooth and rough flooring. The olfactory cues were strawberry and mint. White noise was played to provide background noise and block out any extraneous sounds. On the first day (preconditioning) of the experiment, mice were introduced to the neutral chamber and allowed to explore all three chambers for 1 h. Baseline time spent in the chambers was measured using ANY-maze tracking software (Braintree Scientific, Braintree, MA, USA). Exclusion criteria included mice spending < 20% or > 80% time in a chamber. Drug-chamber pairings for conditioning were counterbalanced across subjects[50]. On the second, third and fourth days, conditioning treatment varied based on experimental group. All mice underwent light anesthesia (2–2.5% isoflurane) prior to all treatments. For the supernatant-induce aversion, mice received anesthesia only followed by confinement into the appropriate pairing chamber for 1 h, following which they were returned to their home cage. Four hours later, mice received either submucosal injection of cell line media or HSC-3 cell line supernatant (30 µl) into the anterior lateral tongue followed by confinement into the opposite pairing chamber for 1 h. For the capsaicin-induced aversion, mice received an oral swabbing of vehicle (0.1% EtOH) followed by confinement into the appropriate pairing chamber for 1 h, following which they were returned to their home cage. Four hours later, mice received oral swabbing of 500 nM capsaicin followed by confinement into the opposite pairing chamber for 1 h. Low dose 500 nM capsaicin was chosen as it was found to be non-aversive in naïve athymic nude mice during the two-bottle choice assay (data not shown). For supernatant/capsaicin-induced aversion, mice received an oral swabbing of vehicle (0.01% EtOH) followed by confinement into the appropriate pairing chamber for 1 h, following which they were returned to their home cage. Three hours later, mice received submucosal injection of HSC-3 cell line supernatant (30 µl) into the anterior lateral tongue. One-hour later the mice received oral swabbing of 500 nM capsaicin followed by confinement into the opposite pairing chamber for 1 h. On the fifth day, mice were once again allowed to freely explore the apparatus for 1 h. Time spent in each chamber was recorded by

ANY-maze. The experimenter conducting the behavioral tests (IMW) was blinded to the treatment groups; the allocation keys were held by NNS.

Primary culture. Bilateral TGs were isolated by removing the skull cap and brain to expose the TGs readily visible in the base of the cranium. Using spring-loaded scissors the TGs were dissected and placed into cold HBSS and dissociated based on the previously described protocol[51]. Briefly, TG were minced and incubated in HBSS containing collagenase type II (Gibco) and dispase type II (Gibco) at 37 °C for 20 min and mechanically dissociated using a fire polished glass Pasteur pipette. A 12.5% by 28% percoll gradient was used to separate myelin and nerve debris from TG neurons. Cells were then plated in DMEM/F12 (Gibco) containing 5% fetal bovine serum and antibiotics (penicillin/streptomycin, 50 U/mL) on 5 mm coverslips. Coverslips were flooded 2 h later with Leibovitz L-15 media (Gibco) containing 10% fetal bovine serum, 5 mM HEPES and 5 mM glucose, and used at room temperature. Experiments were performed within 8 h of tissue harvest.

Calcium imaging. TG neurons plated on 5 mm coverslips were incubated with 5 μM Ca^{2+} indicator fura-2 AM (Invitrogen, Carlsbad, CA, USA) at room temperature for 30 min in a physiological salt buffer (normal bath, 130 NaCl, 3 KCl, 2.5 $CaCl_2$, 0.6 $MgCl_2$, 10 HEPES, 10 Glucose, pH = 7.4, 325 mOsm). Coverslips were placed in a recording chamber and continuously infused with normal bath at room temperature. Imaging was done at 20X magnification in fields containing ≥ 5 neurons and at least 2 coverslips were tested per mouse. To measure the neuronal Ca^{2+} response to TRPV1 activation, capsaicin was applied for 4 s. To measure the neuronal Ca^{2+} response to TRPV1 activation following PAR_2 agonist 2-Furoyl-LIGRLO-amide (2-F), or PAR_2 antagonist GB88, 2-F or 2-F + GB88 was applied for 1 min followed by a 5 min wash with normal bath and then capsaicin was applied for 4 s. To test for cell viability, 30 mM KCl was applied for 4 s at the end of each experiment. Drugs and KCl were applied with a fast-step perfusion system (switching time < 20 ms; Warner Instrument Co, Model SF-77B). A change in intracellular Ca^{2+} concentration ($[Ca^{2+}]_i$) ≥ 30% of baseline was considered as a response to treatment. The magnitude of the response was calculated as (Peak $[Ca^{2+}]_i$) – (Baseline $[Ca^{2+}]_i$). To account for biological variance, percentage of DiI + neurons that responded to capsaicin and the average magnitude of response across DiI + capsaicin-responsive neurons were calculated and the data for each mouse was reported. Fluorescence data was acquired by a Nikon Eclipse Ti microscope at 340 nm and 380 nm excitation wavelengths and analyzed with the TI Element Software (Nikon, Melville, NY, USA). $[Ca^{2+}]_I$ was determined from fura-2AM ratio. Calibration of imaging software to convert Fura-2 ratio following in situ calibration experiments was performed as previously described[52,53].

Immunohistochemistry. To determine changes in protein expression in TG ganglia neurons innervating the tongue, retrograde tracers were injected into the tongue 10 days prior to inoculation or administration of 4NQO or vehicle. Retrograde tracer 1,19-dioctadecyl-3,3,39,39 tetramethylindocarbocyanine perchlorate (DiI; Invitrogen, Carlsbad, CA) was dissolved to 170 mg/mL in DMSO, diluted 1:10 in 0.9% sterile saline, and injected bilaterally using a 30 g needle for a total volume of 5-7μL per tongue of adult male and female mice to label tongue afferents. Retrograde tracer, Fast Blue (Polysciences, Inc, Warrington, PA, USA), was dissolved using Milli-Q water to a final concentration of 2.0% and injected bilaterally using a 30 g needle for a total volume of 5-7μL per tongue of adult male and female C57Bl/6 mice to label tongue afferents. At least 10 days following tongue tracer injection, animals were euthanized through an overdose of inhaled isoflurane and perfused transcardially with phosphate buffered saline (PBS) followed by 4% paraformaldehyde (Sigma Aldrich). TG were dissected, postfixed for 1 h in paraformaldehyde, and cryoprotected in 30% sucrose PBS) at 4 °C. TG were embedded in Tissue-Tek OCT compound (Sakura Finetek, Torrance, CA), sectioned (8 μm), and mounted on Superfrost Plus slides (Fisher Scientific Company, Pittsburgh, PA). Sections were blocked for 1 h in 3% goat serum and incubated in primary antibody in PBS containing 1% bovine serum albumin overnight at room temperature. The primary antibodies used were as follows: guinea pig anti-TRPV1 (1:500, Alomone AGP-118, lot#ANO125), rabbit anti-PAR2 (1:250, Thermo Scientific PA5-77685, lot#VJ3105322). Slides were extensively washed in PBS and incubated in goat anti–rabbit or guinea pig secondary antibodies conjugated to cyanine 2 or 3 (Jackson ImmunoResearch, West Grove, PA) in PBS at 1:250 for 2.5 h, extensively washed, and cover-slipped with FluoroGel II containing DAPI (Electron Microscopy Sciences). Sections were photographed using NIS Elements software and a Nikon Eclipse Ti microscope. For quantification of TRPV1-positive neurons across treatment groups as well as triple labeling of retrograde tracer (DiI), TRPV1-positive and PAR_2-positive neurons, TG neurons with distinct nuclei within the V3 region were counted in every fifth section across three different sections per animal from 3 individual animals with a 20 × objective and identical laser gain settings.

Statistical analysis. An independent samples t-test or analysis of variance (ANOVA) was employed to evaluate the difference between groups defined by genotype and treatment, and mixed models ANOVA analysis was used when repeated measures over time were also included in the analysis. To adjust for multiple comparisons, the post hoc Holm-Sidak test statistic was employed. Statistical significance was set at $p < 0.05$. All statistical analyses were performed using Prism (version 8) statistical software (GraphPad Software Inc., San Diego, CA, USA). Results were presented as mean and standard error of the mean in box/scatter configuration to show the biological variability. Our study is reported in accordance with ARRIVE guidelines (https://arriveguidelines.org).

Received: 1 November 2021; Accepted: 22 February 2022
Published online: 08 March 2022

References

1. Connelly, S. T. & Schmidt, B. L. Evaluation of pain in patients with oral squamous cell carcinoma. *J. Pain* **5**, 505–510. https://doi.org/10.1016/j.jpain.2004.09.002 (2004).
2. Kolokythas, A., Connelly, S. T. & Schmidt, B. L. Validation of the university of California San Francisco oral cancer pain questionnaire. *J. Pain* **8**, 950–953. https://doi.org/10.1016/j.jpain.2007.06.012 (2007).
3. Lam, D. K., Dang, D., Zhang, J., Dolan, J. C. & Schmidt, B. L. Novel animal models of acute and chronic cancer pain: a pivotal role for PAR2. *J. Neurosci.* **32**, 14178–14183. https://doi.org/10.1523/JNEUROSCI.2399-12.2012 (2012).
4. Ghilardi, J. R. *et al.* Selective blockade of the capsaicin receptor TRPV1 attenuates bone cancer pain. *J. Neurosci.* **25**, 3126–3131. https://doi.org/10.1523/JNEUROSCI.3815-04.2005 (2005).
5. Honore, P. *et al.* Repeated dosing of ABT-102, a potent and selective TRPV1 antagonist, enhances TRPV1-mediated analgesic activity in rodents, but attenuates antagonist-induced hyperthermia. *Pain* **142**, 27–35. https://doi.org/10.1016/j.pain.2008.11.004 (2009).
6. Karai, L. J., Russell, J. T., Iadarola, M. J. & Olah, Z. Vanilloid receptor 1 regulates multiple calcium compartments and contributes to Ca2+-induced Ca2+ release in sensory neurons. *J. Biol. Chem.* **279**, 16377–16387. https://doi.org/10.1074/jbc.M310891200 (2004).
7. Niiyama, Y., Kawamata, T., Yamamoto, J., Furuse, S. & Namiki, A. SB366791, a TRPV1 antagonist, potentiates analgesic effects of systemic morphine in a murine model of bone cancer pain. *Br. J. Anaesth.* **102**, 251–258. https://doi.org/10.1093/bja/aen347 (2009).
8. Shinoda, M., Feng, B. & Gebhart, G. F. Peripheral and central P2X receptor contributions to colon mechanosensitivity and hypersensitivity in the mouse. *Gastroenterology* **137**, 2096–2104. https://doi.org/10.1053/j.gastro.2009.06.048 (2009).
9. Nagamine, K. *et al.* Mechanical allodynia and thermal hyperalgesia induced by experimental squamous cell carcinoma of the lower gingiva in rats. *J. Pain* **7**, 659–670. https://doi.org/10.1016/j.jpain.2006.02.013 (2006).
10. Meyer, K. A. Cancer of the stomach and colon. *Ky. Med. J.* **46**, 125–127 (1948).
11. Vaupel, P. W., Frinak, S. & Bicher, H. I. Heterogeneous oxygen partial pressure and pH distribution in C3H mouse mammary adenocarcinoma. *Cancer Res.* **41**, 2008–2013 (1981).
12. Newell, K., Franchi, A., Pouyssegur, J. & Tannock, I. Studies with glycolysis-deficient cells suggest that production of lactic acid is not the only cause of tumor acidity. *Proc. Natl. Acad. Sci. U.S.A.* **90**, 1127–1131. https://doi.org/10.1073/pnas.90.3.1127 (1993).
13. Gillies, R. J., Liu, Z. & Bhujwalla, Z. 31P-MRS measurements of extracellular pH of tumors using 3-aminopropylphosphonate. *Am. J. Physiol.* **267**, C195-203. https://doi.org/10.1152/ajpcell.1994.267.1.C195 (1994).
14. Lautner, M. A., Ruparel, S. B., Patil, M. J. & Hargreaves, K. M. In vitro sarcoma cells release a lipophilic substance that activates the pain transduction system via TRPV1. *Ann. Surg. Oncol.* **18**, 866–871. https://doi.org/10.1245/s10434-010-1328-1 (2011).
15. Brown, D. C., Agnello, K. & Iadarola, M. J. Intrathecal resiniferatoxin in a dog model: efficacy in bone cancer pain. *Pain* **156**, 1018–1024. https://doi.org/10.1097/j.pain.0000000000000115 (2015).
16. Joseph, J. *et al.* Phosphorylation of TRPV1 S801 contributes to modality-specific hyperalgesia in mice. *J. Neurosci.* **39**, 9954–9966. https://doi.org/10.1523/JNEUROSCI.1064-19.2019 (2019).
17. Tu, N. H. *et al.* Legumain induces oral cancer pain by biased agonism of protease-activated receptor-2. *J Neurosci* **41**, 193–210. https://doi.org/10.1523/JNEUROSCI.1211-20.2020 (2021).
18. Amadesi, S. *et al.* Protease-activated receptor 2 sensitizes TRPV1 by protein kinase Cepsilon- and A-dependent mechanisms in rats and mice. *J. Physiol.* **575**, 555–571. https://doi.org/10.1113/jphysiol.2006.111534 (2006).
19. Ruparel, S., Bendele, M., Wallace, A. & Green, D. Released lipids regulate transient receptor potential channel (TRP)-dependent oral cancer pain. *Mol. Pain* **11**, 30. https://doi.org/10.1186/s12990-015-0016-3 (2015).
20. Niiyama, Y., Kawamata, T., Yamamoto, J., Omote, K. & Namiki, A. Bone cancer increases transient receptor potential vanilloid subfamily 1 expression within distinct subpopulations of dorsal root ganglion neurons. *Neuroscience* **148**, 560–572. https://doi.org/10.1016/j.neuroscience.2007.05.049 (2007).
21. Scheff, N. N. *et al.* Granulocyte-colony stimulating factor-induced neutrophil recruitment provides opioid-mediated endogenous anti-nociception in female mice with oral squamous cell carcinoma. *Front. Mol. Neurosci.* **12**, 217. https://doi.org/10.3389/fnmol.2019.00217 (2019).
22. Scheff, N. N. *et al.* Neutrophil-mediated endogenous analgesia contributes to sex differences in oral cancer pain. *Front. Integr. Neurosci.* **12**, 52. https://doi.org/10.3389/fnint.2018.00052 (2018).
23. Scheff, N. N. *et al.* Tumor necrosis factor alpha secreted from oral squamous cell carcinoma contributes to cancer pain and associated inflammation. *Pain* **158**, 2396–2409. https://doi.org/10.1097/j.pain.0000000000001044 (2017).
24. Gatti, R. *et al.* Protease-activated receptor-2 activation exaggerates TRPV1-mediated cough in guinea pigs. *J. Appl. Physiol.* **1985**(101), 506–511. https://doi.org/10.1152/japplphysiol.01558.2005 (2006).
25. Ye, Y. *et al.* Adenosine triphosphate drives head and neck cancer pain through P2X2/3 heterotrimers. *Acta Neuropathol. Commun.* **2**, 62. https://doi.org/10.1186/2051-5960-2-62 (2014).
26. Khasabova, I. A. *et al.* Chemical interactions between fibrosarcoma cancer cells and sensory neurons contribute to cancer pain. *J. Neurosci.* **27**, 10289–10298. https://doi.org/10.1523/JNEUROSCI.2851-07.2007 (2007).
27. Saloman, J. L., Chung, M. K. & Ro, J. Y. P2X(3) and TRPV1 functionally interact and mediate sensitization of trigeminal sensory neurons. *Neuroscience* **232**, 226–238. https://doi.org/10.1016/j.neuroscience.2012.11.015 (2013).
28. Gu, X. F., Lee, J. H., Yoo, S. B., Moon, Y. W. & Jahng, J. W. Intra-oral pre-treatment with capsaicin increases consumption of sweet solutions in rats. *Nutr. Neurosci.* **12**, 149–154. https://doi.org/10.1179/147683009X423319 (2009).
29. Lopshire, J. C. & Nicol, G. D. The cAMP transduction cascade mediates the prostaglandin E2 enhancement of the capsaicin-elicited current in rat sensory neurons: whole-cell and single-channel studies. *J. Neurosci.* **18**, 6081–6092 (1998).
30. Premkumar, L. S. & Ahern, G. P. Induction of vanilloid receptor channel activity by protein kinase C. *Nature* **408**, 985–990. https://doi.org/10.1038/35050121 (2000).
31. Kawabata, A., Kinoshita, M., Kuroda, R. & Kakehi, K. Capsazepine partially inhibits neurally mediated gastric mucus secretion following activation of protease-activated receptor 2. *Clin. Exp. Pharmacol. Physiol.* **29**, 360–361. https://doi.org/10.1046/j.1440-1681.2002.03641.x (2002).
32. Rathee, P. K. *et al.* PKA/AKAP/VR-1 module: A common link of Gs-mediated signaling to thermal hyperalgesia. *J. Neurosci.* **22**, 4740–4745 (2002).
33. Gu, Q. & Lee, L. Y. Hypersensitivity of pulmonary chemosensitive neurons induced by activation of protease-activated receptor-2 in rats. *J. Physiol.* **574**, 867–876. https://doi.org/10.1113/jphysiol.2006.110312 (2006).
34. Constantin, C. E. *et al.* Endogenous tumor necrosis factor alpha (TNFalpha) requires TNF receptor type 2 to generate heat hyperalgesia in a mouse cancer model. *J. Neurosci.* **28**, 5072–5081. https://doi.org/10.1523/JNEUROSCI.4476-07.2008 (2008).
35. Rozas, P. *et al.* Targeted overexpression of tumor necrosis factor-alpha increases cyclin-dependent kinase 5 activity and TRPV1-dependent Ca2+ influx in trigeminal neurons. *Pain* **157**, 1346–1362. https://doi.org/10.1097/j.pain.0000000000000527 (2016).

36. Salvo, E. *et al.* TNFalpha promotes oral cancer growth, pain, and Schwann cell activation. *Sci. Rep.* **11**, 1840. https://doi.org/10.1038/s41598-021-81500-4 (2021).
37. Ye, Y. *et al.* Nerve growth factor links oral cancer progression, pain, and cachexia. *Mol. Cancer Ther.* **10**, 1667–1676. https://doi.org/10.1158/1535-7163.MCT-11-0123 (2011).
38. Ye, Y., Dang, D., Viet, C. T., Dolan, J. C. & Schmidt, B. L. Analgesia targeting IB4-positive neurons in cancer-induced mechanical hypersensitivity. *J. Pain* **13**, 524–531. https://doi.org/10.1016/j.jpain.2012.01.006 (2012).
39. Ji, R. R., Samad, T. A., Jin, S. X., Schmoll, R. & Woolf, C. J. p38 MAPK activation by NGF in primary sensory neurons after inflammation increases TRPV1 levels and maintains heat hyperalgesia. *Neuron* **36**, 57–68. https://doi.org/10.1016/s0896-6273(02)00908-x (2002).
40. Wu, L. *et al.* PAR-2 activation enhances weak acid-induced ATP release through TRPV1 and ASIC sensitization in human esophageal epithelial cells. *Am. J. Physiol. Gastrointest. Liver Physiol.* **309**, G695-702. https://doi.org/10.1152/ajpgi.00162.2015 (2015).
41. Elitt, C. M., Malin, S. A., Koerber, H. R., Davis, B. M. & Albers, K. M. Overexpression of artemin in the tongue increases expression of TRPV1 and TRPA1 in trigeminal afferents and causes oral sensitivity to capsaicin and mustard oil. *Brain Res.* **1230**, 80–90. https://doi.org/10.1016/j.brainres.2008.06.119 (2008).
42. Wu, P., Arris, D., Grayson, M., Hung, C. N. & Ruparel, S. Characterization of sensory neuronal subtypes innervating mouse tongue. *PLoS ONE* **13**, e0207069. https://doi.org/10.1371/journal.pone.0207069 (2018).
43. Shiers, S., Klein, R. M. & Price, T. J. Quantitative differences in neuronal subpopulations between mouse and human dorsal root ganglia demonstrated with RNAscope in situ hybridization. *Pain* **161**, 2410–2424. https://doi.org/10.1097/j.pain.0000000000001973 (2020).
44. Ye, Y. *et al.* Anti-cancer and analgesic effects of resolvin D2 in oral squamous cell carcinoma. *Neuropharmacology* **139**, 182–193. https://doi.org/10.1016/j.neuropharm.2018.07.016 (2018).
45. Naik, K. *et al.* The histopathology of oral cancer pain in a mouse model and a human cohort. *J. Dent. Res.* **100**, 194–200. https://doi.org/10.1177/0022034520961020 (2021).
46. Sagheer, S. H. *et al.* 4NQO induced carcinogenesis: A mouse model for oral squamous cell carcinoma. *Methods Cell. Biol.* **163**, 93–111. https://doi.org/10.1016/bs.mcb.2021.01.001 (2021).
47. Simons, C. T., Dessirier, J. M., Jinks, S. L. & Carstens, E. An animal model to assess aversion to intra-oral capsaicin: increased threshold in mice lacking substance p. *Chem. Senses* **26**, 491–497. https://doi.org/10.1093/chemse/26.5.491 (2001).
48. Johansen, J. P., Fields, H. L. & Manning, B. H. The affective component of pain in rodents: direct evidence for a contribution of the anterior cingulate cortex. *Proc. Natl. Acad. Sci. U.S.A.* **98**, 8077–8082. https://doi.org/10.1073/pnas.141218998 (2001).
49. Johansen, J. P. & Fields, H. L. Glutamatergic activation of anterior cingulate cortex produces an aversive teaching signal. *Nat. Neurosci.* **7**, 398–403. https://doi.org/10.1038/nn1207 (2004).
50. King, T. *et al.* Contribution of afferent pathways to nerve injury-induced spontaneous pain and evoked hypersensitivity. *Pain* **152**, 1997–2005. https://doi.org/10.1016/j.pain.2011.04.020 (2011).
51. Malin, S. A., Davis, B. M. & Molliver, D. C. Production of dissociated sensory neuron cultures and considerations for their use in studying neuronal function and plasticity. *Nat. Protoc.* **2**, 152–160. https://doi.org/10.1038/nprot.2006.461 (2007).
52. Scheff, N. N., Lu, S. G. & Gold, M. S. Contribution of endoplasmic reticulum Ca2+ regulatory mechanisms to the inflammation-induced increase in the evoked Ca2+ transient in rat cutaneous dorsal root ganglion neurons. *Cell Calcium* **54**, 46–56. https://doi.org/10.1016/j.ceca.2013.04.002 (2013).
53. Appel, C. K., Scheff, N. N., Viet, C. T., Schmidt, B. L. & Heegaard, A. M. Decitabine attenuates nociceptive behavior in a murine model of bone cancer pain. *Pain* **160**, 619–631. https://doi.org/10.1097/j.pain.0000000000001442 (2019).

Acknowledgements

We would like to thank Aditi Bhattacharya BDS, MDS, PhD, for her expertise in pathological assessment of the mouse 4NQO tongue tumor tissue and Scheff lab manager, Megan Atherton, for her expertise in rodent breeding and careful review of the manuscript.

Author contributions

All authors listed contributed substantially to the work. N.N.S; designed the research, conducted experiments, performed data analyses, and wrote the manuscript. I.M.W., S.N., and H.W. conducted behavioral and molecular experiments and provided technical support. C.Z.L. reviewed and interpreted histopathology. E.C. and N.H.T. assisted in research design, conducted experiments, and provided technical support. N.W.B. assisted in research design and provided technical assistance. M.N.J. performed data analysis and edited the manuscript. J.C.D. edited the manuscript. B.L.S. assisted in research design and wrote and edited the manuscript.

Funding

Supported by grants from the National Institutes of Health (NS102722, DE026806, DK118971, DE029951, N.W.B., B.L.S.) and Department of Defense (W81XWH1810431, N.W.B., B.L.S.).

Competing interests

N.W.B. is a founding scientist of Endosome Therapeutics Inc. Research in N.W.B.'s laboratory is partly supported by Takeda Pharmaceuticals International. J.C.D. fabricates dolognawmeter™ assay devices through Gnatheon Scientific LLC. The other authors do not have a competing interest.

Additional information

Supplementary Information The online version contains supplementary material available at https://doi.org/10.1038/s41598-022-08005-6.

Correspondence and requests for materials should be addressed to B.L.S.

Reprints and permissions information is available at www.nature.com/reprints.

Publisher's note Springer Nature remains neutral with regard to jurisdictional claims in published maps and institutional affiliations.

Open Access This article is licensed under a Creative Commons Attribution 4.0 International License, which permits use, sharing, adaptation, distribution and reproduction in any medium or format, as long as you give appropriate credit to the original author(s) and the source, provide a link to the Creative Commons licence, and indicate if changes were made. The images or other third party material in this article are included in the article's Creative Commons licence, unless indicated otherwise in a credit line to the material. If material is not included in the article's Creative Commons licence and your intended use is not permitted by statutory regulation or exceeds the permitted use, you will need to obtain permission directly from the copyright holder. To view a copy of this licence, visit http://creativecommons.org/licenses/by/4.0/.

© The Author(s) 2022

Author Manuscript

Author Manuscript

Author Manuscript

Author Manuscript

HHS Public Access

Author manuscript

Biomaterials. Author manuscript; available in PMC 2023 June 01.

Published in final edited form as:

Biomaterials. 2022 June ; 285: 121536. doi:10.1016/j.biomaterials.2022.121536.

Sustained endosomal release of a neurokinin-1 receptor antagonist from nanostars provides long-lasting relief of chronic pain

Rocco Latorre[a,b,1], **Paulina D. Ramírez-Garcia**[c,1], **Alan Hegron**[a,b], **James L. Grace**[c], **Jeffri S. Retamal**[c], **Priyank Shenoy**[c], **Mai Tran**[c], **Luigi Aurelio**[c], **Bernard Flynn**[c], **Daniel P. Poole**[c], **Rafael Klein-Cloud**[a,b], **Dane D. Jensen**[a,d], **Thomas P. Davis**[e], **Brian L. Schmidt**[a,b,d], **John F. Quinn**[c], **Michael R. Whittaker**[c,***], **Nicholas A. Veldhuis**[c,**], **Nigel W. Bunnett**[a,b,*]

[a]Department of Molecular Pathobiology, New York University, New York, 10010, USA

[b]Department of Neuroscience and Physiology, Neuroscience Institute, New York University, New York, 10010, USA

[c]Monash Institute of Pharmaceutical Sciences, Monash University, Parkville, VIC, 3052, Australia

[d]Bluestone Center for Clinical Research, New York University College of Dentistry, New York, 10010, USA

[e]Australian Institute for Bioengineering and Nanotechnology, The University of Queensland, Brisbane, QLD, 4072, Australia

Abstract

Soft polymer nanoparticles designed to disassemble and release an antagonist of the neurokinin 1 receptor (NK_1R) in endosomes provide efficacious yet transient relief from chronic pain. These micellar nanoparticles are unstable and rapidly release cargo, which may limit the duration of analgesia. We examined the efficacy of stable star polymer nanostars containing the NK_1R

*Corresponding author. Department of Molecular Pathobiology, New York University, New York, 10010, USA. nwb2@nyu.edu.
**Corresponding author.Monash Institute of Pharmaceutical Sciences, 381 Royal Parade, Parkville, VIC, 3052, Australia. nicholas.veldhuis@monash.edu. ***Corresponding author. Monash Institute of Pharmaceutical Sciences, 381 Royal Parade, Parkville, VIC, 3052, Australia. michael.whittaker@monash.edu.
[1]Equal first authors.

Credit author statement

Rocco Latorre: Methodology, Validation, Investigation, Writing. Paulina D. Ramírez-Garcia: Methodology, Validation, Investigation, Writing. Alan Hegron: Methodology, Validation, Investigation, Writing. James L. Grace: Methodology, Validation, Investigation. Jeffri S. Retamal: Methodology, Validation, Investigation. Priyank Shenoy: Methodology, Validation, Investigation. Mai Tran: Methodology, Validation, Investigation. Luigi Aurelio: Resources. Bernard Flynn: Resources. Daniel P. Poole: Methodology, Validation, Investigation. Dane D. Jensen: Methodology, Validation, Investigation. Thomas P. Davis: Conceptualization, Funding acquisition. Brian L. Schmidt: Conceptualization, Funding acquisition. John F. Quinn: Conceptualization, Methodology, Writing. Michael R. Whittaker: Conceptualization, Methodology, Validation, Investigation, Writing. Nicholas A. Veldhuis: Conceptualization, Methodology, Validation, Investigation, Writing. Nigel W. Bunnett: Conceptualization, Writing, Funding acquisition, Supervision.

Declaration of competing interest

The authors declare the following financial interests/personal relationships which may be considered as potential competing interests: Nigel W. Bunnett reports financial support was provided by Endosome Therapeutics Inc and Takeda Pharmaceuticals International. Nigel W Bunnett reports a relationship with Endosome Therapeutics Inc and Takeda Pharmaceuticals International that includes: board membership, equity or stocks, funding grants, and travel reimbursement. Declaration of competing interest. NWB is a founding scientist of Endosome Therapeutics Inc. Research in NWB's laboratory is funded, in part, by Takeda Pharmaceuticals International.

Appendix A. Supplementary data

Supplementary data to this article can be found online at https://doi.org/10.1016/j.biomaterials.2022.121536.

Author Manuscript Author Manuscript Author Manuscript Author Manuscript

antagonist aprepitant-amine for the treatment of chronic pain in mice. Nanostars continually released cargo for 24 h, trafficked through the endosomal system, and disrupted NK_1R endosomal signaling. After intrathecal injection, nanostars accumulated in endosomes of spinal neurons. Nanostar-aprepitant reversed mechanical, thermal and cold allodynia and normalized nociceptive behavior more efficaciously than free aprepitant in preclinical models of neuropathic and inflammatory pain. Analgesia was maintained for >10 h. The sustained endosomal delivery of antagonists from slow-release nanostars provides effective and long-lasting reversal of chronic pain.

Keywords

Endosomes; Pain; Nociception; Receptors; Signal transduction

1. Introduction

Chronic pain is common, debilitating and poorly treated by available drugs. Whereas acute pain provides awareness and avoidance of injury and is thus necessary for survival, chronic pain can persist after healing and is maladaptive [1]. The factors that underlie the transition from acute (physiological) to chronic (pathological) pain are poorly understood. In consequence, the treatments for chronic pain are often ineffective or have unacceptable side effects. Although opioids are commonly used to treat acute pain, their analgesic properties wane with continued use (*i.e.*, tolerance), while their on-target side effects of respiratory depression, constipation and sedation remain sustained, are life-threatening and are exacerbated by opioid addiction [2]. The opioid crisis highlights the need to develop improved treatments for chronic pain that are devoid of the side-effects of opioids.

G protein-coupled receptors (GPCRs) control most steps of pain transmission and are major therapeutic targets of treatments for pain [3]. GPCRs at the peripheral terminals of primary sensory neurons detect peptides, proteases, prostaglandins, amines and purines that are generated at sites of injury and disease. GPCRs expressed by second order spinal neurons detect substance P (SP), calcitonin gene-related peptide (CGRP) and glutamate that are released from the central projections of primary sensory neurons. GPCRs regulate the activity of ion channels that control neuronal activity and pain transmission, including members of the transient receptor potential family of cation channels [4].

GPCRs initiate signaling at the plasma membrane, where receptors interact with extracellular agonists and couple to intracellular heterotrimeric G proteins. However, plasma membrane GPCR signaling is transient. GPCR kinases phosphorylate activated receptors, increasing their affinity for β-arrestins (βARRs). βARRs uncouple GPCRs from G proteins, which desensitizes signaling, and couple GPCRs to clathrin and adaptor protein-2, which mediate receptor endocytosis [5]. Desensitization and endocytosis limit GPCR signaling at the surface of cells. Endosomes were formerly considered to be conduits for GPCR trafficking to degradatory or recycling pathways. Recent evidence suggests that GPCRs can form multiprotein signaling complexes within endosomes, including GPCR, Gα and βARRs “megaplexuses”, where Gα subunits convey signals and βARRs act as molecular scaffolds

Author Manuscript Author Manuscript Author Manuscript Author Manuscript

for signaling enzymes, including mitogen-activated protein kinases [6–10]. Evidence derived from use of inhibitors of clathrin-mediated endocytosis, and biosensors that detect signaling events with subcellular resolution, suggests that GPCRs in endosomes control a subset of signals in defined subcellular compartments. The SP neurokinin 1 receptor (NK_1R), CGRP calcitonin-like receptor (CLR), protease-activated receptor-2 (PAR_2) and the δ-opioid receptor signal from endosomes of primary sensory or spinal neurons to control neuronal excitation and pain transmission [11–15].

Since endosomal signals control pain transmission, GPCRs in endosomes might be the optimal therapeutic target for pain [16]. The inadequacy of conventional GPCR antagonists in clinical trials for chronic pain, where activated receptors may redistribute to endosomes due to chronic agonist production [11], might be related to their inability to engage GPCRs in endosomes. Whether conventional GPCR antagonists can penetrate the plasma and endosomal membrane and interact with GPCR conformations within multiprotein complexes in an acidic endosomal environment is seldom studied. Antagonists of the NK_1R, CLR and PAR_2 conjugated to a flexible PEG linker and the lipid cholestanol accumulate into plasma and endosomal membranes, block endosomal signals and provide more effective and long-lasting relief from pain than conventional antagonists [11–15]. The propensity of nanoparticles to accumulate in endosomes offers the prospect of bypassing the plasma membrane and direct delivery of antagonists to endosomes. When encapsulated into soft polymer nanoparticles designed to bypass cell surface receptors and release cargo in acidic endosomes, an antagonist of the NK_1R, aprepitant (AP), provides potent and sustained analgesia in preclinical models of inflammatory and neuropathic pain [17,18]. These micellar nanoparticles rapidly disassemble and release cargo, are inherently unstable and are prone to dilution effects, which might limit the duration of action of analgesics. To surmount these limitations in the present study, we developed an analogue of AP functionalized with PEG-amine for conjugation to nanostars. Nanostars are dilution-stable and can be designed for tunable and sustained cargo release, which could provide a longer lasting analgesia. Core-crosslinked and functional polymeric nanostars are versatile soft matter nanoparticles engineered to be analogs of dendrimers [19]. We previously investigated the pharmacokinetic properties, uptake and association of nanostars with tumors, cancer cells and blood components [20–22]. We also explored the use of nanostars as platforms for the delivery of cancer therapeutics, antioxidants and imaging agents [23–25].

The current study compared the therapeutic efficacy of AP-nanostars and micellar AP-nanoparticles in preclinical models of neuropathic and inflammatory pain by studying evoked and non-evoked nociceptive behavior in mice. The analgesic properties of AP-nanostars with different degrees of hydrolytic stability were explored. The results show that the slow release of AP from nanostars in endosomes of spinal neurons provides a more complete and long-lasting analgesia than attained by free AP or AP encapsulated into micellar nanoparticles.

Author Manuscript Author Manuscript Author Manuscript Author Manuscript

2. Materials and methods

2.1. Synthesis and characterization of micellar nanoparticles

DIPMA nanoparticles were generated and loaded as described [18]. In brief, diblock copolymers were synthesized with a hydrophilic shell of P(PEGMA-*co*-DMAEMA) and a hydrophobic core of P (DIPMA-co-DEGMA) to form pH-responsive DIPMA nanoparticles. Nanoparticles were self-assembled with AP (MK-869 [26]), a hydrophobic NK_1R antagonist, forming DIPMA-aprepitant (DIPMA-AP). Empty nanoparticles (DIPMA-Ø) served as a control. The physicochemical properties of nanoparticles have been described [18,27]. DIPMA nanoparticles enter cells by clathrin- and dynamin-mediated endocytosis and release cargo under acidified conditions of endosomes (>50% cargo release, pH < 6.0).

2.2. Synthesis of nanostars

2.2.1. Materials—Oligo(ethylene glycol) methyl ether acrylate (OEGA, M_n ~480 g/mol, Merck) was deinhibited before use by percolation over basic aluminum oxide. Azobis(isobutyronitrile) (AIBN, Merck) was recrystallized from methanol before use. Sources of other reagents were: *N,N′*-methylenebis(acrylamide) (MBAA, Merck, 98%), 3-vinylbenzaldehyde (VBA, Sigma Aldrich, 97%), pentafluorophenyl acrylate (PFPA, Sigma Aldrich, 98%), trifluoroethanol (TFE, Sigma Aldrich, ≥ =99%), 4-benzoylphenyl acrylate (Benzo, BOC Biosciences), cyanine5 amine (Cy5 amine, Lumiprobe), tetrahydrofuran (THF, LiChrosolv). Chain transfer agent (3-benzylsulfanylthiocarbonylsulfanyl) propionic acid (BSPA) was synthesized as described [18]. Aprepitant amine (AP-NH_2, MIPS-0020668) was synthesized in-house (Fig. S1). Petroleum benzine (b.p 60–80 °C), toluene, chloroform, diethyl ether, acetone and methanol were from Merck Millipore.

2.2.2. Synthesis, purification and activity of aprepitant-NH_2 (AP-NH_2)—AP-NH_2 was synthesized for incorporation into nanostars. AP was from Combi blocks (CA, USA) and BocNH-PEG2-NH_2 was from PurePEG (CA, USA). The synthesis scheme is shown in Fig. S1. The reaction was monitored by liquid chromatography-mass spectrometry (LC-MS) using an Agilent 6100 Series Single Quad LC-MS coupled to an Agilent 1200 Series HPLC. AP (Fig. S1, step 1; 600 mg, 1.123 mmol), 4-(3-(((2*S*,3*R*)-2-((*S*)-1-(3,5-bis(trifluoromethyl)phenyl)ethoxy)-3-(4-fluorophenyl)morpholino)methyl)-5-oxo-4,5-dihydro-1*H*-1,2,4-triazol-1-yl)butanoic acid, potassium iodide (37 mg, 0.245 mmol), potassium carbonate (310 mg, 2.245 mmol) and ethyl-4-bromobutyrate (162 μL, 1.123 mmol) were stirred in DMF (6 mL) at 60 °C for 6 h then at room temperature for 18 h. The mixture was diluted in EtOAc and washed with water, dried ($MgSO_4$), filtered and concentrated to a resin that was chromatographed on silica gel with 60% EtOAc-pet ether to provide the intermediate ester as a clear colorless resin (62% yield, LCMS *m/z* 649.0 $[M+H]^+$). The resin was taken up in MeOH (6.74 mL) and 1 M NaOH solution (3.37 mL) and stirred at room temperature overnight. The mixture was concentrated to remove volatiles and then diluted with water and acidified to pH 7 with 1 M HCl and then extracted with DCM. The combined DCM layers were dried ($MgSO_4$), filtered and concentrated to provide (Fig. S1, step 2) as a resin/foam (400 mg. LCMS: *m/z* 621.0 $[M+H]^+$). *N*-(2-(2-(2-aminoethoxy)ethoxy)ethyl)-4-(3-(((2*S*,3*R*)-2-((*S*)-1-(3,5-bis(trifluoromethyl)phenyl)ethoxy)-3-(4-fluorophenyl)morpholino)methyl)-5-

Author Manuscript Author Manuscript Author Manuscript Author Manuscript

oxo-4,5-dihydro-1*H*-1,2,4-triazol-1-yl)butanamide (Fig. 1, step 3) was prepared by dissolving the acid (Fig. 1, step 2) (105 mg, 0.169 mmol), HATU (64 mg, 0.169 mmol) and BocNH-PEG2-NH2 (42 mg, 0.169 mmol) in DMF (2 mL) and DIPEA (88 μL, 0.507 mmol) and stirred at room temperature for 3 h. The mixture was partitioned between EtOAc and water. The organic layer was washed with water, dried ($MgSO_4$), filtered and concentrated to a resin. The resin was taken up in 3 mL of 1% cHCl in HFIP and left to stand for 4 h and then concentrated. The crude was purified by HPLC to provide 40 mg of resin (32% yield, LCMS: *m/z* 649.0 $[M+H]^+$). ^{19}F NMR (400 MHz, DMSO) δ −61.20 (s, 6F), δ −114.35 (s, 3F); ^1H NMR (400 MHz, DMSO) δ 8.11–7.70 (m, 6H), 7.57–7.49 (m, 2H), 7.45 (s, 2H), 7.30–6.99 (m, 2H), 4.96 (q, J = 6.4 Hz, 1H), 4.31 (d, J = 2.3 Hz, 1H), 4.12 (t, J = 10.7 Hz, 1H), 3.69–3.49 (m, 12H), 3.20 (dd, J = 11.7, 5.9 Hz, 2H), 2.95 (dt, J = 11.2, 5.6 Hz, 2H), 2.79 (dd, J = 31.5, 13.3 Hz, 2H), 2.44–2.34 (m, 1H), 2.13 (t, J = 7.7 Hz, 2H), 1.98–1.74 (m, 2H), 1.39 (d, J = 6.5 Hz, 3H). To assess antagonistic activity, HEK293Tcells expressing human (h) NK_1R were preincubated with graded concentrations of AP and AP-NH_2 for 30 min, and were then challenged with 10 nM SP. Changes in $[Ca^{2+}]$i were monitored using Fura-2/AM [14].

2.2.3. Synthesis of nanostar POEGA arm—A macromolecular chain transfer agent (macro-CTA, POEGA) was synthesized by the reversible addition fragmentation chain transfer (RAFT) polymerization method using the RAFT agent benzylsulfanylthiocarbonylsufanylpropionic acid (BSPA, 0.051 g, 0.19 mmol, 1 eq.), the initiator azobisisobutyronitrile (AIBN, 0.003 g, 0.02 mol, 0.1 eq.), and oligo(ethylene glycol) methyl ether acrylate M_n ~480 g/mol (OEGA, 3.0 g, 6.25 mmol, 32 eq.). The mixture was dissolved in 9 mL toluene and deoxygenated by sparging with nitrogen for 30 min in an ice/water bath. The reaction proceeded at 70 °C, 400 RPM for 4 h. The polymerization was stopped by cooling in an ice/water bath and exposure to air. The resulting arm polymer (BSPA-POEGA) was purified by repeated precipitations in cold petroleum benzine 60–80 °C and then dried for 24 h under vacuum at 37 °C and 1 mbar.

2.2.4. Synthesis of core-crosslinked nanostar polymers—A series of core-crosslinked nanostar polymers was synthesized with the functional monomers 3-vinylbenzaldehyde (VBA), 4-benzoylphenyl acrylate (Benzo) or pentafluorophenyl acrylate (PFPA) incorporated into the core. All reactions were carried out in 5 mL of toluene and deoxygenated by sparging with nitrogen for 30 min in an ice/water bath. Polymerizations proceeded in an oil bath at 70 °C for 24 h and were stopped by cooling on ice/water and exposure to air. Nanostar polymers were synthesized with the following stoichiometries:

Nanostar-VBA: $[POEGA]_0:[MBAA]_0:[VBA]_0:[AIBN]_0$ = 1:8:10:0.3. BSPA-POEGA linear arm (500 mg, 0.0532 mmol), *N,N′*-methylenebisacrylamide (65.7 mg, 0.426 mmol), VBA (70.4 mg, 0.532 mmol), AIBN (2.6 mg, 0.0160 mmol).

Nanostar-Benzo: $[POEGA]_0:[MBAA]_0:[Benzo]_0:[AIBN]_0$ = 1:8:10:0.3. BSPA-POEGA linear arm (500 mg, 0.0532 mmol), *N,N′*-methylenebisacrylamide (65.7 mg, 0.426 mmol), 4-benzophenyl acrylate (134.3 mg, 0.532 mmol), AIBN (2.6 mg, 0.0160 mmol).

Author Manuscript Author Manuscript Author Manuscript Author Manuscript

Nanostar-PFPA: $[POEGA]_0$:$[MBAA]_0$:$[PFPA]_0$:$[AIBN]_0$ = 1:8:10:0.3. BSPA-POEGA linear arm (500 mg, 0.0532 mmol), *N,N′*-methylenebisacrylamide (65.7 mg, 0.426 mmol), PFPA (126.8 mg, 0.532 mmol), AIBN (2.6 mg, 0.0160 mmol).

2.2.5. Purification of nanostar polymers—Nanostars were purified by five successive precipitation and centrifugation steps using chloroform into diethyl ether (2% v/v) to remove unreacted cross-linker, arm polymer and monomers. Nanostar polymers were characterized by ^{1}H NMR and gel permeation chromatography (GPC).

2.2.6. Synthesis of nanostar-Cy5-NH_2—Nanostar-Cy5 conjugates (designated PFPA-Cy5, VBA-Cy5, Benzo-Cy5) were polymerized in DMF (1 mL) in dark at room temperature for 72 h with the following stoichiometries:

VBA-Cy5: Nanostar-VBA (0.02 g), Cy5-NH_3·Cl (1.3 mg, 2.1×10^{-6} mol) and triethylamine (5.0 μL, 3.59×10^{-5} mol).

Benzo-Cy5: Nanostar-Benzo (0.02 g), Cy5-NH_3·Cl (1.2 mg, 2.0×10^{-6} mol) and triethylamine (5.0 μL, 3.59×10^{-5} mol).

PFPA-Cy5: Nanostar-PFPA (0.02 g), Cy5-NH_3·Cl (1.9 mg, 3.23×10^{-6} mol) and triethylamine (5.0 μL, 3.59×10^{-5} mol).

2.2.7. Synthesis of nanostar-AP-NH_2—AP-NH_3 was synthesized and purified as described in supplementary methods. Nanostar-AP conjugates were polymerized in DMSO−d_6 (0.6 mL) in dark at room temperature for 155 h for nanostar-PFPA-AP (designated PFPA-AP), 155 h for nanostar-VBA-AP (VBA-AP) and 84 h for nanostar-Benzo-AP (Benzo-AP). The state of the reaction was periodically assessed using ^{19}F NMR. Stoichiometries of the reactions were as follows:

VBA-AP: Nanostar-VBA (0.02 g), AP-NH_3·Cl (1.5 mg, 2.0×10^{-6} mol) and triethylamine (5.0 μL, 3.59×10^{-5} mol).

Benzo-AP: Nanostar-Benzo (0.02 g), AP-NH_3·Cl (1.6 mg, 2.1×10^{-6} mol) and triethylamine (5.0 μL, 3.59×10^{-5} mol).

PFPA-AP: Nanostar-PFPA (0.02 g), AP-NH3·Cl (2.5 mg, 3.3×10^{-6} mol) and triethylamine (5.0 μL, 3.59×10^{-5} mol).

2.2.8. Purification of nanostars—Nanostar-Cy5 or nanostar-AP was purified by preparative size exclusion chromatography using Bio-Beads S-X1 support and chromatographic grade THF as the mobile phase. Fractions containing nanostar-Cy5 or nanostar-AP conjugates were combined and stored at −20 °C. Successful Cy5 conjugation and the removal of free Cy5 was confirmed by GPC using refractive index (RI) and UV-VIS detection (λ = 646). AP-NH_2 content (conjugated or free contaminant) was determined by ^{19}F NMR using a trifluoroethanol internal standard, while ^{1}H NMR confirmed macromolecular structure. The expected increase in apparent molecular weight of

Author Manuscript Author Manuscript Author Manuscript Author Manuscript

the nanostars on conjugation with AP-NH_2 was confirmed by GPC. Nanostar-AP conjugates were stored in DMSO−d_6 at −20 °C.

2.3. Characterization of nanostars

2.3.1. Gel permeation chromatography (GPC)—Nanostars were characterized using a Shimadzu GPC system comprising three KF-805L columns (300 × 8 mm, bead size: 10 mm, pore size maximum: 5000 Å) and SPD-20A UV/Vis and RID-10A differential refractive-index detectors. The temperature of columns was maintained at 40 °C. The eluent was *N,N*-dimethylacetamide (CHROMASOLV Plus for HPLC) with 0.03% w/v LiBr at a flow rate of 1.0 mL/min. A molecular weight calibration curve was produced using polystyrene standards (500–2 × 10^6 g mol^{-1}). Polymer solutions (~2 mg/mL) were prepared and filtered through 0.45 μm PTFE filters before injection.

2.3.2. Proton-nuclear magnetic resonance (^{1}H NMR) and fluorine-19 nuclear magnetic resonance (^{19}F NMR)—NMR spectra were recorded on a Bruker Advance III (400 MHz for ^{1}H NMR and 376 MHz for ^{19}F NMR) spectrometer using an external lock. The ^{1}H NMR spectra were referenced to the residual nondeuterated solvent and ^{19}F NMR spectra were referenced to trifluoroethanol (TFE). Chemical shifts (δ_H) are reported in parts per million (ppm). $CDCl_3$ and DMSO−d_6 (Cambridge Isotope Laboratories, Inc) were used as NMR solvents. Conversion and degree of polymerization (DP) were calculated by ^{1}H NMR using peak integrals (I) where the subscript number indicates the location of the peak in ppm (I_x). The DP for BSPA-POEGA was calculated using the ^{1}H NMR spectra with $\boldsymbol{n_{OEGA} = \frac{I_{4.07}}{2}}$ normalized to peaks a-c = 5 ($I_{7.32}$). The molecular weight of the polymer (M_n) was calculated using the ^{1}H NMR spectra with $\boldsymbol{M_n = DP \times M_{OEGA} + M_{BSPA}}$.

2.3.3. Dynamic light scattering (DLS) and ζ-potential analysis—Dynamic light scattering and ζ-potential analysis were determined at 25 °C using a Malvern Zetasizer ZS series equipped with a 4 mW laser at λ = 633 nm and a detector angle 173° running DTS software. Viscosity and refractive index were assumed to be 0.899 cP and 1.338 as for PBS and PEG particles: the D_H number, hydrodynamic diameter, and ZETA potential are reported as determined by the DTS software.

2.3.4. Transmission electron microscopy (TEM)—The morphology of nanostars was determined by TEM imaging using a Thermo Scientific L120C electron microscope at an accelerating voltage of 120 kV at room temperature. Formvar coated copper grids (GSCu100F-50, Proscitech) were pretreated in a plasma discharger for 35 s. Nanostars (3 μL, 3 μg/mL) were deposited on grids, immediately blotted, and dried for 1 h followed by negative staining with Ammonium molybdate (5 μL, 5 wt %, 25 s).

2.3.5. pH-dependent release of Cy5-NH_2. Cy5-NH_2 release from nanostars was examined at pH 7.4, 6.0 and 5.0 by UV–visible spectrophotometry—Nanostar-Cy5 conjugate was dried, reconstituted in PBS (pH 7.4, 6.0, 5.0), and placed into the inner sample tube of an individual Spectra-Por Float-A-Lyser G2 Dialysis Device, 3.5–5k MWCO (1.0 mL). Cy5 release study was examined under sink conditions in 1 L PBS buffer (pH 7.4 or 6.0). At defined times, an aliquot (0.5 mL) of solution within the

Author Manuscript Author Manuscript Author Manuscript Author Manuscript

sample tube was removed, analyzed by UV–Vis (λ = 646 nm), and returned to the sample compartment. Changes in the absorbance at λ = 646 nm are reported relative to the starting solution.

2.3.6. Release of AP-NH_2—AP-NH_2 release from nanostars was examined at pH 7.4 by HPLC. Nanostar-AP conjugates were suspended in PBS containing 20% DMSO, adjusted to pH 7.4. Nanostar-AP conjugates (500 μL, 200 μM) were placed into a dialysis device (Spectra-Por Float-A-Lyser G2, 3.5–5k MWCO) and dialyzed against 15 mL of PBS/DMSO. At defined time points, 300 μL of the release solution was collected for HPLC analysis. The same volume of PBS/DMSO was added immediately into the release solution to maintain constant volume. Release was studied under stirring at room temperature. AP-NH_2 release was quantified by HPLC using an ultra-fast liquid chromatograph (UFLC, Shimadzu) with a C18 column (150 × 4.6 mm, 5 μm) using a detection wavelength of 215 nm. The mobile phase was 0.01% phosphoric acid in water and acetonitrile. Samples (300 μL) for analysis were concentrated to a final volume of 100 μL using an ISSI110 SpeedVac Concentrator (Thermo Fisher). AP-NH_2 release was quantified against standards (6.25–200 μM), and compounds were eluted under gradient conditions at a flow rate of 1.5 mL/min.

2.4. Studies of nanostars in cell lines

2.4.1. Cell lines—HEK293T (#CRL-3216™, American Type Culture Collection) cells were cultured in Dulbecco's Modified Eagle's Medium (DMEM) supplemented with heat inactivated fetal bovine serum (FBS, 10%), L-glutamine (2 mM), penicillin (100 U/ml) and streptomycin (100 mg/mL) at 37 °C in 5% CO_2 and 95% O_2. cDNA encoding the hNK_1R with an extracellular N-terminal FLAG-tag was transfected into HEK293Tcells to generate a stable cell line expressing hNK_1R (HEK-hNK_1R) as described [18].

2.4.2. Cell viability assays—HEK293Tcells were plated (25,000 cells/well) into poly-D-lysine-coated 96 well CulturPlates (PerkinElmer, USA). Cells were incubated with vehicle (HBSS), VBA-Ø, Benzo-Ø, PFPA-Ø (1–100 μg/mL) or the positive control Triton X-100 (1%) for 24 h and 48 h. Viability was assessed using AlamarBlue (In Vitro Technologies), propidium iodide (Sigma Aldrich) or Thiazolyl Blue Tetrazolium Bromide (MTT, Sigma Aldrich), according to the manufacturers' instructions. Viability was calculated by subtracting the values of cells treated with the positive control Triton X-100 and expressing the values as a percentage of the vehicle control.

2.4.3. Endocytosis assays—HEK293T cells were plated into 12 mm glass coverslips and cultured for 24 h. Cells were incubated with PFPA-Cy5 nanostars (20 μg/mL) in Hank's balanced salt solution (HBSS) for 30, 60 or 120 min at 37 °C. Cells were washed and fixed in 4% paraformaldehyde (10 min on ice). Cells were incubated in permeabilizing/blocking buffer (5% normal horse serum in PBS containing and 0.3% saponin) for 1 h at room temperature. Cells were incubated with a polyclonal anti-EEA1 antibody (rabbit, #ab2900, Abcam, 1:1000) or polyclonal anti-Rab7 antibody (rabbit, #9367, Cell Signaling, 1:1000) in blocking buffer overnight at 4 °C. Cells were washed and incubated with secondary antibody (donkey anti-rabbit Alexa488, ThermoFisher, 1:1000). Coverslips were mounted using Prolong diamond antifade (ThermoFisher) and images were captured on a Leica

Author Manuscript Author Manuscript Author Manuscript Author Manuscript

TCSSP8 confocal using an HCX PL APO Å~63 NA 2.0 oil objective. Images were analyzed using Fiji [28] with the toolbox plugin JACoP for Manders' overlap coefficient analysis [29].

2.4.4. Enhanced bystander bioluminescence resonance energy transfer (EbBRET) assays—Mini-G proteins coupled to Venus were from N. A. Lambert (Augusta University). Constructs were modified to replace Venus with *Renilla* (R) luciferase 8 (Rluc8). *Renilla* GFP-CAAX (prenylation CAAX box of KRas), tdRGFP-Rab5a and Rluc2-βARR2 were from M. Bouvier (Université de Montréal). HEK293T cells were transfected using PEI with hNK_1R (0.2 μg) and Rluc8-$mG\alpha_{si/s/sq}$ (0.1 μg) [30,31]and either RGFP-CAAX (0.2 μg) for cell surface activation or tdRGFP-Rab5a (0.15 μg) for activation in early endosomes [32]. For EbBRET assays of recruitment of βARR2 to the plasma membrane or early endosomes, HEK293T cells were transfected with PEI with hNK_1R (0.2 μg) and Rluc2-βARR2 (0.1 μg) and RGFP-CAAX (0.2 μg) for plasma membrane recruitment or tdRGFP-Rab5a (0.15 μg) for early endosome recruitment [32]. For EbBRET assays, cells were washed with HBSS containing 10 mM Hepes (pH 7.4). Cells were incubated with Prolume Purple Coelenterazine (2.5 μM, 5 min, 37 °C; NanoLight Technology). EbBRET was recorded for 22.5 min in a Synergy Neo2 Microplate reader (BioTek) (acceptor filter: 515 ± 30 nm; donor filter: 410 ± 80 nm). Baseline was measured for 2.5 min and cells were challenged with SP (10 nM) or vehicle. ΔBRET represents the EbBRET signal in the presence of agonist subtracted by the EbBRET signal in the presence of vehicle.

2.5. Studies of nanostars in mice

2.5.1. Animals—Adult male C57BL/6 mice (6–10 weeks) were from the Monash Animal Research Platform and Jackson Laboratories (#000664) USA. Mice were maintained in a light-controlled (12-h light/dark cycle) temperature-controlled (22 ± 4 °C) environment with *at libitum* access to food and water. Studies on mice were in accordance with the Guide for the Care and Use of Laboratory Animals of the National Institutes of Health and adhered to the ethical guidelines of the International Association for the Study of Pain [33]. Studies were approved by the animal ethics committees of the Monash Institute of Pharmaceutical Sciences, Monash University and of New York University Langone Medical Center. At the end of the studies, animals were euthanized by anesthetic overdose (5% isoflurane) and thoracotomy.

2.5.2. Nanostar biodistribution in animals—PFPA-Cy5 nanostars (1 mg/mL, 5 μL) were administered to mice (i.t., L4/L5) under sedation (2% isoflurane). For assessment of biodistribution in whole animals, mice were sedated again (2% isoflurane) and placed in an *in vivo* imaging system (IVIS spectrum, PerkinElmer, USA). Posterior images were obtained before and at 1 min, 2 h and 8 h post PFPA-Cy5 administration using PerkinElmer Living Image software v4.3.1.

2.5.3. Nanostar imaging in spinal cord sections—At 4 h after administration of PFPA-Cy5 nanostars, mice were transcardially with 4% paraformaldehyde in PBS and frozen sections of spinal cord were prepared as described [18]. Sections were incubated with mouse anti-Hu (1:2000, AB_221448), goat anti-GFAP (1:1000, Abcam, AB_880202)

Author Manuscript Author Manuscript Author Manuscript Author Manuscript

or rat anti-CD11b (1:1000, AB_312785) in PBS containing 0.2% Triton X-100 and 5% NHS (overnight, 4 °C). Sections were washed 3× in PBS for 10 min and incubated with donkey anti-rat Alexa 488 (1:500, ThermoFisher Scientific, AB_2535794), anti-mouse Alexa 568 (1:500, ThermoFisher Scientific AB_2534013) and anti-sheep DyLight™ 405 (1:250, Jackson Immunoresearch, AB_2340740) (2 h, room temperature). Sections were counter-stained with DAPI (5 μg/mL, 5 min), washed and mounted with ProLong Glass mounting medium (ThermoFisher Scientific). Sections were imaged on TCS-SP8 Lightning confocal system (20× HC PL APO NA 0.88 water immersion objective) and images were processed using FIJI.

2.5.4. Drug administration—The following drugs were administered by intrathecal (i.t.) injection (5 μL) into the intervertebral space (L4/L5) of conscious mice: AP (300–1000 nM), AP-NH_2 (1000 nM), DIPMA-AP delivering an equivalent dose of AP (300–1000 nM AP), or nanostars delivering an equivalent dose of AP (1000 nM). Controls included empty nanoparticles (DIPMA-Ø, 100 μg/mL; VBA-Ø, 17 μg/mL; Benzo-Ø, 13 μg/mL; PFPA-Ø, 8.33 μg/mL), or vehicle (artificial cerebrospinal fluid, aCSF). Drugs were injected 10 days after induction of neuropathic pain or 2 days after induction of inflammatory pain.

2.5.5. Neuropathic pain—The spared nerve injury (SNI) procedure [34] with modifications was used to induce neuropathic pain. Under anesthesia (5% isoflurane), the left thigh was shaved and cleaned with isopropyl alcohol and iodide. The skin was incised (1 cm) on the lateral surface of the left thigh and the muscle was bluntly dissected to identify the sural, common peroneal and tibial branches of the sciatic nerve. The common peroneal and tibial nerves were ligated with 6–0 silk adjacent to the trifurcation, and a 1 mm segment of the two nerves was removed immediately distal to the ligature. For sham controls, the trifurcation was identified, but the nerves were untouched. The muscle layer was closed using 5–0 vicryl and the skin was closed with 5–0 surgipro (Ethicon, USA).

2.5.6. Inflammatory pain—An emulsion of Complete Freund's Adjuvant (CFA, 0.5 mg/mL) and saline (0.9% NaCl) was prepared by vortexing for 1 min. CFA or vehicle (0.9% NaCl) was administered by intraplantar (i.pl.) injection (10 μL) into the left hindpaw of sedated mice (2% isoflurane) [11,35].

2.5.7. Assessment of nociception—Investigators were blinded to the procedure (CFA or vehicle, SNI or sham) and treatment. Mice were randomly assigned to treatments (www.randomization.com). Mice were studied during the light cycle (8:00 a.m. to 2:00 p.m.). Prior to experiments, mice were acclimatized to the experimental apparatus and environment for >1 h on 2 successive days.

Mechanical allodynia.: Mechanical nociception was assessed by measuring withdrawal thresholds to stimulation of the plantar surfaces of the hindpaws with calibrated von Frey filaments (VFFs) [13]. Mice were placed on a metal grid. VFF withdrawal thresholds were measured in triplicate to establish a baseline for each mouse. VFF responses were then measured at various times after drug treatment. Results are expressed as nociceptive threshold in grams, as percentage of baseline or as area under curve during the experimental period.

Author Manuscript Author Manuscript Author Manuscript Author Manuscript

Cold allodynia.: Cold nociception was assessed by measuring the acute nociceptive response to evaporative cooling induced by topical application of acetone to the plantar surface of the hindpaw [36]. Mice were placed on a metal grid. Acetone (50 μL) was applied to the plantar surface of the hindpaw using a pipette. The time spent in flicking or licking of the plantar region over 60 s was measured.

Behavioral spectrometer.: Non-evoked nociception was assessed using a behavioral spectrometer, which eliminates operator bias (Behavior Sequencer, Behavioral Instruments, NJ; BiObserve, DE) [37,38]. The spectrometer comprised a 40 cm^2 arena with a CCD camera mounted in the center of the ceiling and a door aperture in the front area of the arena. Mouse movement was assessed by a floor mounted vibration sensor and 32 wall mounted infrared transmitter and receiver pairs. Mice were individually placed in the center of the behavioral spectrometer and their behavior was recorded, tracked, evaluated and analyzed using a computerized video tracking system (Viewer3, BiObserve, DE) for 30 min. Total distance traveled in the open field, average velocity of locomotion, wall distance, ambulation and grooming were recorded and analyzed.

2.6. Statistical analyses

Data are presented as mean ± SEM unless noted otherwise. Student's *t*-test was used for two comparisons. For multiple comparisons, results were compared using one- or two-way ANOVA followed by Tukey's or Dunnett's multiple comparison tests. A $P < 0.05$ was considered significant.

3. Results

3.1. pH-tunable DIPMA-AP nanoparticles provide efficacious relief from neuropathic pain

We have previously determined the efficacy of intrathecal DIPMA-AP for reversal of mechanical allodynia in preclinical models of inflammatory and neuropathic pain in mice and rats [18]; other indices of evoked and non-evoked nociception were not examined. Herein, we compared the effects of graded doses of DIPMA-AP and free AP on mechanical allodynia, cold allodynia and non-evoked nociceptive behavior in a preclinical model of neuropathic pain in mice. The SNI model of neuropathic pain was studied in which the common peroneal and tibial branches of the sciatic nerve of the left hindpaw were transected, leaving the sural branch intact [34]. Control mice underwent sham surgery. To assess mechanical allodynia, withdrawal responses to stimulation of the planar surfaces of the lesioned (left, ipsilateral) and unaffected (right, contralateral) hindpaws with graded VFFs were measured. Cold allodynia was assessed by measuring nociceptive responses (paw flicking and licking over 60 s) to evaporative cooling induced by topical application of acetone to the plantar surface of the ipsilateral hindpaw. Non-evoked nociception was assessed using a behavioral spectrometer, which recorded multiple behaviors and eliminated operator bias [37, 38].

Mechanical allodynia.—The VFF response measured in the ipsilateral paw of SNI mice declined at 3 days post-surgery and was sustained for at least 10 days, indicating development of sustained mechanical allodynia (Fig. 1A). In sham mice, the VFF response

Author Manuscript Author Manuscript Author Manuscript Author Manuscript

declined at 3 days, suggesting post-incisional pain, and recovered to pre-surgical within 7–10 days. In all subsequent experiments, mice were studied 10 days after SNI. Graded doses of DIPMA-AP, an equivalent dose of free AP (300, 500, 1000 nM AP) or DIPMA-Ø was injected intrathecally (all 5 μL), and mechanical allodynia was measured every 30 min for 5 h. These treatments had no effect on VFF withdrawal responses of the contralateral paw (Fig. 1B). Free AP caused a dose-related and partial reversal of VFF withdrawal responses of the ipsilateral paw for up to 3.5 h (Fig. 1C–H). At all doses, the magnitude and duration of the anti-nociceptive effects of DIPMA-AP significantly exceeded that of free AP and was sustained for at least 5 h (Fig. 1C–H). The VFF response (expressed as a percentage of baseline values) at 1 h was 40.3 ± 7.6% and 48.2 ± 9.5% basal after free AP 500 and 1000 nM respectively, but 84 ± 10.2% and 100 ± 10.3% basal after DIPMA-AP 500 and 1000 nM ($P < 0.0001$) respectively. DIPMA-Ø did not affect mechanical allodynia.

Cold allodynia.—At 10 days surgery, application of acetone to the paw caused a nocifensive response that was more sustained for SNI than sham mice, indicating cold allodynia (Fig. 1I and J). DIPMA-AP (500 nM AP) almost normalized cold allodynia at 1 and 2 h in SNI mice, whereas AP was less efficacious at all time points. DIPMA-Ø did not affect cold allodynia.

Non-evoked nociceptive behavior.—At 90 min after intrathecal drug administration, non-evoked nociceptive behavior was measured over 30 min. Compared to sham operated controls, SNI mice exhibited significant decreases in average distance from the wall (Fig. 2A), grooming time (Fig. 2B) and ambulation time (Fig. 2C), whereas track length (Fig. 2D), average velocity (Fig. 2E) and locomotor activity (Fig. 2F) were unaffected. The number of times that the SNI mice crossed a central area of the recording chamber was also significantly diminished in SNI mice (Fig. 2G, H, L). Intrathecal injection of gabapentin (1000 nM), an effective treatment for neuropathic pain, normalized affected behaviors in SNI mice. Free AP (500 nM) failed to normalize distance from wall, grooming and ambulation (Fig. 2A–C) but partially normalized center area crossing (Fig. 2J, L). In contrast, DIPMA-AP (500 nM) fully restored distance from wall (Fig. 2A), grooming time (Fig. 2B), ambulation time (Fig. 2C) and center crossing (Fig. 2L, L) in SNI mice to levels observed in sham mice. Neither AP nor DIPMA-AP affected track length, ambulation velocity or locomotor activity (Fig. 2D–F). DIPMA-Ø did not affect any measured parameter.

These results show that encapsulation into pH-responsive DIPMA nanoparticles enhances the efficacy and duration of effect of AP for reversal of multiple measures of evoked and non-evoked nociception in a preclinical model of chronic neuropathic pain. Since the analgesic properties of DIPMA-AP waned after 5 h, we sought to generate and characterize nanostars as a sustained delivery vehicle for AP.

3.2. Synthesis and characterization of nanostars

Nanostars were synthesized by an arm-first methodology (Fig. 3A). Initially, a macromolecular chain transfer agent (BSPA-POEGA, incorporating a polyacrylate backbone with pendent oligo(ethylene glycol) side chains) was synthesized by polymerizing

Author Manuscript Author Manuscript Author Manuscript Author Manuscript

oligo(ethylene glycol) methyl ether acrylate ($OEGA_{480}$) in the presence of 3-(benzyl sulfanyl thiocarbonyl sulfanyl)-propanoic acid (BSPA) in toluene. The resulting POEGA-BSPA, which includes a non-reactive benzyl group at one chain end and a reactive trithiocarbonate group at the other, was purified by precipitation into cold petroleum ether and drying *in vacuo*. Characterization by GPC (M_n 8600 g/mol, $Đ$ 1.24) and ^{1}H NMR demonstrated suitable molecular weight and functional groups for use in the subsequent synthetic steps (Fig. S2).

To form nanostars, purified BSPA-POEGA was chain extended with one of three distinct functional co-monomers, VBA, Benzo or PFPA, in the presence of *N,N′*-methylenebis(acrylamide) (MBAA) cross-linker (Fig. 3A). The nanostars (each denoted by the functional monomer) were purified by fractional precipitation into 2% (v/v) chloroform in diethyl ether. The molecular weights, molecular weight distributions and shape and uniformity of the nanostars were determined by GPC (Fig. 3B, Fig. S2), ^{1}H NMR (Fig. S2), DLS (Fig. 3B) and TEM (Fig. 3C). Each nanostar exhibited unimodal molecular weight distribution with narrow dispersity and quantitative removal of BSP0A-POEGA arm precursor, with the measured number average molecular weight of 61.9 K–100.9 K. Number-average hydrodynamic diameters determined by DLS were 10.8–16.2 nm, and ζ-potential was close to neutrality (< −5 mV) for each material in PBS. TEM revealed nanostars to be uniformly spherical and well dispersed, although nanostar-VBA images revealed some aggregated material.

3.3. Nanostars demonstrate slow and sustained release of Cy5-NH_2 cargo

To examine the release kinetics, PFPA, VBA and Benzo nanostars were fluorescently labelled with Cy5-NH_2 in the presence of triethylamine (TEA) as base (Fig. S3). Cy5 nanostars were purified by preparative size exclusion chromatography. Successful Cy5 conjugation and removal of residual Cy5 was confirmed by GPC using both RI and UV-VIS detection (λ = 646) (Fig. S3). Narrow molecular weight distribution was preserved throughout this procedure. Measured molecular weights were comparable to those determined for the non-labelled materials, notwithstanding a small decrease in apparent molecular weight for the Benzo nanostar (Fig. 3B). Release kinetics were determined by spectrophotometry at pH 7.4, 6.0 and 5.0. VBA-Cy5 and Benzo-Cy5 released most Cy5 cargo within 10 h, with continued release for at least 24 h (Fig. S4A, B). PFPA-Cy5 released minimal amounts of cargo for up to 48 h (Fig. S4C). The release rate was VBA > Benzo > PFPA. The kinetics of Cy5 release from VBA or Benzo nanostars was similar at pH 7.4, 6.0 and 5.0.

3.4. Nanostars can be conjugated with amine-functionalized AP

AP was alkylated to facilitate functionalization with a PEG2-amine (AP-NH_2) for conjugation to nanostars. AP-NH_2 inhibited SP-evoked Ca^{2+} signaling in HEK293T cells expressing hNK_1R with similar potency and efficacy to AP, and is thus fully functional (Fig. S5). AP-conjugated nanostars, VBA-AP, Benzo-AP and PFPA-AP, were prepared by reacting AP-NH_2 with VBA, Benzo and PFPA, respectively, in the presence of a suitable base (TEA) (Fig. S6). Conjugation of the AP-NH_2 to the nanostar was followed by ^{19}F NMR, with the ^{19}F resonance arising from the 2 × (CF_3) groups of the AP moiety

Author Manuscript Author Manuscript Author Manuscript Author Manuscript

at $\delta = -61.21$ ppm undergoing a well resolved shift of ~ −0.1 ppm upon conjugation, accompanied by significant broadening due to the tethering of the AP-NH_2 to the high molecular weight nanostar. Conjugation reactions were continued over several days until no further incorporation of the AP-NH_2 into the nanostar was observed. AP-conjugated nanostars were purified by preparative size exclusion chromatography using Bio-Beads with THF as the mobile phase. GPC analysis of purified nanostars revealed a slight shift to higher molecular weight upon conjugation, with preservation of unimodal distribution and narrow MWD (Fig. S6). ^{1}H NMR spectroscopic analysis of purified nanostars revealed peaks corresponding to the incorporated aprepitant at 4.9–5.0 ppm (Fig. S7A–C). ^{19}F NMR spectra of the purified AP-conjugated nanostars were recorded in the presence of an internal standard (trifluoroethanol, 0.63 mM), enabling determination of the loaded drug concentration. Physicochemical properties and loading of AP-NH_2 into nanostars are shown in Fig. 3B. TEM revealed the expected nanostar morphology (Fig. S8).

3.5. Nanostars demonstrate slow and sustained release of AP-NH_2 cargo

Time-dependent release of AP-NH_2 from VBA-AP and Benzo-AP was examined at pH 7.4, using HPLC to quantify free AP-NH_2. VBA-AP and Benzo-AP released AP-NH_2 at a similar rate (Fig. S4D–F). Release was more rapid over 10 h and was sustained for at least 24 h. AP-NH_2 release from PFPA-AP nanostars could not be quantified because AP-NH_2 levels were below the sensitivity of detection by HPLC.

3.6. Nanostars are not toxic to HEK293Tcells

To assess potential cytotoxic effects of nanostars, HEK293Tcells were incubated with VBA-Ø, Benzo-Ø and PFPA-Ø (1–100 μg/mL) for 2, 6 and 24 h. Cells were incubated with Triton X-100 as a positive control. Plasma membrane integrity (propidium iodide assay), redox and metabolic activity (Alamar Blue assay) and mitochondrial activity (thiazolyl blue tetrazolium bromide, MTT assay) were assessed. VBA-Ø, Benzo-Ø and PFPA-Ø showed no detectable effects on plasma membrane integrity, redox activity or mitochondrial activity for any tested concentration and studied time point (Fig. S9). Thus, nanostars do not have toxic actions in HEK293Tcells under these conditions.

3.7. Nanostars rapidly traffic to endosomes

The uptake of PFPA-Cy5 nanostars into HEK293Tcells was examined by immunofluorescence and confocal microscopy. Due to the negligible release of Cy5 from the PFPA linker (Fig. S4C), Cy5 fluorescence is likely to denote localization of nanostar material during the period of assay (30–120 min). HEK293Twere incubated with PFPA-Cy5 nanostars for 30, 60 or 120 min, washed and fixed. Early and late endosomes were detected by immunofluorescence staining for early endosomal antigen 1 and Rab7a, respectively. At 30 and 60 min, PFPA-Cy5 nanostars were detected in early endosomes, where colocalization was verified by measurement of the Manders' overlap coefficient (>0.6) (Fig. 4A and B). After 120 min colocalization with early endosomes declined (Manders' overlap coefficient <0.2). PFPA-Cy5 nanostars were most prominently colocalized with late endosomes after 60 min (Manders' overlap coefficient 0.59) and still detected in late endosomes after 120 min (Manders' overlap coefficient 0.45) (Fig. 4C and D). Thus, nanostars internalize into early endosomes and then late endosomes of HEK293Tcells.

Author Manuscript Author Manuscript Author Manuscript Author Manuscript

3.8. Nanostars antagonize endosomal and plasma membrane signaling of the NK_1R in HEK293Tcells

Once activated by SP, the NK_1R couples to heterotrimeric G proteins at the plasma membrane and recruits βARRs, which translocate from the cytosol to the plasma membrane. βARRs couple the NK_1R to clathrin and adaptor protein-2, which mediate endocytosis. SP/NK_1R continues to signal from endosomes of spinal neurons to regulate excitation and pain transmission in the spinal cord [11]. By antagonizing endosomal SP/NK_1R signaling, DIPMA-AP inhibits pain transmission in the spinal cord [18]. We examined whether nanostar-AP similarly inhibits SP-evoked activation of the NK_1R at the plasma membrane and in endosomes. EbBRET was used to study the activation of Gα and recruitment of βARR2 to the plasma membrane and early endosomes of HEK293T cells. SP-dependent activation of $G\alpha_i$ and $G\alpha_q$ was assessed using an EbBRET assay that detects recruitment of mini (m) $G\alpha_{si}$ and $mG\alpha_{sq}$ coupled to Renilla (R)luc8 to the plasma membrane marker CAAX coupled to RGFP or the early endosome marker Rab5a coupled to tandem (td)RGFP. Translocation of mGα to receptors located at the plasma membrane or in endosomes reflects the activation of full length Gα at these locations [30,31]. Recruitment of βARR2 was assessed by measuring EbBRET between Rluc2-βARR2 and RGFP-CAAX or tdRGFP-Rab5a [32].

HEK293T cells expressing hNK_1R and EbBRET sensors were incubated with vehicle (control), VBA-AP, Benzo-AP, PFPA-AP (500 or 1000 nM AP), VBA-Ø, Benzo-Ø or PFPA-Ø for 4 h and were then challenged with SP (10 nM). EbBRET was measured for 1400 s. In vehicle-treated cells, SP stimulated an increase in EbBRET between Rluc8-$mG\alpha_{si}$, Rluc8-$mG\alpha_{sq}$ and Rluc2-βARR2 with RGFP-CAAX (Fig. S10A, D, G) and tdRGFP-Rab5a (Fig. 5A, D, G). VBA-AP (500, 1000 nM) prevented SP-induced recruitment of Rluc8-$mG\alpha_{si}$, Rluc8-$mG\alpha_{sq}$ and Rluc2-βARR2 to RGFP-CAAX (Fig. S10A–I) and tdRGFP-Rab5a (Fig. 5A–I). Benzo-AP (500 nM) inhibited recruitment of Rluc8-$mG\alpha_{si}$ to RGFP-CAAX and tdRGFP-Rab5a, but did not affect recruitment of Rluc8-$mG\alpha_{sq}$ or Rluc2-βARR2. At a higher concentration (1000 nM), Benzo-AP inhibited recruitment of Rluc8-$mG\alpha_{si}$, Rluc8-$mG\alpha_{sq}$ and Rluc2-βARR2 to RGFP-CAAX, but did not inhibit recruitment of Rluc8-$mG\alpha_{sq}$ and Rluc2-βARR2 to tdRGFP-Rab5a. PFPA-AP, VBA-Ø, Benzo-Ø or PFPA-Ø did not inhibit SP-stimulated recruitment of Rluc8-$mG\alpha_{si}$, Rluc8-$mG\alpha_{sq}$ and Rluc2-βARR2 to RGFP-CAAX or tdRGFP-Rab5a (Fig. S11). Thus, when encapsulated into VBA or Benzo nanostars, AP can inhibit SP-evoked activation of G proteins and βARRs at the plasma membrane and in endosomes. The activation of $G\alpha_i$ is more susceptible to inhibition than the activation of $G\alpha_q$ or βARR2. Effective antagonism requires the release of AP from nanostars because PFPA-AP, which does not release AP, had no effect.

3.9. Nanostars accumulate in intracellular membranes of spinal neurons

To investigate the biodistribution of nanostars, Cy5-PFPA nanostars were administered to mice by intrathecal injection. The potential redistribution for nanostar Cy5 fluorescence away from the injection site was evaluated by non-invasive whole body near-infrared imaging. Within 1 min of injection, Cy5 was intensely concentrated at the site of injection (Fig. 6A and B). The signal was retained within the region of the spinal cord for at least 8 h, with minimal reduction in signal intensity between 2 and 8 h post-injection. To

Author Manuscript Author Manuscript Author Manuscript Author Manuscript

examine uptake of nanostars into the spinal cord, tissues were collected from mice 4 h after intrathecal injection of PFPA-Cy5 nanostars. Spinal cord sections were processed to localize markers of neurons (anti-Hu), glial cells (anti-Cd11b) and astrocytes (anti-GFAP) by immunofluorescence and confocal microscopy. Representative images of spinal cord sections (L4/L5) demonstrated that the PFPA-Cy5 remained in the ipsilateral region (Fig. 6B, D, E) and predominantly accumulated in a perinuclear region of spinal neurons identified by the pan-neuronal marker Hu, and showed a punctate distribution consistent with endosomal accumulation (Fig. 6B). In contrast, minimal Cy5 fluorescence distribution was observed in GFAP-positive astrocytes, or Cd11b-positive microglial cells (Fig. 6E).

3.10. VBA-AP and Benzo-AP nanostars provide sustained relief from neuropathic pain

To assess whether nanostar incorporation enhanced and extended the therapeutic efficacy of AP, we compared the effects of VBA-AP, Benzo-AP and free AP on mechanical allodynia, cold allodynia and non-evoked nociceptive behavior in mice with neuropathic pain.

Mechanical allodynia.—VBA-AP, Benzo-AP, PFPA-AP, an equivalent dose of free AP or AP-NH_2 (1000 nM AP) or VBA-Ø, Benzo-Ø or PFPA-Ø was injected intrathecally, and mechanical allodynia was measured. These treatments had no effect on VFF withdrawal responses of the contralateral paw (Fig. 7A). Free AP caused a partial reversal of VFF withdrawal responses of the ipsilateral paw at 2 h (Fig. 7B and C). AP and AP-NH_2 suppressed mechanical allodynia to the same degree (Fig. 7D). The magnitude and duration of the anti-nociceptive effects of VBA-AP and Benzo-AP significantly exceeded that of free AP and were apparent from 2 to at least 10 h (Fig. 7B and C). The VFF response at 6 h was 15.8 ± 6% of baseline values after free AP but 72 ± 9% basal after VBA-AP and 64 ± 7.8% basal after Benzo-AP ($P < 0.0001$). PFPA-AP, which did not release AP, had no effects on mechanical allodynia (Fig. 7B and C). VBA-Ø, Benzo-Ø or PFPA-Ø did not affect mechanical allodynia.

Cold allodynia.—Whereas free AP had a small but insignificant effect on cold allodynia at 2 h, VBA-AP and Benzo-AP reversed cold allodynia from 2 to at least 10 h (Fig. 7E and F). VBA-Ø and Benzo-Ø did not affect cold allodynia.

Non-evoked nociceptive behavior.—Non-evoked nociceptive behavior was measured for 30 min 90 min after intrathecal drug administration. SNI mice exhibited significant decreases in average distance from the wall (Fig. 8A), grooming time (Fig. 8B) and ambulation time (Fig. 8C) compared to sham controls, whereas track length (Fig. 8D), average velocity (Fig. 8E) and locomotor activity (Fig. 8F) were unaffected. Central area crossing was also significantly diminished in SNI mice (Fig. 8G, H, I, L). VBA-AP and Benzo-AP (1000 nM) fully normalized distance from wall (Fig. 8A), grooming time (Fig. 8B), ambulation time (Fig. 8C) and center crossing (Fig. 8J–L) in SNI mice to levels observed in sham mice. VBA-Ø and Benzo-Ø did not affect any measured parameter.

3.11. VBA-AP and Benzo-AP nanostars provide sustained relief from inflammatory pain

To confirm the superior efficacy and duration of analgesia of nanostar AP in a second preclinical model of pain, the effects of VBA-AP, Benzo-AP and free AP on mechanical

Author Manuscript Author Manuscript Author Manuscript Author Manuscript

allodynia, in mice with inflammatory pain was examined. VBA-AP, Benzo-AP or free AP (1000 nmol) was administered by intrathecal injection 48 h after intraplanar injection of CFA. Whereas free AP had a minor inhibitory effect on mechanical allodynia at 2 h, VBA-AP and Benzo-AP inhibited mechanical allodynia to a similar degree for 10 h, although the effects were lost after 24 h (Fig. 9A and B).

4. Discussion

Although opioids that activate the μ-opioid receptor are widely prescribed for the treatment of acute pain, their efficacy wanes with continued use and they can evoke paradoxical hyperalgesia. The over-prescription of opioids, coupled to their addictive properties and severe on-target side effects of respiratory depression, sedation and constipation, underlie the opioid crisis; drug overdose, chiefly opioids, is a leading cause of death world-wide that has worsened during the COVID-19 pandemic. The realization that certain non-μ-opioid GPCRs continue to signal from endosomes to control neuronal activity and pain transmission [11–15], and the propensity of nanoparticles to accumulate in endosomes [12,17,18], raises the possibility of harnessing endosomal acidity to trigger nanoparticle disassembly and GPCR antagonist release for the treatment of pain. Our results show that AP encapsulated into soft polymer DIPMA nanoparticles effectively reverses evoked and non-evoked nociception in a preclinical mouse model of chronic neuropathic pain. The assessment of non-evoked nociception obviates observational and operator bias that plagues studies of evoked nociception in rodents. The demonstration that gabapentin, which is clinically approved for the treatment of neuropathic pain, reverted all measures of non-evoked nociception similar to DIPMA-AP, validates the usefulness of measures of spontaneous nociception. We hypothesize that nanoparticle encapsulation enhances efficacy by delivery of AP to the key therapeutic target, the NK_1R in endosomes of spinal neurons, and that the limited therapeutic efficacy of free AP relates to its inability to effectively engage with conformations of the activated NK_1R within multiprotein signalosomes in the acidified endosomal environment [16]. An advantage of soft polymer DIPMA nanoparticles is that they permit encapsulation of unmodified drugs. Limitations include their inherent instability, which is exacerbated by dilution that exceeds the critical micellar concentration, and immediate disassembly and short-term cargo release at $pH < 6$ [18]. Although administration to confined volumes such as the intrathecal space avoids dilution-related instability, DIPMA nanoparticles are unsuitable for systemic administration because dilution alone would evoke disassembly. Moreover, immediate disassembly in acidic compartments would be expected to limit the duration of therapeutic efficacy of analgesic cargos.

To surmount these limitations, we synthesized nanostars with three distinct reactive groups for conjugation to cargo by RAFT polymerization using an arm first methodology. Nanostars incorporating pentafluorophenyl (PFPA), benzaldehyde (VBA) and benzophenone (Benzo) groups were prepared (Fig. 3). Upon exposure to amine functionalized cargo molecules, these incorporated groups would be expected to form amide, aldimine and ketimine linked nanostar-cargos, respectively, and thus exhibit differential hydrolytic stability. Each nanostar synthesized in this study incorporated a hydrophilic mPEG brush corona, which has the dual function of maintaining drug solubility in an aqueous environment and evading clearance. Nanostars were small (10–20 nm), uniformly spherical and largely unaggregated, and with

Author Manuscript Author Manuscript Author Manuscript Author Manuscript

a small negative charge (−5 mV), properties that would be expected to enhance cellular uptake. The molecular weight, hydrodynamic diameter and ζ-potential of the synthesized nanostars are consistent with previous results on PEGylated nanostars [39–41].

To examine the capacity of the nanostars to undergo differential cargo release depending on the specific amine reactive moiety, the three nanostars (PFPA, VBA, Benzo) were conjugated to the amine functional dye, Cy5-NH_2. The resulting nanostar-dye conjugates enabled examination of the release kinetics from each nanostar by spectrophotometry. Release studies under sink conditions allowed determination of the kinetics of cargo release and the pH-responsivity of the different linkers. In contrast to DIPMA-AP nanoparticles that immediately disassemble at pH < 6.0 [18], VBA and Benzo nanostars continued to release Cy5 cargo for at least 24 h and cargo release was not accelerated under acidic conditions. As anticipated, the aldimine-linked conjugate (VBA-Cy5) released the dye more readily than the ketimine-linked conjugate (Benzo-Cy5). The amide-linked variant, PFPA-Cy5, exhibited minimal dye release over the time course studied. The stable amide-bond linked PFPA-Cy5 also served as a convenient fluorescently-labelled reporter to investigate the trafficking and biodistribution of nanostars.

We synthesized amine functionalized AP for conjugation to nanostars. Structural studies indicate that the triazolinone substituent of AP is oriented toward the extracellular space and creates an extended binding pocket by promoting additional hydrogen bonding with E193 and W184 in the extracellular region of the NK_1R [42]. Modifications to the triazolinone ring are well tolerated and have minimal impact on affinity of AP [43,44]. To enable functionalization of the nanostars with AP, we modified the triazolinone substituent with a 3-carbon linker and PEG2-amine for conjugation to the arm of the nanostar. AP-NH_2 and AP showed similar potency and efficacy for antagonism of SP-evoked Ca^{2+} signaling in HEK293Tcells and reversal of neuropathic pain in mice. Thus, AP-NH_2 retains full activity and was suitable for comparisons to the parent compound AP in subsequent experiments. We observed similar kinetics of AP-NH_2 release from VBA-AP and Benzo-AP nanostars. Since the rate of cargo release likely depends on the nature of the amine reactive moieties, we had expected similar release kinetics of Cy5-NH_2 and AP-NH_2. The observed differences in the relative kinetics of release of AP-NH_2 and Cy5-NH_2 between VBA and Benzo nanostars is thus likely related to the nature of the cargo. A limitation of these *in vitro* measurements of cargo release is that they do not replicate the complex intracellular environment of spinal neurons, where release could be affected by multiple factors. However, these results are in line with the superior ability of VBA-AP and Benzo-AP to suppress NK_1R endosomal signaling in HEK293T cell lines and inhibit nociception in mice when compared to PFPA-AP, which was inactive.

Uptake studies in HEK293Tcells found that PFPA-Cy5 nanostars accumulate in early and late endosomes; endosomes are thus a likely site of cargo release. Further studies will be required to ascertain the ultimate fate of the inert nanostar components in HEK293T cells and in the spinal cord after intrathecal injection. By using EbBRET to assess the recruitment of mGα proteins and βARR2 to the plasma membrane and early endosomes, it was possible to assess the effects of nanostar-AP on NK_1R signaling in subcellular compartments of HEK293T cells. SP stimulated the expected sustained recruitment of $mG\alpha_i$ and $mG\alpha_q$ and

Author Manuscript Author Manuscript Author Manuscript Author Manuscript

βARR2 to the plasma membrane and early endosomes of HEK293T cells. Preincubation of cells with VBA-AP, to allow for nanostar uptake and AP-NH_2 release, prevented SP-evoked activation of $mG\alpha_i$, $mG\alpha_q$ and βARR2 at the plasma membrane and in endosomes. Since late endosomes were the site of nanostar accumulation and likely disassembly, we speculate that freed AP-NH_2 diffuses and thereby antagonizes the NK_1R in early endosomes and at the plasma membrane; the dynamic nature of the tubulovesicular endosomal network likely facilitates the spread of released cargo [45]. Benzo-AP antagonized NK_1R signaling only at higher concentrations, which is consistent with the slower kinetics of Cy5 cargo release. PFPA-AP did not affect NK_1R signaling at any tested concentration, in line with its inability to release cargo; empty nanostars were also inactive. We conclude that release of AP-NH_2 cargo is necessary for antagonism of SP-stimulated NK_1R signaling in HEK293T cells.

When injected intrathecally to mice, PFPA-Cy5 was retained at the site of injection for at least 8 h and was preferentially endocytosed by neurons throughout the spinal cord. Further studies are required to understand the reasons for preferential uptake by neurons rather than glial cells or astrocytes, although the extensive vesicular transport within neurons that is related to synaptic transmission might predispose uptake of nanomaterials. The mechanisms of nanostar uptake into neurons and the possibility of uptake into subtypes of neurons remain to be investigated. We speculate that nanostars enter cells by clathrin- and dynamin-mediated endocytosis since these mechanisms mediate entry of DIPMA nanoparticles to HEK293Tcells [18].

Intrathecal injection of VNA-AP and Benzo-AP provided far more efficacious reversal of evoked and non-evoked nociception in preclinical mouse models of neuropathic and inflammatory pain than free AP, which had minor and transient analgesic effect. Despite differences in the kinetics of Cy5 cargo release *in vitro* and some discrepancy in antagonism of NK_1R signaling in HEK293T cells, the analgesic properties of the same dose of VBA-AP and Benzo-AP were identical. Full dose-response studies will be required to compare fully the analgesic properties of these nanomaterials. However, stable PFPA-AP and empty nanoparticles did not affect nociception, confirming the requirement of AP-NH_2 release for analgesia. VBA-AP and Benzo-AP provided analgesia for at least 10 h, twice the duration of the same dose of DIPMA-AP. The prolonged analgesic efficacy of nanostar-AP is consistent with the slow kinetics of disassembly and cargo release *in vitro*. Sustained and efficacious analgesia of nanostar-AP was attained despite the pH-independence of disassembly *in vitro*. Thus, pH-dependent cargo release in endosomes is not required for analgesia, although it could further enhance pain relief, as is the case for DIPMA-AP nanoparticles. Future pharmacodynamic analyses will be necessary to relate the kinetics of drug release to analgesia.

A limitation of this study is that we did not study the possible toxic effects of nanostars in mice. However, nanostars did not affect several measures of cytotoxicity in HEK293Tcells, and AP-nanostars did not affect withdrawal responses of the contralateral paw, suggesting no effects on normal motor coordination. Moreover, empty nanostars did not affect withdrawal responses and had no effects on multiple measures of normal behavior, which argue against any neurotoxic actions under the conditions of these experiments. DIPMA nanoparticles also do not have detectable toxic actions in HEK293Tcells or after intrathecal injection to

Author Manuscript Author Manuscript Author Manuscript Author Manuscript

mice [18]. Potential long-term neurotoxicity of nanostars will be assessed in future studies. Another limitation is that we only assessed the efficacy of intrathecal administration of nanostars, which had the advantage of drug deliver to targets in spinal neurons. Whether systemically administered nanostars can be used to target peripheral GPCRs for the treatment of chronic pain remains to be studied.

The present investigation extends the use of nanostars beyond the delivery of chemotherapeutics, antioxidants and imaging agents to cancer cells and tumors [20,23–25] to the delivery of GPCR ligands to endosomes of neurons for the treatment of chronic pain. In addition to analgesia, nanoparticle encapsulation and consequent endosomal delivery may enhance other therapeutic actions of AP, including its actions on chemotherapy-induced nausea and vomiting and its antitumor actions. AP has antiproliferative and antimitogenic effects on a variety of cancers (reviewed in Ref. [46]), which may be enhanced by nanoparticle encapsulation. Thus, nanoparticle-AP might ameliorate cancer progression as well as associated pain, while reducing the side effects (nausea and vomiting of standard chemotherapeutic agents). Further studies are required to investigate these possibilities. Although rapid-release DIPMA nanoparticles enhance the therapeutic actions of AP, sustained-release nanostars provide additional benefit. Even longer lasting nanomedicines, such as hydrophobic ion pairing nano-formulations that allow cargo release over weeks [47], may provide even more long-lasting analgesia. Biodegradable nanomaterials have been proposed to be an effective strategy for slow, localized drug release to provide sustained relief of post-surgical pain [48]. Nanostars are an attractive platform for advanced drug delivery due to their modular nature and the potential to conjugate multiple drugs through various linkers, attach targeting moieties and readily adjust the hydrodynamic diameter. Further refinements that could improve the therapeutic benefits of analgesic nanostars could include incorporation of antagonists of multiple GPCRs that signal from endosomes, which could overcome the inherent redundancy of the pathways of pain transmission, and the specific targeting of nanoparticles to neurons that sense and transmit pain. Encapsulation of antagonists of SP, CGRP and glutamate receptors would be expected to strongly inhibit pain transmission in the dorsal horn of the spinal cord, which depends on endosomal signaling of these GPCRs [3,11,15]. Conjugation of an agonists of the ∂-opioid receptor to a liposome shell of mesoporous silica nanoparticles enhances targeting and improves analgesia, which illustrates the utility of nociceptor-targeted analgesics [12].

5. Conclusion

Nanostars that slowly release an antagonist of the NK_1R within endosomes abrogate endosomal signaling and provide sustained antinociception in preclinical models of neuropathic and inflammatory pain. The enhanced efficacy and duration of analgesia of nanostar-aprepitant depends on persistent release of antagonist within endosomes of spinal neurons. The nanostar platform is amenable to co-loading multiple antagonists and targeting to neurons that sense and transmit pain, which would be expected to provide long-lasting and opioid-free analgesia.

Author Manuscript Author Manuscript Author Manuscript Author Manuscript

Supplementary Material

Refer to Web version on PubMed Central for supplementary material.

Acknowledgements

Supported by grants from: National Institutes of Health (NS102722, DE026806, DK118971, DE029951, NWB, BLS) and Department of Defense (W81XWH1810431, W81XWH-22-1-0239, EXpansion Award, NWB, BLS). We thank Eric Le for help with Ca^{2+} mobilization assays and Joseph B. Guttenplan and Shavonne Teng for help with the HPLC analysis of AP-NH_2.

Data availability

The raw data required to reproduce these findings are available upon request. The scripts used for the image analyses are available upon request. The processed data required to reproduce these findings are available upon request.

References

[1]. Basbaum AI, Bautista DM, Scherrer G, Julius D, Cellular and molecular mechanisms of pain, Cell 139 (2) (2009) 267–284. [PubMed: 19837031]

[2]. Shipton EA, Shipton EE, Shipton AJ, A review of the opioid epidemic: what do we do about it? Pain Ther 7 (1) (2018) 23–36. [PubMed: 29623667]

[3]. Geppetti P, Veldhuis NA, Lieu T, Bunnett NW, G protein-coupled receptors: dynamic machines for signaling pain and itch, Neuron 88 (4) (2015) 635–649. [PubMed: 26590341]

[4]. Veldhuis NA, Poole DP, Grace M, McIntyre P, Bunnett NW, The G protein-coupled receptor-transient receptor potential channel axis: molecular insights for targeting disorders of sensation and inflammation, Pharmacol. Rev 67 (1) (2015) 36–73. [PubMed: 25361914]

[5]. Peterson YK, Luttrell LM, The diverse roles of arrestin scaffolds in G protein-coupled receptor signaling, Pharmacol. Rev 69 (3) (2017) 256–297. [PubMed: 28626043]

[6]. Calebiro D, Nikolaev VO, Gagliani MC, de Filippis T, Dees C, Tacchetti C, Persani L, Lohse MJ, Persistent cAMP-signals triggered by internalized G-protein-coupled receptors, PLoS Biol 7 (8) (2009), e1000172. [PubMed: 19688034]

[7]. DeFea KA, Vaughn ZD, O'Bryan EM, Nishijima D, Dery O, Bunnett NW, The proliferative and antiapoptotic effects of substance P are facilitated by formation of a beta -arrestin-dependent scaffolding complex, Proc. Natl. Acad. Sci. U. S. A 97 (20) (2000) 11086–11091. [PubMed: 10995467]

[8]. Irannejad R, Tomshine JC, Tomshine JR, Chevalier M, Mahoney JP, Steyaert J, Rasmussen SG, Sunahara RK, El-Samad H, Huang B, von Zastrow M, Conformational biosensors reveal GPCR signalling from endosomes, Nature 495 (7442) (2013) 534–538. [PubMed: 23515162]

[9]. Nguyen AH, Lefkowitz RJ, Signaling at the endosome: cryo-EM structure of a GPCR-G protein-beta-arrestin megacomplex, FEBS J 288 (8) (2021) 2562–2569. [PubMed: 33605032]

[10]. Nguyen AH, Thomsen ARB, Cahill TJ 3rd, Huang R, Huang LY, Marcink T, Clarke OB, Heissel S, Masoudi A, Ben-Hail D, Samaan F, Dandey VP, Tan YZ, Hong C, Mahoney JP, Triest S, Little J.t., Chen X, Sunahara R, Steyaert J, Molina H, Yu Z, des Georges A, Lefkowitz RJ, Structure of an endosomal signaling GPCR-G protein-beta-arrestin megacomplex, Nat. Struct. Mol. Biol 26 (12) (2019) 1123–1131. [PubMed: 31740855]

[11]. Jensen DD, Lieu T, Halls ML, Veldhuis NA, Imlach WL, Mai QN, Poole DP, Quach T, Aurelio L, Conner J, Herenbrink CK, Barlow N, Simpson JS, Scanlon MJ, Graham B, McCluskey A, Robinson PJ, Escriou V, Nassini R, Materazzi S, Geppetti P, Hicks GA, Christie MJ, Porter CJH, Canals M, Bunnett NW, Neurokinin 1 receptor signaling in endosomes mediates sustained nociception and is a viable therapeutic target for prolonged pain relief, Sci. Transl. Med 9 (392) (2017).

Author Manuscript Author Manuscript Author Manuscript Author Manuscript

[12]. Jimenez-Vargas NN, Gong J, Wisdom MJ, Jensen DD, Latorre R, Hegron A, Teng S, DiCello JJ, Rajasekhar P, Veldhuis NA, Carbone SE, Yu Y, Lopez-Lopez C, Jaramillo-Polanco J, Canals M, Reed DE, Lomax AE, Schmidt BL, Leong KW, Vanner SJ, Halls ML, Bunnett NW, Poole DP, Endosomal signaling of delta opioid receptors is an endogenous mechanism and therapeutic target for relief from inflammatory pain, Proc. Natl. Acad. Sci. U. S. A 117 (26) (2020) 15281–15292. [PubMed: 32546520]

[13]. Jimenez-Vargas NN, Pattison LA, Zhao P, Lieu T, Latorre R, Jensen DD, Castro J, Aurelio L, Le GT, Flynn B, Herenbrink CK, Yeatman HR, Edgington-Mitchell L, Porter CJH, Halls ML, Canals M, Veldhuis NA, Poole DP, McLean P, Hicks GA, Scheff N, Chen E, Bhattacharya A, Schmidt BL, Brierley SM, Vanner SJ, Bunnett NW, Protease-activated receptor-2 in endosomes signals persistent pain of irritable bowel syndrome, Proc. Natl. Acad. Sci. U. S. A 115 (31) (2018) E7438–E7447. [PubMed: 30012612]

[14]. Mai QN, Shenoy P, Quach T, Retamal JS, Gondin AB, Yeatman HR, Aurelio L, Conner JW, Poole DP, Canals M, Nowell CJ, Graham B, Davis TP, Briddon SJ, Hill SJ, Porter CJH, Bunnett NW, Halls ML, Veldhuis NA, A lipid-anchored neurokinin 1 receptor antagonist prolongs pain relief by a three-pronged mechanism of action targeting the receptor at the plasma membrane and in endosomes, J. Biol. Chem 296 (2021), 100345. [PubMed: 33515548]

[15]. Yarwood RE, Imlach WL, Lieu T, Veldhuis NA, Jensen DD, Klein Herenbrink C, Aurelio L, Cai Z, Christie MJ, Poole DP, Porter CJH, McLean P, Hicks GA, Geppetti P, Halls ML, Canals M, Bunnett NW, Endosomal signaling of the receptor for calcitonin gene-related peptide mediates pain transmission, Proc. Natl. Acad. Sci. U. S. A 114 (46) (2017) 12309–12314. [PubMed: 29087309]

[16]. Thomsen ARB, Jensen DD, Hicks GA, Bunnett NW, Therapeutic targeting of endosomal G-protein-coupled receptors, Trends Pharmacol. Sci 39 (10) (2018) 879–891. [PubMed: 30180973]

[17]. Bhansali D, Teng SL, Lee CS, Schmidt BL, Bunnett NW, Leong KW, Nanotechnology for pain management: current and future therapeutic interventions, Nano Today 39 (2021), 101223. [PubMed: 34899962]

[18]. Ramirez-Garcia PD, Retamal JS, Shenoy P, Imlach W, Sykes M, Truong N, Constandil L, Pelissier T, Nowell CJ, Khor SY, Layani LM, Lumb C, Poole DP, Lieu T, Stewart GD, Mai QN, Jensen DD, Latorre R, Scheff NN, Schmidt BL, Quinn JF, Whittaker MR, Veldhuis NA, Davis TP, Bunnett NW, A pH-responsive nanoparticle targets the neurokinin 1 receptor in endosomes to prevent chronic pain, Nat. Nanotechnol 14 (12) (2019) 1150–1159. [PubMed: 31686009]

[19]. Hu J, Qiao R, Whittaker MR, Quinn JF, Davis TP, Synthesis of star polymers by RAFT polymerization as versatile nanoparticles for biomedical Applications, Aust. J. Chem 70 (11) (2017) 1161–1170.

[20]. Bayat N, McOrist N, Ariotti N, Lai M, Sia KC, Li Y, Grace JL, Quinn JF, Whittaker MR, Kavallaris M, Davis TP, Lock RB, Thiol-reactive star polymers functionalized with short ethoxy-containing moieties exhibit enhanced uptake in acute lymphoblastic leukemia cells, Int. J. Nanomed 14 (2019) 9795–9808.

[21]. Glass JJ, Li Y, De Rose R, Johnston AP, Czuba EI, Khor SY, Quinn JF, Whittaker MR, Davis TP, Kent SJ, Thiol-reactive star polymers display enhanced association with distinct human blood components, ACS Appl. Mater. Interfaces 9 (14) (2017) 12182–12194. [PubMed: 28338321]

[22]. Khor SY, Hu J, McLeod VM, Quinn JF, Williamson M, Porter CJ, Whittaker MR, Kaminskas LM, Davis TP, Molecular weight (hydrodynamic volume) dictates the systemic pharmacokinetics and tumour disposition of PolyPEG star polymers, Nanomedicine 11 (8) (2015) 2099–2108. [PubMed: 26343493]

[23]. Esser L, Lengkeek NA, Moffat BA, Vu MN, Greguric I, Quinn JF, Davis TP, Whittaker MR, A tunable one-pot three-component synthesis of an125I and Gd-labelled star polymer nanoparticle for hybrid imaging with MRI and nuclear medicine, Polym. Chem 9 (25) (2018) 3528–3535.

[24]. Goos J, Davydova M, Dilling TR, Cho A, Cornejo MA, Gupta A, Price WS, Puttick S, Whittaker MR, Quinn JF, Davis TP, Lewis JS, Design and preclinical evaluation of nanostars for the passive pretargeting of tumor tissue, Nucl. Med. Biol 84–85 (2020) 63–72.

[25]. Yu SH, Patra M, Ferrari S, Ramirez Garcia P, Veldhuis NA, Kaminskas LM, Graham B, Quinn JF, Whittaker MR, Gasser G, Davis TP, Linker chemistry dictates the delivery of a phototoxic

Author Manuscript Author Manuscript Author Manuscript Author Manuscript

organometallic rhenium(i) complex to human cervical cancer cells from core crosslinked star polymer nanoparticles, J. Mater. Chem. B 6 (47) (2018) 7805–7810. [PubMed: 32255026]

[26]. Kramer MS, Cutler N, Feighner J, Shrivastava R, Carman J, Sramek JJ, Reines SA, Liu G, Snavely D, Wyatt-Knowles E, Hale JJ, Mills SG, MacCoss M, Swain CJ, Harrison T, Hill RG, Hefti F, Scolnick EM, Cascieri MA, Chicchi GG, Sadowski S, Williams AR, Hewson L, Smith D, Carlson EJ, Hargreaves RJ, Rupniak NM, Distinct mechanism for antidepressant activity by blockade of central substance P receptors, Science 281 (5383) (1998) 1640–1645. [PubMed: 9733503]

[27]. Stenzel MH, Davis TP, Star polymer synthesis using trithiocarbonate functional ?-cyclodextrin cores (reversible addition-fragmentation chain-transfer polymerization), J. Polym. Sci. Polym. Chem 40 (24) (2002) 4498–4512.

[28]. Schindelin J, Arganda-Carreras I, Frise E, Kaynig V, Longair M, Pietzsch T, Preibisch S, Rueden C, Saalfeld S, Schmid B, Tinevez JY, White DJ, Hartenstein V, Eliceiri K, Tomancak P, Cardona A, Fiji: an open-source platform for biological-image analysis, Nat. Methods 9 (7) (2012) 676–682. [PubMed: 22743772]

[29]. Bolte S, Cordelieres FP, A guided tour into subcellular colocalization analysis in light microscopy, J. Microsc 224 (Pt 3) (2006) 213–232. [PubMed: 17210054]

[30]. Nehme R, Carpenter B, Singhal A, Strege A, Edwards PC, White CF, Du H, Grisshammer R, Tate CG, Mini-G proteins: novel tools for studying GPCRs in their active conformation, PLoS One 12 (4) (2017), e0175642. [PubMed: 28426733]

[31]. Wan Q, Okashah N, Inoue A, Nehme R, Carpenter B, Tate CG, Lambert NA, Mini G protein probes for active G protein-coupled receptors (GPCRs) in live cells, J. Biol. Chem 293 (19) (2018) 7466–7473. [PubMed: 29523687]

[32]. Namkung Y, Le Gouill C, Lukashova V, Kobayashi H, Hogue M, Khoury E, Song M, Bouvier M, Laporte SA, Monitoring G protein-coupled receptor and beta-arrestin trafficking in live cells using enhanced bystander BRET, Nat. Commun 7 (2016), 12178. [PubMed: 27397672]

[33]. Zimmermann M, Ethical guidelines for investigations of experimental pain in conscious animals, Pain 16 (2) (1983) 109–110. [PubMed: 6877845]

[34]. Cichon J, Sun L, Yang G, Spared nerve injury model of neuropathic pain in mice, Bio Protoc 8 (6) (2018), e2777.

[35]. Stein C, Millan MJ, Herz A, Unilateral inflammation of the hindpaw in rats as a model of prolonged noxious stimulation: alterations in behavior and nociceptive thresholds, Pharmacol. Biochem. Behav 31 (2) (1988) 445–451. [PubMed: 3244721]

[36]. Yoon C, Wook YY, Sik NH, Ho KS, Mo CJ, Behavioral signs of ongoing pain and cold allodynia in a rat model of neuropathic pain, Pain 59 (3) (1994) 369–376. [PubMed: 7708411]

[37]. Brodkin J, Frank D, Grippo R, Hausfater M, Gulinello M, Achterholt N, Gutzen C, Validation and implementation of a novel high-throughput behavioral phenotyping instrument for mice, J. Neurosci. Methods 224 (2014) 48–57. [PubMed: 24384067]

[38]. Castro J, Harrington AM, Lieu T, Garcia-Caraballo S, Maddern J, Schober G, O'Donnell T, Grundy L, Lumsden AL, Miller P, Ghetti A, Steinhoff MS, Poole DP, Dong X, Chang L, Bunnett NW, Brierley SM, Activation of pruritogenic TGR5, MrgprA3, and MrgprC11 on colon-innervating afferents induces visceral hypersensitivity, JCI Insight 4 (20) (2019).

[39]. Ferreira J, Syrett J, Whittaker M, Haddleton D, Davis TP, Boyer C, Optimizing the generation of narrow polydispersity 'arm-first' star polymers made using RAFT polymerization, Polym. Chem 2 (8) (2011) 1671–1677.

[40]. Liu J, Duong H, Whittaker MR, Davis TP, Boyer C, Synthesis of functional core, star polymers via RAFT polymerization for drug delivery applications, Macromol. Rapid Commun 33 (9) (2012) 760–766. [PubMed: 22495770]

[41]. Syrett JA, Haddleton DM, Whittaker MR, Davis TP, Boyer C, Functional, star polymeric molecular carriers, built from biodegradable microgel/nanogel cores, Chem. Commun 47 (5) (2011) 1449–1451.

[42]. Schoppe J, Ehrenmann J, Klenk C, Rucktooa P, Schutz M, Dore AS, Pluckthun A, Crystal structures of the human neurokinin 1 receptor in complex with clinically used antagonists, Nat. Commun 10 (1) (2019) 17. [PubMed: 30604743]

Author Manuscript Author Manuscript Author Manuscript Author Manuscript

[43]. Halik PK, Lipinski PFJ, Matalinska J, Kozminski P, Misicka A, Gniazdowska E, Radiochemical synthesis and evaluation of novel radioconjugates of neurokinin 1 receptor antagonist aprepitant dedicated for NK1R-positive tumors, Molecules 25 (16) (2020).

[44]. Harrison T, Owens AP, Williams BJ, Swain CJ, Williams A, Carlson EJ, Rycroft W, Tattersall FD, Cascieri MA, Chicchi GG, Sadowski S, Rupniak NM, Hargreaves RJ, An orally active, water-soluble neurokinin-1 receptor antagonist suitable for both intravenous and oral clinical administration, J. Med. Chem 44 (24) (2001) 4296–4299. [PubMed: 11708932]

[45]. Hopkins CR, Gibson A, Shipman M, Miller K, Movement of internalized ligand-receptor complexes along a continuous endosomal reticulum, Nature 346 (6282) (1990) 335–339. [PubMed: 2374607]

[46]. Munoz M, Covenas R, The neurokinin-1 receptor antagonist aprepitant: an intelligent bullet against cancer? Cancers 12 (9) (2020) 2682. [PubMed: 32962202]

[47]. Ashton S, Song YH, Nolan J, Cadogan E, Murray J, Odedra R, Foster J, Hall PA, Low S, Taylor P, Ellston R, Polanska UM, Wilson J, Howes C, Smith A, Goodwin RJ, Swales JG, Strittmatter N, Takats Z, Nilsson A, Andren P, Trueman D, Walker M, Reimer CL, Troiano G, Parsons D, De Witt D, Ashford M, Hrkach J, Zale S, Jewsbury PJ, Barry ST, Aurora kinase inhibitor nanoparticles target tumors with favorable therapeutic index in vivo, Sci. Transl. Med 8 (325) (2016), 325ra17.

[48]. Brigham NC, Ji RR, Becker ML, Degradable polymeric vehicles for postoperative pain management, Nat. Commun 12 (1) (2021) 1367.

Author Manuscript Author Manuscript Author Manuscript Author Manuscript

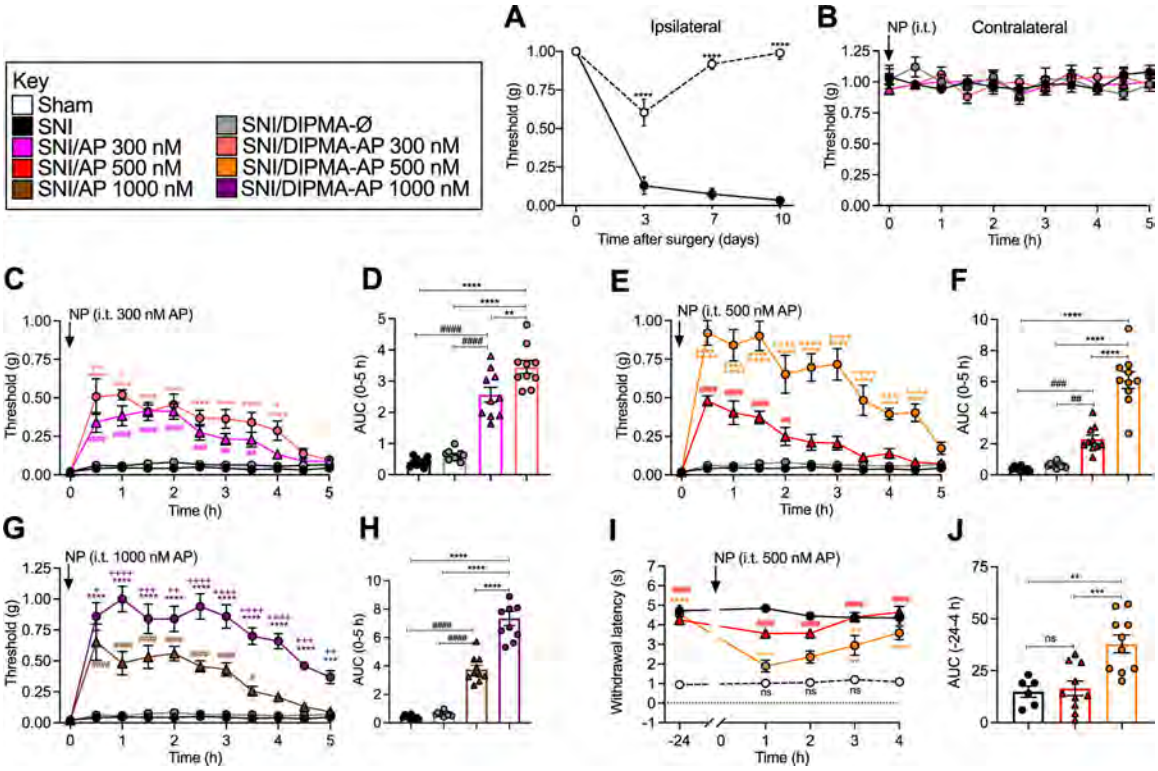

Fig. 1. DIPMA nanoparticles, mechanical and cold allodynia in neuropathic pain.

A. Time course of development of VFF withdrawal responses (mechanical allodynia) of ipsilateral paw in SNI and sham control mice. All subsequent studies were at 10 days post SNI surgery. **B.** Effects of DIPMA-AP, AP or DIPMA-Ø on VFF withdrawal responses of contralateral paw. **C–H.** Effects of DIPMA-AP, AP or DIPMA-Ø on VFF withdrawal responses of ipsilateral paw. **C, E, G** show time course and **D, F, H** show area under curve (AUC) of effects of 300, 500 or 1000 nM DIPMA-AP or free AP. **I, J.** Effects of DIPMA-AP, AP or DIPMA-Ø on acetone withdrawal responses (cold allodynia) of ipsilateral paw in SNI and sham mice. **I** shows time course and **J** shows of effects of 500 nM DIPMA-AP or AP. Mean ± SEM, N = 10 mice. *, +, #$P < 0.05$; **, ++, ##, $P < 0.01$; ***, +++, ###$P <$ 0.005; ****, ++++, ####$P < 0.001$. * DIPMA-AP to SNI, DIPMA-Ø and AP; + DIPMA-AP to AP; # AP to SNI. Two-way ANOVA (mechanical and cold allodynia), one-way ANOVA (AUC) with Tukey's multiple comparisons test.

Author Manuscript Author Manuscript Author Manuscript Author Manuscript

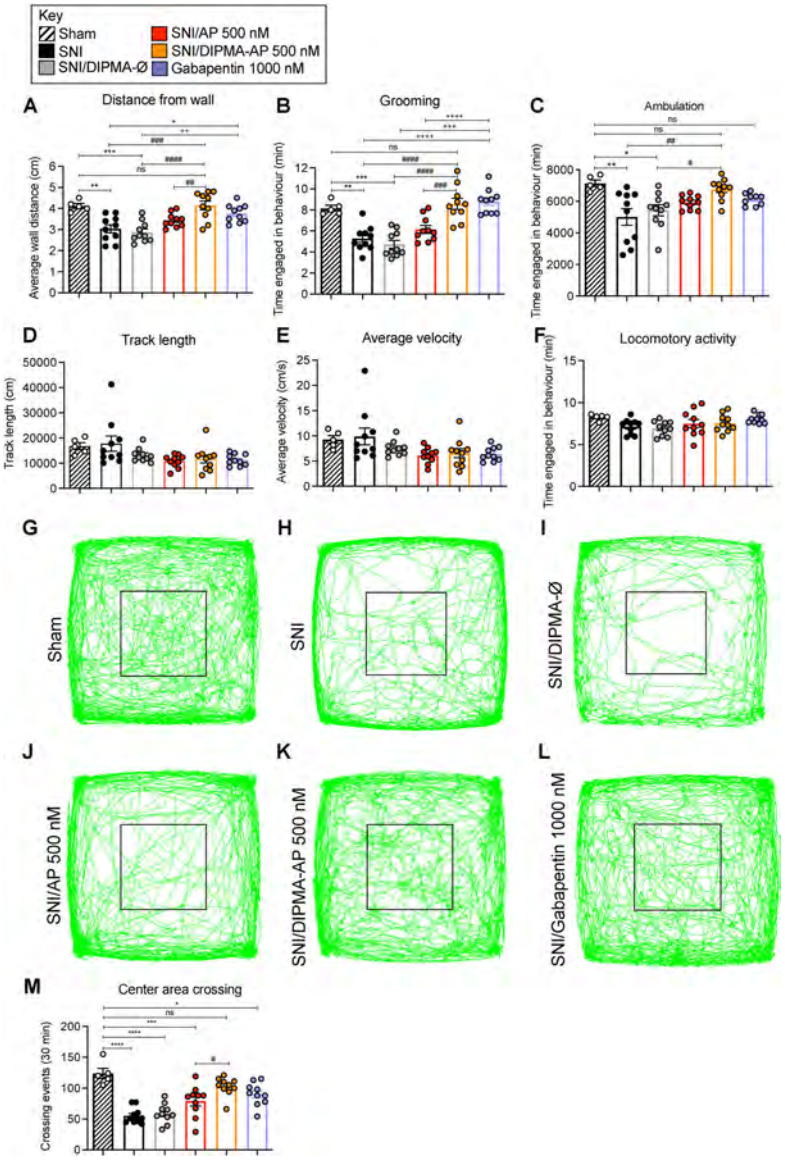

Fig. 2. DIPMA nanoparticles, non-evoked behavior in neuropathic pain.

Non-evoked nociceptive behavior in SNI and sham control mice recorded for 30 min at 90 min after intrathecal injection of DIPMA-AP, AP (500 nM AP), DIPMA-Ø or gabapentin (1000 nM). Distance from wall (**A**), grooming (**B**), ambulation (**C**), track length (**D**), average velocity, (**E**) and locomotor activity (**F**) were recorded. **G-L** are records of tracks of mice. **M** shows crossing events in area marked by black square. Mean ± SEM, N = 10 mice. *, +, #$P < 0.05$; **, ++, ##$P < 0.01$; ***, +++, ###$P < 0.005$; ****, ++++, ####$P < 0.001$. * Sham to all others groups; + gabapentin to sham, SNI and DIPMA-Ø; # DIPMA-AP to sham, SNI, DIPMA-Ø and AP. Two-way ANOVA, Tukey's multiple comparisons test.

Author Manuscript Author Manuscript Author Manuscript Author Manuscript

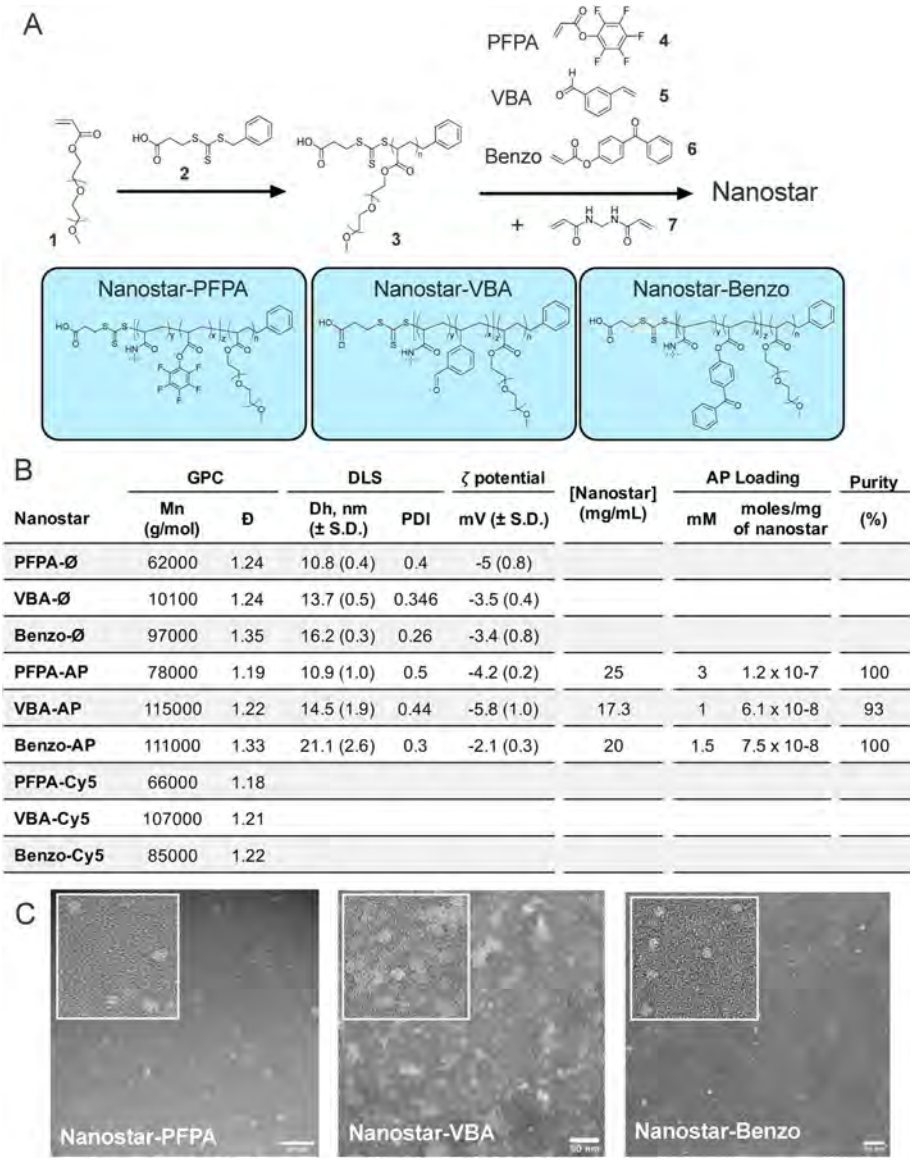

B

Nanostar	GPC Mn (g/mol)	GPC Đ	DLS Dh, nm (± S.D.)	DLS PDI	ζ potential mV (± S.D.)	[Nanostar] (mg/mL)	AP Loading mM	AP Loading moles/mg of nanostar	Purity (%)
PFPA-Ø	62000	1.24	10.8 (0.4)	0.4	-5 (0.8)				
VBA-Ø	10100	1.24	13.7 (0.5)	0.346	-3.5 (0.4)				
Benzo-Ø	97000	1.35	16.2 (0.3)	0.26	-3.4 (0.8)				
PFPA-AP	78000	1.19	10.9 (1.0)	0.5	-4.2 (0.2)	25	3	1.2 x 10-7	100
VBA-AP	115000	1.22	14.5 (1.9)	0.44	-5.8 (1.0)	17.3	1	6.1 x 10-8	93
Benzo-AP	111000	1.33	21.1 (2.6)	0.3	-2.1 (0.3)	20	1.5	7.5 x 10-8	100
PFPA-Cy5	66000	1.18							
VBA-Cy5	107000	1.21							
Benzo-Cy5	85000	1.22							

Fig. 3. Synthesis and characterization of nanostars.

A. Scheme for the arm-first synthesis of core functional nanostars for the preparation of nanostar-AP and nanostar-Cy5 conjugates. **B.** Molecular weight and distribution data, hydrodynamic diameter and ζ-potential (DLS), AP loading and final purity as determined by ^{19}F NMR. **C.** TEM images of nanostars. Scale bar = 50 nm.

Author Manuscript Author Manuscript Author Manuscript Author Manuscript

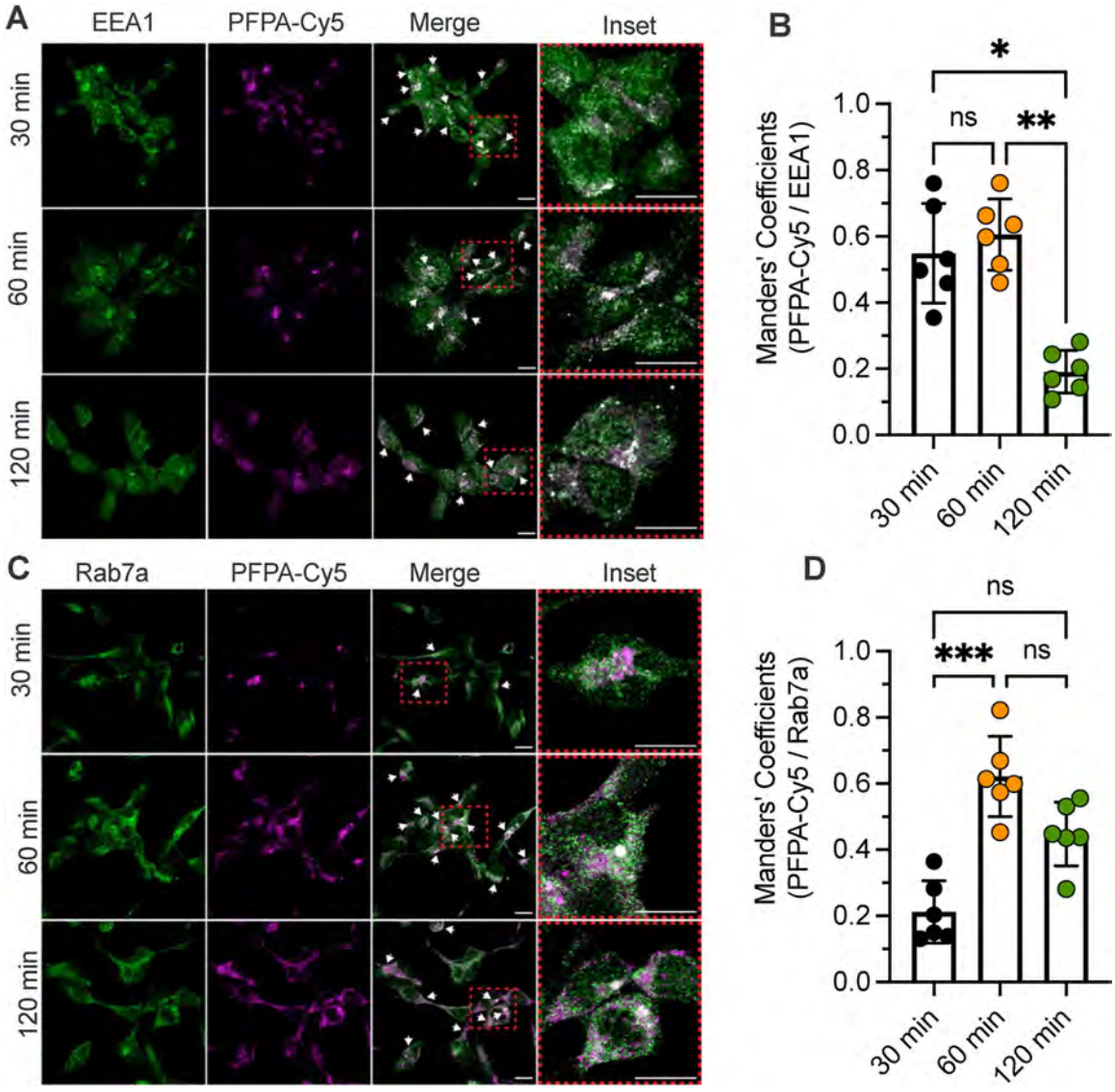

Fig. 4. Endocytosis of Cy5-nanostars in HEK293Tcells.

The uptake and intracellular trafficking of PFPA-Cy5 nanostars in HEK293T cells was examined by immunofluorescence and confocal microscopy. Antibodies to early endosomal antigen 1 (EEA1) and Rab7a were used to detect early and late endosomes, respectively. **A.** Localization of PFPA-Cy5 nanostars and early endosomal antigen 1 at 30, 60 and 120 min. **B.** Manders' overlap coefficient for PFPA-Cy5 nanostars and early endosomal antigen 1. **C.** Localization of PFPA-Cy5 nanostars and Rab7a at 30, 60 and 120 min. **D.** Manders' overlap coefficient for PFPA-Cy5 nanostars and Rab7a. N = 6 independent experiments. $*P < 0.05$, $**P < 0.01$. 1-way ANOVA, Duns's multiple comparison test. Scale bar, 10 μm.

Author Manuscript Author Manuscript Author Manuscript Author Manuscript

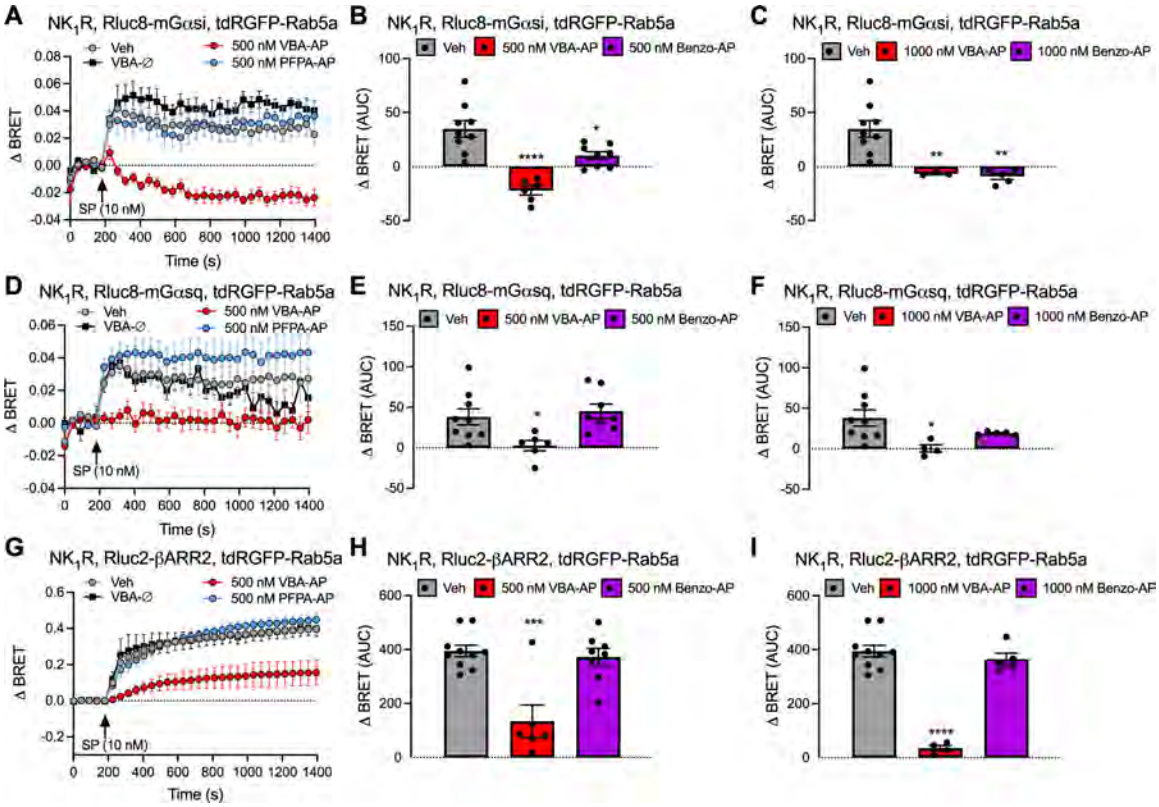

Fig. 5. Nanoparticles and endosomal NK_1R signaling in HEK293T cells.

Effects of SP (10 nM) on EbBRET between Rluc8-mGα_{si} (**A, B, C**), Rluc8-mGα_{sq} (**D, E, F**) and Rlu2-βARR2 (**G, H, I**) with tdRGFP-Rab5a. Cells were preincubated with vehicle (Veh, control), VBA-AP, Benzo-AP, PFPA-AP (500 nM AP loaded in nanoparticles: **A, B, D, E, G, H**; 1000 nM AP loaded in nanoparticles: **C, F, I**) or VBA-Ø for 4 h before stimulation with SP and measurement of EbBRET. **A, D, G**: time course of EbBRET prior and after SP (10 nM) stimulation. **B, C, E, F, H, I**: area under the curves (AUC) of corresponding time course of EbBRET. Mean ± SEM, N = 3–10 independent experiments. $*P < 0.05$, $**P < 0.001$, $***P < 0.001$, $****P < 0.0001$ compared to vehicle. One-way ANOVA, Dunnett's multiple comparisons test.

Author Manuscript Author Manuscript Author Manuscript Author Manuscript

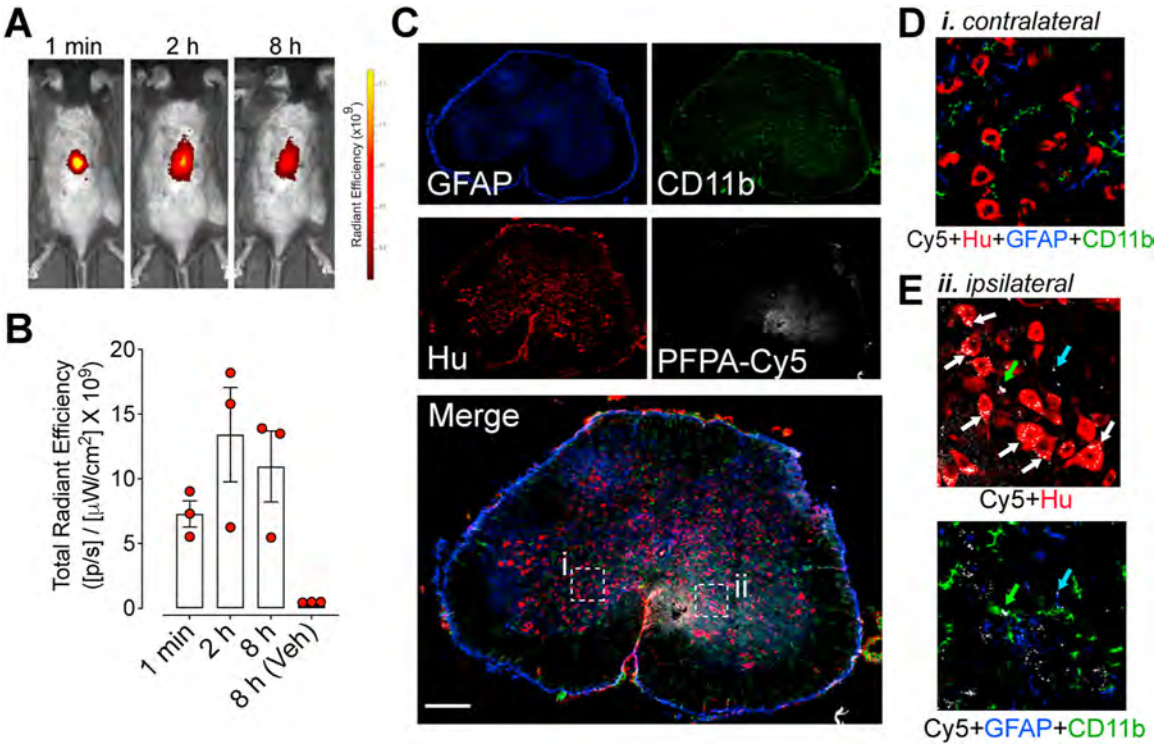

Fig. 6. Spinal cord biodistribution and neuronal uptake of nanostars.

A. Distribution and intensity of PFPA-Cy5 at 1 min, 2 h and 8 h after intrathecal injection of mice. Representative images of experiments on N = 3 mice are shown. Color Scale, Cy5 fluorescence intensity measured as radiant efficiency (units reported as $10^9 \times ps^{-1}\mu W^{-1}cm^{-2}$; p, photons; s, seconds; W, watts). **B.** Quantification of PFPA-Cy5 fluorescence in spinal cord region after intrathecal injection of mice, assessed as the radiant efficiency of the images. Mean ± SEM, N = 3 mice. **C.** Localization of PFPA-Cy5 in the spinal cord 4 h after intrathecal injection, showing single channels followed by merged image of a whole spinal cord section following labelling with anti-GFAP (reactive astrocytes, blue), anti-CD11b (microglia, green), anti-Hu (neurons, red) and PFPA-Cy5 nanostars (white). **D**. Inset (*i*) shows magnified region and lack of Cy5 fluorescence on contralateral side of spinal cord. **E**. Inset (*ii*) shows magnified region and accumulation of Cy5 nanostars predominantly in neurons in ipsilateral region of spinal cord. Representative images 12 sections each from N = 2 mice. (For interpretation of the references to color in this figure legend, the reader is referred to the Web version of this article.)

Author Manuscript Author Manuscript Author Manuscript Author Manuscript

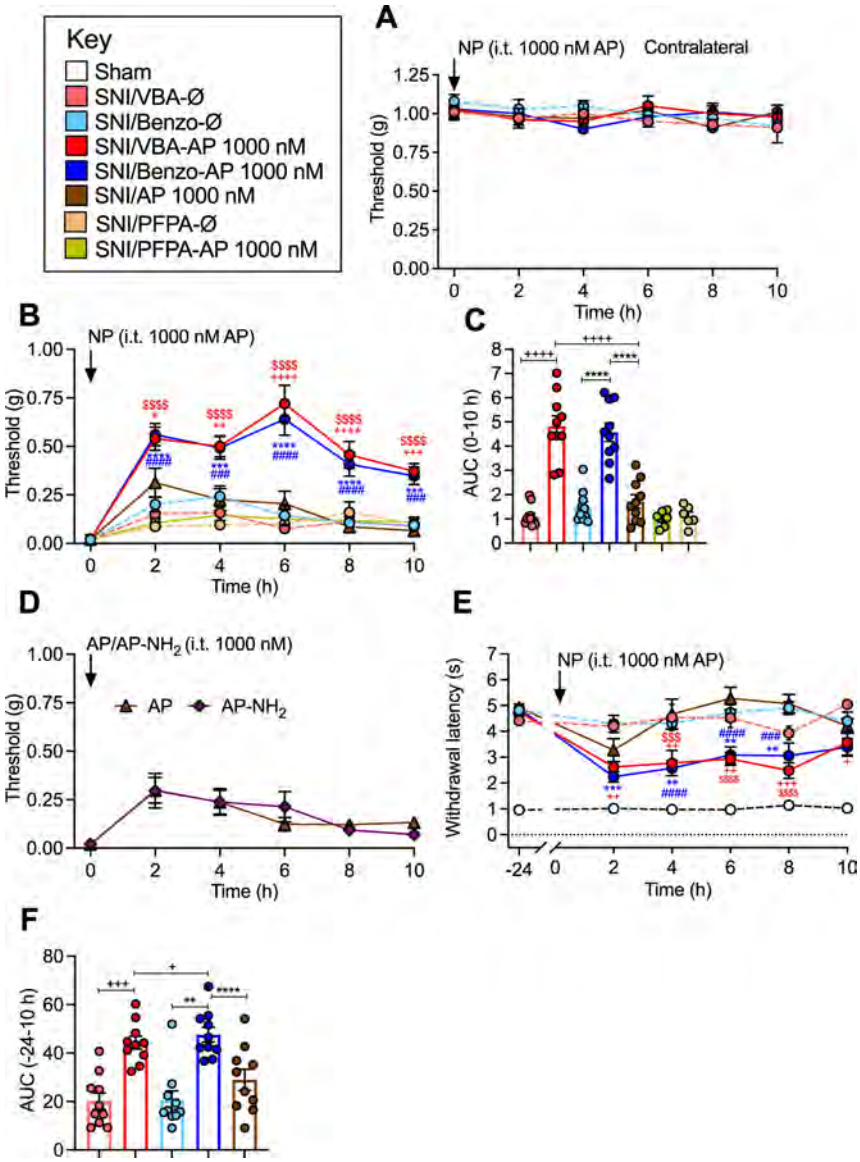

Fig. 7. Nanostars, mechanical and cold allodynia in neuropathic pain.

A. Effects of VBA-AP, Benzo-AP or AP (1000 nM AP), VBA-Ø or Benzo-Ø on VFF withdrawal responses (mechanical allodynia) of contralateral paw. **B, C.** Effects of VBA-AP, Benzo-AP, PFPA-AP, AP (1000 nM AP), VBA-Ø, Benzo-Ø or PFPA-Ø on VFF withdrawal responses of ipsilateral paw. **B** shows time course and **C** shows AUC. **D.** Comparison between AP and AP-NH_2 in SNI mice. **E,F.** Effects of VBA-AP, Benzo-AP, AP (1000 nM AP), VBA-Ø or Benzo-Ø on acetone withdrawal responses (cold allodynia) of ipsilateral paw in SNI mice. **E** shows time course and **F** shows AUC. Mean ± SEM, N = 10 mice. *, +, #, $ $P < 0.05$; **, ++, ##, $ $ $P < 0.01$; ***, +++, ###, $ $ $ $P < 0.005$; ****, ++++, ####, $ $ $ $ $P < 0.001$. * Benzo-AP to AP; + VBA-AP to AP; # Benzo-AP to Benzo-Ø; $ VBA-AP to VBA-Ø. Two-way ANOVA (mechanical and cold allodynia), one-way ANOVA (AUC) with Tukey's multiple comparison test.

Author Manuscript Author Manuscript Author Manuscript Author Manuscript

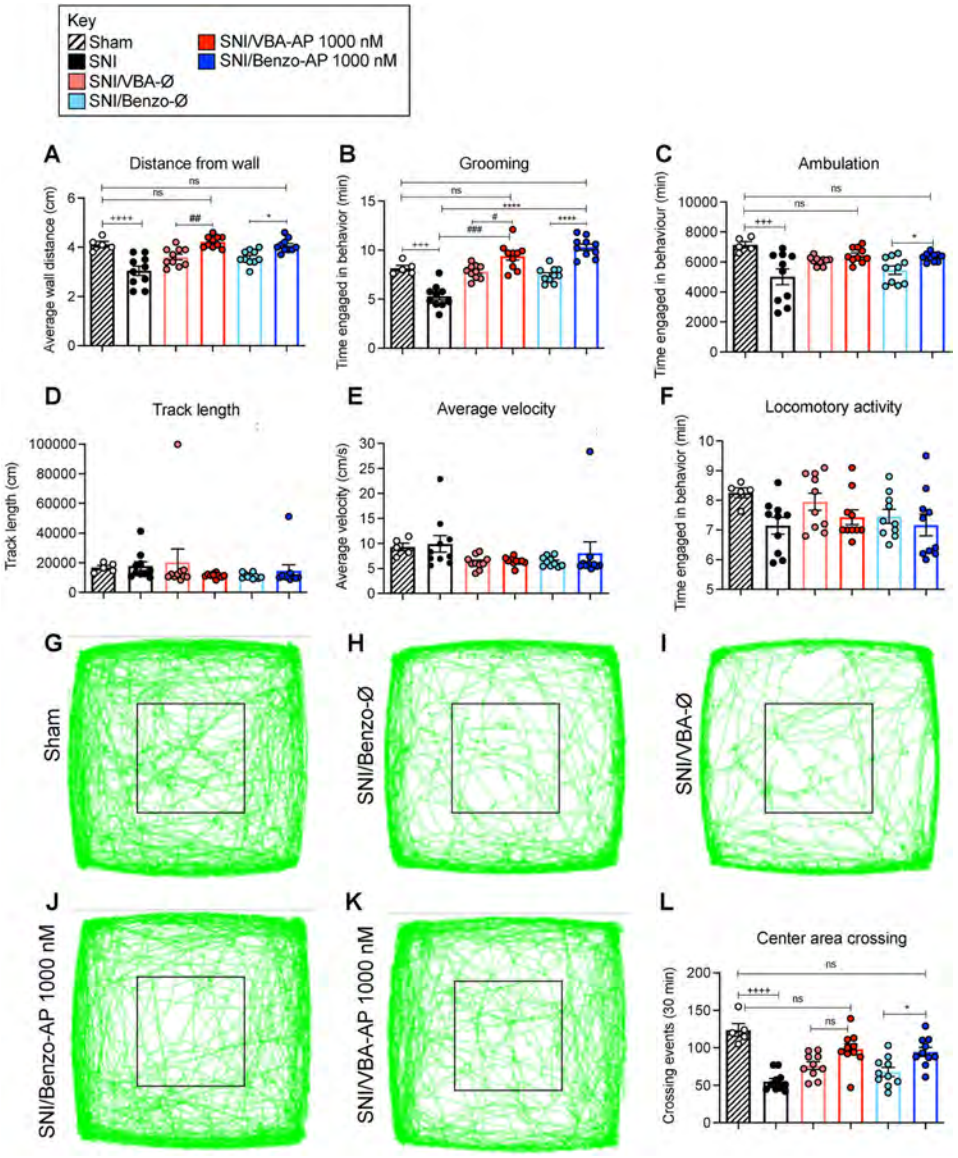

Fig. 8. Nanostars, non-evoked behavior in neuropathic pain.

Non-evoked nociceptive behavior in SNI and sham control mice recorded for 30 min at 90 min after intrathecal injection of VBA-AP, Benzo-AP, AP (1000 nM AP), VBA-Ø or Benzo-Ø. Distance from wall (**A**), grooming (**B**), ambulation (**C**), track length (**D**), average velocity, (**E**) and locomotor activity (**F**) were recorded. **G-K** are records of tracks of mice. **L** shows crossing events in area marked by black square. Mean ± SEM, N = 10 mice. *, +, #$P < 0.05$; **, ++, ##$P < 0.01$; ***, +++, ###$P < 0.005$; ****, ++++, ####$P < 0.001$. * Benzo-AP to Benzo-Ø and, SNI; + Sham to SNI; # VBA-AP to VBA-Ø and SNI. Two-way ANOVA, Tukey's multiple comparisons test.

Author Manuscript Author Manuscript Author Manuscript Author Manuscript

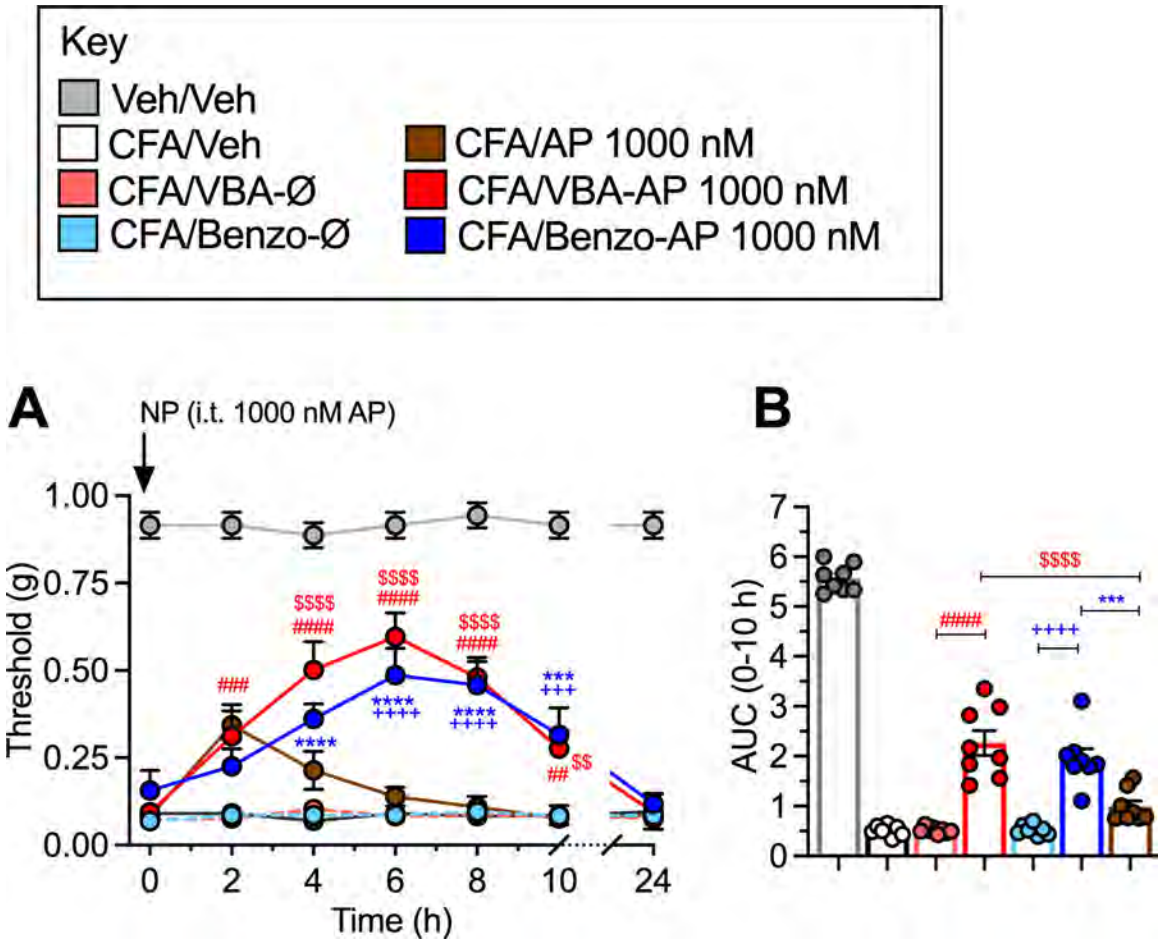

Fig. 9. Nanostars, mechanical allodynia in inflammatory pain.

A-B. . Effects of VBA-AP, Benzo-AP, AP (1000 nM AP), VBA-Ø or Benzo-Ø on VFF withdrawal responses of ipsilateral paw. **A** shows time course and **B** shows AUC. Mean ± SEM, N = 8 mice. *, +, #, $ $P < 0.05$; **, ++, ##, $ $ $P < 0.01$; ***, +++, ###, $ $ $ $P <$ 0.005: ****, ++++, ####, $ $ $ $ $P < 0.001$. * Benzo-AP to Benzo-AP; + Benzo-Ø to AP; # cVBA-AP to VBA-Ø; $ VBA-AP to AP. X-way ANOVA, Dunnett's multiple comparisons test.

Mice expressing fluorescent PAR_2 reveal that endocytosis mediates colonic inflammation and pain

Rocco Latorre[a,b], Alan Hegron[a,b], Chloe J. Peach[a,b], Shavonne Teng[a,b], Raquel Tonello[a,b], Jeffri S. Retamal[a,b,c], Rafael Klein-Cloud[a,b], Diana Bok[a,b,c], Dane D. Jensen[a,b,c], Lena Gottesman-Katz[a,b], Jeanette Rientjes[d], Nicholas A. Veldhuis[e], Daniel P. Poole[e], Brian L. Schmidt[a,b,c], Charalabos H. Pothoulakis[f], Carl Rankin[f], Ying Xie[f], Hon Wai Koon[f], and Nigel W. Bunnett[a,b,1]

[a]Department of Molecular Pathobiology, Neuroscience Institute, New York University, New York, NY 10010; [b]Department of Neuroscience and Physiology, Neuroscience Institute, New York University, New York, NY 10010; [c]Bluestone Center for Clinical Research, New York University College of Dentistry, New York, NY 10010; [d]Gene Modification Platform, Monash University, Clayton, VIC 3168, Australia; [e]Drug Discovery Biology, Monash Institute of Pharmaceutical Sciences, Monash University, Parkville, VIC 3052, Australia; and [f]Vatche and Tamar Manoukian Division of Digestive Diseases, David Geffen School of Medicine, University of California, Los Angeles, CA 90095

Edited by Robert Lefkowitz, Medicine and Biochemistry, Howard Hughes Medical Institute, Durham, NC; received June 30, 2021; accepted December 22, 2021

G protein–coupled receptors (GPCRs) regulate many pathophysiological processes and are major therapeutic targets. The impact of disease on the subcellular distribution and function of GPCRs is poorly understood. We investigated trafficking and signaling of protease-activated receptor 2 (PAR_2) in colitis. To localize PAR_2 and assess redistribution during disease, we generated knockin mice expressing PAR_2 fused to monomeric ultrastable green fluorescent protein (muGFP). PAR_2-muGFP signaled and trafficked normally. PAR_2 messenger RNA was detected at similar levels in *Par2-mugfp* and wild-type mice. Immunostaining with a GFP antibody and RNAScope in situ hybridization using *F2rl1* (PAR_2) and *Gfp* probes revealed that PAR_2-muGFP was expressed in epithelial cells of the small and large intestine and in subsets of enteric and dorsal root ganglia neurons. In healthy mice, PAR_2-muGFP was prominently localized to the basolateral membrane of colonocytes. In mice with colitis, PAR_2-muGFP was depleted from the plasma membrane of colonocytes and redistributed to early endosomes, consistent with generation of proinflammatory proteases that activate PAR_2. PAR_2 agonists stimulated endocytosis of PAR_2 and recruitment of $G\alpha_q$, $G\alpha_i$, and β-arrestin to early endosomes of T84 colon carcinoma cells. PAR_2 agonists increased paracellular permeability of colonic epithelial cells, induced colonic inflammation and hyperalgesia in mice, and stimulated proinflammatory cytokine release from segments of human colon. Knockdown of dynamin-2 (*Dnm2*), the major colonocyte isoform, and Dnm inhibition attenuated PAR_2 endocytosis, signaling complex assembly and colonic inflammation and hyperalgesia. Thus, PAR_2 endocytosis sustains protease-evoked inflammation and nociception and PAR_2 in endosomes is a potential therapeutic target for colitis.

signaling | receptors | proteases | endocytosis | inflammation

G protein–coupled receptors (GPCRs) are the largest family of transmembrane receptors, control most physiological and pathological processes, and are the target of >30% of approved drugs (1). Despite their medical importance, the effects of disease on the function and subcellular distribution of GPCRs are poorly understood. GPCRs at the plasma membrane interact with extracellular ligands and couple to intracellular heterotrimeric G proteins. However, GPCR signaling at the plasma membrane is often transient. GPCR kinases phosphorylate activated receptors, increasing their affinity for β-arrestins (βARRs) (2). βARRs uncouple GPCRs from G proteins, which mediates desensitization, and couple GPCRs to clathrin and adaptor protein 2, which mediate endocytosis. These processes terminate plasma membrane signaling. During disease, the continued generation of agonists could trigger the endocytosis of GPCRs. Although endosomes were once considered merely as a pathway for receptor trafficking, mounting evidence indicates that endosomes are a site of sustained GPCR signaling by Gα- and βARR-mediated mechanisms (3–9). GPCRs can also continue to signal from other intracellular compartments, including the Golgi apparatus (10, 11). The contribution of intracellular GPCR signaling to disease is not fully understood.

We investigated the impact of colitis on endosomal signaling of protease-activated receptor 2 (PAR_2), which mediates the proinflammatory and pronociceptive actions of proteases (12). Trypsin (13), tryptase (14), coagulation factors VIIa and Xa (15), and kallikreins (16) cleave PAR_2 to reveal a tethered ligand that activates the receptor. Cathepsin S, legumain, and elastase cleave at different sites and activate biased mechanisms of PAR_2 signaling (17–19). During colitis, multiple proteases from the host and the microbiome activate PAR_2 (20–25). PAR_2 activation evokes the redistribution of ZO1 and occludin

Significance

Colonic epithelial cells protect against inflammation by forming a barrier against ingress of microbes, digestive enzymes, and metabolic waste from the lumen. Protease-activated receptor-2 (PAR_2) mediates the proinflammatory and pronociceptive actions of proteases. We found that the proteolytic environment of the inflamed mouse colon induces redistribution of PAR_2 from the basolateral plasma membrane to endosomes of colonocytes. Endocytosis allows the assembly of a PAR_2, Gα, and β-arrestin signaling complex that mediates sustained increases in colonocyte paracellular permeability and persistent inflammation and hyperalgesia of the colon. Thus, PAR_2 endocytosis and endosomal signaling disrupts the normal protective function of colonocytes and underlies colonic inflammation and pain. PAR_2 in endosomes is a potential therapeutic target for inflammatory and painful diseases of the colon.

Author contributions: R.L., A.H., C.J.P., R.T., J.S.R., R.K.-C., D.D.J., J.R., N.A.V., D.P.P., C.H.P., Y.X., H.W.K., and N.W.B. designed research; R.L., A.H., C.J.P., S.L.T., R.T., J.S.R., R.K.-C., D.B., D.D.J., L.G.-K., J.R., N.A.V., D.P.P., C.R.R., Y.X., and H.W.K. performed research; J.R., C.H.P., Y.X., and H.W.K. contributed new reagents/analytic tools; R.L., A.H., C.J.P., S.L.T., R.T., J.S.R., R.K.-C., D.D.J., L.G.-K., J.R., N.A.V., D.P.P., B.L.S., C.R.R., Y.X., H.W.K., and N.W.B. analyzed data; and R.L., A.H., C.J.P., R.T., J.S.R., D.D.J., N.A.V., D.P.P., B.L.S., H.W.K., and N.W.B. wrote the paper.

Competing interest statement: N.W.B. is a founding scientist of Endosome Therapeutics, Inc. Research in the laboratories of N.W.B., N.A.V., and D.P.P. is funded in part by Takeda Pharmaceuticals International.

This article is a PNAS Direct Submission.

This article is distributed under Creative Commons Attribution-NonCommercial-NoDerivatives License 4.0 (CC BY-NC-ND).

[1]To whom correspondence may be addressed. Email: nwb2@nyu.edu.

This article contains supporting information online at http://www.pnas.org/lookup/suppl/doi:10.1073/pnas.2112059119/-/DCSupplemental.

Published February 2, 2022.

from tight junctions of colonocytes, leading to increased paracellular permeability, influx of proinflammatory macromolecules and bacteria into the mucosa, and inflammation (26, 27). PAR_2 activation on nociceptors stimulates the release of neuropeptides that cause neurogenic inflammation and pain in the skin (28, 29) and colon (7, 22, 30). Proteases and PAR_2 have been implicated in colonic diseases, including inflammatory bowel disease (IBD), irritable bowel syndrome, and cancer (12). However, the signaling mechanisms by which PAR_2 induces disease are incompletely understood.

Our understanding of the function of PAR_2 is hampered by an inadequate knowledge of its cellular and subcellular localization in health and disease states. Because GPCR antibodies can lack sensitivity and specificity and are unsuitable for studying receptor trafficking in living cells, we generated a knockin mouse expressing PAR_2 fused to monomeric ultrastable green fluorescent protein (muGFP). Colitis resulted in translocation of PAR_2-muGFP from the basolateral membrane of colonocytes to early endosomes. Endocytosis of PAR_2 led to the assembly of a signaling complex (signalosome) comprising PAR_2 and $G\alpha_q$, $G\alpha_i$, or βARR. Endocytosis of PAR_2 was necessary for sustained increases in paracellular permeability, release of proinflammatory cytokines and chemokines, and colonic inflammation and hyperalgesia.

Results

Generation of *Par_2-mugfp* Mice. To gain an understanding of the cellular and subcellular distribution of PAR_2 and how it might be altered during disease, we generated mice expressing mouse PAR_2 fused at the intracellular C terminus to muGFP. muGFP harbors stabilizing mutations (Q69L and N164Y), which improve hydrophobic packing in the core and facilitate hydrogen bonding, and a mutation at the dimer interface (F223D), which prevents dimerization (31). muGFP retains fluorescence after harsh fixation and resists undesirable dimerization. To verify functionality of PAR_2-muGFP, we compared signaling of PAR_2-muGFP and PAR_2 with N-terminal FLAG and C-terminal HA11 epitopes transiently expressed in KNRK cells, which express low levels of PAR_2 and have been used extensively to study PAR_2 functions (13). Trypsin and 2-furoyl-LIGRLO-NH_2 (2F), a PAR_2 agonist that is an analog of the tethered ligand domain, stimulated a concentration-dependent increase in IP-1 formation with similar potency and efficacy in cells expressing PAR_2-muGFP or PAR_2-HA11 (half maximal effective concentration of KNRK-PAR_2-muGFP: trypsin, 5.4×10^8 M; 2F, 9.1×10^8 M; half maximal effective concentration of KNRK-PAR_2-HA11: trypsin, 5.4×10^8 M; 2F, 7.8×10^8 M) (*SI Appendix*, Fig. S1 *A* and *B*). There were no responses to trypsin or 2F in cells expressing muGFP alone. Thus, PAR_2-muGFP signals similarly to PAR_2-HA11 in KNRK cells, suggesting that muGFP does not affect the normal functions of PAR_2.

To generate knockin mice, a targeting construct was generated comprising *Par_2-mugfp*, a floxed PGK neomycin cassette, and a downstream KpnI site for Southern screening (Fig. 1*A*). Five embryonic stem cell clones expressing the construct were identified by Southern blotting (1.25% incorporation); blotting at the 3′ and 5′ arms of homology confirmed correct targeting (Fig. 1*B*). Screening with an internal probe to the NEO cassette excluded random integration or insertion of a concatemer. The presence and the integrity of *loxP* sites and insertion of *Par_2-mugfp* were verified by sequencing. Two clones were injected into BALB/c mouse blastocysts. Chimeras (black and white) were generated from both clones and bred with wild-type C57BL6J female mice to generate black F1 progeny, indicating germline transmission. Expression of *Par_2-mugfp* was confirmed by Southern blotting (Fig. 1*C*) and reverse-transcription polymerase chain reaction (RT-PCR) (Fig. 1*D*).

Characterization of *Par_2-mugfp* Mice. We compared the expression of *F2rl1*, the gene encoding for PAR_2, in *Par_2-mugfp* and wild-type mice using quantitative RT-PCR (qRT-PCR). *F2rl1* expression in the stomach, duodenum, ileum, colon, and dorsal root ganglia (DRG) was not different in *Par_2-mugfp* and wild-type mice (Fig. 1*E*). *F2rl1* was expressed at higher levels in the jejunum of *Par_2-mugfp* mice for unknown reasons. Thus, in most tissues, *F2rl1* is expressed at similar levels in *Par_2-mugfp* and wild-type mice.

Localization of PAR_2-muGFP Immunoreactivity and Messenger RNA. We localized PAR_2-muGFP by indirect immunofluorescence and confocal microscopy using a GFP antibody to amplify the signal. This approach avoided use of GPCR antibodies, which can lack selectivity. In *Par_2-mugfp* mice, GFP immunoreactivity was prominently localized to the basolateral plasma membrane of epithelial cells of the villi and crypts in the duodenum, jejunum, ileum, and lining mucosal folds and crypts in the colon (Fig. 2 *A* and *B*). There was no detectable GFP immunoreactivity in epithelial cells of the small or large intestine of wild-type mice, which confirms selectivity of the GFP antibody (Fig. 2 *A* and *B*). PAR_2-muGFP immunoreactivity was detected at low levels in the enteric nervous system of the small and large intestines of *Par_2-mugfp* mice, but the cellular localization was not further studied.

We used RNAScope in situ hybridization with probes to *F2rl1* and *Gfp* to confirm PAR_2-muGFP localization in the colon. In *Par_2-mugfp* mice, *F2rl1* and *Gfp* were prominently detected in colonocytes (Fig. 2*C*). In wild-type mice, *F2rl1*, but not *Gfp*, was detected in colonocytes. RNAScope was used to detect PAR_2 expression with high sensitivity in DRG neurons. In *Par_2-mugfp* mice, *F2rl1*, and *Gfp* were coexpressed in a subpopulation of DRG neurons (Fig. 2*D*). *F2rl1*, but not *Gfp*, was expressed in DRG neurons of wild-type mice (Fig. 2*E*).

These results confirm the expression of PAR_2 in intestinal epithelial cells and a subpopulation of primary sensory neurons, and they validate the use of *Par_2-mugfp* mice for studies of the cellular localization of this receptor.

Agonist-Evoked Trafficking of PAR_2-muGFP in the Colon. Upon activation, many GPCRs, including PAR_2, undergo endocytosis (3, 7). GPCR trafficking is usually studied in cell lines overexpressing receptors. Little is known about agonist-evoked trafficking of endogenous GPCRs in intact tissues or organisms, largely due to the inadequate specificity or sensitivity of GPCR antibodies. To examine agonist-evoked trafficking of PAR_2 in tissues, isolated segments of colon from *Par_2-mugfp* mice were incubated with trypsin (140 nM), 2F (100 μM), or vehicle (60 min, 37 °C). In vehicle-treated colon, PAR_2-muGFP was principally localized to the basolateral plasma membrane of colonocytes (Fig. 3 *A* and *B*, arrowheads). Trypsin or 2F stimulated depletion of PAR_2-muGFP from the plasma membrane and accumulation in intracellular vesicles (Fig. 3 *A* and *B*, arrows). Vesicles containing PAR_2-muGFP were costained with an antibody to early endosomal antigen 1 (EEA1) and are thus early endosomes (Fig. 3 *C* and *D*; *SI Appendix*, Fig. S2*A*, arrows). Some vesicles were costained with an antibody to Rab7a and are late endosomes (*SI Appendix*, Fig. S2*B*). Quantification of endocytosis, assessed by the cytosol–plasma membrane pixel intensity, confirmed extensive endocytosis of PAR_2-muGFP (Fig. 3 *E* and *F*). Thus, agonists evoke robust endocytosis of endogenous PAR_2 in the intact colon.

Inflammation-Evoked Trafficking of PAR_2-muGFP in the Colon. Little is known about the impact of disease on the subcellular distribution of GPCRs. The continued generation of agonists during chronic disease could induce the redistribution of receptors from the plasma membrane to endosomes. Continued GPCR

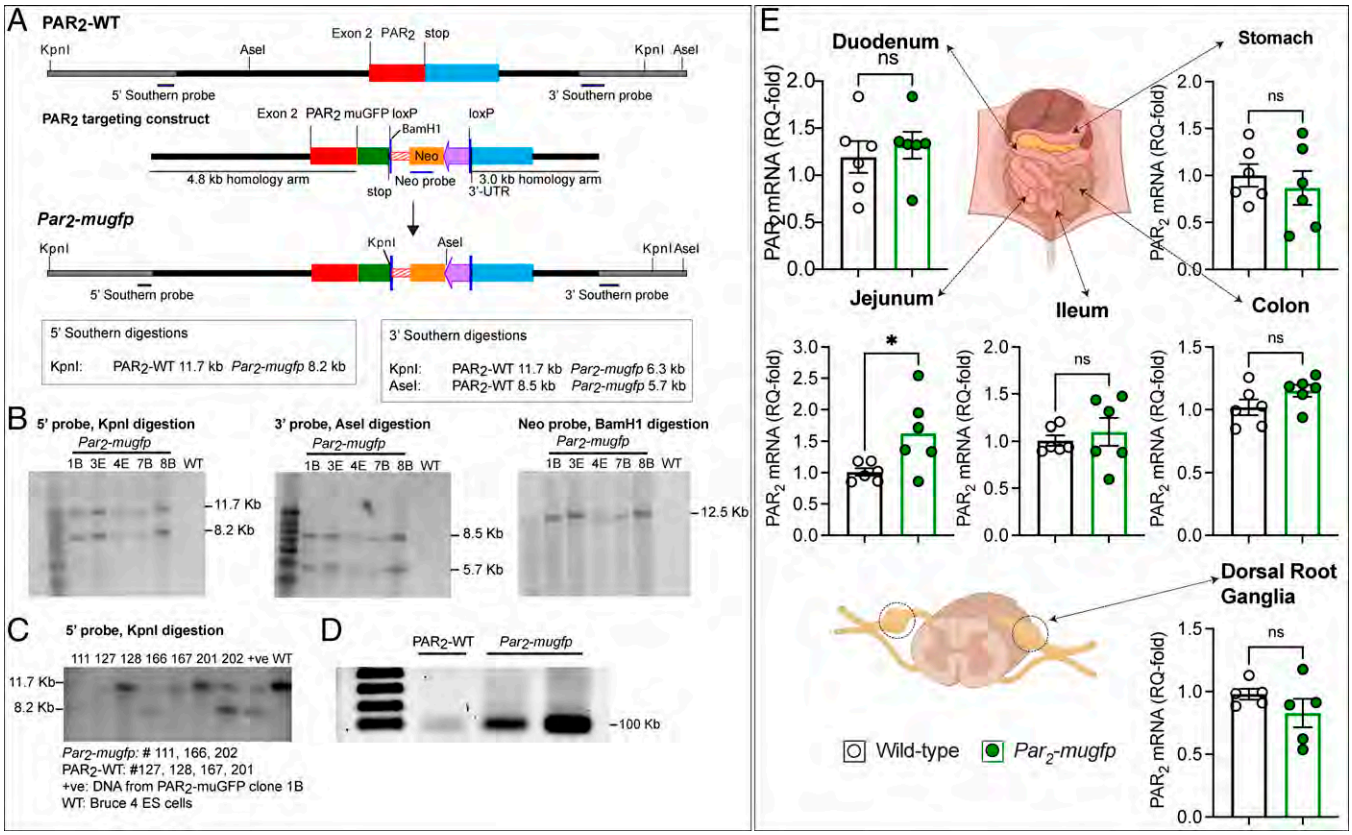

Fig. 1. Generation and characterization of *Par$_2$-mugfp* mice. (*A*) *Par$_2$-mugfp* targeting construct comprising a downstream phosphoglycerine kinase neomycin cassette flanked by *loxP* sites and a downstream KpnI site. (*B*) Southern blot confirming correct targeting. (*C*) Southern blot and (*D*) RT-PCR blot confirming *Par$_2$-mugfp* expression in mice. WT, wild-type. (*E*) Expression of *F2rl1* (*Par$_2$*) mRNA in the digestive tract and DRG of *Par$_2$-mugfp* and wild-type mice determined by qRT-PCR. $n = 6$ mice. Mean ± SEM; ns, nonsignificant. $^*P < 0.05$, Student's *t* test.

signaling from intracellular compartments (e.g., endosomes) underlies disease processes, including persistent pain (5–9). This has implications for therapy, because GPCRs in endosomes might be inaccessible to antagonists that fail to penetrate the plasma and endosomal membranes (e.g., monoclonal antibodies) or cannot effectively engage conformations of GPCRs within multiprotein signaling complexes in acidic endosomes (32). Thus, an understanding of disease-evoked trafficking of GPCRs is required for the design of optimal therapies. We investigated whether PAR_2 redistributes to endosomes of colonocytes during colitis, when multiple host and microbiome proteases are activated (20, 22, 23, 25).

Par$_2$-mugfp mice were treated with 3% dextran sulfate sodium (DSS) in drinking water for 7 d to induce mucosal inflammation of the colon. Controls received plain water. DSS induced signs of colitis, including fecal blood, diarrhea, weight loss, and colon shortening (Fig. 4 *A* and *B*). PAR_2-muGFP was localized at the basolateral plasma membrane of colonocytes in control mice (Fig. 4*C*, arrowheads). At 24 h after DSS treatment, PAR_2-muGFP was depleted from the plasma membrane and prominently detected in intracellular vesicles of colonocytes (Fig. 4*C*, arrows). *Par$_2$-mugfp* mice were also treated with trinitrobenzene sulphonic acid (TNBS; 4 mg/mL in 0.9% NaCl and 50% ethanol, 150-μL enema) to induce transmural inflammation of the colon. Control mice received vehicle (0.9%NaCl and 50% ethanol). After 72 h, TNBS-treated mice had extensive transmural inflammation, with mucosal and submucosal infiltration of neutrophils (Fig. 4 *D* and *E*). PAR_2-muGFP was prominently detected in intracellular vesicles (Fig. 4*F*, arrows) and also present at the plasma membrane (Fig. 4*F*, arrowheads) of colonocytes. In regions of marked inflammation and mucosal disruption, PAR_2-muGFP was detected in immune cells of the mucosa (Fig. 4*G*, arrowheads) and EEA1-positive early endosomes of colonocytes (Fig. 4*G*, arrows).

In two preclinical models of IBD, PAR_2-muGFP redistributes from the plasma membrane to endosomes of colonocytes. This redistribution is likely attributable to the activation of proteases in the inflamed colon.

Mechanism and Pathway of PAR_2 Trafficking in Colonocytes. Activated PAR_2 undergoes clathrin-mediated endocytosis and traffics to early endosomes and lysosomes (13). PAR_2 ubiquitination is necessary for lysosomal targeting (33). Recovery of cellular responsiveness requires Gβγ-dependent activation of protein kinase D, which liberates newly synthesized PAR_2 from the Golgi apparatus and stimulates translocation to the plasma membrane (34, 35).

We used enhanced bystander bioluminescence resonance energy transfer (ebBRET), which capitalizes on the affinity of *Renilla*-tagged proteins, to study the intracellular trafficking of PAR_2 in T84 human colon carcinoma cells (26). To assess PAR_2 endocytosis, we coexpressed PAR_2 coupled to *Renilla* luciferase 8 (Rluc8) and the plasma membrane marker CAAX coupled to *Renilla* GFP (RGFP) or the early endosome marker Rab5a coupled to tandem (td) RGFP. 2F (100 μM) decreased BRET (i.e., proximity) between PAR_2-Rluc8 and RGFP-CAAX and increased BRET between PAR_2-Rluc8 and tdRGFP-Rab5a, consistent with endocytosis (Fig. 5 *B* and *C*). Hypertonic (0.45 M) sucrose, dominant-negative dynamin (Dnm) K44A, and Dnm2 siRNA inhibited endocytosis of PAR_2 (Fig. 5 *D*–*G*). Dnm2 was the predominant Dnm isoform in T84 cells, which expressed Dnm1 and Dnm3 messenger RNA (mRNA) at lower

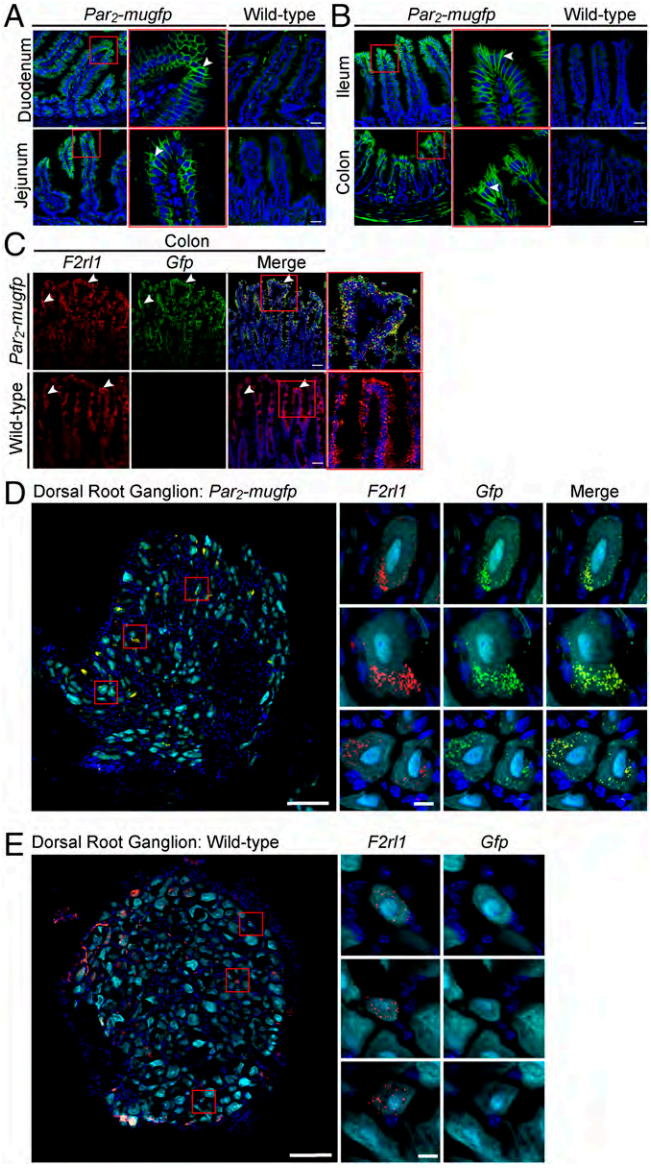

Fig. 2. Localization of PAR_2-muGFP in the intestine and DRG by immunofluorescence and RNAScope in situ hybridization. (*A* and *B*) Localization of GFP immunoreactivity in duodenum and jejunum (*A*) and ileum and colon (*B*) of *Par₂-mugfp* and wild-type mice. (*C*) RNAScope localization of *F2rl1* and *Gfp* mRNA in colon of *Par₂-mugfp* and wild-type mice. Arrowheads indicate immunoreactivity at the basolateral membrane of epithelial cells and mRNA expression within epithelial cells. (*D* and *E*) RNAScope localization of *F2rl1* and *Gfp* mRNA in DRG of *Par₂-mugfp* (*D*) and wild-type (*E*) mice. (Scale bars, 10 μm.) Representative images, independent experiments. $n = 5$ mice.

levels (*SI Appendix*, Fig. S3*A*). siRNA knockdown of Dnm2 was verified by qRT-PCR (*SI Appendix*, Fig. S3*B*).

To study the intracellular trafficking of PAR_2, we expressed BRET1 sensors for PAR2 and subcellular compartments in HEK293T cells (Fig. 5*A*), where BRET1 responses were larger. 2F (10 μM) and trypsin (100 nM) decreased BRET between PAR_2-Rluc8 and Venus-KRas (plasma membrane) and increased BRET between PAR_2-Rluc8 and Venus-Rab5a (early endosome) (Fig. 5 *H–K*; *SI Appendix*, Fig. S4 *A–D*). BRET between PAR_2-Rluc8 and Venus-Rab7a (late endosome) was unaffected (Fig. 5 *L* and *M*; *SI Appendix*, Fig. S4 *E* and *F*). 2F increased BRET between PAR_2-Rluc8 and Venus-Giantin (*cis*-Golgi) and caused a transient decrease and then a sustained increase in BRET between PAR_2-Rluc8 and YFP-TGN-38 (*trans*-Golgi) (Fig. 5 *N–Q*). Trypsin did not affect BRET between PAR_2-Rluc8 and Venus-Giantin but caused a transient decrease in BRET between PAR_2-Rluc8 and YFP-TGN-38 (*SI Appendix*, Fig. S4 *G–J*). 2F and trypsin stimulated BRET between PAR_2-Rluc8 and Venus-Rab11a (recycling endosomes) (Fig. 5 *R* and *S*; *SI Appendix*, Fig. S4 *K* and *L*). DnmK44A inhibited the recruitment of PAR_2 to most compartments.

To determine whether fusion to muGFP affects PAR_2 trafficking, we expressed PAR_2-muGFP in HEK293T cells expressing markers of early and late endosomes and the Golgi apparatus tagged with red fluorescent protein (RFP) and localized PAR_2 and markers by confocal microscopy. 2F (10 μM, 30 min) stimulated trafficking of PAR_2-muGFP from the plasma membrane to early endosomes (Fig. 5*T*; *SI Appendix*, Fig. S5). PAR_2-muGFP was not detected in late endosomes or the Golgi apparatus by microscopy (Fig. 5*U*; *SI Appendix*, Fig. S6).

Assembly of a PAR_2 Signaling Complex with Gα or βARR. GPCRs can assemble Gα and βARR signaling complexes in endosomes, which enable sustained signaling of internalized receptors (3, 4, 36, 37). Within endosomes, Gα subunits can transduce signals and βARRs serve as scaffolds that organize GPCRs and signaling enzymes. Because agonists stimulated trafficking of PAR_2 to early endosomes of T84 and HEK293T cells, we examined the assembly of signaling complexes in this compartment. The activation of $G\alpha_q$, $G\alpha_i$ and $G\alpha_s$ was studied using ebBRET to detect recruitment of mini-Gα (mGα) coupled to Rluc8 to RGFP-CAAX or tdRGFP-Rab5a (Fig. 6*A*). mGα proteins are N-terminally truncated Gα proteins that freely diffuse within the cytosol and bind to active conformations of GPCRs, which reflects Gα activation. $mG\alpha_{sq}$ and $mG\alpha_{si}$ were developed by mutating $mG\alpha_s$ residues to equivalent $G\alpha_q$ and $G\alpha_i$ residues. Recruitment of βARR was assessed by measuring ebBRET between Rluc2-βARR2 and RGFP-CAAX or tdRGFP-Rab5a (Fig. 6*A*). In T84 cells, 2F (100 μM) stimulated the rapid recruitment of $mG\alpha_{sq}$, $mG\alpha_{si}$, or βARR2 to the plasma membrane and endosomes, although βARR2 recruitment to endosomes was slower and more sustained than recruitment to the plasma membrane (Fig. 6 *B–D*). $mG\alpha_s$ was not recruited to the plasma membrane or endosomes.

We studied the mechanisms of assembly of signaling complexes in HEK293T cells. 2F (100 μM) and trypsin (100 nM) stimulated the recruitment of $mG\alpha_{sq}$, $mG\alpha_{si}$, and βARR2 to the plasma membrane and endosomes of HEK293T cells (*SI Appendix*, Fig. S7 *A–F*). Whereas the recruitment of $mG\alpha_{sq}$, $mG\alpha_{si}$ and βARR2 at the plasma membrane declined over 1,400 s, their recruitment to endosomes increased or was sustained. Hypertonic sucrose delayed the recruitment of $mG\alpha_{sq}$, $mG\alpha_{si}$, and βARR2 to the plasma membrane, although ebBRET signals ultimately reached those of controls. In contrast, hypertonic sucrose abolished recruitment of $mG\alpha_{sq}$, $mG\alpha_{si}$, and βARR2 to endosomes.

Conventional BRET is limited to measuring the proximity between two proteins. To simultaneously measure the proximity between PAR_2, an effector (mGα or βARR), and a localization marker, we used NanoLuc Binary Technology (38), NanoBiT BRET (nbBRET) (Fig. 6*E*). A split luciferase assay was developed in which PAR_2 was tagged at the C terminus with the natural peptide fragment of NanoLuc (NP, a 13-residue NanoLuc fragment), and a plasma membrane or endosomal marker was tagged with the large BiT fragment of NanoLuc (LgBiT-CAAX or LgBiT-FYVE, respectively). Luminescence occurs from a complex between PAR_2-NP and LgBiT-CAAX or LgBiT-FYVE, which serves as an energy donor for fluorophore-tagged mGα or βARR. In T84 colonocytes, 2F (100 μM) increased nbBRET between PAR_2, $mG\alpha_{si}$, $mG\alpha_{sq}$, or βARR1 and markers of the plasma membrane or endosome (Fig. 6 *F–H*). In HEK293T cells, 2F and trypsin also stimulated nbBRET

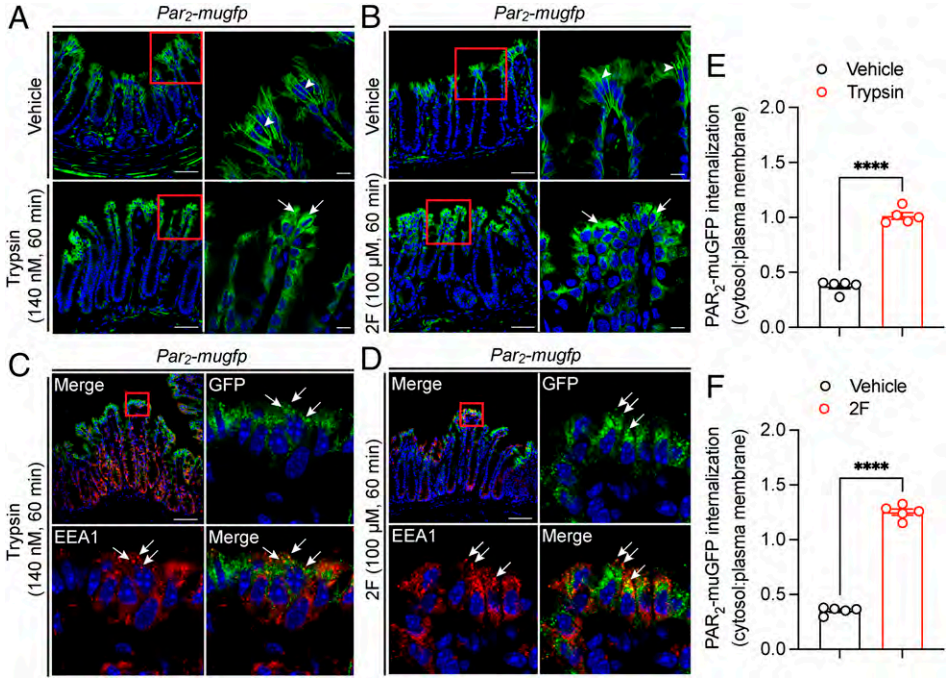

Fig. 3. Agonist-evoked endocytosis of PAR_2-muGFP in the colon. (*A* and *B*) Localization of GFP immunoreactivity in isolated segments of colon from *Par_2-mugfp* mice incubated with vehicle, trypsin (*A*, 140 nM, 60 min) or 2F (*B*, 100 μM, 60 min). (*C* and *D*) Colocalization of GFP and EEA1 in segments treated with trypsin (*C*) or 2F (*D*). Arrowheads denote plasma membrane, and arrows denote endosomes. (Scale bar, 10 μm.) Representative images and independent experiments are shown ($n = 5$ mice). (*E* and *F*) Quantification of PAR_2-muGFP internalization after vehicle, trypsin (*E*), or 2F (*F*) (cytosol–plasma membrane pixel intensity). Mean ± SEM; $n = 5$ mice. ****$P < 0.0001$, Student's *t* test.

between PAR_2, $mG\alpha_{si}$, $mG\alpha_{sq}$, or βARR1 and CAAX or FYVE (Fig. 6 *I–K*; *SI Appendix*, Fig. S8 *A–H*). Recruitment of mGα and βARR to early endosomes lagged behind recruitment to the plasma membrane. nbBRET signals were maintained for at least 1,200 s, suggesting assembly of stable PAR_2/mGα or PAR_2/βARR complexes. Hypertonic sucrose inhibited agonist-stimulated assembly of PAR_2, $mG\alpha_{si}$, $mG\alpha_{sq}$, or βARR1 complexes in early endosomes (*SI Appendix*, Fig. S8 *A*, *B*, *F*, and *G*). DynK44A had similar inhibitory effects on signalosome assembly but to a lesser extent (*SI Appendix*, Fig. S8 *C*, *D*, *G*, and *H*). The PAR_2 antagonist GB88 prevented 2F and trypsin-stimulated signalosome assembly in endosomes of HEK293T cells (*SI Appendix*, Fig. S8 *I* and *J*). Immunofluorescence and confocal microscopy confirmed localization of HA-LgBiT-CAAX at the plasma membrane and HA-LgBiT-FYVE in endosomes (*SI Appendix*, Fig. S8*K*).

In unstimulated HEK293T cells, immunoreactive PAR_2 was localized to the plasma membrane, and immunoreactive $G\alpha_q$ and YFP-βARR1/2 were cytosolic (Fig. 6*L*). In cells exposed to 2F (10 μM, 30 min), PAR_2, $G\alpha_q$, and YFP-βARR1/2 were colocalized in early endosomes.

Our results suggest that agonists induce assembly of a signaling complex comprising PAR_2 and $G\alpha_q$, $G\alpha_i$, or βARR1/2 in early endosomes. This process requires Dnm-dependent endocytosis of PAR_2.

PAR_2 Endocytosis and the Colonic Epithelial Barrier. Tight junctions between colonocytes form a barrier that prevents the ingress of proinflammatory macromolecules and microbes from the lumen. Alterations in tight junction structure contribute to impaired barrier function and inflammation in IBD. PAR_2 agonists promote paracellular permeability of the colon (39) by a mechanism that involves βARR-dependent activation of ERK1/2 and redistribution of ZO1 and occludin from tight junctions (3, 26), suggesting a role for endosomal PAR_2 signaling.

Analysis of the expression of Dnm isoforms in the mouse colon by RNAScope in situ hybridization and RT-qPCR revealed prominent expression of *Dnm2* in colonocytes, whereas *Dnm1* and *Dnm3* mRNA were largely confined to the enteric nervous system (Fig. 7 *A* and *B*). When applied to the basolateral surface of T84 monolayers, trypsin (100 nM) and 2F (10 μM) decreased transepithelial electrical resistance (TEER) after 6 h, consistent with redistribution of tight junctional proteins and increased paracellular permeability (Fig. 7*C*). The PAR_2 antagonist GB88 prevented these effects, confirming a role for PAR_2. Dnm2 siRNA similarly prevented the effects of trypsin and 2F on TEER, implicating a requirement for PAR_2 endocytosis (Fig. 7 *D* and *E*).

PAR_2 Endocytosis, Colonic Inflammation, and Pain. To ascertain whether Dnm2 could contribute to colonic inflammation in vivo, we administered Dnm2 or control small hairpin RNA (shRNA) into the colon of *Par_2-mugfp* mice. After 48 h, RNAScope in situ hybridization revealed ∼50% knockdown of Dnm2 mRNA in colonocytes of mice treated with Dnm shRNA compared to control shRNA (Fig. 8 *A* and *B*). To assess the effects of *Dnm2* knockdown on PAR_2-mediated colonic inflammation and pain, we administered 2F (100 μM) or vehicle into the colon by enema (150 μL). Endocytosis of PAR_2-muGFP, colonic levels of proinflammatory factors, and colonic nociception were assessed. In mice receiving control shRNA, 2F stimulated endocytosis of PAR_2-muGFP in colonocytes after 6 h; Dnm2 shRNA inhibited endocytosis (Fig. 8*C*). In control mice, 2F increased mRNA levels of tumor necrosis factor α (TNF-α), C-X-C motif chemokine ligand 1 (CXCL1), and interleukin-1β (IL-1β) in the colon (Fig. 8 *D–F*). Intracolonic 2F decreased withdrawal responses of the abdomen to calibrated von Frey filaments from 1 to 5 h, which indicates hyperalgesia (Fig. 8 *G* and *H*). These results are consistent with the known proinflammatory and pronociceptive actions of PAR_2 in the colon (7, 22, 30). Dnm2 shRNA inhibited

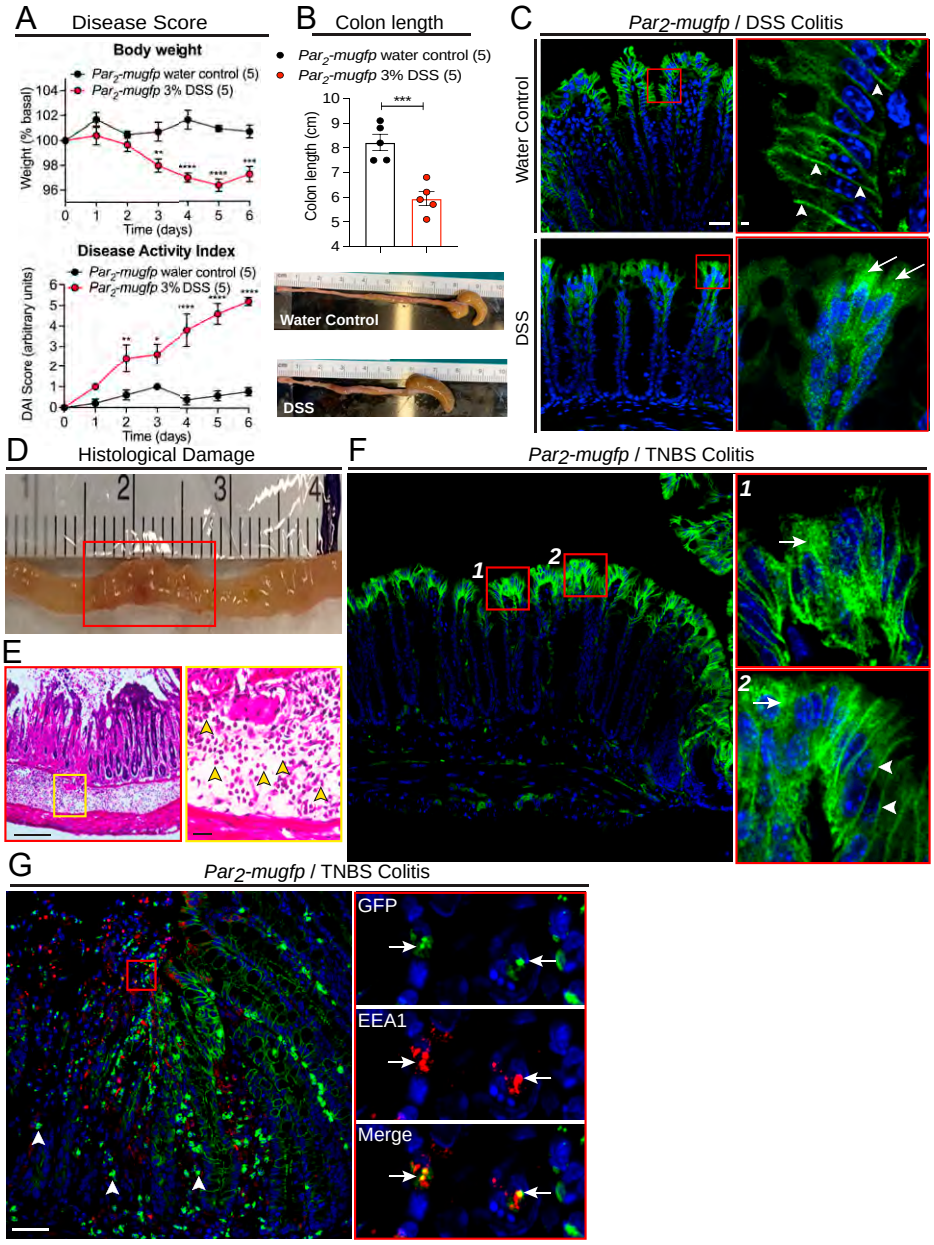

Fig. 4. Colitis-evoked endocytosis of PAR_2.muGFP. (*A–C*) DSS colitis in *Par$_2$-mugfp* mice. (*A*) Body weight and disease activity index (DAI) after DSS or water (control). (*B*) Colon length after DSS or water. Mean ± SEM, $n = 5$ mice. *$P < 0.05$, **$P < 0.01$, ***$P < 0.001$, and ****$P < 0.0001$ compared to water, two-way ANOVA, Tukey's test (*A*), and Student's *t* test (*B*). (*C*) Redistribution of PAR_2-muGFP from the plasma membrane (arrowheads) to endosomes (arrows) after DSS. (*D–F*) TNBS colitis in *Par$_2$-mugfp* mice. (*D*) Grossly inflamed colon. (*E*) Histological sections showing infiltration of neutrophils in the submucosa (yellow arrowheads). (*F*) Redistribution of PAR_2-muGFP from the plasma membrane to endosomes after TNBS. (*G*) Localization of PAR_2-muGFP in infiltrating immune cells (arrowheads) and colocalization of GFP and EEA1 in colonocytes (arrows). (Scale bars, 10 μm.) Representative images and independent experiments are shown ($n = 5$ mice).

2F-stimulated inflammation and nociception. The pronociceptive response to intracolonic 2F was similar in *Par$_2$-mugfp* and wild-type mice but was attenuated in *Par$_2$Na$_v$1.8* mice that lack PAR_2 in $Na_v1.8$-positive nociceptors (7) (Fig. 8 *I* and *J*). These results implicate PAR_2 on $Na_v1.8$-positive neurons in colonic pain and are in line with our report that proteases induce somatic nociception by activating PAR_2 on $Na_v1.8$ neurons (7). The intraplanar injection of trypsin (140 nM, 10 μL) induced mechanical allodynia to a similar degree in the ipsilateral paw but not contralateral paw of *Par$_2$-mugfp* and wild-type mice (*SI Appendix*, Fig. S9 *A* and *B*). Mechanical allodynia was significantly attenuated in *Par$_2^{-/-}$* mice, confirming a role for PAR_2.

IL-8 is proinflammatory cytokine that is released by colonocytes (40). To examine whether PAR_2 evokes inflammation of the human colon, we incubated explants of normal human colonic mucosa with 2F (10 μM, 4 h) and measured IL-8 release into culture medium. 2F stimulated IL-8 release (Fig. 8*K*). Preincubation of explants with dyngo4a (30 μM), a Dnm inhibitor, blocked PAR_2-mediated IL-8 release.

These results suggest that PAR_2 agonists increase paracellular permeability, stimulate cytokine and chemokine release from colonocytes, and sensitize colonic nociceptors. These proinflammatory and pronociceptive actions require Dnm-mediated endocytosis of PAR_2.

Discussion

Although proteases and PAR_2 are implicated in inflammatory diseases, the impact of inflammation on the subcellular distribution and function of PAR_2 has not been investigated. The use of knockin mice expressing PAR_2 fused to muGFP allowed examination of the effects of inflammation on the subcellular trafficking of PAR_2 with high resolution. We detected a major redistribution of PAR_2 from the basolateral membrane to early endosomes of colonocytes in two preclinical models of IBD, which is likely due to increased proteolytic activity in the inflamed colon. By using BRET to probe the formation and composition of PAR_2 signaling complexes, we found that agonists induce the assembly of signalosome comprising PAR_2 and $G\alpha_i$, $G\alpha_q$ or βARR1/2 in colonic epithelial cells. Our results suggest that Dnm2-mediated endocytosis of PAR_2 in the colon is necessary for paracellular permeability, generation of proinflammatory cytokines and chemokines, and sensitization of colonic nociceptors (Fig. 7*E*).

PAR_2 Localization and Trafficking. Mice expressing fluorescent opioid receptors have been extensively used to analyze tissue distribution and the effects of endogenous agonists and drugs on receptor trafficking (41, 42). The use of knockin mice in which *Par₂* was replaced by *Par₂-mugfp* enabled specific and high-resolution analysis of the tissue distribution and subcellular trafficking of PAR_2 in inflamed tissues. Fusion of muGFP did not affect PAR_2 signaling and trafficking in cell lines, and mRNA encoding *Par₂-mugfp* was expressed at similar levels to endogenous *Par₂* in most regions of the digestive tract and sensory ganglia. PAR_2 agonists induced comparable somatic and visceral nociception in *Par₂-mugfp* and wild-type mice. These findings suggest that PAR_2-muGFP functions normally. Within the digestive tract, PAR_2-muGFP immunoreactivity was prominently localized to the basolateral plasma membrane of epithelial cells lining the small and large intestine. RNAScope using probes to *F2rl1* and *Gfp* confirmed expression by enterocytes and colonocytes. The lack of GFP immunoreactivity and mRNA in wild-type mice verified selectivity. The detection of PAR_2 in intestinal epithelial cells confirms reports using receptor antibodies and functional assays (27, 43).

Detection of PAR_2 in DRG neurons required the sensitivity of RNAScope in situ hybridization, which revealed expression in a subset of neurons, in agreement with other reports (7, 44). The activation of PAR_2 in DRG nociceptors stimulates the release of substance P and calcitonin gene–related peptide, which mediate neurogenic inflammation in peripheral tissues and the central transmission of pain (28, 29). Proteases may cause pain in the colon directly by activating PAR_2 on nociceptors or indirectly by activating PAR_2 on colonocytes and stimulating release of pronociceptive factors. The observation that deletion of PAR_2 from $Na_v1.8$ neurons blunts colonic nociception supports a primary role for neuronal PAR_2. Deletion of *Par₂* from $Na_v1.8$ neurons also attenuates protease-evoked somatic nociception (7, 44).

The identity of the proteases that activate PAR_2 and stimulate endocytosis was not addressed in the current study. Protease probes and proteomics have been used to identify serine and cysteine proteases that are activated in the colon of mice with colitis and patients with IBD (20–25). These include proteases from immune cells [e.g., neutrophil elastase and cathepsin S (20–22)], proteases from colonocytes [e.g., trypsins (45)], and proteases from the microbiome. An understanding of whether PAR_2 is principally expressed at the apical or basolateral membrane of intestinal epithelial cells has implications for mechanisms of activation. Luminal proteases from epithelial cells, exocrine glands, or colonic bacteria could activate apical PAR_2, whereas proteases from mucosal immune or epithelial cells could activate PAR_2 at the basolateral membrane. Our finding of predominant basolateral expression is consistent with reports that basolateral, but not apical, application of PAR_2 agonists increases paracellular permeability (43), although PAR_2 has also been detected at the apical membrane (27).

PAR_2 Signaling Complexes. We studied the intracellular trafficking of PAR_2 in colon-derived epithelial cells (T84) and model cell lines (HEK293T) by using BRET to assess the proximity of PAR_2 to subcellular markers and confocal microscopy to localize PAR_2. Our results show that trypsin and 2F deplete PAR_2 from the plasma membrane and induce accumulation in early endosomes, which were identified using several markers (Rab5a, EEA1, FYVE, and CellLights RFP). Dominant-negative DnmK44A, knockdown of Dnm2 (the principal isoform of T84 cells and colonocytes), and hypertonic sucrose blunted endocytosis of PAR_2, suggesting a major role for Dnm2. We did not detect PAR_2 in Rab7a-positive late endosomes, possibly due to receptor degradation. 2F, but not trypsin, increased the BRET signal for PAR_2 in the *cis*-Golgi and stimulated a transient decrease and then a sustained increase in the BRET signal in the *trans*-Golgi. The differential effects of 2F and trypsin likely relate to their different mechanisms of PAR_2 activation. Agonist-evoked depletion of PAR_2 from the *trans*-Golgi is consistent with our studies showing that proteases induce Gβγ- and protein kinase D–dependent mobilization of PAR_2 from the Golgi apparatus to the plasma membrane (34, 35). Agonist-evoked translocation of PAR_2 from the plasma membrane to the Golgi apparatus was not prominent, because we detected PAR_2-muGFP in early endosomes, but not the Golgi apparatus.

Several observations support the hypothesis that PAR_2 agonists induce assembly of a PAR_2 signaling complex with Gα or βARR in early endosomes of T84 and HEK293T cells. ebBRET revealed that 2F and trypsin stimulated the recruitment of $G\alpha_q$, $G\alpha_i$, and βARR2 to early endosomes. NbBRET, a split luciferase BRET assay that allows simultaneous measurements of proximity between PAR_2, an effector (Gα, βARR), and an early endosomal marker, confirmed agonist-evoked recruitment of receptor and effector to early endosomes. Dominant-negative DnmK44A, Dnm2 siRNA, and hypertonic sucrose inhibited the recruitment of PAR_2, $G\alpha_q$, $G\alpha_i$, and βARR1/2 to endosomes. We also detected PAR_2, full-length $G\alpha_q$, and βARR in endosomes by microscopy. Further experiments are needed to determine whether a PAR_2, Gα, and βARR megaplex forms in endosomes. It remains to be determined whether the complex traffics from the plasma membrane to endosomes or PAR_2 recruits Gα and βARR to endosomes. Because GPCRs can form megaplexes with Gα and βARR, the former possibility is more likely. A limitation of our work is that we did not investigate the signals that emanate from internalized PAR_2. We have previously reported that PAR_2 in endosomes regulates kinases (MEKK1 and ERK1/2) in certain subcellular compartments (3, 7). The endosomal complex was stable during the period of measurement (1,200 s), which might give rise to sustained signals in subcellular compartments that control critical functions of colonocytes, including tight junction assembly and release or proinflammatory and pronociceptive factors. Our results do not exclude the possibility that PAR_2 signals from other organelles, such as the Golgi apparatus, as is the case for thyroid-stimulating hormone receptors and opioid receptors (10, 11). Proteases of late endosomes, including cathepsin S and legumain, can activate PAR_2 even in acidic conditions, which could facilitate receptor activation in other subcellular compartments (17, 22). However, the most parsimonious explanation of our results is that signalosomes comprising PAR_2 and $G\alpha_q$, $G\alpha_i$, or βARR1/2 assemble predominantly in early endosomes.

Endosomal PAR_2 Signaling, Colonic Inflammation, and Pain. Our results suggest that endosomal signaling of PAR_2 in the colon increases paracellular permeability and evokes secretion of cytokines and chemokines, which would be expected to amplify

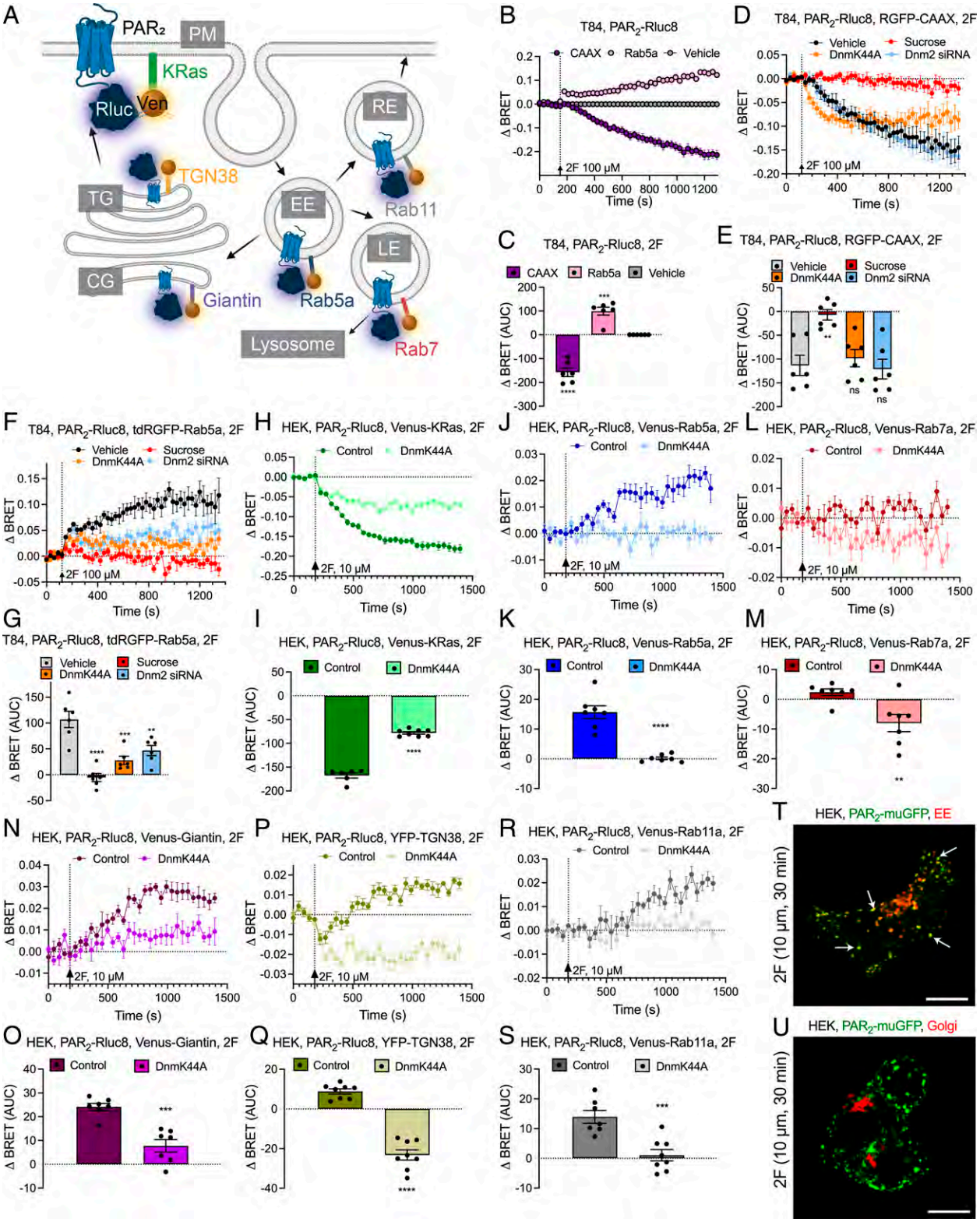

Fig. 5. PAR_2 trafficking to endosomes. (*A*) BRET assays of the proximity between PAR_2-Rluc8 and Venus- or YFP-tagged proteins resident to plasma membrane (PM; CAAX or KRas), early endosomes (EE; Rab5a), late endosomes (LE; Rab7a), recycling endosomes (RE; Rab11a), *cis*-Golgi (CG; giantin), or *trans*-Golgi (TG; TGN38). (*B–G*) Effects of 2F (100 μM) on translocation of PAR_2-Rluc8 from the plasma membrane (RGFP-CAAX) to early endosomes (tdRGFP-Rab5a) of T84 cells treated with vehicle, hypertonic sucrose, or DnmK44A or Dnm2 siRNA. (*H–S*) Effects of 2F (10 μM) on translocation of PAR_2-Rluc8 from the plasma membrane [KRas-Venus (*H* and *I*)] to early endosomes [Rab5a-Venus (*J* and *K*)], late endosomes [Rab7a-Venus (*L* and *M*)], *cis*-Golgi [giantin-Venus (*N* and *O*)], *trans*-Golgi [TGN38-YFP (*P* and *Q*)], and recycling endosomes [Rab11-Venus (*R* and *S*)] in HEK293T cells. Cells were transfected with DnmK44A or untransfected (control). AUC, area under the curve. Mean ± SEM; n = 6–11 independent experiments. $^{**}P < 0.01$, $^{***}P < 0.001$, and $^{****}P < 0.0001$, one-way ANOVA or Tukey's test. (*T* and *U*) Localization of PAR_2-muGFP and CellLight markers of early endosomes (*T*) and the Golgi complex (*U*) in HEK293T cells. Arrows denote colocalization of PAR_2-muGFP and marker of early endosomes. Representative images of n = 5 experiments are shown. (Scale bars, 10 μm.)

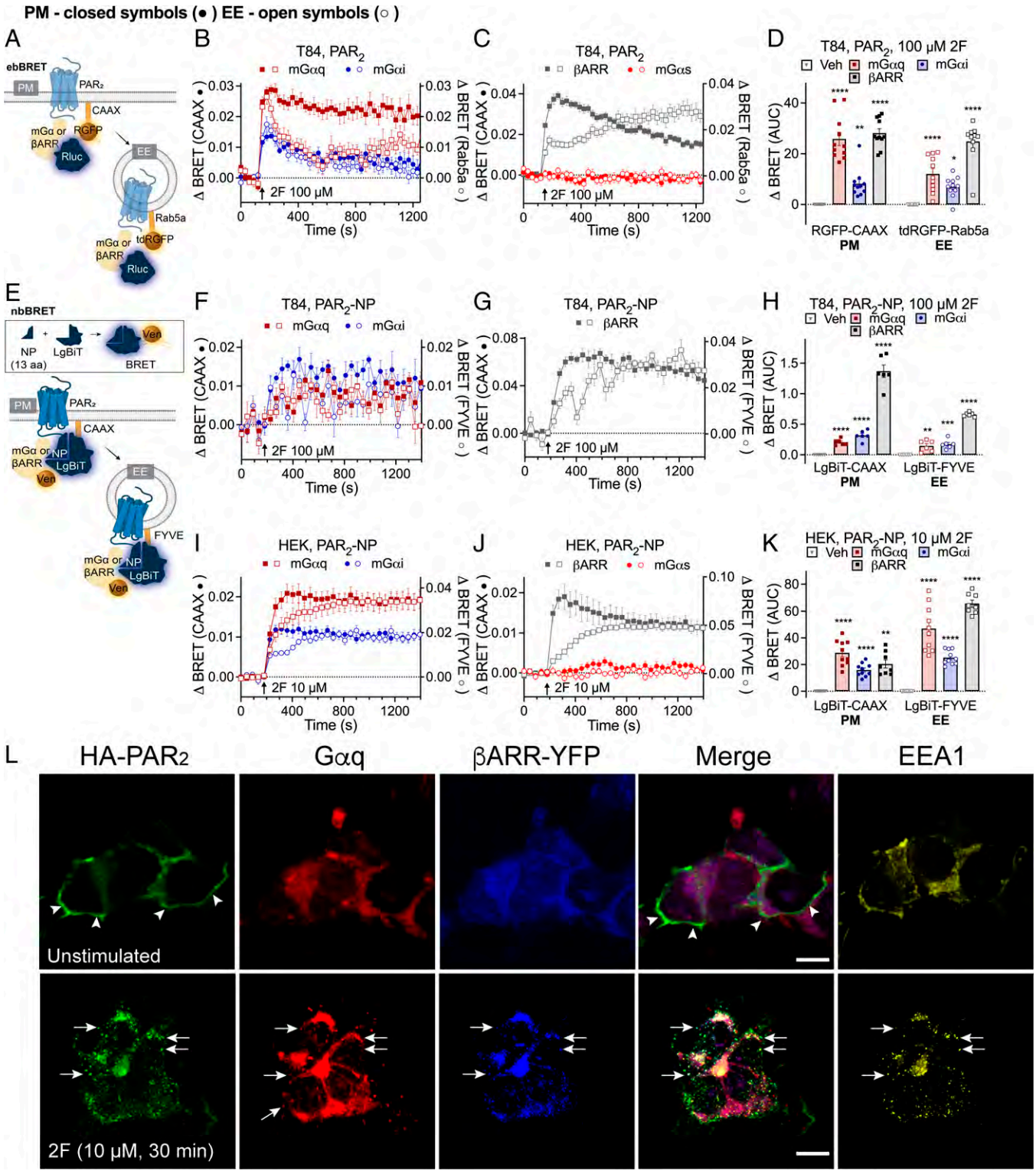

Fig. 6. PAR_2, Gα and βARR signalosome assembly in endosomes. (*A*) EbBRET assays of proximity between effector (Gα; βARR) and proteins resident to plasma membrane (PM; CAAX) or early endosomes (EE; Rab5a). (*B–D*) Effects of 2F (100 μM) on the recruitment of $mG\alpha_{sq}$, $mG\alpha_{si}$, (*B*) βARR2 or $mG\alpha_s$ negative control (*C*) to the plasma membrane (RGFP-CAAX, left axis, closed symbols) or early endosomes (tdRGFP-Rab5a, right axis, open symbols) of T84 cells, and (*D*) area under the curve (AUC). (*E*) NbBRET uses luciferase split into two fragments to detect BRET between receptor and effector (PAR_2 and mGα or βARR) for proteins resident to the PM (CAAX) or early endosomes (FYVE). (*F–H*) Effects of 2F (100 μM) on recruitment of $mG\alpha_{sq}$, $mG\alpha_{si}$ (*F*) or βARR1 (*G*) to the plasma membrane (LgBiT-CAAX) or early endosomes (LgBiT-FYVE) of T84 cells, and (*H*) AUC. (*I–K*) Effects of 2F (10 μM) on recruitment of $mG\alpha_{sq}$, $mG\alpha_{si}$ (*I*), βARR1 or $mG\alpha_s$ (*J*) to the PM (LgBiT-CAAX) or early endosomes (LgBiT-FYVE) of HEK293T cells. (*K*) AUC. Mean ± SEM. n = 6–11 independent experiments. $^*P < 0.05$, $^{**}P < 0.01$, $^{***}P < 0.001$, and $^{****}P < 0.0001$. (*D* and *K*) One-way ANOVA with Dunnett's (*D*) or Holm–Šidák's (*K*) test compared to vehicle. (*H*) Unpaired *t* test. (*L*) Localization of immunoreactive HA-PAR_2, $G\alpha_q$ and EEA1 plus YFP-βARR1 and YFP-βARR2 in HEK293T cells. Cells were unstimulated or incubated with 2F (10 μM, 30 min). Arrowheads, plasma membrane. Arrows, colocalization of HA-PAR_2, $G\alpha_q$ and YFP-βARR1 + 2 in EEA1-positive early endosomes. (Scale bars, 10 μm.) Representative images from $n = 5$ experiments are shown.

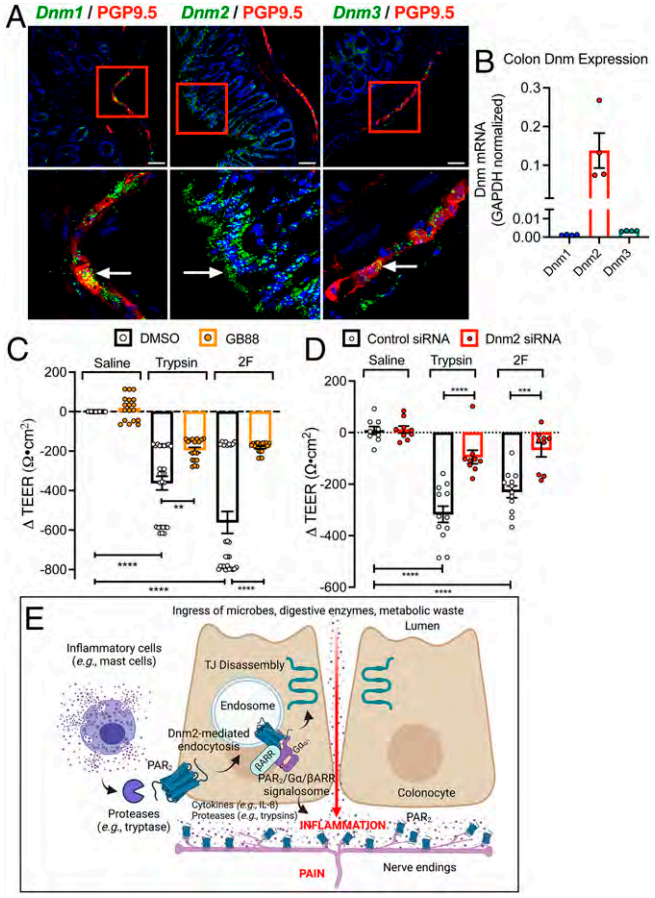

Fig. 7. PAR_2 endosomal signaling and colonic inflammation and pain. (*A*) Localization of *Dnm1-3* in mouse colon by RNAScope in situ hybridization. (Scale bars, 50 μm.) Representative images, independent experiments, $n = 3$ mice. (*B*) Expression of *Dnm1-3* in mouse colon by qRT-PCR. $n = 4$ mice. (*C*) Effects of trypsin (100 nM), 2F (10 μM), or vehicle (saline, control) on TEER of T84 cells after 6 h. Cells were preincubated with GB88 (PAR_2 antagonist) or vehicle (DMSO, control). (*D*) Effects of trypsin (100 nM), 2F (10 μM), or vehicle (saline, control) on TEER of T84 cells after 5 h. Cells were preincubated with Dnm2 or control siRNA. Mean ± SEM. $^{**}P < 0.01$, $^{***}P < 0.001$, and $^{****}P < 0.0001$ by one-way ANOVA, Tukey's test, or Student's *t* test. (*E*) Proposed mechanism by which proteases (e.g., tryptase) from mucosal inflammatory cells (e.g., mast cells) activate PAR_2 at the basolateral membrane of colonocytes to evoke PAR_2 endocytosis and assembly of a PAR_2, Gα, and βARR signalosome in endosomes. Endosomal signaling causes disassembly of tight junctions (TJ) and release of proinflammatory cytokines (e.g., IL-8) and possibly proteases (e.g., trypsins) from colonocytes. The ingress of microbes, proteases, and metabolites from the colonic lumen, and the release of cytokines and proteases from colonocytes, cause inflammation and pain. Proteases activate PAR_2 on nociceptive terminals in the colon to cause pain.

inflammation. In two preclinical mouse models of IBD, PAR_2 was depleted from the basolateral plasma membrane of colonocytes and prominently detected in cytosolic vesicles, including early endosomes. The proteolytic environment of the inflamed intestine is likely to activate PAR_2 and trigger endocytosis and sustained endosomal signaling. In health, tight junctions between colonocytes maintain a barrier that prevents the ingress of macromolecules and microbes from the colonic lumen into the mucosa, which protects against inflammation. Disruption of the barrier would be expected to promote inflammation. When applied to the basolateral surface, trypsin and 2F decreased electrical resistance of polarized monolayers of T84 cells, consistent with a loss of barrier function. The finding that a PAR_2 antagonist and Dnm2 siRNA inhibited this effect suggests a major role for PAR_2 endocytosis and endosomal signaling in redistribution of tight junctional proteins and loss of barrier function. We previously reported that PAR_2 agonists, including mast cell tryptase, stimulate a redistribution of ZO1 and occludin from tight junctions of T84 cells by a mechanism that involves βARRs, MEKK1, and ERK1/2 (26), in line with a role for endosomal signaling of PAR_2 in this process. The observations that Dnm2 knockdown inhibited agonist-induced endocytosis of PAR_2-muGFP in colonocytes and prevented release or proinflammatory cytokines and chemokines in vivo, and that a Dnm inhibitor blocked PAR_2-stimulated secretion of IL-8 from biopsy specimens of human colon, further support a role for PAR_2 endocytosis in colitis. Dnm2 knockdown also abrogated 2F-evoked colonic hyperalgesia, a finding that could be secondary to reduced release from colonocytes of cytokines or proteases that sensitize nociceptors. Because deletion of PAR_2 from $Na_V1.8$-positive neurons blunted 2F-evoked colonic hyperalgesia, the latter is likely. The identity of colonocyte-derived proteases remains to be determined, although colonocytes express isoforms of trypsin that activate PAR_2 (45). Further studies are required to ascertain whether endocytosis is necessary for other actions of PAR_2 in the intestine, such as inflammation associated with bacterial proteolysis and food allergies (46).

Our findings support the hypothesis that proteases in the inflamed colon evoke the assembly of a PAR_2 complex with Gα or βARR in endosomes (Fig. 7*E*). Signals that emanate from this complex disrupt tight junctions and promote release of proinflammatory factors that drive inflammation and pain. The influx of proteases from the colonic lumen could further amplify PAR_2-mediated inflammation and pain. Therapeutic targeting of PAR_2 in endosomes, which might be achieved using lipidated antagonists (7) or endosomally targeted nanoparticles (8), could restrict endosomal signaling and ameliorate IBD and other inflammatory and painful diseases associated with enhanced proteolysis and PAR_2 activation.

Materials and Methods

See *SI Appendix* for details.

Animals. The institutional animal care and use committees of New York University and Monash University approved studies of mice.

***Par_2-mugfp* Mice.** A segment of genomic DNA containing exon 2 of mouse *Par_2* (*F2rl1*) was subcloned from a genomic bacterial artificial chromosome (BAC). The *Par_2-mugfp* gene was synthesized by fusing muGFP to the 3′ end of exon 2. The targeting construct comprised *Par_2-mugfp*, a phosphoglycerine kinase neomycin cassette flanked by loxP sites. The targeting vector was electroporated into C57BL/6J embryonic stem cells. Clones were screened by Southern blotting, sequenced, and injected into mouse blastocysts. Chimeras were bred with wild-type female mice to generate black F1 progeny. Expression of *Par_2-mugfp* was confirmed by Southern blotting and PCR.

qRT-PCR. cDNA was amplified with primers shown in *SI Appendix*, Table S1.

Immunofluorescence. PAR_2-muGFP was localized using a GFP antibody. Endosomes were detected using EEA1 and Rab7a antibodies, and the plasma membrane was identified using E-cadherin antibodies. Neurons were identified using antibodies to NeuN or PGP9.5.

RNAScope In Situ Hybridization. Probes to *F2rl1*, *Gfp*, and *Dnm* isoforms were used for in situ hybridization (*SI Appendix*, Table S1).

Ex Vivo PAR_2 Trafficking. Colon segments were incubated with trypsin, 2F, or vehicle. PAR_2-muGFP was detected by GFP immunofluorescence.

Colitis-Induced PAR_2 Trafficking. Mice were treated with DSS or TNBS to evoke colitis.

Nociception. Investigators were blinded to treatments and genotypes. PAR_2 agonists were administered into the colon or paw. Abdominal or paw withdrawal thresholds von Frey filaments were assessed.

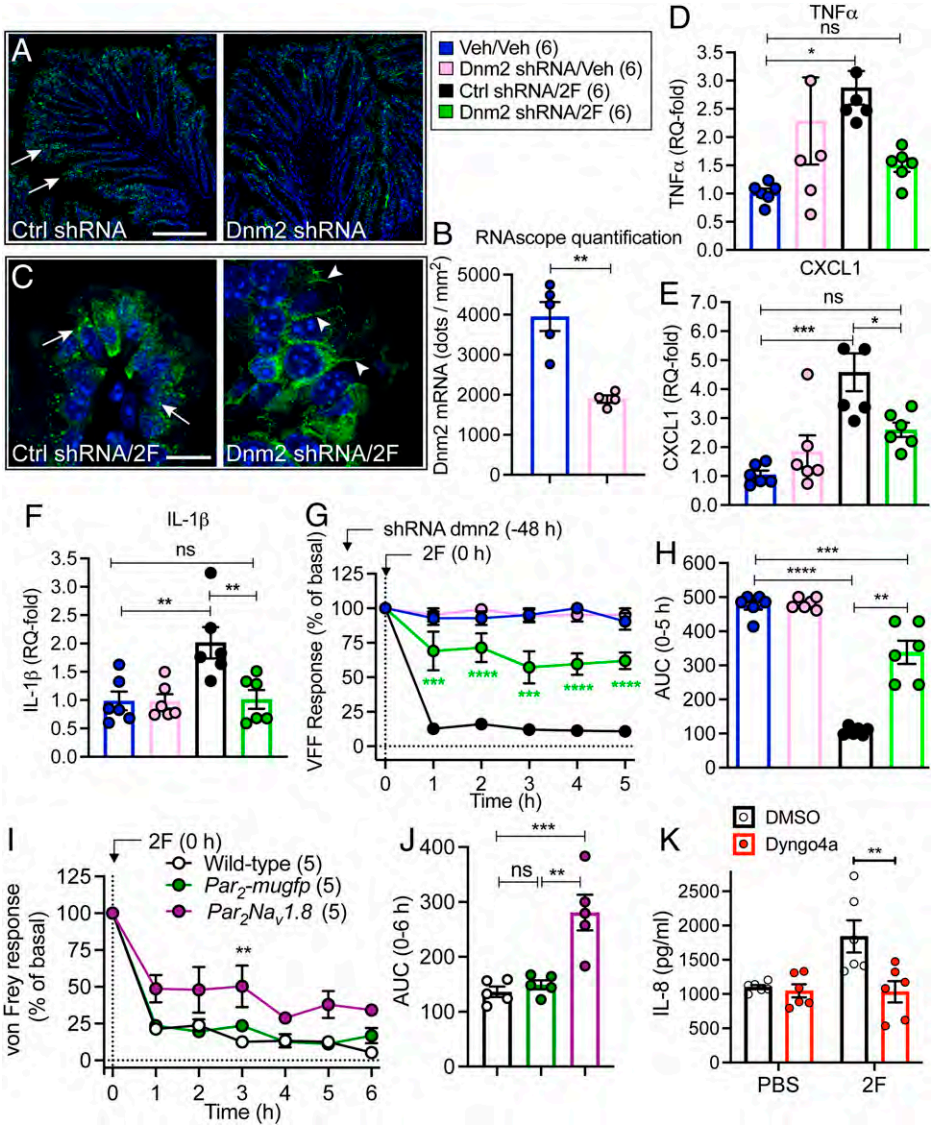

Fig. 8. Contribution of Dnm2 to PAR_2-evoked inflammation and pain in the colon. (*A–H*) Dnm2 or control (Ctrl) shRNA was administered to *Par_2-mugfp* mice by intracolonic injection. Mice were studied after 48 h. (*A*) Localization of *Dnm2* by RNAScope. Representative images are shown. (Scale bars, 100 μm.) (*B*) Quantification of *Dnm2* in the colon. (*C*) Localization of GFP immunoreactivity in the colon at 5 h after intracolonic injection of 2F. Arrows denote endosomes; arrowheads denote cell surface. (Scale bars, 10 μm.) (*A–C*) $n = 5$ mice. (*D–F*) Levels of TNF-α (*D*), CXCL1 (*E*), and IL-1β (*F*) in the colon 5 h after intracolonic injection of 2F. (*G* and *H*) Abdominal von Frey filament withdrawal responses 1–5 h after intracolonic injection of 2F. (*G*) Time course. (*H*) Area under the curve (AUC) from 0 to 5 h. (*D–H*) $n = 6$ mice. (*I* and *J*) Abdominal von Frey filament withdrawal responses of wild-type, *Par_2-mugfp*, and *$Par_2Na_v1.8$* mice 1–6 h after intracolonic injection of 2F. (*I*) Time course. (*J*) Area under curve from 0 to 6 h. $n = 5$ mice. (*K*) Effects of 2F (10 μM) on IL-8 release from explants of human colonic mucosa. Explants were preincubated with dyngo4a or vehicle (DMSO, control). Mean ± SEM; $n = 6$. (*B*) $^{**}P < 0.01$ by Student's *t* test. (*D–J*) $^{*}P < 0.05$, $^{**}P < 0.01$, $^{***}P < 0.001$, and $^{****}P < 0.0001$ by one- and two-way ANOVA or Tukey's test. (*K*) $^{**}P < 0.01$ by Student's *t* test.

In Vivo shRNA Dnm2 Knockdown. Dnm2shRNA or control shRNA was administered into the colon. PAR_2 endocytosis, expression of cytokines and chemokines, and nociception were studied.

Cell Lines, cDNA, and Transfection. Complementary DNA (cDNA) encoding BRET biosensors for PAR_2, mGα, βARR1/2, markers of the plasma membrane, endosomes, and the Golgi apparatus were transfected into T84 cells using Lipofectamine 3000 and into HEK293T cells using PEI. Dominant-negative DnmK44A or Dnm2 or control siRNA (*SI Appendix*, Table S1) was similarly transfected.

PAR_2-muGFP Signaling. KNRK cells expressing PAR_2-muGFP or PAR_2-HA11 were stimulated with PAR_2 agonists, and IP-1 formation was measured.

PAR_2-muGFP Signaling. HEK293T cells expressing PAR_2-muGFP and CellLight organelle markers were challenged with PAR_2 agonists and examined by confocal microscopy.

Trafficking of PAR_2, βARR, and $G\alpha_q$. HEK293T cells stably expressing FLAG-PAR_2-HA were transfected with YFP-βARR1 plus YFP-βARR2. Cells were challenged with PAR_2 agonists, and then PAR_2, $G\alpha_q$, and EEA1 were localized by immunofluorescence and confocal microcopy.

BRET Assays. T84 or HEK293T cells were preincubated with luciferase substrates and challenged with PAR_2 agonists, and BRET was measured using a luminometer.

T84 TEER. T84 cells were cultured on Transwell inserts until TEER was >2,000 Ω. PAR_2 agonists were added to the basolateral compartment, and TEER was measured at 0 and 6 h. GB88 or vehicle was added to the basolateral and apical compartments 30 min before PAR_2 agonists. Dnm2 siRNA or control siRNA and Lipofectamine 3000 were added to both compartments overnight before PAR_2 agonists.

IL-8 Secretion from Human Colonic Mucosa. Institutional review board approval was waived since no patient-identifiable information was obtained. IL-8 secretion was measured by enzyme-linked immunosorbent assay (ELISA) from isolated segments of colonic mucosa collected from patients undergoing resection for treatment of colon cancer.

Statistics. Data are presented as mean ± SEM. Differences were assessed using Student's *t* test for two comparisons and one- or two-way ANOVA and Tukey's, Dunnett's, or Šidák's post hoc test for multiple comparisons. $P < 0.05$ was considered significant at the 95% confidence level.

Data Availability. All study data are included in the article and/or *SI Appendix*.

ACKNOWLEDGMENTS. This study was supported by grants from the NIH (NS102722, DE026806, DK118971, and DE029951 to N.W.B. and B.L.S.), Department of Defense (W81XWH1810431 to N.W.B. and B.L.S.), National Health and Medical Research Council (63303 to N.W.B.), and Australian Research Council Centre of Excellence in Convergent Bio-Nano Science and Technology (N.W.B.). We thank S. O'Brien (University of Birmingham) for guidance with the nbBRET assay. Cartoons were made with BioRender.

1. M. Canals, D. P. Poole, N. A. Veldhuis, B. L. Schmidt, N. W. Bunnett, G-protein-coupled receptors are dynamic regulators of digestion and targets for digestive diseases. *Gastroenterology* **156**, 1600–1616 (2019).
2. Y. K. Peterson, L. M. Luttrell, The diverse roles of arrestin scaffolds in G protein-coupled receptor signaling. *Pharmacol. Rev.* **69**, 256–297 (2017).
3. K. A. DeFea *et al.*, Beta-arrestin-dependent endocytosis of proteinase-activated receptor 2 is required for intracellular targeting of activated ERK1/2. *J. Cell Biol.* **148**, 1267–1281 (2000).
4. R. Irannejad *et al.*, Conformational biosensors reveal GPCR signalling from endosomes. *Nature* **495**, 534–538 (2013).
5. D. D. Jensen *et al.*, Neurokinin 1 receptor signaling in endosomes mediates sustained nociception and is a viable therapeutic target for prolonged pain relief. *Sci. Transl. Med.* **9**, eaal3447 (2017).
6. N. N. Jimenez-Vargas *et al.*, Endosomal signaling of delta opioid receptors is an endogenous mechanism and therapeutic target for relief from inflammatory pain. *Proc. Natl. Acad. Sci. U.S.A.* **117**, 15281–15292 (2020).
7. N. N. Jimenez-Vargas *et al.*, Protease-activated receptor-2 in endosomes signals persistent pain of irritable bowel syndrome. *Proc. Natl. Acad. Sci. U.S.A.* **115**, E7438–E7447 (2018).
8. P. D. Ramírez-García *et al.*, A pH-responsive nanoparticle targets the neurokinin 1 receptor in endosomes to prevent chronic pain. *Nat. Nanotechnol.* **14**, 1150–1159 (2019).
9. R. E. Yarwood *et al.*, Endosomal signaling of the receptor for calcitonin gene-related peptide mediates pain transmission. *Proc. Natl. Acad. Sci. U.S.A.* **114**, 12309–12314 (2017).
10. A. Godbole, S. Lyga, M. J. Lohse, D. Calebiro, Internalized TSH receptors en route to the TGN induce local G_s-protein signaling and gene transcription. *Nat. Commun.* **8**, 1–15 (2017).
11. M. Stoeber *et al.*, A genetically encoded biosensor reveals location bias of opioid drug action. *Neuron* **98**, 963–976 (2018).
12. V. S. Ossovskaya, N. W. Bunnett, Protease-activated receptors: Contribution to physiology and disease. *Physiol. Rev.* **84**, 579–621 (2004).
13. S. K. Bohm *et al.*, Molecular cloning, expression and potential functions of the human proteinase-activated receptor-2. *Biochem. J.* **314**, 1009–1016 (1996).
14. C. U. Corvera *et al.*, Mast cell tryptase regulates rat colonic myocytes through proteinase-activated receptor 2. *J. Clin. Invest.* **100**, 1383–1393 (1997).
15. E. Camerer, W. Huang, S. R. Coughlin, Tissue factor- and factor X-dependent activation of protease-activated receptor 2 by factor VIIa. *Proc. Natl. Acad. Sci. U.S.A.* **97**, 5255–5260 (2000).
16. K. Oikonomopoulou *et al.*, Proteinase-activated receptors, targets for kallikrein signaling. *J. Biol. Chem.* **281**, 32095–32112 (2006).
17. N. H. Tu *et al.*, Legumain induces oral cancer pain by biased agonism of protease-activated receptor-2. *J. Neurosci.* **41**, 193–210 (2021).
18. P. Zhao *et al.*, Cathepsin S causes inflammatory pain via biased agonism of PAR2 and TRPV4. *J. Biol. Chem.* **289**, 27215–27234 (2014).
19. P. Zhao *et al.*, Neutrophil elastase activates protease-activated receptor-2 (PAR2) and transient receptor potential vanilloid 4 (TRPV4) to cause inflammation and pain. *J. Biol. Chem.* **290**, 13875–13887 (2015).
20. B. M. Anderson *et al.*, Application of a chemical probe to detect neutrophil elastase activation during inflammatory bowel disease. *Sci. Rep.* **9**, 13295 (2019).
21. N. Barlow *et al.*, Demonstration of elevated levels of active cathepsin S in dextran sulfate sodium colitis using a new activatable probe. *Neurogastroenterol. Motil.* **27**, 1675–1680 (2015).
22. F. Cattaruzza *et al.*, Cathepsin S is activated during colitis and causes visceral hyperalgesia by a PAR2-dependent mechanism in mice. *Gastroenterology* **141**, 1864–1874 (2011).
23. G. S. Cottrell *et al.*, Protease-activated receptor 2, dipeptidyl peptidase I, and proteases mediate Clostridium difficile toxin A enteritis. *Gastroenterology* **132**, 2422–2437 (2007).
24. A. Denadai-Souza *et al.*, Functional proteomic profiling of secreted serine proteases in health and inflammatory bowel disease. *Sci. Rep.* **8**, 7834 (2018).
25. K. K. Hansen *et al.*, A major role for proteolytic activity and proteinase-activated receptor-2 in the pathogenesis of infectious colitis. *Proc. Natl. Acad. Sci. U.S.A.* **102**, 8363–8368 (2005).
26. C. Jacob *et al.*, Mast cell tryptase controls paracellular permeability of the intestine. Role of protease-activated receptor 2 and beta-arrestins. *J. Biol. Chem.* **280**, 31936–31948 (2005).
27. W. Kong *et al.*, Luminal trypsin may regulate enterocytes through proteinase-activated receptor 2. *Proc. Natl. Acad. Sci. U.S.A.* **94**, 8884–8889 (1997).
28. M. Steinhoff *et al.*, Agonists of proteinase-activated receptor 2 induce inflammation by a neurogenic mechanism. *Nat. Med.* **6**, 151–158 (2000).
29. N. Vergnolle *et al.*, Proteinase-activated receptor-2 and hyperalgesia: a novel pain pathway. *Nat. Med.* **7**, 821–826 (2001).
30. N. Cenac *et al.*, Proteinase-activated receptor-2-induced colonic inflammation in mice: Possible involvement of afferent neurons, nitric oxide, and paracellular permeability. *J. Immunol.* **170**, 4296–4300 (2003).
31. D. J. Scott *et al.*, A novel ultra-stable, monomeric green fluorescent protein for direct volumetric imaging of whole organs using CLARITY. *Sci. Rep.* **8**, 667 (2018).
32. A. R. B. Thomsen, D. D. Jensen, G. A. Hicks, N. W. Bunnett, Therapeutic targeting of endosomal G-protein-coupled receptors. *Trends Pharmacol. Sci.* **39**, 879–891 (2018).
33. C. Jacob *et al.*, c-Cbl mediates ubiquitination, degradation, and down-regulation of human protease-activated receptor 2. *J. Biol. Chem.* **280**, 16076–16087 (2005).
34. D. D. Jensen *et al.*, Protein kinase D and Gβγ subunits mediate agonist-evoked translocation of Protease-activated Receptor-2 from the Golgi apparatus to the plasma membrane. *J. Biol. Chem.* **291**, 11285–11299 (2016).
35. P. Zhao *et al.*, Protein kinase D and Gβγ mediate sustained nociceptive signaling by biased agonists of Protease-Activated Receptor-2. *J. Biol. Chem.* **294**, 10649–10662 (2019).
36. A. H. Nguyen *et al.*, Structure of an endosomal signaling GPCR-G protein-β-arrestin megacomplex. *Nat. Struct. Mol. Biol.* **26**, 1123–1131 (2019).
37. A. R. B. Thomsen *et al.*, GPCR-G protein-β-arrestin super-complex mediates sustained G protein signaling. *Cell* **166**, 907–919 (2016).
38. A. S. Dixon *et al.*, NanoLuc complementation reporter optimized for accurate measurement of protein interactions in cells. *ACS Chem. Biol.* **11**, 400–408 (2016).
39. N. Cenac *et al.*, Induction of intestinal inflammation in mouse by activation of proteinase-activated receptor-2. *Am. J. Pathol.* **161**, 1903–1915 (2002).
40. D. D. Jensen *et al.*, Endothelin-converting enzyme 1 and β-arrestins exert spatiotemporal control of substance P-induced inflammatory signals. *J. Biol. Chem.* **289**, 20283–20294 (2014).
41. D. P. Poole *et al.*, Localization and regulation of fluorescently labeled delta opioid receptor, expressed in enteric neurons of mice. *Gastroenterology* **141**, 982–991 (2011).
42. G. Scherrer *et al.*, Knockin mice expressing fluorescent delta-opioid receptors uncover G protein-coupled receptor dynamics in vivo. *Proc. Natl. Acad. Sci. U.S.A.* **103**, 9691–9696 (2006).
43. N. Cenac *et al.*, PAR2 activation alters colonic paracellular permeability in mice via IFN-gamma-dependent and -independent pathways. *J. Physiol.* **558**, 913–925 (2004).
44. S. N. Hassler *et al.*, The cellular basis of protease-activated receptor 2-evoked mechanical and affective pain. *JCI Insight* **5**, e12793 (2020).
45. G. S. Cottrell, S. Amadesi, E. F. Grady, N. W. Bunnett, Trypsin IV, a novel agonist of protease-activated receptors 2 and 4. *J. Biol. Chem.* **279**, 13532–13539 (2004).
46. A. Caminero *et al.*, Duodenal bacterial proteolytic activity determines sensitivity to dietary antigen through protease-activated receptor-2. *Nat. Commun.* **10**, 1–14 (2019).

AMERICAN JOURNAL OF PHYSIOLOGY
GASTROINTESTINAL AND LIVER PHYSIOLOGY

Am J Physiol Gastrointest Liver Physiol 322: G201–G222, 2022.
First published November 10, 2021; doi:10.1152/ajpgi.00125.2021

MINI-REVIEW

Contributions of bile acids to gastrointestinal physiology as receptor agonists and modifiers of ion channels

Stephen J. Keely,[1]* Andreacarola Urso,[2,3]* Alexandr V. Ilyaskin,[4] Christoph Korbmacher,[4] Nigel W. Bunnett,[5,6] Daniel P. Poole,[7,8] and Simona E. Carbone[7,8]

[1]*Royal College of Surgeons in Ireland, Education and Research Centre, Beaumont Hospital, Dublin, Ireland;* [2]*Department of Surgery, Vagelos College of Physicians and Surgeons, Columbia University, New York, New York;* [3]*Department of Pharmacology, Columbia University, New York, New York;* [4]*Institute of Cellular and Molecular Physiology, Friedrich-Alexander University Erlangen-Nürnberg, Bavaria, Germany;* [5]*Department of Molecular Pathobiology, Neuroscience Institute, New York University, New York, New York;* [6]*Department of Neuroscience and Physiology, Neuroscience Institute, New York University, New York, New York;* [7]*Drug Discovery Biology, Monash Institute of Pharmaceutical Sciences, Monash University, Parkville, Victoria, Australia; and* [8]*Australian Research Council, Centre of Excellence in Convergent Bio-Nano Science and Technology, Monash Institute of Pharmaceutical Sciences, Monash University, Parkville, Victoria, Australia*

Abstract

Bile acids (BAs) are known to be important regulators of intestinal motility and epithelial fluid and electrolyte transport. Over the past two decades, significant advances in identifying and characterizing the receptors, transporters, and ion channels targeted by BAs have led to exciting new insights into the molecular mechanisms involved in these processes. Our appreciation of BAs, their receptors, and BA-modulated ion channels as potential targets for the development of new approaches to treat intestinal motility and transport disorders is increasing. In the current review, we aim to summarize recent advances in our knowledge of the different BA receptors and BA-modulated ion channels present in the gastrointestinal system. We discuss how they regulate motility and epithelial transport, their roles in pathogenesis, and their therapeutic potential in a range of gastrointestinal diseases.

bile acid; FXR; motility; secretion; TGR5

INTRODUCTION

Bile acids (BAs) are amphipathic steroidal molecules found as a major component of bile. BAs are synthesized in hepatocytes, stored in the gall bladder, and released into the small intestine in response to the ingestion of a meal. Classically, BAs are known for their roles in digestion through facilitating the solubilization of fatty acids, stimulating bile flow and intestinal motility, regulating glucose levels, and promoting cholesterol secretion and catabolism (1). BAs modulate their own synthesis, transport, and detoxification and aid in the maintenance of a healthy gut microbiome. Primary BAs, such as cholic acid (CA) and chenodeoxycholic acid (CDCA), are synthesized in the liver and the vast majority are conjugated (e.g., tauro-CA or glyco-CA) before their release into the ileum. In the terminal ileum, ~95% of released BAs are reabsorbed through the ileal BA transporter, IBAT (also known as apical sodium-dependent BA transporter, ASBT). BAs that are not reabsorbed in the ileum enter the colon where they undergo structural modifications catalyzed by anaerobic bacterial enzymes, such as 7α-dehydroxylase, to become secondary BAs (e.g., deoxycholic acid, DCA and lithocholic acid, LCA) (2).

Normally, the BAs are reabsorbed in the terminal ileum and are recycled back to the liver via the enterohepatic circulation. However, disruptions to the enterohepatic circulation, whether due to increased BA synthesis or defective reuptake in the small intestine, results in BA accumulation in the colon. When present at physiological levels, BAs act as important signaling molecules that exert their actions through specific receptors located on the cell surface and in the nucleus. However, given their amphipathic nature and detergent-like properties, increased levels of BAs in the colon can have deleterious effects on the lipid composition of cellular membranes in this region and exert cytotoxic and membranolytic effects (3, 4). Given the detergent-like properties of BAs, caution must be taken when interpreting studies where high concentrations of exogenous BAs have been used. Unless specifically assessed, any observed effects may be attributable to deleterious effects of BAs on the lipid composition of cellular membranes, receptor-mediated effects, or a combination of the two. In this review, we aim to summarize recent advances in the field of BA signaling in the gut

* S. J. Keely and A. Urso contributed equally to this work.
Correspondence: S. E. Carbone (Simona.Carbone@monash.edu).
Submitted 2 April 2021 / Revised 28 October 2021 / Accepted 8 November 2021

0193-1857/22 Copyright © 2022 the American Physiological Society.

Downloaded from journals.physiology.org/journal/ajpgi at New York Univ (216.165.095.084) on September 28, 2023.

with a particular emphasis on how they regulate transport function and motility, and consideration of the effects of physiological versus pathophysiological concentrations of BAs.

BILE ACID RECEPTORS

The discovery that BAs can act as transmitters and mediate cellular signaling processes has been a significant advancement to our understanding of how they exert their functional effects. BAs selectively activate a broad range of G protein-coupled receptors (GPCRs), nuclear receptors, and ion channels. Strategies that indirectly alter their actions at these sites are already used to treat a range of conditions. For example, modulation of luminal BA levels, either through sequestration or altered transport, is currently the main therapeutic approach to treat BA-associated disorders, such as cholestatic itch or gallstones. However, the potential for directly targeting BA-activated receptors and ion channels now offers additional opportunities for therapy. This review provides a summary of GPCRs, nuclear receptors, and ion channels that are influenced by BAs. It aims to contextualize how the distribution, functions, and regulation of BA receptors relate to gastrointestinal (GI) physiology and how their dysregulation is implicated in digestive disease and disorders.

BILE ACID INTERACTION WITH G PROTEIN-COUPLED RECEPTORS

GPCRs are dynamic signaling proteins that are mainly located on the cell surface. They enable cells to detect and respond to a diverse array of extracellular ligands and stimuli. It is now known that BAs can activate several distinct GPCRs, including established bona fide BA receptors (Takeda G protein-coupled receptor 5, TGR5), receptors that interact with BAs in addition to their primary orthosteric agonists (e.g., muscarinic receptors), and putative BA receptors (e.g., Mrgprs). A summary of the current findings is provided in Table 1, with a more detailed description listed in the following sections.

Takeda G Protein-Coupled Receptor 5

TGR5, also known as bile acid receptor, GPBA, GpBAR1, or M-BAR1 is activated by both primary and secondary BAs. TGR5 is G_s-coupled meaning activation of the receptor stimulates adenylyl cyclase to produce cAMP. TGR5 is expressed by a diverse range of cell types in tissues including, but not limited to, gastrointestinal, liver, brown adipose, skeletal muscle, and placental. Within the gastrointestinal tract, TGR5 is expressed by epithelia, enteroendocrine cell subsets, enteric neurons, enteric glia, smooth muscle, monocytes/macrophages, and extrinsic afferents (6, 27). The roles of TGR5 in intestinal motility and secretion will be discussed in detail throughout this review. TGR5 has additional signaling roles in many other gastrointestinal processes that have not been discussed here including inflammation and the development of cancers, and visceral pain (6, 28).

Mas-Related G Protein-Coupled Receptor X4

Mrgprs are a family of orphan GPCRs consisting of more than 50 members. There are several subfamilies, with mouse and human receptors characterized separately. For example, sensory neurons in the dorsal root ganglia (DRG) of mice express MRGPRA1, whereas the ortholog Mas-related G protein-coupled receptor X4 (MRGPRX4) is expressed in human tissues (29). Their contributions to sensation have not been fully characterized, but roles in nociception and itch have been identified. In patients with the gall bladder condition, primary biliary cholangitis, elevated levels of blood BAs are known to cause the symptom of cholestatic itch and BA sequestrants or IBAT inhibitors are used to treat the condition. However, when studying BA activation of the MRGPR family of receptors, interpretation of results may be complicated by differences in the responses of the mouse and human orthologs. For example, recent evidence from in vivo studies in transgenic mice indicates that BA-induced itch is not dependent on the expression of several Mrgprs. Mice lacking a cluster of Mrgpr genes (Mrgpr-cluster$^{-/-}$) exhibit itch in response to DCA in a similar manner to control mice (30). HEK cells transfected with the mouse ortholog MRGPRA1 do not respond to BAs as measured by Ca^{2+} signaling. In contrast, cells expressing the human MRGPRX4 are activated by BAs, and this is the only human receptor to respond (11). Similarly, mice expressing the humanized receptor demonstrate a greater itch response following acute injection of DCA or ursodeoxycholic acid (UDCA) compared with control mice. This same study showed that control mice responded comparably to both BAs, and this is evidence that a Mrgpr-mediated response may not involve activation of TGR5, since UDCA is a poor agonist for the latter receptor (11). It should be noted that longer administration of UDCA is used to treat pruritus associated with cholestasis, with suggested benefits such as stimulation of biliary BA excretion, replacement of the toxic endogenous BA pool, and stabilization of plasma membranes and cytoprotection of cholangiocytes (31).

In the context of the digestive system, the expression of Mrgprs has been described predominantly in primary afferent DRG neurons innervating the intestine. However, some studies have characterized mRNA expression in healthy or inflamed GI tissues. More specifically, expressions of MrgA4, MrgB2, MrgB8, MrgE, and MrgF have been demonstrated by immunohistochemistry in neurochemically defined subsets of enteric neurons (32–35). Activation of Mrgprs in cells such as mast cells could in turn activate closely associated primary afferent and sensory neurons through release of mediators including histamine and proteases. Mrgprs can interact with other cell surface receptors, such as transient receptor potential (TRP) channels to promote cellular responses (36). The relative importance of these interactions in the context of other BA-activated receptors and ion channels is not known. There are populations of primary afferent neurons innervating the gut wall that coexpress Mrgprs and TGR5. Given that both receptors are involved in histamine-independent itch pathways in the skin, this has led some researchers to postulate their function as a visceral "irritant sensing system," suggesting their contribution to pain and symptomology in irritable bowel syndrome (IBS) (6). In a recent study in mice by Castro et al., chronic visceral hypersensitivity (CVH) responses to colorectal distention were induced by intraluminal application of DCA, and agonists of MRGPRA3 and MRGPRC11. Whether DCA was acting on

Downloaded from journals.physiology.org/journal/ajpgi at New York Univ (216.165.095.084) on September 28, 2023.

Table 1. *Effects of BAs on G protein-coupled receptors and nuclear receptors*

Receptor	Bile Acid	Concentration	Tissue Preparation	Response	Effect	Solvent	Refs.
			G protein-coupled receptors				
TGR5 (GPR130, GpBAR1)	DCA OA	1–100 μM 100 μM	Proximal colon from *tgr5*-WT and KO mice	↑ WT KO only 100 μM at DCA	5-HT and CGRP from EC cells to stimulate peristaltic reflex	0.1% Ethanol, distilled water	(5)
	DCA TLCA CCDC	100 μM	DRG neurons innervating colon (mouse)	↑ ↑ ↑	Increased intracellular Ca^{2+} in subpopulations of neurons (%) DCA ∼20%, TLCA∼ 25%, CCDC∼30%	NA	(6)
	CCDC	100 μM, 100 μL rectal enema	Spinal cord (mouse)	↑	Phosphorylated MAP-kinase-ERK-1/2 immunoreactivity (pERK-IR) enhanced in response to colorectal distention	Saline	
	INT-777	10–100 μM	Proximal colon (mouse)	↑	Increased transepithelial resistance and reduced short circuit current, reduced with TTX or neuron-free preparation	DMSO	(7)
	UDCA	3–60 μM		-	Weak TGR5 agonist		
	LCA, DCA	10 and 30 μM	Enteroendocrine cell line, STC-1	↑	Promote GLP-1 secretion	DMSO	(8)
			Cells transfected withTGR5 siRNA	-	Reduced LCA responses at 10 and 30 μM		
			Cells transfected with TGR5 cDNA	↑	Increased LCA responses at 30 μM		
	Range of conjugated & unconjugated BAs	Concentration curve	COS-7 monkey kidney cells expressing human or rat TGR5	↑	Increased cAMP production rank order of potency LCA>DCA>CDCA UDCA and CA ∼20% efficacy at 10 μM	Modified Krebs-Ringer buffer	(9)
	UDCA	10 mM		-UDCA	GLP-1 and PYY release		
	BA mixture	Total BA ∼9 mM, 1 mM each	In vivo intraluminal *tgr5*-WT and KO mice	BA mix: ↑ WT - KO		Isotonic saline	
	LCA RO5527239 (TGR5 agonist)	Concentration curve	CHO cells transfected with TGR5	↑	Increased cAMP production EC_{50} = 457 and 3.6 nM E_{Max}∼110% both	NA	(10)
	DCA RO5527239	Concentration curve	STC-1	↑	Increased cAMP production EC_{50} = 1.59 μM and 321 nM GLP-1 release EC_{50} = 11 μM and 321 nM		
MrgprX4	DCA, UDCA CDCA, CA, OA	2–100 μM	HEK293 cells	↑	Increased $[Ca^{2}]^{+}_{i}$	Water, DMSO, or 0.1 M NaOHNA	(11)
	DCA UDCA	10 μM 100 μM	DRG from +X4 humanized mice	↑	∼5%–6% of +X4 sensory neurons activated by both		
	DCA, t-DCA, UDCA CDCA	1–2 mM	In vivo +X4 humanized mice	↑	Increased cholestatic itch		
Muscarinic M2	t-CDCA, g-DCA, t-DCA, t-CA	100 μM	Ventricular neonatal rat myocytes	↑	Reduced contraction (G_i coupled) (role in TGR5 mediated release of cAMP found to be independent of contraction response)	L-15 media	(12)
	TCA	0–100 μM	Ventricular neonatal rat myocytes	Partial agonist	Radioligand binding, K_d = 17 μM Reduced cAMP production (30% of carbachol response) Reduced contraction (0.2 and 1 mM)	DMSO HBSS	(13)

Continued

Downloaded from journals.physiology.org/journal/ajpgi at New York Univ (216.165.095.084) on September 28, 2023.

Table 1.— *Continued*

Receptor	Bile Acid	Concentration	Tissue Preparation	Response	Effect	Solvent	Refs.
Muscarinic M3	CDCA, LCA, g-LCA, t-LCA, g-DCA, t-DCA, UDCA	30 μM	Ex vivo, precision-cut lung slices	↓	Inhibited acetylcholine contractile responses t-LCA IC_{50} = 3.2 μM	NA	(14)
S1PR2	t-CA, t-DCA, g-DCA, g-CA, t-UDCA	50–100 μM	Primary rat hepatocytes	↑	Activation of ERK1/2 and AKT	DMSO	(15)
	t-CA	100 μM	MLE		Activation of ERK1/2 and AKT Cell proliferation and migration	PBS	(16)
FPR	CDCA	25–400 μM	Human monocytes	↓	Inhibited monocyte chemotaxis to fMLP IC_{50} = 100 μM	Ethanol	(17)
			Human monocytes		Inhibited monocyte Ca flux by fMLP		
			EFTR cell		Inhibited cell migration by fMLP IC50 = 125 μM		
			EFTR cell		Inhibited Ca^{2+} flux by fMLP IC_{50} = 50 μM		
			Human monocytes EFTR cell		Radioligand fMLP binding IC_{50} = 140 μM		
	DCA	25–200 μM	Human monocytes and neutrophils	↓	Inhibited fMLP induced chemotaxis IC_{50} = 100 μM	PBS	(18)
		25 μM			Inhibited fMLP induced Ca^{2+} mobilization		
		5–200 μM			Radioligand fMLP binding		
			Nuclear receptors				
	CDCA>DCA and LCA	50 μM concentration curve for CDCA	CV-1 cells with rat FXR HepG2 cells with human FXR	↑	Transactivation of FXR with luciferase reporter CDCA EC_{50} = 50 μM and 10 μM rat and human FXR	Ethanol	(19)
	CDCA>DCA and LCA	100 μM	CV-1 cells	↑	Reporter gene assay. Increased CAT activity	NA	(20)
	CDCA, g-CDCA, t-CDCA			↑	FRET ligand sensing assay Increased relative fluorescence CDCA EC_{50} = 4.5 μM g- and t-CDCA EC_{50} = 10 μM		
FXR	CA GW4062 (FXR agonist)	200 mg/kg 100 mg/kg	Mice treated in vivo 72 h before to tissue harvest	Ileum, jejunum and duodenum ↑ Liver-	FGF-15 mRNA present in ileum, jejunum and duodenum	NA	(21, 22)
	CDCA	Concentration curve	Human ileum and colon mucosal biopsies	Ileum ↑ Colon–	FGF19 expression EC_{50} = 20 μM		
	CA	50 μM	6-h incubation	Comparison with matched con. CDCA	80% of CDCA response		
	DCA				40%		
	LCA				4%		
	OCA	20 μM			5 times greater than CDCA response		
PXR	LCA 3-keto-LCA	Concentration curve	CV-1 cells with human PXR	↑ ↑	Scintillation proximity binding assay IC_{50} = 9 and 15 μM	NA	(23)
	LCA	100 μM	CV-1 cells with human or mouse PXR and reporter plasmid	↑ (Human)	Reporter gene assay. Increased CAT activity		
	3-keto-LCA		(Cyp3a23)2-tk-CAT	↑			
	CDCA			-			
	CA			-			

Continued

Downloaded from journals.physiology.org/journal/ajpgi at New York Univ (216.165.095.084) on September 28, 2023.

Table 1.— *Continued*

Receptor	Bile Acid	Concentration	Tissue Preparation	Response	Effect	Solvent	Refs.
	DCA			-			
	CDCA	100 μM	CV-1 cells with	↑	Reporter gene activity and	NA	(24)
	DCA		human and	↑	CYP3A4 reporter gene		
	LCA		rodent PXR and	↑	activity		
			reporter plasmids				
	LCA	8 mg/day for 4 days,	PXR-WT and KO	↑ WT	Northern blot analysis		
		oral gavage	mice in vivo	-KO	CYP3A11 mRNA		
VDR	LCA	Concentration curve	HEK293 cells trans-	↑	GAL4-receptor luciferase	NA	(25)
	3-keto-LCA		fected with VDR		assay		
					EC_{50} = 8 and 3 μM		
	LCA		Monkey kidney	↑	Competitive binding assay		
	3-keto-LCA		COS-7		[3H]1,25(OH)2D3		
					K_i = 29 and 8 μM		
	CA, CDCA						
	LCA	0.8 mmol/kg, oral	Ileum tissue of Vdr	↑ WT	Induces mRNA expression	Ethanol and corn oil	(26)
		gavage	WT and KO	-KO	of Cyp24a1		

CA, cholic acid; CDCA, chenodeoxycholic acid; DCA, deoxycholic acid; LCA, lithocholic acid. 3-Keto-LCA is the major metabolite of LCA in rats. UDCA, ursodeoxycholic acid; t-, tauro-conjugated; g-, glyco-conjugated bile acid. Cell lines: rat basophil leukemia cell line transfected with FPR EFTR cell; mouse large cholangiocytes MLE; monkey kidney CV-1 cells; human hepatoma HepG2; enteroendocrine cell line, STC-1. Responses: activation, ↑; inhibition, ↓; no change, -. Solvents: NA, no information available; DMSO stock, dimethyl sulfoxide (DMSO).

Mrgpr receptors was not studied here. Although the expression profiles of TGR5, MRGPRA3, and MRGPRC11 were identified in mouse sensory DRG neurons, expression of MRGPRA1 was not mentioned. The same study examined the response profiles of human DRG neurons. Although they found that cells responded to TGR5-preferring agonists they did not study receptor specificity for these responses and this may be due to limitations in the pharmacological tools currently available. The expression profiles of MRGPRX4 were also not mentioned (6).

Muscarinic Acetylcholine Receptors

Some BAs can interact with muscarinic receptors to influence cholinergic signaling. This is likely the result of structural similarities between some BAs and acetylcholine (ACh), as has been identified for lithocholic acid conjugates (37, 38). Secondary BAs, including taurolithocholic acid (t-LCA), block cholinergic-induced contractions of mouse and human airway smooth muscle evoked by either exogenous ACh or by electrical stimulation of parasympathetic nerve terminals, possibly by acting as antagonists of M3 muscarinic receptors (14). Urso et al. found that this was not through specific activation of TGR5, as BAs continued to relax preconstricted smooth muscle tissues from *tgr5*$^{-/-}$ mice, and selective TGR5 small molecule agonists did not relax tissue from wild-type animals. A role for BAs in muscarinic signaling is further supported by studies in cardiomyocytes, where taurocholate inhibited cAMP-production in a pertussis toxin-sensitive manner to limit contraction. This response was prevented upon pharmacological inhibition or siRNA knockdown of the M2 muscarinic receptor (12, 13). Muscarinic receptors have prominent roles in gastrointestinal motility and secretion. Therefore, it is surprising that not more is known about the implications of BAs interacting with muscarinic receptors in these processes.

Sphingosine-1-Phosphate Receptor 2

Sphingosine-1-phosphate receptor 2 (S1PR2) is one of a series of receptors that respond to the bioactive lipid mediator, lysosphingolipid (S1P). S1PRs are ubiquitously expressed in different tissues and this is reflected by their roles in many processes including angiogenesis, lymphangiogenesis, cell proliferation and motility, immune cell function, and lipid metabolism (39). S1PR2 also has a role as a BA receptor (40). In GPCR screening assays, rodent hepatocytes responded to BAs through extracellular signal-regulated kinase (ERK)1/2 and protein kinase B/Akt signaling. These BA-mediated responses were reduced by an S1PR2-selective antagonist, knockdown of the receptor, and using cells from S1PR2 knockout mice (15). Furthermore, the proliferation of cholangiocytes and onset of liver fibrosis in response to experimental bile duct ligation were attenuated in S1PR2-deficient mice, consistent with the proposed interaction of S1PR2 and BAs (16).

Formyl Peptide Receptors

Formyl peptide receptors (FPRs) are a group of GPCRs involved in innate immune responses. *N*-Formyl-methionyl-leucyl-phenylalanine (fMLP), a major chemotactic factor, is an agonist with different binding affinities for the three FPRs. fMLP binds with high- and low affinities to formyl peptide receptor (FPR) and formyl peptide receptor-like type-1 (FPRL-1), respectively. However, formyl peptide receptor-like type-2 (FPRL-2) does not bind to *N*-formyl peptides. Roles for FPRs in BA-induced signaling have been demonstrated in studies on human monocytes and using human embryonic kidney cells (HEK-293) transfected with FPR and FPRL-1. In these cells, pretreatment with CDCA and DCA inhibited fMLP binding to its receptors and associated elevations in intracellular Ca^{2+} (17, 18). In these same studies, cell migration stimulated by fMLP was inhibited by CDCA and DCA treatment (17, 18). Although these studies did not assess whether TGR5 mediates BA-dependent inhibition of chemotaxis and calcium signaling in these cells, computational modeling experiments have demonstrated antagonist binding sites for DCA on the FPR (41), supporting the idea that direct inhibition of these BA receptors is involved. Intestinal microbiota are known to produce fMLP, and recent studies of interactions between the microbiome, FPRs, and gut motility suggest that FPR-expressing enteric neurons are

Downloaded from journals.physiology.org/journal/ajpgi at New York Univ (216.165.095.084) on September 28, 2023.

important mediators of probiotic-induced gut motility (42). It is therefore plausible that BAs could modulate gastrointestinal physiology through actions on neuronal FPRs. However, direct experimental evidence for such interactions is currently lacking. Furthermore, since FPRs are also expressed by intestinal neutrophils with different expression patterns noted for cells isolated from tissues of patients with Crohn's disease (43), BA/FPR interactions on intestinal immune cells could have important implications for pathogenesis of inflammatory bowel diseases (IBDs).

NUCLEAR RECEPTORS FOR BILE ACIDS

Nuclear receptors are a family of ligand-activated transcription factors, comprised of a ligand-binding domain and a DNA-binding domain to promote or suppress transcription. Activators for these receptors include steroid hormones such as estrogen and progesterone and lipid-soluble mediators such as retinoic acid and vitamin D. In this way they allow factors such as hormones or nutrients to modulate gene expression (44). BAs are ligands for several nuclear receptors with roles in glucose, lipid, and energy metabolism (45). These receptors regulate BA levels in the enterohepatic circulation and mediate processes in inflammation. They represent novel targets for a range of therapies for metabolic, cholestatic liver, and inflammatory bowel diseases (46, 47).

Farnesoid X Receptor

Farnesol was originally thought to be the cognate ligand for farnesoid X receptor (FXR), but this agonist only activates the receptor at supraphysiological concentrations (48). In contrast, conjugated and unconjugated BAs activate FXR at physiological levels with CDCA being one of the most potent agonists (19, 20, 49). FXR is highly expressed in liver and intestinal tissues and has significant roles in mediating both metabolic processes and BA homeostasis. Studies of FXR knockout mice provide evidence for the roles of FXR-dependent BA metabolism, as these mice have elevated levels of circulating BAs and they excrete fewer BAs in their fecal matter (50). In hepatocytes, FXR activation limits the production of primary BAs by various pathways that include downregulating the rate-limiting enzyme for BA synthesis. It also stimulates the secretion of BA from the liver into the gall bladder and limits hepatic reuptake. In intestinal cells, FXR activation promotes downstream pathways that lead to intracellular transport of BAs and reduce BA production in hepatocytes (45, 51). In human ileal enterocytes, BA-mediated activation of FXR stimulates transcription of the hormone fibroblast growth factor 19 (FGF-19, mouse ortholog FGF-15) (21, 22). FGF-19/FGF-15 then activates a downstream pathway in hepatocytes, ultimately inhibiting the production of BAs (45). Maintaining BA homeostasis is important for liver function but when improperly regulated can lead to a range of digestive diseases. For example, BA-diarrhea (BAD) is thought to be caused by alterations in enterohepatic circulation. Given the roles of FXR in stimulating these processes, FXR agonists have been successfully tested for their therapeutic potential to treat this condition (51, 52). The therapeutic potential may extend beyond regulating the enterohepatic circulation of BAs since activation of FXR has been shown to promote antisecretory effects in colonic epithelial cells (53). These additional roles are discussed in more detail later in this review (see BILE ACIDS AND INTESTINAL TRANSPORT OF ELECTROLYTES AND FLUID). In the liver, FXR activation also limits glucogenesis and lipogenesis, therefore, targeting FXR has potential as a therapeutic strategy to treat a range of metabolic conditions, such as nonalcoholic steatohepatitis (54, 55).

Pregnane X Receptor

A range of lipophilic chemicals bind to Pregnane X receptor (PXR) including xenobiotics, endogenous hormones, and BAs (56). PXR is responsible for the metabolism, detoxification, and elimination of such agents. It is highly expressed in the liver and small intestine (24). PXR activation enhances the production of enzymes responsible for BA metabolism/detoxification, represses enzymes involved in BA synthesis, and alters the expression of BA transport proteins (23, 24, 57). LCA also activates PXR (24, 57). Along with FXR, targeting PXR has been proposed as a possible IBD treatment, particularly for patients with Crohn's disease associated with BA-diarrhea [BAD (58)]. In patients with BAD, the activities of enzymes that catalyze BA metabolism are reduced, enzymes that facilitate BA synthesis are elevated and hence the balance of BAs levels is dysregulated. These studies have postulated that PXR or FXR may be deactivated in these patients (59, 60). Dextran sulfate sodium (DSS)-induced colitis is more severe in PXR knockout mice when compared with the wild-type control, and activation of PXR can alleviate the development of inflammation in wild-type mice (61).

Vitamin D Receptor

Typically, vitamin D receptor (VDR) responds to the active form of vitamin D, 1α,25-dihydroxyvitamin D3 $1,25(OH)_2D_3$. The receptor is expressed in the intestine and kidneys where it mediates a range of processes such as calcium homeostasis, cellular differentiation, and immunity.

LCA is a metabolite of CDCA. Although the primary BAs, CDCA and CA, do not activate VDR, LCA is a potent VDR agonist (25). Oral administration of LCA to mice can induce the expression of some of the same targets genes as VDR activation by $1,25(OH)_2D_3$ (26). Although clarity on the physiological relevance for LCA activation of VDR is lacking, it is thought to have a protective role by mediating the elimination and breakdown of LCA, given the cytotoxic and pro-oncogenic nature of the BA (62, 63). Since, intestinal bacteria metabolize CDCA to LCA, it is hypothesized that this provides a mechanism for intestinal bacteria to regulate host VDR function. Recent evidence suggests that the LCA-VDR interactions may have protective roles for the intestinal epithelial barrier (64). This is supported by observations that VDR knockout mice develop dextran sulfate sodium (DSS) colitis more quickly and robustly than wild-type animals (65), and in patients with Crohn's disease or ulcerative colitis colonic epithelial VDR expression is reduced (66).

LCA acts on FXR, PXR, and VDR to modulate BA metabolism, and the downstream effects of these interactions regulate the activities of the cytochrome P450 (CYP) family of enzymes (45). These enzymes protect the body from

Downloaded from journals.physiology.org/journal/ajpgi at New York Univ (216.165.095.084) on September 28, 2023.

a variety of lipophilic chemicals, such as BAs, and their actions are controlled at a transcriptional level by many different signaling molecules. Activation of VDR, by either LCA or $1,25(OH)_2D_3$, induces transcription of the CYP3A4 gene (25). The CYP3A4 enzyme assists in the detoxification of LCA and other BAs by catalyzing their hydroxylation. Hydroxylation of BAs means they are more hydrophilic, facilitating their excretion in fecal matter or urine. The importance of this interaction is demonstrated in VDR knockout mice, where intestinal, circulating, and fecal BA pools are all dysregulated (65, 67). Insertion of the CYP3A4 gene into these mutant mice improves the BA pool size so that the relative levels of BAs in liver and intestine homogenates return to levels comparable with those of wild-type mice. It also reduces the effects of LCA-induced toxicity by stimulating LCA metabolism (68).

Constitutive Androstane Receptor

Constitutive androstane receptor (CAR) is expressed in the liver and intestines where it mediates the detoxification of phenobarbital-like inducers (69). Although endogenous activators for CAR are not well characterized, both androstenol and androstanol have been identified as repressive endogenous ligands for constitutive activity. BAs are unlikely to directly activate CAR (70) but indirect activation has been suggested in LCA-induced liver toxicity models. CAR knockout mice develop more severe damage compared with wild-type controls, highlighting that LCA detoxification could not occur in these mice (71). CAR expression is reduced in the colon from mice with DSS-induced colitis. Similarly, mucosal intestinal biopsies from patients with Crohns' disease and ulcerative colitis also have reduced CAR expression when compared with healthy individuals (72).

FXR, PXR, and CAR regulate overlapping target genes in BA metabolism. To investigate how they coordinate their activities, several studies have used double knockout mice for different combinations of these receptors. They suggest that the receptors jointly protect against BA-induced liver toxicity (71, 73, 74). The gut microbiome regulates the function and expression of CAR and PXR receptors by stimulating the conversion of primary BAs to secondary BAs. Tissues from germ-free (GF) mice express significantly lower mRNA levels for CAR, PXR, and FXR as well as for a range of cytochrome P450 enzymes relative to mice housed under specific pathogen-free (SPF) conditions (75). In conventional mice, daily administration of CAR and PXR agonists changes the biodiversity of their microbiome by reducing two taxa in the *Bifidobacterium* genus (76). Again, this highlights the potential interplay between the gut microbiome, the regulation of BAs levels, the expression this group of receptors, and their activation by BAs.

BILE ACIDS AS MODIFIERS OF ION CHANNEL ACTIVITY

BAs can also exert their effects through interactions with ion channels. Specific ionotropic receptors for BAs have not been identified to date. However, there is good evidence that BAs can modulate the functions of several members of the epithelial sodium channel/degenerin (ENaC/DEG) family. This interaction may be physiologically relevant in tissues where BAs have access to these channels, such as in the intestine and bile ducts. The regulation of these channels by hormones and local factors is highly complex and involves the regulation of channel expression, trafficking, and open probability. Several members of the ENaC/DEG family of ion channels can qualify as ligand-gated ion channels. These include the acid sensing ion channels (ASICs) and the FMRFamide-activated Na^+ channel (FaNaC) that are activated by protons and the tetrapeptide FMRFamide, respectively. For other members of this family, no specific activating ligands have been described with the possible exception of BA-sensitive ion channel (BASIC). A summary of the actions of BAs on ion channels and ionotropic receptors is provided in Table 2.

BA-Sensitive Ion Channel

BA-sensitive ion channel (BASIC) is a member of the ENaC/DEG ion channel family (previously known as intestinal Na^+ channel (INaC) in humans or brain-liver-intestine Na^+ channel (BLINaC) in rodents) (94, 95). BASIC is expressed on the apical membrane of rat cholangiocytes (77, 80). It shows very low basal activity in heterologous expression systems, but is strongly activated by submillimolar concentrations of BAs (77–82). Based on this observation, it is possible that BAs may act as endogenous ligands for the channel in tissues where they are present at high concentrations, such as the bile ducts and the small intestine. However, the stimulatory effect of BA on BASIC does not seem to be as potent and as specific as the stimulatory effect of ligands on classical ionotropic receptors. Moreover, a modulatory effect of BAs on ion channel activity does not seem to be limited to BASIC.

Epithelial Sodium Channel

Epithelial sodium channel (ENaC) is expressed in the apical membrane of epithelia in a range of tissues, including the distal colon and the biliary ducts (96). It mediates transepithelial sodium absorption and therefore regulates fluid volume (97–100). Recent evidence suggests that BA sensitivity is not a unique feature of BASIC but may be a common feature of channels belonging to the ENaC/DEG family. Similar or lower concentrations of BAs needed to activate BASIC can stimulate the rat, mouse, and human ENaC (83–85). Generally, BAs activate ENaC with varying abilities, but some also inhibit the channel (84–86).

It is likely that exposure of ENaC to changing levels of BAs in cholangiocytes and distal colon may modify the function of the channel under physiological conditions. In kidney and distal colon, ENaC plays an important role in mediating sodium absorption. In these tissues, ENaC is mainly stimulated by the mineralocorticoid aldosterone but can also be regulated by additional mediators and local mechanisms (101–104).

Despite the location of ENaC on the apical membrane, BAs may also affect the channel through interactions originating from the basal surface. Preliminary studies demonstrated that LCA applied to the serosal side of the mouse distal colon had a sustained stimulatory effect on ENaC-mediated transepithelial

Downloaded from journals.physiology.org/journal/ajpgi at New York Univ (216.165.095.084) on September 28, 2023.

Table 2. *Effects of bile acids on ion channels and ionotropic receptors*

Ion Channel	Bile Acid	Effect: Stimulation ↑ Inhibition ↓	Concentration Used or EC_{50}/IC_{50}, if Available	Solvent	Cells Expression System	Refs.
		Epithelial sodium channel/degenerin ion channel family				
$BASIC^{rat}$	g-CDCA, t-CDCA g-HDCA, t-HDCA	↑↑↑	1–1.5 mM g-HDCA: $EC_{50} \sim 2$ mM	NA	*X. laevis* oocytes	(77, 78)
	t-CA, t-βMCA	↑				
	UDCA	↑↑↑	$EC_{50} \sim 2.5$ mM			
	t-UDCA, t-HDCA	↑↑↑				
	t-CA, t-LCA t-DCA, t-CDCA	↑↑	1–2 mM t-UDCA: $EC_{50} \sim 2.7$ mM	NA	HEK293 cells	(79)
	t-CDCA, t-HDCA t-UDCA	↑↑	500 μM–1 mM	NA	Normal rat cholangiocytes (NRC)	(80)
$BASIC^{human}$	t-DCA	↑↑↑	500 μM–1 mM	Bath solution	*X. laevis* oocytes	(77, 81, 82)
	t-CDCA	↑↑↑		NA		
	t-CA, t-HDCA	↑				
	t-DCA, t-CDCA	↑↑↑				
	t-CA, t-UDCA t-HDCA, t-LCA	↑	1–2 mM	NA	HEK293 cells	(79)
$BASIC^{mouse}$	t-CA, t-UDCA, t-HDCA t-LCA, t-DCA, t-CDCA	↑↑	1–2 mM t-UDCA: $EC_{50} \sim 4.5$ mM	NA	HEK293 cells	(79)
$\alpha\beta\gamma ENaC^{rat}$	CA	↑↑	1 mM t-DCA: $EC_{50} \sim 260$ μM t-CA: $EC_{50} \sim 410$ μM	DMSO stock	*X. laevis* oocytes	(83)
	t-DCA	↑↑↑		Bath solution		
	g-CA, t-CA	↑↑				
	t-CDCA, t-UDCA	↑				
	t-βMCA, t-HDCA	No effect				
$\alpha\beta\gamma ENaC^{human}$	t-DCA	↑↑↑	250 μM	Bath solution	*X. laevis* oocytes	(84)
	t-CA, t-CDCA	↑↑				
	CA, DCA	↑				
	CDCA	↓				
$\delta\beta\gamma ENaC^{human}$	CA, t-CA, DCA, t-DCA CDCA, t-CDCA	↑↑↑				
$\alpha\beta\gamma ENaC^{mouse}$	DCA, t-CA	↑↑↑	1 mM DCA: $EC_{50} \sim 80$ μM t-CA: $EC_{50} \sim 150$ μM	H_2O stock	*X. laevis* oocytes	(85)
	g-CA	↑↑				
	CA, t-LCA, UCA	↑↑		DMSO stock		
	CDCA, t-CDCA 12βHICA	↑				
	HDCA	↓		H_2O stock		
	t-HDCA	↓↓				
$ENaC^{human}$	t-CA	↑↑	1 mM t-CA: $EC_{50} \sim 200$ μM	H_2O stock	mpkCCD14 cells	
	t-HDCA	↓				
$ENaC^{human}$	UDCA	↓↓	500 μM	NA	NuLi-1 and CuFi-1 airway epithelial cells	(86)
$ASIC1a^{human}$	t-CDCA	↑↑↑	500 μM t-DCA: $EC_{50} \sim 150$ μM	Bath solution	*X. laevis* oocytes	(87)
	t-DCA	↑↑				
	t-CA	↑				
		Other ion channels and ionotropic receptors				
BK_{Ca}^{rabbit}	CA, DCA, LCA, t-LCA	↑↑↑	100 μM	DMSO ethanol stock	Smooth muscle cells	(88)

Continued

Na^+ transport. This is reminiscent of the stimulatory effect of aldosterone (105). The delayed and sustained stimulatory effect of LCA on ENaC may be due to transcriptional regulation involving a nuclear receptor, such as FXR. A dual stimulatory effect of BAs on ENaC from the apical and basolateral side may serve as a compensatory mechanism in the colon to limit fluid loss during diarrhea resulting from impaired ileal BA absorption (for a more detailed discussion

Downloaded from journals.physiology.org/journal/ajpgi at New York Univ (216.165.095.084) on September 28, 2023.

Table 2.— *Continued*

Ion Channel	Bile Acid	Effect: Stimulation ↑ Inhibition ↓	Concentration Used or EC_{50}/IC_{50}, if Available	Solvent	Cells Expression System	Refs.
	CA, g-CA, t-CA		IC_{50} ~ 500-700 μM			
$NMDA^{mouse}$	DCA, t-DCA CDCA, t-CDCA	↓↓↓	IC_{50} ~ 60-70 μM			
	g-CDCA		IC_{50} ~ 130 μM			
	CA, g-CA, t-CA		IC_{50} ~ 500–700 μM	NA	Hypothalamic neurons	(89, 90)
	DCA, t-DCA		IC_{50} ~ 150 μM			
$GABA_A{}^{mouse}$	CDCA, g-CDCA t-CDCA	↓↓↓	IC_{50} ~ 70–80 μM			
	UDCA		IC_{50} ~ 70–100 μM			
$GABA_A$ $\alpha1^{rat}\beta1^{rat}\gamma2L^{mouse}$ $\alpha1^{rat}\beta2^{rat}\gamma2L^{mouse}$ $\alpha1^{rat}\beta3^{human}\gamma2L^{mouse}$ $\alpha1^{rat}\beta3^{human}$ $\beta3^{human}$ $\beta3^{human}\gamma2L^{mouse}$	UDCA	↓↓↓	IC_{50} ~ 70–100 μM IC_{50} ~ 7 μM IC_{50} ~ 200 μM	NA	HEK293 cells	(90)
NMDA $GluN1^{rat}/2A^{rat}$ $GluN1^{rat}/2B^{rat}$	CA, g-CA, t-CA CDCA, g-CDCA t-CDCA	↓	100 μM			
	CA, g-CA, t-CA	↓				
$GluN1^{rat}/2D^{rat}$	CDCA, g-CDCA t-CDCA	↓↓	100 μM t-CDCA: IC_{50} ~ 180 μM	NA	*X. laevis* oocytes	(91)
	CA, g-CA, t-CA	↓	100 μM			
$GluN1^{rat}/3B^{mouse}$	CDCA, g-CDCA t-CDCA	↓↓↓	t-CDCA: IC_{50} ~ 40–80 μM			
	CA, t-CA, CDCA	No effect				
$P2X4^{human}$	t-CDCA	↓↓	250–500 μM t-DCA: IC_{50} ~ 160 μM	Bath solution	*X. laevis* oocytes	(92)
	DCA, t-DCA	↓↓↓				
	t-CA	No effect				
	t-UDCA, t-DCA	↓				
$P2X2^{rat}$	t-CDCA	↓↓	20 μM t-HDCA: IC_{50} ~ 11 μM			
	t-LCA, HDCA t-HDCA, g-HDCA	↓↓↓				
	t-HDCA	No effect	20 μM			
$P2X1^{rat}$	t-LCA	↓	200 μM	H_2O stock	*X. laevis* oocytes	(93)
$P2X3^{rat}$	t-HDCA	No effect	20 μM			
$P2X7^{rat}$	t-LCA		200 μM			
	t-LCA	↑	200 μM			
$P2X4^{rat}$	t-HDCA	No effect	20 μM			
	t-LCA	↑↑	20 μM			
$P2X2^{human}$	t-HDCA	No effect				

CA, cholic acid; CDCA, chenodeoxycholic acid; DCA, deoxycholic acid; HDCA, hyodeoxycholic acid; LCA, lithocholic acid; UCA, ursocholic acid; UDCA, ursodeoxycholic acid; 12βHICA, 12β-hydroxyisocholic acid; βMCA, β-muricholic acid; t-, tauro-conjugated; g-, glyco-conjugated bile acid. Solvents: NA, no information available; bath solution, bile acids/bile salts were directly dissolved in bath solution to obtain the indicated final concentrations; DMSO stock, dimethyl sulfoxide (DMSO) stock solutions were prepared with bile acids at a concentration of 100 mM; H_2O stock, aqueous stock solutions were prepared with bile acid concentrations ranging from 20 to 100 mM; DMSO/ethanol stock, concentrated dimethyl sulfoxide (DMSO) stock solutions were prepared with bile acids at a concentration of 333 mM and then further diluted 1/10 in 95% ethanol.

of the effects of BA on intestinal transport see BILE ACIDS AND INTESTINAL TRANSPORT OF ELECTROLYTES AND FLUID).

Human Acid-Sensing Ion Channel ASIC1a

ASIC1a is another member of the ENaC/DEG family of ion channels. Although BAs do not directly activate ASIC1a, they positively modulate proton-activated ASIC1a currents (87). BAs may not act as classical ligands on the orthosteric site of the channel, but rather modulate the function of already active ASIC1a channels by interacting with a topographically distinct, allosteric site. Using site-directed mutagenesis and computer simulation it has been shown that BAs may directly interact with the transmembrane domains of ENaC/DEG ion channels in the so-called "degenerin region" known to be functionally important for channel gating (81, 84, 87). BA binding to the transmembrane domains of the channel probably stabilizes the channel open conformation leading to increased channel activity. Several ASICs are responsible

Downloaded from journals.physiology.org/journal/ajpgi at New York Univ (216.165.095.084) on September 28, 2023.

for distinct proton-gated currents in neurons regulating gastrointestinal function (106). Thus, it is tempting to speculate that modulation of ASICs by BAs may contribute to gastrointestinal physiology and pathophysiology.

Other Ion Channels and Ionotropic Receptors

BA may also modulate other ion channels and ionotropic receptors. For example, BAs have been shown to modify the function of large-conductance Ca^{2+}- and voltage-activated K^+ (BK) channels via distinct channel subunits and sites (88), they also inhibit currents mediated by ionotropic NMDA and $GABA_A$ receptors (89–91). Recently, it has been demonstrated that the human purinergic receptor $P2X_4$, an ATP-gated nonselective cation channel, is inhibited by unconjugated or tauro-conjugated DCA (92). The inhibitory effect of BAs is not limited to $P2X_4$ and has also been reported for the related $P2X_2$ receptor (93). A comparison of the crystal structure of $P2X_4$ revealed a high degree of similarity in topology and architecture with that of ASIC1 (107), suggesting structural similarities of their BA binding sites. Indeed, tauro-DCA probably interacts with the transmembrane domains of $P2X_4$ thereby stabilizing its closed state (92). $P2X_4$ is abundantly expressed in hepatocytes and cholangiocytes (108, 109) and $P2X_2$ is present in gall bladder and enteric neurons (110, 111). Therefore, BAs may potentially play a role as local modulators of purinoceptors in these systems.

BILE ACIDS AND INTESTINAL TRANSPORT OF ELECTROLYTES AND FLUID

Bile Acids Modulate Intestinal Fluid and Electrolyte Transport in Pathophysiology

Intestinal fluid absorption is critical for effective homeostatic control of whole body fluid and electrolyte balance.

Table 3. *Effects of bile acids on gastrointestinal motility*

GI Region/Application Method/ Measurement	Animal Species	Bile Acid	Concentration Used	Effect:	Refs.
Stomach and small intestine					
Stomach and small intestine/oral gavage/ phenol red	Rat	t-DCA DCA	26–100 mM 5–26 mM	GE ↓ SIT ↓ GE ↓↓ IT ↓↓	(117)
Stomach-cecum/ileum infusion/environmental hydrogen analysis		t-CA DCA	10 mM 10 mM	SCTT ↑ SCTT ↓	(118)
Stomach/nasogastric/paracetamol absorption test	Human (healthy and type 2 diabetes)	CDCA	1.25 g in 100 mL water	GE ↓	(119)
Small intestine					
Jejunum and ileum/intraluminal infusion/ lactulose and in vivo manometry	Human (healthy)	g-CDCA g-CA	15–30 mM 15 mM	SIT ↓ SIT ↓	(120, 121)
Terminal ileum/intraluminal infusion/ex vivo manometry	Rabbit	Rabbit bile t-DCA	0.1–10 mM	MA ↓ MA ↓ at 10 mM	(122)
Colon (in vivo)					
GI and colonic transit/oral/side effect profile	Human (cholesterol gallstone)	UDCA CDCA	7–8 and 14–15 mg/kg/ day (3–12 mo)	BF – BF ↑	(123)
Proximal colon/ rectal perfusion/in vivo manometry and GI sensation	Human (healthy)	CDCA	1 mM	Sensory threshold ↓ PS ↑	(124)
GI and colonic transit/oral capsule/scintigraphy method and bowel function	Human (healthy and IBS-C)	CDCA	500, 1,000 mg	CT ↑ BF ↑	(125) (126)
GI and colonic transit/rectal perfusion/ GI sensation	Human (healthy)	TCA	1,500 and 3,500 mg	Sensory threshold ↓ BF ↑	(127)
Colon (in vitro/ex vivo)					
Colonic motility/bath addition muscle exposure/contraction assay	Mouse *tgr5-wt* and *ko*	UDCA DCA	100 μM 1, 10, 100 μM	WT contraction - WT contraction ↓ KO contraction -	(128, 129)
Colonic motility/ bath addition mucosal exposure/ contraction assay	*tgr5-wt* and *ko*	UDCA DCA LCA OA	100 μM 1, 10, 100 μM 1, 10, 100 μM 100 μM	WT PR - WT PR ↑ KO - WT PR ↑ KO - WT PR ↑ KO -	(129)
Colonic smooth muscle/ bath addition muscle exposure/ contraction assay	Rat	DCA	1, 10, 100 μM	Contraction -	(130)
Colon					
Colon and rectum/intraluminal infusion/ ex vivo manometry	Rabbit	t-CA g-CA	2–16 mM 8–24 mM	MA ↑ MA ↑	(131)
		g-CA DCA	3–30 mM	MA - MA ↑	(132)

CA, cholic acid; CDCA, chenodeoxycholic acid; DCA, deoxycholic acid; LCA, lithocholic acid; UDCA, ursodeoxycholic acid; t-, tauro-conjugated; g-, glyco-conjugated bile acid; Rank order of potency for TGR5 is t-LCA > LCA > DCA > CDCA, UDCA and OA are weak TGR5 agonists. Responses: stimulation, ↑; inhibition, ↓; no change, -. BF, bowel function; CT, colonic transit; GE, gastric emptying; IBS-C, irritable bowel syndrome-constipation predominate; MA, motor activity; PR, peristaltic reflex; PS, propagating sequences; SIT, small intestinal transit.

Downloaded from journals.physiology.org/journal/ajpgi at New York Univ (216.165.095.084) on September 28, 2023.

Na^+ absorption drives fluid uptake across small intestinal villi and surface cells of the colon, whereas Cl^- secretion drives fluid secretion occurring mainly from the crypts. Three main mechanisms drive Na^+ absorption along the gut as follows: while digestion is occurring, small intestinal Na^+-nutrient co-transporters predominate; during the interdigestive period, Na^+/H^+ exchange predominates along the entire length of the intestine; and electrogenic Na^+ absorption is the primary mechanism driving fluid absorption in the distal colon (112). Depending on physiological versus pathophysiological conditions, BAs can activate both proabsorptive and prosecretory pathways to influence ion flux and water retention.

There has long been an association between increased luminal BA levels and the onset of diarrhea in humans. However, the roles of BAs in fluid dysregulation were not recognized until much later than their effects on intestinal motility (see BILE ACIDS AND INTESTINAL MOTILITY). The first preclinical demonstration of such actions came in 1966, where perfusion of DCA, at a concentration of 100 μM, to the rat jejunum inhibited intestinal fluid absorption (113). Based on observations in patients with ileitis and increased BA turnover, Hofmann (114) proposed that the increased levels of luminal BAs were causing the clinical symptoms of diarrhea. This hypothesis was subsequently supported by clinical studies showing that direct administration of dihydroxy BAs to the colorectum induced diarrhea in healthy individuals (115), whereas infusion of conjugated and unconjugated BAs inhibited jejunal water absorption (116).

Typically, only dihydroxy BAs (e.g., DCA and CDCA) alter epithelial transport processes and, in humans, diarrhea only occurs when BAs are present at pathophysiological levels (see Table 3). In the small intestine where their uptake to enterohepatic circulation can occur via IBAT, conjugates of DCA and CDCA exert similar actions to their nonconjugated counterparts but with lower potency. However, in the colon there is a lack of apical uptake pathways and therefore luminal conjugated BAs cannot enter the epithelium unless the barrier becomes compromised, as occurs in conditions of intestinal inflammation. Conjugated BAs can then gain access to the basolateral domain and enter the epithelial cell via basolateral transporters to stimulate increases in free cytosolic Ca^2 (for more details see *Molecular Mechanisms of Bile Acid-Induced Fluid Transport*), thereby activating intracellular mechanisms that promote fluid secretion and inhibit absorption (133, 134). Interestingly, unlike the other dihydroxy BAs, UDCA does not stimulate fluid secretion in the colon and appears to exert antisecretory actions when it is present at sufficiently high levels (135).

Molecular Mechanisms of Bile Acid-Induced Fluid Transport

BAs induce luminal fluid accumulation by inhibiting Na^+ absorption and promoting Cl^- secretion in both the small intestine and colon. This has been demonstrated in many animal models using in vitro and in vivo methods to assess fluid and ion transport in the ileum (136–139) and colon (140, 141). Studies using cultured intestinal epithelial cell lines and on isolated human colonic crypts have provided considerable insights into mechanisms by which BAs induce luminal fluid accumulation and diarrhea. In Caco-2 cells, a model of absorptive epithelial cells, conjugated BAs inhibit Cl^-/OH^- exchange (142). Likewise, when present at high concentrations, CDCA inhibits both Na^+/H^+ exchange (NHE) activity and Cl^-/HCO_3^- exchange in isolated human colonic crypts (143). As discussed in BILE ACIDS AS MODIFIERS OF ION CHANNEL ACTIVITY, BAs can also modify the function of ENaC, which plays a role in Na^+ absorption in the distal colon, particularly when plasma aldosterone levels are increased to minimize renal and intestinal sodium losses. High concentrations of BAs can rapidly induce Cl^- secretion from the crypts across both small intestinal and colonic epithelial cells. This effect appears to involve activation of basolateral K^+ channels, where K^+ leaving the cells provides the electrochemical driving force for Cl^- to exit through channels in the apical membrane. This most likely occurs through the cystic fibrosis transmembrane conductance regulator (CFTR) (144).

The actions of BAs on these transport proteins appear to be predominantly mediated by elevations in intracellular Ca^{2+} (133, 143, 145). BAs have been shown to induce increases in intracellular Ca^{2+} by both influx across the plasma membrane and release from the endoplasmic reticulum (143, 146, 147). However, the upstream mechanisms leading to increased intracellular Ca^{2+} are still not well defined. The fact that only dihydroxy BAs are active might point to the involvement of a receptor. However, neither TGR5, which appears to exert antisecretory actions (7, 148), nor the nuclear receptor, FXR, is a likely candidate. As noted previously in this review, BAs have detergent-like properties and by inducing perturbations in the cell membrane, this may lead to activation of downstream signaling pathways, thereby promoting their prosecretory and antiabsorptive actions (149, 150). It appears that BAs can also directly interact with endoplasmic reticulum membranes to increase cytosolic Ca^{2+} levels (151, 152).

It is clear from studies of isolated epithelial cells that BAs can exert direct actions on intestinal absorption and secretion. However, studies from ex vivo tissues demonstrate that BAs acting on other mucosal cells may also contribute to this dysregulation. As discussed in *Actions of Bile Acids on the Mucosa to Promote Colonic Motility*, luminal BAs can stimulate enterochromaffin cells (ECC) within the mucosa to release serotonin (5-HT). 5-HT can then activate enteric neural pathways, including those that regulate fluid secretion (153–155). Such neural pathways may provide a mechanism by which changes in intestinal fluid and electrolyte transport can be coordinated with changes in motility and permeability (5, 156–158). BAs can also activate mucosal mast cells to release their mediators (159), most notably histamine, and this may be important in mediating Cl^- secretory responses to CDCA (160). It is also important to note that mast cells and enteric nerves exist close to one another in the intestinal mucosa and that interactions between these two cell types are likely to be important in regulating epithelial transport responses to BAs (161, 162).

Roles of Bile Acids in Epithelial Fluid and Electrolyte Transport under Physiological Conditions

In contrast to their acute prosecretory and antiabsorptive effects at high concentrations, BAs have recently been

Downloaded from journals.physiology.org/journal/ajpgi at New York Univ (216.165.095.084) on September 28, 2023.

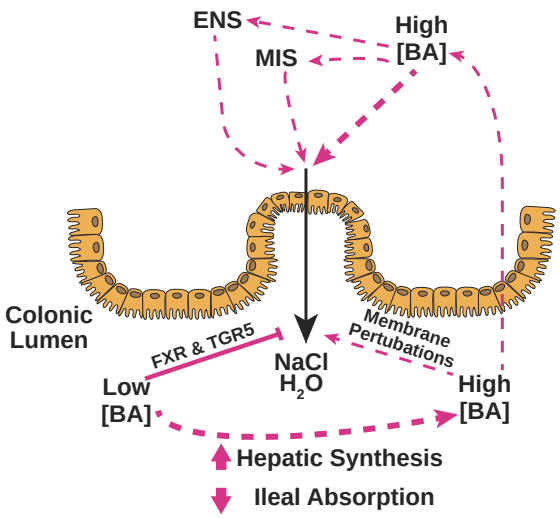

Figure 1. Bile acids (BAs) in regulation of colonic epithelial Cl^- secretion. BAs are normally present in the colon at relatively low concentrations where they act via BA receptors, such as Farnesoid X receptor (FXR) and Takeda G protein-coupled receptor 5 (TGR5), to inhibit salt and water secretion into the lumen (*left*). We propose that such actions serve to promote normal colonic absorptive function. In some pathological conditions, increased delivery of BAs to the colon may result from either increased synthesis of primary BAs by hepatocytes or reduced ileal absorption. The resulting high levels of luminal BAs induce perturbations in the epithelial cell membranes to promote Cl^- secretion and inhibit Na^+ absorption, thereby promoting luminal fluid accumulation (*right*). Such direct effects of BAs on the epithelium are amplified by indirect actions involving the release of neurotransmitters and mediators from the enteric nervous and mucosal immune systems (ENS and MIS, respectively). It is thought that, under such circumstances, increased colonic fluid secretion is a protective mechanism that serves to dilute the abnormally high levels of luminal BAs.

shown to exert antisecretory actions at more physiologically relevant levels (53, 105, 163). Such antisecretory effects are slow in onset (12–24 h) and for DCA occur at concentrations as low as 50 μM, a concentration that is well within the normal physiological range for this BA in the proximal colon (164). Such antisecretory actions of naturally occurring BAs are mimicked by selective FXR agonists and are associated with reduced expression and activity of basolateral Na^+-K^+-ATPase pumps and apical CFTR Cl^- channels (53). We have proposed that under such physiological conditions, BAs may function to inhibit colonic fluid secretion, thereby promoting the normal absorptive function of the colon (summarized in Fig. 1). Thus, by virtue of their opposing actions at low versus high concentrations, dihydroxy BAs may have the capacity to dynamically control the fluidity of the luminal contents. In this context, bacterially mediated deconjugation of luminal BAs would be essential to permit their entry into the cell where FXR activation can occur to induce antisecretory actions. Thus, diet or disease-associated changes in the colonic microbiota that result in altered expression of bile salt hydrolase activity could have important implications for fluid and electrolyte transport (165–169).

Studies have also investigated the potential role for TGR5 in regulating colonic fluid and electrolyte transport. These revealed that TGR5 also exerts antisecretory effects, although its role appears to be distinct to that of FXR. Treatment of muscle-stripped, nerve-free, mucosal preparations of rat colon with the TGR5-selective agonist, INT-777, rapidly and transiently reduced basal Cl^- secretion with a concomitant inhibition in the capacity of the tissue to evoke secretory responses to Ca^{2+}-dependent secretagogues (148). Furthermore, the effects of INT-777 were mimicked by LCA, an endogenous ligand for TGR5. Subsequent studies revealed that TGR5 activation may also dampen colonic Cl^- secretion by inhibiting submucosal neurons. Such actions are proposed to represent a regulatory mechanism that may counterbalance BA-induced fluid secretion (7). A schematic representation of the roles of BAs in regulating colonic intestinal fluid and electrolyte transport is depicted in Fig. 1.

BILE ACIDS AND INTESTINAL MOTILITY

There is strong, consistent evidence that oral delivery or rectal administration of BAs promotes colonic motility. Although early experimental evidence from in vivo studies in rabbit demonstrated that luminal infusion of secondary BAs promotes colonic motility (131, 132), the most compelling evidence comes from clinical studies (124–126). Rectal perfusion of CDCA to healthy individuals reduces the perceived defecatory urge and enhances the frequency of distension-evoked pressure waves or bowel movements (124, 127). Similarly, oral administration of CDCA significantly accelerates colonic transit, but not gastric emptying or colon filling (125). These effects are not limited to healthy patients since in individuals with constipation, oral administration of BAs increases stool frequency and decreases stool consistency (126, 170). This work highlights the therapeutic potential of targeting BA signaling to treat gastrointestinal motility disorders. A summary of the roles of BAs in GI motility and the relative concentrations required to stimulate these actions is presented in Table 3.

Mechanisms for the Prokinetic Actions of BA and the Case for TGR5

Early literature from clinical studies implicates the role of TGR5 in the prokinetic actions of BAs in the colon. Results from clinical trials testing the efficacy of UDCA and CDCA to dissolve and treat gallstones demonstrated that patients treated with CDCA, but not UDCA, experienced diarrhea as a side effect (123, 171, 172). Furthermore, constipation was relieved by treatment with CDCA, but not UDCA (123). This may be explained by the differing agonist activities of the BAs at TGR5, where UDCA has a lower efficacy and potency for TGR5 agonism than CDCA (9, 173). This aligns with evidence from candidate genotype analysis using PCR-based methods, where TGR5 genotype variations are associated with constipation and diarrhea in patients with IBS (174, 175).

Although selective TGR5 agonists are becoming available, the functional effects of TGR5-selective drugs on colonic motility in humans have not yet been investigated. However, studies in mice and dogs demonstrate that TGR5 is expressed throughout the gastrointestinal tract in enteric neurons, epithelial and enteroendocrine cells, and smooth muscle. TGR5 has been identified as a regulator of colonic motility in these species under normal conditions (5, 128, 176). Indeed, there are likely several mechanisms by which BAs can modulate

Downloaded from journals.physiology.org/journal/ajpgi at New York Univ (216.165.095.084) on September 28, 2023.

intestinal motility. Data from in vitro studies suggest that BAs exert prokinetic actions when exposure is limited to the mucosa (5), but exposure to the muscularis externa inhibits intestinal motility (128). In the latter case, BAs may have a direct action on the smooth muscle cells to impair contractile activity (130, 177), or may directly activate inhibitory enteric motor neurons that express TGR5 (128). Such inhibitory actions of BAs on the muscularis externa do not contradict the findings from clinical studies. The absence of transporters, such as ASBT, that permit the absorption of conjugated BAs in the colon limits their access to this tissue layer (178), and most clinical studies involve BA exposure to the gut lumen. Therefore, it is likely that the prokinetic actions of BAs are due to effects initiated in the mucosa. Direct effects of BAs on the muscularis externa may be more relevant in disease conditions, such as inflammation, where loss of barrier function and increased paracellular permeability allows both conjugated and unconjugated BAs to passively pass through the mucosa (179, 180).

Actions of Bile Acids on the Mucosa to Promote Colonic Motility

BAs promote the release of several bioactive mediators from the intestinal mucosa. For example, isolated human ECC release 5-HT following exposure to sodium deoxycholate (57), while mucosal application of BAs to rat jejunum (153) and mouse colon promotes 5-HT release possibly via a TGR5-dependent mechanism (5). This BA-mediated 5-HT release activates neural pathways to promote peristaltic contractions (5).

In addition to 5-HT, it is well documented that BAs also stimulate intestinal L cells to release the peptide hormones glucagon-like peptide-1 (GLP-1) and peptide YY (PYY) (119, 181–185). This involves TGR5-dependent and TGR5-independent mechanisms (8, 9, 186, 187). The release of GLP-1 and PYY is important for regulating appetite and metabolism. One mechanism of action of GLP-1 in metabolism is to promote insulin release, and hence GLP-1 receptor agonists are used clinically to treat diabetes mellitus. GLP-1 and PYY promote digestion and nutrient absorption by delaying gastric emptying and reducing intestinal motility. Infusion of BAs to the lumen of the stomach and small intestine in vivo reduces gastric emptying and intestinal transit in the rat, rabbit, and human (117, 118, 120, 121). The association between BAs, the release of neuropeptides, and delayed small intestinal motility is supported by studies in the rabbit ileum (122) and human stomach (119), where luminal perfusion of BAs increases the plasma concentrations of PYY or GLP-1, respectively, and this is associated with reduced GI motility in these regions.

BAs mediate opposing effects on motility of the small versus large intestines and it is unclear whether neuropeptide release alone can account for these differences. Rectal administration of tauro-CA in humans dose-dependently increases plasma GLP-1 and PYY levels (127, 182) and this is associated with increased defecation frequency (127). GLP-1 or PYY may directly regulate the BA-mediated changes in motility and this could explain the differential actions in the upper gut and colon where they are present at differing concentrations. In vitro studies show that application of GLP-1 inhibits the responses of intestinal muscle strips to electrical stimulation or exogenous application of ACh without influencing basal tone. This inhibition is likely due to an action on enteric inhibitory neurons (188–190), but also involves actions on the smooth muscle cells themselves (189). Myenteric and submucosal neurons functionally express GLP-1 receptors. In studies on whole-mount preparations of rat colon, application of the highly selective agonist, exendin-4, stimulated increases in intracellular calcium in a proportion of neurons from both regions (191). In vivo motility studies indicate that regulation from the central nervous system may also be involved (191, 192). There is conflicting data as to whether PYY stimulates (193, 194) or inhibits GI smooth muscle contractility (195, 196) and these effects may be region-specific (197, 198). PYY is a 36-amino acid polypeptide that is endogenously expressed as either full-length PYY1-36 or as the truncated PYY3-36 form. These peptides have different affinities for the Y receptors that PYY targets (199). Therefore, the presence and activity of PYY variants may account for differences in the contractile responses of different regions to PYY. The cell surface enzyme, dipeptidyl peptidase IV (DPP-IV), both inactivates GLP-1 and converts PYY from its long to its truncated form. Thus, the activity of DPP-IV may play a significant role in shaping the contractile responses to PYY and GLP-1 following BA activation. GLP-1 containing L-cells are evenly distributed across the stomach, small intestine, and colon. In contrast, PYY containing L-cells typically populate the distal small intestine and colon only (195, 200, 201). Whether TGR5 is equivalently expressed by all L-cells regardless of if they contain PYY or GLP-1 remains to be determined, and how these profiles may also contribute to the generation of gut motility patterns is also unknown.

Differing results using taurine-conjugated versus unconjugated isoforms and the use of individual BAs versus mixtures of BAs provide better insight on how they influence motility (see Table 3). In a study by Brown et al. (118), perfusion of the ileum with taurocholic acid (tauro-CA) increased stomach to caecum transit time. In contrast, this transit time decreased with perfusion of DCA. Ullmer et al. found that taurine-conjugated and unconjugated BAs have an equal binding affinity for human-TGR5 in cell lines. However, their effectiveness to increase plasma PYY levels in animals depended on systemic versus luminal application of the agonists (10). The taurine-conjugated TGR5 agonist tauro-RO5527239 did not stimulate secretion of PYY from L-cells, whereas the unconjugated form did. Conjugated forms of BAs or TGR5 agonists have limited ability to access the receptor that is located on the basal side of epithelial cells (186). We speculate that this, in turn, would limit the release of factors, such as PYY, by these cells and thus potentially limit their influence on intestinal motility. Given the importance of the colonic microbiome in determining BA deconjugation, it is clear that changes in bacterial populations that express bile salt hydrolases are likely to significantly impact how BAs modulate fecal transit through the colon. (166–169). BA modulation by the colonic microbiome may therefore be influenced by factors such as diet modification or the onset of disease.

Bile Acids and Intestinal Motility Disorders

Enhanced delivery of BAs to the colon has long been associated with diarrhea (114, 202), with ~25%–33% of patients with chronic functional diarrhea having increased BA delivery to the colon (203). In some rare cases, BA-malabsorption

Downloaded from journals.physiology.org/journal/ajpgi at New York Univ (216.165.095.084) on September 28, 2023.

(BAM) can be due to loss-of-function mutations in intestinal bile acid transporters, such as ASBT and organic solute transporter β (Ostβ) (5, 204–206). However, BAM is most commonly due to structural damage brought about by ileal inflammation from conditions such as Crohn's disease, or following surgical or radiation procedures (207–209). Idiopathic BAM is characterized by increased delivery of BAs in the stool in the absence of structural pathology. Alterations in BA synthesis (174, 210–212) or the enterohepatic circulation (213) are attributed as the causes of BAM and the resultant diarrhea in these conditions. Moreover, studies suggest that 10%–26% of patients with diarrhea predominant IBS (IBS-D) may have BAM as the underlying cause (214). Conversely, recent evidence suggests that some instances of constipation may result from reduced BA delivery to the colon. In a retrospective study, Vijayvargiya et al. (215) reported that 15% of patients with IBS-C had decreased fecal BA levels compared with healthy control patients (45 patients, 108 controls). This evidence for the important roles of BAs in a range of GI motility conditions has prompted research into the therapeutic potential of altering BA delivery to the colon or influencing BA receptor signaling.

More recent clinical studies have shifted away from the direct administration of BAs to patients, to investigating the therapeutic potential of modulating the delivery of endogenous BAs. This approach has produced results consistent with the effects of exogenous administration of BAs. One such strategy is to inhibit the reuptake of BAs in the terminal ileum, using drugs such as IBAT inhibitor, Elobixibat (A3309) (216–218). In vivo studies in constipated dogs (218) and clinical trials conducted in Europe, North America, and Japan have all demonstrated Elobixibat to effectively increase the number of spontaneous bowel movements and to improve stool consistency in patients with chronic constipation (219–222). Elobixibat is now an approved drug for the treatment of constipation in Japan (223). There is limited knowledge as to whether administration of ASBT inhibitors can promote GI motility under control conditions (i.e., nonconstipated patients). However, in vivo experiments in dogs demonstrated that Elobixibat induced giant migrating contractions and increased defecation frequency and fecal wet weight within 10 h of administration (224).

Several other IBAT inhibitors, including volixibat, maralixibat, odevixibat (A4250), and GSK2330672 are in various stages of clinical trials to treat conditions such as nonalcoholic steatohepatitis (225), type 2 diabetes mellitus (226), and cholestatic pruritus in primary biliary cholangitis (227–231). In all of these studies, diarrhea and abdominal pain are cited as treatment-related adverse events, with an incidence ranging from 10% to 80%. Although it is unclear whether a patient subtype is more or less likely to develop these symptoms, the dosage of the drugs can be correlated with the number of reported incidences. Recently published results of a phase 2 clinical trial for GSK2330672 to treat cholestatic pruritus reported diarrhea as an adverse event in 38%, 65%, and 66% of patients receiving 20, 90, and 180 mg of the drug, respectively. This was compared with 11% of patients receiving the placebo (229). This highlights the importance of establishing efficacy, safety, and tolerability of these drugs to treat these conditions. As noted elsewhere, BAs will cause symptoms such as diarrhea when delivered at high, pathophysiological concentrations; therefore, it would be interesting to know how the levels of fecal BAs correlated with symptom severity. In healthy volunteers, volixibat increased fecal BAs by 1.6–3.2 times compared with those that had received placebo. It is worth noting that there was no clear correlation between dosage of volixibat (0.5–5 mg) and excreted BAs. How these levels correlated with symptom severity was not reported. However, these results highlight that there may be variability in the ways in which patients respond to these drugs.

Another approach to modulating endogenous levels of BAs involves the use of BA sequestrants that have opposing effects to ASBT inhibitors and reduce free BA levels in the colon. Such drugs, which include cholestyramine and colesevelam, have been trialed to treat a range of diarrhea-associated conditions including idiopathic BA-diarrhea and BA-associated diarrhea in Crohn's disease and IBS-D (57, 125, 217, 232–234). As FXR activation leads to the inhibition of BA production in hepatocytes, FXR agonists have also been trialed to treat BA-induced diarrhea (52, 86, 235). Two small clinical trials conducted in the UK and the USA have demonstrated the benefits of the FXR agonists obeticholic acid and tropifexor. Daily tropifexor administration had a small but significant effect on slowing ascending colonic motility in patients with primary BA-diarrhea in a recent safety profiling study [60 μg daily, n = 8 (235)]. Obeticholic acid given to patients with primary BA-diarrhea improved stool frequency and formation during a 2-wk treatment period [25 mg, daily, n = 10 (52)]. However, patients with chronic idiopathic diarrhea did not have improved symptoms (n = 8) indicating that neither FXR activation nor limiting physiological levels of BA production have roles in controlling colonic motility (52). This differs to patients with BA-diarrhea, where removing excess BAs reduces the symptoms of the disease. It is important to note that GI motility and secretion are interlinked, where increasing secretion will stimulate motility. FXR agonists limit intestinal fluid secretion in mouse models of secretory diarrhea (53). However, these studies did not specifically study direct GI motor indices.

When considering the potential for targeting BAs for therapeutic purposes, it is important to consider how the gut microbiome interacts with these molecules and their receptors to modulate intestinal motility (236). There is a growing appreciation for the roles of intestinal bacteria in a range of GI disorders. BAs increase intestinal permeability, providing greater opportunity for microbiota to access the gut wall. Although the BAs can modulate motility directly, the inflammation promoted by the infiltrating bacteria can also alter intestinal motility (237). This pairs with the proposed role of TGR5 in regulating intestinal inflammation, which may involve TGR5 expressing-circulating macrophages (179, 180). Recent studies in mice have highlighted that with age-related changes to the microbiome there is an increase in fecal deconjugated BAs. TGR5 activation by conjugated BAs in young mice stimulated an anti-inflammatory phenotype in muscularis macrophages (mMac) protecting normal motility. With aging, the shift of fecal BA content to deconjugated BAs led to reduced TGR5 activation. This resulted in a phenotypic switch of mMac to a more proinflammatory state, stimulating low-grade inflammation in these tissues and thus

Downloaded from journals.physiology.org/journal/ajpgi at New York Univ (216.165.095.084) on September 28, 2023.

delayed GI transit (238). The microbiome-BA balance and its role in intestinal motility seem an obvious consideration when trying to understand complex treatment strategies such as fecal transplants (236). This could have important implications for our understanding of the pathology of a range of GI motility disorders but may also provide novel therapeutic strategies for these conditions.

CONCLUSION

The BA receptor axis is a viable therapeutic target, as evidenced by the clinical use of BA sequestrants and more recently IBAT inhibitors. With the discovery of specific BA receptors, BA-modulated ion channels, and BA transporters, our understanding of the roles of BAs in physiological processes and disease has evolved. BAs have physiological actions as signaling molecules through binding and activation of both cell surface and nuclear receptors and through modifying ion channel function. They also drive pathophysiological changes in disease and may have mechanistic roles in GI disorders including IBS. As outlined in this review, there remains the need for greater understanding of the functional importance of BA receptors, particularly those which have only recently been defined.

GRANTS

S. E. Carbone is supported by an Australian Research Council DECRA Fellow Grant DE200100825. Research in the author's laboratories is supported by National Health and Medical Research Council Australia 1083480 (to D. P. Poole), National Institutes of Health Grants NS102722, DE026806, DE029951, DK118971 (to N. W. Bunnett), Department of Defense Grant W81XWH1810431 (to N. W. Bunnett), the ELAN program of the Interdisciplinary Center for Clinical Research, Erlangen (IZKF) Grant 17-08-01-1-Ilyaskin/P015 (to A.V. Ilyaskin), and by Science Foundation Ireland Grant No. 16/IA/4445 (to S. J. Keely).

DISCLOSURES

N. W. Bunnett is a founding scientist of Endosome Therapeutics Inc. Research in the laboratories of N. W. Bunnett, D. P. Poole, and S. E. Carbone is funded in part by Takeda Pharmaceuticals. None of the other authors has any conflicts of interest, financial or otherwise, to disclose.

AUTHOR CONTRIBUTIONS

S.E.C. analyzed data; D.P.P. and S.E.C. prepared figures; S.J.K., A.U., A.V.I., C.K., N.W.B., D.P.P., and S.E.C. drafted manuscript; S.J.K., A.U., A.V.I., C.K., N.W.B., D.P.P., and S.E.C. edited and revised manuscript; S.J.K., A.U., A.V.I., C.K., N.W.B., D.P.P., and S.E.C. approved final version of manuscript.

REFERENCES

1. **de Aguiar Vallim TQ**, **Tarling EJ**, **Edwards PA.** Pleiotropic roles of bile acids in metabolism. *Cell Metab* 17: 657–669, 2013. doi:10.1016/j.cmet.2013.03.013.
2. **Peleman C**, **Camilleri M**, **Busciglio I**, **Burton D**, **Donato L**, **Zinsmeister AR.** Colonic transit and bile acid synthesis or excretion in patients with irritable bowel syndrome-diarrhea without bile acid malabsorption. *Clin Gastroenterol Hepatol* 15: 720–727.e1, 2017. doi:10.1016/j.cgh.2016.11.012.
3. **Mekhjian HS**, **Phillips SF**, **Hofmann AF.** Colonic absorption of unconjugated bile acids: perfusion studies in man. *Dig Dis Sci* 24: 545–550, 1979. doi:10.1007/BF01489324.
4. **Mikov M**, **Fawcett JP**, **Kuhajda K**, **Kevresan S.** Pharmacology of bile acids and their derivatives: absorption promoters and therapeutic agents. *Eur J Drug Metab Pharmacokinet* 31: 237–251, 2006. doi:10.1007/BF03190714.
5. **Alemi F**, **Poole DP**, **Chiu J**, **Schoonjans K**, **Cattaruzza F**, **Grider JR**, **Bunnett NW**, **Corvera CU.** The receptor TGR5 mediates the prokinetic actions of intestinal bile acids and is required for normal defecation in mice. *Gastroenterology* 144: 145–154, 2013. doi:10.1053/j.gastro.2012.09.055.
6. **Castro J**, **Harrington AM**, **Lieu T**, **Garcia-Caraballo S**, **Maddern J**, **Schober G**, **O'Donnell T**, **Grundy L**, **Lumsden AL**, **Miller P**, **Ghetti A**, **Steinhoff MS**, **Poole DP**, **Dong X**, **Chang L**, **Bunnett NW**, **Brierley SM.** Activation of pruritogenic TGR5, MrgprA3, and MrgprC11 on colon-innervating afferents induces visceral hypersensitivity. *JCI insight* 4: 332, 2019. doi:10.1172/jci.insight.131712.
7. **Duboc H**, **Tolstanova G**, **Yuan PQ**, **Wu V**, **Kaji I**, **Biraud M**, **Akiba Y**, **Kaunitz J**, **Million M**, **Tache Y**, **Larauche M.** Reduction of epithelial secretion in male rat distal colonic mucosa by bile acid receptor TGR5 agonist, INT-777: role of submucosal neurons. *Neurogastroenterol Motil* 28: 1663–1676, 2016. doi:10.1111/nmo.12866.
8. **Katsuma S**, **Hirasawa A**, **Tsujimoto G.** Bile acids promote glucagon-like peptide-1 secretion through TGR5 in a murine enteroendocrine cell line STC-1. *Biochem Biophys Res Commun* 329: 386–390, 2005. doi:10.1016/j.bbrc.2005.01.139.
9. **Kuhre RE**, **Wewer Albrechtsen NJ**, **Larsen O**, **Jepsen SL**, **Balk-Møller E**, **Andersen DB**, **Deacon CF**, **Schoonjans K**, **Reimann F**, **Gribble FM**, **Albrechtsen R**, **Hartmann B**, **Rosenkilde MM**, **Holst JJ.** Bile acids are important direct and indirect regulators of the secretion of appetite- and metabolism-regulating hormones from the gut and pancreas. *Mol Metab* 11: 84–95, 2018. doi:10.1016/j.molmet.2018.03.007.
10. **Ullmer C**, **Alvarez Sanchez R**, **Sprecher U**, **Raab S**, **Mattei P**, **Dehmlow H**, **Sewing S**, **Iglesias A**, **Beauchamp J**, **Conde-Knape K.** Systemic bile acid sensing by G protein-coupled bile acid receptor 1 (GPBAR1) promotes PYY and GLP-1 release. *Br J Pharmacol* 169: 671–684, 2013. doi:10.1111/bph.12158.
11. **Meixiong J**, **Vasavda C**, **Snyder SH**, **Dong X.** MRGPRX4 is a G protein-coupled receptor activated by bile acids that may contribute to cholestatic pruritus. *Proc Natl Acad Sci USA* 116: 10525–10530, 2019. doi:10.1073/pnas.1903316116.
12. **Ibrahim E**, **Diakonov I**, **Arunthavarajah D**, **Swift T**, **Goodwin M**, **McIlvride S**, **Nikolova V**, **Williamson C**, **Gorelik J.** Bile acids and their respective conjugates elicit different responses in neonatal cardiomyocytes: role of Gi protein, muscarinic receptors and TGR5. *Sci Rep* 8: 7110–7112, 2018. doi:10.1038/s41598-018-25569-4.
13. **Sheikh Abdul Kadir SH**, **Miragoli M**, **Abu-Hayyeh S**, **Moshkov AV**, **Xie Q**, **Keitel V**, **Nikolaev VO**, **Williamson C**, **Gorelik J.** Bile acid-induced arrhythmia is mediated by muscarinic M2 receptors in neonatal rat cardiomyocytes. *PLoS One* 5: e9689, 2010. doi:10.1371/journal.pone.0009689.
14. **Urso A**, **D'Ovidio F**, **Xu D**, **Emala CW**, **Bunnett NW**, **Perez-Zoghbi JF.** Bile acids inhibit cholinergic constriction in proximal and peripheral airways from humans and rodents. *Am J Physiol Lung Cell Mol Physiol* 318: L264–L275, 2020. doi:10.1152/ajplung.00242.2019.
15. **Studer E**, **Zhou X**, **Zhao R**, **Wang Y**, **Takabe K**, **Nagahashi M**, **Pandak WM**, **Dent P**, **Spiegel S**, **Shi R**, **Xu W**, **Liu X**, **Bohdan P**, **Zhang L**, **Zhou H**, **Hylemon PB.** Conjugated bile acids activate the sphingosine-1-phosphate receptor 2 in primary rodent hepatocytes. *Hepatology* 55: 267–276, 2012. doi:10.1002/hep.24681.
16. **Wang Y**, **Aoki H**, **Yang J**, **Peng K**, **Liu R**, **Li X**, **Qiang X**, **Sun L**, **Gurley EC**, **Lai G**, **Zhang L**, **Liang G**, **Nagahashi M**, **Takabe K**, **Pandak WM**, **Hylemon PB**, **Zhou H.** The role of sphingosine 1-phosphate receptor 2 in bile-acid-induced cholangiocyte proliferation and cholestasis-induced liver injury in mice. *Hepatology* 65: 2005–2018, 2017. doi:10.1002/hep.29076.
17. **Chen X**, **Yang D**, **Shen W**, **Dong HF**, **Wang JM**, **Oppenheim JJ**, **Howard MZ.** Characterization of chenodeoxycholic acid as an endogenous antagonist of the G-coupled formyl peptide receptors. *Inflamm Res* 49: 744–755, 2000. doi:10.1007/s000110050656.
18. **Chen X**, **Mellon RD**, **Yang L**, **Dong HF**, **Oppenheim JJ**, **Howard MZ.** Regulatory effects of deoxycholic acid, a component of the anti-inflammatory traditional Chinese medicine Niuhuang, on human

Downloaded from journals.physiology.org/journal/ajpgi at New York Univ (216.165.095.084) on September 28, 2023.

leukocyte response to chemoattractants. *Biochem Pharmacol* 63: 533–541, 2002. doi:10.1016/S0006-2952(01)00917-0.
19. **Makishima M**, **Okamoto AY**, **Repa JJ**, **Tu H**, **Learned RM**, **Luk A**, **Hull MV**, **Lustig KD**, **Mangelsdorf DJ**, **Shan B.** Identification of a nuclear receptor for bile acids. *Science* 284: 1362–1365, 1999. doi:10.1126/science.284.5418.1362.
20. **Parks DJ**, **Blanchard SG**, **Bledsoe RK**, **Chandra G**, **Consler TG**, **Kliewer SA**, **Stimmel JB**, **Willson TM**, **Zavacki AM**, **Moore DD**, **Lehmann JM.** Bile acids: natural ligands for an orphan nuclear receptor. *Science* 284: 1365–1368, 1999. doi:10.1126/science.284.5418.1365.
21. **Zhang JH**, **Nolan JD**, **Kennie SL**, **Johnston IM**, **Dew T**, **Dixon PH**, **Williamson C**, **Walters JRF.** Potent stimulation of fibroblast growth factor 19 expression in the human ileum by bile acids. *Am J Physiol Gastrointest Liver Physiol* 304: G940–G948, 2013. doi:10.1152/ajpgi.00398.2012.
22. **Inagaki T**, **Choi M**, **Moschetta A**, **Peng L**, **Cummins CL**, **McDonald JG**, **Luo G**, **Jones SA**, **Goodwin B**, **Richardson JA**, **Gerard RD**, **Repa JJ**, **Mangelsdorf DJ**, **Kliewer SA.** Fibroblast growth factor 15 functions as an enterohepatic signal to regulate bile acid homeostasis. *Cell Metab* 2: 217–225, 2005. doi:10.1016/j.cmet.2005.09.001.
23. **Staudinger JL**, **Goodwin B**, **Jones SA**, **Hawkins-Brown D**, **MacKenzie KI**, **LaTour A**, **Liu Y**, **Klaassen CD**, **Brown KK**, **Reinhard J**, **Willson TM**, **Koller BH**, **Kliewer SA.** The nuclear receptor PXR is a lithocholic acid sensor that protects against liver toxicity. *Proc Natl Acad Sci USA* 98: 3369–3374, 2001. doi:10.1073/pnas.051551698.
24. **Xie W**, **Radominska-Pandya A**, **Shi Y**, **Simon CM**, **Nelson MC**, **Ong ES**, **Waxman DJ**, **Evans RM.** An essential role for nuclear receptors SXR/PXR in detoxification of cholestatic bile acids. *Proc Natl Acad Sci USA* 98: 3375–3380, 2001. doi:10.1073/pnas.051014398.
25. **Makishima M**, **Lu TT**, **Xie W**, **Whitfield GK**, **Domoto H**, **Evans RM**, **Haussler MR**, **Mangelsdorf DJ.** Vitamin D receptor as an intestinal bile acid sensor. *Science* 296: 1313–1316, 2002. doi:10.1126/science.1070477.
26. **Ishizawa M**, **Akagi D**, **Makishima M.** Lithocholic acid is a vitamin D receptor ligand that acts preferentially in the ileum. *Int J Mol Sci* 19: 1975, 2018. doi:10.3390/ijms19071975.
27. **Yoneno K**, **Hisamatsu T**, **Shimamura K**, **Kamada N**, **Ichikawa R**, **Kitazume MT**, **Mori M**, **Uo M**, **Namikawa Y**, **Matsuoka K**, **Sato T**, **Koganei K**, **Sugita A**, **Kanai T**, **Hibi T.** TGR5 signalling inhibits the production of pro-inflammatory cytokines by in vitro differentiated inflammatory and intestinal macrophages in Crohn's disease. *Immunology* 139: 19–29, 2013. doi:10.1111/imm.12045.
28. **Jia W**, **Xie G**, **Jia W.** Bile acid-microbiota crosstalk in gastrointestinal inflammation and carcinogenesis. *Nat Rev Gastroenterol Hepatol* 15: 111–128, 2018. doi:10.1038/nrgastro.2017.119.
29. **Dong X**, **Han S**, **Zylka MJ**, **Simon MI**, **Anderson DJ.** A diverse family of GPCRs expressed in specific subsets of nociceptive sensory neurons. *Cell* 106: 619–632, 2001. doi:10.1016/s0092-8674(01)00483-4.
30. **Meixiong J**, **Vasavda C**, **Green D**, **Zheng Q**, **Qi L**, **Kwatra SG**, **Hamilton JP**, **Snyder SH**, **Dong X.** Identification of a bilirubin receptor that may mediate a component of cholestatic itch. *eLife* 8: e44116, 2019. doi:10.7554/eLife.44116.
31. **Gulamhusein AF**, **Hirschfield GM.** Primary biliary cholangitis: pathogenesis and therapeutic opportunities. *Nat Rev Gastroenterol Hepatol* 17: 93–110, 2020. doi:10.1038/s41575-019-0226-7.
32. **Van Remoortel S**, **Ceuleers H**, **Arora R**, **Van Nassauw L**, **De Man JG**, **Buckinx R**, **De Winter BY**, **Timmermans J-P.** Mas-related G protein-coupled receptor C11 (Mrgprc11) induces visceral hypersensitivity in the mouse colon: a novel target in gut nociception? *Neurogastroenterol Motil* 31: e13623, 2019. doi:10.1111/nmo.13623.
33. **Avula LR**, **Buckinx R**, **Favoreel H**, **Cox E**, **Adriaensen D**, **Van Nassauw L**, **Timmermans JP.** Expression and distribution patterns of Mas-related gene receptor subtypes A-H in the mouse intestine: inflammation-induced changes. *Histochem Cell Biol* 139: 639–658, 2013. doi:10.1007/s00418-013-1086-9.
34. **Avula LR**, **Buckinx R**, **Alpaerts K**, **Costagliola A**, **Adriaensen D**, **Van Nassauw L**, **Timmermans JP.** The effect of inflammation on the expression and distribution of the MAS-related gene receptors MrgE and MrgF in the murine ileum. *Histochem Cell Biol* 136: 569–585, 2011. doi:10.1007/s00418-011-0862-7.
35. **Inclan-Rico JM**, **Kim BS**, **Abdus-Saboor I.** Beyond somatosensation: Mrgprs in mucosal tissues. *Neurosci Lett* 748: 135689, 2021. doi:10.1016/j.neulet.2021.135689.
36. **Luo J**, **Feng J**, **Liu S**, **Walters ET**, **Hu H.** Molecular and cellular mechanisms that initiate pain and itch. *Cell Mol Life Sci* 72: 3201–3223, 2015 [Erratum in *Cell Mol Life Sci* 72: 3587–3588, 2015]. doi:10.1007/s00018-015-1904-4.
37. **Cheng K**, **Chen Y**, **Zimniak P**, **Raufman JP**, **Xiao Y**, **Frucht H.** Functional interaction of lithocholic acid conjugates with M3 muscarinic receptors on a human colon cancer cell line. *Biochim Biophys Acta* 1588: 48–55, 2002. doi:10.1016/s0925-4439(02)00115-1.
38. **Raufman J-P**, **Chen Y**, **Cheng K**, **Compadre C**, **Compadre L**, **Zimniak P.** Selective interaction of bile acids with muscarinic receptors: a case of molecular mimicry. *Eur J Pharmacol* 457: 77–84, 2002. doi:10.1016/s0014-2999(02)02690-0.
39. **Nagahashi M**, **Yuza K**, **Hirose Y**, **Nakajima M**, **Ramanathan R**, **Hait NC**, **Hylemon PB**, **Zhou H**, **Takabe K**, **Wakai T.** The roles of bile acids and sphingosine-1-phosphate signaling in the hepatobiliary diseases. *J Lipid Res* 57: 1636–1643, 2016. doi:10.1194/jlr.R069286.
40. **Keitel V**, **Stindt J**, **Häussinger D.** Bile acid-activated receptors: GPBAR1 (TGR5) and other G protein-coupled receptors. In: *Bile Acids and Their Receptors*, edited by Fiorucci S, Distrutti E. Cham: Springer International Publishing, 2019, p**.** 19–49.
41. **Ferrari C**, **Macchiarulo A**, **Costantino G**, **Pellicciari R.** Pharmacophore model for bile acids recognition by the FPR receptor. *J Comput Aided Mol Des* 20: 295–303, 2006. doi:10.1007/s10822-006-9055-1.
42. **Chandrasekharan B**, **Saeedi BJ**, **Alam A**, **Houser M**, **Srinivasan S**, **Tansey M**, **Jones R**, **Nusrat A**, **Neish AS.** Interactions between commensal bacteria and enteric neurons, via fpr1 induction of ROS, increase gastrointestinal motility in mice. *Gastroenterology* 157: 179–194, 2019. doi:10.1053/j.gastro.2019.03.045.
43. **Anton PA**, **Targan SR**, **Shanahan F.** Increased neutrophil receptors for and response to the proinflammatory bacterial peptide formylmethionyl-leucyl-phenylalanine in Crohn's disease. *Gastroenterology* 97: 20–28, 1989. doi:10.1016/0016-5085(89)91410-8.
44. **Francis GA**, **Fayard E**, **Picard F**, **Auwerx J.** Nuclear receptors and the control of metabolism. *Annu Rev Physiol* 65: 261–311, 2003. doi:10.1146/annurev.physiol.65.092101.142528.
45. **Li T**, **Chiang JY.** Nuclear receptors in bile acid metabolism. *Drug Metab Rev* 45: 145–155, 2013. doi:10.3109/03602532.2012.740048.
46. **Li T**, **Chiang JYL.** Bile acid signaling in metabolic disease and drug therapy. *Pharmacol Rev* 66: 948–983, 2014. doi:10.1124/pr.113.008201.
47. **Schaap FG**, **Trauner M**, **Jansen PL.** Bile acid receptors as targets for drug development. *Nat Rev Gastroenterol Hepatol* 11: 55–67, 2014. doi:10.1038/nrgastro.2013.151.
48. **Forman BM**, **Goode E**, **Chen J**, **Oro AE**, **Bradley DJ**, **Perlmann T**, **Noonan DJ**, **Burka LT**, **McMorris T**, **Lamph WW**, **Evans RM**, **Weinberger C.** Identification of a nuclear receptor that is activated by farnesol metabolites. *Cell* 81: 687–693, 1995. doi:10.1016/0092-8674(95)90530-8.
49. **Wang H**, **Chen J**, **Hollister K**, **Sowers LC**, **Forman MB.** Endogenous bile acids are ligands for the nuclear receptor FXR/BAR. *Mol Cell* 3: 543–553, 1999. doi:10.1016/S1097-2765(00)80348-2.
50. **Sinal CJ**, **Tohkin M**, **Miyata M**, **Ward JM**, **Lambert G**, **Gonzalez FJ.** Targeted disruption of the nuclear receptor FXR/BAR impairs bile acid and lipid homeostasis. *Cell* 102: 731–744, 2000. doi:10.1016/s0092-8674(00)00062-3.
51. **Keely SJ**, **Walters JRF.** The Farnesoid X receptor: good for bad. *Cell Mol Gastroenterol Hepatol* 2: 725–732, 2016. doi:10.1016/j.jcmgh.2016.08.004.
52. **Walters JRF**, **Johnston IM**, **Nolan JD**, **Vassie C**, **Pruzanski ME**, **Shapiro DA.** The response of patients with bile acid diarrhoea to the farnesoid X receptor agonist obeticholic acid. *Aliment Pharmacol Ther* 41: 54–64, 2015. doi:10.1111/apt.12999.
53. **Mroz MS**, **Keating N**, **Ward JB**, **Sarker R**, **Amu S**, **Aviello G**, **Donowitz M**, **Fallon PG**, **Keely SJ.** Farnesoid X receptor agonists attenuate colonic epithelial secretory function and prevent experimental diarrhoea in vivo. *Gut* 63: 808–817, 2014. doi:10.1136/gutjnl-2013-305088.
54. **Neuschwander-Tetri BA**, **Loomba R**, **Sanyal AJ**, **Lavine JE**, **Van Natta ML**, **Abdelmalek MF**, **Chalasani N**, **Dasarathy S**, **Diehl AM**, **Hameed B**, **Kowdley KV**, **McCullough A**, **Terrault N**, **Clark JM**, **Tonascia J**, **Brunt EM**, **Kleiner DE**, **Doo E**; **NASH Clinical Research Network.** Farnesoid X nuclear receptor ligand obeticholic acid for non-cirrhotic, non-alcoholic steatohepatitis (FLINT): a multicentre,

Downloaded from journals.physiology.org/journal/ajpgi at New York Univ (216.165.095.084) on September 28, 2023.

randomised, placebo-controlled trial. *Lancet* 385: 956–965, 2015 [Erratum in *Lancet* 385: 946, 2015].doi:10.1016/S0140-6736(14)61933-4.
55. **Chávez-Talavera O**, **Tailleux A**, **Lefebvre P**, **Staels B.** Bile acid control of metabolism and inflammation in obesity, type 2 diabetes, dyslipidemia, and nonalcoholic fatty liver disease. *Gastroenterology* 152: 1679–1694e.3, 2017. doi:10.1053/j.gastro.2017.01.055.
56. **Cheng J**, **Ma X**, **Gonzalez FJ.** Pregnane X receptor- and CYP3A4-humanized mouse models and their applications. *Br J Pharmacol* 163: 461–468, 2011. doi:10.1111/j.1476-5381.2010.01129.x.
57. **Kidd M**, **Modlin IM**, **Gustafsson BI**, **Drozdov I**, **Hauso O**, **Pfragner R.** Luminal regulation of normal and neoplastic human EC cell serotonin release is mediated by bile salts, amines, tastants, and olfactants. *Am J Physiol Gastrointest Liver Physiol* 295: G260–G272, 2008. doi:10.1152/ajpgi.00056.2008.
58. **Fiorucci S**, **Carino A**, **Baldoni M**, **Santucci L**, **Costanzi E**, **Graziosi L**, **Distrutti E**, **Biagioli M.** Bile acid signaling in inflammatory bowel diseases. *Dig Dis Sci* 66: 674–693, 2021. doi:10.1007/s10620-020-06715-3.
59. **Wilson A**, **Almousa A**, **Teft WA**, **Kim RB.** Attenuation of bile acid-mediated FXR and PXR activation in patients with Crohn's disease. *Sci Rep* 10: 1866, 2020. doi:10.1038/s41598-020-58644-w.
60. **Iwamoto J**, **Saito Y**, **Honda A**, **Miyazaki T**, **Ikegami T**, **Matsuzaki Y.** Bile acid malabsorption deactivates pregnane X receptor in patients with Crohn's disease. *Inflamm Bowel Dis* 19: 1278–1284, 2013. doi:10.1097/MIB.0b013e318281f423.
61. **Shah YM**, **Ma X**, **Morimura K**, **Kim I**, **Gonzalez FJ.** Pregnane X receptor activation ameliorates DSS-induced inflammatory bowel disease via inhibition of NF-κB target gene expression. *Am J Physiol Gastrointest Liver Physiol* 292: G1114–G1122, 2007. doi:10.1152/ajpgi.00528.2006.
62. **Owen RW**, **Dodo M**, **Thompson MH**, **Hill MJ.** Fecal steroids and colorectal cancer. *Nutr Cancer* 9: 73–80, 1987. doi:10.1080/01635588709513914.
63. **Woolbright BL**, **Li F**, **Xie Y**, **Farhood A**, **Fickert P**, **Trauner M**, **Jaeschke H.** Lithocholic acid feeding results in direct hepato-toxicity independent of neutrophil function in mice. *Toxicol Lett* 228: 56–66, 2014. doi:10.1016/j.toxlet.2014.04.001.
64. **Yao B**, **He J**, **Yin X**, **Shi Y**, **Wan J**, **Tian Z.** The protective effect of lithocholic acid on the intestinal epithelial barrier is mediated by the vitamin D receptor via a SIRT1/Nrf2 and NF-κB dependent mechanism in Caco-2 cells. *Toxicol Lett* 316: 109–118, 2019. doi:10.1016/j.toxlet.2019.08.024.
65. **Kim SD**, **Kwon S**, **Lee SK**, **Kook M**, **Lee HY**, **Song K-D**, **Lee H-K**, **Baek S-H**, **Park CB**, **Bae Y-S.** The immune-stimulating peptide WKYMVm has therapeutic effects against ulcerative colitis. *Exp Mol Med* 45: e40, 2013. doi:10.1038/emm.2013.77.
66. **Liu W**, **Chen Y**, **Golan MA**, **Annunziata ML**, **Du J**, **Dougherty U**, **Kong J**, **Musch M**, **Huang Y**, **Pekow J**, **Zheng C**, **Bissonnette M**, **Hanauer SB**, **Li YC.** Intestinal epithelial vitamin D receptor signaling inhibits experimental colitis. *J Clin Invest* 123: 3983–3996, 2013. doi:10.1172/JCI65842.
67. **Schmidt DR**, **Holmstrom SR**, **Fon Tacer K**, **Bookout AL**, **Kliewer SA**, **Mangelsdorf DJ.** Regulation of bile acid synthesis by fat-soluble vitamins A and D. *J Biol Chem* 285: 14486–14494, 2010. doi:10.1074/jbc.M110.116004.
68. **Cheng J**, **Fang Z-Z**, **Kim J-H**, **Krausz KW**, **Tanaka N**, **Chiang JL**, **Gonzalez FJ.** Intestinal CYP3A4 protects against lithocholic acid-induced hepatotoxicity in intestine-specific VDR-deficient mice. *J Lipid Res* 55: 455–465, 2014. doi:10.1194/jlr.M044420.
69. **Wei P**, **Zhang J**, **Egan-Hafley M**, **Liang S**, **Moore DD.** The nuclear receptor CAR mediates specific xenobiotic induction of drug metabolism. *Nature* 407: 920–923, 2000. doi:10.1038/35038112.
70. **Miao J**, **Fang S**, **Bae Y**, **Kemper JK.** Functional inhibitory cross-talk between constitutive androstane receptor and hepatic nuclear factor-4 in hepatic lipid/glucose metabolism is mediated by competition for binding to the DR1 motif and to the common coactivators, GRIP-1 and PGC-1α. *J Biol Chem* 281: 14537–14546, 2006. doi:10.1074/jbc.M510713200.
71. **Zhang J**, **Huang W**, **Qatanani M**, **Evans RM**, **Moore DD.** The constitutive androstane receptor and pregnane X receptor function coordinately to prevent bile acid-induced hepatotoxicity. *J Biol Chem* 279: 49517–49522, 2004. doi:10.1074/jbc.M409041200.
72. **Hudson GM**, **Flannigan KL**, **Erickson SL**, **Vicentini FA**, **Zamponi A**, **Hirota CL**, **Alston L**, **Altier C**, **Ghosh S**, **Rioux KP**, **Mani S**, **Chang TK**, **Hirota SA.** Constitutive androstane receptor regulates the intestinal mucosal response to injury. *Br J Pharmacol* 174: 1857–1871, 2017. doi:10.1111/bph.13787.
73. **Guo GL**, **Lambert G**, **Negishi M**, **Ward JM**, **Brewer HB Jr**, **Kliewer SA**, **Gonzalez FJ**, **Sinal CJ.** Complementary roles of farnesoid X receptor, pregnane X receptor, and constitutive androstane receptor in protection against bile acid toxicity. *J Biol Chem* 278: 45062–45071, 2003. doi:10.1074/jbc.M307145200.
74. **Stedman CAM**, **Liddle C**, **Coulter SA**, **Sonoda J**, **Alvarez JGA**, **Moore DD**, **Evans RM**, **Downes M.** Nuclear receptors constitutive androstane receptor and pregnane X receptor ameliorate cholestatic liver injury. *Proc Natl Acad Sci USA* 102: 2063–2068, 2005. doi:10.1073/pnas.0409794102.
75. **Toda T**, **Saito N**, **Ikarashi N**, **Ito K**, **Yamamoto M**, **Ishige A**, **Watanabe K**, **Sugiyama K.** Intestinal flora induces the expression of Cyp3a in the mouse liver. *Xenobiotica* 39: 323–334, 2009. doi:10.1080/00498250802651984.
76. **Dempsey JL**, **Wang D**, **Siginir G**, **Fei Q**, **Raftery D**, **Gu H**, **Yue Cui J.** Pharmacological activation of PXR and CAR downregulates distinct bile acid-metabolizing intestinal bacteria and alters bile acid homeostasis. *Toxicol Sci* 168: 40–60, 2019. doi:10.1093/toxsci/kfy271.
77. **Wiemuth D**, **Sahin H**, **Falkenburger BH**, **Lefevre CMT**, **Wasmuth HE**, **Gründer S.** BASIC-a bile acid-sensitive ion channel highly expressed in bile ducts. *FASEB J* 26: 4122–4130, 2012. doi:10.1096/fj.12-207043.
78. **Wiemuth D**, **Sahin H**, **Lefevre CM**, **Wasmuth HE**, **Gründer S.** Strong activation of bile acid-sensitive ion channel (BASIC) by ursodeoxycholic acid. *Channels (Austin)* 7: 38–42, 2013. doi:10.4161/chan.22406.
79. **Lenzig P**, **Wirtz M**, **Wiemuth D.** Comparative electrophysiological analysis of the bile acid-sensitive ion channel (BASIC) from different species suggests similar physiological functions. *Pflugers Arch* 471: 329–336, 2019. doi:10.1007/s00424-018-2223-z.
80. **Wiegreffe S**, **Lohrer D**, **Wirtz M**, **Wiemuth D.** The bile acid-sensitive ion channel (BASIC) mediates bile acid-dependent currents in bile duct epithelial cells. *Pflugers Arch* 473: 1841–1850, 2021. doi:10.1007/s00424-021-02622-2.
81. **Ilyaskin AV**, **Kirsch SA**, **Böckmann RA**, **Sticht H**, **Korbmacher C**, **Haerteis S**, **Diakov A.** The degenerin region of the human bile acid-sensitive ion channel (BASIC) is involved in channel inhibition by calcium and activation by bile acids. *Pflugers Arch* 470: 1087–1102, 2018. doi:10.1007/s00424-018-2142-z.
82. **Lefevre CMT**, **Diakov A**, **Haerteis S**, **Korbmacher C**, **Gründer S**, **Wiemuth D.** Pharmacological and electrophysiological characterization of the human bile acid-sensitive ion channel (hBASIC). *Pflugers Arch* 466: 253–263, 2014. doi:10.1007/s00424-013-1310-4.
83. **Wiemuth D**, **Lefèvre CM**, **Heidtmann H**, **Gründer S.** Bile acids increase the activity of the epithelial Na^+ channel. *Pflugers Arch* 466: 1725–1733, 2014. doi:10.1007/s00424-013-1403-0.
84. **Ilyaskin AV**, **Diakov A**, **Korbmacher C**, **Haerteis S.** Activation of the human epithelial sodium channel (ENaC) by bile acids involves the degenerin site. *J Biol Chem* 291: 19835–19847, 2016. doi:10.1074/jbc.M116.726471.
85. **Wang X-P**, **Im SJ**, **Balchak DM**, **Montalbetti N**, **Carattino MD**, **Ray EC**, **Kashlan OB.** Murine epithelial sodium (Na +) channel regulation by biliary factors. *J Biol Chem* 294: 10182–10193, 2019. doi:10.1074/jbc.RA119.007394.
86. **Mroz MS**, **Harvey BJ.** Ursodeoxycholic acid inhibits ENaC and Na/K pump activity to restore airway surface liquid height in cystic fibrosis bronchial epithelial cells. *Steroids* 151: 108461, 2019. doi:10.1016/j.steroids.2019.108461.
87. **Ilyaskin AV**, **Diakov A**, **Korbmacher C**, **Haerteis S.** Bile acids potentiate proton-activated currents in *Xenopus laevis* oocytes expressing human acid-sensing ion channel (ASIC1a). *Physiol Rep* 5: e13132, 2017. doi:10.14814/phy2.13132.
88. **Dopico AM**, **Bukiya AN.** Regulation of Ca^{2+}-sensitive K^+ channels by cholesterol and bile acids via distinct channel subunits and sites. *Curr Top Membr* 80: 53–93, 2017. doi:10.1016/bs.ctm.2017.07.001.
89. **Schubring SR**, **Fleischer W**, **Lin JS**, **Haas HL**, **Sergeeva OA.** The bile steroid chenodeoxycholate is a potent antagonist at NMDA and GABA(A) receptors. *Neurosci Lett* 506: 322–326, 2012. doi:10.1016/j.neulet.2011.11.036.

Downloaded from journals.physiology.org/journal/ajpgi at New York Univ (216.165.095.084) on September 28, 2023.

90. **Yanovsky Y**, **Schubring SR**, **Yao QL**, **Zhao Y**, **Li S**, **May A**, **Haas HL**, **Lin JS**, **Sergeeva OA.** Waking action of ursodeoxycholic acid (UDCA) involves histamine and GABA(A) receptor block. *Plos One* 7: e42512, 2012. doi:10.1371/journal.pone.0042512.
91. **Koch A**, **Bonus M**, **Gohlke H**, **Klöcker N.** Isoform-specific inhibition of *N*-methyl-D-aspartate receptors by bile salts. *Sci Rep* 9: 10068, 2019. doi:10.1038/s41598-019-46496-y.
92. **Ilyaskin AV**, **Sure F**, **Nesterov V**, **Haerteis S**, **Korbmacher C.** Bile acids inhibit human purinergic receptor P2X4 in a heterologous expression system. *J Gen Physiol* 151: 820–833, 2019. doi:10.1085/jgp.201812291.
93. **Schmidt A**, **Joussen S**, **Hausmann R**, **Gründer S**, **Wiemuth D.** Bile acids are potent inhibitors of rat P2X2 receptors. *Purinergic Signal* 15: 213–221, 2019. doi:10.1007/s11302-019-09657-2.
94. **Sakai H**, **Lingueglia E**, **Champigny G**, **Mattei MG**, **Lazdunski M.** Cloning and functional expression of a novel degenerin-like Na^+ channel gene in mammals. *J Physiol* 519: 323–333, 1999. doi:10.1111/j.1469-7793.1999.0323m.x.
95. **Schaefer L**, **Sakai H**, **Mattei MG**, **Lazdunski M**, **Lingueglia E.** Molecular cloning, functional expression and chromosomal localization of an amiloride-sensitive Na^+ channel from human small intestine. *Febs Lett* 471: 205–210, 2000. doi:10.1016/S0014-5793(00)01403-4.
96. **Li Q**, **Kresge C**, **Bugde A**, **Lamphere M**, **Park JY**, **Feranchak AP.** Regulation of mechanosensitive biliary epithelial transport by the epithelial Na^+ channel. *Hepatology* 63: 538–549, 2016. doi:10.1002/hep.28301.
97. **Garty H**, **Palmer LG.** Epithelial sodium channels: function, structure, and regulation. *Physiol Rev* 77: 359–396, 1997. doi:10.1152/physrev.1997.77.2.359.
98. **Schild L.** The epithelial sodium channel and the control of sodium balance. *Biochim Biophys Acta* 1802: 1159–1165, 2010. doi:10.1016/j.bbadis.2010.06.014.
99. **Rossier BC.** Epithelial sodium channel (ENaC) and the control of blood pressure. *Curr Opin Pharmacol* 15: 33–46, 2014. doi:10.1016/j.coph.2013.11.010.
100. **Rotin D**, **Staub O.** Function and regulation of the epithelial Na^+ channel ENaC. *Compr Physiol* 11: 2017–2045, 2021. doi:10.1002/cphy.c200012.
101. **Loffing J**, **Korbmacher C.** Regulated sodium transport in the renal connecting tubule (CNT) via the epithelial sodium channel (ENaC). *Pflugers Arch* 458: 111–135, 2009. doi:10.1007/s00424-009-0656-0.
102. **Rossier BC**, **Stutts MJ.** Activation of the epithelial sodium channel (ENaC) by serine proteases. *Annu Rev Physiol* 71: 361–379, 2009. doi:10.1146/annurev.physiol.010908.163108.
103. **Kleyman TR**, **Kashlan OB**, **Hughey RP.** Epithelial Na^+ channel regulation by extracellular and intracellular factors. *Annu Rev Physiol* 80: 263–281, 2018. doi:10.1146/annurev-physiol-021317-121143.
104. **Kleyman TR**, **Eaton DC.** Regulating ENaC's gate. *Am J Physiol Cell Physiol* 318: C150–C162, 2020. doi:10.1152/ajpcell.00418.2019.
105. **Bertog M**, **Reeh L**, **Bunnett NW**, **Korbmacher C.** Lithocholic acid has a sustained stimulatory effect on the epithelial sodium channel (ENaC) in mouse late distal colon. *Acta Physiol* 219: 164, 2017. doi:10.1111/apha.12870.
106. **Holzer P.** Acid-sensing ion channels in gastrointestinal function. *Neuropharmacology* 94: 72–79, 2015. doi:10.1016/j.neuropharm.2014.12.009.
107. **Gonzales EB**, **Kawate T**, **Gouaux E.** Pore architecture and ion sites in acid-sensing ion channels and P2X receptors. *Nature* 460: 599–605, 2009. doi:10.1038/nature08218.
108. **Doctor RB**, **Matzakos T**, **McWilliams R**, **Johnson S**, **Feranchak AP**, **Fitz JG.** Purinergic regulation of cholangiocyte secretion: identification of a novel role for P2X receptors. *Am J Physiol Gastrointest Liver Physiol* 288: G779–G786, 2005. doi:10.1152/ajpgi.00325.2004.
109. **Besnard A**, **Gautherot J**, **Julien B**, **Tebbi A**, **Garcin I**, **Doignon I**, **Péan N**, **Gonzales E**, **Cassio D**, **Grosse B**, **Liu BK**, **Safya H**, **Cauchois F**, **Humbert L**, **Rainteau D**, **Tordjmann T.** The P2X4 purinergic receptor impacts liver regeneration after partial hepatectomy in mice through the regulation of biliary homeostasis. *Hepatology* 64: 941–953, 2016. doi:10.1002/hep.28675.
110. **Ruan HZ**, **Burnstock G.** P2X2 and P2X3 receptor expression in the gallbladder of the guinea pig. *Auton Neurosci* 111: 89–96, 2004. doi:10.1016/j.autneu.2004.03.002.
111. **Castelucci P**, **Robbins HL**, **Poole DP**, **Furness JB.** The distribution of purine P2X(2) receptors in the guinea-pig enteric nervous system. *Histochem Cell Biol* 117: 415–422, 2002. doi:10.1007/s00418-002-0404-4.
112. **Barrett KE**, **Keely SJ.** Electrolyte secretion and absorption in the small intestine and colon. In: *Textbook of Gastroenterology*, edited by Podolsky D, Camilleri M, Fitz J, Kalloo A, Shanahan F, Wang T. Hoboken, NJ: Wiley-Blackwell, 2015.
113. **Forth W**, **Rummel W**, **Glasner H.** [On the absorption inhibiting effect of bile acids]. *Naunyn Schmiedebergs Arch Pharmakol Exp Pathol* 254: 364–380, 1966.
114. **Hofmann AF.** The syndrome of ileal disease and the broken enterohepatic circulation: cholerheic enteropathy. *Gastroenterology* 52: 752–757, 1967.
115. **Mekjian HS**, **Phillips SF**, **Hofmann AF.** Colonic secretion of water and electrolytes induced by bile acids: perfusion studies in man. *J Clin Invest* 50: 1569–1577, 1971. doi:10.1172/JCI106644.
116. **Wingate DL**, **Krag E**, **Mekhjian HS**, **Phillips SF.** Relationships between ion and water movement in the human jejunum, ileum and colon during perfusion with bile acids. *Clin Sci Mol Med* 45: 593–606, 1973. doi:10.1042/cs0450593.
117. **Feldman S**, **Gibaldi M.** Effect of bile salts on gastric emptying and intestinal transit in the rat. *Gastroenterology* 54: 918–921, 1968.
118. **Brown NJ**, **Read NW**, **Richardson A**, **Rumsey RD**, **Bogentoft C.** Characteristics of lipid substances activating the ileal brake in the rat. *Gut* 31: 1126–1129, 1990. doi:10.1136/gut.31.10.1126.
119. **Hansen M**, **Scheltema MJ**, **Sonne DP**, **Hansen JS**, **Sperling M**, **Rehfeld JF**, **Holst JJ**, **Vilsbøll T**, **Knop FK.** Effect of chenodeoxycholic acid and the bile acid sequestrant colesevelam on glucagon-like peptide-1 secretion. *Diabetes Obes Metab* 18: 571–580, 2016. doi:10.1111/dom.12648.
120. **Penagini R**, **Misiewicz JJ**, **Frost PG.** Effect of jejunal infusion of bile acids on small bowel transit and fasting jejunal motility in man. *Gut* 29: 789–794, 1988. doi:10.1136/gut.29.6.789.
121. **Penagini R**, **Spiller RC**, **Misiewicz JJ**, **Frost PG.** Effect of ileal infusion of glycochenodeoxycholic acid on segmental transit, motility, and flow in the human jejunum and ileum. *Gut* 30: 609–617, 1989. doi:10.1136/gut.30.5.609.
122. **Armstrong DN**, **Krenz HK**, **Modlin IM**, **Ballantyne GH.** Bile salt inhibition of motility in the isolated perfused rabbit terminal ileum. *Gut* 34: 483–488, 1993. doi:10.1136/gut.34.4.483.
123. **Roda E**, **Bazzoli F**, **Labate AM**, **Mazzella G**, **Roda A**, **Sama C**, **Festi D**, **Aldini R**, **Taroni F**, **Barbara L.** Ursodeoxycholic acid vs. chenodeoxycholic acid as cholesterol gallstone-dissolving agents: a comparative randomized study. *Hepatology* 2: 804–810, 1982. doi:10.1002/hep.1840020611.
124. **Bampton PA**, **Dinning PG**, **Kennedy ML**, **Lubowski DZ**, **Cook IJ.** The proximal colonic motor response to rectal mechanical and chemical stimulation. *Am J Physiol Gastrointest Liver Physiol* 282: G443–G449, 2002. doi:10.1152/ajpgi.00194.2001.
125. **Odunsi-Shiyanbade ST**, **Camilleri M**, **McKinzie S**, **Burton D**, **Carlson P**, **Busciglio IA**, **Lamsam J**, **Singh R**, **Zinsmeister AR.** Effects of chenodeoxycholate and a bile acid sequestrant, colesevelam, on intestinal transit and bowel function. *Clin Gastroenterol Hepatol* 8: 159–165, 2010. doi:10.1016/j.cgh.2009.10.020.
126. **Rao AS**, **Wong BS**, **Camilleri M**, **Odunsi-Shiyanbade ST**, **McKinzie S**, **Ryks M**, **Burton D**, **Carlson P**, **Lamsam J**, **Singh R**, **Zinsmeister AR.** Chenodeoxycholate in females with irritable bowel syndrome-constipation: a pharmacodynamic and pharmacogenetic analysis. *Gastroenterology* 139: 1549–1558, 2010. doi:10.1053/j.gastro.2010.07.052.
127. **Wu T**, **Bound MJ**, **Standfield SD**, **Gedulin B**, **Jones KL**, **Horowitz M**, **Rayner CK.** Effects of rectal administration of taurocholic acid on glucagon-like peptide-1 and peptide YY secretion in healthy humans. *Diabetes Obes Metab* 15: 474–477, 2013. doi:10.1111/dom.12043.
128. **Poole DP**, **Godfrey C**, **Cattaruzza F**, **Cottrell GS**, **Kirkland JG**, **Pelayo JC**, **Bunnett NW**, **Corvera CU.** Expression and function of the bile acid receptor GpBAR1 (TGR5) in the murine enteric nervous system. *Neurogastroenterol Motil* 22: 814–e228, 2010. doi:10.1111/j.1365-2982.2010.01487.x.
129. **Alemi F**, **Kwon E**, **Poole DP**, **Lieu T**, **Lyo V**, **Cattaruzza F**, **Cevikbas F**, **Steinhoff M**, **Nassini R**, **Materazzi S**, **Guerrero-Alba R**, **Valdez-Morales E**, **Cottrell GS**, **Schoonjans K**, **Geppetti P**, **Vanner SJ**,

Downloaded from journals.physiology.org/journal/ajpgi at New York Univ (216.165.095.084) on September 28, 2023.

Bunnett NW, **Corvera CU.** The TGR5 receptor mediates bile acid-induced itch and analgesia. *J Clin Invest* 123: 1513–1530, 2013. doi:10.1172/JCI64551.

130. **Hu LD**, **Yu BP**, **Yang B.** Deoxycholic acid inhibits smooth muscle contraction via protein kinase C-dependent modulation of L-type Ca2+ channels in rat proximal colon. *Mol Med Rep* 6: 833–837, 2012. doi:10.3892/mmr.2012.984.
131. **Kirwan WO**, **Smith AN**, **Mitchell WD**, **Falconer JD**, **Eastwood MA.** Bile acids and colonic motility in the rabbit and the human. *Gut* 16: 894–902, 1975. doi:10.1136/gut.16.11.894.
132. **Falconer JD**, **Smith AN**, **Eastwood MA.** The effects of bile acids on colonic motility in the rabbit. *Q J Exp Physiol Cogn Med Sci* 65: 135–144, 1980. doi:10.1113/expphysiol.1980.sp002497.
133. **Dharmsathaphorn K**, **Huott PA**, **Vongkovit P**, **Beuerlein G**, **Pandol SJ**, **Ammon HV.** Cl- secretion induced by bile salts. A study of the mechanism of action based on a cultured colonic epithelial cell line. *J Clin Invest* 84: 945–953, 1989. doi:10.1172/JCI114257.
134. **Keely SJ**, **Scharl MM**, **Bertelsen LS**, **Hagey LR**, **Barrett KE**, **Hofmann AF.** Bile acid-induced secretion in polarized monolayers of T84 colonic epithelial cells: structure-activity relationships. *Am J Physiol Gastrointest Liver Physiol* 292: G290–G297, 2007. doi:10.1152/ajpgi.00076.2006.
135. **Kelly OB**, **Mroz MS**, **Ward JB**, **Colliva C**, **Scharl M**, **Pellicciari R**, **Gilmer JF**, **Fallon PG**, **Hofmann AF**, **Roda A**, **Murray FE**, **Keely SJ.** Ursodeoxycholic acid attenuates colonic epithelial secretory function. *J Physiol* 591: 2307–2318, 2013. doi:10.1113/jphysiol.2013.252544.
136. **Teem MV**, **Phillips SF.** Perfusion of the hamster jejunum with conjugated and unconjugated bile acids: inhibition of water absorption and effects on morphology. *Gastroenterology* 62: 261–267, 1972.
137. **Gracey M**, **Papadimitriou J**, **Burke V**, **Thomas J**, **Bower G.** Effects on small-intestinal function and structure induced by feeding a deconjugated bile salt. *Gut* 14: 519–528, 1973. doi:10.1136/gut.14.7.519.
138. **Volpe BT**, **Binder HJ.** Bile salt alteration of ion transport across jejunal mucosa. *Biochim Biophys Acta* 394: 597–604, 1975. doi:10.1016/0005-2736(75)90145-5.
139. **Freel RW**, **Hatch M**, **Earnest DL**, **Goldner AM.** Dihydroxy bile salt-induced alterations in NaCl transport across the rabbit colon. *Am J Physiol Gastrointest Liver Physiol* 245: G808–G815, 1983. doi:10.1152/ajpgi.1983.245.6.G808.
140. **Binder HJ**, **Rawlins CL.** Effect of conjugated dihydroxy bile salts on electrolyte transport in rat colon. *J Clin Invest* 52: 1460–1466, 1973. doi:10.1172/JCI107320.
141. **Mauricio AC**, **Slawik M**, **Heitzmann D**, **von Hahn T**, **Warth R**, **Bleich M**, **Greger R.** Deoxycholic acid (DOC) affects the transport properties of distal colon. *Pflugers Arch* 439: 532–540, 2000. doi:10.1007/s004249900226.
142. **Alrefai WA**, **Saksena S**, **Tyagi S**, **Gill RK**, **Ramaswamy K**, **Dudeja PK.** Taurodeoxycholate modulates apical Cl^-/OH^- exchange activity in Caco2 cells. *Dig Dis Sci* 52: 1270–1278, 2007. doi:10.1007/s10620-006-9090-8.
143. **Pallagi-Kunstár É**, **Farkas K**, **Maléth J**, **Rakonczay Z Jr**, **Nagy F**, **Molnár T**, **Szepes Z**, **Venglovecz V**, **Lonovics J**, **Rázga Z**, **Wittmann T**, **Hegyi P.** Bile acids inhibit Na^+/H^+ exchanger and Cl^-/HCO_3^- exchanger activities via cellular energy breakdown and Ca^{2+} overload in human colonic crypts. *Pflugers Arch* 467: 1277–1290, 2015. doi:10.1007/s00424-014-1560-9.
144. **Moschetta A**, **Portincasa P**, **Debellis L**, **Petruzzelli M**, **Montelli R**, **Calamita G**, **Gustavsson P**, **Palasciano G.** Basolateral Ca^{2+}-dependent K^+-channels play a key role in Cl^- secretion induced by taurodeoxycholate from colon mucosa. *Biol Cell* 95: 115–122, 2003. doi:10.1016/s0248-4900(03)00011-x.
145. **Devor DC**, **Sekar MC**, **Frizzell RA**, **Duffey ME.** Taurodeoxycholate activates potassium and chloride conductances via an IP3-mediated release of calcium from intracellular stores in a colonic cell line (T84). *J Clin Invest* 92: 2173–2181, 1993. doi:10.1172/JCI116819.
146. **Gerbino A**, **Ranieri M**, **Lupo S**, **Caroppo R**, **Debellis L**, **Maiellaro I**, **Caratozzolo MF**, **Lopez F**, **Colella M.** Ca^{2+}-dependent K^+ efflux regulates deoxycholate-induced apoptosis of BHK-21 and Caco-2 cells. *Gastroenterology* 137: 955–964, 2009. doi:10.1053/j.gastro.2009.03.038.
147. **Chien JM**, **Chou CT**, **Liang WZ**, **Cheng JS**, **Chang HT**, **Tseng HW**, **Kuo SY**, **Kuo CC**, **Chen FA**, **Shieh P**, **Ho CM**, **Lin JR**, **Kuo DH**, **Jan CR.** Effect of deoxycholic acid on Ca^{2+} movement, cell viability and apoptosis in human gastric cancer cells. *Toxicol Mech Methods* 25: 113–119, 2015. doi:10.3109/15376516.2014.990597.
148. **Ward JB**, **Mroz MS**, **Keely SJ.** The bile acid receptor, TGR5, regulates basal and cholinergic-induced secretory responses in rat colon. *Neurogastroenterol Motil* 25: 708–711, 2013. doi:10.1111/nmo.12148.
149. **Akare S**, **Martinez JD.** Bile acid induces hydrophobicity-dependent membrane alterations. *Biochim Biophys Acta* 1735: 59–67, 2005. doi:10.1016/j.bbalip.2005.04.006.
150. **Jean-Louis S**, **Akare S**, **Ali MA**, **Mash EA Jr**, **Meuillet E**, **Martinez JD.** Deoxycholic acid induces intracellular signaling through membrane perturbations. *J Biol Chem* 281: 14948–14960, 2006. doi:10.1074/jbc.M506710200.
151. **Combettes L**, **Berthon B**, **Claret M**, **Erlinger S.** Selective permeabilization of the endoplasmic reticulum by monohydroxylated bile acids in liver. *Hepatology* 9: 663–665, 1989. doi:10.1002/hep.1840090431.
152. **Combettes L**, **Dumont M**, **Berthon B**, **Erlinger S**, **Claret M.** Release of calcium from the endoplasmic reticulum by bile acids in rat liver cells. *J Biol Chem* 263: 2299–2303, 1988.
153. **Peregrin AT**, **Ahlman H**, **Jodal M**, **Lundgren O.** Involvement of serotonin and calcium channels in the intestinal fluid secretion evoked by bile salt and cholera toxin. *Br J Pharmacol* 127: 887–894, 1999. doi:10.1038/sj.bjp.0702615.
154. **Tantisira MH**, **Jodal M**, **Lundgren O.** Intraluminal bile salt increases rate of firing in afferent fibers from the small intestine of the rat. *Experientia* 43: 168–169, 1987. doi:10.1007/BF01942837.
155. **Karlström L**, **Cassuto J**, **Jodal M**, **Lundgren O.** The importance of the enteric nervous system for the bile-salt-induced secretion in the small intestine of the rat. *Scand J Gastroenterol* 18: 117–123, 1983. doi:10.3109/00365528309181570.
156. **Karlström L.** Evidence of involvement of the enteric nervous system in the effects of sodium deoxycholate on small-intestinal transepithelial fluid transport and motility. *Scand J Gastroenterol* 21: 321–330, 1986. doi:10.3109/00365528609003082.
157. **Forsgård RA**, **Korpela R**, **Stenman LK**, **Osterlund P**, **Holma R.** Deoxycholic acid induced changes in electrophysiological parameters and macromolecular permeability in murine small intestine with and without functional enteric nervous system plexuses. *Neurogastroenterol Motil* 26: 1179–1187, 2014. doi:10.1111/nmo.12383.
158. **Sun Y**, **Fihn BM**, **Sjövall H**, **Jodal M.** Enteric neurones modulate the colonic permeability response to luminal bile acids in rat colon in vivo. *Gut* 53: 362–367, 2004. doi:10.1136/gut.2003.015867.
159. **Quist RG**, **Ton-Nu HT**, **Lillienau J**, **Hofmann AF**, **Barrett KE.** Activation of mast cells by bile acids. *Gastroenterology* 101: 446–456, 1991. doi:10.1016/0016-5085(91)90024-f.
160. **Gelbmann CM**, **Schteingart CD**, **Thompson SM**, **Hofmann AF**, **Barrett KE.** Mast cells and histamine contribute to bile acid-stimulated secretion in the mouse colon. *J Clin Invest* 95: 2831–2839, 1995. doi:10.1172/JCI117988.
161. **Arizono N**, **Matsuda S**, **Hattori T**, **Kojima Y**, **Maeda T**, **Galli SJ.** Anatomical variation in mast cell nerve associations in the rat small intestine, heart, lung, and skin. Similarities of distances between neural processes and mast cells, eosinophils, or plasma cells in the jejunal lamina propria. *Lab Invest* 62: 626–634, 1990.
162. **Stead RH**, **Dixon MF**, **Bramwell NH**, **Riddell RH**, **Bienenstock J.** Mast cells are closely apposed to nerves in the human gastrointestinal mucosa. *Gastroenterology* 97: 575–585, 1989. doi:10.1016/0016-5085(89)90627-6.
163. **Keating N**, **Mroz MS**, **Scharl MM**, **Marsh C**, **Ferguson G**, **Hofmann AF**, **Keely SJ.** Physiological concentrations of bile acids down-regulate agonist induced secretion in colonic epithelial cells. *J Cell Mol Med* 13: 2293–2303, 2009. doi:10.1111/j.1582-4934.2009.00838.x.
164. **Hamilton JP**, **Xie G**, **Raufman JP**, **Hogan S**, **Griffin TL**, **Packard CA**, **Chatfield DA**, **Hagey LR**, **Steinbach JH**, **Hofmann AF.** Human cecal bile acids: concentration and spectrum. *Am J Physiol Gastrointest Liver Physiol* 293: G256–G263, 2007. doi:10.1152/ajpgi.00027.2007.
165. **Wei W**, **Wang HF**, **Zhang Y**, **Zhang YL**, **Niu BY**, **Yao SK.** Altered metabolism of bile acids correlates with clinical parameters and the gut microbiota in patients with diarrhea-predominant irritable bowel syndrome. *World J Gastroenterol* 26: 7153–7172, 2020. doi:10.3748/wjg.v26.i45.7153.

Downloaded from journals.physiology.org/journal/ajpgi at New York Univ (216.165.095.084) on September 28, 2023.

166. **Zhan K**, **Zheng H**, **Li J**, **Wu H**, **Qin S**, **Luo L**, **Huang S.** Gut microbiota-bile acid crosstalk in diarrhea-irritable bowel syndrome. *Biomed Res Int* 2020: 3828249, 2020. doi:10.1155/2020/3828249.
167. **Sagar NM**, **Duboc H**, **Kay GL**, **Alam MT**, **Wicaksono AN**, **Covington JA**, **Quince C**, **Kokkorou M**, **Svolos V**, **Palmieri LJ**, **Gerasimidis K**, **Walters JRF**, **Arasaradnam RP.** The pathophysiology of bile acid diarrhoea: differences in the colonic microbiome, metabolome and bile acids. *Sci Rep* 10: 20436, 2020. doi:10.1038/s41598-020-77374-7.
168. **Camilleri M**, **Vijayvargiya P.** The role of bile acids in chronic diarrhea. *Am J Gastroenterol* 115: 1596–1603, 2020. doi:10.14309/ajg.0000000000000696.
169. **Jeffery IB**, **Das A**, **O'Herlihy E**, **Coughlan S**, **Cisek K**, **Moore M**, **Bradley F**, **Carty T**, **Pradhan M**, **Dwibedi C**, **Shanahan F**, **O'Toole PW.** Differences in fecal microbiomes and metabolomes of people with vs without irritable bowel syndrome and bile acid malabsorption. *Gastroenterology* 158: 1016–1028.e8, 2020. doi:10.1053/j.gastro.2019.11.301.
170. **Bazzoli F**, **Malavolti M**, **Petronelli A**, **Barbara L**, **Roda E.** Treatment of constipation with chenodeoxycholic acid. *J Int Med Res* 11: 120–123, 1983. doi:10.1177/030006058301100211.
171. **Fromm H**, **Sarva RP**, **Ravitch MM**, **McJunkin B**, **Farivar S**, **Amin P.** Effects of jejunoileal bypass on the enterohepatic circulation of bile acids, bacterial flora in the upper small intestine, and absorption of vitamin B12. *Metabolism* 32: 1133–1141, 1983. doi:10.1016/0026-0495(83)90060-4.
172. **Sackmann M**, **Pauletzki J**, **Aydemir U**, **Holl J**, **Sauerbruch T**, **Hasford J**, **Paumgartner G.** Efficacy and safety of ursodeoxycholic acid for dissolution of gallstone fragments: comparison with the combination of ursodeoxycholic acid and chenodeoxycholic acid. *Hepatology* 14: 1136–1141, 1991.
173. **Iguchi Y**, **Nishimaki-Mogami T**, **Yamaguchi M**, **Teraoka F**, **Kaneko T**, **Une M.** Effects of chemical modification of ursodeoxycholic acid on TGR5 activation. *Biol Pharm Bull* 34: 1–7, 2011. doi:10.1248/bpb.34.1.
174. **Camilleri M**, **Klee EW**, **Shin A**, **Carlson P**, **Li Y**, **Grover M**, **Zinsmeister AR.** Irritable bowel syndrome-diarrhea: characterization of genotype by exome sequencing, and phenotypes of bile acid synthesis and colonic transit. *Am J Physiol Gastrointest Liver Physiol* 306: G13–G26, 2014. doi:10.1152/ajpgi.00294.2013.
175. **Camilleri M**, **Vazquez-Roque MI**, **Carlson P**, **Burton D**, **Wong BS**, **Zinsmeister AR.** Association of bile acid receptor TGR5 variation and transit in health and lower functional gastrointestinal disorders. *Neurogastroenterol Motil* 23: 995–e458, 2011. doi:10.1111/j.1365-2982.2011.01772.x.
176. **Giaretta PR**, **Suchodolski JS**, **Blick AK**, **Steiner JM**, **Lidbury JA**, **Rech RR.** Distribution of bile acid receptor TGR5 in the gastrointestinal tract of dogs. *Histol Histopathol* 34: 69–79, 2019. doi:10.14670/HH-18-025.
177. **Dopico AM**, **Walsh JV Jr**, **Singer JJ.** Natural bile acids and synthetic analogues modulate large conductance Ca^{2+}-activated K^+ (BKCa) channel activity in smooth muscle cells. *J Gen Physiol* 119: 251–273, 2002. doi:10.1085/jgp.20028537.
178. **Meier Y**, **Eloranta JJ**, **Darimont J**, **Ismair MG**, **Hiller C**, **Fried M**, **Kullak-Ublick GA**, **Vavricka SR.** Regional distribution of solute carrier mRNA expression along the human intestinal tract. *Drug Metab Dispos* 35: 590–594, 2007. doi:10.1124/dmd.106.013342.
179. **Biagioli M**, **Carino A**, **Cipriani S**, **Francisci D**, **Marchiano S**, **Scarpelli P**, **Sorcini D**, **Zampella A**, **Fiorucci S.** The bile acid receptor GPBAR1 regulates the M1/M2 phenotype of intestinal macrophages and activation of GPBAR1 rescues mice from murine colitis. *J Immunol* 199: 718–733, 2017. doi:10.4049/jimmunol.1700183.
180. **Cipriani S**, **Mencarelli A**, **Chini MG**, **Distrutti E**, **Renga B**, **Bifulco G**, **Baldelli F**, **Donini A**, **Fiorucci S.** The bile acid receptor GPBAR-1 (TGR5) modulates integrity of intestinal barrier and immune response to experimental colitis. *PLoS One* 6: e25637, 2011 [Erratum in *PLoS One* 8, 2013. doi:10.1371/journal.pone.0025637.
181. **Adrian TE**, **Ballantyne GH**, **Longo WE**, **Bilchik AJ**, **Graham S**, **Basson MD**, **Tierney RP**, **Modlin IM.** Deoxycholate is an important releaser of peptide YY and enteroglucagon from the human colon. *Gut* 34: 1219–1224, 1993. doi:10.1136/gut.34.9.1219.
182. **Adrian TE**, **Gariballa S**, **Parekh KA**, **Thomas SA**, **Saadi H**, **Al Kaabi J**, **Nagelkerke N**, **Gedulin B**, **Young AA.** Rectal taurocholate increases L cell and insulin secretion, and decreases blood glucose and food intake in obese type 2 diabetic volunteers. *Diabetologia* 55: 2343–2347, 2012. doi:10.1007/s00125-012-2593-2.
183. **Dumoulin V**, **Moro F**, **Barcelo A**, **Dakka T**, **Cuber JC.** Peptide YY, glucagon-like peptide-1, and neurotensin responses to luminal factors in the isolated vascularly perfused rat ileum. *Endocrinology* 139: 3780–3786, 1998. doi:10.1210/endo.139.9.6202.
184. **Meyer-Gerspach AC**, **Steinert RE**, **Keller S**, **Malarski A**, **Schulte FH**, **Beglinger C.** Effects of chenodeoxycholic acid on the secretion of gut peptides and fibroblast growth factors in healthy humans. *J Clin Endocrinol Metab* 98: 3351–3358, 2013. doi:10.1210/jc.2012-4109.
185. **Plaisancié P**, **Dumoulin V**, **Chayvialle JA**, **Cuber JC.** Luminal peptide YY-releasing factors in the isolated vascularly perfused rat colon. *J Endocrinol* 151: 421–429, 1996. doi:10.1677/joe.0.1510421.
186. **Brighton CA**, **Rievaj J**, **Kuhre RE**, **Glass LL**, **Schoonjans K**, **Holst JJ**, **Gribble FM**, **Reimann F.** Bile acids trigger GLP-1 release predominantly by accessing basolaterally located G protein-coupled bile acid receptors. *Endocrinology* 156: 3961–3970, 2015. doi:10.1210/en.2015-1321.
187. **Harach T**, **Pols TW**, **Nomura M**, **Maida A**, **Watanabe M**, **Auwerx J**, **Schoonjans K.** TGR5 potentiates GLP-1 secretion in response to anionic exchange resins. *Sci Rep* 2: 430, 2012. doi:10.1038/srep00430.
188. **Amato A**, **Baldassano S**, **Liotta R**, **Serio R**, **Mulè F.** Exogenous glucagon-like peptide 1 reduces contractions in human colon circular muscle. *J Endocrinol* 221: 29–37, 2014. doi:10.1530/JOE-13-0525.
189. **May AT**, **Crowe MS**, **Blakeney BA**, **Mahavadi S**, **Wang H**, **Grider JR**, **Murthy KS.** Identification of expression and function of the glucagon-like peptide-1 receptor in colonic smooth muscle. *Peptides* 112: 48–55, 2019. doi:10.1016/j.peptides.2018.11.007.
190. **Halim MA**, **Degerblad M**, **Sundbom M**, **Karlbom U**, **Holst JJ**, **Webb DL**, **Hellström PM.** Glucagon-like peptide-1 inhibits prandial gastrointestinal motility through myenteric neuronal mechanisms in humans. *J Clin Endocrinol Metab* 103: 575–585, 2018. doi:10.1210/jc.2017-02006.
191. **O'Brien R**, **O'Malley D.** The Glucagon-like peptide-1 receptor agonist, exendin-4, ameliorated gastrointestinal dysfunction in the Wistar Kyoto rat model of Irritable Bowel Syndrome. *Neurogastroenterol Motil* 32: e13738, 2020. doi:10.1111/nmo.13738.
192. **Tolessa T**, **Gutniak M**, **Holst JJ**, **Efendic S**, **Hellstrom PM.** Glucagon-like peptide-1 retards gastric emptying and small bowel transit in the rat: effect mediated through central or enteric nervous mechanisms. *Dig Dis Sci* 43: 2284–2290, 1998. doi:10.1023/a:1026678925120.
193. **Ferrier L**, **Segain JP**, **Pacaud P**, **Cherbut C**, **Loirand G**, **Galmiche JP**, **Blottière HM.** Pathways and receptors involved in peptide YY induced contraction of rat proximal colonic muscle in vitro. *Gut* 46: 370–375, 2000. doi:10.1136/gut.46.3.370.
194. **Fox-Threlkeld JA**, **Daniel EE**, **Christinck F**, **Woskowska Z**, **Cipris S**, **McDonald TJ.** Peptide YY stimulates circular muscle contractions of the isolated perfused canine ileum by inhibiting nitric oxide release and enhancing acetylcholine release. *Peptides* 14: 1171–1178, 1993. doi:10.1016/0196-9781(93)90172-d.
195. **Lundberg JM**, **Tatemoto K**, **Terenius L**, **Hellström PM**, **Mutt V**, **Hökfelt T**, **Hamberger B.** Localization of peptide YY (PYY) in gastrointestinal endocrine cells and effects on intestinal blood flow and motility. *Proc Natl Acad Sci USA* 79: 4471–4475, 1982. doi:10.1073/pnas.79.14.4471.
196. **Tough IR**, **Forbes S**, **Tolhurst R**, **Ellis M**, **Herzog H**, **Bornstein JC**, **Cox HM.** Endogenous peptide YY and neuropeptide Y inhibit colonic ion transport, contractility and transit differentially via Y_1 and Y_2 receptors. *Br J Pharmacol* 164: 471–484, 2011. doi:10.1111/j.1476-5381.2011.01401.x.
197. **Ferrier L**, **Segain JP**, **Bonnet C**, **Cherbut C**, **Lehur PA**, **Jarry A**, **Galmiche JP**, **Blottiere HM.** Functional mapping of NPY/PYY receptors in rat and human gastro-intestinal tract. *Peptides* 23: 1765–1771, 2002. doi:10.1016/s0196-9781(02)00133-x.
198. **Krantis A**, **Potvin W**, **Harding RK.** Peptide YY (PYY) stimulates intrinsic enteric motor neurones in the rat small intestine. *Naunyn Schmiedebergs Arch Pharmacol* 338: 287–292, 1988. doi:10.1007/BF00173402.
199. **Larhammar D.** Structural diversity of receptors for neuropeptide Y, peptide YY and pancreatic polypeptide. *Regul Pept* 65: 165–174, 1996. doi:10.1016/0167-0115(96)00110-3.
200. **Cho HJ**, **Kosari S**, **Hunne B**, **Callaghan B**, **Rivera LR**, **Bravo DM**, **Furness JB.** Differences in hormone localisation patterns of K and L

Downloaded from journals.physiology.org/journal/ajpgi at New York Univ (216.165.095.084) on September 28, 2023.

type enteroendocrine cells in the mouse and pig small intestine and colon. *Cell Tissue Res* 359: 693–698, 2015. doi:10.1007/s00441-014-2033-3.

201. **Svendsen B**, **Pedersen J**, **Albrechtsen NJ**, **Hartmann B**, **Toräng S**, **Rehfeld JF**, **Poulsen SS**, **Holst JJ.** An analysis of cosecretion and coexpression of gut hormones from male rat proximal and distal small intestine. *Endocrinology* 156: 847–857, 2015. doi:10.1210/en.2014-1710.
202. **Austad WI**, **Lack L**, **Tyor MP.** Importance of bile acids and of an intact distal small intestine for fat absorption. *Gastroenterology* 52: 638–646, 1967.
203. **Valentin N**, **Camilleri M**, **Altayar O**, **Vijayvargiya P**, **Acosta A**, **Nelson AD**, **Murad MH.** Biomarkers for bile acid diarrhoea in functional bowel disorder with diarrhoea: a systematic review and meta-analysis. *Gut* 65: 1951–1959, 2016. doi:10.1136/gutjnl-2015-309889.
204. **Oelkers P**, **Kirby LC**, **Heubi JE**, **Dawson PA.** Primary bile acid malabsorption caused by mutations in the ileal sodium-dependent bile acid transporter gene (SLC10A2). *J Clin Invest* 99: 1880–1887, 1997. doi:10.1172/JCI119355.
205. **Ho RH**, **Leake BF**, **Urquhart BL**, **Gregor JC**, **Dawson PA**, **Kim RB.** Functional characterization of genetic variants in the apical sodium-dependent bile acid transporter (ASBT; SLC10A2). *J Gastroenterol Hepatol* 26: 1740–1748, 2011. doi:10.1111/j.1440-1746.2011.06805.x.
206. **Sultan M**, **Rao A**, **Elpeleg O**, **Vaz FM**, **Abu-Libdeh B**, **Karpen SJ**, **Dawson PA.** Organic solute transporter-β (SLC51B) deficiency in two brothers with congenital diarrhea and features of cholestasis. *Hepatology* 68: 590–598, 2018. doi:10.1002/hep.29516.
207. **Arlow FL**, **Dekovich AA**, **Priest RJ**, **Beher WT.** Bile acids in radiation-induced diarrhea. *South Med J* 80: 1259–1261, 1987. doi:10.1097/00007611-198710000-00015.
208. **Shin A**, **Camilleri M**, **Vijayvargiya P**, **Busciglio I**, **Burton D**, **Ryks M**, **Rhoten D**, **Lueke A**, **Saenger A**, **Girtman A**, **Zinsmeister AR.** Bowel functions, fecal unconjugated primary and secondary bile acids, and colonic transit in patients with irritable bowel syndrome. *Clin Gastroenterol Hepatol* 11: 1270–1275.e1, 2013. doi:10.1016/j.cgh.2013.04.020.
209. **Aldini R**, **Roda A**, **Festi D**, **Sama C**, **Mazzella G**, **Bazzoli F**, **Morselli AM**, **Roda E**, **Barbara L.** Bile acid malabsorption and bile acid diarrhea in intestinal resection. *Dig Dis Sci* 27: 495–502, 1982. doi:10.1007/BF01296727.
210. **Camilleri M**, **Busciglio I**, **Acosta A**, **Shin A**, **Carlson P**, **Burton D**, **Ryks M**, **Rhoten D**, **Lamsam J**, **Lueke A**, **Donato LJ**, **Zinsmeister AR.** Effect of increased bile acid synthesis or fecal excretion in irritable bowel syndrome-diarrhea. *Am J Gastroenterol* 109: 1621–1630, 2014. doi:10.1038/ajg.2014.215.
211. **Lee JM**, **Ong JR**, **Vergnes L**, **de Aguiar Vallim TQ**, **Nolan J**, **Cantor RM**, **Walters JRF**, **Reue K.** Diet1, bile acid diarrhea, and FGF15/19: mouse model and human genetic variants. *J Lipid Res* 59: 429–438, 2018. doi:10.1194/jlr.M078279.
212. **Walters JR**, **Tasleem AM**, **Omer OS**, **Brydon WG**, **Dew T**, **Le Roux CW.** A new mechanism for bile acid diarrhea: defective feedback inhibition of bile acid biosynthesis. *Clin Gastroenterol Hepatol* 7: 1189–1194, 2009. doi:10.1016/j.cgh.2009.04.024.
213. **Montagnani M**, **Love MW**, **Rössel P**, **Dawson PA**, **Qvist P.** Absence of dysfunctional ileal sodium-bile acid cotransporter gene mutations in patients with adult-onset idiopathic bile acid malabsorption. *Scand J Gastroenterol* 36: 1077–1080, 2001. doi:10.1080/003655201750422693.
214. **Wedlake L**, **Thomas K**, **Lalji A**, **Anagnostopoulos C**, **Andreyev HJ.** Effectiveness and tolerability of colesevelam hydrochloride for bile-acid malabsorption in patients with cancer: a retrospective chart review and patient questionnaire. *Clin Ther* 31: 2549–2558, 2009. doi:10.1016/j.clinthera.2009.11.027.
215. **Vijayvargiya P**, **Busciglio I**, **Burton D**, **Donato L**, **Lueke A**, **Camilleri M.** Bile acid deficiency in a subgroup of patients with irritable bowel syndrome with constipation based on biomarkers in serum and fecal samples. *Clin Gastroenterol Hepatol* 16: 522–527, 2018. doi:10.1016/j.cgh.2017.06.039.
216. **Chedid V**, **Vijayvargiya P**, **Camilleri M.** Elobixibat for the treatment of constipation. *Expert Rev Gastroenterol Hepatol* 12: 951–960, 2018. doi:10.1080/17474124.2018.1522248.
217. **Simrén M**, **Tack J.** New treatments and therapeutic targets for IBS and other functional bowel disorders. *Nat Rev Gastroenterol Hepatol* 15: 589–605, 2018. doi:10.1038/s41575-018-0034-5.
218. **Gillberg P-G**, **Dahlström M**, **Starke I**, **Östlund-Lindqvist A-M.** The IBAT inhibition by A3309 a potential mechanism for the treatment of constipation. *Gastroenterology* 138: S224, 2010. doi:10.1016/S0016-5085(10)61017-7.
219. **Chey WD**, **Camilleri M**, **Chang L**, **Rikner L**, **Graffner H.** A randomized placebo-controlled phase IIb trial of a3309, a bile acid transporter inhibitor, for chronic idiopathic constipation. *Am J Gastroenterol* 106: 1803–1812, 2011. doi:10.1038/ajg.2011.162.
220. **Nakajima A**, **Seki M**, **Taniguchi S.** Determining an optimal clinical dose of elobixibat, a novel inhibitor of the ileal bile acid transporter, in Japanese patients with chronic constipation: a phase II, multicenter, double-blind, placebo-controlled randomized clinical trial. *J Gastroenterol* 53: 525–534, 2018. doi:10.1007/s00535-017-1383-5.
221. **Nakajima A**, **Seki M**, **Taniguchi S**, **Ohta A**, **Gillberg PG**, **Mattsson JP**, **Camilleri M.** Safety and efficacy of elobixibat for chronic constipation: results from a randomised, double-blind, placebo-controlled, phase 3 trial and an open-label, single-arm, phase 3 trial. *Lancet Gastroenterol Hepatol* 3: 537–547, 2018. doi:10.1016/S2468-1253(18)30123-7.
222. **Simrén M**, **Bajor A**, **Gillberg P-G**, **Rudling M**, **Abrahamsson H.** Randomized clinical trial: the ileal bile acid transporter inhibitor A3309 vs. placebo in patients with chronic idiopathic constipation—a double-blind study. *Aliment Pharmacol Ther* 34: 41–50, 2011. doi:10.1111/j.1365-2036.2011.04675.x.
223. **Nakajima A**, **Taniguchi S**, **Kurosu S**, **Gillberg PG**, **Mattsson JP**, **Camilleri M.** Efficacy, long-term safety, and impact on quality of life of elobixibat in more severe constipation: post hoc analyses of two phase 3 trials in Japan. *Neurogastroenterol Motil* 31: e13571, 2019. doi:10.1111/nmo.13571.
224. **Taniguchi S**, **Yano T**, **Imaizumi M**, **Manabe N.** Elobixibat, an ileal bile acid transporter inhibitor, induces giant migrating contractions during natural defecation in conscious dogs. *Neurogastroenterol Motil* 30: e13448, 2018. doi:10.1111/nmo.13448.
225. **Newsome PN**, **Palmer M**, **Freilich B**, **Sheikh MY**, **Sheikh A**, **Sarles H**, **Herring R**, **Mantry P**, **Kayali Z**, **Hassanein T**, **Lee H-M**, **Aithal GP**; **Volixibat in Adults study group.** Volixibat in adults with non-alcoholic steatohepatitis: 24-week interim analysis from a randomized, phase II study. *J Hepatol* 73: 231–240, 2020. doi:10.1016/j.jhep.2020.03.024.
226. **Tiessen RG**, **Kennedy CA**, **Keller BT**, **Levin N**, **Acevedo L**, **Gedulin B**, **van Vliet AA**, **Dorenbaum A**, **Palmer M.** Safety, tolerability and pharmacodynamics of apical sodium-dependent bile acid transporter inhibition with volixibat in healthy adults and patients with type 2 diabetes mellitus: a randomised placebo-controlled trial. *BMC Gastroenterol* 18: 3, 2018. doi:10.1186/s12876-017-0736-0.
227. **Mayo MJ**, **Pockros PJ**, **Jones D**, **Bowlus CL**, **Levy C**, **Patanwala I**, **Bacon B**, **Luketic V**, **Vuppalanchi R**, **Medendorp S**, **Dorenbaum A**, **Kennedy C**, **Novak P**, **Gu J**, **Apostol G**, **Hirschfield GM.** A randomized, controlled, phase 2 study of maralixibat in the treatment of itching associated with primary biliary cholangitis. *Hepatol Commun* 3: 365–381, 2019. doi:10.1002/hep4.1305.
228. **Shneider BL**, **Spino C**, **Kamath BM**, **Magee JC**, **Bass LM**, **Setchell KD**, **Miethke A**, **Molleston JP**, **Mack CL**, **Squires RH**, **Murray KF**, **Loomes KM**, **Rosenthal P**, **Karpen SJ**, **Leung DH**, **Guthery SL**, **Thomas D**, **Sherker AH**, **Sokol RJ**; **Childhood Liver Disease Research Network.** Placebo-controlled randomized trial of an intestinal bile salt transport inhibitor for pruritus in alagille syndrome. *Hepatol Commun* 2: 1184–1198, 2018. doi:10.1002/hep4.1244.
229. **United States National Library of Medicine.** *Dose Response Study of GSK2330672 for the Treatment of Pruritus in Participants With Primary Biliary Cholangitis*. 4th May 2021. https://clinicaltrials.gov/show/NCT02966834.
230. **Al-Dury S**, **Wahlström A**, **Wahlin S**, **Langedijk J**, **Elferink RO**, **Ståhlman M**, **Marschall HU.** Pilot study with IBAT inhibitor A4250 for the treatment of cholestatic pruritus in primary biliary cholangitis. *Sci Rep* 8: 6658, 2018. doi:10.1038/s41598-018-25214-0.
231. **Hegade VS**, **Kendrick SFW**, **Dobbins RL**, **Miller SR**, **Thompson D**, **Richards D**, **Storey J**, **Dukes GE**, **Corrigan M**,, **Elferink RPJO**, **Beuers U**, **Hirschfield GM**, **Jones DE.** Effect of ileal bile acid transporter inhibitor GSK2330672 on pruritus in primary biliary cholangitis: a double-blind, randomised, placebo-controlled, crossover, phase 2a study. *Lancet* 389: 1114–1123, 2017. doi:10.1016/S0140-6736(17)30319-7.

Downloaded from journals.physiology.org/journal/ajpgi at New York Univ (216.165.095.084) on September 28, 2023.

232. **Beigel F**, **Teich N**, **Howaldt S**, **Lammert F**, **Maul J**, **Breiteneicher S**, **Rust C**, **Göke B**, **Brand S**, **Ochsenkühn T.** Colesevelam for the treatment of bile acid malabsorption-associated diarrhea in patients with Crohn's disease: a randomized, double-blind, placebo-controlled study. *J Crohns Colitis* 8: 1471–1479, 2014. doi:10.1016/j.crohns.2014.05.009.
233. **Money ME**, **Hofmann AF**, **Hagey LR**, **Walkowiak J**, **Talley NJ.** Treatment of irritable bowel syndrome-diarrhea with pancrealipase or colesevelam and association with steatorrhea. *Pancreas* 38: 232–233, 2009. doi:10.1097/MPA.0b013e31817c1b36.
234. **Camilleri M**, **Acosta A**, **Busciglio I**, **Boldingh A**, **Dyer RB**, **Zinsmeister AR**, **Lueke A**, **Gray A**, **Donato LJ.** Effect of colesevelam on faecal bile acids and bowel functions in diarrhoea-predominant irritable bowel syndrome. *Aliment Pharmacol Ther* 41: 438–448, 2015. doi:10.1111/apt.13065.
235. **Camilleri M**, **Nord SL**, **Burton D**, **Oduyebo I**, **Zhang Y**, **Chen J**, **Im K**, **Bhad P**, **Badman MK**, **Sanders DS**, **Walters JRF.** Randomised clinical trial: significant biochemical and colonic transit effects of the farnesoid X receptor agonist tropifexor in patients with primary bile acid diarrhoea. *Aliment Pharmacol Ther* 52: 808–820, 2020. doi:10.1111/apt.15967.
236. **Ge X**, **Zhao W**, **Ding C**, **Tian H**, **Xu L**, **Wang H**, **Ni L**, **Jiang J**, **Gong J**, **Zhu W**, **Zhu M**, **Li N.** Potential role of fecal microbiota from patients with slow transit constipation in the regulation of gastrointestinal motility. *Sci Rep* 7: 441, 2017. doi:10.1038/s41598-017-00612-y.
237. **Munch A**, **Strom M**, **Soderholm JD.** Dihydroxy bile acids increase mucosal permeability and bacterial uptake in human colon biopsies. *Scand J Gastroenterol* 42: 1167–1174, 2007. doi:10.1080/00365520701320463.
238. **Becker L**, **Spear ET**, **Sinha SR**, **Haileselassie Y**, **Habtezion A.** Age-related changes in gut microbiota alter phenotype of muscularis macrophages and disrupt gastrointestinal motility. *Cell Mol Gastroenterol Hepatol* 7: 243–245.e2, 2019. doi:10.1016/j.jcmgh.2018.09.001.

Downloaded from journals.physiology.org/journal/ajpgi at New York Univ (216.165.095.084) on September 28, 2023.

PLOS ONE

RESEARCH ARTICLE

Granzyme K initiates IL-6 and IL-8 release from epithelial cells by activating protease-activated receptor 2

Dion Kaiserman[1]*, Peishen Zhao[2,3], Caitlin Lorraine Rowe[1], Andrea Leong[2,3], Nicholas Barlow[2], Lars Thomas Joeckel[1], Corinne Hitchen[1], Sarah Elizabeth Stewart[1¤], Morley D. Hollenberg[4], Nigel Bunnett[5], Andreas Suhrbier[6,7], Phillip Ian Bird[1]

1 Department of Biochemistry & Molecular Biology, Biomedicine Discovery Institute, Monash University, Clayton, VIC, Australia, **2** Monash Institute of Pharmaceutical Sciences, Monash University, Parkville, VIC, Australia, **3** Australian Research Council Centre of Excellence in Convergent Bio-Nano Science and Technology, Monash University, Parkville, VIC, Australia, **4** Department of Physiology & Pharmacology, Department of Medicine, University of Calgary, Calgary AB, Canada, **5** Department of Molecular Pathobiology, Department of Neuroscience and Physiology, Neuroscience Institute, New York University, New York, NY, United States of America, **6** QIMR Berghofer Medical Research Institute, Brisbane, QLD, Australia, **7** Australian Infectious Disease Research Centre, University of Queensland, Brisbane, QLD, Australia

¤ Current address: Department of Biochemistry and Genetics, La Trobe Institute for Molecular Science, La Trobe University, Melbourne VIC, Australia
* dion.kaiserman@monash.edu

Check for updates

OPEN ACCESS

Citation: Kaiserman D, Zhao P, Rowe CL, Leong A, Barlow N, Joeckel LT, et al. (2022) Granzyme K initiates IL-6 and IL-8 release from epithelial cells by activating protease-activated receptor 2. PLoS ONE 17(7): e0270584. https://doi.org/10.1371/journal.pone.0270584

Editor: Karl X. Chai, University of Central Florida, UNITED STATES

Received: December 13, 2021

Accepted: June 13, 2022

Published: July 26, 2022

Peer Review History: PLOS recognizes the benefits of transparency in the peer review process; therefore, we enable the publication of all of the content of peer review and author responses alongside final, published articles. The editorial history of this article is available here: https://doi.org/10.1371/journal.pone.0270584

Copyright: © 2022 Kaiserman et al. This is an open access article distributed under the terms of the Creative Commons Attribution License, which permits unrestricted use, distribution, and reproduction in any medium, provided the original author and source are credited.

Data Availability Statement: All relevant data are within the paper and its Supporting Information files.

Abstract

Granzyme K (GzmK) is a tryptic member of the granzyme family of chymotrypsin-like serine proteases produced by cells of the immune system. Previous studies have indicated that GzmK activates protease-activated receptor 1 (PAR1) enhancing activation of monocytes and wound healing in endothelial cells. Here, we show using peptides and full length proteins that GzmK and, to a lesser extent the related protease GzmA, are capable of activating PAR1 and PAR2. These cleavage events occur at the canonical arginine P1 residue and involve exosite interactions between protease and receptor. Despite cleaving PAR2 at the same point as trypsin, GzmK does not induce a classical Ca^{2+} flux but instead activates a distinct signalling cascade, involving recruitment of β-arrestin and phosphorylation of ERK. In epithelial A549 cells, PAR2 activation by GzmK results in the release of inflammatory cytokines IL-6 and IL-8. These data suggest that during an immune response GzmK acts as a pro-inflammatory regulator, rather than as a cytotoxin.

Introduction

Granzymes (Gzm) comprise a family of chymotrypsin-like serine proteases primarily produced by cells of the immune system. There are five human granzymes, each with a distinct substrate specificity: GzmA (dimeric tryptase), GzmB (asp-ase), GzmH (chymase), GzmK (monomeric tryptase), and GzmM (met-ase). Classically, granzymes are described as intracellular cytotoxins that kill compromised cells by activating redundant death pathways when delivered by the pore-forming protein, perforin [1]. More recently, however, numerous non-

Funding: This work was funded by a National Health and Medical Research Council Australia Project Grant 1141421 (PIB & AS), a National Health and Medical Research Council Australia Program Grant 490900 (PIB), National Institutes of Health grants NS102722, DE026806, DK118971 and DE029951 (NB) and Department of Defense grant W81XWH1810431 (NB). The funders had no role in study design, data collection and analysis, decision to publish, or preparation of the manuscript.

Competing interests: The authors have declared that no competing interests exist.

cytotoxic and extracellular roles have been reported for granzymes including: cleavage of extracellular matrix to facilitate migration, direct antiviral effects, immune signalling via activation of cytokines, and activation of cell surface receptors [2].

The protease-activated receptors (PARs) are a family of four G-protein coupled receptors that respond to protease activity. Proteolytic cleavage at a specific site within the amino (N) terminal extracellular domain of the receptor generates a new N-terminus, exposing a short peptide that acts as a tethered ligand to activate the receptor and initiate downstream signalling cascades. PAR activation typically initiates intracellular Ca^{2+} mobilisation and pERK activation, as well as other regulatory pathways including arrestin-recruitment, receptor internalisation and degradation.

Canonical activating cleavage sites of all PARs have been mapped and contain a basic residue at the P1 site. PAR1 is activated by thrombin at Arg41, PAR2 is activated by trypsin at Arg36, and both thrombin and trypsin activate PAR4 at Arg47. PAR3 is also activated by thrombin, at Lys38, but does not appear to signal [3]. As evident from the example of PAR2, distinct proteases may cleave at the same P1 residue within the extracellular domain of a PAR with the same outcome, or they may cleave at distinct residues, resulting in alternative tethered ligand sequences that can activate unique signalling networks. In addition, other cleavage sites, distant from the canonical P1 activation site, may also act to disarm the receptor and prevent receptor activation [3].

There are a number of reports of PAR activation by granzymes. GzmA activates the thrombin receptor (PAR1) on neural cells [4], and cleaves a different receptor, likely PAR2, on monocytes to release cytokines [5]. GzmB cleaves PAR1 and PAR2 to mediate biological effects, however these sites have not been mapped [6,7]. GzmK cleaves and activates PAR1 on endothelial cells and fibroblasts [8–10]. Here we show that GzmK is also capable of cleaving and activating PAR2 on the surface of epithelial cells, invoking cytokine release. Although the cleavage occurs at the canonical site, Ca^{2+} mobilisation is not initiated. Instead, signalling is biased toward ERK phosphorylation and β-arrestin recruitment.

Materials and methods

Cells and cell culture

A549 and COS-1 cells were grown as adherent monolayers in DMEM supplemented with 2 mM L-glutamine, 50 units/ml penicillin and 50 μg/ml streptomycin. HEK293 and KNRK cells were grown in DMEM supplemented with 10% FBS. Cells were passaged at ~80% confluency by washing monolayers with PBS and detaching from the growth support with 0.25% (w/v) trypsin and replating into fresh medium.

Recombinant proteins

Human GzmA and GzmB were purified as previously described [11]. The human GzmK cDNA was modified to replace the signal peptide and prodomain with a 6 × His tag and bovine enterokinase cleavage site and cloned into the *Escherichia coli* expression plasmid pEXP-His. Recombinant protein was expressed in inclusion bodies in BL21 arabinose-inducible *E. coli*. These were collected by centrifugation of the lysed bacterial pellet and washed three times: wash 1 contained 50 mM Tris, pH 7.4, 20 mM EDTA, 20 mM DTT, 1% (v/v) Triton X-100; wash 2 contained 50 mM Tris, pH 7.4, 20 mM EDTA, 1 M NaCl; and wash 3 contained 50 mM Tris, pH 7.4, 20 mM EDTA. The insoluble protein pellet was collected and denatured in 7 M guanidine, 100 mM DTT, and 100 mM Tris, pH 8.3.

The denatured protein was refolded by slow, drop-wise addition into 600 mM L-arginine, 50 mM Tris, pH 7.4, 500 mM NaCl, 1 mM EDTA, 10% (v/v) glycerol, 1 mM L-cysteine and

incubated at room temperature for 72 h. The solution containing soluble and correctly folded pro-granzyme was concentrated by tangential flow filtration before activation as described for GzmA and GzmB.

Granzymes were assayed for activity by gel shift assay with serpin inhibitors and were at least 95% active. Where indicated, granzymes were inactivated by reaction with a 100-fold molar excess of the irreversible serine protease inhibitor, aminoethyl benzene sulfonyl fluoride (AEBSF), for 3 h at 37˚C.

For cytokine release assays, endotoxin was removed by adding Triton X-114 to a final concentration of 1% (v/v), incubating at 4˚C for 30 min, then 37˚C for 10 min followed by centrifugation at 16,000 *g* for 10 min at RT and retaining the upper, aqueous phase. This was repeated 5 times and the resultant preparation assayed for endotoxin using the Pyrogene™ Recombinant Factor C Endotoxin Detection Assay (Lonza Bioscience). All proteases contained <0.05 EU/ml endotoxin.

Peptide cleavage assays

Peptides corresponding to N-terminal fragments of human PAR1 and PAR2 (350 μM) were incubated with granzymes (100 nM) in Hank's Balanced Salt Solution (HBSS) pH 7.4 for 0, 2, 4, and 15 hours at 37˚C. Reactions were quenched with an equal volume of 50% acetonitrile and 0.1% trifluoroacetic acid in water. Degradation was assessed using an Agilent 1260 Infinity HPLC System with Poroshell 120, SB-C18, 2.1 × 30 mm, 2.7 μM column, 5–95% acetonitrile in water over 9 min, 0.1% TFA throughout. The reaction products were identified by mass spectrometry using a Shimadzu LCMS 2020, single quadrupole in electrospray in positive ionization mode with a mass range of 200–2000 *m*/*z*.

Construction and cleavage of NanoLuc®-PAR constructs

The pcDNA3/nLuc®-PAR1-eYFP and pcDNA3/nLuc®-PAR2-eYFP vectors were a gift from Prof. M. Hollenberg (University of Calgary). The consensus site mutations were generated by Q5 site-directed mutagenesis (New England Biolabs) using primers 5'-CTTAGATCCCGCGT–CATTTCTTCTCAG for PAR1 or 5'- CTTAGATCCCGCTAGCTTTCTTCTCAGGAACCCCAATG and 5'-GTGGCATTTGTTGCTTTG for PAR2. COS-1 cells were transfected in 24-well plates by adding 1–2 μg of each plasmid to 5×10^5 COS-1 cells in DMEM supplemented with 2 mM l-glutamine, 50 units/ml penicillin, 50 μg/ml streptomycin, 400 μg/ml DEAE-dextran, and 25 μM chloroquine for 3 h at 37˚C. The medium was replaced with 10% dimethyl sulfoxide in DMEM for 2 min, and cells then returned to complete DMEM.

48 h later cells were washed with PBS and incubated at 37˚C with a serial dilution of granzyme in 500 μl serum free DMEM. Supernatants were collected after 2 h and centrifuged for 5 min at 16,000 g to remove cellular debris. 80 μl was transferred to an opaque 96-well tray and assayed for luciferase activity. Nano-Glo® Luciferase Assay Substrate was diluted in 50 volumes of Nano-Glo® Luciferase Assay Buffer and 20 μl of dilute substrate was mixed with clarified supernatant for 5 min and luminescence measured on a FLUOstar OPTIMA microplate reader (BMG Labtech). Experiments were repeated 3–5 times and are presented as mean ± standard deviation.

Calcium mobilisation assays

KNRK cells and KNRK cells stably expressing human PAR2 [12] were seeded into poly-lysine coated 96 well plates (3×10^5 cells/well). After 24 h, cells were loaded with of the calcium sensitive dye FURA2/AM (1 μM) [Invitrogen, F-1221] in Ca^{2+} buffer (150 mM NaCl, 2.6 mM KCl, 0.1 mM $CaCl_2$, 1.18 mM $MgCl_2$, 10 mM D-glucose, 10 mM HEPES, pH 7.4) containing 4 mM

Probenecid [Sigma Aldrich, P8761] for 1 h at 37˚C. Fluorescence was measured at 340 nm and 380 nm excitation and 530 nm emission using a FlexStation Microplate Reader (Molecular Devices). After a baseline reading for 60 s, cells were treated with vehicle, GzmK (100 nM) or inactive GzmK (100 nM), while trypsin (10 nM) was the positive control, and reading continued for up to 5 min.

To examine whether GzmK has inhibitory effects on trypsin-mediated Ca^{2+} signalling, cells were pre-treated with GzmK or its inactive form (100 nM) for 30 min, washed three times with assay buffer and challenged with trypsin (10 nM). Areas under the curve of protease-mediated Ca^{2+} responses were normalized as the percentage of trypsin response.

To measure endogenous PAR1 and PAR2 activation in A549 cells, cells were seeded into 96 well plates at a density of 3×10^4 cells/well 24 h before the measurement. Cells were then incubated with Fluo-8AM (10 μM) for 1 h at 37˚C. Plates were read using the FDSS/μCELL (Hamamatsu, Japan), with 480 nm excitation 542 nm emission filters every 10 s for 2 min including a 15 s baseline. PAR1 and PAR2 activating peptides were added at 15 s at indicated concentrations. 10 μM ATP was used as a positive control.

ERK phosphorylation assays

KNRK and KNRK-PAR2 cells were seeded into 96 well plates (3×10^5 cells/well). After 24 h, cells were serum starved in 80 μl phenol red free DMEM for at least 12 h to reduce basal ERK activity. Cells were challenged with 10 μl of buffer, GzmK (100 nM), with or without 30 min pre-treatment of EGFR inhibitor AG1478 (100 nM), inactivated GzmK (100 nM), trypsin (10 nM), FBS (10%) for 5 min. Concentration response measurements were also conducted for trypsin and GzmK at increasing protease concentrations. ERK1/2 phosphorylation was detected using the AlphaScreen SureFire ERK1/2 assay kit (PerkinElmer) according to the manufacturer's instructions.

β-arrestin BRET assays

BRET assays were performed essentially as described [13]. Briefly, HEK 293 cells were plated into 10 cm dishes at a density of 2×10^6 cells/plate and transfected with 1 μg PAR2-Rluc8 and 4 μg β-arrestin$_1$-YFP using polyethylenimine (PEI) at a ratio of 1:6 (DNA:PEI). 24 h post-transfection, cells were plated onto a white 96 well plate at a density of 3×10^4 cells/well. 24 h post plating, the medium was replaced with 80 μl 1 × Hank's Buffered Salt Solution, pH 7.4, at 37˚C for 30 min, and treated with either buffer, trypsin (10 nM), GzmA (100 nM) or GzmK, (100 nM) for 2 h. 5 μM coelenterazine was then added and incubated for 5 min. Bioluminescence was measured at 475 ± 30 nm (Rluc8) and fluorescence at 530 ± 30 nm (YFP) on a LUMIstar Omega (BMG Labtech). β-arrestin$_1$ recruitment is indicated as the ratio change between the two wavelengths.

Cytokine ELISAs

A549 cells were seeded in 12 well plates at a density of 0.5×10^6 cells/ml in 1 ml DMEM and incubated at 37˚C for 6 h to allow cell adhesion. DMEM was then exchanged for 1 ml SF-DMEM and cells incubated overnight at 37˚C. The next day, medium was replaced with 500 μl of SF-DMEM containing Gzm or PAR activating peptide for 24 h at 37˚C. Medium was collected and cellular debris removed by centrifugation at 16,000 *g* for 5 min.

ELISA was performed using the human IL-6, human IL-8, human TNFα, and human IL-1β sandwich ELISAs (Life Technologies) according to the manufacturer's instructions. ELISA plates were coated overnight with 100 μl capture antibody in PBS. Plates were washed 3 times with PBS + 0.05% (v/v) Tween-20, then incubated with 200 μl sample diluted in PBS for 2 h at

room temperature. Wells were washed 5 times with PBS, then incubated with 100 μl detection antibody in PBS for 1 h at room temperature. Antibody was removed and wells washed 5 times with PBS + 0.05% Tween-20 and then incubated with streptavidin conjugated to horseradish peroxidase at room temperature for 30 min. Cells were washed 5 times with PBS + 0.05% Tween-20 and then incubated with 100 μl 3,3',5,5'-tetramethylbenzidine and colour development monitored over 15 min. Reactions were stopped by addition of 50 μl H_2SO_4 and colour measured on a FluoStar Omega plate reader at both 450 nm (measurement) and 570 nm (background). Background corrected optical density for untreated cells was subtracted from each measurement and concentration of cytokine was then interpolated from a standard curve. Cytokine release was plotted against treatment concentration and linear regression applied to derive cytokine release per concentration of treatment. ELISA experiments were performed 2–4 times and are presented as mean ± standard deviation.

Results

Cleavage of full-length PAR1 and PAR2 by GzmA and GzmK

Previous studies have indicated that GzmA and GzmK can cleave and activate PARs [4,9,10,14]. To replicate and extend these findings we evaluated GzmA- and K-mediated cleavage of the best-described PARs, PAR1 and PAR2. We examined transiently expressed NanoLuc®-PAR-eYFP constructs in COS-1 cells. In this system luciferase is fused to the N-terminus of the PAR, and yellow fluorescent protein (YFP) is fused to the C-terminus to report receptor localization. Treatment of transfected cells with an exogenous protease that cleaves the PAR extracellular N-terminal domain liberates luciferase, which can then be measured in the medium. To ensure that any cleavage detected occurs at the canonical activation site, we also generated constructs where the Arg41 residue in PAR1, or Arg36 residue in PAR2, was mutated to Ala. We also included enzymatically inactive forms of the granzymes (GzmA-AI and GzmK-AI) in the experiment to confirm that any effects required proteolytic activity as opposed to protein-protein interactions.

We first tested the ability of granzymes to liberate luciferase from NanoLuc®-PAR1-eYFP (Fig 1A). Both GzmA and GzmK cleaved PAR1 in this system. Cleavage by GzmK was more efficient than GzmA, releasing 6 to 7-fold more luciferase (Fig 1A). Inactivation of GzmA or GzmK blocked their ability to release the NanoLuc®, confirming that this is an enzymatic reaction (Fig 1A).

To determine whether cleavage occurred at the consensus site (Arg41) we mutated this residue to alanine (Arg41Ala). As a control for protease cleavage away from the consensus site, we used GzmB, which has been shown to cleave PAR1 [6], but its requirement for an acidic P1 residue suggests it does not cleave at the consensus Arg41. As shown in Fig 1A, GzmB released luciferase from cells, and release was not prevented when PAR1 carried the Arg41Ala (Fig 1A).

Alanine substitution of the P1 residue (Arg41Ala) abolished cleavage by GzmK, confirming that this is the true cleavage point. By contrast, GzmA cleavage was not affected by the Arg41Ala mutation (Fig 1A). This indicates that either GzmA does not cleave at the canonical site, or exosite interactions are sufficient to overcome the decreased affinity caused by loss of Arg41.

In cells expressing NanoLuc®-PAR2-eYFP, both GzmA and GzmK cleaved the full-length protein, and we once again noted that GzmK was significantly more efficient, releasing 4-fold more luciferase (Fig 1B). Importantly, GzmK cleavage was completely abolished by the Arg36Ala P1 mutation. By contrast with PAR1, GzmA cleavage was significantly reduced by the P1 mutation, indicating that GzmA does cleave at the consensus site in PAR2 (Fig 1B).

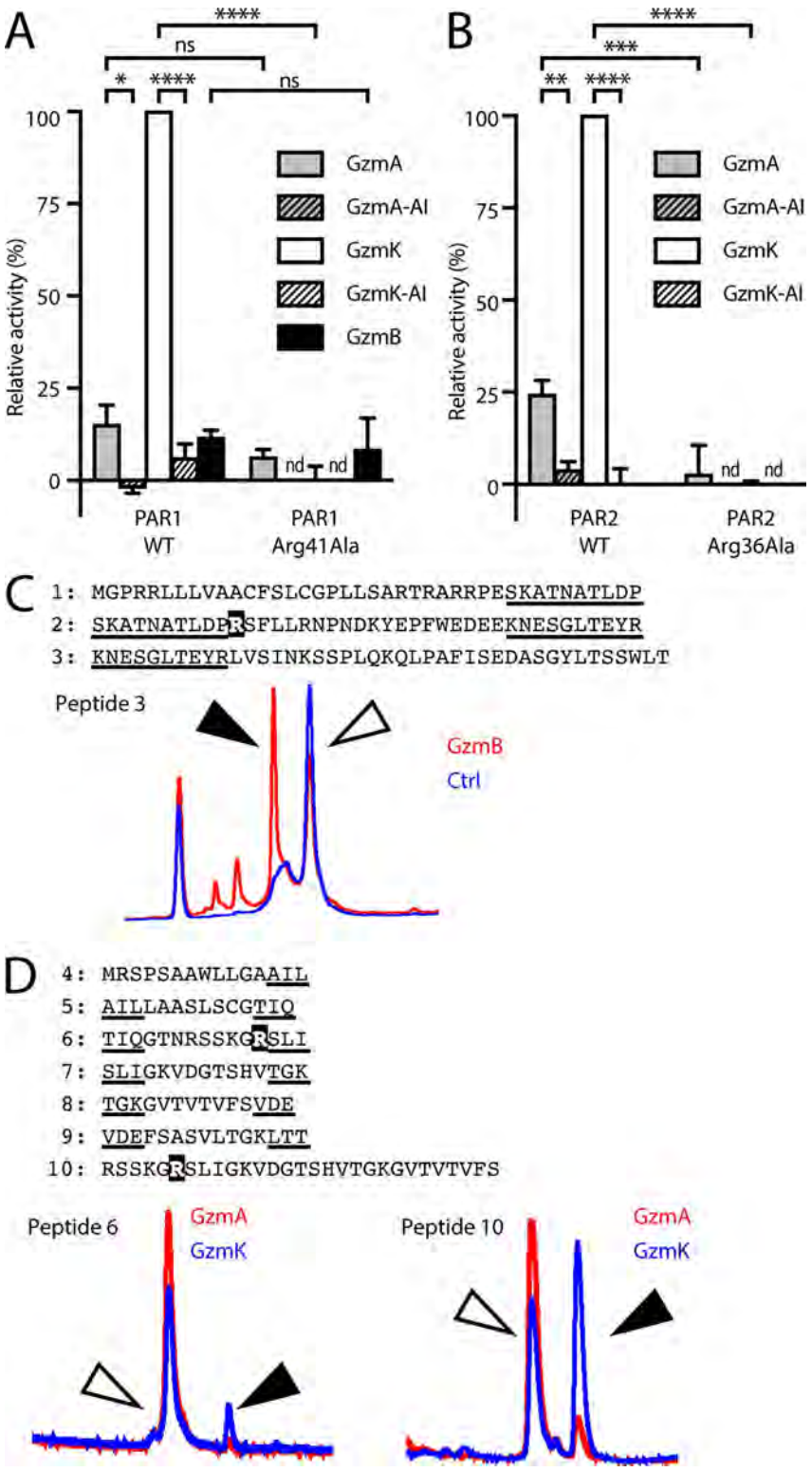

Fig 1. Cleavage of full-length PARs by granzymes. COS-1 cells were transfected with (A) NanoLuc® -PAR1-eYFP; or (B) NanoLuc® -PAR2-eYFP plasmids. Cells were treated with a dilution series of the indicated granzyme or AEBSF-inhibited granzyme in serum-free DMEM for 2 h at 37˚C. Supernatants were assayed for NanoLuc® activity. Data are expressed as a percentage of GzmK-treated WT PAR1 or PAR2. Pairwise Student's t-tests were used to determine significant differences. nd, not determined; ****, $p < 0.0001$; ***, $p < 0.001$; **, $p < 0.01$; *, $p < 0.05$; ns, $p > 0.05$. The

extracellular N-terminal sequences of (C) PAR1 or (D) PAR2 were represented by sets of overlapping peptides: Sequences shared between consecutive peptides are underlined. The PAR2 set also included a longer peptide centred around the consensus cleavage site. The consensus cleavage sites Arg41 and Arg36 are shown in white text on a black background. Peptides were incubated for 15 h with 150 nM each human granzyme and cleavage assessed by HPLC. PAR1 cleavage was observed on GzmB treatment of peptide 3. PAR2 cleavage was observed on GzmA and GzmK treatment of peptides 6 and 10. White arrowhead indicates uncleaved peptide; black arrowhead indicates cleaved peptide.

https://doi.org/10.1371/journal.pone.0270584.g001

Gzms A, B and K cleave PAR-based peptides

In conjunction with the NanoLuc® constructs, we also tested the granzymes' ability to cleave peptides corresponding to the N-terminal domains of PAR1 and PAR2. To accomplish this, we screened granzymes A, B and K against overlapping peptides covering the complete N-terminal domains of PAR1 or PAR2 from the N-terminus to the transmembrane domain. Peptide cleavage was determined by HPLC after 15 h of treatment with 100 nM granzyme and the cleavage sites were identified using mass spectrometry.

For the PAR1 analysis, three overlapping peptides were designed, with the canonical cleavage site Arg41 located in peptide 2. Unexpectedly, neither GzmA nor GzmK cleaved any of the PAR1 peptides, despite cleaving the full length NanoLuc® constructs. This suggests the requirement for further protein-protein interactions between PAR1 and an exosite on the granzyme surface to drive cleavage. Only GzmB cleaved a PAR1 peptide, and this cleavage occurred in peptide 3, which is significantly downstream of the canonical cleavage site (Fig 1C). This suggests that it represents a potential receptor disarming cleavage event.

For the PAR2 analysis we utilised six overlapping peptides from the initiator methionine to the beginning of the first transmembrane domain (Fig 1D). The PAR2 canonical P1 residue Arg36 was located in peptide 6, as well as in peptide 10, a longer sequence surrounding the canonical P1 site. Only the tryptic proteases, GzmA and GzmK, cleaved PAR2 peptides. Cleavage of peptide 6 and peptide 10 was observed (Fig 1D). LC-MS analysis indicated that cleavage by both proteases occurred at the canonical P1 residue Arg36.

As reactions were performed under identical conditions, a direct comparison of cleavage efficiencies could be made. For the shorter peptide 6, the cleaved peptide represented 1.6% of total for GzmA, but 9.6% of total for GzmK, while for the longer peptide 10 the cleavage product represented 6.6% of total for GzmA and 53% of total for GzmK. The increased activity on peptide 10 suggests an interaction of affinity-determining residues four or more residues downstream of the PAR cleavage site with an exosite on the protease. Taken with the NanoLuc®-PAR-eYFP cleavage data this indicates that GzmK is more efficient than GzmA at activating PAR2.

GzmK induces biased PAR2 signalling

Given that cleavage of PAR1 by GzmK has been previously well described in endothelial cells [9], fibroblasts [10] and macrophages [8], we focused on the signalling mechanism and physiological consequences of GzmK cleavage of PAR2.

Cleavage of PAR2 at the canonical P1 site by trypsin leads to multiple intracellular signalling events such as Ca^{2+} mobilisation, ERK phosphorylation and β-arrestin recruitment. To determine whether GzmK elicits similar signalling pathways to trypsin, we used epithelial KNRK cells producing very low levels of endogenous PAR and stably expressing transfected PAR2 [12].

Consistent with the literature, trypsin (10 nM) treatment of KNRK cells expressing PAR2 led to rapid and transient Ca^{2+} mobilisation (Fig 2A and 2B). However, GzmK treatment did not result in a Ca^{2+} flux, which was unexpected given that both the peptide and full-length

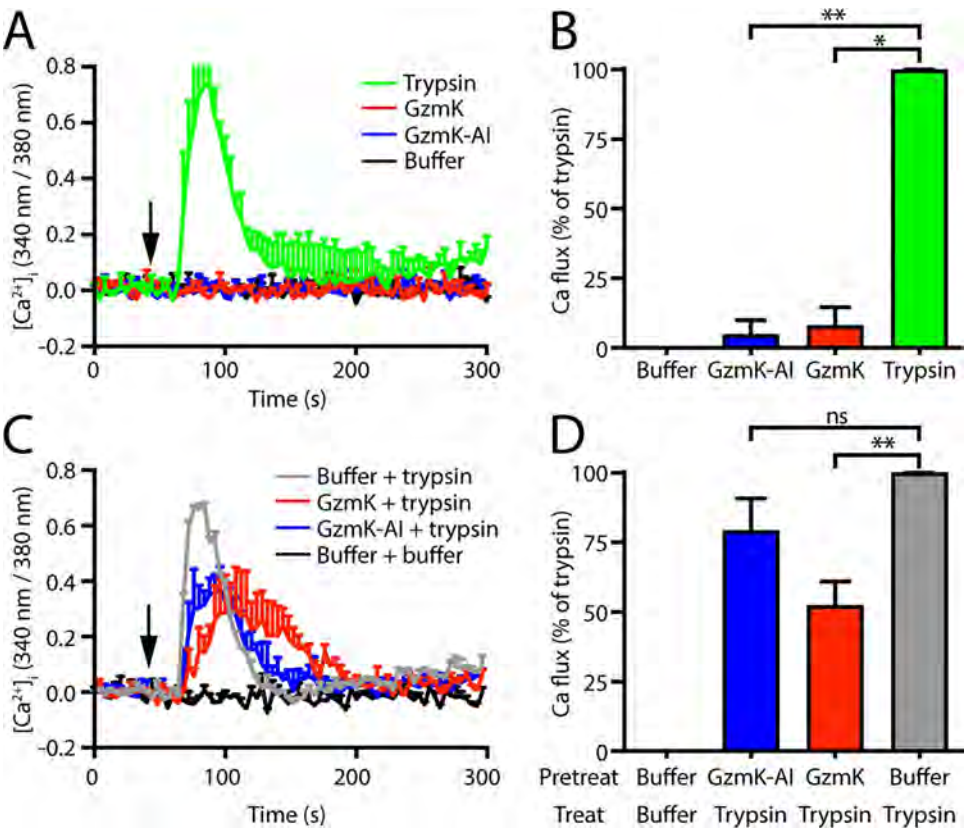

Fig 2. Cleavage of PAR2 by granzyme K does not induce Ca^{2+} flux. KNRK cells expressing human PAR2 (KNRK-PAR2) were treated with the indicated proteases. (A) Fluctuations in intracellular calcium were measured by change in Fura2 fluorescence spectra following treatment. Cells were treated with trypsin, granzyme K (GzmK) or AEBSF-inhibited GzmK (GzmK-AI) or buffer at the indicated time (arrow) and fluorescence measured over a 4 min window. (B) Total response, defined as the area under the curve was determined and standardised to the trypsin response. (C) Cells were pre-treated with GzmK, AEBSF-inhibited GzmK (GzmK-AI), or buffer for 30 min then treated with trypsin and the calcium flux followed by Fura2 fluorescence. (D) Total response, defined as the area under the curve was determined and standardised to the pre-treatment with vehicle response. *, $p < 0.05$; **, $p < 0.01$; ns, $p > 0.05$.

https://doi.org/10.1371/journal.pone.0270584.g002

receptor cleavage data show that it cleaves PAR2 at the same site as trypsin (Fig 1). Although GzmK did not produce a PAR2-mediated Ca^{2+} flux, we considered the possibility that it may have the capacity to interfere with the trypsin-induced response. This was assessed in cells pre-treated with GzmK or buffer alone for 30 min prior to treatment with trypsin (Fig 2C and 2D). We observed a 50% decrease in trypsin-mediated Ca^{2+} release following GzmK treatment (Fig 2C and 2D). GzmK inhibited with the irreversible serine protease inhibitor AEBSF (GzmK-AI) did not affect trypsin signalling, indicating that the suppressing effect requires GzmK activity and is not due to steric interference.

In addition to Ca^{2+} signalling, activation of PAR2 by trypsin also leads to pERK activation, which involves β-arrestin-dependent receptor endocytosis [15]. GzmK treatment triggered both phosphorylation of ERK and recruitment of β-arrestin to a similar extent as trypsin (Fig 3). Activation of ERK in KNRK cells stably expressing PAR2 (KNRK-PAR2), but not the parental line (KNRK), confirmed that ERK signalling is PAR2-dependent (Fig 3A). GzmK activation of PAR2 mediated ERK phosphorylation to a similar extent as trypsin, whereas the inactivated GzmK did not show any ERK response (Fig 3A). Dose response experiments

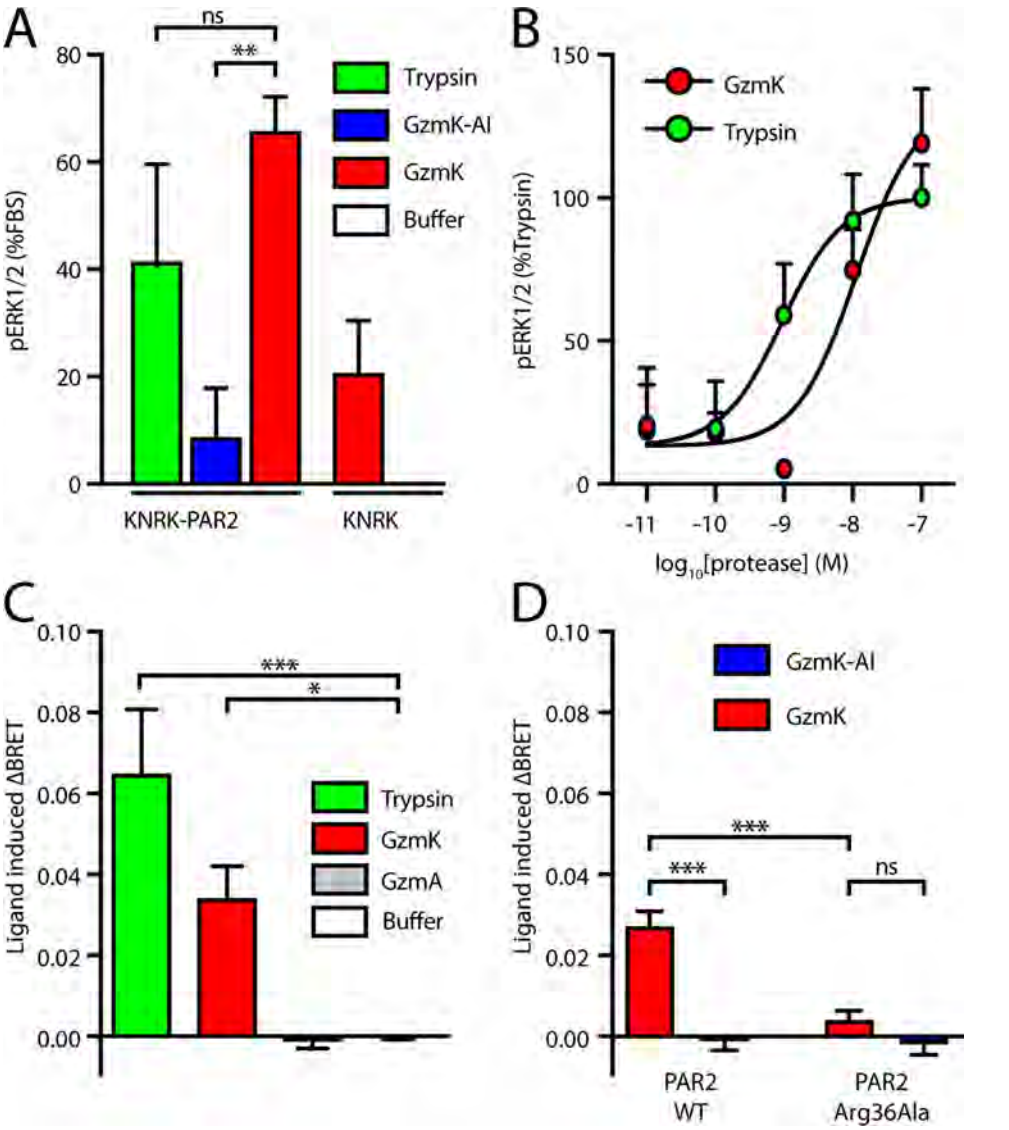

Fig 3. Downstream signalling from PAR2 following cleavage by granzyme K. (A) KNRK cells or KNRK-PAR2 cells were treated with the indicated proteases in serum-free medium and ERK phosphorylation was measured via Alpha-Screen. Data were normalised to the response to medium containing foetal calf serum. (B) ERK phosphorylation induced by a dilution series of granzyme K or trypsin. (C) KNRK cells transfected with PAR2-Rluc and β-arrestin-eYFP. Recruitment of β-arrestin to PAR2 by trypsin or GzmK was measured by BRET ratio. ***, $p < 0.001$; **, $p < 0.01$; *, $p < 0.05$; ns, $p > 0.05$.

https://doi.org/10.1371/journal.pone.0270584.g003

showed that both GzmK and trypsin induce ERK phosphorylation with a potency (EC_{50}) in the low nanomolar range (Fig 3B).

Finally, we investigated the ability of GzmK to recruit arrestin to PAR2. To do this, the bioluminescence resonance energy transfer (BRET) signal between PAR2-Rluc8 and β-arrestin$_1$-YFP was monitored in HEK 293 cells. Our results show that GzmK (100 nM), but not GzmA, stimulates β-arrestin recruitment to a similar extent to trypsin (10 nM) (Fig 3C). The catalytic activity of GzmK is required for this recruitment as the inactive mutant GzmK failed to trigger β-arrestin recruitment (Fig 3C). Mutation of the P1 site Arg 36 severely diminished the recruitment of β-arrestin (Fig 3D), in agreement with earlier data using peptides and N-terminally tagged PAR2 constructs (Fig 1).

Overall, these data show that GzmK activates PAR2, initiating a biased signalling event that includes activation of ERK and recruitment of β-arrestin.

GzmK-mediated interleukin release from epithelial cells involves PAR2

We next investigated the physiological effects of PAR activation by GzmK in an endogenous setting using epithelial A549 cells. We first used activating peptides corresponding to the tethered ligand of PAR1 or PAR2 to determine which PARs respond in our A549 cells. The PAR1 peptide (Thr-Phe-Leu-Leu-Arg-NH_2) induced a weak Ca^{2+} response, whereas the PAR2 peptide (Ser-Leu-Ile-Gly-Lys-Val-NH_2) response was much stronger and sustained for longer (Fig 4). Given these peptides have documented similar potency at activating their respective receptors, our data suggest that PAR2 activity predominates in these cells.

To further explore the physiological effects of granzymes on A549 cells, we treated the A549 cells for 24 h with increasing amounts of GzmA or GzmK and assayed the culture medium for cytokine release. Both GzmA and GzmK induced the release of IL-8, while GzmK but not GzmA induced release of IL-6 (Fig 5A and 5B). Again, GzmK induced substantially (9-fold) more IL-8 release than GzmA, indicating that the cleavage efficiencies identified in the peptide cleavage and luciferase release assays are biologically relevant. In comparing relative levels of cytokine release, we found that GzmK induced release of approximately 9-fold more IL-8 than IL-6.

We next investigated the intracellular signalling events leading to IL-8 release using a series of small molecule inhibitors of PAR1 (vorapaxar), PAR2 (GB88), or MEK signalling (PD184352) (Fig 5C). The release of IL-8 in response to the PAR2-activating peptide was significantly inhibited by PD184352 and abolished by GB88. In cells treated with GzmK, IL-8 release was inhibited 70–80% by GB88 or PD184352, but was unaffected by vorapaxar (Fig 5C), indicating that release is mediated via PAR2 signalling through a MEK-dependent mechanism, and does not involve PAR1. Unlike PAR2 peptide treatment, GB88 did not completely abrogate the response induced by GzmK. This may be due to the higher stability of the protease compared to the PAR2 peptide (or GB88), allowing it to signal for longer.

Discussion

We have shown here, using both synthetic peptides and full-length receptors, that granzymes A, B and K are able to cleave the activation domains of specific PARs. GzmA and GzmK cleave both PAR1 and PAR2, while GzmB cleaves PAR1 but was not tested on PAR2. GzmK is much more efficient at cleaving PAR1 and PAR2 than GzmA, and cleaves both receptors at the canonical site. Activation of PAR2 by GzmK does not trigger Ca^{2+} mobilisation but initiates a biased signalling pathway that involves β-arrestin recruitment and ERK phosphorylation. In lung epithelial cells, GzmK treatment leads to the release of proinflammatory cytokines IL-6 and IL-8, the latter via a PAR2 and MEK-dependent mechanism.

GzmB cleavage of PAR1 was expected from literature reports [6,16]. The critical cleavage site-determining residues for GzmB are an Ile at P4 and Asp at P1 [17]. This is consistent with the motif Ile-Ser-Glu-Asp91 found in the most C-terminal PAR1 peptide tested here, well downstream of the canonical site at Arg41. Cleavage at Asp91 would almost certainly inactivate the receptor. This contradicts previous suggestions that cleavage of PAR1 by GzmB activates the receptor on neurons [6]. However, previous investigations of GzmB have indicated the presence of exosites that facilitate cleavage at suboptimal sites, particularly in extracellular matrix proteins [18–20]. As these still result in cleavage at acidic residues, the only potentially sub-optimal activating P1 residue in PAR1 would therefore be Asp39, two residues upstream of the canonical site. Asp39 is cleaved by matrix metalloprotease 1 to activate PAR1 on the

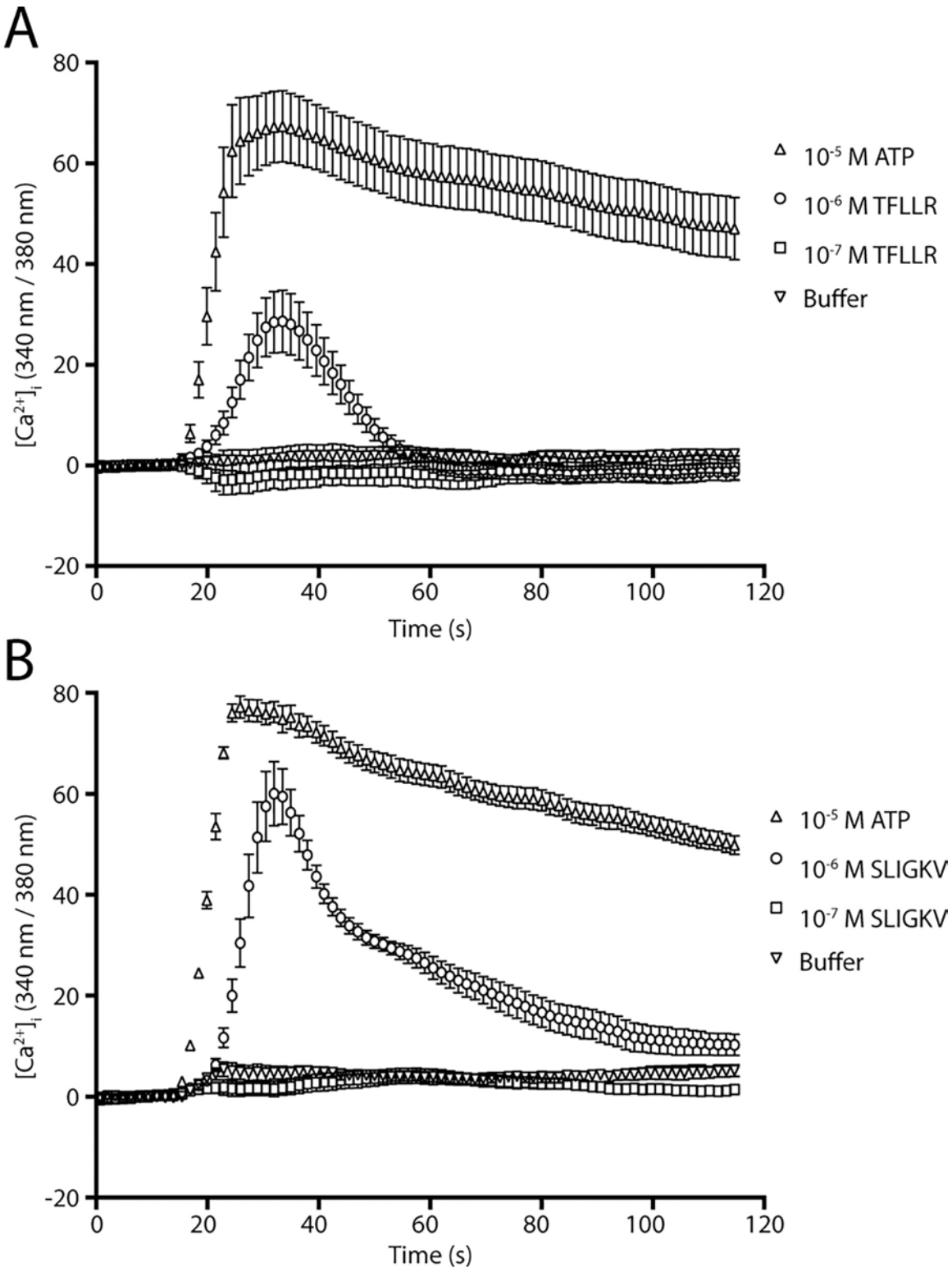

Fig 4. Effect of PAR1 or PAR2 activating peptides on A549 cells. A549 cells were loaded with Fura2 and treated with activating peptides for (A) PAR1 (TFLLR-NH_2), or (B) PAR2 (SLIGKV-NH_2) and calcium flux measured by the change in fluorescence and compared to ATP.

https://doi.org/10.1371/journal.pone.0270584.g004

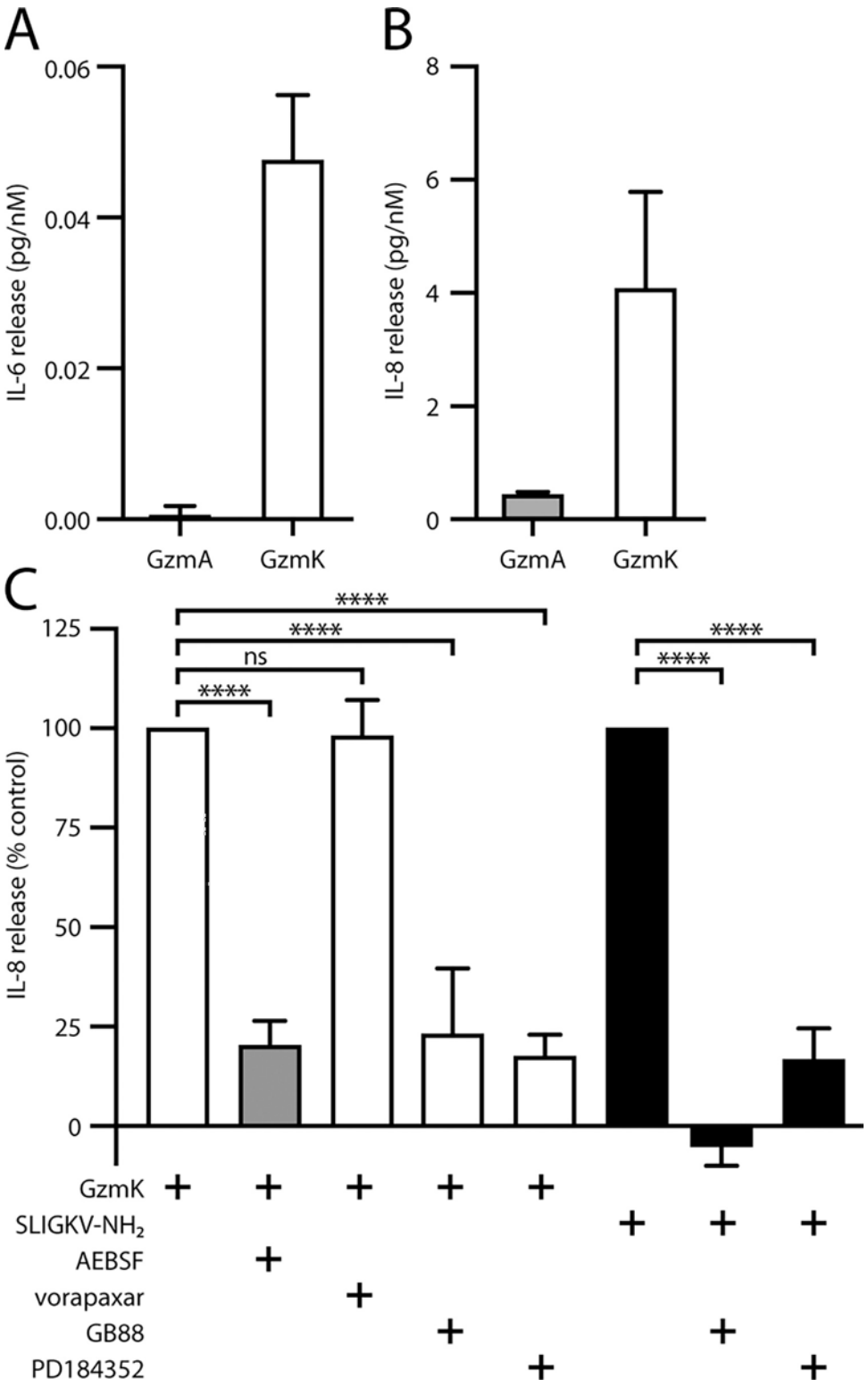

Fig 5. Granzyme K induces chemokine release from A549 cells. A549 cells were treated overnight with a serial dilution of either GzmA or GzmK in serum free medium and cell free supernatants were assayed for either (A) IL-6, or (B) IL-8 by ELISA. (C) A549 cells were pre-treated with inhibitors of PAR1 (vorapaxar), PAR2 (GB88) or MEK signalling (PD184352), then treated with either GzmK (white bars), GzmK-AI (grey bars) or PAR2 activating peptide (black bars) overnight in serum free medium. IL-8 release was measured by ELISA from cell-free supernatants. ****, $p < 0.0001$; ns, $p > 0.05$.

https://doi.org/10.1371/journal.pone.0270584.g005

surface of platelets [21]. Therefore, it is possible that GzmB activity is directed to this site by exosite interactions with the full length PAR1, leading to receptor activation, in agreement with previous neuronal studies [6].

Despite previous speculation about redundant functions of GzmA and GzmK, the work here supports the suggestion that they have distinct biological roles. Both the peptide and full-length receptor cleavage data indicate the GzmK is much more efficient than GzmA at cleaving PAR2. This is possibly due to the presence of Leu at the P2' position, which has been shown to enhance cleavage by GzmK over GzmA [22]. Both GzmA and GzmK cleaved PAR2 peptides at the consensus site, but only cleaved PAR1 in the context of a complete receptor. This suggests a requirement for an exosite on the granzyme to participate in binding to PAR1. Indeed, exosite interactions are known to be an extremely strong component in selecting GzmA substrates in fully folded proteins [23], to the extent that the efficiency of cleavage of a particular substrate sequence differs if it is in a full-length protein compared to a peptide [24].

The downstream signalling effects of PAR cleavage are mediated by the tethered ligand of the neo-amino terminus. Curiously, GzmK and trypsin elicit differential signalling from PAR2 despite cleaving at the canonical P1 residue Arg36. While both proteases lead to ERK phosphorylation and β-arrestin recruitment, only trypsin initiates a Ca^{2+} flux. A similar distinction was seen in the downstream signalling of PAR1 cleaved by GzmK, when compared to thrombin [9]. Biased PAR signalling has been observed with many proteases including elastase, proteinase 3, and various cathepsins [3]. Normally, the observed differences in signalling cascades require cleavage of a PAR at unique non-canonical sites, resulting in unique tethered ligands. This is the case for elastase activation of PAR1 and PAR2 [25–27], cathepsin S activation of PAR2 [13], and activated protein C (APC) activation of PAR1 [28]. How GzmK produces a different outcome while cleaving at the same site remains unclear at present. Although GzmK and trypsin cleave PAR2 at the same site on the receptor, GzmK may stabilise a distinct receptor conformation, which leads to the observed biased signalling profile. This could potentially be due to exosite binding between Gzms and the receptor.

It is interesting that, although GzmK failed to trigger PAR-2 mediated Ca^{2+} mobilisation, pre-incubation of GzmK significantly reduced trypsin mediated Ca^{2+} signalling. It is possible that by binding and cleaving PAR2, GzmK is able to trigger receptor internalisation (which is supported by its ability to recruit β-arrestin to the receptor); or that the binding between the exosite on the receptor and GzmK may prevent efficient cleavage by trypsin of PAR2. Which of these mechanisms contributes to the inhibitory effect of GzmK on trypsin signalling warrants further investigation.

GzmK triggers pERK1/2 activation in a concentration dependent manner, with similar potency to trypsin. pERK1/2 activation is an important downstream signalling endpoint upon PAR2 activation. pERK activation could be mediated via G protein-dependent and/or arrestin-dependent mechanisms [15]. Consistent with this, we have shown that GzmK induces β-arrestin recruitment to PAR2, suggesting a potential involvement of arrestin in GzmK-mediated pERK activation. However, we cannot rule out the participation of other mechanisms. For example, Rho kinase activation contributes to pERK activation during elastase-mediated PAR2 signalling [25]. Whether this pathway also contributes during GzmK-mediated PAR2 signalling remains unclear.

Finally, we have shown here that cleavage of PAR2 by GzmK results in the selective release of the cytokines IL-6 and IL-8 from epithelial cells. The Granville group has also shown that GzmK-mediated PAR1 cleavage induces the release of IL-6 and IL-8 from fibroblasts and endothelial cells to promote an inflammatory environment [8–10]. GzmK-induced PAR1 cleavage can also improve wound healing by keratinocytes [8]. Taken together, these observations raise the possibility that GzmK has redundant functions, or that it has evolved to elicit

similar, specific responses in multiple environments irrespective of the particular PAR expressed.

The biological significance of GzmK is unresolved. GzmK is not an efficient cytotoxin, as micromolar concentrations are required to induce death [29], whereas nanomolar concentrations of GzmB induce death [17]. Furthermore, mice lacking GzmK appear totally healthy, resist viral infection, and have no defect in killing *in vivo* or *in vitro* [30]. Our finding that GzmK via PAR2 selectively induces IL-6 and IL-8 release supports previous suggestions that it has a pro-inflammatory role [31,32]. Among other functions, IL-6 stimulates acute phase protein synthesis and neutrophil production, whereas IL-8 primarily acts as neutrophil attractant. Thus, GzmK may serve as a primary alarmin or an amplifier to support neutrophil recruitment to an injury site. Interestingly, GzmK is found in the circulation of healthy and diseased patients [33], and levels correlate with both disease severity and circulating cytokines during lung infection [34].

Conclusion

Here we have shown that multiple granzymes have the ability to activate PAR1 and PAR2. We have extended the previous observations that GzmK activates PAR1, by showing that it also cleaves PAR2 on the surface of epithelial cells. This initiates signalling cascades involving recruitment of β-arrestin and phosphorylation of ERK, but not intracellular Ca^{2+} fluxes. The physiological result of this signalling is the release of inflammatory cytokines IL-6 and IL-8 from cells. These results provide further support to the argument that GzmK acts as an inflammatory regulator *in vivo*.

Supporting information

S1 Data. Primary data.
(XLSX)

Author Contributions

Conceptualization: Morley D. Hollenberg, Nigel Bunnett, Andreas Suhrbier, Phillip Ian Bird.

Data curation: Dion Kaiserman, Nicholas Barlow.

Formal analysis: Dion Kaiserman, Peishen Zhao.

Funding acquisition: Andreas Suhrbier.

Investigation: Dion Kaiserman, Peishen Zhao, Caitlin Lorraine Rowe, Andrea Leong, Nicholas Barlow, Lars Thomas Joeckel, Phillip Ian Bird.

Methodology: Peishen Zhao, Nicholas Barlow, Lars Thomas Joeckel, Phillip Ian Bird.

Project administration: Dion Kaiserman.

Resources: Peishen Zhao, Nicholas Barlow, Corinne Hitchen, Sarah Elizabeth Stewart, Morley D. Hollenberg, Nigel Bunnett, Andreas Suhrbier, Phillip Ian Bird.

Writing – original draft: Dion Kaiserman, Peishen Zhao, Nicholas Barlow.

Writing – review & editing: Dion Kaiserman, Peishen Zhao, Caitlin Lorraine Rowe, Nicholas Barlow, Lars Thomas Joeckel, Corinne Hitchen, Sarah Elizabeth Stewart, Morley D. Hollenberg, Nigel Bunnett, Andreas Suhrbier, Phillip Ian Bird.

References

1. Voskoboinik I, Whisstock JC, Trapani JA. Perforin and granzymes: function, dysfunction and human pathology. Nat Rev Immunol. 2015; 15(6):388–400. Epub 2015/05/23. https://doi.org/10.1038/nri3839 PMID: 25998963.
2. Joeckel LT, Bird PI. Are all granzymes cytotoxic in vivo? Biol Chem. 2014; 395(2):181–202. Epub 2013/09/05. https://doi.org/10.1515/hsz-2013-0238 PMID: 24002663.
3. Zhao P, Metcalf M, Bunnett NW. Biased signaling of protease-activated receptors. Front Endocrinol (Lausanne). 2014; 5:67. Epub 2014/05/27. https://doi.org/10.3389/fendo.2014.00067 PMID: 24860547; PubMed Central PMCID: PMC4026716.
4. Suidan HS, Bouvier J, Schaerer E, Stone SR, Monard D, Tschopp J. Granzyme A released upon stimulation of cytotoxic T lymphocytes activates the thrombin receptor on neuronal cells and astrocytes. Proc Natl Acad Sci U S A. 1994; 91(17):8112–6. Epub 1994/08/16. https://doi.org/10.1073/pnas.91.17.8112 PMID: 8058766; PubMed Central PMCID: PMC44555.
5. Sower LE, Froelich CJ, Allegretto N, Rose PM, Hanna WD, Klimpel GR. Extracellular activities of human granzyme A. Monocyte activation by granzyme A versus alpha-thrombin. J Immunol. 1996; 156(7):2585–90. Epub 1996/04/01. PMID: 8786323
6. Lee PR, Johnson TP, Gnanapavan S, Giovannoni G, Wang T, Steiner JP, et al. Protease-activated receptor-1 activation by granzyme B causes neurotoxicity that is augmented by interleukin-1beta. J Neuroinflammation. 2017; 14(1):131. Epub 2017/06/29. https://doi.org/10.1186/s12974-017-0901-y PMID: 28655310; PubMed Central PMCID: PMC5488439.
7. Qian Q, Chowdhury BP, Sun Z, Lenberg J, Alam R, Vivier E, et al. Maternal diesel particle exposure promotes offspring asthma through NK cell-derived granzyme B. J Clin Invest. 2020; 130(8):4133–51. Epub 2020/05/15. https://doi.org/10.1172/JCI130324 PMID: 32407293; PubMed Central PMCID: PMC7410053.
8. Turner CT, Zeglinski MR, Richardson KC, Zhao H, Shen Y, Papp A, et al. Granzyme K Expressed by Classically Activated Macrophages Contributes to Inflammation and Impaired Remodeling. J Invest Dermatol. 2019; 139(4):930–9. Epub 2018/11/06. https://doi.org/10.1016/j.jid.2018.09.031 PMID: 30395844.
9. Sharma M, Merkulova Y, Raithatha S, Parkinson LG, Shen Y, Cooper D, et al. Extracellular granzyme K mediates endothelial activation through the cleavage of protease-activated receptor-1. FEBS J. 2016; 283(9):1734–47. Epub 2016/03/05. https://doi.org/10.1111/febs.13699 PMID: 26936634.
10. Cooper DM, Pechkovsky DV, Hackett TL, Knight DA, Granville DJ. Granzyme K activates protease-activated receptor-1. PloS one. 2011; 6(6):e21484. Epub 2011/07/16. https://doi.org/10.1371/journal.pone.0021484 PMID: 21760880; PubMed Central PMCID: PMC3128063.
11. Sun J, Bird CH, Buzza MS, McKee KE, Whisstock JC, Bird PI. Expression and purification of recombinant human granzyme B from Pichia pastoris. Biochem Biophys Res Commun. 1999; 261(2):251–5. Epub 1999/07/30. https://doi.org/10.1006/bbrc.1999.0989 PMID: 10425174.
12. Bohm SK, Kong W, Bromme D, Smeekens SP, Anderson DC, Connolly A, et al. Molecular cloning, expression and potential functions of the human proteinase-activated receptor-2. Biochem J. 1996; 314(Pt 3):1009–16. Epub 1996/03/15. https://doi.org/10.1042/bj3141009 PubMed Central PMCID: PMC1217107. PMID: 8615752
13. Zhao P, Lieu T, Barlow N, Metcalf M, Veldhuis NA, Jensen DD, et al. Cathepsin S causes inflammatory pain via biased agonism of PAR2 and TRPV4. J Biol Chem. 2014; 289(39):27215–34. Epub 2014/08/15. https://doi.org/10.1074/jbc.M114.599712 PMID: 25118282; PubMed Central PMCID: PMC4175355.
14. Sower LE, Klimpel GR, Hanna W, Froelich CJ. Extracellular activities of human granzymes. I. Granzyme A induces IL6 and IL8 production in fibroblast and epithelial cell lines. Cell Immunol. 1996; 171(1):159–63. Epub 1996/07/10. https://doi.org/10.1006/cimm.1996.0187 PMID: 8754861
15. DeFea KA, Zalevsky J, Thoma MS, Dery O, Mullins RD, Bunnett NW. beta-arrestin-dependent endocytosis of proteinase-activated receptor 2 is required for intracellular targeting of activated ERK1/2. J Cell Biol. 2000; 148(6):1267–81. Epub 2000/03/22. https://doi.org/10.1083/jcb.148.6.1267 PMID: 10725339; PubMed Central PMCID: PMC2174299.
16. Wang T, Lee MH, Choi E, Pardo-Villamizar CA, Lee SB, Yang IH, et al. Granzyme B-induced neurotoxicity is mediated via activation of PAR-1 receptor and Kv1.3 channel. PloS one. 2012; 7(8):e43950. Epub 2012/09/07. https://doi.org/10.1371/journal.pone.0043950 PMID: 22952817; PubMed Central PMCID: PMC3430617.
17. Kaiserman D, Bird CH, Sun J, Matthews A, Ung K, Whisstock JC, et al. The major human and mouse granzymes are structurally and functionally divergent. J Cell Biol. 2006; 175(4):619–30. Epub 2006/11/23. https://doi.org/10.1083/jcb.200606073 PMID: 17116752; PubMed Central PMCID: PMC2064598.

18. Buzza MS, Dyson JM, Choi H, Gardiner EE, Andrews RK, Kaiserman D, et al. Antihemostatic activity of human granzyme B mediated by cleavage of von Willebrand factor. J Biol Chem. 2008; 283(33):22498–504. Epub 2008/06/26. https://doi.org/10.1074/jbc.M709080200 PMID: 18577516.

19. Buzza MS, Zamurs L, Sun J, Bird CH, Smith AI, Trapani JA, et al. Extracellular matrix remodeling by human granzyme B via cleavage of vitronectin, fibronectin, and laminin. J Biol Chem. 2005; 280 (25):23549–58. Epub 2005/04/22. https://doi.org/10.1074/jbc.M412001200 PMID: 15843372.

20. Prakash MD, Munoz MA, Jain R, Tong PL, Koskinen A, Regner M, et al. Granzyme B promotes cytotoxic lymphocyte transmigration via basement membrane remodeling. Immunity. 2014; 41(6):960–72. https://doi.org/10.1016/j.immuni.2014.11.012 PMID: 25526309.

21. Trivedi V, Boire A, Tchernychev B, Kaneider NC, Leger AJ, O'Callaghan K, et al. Platelet matrix metalloprotease-1 mediates thrombogenesis by activating PAR1 at a cryptic ligand site. Cell. 2009; 137 (2):332–43. Epub 2009/04/22. https://doi.org/10.1016/j.cell.2009.02.018 PMID: 19379698; PubMed Central PMCID: PMC2807741.

22. Plasman K, Demol H, Bird PI, Gevaert K, Van Damme P. Substrate specificities of the granzyme tryptases A and K. J Proteome Res. 2014; 13(12):6067–77. Epub 2014/11/11. https://doi.org/10.1021/pr500968d PMID: 25383893.

23. Bell JK, Goetz DH, Mahrus S, Harris JL, Fletterick RJ, Craik CS. The oligomeric structure of human granzyme A is a determinant of its extended substrate specificity. Nat Struct Biol. 2003; 10(7):527–34. Epub 2003/06/24. https://doi.org/10.1038/nsb944 PMID: 12819769.

24. Kaiserman D, Stewart SE, Plasman K, Gevaert K, van Damme P, Bird PI. Identification of Serpinb6b as a species-specific mouse granzyme A inhibitor suggests functional divergence between human and mouse granzyme A. J Biol Chem. 2014; 289(13):9408–17. Epub 2014/02/08. https://doi.org/10.1074/jbc.M113.525808 PMID: 24505135; PubMed Central PMCID: PMC3979379.

25. Ramachandran R, Mihara K, Chung H, Renaux B, Lau CS, Muruve DA, et al. Neutrophil elastase acts as a biased agonist for proteinase-activated receptor-2 (PAR2). J Biol Chem. 2011; 286(28):24638–48. Epub 2011/05/18. https://doi.org/10.1074/jbc.M110.201988 PMID: 21576245; PubMed Central PMCID: PMC3137039.

26. Mihara K, Ramachandran R, Renaux B, Saifeddine M, Hollenberg MD. Neutrophil elastase and proteinase-3 trigger G protein-biased signaling through proteinase-activated receptor-1 (PAR1). J Biol Chem. 2013; 288(46):32979–90. Epub 2013/09/21. https://doi.org/10.1074/jbc.M113.483123 PMID: 24052258; PubMed Central PMCID: PMC3829148.

27. Zhao P, Lieu T, Barlow N, Sostegni S, Haerteis S, Korbmacher C, et al. Neutrophil Elastase Activates Protease-activated Receptor-2 (PAR2) and Transient Receptor Potential Vanilloid 4 (TRPV4) to Cause Inflammation and Pain. J Biol Chem. 2015; 290(22):13875–87. Epub 2015/04/17. https://doi.org/10.1074/jbc.M115.642736 PMID: 25878251; PubMed Central PMCID: PMC4447962.

28. Ludeman MJ, Kataoka H, Srinivasan Y, Esmon NL, Esmon CT, Coughlin SR. PAR1 cleavage and signaling in response to activated protein C and thrombin. J Biol Chem. 2005; 280(13):13122–8. Epub 2005/01/25. https://doi.org/10.1074/jbc.M410381200 PMID: 15665002.

29. Zhao T, Zhang H, Guo Y, Zhang Q, Hua G, Lu H, et al. Granzyme K cleaves the nucleosome assembly protein SET to induce single-stranded DNA nicks of target cells. Cell Death Differ. 2007; 14(3):489–99. Epub 2006/09/30. https://doi.org/10.1038/sj.cdd.4402040 PMID: 17008916.

30. Joeckel LT, Allison CC, Pellegrini M, Bird CH, Bird PI. Granzyme K-deficient mice show no evidence of impaired antiviral immunity. Immunol Cell Biol. 2017; 95(8):676–83. Epub 2017/04/22. https://doi.org/10.1038/icb.2017.35 PMID: 28428612.

31. Joeckel LT, Wallich R, Martin P, Sanchez-Martinez D, Weber FC, Martin SF, et al. Mouse granzyme K has pro-inflammatory potential. Cell Death Differ. 2011; 18(7):1112–9. Epub 2011/02/12. https://doi.org/10.1038/cdd.2011.5 PMID: 21311565; PubMed Central PMCID: PMC3131959.

32. Mogilenko DA, Shpynov O, Andhey PS, Arthur L, Swain A, Esaulova E, et al. Comprehensive Profiling of an Aging Immune System Reveals Clonal GZMK(+) CD8(+) T Cells as Conserved Hallmark of Inflammaging. Immunity. 2021; 54(1):99–115 e12. Epub 2020/12/04. https://doi.org/10.1016/j.immuni.2020.11.005 PMID: 33271118.

33. Bade B, Lohrmann J, ten Brinke A, Wolbink AM, Wolbink GJ, ten Berge IJ, et al. Detection of soluble human granzyme K in vitro and in vivo. Eur J Immunol. 2005; 35(10):2940–8. Epub 2005/10/07. https://doi.org/10.1002/eji.200526249 PMID: 16208762.

34. Bratke K, Klug A, Julius P, Kuepper M, Lommatzsch M, Sparmann G, et al. Granzyme K: a novel mediator in acute airway inflammation. Thorax. 2008; 63(11):1006–11. Epub 2008/06/19. https://doi.org/10.1136/thx.2007.091215 PMID: 18559365.

Original research

Agonist that activates the μ-opioid receptor in acidified microenvironments inhibits colitis pain without side effects

Nestor Nivardo Jiménez-Vargas,[1] Yang Yu ,[1] Dane D Jensen,[2,3] Diana Daeun Bok,[3] Matthew Wisdom,[3] Rocco Latorre,[3] Cintya Lopez,[1] Josue O Jaramillo-Polanco,[1] Claudius Degro,[1] Mabel Guzman-Rodriguez,[1] Quentin Tsang,[1] Zachary Snow,[4] Brian L Schmidt,[2] David E Reed,[1] Alan Edward Lomax,[1] Kara Gross Margolis,[4] Christoph Stein,[5] Nigel W Bunnett ,[3,6] Stephen J Vanner[1]

► Additional material is published online only. To view, please visit the journal online (http://dx.doi.org/10.1136/gutjnl-2021-324070).

For numbered affiliations see end of article.

Correspondence to
Professor Nigel W Bunnett, Department of Molecular Pathobiology, New York University College of Dentistry, New York, NY 10010, USA; nwb2@nyu.edu

NNJ-V, YY and DDJ are joint first authors.
NWB and SJV are joint senior authors.

Received 8 January 2021
Revised 15 February 2021
Accepted 9 March 2021
Published Online First 30 March 2021

Check for updates

© Author(s) (or their employer(s)) 2022. No commercial re-use. See rights and permissions. Published by BMJ.

To cite: Jiménez-Vargas NN, Yu Y, Jensen DD, *et al*. *Gut* 2022;**71**:695–704.

ABSTRACT

Objective The effectiveness of μ-opioid receptor (MOPr) agonists for treatment of visceral pain is compromised by constipation, respiratory depression, sedation and addiction. We investigated whether a fentanyl analogue, (±)-N-(3-fluoro-1-phenethylpiperidine-4-yl)-N-phenyl propionamide (NFEPP), which preferentially activates MOPr in acidified diseased tissues, would inhibit pain in a preclinical model of inflammatory bowel disease (IBD) without side effects in healthy tissues.

Design Antinociceptive actions of NFEPP and fentanyl were compared in control mice and mice with dextran sodium sulfate colitis by measuring visceromotor responses to colorectal distension. Patch clamp and extracellular recordings were used to assess nociceptor activation. Defecation, respiration and locomotion were assessed. Colonic migrating motor complexes were assessed by spatiotemporal mapping of isolated tissue. NFEPP-induced MOPr signalling and trafficking were studied in human embryonic kidney 293 cells.

Results NFEPP inhibited visceromotor responses to colorectal distension in mice with colitis but not in control mice, consistent with acidification of the inflamed colon. Fentanyl inhibited responses in both groups. NFEPP inhibited the excitability of dorsal root ganglion neurons and suppressed mechanical sensitivity of colonic afferent fibres in acidified but not physiological conditions. Whereas fentanyl decreased defecation and caused respiratory depression and hyperactivity in mice with colitis, NFEPP was devoid of these effects. NFEPP did not affect colonic migrating motor complexes at physiological pH. NFEPP preferentially activated MOPr in acidified extracellular conditions to inhibit cAMP formation, recruit β-arrestins and evoke MOPr endocytosis.

Conclusion In a preclinical IBD model, NFEPP preferentially activates MOPr in acidified microenvironments of inflamed tissues to induce antinociception without causing respiratory depression, constipation and hyperactivity.

Significance of this study

What is already known on this subject?

► The use of opioids to manage inflammatory bowel disease pain is restricted by side effects of respiratory depression, constipation, sedation and addiction. The μ-opioid receptor (MOPr) mediates the analgesic and detrimental actions of opioids such as fentanyl. We investigated whether a fentanyl analogue, N-(3-fluoro-1-phenethylpiperidine-4-yl)-N-phenyl propionamide (NFEPP), engineered to preferentially bind to the MOPr under acidic conditions found in diseased tissues could selectively inhibit colitis pain without side effects.

What are the new findings?

► In sharp contrast to fentanyl, which inhibited colonic nociception in healthy mice and mice with acute colitis, NFEPP selectively inhibited nociception in mice with colitis but not healthy controls. NFEPP inhibited activity of colonic nociceptors, but only under acidified conditions. Unlike fentanyl, NFEPP did not induce constipation, respiratory depression or altered locomotion. The acidified extracellular fluid of the inflamed colon allowed NFEPP to engage the MOPr and activate antinociceptive signalling pathways.

How might it impact on clinical practice in the foreseeable future?

► Opioids designed to selectively engage receptors in diseased tissues offer the prospect of treating pain without life threatening side effects mediated by receptors in heathy tissues. Since G protein-coupled receptors such as MOPr are the target of over thirty percent of approved drugs, agonists and antagonists designed to selectively engage receptors in diseased tissues might provide enhanced efficacy and specificity for treatment of widespread disorders.

INTRODUCTION

Opioid receptors (OPrs), members of the large family of G protein-coupled receptors, provide an endogenous mechanism for pain control and are thus targets for the treatment of pain.[1] Opioids

Gut: first published as 10.1136/gutjnl-2021-324070 on 30 March 2021. Downloaded from http://gut.bmj.com/ on September 28, 2023 at New York University, Serials Bobst Library Technical Services Serials. Protected by copyright.

that activate the μ-, ∂- and κ-opioid receptors (MOPr, DOPr) on primary sensory, spinal and supraspinal neurons depress activity and inhibit pain. In the inflamed intestine, opioids from infiltrating immune cells activate MOPr and DOPr on primary sensory neurons and suppress inflammatory bowel disease (IBD) pain.[2 3] Drugs that activate MOPr on neurons of the pain pathway are powerful analgesics.[1] However, the usefulness of opioids for the treatment of pain, including IBD pain, is limited by on-target side effects mediated by OPrs in other neurons. MOPr hyperpolarises neurons of the central nervous system, resulting in diminished respiratory drive and sedation.[1] Opioids can also inhibit peristalsis and electrolyte and fluid secretion in the digestive tract by activating MOPr on enteric and central neurons.[4 5] Whereas the analgesic properties of MOPr agonists diminish with continued use (ie, induce tolerance), on-target side effects such as respiratory depression are more sustained, with life-threatening consequences as escalating doses are required to control pain. The addictive properties of opioids exacerbate these problems. The heavy use of opioids is an independent predictor of mortality in IBD patients.[6] Given these problems, non-opioid analgesics have been identified as targets for visceral pain, including antagonists of pronociceptive G protein-coupled receptors and transient receptor potential ion channels.[7]

Insights into the structure and function of MOPrs have facilitated the development of pharmacological approaches to mitigate the detrimental side effects of opioids.[8] Biased agonists, which stabilise MOPr conformations that favour activation of G protein pathways that might underlie analgesia at the expense of β-arrestin (βARR) pathways that may mediate side effects, could provide analgesia with fewer side effects.[9–13] Some G protein biased MOPr agonists show promise in preclinical and human studies,[11 12 14] which has not always been replicated.[15] The premise that different signalling pathways underlie the beneficial and detrimental actions of MOPr agonists and the promise of biased agonists has been questioned.[16] An alternative approach has been to exploit the acidified extracellular environment of diseased tissues (eg, cancer, inflammation) to minimise the side effects of MOPr agonists. Through molecular modelling of MOPr in an acidified environment, a fluorinated analogue of fentanyl, (±)-N-(3-fluoro-1-phenethylpiperidine-4-yl)-N-phenyl propionamide (NFEPP), with a low pKa was developed and found to preferentially activate MOPr in acidified tissues.[17–20] NFEPP inhibits nociception emanating from acidified, diseased tissues without on-target side effects in healthy tissues. It is not known whether NFEPP suppresses inflammatory pain of the colon without affecting defecation, ventilation or locomotion.

Herein, we compared the actions of NFEPP and fentanyl in a preclinical mouse model of IBD. Our results show that NFEPP preferentially activates MOPr in acidified inflamed colon to inhibit nociception without side effects in healthy tissues. Ligands designed to preferentially activate MOPrs in diseased tissues offer the potential for treatment of visceral pain without life-threatening side effects. The approach presented here may be advantageous compared with G protein-biased ligands because G protein activation is an underlying mechanism of opioid-induced respiratory depression and addiction.[21–23]

MATERIALS AND METHODS

Additional materials and methods are included in online supplemental information.

MOPr agonists

NFEPP has been described.[19] Fentanyl was from Sandoz.

Dextran sodium sulfate-induced colitis

Colitis was induced by the administration of 2.5% dextran sodium sulfate (DSS) in drinking water for 5 days.

Visceromotor response to colorectal distention

A telemetric transmitter was implanted to measure electromyographic activity of external oblique muscles. At 10 days after surgery, mice received DSS in the drinking water or water alone for 5 days and were then switched to water alone for 2 days. Visceromotor responses were assessed day 8 after commencing DSS for NFEPP treatment and day 9 for fentanyl treatment. A catheter was inserted 0.5 cm into the colorectum for distension (20, 40, 60, 80 μL). Visceromotor responses were measured 30 min after vehicle, NFEPP or fentanyl (0.2 mg/kg, s.c.). Compliance of the excised colorectum was measured using a pressure transducer.

Colonic pH measurement

pH of colon segments was measured using the pH indicator SNARF 4 F-5 (and 6) carboxylic acid.

Colonic inflammation

Inflammation was assessed by measurement of myeloperoxidase (MPO) activity and by histological scoring.[24]

Tail flick test

Tail flick latency to noxious heat was recorded.

Defecation

Faecal pellets were counted for 1 hour.

Heart rate, oxygen saturation

A pulse oximeter sensor was used to measure heart rate and oxygen saturation.

Locomotion

Distance travelled, speed and resting time were recorded in an open field test.

Patch clamp recording

The excitability of nociceptors was assessed by measuring rheobase.[25]

Extracellular recording

Extracellular recordings were made from the splanchnic nerve innervating isolated segments of mouse distal colon.[25]

Colonic migrating motor complexes

Spatiotemporal maps along of segments of isolated mouse colon were constructed to assess colonic migrating motor complexes (CMMCs).[26]

cDNAs, transfection

Human embryonic kidney 293 (HEK293) cells were transiently transfected using polyethylenimine.[27]

Bioluminescence resonance energy transfer

cAMP formation, βARR2 recruitment and MOPr trafficking to Rab5a-positive endosomes were measured in HEK293 cells using bioluminescence resonance energy transfer (BRET).[27]

Gut: first published as 10.1136/gutjnl-2021-324070 on 30 March 2021. Downloaded from http://gut.bmj.com/ on September 28, 2023 at New York University, Serials Bobst Library Technical Services Serials. Protected by copyright.

Förster resonance energy transfer

Nuclear extracellular signal regulated kinase (ERK) activity was measured in HEK293 cells expressing the Nuc-EKAR Förster resonance energy transfer (FRET) sensor.[27]

Statistics

Results are expressed as mean±SEM Statistical significance was assessed using Student unpaired t-test with Welch's correction or Mann-Whitney test or one-way or two-way analysis of variance (ANOVA) with Tukey's, Bonferroni's or Dunnett's post hoc test.

RESULTS

NFEPP inhibits visceral nociception only in mice with colitis

An agonist that selectively activates MOPr in diseased tissues might obviate on-target side effects mediated by MOPr in healthy tissues. The fentanyl analogue NFEPP was designed to preferentially activate MOPr in the acidified microenvironment of diseased tissues.[19] To assess whether NFEPP would activate MOPr in the inflamed colon and thereby inhibit colitis-induced pain, we compared the efficacy with which NFEPP and fentanyl inhibit visceral nociception in mice with acute colitis and healthy control mice. Mice were treated with DSS (2.5% drinking water, 5 days, 2 days recovery) to induce acute colitis. Time-matched control mice received normal drinking water. Mice were treated with doses of NFEPP, fentanyl (both 0.2 mg/kg, s.c.) or vehicle (control) based on published work.[19] After 30 min, visceral nociception was examined by measuring visceromotor responses to graded colorectal distension (20, 40, 60, 80 µL). Although NFEPP did not affect the visceromotor responses to graded colorectal distension in healthy control mice (% vehicle at 80 µL: NFEPP 108.6%±32.5%, vehicle 100%, N=7, p=0.999, two-way ANOVA, Bonferroni correction), NFEPP inhibited the visceromotor responses in mice with DSS colitis by 65.2%±2.0% (80 µL) (NFEPP 34.8%±2.0%, vehicle 100%, N=5, p<0.001) (figure 1A–D). In contrast, fentanyl inhibited visceromotor responses to colorectal distension both in control mice by 67.8%±11.1% (80 µL: fentanyl 32.3%±11.1%, vehicle 100%, N=6, p<0.01) (figure 1E) and in mice with DSS colitis by 79.7%±15.5% (80 µL: fentanyl 20.3%±15.5%, vehicle 100%, N=4, p<0.001) (figure 1F). The visceromotor responses to colorectal distension at baseline did not differ significantly between control and colitis mice but trended towards higher values in mice with colitis (area under curve; DSS-colitis 7.19±2.65, control 5.27±2.47, N=5–7, p=0.215, two-way ANOVA) (figure 1G). The production of endogenous opioids in the inflamed colon likely explains the absence of significant hyperalgesia in mice with colitis.[28] Compliance of the colorectum from control and colitis mice was not different (increased volume (µL) DSS-colitis 66.1±8.65, control 61.64±9.73, N=4–5, p=0.736, two-way ANOVA) (figure 1H). The results suggest that NFEPP preferentially activates MOPr on nociceptors innervating the inflamed but not healthy colon to inhibit nociception, whereas fentanyl activates MOPr in healthy and diseased mice.

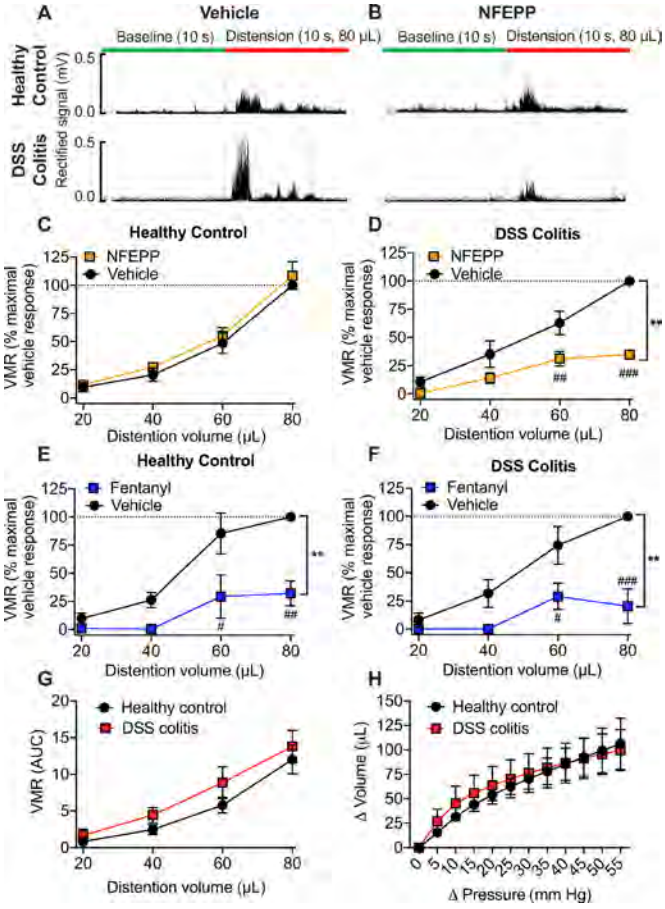

Figure 1 Effects of NFEPP and fentanyl on visceromotor responses to colorectal distension. (A, B) Representative traces showing the effects of vehicle (A) and NFEPP (B) on visceromotor responses to colorectal distension (80 µL) in healthy control and acute DSS colitis mice. (C, D) Effects of vehicle and NFEPP on visceromotor responses to colorectal distension in healthy control mice (C) (N=7, p=0.305) and DSS colitis mice (D) (N=5, p=0.0036). (E, F) Effects of vehicle and fentanyl on visceromotor responses to colorectal distension in healthy control mice (E) (N=6, p=0.0053) and DSS colitis mice (F) (n=4, p=0.0031). Two-way ANOVA, Bonferroni test. (G) Comparison of visceromotor responses to colorectal distension in healthy control (N=7) and DSS colitis (N=5) mice. The area under curve (AUC) of visceromotor responses of control and colitis mice were not significantly different (p=0.215, two-way ANOVA, Bonferroni test. (H) Colorectal compliance in healthy control (N=4) and DSS colitis (N=5) mice. There was no significant difference between control and colitis mice (p=0.736, two-way ANOVA, Bonferroni test). #P<0.05, **##p<0.01, ###p<0.001. In (D–F) # volume distention compared with vehicle, **curve compared with vehicle. ANOVA, analysis of variance; DSS, dextran sodium sulfate; NFEPP, N-(3-fluoro-1-phenethylpiperidine-4-yl)-N-phenyl propionamide; VMR, visceromotor response.

Inflammation acidifies extracellular fluid of the colon

The selectivity of NFEPP depends on its enhanced activity at MOPr in acidified extracellular fluid.[19] To assess whether the inflamed colon is acidified, colon segments from healthy control mice and mice with acute DSS colitis were incubated with the fluorescent pH indicator probe SNARF 4 F-5 (and 6) carboxylic acid, which fluoresces dependent on the protonation state. The inflamed colon (pH 6.71±0.09, N=17) was more acidic (ΔpH 0.33±0.1, p<0.01) than the non-inflamed colon (figure 2A). Colonic MPO activity, an indicator of neutrophil infiltration, was higher in DSS-treated mice (4.08±0.75 U/mg tissue, N=11) than in control mice (0.39±0.13 U/mg tissue, N=11, p<0.001) (figure 2B). Histological examination and measurement of the histological damage score confirmed transmucosal inflammation in the colon of DSS-treated mice (figure 2C,D). Inflammation was more pronounced in the mucosa and submucosa than the muscle layer (figure 2E).

Gut: first published as 10.1136/gutjnl-2021-324070 on 30 March 2021. Downloaded from http://gut.bmj.com/ on September 28, 2023 at New York University, Serials Bobst Library Technical Services Serials. Protected by copyright.

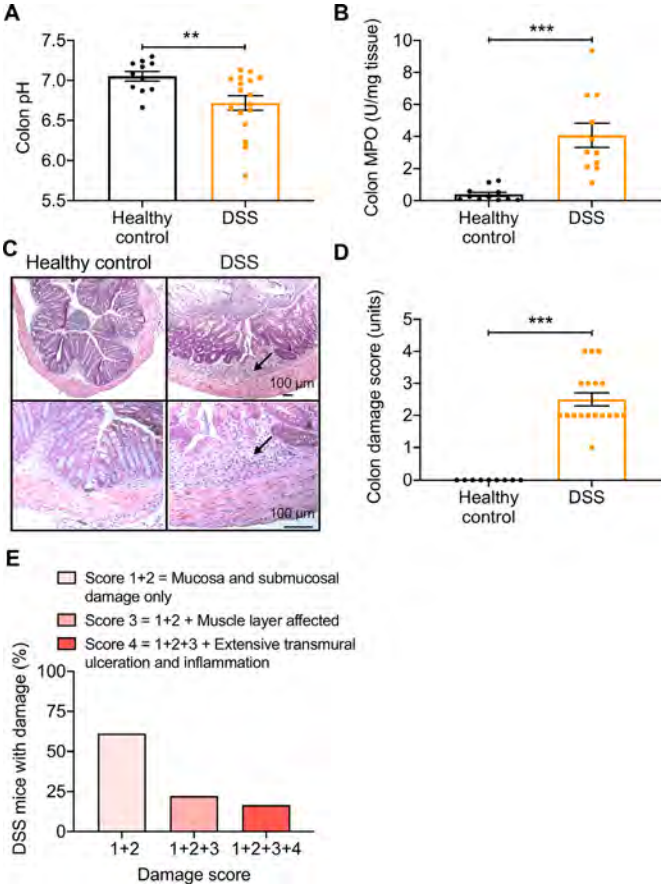

Figure 2 Acidification and inflammation of the colon. (A) pH of extracts of colon from healthy control mice and DSS colitis mice. (B) Myeloperoxidase activity in extracts of colon from healthy control mice and DSS colitis mice. (C–E) Histology (C) and histological damage score (D, E) of the colon from healthy control mice and DSS colitis mice. Arrows in C denote the inflammatory infiltrate in the mucosa of DSS-treated mice. (E) Proportion of specimens with damage score in different layers of colon. N=18 mice. Data points are responses of individual mice. **P<0.01, ***p<0.001. Unpaired Welch's t-test or Mann Whitney test. DSS, dextran sodium sulfate; MPO, myeloperoxidase.

NFEPP does not inhibit somatic thermal nociception, defecation, heart rate, ventilation or locomotion

Conventional agonists activate MOPr in the peripheral and central nervous systems, causing constipation, respiratory depression and sedation.[1 4 5] These on-target side effects limit their usefulness to treatment of IBD pain. We investigated whether NFEPP caused these side effects in healthy control and DSS colitis mice, with the expectation that even defecation might be unaffected in mice with colitis if the pH of the uninflamed musculature is normal. In mice with colitis, NFEPP (0.2 mg/kg, s.c.) did not affect withdrawal responses to noxious heat, assessed by a tail flick assay, whereas fentanyl strongly inhibited the response (p<0.001, figure 3A). These results are in line with the lack of efficacy of NFEPP on visceral nociception in control mice. NFEPP (0.2 or 0.4 mg/kg, s.c.) did not inhibit faecal pellet output in control or colitis mice, whereas fentanyl abolished pellet output in colitis mice (figure 3B,C). NFEPP (0.2 mg/kg, s.c.) did not affect heart rate or blood oxygen saturation in mice with colitis, whereas fentanyl reduced heart rate (ΔBPM 73.33±4.94, N=6, p<0.05 compared with basal) and oxygen saturation (decreased to 85.41%,±1.26, N=6, p<0.05) within 5 min, which returned to basal after 60 min (figure 3D,E). In an open field test of locomotion behaviour, NFEPP did not affect distance travelled, mean speed of travel or resting time (figure 3F–L). In contrast, fentanyl increased distance travelled and speed of travel and decreased resting time as previously shown.[29] These findings suggest that NFEPP does not activate MOPr on peripheral or central neurons of healthy tissues and thus does not cause the typical on-target side effects of fentanyl.

NFEPP preferentially inhibits colonic nociceptors in an acidified extracellular environment

MOPr activates K^+ channels of nociceptors and thereby reduces excitability.[1] Given its pH-dependence, NFEPP might inhibit nociceptors innervating the acidified inflamed colon, without affecting nociceptors in healthy tissues with normal extracellular pH.[17–20] To examine this possibility, we exposed mouse DRG neurons equilibrated at pH 6.5, 6.8 or 7.4 to NFEPP (300 nM), the MOPr agonist DAMGO (100 nM) or vehicle (control) for 15 min (figure 4A). Concentrations were based on published work.[19] Neurons were washed and excitability was assessed by measuring the rheobase (minimum input current required to fire an action potential) of small diameter neurons by patch clamp. NFEPP increased rheobase by 21.32%±8.62% at pH 6.5 and by 29%±8.62% at pH 6.8 when compared with vehicle (p<0.05) but had no effect at pH 7.4 (figure 4B–E). DAMGO increased rheobase by 25.21%±8.07% compared with vehicle (p<0.05) at pH 7.4 (figure 4E) as reported.[25 30] DAMGO had no effect at pH 6.5 (figure 4C). We then examined the duration of NFEPP-mediated inhibition of nociceptor excitability. After measurement of baseline rheobase at pH 7.4, neurons were incubated with NFEPP (300 nM) or vehicle at pH 6.5 for 10 min, and then rapidly switched to agonist-free buffer at pH 7.4. Rheobase was measured at 0, 15 or 30 min after NFEPP or vehicle (figure 4F). At T=0 min, NFEPP increased the rheobase compared with baseline (53.84%±10.5%, p<0.01) and vehicle (36.36%±9.31%, p<0.05) (figure 4F). However, the effect of NFEPP was not sustained at T=15 or T=30 min. When neurons were incubated with NFEPP (300 nM, 15 min) at pH 6.5 and then washed, there was an immediate increase in rheobase (figure 4G). After washing and recovery for 30 min at pH 6.5, the effect of NFEPP was also not sustained.

Although G protein-coupled receptors were once thought to signal exclusively from the plasma membrane, accumulating evidence suggests certain receptors signal from endosomes to control pain transmission.[3 25 27 31–33] Inhibitors of endocytosis blunt the inhibitory actions of DOPr agonists on excitability of DRG neurons, suggesting that endosomal signalling of DOPr underlies the sustained inhibitory effects of certain opioids.[3] However, the clathrin inhibitor PitStop2 did not block the immediate effect (T=0 min) of NFEPP on rheobase at pH 6.5 (figure 4G). Thus, endosomal signalling does not mediate the inhibitory actions of NFEPP-activated MOPr in primary afferent neurons.

To determine whether NFEPP could similarly depress the activation of the peripheral processes of nociceptors that would innervate diseased, acidified tissues, we made extracellular recordings from lumbar splanchnic nerves innervating isolated segments of mouse colon. Nociceptors were characterised by their responsiveness to stimulation of the colon or mesentery with von Frey filaments (VFF) (1 g). Tissues were equilibrated at pH 6.5 or 7.4 (10 min) and basal VFF responses were measured and found to be the same (figure 4H,I). NFEPP (300 nM) or vehicle (control) was superfused into the organ bath for 5 min

Gut: first published as 10.1136/gutjnl-2021-324070 on 30 March 2021. Downloaded from http://gut.bmj.com/ on September 28, 2023 at New York University, Serials Bobst Library Technical Services Serials. Protected by copyright.

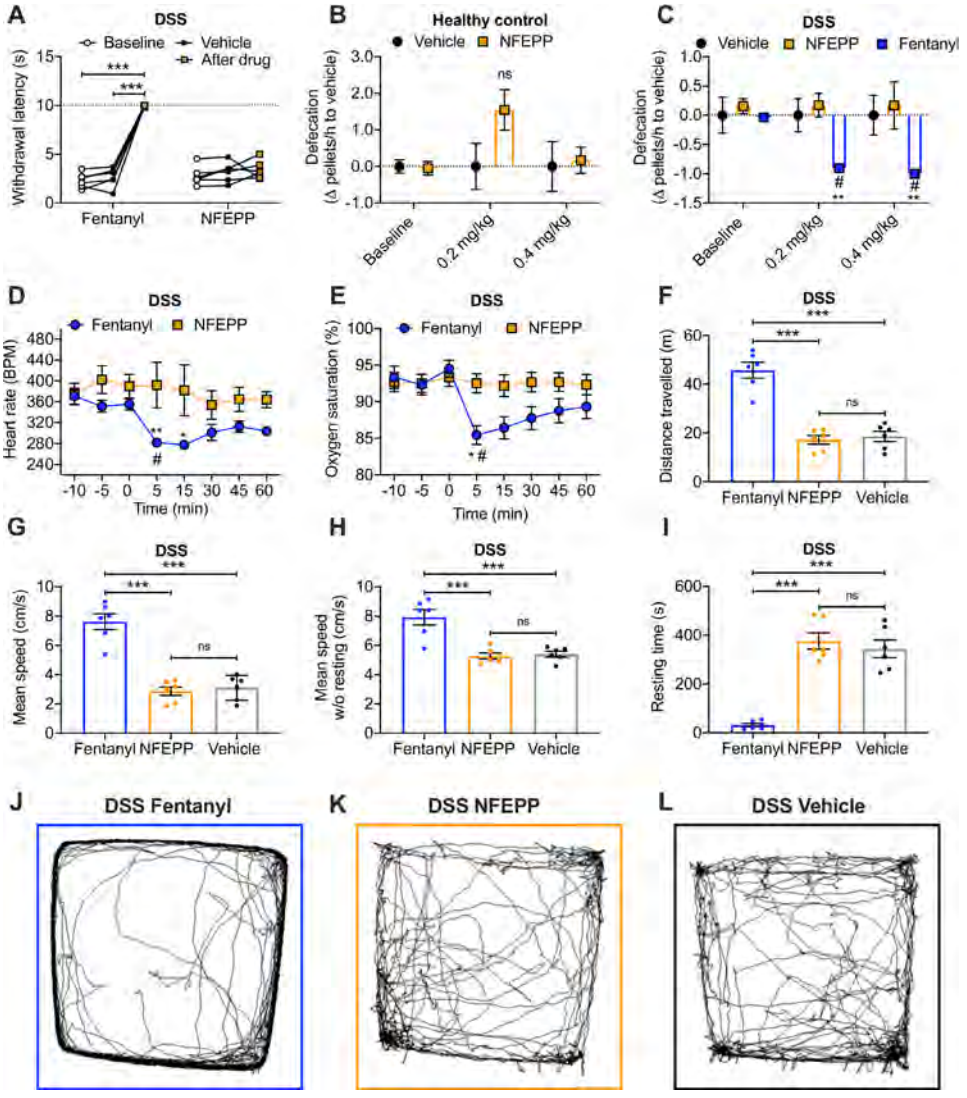

Figure 3 Evaluation of on-target side effects of NFEPP and fentanyl. The effects of NFEPP and fentanyl on withdrawal responses to noxious heat in a tail flick assay (A), N=6 mice per treatment, defecation (B, C), N=6–11 mice per treatment, heart rate (D), N=6 mice per treatment, oxygen saturation (E), N=6 mice per treatment and locomotion (open field test) (F–L), N=6 mice per treatment. (J–L) Are representative travel maps of mice treated with fentanyl, NFEPP or vehicle. Data are from DSS mice with the exception of (B), which is from control mice. Data points are responses of individual mice. #*P<0.05, **p<0.01, ***p<0.001. One-way or two-way ANOVA, Tukey's or Bonferroni's or Dunnett's tests. In C, #compared with vehicle, **fentanyl compared with NFEPP. in D, E, #compared with baseline, *fentanyl compared with NFEPP. ANOVA, analysis of variance; DSS, dextran sodium sulfate; NFEPP, N-(3-fluoro-1-phenethylpiperidine-4-yl)-N-phenyl propionamide; ns, not significant.

and then VFF responses were measured. At pH 6.5, NFEPP attenuated afferent responses to VFF probing compared with basal responses (27.3%±3.5% inhibition, p<0.01) (figure 4H). This effect was reversed after a 15 min washout at pH 7.4 (figure 4H). In contrast, the exposure to NFEPP at pH 7.4 had no effect on afferent mechanical sensitivity (figure 4I). Thus, NFEPP preferentially activates MOPr at the soma and in peripheral processes of nociceptors in acidic environments to transiently depress excitability and mechanical sensitivity.

NFEPP does not alter CMMCs at physiological extracellular pH

Fentanyl and morphine activate MOPr on interneurons of the myenteric plexus, which inhibits release of acetylcholine and nitric oxide and thereby depresses peristaltic contractions of the colon.[4] We made spatiotemporal maps of isolated segments of mouse colon to analyse whether NFEPP would affect the frequency, velocity and length of CMCCs in a pH-dependent manner. Segments of colon were equilibrated in organ baths at extracellular pH 7.4 or 6.8. Spatiotemporal maps were made under basal conditions, in tissues exposed to NFEPP (300 nM), and after NFEPP washout. Under basal conditions, the frequency, velocity and length of CMMCs were not significantly different at pH 7.4 or 6.8 (figure 5A,D,G–I). pH-dependent differences were detected in NFEPP-treated tissues. At pH 7.4, NFEPP had no significant effect on frequency, velocity or length of migrating motor complexes compared with baseline (figure 5B,G–I). These parameters were also unchanged after drug washout (figure 5C,G–I). At pH 6.8 NFEPP abolished migrating motor complexes (figure 5E,G–I). The frequency, velocity and length of migrating motor complexes recovered after drug wash-out (figure 5F,G–I). These findings suggest that NFEPP does not alter colonic peristalsis at physiological pH but may inhibit peristalsis in acidified tissues.

Gut: first published as 10.1136/gutjnl-2021-324070 on 30 March 2021. Downloaded from http://gut.bmj.com/ on September 28, 2023 at New York University, Serials Bobst Library Technical Services Serials. Protected by copyright.

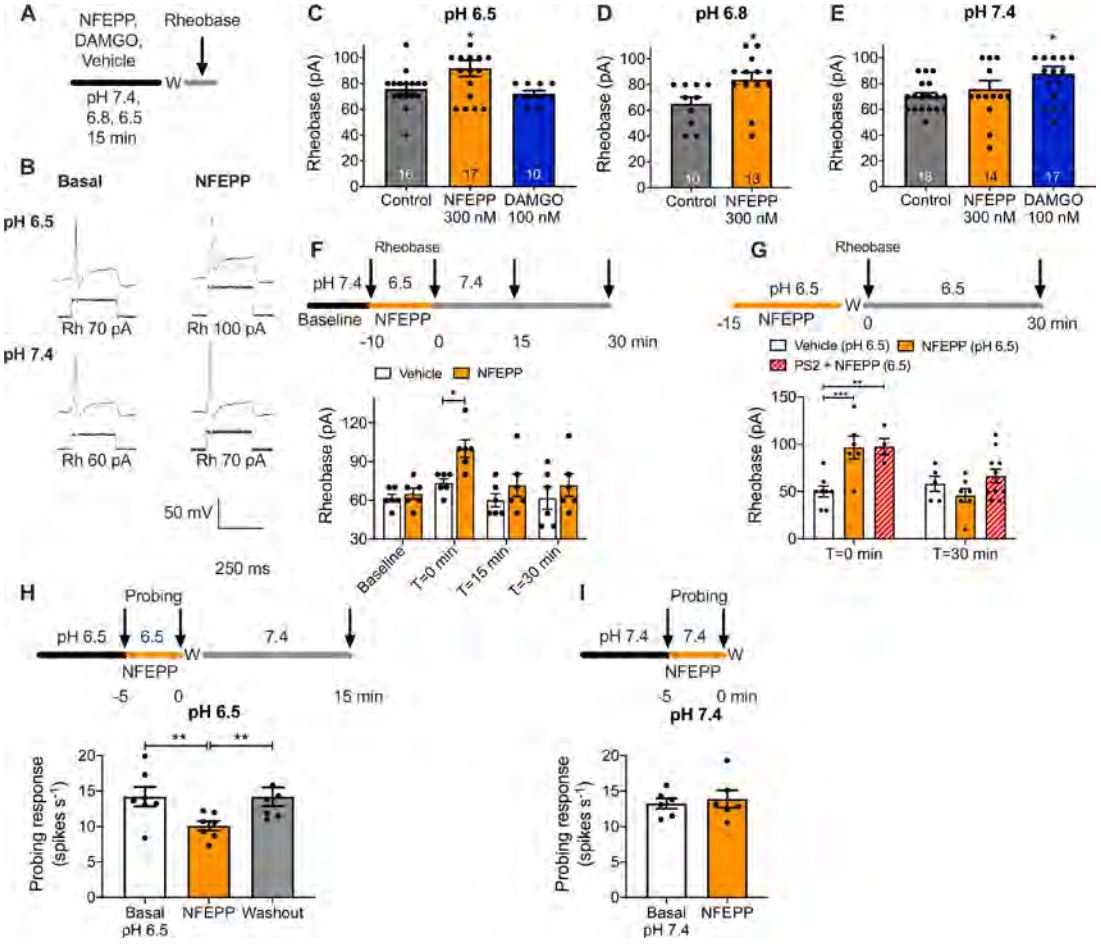

Figure 4 pH-dependent effects of NFEPP on nociceptor excitability. (A–G) Rheobase measurements of excitability of DRG neurons, showing effects of NFEPP and DAMGO at extracellular pH 7.4, 6.8 or 6.5. DRG neurons were preincubated with NFEPP and rheobase (Rh) was measured after washing. (A) protocol. (B) Representative traces under control conditions and after NFEPP at pH 6.5 or pH 7.4. (C–E) effects of NFEPP and DAMGO on rheobase at pH 6.5 (C), 6.8 (D) and 7.4 (E). Data points are responses of individual neurons from n=5–6 mice for each treatment. *P<0.05, 1-way ANOVA, Dunnett's test. (F, G) Duration of NFEPP effects. Neurons were incubated with NFEPP at pH 6.5 and then recovered at pH 7.4 (F) or pH 6.5 (G). Some neurons were treated with PitStop2 (pS2) in G). Data points are responses of individual neurons from N=6–7 mice for each treatment. *P<0.05, **p<0.01, ***p<0.001, two-way ANOVA, Tukey's test. (H, I) Excitability of colonic afferent nociceptors to mechanical stimulation of the mesentery with VFF. Basal responses, effects of NFEPP and recovery of responsiveness on mechano-sensitivity at pH 6.5 (H) and 7.4 (I). Data points are responses of individual receptive fields from n=4 mice. (H) **P<0.01, one-way ANOVA, Bonferroni test. (I) p=0.371, paired t-test. ANOVA, analysis of variance; NFEPP, N-(3-fluoro-1-phenethylpiperidine-4-yl)-N-phenyl propionamide; VFF, von Frey filaments.

NFEPP activates MOPr in an acidified extracellular environment

MOPr couples to $G_{\alpha i}$, which inhibits cAMP formation, and recruits βARRs.[34] We assessed the pH-dependence with which NFEPP might activate these signalling and trafficking pathways. The effects of NFEPP on forskolin-stimulated cAMP generation at extracellular pH 7.4, 6.8 or 6.5 was assessed in HEK293 cells expressing MOPr. NFEPP (300 nM) inhibited cAMP formation at pH 6.5 and 6.8 but not at pH 7.4 for at least 20 min (figure 6A,B). The inhibitory effects of NFEPP at pH 6.5 or 6.8 were comparable to that of the MOPr agonist DAMGO (100 nM) at pH 7.4. Although higher concentrations of NFEPP inhibited cAMP formation at pH 7.4, the effects were less potent and efficacious than at pH 6.5 or 6.8 (figure 6C).

βARRs associate with G protein-coupled receptors to mediate desensitisation, endocytosis and endosomal signalling.[35] To examine the pH-dependence of βARR recruitment to MOPr, we coexpressed in HEK293 cells MOPr tagged with *Rinella* luciferase (MOPr-Rluc8) and βARR2 tagged with yellow fluorescent protein (βARR-YFP). BRET was measured to monitor the proximity between MOPr-Rluc8 and βARR2-YFP. NFEPP (300 nM) increased MOPr-Rluc8/βARR2-YFP BRET at pH 6.5 and 6.8 but not at pH 7.4 (figure 6D,E). To assess pH-dependent MOPr endocytosis, we used BRET to examine the proximity between MOPr-Rluc8 and Rab5a (a resident protein of early endosomes) tagged with Venus (Rab5a-Venus). NFEPP (300 nM) increased MOPr-Rluc8/Rab5a-Venus BRET at pH 6.5 and 6.8, but not at pH 7.4 (figure 6F,G). Thus, NFEPP preferentially activates MOPr under acidic extracellular conditions, leading to inhibition of cAMP formation, recruitment of βARR2 and endocytosis.

Some G protein-coupled receptors, including OPrs, signal in endosomes by G protein-mediated and βARR-mediated mechanisms.[3 25 27 31–33] Receptors in endosomes generate compartmentalised signals that regulate neuronal excitability and pain. For neuropeptide receptors, the acidic microenvironment of the endosome (pH 5.5–6) promotes peptide/receptor dissociation and peptide degradation, which terminate endosomal signalling.[36–40] NFEPP (a non-peptide) might robustly activate MOPr in acidic early endosomes given its pH-dependent

Gut: first published as 10.1136/gutjnl-2021-324070 on 30 March 2021. Downloaded from http://gut.bmj.com/ on September 28, 2023 at New York University, Serials Bobst Library Technical Services Serials. Protected by copyright.

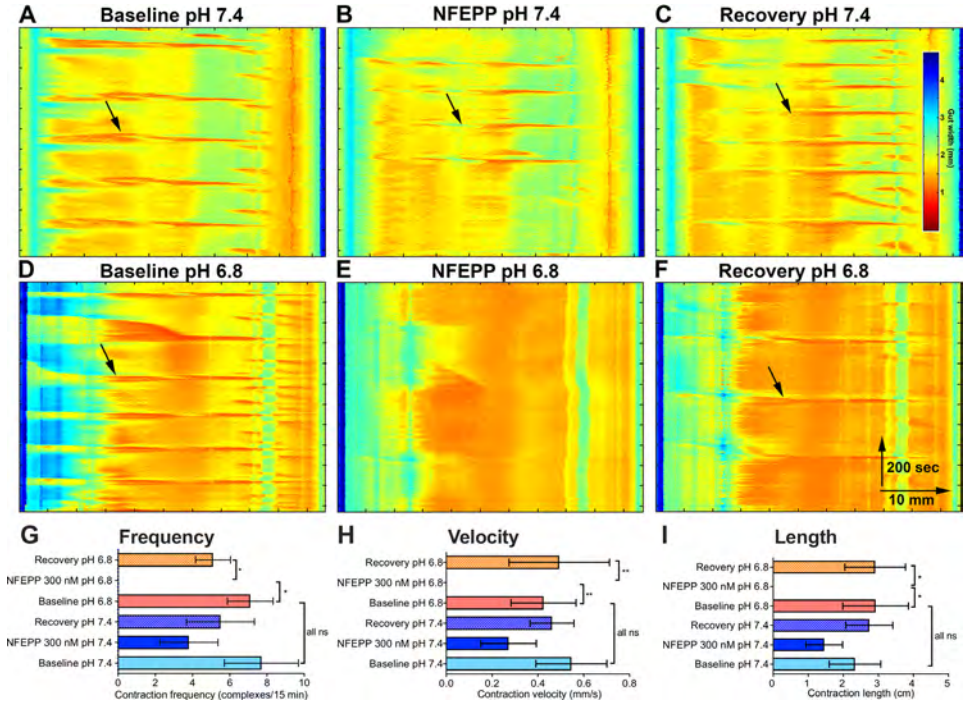

Figure 5 pH-dependent effects of NFEPP on colonic migrating motor complexes. (A–F) Representative spatiotemporal maps of mouse colon at pH 7.4 (A–C) and pH 6.8 (D–F) under baseline conditions (A, D), in the presence of NFEPP 300 nM, (B, D) and after drug wash-out and recovery (C, F). Black arrows indicate sample contractions. (G) Frequency. (H) Velocity. (I) Contraction length. N=6 mice per group. *P<0.05, **p<0.01, Student's unpaired t-tests with Welch's correction were used to compare means. NFEPP, N-(3-fluoro-1-phenethylpiperidine-4-yl)-N-phenyl propionamide; ns, not significant.

properties and presumed resistance to peptidases. To assess endosomal signalling, we expressed in HEK293 cells MOPr and a genetically encoded FRET biosensor for ERK activity in the nucleus (Nuc-EKAR), which is regulated by endosomal receptor signalling.[25 27 33] We measured ERK activity by FRET, which allowed analysis of signalling with high spatial and temporal fidelity. When incubated with cells at pH 6.5 or 6.8, but not at pH 7.4, NFEPP (300 nM) stimulated a sustained activation of nuclear ERK (figure 6H,I). The clathrin inhibitor PitStop2 (30 µM) and the dynamin inhibitor Dyngo4a (50 µM) blocked NFEPP-stimulated nuclear ERK activity (figure 6J,K). The inactive analogues, PitØ and DynØ, had no effect (figure 6J,K). The results suggest that NFEPP-induced MOPr signalling in endosomes activates nuclear ERK.

DISCUSSION

The main finding of our study is that NFEPP, which preferentially activates MOPr in the acidic extracellular environment of diseased tissues, selectively inhibits distension-evoked nociception in the inflamed mouse colon but not in the healthy colon. This finding is consistent with the acidification of the inflamed colon. Under acidic but not physiological conditions, NFEPP also inhibited excitability of nociceptors and suppressed mechanosensitivity of colonic afferent fibres. NFEPP did not affect defecation, ventilation or locomotion in mice with colitis, and did not affect peristaltic contractions of the isolated colon at physiological pH. In line with these findings, NFEPP evoked MOPr $G_{\alpha i}$ signalling, βARR recruitment and endocytosis only under acidic conditions. In contrast, fentanyl inhibited distention-evoked nociception in both the inflamed and healthy colon and induced the expected side effects of a conventional MOPr agonist.

Ischaemia, inflammation and cancer are associated with acidification of the extracellular fluid. During acute and chronic inflammation, the influx of activated immune cells, increased energy expenditure and oxygen use, and accelerated rate of glycolysis result in accumulation of lactic acid, which can acidify extracellular fluid by several pH units.[41] The hypoxic and proliferative zones of solid tumours are also markedly acidified.[42] Extracellular acidification can itself alter the inflammatory response and influence proliferation and metastasis of tumours.[42 43] In the present study, we exploited the acidification of the inflamed colon to increase the selectivity of a MOPr agonist for the treatment of pain, without side effects in healthy tissues. We observed that acute colitis caused a mild acidification of the colon (pH 6.7). pH was measured by incubating the pH indicator probe SNARF 4F-5 (and 6) carboxylic acid with segments of colon in vitro, which might explain the lower-than-expected pH of the uninflamed colon (pH 7.05). Our results support reports of colonic acidosis in patients with ulcerative colitis and Crohn's disease.[44] NFEPP was designed by modelling the docking of fentanyl with MOPr.[19] Since its pKa exceeds 8, fentanyl is protonated and binds to and activates MOPr in healthy (pH 7.4) and inflamed (pH 5–7) tissues. Replacement of hydrogen of fentanyl by fluorine in NFEPP decreased the pKa of NFEPP to 6.8, which resulted in preferential NFEPP activation of MOPr in acidified extracellular fluid (pH 5.5–6.5). We observed that NFEPP more potently activated MOPr at pH 6.5 and 6.8 than at pH 7.4, leading to inhibition of cAMP formation, recruitment of βARR2, and stimulation of MOPr endocytosis.

The ability of fentanyl to interact with MOPr at the pH of both normal and inflamed tissues accounts for its capacity to inhibit mechanically evoked nociception in the non-inflamed and inflamed colon, and explains the side effects of constipation, respiratory depression and altered locomotion that are mediated by MOPr in the peripheral and central nervous systems. The preference of NFEPP for activating MOPr in the acidified

Gut: first published as 10.1136/gutjnl-2021-324070 on 30 March 2021. Downloaded from http://gut.bmj.com/ on September 28, 2023 at New York University, Serials Bobst Library Technical Services Serials. Protected by copyright.

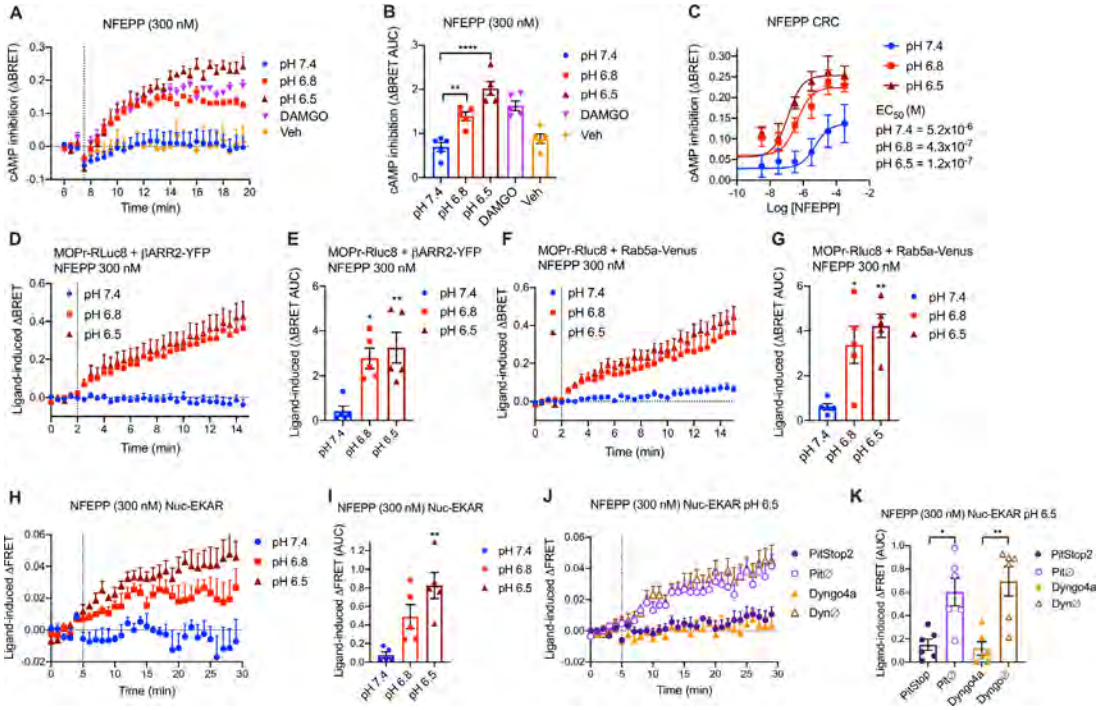

Figure 6 pH-dependent effects of NFEPP on MOPr signalling and endocytosis in HEK293 cells. (A–C) pH-dependency of NFEPP-induced inhibition of forskolin-stimulated formation of cAMP compared with effects of DAMGO at pH 7.4. (A) Time course. (B) Areas under curves (AUC). (C) Concentration-response curve (CRC). (D, E) pH-dependency of NFEPP-induced recruitment of βARR2 to MOPr. (D) Time course. (E) Areas under curves. (F, G) pH-dependency of NFEPP-induced recruitment of MOPr to Rab5a early endosomes. (F) Time course. (G) Areas under curves. (H-K) (H, I) pH-dependency of NFEPP-induced activation of nuclear ERK (Nuc-EKAR). (H) Time course. (I) Areas under curves. (J, K) Effects of PitStop2, Dyngo4a and inactive analogues (PitØ, DynØ) on NFEPP-induced activation of nuclear ERK at pH 6.5. (J) Time course. (K) Areas under curves. Data points are responses of independent experiments. N=5 independent experiments. *P<0.05, **p<0.01, ****p<0.0001, one-way ANOVA, Tukey's test. ANOVA, analysis of variance; ERK, extracellular signal regulated kinase; MOPr, μ-opioid receptor; NFEPP, N-(3-fluoro-1-phenethylpiperidine-4-yl)-N-phenyl propionamide.

extracellular fluid accounts for its selectivity for inhibiting nociception in the inflamed but not non-inflamed colon, and accounts for the lack of observed on-target side effects. We observed that NFEPP decreased the excitability of dorsal root ganglion nociceptors and suppressed mechanically evoked activation of colonic nociceptors in acidic but not physiological conditions. These findings are in line with the capacity of NFEPP to inhibit colonic nociception in mice with colitis. Together, our results suggest that NFEPP selectively activates MOPr at the terminals of nociceptors innervating the inflamed and acidified colonic mucosa. Most experiments in mice compared a single dose of fentanyl and NFEPP. Higher doses of NFEPP may activate MOPr in normal tissues since we observed that NFEPP could activate MOPr expressed in HEK293 cells at normal extracellular pH, although with a reduced potency and efficacy. Further studies are required to examine this possibility.

The effects of NFEPP on colonic motility and defecation deserves further study. Whereas NFEPP did not inhibit defecation in mice with colitis, NFEPP did suppress propulsive contractions of isolated segments of colon at acidic pH. One explanation of the lack of effect of NFEPP on defecation in mice with colitis is that inflammation and thus acidosis is restricted to the mucosa whereas the muscularis externa and myenteric plexus remain at physiological pH. In contrast, in studies of the isolated colon the entire bath and thus all layers were acidified. We observed that the mucosa was the predominant site of DSS-evoked inflammation, which supports the hypothesis that the muscularis externa is not acidified and thus NFEPP does not activate MOPr in myenteric neurons to suppress motility. In addition, MOPr can also regulate defecation by a central mechanism, which would not be activated by NFEPP.[5] A limitation of our experiments is that we were only able to measure pH of the entire colon wall rather than different layers (mucosa, submucosa, muscularis externa), and thus cannot be certain that the pH of the muscularis mucosa is unaffected in mice with DSS colitis. pH-dependent peptide probes, which have been used to localise acidified tumour microenvironments in intact tissues,[42] may enable precise mapping of acidified regions of the inflamed colon. It will also be important to study the effects of NFEPP on defecation in preclinical models of transmural colitis, such as the trinitrobenzene sulphonic acid model, to explore further the potential effects of NFEPP on motility in colitis. Such studies are clinically relevant since whereas ulcerative colitis is largely confined to the mucosa and submucosa, Crohn's disease is transmural. It will be of interest to study the efficacy of NFEPP in preclinical models of chronic colitis and in postinflammatory states that are relevant to irritable bowel syndrome. It will be important to determine if NFEPP, like some other opioids, can predispose the development of toxic megacolon.[45] Whether repeated administration of NFEPP attenuates responsiveness (ie, induces tolerance) remains to be studied. Our results showing that NFEPP selectively inhibits inflammatory pain in the colon are in agreement with other reports of NFEPP selectivity and efficacy for treatment of somatic inflammatory and neuropathic pain, acid-induced abdominal pain, and cancer pain in mice and rats.[18–20 46]

We examined the effects of NFEPP on MOPr signalling and trafficking in HEK293 cells. Our results show that NFEPP activates MOPr at pH 6.5 and 6.8 to inhibit formation of cAMP, recruit βARR2 and stimulate MOPr trafficking to early endosomes

Gut: first published as 10.1136/gutjnl-2021-324070 on 30 March 2021. Downloaded from http://gut.bmj.com/ on September 28, 2023 at New York University, Serials Bobst Library Technical Services Serials. Protected by copyright.

expressing Rab5a. Once viewed as a conduit for receptor trafficking, endosomes are now considered an important site of signal transduction of G protein-coupled receptors that control pain transmission.[3 25 27 31–33] Both MOPr and DOPr can signal from endosomes,[32] and endosomal signalling of DOPr mediates the sustained antinociceptive actions of opioids, including those released from the inflamed colon.[3] The capacity of NFEPP to promote MOPr endocytosis and to engage MOPr at the pH of early endosomes may predispose NFEPP to activate MOPr in endosomes. In support of this possibility, we observed that NFEPP activated ERK in the nucleus, and that inhibitors of clathrin- and dynamin-mediated endocytosis abolished this signal, which thus requires endosomal signalling. DOPr similarly signals from endosomes to activate nuclear ERK.[3] DOPr agonists cause a sustained inhibition of nociceptor excitability, which is suppressed by endocytic inhibitors and thus requires endosomal signalling.[3] In contrast, the inhibitory actions of NFEPP on nociceptor excitability were not sustained despite its ability to activate MOPr in endosomes of HEK293 cells. Other MOPr agonists similarly exert transient inhibitory effects. Together, these findings suggest that NFEPP inhibits nociception primarily be activating MOPr at the plasma membrane of acidified tissues.

Agonists designed to preferentially engage MOPr in diseased tissues offer the potential for effective pain relief without the side effects that are mediated by MOPr in healthy tissues. These drugs would represent a major advance in the treatment of painful digestive diseases, including IBD, irritable bowel syndrome, pancreatitis and pancreatic cancer. Further work is required before NFEPP can be advanced to clinical trials, including toxicology, pharmacokinetic analysis, and studies of efficacy in preclinical models of painful inflammatory and functional diseases of the digestive system. Since G protein-coupled receptors are the single largest target of approved drugs, similar principles might allow the enhanced targeting of other ligands for the treatment of diverse diseases with fewer on-target side effects.

Author affiliations
[1]Gastrointestinal Diseases Research Unit, Kingston General Hospital, Queens University, Kingston, Ontario, Canada
[2]Bluestone Center for Clinical Research, New York University College of Dentistry, New York, New York, USA
[3]Department of Molecular Pathobiology, New York University College of Dentistry, New York, New York, USA
[4]Department of Pediatrics, Columbia University in the City of New York, New York, New York, USA
[5]Department Experimental Anaesthesiology, Charité Campus Benjamin Franklin, Berlin, Germany
[6]Department of Neuroscience and Physiology, Neuroscience Institute, Grossman School of Medicine, New York University, New York, New York, USA

Funding Supported by grants from National Institutes of Health (NS102722, DE026806, DK118971, DE029951, NWB, BLS; RO1NS01554, KGM), Department of Defence (W81XWH1810431, NWB, BLS; PR160365, KGM), Crohn's Colitis Canada (SJV, AEL, DER) and Deutsche Forschungsgemeinschaft (STE 477/19-1, EXC 2046 AA1-1, CS).

Competing interests NWB is a founding scientist of Endosome Therapeutics Inc.

Patient consent for publication Not required.

Ethics approval Queen's University and Columbia University ethics committees approved procedures on C57BL/6 mice (male, 6–8 weeks).

Provenance and peer review Not commissioned; externally peer reviewed.

Data availability statement Data are available on reasonable request. Data are available from the corresponding authors on reasonable request.

Supplemental material This content has been supplied by the author(s). It has not been vetted by BMJ Publishing Group Limited (BMJ) and may not have been peer-reviewed. Any opinions or recommendations discussed are solely those of the author(s) and are not endorsed by BMJ. BMJ disclaims all liability and responsibility arising from any reliance placed on the content. Where the content includes any translated material, BMJ does not warrant the accuracy and reliability of the translations (including but not limited to local regulations, clinical guidelines, terminology, drug names and drug dosages), and is not responsible for any error and/or omissions arising from translation and adaptation or otherwise.

ORCID iDs
Yang Yu http://orcid.org/0000-0001-8388-5825
Nigel W Bunnett http://orcid.org/0000-0003-3367-0644

REFERENCES

1 Corder G, Castro DC, Bruchas MR, *et al*. Endogenous and exogenous opioids in pain. *Annu Rev Neurosci* 2018;41:453–73.
2 Valdez-Morales E, Guerrero-Alba R, Ochoa-Cortes F, *et al*. Release of endogenous opioids during a chronic IBD model suppresses the excitability of colonic DRG neurons. *Neurogastroenterol Motil* 2013;25:39–e4.
3 Jimenez-Vargas NN, Gong J, Wisdom MJ, *et al*. Endosomal signaling of delta opioid receptors is an endogenous mechanism and therapeutic target for relief from inflammatory pain. *Proc Natl Acad Sci U S A* 2020;117:15281–92.
4 Galligan JJ, Sternini C. Insights into the role of opioid receptors in the Gi tract: experimental evidence and therapeutic relevance. *Handb Exp Pharmacol* 2017;239:363–78.
5 Tsuchida D, Fukuda H, Koda K, *et al*. Central effect of mu-opioid agonists on antral motility in conscious rats. *Brain Res* 2004;1024:244–50.
6 Targownik LE, Nugent Z, Singh H, *et al*. The prevalence and predictors of opioid use in inflammatory bowel disease: a population-based analysis. *Am J Gastroenterol* 2014;109:1613–20.
7 Camilleri M. Toward an effective peripheral visceral analgesic: responding to the National opioid crisis. *Am J Physiol Gastrointest Liver Physiol* 2018;314:G637–46.
8 Stein C. New concepts in opioid analgesia. *Expert Opin Investig Drugs* 2018;27:765–75.
9 Bohn LM, Gainetdinov RR, Lin FT, *et al*. Mu-Opioid receptor desensitization by beta-arrestin-2 determines morphine tolerance but not dependence. *Nature* 2000;408:720–3.
10 Bohn LM, Lefkowitz RJ, Gainetdinov RR, *et al*. Enhanced morphine analgesia in mice lacking beta-arrestin 2. *Science* 1999;286:2495–8.
11 Manglik A, Lin H, Aryal DK, *et al*. Structure-Based discovery of opioid analgesics with reduced side effects. *Nature* 2016;537:185–90.
12 Schmid CL, Kennedy NM, Ross NC, *et al*. Bias factor and therapeutic window correlate to predict safer opioid analgesics. *Cell* 2017;171:e13:1165–75.
13 Suomivuori C-M, Latorraca NR, Wingler LM, *et al*. Molecular mechanism of biased signaling in a prototypical G protein-coupled receptor. *Science* 2020;367:881–7.
14 Singla N, Minkowitz HS, Soergel DG, *et al*. A randomized, phase IIb study investigating oliceridine (TRV130), a novel μ-receptor G-protein pathway selective (μ-GPS) modulator, for the management of moderate to severe acute pain following abdominoplasty. *J Pain Res* 2017;10:2413–24.
15 Hill R, Disney A, Conibear A, *et al*. The novel μ-opioid receptor agonist PZM21 depresses respiration and induces tolerance to antinociception. *Br J Pharmacol* 2018;175:2653–61.
16 Servick K. Safety benefits of 'biased' opioids scrutinized. *Science* 2020;367:966.
17 Del Vecchio G, Labuz D, Temp J, *et al*. pK_a of opioid ligands as $_a$ discriminating factor for side effects. *Sci Rep* 2019;9:19344.
18 Rodriguez-Gaztelumendi A, Spahn V, Labuz D, *et al*. Analgesic effects of a novel pH-dependent μ-opioid receptor agonist in models of neuropathic and abdominal pain. *Pain* 2018;159:2277–84.
19 Spahn V, Del Vecchio G, Labuz D, *et al*. A nontoxic pain killer designed by modeling of pathological receptor conformations. *Science* 2017;355:966–9.
20 Spahn V, Del Vecchio G, Rodriguez-Gaztelumendi A, *et al*. Opioid receptor signaling, analgesic and side effects induced by a computationally designed pH-dependent agonist. *Sci Rep* 2018;8:8965.
21 Hill R, Disney A, Conibear A, *et al*. The novel μ-opioid receptor agonist PZM21 depresses respiration and induces tolerance to antinociception. *Br J Pharmacol* 2018;175:2653–61.
22 Kliewer A, Schmiedel F, Sianati S, *et al*. Phosphorylation-Deficient G-protein-biased μ-opioid receptors improve analgesia and diminish tolerance but worsen opioid side effects. *Nat Commun* 2019;10:367.
23 Negus SS, Freeman KB. Abuse potential of biased mu opioid receptor agonists. *Trends Pharmacol Sci* 2018;39:916–9.
24 Wallace JL, Keenan CM. An orally active inhibitor of leukotriene synthesis accelerates healing in a rat model of colitis. *Am J Physiol* 1990;258:G527–34.
25 Jimenez-Vargas NN, Pattison LA, Zhao P, *et al*. Protease-Activated receptor-2 in endosomes signals persistent pain of irritable bowel syndrome. *Proc Natl Acad Sci U S A* 2018;115:E7438–47.
26 Israelyan N, Del Colle A, Li Z, *et al*. Effects of serotonin and slow-release 5-hydroxytryptophan on gastrointestinal motility in a mouse model of depression. *Gastroenterology* 2019;157:507–21.
27 Jensen DD, Lieu T, Halls ML, *et al*. Neurokinin 1 receptor signaling in endosomes mediates sustained nociception and is a viable therapeutic target for prolonged pain

Gut: first published as 10.1136/gutjnl-2021-324070 on 30 March 2021. Downloaded from http://gut.bmj.com/ on September 28, 2023 at New York University, Serials Bobst Library Technical Services Serials. Protected by copyright.

relief. *Sci Transl Med* 2017;9. doi:10.1126/scitranslmed.aal3447. [Epub ahead of print: 31 May 2017].
28 Boué J, Basso L, Cenac N, *et al*. Endogenous regulation of visceral pain via production of opioids by colitogenic CD4(+) T cells in mice. *Gastroenterology* 2014;146:166–75.
29 Varshneya NB, Walentiny DM, Moisa LT, *et al*. Opioid-Like antinociceptive and locomotor effects of emerging fentanyl-related substances. *Neuropharmacology* 2019;151:171–9.
30 Guerrero-Alba R, Valdez-Morales EE, Jiménez-Vargas NN, *et al*. Co-Expression of μ and δ opioid receptors by mouse colonic nociceptors. *Br J Pharmacol* 2018;175:2622–34.
31 Ramírez-García PD, Retamal JS, Shenoy P, *et al*. A pH-responsive nanoparticle targets the neurokinin 1 receptor in endosomes to prevent chronic pain. *Nat Nanotechnol* 2019;14:1150–9.
32 Stoeber M, Jullié D, Lobingier BT, *et al*. A genetically encoded biosensor reveals location bias of opioid drug action. *Neuron* 2018;98:963–76.
33 Yarwood RE, Imlach WL, Lieu T, *et al*. Endosomal signaling of the receptor for calcitonin gene-related peptide mediates pain transmission. *Proc Natl Acad Sci U S A* 2017;114:12309–14.
34 Williams JT, Ingram SL, Henderson G, *et al*. Regulation of μ-opioid receptors: desensitization, phosphorylation, internalization, and tolerance. *Pharmacol Rev* 2013;65:223–54.
35 Peterson YK, Luttrell LM. The diverse roles of arrestin scaffolds in G protein-coupled receptor signaling. *Pharmacol Rev* 2017;69:256–97.
36 Cottrell GS, Padilla BE, Amadesi S, *et al*. Endosomal endothelin-converting enzyme-1: a regulator of beta-arrestin-dependent ERK signaling. *J Biol Chem* 2009;284:22411–25.
37 Gupta A, Fujita W, Gomes I, *et al*. Endothelin-Converting enzyme 2 differentially regulates opioid receptor activity. *Br J Pharmacol* 2015;172:704–19.
38 Jensen DD, Halls ML, Murphy JE, *et al*. Endothelin-Converting enzyme 1 and β-arrestins exert spatiotemporal control of substance P-induced inflammatory signals. *J Biol Chem* 2014;289:20283–94.
39 Padilla BE, Cottrell GS, Roosterman D, *et al*. Endothelin-Converting enzyme-1 regulates endosomal sorting of calcitonin receptor-like receptor and beta-arrestins. *J Cell Biol* 2007;179:981–97.
40 Roosterman D, Cottrell GS, Padilla BE, *et al*. Endothelin-Converting enzyme 1 degrades neuropeptides in endosomes to control receptor recycling. *Proc Natl Acad Sci U S A* 2007;104:11838–43.
41 Erra Díaz F, Dantas E, Geffner J. Unravelling the interplay between extracellular acidosis and immune cells. *Mediators Inflamm* 2018;2018:1–11.
42 Rohani N, Hao L, Alexis MS, *et al*. Acidification of tumor at stromal boundaries drives transcriptome alterations associated with aggressive phenotypes. *Cancer Res* 2019;79:1952–66.
43 Rajamäki K, Nordström T, Nurmi K, *et al*. Extracellular acidosis is a novel danger signal alerting innate immunity via the NLRP3 inflammasome. *J Biol Chem* 2013;288:13410–9.
44 Nugent SG, Kumar D, Rampton DS, *et al*. Intestinal luminal pH in inflammatory bowel disease: possible determinants and implications for therapy with aminosalicylates and other drugs. *Gut* 2001;48:571–7.
45 Katagiri N, Sakai R, Izutsu T, *et al*. Postoperative pain management in patients with ulcerative colitis. *Anesth Prog* 2020;67:158–63.
46 Baamonde A, Menéndez L, González-Rodríguez S, *et al*. A low pKa ligand inhibits cancer-associated pain in mice by activating peripheral mu-opioid receptors. *Sci Rep* 2020;10:18599.

Gut: first published as 10.1136/gutjnl-2021-324070 on 30 March 2021. Downloaded from http://gut.bmj.com/ on September 28, 2023 at New York University, Serials Bobst Library Technical Services Serials. Protected by copyright.

Cellular/Molecular

Opioid-Induced Pronociceptive Signaling in the Gastrointestinal Tract Is Mediated by Delta-Opioid Receptor Signaling

Josue Jaramillo-Polanco,[1*] Cintya Lopez-Lopez,[1*] Yang Yu,[1] Emma Neary,[1] Alan Hegron,[2] Meritxell Canals,[3,4] Nigel W. Bunnett,[2] David E. Reed,[1] Alan E. Lomax,[1] and Stephen J. Vanner[1]

[1]Gastrointestinal Diseases Research Unit, Kingston General Hospital, Queen's University, Kingston, Ontario K7L 2V7, Canada, [2]Department of Molecular Pathobiology, Department of Neuroscience and Physiology, Neuroscience Institute, New York University, New York, New York 10010, [3]Division of Physiology, Pharmacology and Neuroscience, School of Life Sciences, Queen's Medical Centre, University of Nottingham, Nottingham, NG7 2UH, United Kingdom, and [4]Centre of Membrane Protein and Receptors, Universities of Birmingham and Nottingham, Nottingham, NG7 2UH, United Kingdom

Opioid tolerance (OT) leads to dose escalation and serious side effects, including opioid-induced hyperalgesia (OIH). We sought to better understand the mechanisms underlying this event in the gastrointestinal tract. Chronic *in vivo* administration of morphine by intraperitoneal injection in male C57BL/6 mice evoked tolerance and evidence of OIH in an assay of colonic afferent nerve mechanosensitivity; this was inhibited by the δ-opioid receptor (DOPr) antagonist naltrindole when intraperitoneally injected in previous morphine administration. Patch-clamp studies of DRG neurons following overnight incubation with high concentrations of morphine, the μ-opioid receptors (MOPr) agonist [D-Ala^2, N-Me-Phe^4, Gly^5-ol]-Enkephalin (DAMGO) or the DOPr agonist [D-Ala^2, D-Leu^5]-Enkephalin evoked hyperexcitability. The pronociceptive actions of these opioids were blocked by the DOPr antagonist SDM25N but not the MOPr antagonist D-Pen-Cys-Tyr-D-Trp-Orn-Thr-Pen-Thr-NH_2. The hyperexcitability induced by DAMGO was reversed after a 1 h washout, but reapplication of low concentrations of DAMGO or [D-Ala^2, D-Leu^5]-Enkephalin restored the hyperexcitability, an effect mediated by protein kinase C. DOPr-dependent DRG neuron hyperexcitability was blocked by the endocytosis inhibitor Pitstop 2, and the weakly internalizing DOPr agonist ARM390 did not cause hyperexcitability. Bioluminescence resonance energy transfer studies in HEK cells showed no evidence of switching of G-protein signaling from G_i to a G_s pathway in response to either high concentrations or overnight incubation of opioids. Thus, chronic high-dose opioid exposure leads to opioid tolerance and features of OIH in the colon. This action is mediated by DOPr signaling and is dependent on receptor endocytosis and downstream protein kinase C signaling.

Key words: colonic afferent nerves; delta-opioid receptor; dorsal root ganglia; mu-opioid receptor; opioid tolerance; opioid-induced hyperalgesia

Significance Statement

Opioids are effective in the treatment of abdominal pain, but escalating doses can lead to opioid tolerance and potentially opioid-induced hyperalgesia. We found that δ-opioid receptor (DOPr) plays a central role in the development of opioid tolerance and opioid-induced hyperalgesia in colonic afferent nociceptors following prolonged exposure to high concentrations of MOPr or DOPr agonists. Furthermore, the role of DOPr was dependent on OPr internalization and activation of a protein kinase C signaling pathway. Thus, targeting DOPr or key components of the downstream signaling pathway could mitigate adverse side effects by opioids.

Received Oct. 11, 2021; revised Feb. 22, 2022; accepted Feb. 23, 2022.

Author contributions: J.J.-P., C.L.-L., Y.Y., A.H., M.C., N.W.B., D.E.R., A.E.L., and S.J.V. designed research; J.J.-P., C.L.-L., Y.Y., E.N., and A.H. performed research; J.J.-P., C.L.-L., Y.Y., and A.H. analyzed data; J.J.-P., C.L.-L., Y.Y., A.H., M.C., N.W.B., D.E.R., A.E.L., and S.J.V. wrote the paper.

S.J.V., A.E.L., and D.E.R. were supported by Crohn's and Colitis Canada. N.W.B. was supported by National Institutes of Health Grants NS102722, DE026806, DK118971, and DE029951.

*J.J.-P. and C.L.-L. contributed equally to this work as co-first authors.

The authors declare no competing financial interests.

Correspondence should be addressed to Stephen J. Vanner at stephen.vanner@kingstonhsc.ca.

https://doi.org/10.1523/JNEUROSCI.2098-21.2022

Copyright © 2022 the authors

Introduction

Chronic abdominal pain is a debilitating symptom in gastrointestinal disorders, such as irritable bowel syndrome and inflammatory bowel disease. While opioid drugs are effective, they cause serious side effects (Bielefeldt et al., 2009; Targownik et al., 2014). Opioid tolerance (OT), where increasing opioid doses are required to maintain the same level of analgesia, underlies escalating opioid dosing and the resulting risk of serious side effects (Allouche et al., 2014; Cahill et al., 2016; Stein, 2016, 2018).

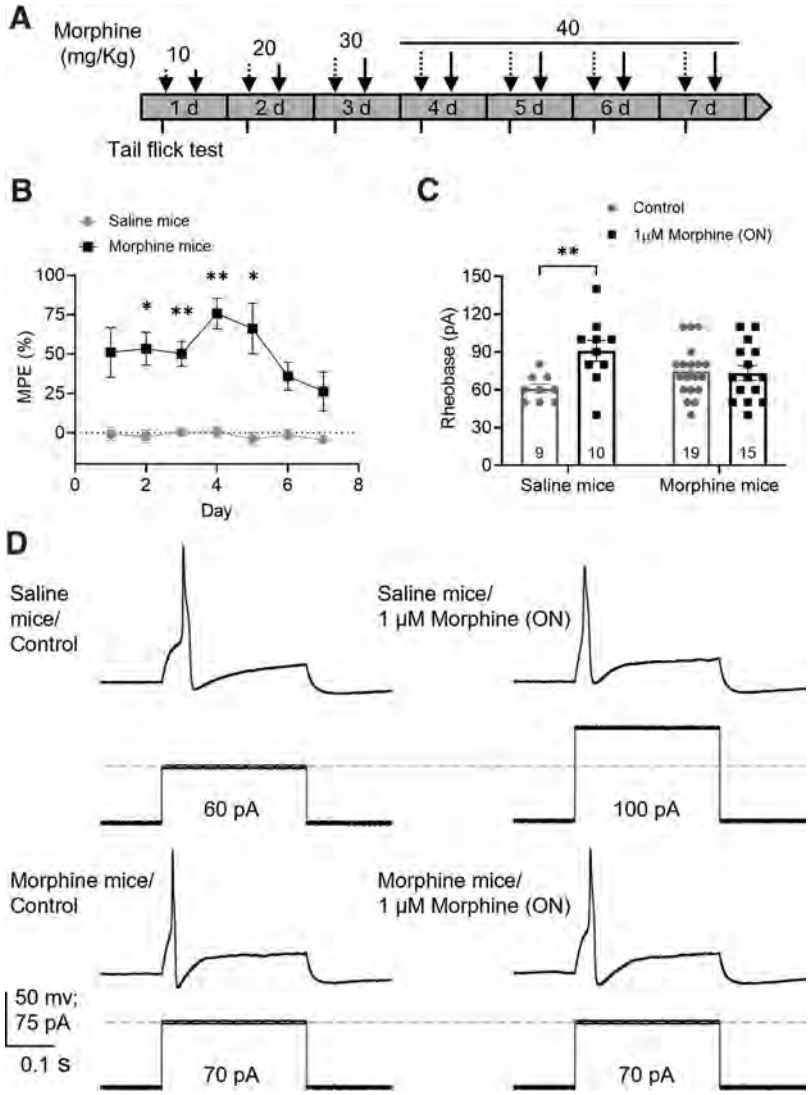

Figure 1. Chronic morphine treatment induces tolerance in mouse DRG neurons. ***A***, Schematic protocol of chronic morphine treatment. Dashed arrows indicate morning i.p. injections. Solid arrows indicate afternoon i.p. injections. Tail-flick assay (short ticks) was performed before and after morning injections. ***B***, *In vivo* tail-flick test showed that morphine had an antinociceptive effect compared with saline ($F_{(1,10)} = 117.5$, $p < 0.0001$, two-way repeated-measures ANOVA with Bonferroni's *post hoc* test); this effect declined after day 4 despite high doses suggesting OT. Results are expressed as the mean of % MPE ± SEM, saline mice = 6; morphine mice = 6. ***C***, Effect of overnight 1 μM morphine on rheobase of DRG neurons measured by patch clamp from saline and morphine-treated mice shows tolerance to morphine in neurons from morphine-treated mice ($F_{(1,49)} = 5.57$, $p = 0.022$, two-way ANOVA with Bonferroni's *post hoc* test). Number of cells appears in each bar. $^{*}p \leq 0.05$. $^{**}p \leq 0.01$. ***D***, Representative recordings of the rheobase (minimal current to elicit an action potential) of DRG neurons from saline and morphine-treated mice exposed to vehicle (control) or morphine overnight.

Moreover, there is evidence that increasing doses can lead to a paradoxical switch in signaling leading to enhanced pain (Mattioli et al., 2014), a condition called opioid-induced hyperalgesia (OIH), although this phenomenon is poorly understood.

Nociceptive signaling in the intestine is mediated by the small C-fiber and larger Aδ-fiber DRG neurons (Robinson and Gebhart, 2008; Kyloh et al., 2011) whose distal axons innervate the intestine and central axons project to second-order neurons in the dorsal horn of the spinal cord. Opioid drugs and endogenous opioids bind to G-protein-coupled μ-, δ-, or κ-opioid receptors (MOPr, DOPr, KOPr) on the plasma membrane of these neurons (Stein, 2016; Spahn et al., 2018). In addition to conventional G-protein-mediated signaling, recent evidence also revealed that β-arrestins (βarrs) couple receptors to clathrin and adaptor protein-2 and guide receptors and ligands to endosomes where further signaling occurs (Jensen et al., 2017; Jimenez-Vargas et al., 2018, 2020; Stoeber et al., 2018).

A large body of work has shown that the molecular mechanisms underlying OT are remarkably complex, and several mechanisms have been proposed, including opioid receptor interactions, receptor phosphorylation, G-protein uncoupling, and altered receptor internalization/recycling (Varga et al., 2004; Williams et al., 2013; Allouche et al., 2014; Galligan and Akbarali, 2014). Several studies have highlighted the importance of βarr2 in the development of morphine antinociceptive tolerance (Bohn et al., 1999; Raehal and Bohn, 2011; Kliewer et al., 2019; Grim et al., 2020; He et al., 2021). Interestingly, the mechanisms of tolerance may be tissue-dependent, further highlighting the need for studies in the intestine.

The analgesic actions of conventional opioid drugs in the intestine, such as morphine, are thought to be mediated primarily by MOPr activation, although DOPr signaling may also have important analgesic actions despite being less well studied (Pergolizzi et al., 2020). Recent clinical studies have shown that drugs targeting multiple opioid receptors, such as a novel agent with mixed effects (MOPr agonist/DOPr antagonist), in the GI tract may have sustained efficacy (Lacy, 2018), but their mechanism of action is poorly understood. To better understand the mechanisms of OT in nociceptive signaling in the intestine and the roles of MOPr and DOPr, we used a model of chronic morphine administration to induce OT and features of OIH. We found evidence of a significant functional MOPr–DOPr interaction underlying these phenomena and sought to understand the mechanisms involved.

Materials and Methods

Materials. SDM25N hydrochloride (SDM25N), D-Pen-Cys-Tyr-D-Trp-Orn-Thr-Pen-Thr-NH_2 (CTOP), naloxone hydrochloride (NLX), AR-M1000390 hydrochloride (ARM390), H 89 hydrochloride (H89), and GF 109203× (GFX) were from Tocris Bioscience. Pitstop 2 (PS2) was from Abcam, and other reagents, including [D-Ala^2, D-Leu^5]-Enkephalin (DADLE), and [D-Ala^2, N-Me-Phe^4, Gly^5-ol]-Enkephalin (DAMGO), and naltrindole hydrochloride (NTI), were from Sigma Aldrich, unless stated otherwise.

Animals. All studies were approved by the Queen's University animal care committees in accordance with guidelines from their National Council of Animal Care. C57BL/6 mice (males and in a small series, females; 8-12 weeks, Charles River Laboratories) were maintained under controlled temperature (22 ± 1°C) and light (12 h light/dark cycle) with free access to food and water.

Chronic morphine treatment. Morphine (Sandoz) was administered by intraperitoneal (i.p.) injection twice daily (9:00 A.M. and 6:00 P.M.) for 7 d, at increasing dose (10 mg/kg first day, 20 mg/kg second day, 30 mg/kg third day, 40 mg/kg fourth to seventh day; see Fig. 1*A*) (Mattioli et al., 2014). Control mice were injected with saline solution

(NaCl 0.9% i.p.) twice daily for 7 d. On day 8, under general anesthetic (ketamine/xylazine), mice were killed, and the DRGs and colons were excised. Where indicated, mice were preinjected with 2.5 mg/kg i.p. NTI 20 min before morphine injections (Matthes et al., 1998). Mice weight was monitored each day during the protocol.

Tail-flick assay. The *in vivo* antinociceptive effect of chronic morphine treatment was tested using the tail-flick assay. Mice were gently placed head first into a restrainer with air holes with both legs inside the restrainer and tail exposed, and the distal one-third of the tail was immersed in a water bath at 52°C. The latency to tail-flick was video recorded before (to determine the baseline) and 30 min after the morning injection with a cutoff time of 10 s to prevent tissue damage. Each assay was performed in triplicate. The latency was measured later in videos starting from the immersion of the tail in the water until the first tail-flick. The investigator analyzing videos was blinded to treatments. Data are presented as percent of maximum possible effect (% MPE) = [(post-drug latency − baseline latency) ÷ (10 − baseline latency)] × 100 (Mattioli et al., 2014; Kang et al., 2017). Attenuation of the maximal antinociceptive effect of morphine overtime was considered as OT.

Retrograde labeling of colon-projecting DRG neurons. To identify colon-projecting DRG neurons, surgeries were performed to inject the retrograde tracer Fast Blue (17740-1, Polysciences) into the colon wall. Female mice were anesthetized via isoflurane inhalation (1.5%-2.5% isoflurane; oxygen flow: 1 L/min), placed on a heating pad, and subjected to midline laparotomy. The colon was carefully exposed, and Fast Blue (1.7% w/v in sterile water) was injected in small volumes (1-2 µl) into multiple sites on the colon wall. The gut was wiped down after each injection to remove excess dye. Bupivacaine (2 mg/kg intradermally) and tramadol (20 mg/kg subcutaneously) were given before surgery, and tramadol (20 mg/kg subcutaneously) was given daily for 3 d as a postoperative analgesic. Mice were killed 7-14 d after surgery, and DRGs (T9-T13) were acutely dissociated for patch-clamp recordings.

Isolation of DRG neurons. DRG neurons were acutely dissociated, as previously described (Ibeakanma et al., 2011). Briefly, mice were killed after ketamine/xylazine i.p. injection, and DRGs from T9-T13 were dissected and collected on Hanks' balanced salt solution. Neurons were enzymatically and mechanically dissociated in F-12 supplemented media (10% FBS, penicillin, streptomycin), plated on Poly-D lysine/laminin-coated coverslips, and placed at 37°C (95% O_2 and 5% CO_2) for 2 h before being incubated overnight with F-12 supplemented media. Electrophysiological recordings were performed the following day. Each treatment was tested on DRG neurons from 6-8 male mice, with exception of the recordings on retrogradely labeled DRG neurons that were obtained from 2 female mice.

Patch-clamp recordings. All experiments were performed at room temperature as previously described (Valdez-Morales et al., 2013). Patch pipettes were pulled (PC-100 Puller, Narishige) and fire-polished (3-5 MΩ) from borosilicate glass capillaries (Warner Instruments). Voltage-clamp recordings were performed by using Multiclamp 700B amplifier, digitized by Digidata 1440A AD converter, and recorded using pClamp 10.5 software (all by Molecular Devices). Dissociated DRG neurons were incubated acutely (30 min) or overnight at 37°C with morphine, the selective MOPr agonist DAMGO (Yekkirala et al., 2010) or the selective DOPr agonists DADLE (Raynor et al., 1994) or ARM390 (Marie et al., 2003). The OPr antagonists NLX (Wang et al., 2008), CTOP (Raynor et al., 1994), and SDM25N (McLamore et al., 2001), PKA inhibitor H89 (Davies et al., 2000), PKC inhibitor GFX (Toullec et al., 1991), or the selective inhibitor of clathrin-mediated endocytosis PS2 (Robertson et al., 2014) were incubated 30 min before the application of agonists. All cells with a membrane capacitance ≤30 pF and a resting membrane potential more negative than −40 mV were analyzed (Moore et al., 2002; Stewart et al., 2003). Where indicated, colon-projecting DRG neurons were identified by the Fast Blue fluorescence emitted from labeled cell bodies under short exposure to UV light with a 365 nm filter.

Perforated patch-clamp recordings were obtained with amphotericin B (0.24 mg/ml) (Ibeakanma et al., 2011), and neuronal excitability was assessed by measuring the rheobase and the action potential discharge at twice rheobase. The extracellular solution composition was as follows (in mM): 140 NaCl, 5 KCl, 1 $MgCl_2$, 2 $CaCl_2$, 10 HEPES, 10 D-glucose, pH 7.4. The pipette solution composition was as follows (mM): 110 K-gluconate, 30 KCl, 10 HEPES, 1 $MgCl_2$, 2 $CaCl_2$, pH 7.25.

Ex vivo *colonic afferent nerve recordings.* Distal colon along with attached mesentery (containing the interior mesenteric ganglion) was removed intact and placed in an organ bath continuously superfused with carbogenated (5% CO_2 and 95% O_2) Krebs buffer (composition, in mM as follows: NaCl, 118.4; $NaHCO_3$, 24.9; $MgSO_4$, 1.2; KH_2PO_4, 1.2; glucose, 11.7; $CaCl_2$, 1.9) at 34°C. Krebs contained the L-type calcium channel blocker nifedipine (3 µM) and the muscarinic acetylcholine receptor antagonist atropine (5 µM) to suppress smooth muscle activity (Zar et al., 1990), as well as the cyclooxygenase inhibitor indomethacin (3 µM) to suppress potential inhibitory actions of endogenous prostaglandins (Peiris et al., 2017). The preparations were opened longitudinally along the mesenteric border and pinned flat with the mucosal side up. Lumbar splanchnic nerve was identified in the neurovascular bundle, teased apart into 5-6 fibers, and individually drawn into a glass suction electrode attached to a Neurolog headstage (NL100, Digitimer). Afferent nerve signals were amplified ×10,000 (NL104), filtered (150-800 Hz, NL125 band pass filter), and recorded on a computer via a Micro 1401 interface and Spike 2 software (version 7, Cambridge Electronic Design).

Receptive fields were identified by systematically stroking the mucosal surface or the mesenteric attachment with a brush. Once identified, receptive fields were tested with three distinct mechanical stimuli to allow classification: probing (with 1 g von Frey filament), mucosal stroking (0.4 g von Frey filament), and circumferential stretch. The circumferential stretch was applied manually by holding the gut wall with forceps and stretching gently. Vascular afferents that only respond to probing on the gut wall or the mesenteric attachment were included in this study since they are thought to be nociceptors (Brookes et al., 2013). Following a 30 min equilibration period, control probing responses (1 g) of each unit were examined by probing 3 times, each for 3 s with 10 s intervals between probings. Morphine (1 µM) was superfused into the organ bath for 15 min before reassessment of the probing response. Single-unit analysis was performed offline using the spike sorting function of Spike2 to discriminate the afferent nerve activity of individual units. The afferent nerve response to probing was assessed as average firing frequency during a 3 s period using a custom-made script in Spike2. Baseline activity was assessed as average firing frequency during a 120 s period after equilibration and reassessed in the presence of morphine. The investigator recording from afferent nerves was blinded to the treatments.

cDNAs. DOPr and MOPr were from GenoCopoeia. GRK2 was from D. Jensen (Columbia University). RGFP-CAAX, Rluc2-Gαi/s/q, GFP10-Gγ2, Gβ1, and Rluc2-βarrestin-2 were from M. Bouvier (Université de Montréal) (Gales et al., 2006; Namkung et al., 2016).

Cell culture and transfection. For bioluminescence resonance energy transfer (BRET) assays of G protein activation, HEK293T cells were cultured and transfected, as described previously (Jimenez-Vargas et al., 2020), using JetPEI (Polyplus Transfection) with DOPr and MOPr (0.2 µg), GRK2 (0.2 µg) and Rluc2-$G\alpha_{i/s/q}$ (0.2 µg), and GFP10-Gγ2 (0.4 µg) with Gβ1 (0.1 µg). For ebBRET of βarr2 recruitment to the membrane, HEK293T cells were transfected with DOPr and MOPr (0.2 µg), GRK2 (0.2 µg), Rluc2-βarr2 (0.1 µg), and RGFP-CAAX (0.4 µg) for plasma membrane recruitment (Namkung et al., 2016).

BRET assays G protein activations and βarr recruitment to the plasma membrane. Transfected HEK293T cells were incubated overnight with vehicle, DADLE 10 µM, or DAMGO 10 µM. On the day of the assay, HEK293T cells were washed with Dulbecco's PBS, and then Tyrode's buffer was added, and cells were incubated for 30 min at 37°C. After the addition of Prolume Purple Coelenterazine (2.5 µM; NanoLight Technology), the cells were incubated for 5 min at 37°C. BRET was recorded for 22.5 min in a Synergy Neo2 Microplate reader (BioTek) (acceptor filter: 515 ± 30 nm; donor filter: 410 ± 80 nm). Cells were challenged with vehicle, DADLE 10 nM, DADLE 10 µM, DAMGO 10 nM, or DAMGO 10 µM after 2.5 min. Δ-BRET represents the BRET signal in the presence of agonist subtracted by the BRET signal in the presence of vehicle.

Statistical analyses. Data were analyzed using Prism 9 Software (GraphPad Software), and results are expressed as mean ± SEM. Normal distribution was assessed by parametric testing D'Agostino-

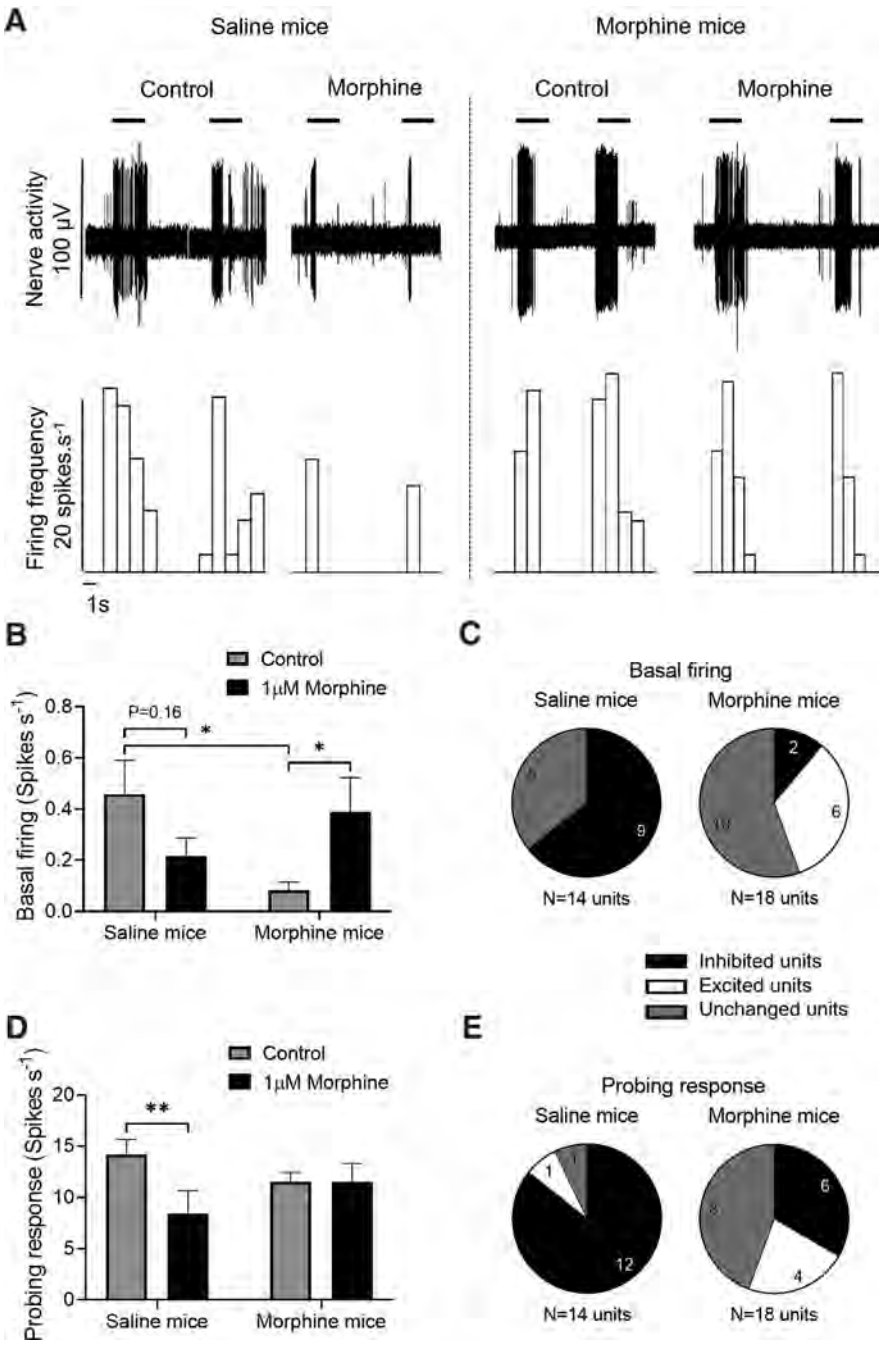

Figure 2. Chronic morphine treatment induces tolerance and OIH in mouse colon. Effect of acute application of 1 μM morphine on the basal activity and probing response of colonic afferent axons from saline and morphine-treated mice. ***A***, Representative recording of colonic nerve response to 1 g von Frey filament probing before and after administration of 1 μM morphine. ***B***, Acute morphine application did not affect the basal firing in afferent axons from saline-treated mice, while it increased firing in afferent axons from morphine-treated mice ($F_{(1,28)} = 10.06$, $p = 0.0037$, two-way repeated-measures ANOVA with Bonferroni's *post hoc* test). ***C***, Analysis of basal nerve activity showed an increased number of excited units on morphine-treated mice, whereas most of the units were inhibited in saline-treated mice (χ^2, df = 5.269, 1; $p = 0.022$). ***D***, Acute application of 1 μM morphine inhibited the colonic afferent nerve response to probing in saline-treated mice but not in morphine-treated mice ($F_{(1,30)} = 6.35$, $p = 0.0173$, two-way repeated-measures ANOVA with Bonferroni's *post hoc* test). ***E***, Chronic exposure to morphine increased the number of units that were excited on probing response after acute morphine application (χ^2, df = 8.283, 1; $p = 0.004$). ***B***, ***D***, Error bars indicate mean ± SEM. *$p \leq 0.05$. **$p \leq 0.01$.

Pearson. Differences between two groups were examined using unpaired *t* test, whereas multiple groups were examined using one-way ANOVA with Dunnett's or Tukey's *post hoc* test as indicated, or two-way ANOVA with Bonferroni's *post hoc* test for multiple comparisons. A *p* value ≤ 0.05 was considered significant. After classification of unit responses, data were loaded into a contingency table and then analyzed with the χ^2 test for trend. A *p* value ≤ 0.05 was considered significant.

Results

OT and colonic OIH

Mice were treated with morphine for 7 d, using an established model of OIH (Fig. 1*A*) (Ferrini et al., 2013; Mattioli et al., 2014). Tolerance of somatic nerves was assessed using a tail-flick test in conscious mice. Morphine's antinociceptive effect was maximum on day 4 and declined over the following days despite high opioid doses (Fig. 1*B*; $p = 0.002$, two-way repeated-measures ANOVA, $N = 6$ saline-, 6 morphine-treated mice), suggesting development of OT (Mattioli et al., 2014; Kang et al., 2017). Patch-clamp recordings from DRG neurons isolated from morphine- and saline-treated mice demonstrated that overnight application of morphine (1 μM) inhibited neurons from saline-treated mice (rheobase increased by 49%; $p = 0.006$, two-way ANOVA, $n = 9$ control cells, 10 morphine-incubated cells/6 mice) but had no effect on neurons from mice treated with chronic morphine (Fig. 1*C*,*D*; $p > 0.99$, two-way ANOVA, $n = 15$ control cells, 19 morphine-incubated cells/6 mice).

To determine the effect of chronic morphine administration on excitability of afferent nerves innervating the colon, recordings were obtained from colons dissected from saline- and morphine-treated mice (Fig. 2*A*). Chronic morphine treatment decreased basal firing of afferent nerves (Fig. 2*B*; $p = 0.028$, two-way repeated-measures ANOVA, $n = 12$ units/6 saline-treated mice, 18 units/6 morphine-treated mice). However, while the acute application of morphine (1 μM) reduced the basal firing activity of afferent nerves from saline-treated mice ($p = 0.16$, two-way repeated-measures ANOVA, $n = 12$ units/6 saline-treated mice), it evoked a paradoxical increase in basal firing in afferent nerves from morphine-treated mice (Fig. 2*B*; $p = 0.018$, two-way repeated-measures ANOVA, $n = 18$ units/6 morphine-treated mice). Similarly, morphine also inhibited the mechanosensitive response (von Frey filament, 1 g) in saline-treated mice but did not alter mechanosensitive responses in the morphine-treated mice (Fig. 2*D*; $p = 0.004$, two-way repeated-measures ANOVA, $n = 14$ units/6 saline-treated mice). Based on responses to the superfusion of morphine, units were classified in three groups: excited (>20% increase over baseline or control probing response), inhibited (>20%

decrease from baseline or control probing response), and unchanged (<20% change) (Yu et al., 2019). Compared with saline-treated mice in which acute morphine application inhibited both basal firing (Fig. 2*C*; χ^2, df = 5.269, 1; $p = 0.022$) and mechanosensitivity (Fig. 2*E*; χ^2, df = 8.283, 1; $p = 0.004$) in most afferent units, morphine-treated mice had significantly fewer units with decreased firing and a greater number with increased or unchanged excitability.

Together, these studies demonstrate the development of OT in response to chronic morphine and provide evidence of a paradoxical increase in basal and mechanosensitive afferent nerve firing in response to the acute application of morphine, suggesting OIH.

Pronociceptive signaling evoked by morphine is mediated by DOPr

To examine mechanisms underlying the development of OT and morphine-induced hyperexcitability in colonic afferents neurons, DRG neurons from naive mice were treated with morphine at a low (10 nM) or a high (30 μM) concentration either acutely (30 min) or overnight, and patch-clamp recordings were then obtained. Concentrations in the nanomolar range activate the classical G_i-mediated inhibitory pathway (Roeckel et al., 2017), whereas concentrations in the micromolar to millimolar range have been used to induce a pronociceptive effect (Akaishi et al., 2000; Forster et al., 2009; Rowan et al., 2014). Acute application of low and high concentrations of morphine decreased neuron excitability compared with control; rheobase increased by 24% ($p = 0.038$, one-way ANOVA, $n = 15$-21) and 30% ($p = 0.004$, one-way ANOVA, $n = 21$ on each group), respectively (Fig. 3*A*). Overnight incubation with high concentrations of morphine induced an increase in neuron excitability compared with control; rheobase decreased by 18% (Fig. 3*B*; $p = 0.039$, one-way ANOVA, $n = 22$ on each group). These data parallel the findings in afferent nerve recordings (Fig. 2), demonstrating that prolonged exposure to high concentration of opioids induces tolerance and a paradoxical increase in excitability of nociceptive neurons. The pronociceptive effect evoked by chronic morphine exposure was blocked by SDM25N (DOPr antagonist, 100 nM) (McLamore et al., 2001) but not by CTOP (MOPr antagonist, 100 nM) (Raynor et al., 1994), suggesting that the increased excitability induced by prolonged *in vitro* exposure to a high concentration of morphine is mediated by DOPr (Fig. 3*C*; for SDM25N: $p = 0.019$; for CTOP: $p > 0.99$, two-way ANOVA, $n = 10$-15).

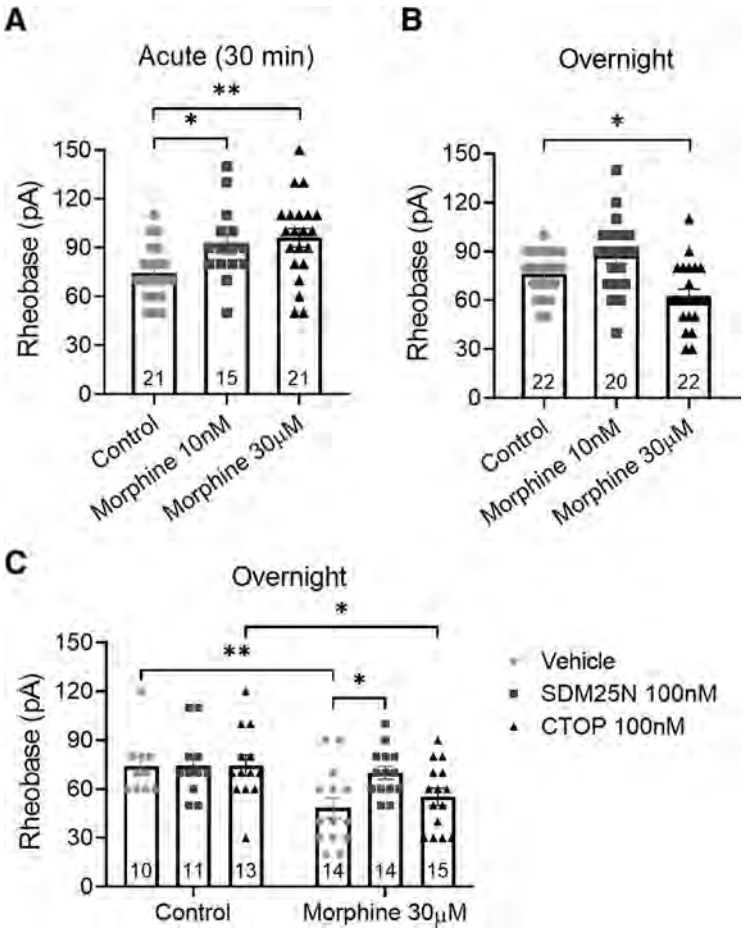

Figure 3. Overnight incubation with high concentrations of morphine has a pronociceptive effect on naive DRG neurons mediated by DOPr. ***A***, Effect of the acute incubation of morphine on the excitability of DRG neurons measured by perforated patch clamp. Both low and high concentrations of morphine increased neuron rheobase compared with control ($F_{(2,54)} = 5.79$, $p = 0.0053$, one-way ANOVA with Dunnett's *post hoc* test). ***B***, Overnight incubation of low-concentration morphine had no effect on rheobase, while high concentration decreased neuron rheobase compared with control ($F_{(2,61)} = 8.93$, $p = 0.0004$, one-way ANOVA with Dunnett's *post hoc* test). ***C***, DOPr antagonist SDM25N but not MOPr antagonist CTOP prevented the pronociceptive effect induced by high-concentration morphine ($F_{(1,71)} = 12.45$, $p = 0.0007$, two-way ANOVA with Bonferroni's *post hoc* test). Number of cells appears in each bar. Error bars indicate mean ± SEM. $^*p \leq 0.05$. $^{**}p \leq 0.01$.

To determine whether DOPr activation is also necessary for morphine-induced hyperalgesia *in vivo*, we examined the effect of the DOPr antagonist NTI (2.5 mg/kg) (Matthes et al., 1998). The DOPr antagonist was administered daily 20 min before morphine injections (Fig. 4*A*), and results from these mice were compared with those treated with morphine alone. The tail-flick test showed that NTI reduced the antinociceptive effect (MPE) of morphine at day 3, suggesting the involvement of DOPr in morphine-induced analgesia (Fig. 4*B*; $p = 0.031$, two-way repeated-measures ANOVA, $N = 7$ morphine-, 7 NTI + morphine-treated mice). Importantly, the analgesic effect of morphine was reduced on day 7 in morphine-treated mice ($p = 0.003$, two-way repeated-measures ANOVA, $N = 7$ mice), whereas NTI prevented this tolerance ($p = 0.15$, two-way repeated-measures ANOVA, $N = 7$ mice). In patch-clamp studies of DRG neurons, acute morphine application increased the excitability of nociceptive neurons from morphine-treated mice (rheobase decreased 26%, $p = 0.049$, two-way ANOVA, $n = 15$ control cells, 16 morphine-incubated cells/7 mice), but it did not affect the excitability of neurons from NTI + morphine mice ($p > 0.99$, two-way ANOVA, $n = 17$ control cells, 15 morphine-incubated cells/7 mice), demonstrating that blocking DOPr with NTI *in vivo* prevented the increase in DRG neuron excitability induced by chronic morphine (Fig. 4*C*). *Ex vivo* afferent nerve recordings in colons from mice receiving morphine alone showed that basal firing and mechanosensitivity were unaffected by the acute application of morphine (i.e., exhibited tolerance) (Fig. 4*D*,*F*; $p > 0.99$ and 0.25, respectively, two-way repeated-measures ANOVA, $n = 15$ units/7 morphine-treated mice), whereas in colons from NTI + morphine mice, the acute morphine application inhibited mechanosensitivity

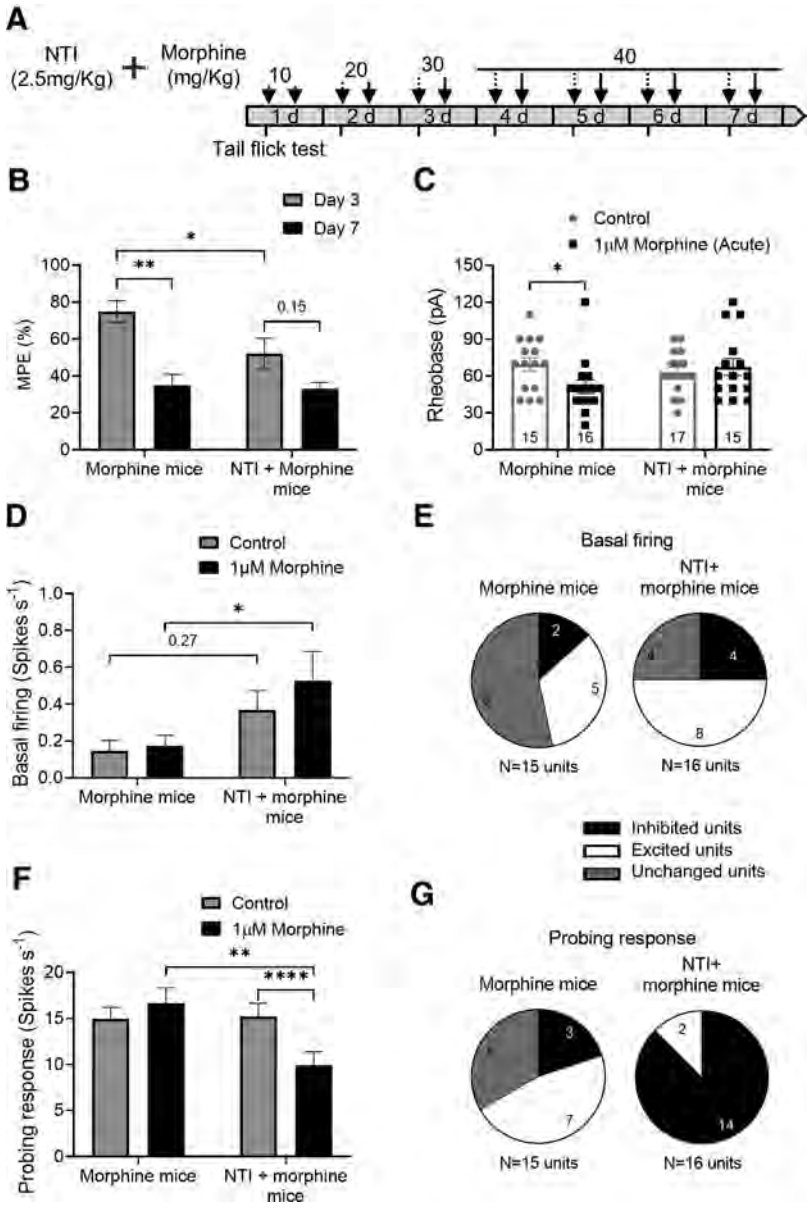

Figure 4. The DOPr inhibitor NTI prevents tolerance and the pronociceptive effect induced by chronic morphine. ***A***, Schematic protocol of chronic morphine treatment in the presence of DOPr antagonist NTI. ***B***, *In vivo* tail-flick test on NTI + morphine-treated mice showed an inhibition on the maximum antinociceptive effect reached on day 3 by morphine-treated mice ($F_{(1,12)} = 5.52$, $p = 0.037$, two-way repeated-measures ANOVA with Bonferroni's *post hoc* test). This maximum antinociceptive effect decreased on day 7 only in morphine-treated mice ($F_{(1,12)} = 17.67$, $p = 0.0012$, two-way repeated-measures ANOVA with Bonferroni's *post hoc* test). Results are expressed as mean of % MPE ± SEM, morphine mice = 7; NTI + morphine mice = 7. ***C***, Acute morphine incubation decreased rheobase of neurons from morphine-treated mice but did not have any effect on neurons from NTI + morphine-treated mice ($F_{(1,59)} = 4.163$, $p = 0.046$, two-way ANOVA with Bonferroni's *post hoc* test). Number of cells appears in each bar. ***D-G***, Effect of acute application of 1 μM morphine on the basal activity and probing response of colonic afferent axons from morphine (6 mice) and NTI + morphine-treated mice (5 mice). ***D***, No changes were observed on basal firing in afferent nerves from morphine-or NTI + morphine-treated mice ($F_{(1,29)} = 1.53$, $p = 0.226$, two-way repeated-measures ANOVA with Bonferroni's *post hoc* test). ***E***, Quantification of units showed no difference between groups in terms of basal activity (χ^2, df = 2.28, 1; $p = 0.131$). ***F***, Acute application of morphine inhibited the afferent response to probing only in NTI + morphine mice ($F_{(1,29)} = 21.44$, $p < 0.0001$, two-way repeated-measures ANOVA with Bonferroni's *post hoc* test). ***G***, Most of the units were inhibited in response to probing after acute morphine exposure on NTI + morphine mice compared with those from morphine-treated mice, which showed a higher number of excited units (χ^2, df = 14.06, 1; $p = 0.0002$). Error bars indicate mean ± SEM. *$p \leq 0.05$. **$p \leq 0.01$. ****$p \leq 0.0001$.

(Fig. 4*F*; $p < 0.0001$, two-way repeated-measures ANOVA, $n = 16$ units/7 NTI + morphine-treated mice). The number of afferent units with different responses to acute morphine application in terms of basal firing between morphine mice and NTI + morphine mice was similar (Fig. 4*E*; χ^2, df = 2.280, 1; $p = 0.13$). However, acute morphine decreased the number of excited mechanosensitive units and increased the number of inhibited units in NTI + morphine mice (Fig. 4*G*; χ^2, df = 14.06, 1; $p = 0.0002$), suggesting that blocking DOPr activation significantly reduced OIH in morphine-treated mice.

The role of MOPr and DOPr signaling in the paradoxical increased DRG neuron excitability induced by opioids

We have previously shown that MOPr and DOPr are functionally expressed on colonic DRG neurons and coexpressed on a significant proportion of these neurons (Guerrero-Alba et al., 2018). To examine their specific roles in the development of opioid-induced neuronal hyperexcitability, the effects of the MOPr agonist DAMGO and the DOPr agonist DADLE were examined using acute application (30 min) and overnight incubation (Figs. 5 and 6, respectively) with low (10 nM) and high (10 μM) agonist concentrations. DAMGO and DADLE have similar binding affinities for their receptors ($IC_{50} \sim 2$ nM), evoking inhibition at nanomolar concentrations (Raynor et al., 1994; Guerrero-Alba et al., 2018), and we sought to determine whether higher concentrations can evoke an excitatory effect. Following acute application of 10 nM or 10 μM DAMGO, neuronal excitability was decreased compared with control (Fig. 5*A*; $p = 0.002$ and 0.009, respectively, two-way ANOVA, $n = 28$-30). This decreased excitability was selectively blocked by 100 nM CTOP (Fig. 5*A*; $p = 0.0012$ and 0.02, respectively, two-way ANOVA, $n = 18$-30), but not by 100 nM SDM25N (Fig. 5*B*; $p > 0.99$, two-way ANOVA, $n = 20$-30). Acute application of 10 nM DADLE also decreased neuron excitability, whereas 10 μM DADLE increased neuron excitability (Fig. 5*C*; $p = 0.026$ and 0.018, two-way ANOVA, $n = 23$-26). Both effects were blocked by SDM25N (Fig. 5*C*; $p = 0.003$ and 0.046, two-way ANOVA, $n = 23$-26), whereas CTOP failed to block the excitatory effect by 10 μM DADLE (Fig. 5*D*; $p > 0.99$, two-way ANOVA, $n = 14$ on each group).

After overnight exposure, 10 nM DAMGO decreased neuron excitability compared with control, whereas 10 μM DAMGO increased excitability (Fig. 6*A*; $p < 0.0001$ and 0.03, respectively, two-way ANOVA, $n = 23$-25). Importantly, this excitatory effect of DAMGO was blocked by the DOPr antagonist SDM25N (Fig. 6*B*; $p < 0.0001$, two-way ANOVA, $n = 10$-13) but not by the MOPr antagonist CTOP (Fig. 6*A*; $p > 0.99$, two-way ANOVA, $n = 22$-23); 10 nM DADLE had no

effect on the mean rheobase suggesting desensitization, whereas 10 μM DADLE increased neuron excitability (Fig. 6*C*; $p = 0.296$ and 0.004, respectively, two-way ANOVA, $n = 23$-28). This pronociceptive effect was also blocked by SDM25N (Fig. 6*C*; $p = 0.006$, two-way ANOVA, $n = 23$-33) but also by CTOP (Fig. 6*D*; $p = 0.008$, two-way ANOVA, $n = 19$ on each group), an unexpected finding given that CTOP did not block the pronociceptive action evoked by DADLE (Fig. 5*D*). Together, our data suggest that DOPr is involved in the paradoxical increased neuronal excitability induced by MOPr and DOPr agonists.

To confirm our fundamental observation in gut specific neurons, we performed patch-clamp recordings on colon-projecting DRG neurons (Fast Blue-labeled) from female mice. The DOPr agonist DADLE 10 μM overnight incubated increased DRG neuron excitability compared with vehicle (Fig. 6*E*; $p = 0.0035$, unpaired *t* test, $n = 8$ on each group).

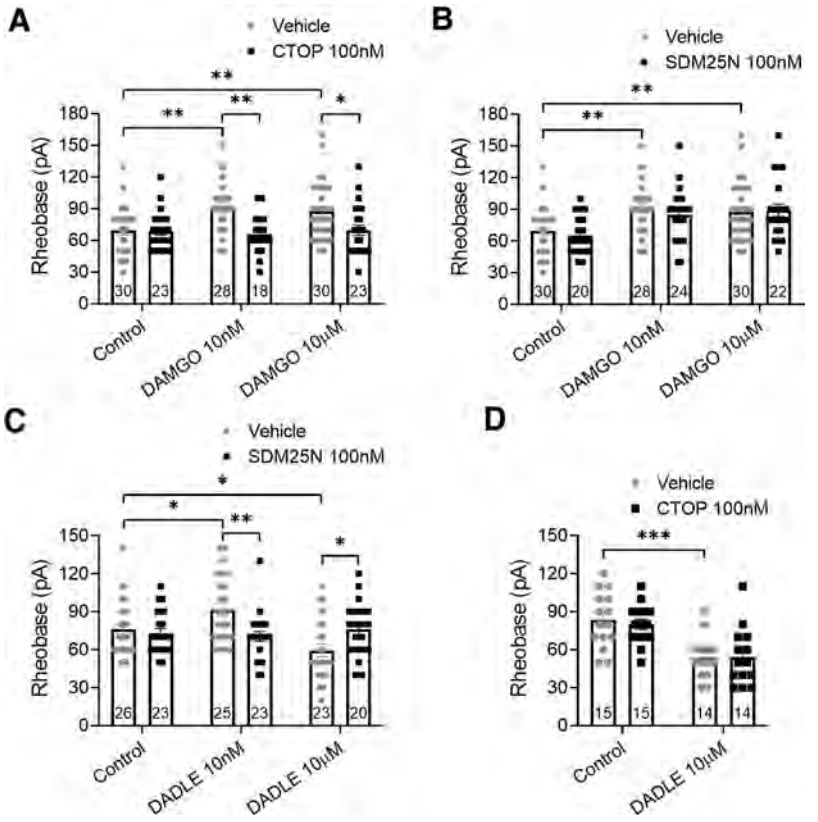

Figure 5. Acute application of MOPr and DOPr agonists shows that pronociceptive actions are mediated by DOPr. ***A***, ***B***, Effect of low-concentration (10 nM) and high-concentration (10 μM) DAMGO applied acutely (30 min) on neuron excitability. Patch-clamp recordings show that low and high concentrations of DAMGO increased neuron rheobase. This antinociceptive effect was inhibited by MOPr antagonist CTOP (***A***: $F_{(2,146)} = 3.655$, $p = 0.028$) but not by DOPr antagonist SDM25N (***B***: $F_{(2,148)} = 0.339$, $p = 0.713$). ***C***, ***D***, A low concentration of DADLE increased neuron rheobase, whereas a high concentration decreased neuron rheobase. DOPr antagonist SDM25N blocked both effects induced by DADLE (***C***: $F_{(1,134)} = 8.35$, $p = 0.0004$), whereas CTOP was unable to block the pronociceptive effect evoked by high-concentration DADLE (***D***: $F_{(1,54)} = 0.1555$, $p = 0.695$). Number of cells appears in each bar. Error bars indicate mean ± SEM. *$p \leq 0.05$; **$p \leq 0.01$; ***$p \leq 0.001$; two-way ANOVA with Bonferroni's *post hoc* test.

The DOPr-mediated pronociceptive effect is endocytosis-dependent

To examine the intracellular signaling underlying hyperexcitability evoked by overnight incubation with high concentrations of DAMGO and DADLE, we used the opioid receptor antagonist NLX and the inhibitor of endocytosis, PS2. NLX is an alkaloid that can permeate the plasma membrane and also affect the intracellular signaling of opioid receptors (Wang et al., 2008), whereas PS2 is an inhibitor of clathrin-mediated endocytosis (Robertson et al., 2014). The pronociceptive effects of DAMGO and DADLE were blocked by 1 μM NLX (Fig. 7*A*; $p < 0.0001$ and 0.002 respectively, two-way ANOVA, $n = 12$-16) and also by 20 μM PS2 (Fig. 7*B*; $p = 0.027$ and 0.016 respectively, two-way ANOVA, $n = 14$-19). To further characterize the involvement of endocytic pathways in the increased neuronal excitability evoked by high concentrations of opioid agonists and mediated by DOPr, DRG neurons were incubated acutely (30 min) and overnight with high concentration of a weakly internalizing DOPr agonist ARM390 (10 μM) (Marie et al., 2003; Pradhan et al., 2009). We previously showed that DADLE and SNC80 but not ARM390 (100 nM) induced βarr recruitment as well as DOPr internalization (Jimenez-Vargas et al., 2020). Acute incubation with ARM390 did not alter the mean rheobase of DRG neurons, whereas overnight incubation decreased neuron excitability despite the high concentration (Fig. 7*C*; $p = 0.039$, one-way ANOVA, $n = 20$ or 21). Together, these data suggest that the neuronal hyperexcitability induced by opioids is dependent on DOPr internalization.

Overnight exposure to a high concentration of opioids switches MOPr and DOPr signaling in response to acute opioid re-exposure to a pronociceptive pathway

To further examine the mechanisms underlying the switch of opioid signaling to a pronociceptive pathway, we studied the response to low-concentration (10 nM) MOPr and DOPr agonists following overnight incubation of DRG neurons with high concentrations (10 μM) of DAMGO or DADLE (Fig. 8*A*). As shown in Figure 6, sustained exposure to 10 μM DADLE increased neuron excitability. However, after 1 h washout of DADLE, neuron excitability recovered to control levels (Fig. 8*B*). Neurons were then re-exposed to acute application (30 min) of 10 nM of either a DOPr or MOPr agonist. DADLE 10 nM but not DAMGO increased neuron excitability rather than decreasing it ($p = 0.002$ and $p > 0.99$, respectively, one-way ANOVA, $n = 16$ or 17), as previously observed in naive neurons (Fig. 5), suggesting a switch in receptor downstream signaling pathways as a result of the prior overnight exposure to DADLE (Fig. 8*B*). Interestingly, following overnight incubation with 10 μM DAMGO, re-exposure to both 10 nM DAMGO or DADLE increased neuron excitability (Fig. 8*C*; $p = 0.003$ on both cases, one-way ANOVA, $n = 10$-12).

PKC mediates the pronociceptive effect by opioids after overnight exposure to 10 μM DADLE

To further understand the intracellular mechanism underlying neuronal hyperexcitability after opioid re-exposure, we explored the role of PKA and PKC signaling. Opioid inhibition of neurons occurs via G_i-protein linked to PKA pathway, whereas PKCε signaling has been implicated in pronociceptive responses induced by opioids (Joseph et al., 2010). Following washout of the

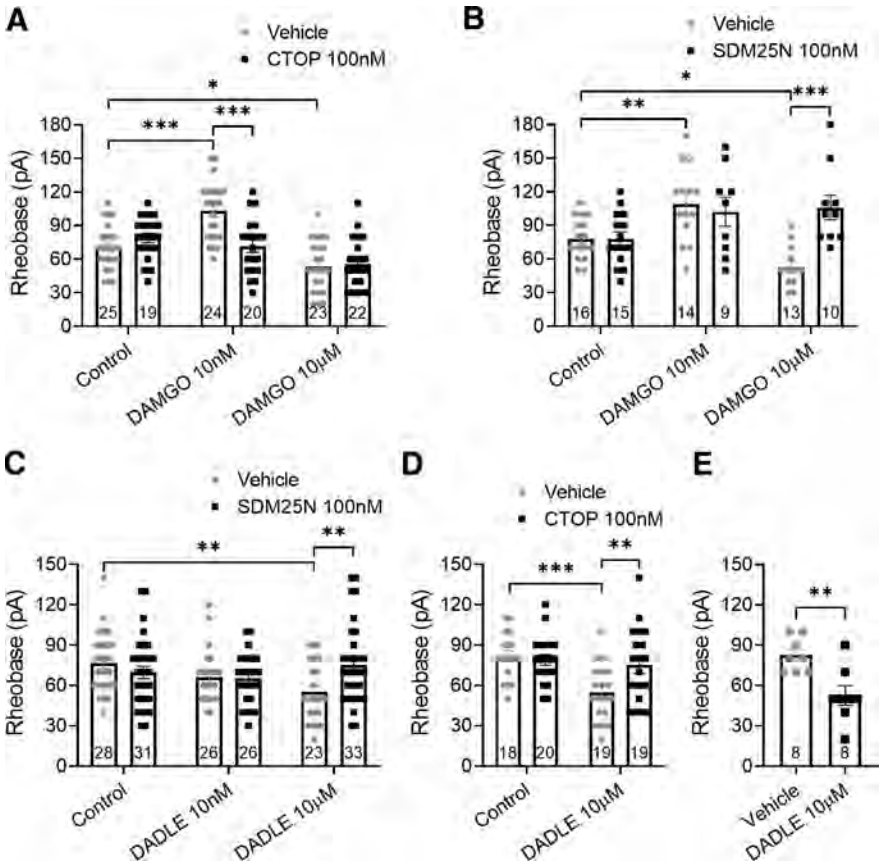

Figure 6. DOPr mediates the pronociceptive effect induced by high concentrations of MOPr and DOPr agonists applied overnight. ***A***, ***B***, Effect of low-concentration (10 nM) and high-concentration (10 μM) DAMGO overnight incubated on DRG neuron excitability. DRG neuron rheobase increased with low-concentration but decreased with high-concentration DAMGO. ***A***, CTOP prevented the antinociceptive effect by 10 nM DAMGO but had no effect on the pronociceptive effect by 10 μM DAMGO ($F_{(2,127)} = 9.898$, $p < 0.0001$). ***B***, SDM25N inhibited only the pronociceptive effect by 10 μM DAMGO ($F_{(2,71)} = 8.144$, $p = 0.0007$). ***C***, ***D***, Low-concentration DADLE had no effect on neuron rheobase, while high concentrations decreased neuron rheobase; this pronociceptive effect by high-concentration DADLE was inhibited by both SDM25N (***C***: $F_{(2,161)} = 5.022$, $p = 0.0077$) and CTOP (***D***: $F_{(1,72)} = 5.605$, $p = 0.0206$). ***E***, Effect of 10 μM DADLE on DRG neurons innervating the colon of female mice. High-concentration DADLE decreased the rheobase of Fast Blue-labeled neurons ($t_{(14)} = 3.506$, $p = 0.0035$, unpaired *t* test). Number of cells appears in each bar. Error bars indicate mean ± SEM. ***A–D***, $^*p \leq 0.05$; $^{**}p \leq 0.01$; $^{***}p \leq 0.001$; two-way ANOVA with Bonferroni's *post hoc* test.

excitatory effect of overnight 10 μM DADLE or DAMGO incubation, PKA or PKC inhibitors were applied to DRG neurons 30 min before acute incubation with 10 nM opioids (Fig. 8*D*). H89
1 μM failed to block the pronociceptive effect of 10 nM DADLE re-exposure (Fig. 8*E*,*G*; rheobase decreased compared with H89 control; $p = 0.02$ and $p = 0.012$ respectively, one-way ANOVA, $n = 12$-16), but blocked the pronociceptive effect of 10 nM DAMGO re-exposure (Fig. 8*G*; rheobase not different compared with H89 control, $p = 0.15$, one-way ANOVA, $n = 16$ or 17). GFX 1 μM blocked the pronociceptive effect of 10 nM DADLE re-exposure following either overnight 10 μM DADLE or DAMGO incubation (Fig. 8*F*,*H*; rheobase not different from GFX control, $p = 0.63$ and $p = 0.09$, respectively, one-way ANOVA, $n = 12$-18), suggesting that PKC signaling plays a role in the pronociceptive responses mediated by DOPr.

$G\alpha_i$ signaling and βarr2 recruitment are lost after sustained exposure to opioids

BRET assays were performed in HEK293T cells to measure the activation of $G\alpha_i$, $G\alpha_s$, and $G\alpha_q$ proteins following acute opioid agonists re-exposure. Acute application of DADLE and DAMGO to cells not previously exposed to opioids activated $G\alpha_i$ subunits but minimal $G\alpha_q$ and not $G\alpha_s$ proteins. DADLE evoked a larger response than DAMGO (Fig. 9). $G\alpha_i$ subunit activation by acute opioids decreased when cells were previously exposed to a high concentration of DADLE (10 μM) or DAMGO (10 μM) (Fig. 9*A–D*; one-way ANOVA), suggesting possible desensitization of $G\alpha_i$ signaling after prolonged opioid exposure. We did not find evidence of $G\alpha_s$ or $G\alpha_q$ protein activation after opioid re-exposure (Fig. 9*E–L*; one-way ANOVA).

βarr2 recruitment to the plasma membrane was also measured in HEK293T cells. Acute application of DADLE (Fig. 9*M*,*N*) or high concentration of DAMGO (Fig. 9*P*) evoked significant recruitment of βarr2 to the plasma membrane. This recruitment was absent when cells were re-exposed to opioids after overnight incubation with high concentration of DADLE or DAMGO (Fig. 9*M–P*; one-way ANOVA).

Discussion

The opioid crisis in the developed world has fueled ongoing interest in strategies to mitigate the serious and potentially lethal side effects of opioid drugs. These side effects are driven by escalating dosing as a result of OT and possibly the less well-described phenomenon of OIH, where opioids are thought to paradoxically increase nociceptive signaling following chronic exposure to high doses (Farmer et al., 2017). An important site of analgesia derived from systemic opioids is the peripheral nociceptive DRG neuron, such as those innervating the intestine (Guerrero-Alba et al., 2018). Here we focus on peripheral nociceptive signaling mechanisms in the colon using *in vivo* models of OT and corresponding *in vitro* models of OPr desensitization. We provide evidence of decreased antinociceptive and enhanced pronociceptive signaling from afferent nerves following chronic morphine exposure and corresponding changes in *in vitro* studies of isolated DRG neurons. Moreover, we found evidence of a functional MOPr–DOPr interaction where these events were driven by activation of DOPr in response to high doses of either MOPr or DOPr agonists.

Morphine is a common analgesic used to manage pain over days to weeks in multiple clinical settings. In our *in vivo* studies with morphine exposure for only 7 d, we observed decreased analgesia and enhanced pronociceptive signaling in colonic afferent nerves, when the nerves were challenged with an acute application of morphine. These findings were evident after quantification of the number of individual units differentially altered by acute morphine in basal afferent nerve firing and mechanical probing responses, suggesting that both basal firing and mechanosensitive properties are affected. In parallel, patch-clamp

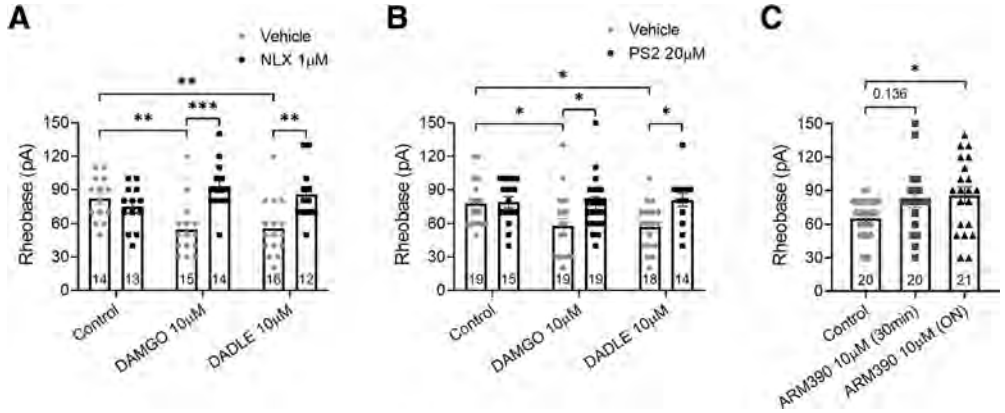

Figure 7. Opioid-induced DRG neuronal hyperexcitability is dependent on receptor endocytosis. ***A***, Patch-clamp recordings show that the OPr antagonist naloxone (NLX) prevented the decrease in the rheobase evoked by high-concentration DAMGO and DADLE applied overnight ($F_{(2,78)} = 8.143$, $p = 0.0006$, two-way ANOVA with Bonferroni's *post hoc* test). ***B***, The clathrin inhibitor PS2 also prevented the decrease on the rheobase evoked by high-concentration opioids ($F_{(1,98)} = 10.63$, $p = 0.0015$, two-way ANOVA with Bonferroni's *post hoc* test). ***C***, Acute application of a weakly internalizing DOPr agonist ARM390 at equally high concentration did not alter neuron rheobase, whereas overnight incubation increased neuron rheobase ($F_{(2,58)} = 3.064$, $p = 0.054$, one-way ANOVA with Dunnett's *post hoc* test). Number of cells appears in each bar. Error bars indicate mean ± SEM. *$p \leq 0.05$. **$p \leq 0.01$. ***$p \leq 0.001$.

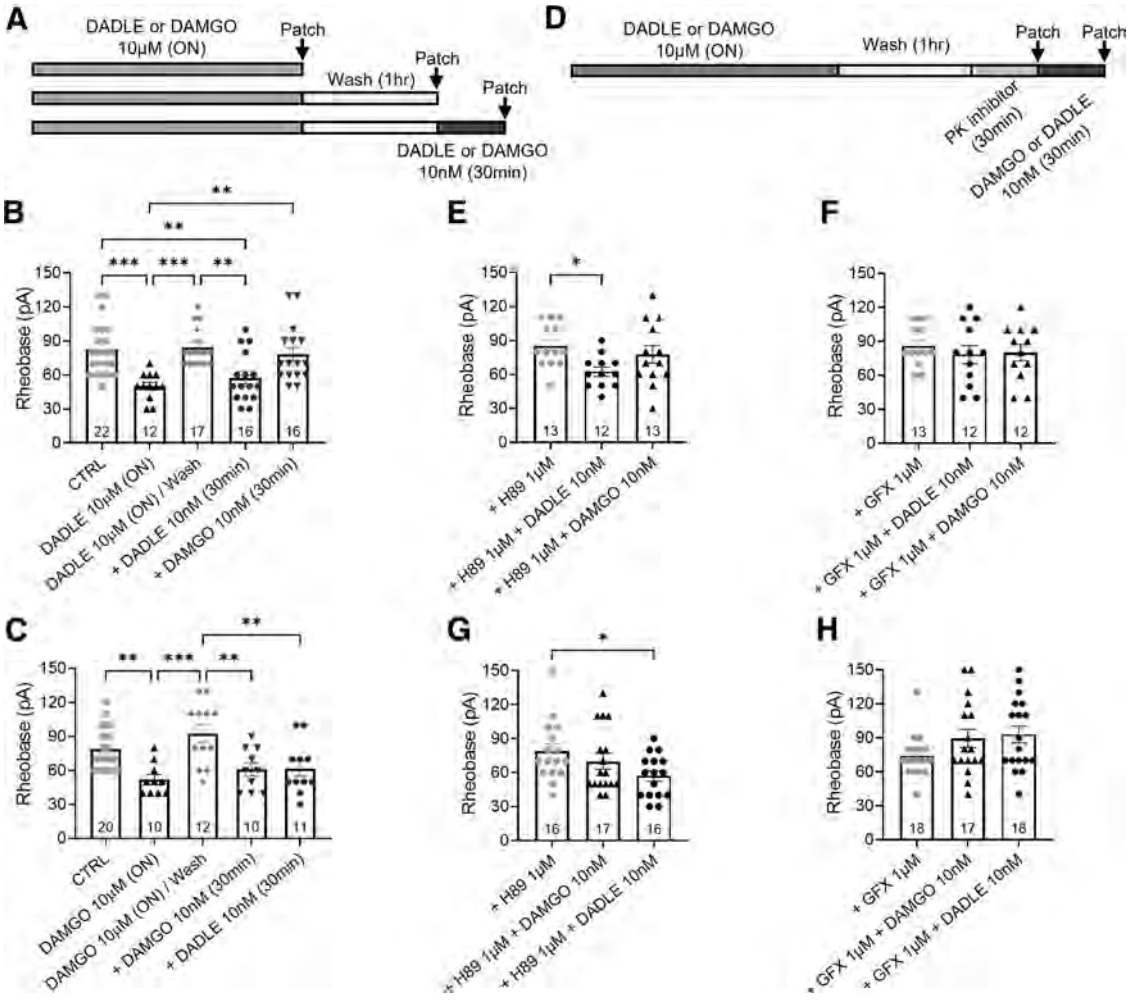

Figure 8. Overnight exposure to high-concentration opioids switches low-concentration DOPr and MOPr agonist responses to a PKC-dependent pronociceptive pathway. ***A***, Schematic protocol showing the paradigm used in ***B*** and ***C***. Arrows indicate perforated patch-clamp recordings at different treatment points. ***B***, The pronociceptive effect induced by high-concentration DADLE is lost after 1 h washout with control media, re-exposure to a low-concentration DADLE paradoxically decreased neuron rheobase ($F_{(4,78)} = 8.474$, $p < 0.0001$). ***C***, After washout of high-concentration DAMGO overnight, acute re-exposure to DAMGO or DADLE paradoxically decreased neuron rheobase ($F_{(4,58)} = 7.111$, $p < 0.0001$). ***D***, Schematic protocol showing the paradigm used in ***E–H***. Arrows indicate perforated patch-clamp recordings after incubation with PKA or PKC inhibitors with or without opioid re-exposure. ***E***, ***F***, Following the washout of overnight high-concentration DADLE, PKC inhibitor GFX (***F***: $F_{(2,34)} = 0.382$, $p = 0.686$) but not PKA inhibitor H89 (***E***: $F_{(2,35)} = 3.681$, $p = 0.035$) prevented the paradoxical increased excitability induced by acute re-exposure to low-concentration DADLE. ***G***, ***H***, Following washout of overnight high-concentration DAMGO, PKA inhibitor H89 (***G***: $F_{(2,53)} = 4.1$, $p = 0.022$) only prevented the pronociceptive effect induced by acute re-exposure to low-concentration DAMGO while PKC inhibitor GFX (***H***: $F_{(2,50)} = 2.246$, $p = 0.116$) prevented the increased excitability induced by acute re-exposure to both low-concentration DAMGO or DADLE. Number of cells appears in each bar. Error bars indicate mean ± SEM. *$p \leq 0.05$; **$p \leq 0.01$; ***$p \leq 0.001$; one-way ANOVA with Dunnett's *post hoc* test.

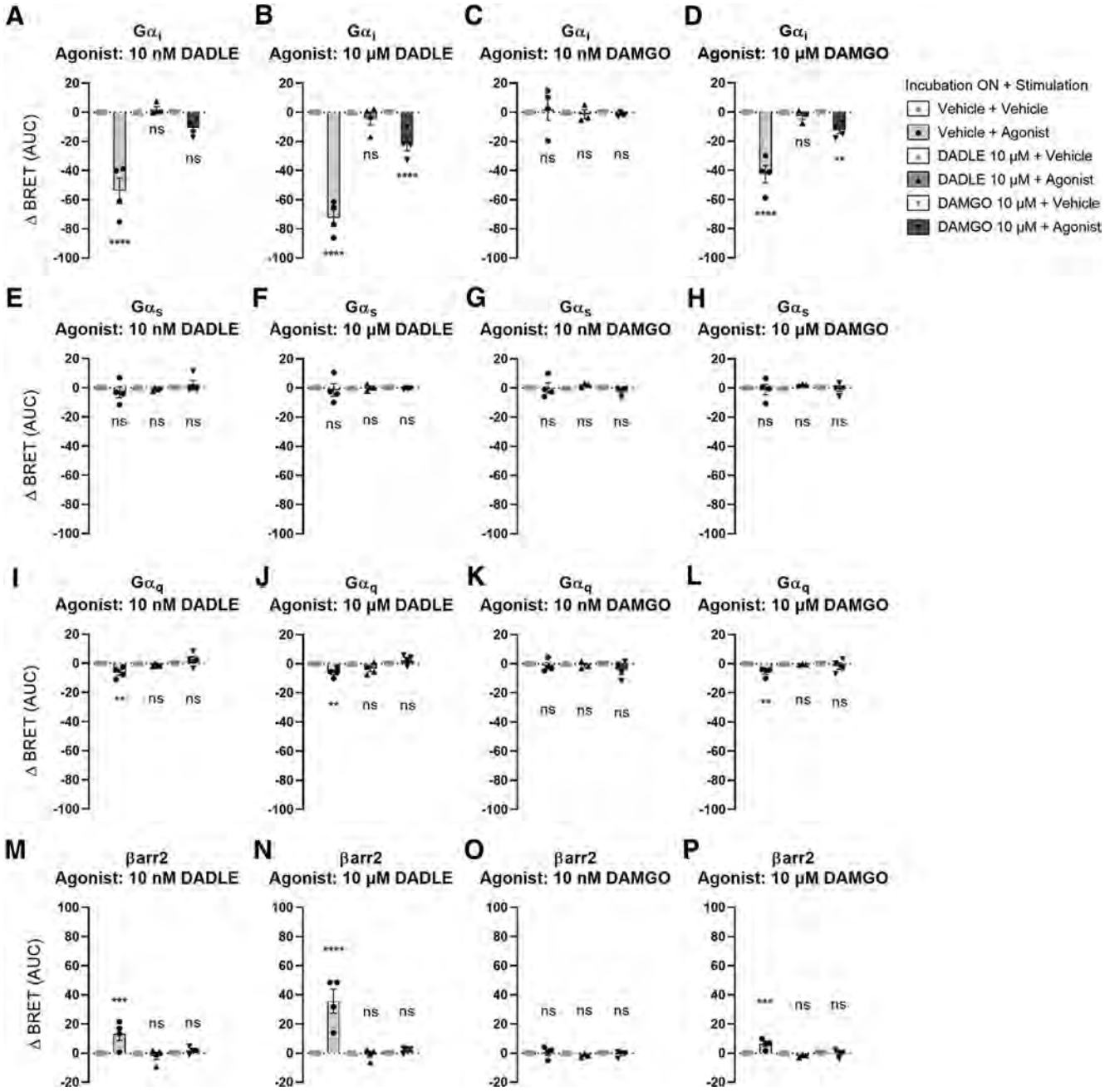

Figure 9. Overnight incubation with high-concentration opioids decreased acute Gα_i activation and βarr2 recruitment. Transfected HEK293T cells were treated overnight with vehicle, high-concentration (10 μM) DADLE or DAMGO, washed for 30 min, and then stimulated with vehicle, or agonist with low-concentration (10 nM) DAMGO or DADLE or high-concentration (10 μM) DAMGO or DADLE. BRET was recorded over time to measure activation of Gα_i (***A***: $F_{(5,24)} = 45.25$, $p < 0.0001$; ***B***: $F_{(5,24)} = 99.2$, $p < 0.0001$; ***C***: $F_{(5,23)} = 0.1771$, $p = 0.9685$; ***D***: $F_{(5,23)} = 51.16$, $p < 0.0001$), Gα_s (***E***: $F_{(5,24)} = 0.8942$, $p = 0.5007$; ***F***: $F_{(5,24)} = 0.1545$, $p = 0.9766$; ***G***: $F_{(5,23)} = 0.9256$, $p = 0.4824$; ***H***: $F_{(5,23)} = 0.477$, $p = 0.7896$), and Gα_q (***I***: $F_{(5,24)} = 7.611$, $p < 0.0002$; ***J***: $F_{(5,24)} = 8.63$, $p < 0.0001$; ***K***: $F_{(5,23)} = 1.63$, $p = 0.1919$; ***L***: $F_{(5,23)} = 6.034$, $p = 0.001$) by dissociation of Rluc2-Gα with GFP10-Gγ2 after agonist stimulation. Consequently, a decrease of BRET reflects an activation of Gα protein. Following the same cell treatment, recruitment of Rluc2-βarr2 to the plasma membrane (rGFP-CAAX) was also measured using ebBRET (***M***: $F_{(5,24)} = 8.966$, $p < 0.0001$; ***N***: $F_{(5,24)} = 24.1$, $p < 0.0001$; ***O***: $F_{(5,23)} = 0.7804$, $p = 0.574$; ***P***: $F_{(5,23)} = 13.28$, $p < 0.0001$), an increase of ebBRET reflecting the recruitment of βarr2 at the plasma membrane. Data were collected from 3-7 independent experiments. Bars represent mean of the area under the curve ± SEM. *$p \leq 0.05$; **$p \leq 0.01$; ***$p \leq 0.001$; ****$p \leq 0.001$; one-way ANOVA with multiple comparisons and Tukey's *post hoc* test.

studies of individual DRG neurons from the same animals demonstrated receptor desensitization in response to the acute application of morphine. Furthermore, chronic incubation (overnight) with high-dose morphine recapitulates the switch from antinociceptive to pronociceptive signaling following an acute morphine challenge (Fig. 3*C*), a phenomenon observed by others (Khomula et al., 2019).

The analgesic actions of morphine and related compounds are mediated largely by MOPrs. Our studies, however, identified that the switch to pronociceptive pathways is mediated by DOPr signaling, based on several findings. Our *in vitro* studies of isolated DRG neurons demonstrated that the selective DOPr antagonists blocked the pronociceptive actions of overnight morphine incubation, whereas the MOPr antagonist had no effect. We observed a similar phenomenon *in vivo* where the pronociceptive actions of acute application of morphine following chronic exposure were blocked by the selective DOPr antagonist NTI, suggesting that DOPr plays a significant role in the development of

hyperalgesia. We then used selective MOPr and DOPr agonists and their respective antagonists to recapitulate these findings. The higher concentrations we used may have exceeded concentrations reported to be selective (Raynor et al., 1994). Previous studies suggest that morphine and DAMGO at high concentrations can activate DOPr (Jordan et al., 2000; Zhao et al., 2003). Nonetheless, we found that the classical inhibition evoked by acute application at these high concentrations was blocked by their respective antagonists (Fig. 5).

Our studies may suggest a functional MOPr–DOPr interaction following sustained application of high-dose agonists. We previously showed that MOPr and DOPr are coexpressed on a significant proportion of nociceptive DRG neurons (Guerrero-Alba et al., 2018). The concept of MOPr–DOPr interaction underlying OPr-mediated inhibition is well described in previous studies (DiCello et al., 2020), although the mechanisms are poorly understood and may be multifactorial. Additionally, selectivity studies found that MOPr agonists morphine and DAMGO showed higher affinity to cells coexpressing MOPr-DOPr receptors compared with cells expressing only MOPr (Yekkirala et al., 2010). In our studies, where neurons were exposed to high concentrations of DADLE and DAMGO overnight and then excitability allowed to recover during a washout, we found diverging effects when we re-exposed these neurons to low concentrations of the agonists. DAMGO overnight exposure primed the neurons to a pronociceptive action in response to a subsequent challenge with both the MOPr and DOPr agonists, whereas overnight DADLE only resulted in a pronociceptive response to subsequent DADLE, but not DAMGO. These findings further support the concept that the pronociception evoked high-dose opioids are selectively mediated by activation of DOPr by either MOPr or DOPr agonists.

DOPr agonists are being developed for the treatment of chronic pain, as well as psychiatric disorders (Gendron et al., 2015). Like other GPCRs, DOPrs exhibit agonist-selective recruitment of arrestins, resulting in functional selectivity between agonists. Arrestins are multifaceted proteins that play an important role in DOPr trafficking and signaling. Recent studies suggest that weakly internalizing DOPr agonists have sustained signaling from the plasma membrane and exhibit sustained antinociception, whereas those that externalize and recruit arrestins exhibit rapid tolerance. OPr internalization has received considerable attention in studies of DOPr antinociceptive signaling and have shown that tolerance is induced by high internalizing DOPr agonist through βarr recruitment (Pradhan et al., 2010, 2016; Vicente-Sanchez et al., 2018), but the cellular mechanisms underlying DOPr hyperalgesia have not been studied. We found that the weakly internalizing DOPr agonist ARM390 did not evoke neuronal hyperexcitability, unlike DADLE, and that the actions of DADLE were blocked by the clathrin inhibitor PS2. Thus, our studies suggest that the DOPr-mediated pronociceptive signaling is also dependent on receptor internalization.

Opioid inhibitory effects are classically linked to $G\alpha_i$ and $G_{\beta\gamma}$ protein signaling, and downstream inhibition of adenylate cyclase and PKA activity, although other signaling pathways have been implicated (Al-Hasani and Bruchas, 2011). We did not find a switch in $G\alpha_i$ to $G\alpha_s$ or $G\alpha_q$ signaling; however, our results suggest that DOPr-mediated pronociceptive signaling is PKC-dependent, which is similar to findings in other studies using MOPr selective agonists (Joseph et al., 2010). It has been reported that PKC activation can be downstream of $G\alpha_i$ pathway via $G_{\beta\gamma}$ subunits or calcium entry (Camps et al., 1992; Nishizuka, 1992). Further studies are needed to determine the role of PKC in the mechanisms of phosphorylation and internalization of OR that might lead to OT and OIH.

There are several potential limitations of the current study. All opioid agonists are analgesic, yet selective activation of MOPr and DOPr exhibits different behavioral effects. DOPr agonists have anxiolytic and antidepressant activity (Valentino and Volkow, 2018), and MOPr agonists induce euphoria and stress coping. And while such actions could alter the outcome of behavioral studies, there is little evidence they have impacted the current study. Our electrophysiological measurements of tolerance and OIH were obtained using *ex vivo* peripheral afferent nerve preparations and *in vitro* patch-clamp studies of isolated neurons following chronic treatment and thus would not be directly influenced by the psychological impact of DOPr or MOPr signaling. While the tail flick test measures of tolerance could be influenced by psychological changes, our electrophysiological studies showed parallel correlates of tolerance and OIH in the same animals. Another potential limitation is the lack of *in vivo* dose ranging studies and correlation with the concentrations used in the *in vitro* studies. Further studies are needed in this regard, but the current studies show evidence of the observed *in vitro* correlates of tolerance and OIH in the *in vivo* studies, and the doses used were well tolerated by the animals and thus are likely comparable with those used in humans. A final issue relates to the identity of the DRG neurons studied. While the studies conducted using afferent recordings from the colon and patch-clamp studies of neurons retrogradely labeled from the colon of male and female mice demonstrate the pronociceptive actions of DOPr in gut-specific neurons, most of the patch-clamp studies were conducted on nonlabeled neurons; thus, many of these would be somatosensory neurons. Thus, it is likely that the findings described in this study relate not only to visceral neurons but also to the peripheral somatosensory system.

In conclusion, DOPr plays a major role in the development of OT and OIH in colonic afferent nociceptors. The development of OIH requires prolonged exposure to high opioid concentrations, leading to activation of mechanisms, such as OPr internalization and activation of PKC signaling pathway. Targeting key components on these identified pathways could mitigate the development of OT and OIH in the colon.

References

Akaishi T, Saito H, Ito Y, Ishige K, Ikegaya Y (2000) Morphine augments excitatory synaptic transmission in the dentate gyrus through GABAergic disinhibition. Neurosci Res 38:357–363.

Al-Hasani R, Bruchas MR (2011) Molecular mechanisms of opioid receptor-dependent signaling and behavior. Anesthesiology 115:1363–1381.

Allouche S, Noble F, Marie N (2014) Opioid receptor desensitization: mechanisms and its link to tolerance. Front Pharmacol 5:280.

Bielefeldt K, Davis B, Binion DG (2009) Pain and inflammatory bowel disease. Inflamm Bowel Dis 15:778–788.

Bohn LM, Lefkowitz RJ, Gainetdinov RR, Peppel K, Caron MG, Lin FT (1999) Enhanced morphine analgesia in mice lacking beta-arrestin 2. Science 286:2495–2498.

Brookes SJ, Spencer NJ, Costa M, Zagorodnyuk VP (2013) Extrinsic primary afferent signalling in the gut. Nat Rev Gastroenterol Hepatol 10:286–296.

Cahill CM, Walwyn W, Taylor AM, Pradhan AA, Evans CJ (2016) Allostatic mechanisms of opioid tolerance beyond desensitization and downregulation. Trends Pharmacol Sci 37:963–976.

Camps M, Carozzi A, Schnabel P, Scheer A, Parker PJ, Gierschik P (1992) Isozyme-selective stimulation of phospholipase C-beta 2 by G protein beta gamma-subunits. Nature 360:684–686.

Davies SP, Reddy H, Caivano M, Cohen P (2000) Specificity and mechanism of action of some commonly used protein kinase inhibitors. Biochem J 351:95–105.

DiCello JJ, Carbone SE, Saito A, Rajasekhar P, Ceredig RA, Pham V, Valant C, Christopoulos A, Veldhuis NA, Canals M, Massotte D, Poole DP (2020) Mu and delta opioid receptors are coexpressed and functionally interact in the enteric nervous system of the mouse colon. Cell Mol Gastroenterol Hepatol 9:465–483.

Farmer AD, Gallagher J, Bruckner-Holt C, Aziz Q (2017) Narcotic bowel syndrome. Lancet Gastroenterol Hepatol 2:361–368.

Ferrini F, Trang T, Mattioli TA, Laffray S, Del'Guidice T, Lorenzo LE, Castonguay A, Doyon N, Zhang WB, Godin AG, Mohr D, Beggs S, Vandal K, Beaulieu JM, Cahill CM, Salter MW, De Koninck Y (2013) Morphine hyperalgesia gated through microglia-mediated disruption of neuronal Cl^- homeostasis. Nat Neurosci 16:183–192.

Forster AB, Reeh PW, Messlinger K, Fischer MJ (2009) High concentrations of morphine sensitize and activate mouse dorsal root ganglia via TRPV1 and TRPA1 receptors. Mol Pain 5:17.

Gales C, Van Durm JJ, Schaak S, Pontier S, Percherancier Y, Audet M, Paris H, Bouvier M (2006) Probing the activation-promoted structural rearrangements in preassembled receptor-G protein complexes. Nat Struct Mol Biol 13:778–786.

Galligan JJ, Akbarali HI (2014) Molecular physiology of enteric opioid receptors. Am J Gastroenterol Suppl 2:17–21.

Gendron L, Mittal N, Beaudry H, Walwyn W (2015) Recent advances on the delta opioid receptor: from trafficking to function. Br J Pharmacol 172:403–419.

Grim TW, Schmid CL, Stahl EL, Pantouli F, Ho JH, Acevedo-Canabal A, Kennedy NM, Cameron MD, Bannister TD, Bohn LM (2020) A G protein signaling-biased agonist at the mu-opioid receptor reverses morphine tolerance while preventing morphine withdrawal. Neuropsychopharmacology 45:416–425.

Guerrero-Alba R, Valdez-Morales EE, Jimenez-Vargas NN, Bron R, Poole D, Reed D, Castro J, Campaniello M, Hughes PA, Brierley SM, Bunnett N, Lomax AE, Vanner S (2018) Coexpression of mu and delta opioid receptors by mouse colonic nociceptors. Br J Pharmacol 175:2622–2634.

He L, Gooding SW, Lewis E, Felth LC, Gaur A, Whistler JL (2021) Pharmacological and genetic manipulations at the micro-opioid receptor reveal arrestin-3 engagement limits analgesic tolerance and does not exacerbate respiratory depression in mice. Neuropsychopharmacology 46:2241–2249.

Ibeakanma C, Ochoa-Cortes F, Miranda-Morales M, McDonald T, Spreadbury I, Cenac N, Cattaruzza F, Hurlbut D, Vanner S, Bunnett N, Vergnolle N, Vanner S (2011) Brain-gut interactions increase peripheral nociceptive signaling in mice with postinfectious irritable bowel syndrome. Gastroenterology 141:2098–2108.e5.

Jensen DD, Lieu TM, Halls ML, Veldhuis NA, Imlach WL, Mai QN, Poole DP, Quach T, Aurelio L, Conner J, Klein Herenbrink C, Barlow N, Simpson JS, Scanlon MJ, Graham B, McCluskey A, Robinson PJ, Escriou V, Nassini R, Materazzi S, et al. (2017) Neurokinin 1 receptor signaling in endosomes mediates sustained nociception and is a viable therapeutic target for prolonged pain relief. Sci Transl Med 9:eaal3447.

Jimenez-Vargas NN, Pattison LA, Zhao P, Lieu TM, Latorre R, Jensen DD, Castro J, Aurelio L, Le GT, Flynn B, Klein Herenbrink C, Yeatman HR, Edgington-Mitchell L, Porter CJ, Halls ML, Canals M, Veldhuis NA, Poole DP, McLean P, Hicks GA, et al. (2018) Protease-activated receptor-2 in endosomes signals persistent pain of irritable bowel syndrome. Proc Natl Acad Sci USA 115:E7438–E7447.

Jimenez-Vargas NN, Gong J, Wisdom MJ, Jensen DD, Latorre R, Hegron A, Teng S, DiCello JJ, Rajasekhar P, Veldhuis NA, Carbone SE, Yu Y, Lopez-Lopez C, Jaramillo-Polanco J, Canals M, Reed DE, Lomax AE, Schmidt BL, Leong KW, Vanner SJ, et al. (2020) Endosomal signaling of delta opioid receptors is an endogenous mechanism and therapeutic target for relief from inflammatory pain. Proc Natl Acad Sci USA 117:15281–15292.

Jordan BA, Cvejic S, Devi LA (2000) Opioids and their complicated receptor complexes. Neuropsychopharmacology 23:S5–S18.

Joseph EK, Reichling DB, Levine JD (2010) Shared mechanisms for opioid tolerance and a transition to chronic pain. J Neurosci 30:4660–4666.

Kang M, Mischel RA, Bhave S, Komla E, Cho A, Huang C, Dewey WL, Akbarali HI (2017) The effect of gut microbiome on tolerance to morphine mediated antinociception in mice. Sci Rep 7:42658.

Khomula EV, Araldi D, Levine JD (2019) In vitro nociceptor neuroplasticity associated with in vivo opioid-induced hyperalgesia. J Neurosci 39:7061–7073.

Kliewer A, Schmiedel F, Sianati S, Bailey A, Bateman JT, Levitt ES, Williams JT, Christie MJ, Schulz S (2019) Phosphorylation-deficient G-protein-biased mu-opioid receptors improve analgesia and diminish tolerance but worsen opioid side effects. Nat Commun 10:367.

Kyloh M, Nicholas S, Zagorodnyuk VP, Brookes SJ, Spencer NJ (2011) Identification of the visceral pain pathway activated by noxious colorectal distension in mice. Front Neurosci-Switz 5:16.

Lacy BE (2018) Review article: an analysis of safety profiles of treatments for diarrhoea-predominant irritable bowel syndrome. Aliment Pharmacol Ther 48:817–830.

Marie N, Landemore G, Debout C, Jauzac P, Allouche S (2003) Pharmacological characterization of AR-M1000390 at human delta opioid receptors. Life Sci 73:1691–1704.

Matthes HW, Smadja C, Valverde O, Vonesch JL, Foutz AS, Boudinot E, Denavit-Saubie M, Severini C, Negri L, Roques BP, Maldonado R, Kieffer BL (1998) Activity of the delta-opioid receptor is partially reduced, whereas activity of the kappa-receptor is maintained in mice lacking the mu-receptor. J Neurosci 18:7285–7295.

Mattioli TA, Leduc-Pessah H, Skelhorne-Gross G, Nicol CJ, Milne B, Trang T, Cahill CM (2014) Toll-like receptor 4 mutant and null mice retain morphine-induced tolerance, hyperalgesia, and physical dependence. PLoS One 9:e97361.

McLamore S, Ullrich T, Rothman RB, Xu H, Dersch C, Coop A, Davis P, Porreca F, Jacobson AE, Rice KC (2001) Effect of N-alkyl and N-alkenyl substituents in noroxymorphindole, 17-substituted-6,7-dehydro-4,5alpha-epoxy-3,14-dihydroxy-6,7:2',3'-indolomorphina ns, on opioid receptor affinity, selectivity, and efficacy. J Med Chem 44:1471–1474.

Moore BA, Stewart TM, Hill C, Vanner SJ (2002) TNBS ileitis evokes hyperexcitability and changes in ionic membrane properties of nociceptive DRG neurons. Am J Physiol Gastrointest Liver Physiol 282:G1045–G1051.

Namkung Y, Le Gouill C, Lukashova V, Kobayashi H, Hogue M, Khoury E, Song M, Bouvier M, Laporte SA (2016) Monitoring G protein-coupled receptor and beta-arrestin trafficking in live cells using enhanced bystander BRET. Nat Commun 7:12178.

Nishizuka Y (1992) Intracellular signaling by hydrolysis of phospholipids and activation of protein kinase C. Science 258:607–614.

Peiris M, Hockley JR, Reed DE, Smith ES, Bulmer DC, Blackshaw LA (2017) Peripheral KV7 channels regulate visceral sensory function in mouse and human colon. Mol Pain 13:1744806917709371.

Pergolizzi JV Jr, Raffa RB, Rosenblatt MH (2020) Opioid withdrawal symptoms, a consequence of chronic opioid use and opioid use disorder: current understanding and approaches to management. J Clin Pharm Ther 45:892–903.

Pradhan AA, Walwyn W, Nozaki C, Filliol D, Erbs E, Matifas A, Evans C, Kieffer BL (2010) Ligand-directed trafficking of the delta-opioid receptor in vivo: two paths toward analgesic tolerance. J Neurosci 30:16459–16468.

Pradhan AA, Becker JA, Scherrer G, Tryoen-Toth P, Filliol D, Matifas A, Massotte D, Gaveriaux-Ruff C, Kieffer BL (2009) In vivo delta opioid receptor internalization controls behavioral effects of agonists. PLoS One 4:e5425.

Pradhan AA, Perroy J, Walwyn WM, Smith ML, Vicente-Sanchez A, Segura L, Bana A, Kieffer BL, Evans CJ (2016) Agonist-specific recruitment of arrestin isoforms differentially modify delta opioid receptor function. J Neurosci 36:3541–3551.

Raehal KM, Bohn LM (2011) The role of beta-arrestin2 in the severity of antinociceptive tolerance and physical dependence induced by different opioid pain therapeutics. Neuropharmacology 60:58–65.

Raynor K, Kong H, Chen Y, Yasuda K, Yu L, Bell GI, Reisine T (1994) Pharmacological characterization of the cloned kappa-, delta-, and mu-opioid receptors. Mol Pharmacol 45:330–334.

Robertson MJ, Deane FM, Stahlschmidt W, von Kleist L, Haucke V, Robinson PJ, McCluskey A (2014) Synthesis of the Pitstop family of clathrin inhibitors. Nat Protoc 9:1592–1606.

Robinson DR, Gebhart GF (2008) Inside information: the unique features of visceral sensation. Mol Interv 8:242–253.

Roeckel LA, Utard V, Reiss D, Mouheiche J, Maurin H, Robe A, Audouard E, Wood JN, Goumon Y, Simonin F, Gaveriaux-Ruff C (2017)

Morphine-induced hyperalgesia involves mu opioid receptors and the metabolite morphine-3-glucuronide. Sci Rep 7:10406.
Rowan MP, Bierbower SM, Eskander MA, Szteyn K, Por ED, Gomez R, Veldhuis N, Bunnett NW, Jeske NA (2014) Activation of mu opioid receptors sensitizes transient receptor potential vanilloid type 1 (TRPV1) via beta-arrestin-2-mediated cross-talk. PLoS One 9:e93688.
Spahn V, Del Vecchio G, Rodriguez-Gaztelumendi A, Temp J, Labuz D, Kloner M, Reidelbach M, Machelska H, Weber M, Stein C (2018) Opioid receptor signaling, analgesic and side effects induced by a computationally designed pH-dependent agonist. Sci Rep 8:8965.
Stein C (2016) Opioid receptors. Annu Rev Med 67:433–451.
Stein C (2018) New concepts in opioid analgesia. Expert Opin Investig Drugs 27:765–775.
Stewart T, Beyak MJ, Vanner S (2003) Ileitis modulates potassium and sodium currents in guinea pig dorsal root ganglia sensory neurons. J Physiol 552:797–807.
Stoeber M, Jullie D, Lobingier BT, Laeremans T, Steyaert J, Schiller PW, Manglik A, von Zastrow M (2018) A genetically encoded biosensor reveals location bias of opioid drug action. Neuron 98:963–976.e965.
Targownik LE, Nugent Z, Singh H, Bugden S, Bernstein CN (2014) The prevalence and predictors of opioid use in inflammatory bowel disease: a population-based analysis. Am J Gastroenterol 109:1613–1620.
Toullec D, Pianetti P, Coste H, Bellevergue P, Grand-Perret T, Ajakane M, Baudet V, Boissin P, Boursier E, Loriolle F (1991) The bisindolylmaleimide GF 109203X is a potent and selective inhibitor of protein kinase C. J Biol Chem 266:15771–15781.
Valdez-Morales E, Guerrero-Alba R, Ochoa-Cortes F, Benson J, Spreadbury I, Hurlbut D, Miranda-Morales M, Lomax AE, Vanner S (2013) Release of endogenous opioids during a chronic IBD model suppresses the excitability of colonic DRG neurons. Neurogastroent Motil 25:39–46.e4.
Valentino RJ, Volkow ND (2018) Untangling the complexity of opioid receptor function. Neuropsychopharmacology 43:2514–2520.
Varga EV, Navratilova E, Stropova D, Jambrosic J, Roeske WR, Yamamura HI (2004) Agonist-specific regulation of the delta-opioid receptor. Life Sci 76:599–612.
Vicente-Sanchez A, Dripps IJ, Tipton AF, Akbari H, Akbari A, Jutkiewicz EM, Pradhan AA (2018) Tolerance to high-internalizing delta opioid receptor agonist is critically mediated by arrestin 2. Br J Pharmacol 175:3050–3059.
Wang HY, Frankfurt M, Burns LH (2008) High-affinity naloxone binding to filamin a prevents mu opioid receptor-Gs coupling underlying opioid tolerance and dependence. PLoS One 3:e1554.
Williams JT, Ingram SL, Henderson G, Chavkin C, von Zastrow M, Schulz S, Koch T, Evans CJ, Christie MJ (2013) Regulation of mu-opioid receptors: desensitization, phosphorylation, internalization, and tolerance. Pharmacol Rev 65:223–254.
Yekkirala AS, Kalyuzhny AE, Portoghese PS (2010) Standard opioid agonists activate heteromeric opioid receptors: evidence for morphine and [d-Ala (2)-MePhe(4)-Glyol(5)]enkephalin as selective mu-delta agonists. ACS Chem Neurosci 1:146–154.
Yu Y, Villalobos-Hernandez EC, Pradhananga S, Baker CC, Keating C, Grundy D, Lomax AE, Reed DE (2019) Deoxycholic acid activates colonic afferent nerves via 5-HT3 receptor-dependent and -independent mechanisms. Am J Physiol Gastrointest Liver Physiol 317:G275–G284.
Zar MA, Iravani MM, Luheshi GN (1990) Effect of nifedipine on the contractile responses of the isolated rat bladder. J Urol 143:835–839.
Zhao GM, Qian X, Schiller PW, Szeto HH (2003) Comparison of [Dmt1] DALDA and DAMGO in binding and G protein activation at mu, delta, and kappa opioid receptors. J Pharmacol Exp Ther 307:947–954.

nature COMMUNICATIONS

ARTICLE

https://doi.org/10.1038/s41467-022-28204-z OPEN

Schwann cell endosome CGRP signals elicit periorbital mechanical allodynia in mice

Francesco De Logu[1,10], Romina Nassini[1,2,10], Alan Hegron[3,10], Lorenzo Landini[1], Dane D. Jensen[3,4], Rocco Latorre[3], Julia Ding[5], Matilde Marini[1], Daniel Souza Monteiro de Araujo[1], Paulina Ramírez-Garcia[6], Michael Whittaker[6], Jeffri Retamal[6], Mustafa Titiz[1], Alessandro Innocenti[7], Thomas P. Davis[6,8], Nicholas Veldhuis[6], Brian L. Schmidt[3,4,9], Nigel W. Bunnett[3,9]✉ & Pierangelo Geppetti[1,2]✉

Efficacy of monoclonal antibodies against calcitonin gene-related peptide (CGRP) or its receptor (calcitonin receptor-like receptor/receptor activity modifying protein-1, CLR/RAMP1) implicates peripherally-released CGRP in migraine pain. However, the site and mechanism of CGRP-evoked peripheral pain remain unclear. By cell-selective RAMP1 gene deletion, we reveal that CGRP released from mouse cutaneous trigeminal fibers targets CLR/RAMP1 on surrounding Schwann cells to evoke periorbital mechanical allodynia. CLR/RAMP1 activation in human and mouse Schwann cells generates long-lasting signals from endosomes that evoke cAMP-dependent formation of NO. NO, by gating Schwann cell transient receptor potential ankyrin 1 (TRPA1), releases ROS, which in a feed-forward manner sustain allodynia via nociceptor TRPA1. When encapsulated into nanoparticles that release cargo in acidified endosomes, a CLR/RAMP1 antagonist provides superior inhibition of CGRP signaling and allodynia in mice. Our data suggest that the CGRP-mediated neuronal/Schwann cell pathway mediates allodynia associated with neurogenic inflammation, contributing to the algesic action of CGRP in mice.

[1] Department of Health Sciences, Clinical Pharmacology and Oncology Section, University of Florence, Florence 50139, Italy. [2] Headache Center, Careggi University Hospital, Florence 50139, Italy. [3] Department of Molecular Pathobiology, College of Dentistry, New York University, New York, NY 10010, USA. [4] Bluestone Center for Clinical Research, New York University College of Dentistry, New York, NY 10010, USA. [5] Department of Anesthesiology, Columbia University, New York, NY 10010, USA. [6] Drug Discovery Biology Theme and Australian Research Council Centre of Excellence in Convergent Bio-Nano Science and Technology, Monash Institute of Pharmaceutical Sciences, Monash University, Parkville, VIC 3052, Australia. [7] Plastic and Reconstructive Microsurgery - Careggi University Hospital, Florence 50139, Italy. [8] Australian Institute for Bioengineering and Nanotechnology, The University of Queensland, Brisbane, QLD 4072, Australia. [9] Department of Neuroscience and Physiology and Neuroscience Institute, School of Medicine, New York University, New York, NY 10010, USA. [10] These authors contributed equally: Francesco De Logu, Romina Nassini, Alan Hegron. ✉email: nwb2@nyu.edu; pierangelo.geppetti@unifi.it

For almost a century it has been known that cutaneous tissue injury elicits a local vascular response, referred to as neurogenic inflammation, that is associated to a wider area of increased sensitivity to mechanical stimuli[1]. A subset of C-fiber primary afferents, which mediate neurogenic inflammation, is the main source of the neuropeptides substance P (SP) and calcitonin gene-related peptide (CGRP)[2,3]. In rodents, noxious stimuli such as capsaicin, a pungent agonist of the transient receptor potential vanilloid 1 (TRPV1) channel[4], evoke the peripheral release of CGRP which induces arteriolar vasodilatation[2] and of SP which elicits plasma protein extravasation[5], and produce sensory responses, which encompasses acute nociception and prolonged mechanical allodynia[6]. Capsaicin administration to the human skin elicits a similar pattern of responses, consisting of local cutaneous vasodilatation and focal and transient burning pain (min) associated with widespread, sustained mechanical hypersensitivity (hrs)[7]. While CGRP has been identified as the mediator of neurogenic vasodilatation in rodents[2] and humans[8], the cellular and molecular mechanisms underlying mechanical allodynia associated with neurogenic inflammation are unknown.

Mechanistic studies in animal models and humans have highlighted the role of CGRP in migraine pain[9]. Thus, small molecule antagonists of the CGRP receptor and monoclonal antibodies against CGRP or its receptor can relieve migraine pain[10]. The poor blood-brain barrier penetration of some small-molecule antagonists[11,12] and of monoclonal antibodies[13,14] suggests a peripheral contribution to CGRP-mediated migraine pain. However, little is known about the proalgesic actions of CGRP in the periphery. In mice, intraplantar injection of CGRP evokes mechanical allodynia[15] and systemic CGRP causes facial grimace[16]. Periorbital CGRP injection, while failing to evoke spontaneous nociceptive behavior, produces sustained (~4 h) periorbital mechanical allodynia (PMA)[17]. CGRP released from trigeminal peripheral terminals mediates PMA in mice[18] evoked by systemic (intraperitoneal) administration of the pro-headache agent glyceryl trinitrate (GTN)[19]. Facial cutaneous allodynia is one component of the migraine attack[20,21]. Although the process that initiates migraine pain may originate in the central nervous system (CNS)[22,23], the cell type and signaling pathway by which CGRP acts in the periphery to cause pain are unknown.

The CGRP receptor is a heterodimer of calcitonin receptor-like receptor (CLR), a G protein-coupled receptor (GPCR), and receptor activity-modifying protein 1 (RAMP1), a single transmembrane domain CLR chaperone[24]. These two components coexist in cells that mediate the actions of CGRP, for example, vascular myocytes[2]. Satellite glial cells and Schwann cells express CLR/RAMP1 and are closely associated with peptidergic sensory neurons[25]. While the extracellular space between the soma of trigeminal neurons and satellite glial cells is not a recognized locus for neurotransmission, the varicosities of C-fibers and the ensheathing Schwann cells are sites where neuropeptides, including CGRP[26], are normally released. Schwann cells from rat sciatic nerve respond to CGRP by increasing intracellular cAMP levels[27] and CLR/RAMP1 are expressed by Schwann cells that wrap CGRP + ve terminals of rat nociceptors[25,28,29]. Schwann cells mediate mechanical allodynia in mouse models of neuropathic and cancer pain[30,31]. Cutaneous Schwann cells can also directly activate sensory nerves to promote mechanical nociception[32]. Although GPCRs are usually considered to signal principally from the plasma membrane, GPCR kinases and β-arrestins (βARRs) rapidly terminate this signaling. Persistent endosomal signaling of GPCRs, including CLR/RAMP1, underlies sustained neuronal activation and nociception in the CNS[33–35].

Herein, we hypothesized that mechanical allodynia associated with neurogenic inflammation is mediated by CGRP which targets CLR/RAMP1 in Schwann cells ensheathing peripheral endings of nociceptors. By selective RAMP1 gene deletion in Schwann cells, we reveal that CGRP released from trigeminal terminals causes PMA by paracrine signaling to the surrounding Schwann cells. We also hypothesized that persistent CGRP/CLR/RAMP1 signaling from endosomes in Schwann cells underlies sustained PMA. By using inhibitors of clathrin- and dynamin-mediated endocytosis and stimulus-responsive nanoparticles designed to release CLR/RAMP1 antagonists in acidified endosomes, we found that CLR/RAMP1 endosomal signaling results in a cAMP-dependent release of nitric oxide (NO), which activates transient receptor potential ankyrin 1 (TRPA1), a proalgesic channel and sensor of oxidative stress[36].

Results

CGRP evokes PMA by activating Schwann cell CLR/RAMP1. We detected CLR and RAMP1 mRNA and immunoreactivity in primary cultures of human Schwann cells (HSCs) or mouse Schwann cells (MSCs) taken from the sciatic or trigeminal nerve (Fig. 1a, Supplementary Fig. 1a). The S100 + ve mouse Schwann cell line (IMS32) recapitulated features of primary MSCs, including expression of CLR and RAMP1 mRNA and immunoreactivity (Supplementary Fig. 1a, b) and TRPA1-dependent Ca^{2+} response to allyl isothiocyanate (Supplementary Fig. 1c). Immunoreactive CLR and RAMP1 were also detected in S100 + ve Schwann cells in nerve bundles in biopsies of human abdominal and mouse periorbital skin (Fig. 1b).

In C57BL/6 J male mice, periorbital CGRP elicited PMA (Supplementary Fig. 1d). Periorbital CGRP also evoked PMA in female mice (Supplementary Fig. 1d). Periorbital CGRP did not elicit allodynia in the hind paw (Supplementary Fig. 1e). Unless otherwise specified, all drugs were administered by subcutaneous periorbital injection (Supplementary Table 1). To assess the role of Schwann cell CLR/RAMP1 in CGRP-evoked PMA, Schwann cell-specific Cre mice (*Plp-Cre^{ERT}*) were crossed with RAMP1 floxed mice (*Ramp1$^{fl/fl}$*) to generate *Plp-Cre^{ERT+};Ramp1$^{fl/fl}$* and *Plp-Cre^{ERT-};Ramp1$^{fl/fl}$* (Control) mice. For selective deletion of RAMP1 in Schwann cells of the periorbital region, 4-hydroxytamoxifen (4-OHT) was administered daily for 3 days to *Plp-Cre^{ERT+};Ramp1$^{fl/fl}$* and Control mice. CGRP elicited PMA in both male and female Control mice that was similarly attenuated in *Plp-Cre^{ERT+};Ramp1$^{fl/fl}$* mice (Fig. 1c). In *Plp-Cre^{ERT+};Ramp1$^{fl/fl}$* mice 4-OHT treatment down-regulated RAMP1 immunoreactivity in S100 + ve cells surrounding trigeminal but not sciatic nerve fibers (Fig. 1d) and did not prevent paw mechanical allodynia evoked by intraplantar CGRP, which was prevented by intraplantar 4-OHT (Supplementary Fig. 1f).

Intravenous CGRP provokes delayed headache attacks in patients[37]. Intraperitoneal CGRP caused PMA and paw allodynia in male and female C57BL/6 J mice without gender difference (Fig. 1e, Supplementary Fig. 1g). In *Plp-Cre^{ERT+};Ramp1$^{fl/fl}$* mice treated with periorbital 4-OHT PMA, but not paw allodynia, was similarly reduced in males and females in response to intraperitoneal CGRP (Fig. 1f, g and Supplementary Fig. 1h, i). Systemic (intraperitoneal) 4-OHT reduced both PMA and paw allodynia by intraperitoneal CGRP (Supplementary Fig. 1j, k). These results reveal an essential role for CLR/RAMP1 of Schwann cells surrounding periorbital trigeminal endings in PMA elicited by local and systemic CGRP.

Stimulation of peptidergic trigeminal neurons evokes PMA by activating Schwann cell CLR/RAMP1. To explore the ability of endogenous CGRP to elicit PMA, we administered capsaicin, which activates TRPV1[4] thus releasing CGRP and SP from peptidergic nociceptors[3]. Periorbital capsaicin elicited acute

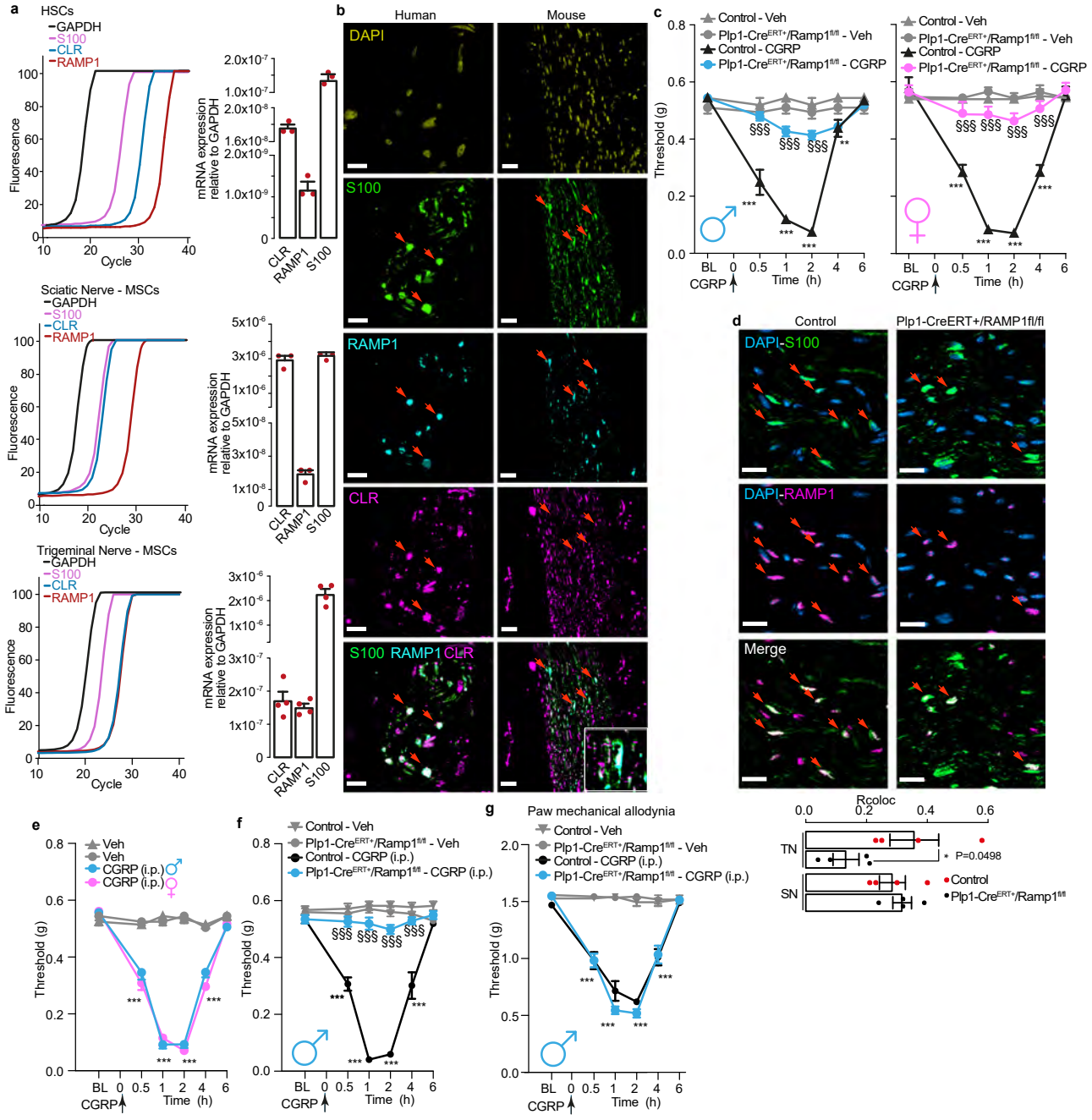

Fig. 1 Schwann cell RAMP1 mediates PMA evoked by CGRP. a Representative real-time PCR plot and cumulative data for GAPDH, S100, CLR and RAMP1 mRNA in HSCs ($n = 3$ independent experiments) and MSCs from trigeminal or sciatic nerve (MSCs from sciatic nerve $n = 3$ independent experiments; MSCs from trigeminal nerve, $n = 4$ independent experiments). **b** Representative images of DAPI and immunoreactive S100, RAMP1 and CLR in human and mouse cutaneous nerve bundles (scale, 10 µm human, 50 µm mouse) ($n = 3$ subjects). **c** PMA induced by CGRP (1.5 nmol) or vehicle in male and female *Plp1-Cre^{ERT+}/Ramp1$^{fl/fl}$* and Control mice treated with periorbital 4-OHT ($n = 8$ mice per group). **d** Representative images and colocalization value (Rcoloc) of S100 and RAMP1 in periorbital nerve and sciatic nerve trunks from *Plp1-Cre^{ERT+};Ramp1$^{fl/fl}$* and Control mice (scale, 20 µm) ($n = 4$ replicates). TN (trigeminal nerve), SN (sciatic nerve). **e** PMA induced by intraperitoneal (i.p.) CGRP (0.1 mg/kg) or vehicle in male and female C57BL/6 J mice ($n = 8$ mice per group). **f** PMA and (**g**) paw mechanical allodynia induced by intraperitoneal (i.p.) CGRP (0.1 mg/kg) or vehicle in male *Plp1-Cre^{ERT+}/Ramp1$^{fl/fl}$* and Control mice ($n = 8$ mice per group) treated with periorbital 4-OHT. Mean±SEM. $^{*}P < 0.05$, $^{**}P < 0.01$, $^{***}P < 0.001$ vs. Veh, Control-Veh, and TN-Control, $^{§§§}P < 0.001$. vs. Control-CGRP. 2-way (**c**, **e**, **f**, **g**) or 1-way (d) ANOVA, Bonferroni correction. Source data are provided as a Source Data file.

(~10 min) nociceptive behavior (Fig. 2a) and, like CGRP, caused prolonged (~4 h) PMA (Fig. 2b). Allodynia was detected in the periorbital area but not in the hind paw (Supplementary Fig. 2a), indicating a local action. TRPV1 deletion (*Trpv1*$^{-/-}$ mice) (Fig. 2c, d) or pretreatment with the TRPV1 antagonist capsazepine (Fig. 2e, f), prevented acute nociception and PMA. An antagonist (L-733,060) of the SP neurokinin 1 (NK_1) receptor, which prevented SP-evoked PMA (Fig. 2g), failed to diminish capsaicin-evoked acute nociception and PMA (Fig. 2h, Supplementary Fig. 2b). The histamine H_1 receptor antagonist, astemizole, inhibited SP-evoked PMA (Supplementary Fig. 2c) but did not affect CGRP- or capsaicin-evoked PMA (Supplementary Fig. 2d, e). Pretreatment with the CLR/RAMP1 antagonists, CGRP8-37 or olcegepant, prevented PMA (Fig. 2i, j) but not acute

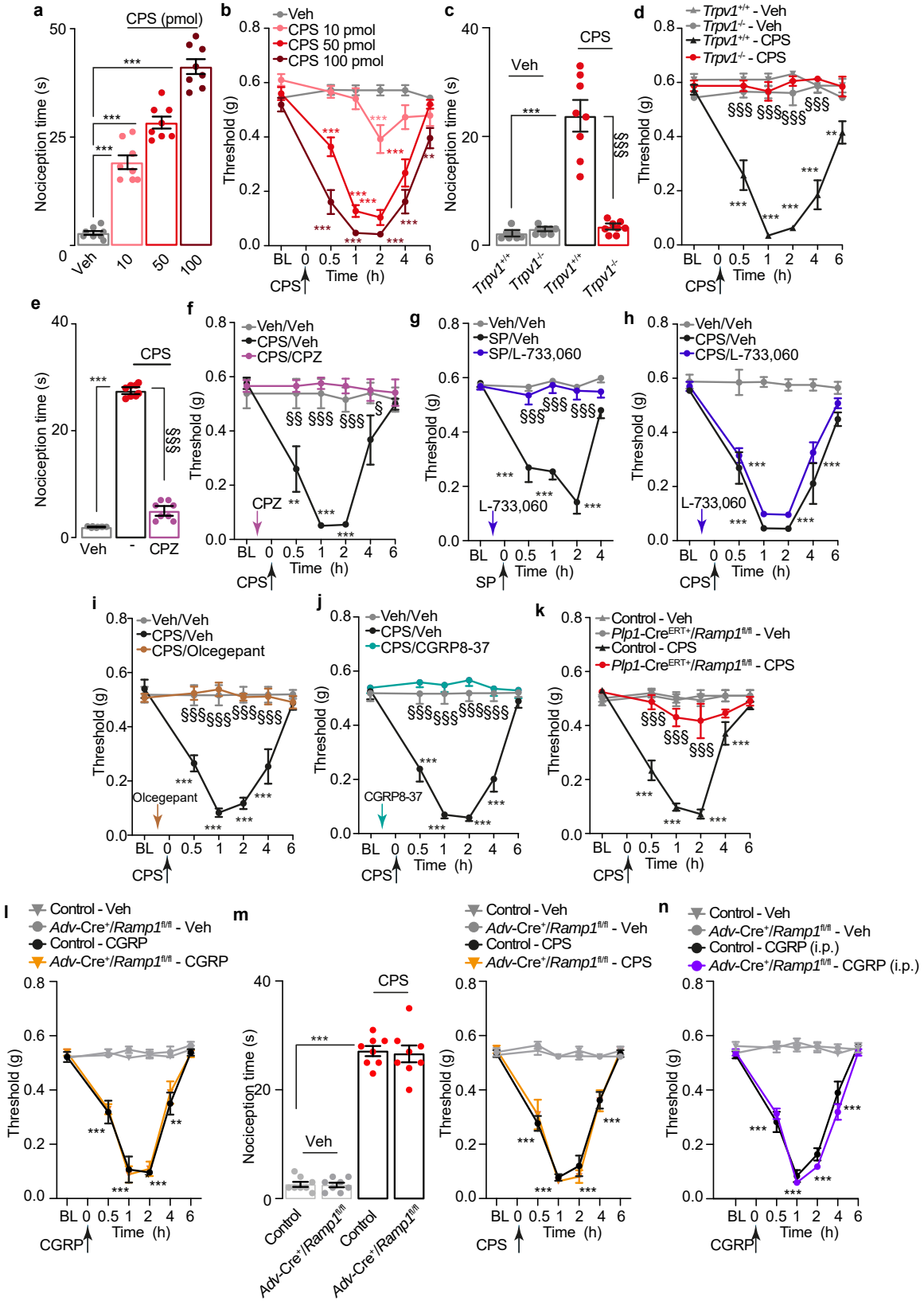

nociception evoked by capsaicin (Supplementary Fig. 2b). Importantly, 4-OHT markedly inhibited capsaicin-evoked PMA (Fig. 2k) but not acute nociception (Supplementary Fig. 2f) in *Plp-Cre*$^{ERT+}$;*Ramp1*$^{fl/fl}$ mice observed in Control mice. CGRP-evoked PMA or capsaicin-evoked acute nociception and PMA were similar in mice with selective deletion of RAMP1 in nociceptors (*Advillin-Cre*$^{+}$;*Ramp1*$^{fl/fl}$, *Adv-Cre*$^{+}$;*Ramp1*$^{fl/fl}$) and Control mice (Fig. 2l, m). Both PMA and paw allodynia were similar in *Adv-Cre*$^{+}$;*Ramp1*$^{fl/fl}$ and Control mice after intraperitoneal CGRP (Fig. 2n and Supplementary Fig. 3a). Thus, CGRP but not SP mediates allodynia resulting from excitation of TRPV1 + ve peptidergic nociceptors, and PMA evoked by both

Fig. 2 Capsaicin induces PMA via CGRP and CLR/RAMP1 in Schwann cells. a Acute nociception and (**b**) PMA after periorbital injection of capsaicin (CPS) or vehicle in C57BL/6 J mice. **c** Acute nociception and (**d**) PMA after CPS (50 pmol) or vehicle in *Trpv1*$^{+/+}$ and *Trpv1*$^{-/-}$ mice. **e** Acute nociception and (**f**) PMA after CPS (50 pmol) or vehicle in C57BL/6 J mice pretreated with capsazepine (CPZ, 100 pmol) or vehicle. **g**, **h** PMA after periorbital SP (3.5 nmol), CPS (50 pmol) or vehicle in C57BL/6 J mice pretreated (0.5 h) with L-733,060 (20 nmol) or vehicle. **i**, **j** PMA after CPS (50 pmol) or vehicle in C57BL/6 J mice pretreated (0.5 h) with olcegepant (1 nmol) or CGRP8-37 (10 nmol) or vehicle. **k** PMA after CPS (50 pmol) or vehicle in *Plp1-Cre*$^{ERT+/}$*Ramp1*$^{fl/fl}$ or Control mice treated with periorbital 4-OHT or vehicle. **l** PMA after periorbital CGRP (1.5 nmol) or vehicle and (**m**) acute nociceptive response and PMA after periorbital CPS (50 pmol) or vehicle in *Adv-Cre*$^{+/}$*Ramp1*$^{fl/fl}$ or Control mice. **n** PMA induced by intraperitoneal (i.p.) CGRP (0.1 mg/kg) or vehicle in *Adv-Cre*$^{+/}$*Ramp1*$^{fl/fl}$ or Control mice. Mean±SEM., $n = 8$ mice per group. $^{**}P < 0.01$, $^{***}P < 0.001$ vs. Veh/Veh, Trpv1$^{+/+}$-Veh and Control-Veh; $^{§}P < 0.05$, $^{§§}P < 0.01$, $^{§§§}P < 0.001$ vs. Trpv1$^{+/+}$-CPS, CPS/Veh, SP/Veh, Control-CPS, Control-CGRP. 1-way (**a**, **c**, **e** and **m** left panel) or 2-way (**b**, **d**, **f**–**l**, **m** right panel and **n**) ANOVA, Bonferroni correction. Source data are provided as a Source Data file.

endogenous and exogenous CGRP depends on CLR/RAMP1 of Schwann cells surrounding peripheral terminals of nociceptors, while the receptor of sensory nerve fibers is not implicated.

Schwann cell CLR/RAMP1 mediates the CGRP-dependent PMA evoked by GTN. Systemic GTN administration provokes sustained headaches in humans[19]. In mice intraperitoneal GTN elicits PMA[18] that is, in part mediated by CGRP release from periorbital trigeminal terminals[18]. Here, systemic GTN elicited PMA (Fig. 3a) and paw allodynia (Fig. 3b) that were similar in Control and *Adv-Cre*$^{+}$;*Ramp1*$^{fl/fl}$ mice. Olcegepant transiently and partially inhibited PMA (Fig. 3a), while did not affect GTN-evoked paw allodynia (Fig. 3b) in both mouse strains. RAMP1 deletion from trigeminal Schwann cells (*Plp-Cre*$^{ERT+}$;*Ramp1*$^{fl/fl}$ mice) partially inhibited PMA (Fig. 3c), but not paw allodynia (Fig. 3d). Importantly, treatment with olcegepant reduced GTN-evoked PMA in Control mice, but failed to further inhibit the response in *Plp-Cre*$^{ERT+}$;*Ramp1*$^{fl/fl}$ mice (Fig. 3c). Paw allodynia was unchanged by olcegepant (Fig. 3d). Together, the findings suggest that Schwann cell CLR/RAMP1 mediates the CGRP-dependent component of PMA in a mouse headache model.

Clathrin- and dynamin-mediated endocytosis of CLR/RAMP1 in Schwann cells mediates PMA. We investigated the CLR/RAMP1 signaling pathway in Schwann cells that mediates CGRP-evoked PMA. The CGRP-stimulated cAMP formation was measured in HSCs using a virally encoded cAMP cADDis reporter. CGRP stimulated a prompt concentration-dependent increase in cAMP formation in HSCs that was sustained for >300 s (Fig. 4a, b; Supplementary Movie 1). The CLR/RAMP1 antagonist olcegepant caused a concentration-dependent inhibition of CGRP-stimulated cAMP formation (Fig. 4c–e).

Endosomal signaling of GPCRs, including CLR/RAMP1, controls nociception[33–35]. To assess CLR/RAMP1 endocytosis in Schwann cells, we incubated HSCs expressing the early endosome marker Rab5a-GFP with TAMRA-CGRP. In vehicle-treated cells, live-cell imaging revealed uptake of TAMRA-CGRP into Rab5a-GFP + ve early endosomes within 10 min that continued for 30 min (Fig. 4f, Supplementary Movie 2). Inhibitors of clathrin (PitStop2, PS2) or dynamin (Dyngo4a, Dy4) prevented the translocation of TAMRA-CGRP to endosomes causing retention of weak TAMRA-CGRP fluorescence at the cell surface (Fig. 4e, f; Supplementary Movies 3 and 4). Quantification of TAMRA-CGRP fluorescence intensity in Rab5a-GFP + ve endosomes or the proportion of endosomes containing TAMRA-CGRP confirmed that PS2 and Dy4 inhibited endocytosis of TAMRA-CGRP (Fig. 4g, h). Inactive analogs had no effect. Hypertonic sucrose (0.45 M) inhibits clathrin-mediated endocytosis, including agonist-stimulated endocytosis of GPCRs[38]. Hypertonic sucrose also inhibited the uptake of TAMRA-CGRP in HSCs (Fig. 4g, h, Supplementary Movie 5). Injection of PS2 or Dy4, but not their inactive analogs, prevented CGRP-evoked PMA, both in male and female mice (Fig. 4i, j and Supplementary Fig. 3b, c). PS2 or Dy4 also reversed capsaicin-evoked PMA (Fig. 4k, l). Thus, CGRP stimulates clathrin- and dynamin-mediated endocytosis of CLR/RAMP1 in Schwann cells, which sustains CGRP-evoked PMA.

CLR activates Gα$_s$, Gα$_q$, and Gα$_i$ and recruits βARR2 to the plasma membrane and endosomes. GPCRs, including CLR/RAMP1, can signal from endosomes by Gα$_s$, Gα$_q$, and βARR-mediated mechanisms[33–35]. We used enhanced bystander bioluminescence resonance energy transfer (EbBRET) to study the activation of Gα and recruitment of βARR to the plasma membrane and early endosomes of HEK293T cells expressing human (h) CLR and RAMP1 (HEK-hCLR/RAMP1). CGRP-dependent activation of Gα$_s$, Gα$_{sq}$, and Gα$_{si}$ was assessed using an EbBRET assay that detects recruitment of mini (m) Gα coupled to *Renilla* (R)luc8 to the plasma membrane marker CAAX coupled to RGFP or the early endosome marker Rab5a coupled to tandem (td) RGFP. mGα proteins are N-terminally truncated Gα proteins that freely diffuse throughout the cytoplasm and bind to active conformations of GPCRs. Their translocation to GPCRs reflects Gα activation. mGα$_{sq}$ and mGα$_{si}$ were developed by mutating mGα$_s$ residues to equivalent Gα$_q$ and Gα$_i$ residues. Recruitment of βARR was assessed by measuring EbBRET between Rluc2-βARR2 and RGFP-CAAX or tdRGFP-Rab5a. CGRP induced a rapid increase in EbBRET between Rluc8-mGα$_s$, Rluc8-mGα$_{sq}$, Rluc8-mGα$_{si}$, and Rluc2-βARR2 with RGFP-CAAX, which was maximal at ~300 s and declined over 1000 s (Fig. 5a, b). CGRP increased EbBRET between Rluc8-mGα$_s$, Rluc8-mGα$_{sq}$, Rluc8-mGα$_{si}$ and Rluc2-βARR2 with tdRGFP-Rab5a that was fully sustained for 1300 s (Fig. 5c, d). EbBRET was similarly used to study the activation of Gα and recruitment of βARR2 to the plasma membrane and endosomes of HSCs transfected with hCLR/RAMP1 (CLR/RAMP1 overexpression was required to amplify BRET signals). In HSCs, CGRP increased EbBRET between Rluc8-mGα$_s$, Rluc8-mGα$_{sq}$, Rluc8-mGα$_{si}$ and Rluc2-βARR2 with RGFP-CAAX and tdRGFP-Rab5a (Fig. 5e–h). EbBRET signals were sustained for 1300 s.

To investigate the contribution of endocytosis to the activation of Gα proteins and βARRs in endosomes, we preincubated cells with hypertonic sucrose. CGRP increased EbBRET between hCLR-Rluc8 and tdRGFP-Rab5a in HEK-hCLR/RAMP1 cells, consistent with CLR endocytosis (Fig. 5i). Hypertonic sucrose inhibited these changes, which indicates an inhibition of endocytosis (Fig. 5i). Hypertonic sucrose caused a delayed yet more sustained activation of Rluc8-mGα$_s$, Rluc8-mGα$_{sq}$, Rluc8-mGα$_{si}$, and Rluc2-βARR2 at the plasma membrane (Supplementary Fig. 4a–f), and an almost complete inhibition of activation of Rluc8-mGα$_s$, Rluc8-mGα$_{sq}$, Rluc8-mGα$_{si}$ and Rluc2-βARR2 in endosomes (Fig. 5j, k). Sucrose similarly delayed CGRP-induced recruitment of Rluc8-mGα$_s$, Rluc8-mGα$_{sq}$, Rluc8-mGα$_{si}$ and

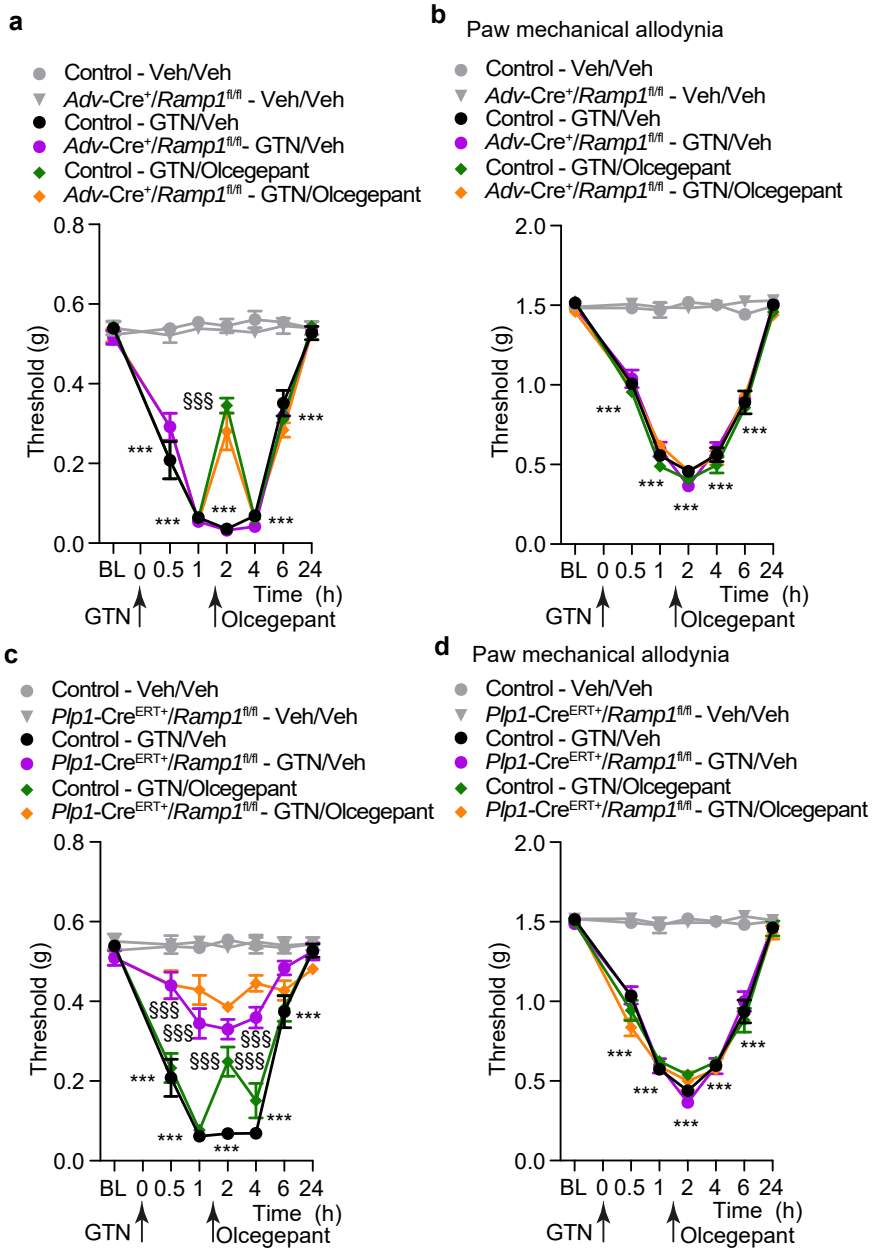

Fig. 3 GTN induces PMA via CGRP released from periorbital trigeminal terminals and, CLR/RAMP1 in Schwann cells. a PMA and (**b**) paw mechanical allodynia induced by intraperitoneal (i.p.) GTN (10 mg/kg) or vehicle in *Adv-Cre*$^{+/}$*Ramp1*$^{fl/fl}$ or Control mice post-treated (1.5 hs after GTN) with olcegepant (1 nmol) or vehicle. (**c**) PMA and (**d**) paw mechanical allodynia induced by GTN (10 mg/kg, i.p.) or vehicle in *Plp1-Cre*$^{ERT+/}$*Ramp1*$^{fl/fl}$ or Control (treated with periorbital 4-OHT or vehicle) post-treated (1.5 hs after GTN) with olcegepant (1 nmol) or vehicle. Mean±SEM., $n = 8$ mice per group. ***$P < 0.001$ vs. Control-Veh/Veh; $^{§§§}P < 0.001$ vs. Control-GTN/Veh. 2-way ANOVA, Bonferroni correction. Source data are provided as a Source Data file.

Rluc2-βARR2 to the plasma membrane (Supplementary Fig. 4g–l) and almost completely inhibited activation of $G\alpha_{s,sq,si}$ and βARR2 in endosomes of HSCs expressing hCLR/RAMP1 (Fig. 5l, m).

To examine the contribution of endosomal CLR/RAMP1 signaling to CGRP-induced cAMP formation, we preincubated HSCs expressing the cADDis cAMP reporter with sucrose or vehicle. In vehicle-treated cells, CGRP stimulated a rapid (1 min) increase in cAMP formation that was sustained for 30 min (Fig. 5n, o). Sucrose reduced but did not abolish the initial response, yet strongly inhibited the sustained phase of CGRP-stimulated cAMP formation (Fig. 5n, o). Thus, CGRP initially activates Gα and βARR at the plasma membrane, which is followed by sustained activation of Gα and βARR in early endosomes. Endocytosis is necessary for the recruitment of Gα and βARR to endosomes. $G\alpha_s$ continues to signal in endosomes, leading to sustained cAMP formation.

CLR/RAMP1 activation in Schwann cells releases NO, which initiates but does not sustain PMA. We investigated the mechanisms that sustain PMA following CLR/RAMP1 activation and endocytosis in Schwann cells. Pre- but not post-treatment (60 min after CGRP or capsaicin) with CLR/RAMP1 antagonists, olcegepant or CGRP8-37, attenuated PMA evoked by capsaicin and in accordance with previous studies[17,18] PMA evoked by CGRP (Supplementary Fig. 5a–f). Similarly, inhibitors of clathrin- and dynamin-mediated endocytosis had no effect when administered

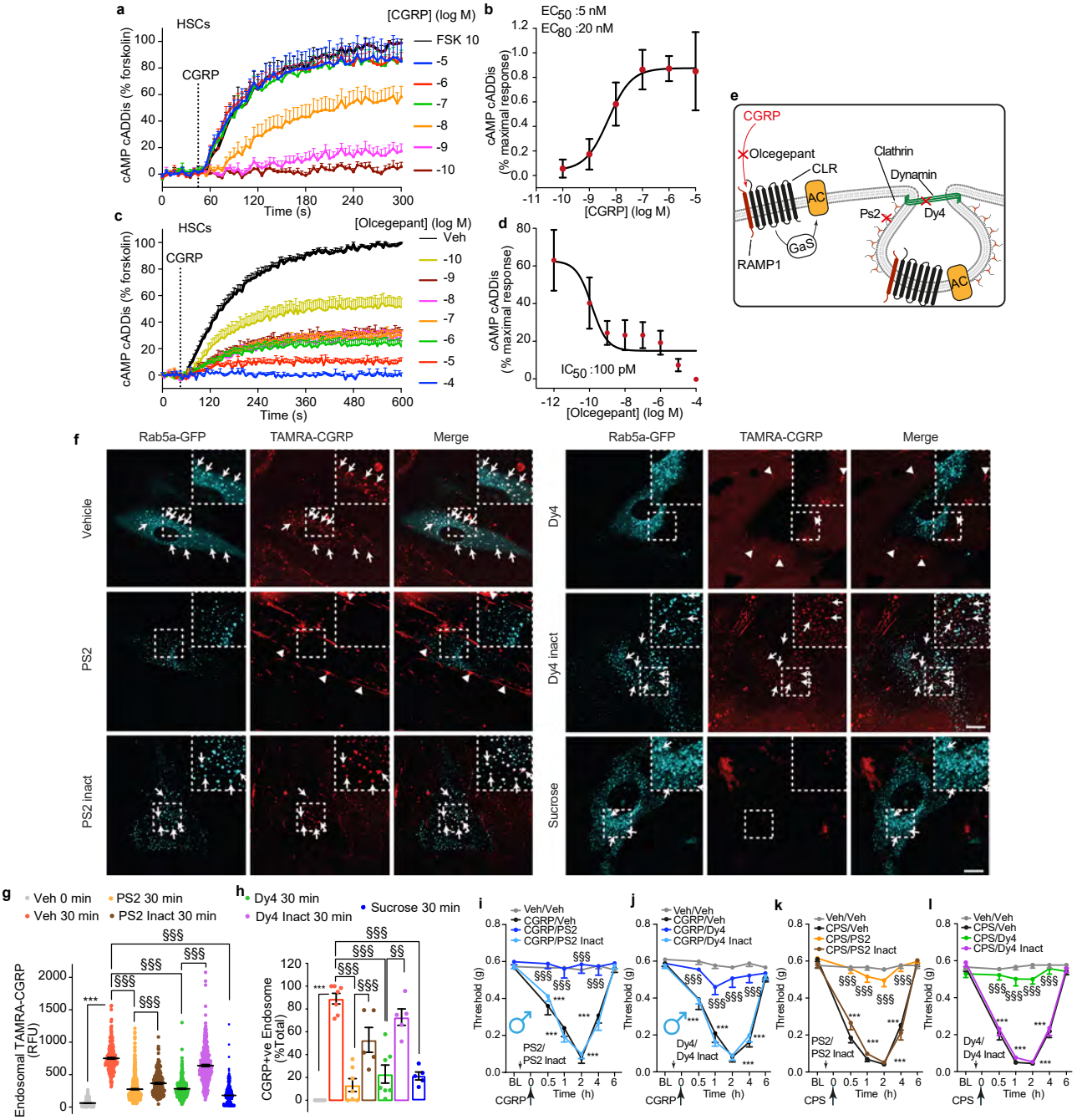

Fig. 4 Functional CLR/RAMP1 is expressed by HSCs and undergoes clathrin- and dynamin-mediated endocytosis, which underlies nociception. **a**, **b** Effects of graded concentrations of CGRP on cAMP formation ($n = 5$ independent experiments). **c**, **d** Effects of graded concentrations of olcegepant on CGRP (100 nM)-evoked cAMP formation ($n = 4$ independent experiments). **e** Pharmacological targets. **f** Representative images of HSCs expressing Rab5a-GFP at 30 min after incubation with TAMRA-CGRP (100 nM). Arrows denote colocalization of TAMRA-CGRP and Rab5a-GFP. Arrowheads denote retention of a weak TAMRA-CGRP signal at the plasma membrane. Cells were preincubated with vehicle, Dyngo-4a (Dy4), Pitstop 2 (PS2), inactive analogs (PS2 and Dy4 inact) (all 30 μM) or sucrose (0.45 M) ($n = 4$ independent experiments). Scale, 10 μm. **g** Quantification of localization of TAMRA-CGRP in endosomes (data represent $n = 949$ veh 0 min, $n = 1209$ veh 30 min, $n = 1111$ Dy4 30 min, $n = 1016$ Dy4 inact 30 min, $n = 1700$ PS2 30 min, $n = 714$ PS2 inact 30 min, $n = 1896$ sucrose) and (**h**) quantification of the number of TAMRA-CGRP+ve endosomes (data represent $n = 5$ veh 0 min, $n = 7$ veh 30 min, $n = 7$ Dy4 30 min, $n = 5$ Dy4 inact 30 min, $n = 7$ PS2 30 min, $n = 5$ PS2 inact 30 min, $n = 5$ sucrose). **i**, **j** PMA induced by periorbital CGRP (1.5 nmol) or vehicle in C57BL/6 J male mice pretreated (0.5 h) with PS2, Dy4, PS2 or Dy4 inact (all 500 pmol) ($n = 8$ mice per group). **k**, **l** PMA induced by periorbital capsaicin (CPS, 50 pmol) or vehicle in C57BL/6 J male mice pretreated (0.5 h) with PS2, Dy4, PS2 or Dy4 inact (all 500 pmol) ($n = 8$ mice per group). Mean±SEM. $^{***}P < 0.001$ vs. Veh 0 min, and Veh/Veh; $^{§§}P < 0.01$, $^{§§§}P < 0.001$ vs. Veh 30 min, PS2 30 min, Dy4 30 min, CGRP/PS2 inact, CGRP/Dy4 inact, CPS/PS2 inact, CPS/Dy4 inact. 1-way (**g**, **h**) or 2-way (**i**–**l**) ANOVA, Bonferroni correction. Source data are provided as a Source Data file.

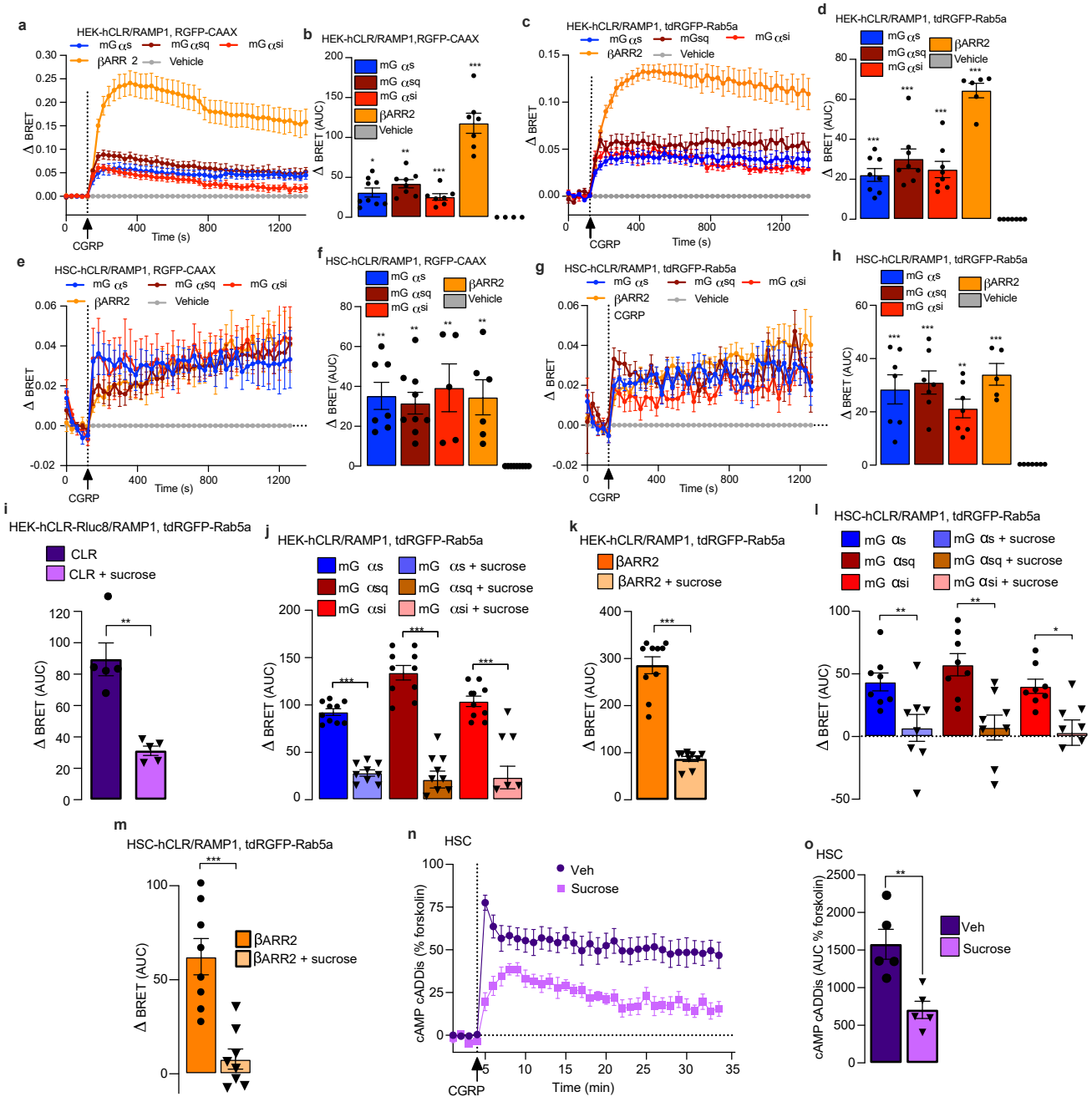

Fig. 5 CGRP leads to Gα protein activation and βARR2 recruitment at the plasma membrane and in early endosomes in HEK-hCLR/RAMP1 cells and HSCs-hCLR/RAMP1. Endosomal signaling generates sustained formation of cAMP in HSCs. (**a**–**d**) CGRP (100 nM) increased EbBRET between Rluc8-mGα$_s$, Rluc8-mGα$_{sq}$, Rluc8-mGα$_{si}$, and Rluc2-βARR2 with RGFP-CAAX (**a**, **b**) and tdRGFP-Rab5a (**c**, **d**) in HEK-hCLR/RAMP1 cells. **a**, **c** time course. **b**, **d** area under curve (AUC) (**a**, **b** $n = 10$ mGα$_s$, $n = 8$ mGα$_{sq}$, $n = 7$ mGα$_{si}$, $n = 7$ βARR2, $n = 9$ veh; **c**, **d** $n = 8$ mGα$_s$, $n = 8$ mGα$_{sq}$, $n = 8$ mGα$_{si}$, $n = 6$ βARR2, $n = 9$ veh). **e**–**h** CGRP (100 nM) increased EbBRET between Rluc8-mGα$_s$, Rluc8-mGα$_{sq}$, Rluc8-mGα$_{si}$, and Rluc2-βARR2 with RGFP-CAAX (**e**, **f**) and tdRGFP-Rab5a (**g**, **h**) in HSC-hCLR/RAMP1 cells. **e**, **g** time course. **f**, **h** AUC (**e**, **f** $n = 7$ mGα$_s$, $n = 9$ mGα$_{sq}$, $n = 5$ mGα$_{si}$, $n = 6$ βARR2, $n = 9$ veh; **g**, **h** $n = 7$ mGα$_s$, $n = 7$ mGα$_{sq}$, $n = 7$ mGα$_{si}$, $n = 5$ βARR2, $n = 7$ veh). (**i**) Hypertonic sucrose (0.45 M) inhibited CGRP (100 nM)-stimulated EbBRET between hCLR-Rluc8 and tdRGFP-Rab5a in HEK-hCLR/RAMP1 cells ($n = 5$ independent experiments). (**j**, **k**) Hypertonic sucrose (0.45 M) inhibited CGRP (100 nM)-stimulated EbBRET between Rluc8-mGα$_s$, Rluc8-mGα$_{sq}$, Rluc8-mGα$_{si}$ and Rluc2-βARR2 with tdRGFP-Rab5a in HEK-hCLR/RAMP1 cells (**j**, **k** $n = 10$ independent experiments). (**l**, **m**) Sucrose (0.45 M) inhibited CGRP (100 nM)-stimulated EbBRET between Rluc8-mGα$_s$, Rluc8-mGα$_{sq}$, Rluc8-mGα$_{si}$, and Rluc2-βARR2 with tdRGFP-Rab5a in HSC-hCLR/RAMP1 cells. ($n = 8$ independent experiments). (**n**, **o**) Sucrose (0.45 M) inhibited CGRP (100 nM)-stimulated formation of cAMP in HSCs. **n** time course. o, AUC ($n = 5$ independent experiments). Mean±SEM.. $^*P < 0.05$, $^{**}P < 0.01$, $^{***}P < 0.001$, vs. Veh. 1-way ANOVA, Dunnett's correction (**b**, **d**, **f**, **h**) or parametric unpaired *t* test (**i**–**m**, **o**). Source data are provided as a Source Data file.

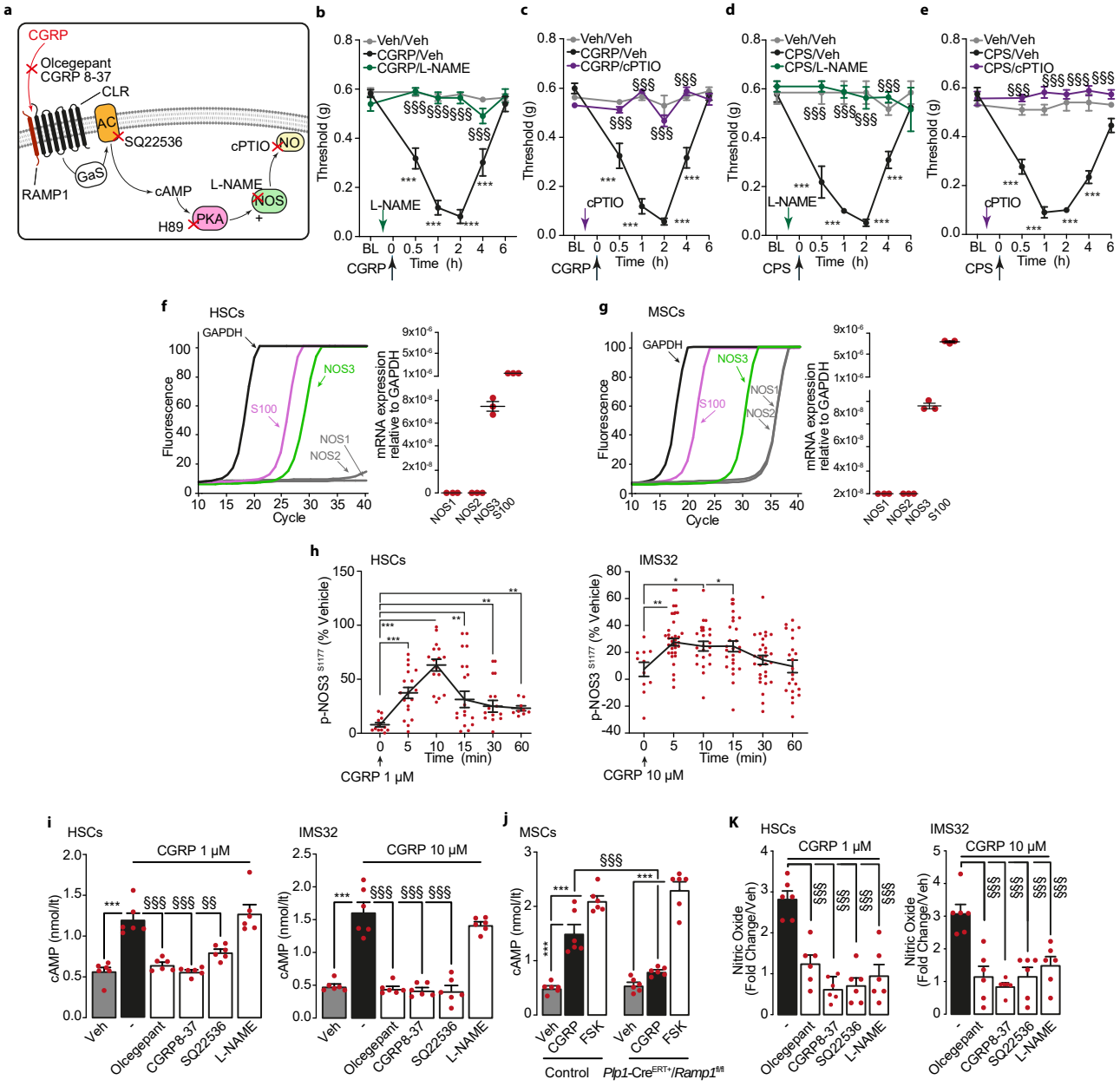

Fig. 6 Endogenous and exogenous CGRP induces PMA via NO production. a Pharmacological targets. **b**–**e** PMA after periorbital injection of CGRP (1.5 nmol), capsaicin (CPS, 50 pmol) or vehicle in C57BL/6 J mice pretreated (0.5 h) with L-NAME (1 µmol) and cPTIO (200 nmol) or vehicle ($n = 8$ mice per group). **f**, **g** Real-time PCR plot and cumulative data for GAPDH, S100, NOS1, NOS2 and NOS3 in primary HSCs and MSCs ($n = 3$ independent experiments). **h** In-cell p-NOS3^{s1177} ELISA in HSCs and IMS32 cells before (time 0, $n = 11$ independent experiments in both HSCs and IMS32) or after CGRP (time 5, $n = 18$ and $n = 31$, time 10, $n = 16$ and $n = 21$, time 15, $n = 15$ and $n = 25$, time 30, $n = 12$ and $n = 29$, time 60, $n = 9$ and $n = 22$ independent experiments in HSCs and IMS32, respectively). cAMP assay in (**i**) HSCs, IMS32 and (**j**) MSCs from *Plp1-Cre$^{ERT+/}$Ramp1$^{fl/fl}$* or Control mice treated with intraperitoneal 4-OHT, **k** nitric oxide assay in HSCs and IMS32 cells treated with CGRP or vehicle ($n = 6$ independent experiments). Some cells were treated with olcegepant (1 µM), CGRP8-37 (1 µM), SQ22536 (100 µM), L-NAME (100 µM) or vehicle ($n = 6$ independent experiments). Mean±SEM. (−) represents the combination of different vehicles. *$P < 0.05$, **$P < 0.01$, ***$P < 0.001$ vs. Veh/Veh, time 0 (min); §§§$P < 0.001$ vs. CGRP/Veh, CGRP 1 µM and 10 µM. 1-way (**h**–**k**) or 2-way (**b**–**e**) ANOVA, Bonferroni correction. Source data are provided as a Source Data file.

60 min after CGRP or capsaicin (Supplementary Fig. 5g–j). Thus, once induced by CGRP, CLR/RAMP1 antagonists or inhibitors of CRL/RAMP1 internalization are unable to attenuate PMA. Pre- but not post-treatment with the protein kinase A (PKA) inhibitor, H89, reduced PMA by CGRP and capsaicin (Supplementary Fig. 5k–n). NO has been implicated in CGRP-mediated vascular responses[2]. Although NO can release CGRP with proalgesic functions, the contribution of NO to CGRP-evoked allodynia is uncertain. Pre-treatment with an NO synthase (NOS) inhibitor (L-NAME) or an NO scavenger (cPTIO) (Fig. 6a), abrogated CGRP-evoked PMA (Fig. 6b, c). L-NAME and cPTIO pretreatment also attenuated capsaicin-evoked PMA (Fig. 6d, e). However, L-NAME and cPTIO did not affect PMA when administered 60 min after CGRP (Supplementary Fig. 5o, p) or capsaicin (Supplementary Fig. 5q, r). Thus, PKA-dependent NO release[39] is necessary to initiate, but is not sufficient to sustain, CGRP-evoked allodynia.

In vitro findings recapitulated in vivo results. HSCs, MSCs, and IMS32 cells predominantly expressed NOS3 (eNOS) mRNA, with

little or no expression of NOS1 and NOS2 (nNOS and iNOS, respectively) mRNA (Fig. 6f, g; Supplementary Fig. 5s). In both HSCs and IMS32 cells CGRP elicited a transient increase in NOS3 phosphorylation (*i.e.*, activation), consistent with NO generation, which peaked at 5–10 min and declined within 30–60 min (Fig. 6h), and a cAMP increase that was prevented by olcegepant, CGRP8-37 and an adenylyl cyclase inhibitor (SQ22536), but not by L-NAME (Fig. 6i). The increase in cAMP evoked by CGRP but not that elicited by forskolin was reduced in cultured MSCs obtained from *Plp-Cre^{ERT+};Ramp1$^{fl/fl}$* mice as compared to Control mice treated with intraperitoneal 4-OHT (Fig. 6j). In contrast, the CGRP-evoked increase in NO was attenuated by all these interventions, including NOS inhibition (Fig. 6k). The cAMP increase evoked by forskolin was unaffected by CLR/RAMP1 antagonism and NOS inhibition, and olcegepant failed to inhibit NO release by the NO donor NONOate (Supplementary Fig. 5t, u), indicating selectivity. NO release evoked by CGRP, but not that evoked by NONOate was inhibited by PS2 and Dy4, but not their inactive analogs (Supplementary Fig. 5v), further supporting selectivity. These results suggest that clathrin- and dynamin-dependent endocytosis and endosomal CLR/RAMP1 signaling evoke NOS activation and NO generation in Schwann cells.

Schwann cell TRPA1 mediates CGRP-evoked PMA. NO belongs to a series of reactive oxygen species (ROS) that target TRPA1[40]. TRPA1 is coexpressed with TRPV1 and CGRP in a subpopulation of primary sensory neurons[41]. TRPA1 is expressed in Schwann cells of nerve bundles of human skin and mouse sciatic nerve, where it mediates mechanical allodynia in rodent models of pain[30,42]. Immunoreactive TRPA1 was coexpressed with RAMP1 in S100 + ve Schwann cells in human abdominal and mouse periorbital cutaneous nerves bundles (Fig. 7a). Thus, CLR/RAMP1 might engage signaling pathways that activate TRPA1 in trigeminal Schwann cells to initiate allodynia (Fig. 7b). This hypothesis was supported by the observation that both CGRP- and capsaicin-evoked PMA were reduced in *Trpa1$^{-/-}$* mice and in mice with sensory neuron-specific deletion of TRPA1 (*Adv-Cre^{+};Trpa1$^{fl/fl}$*) (Fig. 7c, d and Supplementary Fig. 6a, b).

We next investigated the signaling pathway by which the CLR/RAMP1 activates TRPA1. In HSCs and IMS32 cells, CGRP stimulated a slowly developing yet sustained increase in Ca^{2+} response (Fig. 7e, f) and increased H_2O_2 levels (Supplementary Fig. 6c). Olcegepant, CGRP8-37, SQ22536, H89, L-NAME, Ca^{2+}-free medium, a ROS scavenger (PBN) or a NOX1 inhibitor (ML171) attenuated Ca^{2+} responses (Fig. 7e, f) and H_2O_2 levels (Supplementary Fig. 6c). A TRPA1 antagonist (A967079) inhibited CGRP-stimulated Ca^{2+} (Fig. 7e, f) and H_2O_2 responses (Supplementary Fig. 6c) but did not affect CGRP-stimulated NO formation (Fig. 7g). CGRP-evoked Ca^{2+} responses were reduced in Schwann cells from *Trpa1$^{-/-}$* mice (Supplementary Fig. 6d). These results support the hypothesis that CGRP liberates NO, which activates Schwann cell TRPA1; activated TRPA1 promotes a Ca^{2+}-dependent H_2O_2 generation that sustains a feed-forward mechanism comprising TRPA1 channel engagement and ROS release.

In vivo results corroborated this hypothesis. Whereas CLR/RAMP1 antagonists or NO inhibitors attenuated PMA only if given before CGRP or capsaicin, both pre- and post-treatment with a TRPA1 antagonist, a ROS scavenger and a NOX1 inhibitor reduced PMA (Fig. 7h–j; Supplementary Fig. 6e–g). Although pretreatment with TRPA1 or ROS inhibitors did not affect the acute nociception, they inhibited capsaicin-evoked PMA (Supplementary Fig. 6h–j). Post-treatment also attenuated capsaicin-evoked PMA (Supplementary Fig. 6h–j). These findings highlight the mechanistic differences between acute nociception and delayed PMA. After an initial and transient NO-dependent phase, PMA is sustained by persistent ROS liberation, which targets TRPA1 in Schwann cells. This hypothesis is robustly supported by the observation that PMA evoked by CGRP or capsaicin was markedly attenuated in mice with selective deletion of TRPA1 in Schwann cells (*Plp-Cre^{ERT+};Trpa1$^{fl/fl}$*) (Fig. 7k; Supplementary Fig. 6k).

Targeting endosomal CGRP signaling provides superior relief of CGRP- and capsaicin-evoked PMA. The finding that persistent GPCR signaling from endosomes mediates pain transmission suggests that GPCRs in endosomes rather than at the plasma membrane are a valid and perhaps superior target for the treatment of pain[33–35]. Nanoparticles have been used to deliver chemotherapeutics to tumor, where endocytosis and endosomal escape are necessary for drug delivery to cytosolic and nuclear targets[43]. The realization that GPCRs within endosomes are a therapeutic target, raises the possibility of exploiting the acid microenvironment of endosomes as a stimulus for nanoparticle disassembly and release of antagonist cargo[34].

To target CLR in endosomes, we generated self-assembling soft polymer nanoparticles containing a CLR antagonist. Diblock copolymers were synthesized with a hydrophilic shell of P(PEGMA-co-DMAEMA) and a hydrophobic core of P(DIPMA-co-DEGMA) (Fig. 8a). Gel permeation chromatography and ^{1}H-nuclear magnetic resonance (^{1}H-NMR) confirmed the molecular weight and composition of nanoparticles (Supplementary Fig. 7a–d). Nanoparticles were self-assembled with MK-3207, a potent hydrophobic antagonist of human CLR/RAMP1, forming DIPMA-MK-3207 (Fig. 8a). Empty nanoparticles (DIPMA-Ø) were used as a control. Nanoparticles were uniformly spherical, with the similar diameter (30–35 nm) and ζ-potential (−0.4–1.3 mV) (Fig. 8b, c). DIPMA nanoparticles demonstrate a pH-dependent cargo release at pH < ~6.5, consistent with the protonation of the DIPMA tertiary amine (pK_a 6.1), charge repulsion, and disassembly[34]. DIPMA nanoparticles enter cells by clathrin- and dynamin-mediated endocytosis and disassemble in acidic early endosomes[34]. To determine whether DIPMA nanoparticles target endosomes containing CLR/RAMP1, HSCs expressing early endosomal antigen-1-GFP (EEA1-GFP) were incubated with DIPMA-Cy5 for 30 min to allow the accumulation in EEA1-GFP + ve endosomes (Fig. 7d, Supplementary Movie 6). Cells were then incubated with TAMRA-CGRP, which was detected in endosomes containing Cy5-DIPMA within 5–10 min (Fig. 8d, Supplementary Movie 6). Thus, DIPMA nanoparticles accumulate with CLR/RAMP1 in early endosomes of Schwann cells.

To determine whether DIPMA-MK-3207 can antagonize CLR in endosomes, we measured CGRP-stimulated cAMP formation using the CAMYEL cAMP BRET sensor, which detects total cellular cAMP. HEK293T cells expressing rat CLR/RAMP1 (HEK-rCRL/RAMP1) were preincubated with graded concentrations of DIPMA-MK-3207 or free MK-3207, DIPMA-Ø or vehicle (control) for 30 min. Beginning at 0 min, baseline BRET was measured for 5 min, and cells were then challenged with CGRP. At 10 min, cells were washed to remove extracellular CGRP, and BRET was measured up to 35 min. In vehicle-treated cells, CGRP stimulated a prompt increase in cAMP formation (1st phase, 6–10 min) that gradually declined after agonist removal from the extracellular fluid (2nd phase, 11–35 min) (Fig. 8e). DIPMA-Ø did not affect this response. Free MK-3207 and DIPMA-MK-3207 (100, 316 nM) both inhibited CGRP-evoked cAMP in the 1st phase to a similar extent (Fig. 8f). During the 2nd phase, free MK-3207 was inactive at all concentrations whereas DIPMA-MK3207 (31.6, 100, 316 nM) strongly inhibited responses (Fig. 8g). The results suggest that

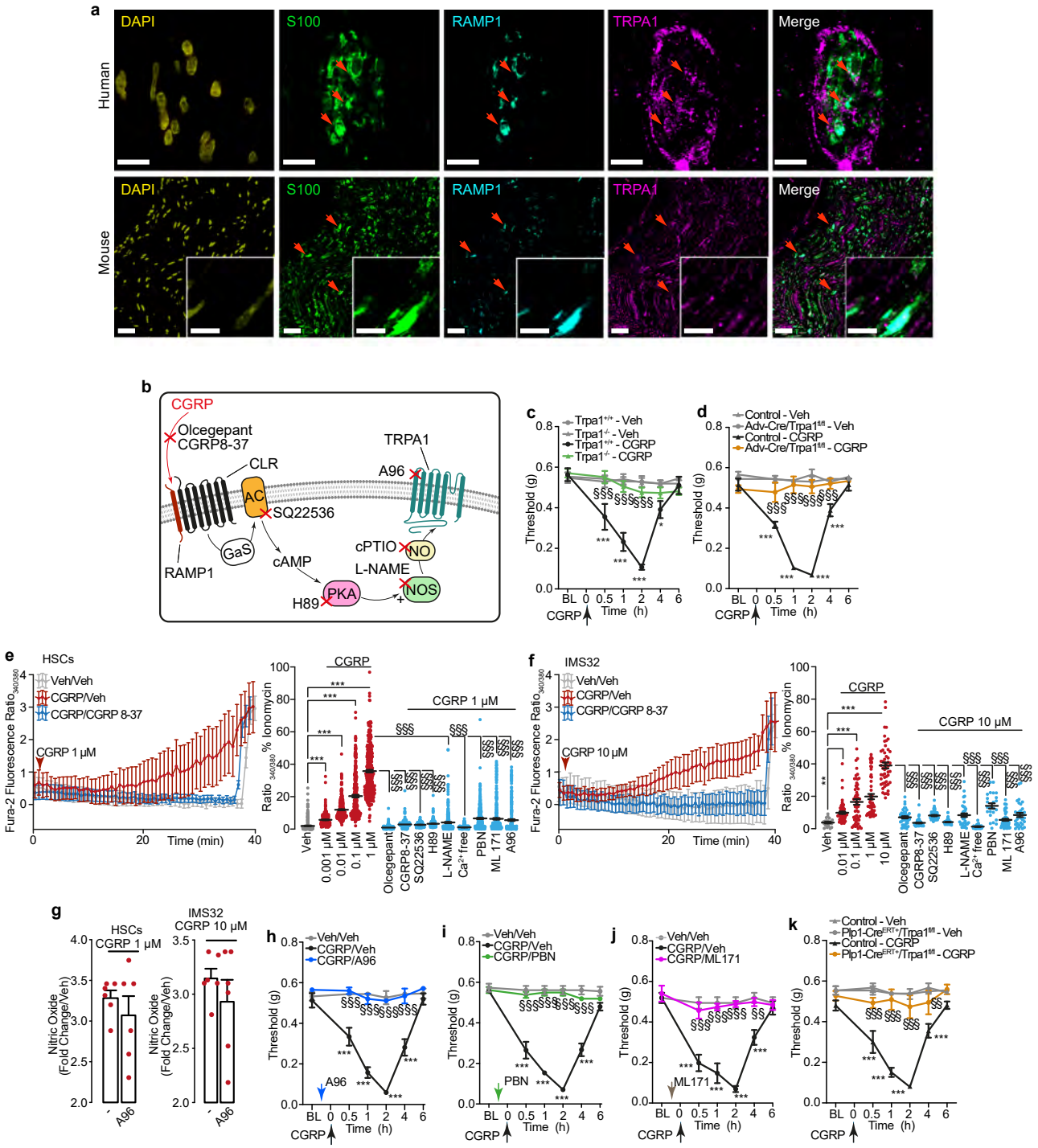

Fig. 7 CGRP induces ROS release via Schwann cell TRPA1 activation. a Representative images of localization of immunoreactive DAPI, S100, RAMP1 and TRPA1 in human abdominal and mouse periorbital cutaneous nerve bundles (Scale: 10 µm human, 50 µm mouse, inset 10 µm) ($n = 3$ subjects). **b** Pharmacological targets. **c**, **d** PMA after periorbital injection of CGRP (1.5 nmol) or vehicle in (**c**) *Trpa1*$^{+/+}$ and *Trpa1*$^{-/-}$ mice and in (**d**) *Adv-Cre*$^{+}$/*Trpa1*$^{fl/fl}$ or Control mice ($n = 8$ mice per group). **e**, **f** Ca^{2+} response in HSCs and IMS32 cells exposed to CGRP (0.001 µM, HSCs $n = 284$; 0.01 µM, HSCs $n = 291$, IMS32 $n = 62$; 0.1 µM, HSCs $n = 297$, IMS32 $n = 53$; 1 µM, HSCs $n = 362$, IMS32 $n = 57$; 10 µM, IMS32 $n = 53$ cells) in the presence of olcegepant (100 nM, HSCs $n = 291$, IMS32 $n = 44$ cells), CGRP8-37 (100 nM, HSCs $n = 359$, IMS32 $n = 55$ cells), SQ22536 (100 µM, HSCs $n = 225$, IMS32 $n = 47$ cells), H89 (1 µM, HSCs $n = 292$, IMS32 $n = 58$ cells), L-NAME (10 µM HSCs $n = 285$, IMS32 $n = 38$), Ca^{2+}-free medium (HSCs $n = 290$, IMS32 $n = 28$ cells), PBN (50 µM, HSCs $n = 309$, IMS32 $n = 24$ cells), ML171 (1 µM, HSCs $n = 320$, IMS32 $n = 49$ cells), A967079 (A96, 50 µM, HSCs $n = 276$ IMS32 $n = 533$ cells) or vehicle (HSCs $n = 297$, IMS32 $n = 41$ cells). **g** Nitric oxide release in HSCs and IMS32 cells exposed to CGRP (1 or 10 µM) in the presence of A96 (50 µM) or vehicle (n = 6 independent experiments). (**h**–**j**) PMA after CGRP (1.5 nmol) or vehicle in C57BL/6 J male mice pre-treated (0.5 h) with **h** A96 (300 nmol), **i** PBN (670 nmol) or (**j**) ML171 (250 nmol) or vehicle. **k** PMA after CGRP (1.5 nmol) or vehicle in *Plp1-Cre*$^{ERT+}$/*Trpa1*$^{fl/fl}$ or Control mice treated with 4-OHT (**h**–**k** $n = 8$ mice per group). Mean±SEM. (−) represents the combination of different vehicles. $^{*}P < 0.05$, $^{**}P < 0.01$, $^{***}P < 0.001$ vs. *Trpa1*$^{+/+}$-Veh, Control-Veh, Veh and Veh/Veh; $^{§§}P < 0.01$, $^{§§§}P < 0.001$ vs. *Trpa1*$^{+/+}$-CGRP, Control-CGRP, CGRP 1 µM and 1 µM, CGRP/Veh. 2-way (**c**, **d**, **h**-**k**) or 1-way (**e**, **f**) ANOVA, Bonferroni correction. Source data are provided as a Source Data file.

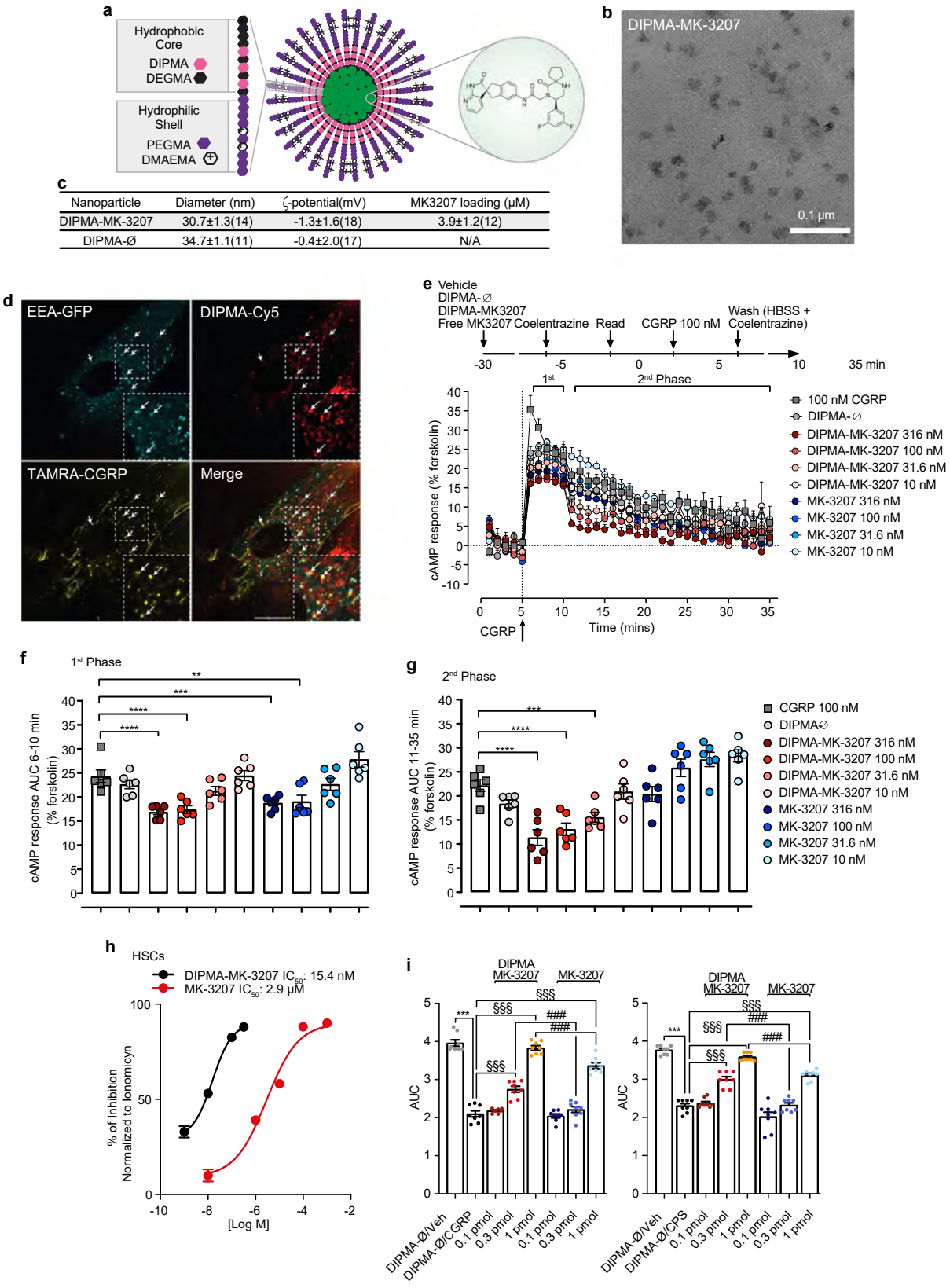

DIPMA-MK3207 can antagonize the sustained phase of CGRP-stimulated formation of cAMP, which is attributable to endosomal CLR/RAMP1 signaling.

To assess the antagonism of the pain signaling pathway in HSCs, we measured CGRP-evoked changes in Ca^{2+} response, which depend on endosomal CGRP signaling and activation of TRPA1. HSCs were preincubated with graded concentrations of DIPMA-MK-3207 or MK-3207 for 20 min to allow the accumulation in endosomes, and washed to remove extracellular compounds. At 10 min after washing, cells were challenged with CGRP and Ca^{2+} response was measured as an index of TRPA1 activity. DIPMA-MK-3207 inhibited CGRP-evoked increase in Ca^{2+}

Fig. 8 DIPMA-MK-3207 nanoparticles target endosomal CLR/RAMP1 signaling and provide superior relief from CGRP-evoked PMA. a pH-responsive DIPMA-MK-3207. **b** Transmission electron micrograph image of DIPMA-MK-3207 (Scale: 0.1 µm), from two different nanoparticle preparations (3 images captured per sample). **c** Physicochemical properties of DIPMA-MK-3207 and DIPMA-Ø. **d** Uptake of DIPMA-Cy5 into HSCs expressing EEA1-GFP. Cells were preincubated with DIPMA-Cy5 (40–60 ng/ml) for 30 min and were then incubated with TAMRA-CGRP (100 nM) for 30 min. Arrows denote accumulation of TAMRA-CGRP in early endosomes containing DIPMA-Cy5. Representative images from $n = 5$ independent experiments (Scale: 10 µm). **e–g** Effects of DIPMA-MK-3207, MK-3207, DIPMA-Ø or vehicle on CGRP- (100 nM) stimulated cAMP formation in HEK-rCLR/RAMP1 cells. **e** Time course and **f**, **g** integrated response (AUC) before (1st phase) and after (2nd phase) washing to remove extracellular CGRP ($n = 6$ independent experiments). **h** Concentration-response curves of the inhibition by DIPMA-MK-3207 or free MK-3207 on the Ca^{2+} response to CGRP in HSCs (DIPMA-MK-3207: −9M, $n = 145$; −8M, $n = 361$; −7M, $n = 213$: −6.5 M, $n = 150$; or free MK-3207: −8M, $n = 83$; −6M, $n = 106$; −5M, $n = 87$; −4M, $n = 127$: −3M, $n = 127$ cells). **i** PMA, expressed as AUC, after periorbital injection of CGRP (1.5 nmol), capsaicin (CPS, 50 pmol) or vehicles in C57BL/6 J male mice pre-treated (0.5 h) with DIPMA-MK-3207, MK-3207 (0.1, 0.3, 1 pmol), DIPMA-Ø or vehicle ($n = 8$ mice per group). Mean±SEM. $^{***}P < 0.001$ vs. DIPMA-Ø/Veh, $^{###}P < 0.001$ vs. MK-3207 0.3 pmol and MK-3207 1 pmol. **f**, **g**, **i** 1-way ANOVA, Bonferroni correction. Source data are provided as a Source Data file.

response (IC_{50} 15.4 nM, 95% confidence interval, 10.9–21.0 nM) more potently than free MK-3207 (IC_{50} 2.9 µM, 95% confidence interval, 1.9–4.2 µM, $P < 0.0001$) (Fig. 8h). To assess antinociception, DIPMA-MK-3207 or free MK-3207 (0.1, 0.3, 1.0 pmol) was injected into the periorbital region 30 min before periorbital injection of CGRP or capsaicin. DIPMA-MK-3207 (0.3, 1.0 pmol) more effectively inhibited PMA than the same doses of free MK-3207 (Fig. 8i). DIPMA-Ø had no effect. Thus, endosomal targeting enhances the efficacy of a CLR/RAMP1 antagonist in a preclinical model of migraine pain.

Discussion

The major findings of the present study are that CGRP causes PMA by activating CLR/RAMP1 of Schwann cells, CLR/RAMP1 signals from endosomes of Schwann cells to activate pain pathways, and endosomal CLR/RAMP1 can be targeted using nanoparticles and endocytosis inhibitors to relieve CGRP-evoked PMA. CLR/RAMP1 stimulation and trafficking to endosomes results in a persistent cAMP-dependent NOS activation and generation of NO, a mediator of migraine pain[19]. The role of NO in PMA is crucial, yet transient, as it is temporally limited to the engagement of TRPA1/NOX1, which releases ROS with a dual function. On one hand, ROS target TRPA1/NOX1 of Schwann cells to maintain ROS generation by a feed-forward mechanism. On the other hand, as suggested by experiments with selective TRPA1 deletion in primary sensory neurons, ROS target TRPA1 on nociceptors to signal allodynia to the CNS.

Periorbital capsaicin injection elicited acute nociception mediated by TRPV1 excitation and ensuing afferent discharge, which signals pain to the CNS. In a larger cutaneous area, capsaicin evoked delayed and prolonged PMA. While the acute pain response is most likely dependent on ion influx associated with TRPV1 activation, the mechanism underlying mechanical hypersensitivity[7,44] has remained elusive. Our findings support the existence of a paracrine mechanism that underlies PMA associated with neurogenic inflammation. We suggest that capsaicin locally activates TRPV1 + ve nerve fibers to generate action potentials that propagate antidromically into collateral fibers which release CGRP in a broader area, thus eliciting widespread PMA. PMA depends on the interaction between peptidergic nerve fibers, surrounding Schwann cells and nociceptive neurons that convey allodynic signals to the CNS. CGRP liberated from the varicosities of trigeminal TRPV1 + ve nerve fibers binds to CLR/RAMP1 of adjacent Schwann cells.

CNS perturbations may target the trigeminovascular system and initiate the migraine attack[22,23]. These central mechanisms may underlie the delayed facial allodynia associated with migraine[20,21]. However, the beneficial effect of anti-CGRP medicines that do not cross the blood-brain barrier suggests that CGRP acts in the periphery to elicit pain. The peripheral site of the algesic action of CGRP released from peptidergic C-fibers has been proposed as the CLR/RAMP1 on adjacent non-peptidergic Aδ-fibers[45] and more precisely at the level of the node of Ranvier[28]. The present results in *Adv-Cre*$^{+}$;*Ramp1*$^{fl/fl}$ mice suggest that CGRP does not act on trigeminal nociceptors to cause PMA in mice. This is consistent with failure of CGRP administration to elicit any itch, pain or axon reflex responses in humans[46]. Instead, our results support the hypothesis that CGRP released from trigeminal nociceptors targets CLR/PAMP1 on Schwann cells that wrap their terminals to evoke PMA. A limitation of our study is that we only assessed PMA that mimics one component of migraine pain. We cannot exclude the possibility that central mechanisms contribute to other pain symptoms of migraine, and that some of the locally administered antagonists used in the present study penetrated the CNS, where they could also influence pain transmission. Although human Schwann cells express CLR/RAMP1 and show functional responses to CGRP that can account for allodynia in mice, further work is needed to understand whether similar mechanisms account for migraine pain in humans.

Another limitation of the present study is that we cannot pinpoint which type of neuron conveys the signals that underlie mechanical allodynia in the trigeminal region. Specifically, we were unable to distinguish between TRPV1-expressing nerve fibers that release CGRP and TRPA1-expressing nerve fibers that are targeted by Schwann cell ROS and convey allodynic signals centrally, since TRPV1 and TRPA1 may coexist in the same population of CGRP-expressing Aδ- or C-fiber primary sensory neurons[2,41]. Most Schwann cells in Remak bundles contain multiple unmyelinated axons from C-fiber nociceptors, including CGRP + ve fibers, which release the bulk of CGRP[2], and non-peptidergic isolectin B4 + ve fibers[47]. Thus, CGRP-evoked release of ROS from Schwann cells could induce allodynia by targeting TRPA1 on three neuronal subtypes, including the same Aδ- or C-fiber that releases CGRP, a different C-fiber of the same Remak bundle, or a different adjacent Aδ-fiber. The observation that both C-fiber and Aδ-fiber nociceptors contribute to capsaicin-evoked hypersensitivity in humans[48] supports the hypothesis that both types of neurons[28,45] are implicated in CGRP-mediated allodynia, thus highlighting the complex neural transmission of mechanical allodynia associated with neurogenic inflammation.

CLR/RAMP1 signals from endosomes by G-protein-mediated mechanisms that activate a subset of compartmentalized signals, including cytosolic protein kinase C and nuclear extracellular signal-regulated kinase; these kinases regulate excitation of spinal neurons and pain transmission[35]. Our results show that CLR/RAMP1 activates $G\alpha_s$, $G\alpha_q$ and $G\alpha_i$ and recruits βARRs in endosomes of Schwann cells, determined by EbBRET. Inhibitors of clathrin- and dynamin-mediated endocytosis blocked the recruitment of CLR/RAMP1, Gα and βARR to endosomes, which presumably requires CLR/RAMP1 endocytosis. GPCR/Gα signaling complexes have also been detected in endosomes by using

conformationally selective nanobodies[49]. The observation that endocytosis inhibitors attenuated CGRP-stimulated cAMP formation and activation of NOS and TRPA1 reveals a central role for CLR/RAMP1 signaling in endosomes of Schwann cells in CGRP-evoked periorbital pain. Endocytosis of other Gs-coupled GPCRs is also necessary for the full repertoire of cAMP-mediated signaling outcomes, which entails endosomal recruitment of adenylyl cyclase 9[50] and assembly of metastable accumulations of PKA[51]. We found that a nanoparticle-encapsulated CLR/RAMP1 antagonist, which targeted CLR/RAMP1 in endosomes and released cargo in the acidified endosomal microenvironment[34], also attenuated CGRP-stimulated cAMP formation and blunted TRPA1 activation.

The observation that periorbital injection of inhibitors of clathrin and dynamin and of DIPMA-MK-3207 prevented CGRP- and capsaicin-evoked PMA provides the evidence for a prominent role of endosomal CGRP signaling of pain from a peripheral site. The finding that nanoparticle encapsulation enhanced the potency of a CGRP antagonist for inhibition of endosomal signaling and resultant nociception supports the hypothesis that CLR/RAMP1 in endosomes mediates facial allodynia which contributes to migraine pain. Nanoparticle encapsulation similarly boosts the efficacy of an NK_1 receptor antagonist in preclinical models of inflammatory and neuropathic pain[34]. An antagonist of CLR/RAMP1 conjugated to a membrane lipid cholestanol also accumulates in endosomes and provides superior relief from pain[35], which reinforces the importance of CLR/RAMP1 endosomal signaling for pain transmission.

Limitations of the present study include uncertainty about the nature of the CLR/RAMP1 signaling complex in endosomes of Schwann cells, which warrants further investigation by proteomics approaches. Although some of the pharmacological inhibitors used to dissect the signaling pathway can have non-specific actions, we bolstered confidence in selectivity by using inhibitors of the same pathway and by genetic deletion of GPCRs and TRP channels. Our findings reveal a prominent role for CLR/RAMP1 in Schwann cells for CGRP-evoked periorbital pain. Future studies will investigate the role of this pathway in preclinical models of migraine pain.

Monoclonal antibodies to CGRP, although beneficial, are not effective in all patients[10]. While non-CGRP-dependent mechanisms might explain this failure[52], monoclonal antibodies likely do not inhibit CGRP signaling in endosomes. The small molecule CLR/RAMP1 antagonist, rimegepant, was found to resolve migraine attacks in patients treated with the anti-CLR/RAMP1 monoclonal antibody, erenumab[53]. This unexpected result was interpreted by the inherent membrane permeability of the lipophilic antagonist rimegepant[54] that might favor inhibition of CGRP signaling in endosomes[53], while neither receptor-targeted nor ligand-targeted monoclonal antibodies internalized with CLR/RAMP1 activated by CGRP[55]. Our results showing a superior inhibition of CGRP signaling in Schwann cells and of PMA by DIPMA-MK-3207, which selectively targets receptor activity in endosomes, reveal a better approach to control allodynia.

In 1936, Sir Thomas Lewis postulated[1] that in human skin action potentials are carried antidromically from the injured nerve terminal to collateral branches from where a chemical substance is released that produces the flare and increases the sensitivity of other fibers responsible for pain. CGRP has been previously identified as the mediator of neurogenic vasodilatation in rodents[2], and in humans[8]. Herein, we propose that CGRP is the 'chemical substance' that, via the essential role of endosomal CLR/RAMP1, TRPA1/NOX1 and oxidative stress of surrounding Schwann cells, sustains the enhanced sensitivity of primary sensory neurons associated with neurogenic inflammation (Fig. 9). The present results suggest that peripherally acting anti-CGRP medicines reduce migraine pain in part by targeting the facial allodynia that originates from CGRP-mediated endosomal signaling in Schwann cells.

Methods

The research conducted complies with all relevant ethical regulations. Animal experiments were carried out in accordance with European Union (EU) guidelines for animal care procedures and the Italian legislation (DLgs 26/2014) application of the EU Directive 2010/63/EU. The study was approved by the National Committee for the Protection of Animals used for Scientific Purposes of the Italian Ministry of Health (research permits #383/2019-PR and #765/2019-PR). The use of formalin-fixed paraffin-embedded (FFPE) sections of human abdominal cutaneous tissues was approved by the Local Ethics Committee of the Florence University Hospital (Area Vasta Toscana Centro) (18271_bio/2020), according to the Helsinki Declaration, and all patients gave their informed consent. Participants did not receive any form of compensation. Biopsies of human abdominal skin analyzed derived from three different patients [female, median age 58 years (range 56–61 years)].

Experimental model and subject details

Animals. Male and female mice were used throughout (25–30 g, 5–8 weeks). The following strains of mice were used C57BL/6 J mice (Charles River, RRID:IMSR_JAX:000664); wild-type (*Trpa1*$^{+/+}$) and TRPA1-deficient (*Trpa1*$^{-/-}$; B6129P-Trpa1^{tm1Kykw}/J; RRID:IMSR_JAX:006401, Jackson Laboratory) mice;[56] wild-type (*Trpv1*$^{+/+}$) and TRPV1-deficient (*Trpv1*$^{-/-}$; B6129X1-Trpv1^{tm1Jul}/J, RRID:IMSR_JAX:003770, Jackson Laboratory) mice. Genetically modified mice were maintained as heterozygotes on a C57BL/6 J background.

To generate mice in which the *Trpa1* and *Ramp1* genes were conditionally silenced in Schwann cells/oligodendrocytes, homozygous 129S-*Trpa1*^{tm2Kykw}/J (*floxed Trpa1, Trpa1*$^{fl/fl}$, RRID:IMSR_JAX:008649 Jackson Laboratory) and C57BL/6N-*Ramp1*$^{<tm1c(EUCOMM)Wtsi>/H}$ (*floxed Ramp1*, *Ramp1*$^{fl/fl}$ Stock No: EM:07401, MRC HARWELL Mary Lion Center)[57] were crossed with hemizygous B6.Cg-Tg(*Plp1-Cre*^{ERT})3Pop/J mice (*Plp1-Cre*^{ERT}, RRID:IMSR_JAX:005975 Jackson Laboratory), expressing a tamoxifen-inducible Cre in myelinating cells (Plp1, proteolipid protein myelin 1)[30]. The progeny (*Plp1-Cre*^{ERT};*Trpa1*$^{fl/fl}$ and *Ramp1-Cre*^{ERT};*Trpa1*$^{fl/fl}$) was genotyped by PCR for *Trpa1, Ramp1* and *Plp1-Cre*^{ERT}. Mice negative for *Plp1-Cre*^{ERT} (*Plp1-Cre*$^{ERT-}$;*Trpa1*$^{fl/fl}$ and *Plp1-Cre*$^{ERT-}$;*Ramp1*$^{fl/fl}$) were used as control. Both positive and negative mice to *Cre*^{ERT} and homozygous for floxed *Trpa1* (*Plp1-Cre*^{ERT};*Trpa1*$^{fl/fl}$ and *Plp1-Cre*$^{ERT-}$;*Trpa1*$^{fl/fl}$, respectively) and floxed *Ramp1* (*Plp1-Cre*^{ERT};*Ramp1*$^{fl/fl}$ and *Plp1-Cre*$^{ERT-}$;*Ramp1*$^{fl/fl}$) mice were treated with 4-hydroxytamoxifen (4-OHT) by subcutaneous periorbital (p.orb.) injection (0.02 mg/10 µl in corn oil once a day for 3 consecutive days). Some *Plp1-Cre*^{ERT};*Ramp1*$^{fl/fl}$ and *Plp1-Cre*$^{ERT-}$;*Ramp1*$^{fl/fl}$ mice were treated with intraperitoneal (i.p.) or intraplantar (i.pl.) 4-OHT (1 mg/100 µl or 0.02 mg/10 µl in corn oil once a day for 3 consecutive days, respectively).

Treatments resulted in Cre-mediated ablation of *Trpa1* and *Ramp1* in PLP-expressing Schwann cells/oligodendrocytes. To selectively delete the *Trpa1* and *Ramp1* gene in primary sensory neurons, *Trpa1*$^{fl/fl}$ and *Ramp1*$^{fl/fl}$ mice were crossed with hemizygous *Advillin-Cre* mice *(Adv-Cre)*[30,58,59]. Both positive and negative mice to *Cre*^{ERT} and homozygous for floxed *Trpa1* (*Adv-Cre*$^{+}$;*Trpa1*$^{fl/fl}$ and *Adv-Cre*$^{-}$;*Trpa1*$^{fl/fl}$, respectively) and floxed *Ramp1* (*Adv-Cre*$^{+}$;*Ramp1*$^{fl/fl}$ and *Adv-Cre*$^{-}$;*Ramp1*$^{fl/fl}$) were used.

The group size of $n = 8$ animals for behavioral experiments was determined by sample size estimation using G*Power (v3.1)[60] to detect size effect in a post-hoc test with type 1 and 2 error rates of 5 and 20%, respectively. Mice were allocated to vehicle or treatment groups using a randomization procedure (http://www.randomizer.org/). Four independent and blinded investigators performed the treatments, behavioral experiments, genotyping and data analysis, respectively. No animals were excluded from experiments.

The behavioral studies followed the animal research reporting in vivo experiment (ARRIVE) guidelines[61]. Mice were housed in a temperature (20 ± 2 °C) and humidity (50 ± 10%) controlled vivarium (12 h dark/light cycle, free access to food and water, five animals per cage). At least 1 h before behavioral experiments, mice were acclimatized to the experimental room and behavior was evaluated between 9:00 am and 5:00 pm. All the procedures were conducted following the current guidelines for laboratory animal care and the ethical guidelines for investigations of experimental pain in conscious animals set by the International Association for the Study of Pain[62]. Animals were anesthetized with a mixture of ketamine and xylazine (90 mg/kg and 3 mg/kg, respectively, i.p.) and euthanized with inhaled CO_2 plus 10–50% O_2.

Cell lines. Primary cultures of human Schwann cells (HSCs, #1700, ScienCell Research Laboratories) were grown and maintained in Schwann cell medium (#1701, ScienCell Research Laboratories) at 37 °C in 5% CO_2 and 95% O_2. Cells were passaged at 90% confluency and discarded after 12 passages. HEK293T (#CRL-3216™, American Type Culture Collection) cells were cultured in Dulbecco's Modified Eagle's Medium (DMEM) supplemented with heat-inactivated fetal bovine serum (FBS, 10%), L-glutamine (2 mM), penicillin (100 U/ml) and streptomycin (100 mg/ml) at 37 °C in 5% CO_2 and 95% O_2. The mouse Schwann cell

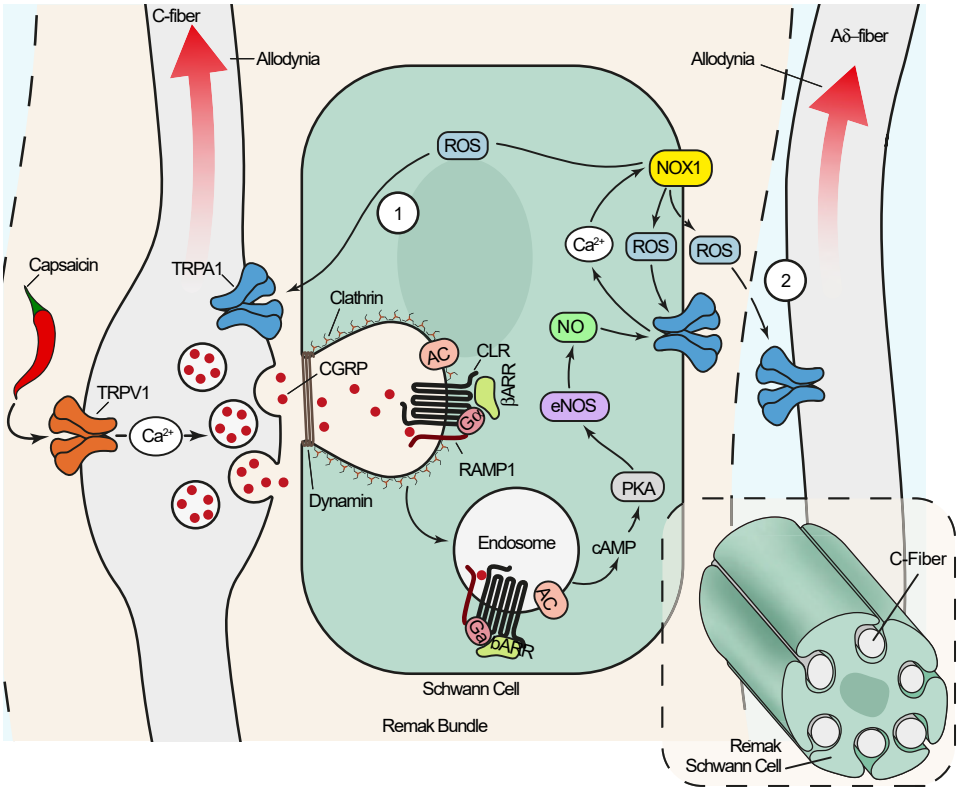

Fig. 9 Schematic representation of the pathway that signal prolonged cutaneous allodynia elicited by CGRP released and associated with neurogenic inflammation. The pro-migraine neuropeptide, CGRP, released from trigeminal cutaneous afferents, activates CLR/RAMP1 on Schwann cells. CLR/RAMP1 traffics to endosomes, where sustained G protein signaling increases cAMP and stimulates PKA that results in nitric oxide synthase activation. The ensuing release of nitric oxide targets the oxidant-sensitive channel, TRPA1, in Schwann cells, which elicits persistent ROS generation. ROS triggers TRPA1 on adjacent C- (1) or Aδ-fiber (2) afferents resulting in periorbital allodynia, a hallmark of migraine pain. The inset shows several unmyelinated axons invaginated into a Schwann cell forming a Remak bundle.

line (IMS32 cells, #PMC-SWN-IMS32-COS, Cosmo Bio USA) was grown and maintained in Schwann cell medium (#PMC-SWN-MM-COS, Cosmo Bio USA) at 37 °C in 5% CO_2 and 95% O_2[63,64]. All cells were used when received without further authentication.

Pharmacological reagents. Supplementary Table 1 and 2 provide doses, routes of administration and concentrations and of all pharmacological reagents.

Behavioral experiments

Treatment protocol. Subcutaneous injections were made in the periorbital area 2–3 mm from the external eyelid corner[17]. Briefly, the mouse was lifted by the base of the tail and placed on a solid surface with one hand and the tail was pulled back. Then, it was quickly and firmly picked up by the scruff of the neck with the thumb and index finger of the other hand. The injection was made rapidly by a single operator with minimal animal restraint. Mice received unilateral (right side) injections (10 µl/site) of CGRP (1.5 nmol in 0.9% NaCl), SP (3.5 nmol in 0.9% NaCl), capsaicin (10, 50, 100 pmol in 0.1% dimethyl sulfoxide, DMSO), or vehicles (control). Mice received bilateral injections (10 µl/site, right side same site as stimulus, left side symmetrical to right side) of antagonists and inhibitors. CGRP (1.5 nmol in 0.9% NaCl) or vehicle was also administered by intraplantar (i.pl., 20 µl/site) or systemic (0.1 mg/kg, i.p.) injection. GTN was administered at 10 mg/kg, i.p. injection.

Acute nociception. Immediately after the p.orb. injection, mice were placed inside a plexiglass chamber and spontaneous nociception was assessed for 10 min by measuring the time (s) that the animal spent rubbing the injected area of the face with its paws[17,65].

Periorbital mechanical allodynia. PMA was assessed using the up-down paradigm[66,67] in the same mice in which acute nociceptive responses were monitored. Briefly, mice were placed in a restraint apparatus designed for the evaluation of periorbital mechanical thresholds[17]. One day before the first behavioral observation, mice were habituated to the apparatus. PMA was evaluated in the periorbital region over the rostral portion of the eye (i.e., the area of the periorbital region facing the sphenoidal rostrum)[68] before (basal threshold) and after (0.5, 1, 2, 4, 6, 8 h) treatments. On the day of the experiment, after 20 min of adaptation inside the chamber, a series of 7 von Frey filaments in logarithmic increments of force (0.02, 0.04, 0.07, 0.16, 0.4, 0.6, and 1.0 g) were applied to the periorbital area perpendicular to the skin, with sufficient force to cause slight buckling, and held for approximately 5 s to elicit a positive response. Mechanical stimuli were applied homolaterally outside the periorbital area at a distance of 6–8 mm from the site where stimuli were injected. The response was considered positive by the following criteria: mouse vigorously stroked its face with the forepaw, head withdrawal from the stimulus, or head shaking. Mechanical stimulation started with the 0.16 g filament. The absence of response after 5 s led to the use of a filament with increased force, whereas a positive response led to the use of a weaker (*i.e.* lighter) filament. Six measurements were collected for each mouse or until four consecutive positive or negative responses occurred. The 50% mechanical withdrawal threshold (expressed in g) was then calculated from these scores by using a δ value of 0.205, previously determined.

Paw mechanical allodynia. Paw mechanical allodynia was evaluated by measuring the paw withdrawal threshold by using the up-down paradigm[66,67]. Mice were acclimatized (1 h) in individual clear plexiglass boxes on an elevated wire mesh platform, to allow for access to the plantar surfaces of the hind paws. von Frey filaments of increasing stiffness (0.07, 0.16, 0.4, 0.6, and 1.0, 1.4 and 2 g) were applied to the hind paw plantar surfaces of mice with enough pressure to bend the filament. The absence of a paw being lifted after 5 s led to the use of the next filament with an increased force, whereas a lifted paw indicated a positive response, leading to the use of a subsequently weaker filament. Six measurements were collected for each mouse or until four consecutive positive or negative responses occurred. The 50% mechanical withdrawal threshold (expressed in g) was then calculated.

Primary culture of mouse Schwann cells. Mouse Schwann cells (MSC) were isolated from sciatic or trigeminal nerves of C57BL/6 J, and from sciatic nerve of *Trpa1*$^{+/+}$ and *Trpa1*$^{-/-}$, *Plp1-Cre*$^{ERT+}$;*Ramp1*$^{fl/fl}$ and *Plp1-Cre*$^{ERT-}$;*Ramp1*$^{fl/fl}$ mice[30,69]. The epineurium was removed, and nerve explants were divided into 1 mm segments and dissociated enzymatically using collagenase (0.05%) and hyaluronidase (0.1%) in Hank's Balanced Salt Solution (HBSS, 2 hr, 37 °C). Cells were collected by centrifugation (150xg, 10 min, room temperature) and the pellet was resuspended

and cultured in DMEM containing fetal calf serum (10%), L-glutamine (2 mM), penicillin (100 U/ml), streptomycin (100 mg/ml), neuregulin (10 nM) and forskolin (2 μM). Three days later, cytosine arabinoside (Ara-C, 10 mM) was added to remove fibroblasts. Cells were cultured at 37 °C in 5% CO_2 and 95% O_2. The culture medium was replaced every 3 days and cells were used after 15 days of culture.

qRT-PCR. Total RNA was extracted from HSCs, IMS32 and sciatic or trigeminal MSCs cells using the RNeasy Mini kit (Qiagen SpA), according to the manufacturer's protocol. RNA concentration and purity were assessed spectrophotometrically by measuring the absorbance at 260 nm and 280 nm. RNA was reverse transcribed with the Qiagen QuantiTect Reverse Transcription Kit (Qiagen SpA) following the manufacturer's protocol. For mRNA relative quantification, rt-PCR was performed on Rotor Gene® Q (Qiagen SpA, Rotor-Gene® Q- Software Version 2.3.1.49). The relative abundance of mRNA transcripts was calculated using the delta CT method and normalized to GAPDH levels. The sets of primers for human and mouse cells are listed in the Supplementary Table 3.

Calcium imaging. HSCs, IMS32 and sciatic nerve MSCs cells were plated on poly-L-lysine-coated (8.3 μM) 35 mm glass coverslips and maintained at 37 °C in 5% CO_2 and 95% O_2 for 24 h. Cells were loaded (40 min) with Fura-2 AM-ester (5 μM) added to the buffer solution (37 °C) containing (in mM) 2 $CaCl_2$; 5.4 KCl; 0.4 $MgSO_4$; 135 NaCl; 10 D-glucose; 10 HEPES and bovine serum albumin (BSA, 0.1%) at pH 7.4. Cells were washed and transferred to a chamber on the stage of a fluorescent microscope for recording (Olympus IX 81) and exposed to CGRP (0.01–10 μM) or vehicle (0.9% NaCl) and the Ca^{2+} response was monitored for approximately 40 min. In another set of experiments, IMS32 cells were exposed to AITC (30 μM) or vehicle (0.03% DMSO). The Ca^{2+} response to CGRP was monitored in the presence of CGRP8-37 (100 nM), olcegepant (100 nM), SQ22536 (100 μM), L-NAME (10 μM), A967079 (50 μM), PBN (50 μM), H89 (1 μM), ML171 (1 μM) or vehicle (0.1 % DMSO), and in the presence of DIPMA-MK-3207 (1–1000 nM) and MK-3207 free drug (0.01–1000 μM) or DIPMA-empty. Cells were preincubated with DIPMA-MK-3207 or MK-3207 for 20 min at room temperature to allow nanoparticle accumulation in endosomes. Some experiments used Ca^{2+}-free buffer solution containing EDTA (1 mM). Results were expressed as percent increase in $ratio_{340/380}$ over baseline normalized to the maximum effect induced by ionomycin (5 μM) added at the end of each experiment.

Protein extraction and western immunoblot assay. HSCs and IMS32 cells were plated on 60 mm culture dish and maintained in 5% CO_2 and 95% O_2 (37 °C, until confluence). HSCs and IMS32 cells were homogenized in RIPA buffer [NaCl (150 mM), Tris-base (50 mM), EGTA (5 mM), Triton X-100 (1%), sodium deoxycholate (0.5%), sodium dodecyl sulfate (0.1%)] containing dithiothreitol (1 mM) and complete protease inhibitor cocktail. Lysates were centrifuged at 16,128x *g* at 4 °C for 10 min. Protein concentration in supernatants was determined using BCA protein assay (Thermo Scientific). Samples with equal amounts of proteins (20 μg) were then separated by NuPAGE 4–12% bis-tris gel electrophoresis (Life Technologies), and the proteins were transferred to a nitrocellulose (Bio-Rad). Membranes were incubated with dry milk (5%) in Tris buffer [(TBST; Tris (20 mM) at pH 7.5, NaCl (150 mM)] containing Tween 20 (0.1%) for 1 h at room temperature, and incubated with the following primary antibodies: RAMP1 [ERP10867] (#ab156575, rabbit monoclonal, 1:1000, Abcam, Lot: GR3196403-5), CRLR (#NBP1-59073, rabbit polyclonal, 1:500, Novus Biological, Lot: 8312) or β-actin (#ab6276, mouse monoclonal, 1:5000, Abcam, Lot: GR 141-7) at 4 °C overnight. Membranes were then probed with goat anti-mouse or donkey antirabbit IgG conjugated with horseradish peroxidase (HRPO, 1:10,000, Bethyl Laboratories Inc., Cat#A90-516P and Cat#A120-208P) for 2 hr at room temperature. Finally, membranes were washed three times with TBST, and bound antibodies were detected using chemiluminescence reagents (Pierce™ ECL, Thermo Scientific), and revealed using an imaging system (ChemiDoc version 2.3.0.07 BioRad). The density of specific bands was measured using an image processing program (ImageJ 1.32 J, National Institutes of Health) and normalized to β-actin.

In-cell ELISA assay. HSCs or IMS32 cells were plated in 96-well black wall clear bottom plates (Corning Life Sciences) (5×10^5 cells/well) and maintained at 37 °C in 5% CO_2 and 95% O_2 for 24 h. HSCs and IMS32 cells were exposed to CGRP (1 and 10 μM, respectively) or its vehicle (phosphate-buffered saline, PBS) for 5, 10, 15, 30 and 60 min, at 37 °C, then washed with DMEM pH 2.5 and fixed in 4% paraformaldehyde for 30 min. Cells were then washed with TBST (0.05%) and blocked with donkey serum (5%) for 4 h at room temperature and incubated overnight 4 °C with $eNOS^{pS1177}$ (#ab184154, rabbit polyclonal, 1:100, Abcam, Lot: GR3257047-9). Cells were then washed and incubated with donkey anti-rabbit IgG conjugated with horseradish peroxidase (HRPO, 1:2000, Bethyl Laboratories Inc.) for 2 h at room temperature. Cells were then washed and stained using SIGMA-FAST OPD for 30 min protected from light. After the incubation period, the absorbance was measured at 450 nm. Change in NOS3 phosphorylation was calculated as a percentage of the signal in vehicle-treated cells.

cAMP ELISA assay. cAMP level was determined by the CatchPoint™ cyclic-AMP fluorescent assay kit (#R8088, Molecular Device) according to the manufacturer's protocol. Briefly, HSCs or IMS32 cells were plated in 96-well black wall clear bottom plates (Corning Life Sciences) (5×10^5 cells/well) and maintained in 5% CO_2 and 95% O_2 (24 h, 37 °C). The cultured medium was replaced with HBSS added with olcegepant (100 nM), CGRP8-37 (100 nM), SQ22536 (100 μM), L-NAME (10 μM) or vehicle (0.1% DMSO in HBSS) for 20 min at room temperature. HSCs or IMS32 cells were then stimulated with CGRP (1 and 10 μM, respectively), forskolin (1 μM, positive control) or their vehicles (HBSS) and maintained for 40 min at room temperature protected from light. Signal was detected 60 min after exposure to the stimuli. cAMP level was calculated using cAMP standards and expressed as nmol/1.

Nitric oxide assay. Nitric oxide was determined by using the fluorometric-orange assay kit (#ab219932, Abcam) according to the manufacturer's protocol. HSCs or IMS32 cells were plated 96-well black wall clear bottom plates (Corning Life Sciences) (5×10^5 cells/well) and maintained in 5% CO_2 and 95% O_2 (24 h, 37 °C). The cultured medium was replaced with Hanks' balanced salt solution (HBSS) added with olcegepant (100 nM), CGRP8-37 (100 nM), SQ22536 (100 μM), L-NAME (10 μM), A967079 (50 μM), PS2 or Dy4 (both 30 μM), PS2 inact or Dy4 inact (30 μM) or vehicle (0.1% DMSO in HBSS) for 20 min at room temperature. HSCs or IMS32 cells were then stimulated with CGRP (1 and 10 μM, respectively), diethylamine NONOate (1 mM, positive control) or their vehicles (HBSS) and maintained for 40 min at room temperature protected from light. Signal was detected 60 min after exposure to the stimuli. Change in nitric oxide level was calculated as percentage of the vehicle.

H_2O_2 assay. H_2O_2 was determined by using the Amplex Red assay (#A12222, Thermo Fisher, Invitrogen). HSCs or IMS32 cells were plated in 96-well black wall clear bottom plates (Corning Life Sciences) (5×10^5 cells/well) and maintained in 5% CO_2 and 95% O_2 (24 h, 37 °C). The cultured medium was replaced with Krebs-Ringer phosphate (KRP, composition in mM: 2 $CaCl_2$; 5.4 KCl; 0.4 $MgSO_4$; 135 NaCl; 10 D-glucose; 10 HEPES [pH 7.4]) added with olcegepant (100 nM), CGRP8-37 (100 nM), SQ22536 (100 μM), L-NAME (10 μM), A967079 (50 μM), PBN (50 μM) or vehicle (0.1% DMSO in KRP) for 20 min at room temperature. HSCs or IMS32 cells were then stimulated with CGRP (1 and 10 μM, respectively) or its vehicle (KRP) added with Amplex red (50 μM) and horseradish peroxidase (HRP, 1 U/ml) and maintained for 40 min at room temperature protected from light. Some experiments were performed in Ca^{2+}-free KRP containing EDTA (1 mM). Signal was detected 60 min after exposure to the stimuli. H_2O_2 release was calculated using H_2O_2 standards and expressed as nmol/1.

Immunofluorescence. Anesthetized mice were transcardially perfused with PBS and 4% paraformaldehyde. Trigeminal and sciatic nerves were removed, postfixed for 24 h, and paraffin-embedded. Human and mouse formalin-fixed paraffin-embedded (FFPE) sections (5 μm) were incubated with primary antibodies: TRPA1 (#ab58844, rabbit polyclonal, 1:400, Abcam, Lot: GR165165-21), S100 (#ab14849, mouse monoclonal [4B3], 1:300, Abcam, Lot: GR3233892-2), CLR (#NLS6731, rabbit polyclonal, 1:30, Novus Biologicals, Lot: QC58878-190422), RAMP1- Alexa Fluor 594 (#ab241335, rabbit polyclonal, 1:200, Abcam Lot: GR3247267-4), diluted in fresh blocking solution (PBS, pH 7.4, 2.5% normal goat serum, [NGS]). Sections were then incubated with the fluorescent polyclonal secondary antibodies Alexa Fluor 488 and 555 (#A32731, Lot: VA295501, #A32727, Lot: UL287768, 1:600; Invitrogen), and coverslipped using the mounting medium with DAPI (Abcam). Images were acquired by a Zeiss Axio Imager 2, Zeiss ZEN imaging 2020. The Pearson correlation (Rcoloc) value for RAMP1 and S100 in the colocalization studies were calculated using the colocalization Plugin of the ImageJ software (ImageJ 1.32 J, National Institutes of Health).

cAMP cADDIS assay. HSCs were plated on poly-D-lysine-coated 96-well black wall clear bottom plates (Corning Life Sciences) (25×10^3 cells/well) and incubated in 5% CO_2 and 95% O_2 for 4–6 h. HSCs were transduced with the baculovirus mediated Green Upward cADDIS cAMP reporter (25 μl/well, Montana Molecular) following manufacturer's instructions, and cells were incubated in 5% CO_2 and 95% O_2 (48 h, 37 °C). HSCs were washed twice in HBSS plus HEPES (10 mM) pH 7.4. Cells were incubated in HBSS/HEPES with the CLR/RAMP1 antagonists olcegepant (100 pM–100 μM) or vehicle (control) for 30 min. Plates were mounted in a FlexStation3 plate reader (Molecular Devices) and fluorescence (485–500 excitation, 515–530 emission with cutoff at 510) was monitored. The baseline was measured for 1 min, and cells were stimulated with human CGRPα (100 pM-10 μM) or forskolin (10 μM, positive control). For single-cell imaging, HSCs were plated on poly-D-lysine-coated 35 mm glass-bottom dishes (MatTek, Ashland) (40×10^3 cells/dish) and incubated in 5% CO_2 and 95% O_2 (overnight, 37 °C). HSCs cells were transduced with Green Upward cADDIS and incubated for 48 h. HSCs were washed twice in HBSS/HBS and mounted on a Leica DMI8 microscope (Wetzlar, Germany). Fluorescence (470/40 excitation, 527/30 emission) was measured every 5 s. The baseline was measured for 30 s, and HSCs were challenged with human CGRPα (100 nM). Images were analyzed with ImageJ (NIH). To inhibit endocytosis, cells were incubated in HBSS containing 0.45 M sucrose or normal HBSS (control) for 30 min at 37 °C before cAMP assays.

CAMYEL BRET cAMP assay. HEK293T cells stably expressing the CAMYEL BRET sensor (~2×10^6) were seeded into 90 mm Petri dish (Corning™, USA) in DMEM/FBS/

Geneticin and incubated in 5% CO_2 and 95% O_2 (24 h, 37 °C). Prior to the transfection, the medium was changed to fresh DMEM/FBS/Geneticin and rat CLR/RAMP1 was transfected (2.5 µg CLR/RAMP1 DNA/dish) using JetPEI (Polyplus Transfection, France) at a 1:6 ratio. After 24 h, cells were plated in poly-L-lysine coated black 96 well CulturPlate (Perkin Elmer, USA) and incubated in 5% CO_2 and 95% O_2 (24 h, 37 °C). BRET was assessed using a LUMIstar (BMG LABTECH, Germany). On the day of the assay, cells were equilibrated in HBSS for 30 min, supplemented with 12 mM HEPES at 37 °C in CO_2-free incubator. DIPMA-MK-3207 or free MK-3207 was incubated for 25 min, followed by the addition of coelentrazine-h (50 µM) for 5 min. Baseline was then measured for 5 min, followed by stimulation with CGRP (100 nM, ~EC_{50}), vehicle (HBSS) or forskolin (1 µM, positive control), and further measurements for 5 min. Buffer was then replaced by HBSS with coelentrazine-h (50 µM) and measurements were resumed for further 25 min.

Synthesis of TAMRA-CGRP and endocytosis of TAMRA-CGRP and Cy5-DIPMA nanoparticles. TAMRA-CGRP was synthesized by JPT Peptide Technologies (Berlin, Germany). A lysine residue conjugated to TAMRA was added to the C-terminus of human CGRPα (A1CDTATCVTHRLAGLLSRSGGVVKNNFVPT NVGSKAF37-K-TAMRA). Peptide purity was > 94%. HSCs were plated on poly-D-lysine-coated 35 mm glass-bottom dishes (MatTek) (50×10^3 cells/dish) and incubated in 5% CO_2 and 95% O_2 (overnight, 37 °C). HSCs were transduced with the BacMan CellLight Early Endosomes Rab5a-GFP marker (5 µl/dish) and incubated in 5% CO_2 and 95% O_2 (48 h, 37 °C). HSCs were washed twice in HBSS/HEPES. Cells were incubated with the endocytosis inhibitors PS2 or Dy4 (both 30 µM), PS2 inact or Dy4 inact (30 µM), sucrose (0.45 M) or vehicle (control) for 30 min. Cells were imaged using Leica SP8 confocal microscope (Wetzlar), LAS X imaging software. Images were captured every 15 s. Baseline fluorescence was recorded for 2 min. TAMRA-CGRP (1 µM) was added and cells were imaged for 30 min. TAMRA-CGRP internalization to early endosomes at 30 min was quantified using ImageJ (National Institutes of Health). Regions of interest (ROIs) were defined by thresholding the channel for early endosomes (GFP) and particles were analyzed for size (≥0.2 μm^2) and for roundness (0.2–1). ROIs were then overlayed on the TAMRA-CGRP channel and mean fluorescence was quantified for each ROI. Data are presented as relative fluorescent units (RFUs) per endosome and percentage of CGRP- + ve endosomes (endosomes with TAMRA-CGRP fluorescence >350 RFU) to total endosomes. Imaging experiments were repeated 5–7 times per group and a minimum of 4 cells were imaged for each experiment. To assess the internalization nanoparticles, HSCs were plated as described and incubated with DIPMA-Cy5 nanoparticles (40–60 µg/ml) for 1 h. Cells were washed and imaged as stated.

EbBRET assays of G protein and βARR recruitment to the plasma membrane and endosomes cDNAs. Mini-G proteins coupled to Venus were from N. A. Lambert (Augusta University). Constructs were modified to replace Venus with Rluc8. *Renilla* (R) GFP-CAAX (prenylation CAAX box of KRas), tdRGFP-Rab5a, Rluc2-βARR2 and human CLR-Rluc8 were from M. Bouvier (Université de Montréal).

Transfection. For EbBRET assays of trafficking of mini-G proteins to the plasma membrane or early endosomes, HEK293T cells were transfected using JetPEI (Polyplus Transfection, France) with bicistronic human myc-CLR-NanoBiT/HA-RAMP1 (0.2 µg) (NanoBiT: GVTGWRLCERILA) and Rluc8-m$G\alpha_{si/s/sq}$ (0.1 µg)[70,71] and either RGFP-CAAX (0.2 µg)[72] for cell surface activation or tdRGFP-Rab5a (0.15 µg) for activation in early endosomes. Schwann cells were transfected using lipofectamine 3000 with bicistronic human myc-CLR-NanoBiT/HA-RAMP1 (1 µg) and Rluc8-m$G\alpha_{si/s/sq}$ (2 µg) and either RGFP-CAAX (1.5 µg) or tdRGFP-Rab5a (1.5 µg). For EbBRET assays of recruitment of βARR2[72] to the plasma membrane or early endosomes, HEK293T cells were transfected with JetPEI with bicistronic human myc-CLR-NanoBiT/HA-RAMP1 (0.2 µg) and Rluc2-βARR2 (0.1 µg) and RGFP-CAAX (0.2 µg) for plasma membrane recruitment or tdRGFP-Rab5a (0.15 µg) for early endosome recruitment. Schwann cells were transfected using lipofectamine 3000 with bicistronic human myc-CLR-NanoBiT/HA-RAMP1 (1 µg) and Rluc2-βARR2 (2 µg) and RGFP-CAAX (1.5 µg) or tdRGFP-Rab5a (1.5 µg). For EbBRET assay of trafficking of CLR from the plasma membrane to early endosomes, HEK293T cells were transfected using JetPEI with human myc-CLR-Rluc8 (0.7 µg), human myc-RAMP1 (0.5 µg) and either plasma membrane marker RGFP-CAAX (0.2 µg) or early endosome marker tdRGFP-Rab5a (0.15 µg).

BRET assays. HEK293T cells and HSCs were washed with HBSS buffer complemented with 10 mM HEPES at pH 7.4. Prolume Purple Coelenterazine (2.5 µM, NanoLight Technology) was added, and cells were incubated for 5 min at 37 °C. EbBRET was recorded for 22.5 min in a Synergy Neo2 Microplate reader (BioTek) (acceptor filter: 515 ± 30 nm; donor filter: 410 ± 80 nm). The baseline was measured for 2.5 min, and cells were challenged with human CGRPα (100 nM) or vehicle. ΔBRET represents the EbBRET signal in the presence of agonist subtracted by the EbBRET signal in the presence of the vehicle. To inhibit endocytosis, cells were incubated in HBSS containing 0.45 M sucrose or normal HBSS (control) for 30 min at 37 °C before EbBRET assays.

Synthesis and Characterization of Nanoparticles

Synthesis of P(PEGMA-co-DMAEMA)-b-P(DIPMA-co-DEGMA). The polymer was synthesized in a two-step sequential polymerization by the reversible addition-fragmentation chain (RAFT) method[73], as previously described[34]. First, the hydrophilic block, P(PEGMA-co-DMAEMA), was synthesized using the RAFT agent, 2-cyanoprop-2-yl dithiobenzoate (CPBD, 0.0736 g, 3.34×10^{-4} mol) and the initiator azobisisobutyronitrile (AIBN, 0.0054 g, 3.34×10^{-5} mol) in a ratio of 1:0.1. The monomers poly(ethylene glycol) monomethyl ether methacrylate (PEGMA, 6 g, 0.02 mol) and 2-[*N,N*-(dimethylamino)ethyl] methacrylate (DMAEMA, 0.314 g, 0.001 mol) were used at a ratio of 10:1. The mixture, dissolved in toluene, was deoxygenated by sparging with nitrogen and left to react at 70 °C, 75x *g* for 21 h. The remaining monomers were removed by dialysis (MWCO 3500, Membrane Filtration Products) against acetone for 96 h and the final product was dried for 24 h in a vacuum oven at 37 °C and 1 mbar.

The chain extension reaction to incorporate the monomers 2-[*N,N*-(diisopropylamino)ethyl] methacrylate (DIPMA) and di(ethylene glycol) methyl ether methacrylate (DEGMA) was initiated by AIBN (0.0009 g, 5.35×10^{-6} mol), using the hydrophilic block P(PEGMA-co-DMAEMA, 0.4455 g, 3.56×10^{-5} mol) and the monomers DIPMA (0.7603 g, 3.56×10^{-3} mol) and DEGMA (0.0738 g, 3.92×10^{-4} mol), at a ratio of 0.15:1:100:11. The mixture was dissolved in toluene, deoxygenate d and left to react at 70 °C, 75 × *g* for 17.5 h. The final product, P(PEGMA-co-DMAEMA)-b-P(DIPMA-co-DEGMA), was purified as described above.

Synthesis of P(PEGMA-co-DMAEMA)-b-P(DIPMA-co-DEGMA-co-Cy5). The chain extension of P(PEGMA-co-DMAEMA, 0.5 g, 3.85×10^{-5} mol) was done in toluene by adding DIPMA (0.82 g, 3.85×10^{-3} mol), DEGMA (0.080 g, 4.23×10^{-4} mol) and 4,4-dimethyl-2-vinyl-2-oxazolin-5-one (VDM, 0.027 g, 1.92×10^{-4} mol), in the presence of AIBN (1 mg, 5.77×10^{-6} mol) at a ratio of 1:100:11:5:0.15. The mixture was deoxygenated and left to react at 70 °C, 75 xg for 18 h. Cy5 coupling was performed by mixing 250 µl of the reaction with Cyanine5 amine (Cy5, 0.008 g, 1.20×10^{-5} mol). The mixture was left to react at room temperature, 75x *g* for 72 h under dark conditions and the final product was purified as described above.

Analysis of diblock copolymer

Gel permeation chromatography (GPC). The molecular weights of polymers were determined by GPC using a liquid chromatography system equipped with a (RID-10A) differential refractive index detector ($\lambda = 633$ nm) and SPD-20A ultraviolet detector (Shimadzu). Samples were fractionated using 5.0 µm bead-size guard column (50 × 7.8 mm) and three Shodex KF-805L columns (300 × 8 mm, 10 µm $n =$ bead-size, 5000 Å pore size) in series at 40 °C and eluted in *N,N*-dimethylacetamide (DMAC, HPLC grade, with 0.03% w/v LiBr) at a flow rate of 1 ml/min. A molecular weight calibration curve was produced using polystyrene standards ranging from 500 to 2×10^6 Da.

Proton-nuclear magnetic resonance (^{1}H-NMR). The conversion and composition of polymers were assessed by ^{1}H-NMR using a Bruker Avance III 400 Ultrashield Plus spectrometer (USA) at 400 mHz running Topspin, version 1.3 and deuterated chloroform (chloroform-d) as solvent. Conversions (Conv%) and repeating monomer units (n) were calculated using peak integrals (I) where the subscript number indicates the location of the peak in ppm (I_x). The Conv% were calculated using the ^{1}H-NMR spectra before starting the reactions ($t = 0$) and after the reactions were stopped ($t = f$) (^{1}H-NMR spectra not shown), with $Conv\% = \left(1 - \left(\frac{I_{6.24(t=f)}}{I_{6.24(t=0)}}\right)\right) \times 100$. For P(PEGMA-co-DMAEMA), n was calculated using the ^{1}H-NMR spectra with $n_{PEGMA} = \frac{I_{4.25} - I_{2.5}}{I_{7.8-7.9}}$ and $n_{DMAEMA} = \frac{I_{2.5}}{I_{7.8-7.9}}$. For P(PEGMA-co-DMAEMA)-b-(DIPMA-co-DEGMA), n were calculated using the ^{1}H-NMR spectra with $n_{DIPMA} = \frac{I_3 + I_{2.6}}{2 \times I_{4-4.}} \times (n_{PEGMA} + n_{DMAEMA})$ and $n_{DEGMA} = \frac{I_{3.396}}{I_{3.378}} \times n_{PEGMA}$ (Supplementary Fig. 6) For P(PEGMA-co-DMAEMA)-b-(DIPMA-co-DEGMA-co-VDM), n was calculated as described for P(PEGMA-co-DMAEMA)-b-(DIPMA-co-DEGMA) (^{1}H-NMR spectra not shown).

Self-assembly of nanoparticles (NPs). The diblock copolymer, P(PEGMA-co-DMAEMA)-b-P(DIPMA-co-DEGMA) was used to self-assemble pH-responsive NPs. For the self-assembly of NPs loaded with MK-3207 (DIPMA- MK-3207) a mixture of 5 mg of the diblock copolymer and 53.5 µg of MK-3207 was dissolved in 0.5 ml of dimethylformamide (DMF). Empty NPs (DIPMA-Ø) were self-assembled without adding MK-3207. The mixture was then added into 4.5 ml of PBS under stirring at a flow rate of 1.2 ml/h, using a syringe pump (Harvard Apparatus). Assemblies of DIPMA-MK-3207 and DIPMA-Ø were dialyzed against PBS for 24 h (MWCO 3500, Membrane Filtration Products). The assembly of NPs for live-cell imaging and biodistribution studies was done as described for DIPMA-Ø using the diblock copolymer P(PEGMA-co-DMAEMA)-b-P(DIPMA-co-DEGMA-co-Cy5), which couples Cy5 on the hydrophobic block, resulting in NPs with Cy5 incorporated in the core (DIPMA-Cy5).

Characterization of NPs

Dynamic light scattering (DLS). The size distribution of DIPMA-MK-3207 and DIPMA-Ø (1 mg/ml) was determined by DLS (Zetasizer Nano ZS ZEN3600 particle size analyser), using polystyrene cuvettes at 25 °C and 173° backscatter angle.

Ultra-performance liquid chromatography-mass spectrometry (LC-MS). MK-3207 loading into the core of NPs was assessed by LC-MS using a Waters Micromass Quattro Premier triple quadrupole mass spectrometer coupled to a Waters Acquity UPLC (USA). Freeze-dried DIPMA- MK-3207 (1 ml, 1 mg/ml) were dissolved in a mixture of DMSO and formic acid 0.1% (5:2). The samples were prepared for analysis by mixing an aliquot of each preparation with internal standard solution (diazepam, 5 µg/ml) in a 5:2 proportion and made up to 500 µl with the dilution solvent (acetonitrile 50%: formic acid 0.1%, 1:1). Samples were fractionated on a Supelco Ascentis Express RP Amide column (50 mm by 2.1 mm, 2.7 µm particle size) equipped with a Phenomenex SecurityGuard precolumn fitted with a Synergi Polar cartridge, maintained at 40 °C. MK-3207 loading was quantified against MK-3207 standards (0.016–20 µM). Compounds were eluted under gradient conditions with a mobile phase of formic acid (0.05%) and acetonitrile. Mass spectrometry was conducted in positive electrospray ionization conditions and elution of compounds were monitored with multiple-reaction monitoring.

Transmission electron microscopy (TEM). The morphology of NPs was determined by TEM imaging using a Tecnai F20 transmission electron microscope at an accelerating voltage of 120 kV at room temperature. Carbon-coated grids were prepared by plasma discharge (35 s). DIPMA-MK-3207 samples (5 µl, 1 mg/ml) were placed on the grid for 20 s. Samples were negatively stained with uranyl acetate (5 µl, 0.5 wt %, 25 s).

Statistical analysis. Results are expressed as mean ± standard error of the mean (SEM). For multiple comparisons, a one-way analysis of variance (ANOVA) followed by the post-hoc Bonferroni's test or Dunnett's test was used. Two groups were compared using Student's *t*-test. For behavioral experiments with repeated measures, the two-way mixed model ANOVA followed by the post-hoc Bonferroni's test was used. Statistical analyses were performed on raw data using Graph Pad Prism 8 (GraphPad Software Inc.). IC_{50} values and confidence intervals were determined from non-linear regression models using Graph Pad Prism 8 (GraphPad Software Inc.). *P* values less than 0.05 ($P < 0.05$) were considered significant. Statistical tests used and the sample size for each analysis are listed in the Fig. legend.

Reporting Summary. Further information on research design is available in the Nature Research Reporting Summary linked to this article.

Data availability

Source data are provided with this paper.

Received: 28 July 2021; Accepted: 14 January 2022
Published online: 03 February 2022

References

1. Lewis, T. Experiments Relating to Cutaneous Hyperalgesia and Its Spread Through Somatic Nerves. *Clin. Sci.* **2**, 373–414 (1936).
2. Russell, F. A., King, R., Smillie, S. J., Kodji, X. & Brain, S. D. Calcitonin gene-related peptide: physiology and pathophysiology. *Physiol. Rev.* **94**, 1099–1142 (2014).
3. Geppetti P., Holzer P. Neurogenic Inflammation. Boca Raton (1996).
4. Szallasi, A. & Blumberg, P. M. Vanilloid (Capsaicin) receptors and mechanisms. *Pharmacol. Rev.* **51**, 159–212 (1999).
5. Steinhoff, M. S., von Mentzer, B., Geppetti, P., Pothoulakis, C. & Bunnett, N. W. Tachykinins and their receptors: contributions to physiological control and the mechanisms of disease. *Physiol. Rev.* **94**, 265–301 (2014).
6. La, J. H. et al. Differential involvement of reactive oxygen species in a mouse model of capsaicin-induced secondary mechanical hyperalgesia and allodynia. *Mol. Pain.* **13**, 1744806917713907 (2017).
7. Ali, Z., Meyer, R. A. & Campbell, J. N. Secondary hyperalgesia to mechanical but not heat stimuli following a capsaicin injection in hairy skin. *Pain* **68**, 401–411 (1996).
8. Sinclair, S. R. et al. Inhibition of capsaicin-induced increase in dermal blood flow by the oral CGRP receptor antagonist, telcagepant (MK-0974). *Br. J. Clin. Pharmacol.* **69**, 15–22 (2010).
9. Edvinsson, L., Haanes, K. A., Warfvinge, K. & Krause, D. N. CGRP as the target of new migraine therapies - successful translation from bench to clinic. *Nat. Rev. Neurol.* **14**, 338–350 (2018).
10. Ashina, H. Migraine. *N. Engl. J. Med.* **383**, 10 (2020).
11. Doods, H., Arndt, K., Rudolf, K. & Just, S. CGRP antagonists: unravelling the role of CGRP in migraine. *Trends Pharmacol. Sci.* **28**, 580–587 (2007).
12. Hostetler, E. D. et al. In vivo quantification of calcitonin gene-related peptide receptor occupancy by telcagepant in rhesus monkey and human brain using the positron emission tomography tracer [11C]MK-4232. *J. Pharmacol. Exp. Ther.* **347**, 478–486 (2013).
13. Noseda, R. et al. Fluorescently-labeled fremanezumab is distributed to sensory and autonomic ganglia and the dura but not to the brain of rats with uncompromised blood brain barrier. *Cephalalgia* **40**, 229–240 (2020).
14. Johnson, K. W., Morin, S. M., Wroblewski, V. J. & Johnson, M. P. Peripheral and central nervous system distribution of the CGRP neutralizing antibody [(125)I] galcanezumab in male rats. *Cephalalgia* **39**, 1241–1248 (2019).
15. Mogil, J. S. et al. Variable sensitivity to noxious heat is mediated by differential expression of the CGRP gene. *Proc. Natl. Acad. Sci. USA* **102**, 12938–12943 (2005).
16. Rea, B. J. et al. Peripherally administered calcitonin gene-related peptide induces spontaneous pain in mice: implications for migraine. *Pain* **159**, 2306–2317 (2018).
17. De Logu, F. et al. Migraine-provoking substances evoke periorbital allodynia in mice. *J. Headache Pain* **20**, 18 (2019).
18. Marone, I. M. et al. TRPA1/NOX in the soma of trigeminal ganglion neurons mediates migraine-related pain of glyceryl trinitrate in mice. *Brain* **141**, 2312–2328 (2018).
19. Ashina, M., Hansen, J. M., BO, A. D. & Olesen, J. Human models of migraine - short-term pain for long-term gain. *Nat. Rev. Neurol.* **13**, 713–724 (2017).
20. Lipton, R. B. et al. Cutaneous allodynia in the migraine population. *Ann. Neurol.* **63**, 148–158 (2008).
21. Burstein, R., Yarnitsky, D., Goor-Aryeh, I., Ransil, B. J. & Bajwa, Z. H. An association between migraine and cutaneous allodynia. *Ann. Neurol.* **47**, 614–624 (2000).
22. Goadsby, P. J. et al. Pathophysiology of Migraine: A Disorder of Sensory Processing. *Physiol. Rev.* **97**, 553–622 (2017).
23. May, A. & Burstein, R. Hypothalamic regulation of headache and migraine. *Cephalalgia* **39**, 1710–1719 (2019).
24. McLatchie, L. M. et al. RAMPs regulate the transport and ligand specificity of the calcitonin-receptor-like receptor. *Nature* **393**, 333–339 (1998).
25. Lennerz, J. K. et al. Calcitonin receptor-like receptor (CLR), receptor activity-modifying protein 1 (RAMP1), and calcitonin gene-related peptide (CGRP) immunoreactivity in the rat trigeminovascular system: differences between peripheral and central CGRP receptor distribution. *J. Comp. Neurol.* **507**, 1277–1299 (2008).
26. Beckers, H. J., Klooster, J., Vrensen, G. F. & Lamers, W. P. Ultrastructural identification of trigeminal nerve terminals in the pterygopalatine ganglion of rats: an anterograde tracing and immunohistochemical study. *Brain Res.* **557**, 22–30 (1991).
27. Cheng, L., Khan, M. & Mudge, A. W. Calcitonin gene-related peptide promotes Schwann cell proliferation. *J. Cell Biol.* **129**, 789–796 (1995).
28. Edvinsson, J. C. A. et al. C-fibers may modulate adjacent Adelta-fibers through axon-axon CGRP signaling at nodes of Ranvier in the trigeminal system. *J. Headache Pain.* **20**, 105 (2019).
29. Toth, C. C. et al. Locally synthesized calcitonin gene-related Peptide has a critical role in peripheral nerve regeneration. *J. Neuropathol. Exp. Neurol.* **68**, 326–337 (2009).
30. De Logu, F. et al. Schwann cell TRPA1 mediates neuroinflammation that sustains macrophage-dependent neuropathic pain in mice. *Nat. Commun.* **8**, 1887 (2017).
31. De Logu F., et al. Peripheral Nerve Resident Macrophages and Schwann Cells Mediate Cancer-induced Pain. *Cancer. Res.* **81**, 3387–3401 (2021).
32. Abdo, H. et al. Specialized cutaneous Schwann cells initiate pain sensation. *Science* **365**, 695–699 (2019).
33. Jensen D. D., et al. Neurokinin 1 receptor signaling in endosomes mediates sustained nociception and is a viable therapeutic target for prolonged pain relief. *Sci. Transl. Med.* **9**, eaal3447 (2017).
34. Ramírez-García, P. D. et al. A pH-responsive nanoparticle targets the neurokinin 1 receptor in endosomes to prevent chronic pain. *Nat. Nanotechnol.* **14**, 1150–1159 (2019).
35. Yarwood, R. E. et al. Endosomal signaling of the receptor for calcitonin gene-related peptide mediates pain transmission. *Proc. Natl. Acad. Sci. USA* **114**, 12309–12314 (2017).
36. Talavera, K. et al. Mammalian Transient Receptor Potential TRPA1 Channels: From Structure to Disease. *Physiol. Rev.* **100**, 725–803 (2020).
37. Lassen, L. H. et al. CGRP may play a causative role in migraine. *Cephalalgia* **22**, 54–61 (2002).
38. Guo, S. et al. Selectivity of commonly used inhibitors of clathrin-mediated and caveolae-dependent endocytosis of G protein–coupled receptors. Biochimica et Biophysica Acta (BBA). *Biomembranes* **1848**, 2101–2110 (2015).
39. Hosaka, K. et al. Calcitonin gene-related peptide activates different signaling pathways in mesenteric lymphatics of guinea pigs. *Am. J. Physiol. Heart Circ. Physiol.* **290**, H813–H822 (2006).
40. Miyamoto, T., Dubin, A. E., Petrus, M. J. & Patapoutian, A. TRPV1 and TRPA1 mediate peripheral nitric oxide-induced nociception in mice. *PLoS One* **4**, e7596 (2009).
41. Bhattacharya, M. R. et al. Radial stretch reveals distinct populations of mechanosensitive mammalian somatosensory neurons. *Proc. Natl. Acad. Sci. USA* **105**, 20015–20020 (2008).

42. De Logu, F. et al. Schwann cells expressing nociceptive channel TRPA1 orchestrate ethanol-evoked neuropathic pain in mice. *J. Clin. Invest.* **129**, 5424–5441 (2019).
43. Farokhzad, O. C. & Langer, R. Impact of nanotechnology on drug delivery. *ACS nano* **3**, 16–20 (2009).
44. LaMotte, R. H., Shain, C. N., Simone, D. A. & Tsai, E. F. Neurogenic hyperalgesia: psychophysical studies of underlying mechanisms. *J. Neurophysiol.* **66**, 190–211 (1991).
45. Melo-Carrillo, A. et al. Fremanezumab-A Humanized Monoclonal Anti-CGRP Antibody-Inhibits Thinly Myelinated (Adelta) But Not Unmyelinated (C) Meningeal Nociceptors. *J. Neurosci.* **37**, 10587–10596 (2017).
46. Weidner, C. et al. Acute effects of substance P and calcitonin gene-related peptide in human skin-a microdialysis study. *J. Invest. Dermatol.* **115**, 1015–1020 (2000).
47. Murinson, B. B., Hoffman, P. N., Banihashemi, M. R., Meyer, R. A. & Griffin, J. W. C-fiber (Remak) bundles contain both isolectin B4-binding and calcitonin gene-related peptide-positive axons. *J. Comp. Neurol.* **484**, 392–402 (2005).
48. Ziegler, E. A., Magerl, W., Meyer, R. A. & Treede, R. D. Secondary hyperalgesia to punctate mechanical stimuli. Central sensitization to A-fibre nociceptor input. *Brain* **122**, 2245–2257 (1999).
49. Irannejad, R. et al. Conformational biosensors reveal GPCR signalling from endosomes. *Nature* **495**, 534–538 (2013).
50. Lazar A. M. et al. G protein-regulated endocytic trafficking of adenylyl cyclase type 9. *Elife* **9**, e58039 (2020).
51. Peng G. E., Pessino V., Huang B., von Zastrow M. Spatial decoding of endosomal cAMP signals by a metastable cytoplasmic PKA network. *Nat. Chem. Biol.* **17**, 558–566 (2021).
52. Olesen, J., Burstein, R., Ashina, M. & Tfelt-Hansen, P. Origin of pain in migraine: evidence for peripheral sensitisation. *Lancet. Neurol.* **8**, 679–690 (2009).
53. Mullin, K. et al. Potential for treatment benefit of small molecule CGRP receptor antagonist plus monoclonal antibody in migraine therapy. *Neurology* **94**, e2121–e2125 (2020).
54. Luo, G. et al. Discovery of (5S,6S,9R)-5-amino-6-(2,3-difluorophenyl)-6,7,8,9-tetrahydro-5H-cyclohepta[b]pyri din-9-yl 4-(2-oxo-2,3-dihydro-1H-imidazo[4,5-b]pyridin-1-yl)piperidine-1-carboxylate (BMS-927711): an oral calcitonin gene-related peptide (CGRP) antagonist in clinical trials for treating migraine. *J. Med. Chem.* **55**, 10644–10651 (2012).
55. Manoukian, R. et al. Effects of monoclonal antagonist antibodies on calcitonin gene-related peptide receptor function and trafficking. *J. Headache Pain* **20**, 44 (2019).
56. Kwan, K. Y. et al. TRPA1 contributes to cold, mechanical, and chemical nociception but is not essential for hair-cell transduction. *Neuron* **50**, 277–289 (2006).
57. Skarnes, W. C. et al. A conditional knockout resource for the genome-wide study of mouse gene function. *Nature* **474**, 337–342 (2011).
58. Guan, Z. et al. Injured sensory neuron-derived CSF1 induces microglial proliferation and DAP12-dependent pain. *Nat. Neurosci.* **19**, 94–101 (2016).
59. Zurborg, S. et al. Generation and characterization of an Advillin-Cre driver mouse line. *Mol. Pain* **7**, 66 (2011).
60. Faul, F., Erdfelder, E., Lang, A. G. & Buchner, A. G*Power 3: a flexible statistical power analysis program for the social, behavioral, and biomedical sciences. *Behav. Res. Methods* **39**, 175–191 (2007).
61. Kilkenny, C., Browne, W. J., Cuthill, I. C., Emerson, M. & Altman, D. G. Improving bioscience research reporting: the ARRIVE guidelines for reporting animal research. *PLoS Biol.* **8**, e1000412 (2010).
62. Zimmermann, M. Ethical guidelines for investigations of experimental pain in conscious animals. *Pain* **16**, 109–110 (1983).
63. Watabe, K. et al. Spontaneously immortalized adult mouse Schwann cells secrete autocrine and paracrine growth-promoting activities. *J. Neurosci. Res* **41**, 279–290 (1995).
64. Watabe, K. et al. Tissue culture methods to study neurological disorders: establishment of immortalized Schwann cells from murine disease models. *Neuropathology* **23**, 68–78 (2003).
65. Luccarini, P., Childeric, A., Gaydier, A. M., Voisin, D. & Dallel, R. The orofacial formalin test in the mouse: a behavioral model for studying physiology and modulation of trigeminal nociception. *J. Pain* **7**, 908–914 (2006).
66. Dixon, W. J. Efficient analysis of experimental observations. *Annu. Rev. Pharmacol. Toxicol* **20**, 441–462 (1980).
67. Chaplan, S. R., Bach, F. W., Pogrel, J. W., Chung, J. M. & Yaksh, T. L. Quantitative assessment of tactile allodynia in the rat paw. *J. Neurosci. Methods* **53**, 55–63 (1994).
68. Elliott, M. B., Oshinsky, M. L., Amenta, P. S., Awe, O. O. & Jallo, J. I. Nociceptive neuropeptide increases and periorbital allodynia in a model of traumatic brain injury. *Headache* **52**, 966–984 (2012).
69. Tao, Y. Isolation and culture of Schwann cells. *Methods Mol. Biol.* **1018**, 93–104 (2013).
70. Nehme, R. et al. Mini-G proteins: Novel tools for studying GPCRs in their active conformation. *PLoS One* **12**, e0175642 (2017).
71. Wan, Q. et al. Mini G protein probes for active G protein-coupled receptors (GPCRs) in live cells. *J. Biol. Chem.* **293**, 7466–7473 (2018).
72. Namkung, Y. et al. Monitoring G protein-coupled receptor and beta-arrestin trafficking in live cells using enhanced bystander BRET. *Nat. Commun* **7**, 12178 (2016).
73. Chiefari, J. et al. Living Free-Radical Polymerization by Reversible Addition −Fragmentation Chain Transfer: The RAFT Process. *Macromolecules* **31**, 5559–5562 (1998).

Acknowledgements

Supported by grants from European Research Council (ERC) under the European Union's Horizon 2020 research and innovation programme (grant agreement No. 835286, P.G.); National Institutes of Health (NS102722, DE026806, DK118971, DE029951, N.W.B., B.L.S.) and Department of Defense (W81XWH1810431, N.W.B., B.L.S.).

Author contributions

F.D.L., R.N., A.H., L.L., D.D.J., R.L., J.D., M.M., D.S.M.dA., P.R.-G., M.W., J.R., M.T., A.I., N.V., T.P.D., B.L.S., N.W.B., P.G., designed and conducted the experiments, performed the analysis, discussed the results, and wrote the paper.

Competing interests

N.W.B. is a founding scientist of Endosome Therapeutics Inc. P.G. is a member of the Scientific Advisory Board of Endosome Therapeutics Inc. The laboratory of N.V. and M.W. has been funded in-part by Endosome Therapeutics Inc. R.N., F.D.L. and P.G. are founding scientists of FloNext Srl. P.G. has been in advisory boards and/or received fees for lectures from Novartis, Amgen, TEVA, AbbVie. The remaining authors declare no competing interests.

Additional information

Supplementary information The online version contains supplementary material available at https://doi.org/10.1038/s41467-022-28204-z.

Correspondence and requests for materials should be addressed to Nigel W. Bunnett or Pierangelo Geppetti.

Peer review information *Nature Communications* thanks Lars Edvinsson and the other anonymous reviewer(s) for their contribution to the peer review of this work.

Reprints and permission information is available at http://www.nature.com/reprints

Publisher's note Springer Nature remains neutral with regard to jurisdictional claims in published maps and institutional affiliations.

Open Access This article is licensed under a Creative Commons Attribution 4.0 International License, which permits use, sharing, adaptation, distribution and reproduction in any medium or format, as long as you give appropriate credit to the original author(s) and the source, provide a link to the Creative Commons license, and indicate if changes were made. The images or other third party material in this article are included in the article's Creative Commons license, unless indicated otherwise in a credit line to the material. If material is not included in the article's Creative Commons license and your intended use is not permitted by statutory regulation or exceeds the permitted use, you will need to obtain permission directly from the copyright holder. To view a copy of this license, visit http://creativecommons.org/licenses/by/4.0/.

© The Author(s) 2022

scientific reports

Check for updates

OPEN

TGR5 agonists induce peripheral and central hypersensitivity to bladder distension

Ashlee Caldwell[1,2,3,5], Luke Grundy[1,2,5], Andrea M. Harrington[1,2], Sonia Garcia-Caraballo[1,2], Joel Castro[1,2], Nigel W. Bunnett[4] & Stuart M. Brierley[1,2,3]✉

The mechanisms underlying chronic bladder conditions such as interstitial cystitis/bladder pain syndrome (IC/BPS) and overactive bladder syndrome (OAB) are incompletely understood. However, targeting specific receptors mediating neuronal sensitivity to specific stimuli is an emerging treatment strategy. Recently, irritant-sensing receptors including the bile acid receptor TGR5, have been identified within the viscera and are thought to play a key role in neuronal hypersensitivity. Here, in mice, we identify mRNA expression of TGR5 (*Gpbar1*) in all layers of the bladder as well as in the lumbosacral dorsal root ganglia (DRG) and in isolated bladder-innervating DRG neurons. In bladder-innervating DRG neurons *Gpbar1* mRNA was 100% co-expressed with *Trpv1* and 30% co-expressed with *Trpa1*. In vitro live-cell calcium imaging of bladder-innervating DRG neurons showed direct activation of a sub-population of bladder-innervating DRG neurons with the synthetic TGR5 agonist CCDC, which was diminished in *Trpv1*$^{-/-}$ but not *Trpa1*$^{-/-}$ DRG neurons. CCDC also activated a small percentage of non-neuronal cells. Using an ex vivo mouse bladder afferent recording preparation we show intravesical application of endogenous (5α-pregnan-3β-ol-20-one sulphate, Pg5α) and synthetic (CCDC) TGR5 agonists enhanced afferent mechanosensitivity to bladder distension. Correspondingly, in vivo intravesical administration of CCDC increased the number of spinal dorsal horn neurons that were activated by bladder distension. The enhanced mechanosensitivity induced by CCDC ex vivo and in vivo was absent using *Gpbar1*$^{-/-}$ mice. Together, these results indicate a role for the TGR5 receptor in mediating bladder afferent hypersensitivity to distension and thus may be important to the symptoms associated with IC/BPS and OAB.

Chronic bladder pathologies such as interstitial cystitis/bladder pain syndrome (IC/BPS) and overactive bladder syndrome (OAB) affect up to 16% of the population, significantly decreasing the quality of life for sufferers[1–4]. Although there are important differences between these conditions, the common symptoms of frequency, urgency and discomfort[1,5] are strongly indicative of neuronal hypersensitivity within bladder sensory pathways. Treatment options for each of these conditions are limited, suggesting a more complete understanding of the mechanisms underlying bladder sensory signalling is required.

The primary sensory afferents innervating the urinary bladder have cell bodies within the dorsal root ganglia (DRG)[6,7]. Sensory nerve endings for these afferent neurons are located throughout all layers of the bladder wall including the detrusor smooth muscle, the mucosal/interstitial tissue, and the urothelium[8,9]. Activation of these sensory nerve endings by various mechanical, chemical, or inflammatory stimuli results in sensory input into the dorsal horn of the spinal cord, where the bladder afferent neurons terminate[6,10,11]. From here, signals are relayed into autonomic and central pathways via activation of second order neurons, facilitating bladder relaxation and conscious sensory perception, respectively[11,12]. The specificity of the sensory input into central pathways is driven by the combination of receptors and ion channels expressed on the sensory terminals, allowing for the differentiation of distinct stimuli. Specific targeting of receptors on sensory nerve endings therefore presents an

[1]Visceral Pain Research Group, College of Medicine and Public Health, Flinders Health and Medical Research Institute (FHMRI), Flinders University, Bedford Park, South Australia 5042, Australia. [2]Hopwood Centre for Neurobiology, Lifelong Health Theme, Level 7, South Australian Health and Medical Research Institute (SAHMRI), North Terrace, Adelaide, South Australia 5000, Australia. [3]Discipline of Medicine, University of Adelaide, Level 7, SAHMRI, North Terrace, Adelaide, South Australia 5000, Australia. [4]Department of Molecular Pathobiology, Department of Neuroscience and Physiology, Neuroscience Institute, New York University, New York, NY, USA. [5]These authors contributed equally: Ashlee Caldwell and Luke Grundy. ✉email: stuart.brierley@flinders.edu.au

opportunity to modulate the intensity of bladder sensory signals. Pharmacological modulation of receptors is an invaluable method of treatment development for a variety of conditions, in particular G-protein coupled receptors (GPCRs) constitute the majority of current and potential pharmaceutical receptor targets[13]. This includes targets to treat itch, which can be induced by both histaminergic and non-histaminergic mechanisms, the latter of which includes bile acids and agonists of Mas-gene-related G protein-coupled receptors (Mrgprs)[14].

Itch-inducing GPCRs have recently been highlighted as potential pharmacological targets in visceral hypersensitivity conditions[15]. We have demonstrated that activation of histamine receptor H_1R, or the Mrgpr subtypes MrgprA3 and MrgprC11 modulate bladder afferent sensitivity to distension[16,17]. Takeda G-Protein Receptor 5 (TGR5), also known as Membrane-Bile Acid Receptor (M-BAR) or G-protein-coupled Bile Acid Receptor 1 (GPBAR1), is a membrane-bound G-protein coupled bile acid receptor[18,19]. TGR5 is expressed throughout the viscera and the nervous system, including the gastrointestinal tract[20–22], the bladder[23], as well as neurons and glial cells in the DRG[24–26]. TGR5 has been recently proposed as the integral receptor required for pruritus associated with chronic and pregnancy-related liver diseases, with TGR5 activation in DRG neurons resulting in neuronal hyperexcitability and the release of neurotransmitters in the dorsal horn[20,24,26]. Furthermore, TGR5 has been implicated in the pathology of irritable bowel syndrome (IBS), a common co-morbidity of OAB and IC/BPS[26]. In addition to bile acids, TGR5 can be activated by neurosteroids such as progesterone and progesterone metabolites[27,28] to evoke itch sensations via a TGR5-dependent mechanism[28,29]. Progesterone metabolites are conjugated and excreted via the urine, while bile acids have also been identified in the urine[30–34]. However, the role of TGR5 in regulating bladder afferent hypersensitivity is currently unknown.

Given the presence of endogenous TGR5 agonists in the bladder and the implicated roles for TGR5 in irritant sensation, we sought to investigate the expression and function of TGR5 in bladder afferent sensitivity. Here we show that TGR5 is expressed in a sub-population of bladder-innervating DRG neurons that co-express TRPV1, and to a lesser extent TRPA1. Endogenous and synthetic TGR5 agonists enhanced bladder afferent responses to bladder distension both ex vivo and in vivo, effects which are lost in mice lacking the TGR5 receptor (*Gpbar1*$^{-/-}$). This study shows for the first time the ability of TGR5 to regulate bladder afferent mechanosensitivity.

Methods

Ex vivo bladder afferent nerve recordings. Nerve recordings were performed in an ex vivo model as previously described[16,17,35–37]. Mice were humanely killed via CO_2 inhalation, and the entire lower abdomen was removed and submerged in a modified organ bath under continual perfusion with gassed (95% O_2 and 5% CO_2) Krebs-bicarbonate solution (composition in mmol/L: 118.4 NaCl, 24.9 $NaHCO_3$, 1.9 $CaCl_2$, 1.2 $MgSO_4$, 4.7 KCl, 1.2 KH_2PO_4, 11.7 glucose) at 35 °C. The bladder, urethra, and ureters were exposed by removing excess tissue. Ureters were tied with 4–0 perma-hand silk (Ethicon, #LA53G). The bladder was catheterised (PE 50 tubing) via the urethra and connected to a syringe pump (NE-1000) to allow a controlled fill rate of 30 µL/min with saline (NaCl, 0.9%). To enable intravesical pressure recording during graded distension, a second catheter was inserted through the dome of the bladder, secured with silk, and connected to a pressure transducer (NL108T2; Digitimer). Pelvic nerves, isolated from all other nerve fibres between the pelvic ganglia and the spinal cord, were dissected into fine multiunit branches and a single branch was placed within a sealed glass pipette containing a microelectrode (WPI) attached to a Neurolog headstage (NL100AK; Digitimer). Nerve activity was amplified (NL104), filtered (NL 125/126, band pass 50–5000 Hz, Neurolog; Digitimer), and digitised (CED 1401; Cambridge Electronic Design, Cambridge, UK) to a PC for offline analysis using Spike2 software (Cambridge Electronic Design, Cambridge, UK). The number of action potentials crossing a pre-set threshold at twice the background electrical noise was determined per second to quantify the afferent response. Single-unit analysis was performed offline using Spike2 software by matching individual spike waveforms through linear interpolation. A single unit was deemed to be responsive if a greater than 20% increase in afferent responsiveness was detected.

Afferent recording experimental protocols. As described previously[16,17,35–37], at the start of each afferent recording experiment, control bladder distensions were performed with an intravesical infusion of saline (NaCl, 0.9%) at a rate of 30 µL/min to a maximum pressure of 30 mmHg at 10 min intervals to assess the viability of the preparation and reproducibility of the intravesical pressure and neuronal responses to distension. The volume in the bladder was extrapolated from the known fill rate (30 µL/min) and the time taken (s) to reach maximum pressure (30 mmHg). Compliance was determined by plotting intravesical pressure against the calculated volume. After a stable baseline was maintained, the saline in the infusion pump was replaced by 5α-pregnan-3β-ol-20-one sulphate (Pg5α; 300 µM; Steraloids, #P3865-000) or 3-(2-chlorophenyl)-*N*-(4-chlorophenyl)-*N*,5-dimethyl-4-isoxazolecarboxamide (CCDC; 300 µM; Biovision, #1722-5, CAS: 1197300-24-5). Pg5α is a progesterone sulphate previously identified as an endogenous TGR5 agonist[28], whilst CCDC is a potent synthetic TGR5 agonist reported to be TGR5-specific[38]. For both Pg5 α and CCDC, stock solutions were made to 10 mM with 1% DMSO. Stock solutions were diluted to final working concentrations in 0.9% saline. Control refers to 0.9% saline containing 0.03% DMSO. The single nerve bundle isolated and inserted into the glass electrode during the dissection process was contained within the recording electrode for the entire experiment, allowing afferent nerve responses to be compared in the same nerve fibres during intra-bladder incubation with saline and Pg5α (300 µM) or CCDC (300 µM).

In vivo spinal dorsal horn activation. *In vivo bladder distension.* In vivo bladder infusion in anaesthetised mice were performed as previously described[16,37]. 12-week-old female mice were anaesthetised (isoflurane 2–4% in oxygen) and a catheter (PE 50 tubing) was inserted into the bladder via the urethra. Correct catheter placement was determined by inserting the catheter gently until meeting resistance (bladder dome) and receding slightly (2–3 mm) to avoid damaging the bladder wall. Urine was removed using a suction syringe and the

Antigen	Species raised in	Manufacturer code	Manufacturer	Dilution	RIID	
Primary						
Phospho-p44/42 MAPK (Erk1/2) (Thr202/Tyr204) (D13.14.4E) XP(tm) mAb (pERK)	Rabbit	4370	Cell Signalling	1:100	AB_2315112	
Antigen	**Species raised in**	**AF conjugate**	**Manufacturer code**	**Manufacturer**	**Dilution**	**RIID**
Secondary						
Rabbit IgG H + L	Chicken	594	A21442	ThermoFisher	1:200	AB_141840

Table 1. Primary and secondary antisera details.

catheter removed. A new catheter (PE 50 tubing), primed with either vehicle (saline; N = 5 mice) or CCDC (100 µM; N = 5 mice), was inserted and 100 µL of solution infused gently, to fill but not fully distend the bladder, and allowed to incubate for 5 min. The solution was then carefully removed from the bladder to ensure minimum liquid remained in the bladder. A third, dry catheter (PE 50 tubing) was inserted, and a small length of 4-0 perma-hand silk (Ethicon, #LA53G) was knotted over the urethral opening to fix the catheter into place and minimise loss of pressure. A 5-min stabilisation period was allowed between tying the catheter and performing the distensions to limit false-positive pERK signalling from the act of tying. A sphygmomanometer was attached between the catheter and a 10 mL air-filled suction syringe. 5 × 20-s bladder distensions were performed at 10-s intervals, at a holding pressure of 40 mmHg. Following the fifth 20-s distension, mice were administered an euthanasia agent overdose (intraperitoneal injection, 0.125 mL/250 g Lethabarb®; Virbac Australia) followed by rapid transcardial perfuse fixation.

Transcardial perfuse fixation and tissue dissection. As described previously[16,17,35–37], following euthanasia overdose, the thoracic cavity was opened and 0.5 mL heparinised saline (50 IU in 5 mL; Pfizer) was injected into the left ventricle. A 22-gauge needle attached to tubing and a peristaltic perfusion pump was then inserted in or near the injection site in the left ventricle. The right atrium was cut open to allow for perfusate drainage. Warm phosphate buffer (0.1 M; 21.7 mM NaH_2PO_4 [Chem Supply, #SA061-500G], 81 mM Na_2HPO_4 [VWR Chemicals, #102494C], pH 7.2) was then perfused, followed by ice-cold 4% paraformaldehyde (PFA; Sigma-Aldrich, #158127) in 0.1 M phosphate buffer. After complete PFA perfusion, the lumbosacral spinal cord was removed and postfixed in 4% PFA in 0.1 M phosphate buffer at 4 °C for 18–20 h. Spinal cords were then cryoprotected in 30% sucrose/phosphate buffer (Sigma-Aldrich, #S9378) for two days at 4 °C, followed by a 48-h incubation at 4 °C in 50% optimal cutting temperature compound (OCT; VWR, #C361603E)/30% sucrose/phosphate buffer solution before freezing in 100% OCT using liquid nitrogen-cooled 2-methylbutane Sigma-Aldrich, #M32631). The frozen spinal cord segments were cryosectioned (10 µm thickness) and placed onto gelatin-coated slides for processing of immunofluorescence labelling. Sectioning was performed serially and distributed over 6 slides, which were used for immunofluorescence localisation of phosphorylated-MAP-kinase ERK 1/2 (pERK). The number of pERK-immunoreactive neurons were counted in spinal cord sections from L6-S1, with spinal segments determined ex vivo by the shape of the dorsal horn[39].

Immunohistochemistry of phosphorylated-MAP-kinase ERK 1/2 within the spinal cord. The dorsal horn neurons activated by bladder distension were identified by immunofluorescent labelling for neuronal activation marker, phosphorylated-MAP-kinase ERK 1/2 (pERK), using a method described previously[16,36,37,40,41]. The details for the primary and secondary antisera can be found in Table 1. pERK activation was determined rather than c-Fos as ERK phosphorylation occurs within minutes of the peripheral stimuli and thus correlates better to the short-duration peripheral stimuli applied. Further, spinal neuronal activation in response to a range of peripheral stimuli is increasingly being identified via pERK activation quantification[36,37,41,42]. After air drying for one hour, excess OCT was removed from sections by washing with 0.2% Triton X-100 (Sigma-Aldrich, #T8787) in 0.1 M phosphate-buffered saline (PBS-T). Non-specific secondary antibody binding was blocked with 5% normal chicken serum diluted in 0.2% PBS-T. Tissue sections were then incubated with pERK primary antisera diluted in PBS-T at room temperature overnight (18 h). Sections were washed in PBS-T and incubated with secondary antibody conjugated to AlexaFluor 594 for 1 h at room temperature, followed by a PBS-T wash before mounting in ProLong Diamond Antifade (Life Technologies, #P-36962) and coverslipping. Negative controls were prepared as above with omission of the primary antibody. Slides were allowed to set for 24 h prior to visualisation.

Microscopy. Fluorescence was visualised with an epifluorescence microscope (Olympus, Tokyo, Japan) using a 10 × objective and 3-s exposure. ImageJ software (NIH) was used for image analysis. Aside from making moderate adjustments for brightness and contrast, the images were not manipulated in any way.

Spinal cord pERK neuronal counts and analysis. Neuronal counts were analysed as described previously[16] and utilized previously saved digital photomicrographs, with only neurons with intact nuclei counted. The number of pERK-immunoreactive (pERK-IR) neurons in a quadrant of the L6-S1 dorsal horn was obtained from a minimum of 6 sections/animal viewed at 10 × magnification. The mean number of pERK-IR neurons (± SEM) was compared between vehicle- and CCDC-treated mice.

Retrograde tracing. As described previously[16], small, aseptic, abdominal incision was made in anaesthetised (2–4% isoflurane in oxygen) mice. Cholera Toxin subunit B conjugated to AlexaFluor 488 (CTB-488, 0.5% diluted in 0.1 M phosphate-buffered saline [PBS] pH 7.4; ThermoFisher Scientific) was injected into the bladder wall at three sites (3 µL/injection) using a 5 µL Hamilton syringe attached to a 30-gauge needle[36,37]. The needle was inserted subserosally, parallel with the bladder muscle, to prevent injection of CTB into the bladder lumen. The abdominal incision was sutured closed and antibiotic (Amoxicillin; 50 mg/kg; Amoxil, AUSTR11137) and analgesic (Buprenorphine (Temvet); 0.1 mg/kg; Troy Laboratories Pty Ltd, APVMA #67612) given subcutaneously as mice regained consciousness. Mice were then individually housed and allowed to recover. 4 days post-surgery, mice were humanely killed for subsequent removal of the lumbosacral (LS; L5-S1) dorsal root ganglia (DRG) and isolation and culture of the neurons to visualise CTB-labelled bladder-innervating neurons within the DRG population.

Cell culture of bladder-innervating DRG neurons. As described previously[16], four days after retrograde tracing, mice were humanely euthanised via CO_2 inhalation and lumbosacral (LS; L5-S1) dorsal root ganglia (DRG) were removed. DRG were digested in Hanks' balanced salt solution (HBSS; pH 7.4; Life Technologies, #14170161) containing 4 mg/mL dispase (GIBCO, ThermoFisher Scientific, #17105041) and 3 mg/mL collagenase II (GIBCO, ThermoFisher Scientific, #17101015) at 37 °C for 30 min. The collagenase-dispase solution was aspirated and replaced with HBSS containing collagenase (3 mg/mL) only for 10 min at 37 °C, followed by washes in HBSS. DRG were then mechanically disrupted and cells dissociated in 600 µL complete DMEM (Dulbecco's Modified Eagle Media [DMEM; GIBCO, ThermoFisher Scientific, #11995065]; 10% Foetal Calf Serum [Invitrogen, ThermoFisher Scientific, MA, USA]; 2 mM l -glutamine [GIBCO, ThermoFisher Scientific, #25030081], 100 µM MEM non-essential amino acids [GIBCO, ThermoFisher Scientific, #11140076], 100 mg/mL penicillin/streptomycin [GIBCO, ThermoFisher Scientific, #15070063], and 96 µg/L nerve growth factor-7S [Sigma, N0513-0.1MG]) via trituration through fire-polished Pasteur pipettes of descending diameter, and centrifuged at 50×*g* for 1 min[36,37,40,43]. Neurons were resuspended in complete DMEM (360 µL) and spot-plated onto 13 mm coverslips (30 µL/coverslip) coated with laminin (20 µg/mL; Sigma-Aldrich, #L2020) and poly-d-lysine (800 µg/mL; ThermoFisher Scientific) in a 12-well plate. Coverslips were incubated at 37 °C in 5% CO_2 for 2–3 h to allow adherence of neurons before gently flooding each well with 1.7 mL complete DMEM. Cultured neurons were maintained in an incubator at 37 °C in 5% CO_2 for 18–48 h for calcium imaging or cell picking for single-cell PCR as described below.

Single-cell RT-PCR of individual bladder-innervating dorsal root ganglia neurons. Under continuous perfusion of sterile and RNA-/DNase-free PBS, single retrogradely traced bladder dorsal root ganglia (DRG) neurons were identified using a fluorescence microscope and collected into the end of a fine glass capillary using a micromanipulator[16,37]. The glass capillary was then broken into a sterile Eppendorf tube containing 10 µL of lysis buffer with DNAse (TaqMan Gene Expression Cells-to-CT Kit; Invitrogen, #4399002). For each coverslip of cultured DRG neurons, a bath control was also taken and analysed together with cells. Following lysis and termination of DNAse treatment, samples were immediately frozen on dry ice and stored at − 80 °C until cDNA synthesis was performed. RNA was reverse transcribed to cDNA using SuperScript™ IV VILO™ Master Mix (Invitrogen, #11766500) as per the manufacturer's instructions. cDNA was stored at − 20 °C for qRT-PCR. *Tubb3* (tubulin-3) expression served as a neuronal marker and positive control, and *Gfap* (glial fibrillary acidic protein) expression served as a glial cell marker for exclusion. Expression was considered positive if a complete curve was observed before 50 cycles[16].

Analysis of mRNA expression in whole LS DRG, isolated urothelial cells and bladder mucosal and detrusor layers. *Tissue collection.* As described previously[16] 16- to 18-week-old mice were humanely euthanised via CO_2 inhalation and the bladder and lumbosacral (L5-S1) dorsal root ganglia (DRG) removed. DRG were frozen in dry ice in pairs by spinal level (L5, L6, S1) and stored at − 80 °C for RNA extraction and quantitative reverse-transcription polymerase chain reaction (qRT-PCR). The bladder was dissected in sterile PBS with a single cut from the urethral opening along one side to the dome, stretched out, and pinned flat, urothelial side up. For RT-qPCR of the bladder layers, the mucosa and detrusor were gently peeled apart, frozen in dry ice, and stored at -80˚C for RNA extraction and qRT-PCR.

Isolation of mouse urothelial cells. For urothelial cell qRT-PCR, urothelial cells were isolated as performed previously[16,35,44,45]. Following stretching and pinning of the opened bladder as per bladder layer separation, the bladder was incubated with DMEM containing 2.5 mg/mL dispase, 10% Foetal Calf Serum, and 1 µM/mL HEPES (Sigma, #H3375, pH 7.0) at room temperature for 3 h. Cells were collected by gentle scraping of the urothelium with a blunt scalpel and dissociated in 0.025% trypsin EDTA (GIBCO, ThermoFisher Scientific, #25200072) at 37 °C in 5% CO_2 for 15 min with gentle intermittent trituration[16]. The trypsin was deactivated by adding the cell suspension to DMEM containing 10% Foetal Calf Serum before centrifugation (15 min, 1500 rpm, 4 °C). Cells were then resuspended in keratinocyte serum-free media (KSFM; Invitrogen, #17005042). Cell count and viability were determined using the Countess Automated Cell Counter (Invitrogen, ThermoFisher Scientific). Cells were then pelleted, frozen in dry ice, and stored at − 80 °C for RNA extraction and qRT-PCR.

RNA extraction and cDNA synthesis. As described previously[16] RNA was extracted using the PureLink RNA Micro kit (Invitrogen, Victoria, Australia, #12183-016; DRG pairs and isolated urothelial cells) or the PureLink RNA Mini kit (Invitrogen, #12183018A; bladder mucosa and detrusor) with DNAse treatment (Life Technolo-

Gene Alias	Gene target	Assay ID
β-Actin (reference gene)	*Actb*	Mm00607939_s1
Gapdh (reference gene)	*Gapdh*	Mm99999915_g1
Tubulin-3 (neuronal marker)	*Tubb3*	Mm00727586_s1
Glial fibrillary acidic protein (glial marker)	*Gfap*	Mm01253033_m1
Takeda G-protein Receptor 5	*Gpbar1*	Mm04212121_s1
Transient receptor potential vanilloid 1	*Trpv1*	Mm01246300_m1
Transient receptor potential ankyrin 1	*Trpa1*	Mm01227437_m1

Table 2. Primers used for qRT-PCR receptor expression assays.

gies, #12185-010) according to the manufacturer's instructions. A NanoDrop Lite spectrophotometer (Thermofisher Scientific) determined RNA quantity and purity. RNA was reverse transcribed to cDNA using SuperScript VILO Master Mix (Invitrogen, #11755250) as per the manufacturer's instructions. The cDNA was stored at − 20 °C until use.

Quantitative reverse-transcription polymerase chain reaction (qRT-PCR). As described previously[16] QRT-PCR was performed using Taqman Gene Expression Master Mix (Applied Biosystems, Victoria, Australia, #4369016) with commercially available hydrolysis probes (TaqMan; Life Technologies, see Table 2 for details) and RNAse-free water (AMBION, Victoria, Australia, #AM9916). For each reaction, 10 µL of MasterMix, 1 µL of TaqMan primer assay, 4 µL of water, and 5 µL of cDNA (1:2 dilution in RNA-free H_2O) from each sample was tested in duplicate for each target. Reference genes *Actb* (DRG pairs) and *Gapdh* (mucosa, detrusor, and urothelial cells) were used as endogenous controls. Assays were run for 45 cycles on a 7500 Fast Real-Time PCR machine (Applied Biosystems), using 7500 Fast software, v2.0.6. mRNA quantities are expressed as $2^{-\Delta Ct}$ relative to reference gene. Using Prism 8 software (GraphPad, San Diego, CA), data were analysed by one-way analysis of variance (ANOVA) with Tukey's multiple comparison test.

Calcium imaging of cultured LS DRG neurons. As described previously[16,46] cultured LS DRG neurons (18–48 h post-plating) were loaded with 2 µM Fura-2-acetoxymethyl ester (Fura-2; Invitrogen, ThermoFisher Scientific, #F1221) in pluronic F-127 (Invitrogen, ThermoFisher Scientific, #P3000MP) and incubated for 30 min at 37 °C before washing with HEPES buffer (10 mM HEPES sodium salt [4-(2-hydroxyethyl)piperazine-1-ethanesulfonic acid sodium salt; Sigma, #H7006-100G], 140 mM NaCl [Chem Supply, #SA046-3KG], 4 mM KCl [Chem Supply, #PA054-500G], 5 mM d-glucose anhydrous [Chem Supply, #GA018-500G], 2 mM $CaCl_2$ [Scharlau, #CA01951000], and 2 mM $MgCl_2$ [Sigma, #M8266-100G], pH 7.40) for 10 min and imaging at room temperature (23 °C). Fura-2 was excited at 340 and 380 nm and emissions were measured at 510 nm using a Nikon TE300 Eclipse microscope equipped with a Sutter DG-4/OF wavelength switcher, an Omega XF04 filter set for Fura-2, a Photonic Science ISIS-3 intensified CCD camera, and Universal Interface Card MetaFluor software. Retrogradely traced bladder-innervating DRG neurons were identified by the presence of the CTB-488 tracer, visible under excitation at 480 nm. 480 nm excitation was used for initial bladder neuron identification only; to prevent unnecessary photobleaching, images were not obtained at 480 nm during the experiment. Fluorescence images were obtained every 5 s leading up to and immediately following drug application, and every 20 s for washout period, using a 20× objective. Data were recorded and further analysed using MetaFluor software.

After an initial baseline reading to ensure cell fluorescence was stable, indicating healthy cells, DRG neurons were stimulated with CCDC (100 µM; Biovision, #1722-5, CAS: 1197300-24-5), and changes in intracellular calcium $[Ca^{2+}]_i$ were monitored in real time. For experiments assessing downstream TRP channel signalling, application and washout of CCDC was followed by application of TRPA1 agonist allyl isothiocyanate (AITC; 100 µM; Aldrich, #377430, CAS: 57-06-7) then TRPV1 agonist Capsaicin (50 nM; Sigma, #M2028, CAS: 404-86-4). After agonist additions, HEPES buffer containing high KCL (40 mM) was applied as a positive control to induce calcium overload driven by neuronal depolarisation. $[Ca^{2+}]_i$ is expressed as the ratio between the fluorescence signals at 340 and 380 nm. Baseline $[Ca^{2+}]_i$ was determined by averaging 8–12 fluorescence ratio readings immediately prior to stimulation. Maximum peak response was calculated by subtracting the relevant baseline score from the maximum fluorescence ratio measurement following compound application. Baseline fluorescence was normalised to a ratio of 1 for example traces.

Data availability, experimental design, data analysis and statistics. The datasets used and/or analysed during the current study are available from the corresponding author on reasonable request. Data are presented as described previously[16] with the mean ± SEM or the % of neurons or afferents or the maximum imp/s before and after. N indicates the number of animals, whilst n indicates the number of independent neurons or afferents. Statistical significance was reported at a level of $^{*}P<0.05$, $^{**}P<0.01$, $^{***}P<0.001$, $^{****}P<0.0001$. In some cases, # is used to indicate significance of at least $P<0.05$ for multiple comparisons. Data were analysed using Prism 8 (GraphPad, San Diego, CA, USA), using one- or two-way analysis of variance (ANOVA) with Tukey's or Sidak's post hoc analyses dependent on data distribution, or student t-tests, for parametric data. Non-parametric data were analysed using Kruskal–Wallis test with Dunn's multiple comparisons, Mann–Whitney

analysis, or Wilcoxon matched-pairs signed rank test. Data were tested for Gaussian distribution to determine the correct statistical tests. The specific tests used to analyse each data set are indicated within individual figure legends.

Ethics and animals. Animal studies were performed and reported in compliance with the ARRIVE guidelines. In this study, we used 12- to 18-week-old male and female C57BL/6J mice provided via an in-house breeding colony at the South Australian Health and Medical Research Institute (SAHMRI). Mice at SAHMRI were originally acquired from an in-house C57BL/6J breeding programme (JAX strain #000664; originally purchased from The Jackson Laboratory; breeding barn MP14; Bar Harbor, ME) and then bred within the specific and opportunistic pathogen-free animal care facility at SAHMRI. Some experiments utilised TRPV1 knockout (*trpv1*$^{-/-}$), TRPA1 knockout (*trpa1*$^{-/-}$), or TGR5 knockout (*Gpbar1*$^{-/-}$) mouse strains with a C57BL/6J genetic background, also bred in-house at SAHMRI. *Trpv1*$^{-/-}$ mice were originally acquired from an in-house breeding program at The Jackson Laboratory (JAX stock #003770; Bar Harbor, ME), *Trpa1*$^{-/-}$ mice were gifted to us by the original developer, Prof David Corey (Harvard University, Cambridge, MA, USA), and *Gpbar1*$^{-/-}$ mice were gifted to use by Prof Johan Auwerx and Prof Kristina Schoonjans, Ecole Polytechnique de Lausanne (Lausanne, Switzerland). *Gpbar1*$^{-/-}$ mice were also crossed onto *Na$_V$1.8*cre- line to generate a sensory neuron specific *Gpbar1*$^{-/-}$ (*Na$_V$1.8-Gpbar1*$^{-/-}$). These genetically modified mouse lines were all then bred in-house at SAHMRI as per the wildtype mice. Na$_V$1.8Cre-*Gpbar1*$^{-/-}$ mice were gifted to us by Prof Nigel Bunnett (Monash University, Victoria, Australia), then housed at SAHMRI's Preclinical, Imaging, and Research Laboratories (PIRL) facility for procedures.

All experiments were approved by and performed in accordance with the SAHMRI Animal Ethics Committee approvals (SAM195 and SAM190). Mice were group housed (5 mice per cage) within individual ventilated cages filled with chip coarse dust-free aspen bedding (PuraChips Aspen coarse 63L; Cat# ASPJMAEB-CA, Able Scientific, Australia). Cages were stored on individual ventilated cage racks within a temperature-controlled environment of 22 °C and a 12-h light/12-h dark cycle. Mice had free access to LabDiet JL Rat and Mouse/Auto6F chow (Speciality Feeds, Australia) and autoclaved reverse osmosis water. Sample sizes of each experiment are detailed in the corresponding figure legends.

Results

The TGR5 agonist Pg5α causes bladder afferent hypersensitivity. To determine if activation of the TGR5 receptor could influence bladder sensation we determined the impact of peripheral TGR5 activation in an ex vivo bladder afferent preparation. Intravesical application of Pg5α, a progesterone sulphate previously identified as an endogenous TGR5 agonist[28], resulted in a significant increase in bladder afferent firing in response to graded bladder distension compared to saline (Fig. 1A), indicating mechanical hypersensitivity following TGR5 activation. No change was observed in bladder compliance (pressure/volume relationship) between saline and Pg5α experiments (Fig. 1B), indicating that afferent hypersensitivity was not caused by changes in detrusor muscle tone.

Single-unit analysis of the bladder afferent nerve fibres revealed that 44.4% (20/45) of the mechanosensitive bladder afferents demonstrated mechanical hypersensitivity following instillation of Pg5α ('responders'), whereas 55.6% (25/45) of mechanosensitive afferents were unresponsive to Pg5α ('non-responders') (Fig. 1C). Pg5α-responsive afferents showed a significantly increased afferent firing rate at pressures of 20 mmHg and above (Fig. 1Di) and a significant increase in the maximum peak of afferent firing in response to distension following Pg5α instillation (Fig. 1Dii). In comparison, no change in afferent firing was observed between saline and Pg5α experiments for non-responding afferents, neither at any particular distension pressure (Fig. 1Ei) nor in the maximum peak response (Fig. 1Eii). These data demonstrate that the progesterone metabolite Pg5α causes mechanical hypersensitivity of a sub-population of bladder afferents in response to graded bladder distension (Fig. 1F).

The synthetic TGR5 agonist CCDC replicates Pg5α-induced increases in bladder afferent mechanosensitivity. We next aimed to further define and confirm the specific involvement of the TGR5 receptor in mediating bladder afferent mechanosensitivity. To this end, we used a potent, synthetic TGR5 agonist, 3-(2-chlorophenyl)-*N*-(4-chlorophenyl)-*N*,5-dimethyl-4-isoxazolecarboxamide (CCDC), reported to be TGR5-specific[38] to confirm the results obtained with Pg5α. Similar to Pg5α, on applying CCDC to the ex vivo bladder afferent preparation we observed an increase in afferent mechanosensitivity to bladder distension compared to saline (Fig. 2A). No change to muscle compliance was observed between saline and CCDC intravesical instillation (Fig. 2B), demonstrating that the effect of CCDC on mechanosensitivity is a direct afferent effect and not secondary to muscular changes. Single unit analysis of the mechanosensitive bladder afferents showed 50% (20/40) of afferents responded to CCDC with mechanical hypersensitivity to bladder distension compared to saline ('responders'), while 50% (20/40) showed no change in mechanosensitivity following CCDC instillation ('non-responders') compared to saline (Fig. 2C). CCDC-responsiveness was indicated by a mechanical hypersensitivity compared to saline at pressures of 10 mmHg and above (Fig. 2Di) and by a significant increase in the maximum peak of afferent firing (Fig. 2Dii) following CCDC instillation compared to saline. No changes in afferent firing at any individual pressures (Fig. 2Ei) or at maximum peak (Fig. 2Eii) were observed in the non-responding afferents. These data demonstrate that CCDC causes mechanical hypersensitivity of a sub-population of bladder afferents (Fig. 2F).

CCDC-induced bladder afferent mechanical hypersensitivity is reduced in *Gpbar1*$^{-/-}$ mice. To confirm that the CCDC-evoked mechanical hypersensitivity in ex vivo bladder afferents we observed were mediated by TGR5, we determined the effect of CCDC on bladder afferents in a *Gpbar1*$^{-/-}$ mouse model. In

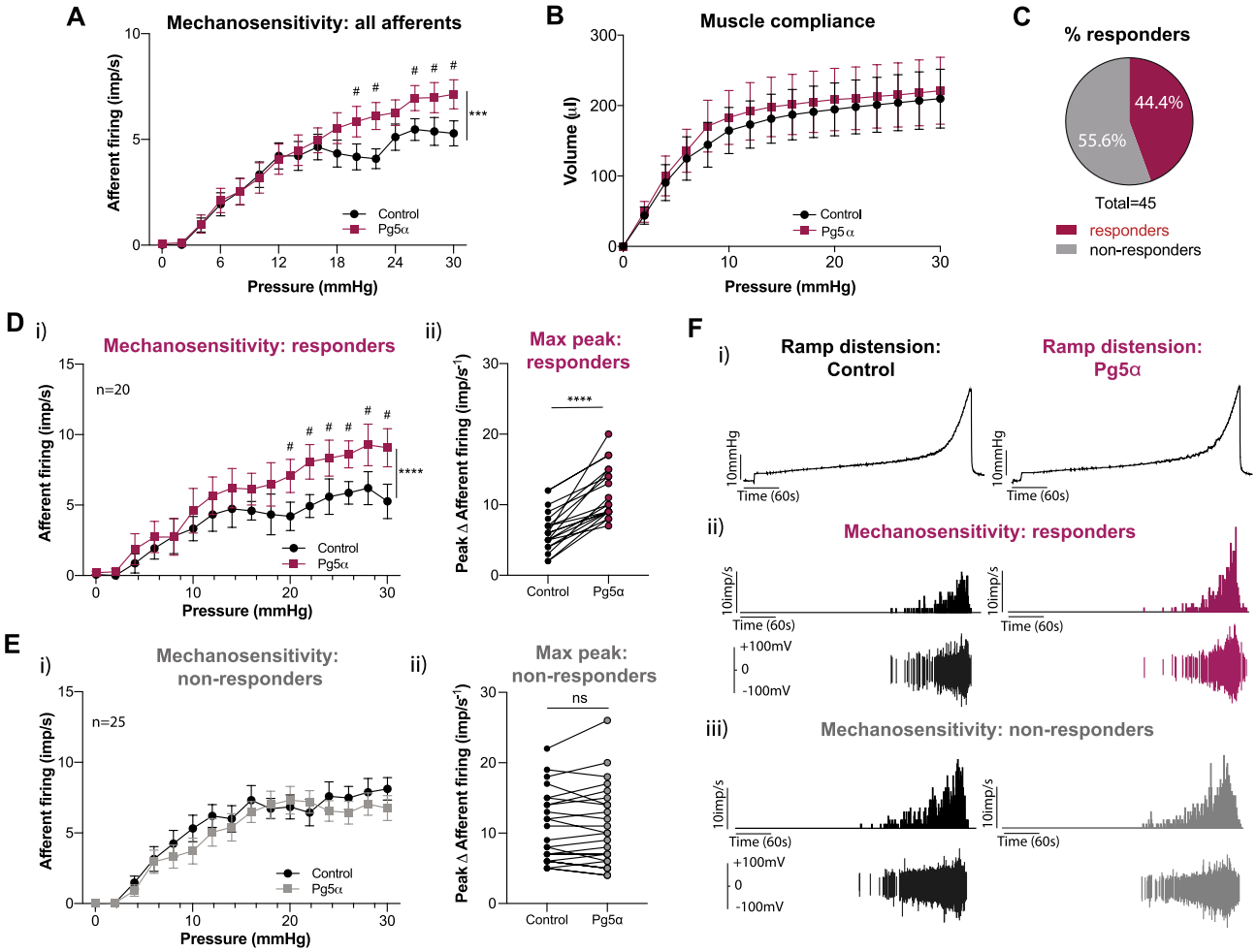

Figure 1. Pg5α enhances bladder afferent responses to mechanical stimuli ex vivo. (**A**) Whole nerve afferent firing was measured in response to graded bladder distension in an ex vivo preparation in the presence of saline (control) or progesterone sulphate '5α-pregnan-3β-ol-20-one sulphate' (Pg5α; 300 µM). Application of Pg5α increased the overall bladder afferent firing rate (impulses per second; imp/s) in response to bladder distension compared to saline (n = 45 single units from N = 5 mice; $^{***}P < 0.001$ and $^{\#}P < 0.05$ at individual distension pressures). (**B**) The intraluminal pressure measured as volume during bladder distension did not differ between saline and Pg5α (ns, $P > 0.05$), indicating no change in muscle compliance. (**C**) Of the 45 mechanosensitive bladder afferents recorded, 44.4% (20 out of 45) increased their responsiveness to distension following Pg5α (responders), whilst 55.6% (25 out of 45) were unchanged (non-responders). A single unit was deemed to be responsive if a greater than 20% increase in afferent responsiveness was detected. (**D**) Responding afferents had (i) significantly enhanced afferent firing rates at pressures of 20 mmHg and above ($^{\#}P < 0.05$) and (ii) a significantly higher maximum peak in afferent firing in the presence of Pg5α compared to saline ($^{****}P < 0.0001$). (**E**) Non-responding mechanosensitive afferents had (**i**) no significant difference in afferent firing at any distension pressure and (**ii**) no significant difference in the maximum peak of afferent firing between distensions with saline or Pg5α (*ns*, $P > 0.05$). **F**) Representative examples demonstrating the (**i**) graded increase in pressure with volume over time in response to bladder distension, (**ii**) a Pg5α-responsive afferent during bladder distension in the presence of saline and Pg5α, and (**iii**) Pg5α non-responsive mechanosensitive afferent during bladder distension in the presence of saline and Pg5α. Data are represented as mean ± SEM (**A**,**B**,**Di**,**Ei**), or percentage of afferents (**C**), or maximum imp/s before and after Pg5α (**Dii**,**Eii**). 'Responders' were defined by a greater than 25% increase in afferent firing (**C**,**D**,**E**,**F**). P values are based on two-way ANOVA (**A**,**B**,**Di**,**Ei**, with subsequent Sidak's post hoc test significance at individual data points indicated (**A**,**Di**, # represents significance of at least $P < 0.05$), or Wilcoxon matched-pairs signed rank test (**Dii**,**Eii**).

Gpbar1$^{-/-}$ mice, the mechanical hypersensitivity to distension following CCDC compared to saline was completely abolished (Fig. 3A). As in wildtype mice there was no change in muscle compliance between CCDC and saline experiments (Fig. 3B), confirming that the absence of altered sensitivity was not caused by changes in bladder muscle function. Interestingly, single unit analysis of the afferents showed that while the majority of afferents (82.9%; 29/35) reflected the overall lack of sensitivity to CCDC, mechanical hypersensitivity was observed in 17.1% (6/35) of mechanosensitive afferent fibres (Fig. 3C). These CCDC-responsive neurons demonstrated mechanical hypersensitivity specifically at 10 mmHg (Fig. 3Di) and an increase in the maximum peak

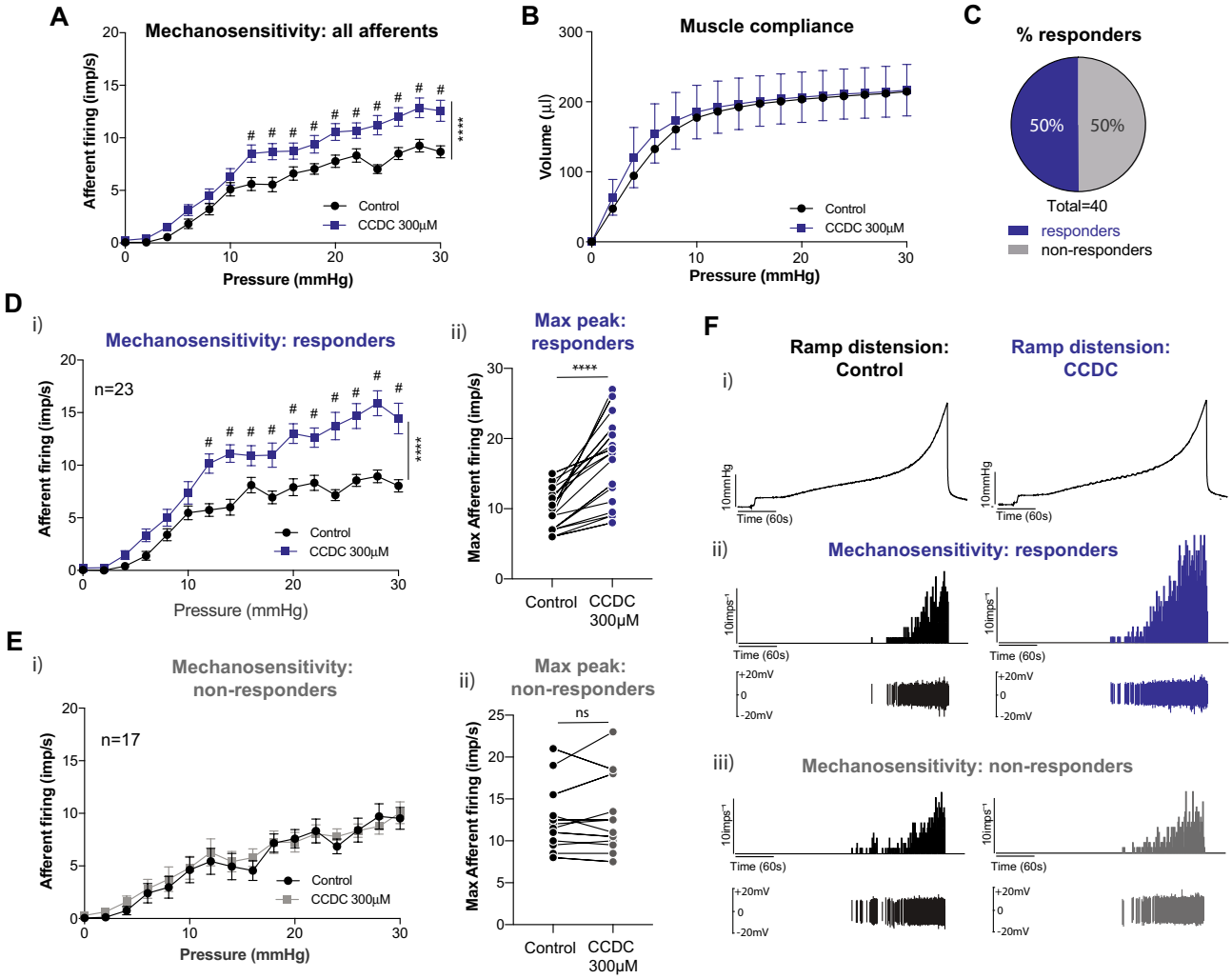

Figure 2. The synthetic TGR5 agonist CCDC enhances bladder afferent mechanosensitivity. (**A**) Afferent firing was recorded in response to graded bladder distension in an ex vivo preparation, comparing responses in the presence of saline (control) or the synthetic TGR5 agonist CCDC. Application of CCDC (300 μM) caused a significant increase in the overall afferent firing rate (impulses per second; imp/s) at distension pressures at and above 12 mmHg (n = 40 single units from N = 4 mice; $^{****}P < 0.0001$, and $^{\#}P < 0.05$ at individual distension pressures). (**B**) No differences were observed in the pressure to volume relationship between saline and CCDC (ns, $P > 0.05$). (**C**) Of the 40 mechanosensitive bladder afferents recorded, 50% (20 out of 40) displayed enhanced responses to distension after CCDC (responders), whilst 50% (20 out of 40) were unchanged. (**D**) CCDC-responsive afferents (n = 20) demonstrated a significant increase in mechanosensitivity following CCDC application. (**i**) Responders showed significantly increased mechanosensitivity to distension at pressures at and above 12 mmHg (**** $P < 0.0001$). (**ii**) The maximum peak of afferent firing with CCDC was significantly higher compared with saline ($^{****}P < 0.0001$). (**E**) CCDC-unresponsive mechanosensitive afferents (non-responders; n = 20) showed no difference in mechanosensitivity between saline and CCDC, with (**i**) no difference in imp/s at any distension pressure (ns, $P > 0.05$) and (**ii**) no change observed in the maximum imp/s to bladder distension (ns, $P > 0.05$). (**F**) (**i**) Example experimental traces showing the graded increase in pressure that occurs with increasing volume over time with saline, followed by CCDC. (**ii**) Graded increases in afferent firing in response to bladder distension, with a visible increase in imp/s following administration of CCDC (100 μM). (**iii**) Graded increase in afferent firing in response to bladder distension, with no change in response between saline and CCDC administrations. Data are represented as mean ± SEM (**A**,**B**,**Di**,**Ei**), percentage of afferents (**C**), or maximum imp/s (**Dii**) and **Eii**). 'Responders' were defined by a greater than 25% increase in afferent firing (**C**,**D**,**E**). P values above are based on two-way ANOVA (**A**,**B**,**Di**,**Ei**), with subsequent Sidak's post hoc test significance at individual data points indicated (**A**,**Di**, # represents significance of at least $P < 0.05$), or Wilcoxon matched-pairs signed rank test (**Dii**,**Eii**).

of afferent firing (Fig. 3Dii). In line with the overall bladder afferent data, the vast majority of mechanosensitive single units (82.9%; 29/35) showed no difference in mechanosensitivity following CCDC instillation compared to saline (Fig. 3Ei-ii).

In vivo intravesical CCDC in wild-type mice increases the number of activated dorsal horn neurons to bladder distension, an effect not apparent in *Gpbar1*$^{-/-}$ mice. Our results thus far have established a role for TGR5 agonists in peripheral bladder afferent hypersensitivity. To determine whether this mechanical hypersensitivity is conveyed to the central nervous system, we assessed dorsal horn neuronal activation in response to in vivo bladder distension at 40 mmHg induced pERK-immunoreactivity in lumbosacral (LS) dorsal horn neurons (Fig. 4A). We observed LS dorsal horn pERK-immunoreactive (-IR) neurons in response to saline bladder distension at 40 mmHg in wild-type mice (Fig. 4Ai). The pERK-IR neurons were identified predominantly in the regions of the dorsal grey commissure and the superficial dorsal horn, with some pERK-IR neurons in the lateral spinal nuclei and the sacral parasympathetic nucleus in sacral spinal segments (Fig. 4Aii). Following intra-bladder CCDC application we observed a significant increase in the number of pERK-IR neurons within LS dorsal horn which were distributed throughout the same regions of the dorsal horn as seen in the saline experiments (Fig. 4Ai, Aiii). As these regions are known to play a role in bladder afferent input, integration, and projection of autonomic and nociceptive visceral signalling[36,47], an increase in pERK-IR neurons indicates an increase in central sensitivity to bladder distension and hence projection of the peripheral mechanosensitivity observed ex vivo in wild-type mice.

LS spinal dorsal horn neuronal pERK-IR induced by in vivo bladder distensions following intravesical incubation with CCDC or saline was also determined in *Gpbar1*$^{-/-}$ mice. The CCDC-induced enhanced spinal dorsal horn neuronal response to bladder distension was abolished in the *Gpbar1*$^{-/-}$ model, with no difference in the number of LS dorsal horn pERK-IR neurons between CCDC and saline in these mice (Fig. 4Bi). The pERK-IR neurons activated by bladder distension following intravesical instillation of both saline and CCDC were observed in the same dorsal horn regions as seen in the wildtype, suggesting no differences in spinal bladder afferent signalling pathways in the *Gpbar1*$^{-/-}$ mice (Fig. 4Bii,Biii). Taken together, these results demonstrate that activation of the TGR5 receptor is able to mediate an increase in peripheral and spinal sensitivity to bladder distension indicative of sensory neuron activation.

***Gpbar1* (TGR5) mRNA is expressed in the bladder and bladder innervating DRG neurons.** To begin unravelling the mechanisms through which TGR5 agonists CCDC and Pg5α exert mechanical hypersensitivity of bladder afferents we determined the relative mRNA expression of the TGR5 gene *Gpbar1* within the bladder and bladder-innervating sensory neurons. *Gpbar1* mRNA expression was identified throughout the bladder wall; in isolated urothelial cells, the mucosa, and the detrusor smooth muscle (Fig. 5A), as well as in isolated LS (L5-S1) DRG (Fig. 5B). *Gpbar1* expression was absent in all tissues from *Gpbar1*$^{-/-}$ mice (Fig. 5A,B), whilst the relative abundance of either Transient receptor potential (TRP) vanilloid 1 (*trpv1*) or ankyrin 1 (*trpa1*) observed in LS DRG from *Gpbar1*$^{-/-}$ mice was unchanged compared to wildtype (Fig. 5B). TRP channels are common downstream targets for GPCR signalling cascades, with previous studies identifying downstream coupling of irritant-sensing receptors with TRPV1 and TRPA1[16,24,26,48,49]. To assess potential TRP channel coupling with TGR5 in bladder neurons, we used single cell RT-PCR to determine the co-expression of *Gpbar1* with *trpv1* and *trpa1*. Single cell RT-PCR identified *Gpbar1* expression in 13.0% (10/77) of retrogradely traced bladder afferent neurons (Fig. 5C). 84.4% (65/77) and 18.5% (12/77) of bladder-innervating DRG expressed *trpv1* and *trpa1* mRNA, respectively (Fig. 5C). Of the bladder DRG neurons expressing *Gpbar1* mRNA, 100% co-expressed *trpv1*, and only 30% co-expressed *trpa1* (Fig. 5Cii,Ciii), despite previous functional data in other DRG neurons showing distinct coupling of TGR5 with TRPA1[24].

In vitro application of CCDC to bladder-innervating DRG neurons increases intracellular Ca^{2+}. To gain insights into the mechanism of action of neuronal TGR5 in mediating bladder afferent sensitivity, we performed live cell calcium imaging in LS DRG neurons isolated from retrogradely bladder-traced mice. Following direct application of CCDC to the neurons, a significant increase in intracellular Ca^{2+}, indicated by an increase in the Fura-2 fluorescence ratio (Fig. 6Ai,Aii), was observed in 58.82% (40/68) of bladder-traced DRG neurons (Fig. 6Bi). Interestingly, the percentage of bladder-traced neurons responding to CCDC was substantially higher than the percentage on non-traced neurons, of which only 24.65% (126/511) responded (Fig. 6Bi). The average magnitude of CCDC-induced increases in intracellular Ca^{2+} was also greater in bladder-traced compared to non-traced neurons, as indicated by a significantly higher maximum peak value of Fura-2 fluorescence and area under the curve of response (Fig. 6Bii,Biii). These results demonstrate the TGR5 agonist CCDC is able to cause direct activation of LS DRG neurons and indicate the possibility that bladder-innervating DRG neurons are tuned to evoke greater responses to TGR5 agonists.

In vitro CCDC-induced increases in intracellular Ca^{2+} in bladder-innervating DRG neurons are partially mediated by TRPV1. Coupling between TGR5 and TRPA1 has been previously demonstrated in cutaneous[24] and colon[26] innervating DRG neurons. Here our single-cell mRNA expression data from bladder-innervating DRG neurons demonstrated 100% co-expression of *trpv1* with *Gpbar1* compared to only 30% co-expression of *trpa1* with *Gpbar1* (Fig. 5C), suggesting a distinct intracellular signalling pathway in bladder-innervating DRG neurons. To functionally explore potential coupling between TGR5 and TRP channels in bladder afferent DRG neurons in vitro, we determined co-activation of TGR5, TRPA1, and TRPV1 in individual neurons with successive administration of CCDC, AITC (TRPA1 agonist), and capsaicin (TRPV1 agonist) using live cell calcium imaging (Fig. 7A,B). In line with our single-cell co-expression data, 87.5% (21/24) of bladder

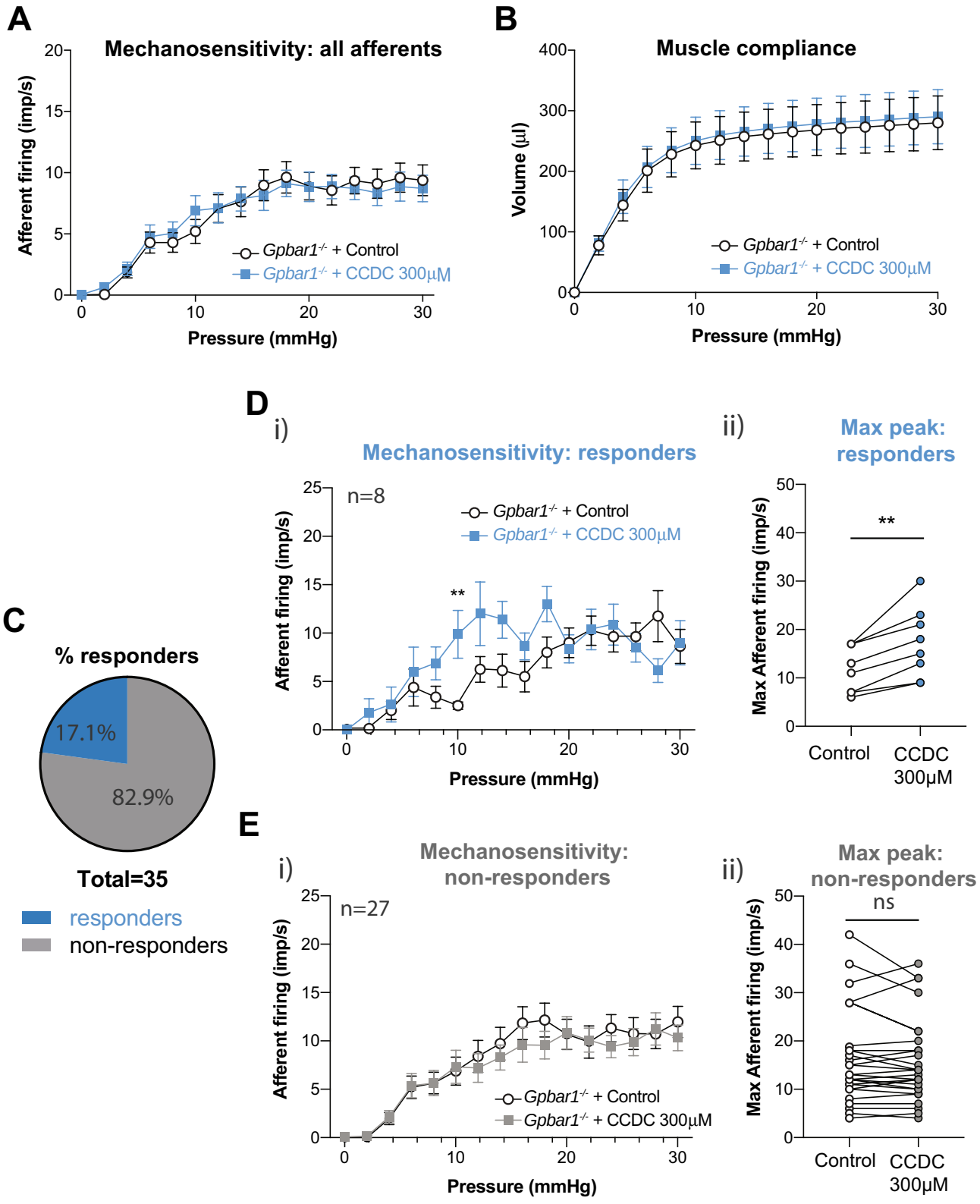
A
Mechanosensitivity: all afferents
Afferent firing (imp/s)
Pressure (mmHg)
Gpbar1-/- + Control
Gpbar1-/- + CCDC 300µM
B
Muscle compliance
Volume (µl)
Pressure (mmHg)
Gpbar1-/- + Control
Gpbar1-/- + CCDC 300µM
C
% responders
17.1%
82.9%
Total=35
responders
non-responders
D
i)
Mechanosensitivity: responders
n=8
Afferent firing (imp/s)
Pressure (mmHg)
Gpbar1-/- + Control
Gpbar1-/- + CCDC 300µM
**
ii)
Max peak: responders
Max Afferent firing (imp/s)
**
Control
CCDC 300µM
E
i)
Mechanosensitivity: non-responders
n=27
Afferent firing (imp/s)
Pressure (mmHg)
Gpbar1-/- + Control
Gpbar1-/- + CCDC 300µM
ii)
Max peak: non-responders
Max Afferent firing (imp/s)
ns
Control
CCDC 300µM

◂**Figure 3.** CCDC-induced hypersensitivity to distension is abolished in *Gpbar1 (TGR5)*$^{-/-}$ mice. (**A**) Bladder distensions were performed with saline (control) and CCDC (100 μM) *in* ex vivo preparations from *Gpbar1*$^{-/-}$ mice. No difference in afferent firing (impulses per second; imp/s) was observed following administration of CCDC compared to saline in the *Gpbar1*$^{-/-}$ mice (n = 35 single units from N = 4; ns, $P > 0.05$). (**B**) The pressure to volume relationship during bladder distension is unchanged following CCDC administration compared to saline, indicating no change in muscle compliance in preparations from *Gpbar1*$^{-/-}$ mice (ns, $P > 0.05$). (**C**) Whilst the majority of afferents (82.9%) reflected the overall results with no change in afferent firing (29 out of 35; non-responders), 6 out of 35 (17.1%) afferents displayed enhanced responses to distension following CCDC with an increase in mechanosensitivity. (**D**) In CCDC-responsive afferents, (**i**) a significant increase in imp/s was observed following CCDC administration overall (**$P < 0.01$) and specifically at a distension pressure of 10 mmHg (**$P < 0.01$). (**ii**) the maximum imp/s following CCDC administration was significantly increased compared to saline in responders (**$P < 0.01$). (**E**) In non-responding afferents, (**i**) no change in imp/s at any distension pressure was observed in non-responders between CCDC and saline distensions (ns, $P > 0.05$), whilst (**ii**) no significant difference was observed between the maximum imp/s of non-responders following administration of CCDC compared to saline (ns, $P > 0.05$). P values above are based on two-way ANOVA (**A**,**B**,**Di**,**Ei**), with subsequent Sidak's post hoc test significance at individual data points indicated on (**Di**), Wilcoxon matched-pairs signed rank test (**Dii**,**Eii**).

traced neurons that responded to CCDC also responded to capsaicin, whilst 33.3% (8/24) of CCDC-responsive bladder-traced neurons also responded to AITC (Fig. 7B). Only 16.7% (4/24) of CCDC-responsive bladder-traced neurons were unresponsive to both AITC and capsaicin (Fig. 7B).

To further explore the potential functional relationships between TGR5 and TRP channels TRPV1 and TRPA1, we measured bladder-traced DRG neuronal responses to CCDC in vitro using *trpv1*$^{-/-}$ and *trpa1*$^{-/-}$ mice. The percentage of bladder-traced DRG neurons responding to CCDC was reduced by approximately 50% in *trpv1*$^{-/-}$ mice (27.3%) compared to wildtype mice (58.8%), with no obvious change observed in the *trpa1*$^{-/-}$ mice (60.9%) compared to wildtype mice (Fig. 7C). The profile and magnitude of CCDC responses between wildtype and *trpv1*$^{-/-}$ and *trpa1*$^{-/-}$ mice was also examined (Fig. 7Di–iii). Whilst the few *trpv1*$^{-/-}$ neurons that responded to CCDC show a trend towards reduced response amplitudes, there was no statistical differences in the average maximum peak of Fura-2 fluorescence (Fig. 7Dii) and area under the curve (Fig. 7Diii) of the CCDC responses. Overall, these data implicate an interaction between TRPV1 and TGR5 in subsets of bladder-innervating DRG neurons. However, as CCDC responses are also observed in some *trpv1*$^{-/-}$ DRG neurons, this suggests interactions with other channels also occur.

In vitro CCDC-induced increases in intracellular Ca^{2+} in bladder-innervating DRG neurons remain in *Gpbar1*$^{-/-}$ mice. To confirm the in-vitro effects of CCDC on isolated bladder-innervating DRG neurons were due to activation of the TGR5 receptor we examined CCDC responses firstly in cells isolated from *Gpbar1*$^{-/-}$ mice and subsequently in *Na_V1.8Cre-Gpbar1*$^{-/-}$ mice. To our surprise, responses to CCDC remained in neurons from these mice (Fig. 8). The percentage of cells responding to CCDC from *Gpbar1*$^{-/-}$ and *Na_V1.8Cre-Gpbar1*$^{-/-}$ mice was roughly equivalent to that from wild-type mice (Fig. 8Ai–iii,Bi–ii). The total fluorescent response to CCDC, depicted as the area under the response curve (AUC) was significantly reduced in cells from *Na_V1.8Cre-Gpbar1*$^{-/-}$ (neuronal knockout of *Gpbar1*) but not *Gpbar1*$^{-/-}$ (global knockout of *Gpbar1*) mice (Fig. 8Aiii,C), however, a robust response still remained. No significant differences in the maximum peak of Fura-2 fluorescence in response to CCDC were observed in cells from wildtype, *Gpbar1*$^{-/-}$ or *Na_V1.8Cre-Gpbar1*$^{-/-}$ mice (Fig. 8D).

CCDC-evokes increases in intracellular Ca^{2+} in a small proportion of non-neuronal cells. We have shown that the effects of CCDC in the intact bladder, namely mechanical hypersensitivity of pelvic afferents and spinal cord activation, is prevented in *Gpbar1*$^{-/-}$ mice. Therefore, we investigated if the *in-vitro* effects we observed with CCDC in neurons from *Na_V1.8Cre-Gpbar1*$^{-/-}$ and *Gpbar1*$^{-/-}$ mice resulted from additional cell types responding to CCDC that are not present in the bladder (Fig. 9). We observed that a small population (3%) of non-neuronal cells from wildtype mice responded to CCDC (Fig. 9ABi–iii). Surprisingly, non-neuronal responses to CCDC were retained in cells from *Gpbar1*$^{-/-}$ and *Na_V1.8Cre-Gpbar1*$^{-/-}$ mice (Fig. 9Bi). Furthermore, the area under the response curve (AUC, Fig. 9Bii) and the maximum peak of Fura-2 fluorescence in response to CCDC (Fig. 9Biii) were not significantly reduced in cells from *Gpbar1*$^{-/-}$ nor *Na_V1.8Cre-Gpbar1*$^{-/-}$ mice.

Discussion

The overlapping symptoms of OAB and IC/BPS, including frequency, urgency and discomfort indicate an increase in the sensitivity of bladder afferent neurons to bladder filling. Identifying the receptors and channels involved in bladder afferent neuronal activation, and the impact these have on behavioural responses in states of health and hypersensitivity, is a crucial step to developing efficacious treatment options for patients suffering bladder hypersensitivity disorders. Here, we have identified a role for the bile acid receptor TGR5 in mediating bladder afferent mechanical hypersensitivity in vivo and ex vivo. Intravesical administration of the progesterone metabolite Pg5α and the synthetic TGR5 agonist CCDC increased afferent sensitivity to bladder distension at both peripheral and spinal levels, responses which we show to be reduced or absent in mice lacking the gene for TGR5 (*Gpbar1*).

These findings are important as endogenous TGR5 agonists, including bile acids and progesterone metabolites are present at low levels in the urine of healthy subjects[33,34] and are increased dramatically under different

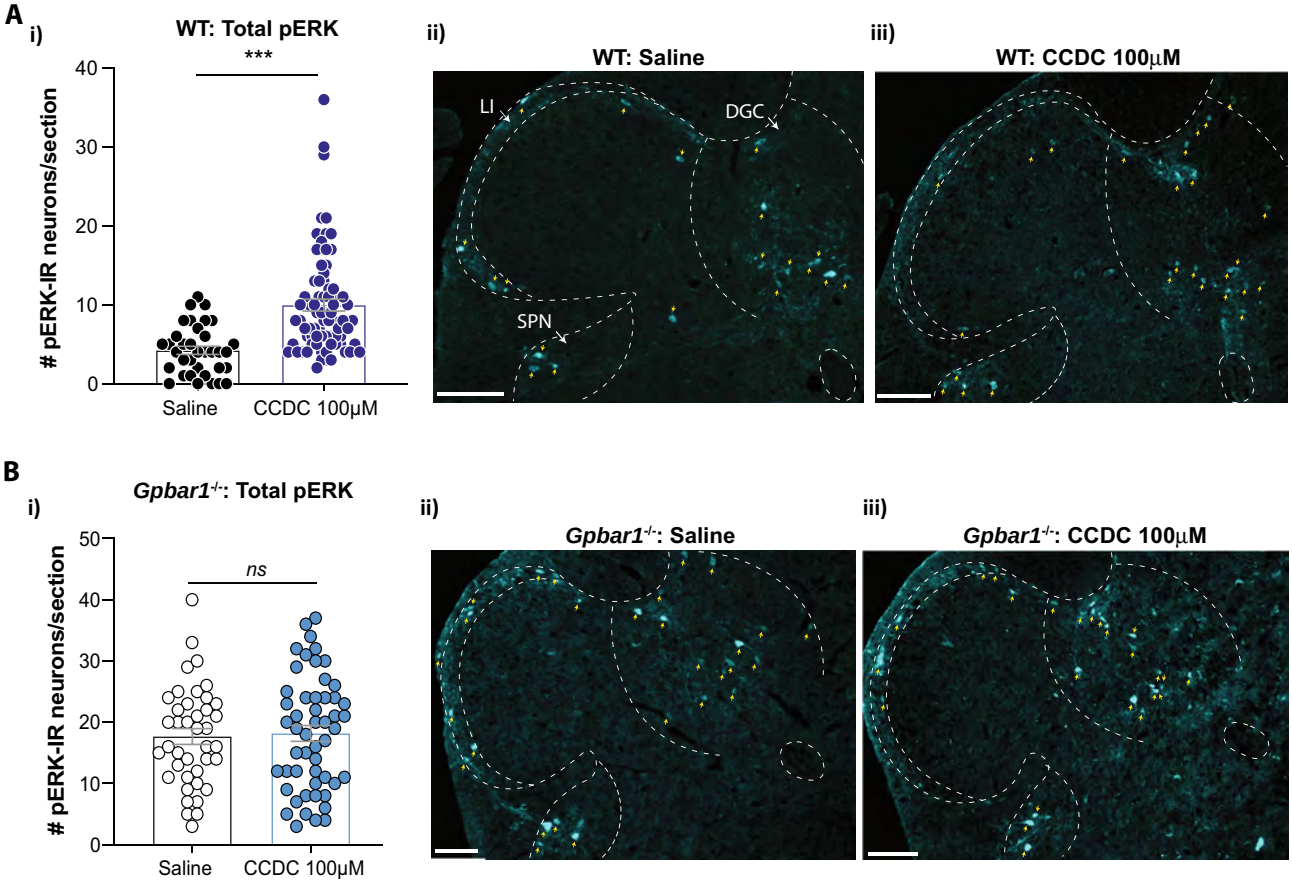

Figure 4. Intravesical bladder CCDC administration increases spinal dorsal horn pERK immunoreactivity in response to bladder distension. (**A**) (**i**) In vivo bladder distensions in wildtype mice following intravesical saline (control) or CCDC (100 μM) administration. Group data showing the number of pERK-immunoreactive (pERK-IR) dorsal horn neurons in 10 μm sections of the lumbosacral spinal cord. Compared to saline (N = 4), the number of pERK-IR neurons in the LS dorsal horn per section was significantly greater in response to bladder distension following intravesical administration of CCDC (N = 6; $^{***}P < 0.001$). (**ii–iii**) Images are representative dorsal horn sections from the S1 region from (**ii**) saline-treated and (**iii**) CCDC-treated wildtype mice, with dashed lines to delineate the superficial dorsal horn (SDH) and dorsal grey commissure (DGC), and yellow arrows pointing to pERK-IR neurons. (**B**) (**i**) In *Gpbar1*$^{-/-}$ mice there was no difference observed in the number of pERK-IR neurons in the LS dorsal horn per section following bladder distension following intravesical administration of either saline (N = 3) or CCDC (N = 4; ns, $P > 0.05$). Images are representative dorsal horn sections from the S1 regions from (**ii**) saline-treated and (**iii**) CCDC-treated *Gpbar1*$^{-/-}$ mice, with dashed lines to delineate the superficial dorsal horn (SDH) and dorsal grey commissure (DGC), and yellow arrows pointing to pERK-IR neurons. Data are represented as mean ± SEM, with each dot representing the total number of pERK-IR neurons within a single dorsal horn quadrant from one section. *P* values were determined by Mann–Whitney non-parametric test (**Ai**,**Bi**). Scale bar 100 μm throughout. *CC* central canal, *SPN* sacral parasympathetic nucleus, *LSN* lateral spinal nucleus.

conditions, including pregnancy and liver disease[32,50]. As such, the increased sensitivity of these mechanosensitive bladder afferents following intravesical administration of Pg5α suggests an endogenous role for TGR5 agonists in mediating afferent hypersensitivity. The CCDC-induced increase in bladder afferent firing to distension largely mirrored that of PG5α, although the sensitisation was observable from earlier distension pressures following CCDC administration compared to PG5α. Importantly, the overall bladder afferent hypersensitivity induced by CCDC was abolished in *Gpbar1*$^{-/-}$ mice and the percentage of responding afferents greatly reduced.

These findings of afferent sensitisation by TGR5 agonists have physiological relevance as projections from bladder afferents terminate within the lumbosacral spinal dorsal horn[10,51]. Following peripheral activation, these neurons release neurotransmitters within the dorsal horn which act on second order neurons. Sub-populations of second order spinal neurons involved in bladder sensory pathways have been identified within the superficial dorsal horn (SDH), the dorsal grey commissure (DGC) and the sacral parasympathetic nucleus (SPN)[6,16,36,51–55]. These second order neurons relay peripheral bladder sensory input to the brain, resulting in autonomic micturition reflexes and cognitive perception[6,36,47,56]. Here, we demonstrate in sacral spinal segments that following CCDC and bladder distension there is an increase in the number of pERK-IR neurons within the SDH, the DGC, the lateral spinal nuclei and the SPN. This indicates peripheral bladder afferent hypersensitivity induced

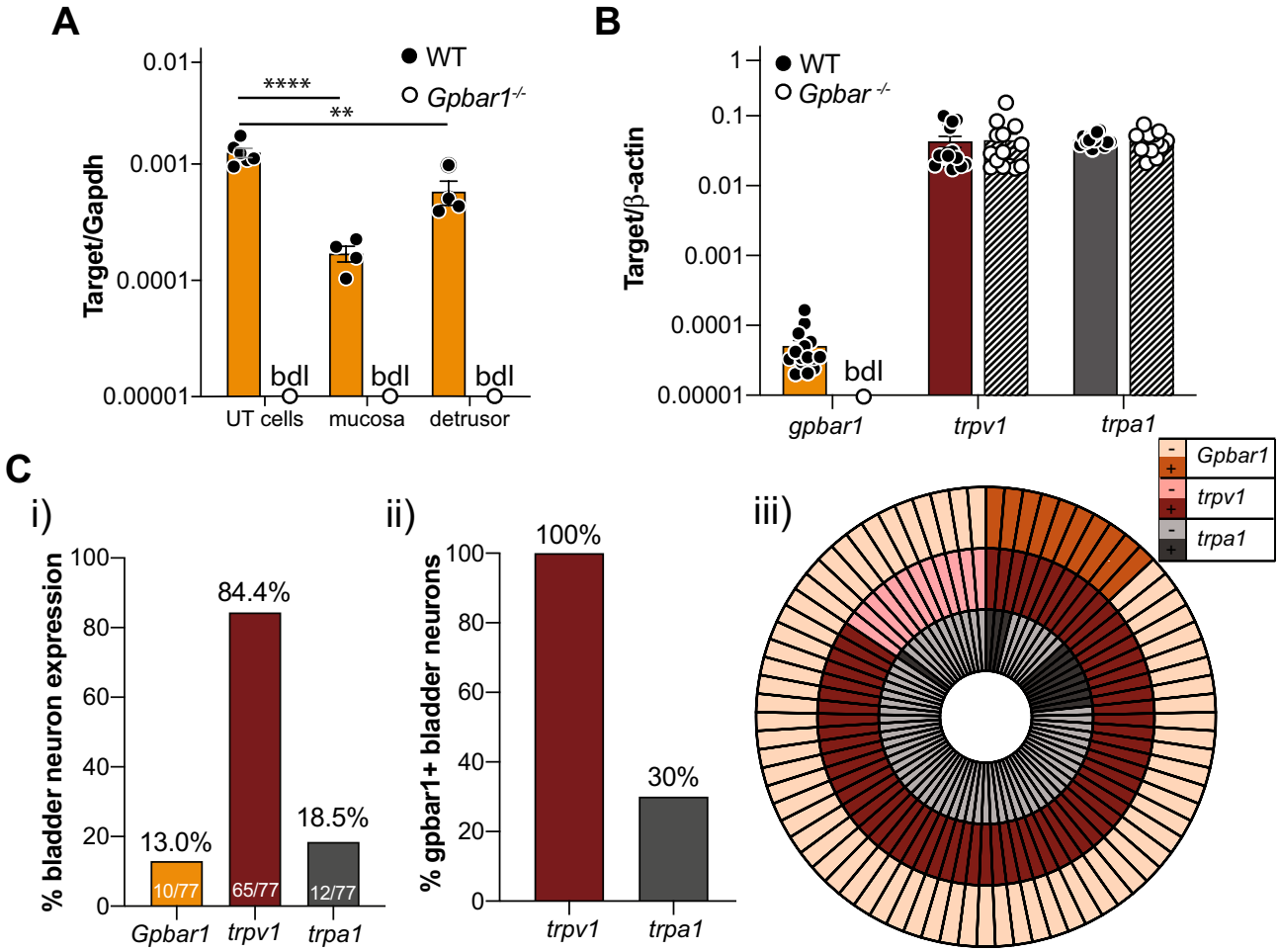

Figure 5. Relative mRNA expression in bladder tissue, lumbosacral DRG and isolated bladder-innervating DRG neurons. (**A**) qRT-PCR was used to determine the relative abundance of the TGR5 gene *Gpbar1* in urothelial cells, mucosal urothelium, and detrusor smooth muscle of the bladder of wild-type and *Gpbar1*$^{-/-}$ mice. *Gpbar1* was expressed in all layers of the wildtype bladder, with relative abundance in the isolated urothelial cells (UT cells; N = 6 mice) significantly higher than in the mucosa (N = 4 mice; ****$P < 0.0001$) and detrusor (N = 4 mice; **$P < 0.01$). No significant difference was observed between mucosa and detrusor layers (ns, $P = 0.0833$). *Gpbar1* mRNA expression was below detectable levels (bdl) in all tissues tested from *Gpbar1*$^{-/-}$ mice. (**B**) Relative mRNA expression of *Gpbar1*, *trpv1* and *trpa1* in lumbosacral (LS) dorsal root ganglia (DRG) from wildtype and *Gpbar1*$^{-/-}$ mice. *Gpbar1* is expressed in LS DRG from WT mice. *Gpbar1* levels were below the detectable limit (bdl) in *Gpbar1*$^{-/-}$ mice. No differences were observed between wildtype and *Gpbar1*$^{-/-}$ mice for the highly expressed genes *trpv1* or *trpa1*. (**C**) (**i**) *Gpbar1*, *trpv1* and *trpa1* mRNA expression in isolated, retrogradely traced bladder-innervating DRG neurons was determined with single cell RT-PCR. 13% of bladder neurons (10 out of 77 neurons, N = 3) expressed *Gpbar1*, while 84.4% (65 out of 77 neurons) expressed *trpv1* and 18.5% (12 out of 77 neurons) expressed *trpa1*. (**ii**) Of the 10 bladder-innervating DRG neurons expressing *Gpbar1*, 100% (10 out of 10) co-expressed *trpv1*, while 30% (3 out of 10) co-expressed *trpa1*. (**iii**) Polar plot depicting the expression profile (dark shading: expressing target; light shading: not expressing target) of each bladder-innervating DRG neuron with respect to *Gpbar1* (outer ring), *Trpv1* (middle ring) and *Trpa1* (inner ring). Data are represented as mean ± SEM ($2^{-\Delta Ct}$) on a log10 scale (**A**,**B**), or percentage of neurons (**Ci**,**Cii**). *P* values above are based on one-way ANOVA with Tukey's multiple comparison test, with *Gpbar1*$^{-/-}$ not included in the analysis.

by TGR5 agonism is relayed into the spinal cord and subsequent central pathways. These findings correlate well with our previous studies whereby intravesical application of histamine or Mrgpr agonists increases bladder afferent responses to bladder distension, resulting in increased neuronal activation within the spinal cord dorsal horn regions associated with micturition and nociception[16,17].

Our mRNA expression results confirm *Gpbar1* expression in all layers of the mouse urinary bladder, building on a previous study showing expression of the TGR5 gene *Gpbar1* mRNA in whole rat bladder[23]. Whilst TGR5 is known to play an important role in smooth muscle relaxation, particularly in the gallbladder and the stomach[57–59], it is particularly important to note that in the current study bladder muscle compliance was unchanged following intravesical administration of either Pg5α or CCDC. This indicates the Pg5α- or CCDC-induced hypersensitivity of bladder afferents to distension occurs at the level of the afferent ending. Importantly

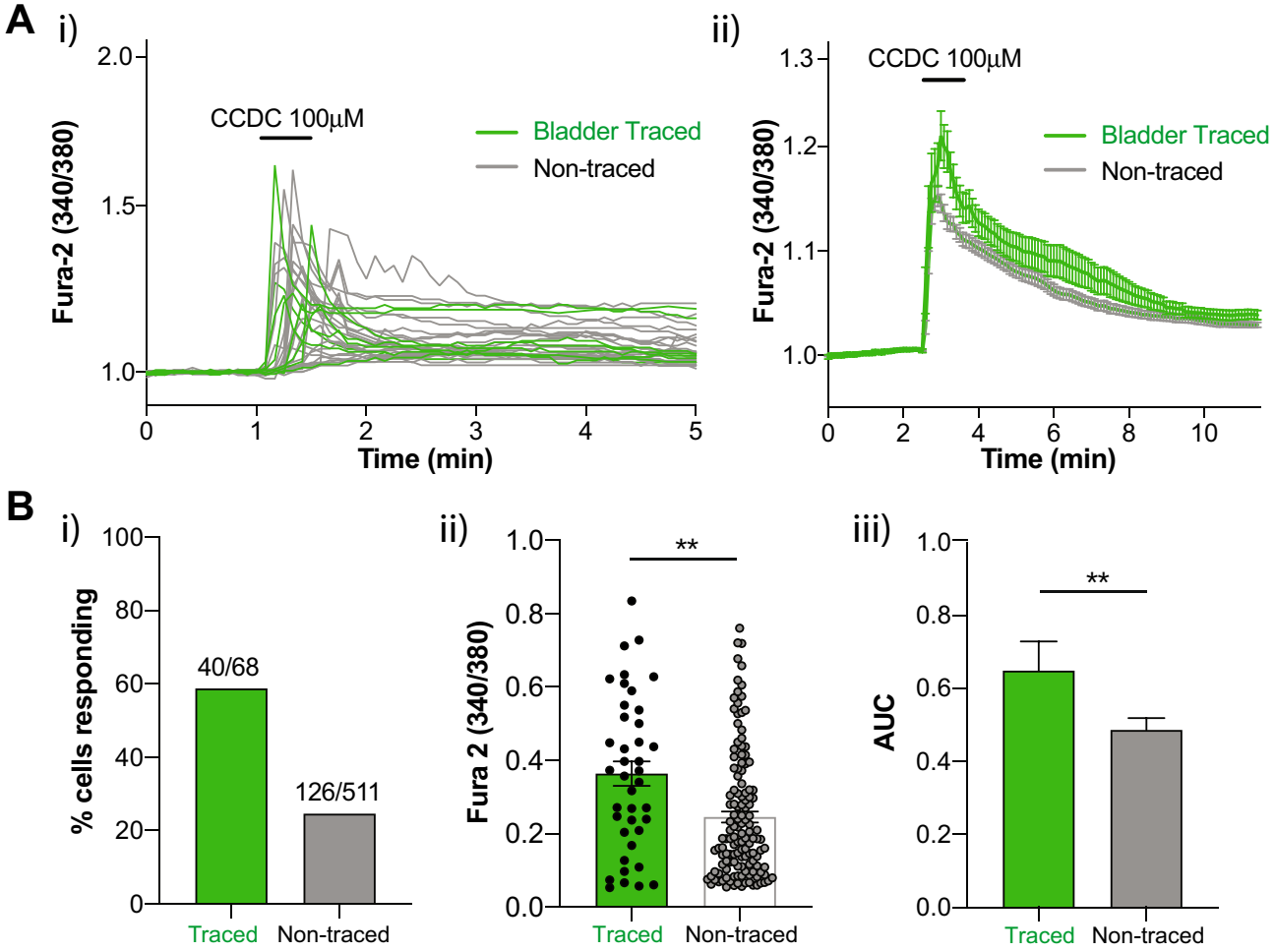

Figure 6. In vitro activation of TGR5 in primary DRG neurons results in increased intracellular Ca^{2+}. (**A**) Live cell calcium imaging was performed on retrogradely traced, isolated LS DRG neurons from wild-type mice to measure intracellular Ca^{2+} changes in response to direct CCDC (100 μM) application. (**i**) An example experiment showing bladder traced (green) and non-traced (grey) DRG neurons from a single coverslip, with each line representing a single neuron over time and an increase in the Fura-2 fluorescence ratio (340/380) indicating an increase in intracellular Ca^{2+} from baseline normalised to a ratio of 1. (**ii**) Mean ± SEM of intracellular Ca^{2+} responses to CCDC (100 μM) in traced (n = 40) and non-traced (n = 126) neurons. (**B**) (**i**) 58.82% of bladder traced neurons (40 out of 68; N = 7) responded to CCDC application with an increase in intracellular Ca^{2+}, compared to only 24.65% of non-traced neurons (126 out of 511). The response to CCDC for traced and non-traced neurons showed (**ii**) a significantly higher maximum peak (****$P < 0.0001$) and (**iii**) a significantly larger area under the curve (AUC, **$P < 0.01$) in bladder-innervating DRG neurons compared to non-traced DRG neurons.

our single cell RT-PCR data show *Gpbar1* expression in 13% of bladder-innervating DRG neurons, which is comparable to recent studies in cutaneous- and colon-innervating DRG neurons showing 8% and 19% are positive for *Gpbar1* mRNA expression, respectively[24,26]. Both studies further analysed co-expression with *Trpa1* and *Trpv1*, which are common downstream targets for GPCR signalling and have both been shown to play a role in mediating itch and pain sensation[15,48]. These previous studies indicate that TRPA1 is the key downstream effector coupled to neuronal TGR5, with both cutaneous and colonic afferent hypersensitivity to CCDC abolished in *trpa1*$^{-/-}$ mice[24,26]. Previous expression data largely supports this, as cutaneous- and colon-innervating DRG neurons show high co-expression with both *trpa1* (100% in cutaneous and 83% in colonic *Gpbar1*-positive DRG neurons) and *trpv1* (60% in cutaneous and 78% in colonic *Gpbar1*-positive DRG neurons)[24,26]. Another study assessing *Gpbar1* mRNA expression in small diameter DRG neurons showed lower associations with both *trpa1* (41% of *Gpbar1*-positive small diameter DRG neurons) and *trpv1* (32% of *Gpbar1*-positive small diameter DRG neurons)[29]. Interestingly, we show bladder-innervating DRG neurons differ to cutaneous and colon-innervating DRG neurons, with 100% of bladder-innervating *Gpbar1*-expressing DRG neurons co-expressing *trpv1,* but only 30% co-expressing *trpa1*.

Our in vitro functional calcium imaging data showed CCDC activated a population of bladder-innervating DRG neurons, and that the magnitude of these CCDC responses were greater in bladder-innervating neurons than non-bladder innervating neurons, suggesting an enhanced role in bladder pathways. Bladder-innervating

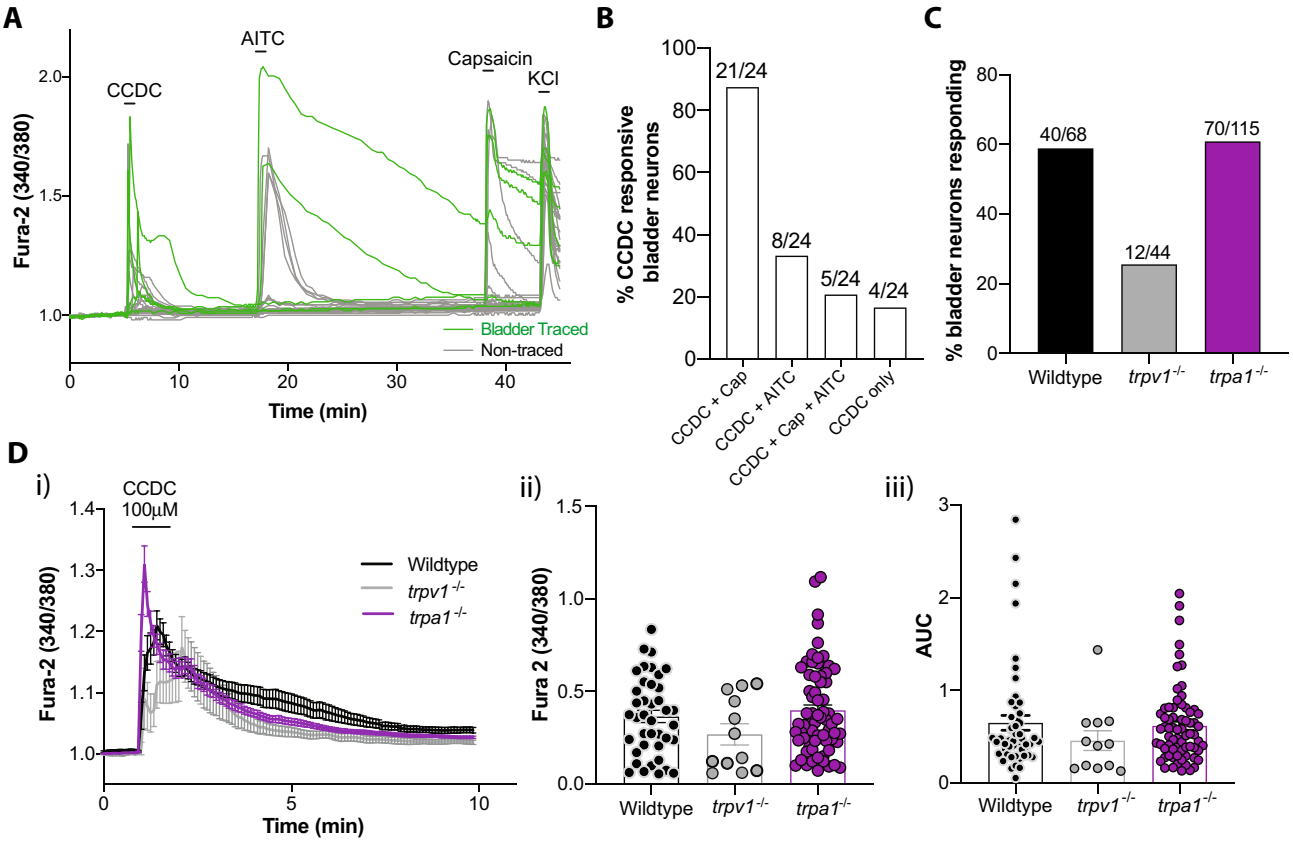

Figure 7. Intracellular calcium responses to CCDC in *trpv1*$^{-/-}$ and *trpa1*$^{-/-}$ mice. (**A**) Live cell calcium imaging was performed on isolated, bladder-traced DRG neurons from WT, *trpv1*$^{-/-}$ and *trpa1*$^{-/-}$ mice to determine changes in intracellular Ca^{2+} in response to direct application of CCDC. An example experiment showing bladder traced (green) and non-traced (grey) neurons from a single coverslip, with each line representing a single neuron over time and an increase in the Fura-2 fluorescence ratio (340/380) indicating an increase in intracellular Ca^{2+}, from baseline normalised to a ratio of 1. The TRPA1 agonist AITC (100 µM) and TRPV1 agonist capsaicin (50 nM) were applied in succession following CCDC (100 µM) and washout periods to determine co-activation of neurons. KCl was added at the end of each experiment as a positive neuronal control. (**B**) The percentage of neurons co-responding with CCDC to each compound. Of the CCDC-responsive neurons 87.5% (21/24) also responded to capsaicin, whilst 33.3% (8/24) of CCDC-responsive bladder-traced neurons also responded to AITC. Only 16.7% (4/24) of CCDC-responsive bladder-traced neurons were unresponsive to both AITC and capsaicin. (**C**) The percentage of bladder-traced neurons responding to CCDC in WT, *trpv1*$^{-/-}$ and *trpa1*$^{-/-}$ mice. Compared to 58.8% observed in wildtype neurons, only 27.3% of *trpv1*$^{-/-}$ bladder-traced neurons (12 out of 44; N = 4) responded to CCDC, whilst 60.9% of bladder-traced neurons from *trpa1*$^{-/-}$ mice responded to CCDC (70 out of 115; N = 5). (**D**) (**i**) An average response curve for each population was determined from the CCDC-responsive bladder-innervating DRG neurons, to visually compare the neuronal responses between wildtype (black), *trpv1*$^{-/-}$ (grey), and *trpa1*$^{-/-}$ (purple) bladder neurons. (**ii**) maximum peak fluorescence and (**iii**) area under the curve (AUC) of fluorescence were compared across neurons from wildtype (black), *trpv1*$^{-/-}$ (grey), and *trpa1*$^{-/-}$ (purple) mice. No significant differences between either *trpv1*$^{-/-}$ or *trpa1*$^{-/-}$ neurons and wild-type neurons were observed. Data are represented as percentage of neurons (**B**,**C**) or mean ± SEM (**Di**,**Dii**,**Diii**). *P* values were determined using Kruskal–Wallis non-parametric ANOVA tests with subsequent Dunn's post hoc multiple comparisons tests.

DRG neuron responses to CCDC supports previous studies whereby CCDC activates sub-populations of colonic and cutaneous DRG neurons[24,26]. However, unlike these previous studies, significant functional co-expression was observed between TGR5 and TRPV1 (CCDC and capsaicin responsive) with less interaction observed between TGR5 and TRPA1 (CCDC and AITC responsive). These data correspond with our mRNA expression data which demonstrates extensive *Gpbar1 and trpv1 co-expression,* suggesting an alternative downstream coupling mechanism for TGR5 to that seen in colonic or cutaneous DRG neurons. The potential associations of in vitro CCDC activity with TRPA1 and TRPV1 were further dissected using DRG from *trpa1*$^{-/-}$ and *trpv1*$^{-/-}$ mice. Data from these DRG neurons demonstrate that CCDC-induced activation of bladder-innervating DRG neurons was greatly reduced in *trpv1*$^{-/-}$ DRG neurons, whilst no significant differences in CCDC responses were observed in the absence of *trpa1*. Together, these data indicate that TGR5 signalling in bladder afferents is partially mediated by TRPV1 as a potential downstream effector.

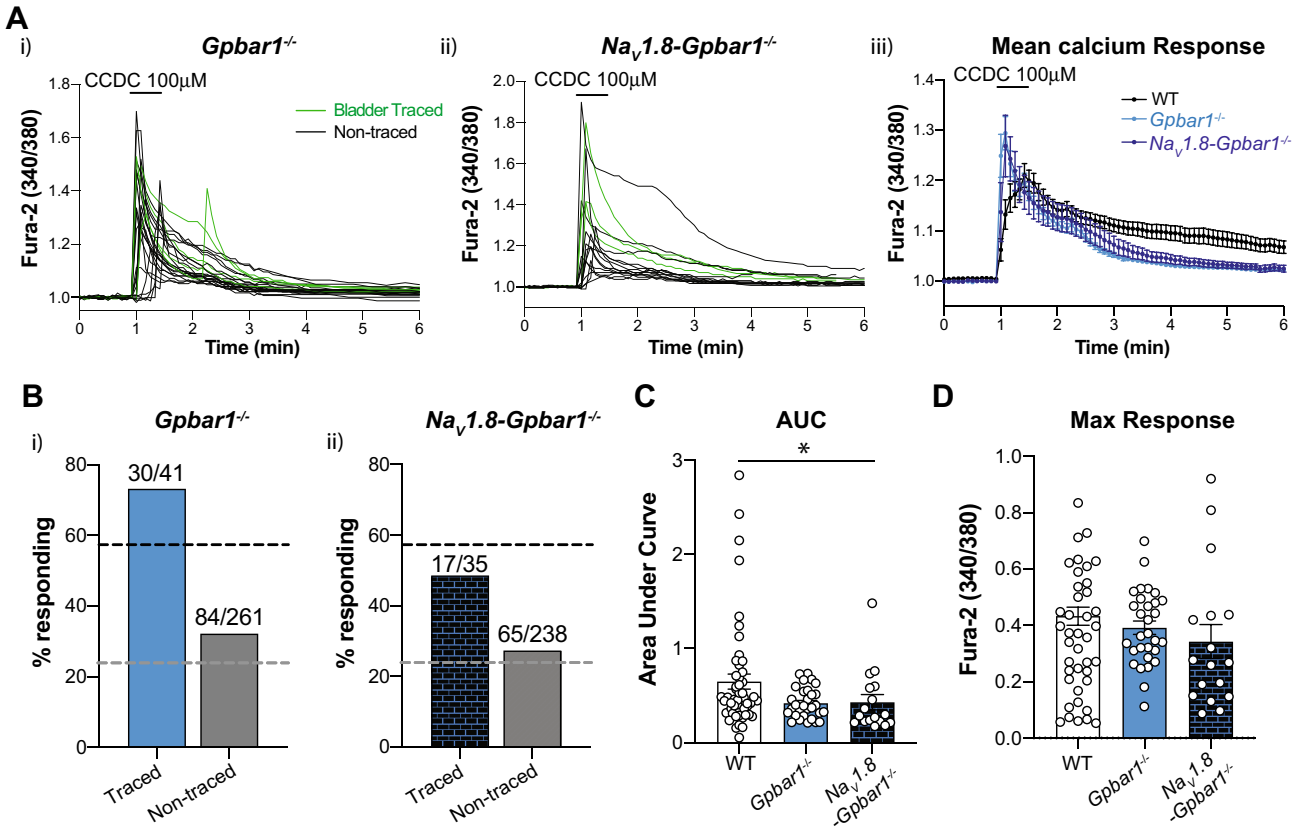

Figure 8. Intracellular calcium responses to CCDC in neuronal cultures from *Gpbar1*$^{-/-}$ and *Na*$_V$*1.8-Gpbar1*$^{-/-}$ mice. (**A**) Intracellular calcium changes were measured in bladder-traced (green) and untraced (black) lumbosacral dorsal root ganglia (LS DRG) neurons from *Gpbar1*$^{-/-}$ and *Na*$_V$*1.8-Gpbar1*$^{-/-}$ mice in response to CCDC (100 μM). Example experiments from (**i**) *Gpbar1*$^{-/-}$ and (**ii**) *Na*$_V$*1.8-Gpbar1*$^{-/-}$ mice showing bladder traced (green) and non-traced (black) neurons from a single coverslip responding to CCDC (100 μM). Each line represents a single neuron and an increase in the Fura-2 fluorescence ratio (340/380) indicates an increase in intracellular Ca^{2+}. (**iii**) Mean ± SEM of intracellular Ca^{2+} responses to CCDC (100 μM) in bladder-innervating neurons from Wildtype, *Gpbar1*$^{-/-}$ and *Na*$_V$*1.8-Gpbar1*$^{-/-}$ mice. (**B**) The percentage (%) of neurons responding to 100 μM CCDC in *Gpbar1*$^{-/-}$ and *Na*$_V$*1.8-Gpbar1*$^{-/-}$ mice. (**i**) 73.2% (30 out of 41) of bladder-traced *Gpbar1*$^{-/-}$ neurons, and (**ii**) 48.6% (17 out of 35) of bladder-traced *Na*$_V$*1.8-Gpbar1*$^{-/-}$ neurons responded to CCDC. Dashed black and grey lines represent % of bladder-innervating neurons and untraced neurons from wildtype mice responding to CCDC (100 μM). (**C**) The average intracellular calcium change over time (AUC) in response to 100 μM CCDC was determined for *Gpbar1*$^{-/-}$ (light blue) and *Na*$_V$*1.8-Gpbar1*$^{-/-}$ (dark blue) bladder-traced LS DRG neurons and compared to wildtype (white). No statistical difference in the area under the curve (AUC) was observed between wildtype and *Gpbar1*$^{-/-}$ responses (ns, $P > 0.05$), whereas *Na*$_V$*1.8-Gpbar1*$^{-/-}$ bladder-traced responses had a significantly reduced AUC compared to wildtype (*$P < 0.05$). No significant difference was observed in the AUC between *Gpbar1*$^{-/-}$ and *Na*$_V$*1.8-Gpbar1*$^{-/-}$ responses. (**D**) Maximum fluorescent responses to CCDC (100 μM) were not significantly different between wildtype, *Gpbar1*$^{-/-}$ and *Na*$_V$*1.8-Gpbar1*$^{-/-}$ bladder-traced neurons (ns, $P > 0.05$). Data are represented as percentage of cells (**B**) or mean ± SEM (**C**,**D**) with individual data points in (**C**,**D**) representing values from individual cells. *P* values above were determined by Kruskal–Wallis non-parametric analysis of variance with Dunn's multiple comparisons tests (**C**,**D**).

Our ex vivo and in vivo data with CCDC are relatively clear cut in the role TGR5 plays in bladder afferent hypersensitivity, with agonist responses reduced or absent in *Gpbar1*$^{-/-}$ mice. However, the proportion of bladder-innervating DRG neurons responding to CCDC is greater than the single cell mRNA expression data predicts. Furthermore, in these calcium imaging studies CCDC responses were still observed in DRG from *Gpbar1*$^{-/-}$ *(global knockout of Gpbar1) and Na*$_V$*1.8-Gpbar1*$^{-/-}$ (neuronal knockout of *Gpbar1* as 98% of bladder-innervating DRG neurons express $Na_V1.8$[37]) mice. Whilst CCDC is a synthetic agonist developed to be TGR5-specific[38] it is unclear if it can also act via additional receptors. For example, in addition to TGR5[28] progesterone metabolites can act on progesterone receptors and $GABA_A$ receptors[60,61], although $GABA_A$ receptor agonists inhibit rather than sensitize visceral afferents[62]. In addition, recent data show that some bile acids can also act through MrgprX4[25,63]. In the current study we also found that CCDC activated a small percentage of non-neuronal cells and that these responses were similar between wildtype, *Gpbar1*$^{-/-}$ *and Na*$_V$*1.8-Gpbar1*$^{-/-}$ DRG neurons. A recent study has shown in human and monkey that TGR5 is highly expressed in satellite glial cells

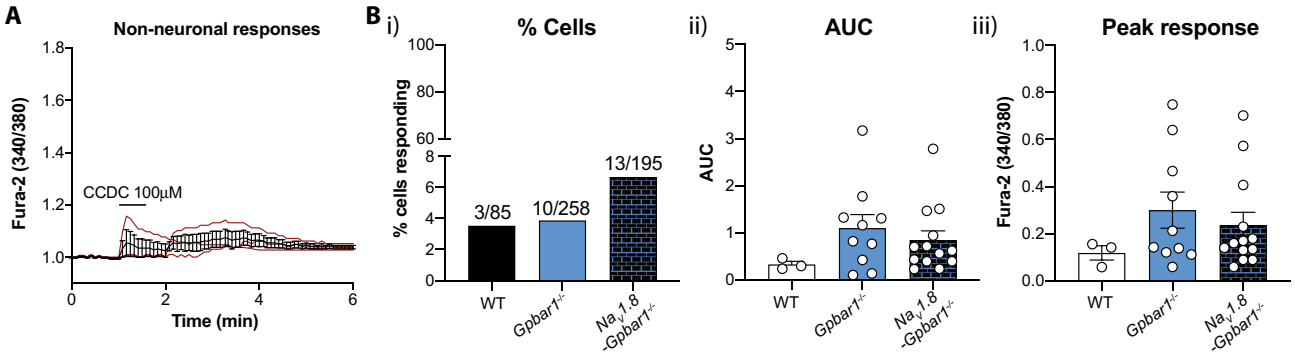

Figure 9. Intracellular calcium responses to CCDC in non-neuronal cells from wildtype, *Gpbar1*$^{-/-}$ and *Na*$_V$*1.8-Gpbar1*$^{-/-}$ mice. (**A**) Intracellular calcium changes were measured in non-neuronal cells from wildtype (WT: black), *Gpbar1*$^{-/-}$ (light blue) and *Na*$_V$*1.8-Gpbar1*$^{-/-}$ (dark blue) mice in response to CCDC (100 μM). Mean ± SEM of intracellular Ca^{2+} responses to CCDC (100 μM) in non-neuronal cells from wildtype mice. Red lines represent the three individual responding cells (3/85). (**B**) (**i**) The percentage (%) of non-neuronal cells responding to CCDC (100 μM). 3.5% (3 out of 85), 3.88% (10 out of 258) and 6.67% (13 out of 195) of non-neuronal cells from wildtype, *Gpbar1*$^{-/-}$, and Na_V1.8-*Gpbar1*$^{-/-}$ respectively responded to CCDC (100 μM). (**ii**) No significant differences were observed in either the average intracellular calcium response over time or (**ii**) the peak fluorescent response to 100 μM CCDC between non-neuronal cells from wildtype, *Gpbar1*$^{-/-}$ (light blue) and Na_V1.8-*Gpbar1*$^{-/-}$ (dark blue) mice. Data are represented as percentage of cells (**Bi**) or Mean ± SEM (**Bii**,**Biii**), with individual data points representing values from individual cells. Significance was determined by Kruskal–Wallis non-parametric analysis of variance with Dunn's multiple comparisons tests (**Bii**,**Biii**).

surrounding DRG neurons but not the DRG neurons, whereas in mouse TGR5 is expressed by DRG neurons[25,63]. It is possible that some of the disparity observed in our DRG calcium imaging studies are related to indirect actions, whereby satellite glial cells release factors in response to CCDC application and that these factors then act on and activate DRG neurons. These discrepancies aside overall our mRNA expression, ex vivo and in vivo functional evidence indicate that the physiological actions of both the synthetic and the endogenous TGR5 agonists are mainly due to activation of TGR5. In particular, the enhanced dorsal horn neuronal activation in response to CCDC and bladder distension is completely lost in *Gpbar1*$^{-/-}$ mice, suggesting TGR5 expressing bladder-innervating DRG neurons are crucial for these sensitizing actions of CCDC in vivo.

How bile acid or progesterone metabolite urinary content is altered during bladder hypersensitivity is not yet known. However, an important consideration in determining any role for TGR5 in OAB and IC/BPS is the permeability of the urothelium. Increased urothelial permeability is a common finding in IC/BPS, which may allow increased access of urinary contents, such as bile acids and progesterone metabolites, to access the underlying tissue and nerve endings within the bladder wall[1,64]. Further studies are required to determine the impact of TGR5 signalling in bladder afferents during states of hypersensitivity and any changes specific to this pathway including receptor expression and agonist concentrations in the urine and tissue.

In conclusion, this study has identified the expression and function of the bile acid receptor TGR5 in bladder-innervating afferent DRG neurons. Intravesical administration of TGR5 agonists in the urinary bladder results in TGR5-dependent enhanced mechanosensitivity to bladder distension and increased spinal dorsal horn neuronal activity, indicating a role for TGR5 in mediating the sensitivity of bladder sensory signalling pathways. Further, we have shown that TGR5 activation in bladder-innervating neurons is partially mediated by TRPV1. As irritant-sensing GPCRs are now known to enhance bladder mechanosensitivity, TGR5 and its related receptors may represent potential targets for future treatment in conditions of bladder hypersensitivity.

Received: 3 March 2022; Accepted: 2 June 2022
Published online: 15 June 2022

References

1. Grundy, L., Caldwell, A. & Brierley, S. M. Mechanisms underlying overactive bladder and interstitial cystitis/painful bladder syndrome. *Front. Neurosci.* **12**, 931 (2018).
2. Hanno, P. M. Interstitial cystitis-epidemiology, diagnostic criteria, clinical markers. *Rev. Urol.* **4**(Suppl 1), S3-8 (2002).
3. Yee, C. H. *et al.* Survey on prevalence of lower urinary tract symptoms in an Asian population. *Hong Kong Med. J.* **25**, 13–20 (2019).
4. Truzzi, J. C. *et al.* Overactive bladder—18 years—Part I. *Int. Braz. J. Urol.* **42**, 188–198 (2016).
5. Ackerman, A. L., Lai, H. H., Parameshwar, P. S., Eilber, K. S. & Anger, J. T. Symptomatic overlap in overactive bladder and interstitial cystitis/bladder pain syndrome: Development of a new algorithm. *BJU Int.* **123**, 682–693 (2019).
6. Fowler, C. J., Griffiths, D. & de Groat, W. C. The neural control of micturition. *Nat. Rev. Neurosci.* **9**, 453–466 (2008).
7. de Groat, W. C. & Yoshimura, N. Anatomy and physiology of the lower urinary tract. *Handb. Clin. Neurol.* **130**, 61–108 (2015).
8. Spencer, N. J. *et al.* Identifying unique subtypes of spinal afferent nerve endings within the urinary bladder of mice. *J. Comp. Neurol.* **526**, 707–720 (2018).
9. Rahnama'i, M. S. *et al.* Distribution and sub-types of afferent fibre in the mouse urinary bladder. *J. Chem. Neuroanat.* **79**, 1–11 (2017).
10. Grundy, L. *et al.* Translating peripheral bladder afferent mechanosensitivity to neuronal activation within the lumbosacral spinal cord of mice. *Pain* **160**, 793–804 (2019).

11. de Groat, W. C., Griffiths, D. & Yoshimura, N. Neural control of the lower urinary tract. *Compr. Physiol.* **5**, 327–396 (2015).
12. Andersson, K. E. & Arner, A. Urinary bladder contraction and relaxation: Physiology and pathophysiology. *Physiol. Rev.* **84**, 935–986 (2004).
13. Hauser, A. S., Attwood, M. M., Rask-Andersen, M., Schioth, H. B. & Gloriam, D. E. Trends in GPCR drug discovery: New agents, targets and indications. *Nat. Rev. Drug Discov.* **16**, 829–842 (2017).
14. Meixiong, J. & Dong, X. Mas-related G protein-coupled receptors and the biology of itch sensation. *Annu. Rev. Genet.* **51**, 103–121 (2017).
15. Brizuela, M., Castro, J., Harrington, A. M. & Brierley, S. M. Pruritogenic mechanisms and gut sensation: Putting the "irritant" into irritable bowel syndrome. *Am. J. Physiol. Gastrointest. Liver Physiol.* **320**, G1131-g1141 (2021).
16. Grundy, L. *et al.* Histamine induces peripheral and central hypersensitivity to bladder distension via the histamine H1 receptor and TRPV1. *Am. J. Physiol. Renal. Physiol.* **318**, F298–F314 (2020).
17. Grundy, L. *et al.* Activation of MrgprA3 and MrgprC11 on bladder-innervating afferents induces peripheral and central hypersensitivity to bladder distension. *J. Neurosci.* **41**, 3900–3916 (2021).
18. Maruyama, T. *et al.* Identification of membrane-type receptor for bile acids (M-BAR). *Biochem. Biophys. Res. Commun.* **298**, 714–719 (2002).
19. Kawamata, Y. *et al.* A G protein-coupled receptor responsive to bile acids. *J. Biol. Chem.* **278**, 9435–9440 (2003).
20. Alemi, F. *et al.* The receptor TGR5 mediates the prokinetic actions of intestinal bile acids and is required for normal defecation in mice. *Gastroenterology* **144**, 145–154 (2013).
21. Yoneno, K. *et al.* TGR5 signalling inhibits the production of pro-inflammatory cytokines by in vitro differentiated inflammatory and intestinal macrophages in Crohn's disease. *Immunology* **139**, 19–29 (2013).
22. Poole, D. P. *et al.* Expression and function of the bile acid receptor GpBAR1 (TGR5) in the murine enteric nervous system. *Neurogastroenterol. Motil.* **22**(814–25), e227–e228 (2010).
23. Zhu, J. *et al.* Hydrophobic bile acids relax rat detrusor contraction via inhibiting the opening of the Na(+)/Ca(2)(+) exchanger. *Sci. Rep.* **6**, 21358 (2016).
24. Lieu, T. *et al.* The bile acid receptor TGR5 activates the TRPA1 channel to induce itch in mice. *Gastroenterology* **147**, 1417–1428 (2014).
25. Yu, H. *et al.* MRGPRX4 is a bile acid receptor for human cholestatic itch. *Elife* **8**, 25 (2019).
26. Castro, J. *et al.* Activation of pruritogenic TGR5, MrgprA3, and MrgprC11 on colon-innervating afferents induces visceral hypersensitivity. *JCI Insight* **4**, 25 (2019).
27. Keitel, V. *et al.* Effect of maternal cholestasis on TGR5 expression in human and rat placenta at term. *Placenta* **34**, 810–816 (2013).
28. Abu-Hayyeh, S. *et al.* Prognostic and mechanistic potential of progesterone sulfates in intrahepatic cholestasis of pregnancy and pruritus gravidarum. *Hepatology* **63**, 1287–1298 (2016).
29. Alemi, F. *et al.* The TGR5 receptor mediates bile acid-induced itch and analgesia. *J. Clin. Invest.* **123**, 1513–1530 (2013).
30. Alnouti, Y. Bile Acid sulfation: A pathway of bile acid elimination and detoxification. *Toxicol. Sci.* **108**, 225–246 (2009).
31. Baumgartner, U. *et al.* Pattern of bile acid regurgitation and metabolism during perfusion of the bile duct obstructed rat liver. *J. Hepatol.* **22**, 208–218 (1995).
32. Meng, L. J. *et al.* Profiles of bile acids and progesterone metabolites in the urine and serum of women with intrahepatic cholestasis of pregnancy. *J. Hepatol.* **27**, 346–357 (1997).
33. Bathena, S. P. *et al.* Urinary bile acids as biomarkers for liver diseases I Stability of the baseline profile in healthy subjects. *Toxicol. Sci.* **143**, 296–307 (2015).
34. Stanczyk, F. Z. All progestins are not created equal. *Steroids* **68**, 879–890 (2003).
35. Grundy, L., Daly, D. M., Chapple, C., Grundy, D. & Chess-Williams, R. TRPV1 enhances the afferent response to P2X receptor activation in the mouse urinary bladder. *Sci. Rep.* **8**, 197 (2018).
36. Grundy, L. *et al.* Chronic linaclotide treatment reduces colitis-induced neuroplasticity and reverses persistent bladder dysfunction. *JCI Insight* **3**, 25 (2018).
37. Grundy, L. *et al.* Tetrodotoxin-sensitive voltage-gated sodium channels regulate bladder afferent responses to distension. *Pain* **159**, 2573–2584 (2018).
38. Evans, K. A. *et al.* Discovery of 3-aryl-4-isoxazolecarboxamides as TGR5 receptor agonists. *J. Med. Chem.* **52**, 7962–7965 (2009).
39. Lein, E. S. *et al.* Genome-wide atlas of gene expression in the adult mouse brain. *Nature* **445**, 168–176 (2007).
40. Inserra, M. C. *et al.* Multiple sodium channel isoforms mediate the pathological effects of Pacific ciguatoxin-1. *Sci. Rep.* **7**, 42810 (2017).
41. Castro, J. *et al.* alpha-Conotoxin Vc1.1 inhibits human dorsal root ganglion neuroexcitability and mouse colonic nociception via GABAB receptors. *Gut* **66**, 1083–1094 (2017).
42. Jiang, G. Y. *et al.* Neurochemical characterization of pERK-expressing spinal neurons in histamine-induced itch. *Sci. Rep.* **5**, 12787 (2015).
43. Osteen, J. D. *et al.* Selective spider toxins reveal a role for the Nav1.1 channel in mechanical pain. *Nature* **534**, 494–499 (2016).
44. Grundy, L. *et al.* NKA enhances bladder-afferent mechanosensitivity via urothelial and detrusor activation. *Am. J. Physiol. Renal Physiol.* **315**, F1174–F1185 (2018).
45. Chess-Williams, R., Sellers, D. J., Brierley, S. M., Grundy, D. & Grundy, L. Purinergic receptor mediated calcium signalling in urothelial cells. *Sci. Rep.* **9**, 16101 (2019).
46. Konthapakdee, N. *et al.* Serotonin exerts a direct modulatory role on bladder afferent firing in mice. *J. Physiol.* **597**, 5247–5264 (2019).
47. Todd, A. J. Neuronal circuitry for pain processing in the dorsal horn. *Nat. Rev. Neurosci.* **11**, 823–836 (2010).
48. Wilson, S. R. *et al.* TRPA1 is required for histamine-independent, Mas-related G protein-coupled receptor-mediated itch. *Nat. Neurosci.* **14**, 595–602 (2011).
49. Shim, W. S. *et al.* TRPV1 mediates histamine-induced itching via the activation of phospholipase A2 and 12-lipoxygenase. *J. Neurosci.* **27**, 2331–2337 (2007).
50. van Berge Henegouwen, G. P., Brandt, K. H., Eyssen, H. & Parmentier, G. Sulphated and unsulphated bile acids in serum, bile, and urine of patients with cholestasis. *Gut* **17**, 861–869 (1976).
51. de Groat, W. C. & Yoshimura, N. Afferent nerve regulation of bladder function in health and disease. *Handb. Exp. Pharmacol.* **20**, 91–138 (2009).
52. Park, S. K. *et al.* Synaptic connectivity of urinary bladder afferents in the rat superficial dorsal horn and spinal parasympathetic nucleus. *J. Comp. Neurol.* **527**, 3002–3013 (2019).
53. Nadelhaft, I., Vera, P. L., Card, J. P. & Miselis, R. R. Central nervous system neurons labelled following the injection of pseudorabies virus into the rat urinary bladder. *Neurosci. Lett.* **143**, 271–274 (1992).
54. Birder, L. A. & de Groat, W. C. Induction of c-fos expression in spinal neurons by nociceptive and nonnociceptive stimulation of LUT. *Am. J. Physiol.* **265**, R326–R333 (1993).
55. Birder, L. A., Roppolo, J. R., Erickson, V. L. & de Groat, W. C. Increased c-fos expression in spinal lumbosacral projection neurons and preganglionic neurons after irritation of the lower urinary tract in the rat. *Brain Res.* **834**, 55–65 (1999).
56. Grundy, L. & Brierley, S. M. Cross-organ sensitization between the colon and bladder: To pee or not to pee?. *Am. J. Physiol. Gastrointest. Liver Physiol.* **314**, G301–G308 (2018).

57. Lavoie, B. *et al.* Hydrophobic bile salts inhibit gallbladder smooth muscle function via stimulation of GPBAR1 receptors and activation of KATP channels. *J. Physiol.* **588**, 3295–3305 (2010).
58. Rajagopal, S. *et al.* Activation of G protein-coupled bile acid receptor, TGR5, induces smooth muscle relaxation via both Epac- and PKA-mediated inhibition of RhoA/Rho kinase pathway. *Am. J. Physiol. Gastrointest. Liver Physiol.* **304**, G527–G535 (2013).
59. Li, T. *et al.* The G protein-coupled bile acid receptor, TGR5, stimulates gallbladder filling. *Mol. Endocrinol.* **25**, 1066–1071 (2011).
60. Callachan, H. *et al.* Modulation of the GABAA receptor by progesterone metabolites. *Proc. R. Soc. Lond. B Biol. Sci.* **231**, 359–369 (1987).
61. Schumacher, M. *et al.* Revisiting the roles of progesterone and allopregnanolone in the nervous system: Resurgence of the progesterone receptors. *Prog. Neurobiol.* **113**, 6–39 (2014).
62. Loeza-Alcocer, E., McPherson, T. P. & Gold, M. S. Peripheral GABA receptors regulate colonic afferent excitability and visceral nociception. *J. Physiol.* **597**, 3425–3439 (2019).
63. Meixiong, J., Vasavda, C., Snyder, S. H. & Dong, X. MRGPRX4 is a G protein-coupled receptor activated by bile acids that may contribute to cholestatic pruritus. *Proc. Natl. Acad. Sci. USA* **116**, 10525–10530 (2019).
64. Keay, S. K., Birder, L. A. & Chai, T. C. Evidence for bladder urothelial pathophysiology in functional bladder disorders. *Biomed. Res. Int.* **2014**, 865463 (2014).

Acknowledgements

Work was supported by a National Health and Medical Research Council of Australia (NHMRC) Project Grant (APP1140297 to S.M.B), an NHMRC R.D Wright Biomedical Research Fellowship (APP1126378 to S.M.B), a National Institutes of Health grant (U01 NS113871 to S.M.B), and an Australian Research Council (ARC) Discovery Project (DP180101395 to A.M.H and S.M.B). Supported by grants from National Institutes of Health (NS102722, DE026806, DK118971, DE029951, NWB), Department of Defence (W81XWH1810431, NWB), National Health and Medical Research Council (63303, NWB).

Author contributions

A.C., L.G., A.M.H. and S.G.-C. performed the experiments. A.C., L.G., A.M.H., S.G.-C., J.C. and S.M.B. analysed the experiments. N.W.B. provided critical reagents, genetically modified mice and intellectual input. S.M.B. designed the statistical plan/analyses and supervised the study. A.M.H., N.W.B. and S.M.B. obtained funding for the study. A.C., L.G. and S.M.B. wrote the manuscript text and prepared the figures. A.C., L.G., A.M.H., S.G.-C., J.C., N.W.B. and S.M.B. reviewed and interpreted the data and contributed to the final manuscript.

Competing interests

NWB is a founding scientist of Endosome Therapeutics Inc. Research in NWB's laboratory is funded, in part, by Takeda Pharmaceuticals International. All other authors do not have conflict of interests related to this work.

Additional information

Correspondence and requests for materials should be addressed to S.M.B.

Reprints and permissions information is available at www.nature.com/reprints.

Publisher's note Springer Nature remains neutral with regard to jurisdictional claims in published maps and institutional affiliations.

Open Access This article is licensed under a Creative Commons Attribution 4.0 International License, which permits use, sharing, adaptation, distribution and reproduction in any medium or format, as long as you give appropriate credit to the original author(s) and the source, provide a link to the Creative Commons licence, and indicate if changes were made. The images or other third party material in this article are included in the article's Creative Commons licence, unless indicated otherwise in a credit line to the material. If material is not included in the article's Creative Commons licence and your intended use is not permitted by statutory regulation or exceeds the permitted use, you will need to obtain permission directly from the copyright holder. To view a copy of this licence, visit http://creativecommons.org/licenses/by/4.0/.

© The Author(s) 2022